2017

Arynes And Heteroarynes In The Synthesis Of Dibenzocinnolines, Diazaxanthyledenes, And Triptycenes

Sung-Eun Suh
University of Pennsylvania, orgsynsuh@gmail.com

Arynes And Heteroarynes In The Synthesis Of Dibenzocinnolines, Diazaxanthyledenes, And Triptycenes

Abstract
Arynes are known as useful synthons in organic synthesis. In particular, reactions accompanying multiple arynes have been employed for the construction of arenes and heteroarenes of complex molecules. Employing known reactivity modes of arynes such as cycloadditions, nucleophilic addition, bond insertion, Alder-ene, annulation, desaturation, and polymerization, a wide variety of transformation of reactive starting materials led to the development of novel fluorophores and energy materials, as well as the synthesis of natural products.

Harnessing the highly reactive arynes, the triple aryne-tetrazine (TAT) reaction was disclosed as a novel metal-free synthetic method for the preparation of dibenzo[de,g]cinnoline derivatives in a single operation. Dibenzo[de,g]cinnolines have been shown as potential fluorescent probes in cells. For the mechanism, multiple mechanistic steps of the TAT reaction were scrutinized by isolation of intermediates and byproducts as well as a computational study on the transition states and the competitive reactions pathways.

A facile two-step synthesis of the reported structure of xylopyridine A was developed from a pyridyne precursor and 2-fluorobenzoic acid utilizing a pyridyne insertion reaction followed by reductive coupling. Simple transformation of the reported xylopyridine A structure have given photoactivatable dyes and specific organelle staining probes in either live or fixed cells and tissues, exhibiting high quantum yields, photostability, cell permeability and low toxicity. On the basis of these results, the synthesis of multistage photoactivatable dyes was designed and studied.

Utilization of arynes allowed access to the synthesis of 9-substituted triptycene derivatives which have been recognized as three-way junction binders. Accompanying solid-phase peptide synthesis, the rapid diversification of the triptycene scaffold was achieved for screening in a nucleic acid junction binding assay.

Degree Type
Dissertation

Degree Name
Doctor of Philosophy (PhD)

Graduate Group
Chemistry

First Advisor
David M. Chenoweth

Keywords
Aryne, Benzyne, Dibenzo[de,g]cinnoline, The TAT Reaction, Triptycene, Xylopyridine A

ARYNES AND HETEROARYNES IN THE SYNTHESIS OF DIBENZOCINNOLINES, DIAZAXANTHYLEDENES, AND TRIPTYCENES

Sung-Eun Suh

A DISSERTATION
in

Chemistry

Presented to the Faculties of the University of Pennsylvania

in

Partial Fulfillment of the Requirements for the
Degree of Doctor of Philosophy

2017

Supervisor of Dissertation

_____

David M. Chenoweth
Assistant Professor of Chemistry

Graduate Group Chairperson

_____

Gary A. Molander
Hirschmann-Makineni Professor of Chemistry and Department Chair

Dissertation Committee:

Amos B. Smith III, Rhodes-Thompson Professor of Chemistry
Jeffrey D. Winkler, Merriam Professor of Chemistry
Eric J. Schelter, Associate Professor of Chemistry

ARYNES AND HETEROARYNES IN THE SYNTHESIS OF DIBENZOCINNOLINES, DIAZAXANTHYLEDENES, AND TRIPTYCENES

To Yeeun

ACKNOWLEDGEMENTS

I would like to thank my advisor, Professor David M. Chenoweth, for his patience, support and enthusiasm for the last five years. It was very fortunate that David let me to join his group. I will always remember when he told me "you should follow your own instincts." Even if he had much better ideas and insight, he first gave me numerous chances to plan and design some of my projects with his patience. Under his supervision, I was always excited to learn how to apply our synthetic achievements to the development of biological tools. He will continue to be my mentor and friend every day. I would also thank to my committee members. Dr. Amos B. Smith III, my committee chair, who was always willing to advise and help me when I was concerned about my future plans. Dr. Jeffrey D. Winkler always asked me sharp questions about my projects during the committee meetings, which trained me to think critically about my research. Not only Dr. Eric J. Schelter provided numerous scientific insights, but he also encouraged and supported me. Besides the committee members, I appreciate Dr. Madeleine M. Joullié for her willingness to advise me. I will always remember what you told me, "your safety is always first, chemistry can always wait." I have to thank Dr. E. James Petersson for teaching me about biological experiments and applications during fluorophore meetings and chemical biology class. My masters advisor, Dr. Cheon-Gyu Cho, deserves great thanks for guiding me in the real practical organic chemistry world outside textbooks, as well as training me to be equipped with synthetic skills.

I appreciate all lab members in the Chenoweth group. I was happy to work with Dr. Robert-André Rarig, Dr. Stephanie Barros, Dr. Mai Tran, Dr. Yitao Zhang, Adrienne Pesce, Roy Malamakal, Chanat Jay Aonbangkhen, Ina Yoon, Daniel Wu, Joomyung Vicky Jun, Alexander Kasznel, Samuel Melton, Dr. Jinxing Li, Alexander Simafranca, Moses Adenaike, and Gabriel Angrand. I am not able to mention everything that they have helped me from research to graduate life. I would like to especially thank Vicky (sitting next to me) for listening to my boring stories about Korean history, daily concerns, and future plans. I would also like to give a special thanks to Roy for sharing how Ph.D. life was going

during late nights. Additionally, I would like to thank my friends, Dr. Wonsuk Kim, Dr. Inji Shin, Dr. Taejong Paik, Dr. Heeoon Han, Dr. Jongwoo Park, Dr. Chan-Woo Lee, Dr. Jisun Lee, Dr. Young Eun Lee, Dr. Hongseok Yun, Dr. DaWeon Ryu, Dr. Jee Eon Kim, Dr. Sun Min Kim, Dr. Byeong-Seon Kim, Dr. Kwang-Im Oh, Dr. Youngkuk Kim, Houng Kang, Yumin Lee, Dabin Kim, Paul Sung, Joseph Han, Dr. Jaruwan Chatwichien, Yohei Yamashita, Claire Gober, Yike Zou, Qi Liu, Chun Liu, Dr. Doory Kim, Yeunook Bae, Eui-Hyuk Choi, Sunghoon Lee, and Jongwon Lee. I will never forget our friendship.

For the facilities at Penn, I would like to thank Dr. Patrick J. Carroll, Dr. Rakesh Kohli, Dr. Charles W. Ross III, Dr. George Furst, Dr. Jun Gu, Dr. Simon Berritt, and Ryan S. Kubanoff. They were fantastic! Special thanks to Dr. Kohli and Dr. Ross for giving me a chance to work as a laboratory research associate in Mass Spectrometry Laboratory. I also appreciate Dr. Judith N. Currano and Kristen Muscat for catching what I missed and helping me so many times. I sincerely thank my collaborators: Dr. J. Nicholas Betley, Elen Hernandez, Dr. Kendall N. Houk, Dr. Shuming Chen, Dr. Robert O. Heuckeroth, Silvia Huerta, Dr. Adam I. Marcus, and Najdat Zohbi. Discussions with them have enriched my knowledge outside of the "chemistry" box.

This thesis is dedicated to my lovely wife and a passionate painter, Yeeun Kang. Her bright energy and art have been refreshing my thoughts and allowing me to stay positive no matter how my experiment goes. I have to thank my parents, parents-in-law, brother-in-law, and all family members of my brother. Without their love and encouragement, I could not have finished my thesis.

ABSTRACT

ARYNES AND HETEROARYNES IN THE SYNTHESIS OF DIBENZOCINNOLINES, DIAZAXANTHYLEDENES, AND TRIPTYCENES

Sung-Eun Suh

David M. Chenoweth

Arynes are known as useful synthons in organic synthesis. In particular, reactions accompanying multiple arynes have been employed for the construction of arenes and heteroarenes of complex molecules. Employing known reactivity modes of arynes such as cycloadditions, nucleophilic addition, bond insertion, Alder-ene, annulation, desaturation, and polymerization, a wide variety of transformation of reactive starting materials led to the development of novel fluorophores and energy materials, as well as the synthesis of natural products.

Harnessing the highly reactive arynes, the triple aryne-tetrazine (TAT) reaction was disclosed as a novel metal-free synthetic method for the preparation of dibenzo[*de*,*g*]cinnoline derivatives in a single operation. Dibenzo[*de*,*g*]cinnolines have been shown as potential fluorescent probes in cells. For the mechanism, multiple mechanistic steps of the TAT reaction were scrutinized by isolation of intermediates and byproducts as well as a computational study on the transition states and the competitive reactions pathways.

A facile two-step synthesis of the reported structure of xylopyridine A was developed from a pyridyne precursor and 2-fluorobenzoic acid utilizing a pyridyne insertion reaction followed by reductive coupling. Simple transformation of the reported xylopyridine A structure have given

photoactivatable dyes and specific organelle staining probes in either live or fixed cells and tissues, exhibiting high quantum yields, photostability, cell permeability and low toxicity. On the basis of these results, the synthesis of multistage photoactivatable dyes was designed and studied.

Utilization of arynes allowed access to the synthesis of 9-substituted triptycene derivatives which have been recognized as three-way junction binders. Accompanying solid-phase peptide synthesis, the rapid diversification of the triptycene scaffold was achieved for screening in a nucleic acid junction binding assay.

TABLE OF CONTENTS

LIST OF TABLES

CHAPTER 2

APPENDIX 1

APPENDIX 2

APPENDIX 3

CHAPTER 5

APPENDIX 4

CHAPTER 7

APPENDIX 6

CHAPTER 8

APPENDIX 7

LIST OF FIGURES

CHAPTER 1

CHAPTER 2

APPENDIX 1

CHAPTER 3

APPENDIX 2

CHAPTER 4

APPENDIX 3

CHAPTER 5

APPENDIX 4

CHAPTER 6

APPENDIX 5

CHAPTER 7

APPENDIX 6

CHAPTER 8

APPENDIX 7

CHAPTER 9

APPENDIX 8

LIST OF SCHEMES

CHAPTER 1

CHAPTER 3

CHAPTER 4

CHAPTER 5

CHAPTER 7

CHAPTER 8

CHAPTER 9

Chapter 1

Multiple Aryne Synthons for Ring Construction

1.1 Introduction

1.1.1 Prologue

For more than 70 years, aryne-engaged reactions have been highly praised as one of the most rapid ring-constructing methodologies.[1] Along with providing brisk reaction speed, arynes possess diverse reactivity modes, participating in [2+2], [3+2], [4+2], [5+2], and [2+2+2] cycloadditions[1a] as well as nucleophilic addition,[1l] σ-bond insertion,[1g] Alder-ene reactions,[2] annulation,[3] desaturation,[4] and polymerization.[5] To accompany other substrates, multicomponent or domino aryne reactions have been developed.[1f,n] Furthermore, intermolecular reactions of more than two arynes and substrates have shortened the number of reaction steps toward target molecules, constructed polycyclic compounds, and led to the discovery of new synthetic methodologies.

1.1.2 History of Benzyne Generation Methods

The first preliminary evidence for the existence of arynes was reported in 1902.[6] Stoermer and Kahlert demonstrated that 3-bromobenzofuran with KOH/EtOH affords the unexpected 2-ethoxybenzofuran not 3-ethoxybenzofuran. To explain the result, they proposed a triple bond on the furan ring of the intermediate; however, the mechanism was unclear. In 1953, Roberts and co-workers proposed benzyne formation and provided evidence based on their observations.[7]

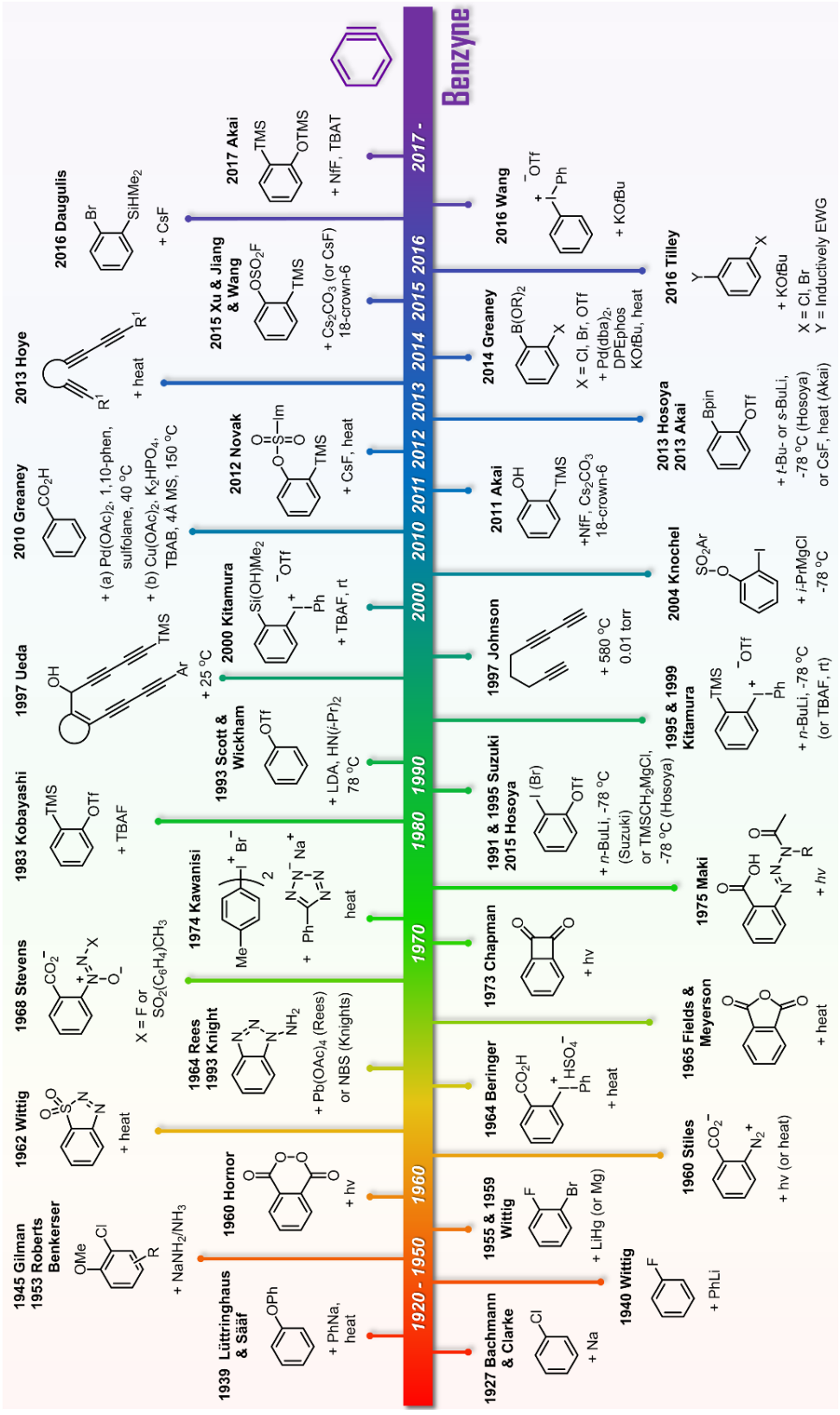

Figure 1.1. Timeline of representative benzyne generation methods.

Twenty-six years before the term "benzyne" was coined by Roberts, Bachman and Clarke reported the [2+2+2] cycloaddition of three equivalents of benzyne, which is called "free phenylene" in the report (Figure 1.1).[8] Two equivalents of free phenyl radicals, which are generated from the Wurtz-Fittig reaction of chlorobenzenes, react with sodium metal to generate benzene and benzyne. The authors observed triphenylene as the cycloaddition product. In 1939, Lüttringhaus and Sääf disclosed that benzyne generation from the reaction of diphenylether and phenylsodium might explain the unforeseen rearrangements.[9] In the early 1940s, Wittig and co-workers proposed the possible generation of a triple bond on the benzene ring from the reaction of fluorobenzyne and phenyl lithium even though the authors were unsure about the formation of benzyne.[10] In 1945, Gilman and Avakian reported the unexpected synthesis of aniline.[11] In this report, addition of sodium amide to 1-chloro-2-methoxybenzene did not yield the desired *ortho*-substitution product, and only *meta*-amination was observed. After 8 years, Benkeser and Schroll explained that the addition of the amide to the *meta* position of 1-chloro-2-methoxybenzene followed by a 1,2-hydride shift and elimination may lead to the formation of the *meta*-substituted product.[12] However, this mechanism was improbable because the formation of benzyne from the addition of sodium amide to 1-chloro-2-methoxybenzene was proven by Roberts in the same year.[7] In 1955, Wittig and Pohmer excluded strong base for the formation of benzyne and employed 1-bromo-2-fluorobenzene as a benzyne precursor.[13] The addition of lithium amalgam generated benzyne, which reacted with furan to afford epoxynaphthalene. After 4 years, in place of lithium amalgam, magnesium was used to make benzyne, which undergoes a Diels-Alder reaction with anthracene to afford triptycene.[14]

The first metal-free benzyne generation method was introduced by Stiles and Miller in 1960.[15] Phenyldiazonium-2-carboxylate was formed by the reaction of anthranilic acid and

isoamylnitrite with the release of N_2 and CO_2 gas. Two years later, Wittig and Hoffmann developed benzo[*d*][1,2,3]thiadiazole 1,1-dioxide, which released SO_2 and N_2 gas to form benzyne.[16] In 1965, Fields and Meyerson reported the thermal decomposition of phthalic anhydride to generate benzyne with CO and CO_2 gas.[17] Three years later, Stevens reported 2-azoxybenzoic acid as a benzyne precursor, which was decomposed into benzyne with CO_2 gas and diimide as the byproducts.[18]

A hypervalent iodine-benzyne precursor (i.e., diphenyliodonium-2-carboxylate) was reported by Beringer and Huang in 1964.[19] Although the phenyliodonio group is a good leaving group, the generation of benzyne still required a high reaction temperature (i.e., approximately 200 °C). In the 1990s, phenyl[*o*-(trimethylsilyl)phenyl]iodonium triflate was developed by Kitamura and co-workers.[20] Replacing the carboxylic group of diphenyliodonium-2-carboxylate, Beringer's hypervalent iodine-benzyne precursor containing a silyl group enabled a lower reaction temperature (*n*-BuLi at –78 °C or TBAF at room temperature). In 1974, Kawanisi and co-workers also proposed the diaryliodonium benzyne precursor, which does not have any *ortho* substituent.[21] Benzyne was generated by adding sodium 5-phenyltetrazolide to diaryliodonium halides. Recently, Wang and Huang utilized diaryliodonium triflate as the benzyne precursor and potassium *t*-butoxide as the base for *N*-arylation of secondary amides.[22]

In 1964, Rees and Campbell reported the first oxidative method for benzyne generation in their short communication.[23] 1-Aminobenzotriazole goes through oxidation with lead(IV) acetate, evolving two equivalents of N_2 gas. After 29 years, Knight and Berkett succeeded in excluding the toxic lead oxidant and used NBS for the generation of benzyne.[24]

In 1960, Horner and Brüggemann reported the first photolytic method for benzyne generation.[25] Upon exposure to UV irradiation, phthaloyl peroxide releases CO_2 to form

benzyne at room temperature. In 1973, the report by Chapman and co-workers disclosed that irradiation of benzocyclobutenedione generated benzyne with two equivalents of CO_2 gas.[26] After two years, Maki and co-workers designed a novel photolytic benzyne precursor.[27] *o*-(*N*-acetyl-*N*-alky1triazeno)benzoic acids can be photochemically degraded into benzyne and side products, such as *N*-methylacetamide, N_2, and CO_2. In 2014, Schnarr and co-workers revisited this method and successfully performed the click reaction involving azides and Maki's benzyne precursor.[28]

Since Kobayashi developed silylaryl triflate aryne precursors in 1983, the scope of aryne derivatives has been broadened, and the synthetic utilization of arynes has become more accessible due to its mild reaction conditions.[29] Exploiting the strength of the Si-F bond, benzyne can be generated upon addition of a fluoride source at room temperature. The Suzuki,[30] Hosoya,[31] Akai,[32] and Greaney[33] groups have explored replacing the silyl group in Kobayashi's benzyne precursor with a halogen or bolyl group to enrich the application of aryne. Furthermore, in place of the triflate group, the Knochel,[34] Novak,[35] Xu, Jiang, Wang,[36] and Daugulis[37] groups installed halo or other sulfonate groups to broaden the scope of aryne reactions.

The method for generating benzyne by addition of a strong base to a benzyne precursor has been modified and is still used today. Scott, Wickham, and co-workers employed phenyl trifluoromethanesulfonate,[38] and Tilley and co-workers attached inductively electron-withdrawing group on *meta* position of phenyl halides.[39] Beyond the harsh conditions, the Greaney group recently developed novel benzyne generation methods. In 2010, the authors reported that benzoic acid undergoes palladium- or copper-catalyzed tandem C-H activation and decarboxylation to afford benzyne.[40] Akai and co-workers used perfluorobutanesulfonyl

fluoride (NfF) and cesium carbonate for the *in situ* formation of nonaflate followed by generation of benzyne from 2-(trimethylsilyl)phenol in 2011.[41] Recently, they modified 2-(trimethylsilyl)phenol to prepare a more stable precursor. NfF and TBAT have been employed to generate benzyne from 2-(trimethylsilyl)phenyl trimethylsilyl ethers.[42]

A hexadehydro-Diels–Alder (HDDA) reaction was independently reported by both the Ueda[43] and Johnson[44] groups in 1997. Johnson and Bradley employed nona-1,3,8-triyne with vacuum pyrolysis at 580 °C to afford indane and indene in 86% and 14% yield, respectively. The authors also performed the reaction with nona-1,3,8-triyne-1,9-d_2 to support the mechanism of benzyne formation. More strained acyclic tetraynes for the HDDA reactions were used by Ueda and co-workers. In their first report, the HDDA reaction was finished at room temperature within two to three days. By 2008, they had reported HDDA of various tetrayne derivatives as well as mechanistic studies.[45] In 2012, Hoye and co-workers reestablished the HDDA of tetra- and triyne with a broad substrate scope, experimental mechanistic evidence, computational studies, aryne-trapping reactions, and substitution effects.[46] Since this report, numerous applications of HDDA have been reported by several groups including the Hoye group.

1.1.3 Scope

This review addresses each type of reaction that yields products bearing more than two aryne synthons. Here, the reported reactions encompass both intramolecular and intermolecular mechanisms and include both multistep and one-pot addition of arynes. Very detailed reviews have been previously published on multicomponent aryne reactions,[1b,f,k,n] aryne reactions in natural product synthesis,[1c,e] transition metal-catalyzed aryne reactions,[1p] utilities of aryne in the

synthesis of heterocycles,[1d,f,g] polycyclic aromatic compounds,[1h,j] biaryls,[1o] and general information[1a,i,l,m] on aryne reactions.

We focus on introducing the general reaction schemes, mechanisms, and notable information in the references. In the absence of proposed mechanisms, we carefully refer to other reports to visualize a plausible mechanism. Some structures, such as phenylenes, were impossible to include in this review due to their numerous examples. In this case, some representative structures have been selected for discussion. For unclear mechanisms in references, the original authors' explanation has been followed. For example, the aryne insertion reaction would look identical to a [2+2] cycloaddition followed by a ring opening reaction if the detailed mechanistic study was not included in the report. Transition-metal catalyzed cycloadditions are categorized as formal cycloadditions in the cycloaddition section. For sections 2 to 9, the categories are named after the first aryne reaction in the mechanism. All aryne synthons in the intermediates, transition states, and products are colored blue.

1.2 [2+2] Cycloadditions

1.2.1 Biphenylene Synthesis

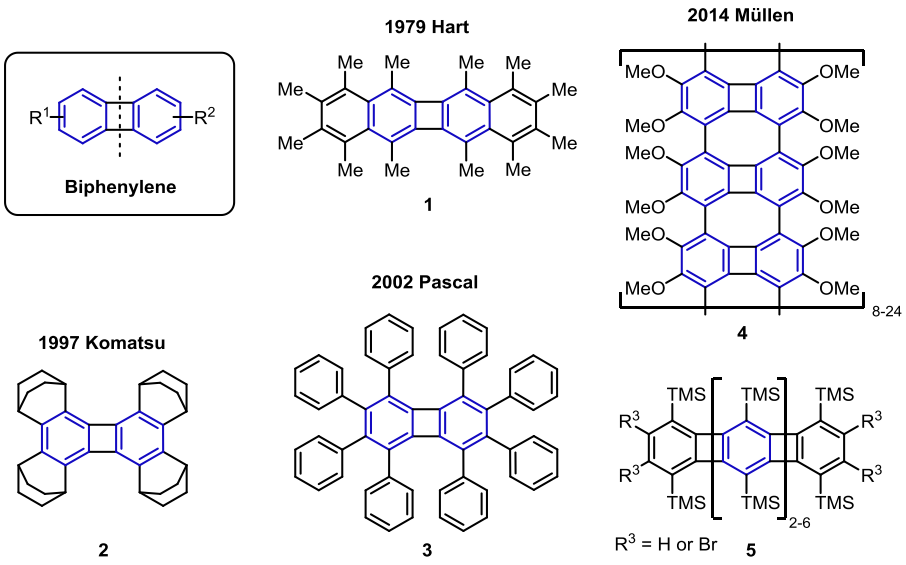

Figure 1.2. Representative biphenylenes.

The synthesis of biphenylenes (called "diphenylenes" in the report) from benzynes was introduced by Heaney, Mann, and Millar in 1957.[47] (2-Bromophenyl)magnesium iodide was used for the generation of benzynes and in situ [2+2] cycloaddition of two equivalent of benzynes afforded biphenylenes. Several syntheses with various substituted arynes were subsequently reported.[48] The representative biphenylenes are depicted in Figure 1.2. 2,3-Dibromo-1,4,5,6,7,8-hexamethylnaphthalene was used with *n*-BuLi to synthesize dodecamethylbinaphthylene **1** by Hart and Teuerstein.[49] Komatsu and co-workers synthesized biphenylene **2** bearing four bicyclo[2.2.2]octane units.[50] Interestingly, **2** was prepared from *o*-dibromobenzyne with *n*-BuLi but aryl diazonium carboxylate did not work. Pascal and co-workers found that 3% of 1,2,3,4,5,6,7,8-octaphenylbiphenylene **3** was obtained from aryl diazonium carboxylate.[51] Müllen and co-workers used 1,4,5,8-tetraiodo-2,3,6,7-

tetraalkoxybiphenylenes and 1,4,5,8-tetra(trimethylsilyl)-2,3,6,7-tetraalkoxybiphenylenes to synthesize nanographenes **4** and **5**, respectively.[52]

1.2.2 [2+2]/[2+2] Cycloadditions

Scheme 1.1. Aly's Bis-acridine Synthesis via double [2+2] cycloadditions.

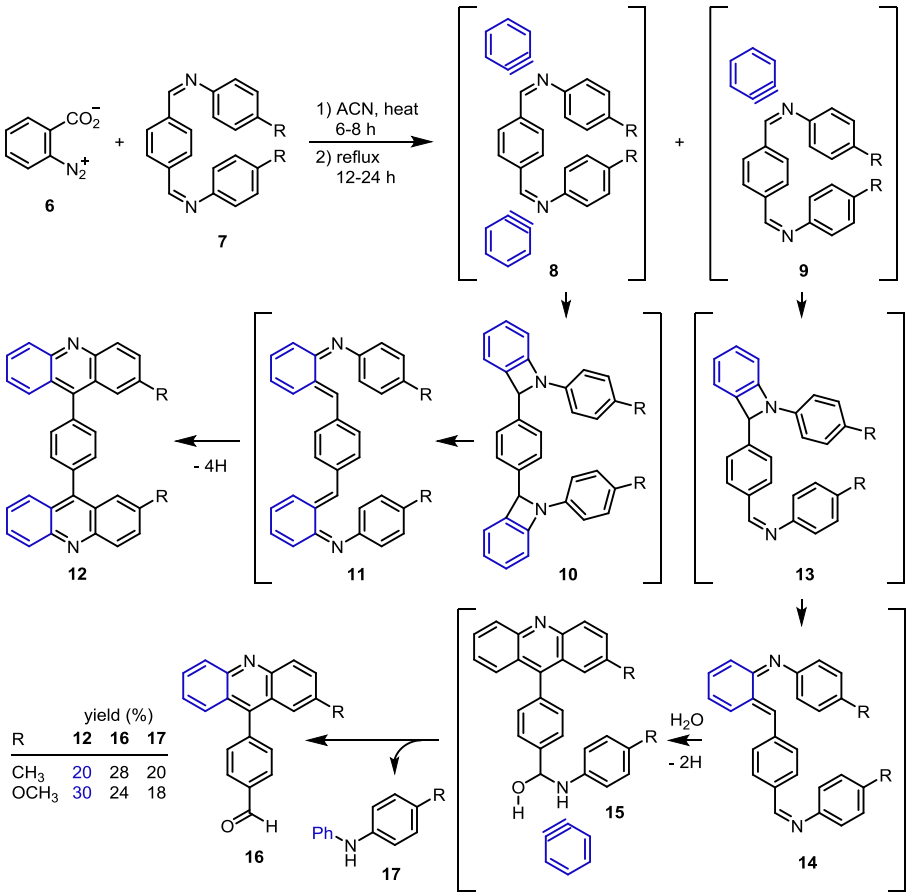

In 1999, Aly and co-workers reported double formal [2+2] cycloadditions of *N,N'*-bis-(aryl)-benzene-1,4-diyldimethylidene-diamines **7**, and two equivalents of benzyne were generated from benzenediazonium carboxylate **6** (Scheme 1.1).[53] The reactions afforded double [2+2] cycloadducts (1,4-bis(2'-substituted-acridine-10-yl)benzenes **12**) with two other products including 10-(4′ -formylphenyl)-2-substituted-acridines **16** and *N*-phenyl-arylamines

17. [2+2] cycloaddition between imines **7** and benzyne first forms azetidine ring (**10** or **13**), which is then opened by retro-[2+2] cycloaddition followed by electrocyclization to yield **12** (for double cyclization) and both **16** and **17** (for mono cyclization) in the proposed mechanism.

Scheme 1.2. Caubere's Benzocyclobutabiphenylenes Synthesis via Stepwise [2+2]/[2+2] Cycloadditions.

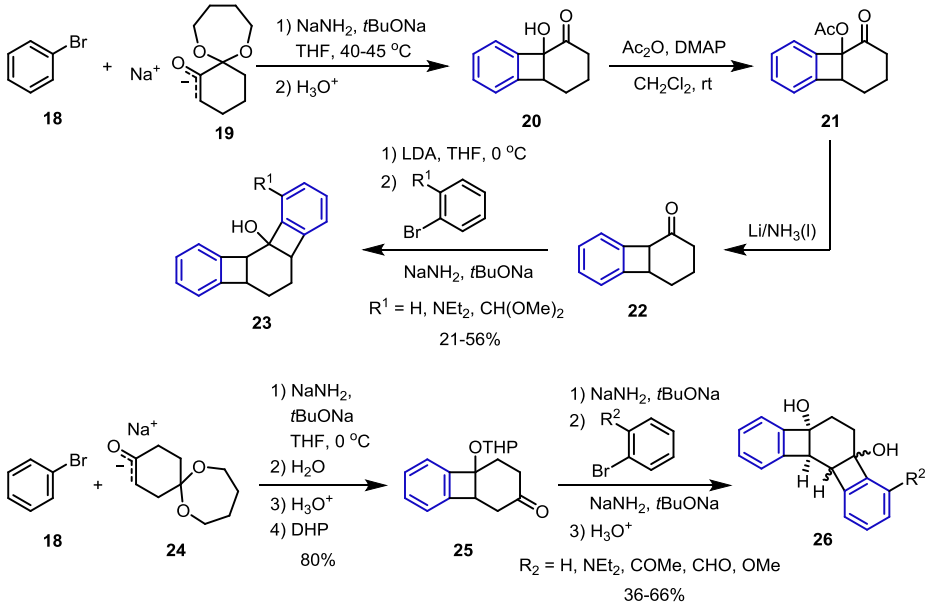

Consecutive [2+2] cycloadditions of enolates (**19** and **24**) and benzyne were performed by Caubere and co-workers in 1991 (Scheme 1.2).[54] Enolate **19** undergoes the first [2+2] cycloaddition with benzyne to afford hexahydrobiphenylene **20**. The new enolate formed after acetylation and deacetoxylation reacted with another benzyne to afford hexahydrobenzocyclobutabiphenylene **23**. The enolate **24** after THP protection of hexahydrobiphenylene was reacted with benzyne to yield the corresponding hexahydrobenzocyclobutabiphenylene **26**.

Scheme 1.3. Yu and Liu's Double [2+2] Cycloaddition Reactions of Norbornadiene with Benzynes.

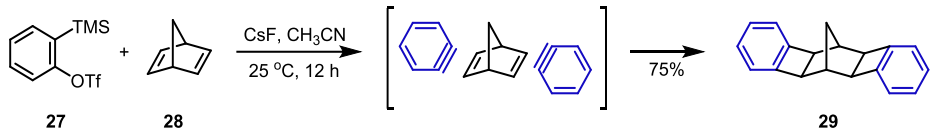

Norbornadienes have been used as [2+2] and [4+2] cycloaddition partners due to their strain (Scheme 1.3). Double [2+2] cycloadditions of norbornadiene **28** and two equivalent of benzynes were employed by Yu, Lin, and co-workers.[2b] When one equivalent of benzyne was used, 73% of the mono-cycloadduct **29** was obtained.

1.2.3 [2+2]/[2+2]/[2+2] Cycloadditions

As discussed in section 2.1, biphenylenes were obtained from [2+2] cycloaddition of two benzynes. Friedman reported that two biphenylenes **30** underwent ring opening followed

Scheme 1.4. Tetra- and Hexaphenylene Synthesis.

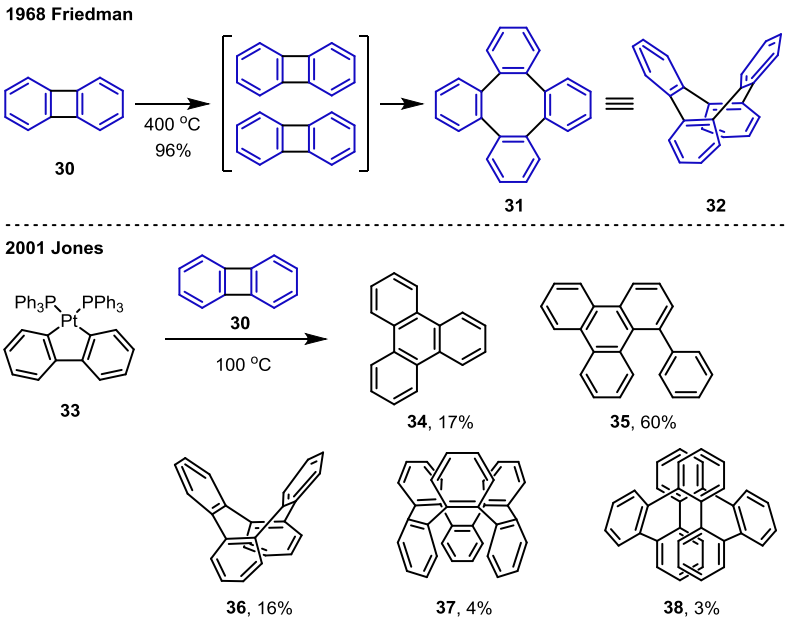

by dimerization at 400 °C to afford tetraphenylene **32** in 96% yield (Scheme 1.4).[48a] Subsequently, several transition metal-catalyzed reactions with substituents has been developed for this conversion. In 2001, Jones and co-workers found two isomers of hexaphenylene (**37** and **38**) from the reaction of biphenylenes **30** and platinum complex **33**.[55]

1.2.4 [2+2]/[2+2]/[4+2] Cycloadditions

Scheme 1.5. Shindo's One-Pot Triptycene Synthesis via Triple Cycloadditions.

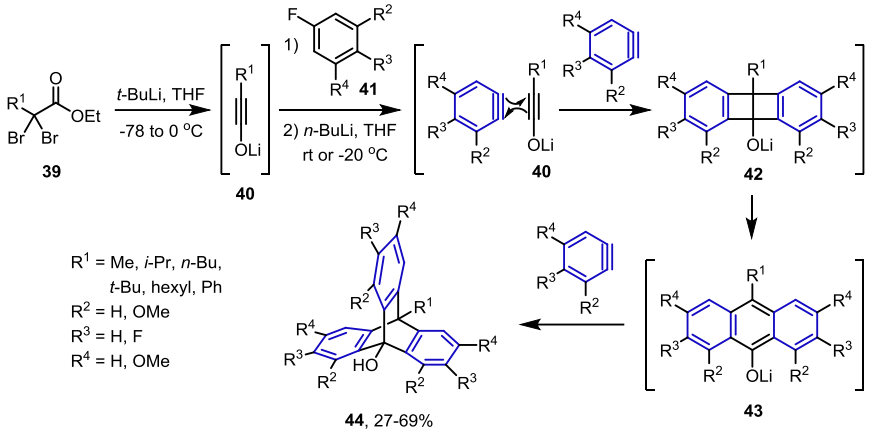

As shown in Scheme 1.2, enolates can be [2+2] cycloaddition partners for aryne. Recently, Shindo and co-workers used benzyne and lithium ynolates **40** generated from the reaction of precursor **39** and t-BuLi to synthesize triptycenes **44** in one pot (Scheme 1.5).[56] In the plausible mechanism, ynolates **40** reacted with benzyne via formal [2+2] cycloaddition, and the resulting enolates further reacted with a second benzyne in a [2+2] cycloaddition reaction to afford **42**. Retro-[2+2] cycloaddition of the strained Dewar anthracene **42** leads to anthracene **43** followed by [4+2] cycloaddition with the third benzyne to afford triptycenes **44**. This approach is a rapid method for synthesizing tri *ortho*-substituted C3-symmetrical triptycenes. The computational study explained the regioselectivity of this triple aryne reaction.

1.2.5 [2+2]/[4+2] Cycloadditions

Scheme 1.6. Fleming's Anthracene Synthesis.

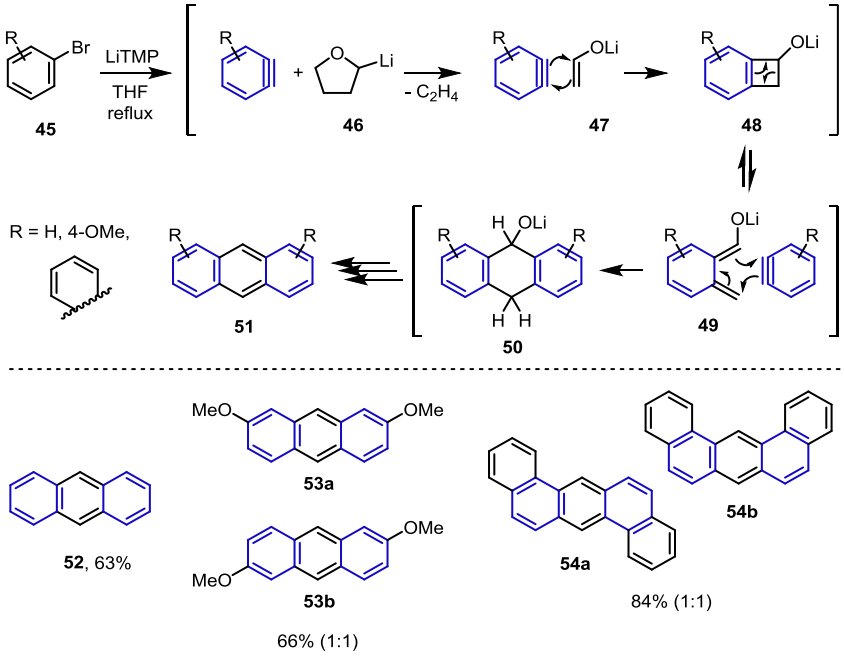

In 1975, Fleming and Mah reported the anthracene synthesis using THF and bromophenols **45** with LiTMP (Scheme 1.6).[57] THF was degraded into ethylene gas and enolates **47** by LiTMP. The resulting enolates **47** react with benzyne to form *ortho*-quinodimethane intermediates **49**. Intermediates **49** undergo a [4+2] cycloadditions with the second benzyne followed by oxidation to afford anthracenes (**51**-**54b**).

9-Arylxanthenes **59** were synthesized by Yoshida, Kunai, and co-workers utilizing two equivalents of benzynes and 9-arylaldehydes **55** (Scheme 1.7).[58] The [2+2] cycloaddition of aldehydes **55** and benzyne yields quinone methide intermediates **58** bearing a fixed *cis*-diene. Then, the diene reacts with another benzyne via [4+2] cycloaddition followed by oxidation to afford the desired 9-arylxanthenes **59** in the proposed mechanism.

Scheme 1.7. Yoshida and Kunai's 9-Arylxanthene Synthesis.

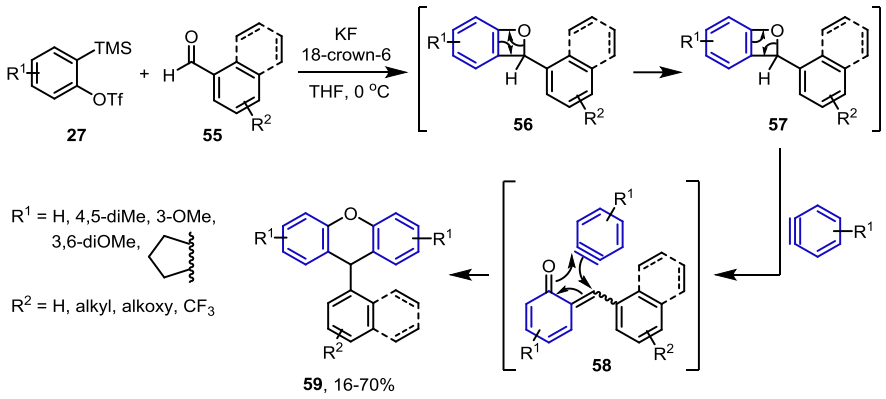

1.2.6 [2+2] Cycloaddition/Nucleophilic Addition

Scheme 1.8. Gogoi's Conversion from Coumarins to Isocoumarins.

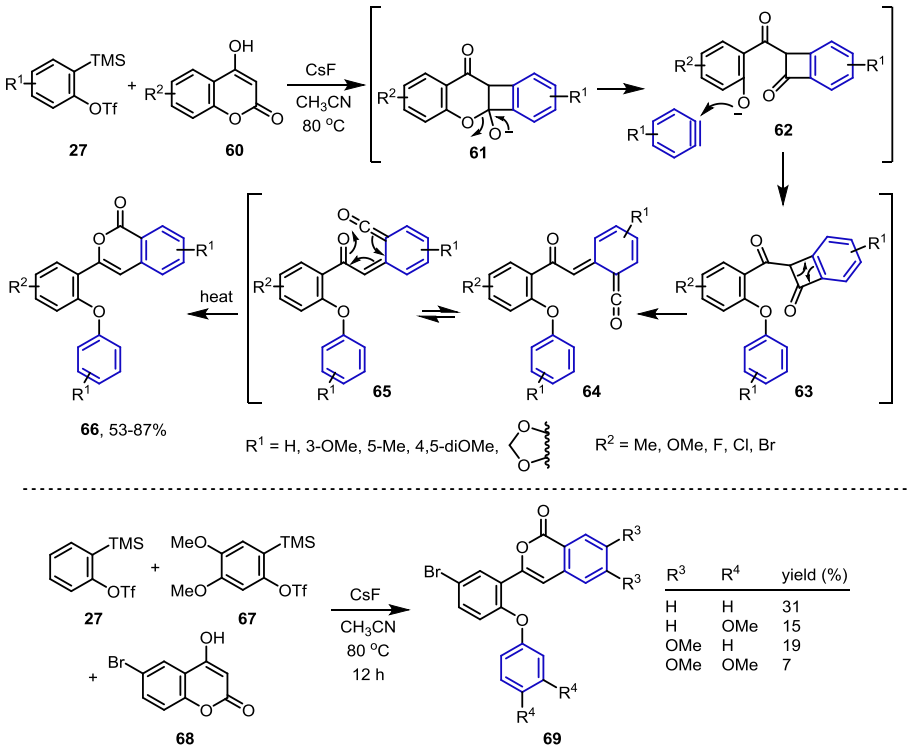

The synthesis of isocoumarins **66** from coumarins **60** was demonstrated by Gogoi and co-workers in 2017 (Scheme 1.8).[59] [2+2] Cycloaddition of benzyne and 4-hydroxycoumarins

60 affords the four-membered intermediate **61** followed by ring opening of coumarin **61** and nucleophilic addition to another benzyne. The resulting cyclobutanone intermediates **63** undergo retro-[2+2] cycloaddition to ketene intermediates **64**. Then, a pericyclic reaction closes the ring to form isocoumarins **66**. When coumarin **68** and two different aryne precursors **27** and **67** are employed, three component reaction adduct **69** was obtained as four different products due to their crossover reactions between two competitive arynes.

Scheme 1.9. Biehl's Arylindane Synthesis.

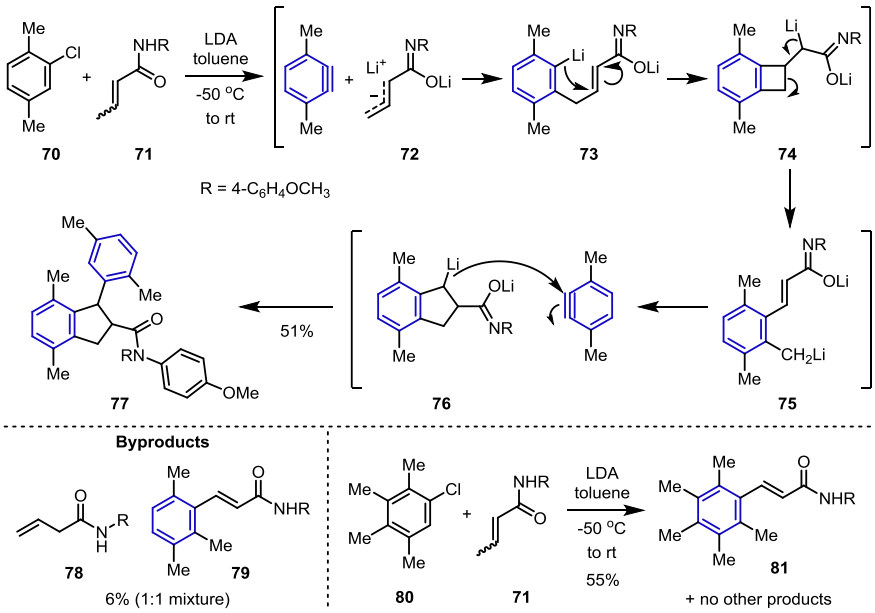

Biehl and co-workers have reported the synthesis of arylindane **77** from crotonamide **71** and benzyne (Scheme 1.9).[60] Lithiation of crotonamide **71** leads to dianion intermediate **72**, which reacts with benzyne via the formal [2+2] cycloaddition to yield benzocyclobutane intermediates **74**. Intermediate **74** undergoes ring opening followed by either five-membered ring formation or quenching with a proton source to afford indane intermediate **76** or cinnamamide **79**. Indane dianion **76** was added to an additional benzyne to afford arylindane

compound **77**. Unlike 3,6-dimethylbenzyne, 3,4,5,6-tetramethylbenzyne only yielded **81** with no double benzyne adducts.

Scheme 1.10. Studer's Carbazole Synthesis Cotrolled by Fluoride Sources.

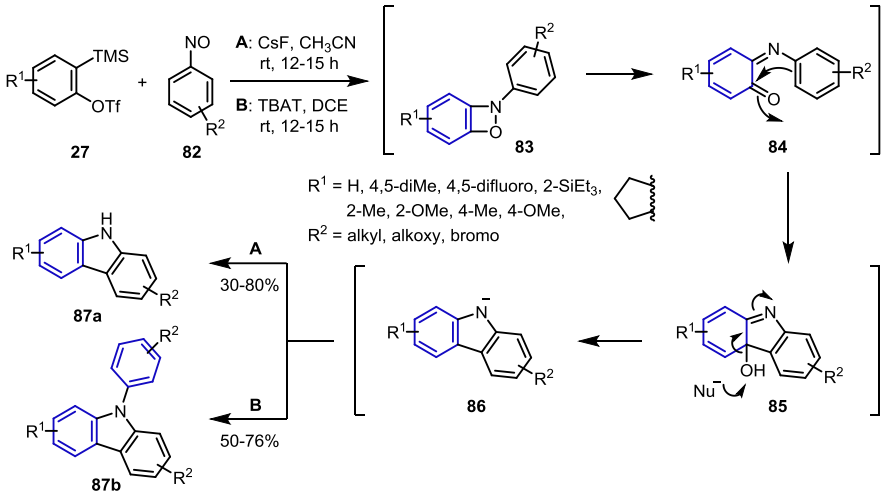

Studer and co-workers developed the synthesis of carbazoles (**87a** and **87b**) from nitrobenzenes **82** and arynes (Scheme 1.10).[61] In the proposed mechanism, [2+2] cycloaddition of aryne and nitrobenzenes **82** forms four-membered ring intermediates **83**, and the subsequent ring opening of **83** yield hydroxylcarbazole intermediates **85**. Elimination and hydrolysis of **86** affords carbazoles **87a** when CsF is used. However, in the presence of tetrabutylammonium difluorotriphenylsilicate (TBAT), consecutive elimination of **85** and nucleophilic addition to the second aryne result in the formation of *N*-arylcarbazole **87b**.

1.3 [3+2] Cycloadditions

1.3.1 [3+2]/[3+2] Cycloadditions

Scheme 1.11. Nakayama's Synthesis of Dibenzotetrathiafulvalene and Related Compounds.

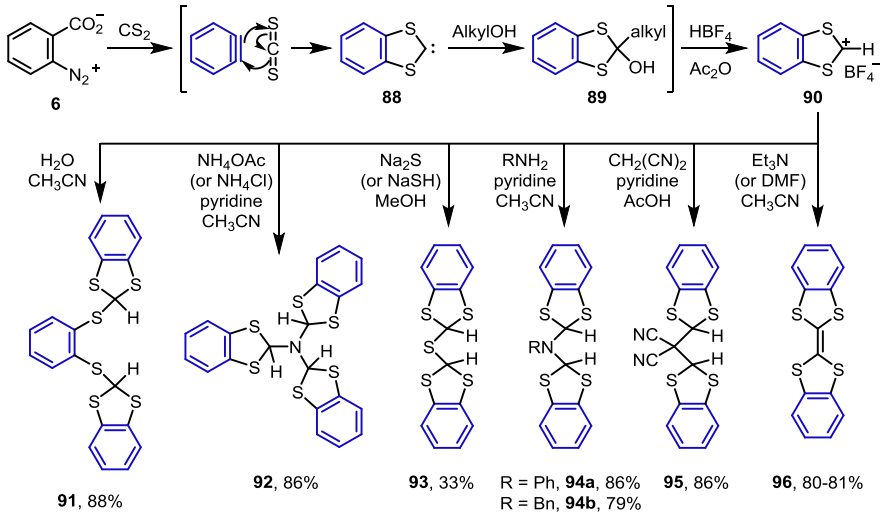

In 1970, Meyerson and Fields described the generation of benzo-1,3-dithiolium carbene **88** via [3+2] cycloaddition of benzyne and carbon disulfide (Scheme 1.11).[62] To harness the reactivity of **88**, several salt forms of **88** were reported.[63] In 1974, the formation of fluoroborate salt **90** from carbene **88** was developed by Nakayama and co-workers. In their report in 1976, Nakayama revisited the previous synthetic application of carbene **88** to modify or reproduce the result with fluoroborate salt **90**.[64] This salt (**90**) was used to modify the previous synthetic applications of the other salt forms of **88**. Hydrolysis of **90** afforded trimer **91**. Another trimer structure (**92**) was obtained from ammonium acetate or ammonium chloride and **90** under basic conditions. Insertion of a sulfur atom between two equivalents of **90** was observed by adding sodium sulfide. Using pyridine, a primary amine or malononitrile group was inserted between

two equivalents of **90**, yielding both **94a** and **94b** or **95**. Dimerization of **90** occurred when only trimethyl amine or DMF was employed in the reaction.

Scheme 1.12. Cariou and Dodd's Double [3+2] Cycloadditions of Azides and Arynes.

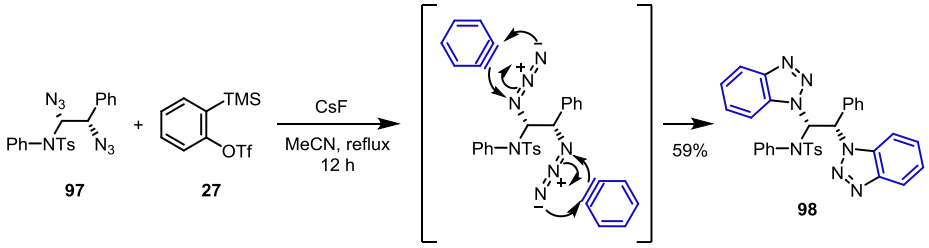

Scheme 1.13. Nakayama's Synthesis of Tetracyclic Sulfonium Salts and Dibenzo-1,3,6,-trithiocin Derivatives.

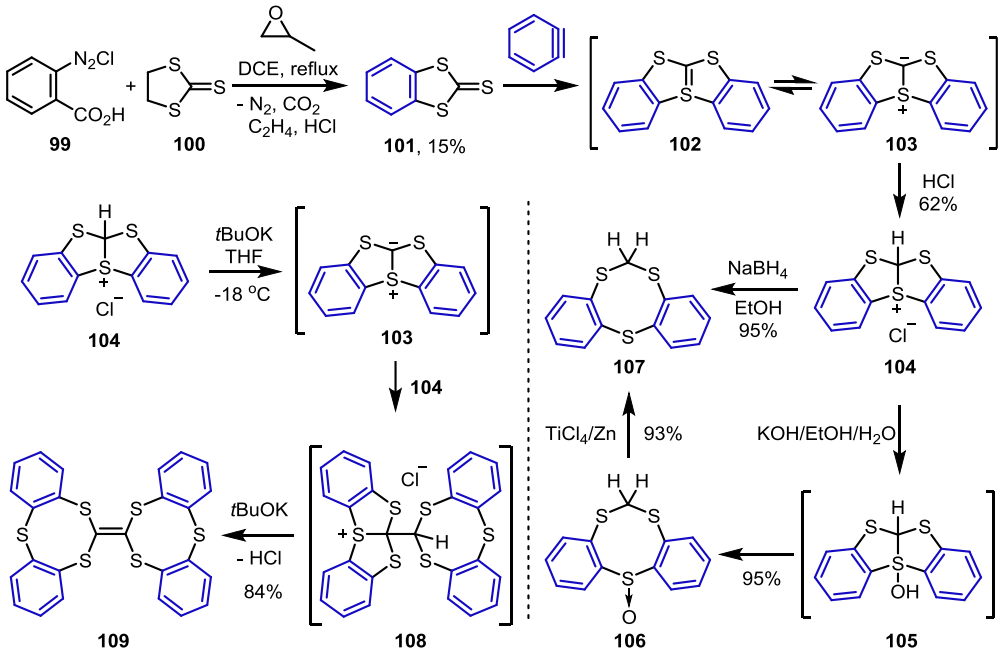

Click reactions of azides and alkyne are well-known [3+2] cycloadditions. The first aryne click reaction (i.e., a cycloaddition of azides and arynes) was reported by Larock and co-workers in 2008.[65] Subsequently, several aryne click reaction have been reported. Dodd, Cariou,

and co-workers reported double click reactions of diazido adduct **97** and benzyne to yield **98** (Scheme 1.12).[66]

Nakayama and co-workers employed trithiocarbonate **100** for [3+2] cycloaddition with benzyne to afford 1,3-benzodithiole-2-thione **101** followed by a second [3+2] cycloaddition with benzyne to form the tetracyclic intermediate **102** (Scheme 1.13).[67] After work-up with HCl, tetracyclic sulfonium chloride **104** was prepared. This core structure was transformed to dibenzo[*d*,*g*][1,3,6]trithiocin **107** by addition of hydride to **104** or two-step hydrolysis/reduction of **104**. Dimer product **109** was successfully prepared from deprotonation of **104** using a strong base at -18 °C.

Scheme 1.14. Larock's Conversion from Bishydrazonobenzene to Dibenzoylbenzene.

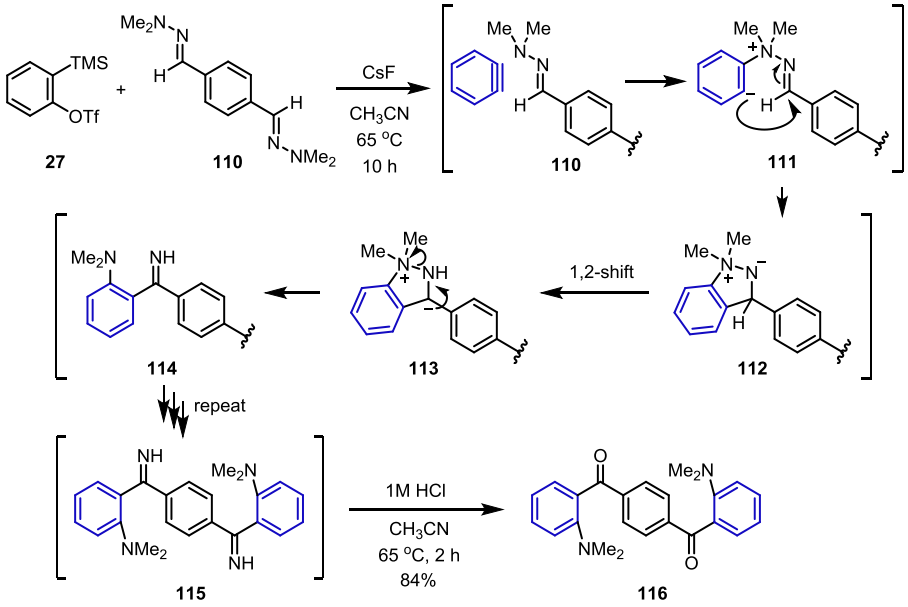

Larock and Dubrovskiy reported the synthesis of dibenzoylbenzene **116** from bishydrazonobenzene **110** (Scheme 1.14).[68] [3+2] Cycloaddition of hydrazone **110** and

benzyne leads to the five-membered intermediate **112** followed by rearrangement of **112** and hydrolysis of **114** to yield dibenzoylbenzene **116**.

1.3.2 [3+2] Cycloaddition/Nucleophilic Addition

Scheme 1.15. Larock's Pyridoindole Synthesis.

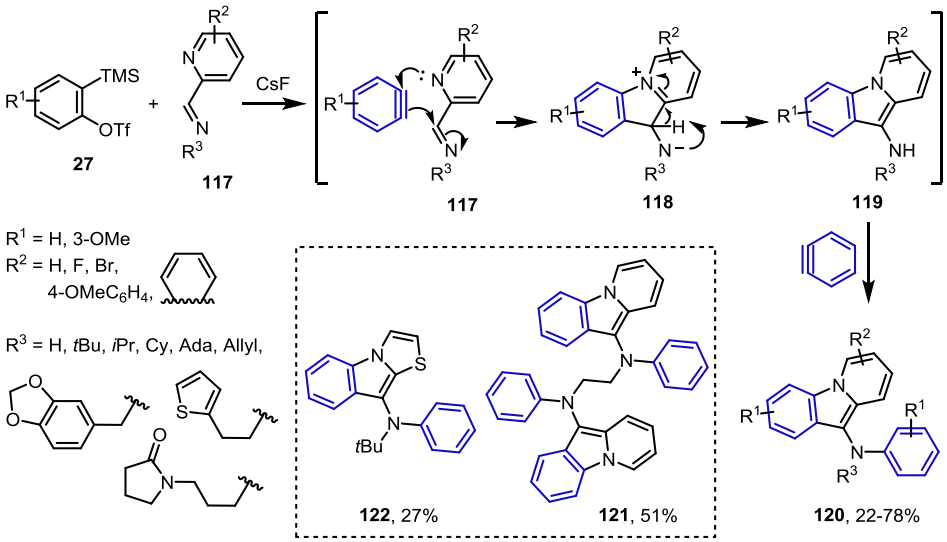

Less than a year earlier, a report by Larock and co-workers presented the unusual pyridoindole synthesis from N-pyridin-2-yl-methanimines **117** and arynes (Scheme 1.15).[3b] The formal [3+2] cycloaddition was initiated by the addition of nitrogen from pyridines **117** to benzyne. The resulting carbanion attacks the imine intramolecularly to form a five-membered ring **118**, which is rearranged by α-deprotonation to yield pyridoindoles **119**. The next mechanistic step is proposed to be nucleophilic addition of secondary amines **119** to another benzyne to afford **120**. In place of the pyridyl group, a thiazolyl group was employed to yield thiazolo[3,2-*a*]indole **122**. When diimine was used as the starting material, double annulation product **121** was formed.

Scheme 1.16. Synthesis of 1-Arylindazoles.

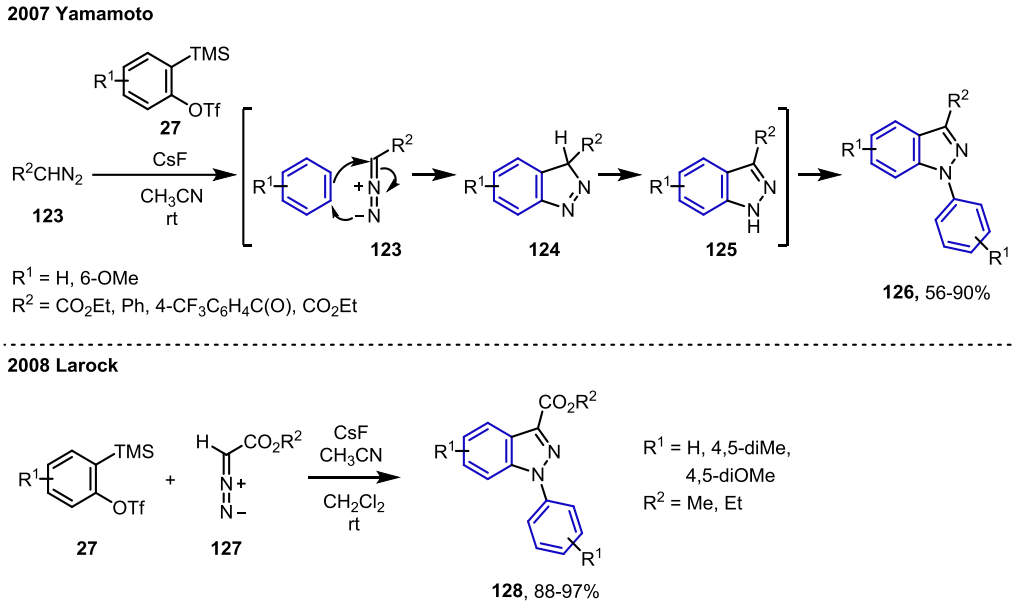

The 1-arylindazole synthesis has been demonstrated by Yamamoto and Jin (Scheme 1.16).[69] Similar to Huisgen cycloaddition, diazomethanes **123**, an isostere of azides, undergoes 1,3-dipolar cycloaddition with benzyne and subsequent proton transfer. The corresponding 1*H*-indazoles **124** further reacted with a second benzyne via *N*-arylation to yield **126** when two equivalents of benzyne were added. In the same year, Larock and co-workers also reported the same reactions to prepare **128** with a different substrate scope.[70]

Without the catalyst, the reaction between diazomethanes and benzynes afforded 1-arylindazoles. Using a silver catalyst, Liu and Wang successfully achieved 2-arylindazoles **134** in 2012 (Scheme 1.17).[71] According to their proposed mechanism, the mechanistic pathway differed from the non-catalytic pathway in Scheme 1.16 due to the coordination of Ag(I) to the 1-position of indazole **131**. This trapping inhibits the addition to the second benzyne at the 1-position of **131**. In lieu of the addition to the 1-position, *N*-arylation becomes more accessible at the 2-position of **132**, yielding **134**.

Scheme 1.17. Liu's 2-Phenyl-3-carbonylindazoles Synthesis.

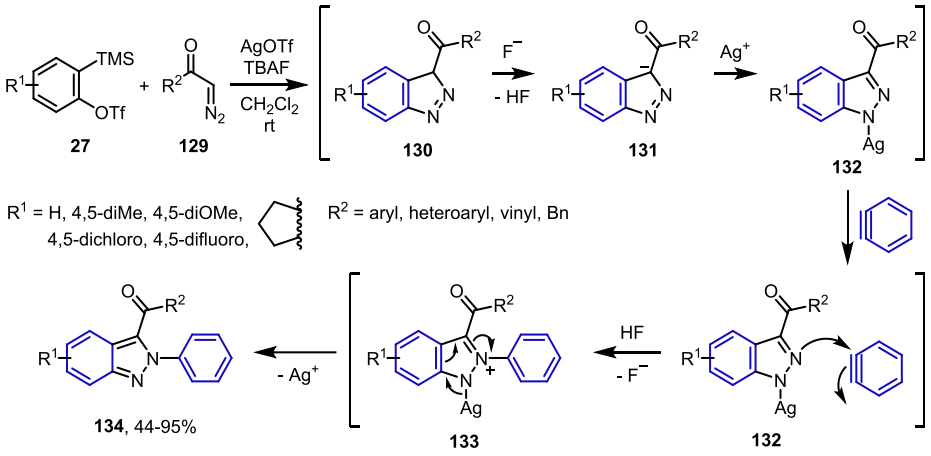

Scheme 1.18. Xia's Tandem [3+2] Cycloaddition/Nucleophilic Addition.

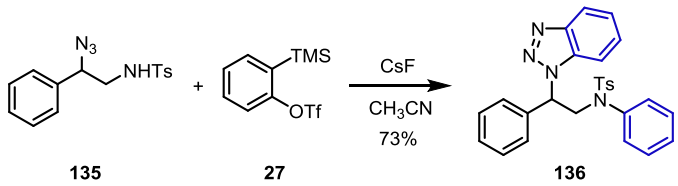

Scheme 1.19. Studer's Synthesis of Fully Substituted Alkenes.

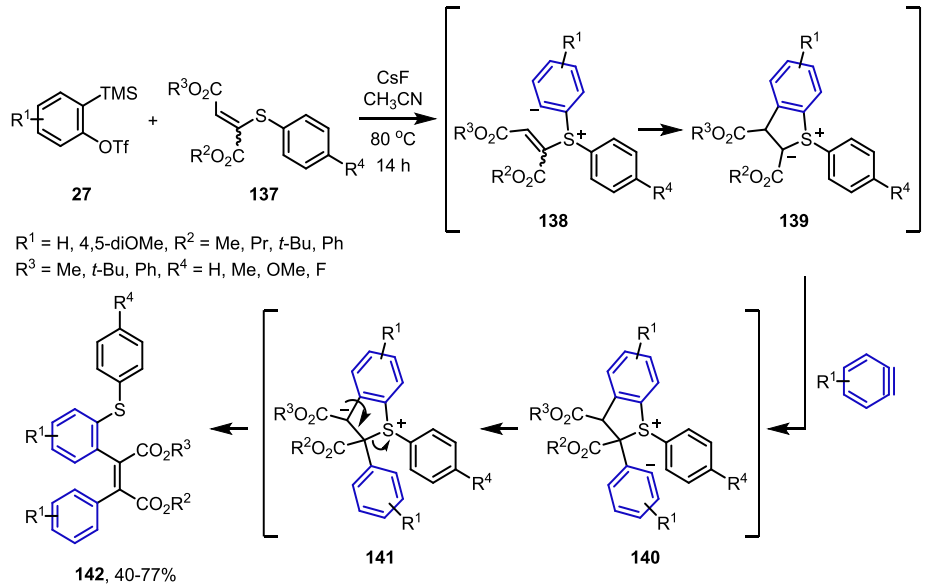

As shown in Scheme 1.12, the click reactions of azido compounds and benzynes yield benzotriazoles. In addition, double aryne click reactions of azido derivatives and other multiple aryne reactions including a click reaction have been reported. Tandem Huisgen cycloaddition of azide adduct **135** and nucleophilic addition to benzyne was introduced in the end of the report by Xia and co-workers (Scheme 1.18).[72]

Studer and co-workers reported that vinyl sulfide derivatives **137** undergo [3+2] cycloaddition with benzyne, affording ylide intermediates **139** (Scheme 1.19).[73] The following 1,4-proton transfer of **140** and β-elimination of **141** afford the desired alkene products **142**. In the report, when 1,2 equivalents of benzyne and 5 equivalents of water were employed, the second arylation of **139** was blocked.

The first example of a tandem [3+2] cycloaddition and N-O bond insertion reaction was reported by Okuma and co-workers (Scheme 1.20).[74] Quinoline N-oxides **143** were used for the synthesis of oxazepino[4,5-*a*]quinolones **145** and 2-(2-hydroxyphenyl)quinolones **146**. Initial [3+2] cycloaddition of nitrones **143** and benzyne forms the five-membered intermediates

Scheme 1.20. Okuma's Oxazepino[4,5-a]quinolone Synthesis.

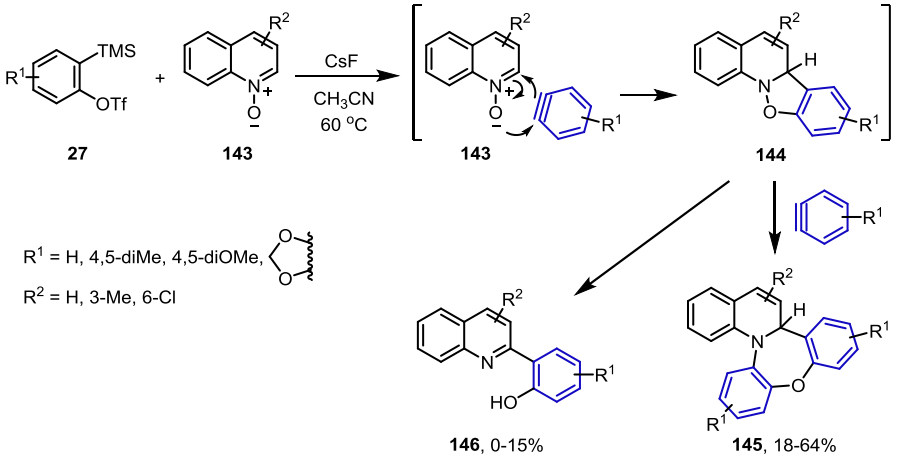

144, which is allowed to go through either benzyne insertion or rearrangement to 7-membered heterocyclic products **145** and ring-opened products **146**.

1.4 [4+2] Cycloadditions

1.4.1 [4+2]/[2+2] Cycloadditions

Scheme 1.21. He and Wang's [4+2]/[2+2] Cycloadditions.

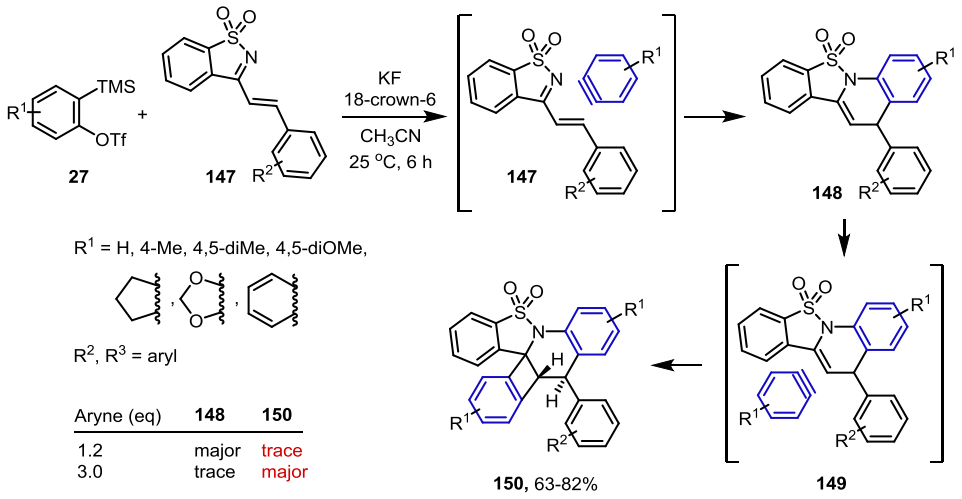

He, Wang, and co-workers developed tandem aza-[4+2] and [2+2] cycloadditions of benzyne and 1-sulfonyl-1-azadienes **147** (Scheme 1.21).[75] Depending on the amount of benzyne, the reaction was tunable to afford aza-[4+2] adducts **148** and aza-[4+2]/[2+2] adducts **150**.

In 1984, Wege and Anthony demonstrated tandem [2+2]/[4+2] cycloadditions of benzofuran **151** and benzyne (Scheme 1.22).[48e] A [2+2] cycloadduct **152** and a [2+2]/[4+2] cycloadduct **153** were isolated. After thirty years, Liu and Yu reported their results for the tandem [4+2]/[2+2] or [2+2]/4+2] cycloadditions of indene **154** and benzyne to afford **155**.[2b] Simultaneously, Biju and co-workers disclosed the scope of the reactions of benzofurans and

indenes (**156**) in the synthesis of **158** and proposed a mechanism involving a [4+2] cycloaddition that is preceded by a [2+2] cycloaddition.[76] However, the mechanistic pathway remains unclear due to non-isolable [2+2] intermediates **157** from **156**.

Scheme 1.22. [4+2]/[2+2] or [2+2]/4+2] Cycloadditions of Indene or Benzofurans with Arynes.

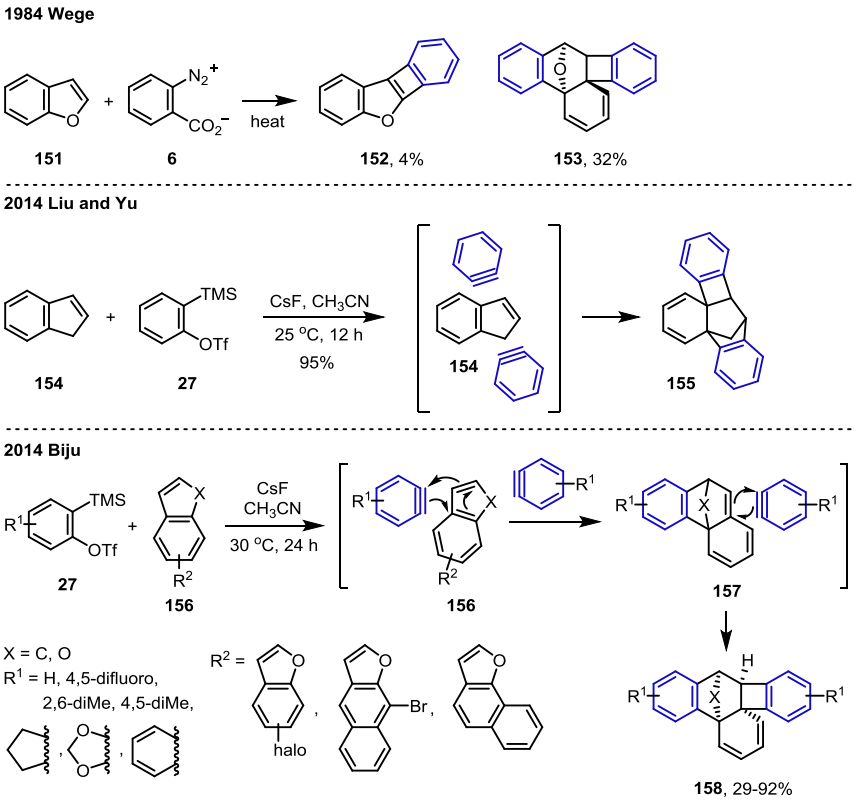

Mead and co-workers discovered the reactivity of 1-azadiene **159** with benzynes (Scheme 1.23).[77] The azadiene **159** reacts with benzyne via either [2+2] or [4+2] cycloaddition to yield benzoazetidine **160** or quinolone **161**. For the [4+2] adduct **161**, one more [2+2] cycloaddition was observed by isolation of benzoquinoline **162**. Interestingly, no benzoazetidine **160** was observed at 130 °C.

Scheme 1.23. Mead's Synthesis of Benzoazetidine, Quinolines, and Benzoquinolines.

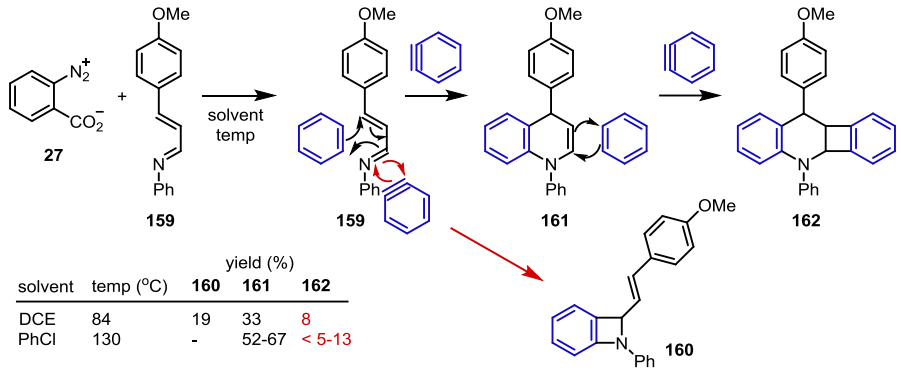

Scheme 1.24. Sugihara and Nakayama's [4+2]/[2+2] Cycloadditions of Adamantylidenecyclopentadiene with Aryne.

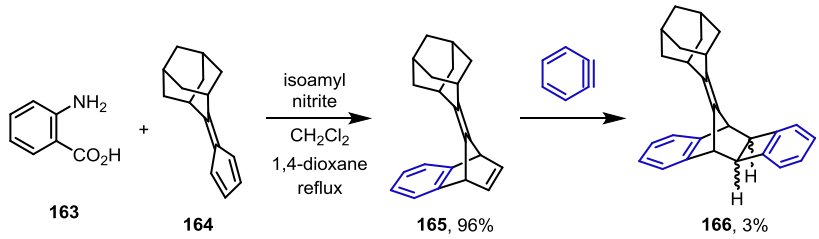

The aryne reaction of adamantylfulvene **164** was reported by Sugihara, Kobiki, and Nakayama (Scheme 1.24).[78] When 1.5 equivalents of benzyne was employed, the [4+2] adduct **165** was the major product, and the tandem [4+2]/[2+2] adduct **166** was the minor product.

1.4.2 [4+2]/[4+2] Cycloadditions

Barrett and co-workers reported the synthesis of binapthyl **170** and either dinaphthyl ether (**173a** and **173b**) or napthylaryl ether (**174a** and **174b**) (Scheme 1.25).[79] The reaction goes through double [4+2] cycloaddition reactions of aryne with 2,2'-bifuryl **168** or 2-methoxyfuran **172** as one of the synthetic efforts to prepare binaphthyl or dinaphthyl ether-

containing natural products, such as palmarumycin CP_1, diepoxin σ, preussomerin G, and spiroxin C.

Scheme 1.25. Barrett's Synthetic Approach to the Synthesis of Binaphthyl or Dinaphthyl Ether-Containing Natural Products.

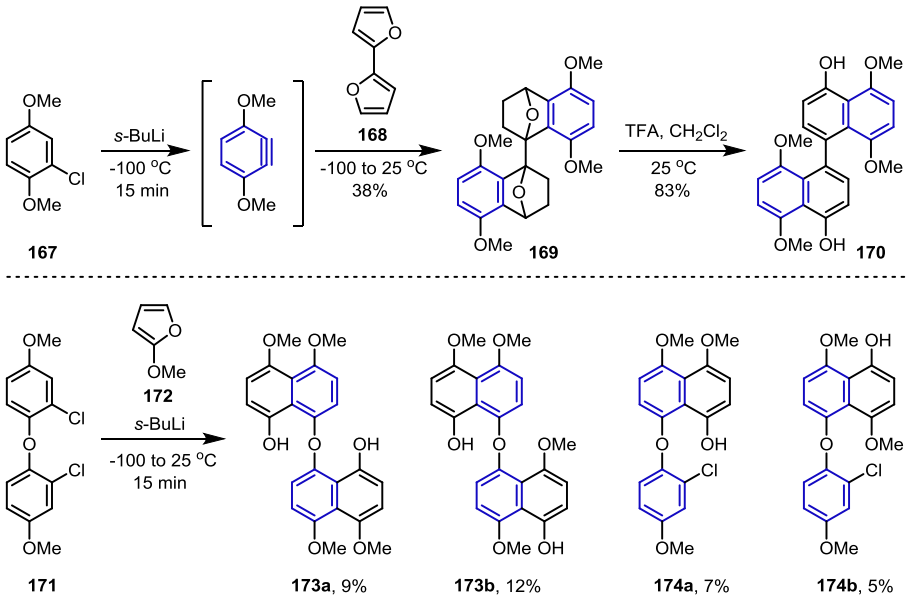

Scheme 1.26. Ōki's Synthesis of Bitriptycyl Derivative.

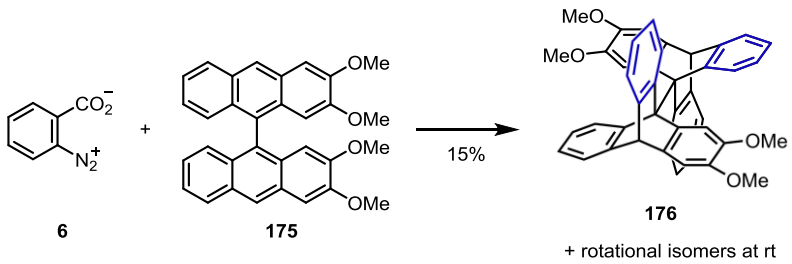

Ōki and co-workers used tetramethoxybianthryl **175** and benzyne to synthesize bitriptycenes **176** (Scheme 1.26).[80] Two rotational isomers were separated with **176** by HPLC. The demethylation of **176** with sodium ethanethiolate at room temperature only yielded the

methoxy groups of the 3 and 3' positions facing outward being converted to hydroxyl groups. The 2- and 2'-methoxy groups were intact due to steric hindrance.

Gold-catalyzed double [4+2] cycloadditions of *ortho*-alkynyl(oxo)benzenes **177** and benzynes were developed by Asao and co-workers (Scheme 1.27).[81] In the proposed mechanism, the coordination of alkyne to AuCl followed by nucleophilic addition of the oxygen atom of the carbonyl group of **178** to the alkyne forms zwitterionic intermediates **179**. The [4+2] cycloaddition of **179** and benzyne affords the bicyclic intermediates **181**, which undergoes rearrangement to anthracenes **182**. Another benzyne [4+2] cycloaddition of **182** affords the corresponding triptycenes (**183a** and **183b**).

Scheme 1.27. Asao's Triptycene Synthesis.

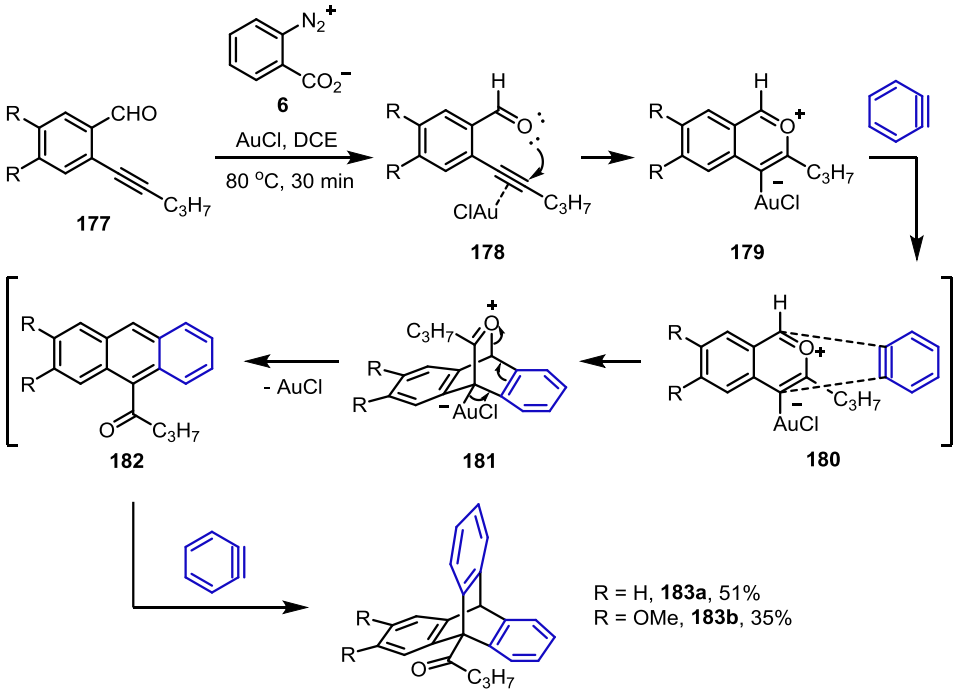

Anthracene synthesis from oxazoles **184** and benzyne was introduced by Bhatt and Reddy in 1980 (Scheme 1.28).[82] The double [4+2] cycloadditions of benzyne and oxazoles **184**

yields 9,10-dihydro-9,10-epoxyanthracenes **187**, which reduces **187** with zinc and acetic acid to afford anthracenes **188**.

Scheme 1.28. Bhatt's Anthracene Synthesis.

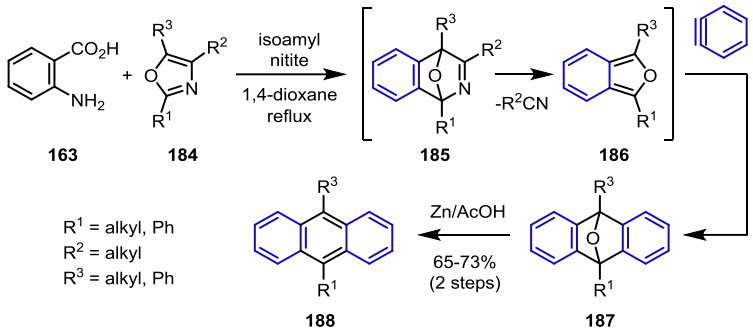

Scheme 1.29. Coquerel and Rodriguez's Nornitidine Synthesis.

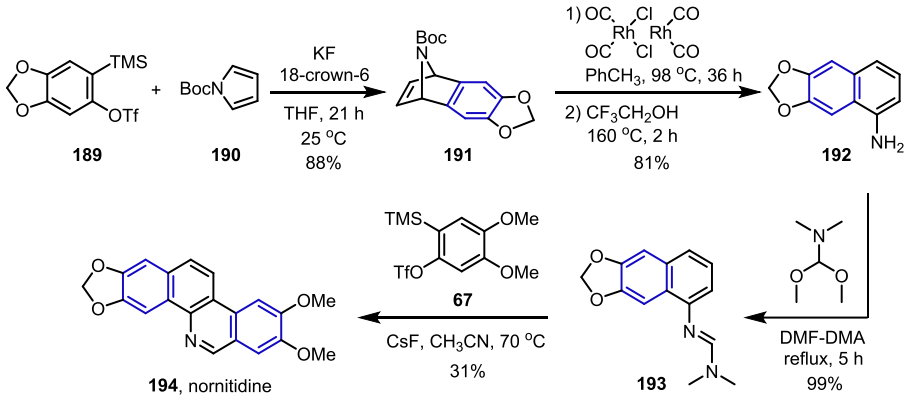

In 2015, Coquerel, Rodriguez, and co-workers employed two arynes to synthesize the alkaloid natural product nornitidine **194** (Scheme 1.29).[83] *N*-Boc-pyrrole **190** reacted with aryne **189** via [4+2] cycloaddition to yield azabicyclic compound **191**. Rhodium-catalyzed ring opening of **191** followed by deprotection afforded naphthylamine **192**. Amine **192** reacted with *N,N*-dialkylformamide dimethylacetal to yield *N,N*-dimethylformamidine **193**, which further reacted with another aryne **67** to afford nornitidine **194**.

Scheme 1.30. Kuck and Cao's Synthesis of Bis-tribenzotriquinacene and Monoanthro-dibenzotriquinacene.

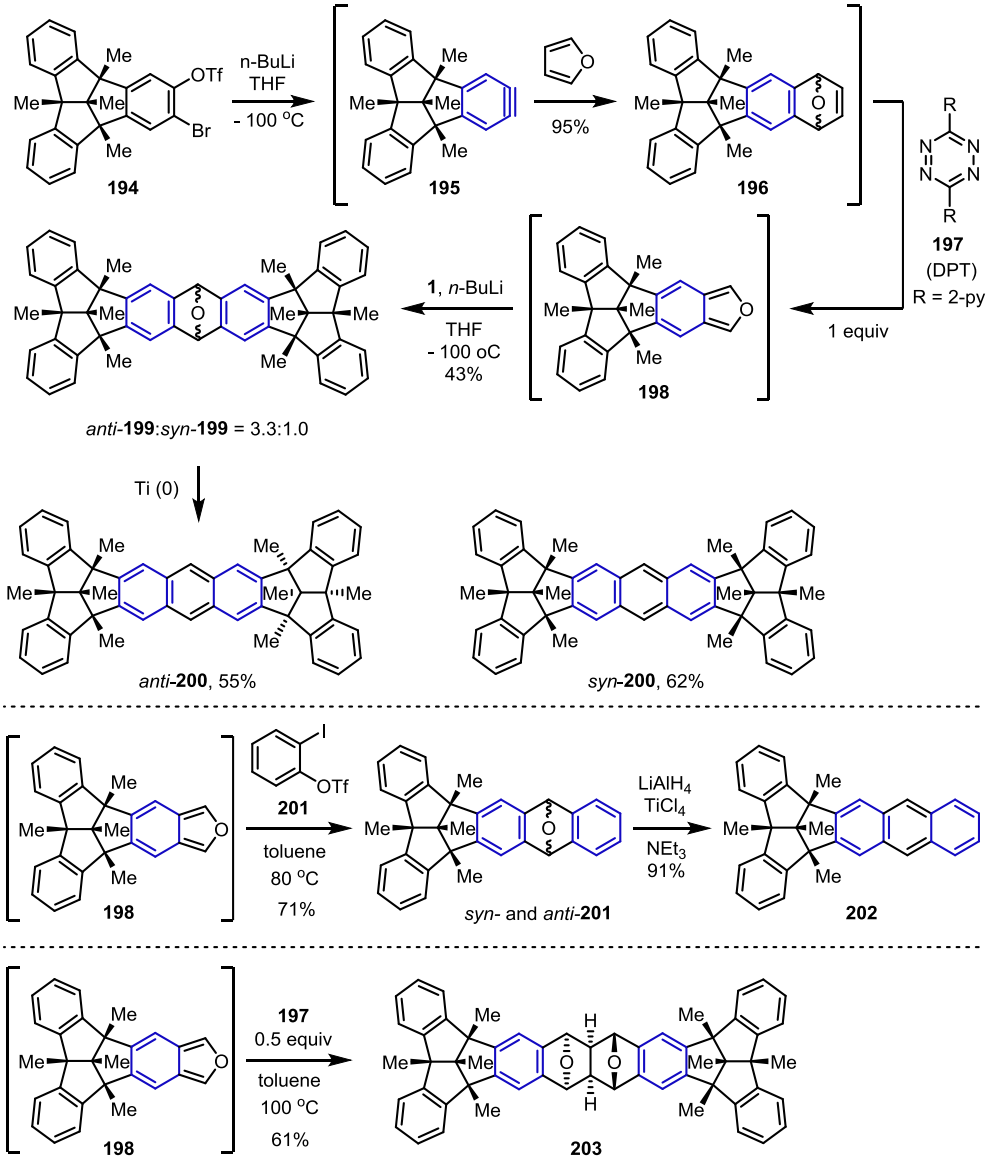

Kuck and Cao reported the synthesis of bis-tribenzotriquinacenes **200**, monoanthro-dibenzotriquinacene **202**, and hexadecacycle **203** (Scheme 1.30).[84] Tribenzotriquinacene (TBTQ)-based aryne **195** reacted with furan via [4+2] cycloaddition to form oxabicycle **196**, and the subsequent acetylene extrusion by [4+2] cycloaddition of 3,6-di-(2-pyridyl)-1,2,4,5-tetrazine (DPT) of **196** affords isobenzofuran **198**. Further [4+2] cycloaddition of **198** and the

second aryne **196** and *in situ* titanium reduction afford bis-tribenzotriquinacenes (*anti*- and *syn*-**199**). The addition of benzyne rather than **195** to **198** and deoxygenation of *syn*- and *anti*-**201** resulted in the formation of **202**. 0.5 equivalents of DPT were added to **4** to achieve **203**.

The synthesis of dihydroethenopentacene **206** from tetramethylidene **204** and benzyne was reported by Uno and co-workers in 2005 (Scheme 1.31).[85] The double [4+2] cycloadditions of **204** and two equivalents of benzynes afforded intermediates **205**, which were subjected to DDQ oxidation to form dihydroethenopentacene **206**. In the same year, Ono and co-workers also used this method to prepare the substituted dihydroethenopentacene derivatives **207**.[86] The syntheses of heptacene **208** and hexacene **209** were developed by Neckers and co-workers in 2006[87] and Neckers, Shah, and co-workers in 2007,[88] respectively. In 2010, Yamada and co-workers used a similar method to prepare tetraaryl-substituted pentacenes **210**.[89]

Scheme 1.31. Synthesis of Dihydroethenopentacene Derivatives.

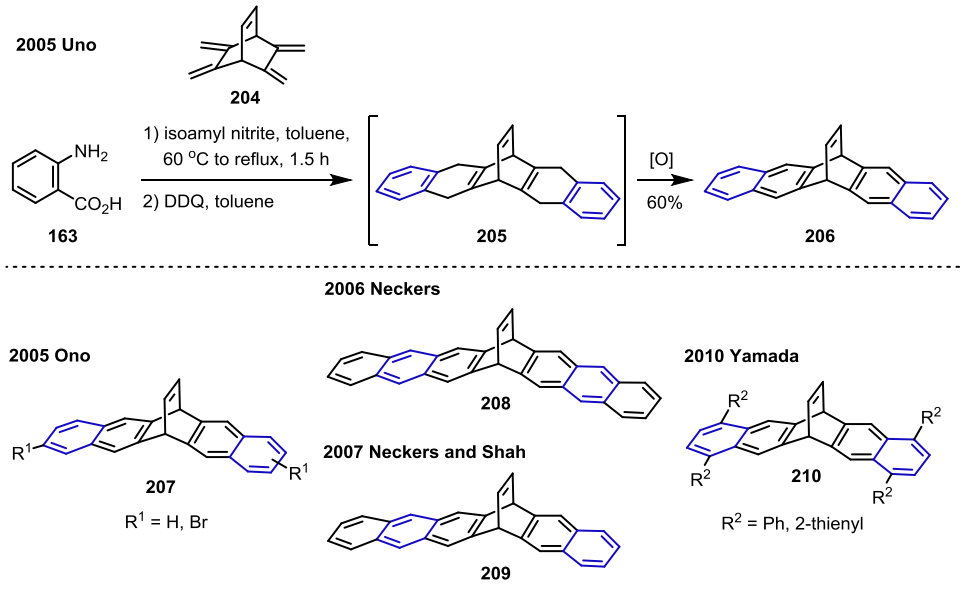

Gribble and Lopshuk employed münchnone **212** as the starting material in double aryne [4+2] cycloadditions to prepare dihydroepiminopentacene **214** and dihydroepiminoanthracene **217** (Scheme 1.32).[90] **214** was obtained in 89% yield when 0.7 equivalents of naphthyne were added. The reaction with 3.0 equivalents of **212** accompanying the subsequent oxidation with silica gel and/or in air affords dione **215**. The desired dihydroepiminoanthracene **217** was obtained, and benzoisoindole **216** were isolated as the intermediates using benzyne and 1.5 equivalents of **212**.

Scheme 1.32. Gribble's Dihydroepiminopentacene Synthesis.

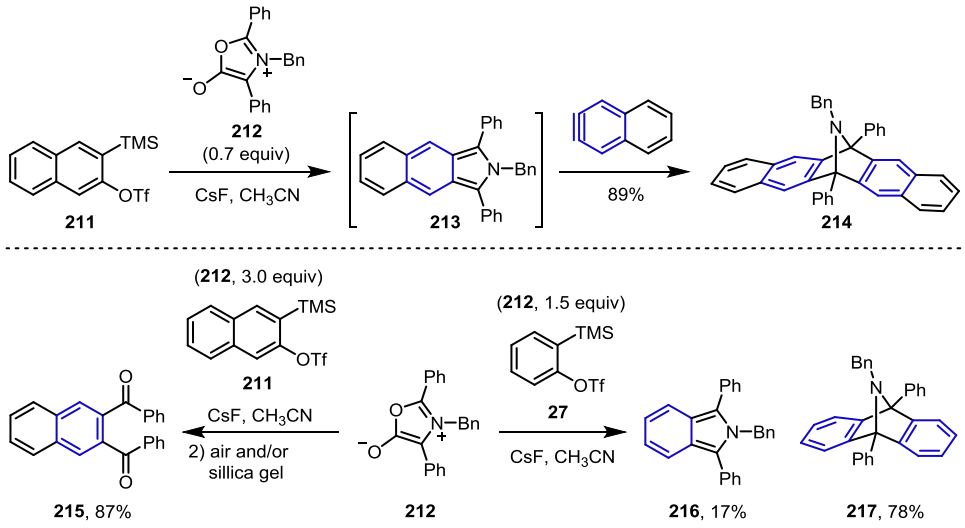

Sha and Wu reported the synthesis of xanthenes **224a** and benzophenones **224b** from 3-vinylchromones **218** and arynes (Scheme 1.33).[91] Acid reversibly drives **218** to tautomers **219**. The [4+2] cycloaddition of **219** affords oxo-bridged tricycles **222**, which undergo further [4+2] cycloaddition and ring opening of **223** to form xanthenes **224a**. In another pathway, **220** reacts with benzyne through [4+2] cycloaddition to afford benzophenones **224b**. Addition of 1.1

equivalents of TfOH led to **224a** as the major products and **224b** as the minor products but 2.5 equivalents of TFA only yielded **224b**.

Scheme 1.33. Sha and Wu's Xanthene and Benzophenone Synthesis.

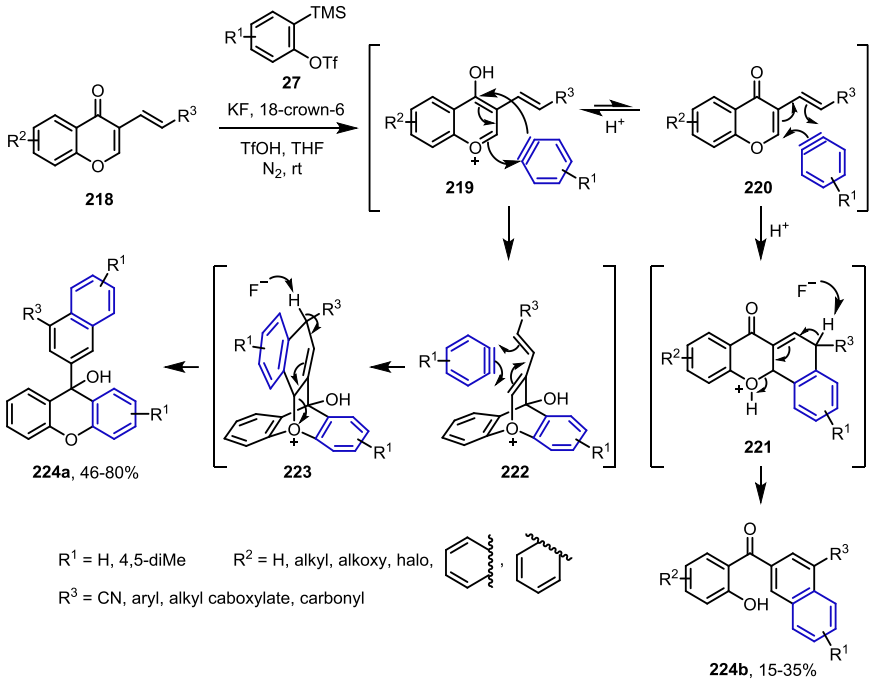

Garcia-Garibay and co-workers synthesized acetone-protected triptycene **226** from anthracene **225** in 2002 (Figure 1.3).[92] Tandem deprotection of **226** and Sonogashira coupling with an aromatic spacer led to bis-triptycene derivatives **227**-**230**. In addition to the Sonogashira coupling method, several other approaches to the synthesis of various bridged triptycenes (**231** and **232**) have been developed.[93] In 2014, the report by Mastalerz and co-workers showed the formation of a trace amount of double benzyne adduct *rac*-**237** from the [4+2] cycloaddition reaction of *ortho*--methoxybenzynes and two side rings of 1,8-dimethoxyanthracene **233**.[94]

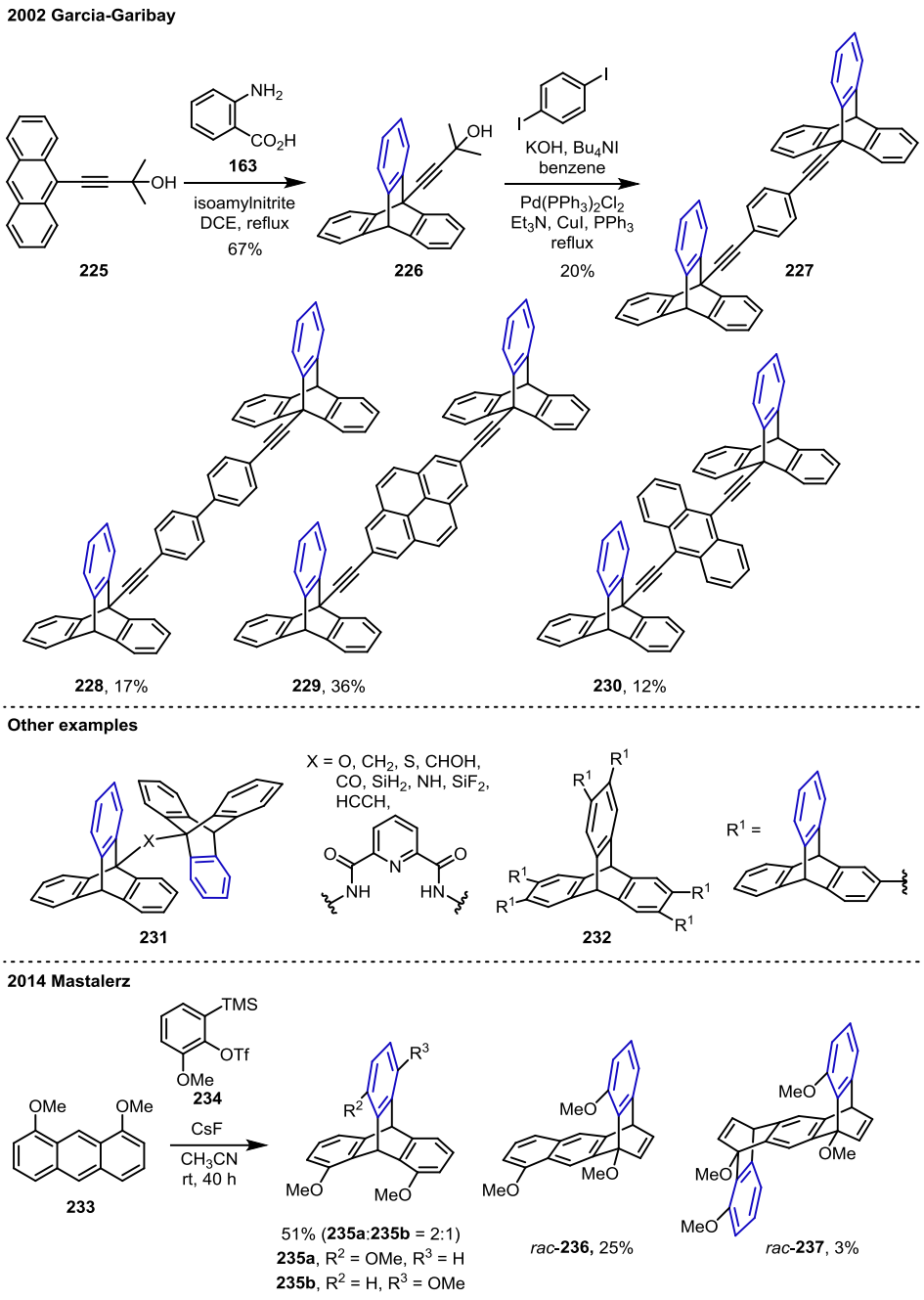

Figure 1.3. Representative iptycene synthesis.

Scheme 1.34. Rubin's Fullerene Synthesis.

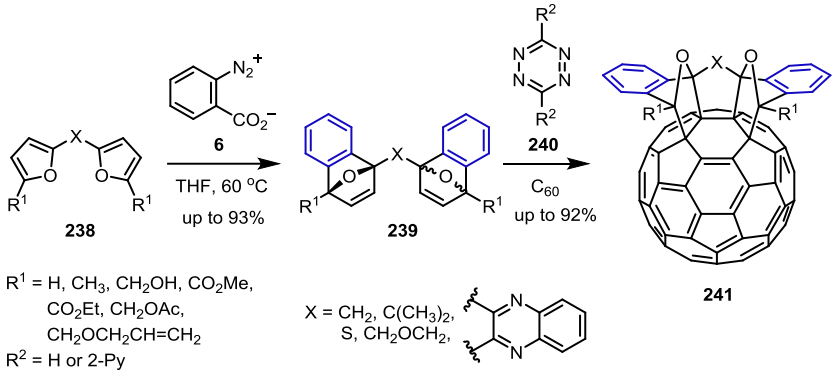

Scheme 1.35. Fabris' Dimerization Reaction.

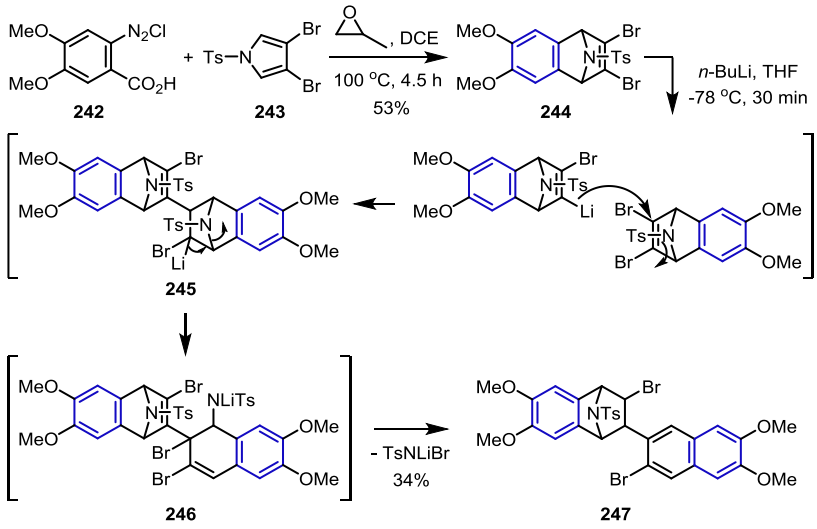

After applying the double benzyne [4+2] cycloaddition strategy to fullerene, Rubin and co-workers functionalized the fullerene (Scheme 1.34).[95] Bisfurans **238** reacted with benzynes to yield 1,4-dihydro-1,4-epoxynaphthalene derivatives **239**, which underwent tandem acetylene extrusion by dipyridyltetrazine **240** and double [4+2] cycloadditions to yield the corresponding fullerenes **241**.

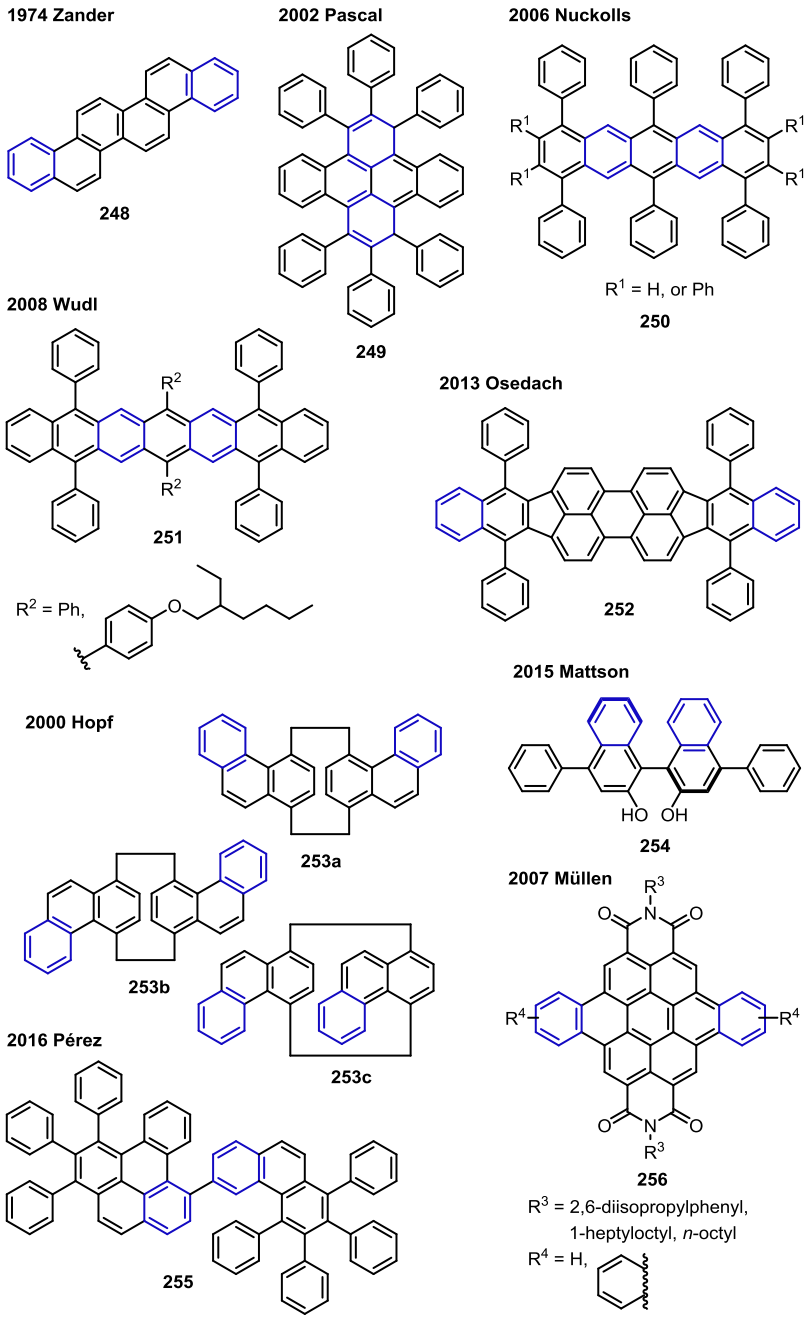

Figure 1.4. Representative [4+2]/[4+2] cycloaddition adducts.

Fabris and co-workers described the dimerization of two epiminonaphthalenes **244** that were formed by [4+2] cycloadditions of *N*-tosyl-protected pyrrole **243** and aryne (Scheme

1.35).[96] Dimerization of **244** was performed by addition of *n*-BuLi followed by elimination of Ts-NLiBr from **246** to yield dimer **247**.

Other double [4+2] cycloadducts are described in Figure 1.4. Znder and Franke reported the synthesis of benzo[*c*]picene **248** from double aryne cycloaddition of 1,5-divinylnaphthalene.[97] Pascal and co-workers employed a fully phenyl-substituted Stiles benzyne precursor (i.e., 3,4,5,6-tetraphenylanthranilic acid) to synthesize polycycle **249**.[51] Using the Kitamura hypervalent iodine-benzyne precursor, Nuckolls and co-workers synthesized hexaphenyl pentacene and decaphenyl pentacene (**250**).[98] Wudl and co-workers have attempted to synthesize heptacenes, and they reported the synthesis of **251** from arynes and 2,5-diaryl-6-oxo-1,3,4-oxadiazine-6-one with the release of N_2 and CO_2 gas.[99] Dibenzo([*f,f*']-4,4',7,7'-tetraphenyl)diindeno[1,2,3-*cd*:1',2',3'-*lm*]perylene (DBP) **252** is a well-known organic field effect transistor material. To synthesize DBP **252**, several coupling reactions on fissure, bay, cove, and fjord regions of the precursors of **252** have been employed.[100] Osedach and co-workers used benzynes for double [4+2] cycloadditions on two terminal bay regions of **252**.[101] Hopf and co-workers synthesized phenanthrenophanes (**253a**-**253c**) using the double [4+2] cycloaddition reaction of diethenyl[2.2]paracyclophanes and benzynes.[2g] Mattson and co-workers used benzyne for [4+2] cycloaddition of benzoylacetone to prepare 4-phenyl-2-naphthol.[102] The resulting naphthols were coupled to one another to afford BINOL **254**. Pérez and co-workers designed a highly substituted Kobayashi benzyne (i.e., 5,6,7,8-tetraphenyl-4-(trimethylsilyl)phenanthrene-3-yl triflate) and synthesized **255** but the mechanism remains controversial.[103] Müllen and co-workers have focused on the synthesis of perylenes, and we

introduce one example.[104] They employed double aryne [4+2] cycloaddition for the synthesis of perylene imides **256**.

1.4.3 [4+2]/[4+2]/[4+2] Cycloadditions

Scheme 1.36. Seitz's Triple [4+2] Aryne Cycloaddition for the Synthesis of Triptycene.

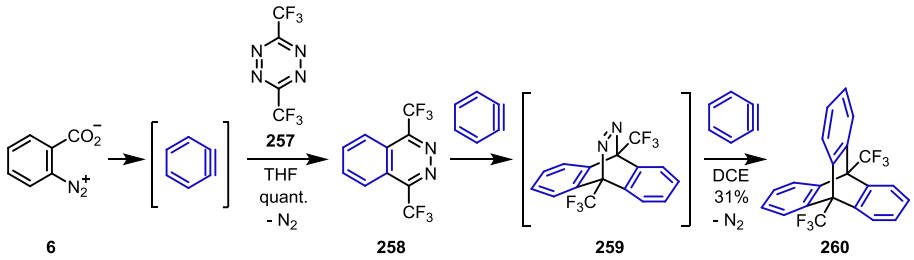

Seitz and Laue obtained 3,6-bis(trifluoromethyl)phthalazine **258** from the reaction of 3,6-bis(trifluoromethyl)tetrazine **257** and benzyne in 1987 (Scheme 1.36).[105] After 9 years, they reported the synthesis of 9,10-bis(trifluoromethyl)triptycene **260** from two equivalents of

Scheme 1.37. Fabris' Triple [4+2] Aryne Cycloaddition Reaction.

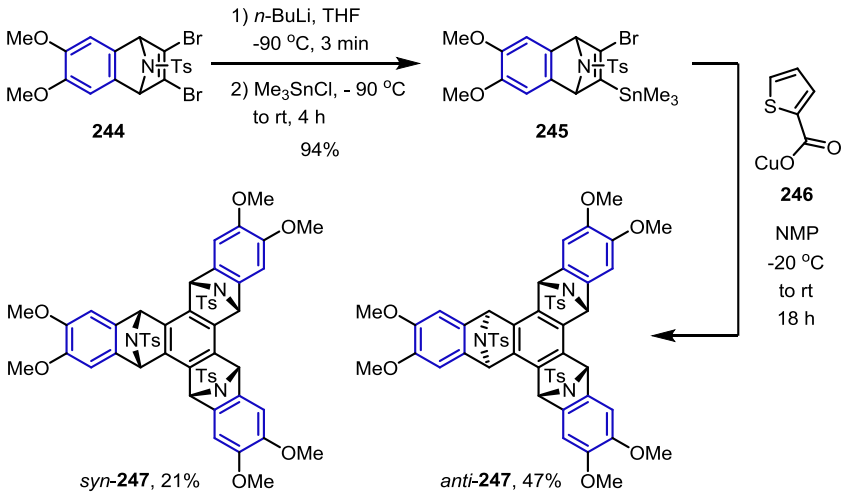

Scheme 1.38. Mislow's Tris(9-triptycyl) Derivative Synthesis.

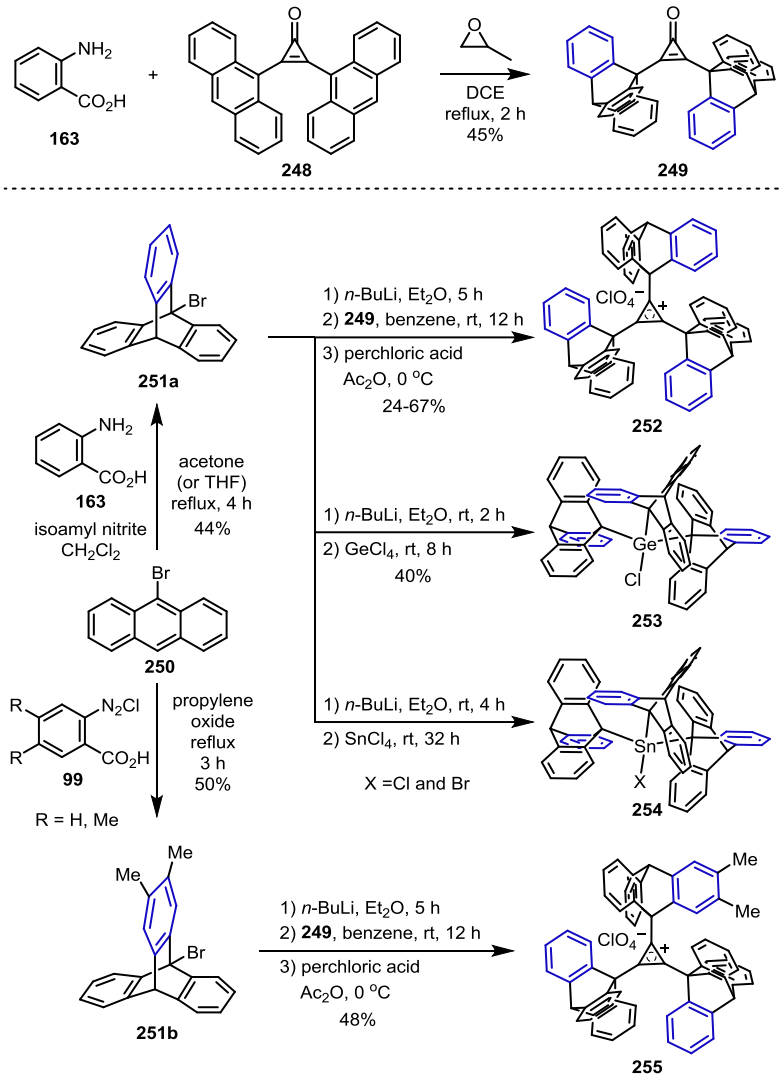

benzynes and **258**.[106] A total of three equivalents of benzynes reacted with **257** to afford **260** in 31% yield over two reaction steps.

Epiminonaphthalenes **244** that were developed by Fabris and co-workers (Scheme 1.35) were used for the synthesis of benzocyclotrimers (*syn*- and *anti*-**247**) (Scheme 1.37).[96] After transmetalation and stannylation of **244**, the cyclotrimerization of stannane **245** with copper(I) 2-thiophenecarboxylate **246** affords *syn*- and *anti*-**247**. The total yield of **247** (68%)

was calculated based on the sum of the *syn*- and *anti*-isomer yields (i.e., 21% and 47%, respectively).

Mislow and co-workers reported the synthesis of tris(9-triptycyl) scaffolds bearing cyclopropenium, germanium, or stannum as the center component (Scheme 1.38).[93k] To prepare bis(9-triptycyl)cyclpropenone **249**, bis(9-anthryl)cyclopropenone **248** reacted with benzynes via double [4+2] cycloadditions. After transmetalation of 9-bromotriptycenes (**251a** and **251b**) generated from 9-bromoanthracene **250**, lithiated triptycene intermediates were added to **249** to yield tris(9-triptycyl)cyclopropeniums. Cyclopropenium perchlorates (**252** and **255**) were isolated by treating the cyclopropeniums with perchloric acid. Furthermore, the addition of lithiated triptycene to $GeCl_4$ or $SnCl_4$ led to tris(9-triptycyl)germanium chloride **253**, tris(9-triptycyl)germanium chloride and bromide **254**.

1.4.4 [4+2]/[4+2]/[4+2]/[4+2] Cycloadditions

Scheme 1.39. Müllen's Synthesis of Nonacene Precursor.

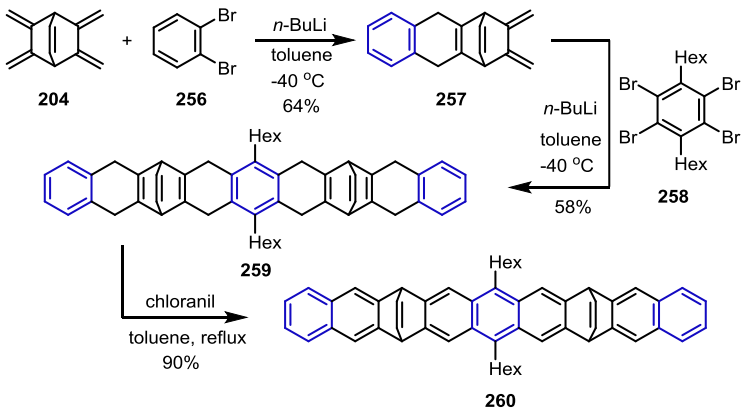

Scheme 1.40. Müllen and Li's Synthesis of Tetranaphthoterrylene Tetracarboxdiimide.

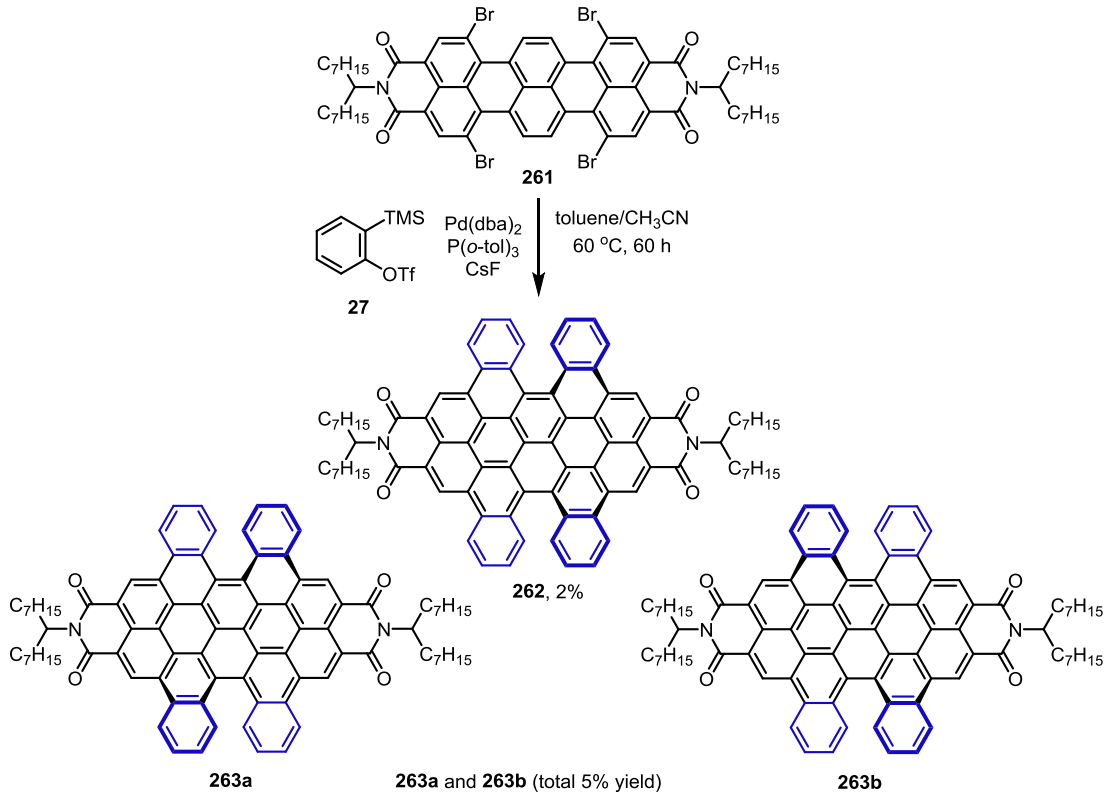

As shown in Scheme 1.31, tetramethylidene **204** has been used for the synthesis of linear acenes. Müllen and Herwig employed one equivalent of benzyne to trap dimethylidene intermediate **257**, which underwent double [4+2] cycloaddition with bisaryne followed by oxidation to afford nonacene precursor **260** (Scheme 1.39).[107]

As discussed in Figure 1.4, the synthesis of dibenzocoronenebis(dicarboximide)s **256** from two equivalents of benzynes and 1,7-dibromoperylenebis(dicarboximide) has been reported by Müllen and co-workers (Scheme 1.40).[108] After four years, Müllen, Li, and co-workers reported formal quadruple benzyne [4+2] cycloadditions with tetrabromoterrylenebis(dicarboximide) **261** to yield tetranaphthoterrylene tetracarboxdiimides

(**262**, **263a**, and **263b**) as three isomers. The prominent review for perylene synthesis was reported by Müllen and co-workers in 2010.[109]

1.4.5 [4+2]/[4+2] Cycloadditions/ Nucleophilic Addition

Scheme 1.41. Zhang's *N*-Phenylanthracenamine Synthesis.

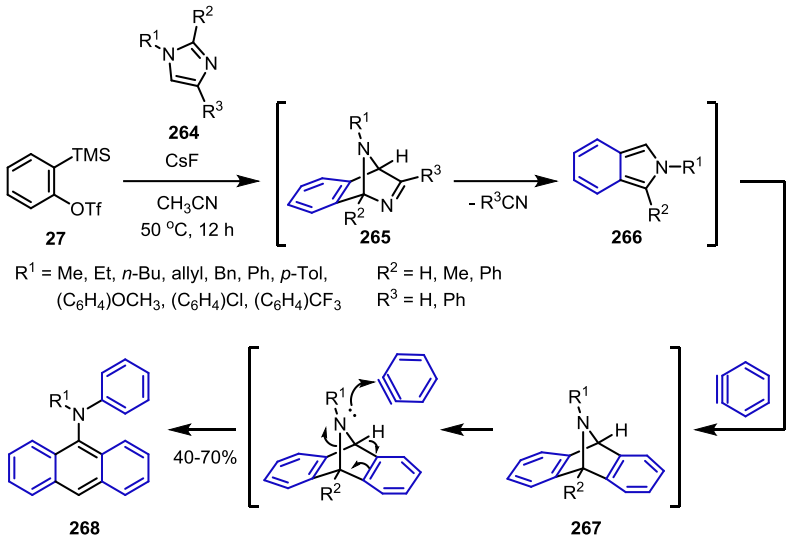

In 2007, Zhang and Xie reported one-pot double benzyne [4+2] cycloaddition and nucleophilic addition of imidazoles **264** (Scheme 1.41).[110] The first [4+2] cycloaddition of benzyne and **264** affords bicyclic intermediates **265**, which undergo expulsion of R^3CN to afford isoindole intermediates **266**. The corresponding intermediates **266** reacts with another benzyne via [4+2] cycloaddition and subsequent nucleophilic addition to the third benzyne to yield *N*-phenylanthracenamines **268**.

1.4.6 [4+2] Cycloaddition/Nucleophilic Addition

Scheme 1.42. Rickborn's Benzyne-Oxazole Reaction.

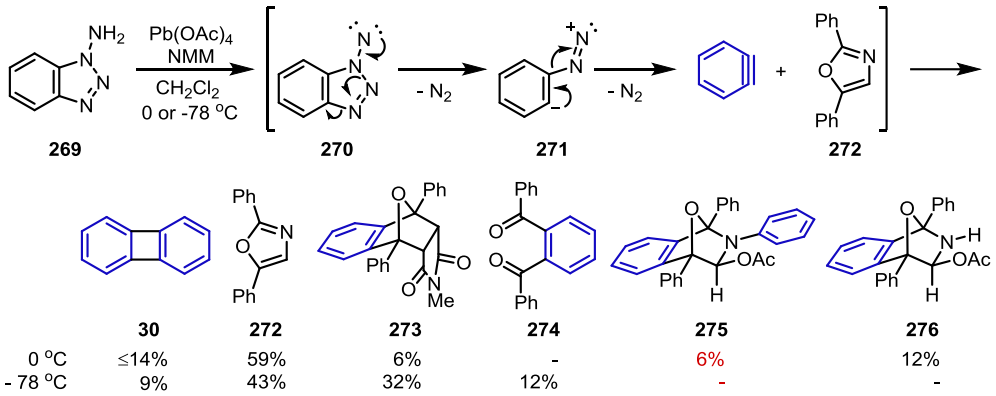

In 1990, Rickborn and co-workers utilized Rees' method to generate benzyne from the oxidation of 1-aminobenzotriazole **269** to study the reactivity between oxazole **272** and benzyne (Scheme 1.42).[111] The [2+2] cycloadduct **30** and benzyne-oxazole-NMM adduct **273** were obtained. Additionally, dione **274** was formed at 0 °C, and both the benzyne-oxazole-OAc adduct **276** and double benzyne adduct **275** were obtained at –78 °C.

Scheme 1.43. Zhu's One-Pot [4+2] Cycloaddition and Nucleophilic Addition.

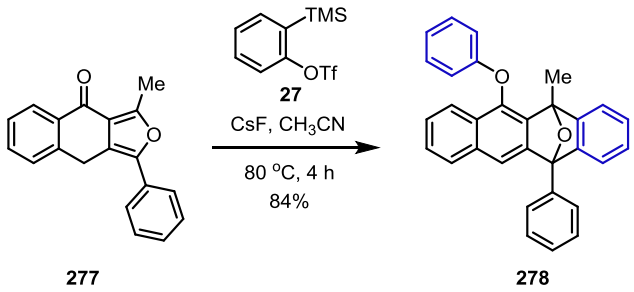

Zhu and co-workers synthesized cyclohexanone-fused furan **277** from alkynone using a gold catalyst (Scheme 1.43).[112] Further transformation of **277** afforded bis(benzyne) adduct

278. The mechanism was not studied but is assumed to involve tandem [4+2] cycloaddition and nucleophilic addition or these reactions in the reverse order.

1.4.7 [4+2] Cycloaddition/Nucleophilic Addition/[4+2] Cycloaddition

Scheme 1.44. Chenoweth's Triple Aryne-Tetrazine Reaction.

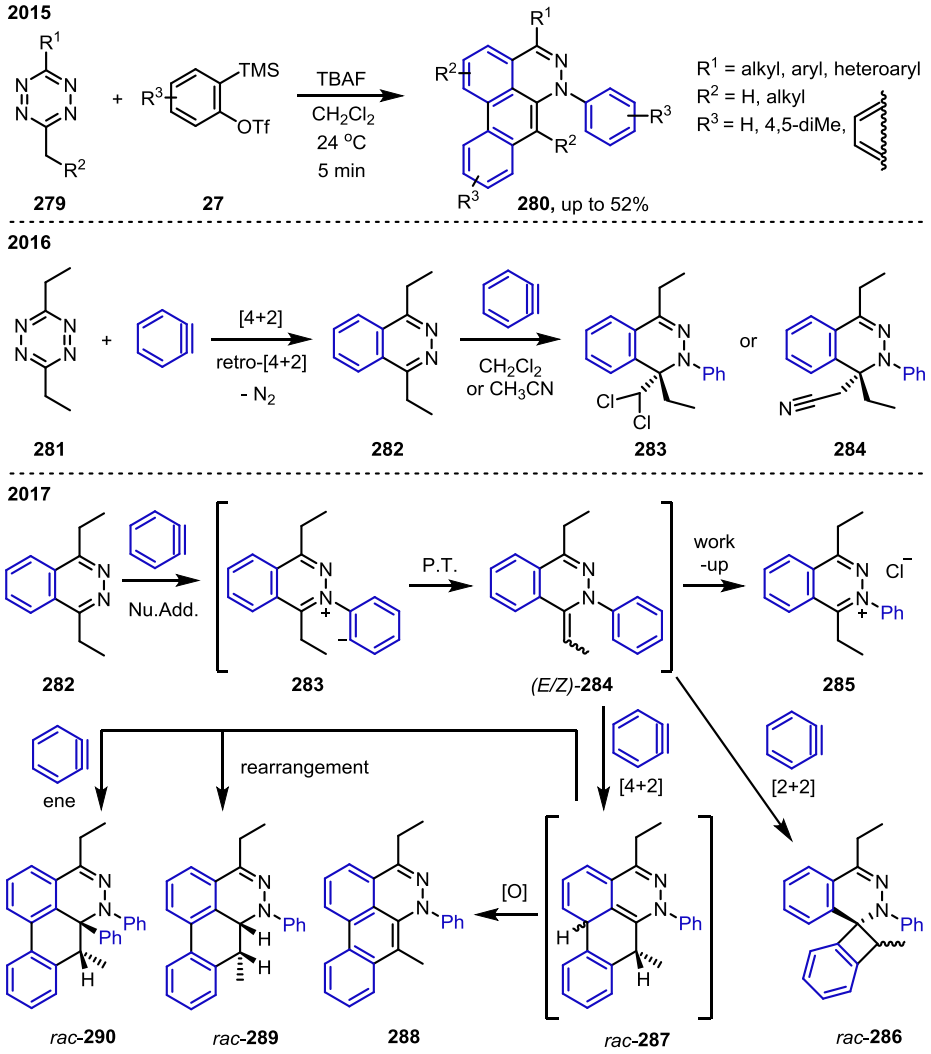

In 2015, we reported the triple aryne-tetrazine (TAT) reaction affording dibenzo[*de,g*]cinnolines **280** (Scheme 1.44).[113] Tetrazines **279** reacted with three equivalent of

aynes to yield **280**. Then, we observed solvent adducts that were formed via a multicomponent reaction (MCR) of solvent, benzyne, and phthalazine **282.**[114] Dichloromethane- and acetonitrile adducts (**283** and **284**) were isolated, and the reaction mechanism was confirmed by hydrogen–deuterium exchange experiments. Recently, we scrutinized the reaction mechanism, isolated the intermediates and byproducts, and conducted a crossover experiment and computational study with Houk and Chen.[115] For the proposed mechanism, [4+2] and retro-[4+2] cycloaddition of tetrazine **281** and benzyne affords the corresponding phthalazine **282,** and the subsequent nucleophilic addition of **282** to benzyne yields zwitterionic intermediate **283**. The intermolecular water-mediated proton transfer of **283** led to (*E*/*Z*)-**284**, which undergoes both [2+2] and [4+2] cycloaddition to afford a [2+2] adduct *rac*-**286** and intermediate *rac*-**287**. **285** was obtained after work-up. The intermediate *rac*-**287** is diversified into rearranged product *rac*-**289**, ene-product *rac*-**290**, and **288**.

Coquerel, Rodriguez, and co-workers employed *N*-aryl aldimines **291** for pseudo MCR with arynes (Scheme 1.45).[116] [4+2] cycloaddition of aryne and aldimine **291** followed by nucleophilic addition to aryne yield *N*-arylated 1,2-dihydroisoquinolines **294.** For the specific substituent, one more [4+2] cycloaddition of **294** affords the 5,6-dihydrobenzo[*c*]phenanthridine **296**. Addition of benzyne to *N*-pyrazolyl ketamine **297** affords spirooxindole scaffold **299** bearing two aryne synthons. The reaction performed in THF produced etherated spirooxindole **298**. *N*-pyrazolyl cyclopentanoneimine **300** did not proceed through a [4+2] cycloaddition but triple *N*-arylation to afford **301**.

Scheme 1.45. Coquerel and Rodriguez's Pesudo MCR between Imines and Arynes.

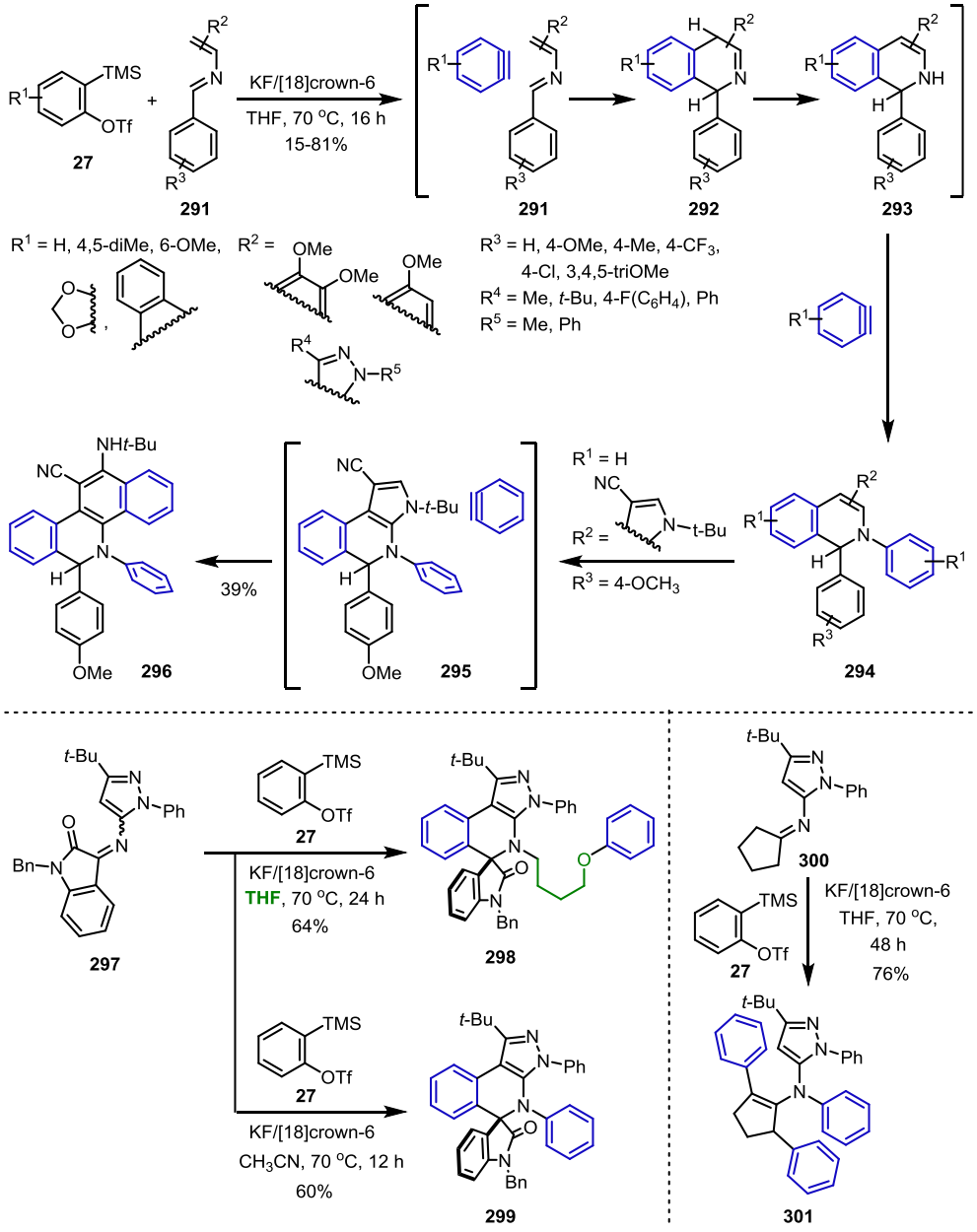

1.4.8 [4+2] Cycloaddition/Ene Reaction

Scheme 1.46. Liu and Yu's Diphenyldihydrophenanthrene Synthesis.

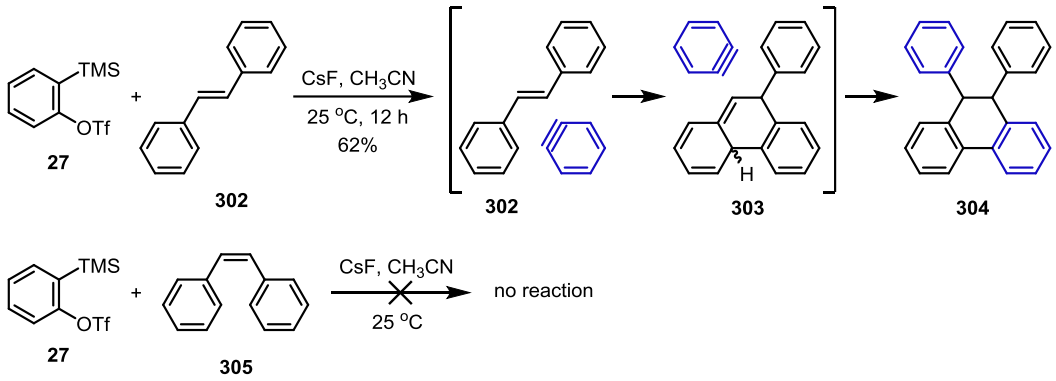

Scheme 1.47. Li and Jia's Tandem [4+2] Cycloaddition/Formal Ene Reaction of Oxindoles and Arynes.

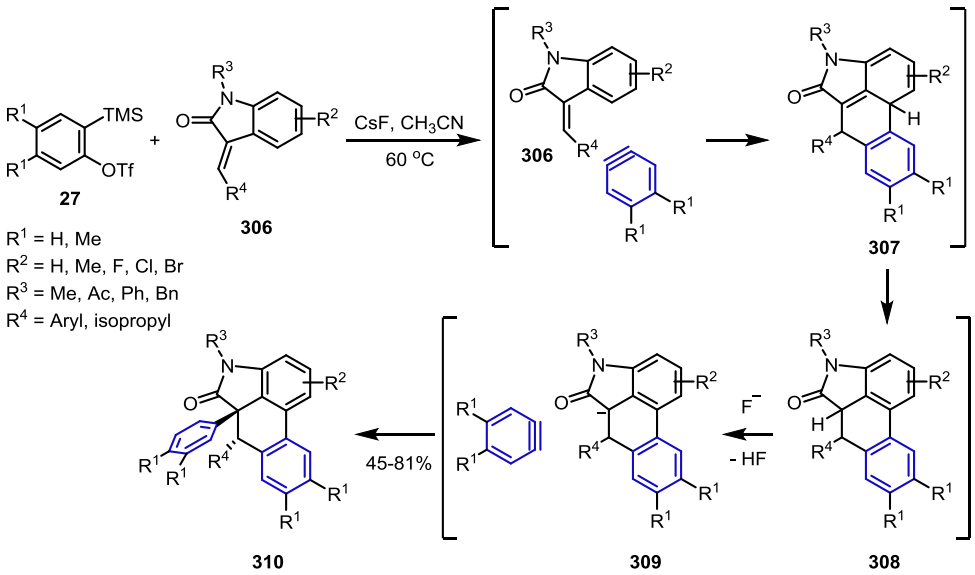

In the synthesis of 9,10-diphenyl-9,10-dihydrophenanthrene **304** from *trans*-stilbene **302** and benzyne by Liu, Yu, and co-workers, the reaction of benzyne with the diene of stilbene **302** via [4+2] cycloaddition followed by an ene reaction affords desired product **304** (Scheme 1.46).[2b] The possibility of [2+2+2] cycloaddition of two benzynes and stilbene was not

mentioned in the literature. However, this reaction pathway does not appear to be plausible because their control experiment disclosed that *cis*-stilbene **305** did not react with benzynes.

Li, Jia, and co-workers reported the synthesis of arylidenoxindole derivatives **310** by employing two equivalents of benzynes and oxindole **306** (Scheme 1.47).[117] [4+2] cycloaddition of benzyne affords intermediate **307**. The proposed mechanism of the transformation from **308** to **310** involves a [1,3]-H shift of **308** and subsequent deprotonation/nucleophilic addition to benzyne to yield **310**. Another possible pathway for this transformation involves a direct ene reaction of **307** to afford **310**.

Scheme 1.48. Liu's Tandem [4+2] Cycloaddition/Formal Ene Reaction of Benzylidenephthalans and Arynes.

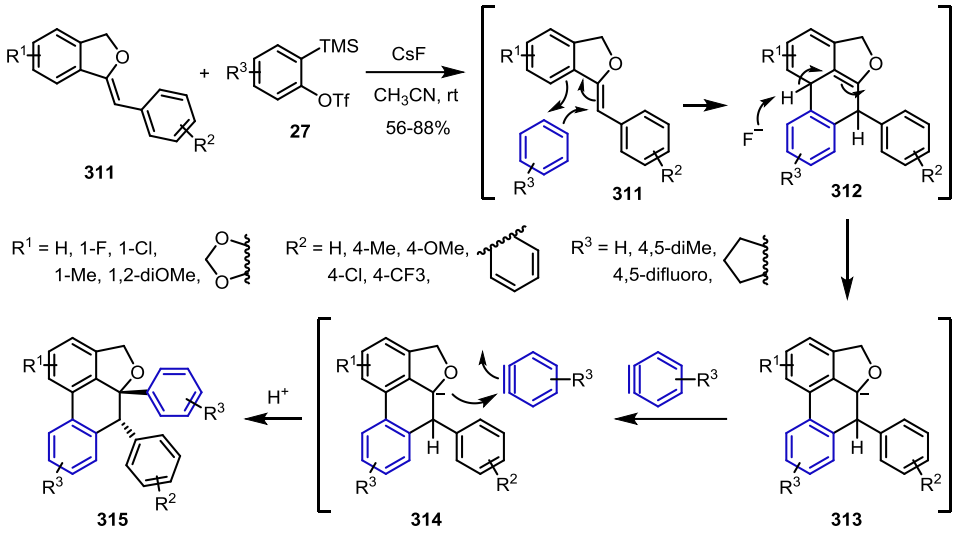

The synthesis of phenanthro[10,1-*bc*]furans **315** from benzylidenephthalans **311** and arynes was developed by Liu and co-workers (Scheme 1.48).[118] In comparison to Scheme 1.47, benzylidenephthalans **311** resembles oxindoles **306** and thus, the proposed mechanisms are also

similar to one another. After [4+2] cycloaddition of **311** and benzyne, deprotonation and rearomatization of **302** led to intermediate **313,** which afforded **315** via nucleophilic addition to another benzyne. As shown in the previous scheme, a direct ene reaction of **312** should yield **315**.

Scheme 1.49. Biju's Aryldihydrophenanthrene Synthesis.

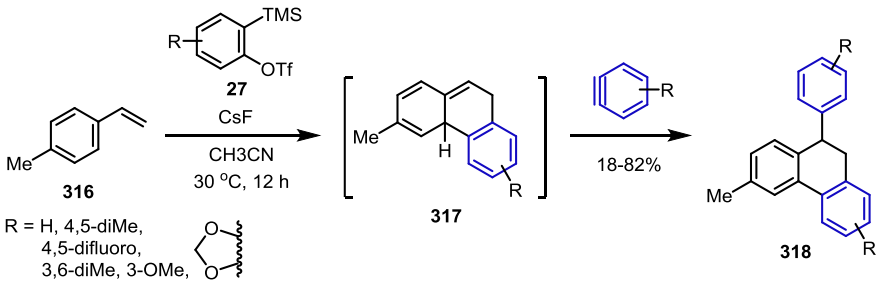

Biju and co-workers reported the synthesis of aryldihydrophenanthrenes **318** via tandem [4+2] cycloaddition and ene reaction of styrenes **316** and arynes (Scheme 1.49).[119] In general, aryne-engaged synthetic approaches to the synthesis of phenanthrenes or dihydrophenanthrenes involve [2+2+2] cycloaddition of two equivalent of arynes with one equivalent of alkynes or alkenes. However, [4+2] cycloaddition with **316** and benzyne followed by either an ene reaction or stepwise deprotonation/nucleophilic addition of **317** afford **318** in this study. A [2+2+2] cycloaddition method for the preparation of phenanthrene derivatives will be discussed in Section 6.2.

1.5 [5+2] Cycloadditions

1.5.1 [5+2]/[2+2] Cycloadditions

Scheme 1.50. Yoo's 1,4-Benzodiazepines Derivatives Synthesis.

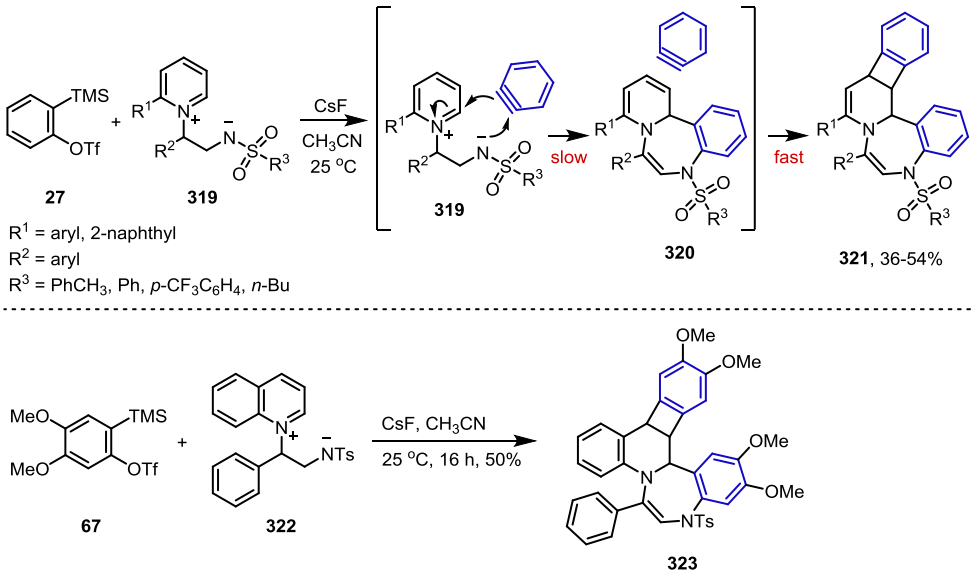

Recently, Yoo and co-workers reported tandem [5+2]/[2+2] cycloadditions for the synthesis of 1,4-benzodiazepines derivatives **321** (Scheme 1.50).[120] Higher-order cycloaddition is very rare in aryne chemistry, and [5+2] cycloaddition has not been described prior to this published study. Zwitterion pyridinium **319** reacted with benzyne via [5+2] cycloaddition, and the corresponding 1,4-benzodiazepine **320** goes through [2+2] cycloaddition with another benzyne to yield 1,4-benzodiazepines **321**. Polycycle **323** was obtained when dimethoxy aryne precursor **67** and **322** were employed. The [5+2] cycloaddition is most likely the rate-determining step based on their mechanistic study.

1.6 [2+2+2] Cycloadditions

1.6.1 Triphenylene Synthesis

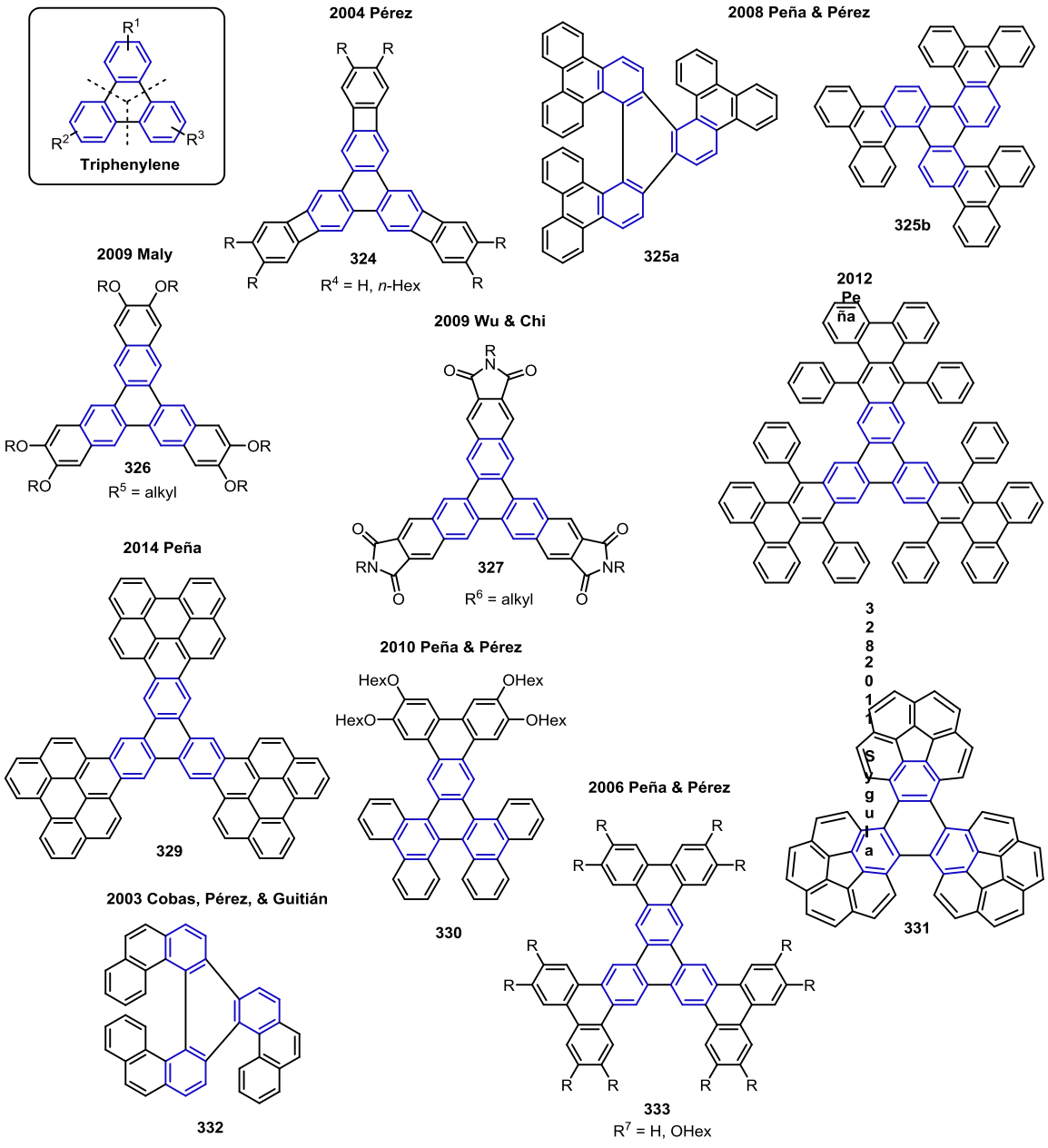

Figure 1.5. Representative triphenylenes.

As shown in Figure 1.1, Bachman and Clarke introduced the generation of benzyne from chlorobenzene and sodium metal in 1927.[8] In the report, they reported the formation of triphenylene via [2+2+2] cycloaddition. Subsequently, several highly strained and gigantic triphenylenes have been synthesized (Figure 1.5).[121] Triphenylene synthesis[3a,d,33,40,47,48f,122] was not discussed in this review but a valuable review on the synthesis of triphenylenes and other polycyclic aromatic compounds was recently reported by Pérez, Peña, and Guitián in 2013.[1h]

1.6.2 Phenanthrene, Phenanthridine, and Related Compounds Synthesis

The synthesis of phenanthrenes/dihydrophenanthrene via [2+2+2] cycloaddition of two equivalents of arynes with one equivalent of alkynes or alkenes has been reported.[2b,41,119,121h,j,122w,123] Utilizing nitriles as the partner of arynes, the limited scope of phenanthridine synthesis from various arynes has been developed.[3e,124] Representative structures of phenanthrenes, dihydrophenanthrene, and phenanthridine are shown in Figure 1.6.[3e,121h,j,123c,i,n,124]

Gold/copper-catalyzed formal [2+2+2] cycloaddition of arynes and acetylenes **335** was employed for the synthesis of alkynylated biphenyl derivatives **339** by Zhang and co-workers in 2008 (Scheme 1.51).[123l] Only diphenylacetylene was isolated in good yield when the gold catalyst was excluded from the reaction. Subsequently, Yoshida and co-workers observed suppression of diphenylacetylene formation when CuCl rather than CuI was employed.[125] In the reaction, the desired alkynylated biphenyl products **340** were obtained in good yield. They obtained fluorenylidene **346** from ethyl propiolate **341** and benzynes in their effort to synthesize

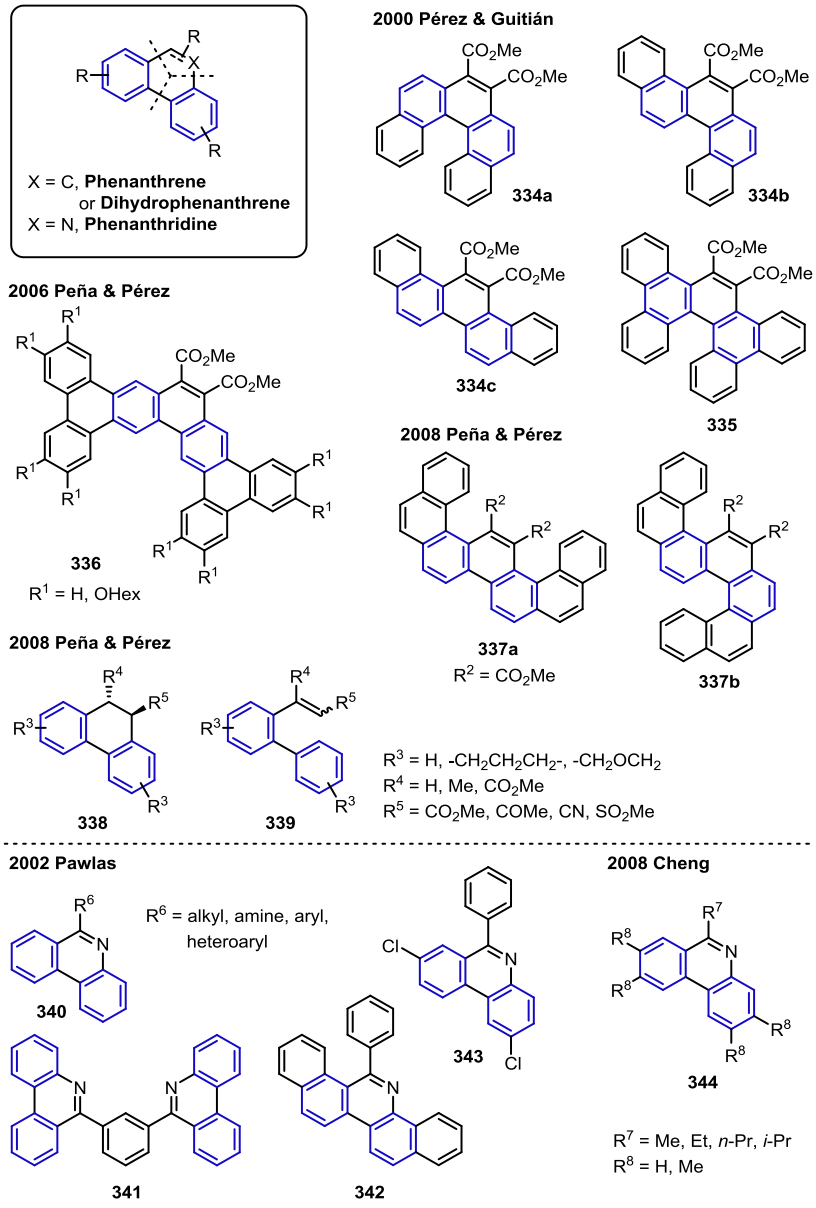

Figure 1.6. Representative phenanthrene, phenanthridine, and related compounds.

alkynylbiphenyl. This result supports the presence of intermediate **344** in the mechanism. In 2010, they extended the scope of acetylenes for the reaction and succeeded in synthesizing bromoalkynylation products **347** from bromoacetyelenes with $CuBr_2$.[126]

Scheme 1.51. Synthesis of Alkynylbiphenyl Derivatives.

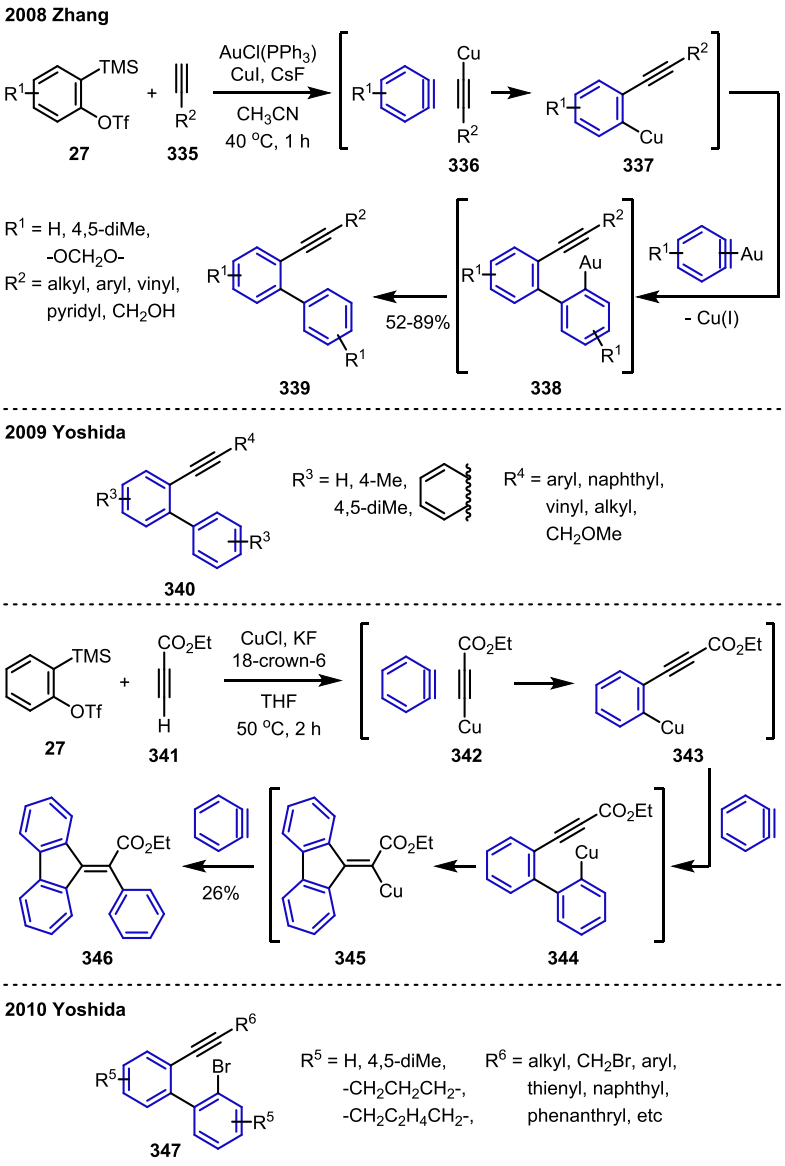

Using $Pd(OAc)_2$ and a bicyclic phosphite ligand (i.e., 4-ethyl-2,6,7-trioxa-1-phosphabicyclo[2.2.2]octane (ETPO)), Kunai, Yoshida, and co-workers conducted formal [2+2+2] cycloaddition of hexamethylditin **348** and two equivalents of arynes (Scheme 1.52).[127] After formation of palladabenzocyclopropene **349**, another aryne was inserted into the

cyclopropene ring. Ditin **348** was added to cyclopropene **349** and biphenyl ring **350** to afford distannylarene **351** and distannylbiaryl **352**, respectively.

Scheme 1.52. Kunai and Yoshida's Synthesis of Distannylbiaryls and Distannylarenes.

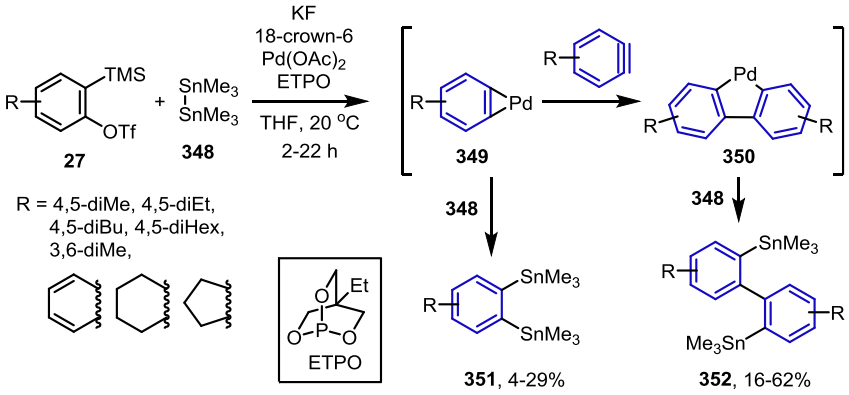

1.7 Nucleophilic Additions

1.7.1 Nucleophilic Addition/[3+2] Cycloaddition

Yao and co-workers accomplished the synthesis of dihydrobenzo[*d*]isoxazoles **356** and dihydrobenzo[*d*]oxazoles **360** from nitrones and arynes (Scheme 1.53).[128] The nitrogen of nitrones **353** were added to aryne to generate zwitterionic intermediate **354**, which underwent proton transfer and ring closure to yield dihydrobenzo[*d*]isoxazole **356**. The N-O bond can be cleaved via a radical pathway or an ionic pathway. The addition of TEMPO to the reaction still led to **360** but the TEMPO adduct was not observed. Therefore, this experiment may indicate that the ionic pathway is more favorable. The resulting spirocyclic intermediate **358** is opened

and rearranged to form dihydrobenzo[*d*]oxazole **360**. The ratio of **356** and **360** was controlled by temperature. **356** was a major product at 10 or 40 °C, and **360** was formed as a major product at 80 °C.

Scheme 1.53. Yao's Synthesis of Dihydrobenzo[*d*]isoxazoles and Dihydrobenzo[*d*]oxazoles.

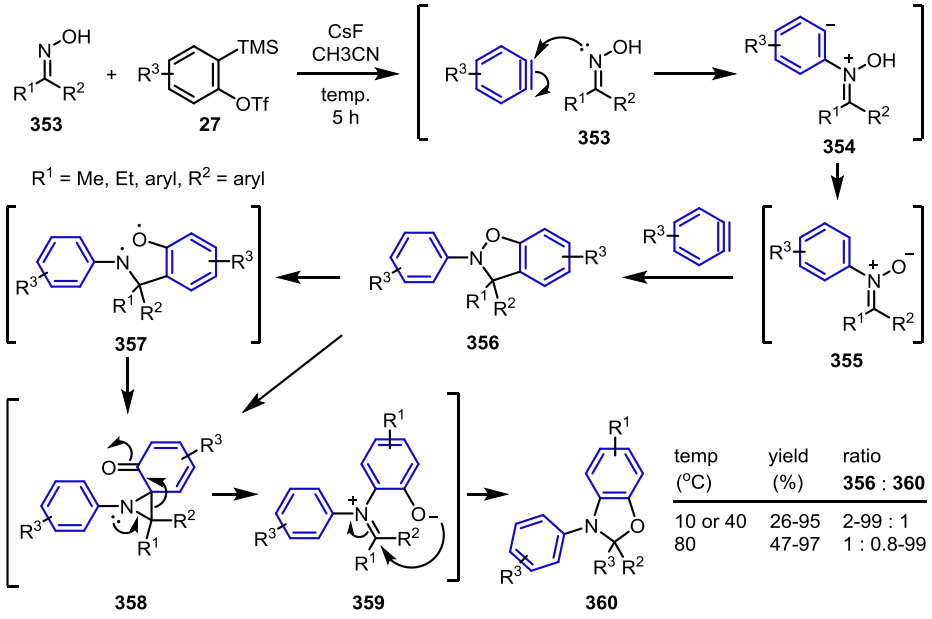

1.7.2 Nucleophilic Addition/[4+2] Cycloaddition

Scheme 1.54. Aly's Phenylisoindolophenathridine Synthesis.

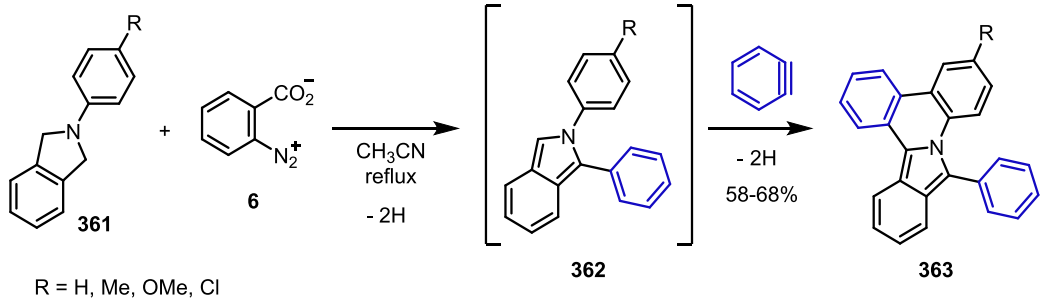

Phenylisoindolophenathridines **363** were synthesized by Aly and co-workers (Scheme 1.54).[129] In the proposed mechanism, arylisoindoline **361** was oxidized to isoindole **362** followed by nucleophilic addition to benzyne to afford diarylisoindole intermediate **362**. [4+2] cycloaddition of **362** followed by oxidation led to phenylisoindolophenathridine **363**. Interestingly, *N*-phenylanthracenamine was not observed. A shown in Scheme 1.41, the arylisoindole intermediate **266** reacted with two equivalents of benzynes to form *N*-phenylanthracenamine **268**. The mechanism was not studied but the first oxidation step most likely plays a key role in inhibiting the pathway to *N*-phenylanthracenamine.

Scheme 1.55. Biehl's Anthrone Imine Synthesis.

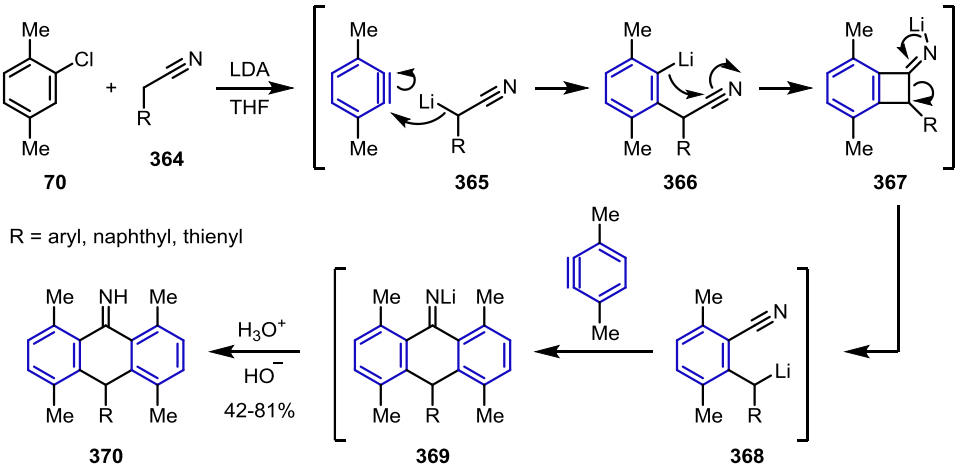

Biehl and co-workers used two equivalents of 3,6-dimethylbenzyne for the annulation of nitriles **364** to produce anthrone imines **370** (Scheme 1.55).[130] Lithiation of nitrile **365** followed by nucleophilic addition of **365** to benzyne led to intermediate **366**. Intramolecular addition and subsequent ring opening yield intermediate **368**, which undergoes [4+2] cycloaddition with another aryne to afford desired anthrone imines **370**.

Scheme 1.56. Huang and Wu's Isoquinolines Synthesis.

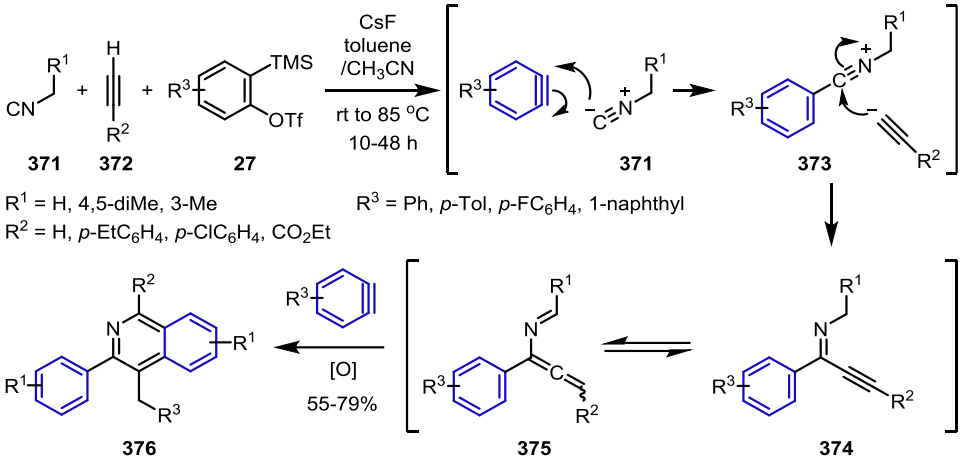

In 2009, Huang and Sha discovered the multicomponent reaction of isocyanides **371**, alkynes **372**, and benzynes (Scheme 1.56).[131] After the addition of **371** to aryne, the alkynyl anion

Scheme 1.57. Katritzky's One-Pot Nucleophilic Addition/[4+2] Cycloaddition.

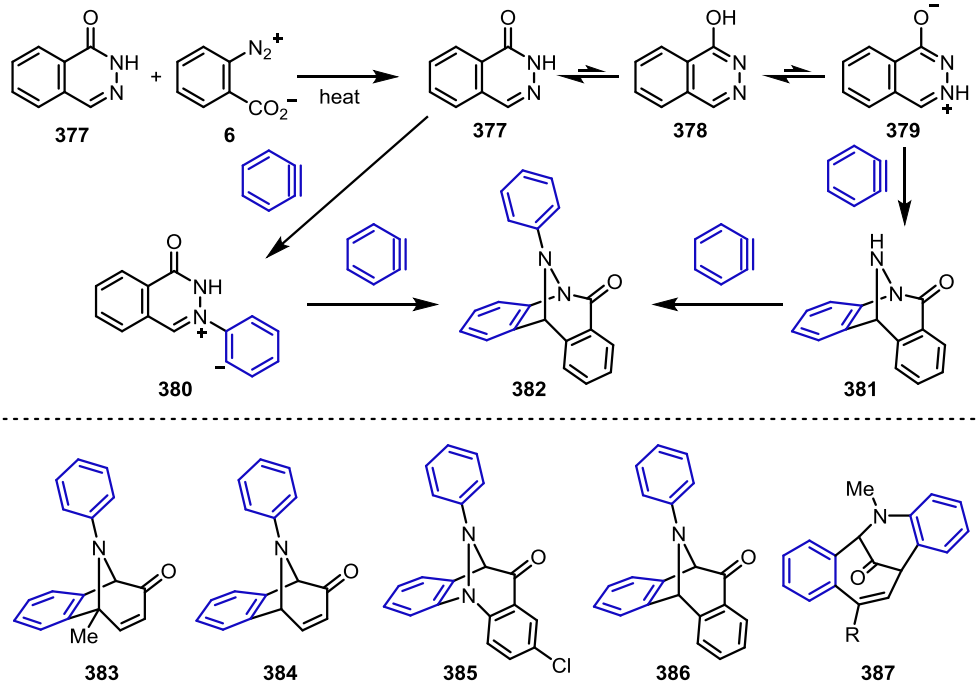

attacks the resulting intermediate **373**, yielding 1-alkynyl imine **374**. Isomerization of **374** affords aza-diene **375**, which undergoes [4+2] cycloaddition of aryne and oxidation to afford isoquinolines **376**. Subsequently, Wu, Huang, and Sha extended the reaction scope and introduced a plausible mechanism based on their studies.[132]

In 1972, Katritzky and co-workers embarked on the formation of tricyclic compounds using hydroxypyridine and two equivalents of benzynes (Scheme 1.57).[133] Then, they have reported the synthesis of several tricyclic compounds and proposed the representative mechanism of one of the reactions in 1975.[134] According to the report, the nitrogen of phthalazin-l(2*H*)-one **377** was added to benzyne, and the following [4+2] cycloaddition yielded the desired cycloadduct **382**. In another possible pathway, **377** undergoes [4+2] cycloaddition of benzyne followed by nucleophilic addition to benzyne to afford **382**. The synthesis of other double benzyne adducts (**383**-**387**) has been reported by Katiritzky.[134-135]

1.7.3 Nucleophilic Addition/[4+2] Cycloaddition/Nucleophilic Addition

Scheme 1.58. Larock's Conversion from Pyrrole to Diphenylaminonaphthalene.

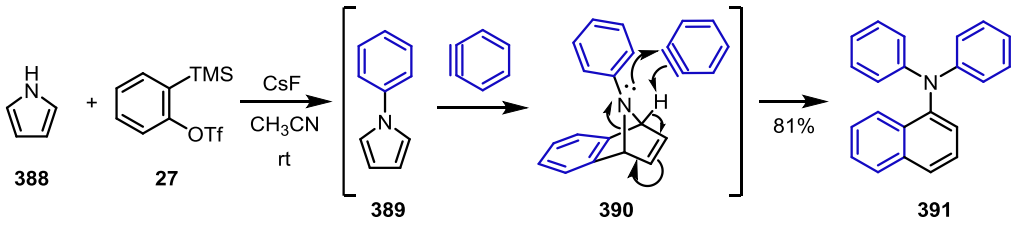

One year prior to Zhang's *N*-phenylanthracenamine synthesis, Larock and Liu reported the synthesis of diphenylaminonaphthalene **391** from pyrrole **388** (Scheme 1.58).[136] *N*-arylation

of pyrrole **388** occurs along with a simultaneous [4+2] cycloaddition followed by one more *N*-arylation to afford diphenylaminonaphthalene **391**.

1.7.4 Nucleophilic Addition/[4+2]/[4+2] Cycloadditions/Nucleophilic Addition

Scheme 1.59. Okuma's Synthesis of Diphenylaminoanthracene, Xanthene, Xanthone, and Quaternary Ammonium Salts.

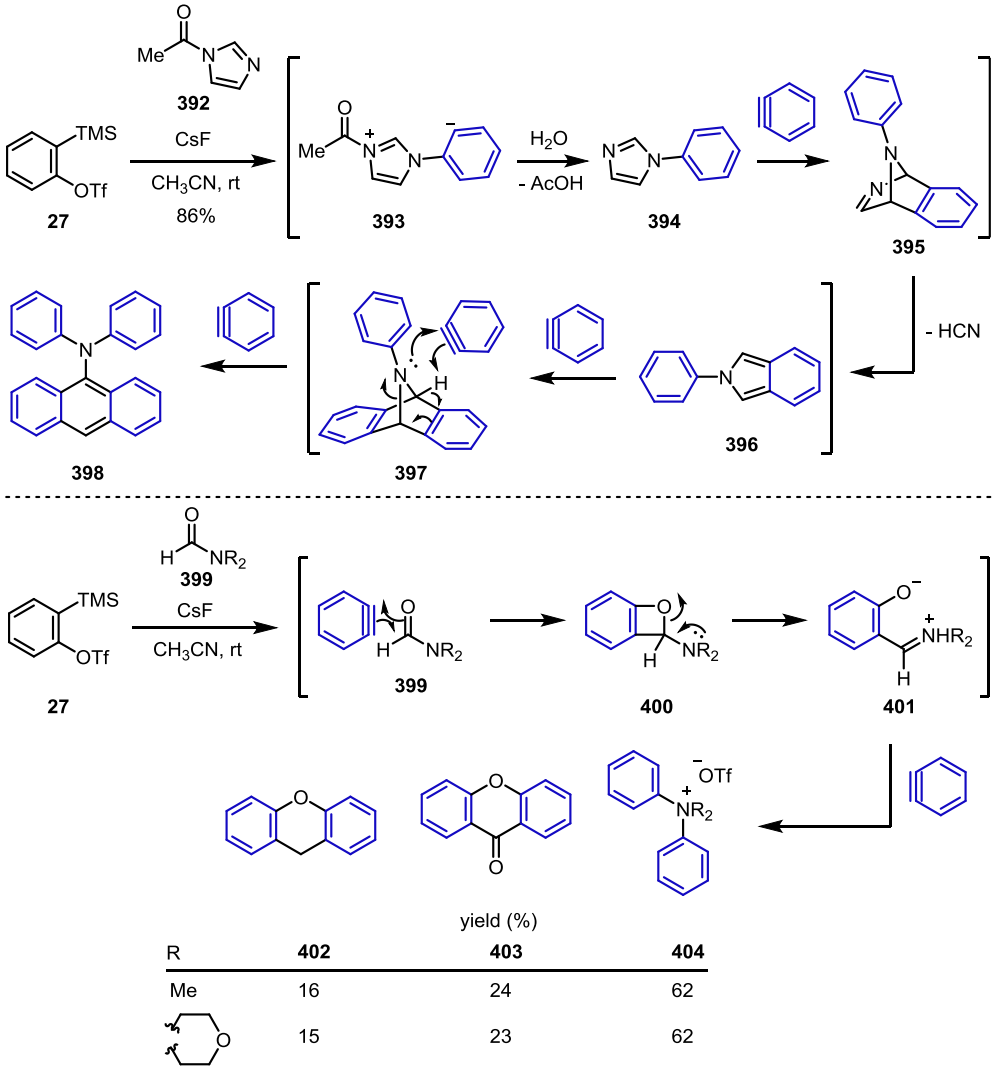

R	402	403	404
Me	16	24	62
	15	23	62

In 2011, Okuma and co-workers reported the synthesis of quadruple benzyne adducts from acetylimidazole **392** or formaides **399** (Scheme 1.59).[48b] As shown in Schemes 1.41 and 1.58, once the *N*-substituted furans **266** or benzofuran ring **389** is formed, consecutive [4+2] cycloaddition of benzyne and *N*-arylation yield *N*-phenylanthracenamines **268** or *N,N*-diphenylnaphthalenamine **391**. Similarly, *N*-phenylbenzofuran **396** was formed as an intermediate via *N*-arylation of **392**, deprotection of acetyl-protected imidazole **393**, and [4+2] cycloaddition of **394**. *N*-phenylbenzofuran **396** reacted with two more benzynes to afford *N,N*-diphenylanthracenamine **398**.

In the same report, the synthesis of xanthene **402**, xanthone **403**, and quaternary ammonium salts **404** from formaides **399** as a single starting material was demonstrated. After formal [2+2] cycloaddition of benzyne with **399** and the subsequent ring opening of **400**, intermediate **401** reacted with benzyne via [4+2] cycloaddition or hydrolysis, which resulted in the formation of xanthene **402**, xanthone **403**, and quaternary ammonium salts **404**.

1.7.5 Nucleophilic Addition/Nucleophilic Addition

Di- or triarylamines **410** were synthesized from isocyanates **405** and arynes by Hsieh and co-workers (Scheme 1.60).[137] The addition of lutidine to **405** generates zwitterion **406**, which attacks aryne to form intermediate **407**. Hydrolysis of **407** affords carbamic acid **408**, and the subsequent decarboxylation of **408** and nucleophilic addition of **409** to aryne afford di- or triarylamines **410**. The mechanism of the reaction with lutidine or pyridine catalyst is not conclusive. However, isocyanate typically requires a pre-nucleophile to be an active nucleophile.

Water is the crucial factor for this reaction because the yield of the desired product **410** decreases in the absence of water.

Scheme 1.60. Hsieh's Conversion from Isocyanate to Tertiaryamines.

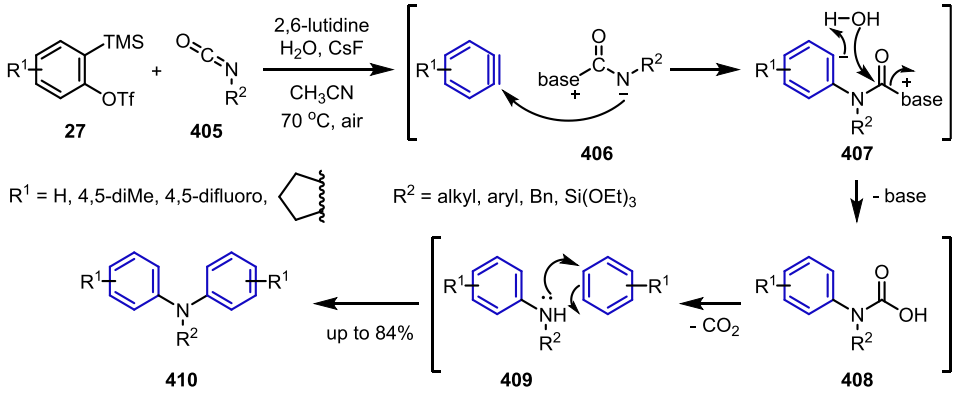

In 1998, Biehl and co-workers conducted the aryne reaction by employing *o*-chlorophenylmethanol **411** and 2-phenylacetonitrile **412** for the synthesis of 6-benzyl-2-hydroxymethylbenzonitriles **419**, 3-arylmethyl-4-methylphthalimides **420**, and 1-hydroxymethyl-6-aryl-2*H*-anthra[9,1-*bc*]furans **421** (Scheme 1.61).[138] After lithiation of **411** and **412**, arylcyanomethyl lithium **414** is added to aryne **413** to yield intermediate **415**. Intermediate **415** also undergoes cyclization and ring opening to afford intermediate **417**. Hydrolysis of **417** affords **419** but cyclization of **417** followed by hydrolysis of **421** produces **421**. In addition, intermediate **417** undergoes another aryne addition and annulation to form a new 6-membered ring in **419**. Then, one of the lithiated methanol groups attacks imine, and thus, the following hydrolysis forms **420**. **420** was the major product, and **422** was only observed when 2-(4-methoxyphenyl)acetonitrile was used.

Scheme 1.61. Biehl's Mono and Double [4+2] Cycloaddition Reactions.

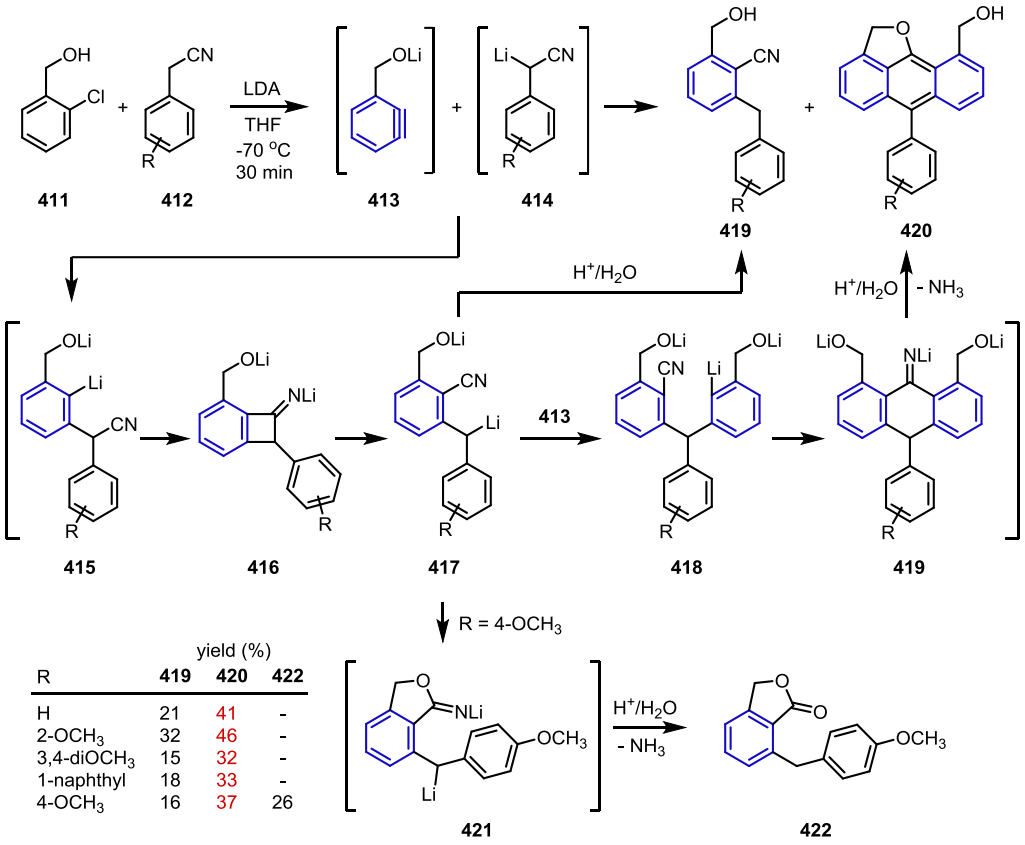

R	yield (%) 419	420	422
H	21	41	-
2-OCH_3	32	46	-
3,4-diOCH_3	15	32	-
1-naphthyl	18	33	-
4-OCH_3	16	37	26

Scheme 1.62. Chandrasekhar's Solvent-Dependent Tunable Multiaryne Reaction.

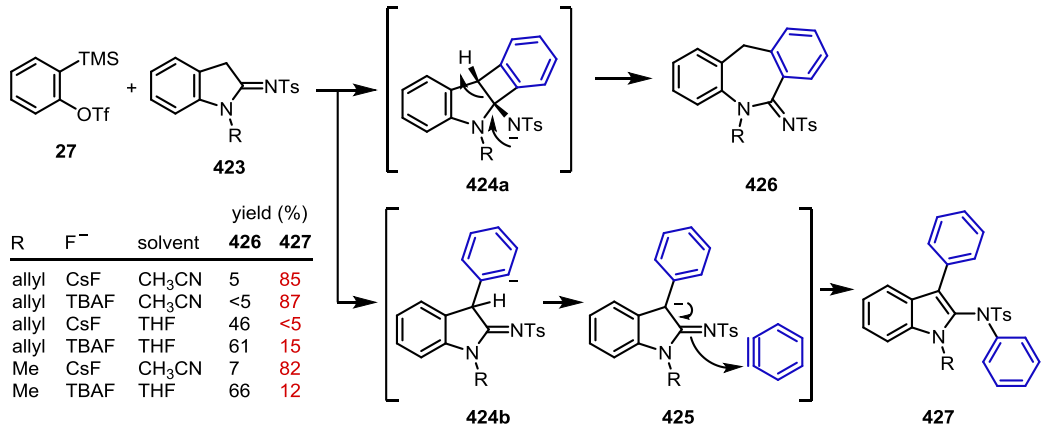

R	F^-	solvent	yield (%) 426	427
allyl	CsF	CH_3CN	5	85
allyl	TBAF	CH_3CN	<5	87
allyl	CsF	THF	46	<5
allyl	TBAF	THF	61	15
Me	CsF	CH_3CN	7	82
Me	TBAF	THF	66	12

The tunable synthesis of dibenzo[*b,e*]azepin-6-imines **426** and highly substituted indoles **427** was reported by Chandrasekhar and co-workers (Scheme 1.62).[139] 2-Sulfonyliminoindoline **423** reacted with benzyne via either [2+2] cycloaddition toward **426** or double nucleophilic additions to benzynes to yield **427**. Interestingly, the reaction was tunable using acetonitrile or THF as the solvent. Acetonitrile and THF conditions afforded **426** and **427** as major products, respectively. When the reaction was performed in deuterated acetonitrile, solvent-assisted protonation was proposed as one of the mechanistic steps in the synthesis of **427.**

Knochel's benzyne precursor **428** was used for the one-pot synthesis of 2,2'-bis-substituted biphenyls **431** by Studer and co-workers in 2015 (Scheme 1.63).[140] Benzyne and ArMgCl **430** are generated from **428** and **429** and coupled *in situ* using a Grignard reagent. Intermediate **430** was dimerized using Li_2CuCl_4 and oxygen gas. The addition of DMF rather than Li_2CuCl_4 and oxygen gas led to intermediate **430** not to the dimer but to benzaldehyde.

Scheme 1.63. Studer's Biaryl Synthesis.

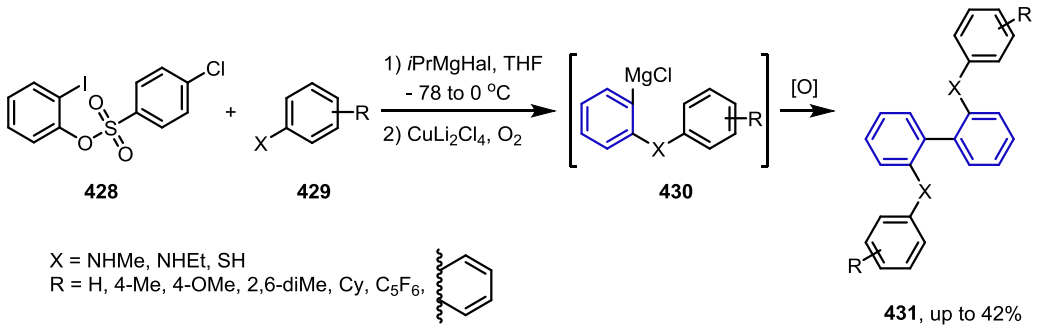

Scheme 1.64. Larock's Phenylcarbazole Synthesis.

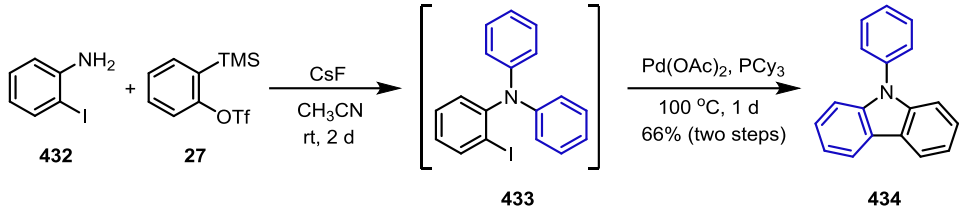

The synthesis of carbazole and dibenzofuran was reported by Larock and Liu (Scheme 1.64).[141] In the report, the reaction between 2-iodoaniline **432** and more than two equivalents of benzyne produces *N*-phenylcarbazole **434**. This one-pot reaction involves double *N*-arylation of **432** and Pd-catalyzed annulation of the resulting triaryl amine intermediate **433** to afford **434**.

Scheme 1.65. Kunai and Yoshida's Multicomponent Reaction.

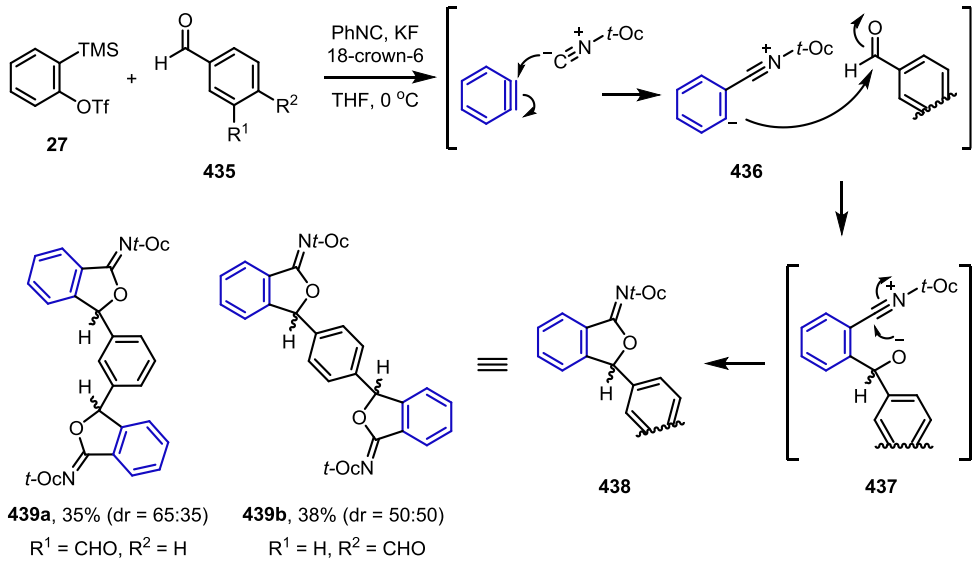

1,3- and 1,4-Phenylene-bis(dihydroisobenzofuranimine)s (**439a** and **439b**) were synthesized from benzynes, isocyanides, and benzaldehydes **435** by Kunai, Yoshida, and co-workers (Scheme 1.65).[142] In this mechanism, the addition of isocyanide to benzyne followed by

addition of anion of zwitterion **436** to iso- or terephthalaldehyde **435** yield intermediate **437**. Annulation of **437** affords **439a** or **439b**.

Scheme 1.66. Castedo's N-Phenylation of Alkaloid Natural Products.

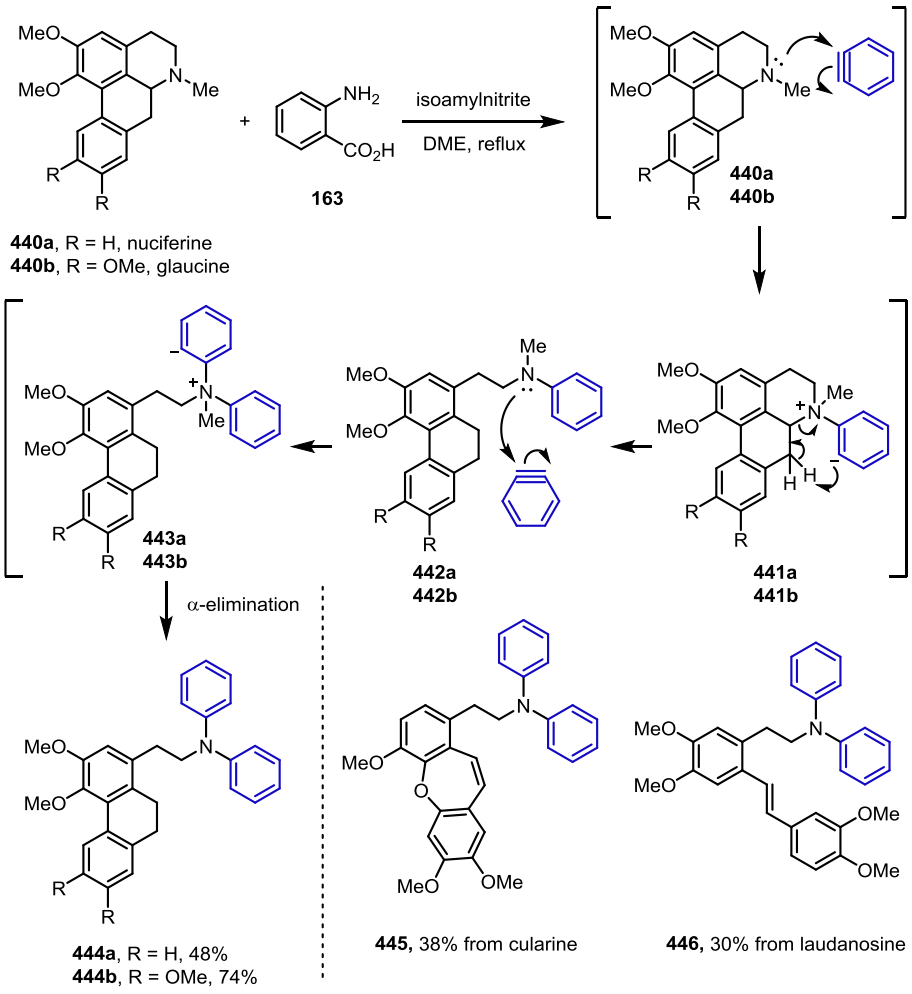

In 1993, Castedo and co-workers modified alkaloid natural products by employing benzynes (Scheme 1.66).[2c] Diphenylamines were obtained from nuciferine **440a**, glaucine **440b**, cularine, and laudanosine. In the proposed mechanism for double arylation of **440a** or **440b**, *N*-phenylation followed by β-elimination of **441a** or **441b** affords ring-opened intermediate **442a**

or **442b**. Further *N*-phenylation of **443a** or **443b** and subsequent α-elimination affords diphenylamine derivatives **444a** and **444b**. Similarly, **445** and **446** were individually obtained from cularine and laudanosine.

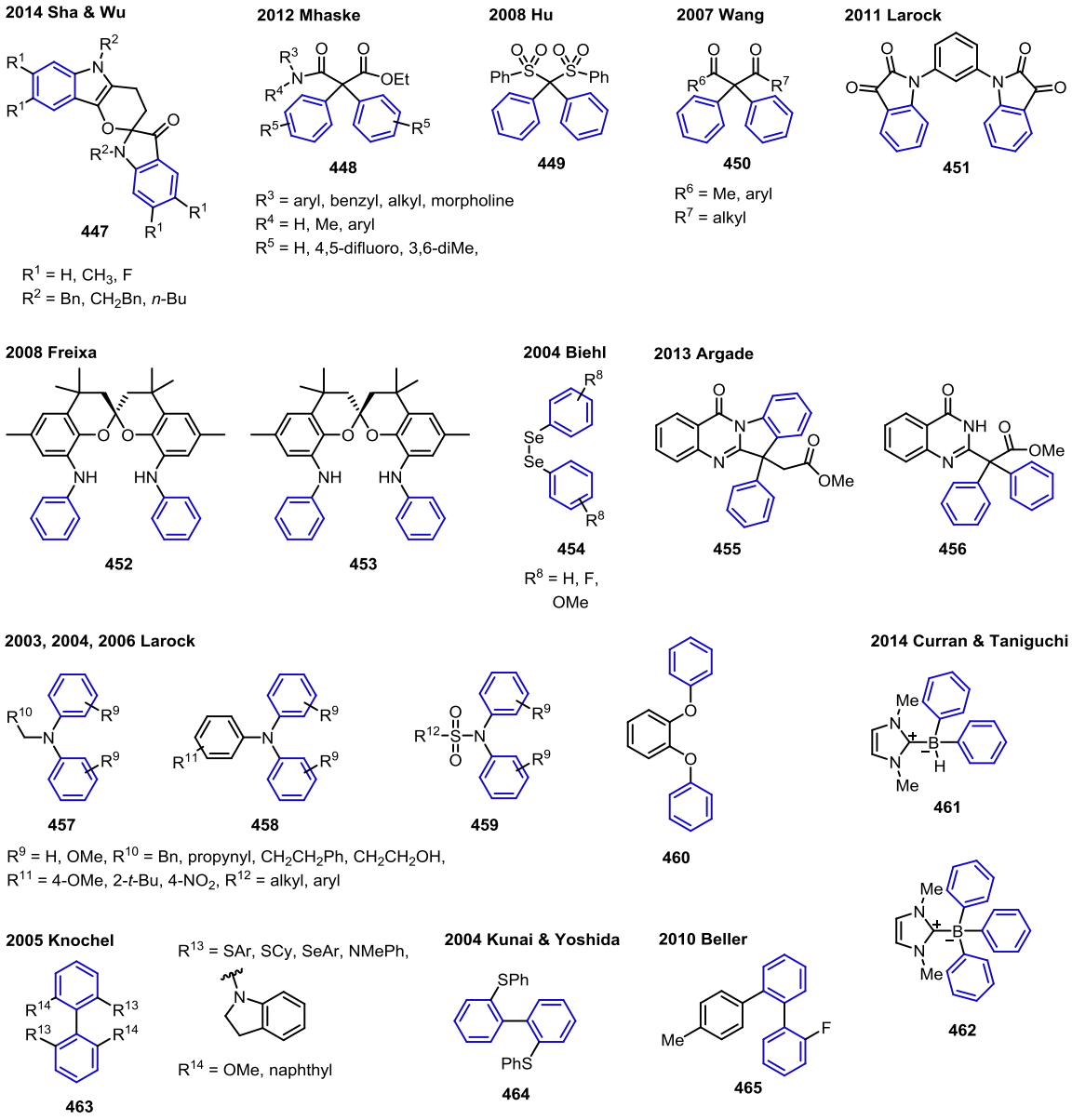

Figure 1.7. Double nucleophilic addition products.

Double nucleophilic additions of arynes are one of the most plentiful multiple aryne reactions in the literature. Representative products of double nucleophilic additions are shown in Figure 1.7. Sha, Wu, and co-workers reported the synthesis of spiro-products **447** from the reaction of benzynes and aziridines.[143] Double α-arylations of malonamide esters, bis(phenylsulfonyl)methanes, and 1,3-diones to **448**,[144] **449**,[145] and **450**,[146] respectively, have been independently reported by the Mihaske, Hu, and Wang groups. Larock and Rogness introduced the synthesis of 1,10-(1,3-Phenylene)bis-(indoline-2,3-dione) **451**.[147] In the report, double annulation of bis(*N*-substituted methyl oxamates) was initiated by nucleophilic addition of arynes. Freixa and co-workers conducted double *N*-arylation of *rac*-4,4,4',4',6,6'-hexamethylspiro-2,2'-bi(chroman) diamine with two equivalents of benzyne to afford **452** and **453**.[148] Biehl successfully synthesized areneselenol using arylation of selenourea and elimination of cyanamide. 1,2-Diaryldiselane **454** was obtained by oxidative homocoupling of two areneselenols.[149] The effort of Argade and Vaidya to synthesize the natural product cruciferane revealed the formation of aryne adducts **455** and **456**.[150] **455** was formed by consecutive insertion-type nucleophilic additions and *C*-arylation, and **466** was obtained via double *C*-arylation. In the multiple reports from the Larock group, double *N*-arylations and double *O*-arylation are reported with aryne adducts **457**-**460**.[136,151] Hydroboration of arynes with double and triple *B*-arylated compounds (**461** and **462**) were reported in the study by Curran and Taniguchi.[152] Due to the efforts of the Kunai/Yoshida and Knochel groups, the syntheses of biaryl compounds (**463**[153] and **464**[154]) containing dithiols, diselenols, and diamines have been developed. Beller reported domino Grignard-double-coupling fluorination for the synthesis of 2-(4-methylbiphenyl)-fluorobenzene using two equivalents of benzynes and 4-tolylmagnesium bromide.[155]

1.7.6 Nucleophilic Addition/Nucleophilic Addition/Nucleophilic Addition

Scheme 1.67. Yoshida's Triarylation of Chlorotriazines.

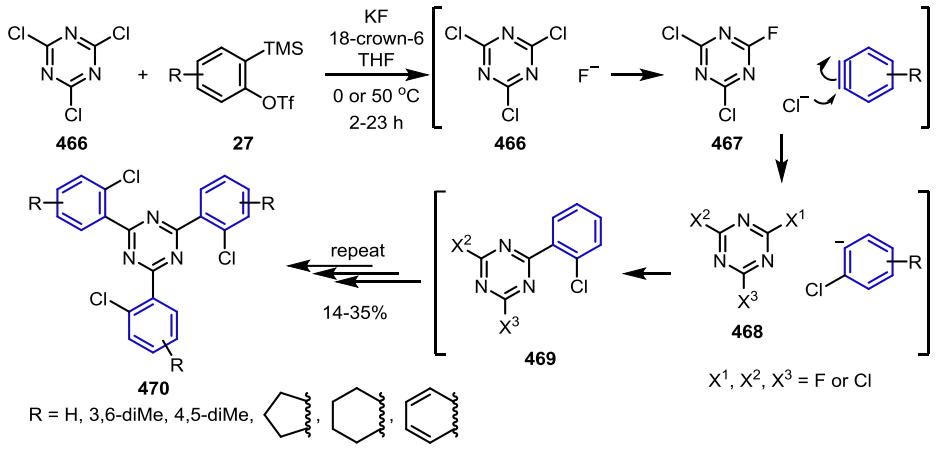

In 2009, Yoshida and co-workers reported the synthesis of chlorotriazines **470** from cyanuric chloride **466** and arynes (Scheme 1.67).[156] Nucleophilic aromatic substitution of **466** with fluoride yields cyanuric intermediate **467** and chloride. The chloride was added to aryne, and **467** or **468** undergoes nucleophilic aromatic substitution with chlorobezenoid to yield **469**. Repeating the process affords chlorotriazines **470**.

Mehta, Srihari, and co-workers used indolin-2-ones **471** and benzynes to synthesize triarylated oxindoles **478** and dibenzo[*b*,*e*]azepin-6-ones **480** (Scheme 1.68).[157] *N*-arylation of **471** and the subsequent deprotonation of **472** yield 1-phenylindolin-2-ones **473**, which undergo diarylation on the alpha carbon. The corresponding benzenide intermediates **477** go through protonation to afford **478**. The addition of the benzenide **477** to the carbonyl group leads to four-membered ring intermediate **479**. Ring opening of **479** results in expansion of the ring to afford **480**. At room temperature, only **478** was formed but **480** was the major product at 90 °C. The related products (**481**-**489**) are shown at the bottom of Scheme 1.68.

Scheme 1.68. Mehta and Srihari's Oxindole and Dibenzo[*b,e*]azepin-6-one Synthesis.

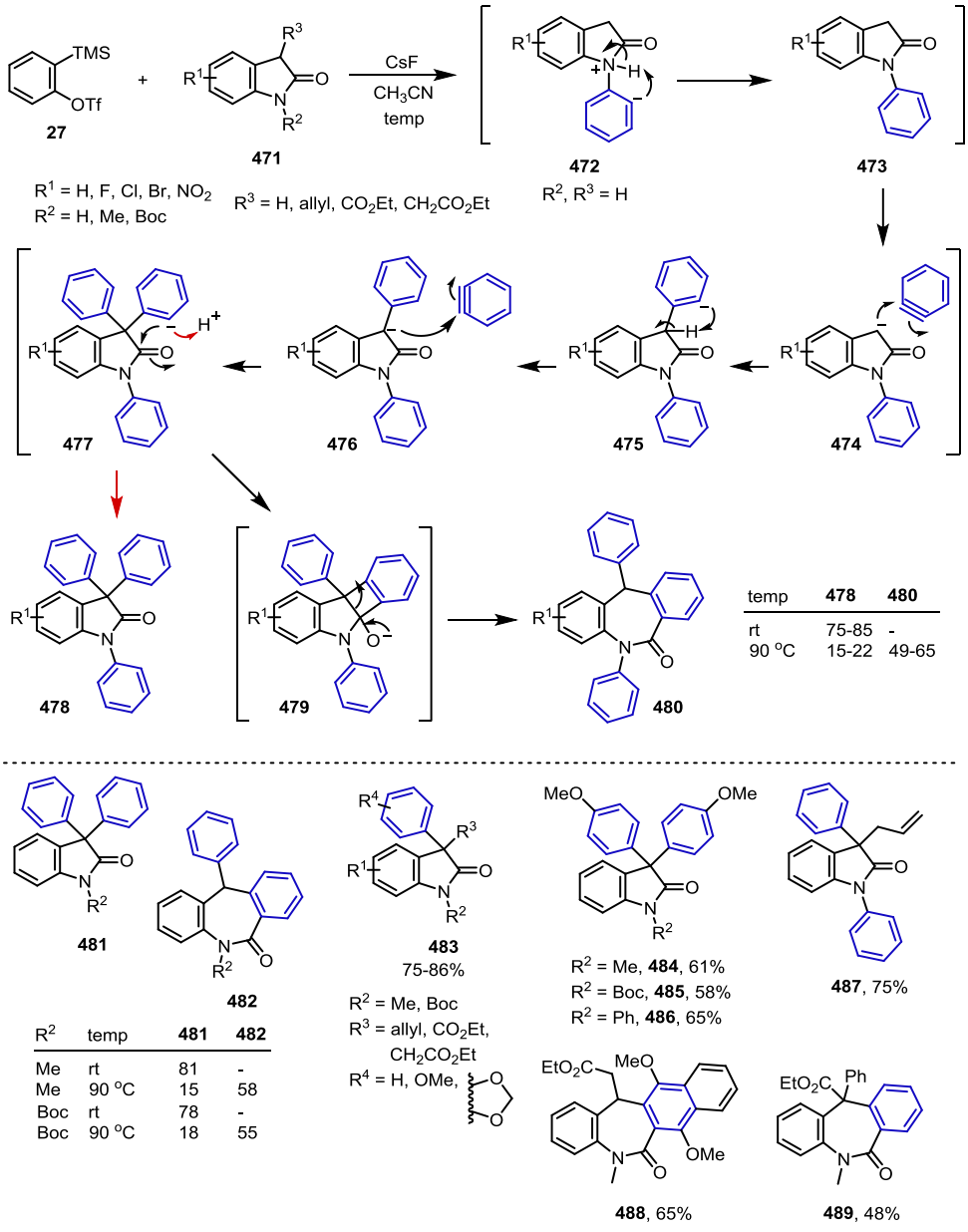

1.7.7 Nucleophilic Addition/Ene Reaction

Scheme 1.69. Biju's Synthesis of Indoles and Arylindoles.

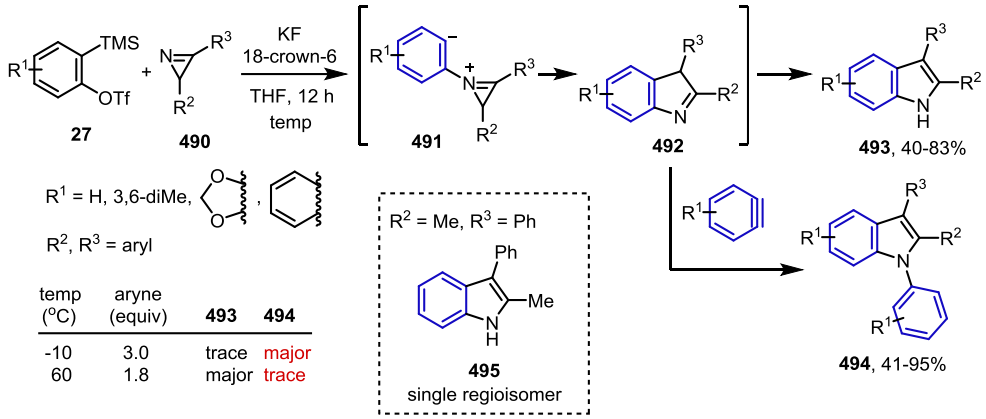

Biju and co-workers conducted the reaction of azirines **490** and arynes to synthesize indoles **493** and arylindoles **494** (Scheme 1.69).[158] The nitrogen atom of azirine **490** attacks aryne, and the resulting aryl anion **491** is added to iminium to form 3*H*-indole intermediate **492**. A 1,3-hydrogen shift of **492** affords indole **493**, and an aryne ene reaction of **492** yields arylindole **494**. The addition of three equivalents of aryne at –10 °C produced **494** as the major product. Interestingly, indole **493** was obtained as the major product with 1.8 equivalents of aryne at 60 °C.

1.8 Insertion Reactions

1.8.1 Insertion Reaction/[4+2] Cycloaddition

Using diarylcyclopropenones **496** and arynes, Werz and co-workers reported the formation of spiroxanthenes **502** (Scheme 1.70).[159] Insertion of aryne to the cyclopropenones

496 yields spirobenzoxete intermediates **497**, which undergo rearrangement and a subsequent aryne insertion reaction of **499** to afford the desired spirocyclic xanthenes **502**. The process was expected to follow either a biradical or ionic mechanism. The biradical pathway is described with red arrows in Scheme 1.70.

Scheme 1.70. Werz's Spriocyclic Xanthene Synthesis.

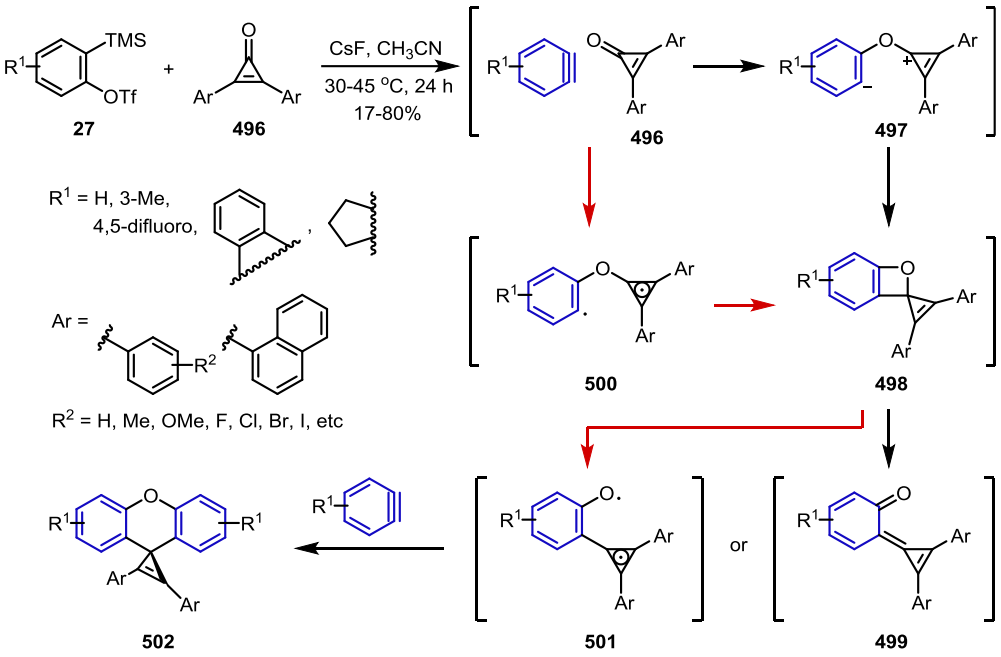

Scheme 1.71. Okuma's Selenoxanthene Synthesis.

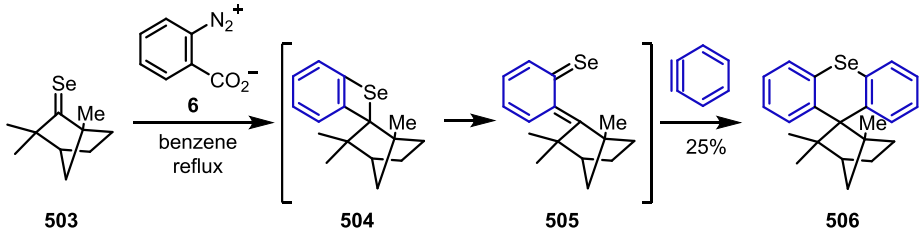

Okuma and co-workers reported the reactivity of selones with benzynes (Scheme 1.71).[160] In the report, the double benzyne reaction of selenofenchone **503** was observed. After insertion of **503** to benzyne, intermediate **505** reacts with another benzyne via [4+2] cycloaddition to afford spiro(fenchone-9,9'-selenoxanthene) **506** in 25% yield. The structure of **506** was confirmed by X-ray crystallographic analysis.

1.8.2 Insertion Reaction/Nucleophilic Addition

Scheme 1.72. Shi, Wu, and Wu's Tandem Aryne Insertion/Nucleophilic Reaction with Carbodiimides.

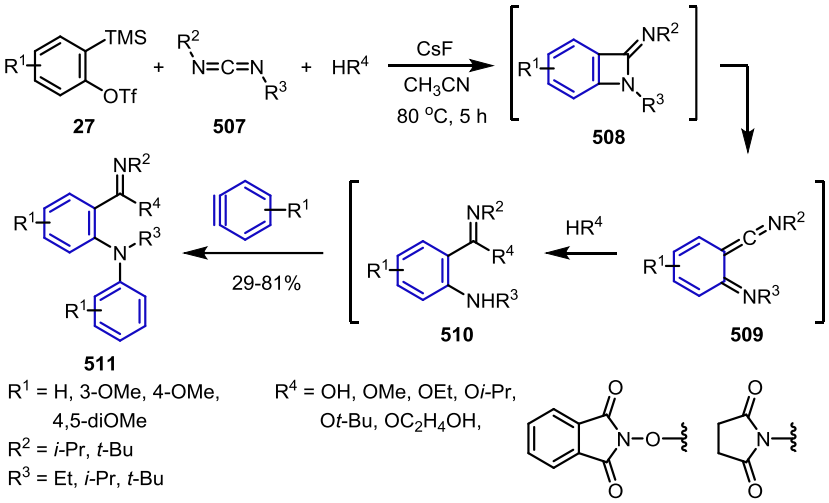

Carbodiimides **507** were used to synthesize 2-arylaminobenzimidates **511** by Shi, Wu, and Wu (Scheme 1.72).[161] Insertion of aryne to **507** occurs through a four-membered intermediate (**508**) to afford aza-*o*-quinomethide **509**. Intermediate **509** reacts with water or alcohol to yield 2-aminobenzimidate **510**, which undergoes *N*-arylation to afford **511**.

Scheme 1.73. Alajarin, López-Ortiz, and Lopez-Leonardo's Tandem P=N and P=S Bond Insertion/Nucleophilic Addition.

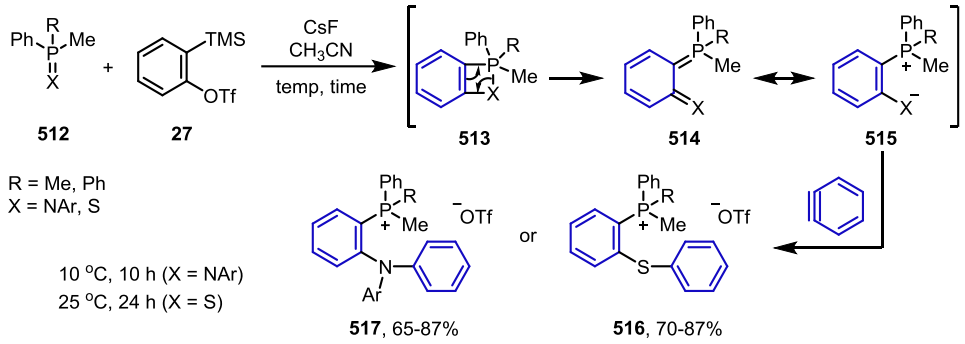

Scheme 1.74. Larock's Xanthene Synthesis.

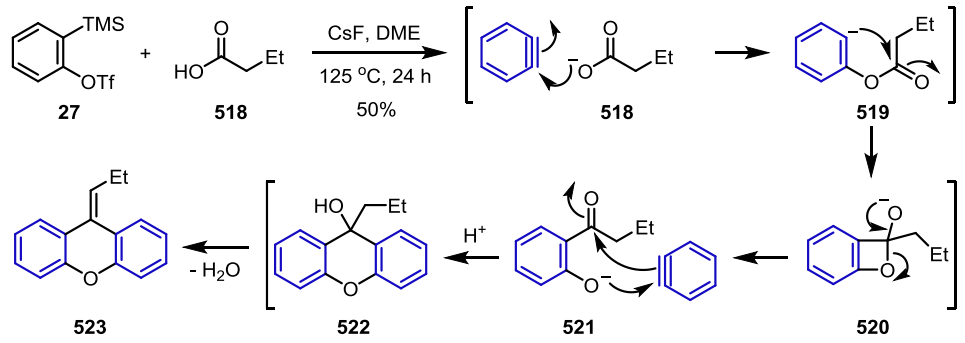

The benzyne insertion reaction worked for P=N and P=S bonds. In 2014, insertion of iminophosphoranes or phosphane sulfides **512** was disclosed by Alajarin, López-Ortiz, Lopez-Leonardo, and co-workers (Scheme 1.73).[162] Benzyne was inserted into the P=N or P=S bond of **512**, and the resulting intermediate **514** underwent nucleophilic addition to benzyne to afford **516** from iminophosphoranes or **517** from phosphane sulfides.

Scheme 1.75. Greaney's Insertion/Nucleophilic Addition of Thioureas.

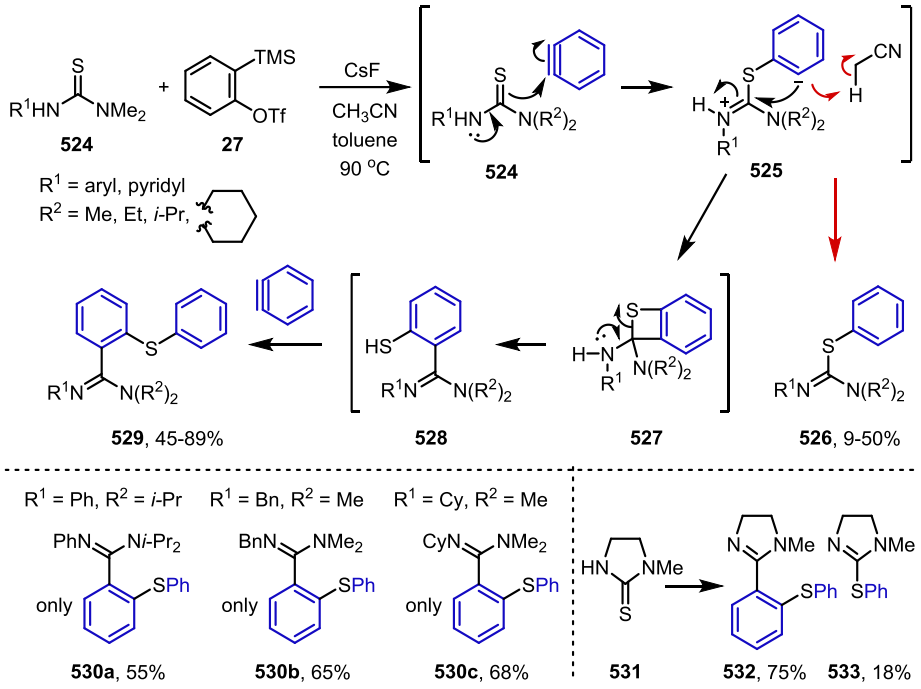

The report by Larock and Dubrovskiy described the synthesis of 9-propylidene-9*H*-xanthene **523** from butyric acid **518** and benzynes (Scheme 1.74).[163] After insertion of benzyne to **518**, the resulting phenoxide **521** was added to benzyne for annulation to afford intermediate **522**. The loss of water produces **523**.

In 2011, Greaney and Biswas reported the synthesis of phenyl carbamimidothioates **526** and 2-(phenylthio)benzimidamides **529** from thiourea **524** and benzynes (Scheme 1.75).[164] Insertion of benzyne to **524** and subsequent nucleophilic addition of **528** to benzyne afford **3**, and *S*-arylation of **524** followed by quenching zwitterionic intermediate **525** with acetonitrile afford **526**. Interestingly, for some substituents, only **530a**-**530c** were isolated from the crude mixture. The aryne insertion reaction of cyclic thiourea **531** proceeded to afford **532** and **533** in 75% and 18%, respectively.

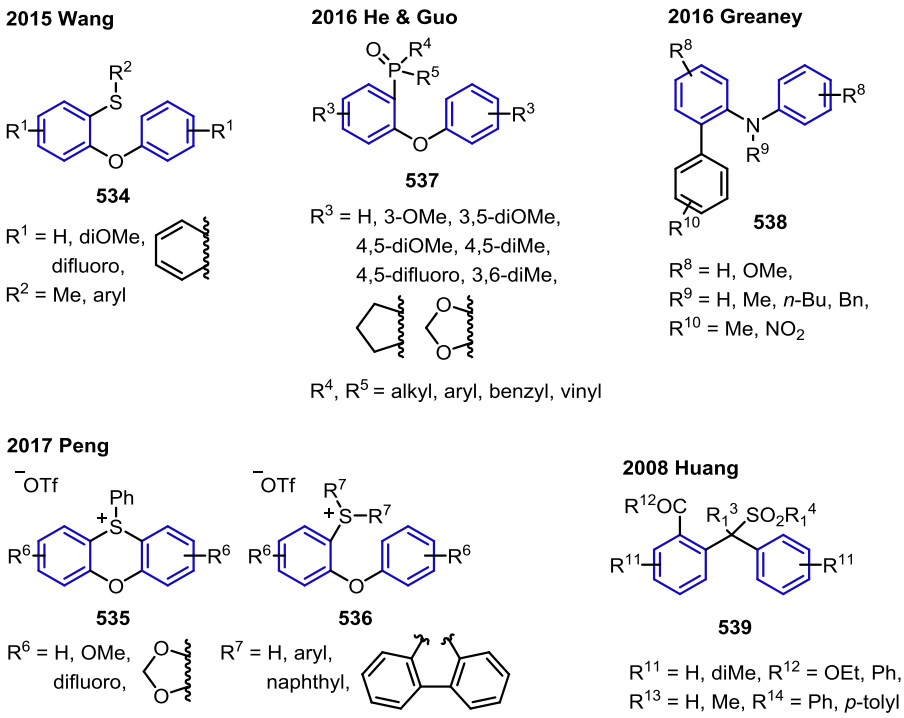

Figure 1.8. Insertion reaction/nucleophilic addition products.

Other tandem insertion reactions and nucleophilic additions have been reported (Figure 1.8). Wang and co-workers reported aryne insertion to sulfoxides and the subsequent *O*-arylation to afford **534**.[165] The Peng group broadened the scope of the sulfoxides for this reaction with **535** and **536**.[166] Tandem insertion of phosphinic acid to aryne and *O*-arylation was reported with products **537** by He, Guo and co-workers.[167] Greaney and co-workers disclosed new biaryl synthetic methods with **538**, employing a benzyne Truce–Smiles rearrangement of sulfonamides.[168] The synthesis of *o*-keto benzyl sulfones **539** from aryne insertion of β-keto sulfones and *in situ C*-arylation was developed by the Huang group.[169]

1.8.3 Insertion Reaction/Nucleophilic Addition/Nucleophilic Addition

Scheme 1.76. Conversion from β–Lactam to Acridone and Dihydroquinolinone.

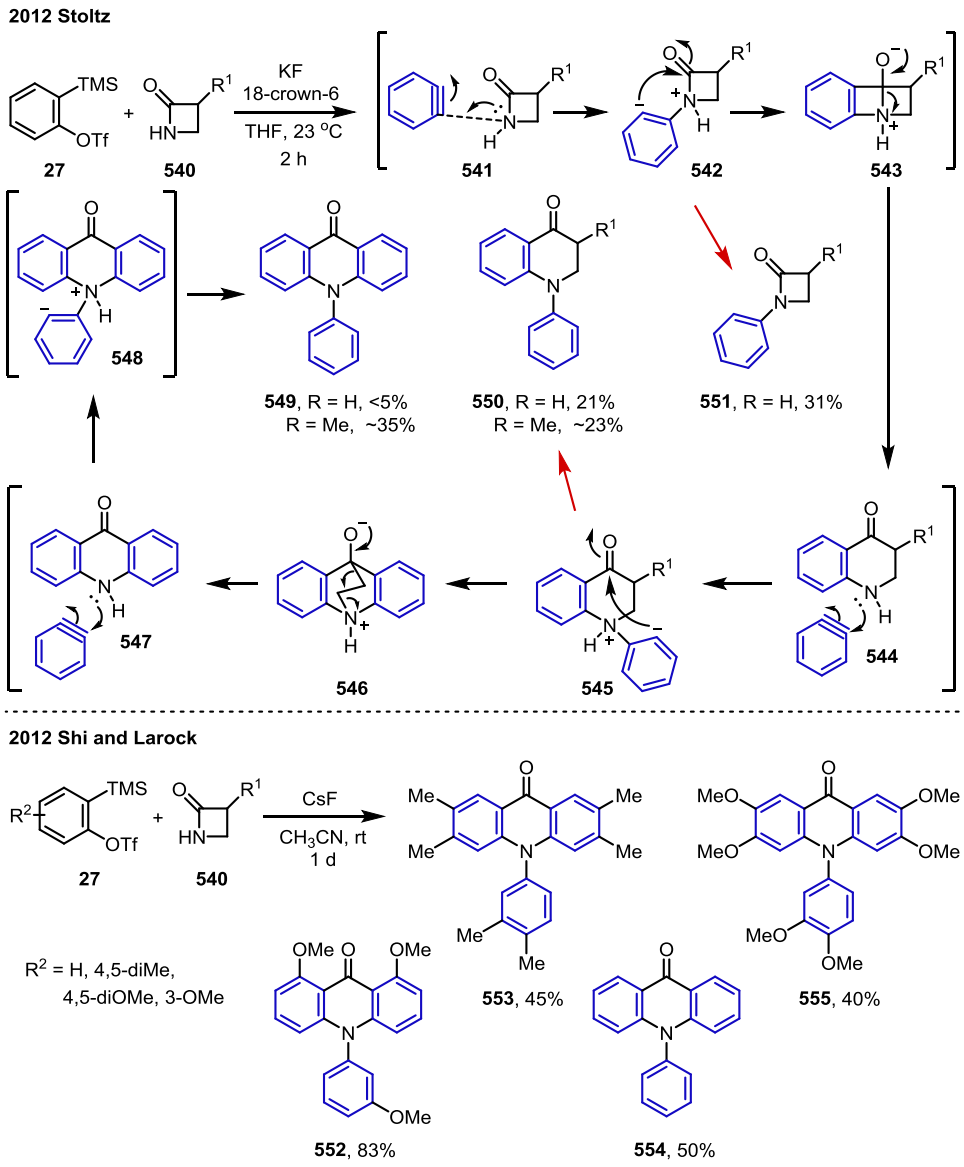

In 2012, Stoltz and Kim reported the synthesis of 10-phenylacridin-9(10*H*)-one **549** and dihydroquinolinone **550** from β-lactams **540** and benzynes (Scheme 1.76).[170] The initial insertion of **540** to benzyne led to azeidinium intermediates **542**, which undergo nucleophilic addition of **544** to afford zwitterionic intermediate **545**. Proton abstraction of **545** affords

dihydroquinolinone **550**, and then, benzenide attacks the carbonyl group to form bicyclic intermediate **546**. After extrusion of ethylene gas, the resulting acridone reacts with the third benzyne followed by proton abstraction to yield 10-phenylacridin-9(10*H*)-one **549**. In addition, 1-phenylazetidin-2-one **551** was obtained from the reaction of non-substituted lactam with benzyne. Just prior to this report, Shi, Larock, and co-workers reported the same synthesis that afforded four different kinds of aryne adducts (**552**-**555**).[171]

1.8.4 Insertion Reaction/Insertion Reaction

The synthesis of macrocycles was developed by Vincente, Saura-Llamas, and co-workers (Scheme 1.77).[172] Double aryne insertion reaction into dimeric cyclopalladated complex **557** leads to the formation of dimer **558** of the ten-membered palladacycle, which is diversified into

Scheme 1.77. Vicente and Saura-Llamas's Macrocycle Synthesis.

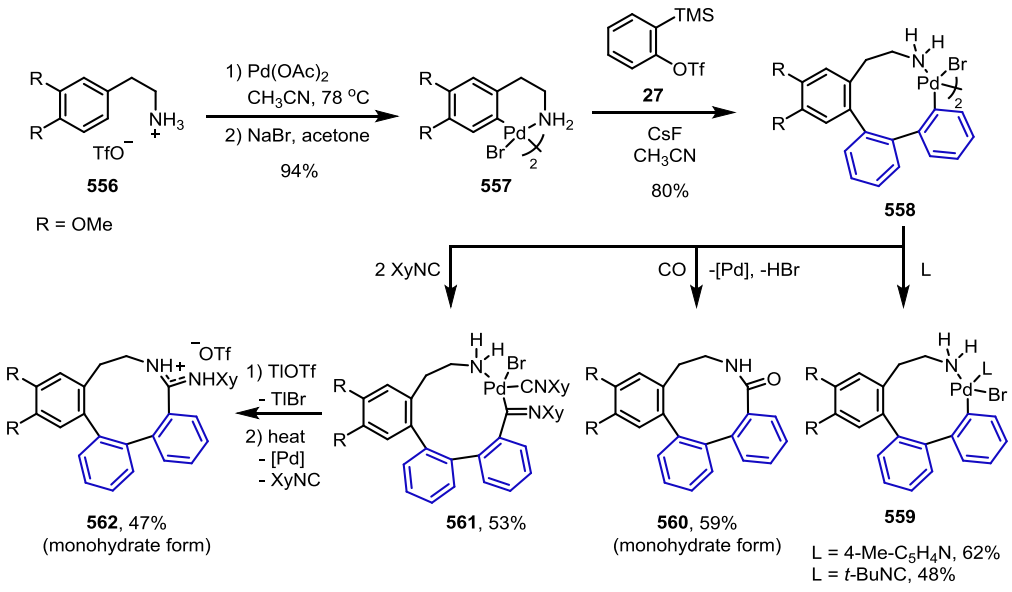

Scheme 1.78. Chenoweth's Two-Step Synthesis of the Reported Xylopyridine A Structure.

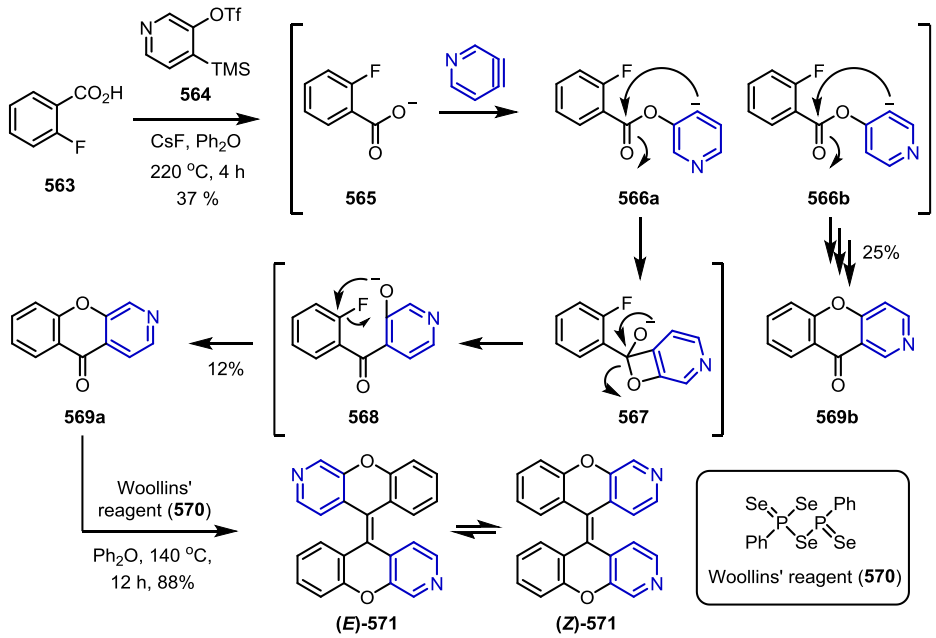

ten-membered C,N-palladacycle **559** by ligand exchange, ten-membered tribenzazecine **560** by CO insertion, and eleven-membered palladacycle **561** by addition of 2,6-dimethylphenyl isocyanide (XyNC). Employing TlTfO and heating **561** results in the isolation of ten-membered amidinium salt **562**.

In 2013, we reported the five-step synthesis of the reported structure of xylopyridine A (*E*-**571** and *Z*-**571**) in Scheme 1.78, which exists in both the *E* and *Z* forms.[173] After four years, we recently significantly shortened the number of steps by employing a pyridyne insertion reaction.[174] Deprotonation of 2-fluorobenzoic acid **563** yields carboxylate intermediate **565**, which was inserted into pyridyne to afford intermediates **586a** and **586b**. Intramolecular nucleophilic aromatic substitution of **568** results in the formation of **569a**. We observed **569b** as the isomer of **569a**. Dimerization of **569a** was performed via Woollins' coupling to (*E*/*Z*)-**571**.

Scheme 1.79. Yamazaki's Bis-Perfluoroalkanamide Synthesis.

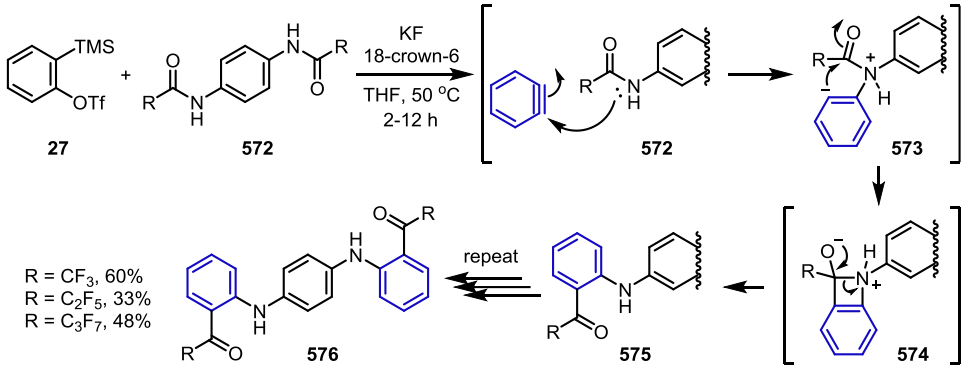

Yamazaki and co-workers demonstrated double aryne insertions to the C-N bonds of amides **572** (Scheme 1.79).[175] A mechanism was not proposed in the report but it presumably follows the typical C-N bond insertion pathway. The nitrogen atom of **572** attacks benzyne, and the resulting anions **573** on the phenyl group are added to the carbonyl group to form four-membered ring intermediates **574**. Ring opening of **574** affords the desired products **575**. Repeating the process may afford double aryne-inserted products **576**.

Representative double or triple insertion reaction products are shown in Figure 1.9. Murai, Chatani, and co-workers revealed the cobalt-catalyzed double aryne insertion to one equivalent or two equivalents of carbon monoxide to afford **577** and **578**.[176] Glorius and Biju reported carbene-catalyzed formal double aryne insertion to terephthalaldehyde to yield 1,4-dibenzoylbenzene **579**.[177] Using benzynes, Zeng and co-workers developed the ring expansion strategy.[178] In their report, the cyclohexanone ring was expanded with single or double aryne insertion reactions. For double aryne insertion, nine-membered ring-containing compound **580** was obtained and confirmed by X-ray crystallographic analysis. Okuma observed double aryne insertion adducts **581** (open-ring form) and **582** (closed-ring form) from the reaction of 4,4,4-trifluorobutane-1,3-dione and benzynes.[179]

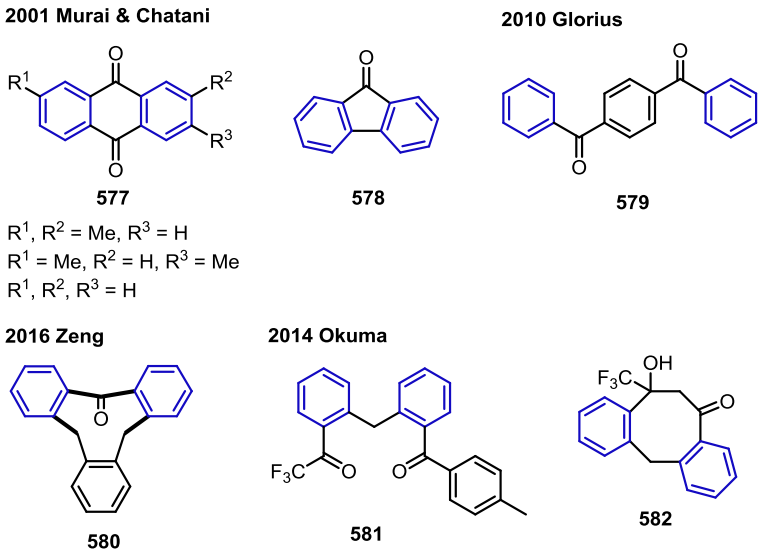

Figure 1.9. Double or triple insertion reaction.

1.8.5 Insertion Reaction/Ene Reaction

Scheme 1.80. He's Quinolone Synthesis.

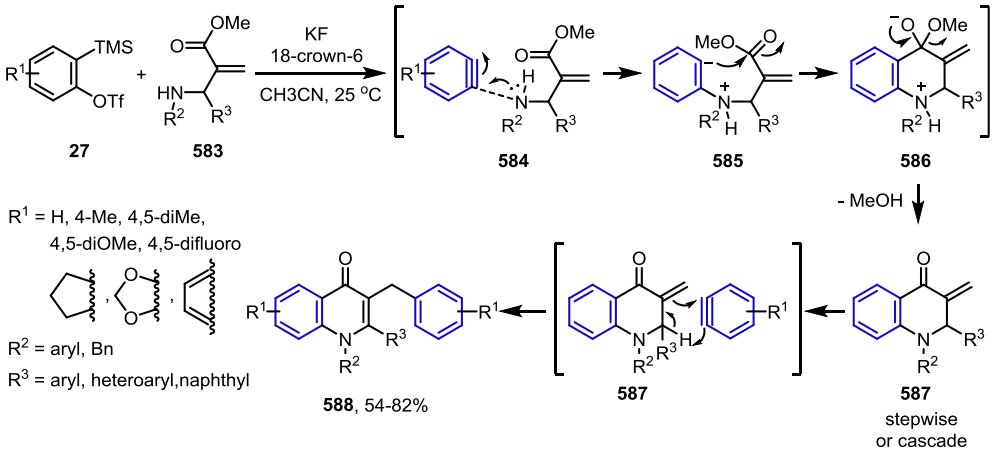

He and co-workers discovered the synthesis of 4-quinolones **588** from aza-Morita–Baylis–Hillman (AMBH) adducts **583** and arynes (Scheme 1.80).[2a] The nitrogen of the AMBH adducts **583** are added to aryne, and the resulting anions **585** undergo 1,2-addition to

the carbonyl group for annulation. The corresponding enones **587** undergo an ene reaction with aryne to afford 4-quinolones **588**. Intermediate **587** was isolated by addition of only 1.2 equivalents of aryne. When isolated **587** was resubjected to aryne, **588** was obtained in good yield.

1.8.6 Miscellaneous

Scheme 1.81. Ramtohul's Acridone Synthesis.

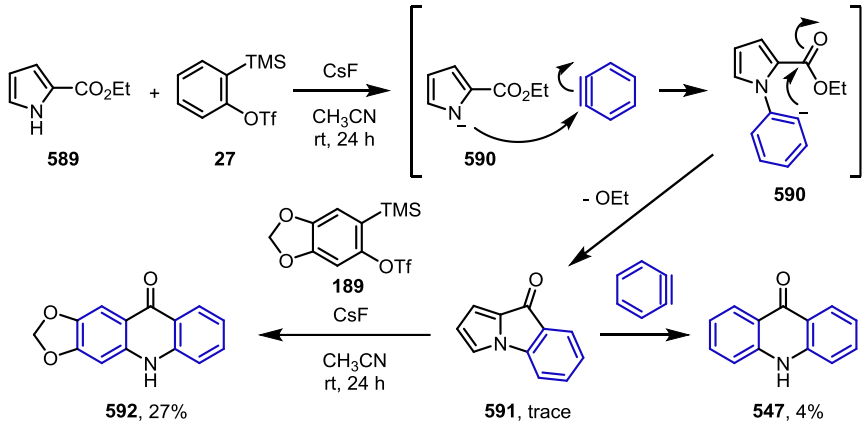

The synthesis of acridones **547** and **592** from ethyl pyrrole-2-carboxylate **589** and aryne precursors (**27** and **189**) was reported by Ramtohul and Giacometti (Scheme 1.81).[3f] Deprotonation of **589** and the subsequent insertion reaction afford pyrroloindolone **591**, which was isolated with **547**. When **591** was resubjected to the reaction with **189**, unsymmetric acridone **592** was obtained. The mechanism remains unclear for the second aryne addition in the report.

1.9 Ene Reactions

1.9.1 Ene Reaction/Nucleophilic Addition

As shown in Scheme 1.66, Castedo and co-workers studied the reactivity between alkaloids and benzynes (Scheme 1.82).[2c] In the report, they found that dehydronoraporphine **593** reacts with benzyne via an aza-ene reaction to yield arylated intermediate **594**. Restoring the aromaticity of **594** and subsequent nucleophilic addition of **595** to benzyne afforded diarylated product **596**.

Scheme 1.82. Castedo's Ene Reaction and Nucleophilic Addition of Dehydronoraporphine.

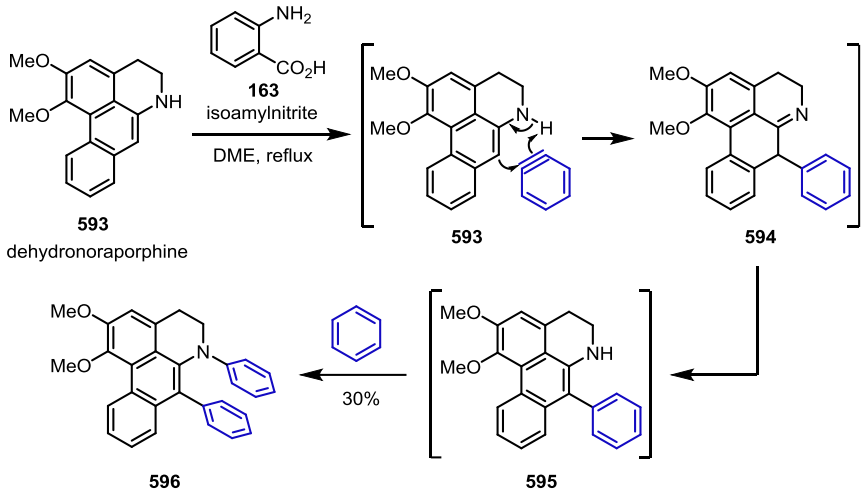

1.9.2 Ene Reaction/Ene Reaction

Liu, Yin, and co-workers reported the aryne-ene reaction of aryne and various olefins (Scheme 1.83).[2d] In the report, double arylation of 1,5-cyclooctadiene **597** was demonstrated.

The proposed mechanism involved the double aryne-ene reaction of 1,5-cyclooctadiene **597** to afford 3,7-diphenylcycloocta-1,5-diene **598**.

Scheme 1.83. Liu and Yin's Double Ene reactions.

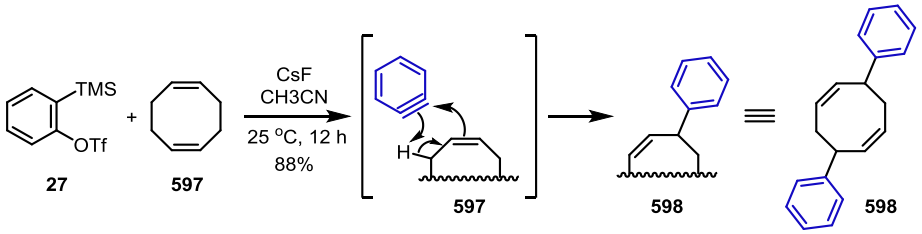

Other double ene products are shown in Figure 1.10. In 1972, Friedman and Brinkley reported that toluene undergoes an ene reaction with aryne twice to yield **599**.[2h] As shown in Figure 1.4, the Hopf group reported double [4+2] cycloaddition of diethenyl[2.2]paracyclophanes and benzynes. In this report, they observed that 4-vinyl[2.2]paracyclophanes undergo double aryne ene reactions to afford **600**. In 2012, Greneay and co-workers obtained the double ene-products **601a** and **601b** (regioisomer of **601a**) from the reaction of ditritylbenzene-1,4-diamine and benzynes.[2f]

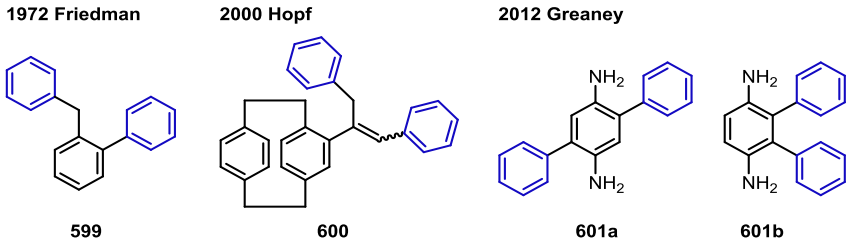

Figure 1.10. Double ene reaction products.

1.10 Polymerization

Scheme 1.84. Inoue & Ihara's Copolymerization of Benzyne and Pyridine.

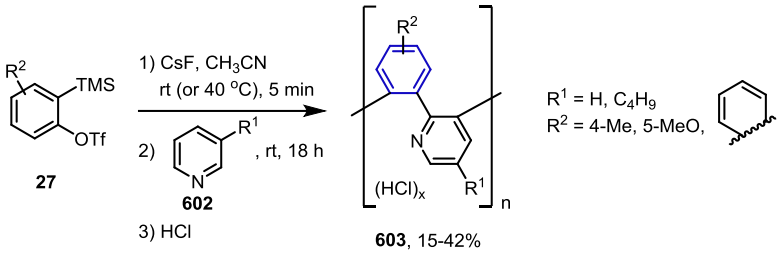

Scheme 1.85. Swager's Synthesis of Dihydroindenofluorene Polymer by Using Bisaryne-Engaged Monomer.

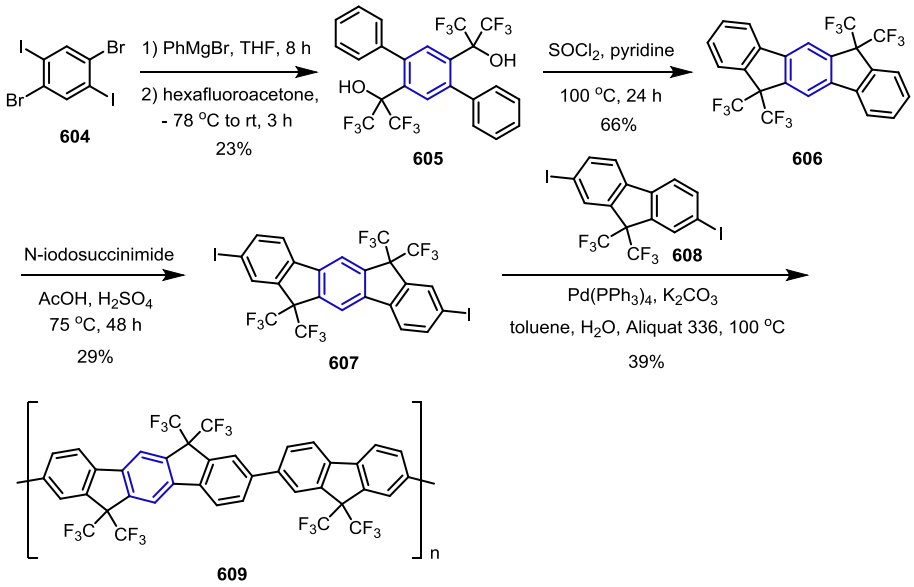

In 2005, Ihara and co-workers reported the synthesis of copolymers **603** from arynes and pyridines **602** (Scheme 1.84).[5d] To synthesize poly(*o*-phenylene), Kobayashi benzyne precursor **27** and CsF were used with several nucleophiles, transition metals, and radical initiators but the

reaction did not proceed. However, they employed pyridine and successfully synthesized copolymer **603** containing *ortho*-phenylene and 2,3-dihydropyridine.

Swager and Amara used bisaryne precursor **604** for the synthesis of polymers **609** bearing indenofluorene and fluorene in 2006 (Scheme 1.85).[5e] The generation of bisaryne from 1,4-dibromo-2,5-diodobenzene **604** with PhMgBr was performed, and this Grignard reagent was also accompanied by hexafluoroacetone and bisaryne for an *in situ* three-component reaction to yield **605**. After the intramolecular Friedel–Crafts reaction of **605**, the corresponding indenofluorene **606** was iodinated to afford monomer **607**. Pd-catalyzed polymerization of **607** and diiodofluorine **608** afforded polymers **609**.

Scheme 1.86. Nozaki and Ito's Formal Aryne Polymerization.

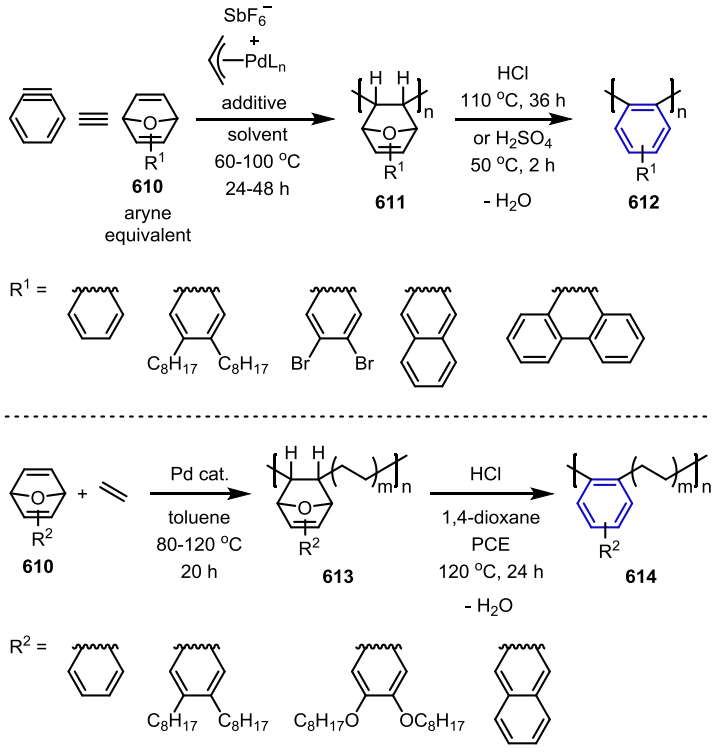

In 2014 and 2015, Nozaki, Ito, and co-workers employed [2.2.1]oxabicyclic alkenes **610** as aryne equivalents for the synthesis of polymers **612** or **614** bearing *o*-arylene or both *o*-arylene and ethylene (Scheme 1.86).[5b,f] Pd-catalyzed polymerization of **610** affords polymer **611**, which undergoes dehydration to yield poly(*o*-arylene)s **612**. When ethylene was added for polymerization, formal aryne-ethylene copolymer **614** was obtained.

Scheme 1.87. Garg and Maynard's Synthesis of Benzonorbornadiene Polymers by Using Aryne-Engaged Monomer.

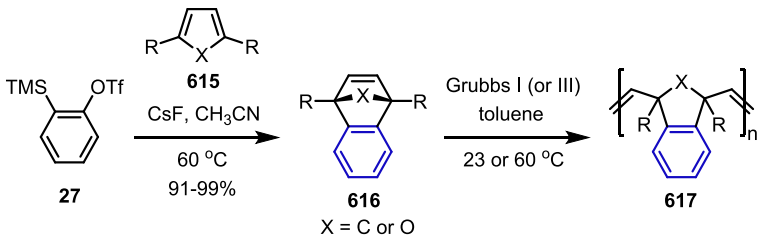

Scheme 1.88. Uchiyama and Mikami's Aryne Polymerization.

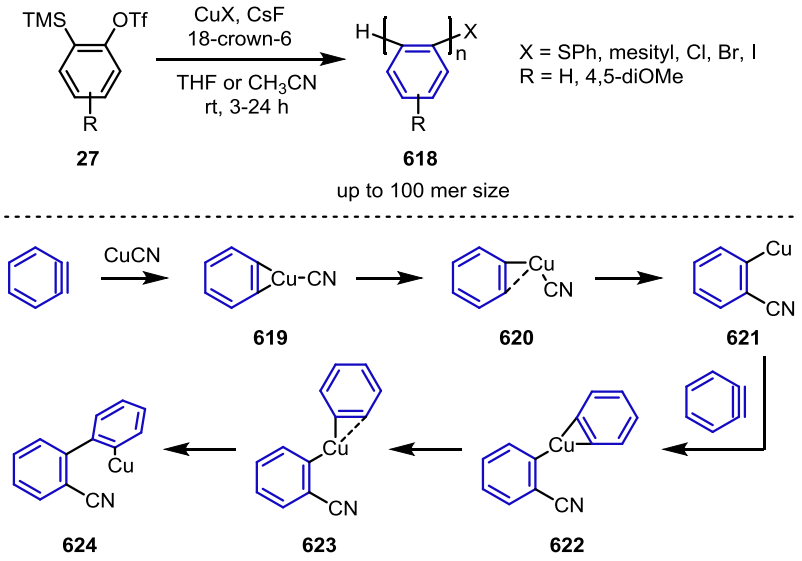

In 2015, benzyne precursor **27** was used for the formation of polymer **617** bearing 1,4-epoxynaphthalene or benzonorbornadiene by Garg, Maynard, and co-workers (Scheme 1.87).[5c] Benzyne [4+2] cycloaddition of cyclopenta-1,3-diene or furan (**615**) yields monomer **616**. Ring-opening metathesis of **616** with Grubbs I or III catalyst affords poly(benzonorbornadiene)s or poly(1,4-epoxynaphthalene)s (**617**).

In 2015, Uchiyama, Mikami, and Mizukoshi reported the first direct aryne polymerization using Kobayashi benzyne precursors **27** and copper catalysts (Scheme 1.88).[5a] Based on DFT calculations of the polymerization mechanism, benzyne and CuCN form triangular complex **619**, and then, the triple bond of benzyne inserts into the Cu-CN bond to afford intermediate **621**. The addition of another benzyne to **621** follows the same mechanistic pathway to afford biaryl intermediate **624**.

1.11 Conclusion

In this review, we attempted to cover all existing multiple aryne-engaged reactions and provide the reaction scopes and mechanisms. Arynes are very powerful tools for the rapid construction of cyclic and heterocyclic molecules. The reaction scope is also notably broad from pericyclic reactions to polar reactions. In particular, combinations of more than two aryne reactions have become efficient methods for building complex molecules. Despite the potential of aryne reactions, many questions remain to be studied and explored in the area of multiaryne reactions. We hope that this review stimulates the interest of the audience outside the area of

aryne chemistry as well as helps chemists conducting research in this area by providing insight and ideas.

1.12 References

(1) (a) Sanz, R. *Org. Prep. Proced. Int.* **2008,** *40*, 215-291. (b) Bhojgude, S. S.; Biju, A. T. *Angew. Chem. Int. Ed.* **2012,** *51*, 1520-1522. (c) Gampe, C. M.; Carreira, E. M. *Angew. Chem. Int. Ed.* **2012,** *51*, 3766-3778. (d) Okuma, K. *Heterocycles* **2012,** *85*, 515-544. (e) Tadross, P. M.; Stoltz, B. M. *Chem. Rev.* **2012,** *112*, 3550-3577. (f) Yoshida, H.; Takaki, K. *Heterocycles* **2012,** *85*, 1333-1349. (g) Dubrovskiy, A. V.; Markina, N. A.; Larock, R. C. *Org. Biomol. Chem.* **2013,** *11*, 191-218. (h) Pérez, D.; Peña, D.; Guitián, E. *Eur. J. Org. Chem.* **2013,** *2013*, 5981-6013. (i) Wu, C.; Shi, F. *Asian J. Org. Chem.* **2013,** *2*, 116-125. (j) Wu, D.; Ge, H.; Liu, S. H.; Yin, J. *RSC Adv.* **2013,** *3*, 22727-22738. (k) Biju, A.; Bhunia, A. *Synlett* **2014,** *25*, 608-614. (l) Yoshida, H. *Compr. Org. Synth. (2nd Ed.)* **2014,** *4*, 517-579. (m) Yoshida, S.; Hosoya, T. *Chem. Lett.* **2015,** *44*, 1450-1460. (n) Bhojgude, S. S.; Bhunia, A.; Biju, A. T. *Acc. Chem. Res.* **2016,** *49*, 1658-1670. (o) Garcia-Lopez, J. A.; Greaney, M. F. *Chem. Soc. Rev.* **2016,** *45*, 6766-6798. (p) Karmakar, R.; Lee, D. *Chem. Soc. Rev.* **2016,** *45*, 4459-4470.

(2) (a) Santhosh Reddy, R.; Lagishetti, C.; Kiran, I. N.; You, H.; He, Y. *Org. Lett.* **2016,** *18*, 3818-3821. (b) Chen, Z.; Han, X.; Liang, J.-H.; Yin, J.; Yu, G.-A.; Liu, S.-H. *Chin. Chem. Lett.* **2014,** *25*, 1535-1539. (c) Paz, M.; Saá, C.; Guitián, E.; Castedo, L.; Saá, J. M. *Heterocycles* **1993,** *36*, 1217-1223. (d) Chen, Z.; Liang, J.; Yin, J.; Yu, G.-A.; Liu, S. H. *Tetrahedron Lett.* **2013,** *54*, 5785-5787. (e) Tabushi, I.; Yamada, H.; Yoshida, Z.; Oda, R. *Bull. Chem. Soc. Jpn.* **1977,** *50*, 285-290. (f) Pirali, T.; Zhang, F.; Miller, A. H.; Head, J. L.; McAusland, D.; Greaney, M. F. *Angew. Chem. Int. Ed.* **2012,** *51*, 1006-1009. (g) Aly, A. A.; Hopf, H.; Ernst, L. *Eur. J. Org. Chem.* **2000**, 3021-3029. (h) Brinkley, J. M.; Friedman, L. *Tetrahedron Lett.* **1972,** *13*, 4141-4142.

(3) (a) Liu, Z.; Zhang, X.; Larock, R. C. *J. Am. Chem. Soc.* **2005,** *127*, 15716-15717. (b)

Rogness, D. C.; Markina, N. A.; Waldo, J. P.; Larock, R. C. *J. Org. Chem.* **2012,** *77*, 2743-2755. (c) Rogness, D. C.; Larock, R. C. *J. Org. Chem.* **2010,** *75*, 2289-2295. (d) Liu, Z.; Larock, R. C. *J. Org. Chem.* **2007,** *72*, 223-232. (e) Gerfaud, T.; Neuville, L.; Zhu, J. *Angew. Chem. Int. Ed.* **2009,** *48*, 572-577. (f) Ramtohul, Y.; Giacometti, R. *Synlett* **2009,** *2009*, 2010-2016.

(4) Niu, D.; Willoughby, P. H.; Woods, B. P.; Baire, B.; Hoye, T. R. *Nature* **2013,** *501*, 531-534.

(5) (a) Mizukoshi, Y.; Mikami, K.; Uchiyama, M. *J. Am. Chem. Soc.* **2015,** *137*, 74-77. (b) Ito, S.; Wang, W.; Nozaki, K. *Polym. J.* **2015,** *47*, 474-480. (c) Medina, J. M.; Ko, J. H.; Maynard, H. D.; Garg, N. K. *Macromolecules* **2017,** *50*, 580-586. (d) Ihara, E.; Kurokawa, A.; Koda, T.; Muraki, T.; Itoh, T.; Inoue, K. *Macromolecules* **2005,** *38*, 2167-2172. (e) Amara, J. P.; Swager, T. M. *Macromolecules* **2006,** *39*, 5753-5759. (f) Ito, S.; Takahashi, K.; Nozaki, K. *J. Am. Chem. Soc.* **2014,** *136*, 7547-7550.

(6) Stoermer, R.; Kahlert, B. *Ber. Dtsch. Chem. Ges.* **1902,** *35*, 1633-1640.

(7) Roberts, J. D.; H. E. Simmons, J.; Carlsmith, L. A.; Vaughan, C. W. *J. Am. Chem. Soc.* **1953,** *75*, 3290-3291.

(8) Bachman, W. E.; Clarke, H. T. *J. Am. Chem. Soc.* **1927,** *49*, 2089-2098.

(9) Lüttringhaus, A.; Sääf, G. v. *Eur. J. Org. Chem.* **1939,** *542*, 241-258.

(10) (a) Wittig, G.; Pieper, G.; Fuhrmann, G. *Ber. Dtsch. Chem. Ges.* **1940,** *73*, 1193-1197. (b) Wittig, G.; Fuhrmann, G. *Ber. Dtsch. Chem. Ges.* **1940,** *73*, 1197-1218. (c) Wittig, G. *Naturwissenschaften* **1942,** *30*, 696-703.

(11) Gilman, H.; Avakian, S. *J. Am. Chem. Soc.* **1945,** *67*, 349-351.

(12) Benkeser, R. A.; Schroll, G. *J. Am. Chem. Soc.* **1953,** *75*, 3196-3197.

(13) Wittig, G.; Pohmer, L. *Angew. Chem.* **1955,** *67*, 348.

(14) Wittig, G. *Org. Synth.* **1959,** *39*, 75.

(15) Stiles, M.; Miller, R. G. *J. Am. Chem. Soc.* **1960,** *82*, 3802-3802.

(16) Wittig, G.; Hoffmann, R. W. *Chem. Ber.* **1962,** *95*, 2718-2728.

(17) Fields, E. K.; Meyerson, S. *Chemical Communications (London)* **1965**, 474-476.

(18) Stevens, T. E. *J. Org. Chem.* **1968,** *33*, 855-856.

(19) Beringer, F. M.; Huang, S. J. *J. Org. Chem.* **1964,** *29*, 445-448.

(20) (a) Kitamura, T.; Yamane, M. *J. Chem. Soc., Chem. Commun.* **1995**, 983-984. (b)

Kitamura, T.; Yamane, M.; Inoue, K.; Todaka, M.; Fukatsu, N.; Meng, Z.; Fujiwara, Y. *J. Am. Chem. Soc.* **1999,** *121*, 11674-11679. (c) Kitamura, T.; Meng, Z.; Fujiwara, Y. *Tetrahedron Lett.* **2000,** *41*, 6611-6614.

(21) Akiyama, T.; Imasaki, Y.; Kawanisi, M. *Chem. Lett.* **1974,** *6*, 229-230.

(22) Wang, M.; Huang, Z. *Org. Biomol. Chem.* **2016,** *14*, 10185-10188.

(23) Campbell, C. D.; Ree, C. W. *Proc. Chem. Soc.* **1964**, 296.

(24) Birkett, M. A.; Knight, D. W. *Tetrahedron Lett.* **1993,** *34*, 6939-6940.

(25) Horner, L.; Brüggemann, H. *Eur. J. Org. Chem.* **1960,** *635*, 22-30.

(26) Chapman, O. L.; Mattes, K.; McIntosh, C. L.; Pacansky, J.; Calder, G. V.; Orr, G. *J. Am. Chem. Soc.* **1973,** *95*, 6134-6135.

(27) (a) Maki, Y.; Furuta, T.; Kuzuya, M.; Suzuki, M. *J. Chem. Soc., Chem. Commun.* **1975**, 616-617. (b) Maki, Y.; Furuta, T.; Suzuki, M. *J. Chem. Soc., Perkin Trans. 1* **1979**, 553-557.

(28) Gann, A. W.; Amoroso, J. W.; Einck, V. J.; Rice, W. P.; Chambers, J. J.; Schnarr, N. A. *Org. Lett.* **2014,** *16*, 2003-2005.

(29) Himeshima, Y.; Sonoda, T.; Kobayashi, H. *Chem. Lett.* **1983**, 1211-1214.

(30) (a) Hosoya, T.; Hasegawa, T.; Kuriyama, Y.; Matsumoto, T.; Suzuki, K. *Synlett* **1995**, 177-179. (b) Matsumoto, T.; Hosoya, T.; Katsuki, M.; Suzuki, K. *Tetrahedron Lett.* **1991,** *32*, 6735-6736.

(31) (a) Yoshida, S.; Uchida, K.; Hosoya, T. *Chem. Lett.* **2015,** *44*, 691-693. (b) Sumida, Y.; Kato, T.; Hosoya, T. *Org. Lett.* **2013,** *15*, 2806-2809.

(32) Takagi, A.; Ikawa, T.; Saito, K.; Masuda, S.; Ito, T.; Akai, S. *Org. Biomol. Chem.* **2013,** *11*, 8145-8150.

(33) García-López, J.-A.; Greaney, M. F. *Org. Lett.* **2014,** *16*, 2338-2341.

(34) Sapountzis, I.; Lin, W.; Fischer, M.; Knochel, P. *Angew. Chem. Int. Ed.* **2004,** *43*, 4364-4366.

(35) Kovács, S.; Csincsi, Á. I.; Nagy, T. Z.; Boros, S.; Timári, G.; Novák, Z. *Org. Lett.* **2012,** *14*, 2022-2025.

(36) Chen, Q.; Yu, H.; Xu, Z.; Lin, L.; Jiang, X.; Wang, R. *J. Org. Chem.* **2015,** *80*, 6890-6896.

(37) Mesgar, M.; Daugulis, O. *Org. Lett.* **2016,** *18*, 3910-3913.

(38) Wickham, P. P.; Reuter, K. H.; Senanayake, D.; Guo, H.; Scott, W. J. *Tetrahedron Lett.*

1993, *34*, 7521-7524.

(39) Dong, Y.; Lipschutz, M. I.; Tilley, T. D. *Org. Lett.* **2016,** *18*, 1530-1533.

(40) Cant, A. A.; Roberts, L.; Greaney, M. F. *Chem. Commun.* **2010,** *46*, 8671-8673.

(41) Ikawa, T.; Nishiyama, T.; Nosaki, T.; Takagi, A.; Akai, S. *Org. Lett.* **2011,** *13*, 1730-1733.

(42) Ikawa, T.; Masuda, S.; Nakajima, H.; Akai, S. *J. Org. Chem.* **2017,** *82*, 4242-4253.

(43) Miyawaki, K.; Suzuki, R.; Kawano, T.; Ueda, I. *Tetrahedron Lett.* **1997,** *38*, 3943-3946.

(44) Bradley, A. Z.; Johnson, R. P. *J. Am. Chem. Soc.* **1997,** *119*, 9917-9918.

(45) (a) Miyawaki, K.; Kawano, T.; Ueda, I. *Tetrahedron Lett.* **1998,** *39*, 6923-6926. (b) Miyawaki, K.; Kawano, T.; Ueda, I. *Tetrahedron Lett.* **2000,** *41*, 1447-1451. (c) Kawano, T.; Inai, H.; Miyawaki, K.; Ueda, I. *Tetrahedron Lett.* **2005,** *46*, 1233-1236. (d) Torikai, K.; Otsuka, Y.; Nishimura, M.; Sumida, M.; Kawai, T.; Sekiguchi, K.; Ueda, I. *Bioorg. Med. Chem.* **2008,** *16*, 5441-5451.

(46) Hoye, T. R.; Baire, B.; Niu, D.; Willoughby, P. H.; Woods, B. P. *Nature* **2012,** *490*, 208-212.

(47) Heaney, H.; Millar, I. T. *Org. Synth.* **1960,** *40*, 105.

(48) (a) Logullo, F. M.; Seitz, A. H.; Friedman, L. *Org. Synth.* **1968,** *48*, 12. (b) Okuma, K.; Nojima, A.; Nakamura, Y.; Matsunaga, N.; Nagahora, N.; Shioji, K. *Bull. Chem. Soc. Jpn.* **2011,** *84*, 328-332. (c) Sato, T.; Narazaki, A.; Kawaguchi, Y.; Niino, H. *Chem. Lett.* **2008,** *37*, 334-335. (d) Okuma, K.; Fukuzaki, Y.; Nojima, A.; Sou, A.; Hino, H.; Matsunaga, N.; Nagahora, N.; Shioji, K.; Yokomori, Y. *Bull. Chem. Soc. Jpn.* **2010,** *83*, 1238-1247. (e) Anthony, I. J.; Wege, D. *Aust. J. Chem.* **1984,** *37*, 1283-1292. (f) Nishinaga, T.; Inoue, R.; Matsuura, A.; Komatsu, K. *Org. Lett.* **2002,** *4*, 1435-1438. (g) Brown, R. E. C.; Coulston, K. J.; Eastwood, F. W.; Vogel, C. *Aust. J. Chem.* **1988,** *41*, 1687-1695. (h) Tutara, A.; Cakmaka, O.; Karakasa, M.; Onala, A.; Ide, S. *J. Chem. Res.* **2004,** *2004*, 545-549. (i) Vagin, S. I.; Frickenschmidt, A.; Kammerer, B.; Hanack, M. *Chemistry* **2007,** *13*, 985-991. (j) Ward, E. R.; Pearson, B. D. *J. Chem. Soc.* **1959**, 1676-1680. (k) Avila, D. V.; Davies, A. G.; Girbal, M. L.; Ng, K. M. *J. Chem. Soc., Perkin Trans. 2* **1990**, 1693-1699. (l) R. L. Hillard, I.; Vollhardt, K. P. C. *J. Am. Chem. Soc.* **1976,** *98*, 3579-3582. (m) Whitney, S. E.; Rickborn, B. *J. Org. Chem.* **1988,** *53*, 5595-5596. (n) Mazza, D. D.; Reinecke, M. G. *J. Org. Chem.* **1988,** *53*, 5799-5806. (o) Wittig, G.; Meske-Schüller, J. *Liebigs Ann. Chem. Bd.* **1968,** *711*, 65-75. (p) Rees, C. W.; West, D. E. *J. Chem. Soc. C* **1970**, 583-589. (q) Barton, J. W.;

Grinham, A. R. *J. Chem. Soc., Perkin Trans. 1* **1972**, 634-637. (r) Campbell, C. D.; Rees, C. W. *J. Chem. Soc. C* **1969**, 742-747. (s) Campbell, C. D.; Rees, C. W. *J. Chem. Soc. C* **1969**, 748-776=751. (t) Barton, J. W.; Jones, M. S. A. *J. Chem. Soc. C* **1967**, 1276-1278. (u) Sato, M.; Ebine, S.; Tsunetsugu, J. *J. Chem. Soc., Perkin Trans. 1* **1977**, 1282-1287. (v) Keating, M.; Peek, M. E.; Rees, C. W.; Storr, R. C. *J. Chem. Soc., Perkin Trans. 1* **1972**, 1315-1316. (w) Jayalekshmy, P.; Mazur, S. *J. Am. Chem. Soc.* **1976,** *98*, 6710-6711. (x) Zeng, Y.; Li, G.; Hu, J. *Angew. Chem. Int. Ed.* **2015,** *54*, 10773-10777. (y) Newman, M. S.; Logue, M. W. *J. Org. Chem.* **1971,** *36*, 1398-1401.

(49) Hart, H.; Teuerstein, A. *Synthesis* **1979**, 693-695.

(50) Matsuura, A.; Nishinaga, T.; Komatsu, K. *Tetrahedron Lett.* **1997,** *38*, 4125-4128.

(51) Jun Lu, J. Z.; Shen, X.; Ho, D. M.; Robert A. Pascal, J. *J. Am. Chem. Soc.* **2002,** *124*, 8035-8041.

(52) Schlütter, F.; Nishiuchi, T.; Enkelmann, V.; Müllen, K. *Angew. Chem. Int. Ed.* **2014,** *53*, 1538-1542.

(53) Aly, A. A.; Mohamed, N. K.; Hassan, A. A.; Mourad, A.-F. E. *Tetrahedron* **1999,** *55*, 1111-1118.

(54) Zouaoui, M. A.; Mouaddib, A.; Jamart-Gregoire, B.; Ianelli, S.; Nardelli, M.; Caubere, P. *J. Org. Chem.* **1991,** *56*, 4078-4081.

(55) Simhai, N.; Iverson, C. N.; Edelbach, B. L.; Jones, W. D. *Organometallics* **2001,** *20*, 2759-2766.

(56) Umezu, S.; Gomes, G. d. P.; Yoshinaga, T.; Sakae, M.; Matsumoto, K.; Iwata, T.; Alabugin, I.; Shindo, M. *Angew. Chem. Int. Ed.* **2017,** *56*, 1298-1302.

(57) Fleming, I.; Mah, T. *J. Chem. Soc., Perkin Trans. 1* **1975**, 964-965.

(58) Yoshida, H.; Watanabe, M.; Fukushima, H.; Ohshita, J.; Kunai, A. *Org. Lett.* **2004,** *6*, 4049-4051.

(59) Neog, K.; Dutta, D.; Das, B.; Gogoi, P. *Org. Lett.* **2017,** *19*, 730-733.

(60) Deshmukh, A. R.; Zhang, H.; Tran, L. d.; Biehl, E. R. *J. Org. Chem.* **1992,** *57*, 2485-2486.

(61) Chakrabarty, S.; Chatterjee, I.; Tebben, L.; Studer, A. *Angew. Chem. Int. Ed.* **2013,** *52*, 2968-2971.

(62) Fields, E. K.; Meyerson, S. *Tetrahedron Lett.* **1970,** *11*, 629-631.

(63) Nakayama, J. *J. Chem. Soc., Chem. Commun.* **1974**, 166.

(64) Nakayama, J.; Fujiwara, K.; Hoshino, M. *Bull. Chem. Soc. Jpn.* **1976,** *49*, 3567-3573.

(65) Shi, F.; Waldo, J. P.; Chen, Y.; Larock, R. C. *Org. Lett.* **2008,** *10*, 2409-2412.

(66) Nocquet-Thibault, S.; Rayar, A.; Retailleau, P.; Cariou, K.; Dodd, R. H. *Chemistry* **2015,** *21*, 14205-14210.

(67) Nakayama, J.; Kimata, A.; Taniguchi, H.; Takahashi, F. *Bull. Chem. Soc. Jpn.* **1996,** *69*, 2349-2354.

(68) Dubrovskiy, A. V.; Larock, R. C. *J. Org. Chem.* **2012,** *77*, 11232-11256.

(69) Jin, T.; Yamamoto, Y. *Angew. Chem. Int. Ed.* **2007,** *46*, 3323-3325.

(70) Liu, Z.; Shi, F.; Martinez, P. D. G.; Raminelli, C.; Larock, R. C. *J. Org. Chem.* **2001,** *66*, 1403-1412.

(71) Wang, C. D.; Liu, R. S. *Org. Biomol. Chem.* **2012,** *10*, 8948-8952.

(72) Sun, H.; Yang, C.; Lin, R.; Xia, W. *Adv. Synth. Catal.* **2014,** *356*, 2775-2780.

(73) Li, Y.; Muck-Lichtenfeld, C.; Studer, A. *Angew. Chem. Int. Ed.* **2016,** *55*, 14435-14438.

(74) Okuma, K.; Hirano, K.; Shioga, C.; Nagahora, N.; Shioji, K. *Bull. Chem. Soc. Jpn.* **2013,** *86*, 615-619.

(75) Kiran, I. N.; Reddy, R. S.; Lagishetti, C.; Xu, H.; Wang, Z.; He, Y. *J. Org. Chem.* **2017,** *82*, 1823-1832.

(76) Bhojgude, S. S.; Thangaraj, M.; Suresh, E.; Biju, A. T. *Org. Lett.* **2014,** *16*, 3576-3579.

(77) Mead, K.; Stokes, S.; Bekkam, M.; Rupp, M. *Synlett* **2012,** *23*, 389-392.

(78) Nakayama, J.; Sugihara, Y.; Kobiki, A. *Heterocycles* **2009,** *78*, 103-115.

(79) Biland-Thommen, A. S.; Raju, G. S.; Blagg, J.; White, A. J. P.; Barrett, A. G. M. *Tetrahedron Lett.* **2004,** *45*, 3181-3184.

(80) Toyota, S.; Yasutomi, A.; Ōki, M. *Tetrahedron Lett.* **1995,** *36*, 6297-6300.

(81) Sato, K.; Menggenbateer; Kubota, T.; Asao, N. *Tetrahedron* **2008,** *64*, 787-796.

(82) Reddy, G. S.; Bhatt, M. V. *Tetrahedron Lett.* **1980,** *21*, 3627-3628.

(83) Castillo, J. C.; Quiroga, J.; Abonia, R.; Rodriguez, J.; Coquerel, Y. *Org. Lett.* **2015,** *17*, 3374-3377.

(84) Niu, W. X.; Yang, E. Q.; Shi, Z. F.; Cao, X. P.; Kuck, D. *J. Org. Chem.* **2012,** *77*, 1422-1434.

(85) Uno, H.; Watanabe, H.; Yamashita, Y.; Ono, N. *Org. Biomol. Chem.* **2005,** *3*, 448-453.

(86) Yamada, H.; Yamashita, Y.; Kikuchi, M.; Watanabe, H.; Okujima, T.; Uno, H.; Ogawa, T.; Ohara, K.; Ono, N. *Chemistry* **2005,** *11*, 6212-6220.

(87) Mondal, R.; Shah, B. K.; Neckers, D. C. *J. Am. Chem. Soc.* **2006,** *128*, 9612-9613.

(88) Mondal, R.; Adhikari, R. M.; Shah, B. K.; Neckers, D. C. *Org. Lett.* **2007,** *9*, 2505-2508.

(89) Katsuta, S.; Yamada, H.; Okujima, T.; Uno, H. *Tetrahedron Lett.* **2010,** *51*, 1397-1400.

(90) Lopchuk, J. M.; Gribble, G. W. *Tetrahedron Lett.* **2014,** *55*, 2809-2812.

(91) Huang, X.-J.; Tao, Y.; Li, Y.-K.; Wu, X.-Y.; Sha, F. *Tetrahedron* **2016,** *72*, 8565-8577.

(92) Godinez, C. E.; Zepeda, G.; Garcia-Garibay, M. A. *J. Am. Chem. Soc.* **2002,** *124*, 4701–4707.

(93) (a) Iwamura, H.; Mislow, K. *Acc. Chem. Res.* **1988,** *21*, 175-182. (b) Cozzi, F.; Guenzi, A.; Johnson, C. A.; Mislow, K.; Hounshell, W. D.; Blount, J. F. *J. Am. Chem. Soc.* **1981,** *103*, 957-958. (c) Kawada, Y.; Iwamura, H. *J. Am. Chem. Soc.* **1981,** *103*, 958-960. (d) Bürgi, H. B.; Hounshell, W. D.; Nachbar, R. B., Jr.; Mislow, K. *J. Am. Chem. Soc.* **1983,** *105*, 1427-1438. (e) Guenzi, A.; Johnson, C. A.; Cozzi, F.; Mislow, K. *J. Am. Chem. Soc.* **1983,** *105*, 1438-1448. (f) Kawada, Y.; Iwamura, H. *J. Am. Chem. Soc.* **1983,** *105*, 1449-1459. (g) Kawada, Y.; Yamazaki, H.; Koga, G.; Murata, S.; Iwamura, H. *J. Org. Chem.* **1986,** *51*, 1472-1477. (h) Kawada, Y.; Iwamura, H. *Tetrahedron Lett.* **1981,** *22*, 1533-1536. (i) Chance, J. M.; Geiger, J. H.; Mislow, K. *J. Am. Chem. Soc.* **1989,** *111*, 2326-2327. (j) Kawada, Y.; Iwamura, H. *J. Org. Chem.* **1980,** *45*, 2547-2548. (k) Chance, J. M.; Geiger, J. H.; Okamoto, Y.; Aburatani, R.; Mislow, K. *J. Am. Chem. Soc.* **1990,** *112*, 3540-3547. (l) Iwamura, H.; Ito, T.; Ito, H.; Toriumi, K.; Kawada, Y.; Osawa, E.; Fujiyoshi, T.; Jaime, C. *J. Am. Chem. Soc.* **1984,** *106*, 4712-4717. (m) Johnson, C. A.; Guenzi, A.; Nachbar, R. B., Jr.; Blount, J. F.; Wennerstrom, O.; Mislow, K. *J. Am. Chem. Soc.* **1982,** *104*, 5163-5168. (n) Johnson, C. A.; Guenzi, A.; Mislow, K. *J. Am. Chem. Soc.* **1981,** *103*, 6240-6242. (o) Hounshell, W. D.; Johnson, C. A.; Guenzi, A.; Cozzi, F.; Mislow, K. *Proc. Natl. Acad. Sci. U. S. A.* **1980,** *77*, 6961-6964. (p) Reinhard, D.; Rominger, F.; Mastalerz, M. *J. Org. Chem.* **2015,** *80*, 9342-9348. (q) Wang, G.; Ma, L.; Xiang, J.; Wang, Y.; Chen, X.; Che, Y.; Jiang, H. *J. Org. Chem.* **2015,** *80*, 11302-11312. (r) Setaka, W.; Nirengi, T.; Kabuto, C.; Kira, M. *J. Am. Chem. Soc.* **2008,** *130*, 15762-15763.

(94) Elbert, S. M.; Rominger, F.; Mastalerz, M. *Chemistry* **2014,** *20*, 16707-16720.

(95) Sander, M.; Jarrosson, T.; Chuang, S.-C.; Khan, S. I.; Rubin, Y. *J. Org. Chem.* **2007,** *72*, 2724-2731.

(96) Bolzan, A.; Bortoluzzi, M.; Borsato, G.; Fabbro, C.; Daştan, A.; Lucchi, O. D.; Fabris, F. *Helv. Chim. Acta* **2015,** *98*, 1067-1074.

(97) Zander, M.; Franke, W. H. *Chem. Ber.* **1974,** *107*, 727-730.

(98) Miao, Q.; Chi, X.; Xiao, S.; Zeis, R.; Lefenfeld, M.; Siegrist, T.; Steigerwald, M. L.; Nuckolls, C. *J. Am. Chem. Soc.* **2006,** *128*, 1340-1345.

(99) Chun, D.; Cheng, Y.; Wudl, F. *Angew. Chem. Int. Ed.* **2008,** *47*, 8380-8385.

(100) Debad, J. D.; Morris, J. C.; Lynch, V.; Magnus, P.; Bard, A. J. *J. Am. Chem. Soc.* **1996,** *118*, 2374-2379.

(101) Osedach, T. P.; Andrew, T. L.; Bulović, V. *Energy Environ. Sci.* **2013,** *6*, 711-718.

(102) Wieting, J. M.; Fisher, T. J.; Schafer, A. G.; Visco, M. D.; Gallucci, J. C.; Mattson, A. E. *Eur. J. Org. Chem.* **2015,** *2015*, 525-533.

(103) Pozo, I.; Cobas, A.; Peña, D.; Guitian, E.; Pérez, D. *Chem. Commun.* **2016,** *52*, 5534-5537.

(104) Avlasevich, Y.; Müller, S.; Erk, P.; Müllen, K. *Chemistry* **2007,** *13*, 6555-6561.

(105) Seitz, G.; Hoferichter, R.; Mohr, R. *Angew. Chem. Int. Ed.* **1987,** *26*, 332-334.

(106) Laue, J.; Seitz, G. *Liebigs Ann.* **1996**, 773-775.

(107) Herwig, P. T.; Müllen, K. *Adv. Mater.* **1999,** *11*, 480-483.

(108) Eversloh, C. L.; Liu, Z.; Müller, B.; Stangl, M.; Li, C.; Müllen, K. *Org. Lett.* **2011,** *13*, 5528-5531.

(109) Avlasevich, Y.; Li, C.; Müllen, K. *J. Mater. Chem.* **2010,** *20*, 3814-3826.

(110) Xie, C.; Zhang, Y. *Org. Lett.* **2007,** *9*, 781-784.

(111) Whitney, S. E.; Winters, M.; Rickborn, B. *J. Org. Chem.* **1990,** *55*, 929-935.

(112) Zhang, C.; Jiang, H.; Zhu, S. *Chem. Commun.* **2017,** *53*, 2677-2680.

(113) Suh, S. E.; Barros, S. A.; Chenoweth, D. M. *Chem. Sci.* **2015,** *6*, 5128-5132.

(114) Suh, S. E.; Chenoweth, D. M. *Org. Lett.* **2016,** *18*, 4080-4083.

(115) Suh, S.-E.; Chen, S.; Houk, K. N.; Chenoweth, D. M. *Manuscript in Preparation* **2017**.

(116) Castillo, J. C.; Quiroga, J.; Abonia, R.; Rodriguez, J.; Coquerel, Y. *J. Org. Chem.* **2015,** *80*, 9767-9773.

(117) Su, S.; Wang, N.; Li, C.; Song, B.; Jia, X.; Li, J. *Asian J. Org. Chem.* **2014,** *3*, 269-272.

(118) Siyang, H. X.; Wu, X. R.; Liu, H. L.; Wu, X. Y.; Liu, P. N. *J. Org. Chem.* **2014,** *79*, 1505-1510.

(119) Bhojgude, S. S.; Bhunia, A.; Gonnade, R. G.; Biju, A. T. *Org. Lett.* **2014,** *16*, 676-679.

(120) Shin, J.; Lee, J.; Ko, D.; De, N.; Yoo, E. J. *Org. Lett.* **2017,** *19*, 2901-2904.

(121) (a) Alonso, J. M.; Díaz-Álvarez, A. E.; Criado, A.; Pérez, D.; Peña, D.; Guitián, E. *Angew. Chem. Int. Ed.* **2012,** *51*, 173-177. (b) Pavliček, N.; Schuler, B.; Collazos, S.; Moll, N.; Pérez, D.; Guitián, E.; Meyer, G.; Peña, D.; Gross, L. *Nature chemistry* **2015,** *7*, 623-628. (c) Peña, D.; Cobas, A.; Pérez, D.; Guitián, E.; Castedo, L. *Org. Lett.* **2003,** *5*, 1863-1866. (d) Yin, J.; Qu, H.; Zhang, K.; Luo, J.; Zhang, X.; Chi, C.; Wu, J. *Org. Lett.* **2009,** *11*, 3028-3031. (e) Rodríguez-Lojo, D.; Peña, D.; Pérez, D.; Guitián, E. *Org. Biomol. Chem.* **2010,** *8*, 3386-3388. (f) Iglesias, B.; Cobas, A.; Pérez, D.; Guitián, E. *Org. Lett.* **2004,** *6*, 3557-3560. (g) Lynett, P. T.; Maly, K. E. *Org. Lett.* **2009,** *11*, 3726-3729. (h) Romero, C.; Peña, D.; Pérez, D.; Guitián, E. *Chemistry* **2006,** *12*, 5677-5684. (i) Yanney, M.; Fronczek, F. R.; Henry, W. P.; Beard, D. J.; Sygula, A. *Eur. J. Org. Chem.* **2011,** *2011*, 6636-6639. (j) Romero, C.; Peña, D.; Pérez, D.; Guitián, E. *J. Org. Chem.* **2008,** *73*, 7996-8000. (k) Schuler, B.; Collazos, S.; Gross, L.; Meyer, G.; Pérez, D.; Guitián, E.; Peña, D. *Angew. Chem. Int. Ed.* **2014,** *53*, 9004-9006.

(122) (a) Chen, L.; Zhang, C.; Wen, C.; Zhang, K.; Liu, W.; Chen, Q. *Catal. Commun.* **2015,** *65*, 81-84. (b) Zhou, Z.-h.; Yamamoto, T. *J. Organomet. Chem.* **1991,** *414*, 119-127. (c) Rudiger, E. C.; Rominger, F.; Steuer, L.; Bunz, U. H. F. *J. Org. Chem.* **2016,** *81*, 193-196. (d) Tan, Q.; Chen, H.; Xia, H.; Liu, B.; Xu, B. *Chem. Commun.* **2016,** *52*, 537-540. (e) Barnett, L.; Ho, D. M.; Baldridge, K. K.; Jr., R. A. P. *J. Am. Chem. Soc.* **1999,** *121*, 727–733. (f) Jayanth, T. T.; Cheng, C. H. *Chem. Commun.* **2006**, 894-896. (g) Naritomi, M.; Murofushi, H.; Nakashima, N. *Bull. Chem. Soc. Jpn.* **2004,** *77*, 2121-2127. (h) Chen, Y.-L.; Wong, M.-S.; Wong, W.-Y.; Lee, A. W. M. *Tetrahedron Lett.* **2007,** *48*, 2421-2425. (i) Shibata, K.; Kulkarni, A. A.; Ho, D. M.; Robert A. Pascal, J. *J. Am. Chem. Soc.* **1994,** *116*, 5983-5984. (j) Seibel, J.; Allemann, O.; Siegel, J. S.; Ernst, K. H. *J. Am. Chem. Soc.* **2013,** *135*, 7434-7437. (k) Wang, Y.; Stretton, A. D.; McConnell, M. C.; Wood, P. A.; Parsons, S.; Henry, J. B.; Mount, A. R.; Galow, T. H. *J. Am. Chem. Soc.* **2007,** *129*, 13193-13200. (l) Bennett, M. A.; Kopp, M. R.; Wenger, E.; Willis, A. C. *J. Organomet. Chem.* **2003,** *667*, 8-15. (m) Abou-Teim, O. S. *Asian J. Chem.* **2006,** *18*, 109-112.

(n) Campbell, M. C.; Humphries, R. E.; Munn, N. M. *J. Org. Chem.* **1992,** *57*, 641-644. (o) Fossatelli, M.; Brandsma, L. *Synthesis* **1992**, 756. (p) Soe, W.-H.; Manzano, C.; Renaud, N.; Mendoza, P. d.; Sarkar, A. D.; Ample, F.; Hliwa, M.; Echavarren, A. M.; Chandrasekhar, N.; Joachim, C. *ACS Nano* **2011,** *5*, 1436-1440. (q) Peña, D.; Cobas, A.; Pérez, D.; Guitián, E. *Synthesis* **2002**, 1454-1458. (r) Peña, D.; Pérez, D.; Guitián, E.; Castedo, L. *Org. Lett.* **1999,** *1*, 1555-1557. (s) Peña, D.; Cobas, A.; Pérez, D.; Guitián, E.; Castedo, L. *Org. Lett.* **2000,** *2*, 1629-1632. (t) Peña, D.; Escudero, S.; Pérez, D.; Guitián, E.; Castedo, L. *Angew. Chem. Int. Ed.* **1998,** *37*, 2659-2661. (u) Michel, B.; Greaney, M. F. *Org. Lett.* **2014,** *16*, 2684-2687. (v) Jafarpour, F.; Hazrati, H.; Nouraldinmousa, S. *Org. Lett.* **2013,** *15*, 3816-3819. (w) Peña, D.; Pérez, D.; Guitián, E.; Castedo, L. *J. Am. Chem. Soc.* **1999,** *121*, 5827-5828. (x) Kim, H. S.; Gowrisankar, S.; Kim, E. S.; Kim, J. N. *Tetrahedron Lett.* **2008,** *49*, 6569-6572. (y) Jayanth, T. T.; Jeganmohan, M.; Cheng, C.-H. *J. Org. Chem.* **2004,** *69*, 8445-8450.

(123) (a) Yoshikawa, E.; Yamamoto, Y. *Angew. Chem. Int. Ed.* **2000,** *39*, 173-175. (b) Hsieh, J.-C.; Rayabarapu, D. K.; Cheng, C.-H. *Chem. Commun.* **2004**, 532-533. (c) Peña, D.; Pérez, D.; Guitián, E.; Castedo, L. *Synlett* **2000**, 1061-1063. (d) Peña, D.; Pérez, D.; Guitián, E.; Castedo, L. *Eur. J. Org. Chem.* **2003,** *2003*, 1238-1243. (e) Jayanth, T. T.; Jeganmohan, M.; Cheng, M.-J.; Chu, S.-Y.; Cheng, C.-H. *J. Am. Chem. Soc.* **2006,** *128*, 2232-2233. (f) Ni, S.; Shu, W.; Ma, S. *Synlett* **2013,** *24*, 2310-2314. (g) Hsieh, J. C.; Cheng, C. H. *Chem. Commun.* **2005**, 2459-2461. (h) Caeiro, J.; Peña, D.; Cobas, A.; Pérez, D.; Guitián, E. *Adv. Synth. Catal.* **2006,** *348*, 2466-2474. (i) Quintana, I.; Boersma, A. J.; Peña, D.; Pérez, D.; Guitián, E. *Org. Lett.* **2006,** *8*, 3347-3349. (j) Saito, N.; Shiotani, K.; Kinbara, A.; Sato, Y. *Chem. Commun.* **2009**, 4284-4286. (k) Romero, C.; Peña, D.; Pérez, D.; Guitián, E.; Termine, R.; Golemme, A.; Omenat, A.; Barberá, J.; Serrano, J. L. *J. Mater. Chem.* **2009,** *19*, 4725-4731. (l) Xie, C.; Zhang, Y.; Yang, Y. *Chem. Commun.* **2008**, 4810-4812. (m) Hwu, J. R.; Swain, S. P. *Chemistry* **2013,** *19*, 6556-6560. (n) Peña, D.; Pérez, D.; Guitián, E.; Castedo, L. *J. Org. Chem.* **2000,** *65*, 6944–6950. (o) Yoshikawa, E.; Radhakrishnan, K. V.; Yamamoto, Y. *J. Am. Chem. Soc.* **2000,** *122*, 7280-7286. (p) Radhakrishnan, K. V.; Yoshikawa, E.; Yamamoto, Y. *Tetrahedron Lett.* **1999,** *40*, 7533-7535. (q) Sakai, H.; Kubota, T.; Yuasa, J.; Araki, Y.; Sakanoue, T.; Takenobu, T.; Wada, T.; Kawai, T.; Hasobe, T. *The Journal of Physical Chemistry C* **2016,** *120*, 7860-7869.

(124) (a) Pawlas, J.; Begtrup, M. *Org. Lett.* **2002,** *4*, 2687-2690. (b) Hsieh, J.-C.; Cheng, C.-H.

Chem. Commun. **2008**, 2992-2994.

(125) Yoshida, H.; Morishita, T.; Nakata, H.; Ohshita, J. *Org. Lett.* **2009,** *11*, 373-376.

(126) Morishita, T.; Yoshida, H.; Ohshita, J. *Chem. Commun.* **2010,** *46*, 640-642.

(127) Yoshida, H.; Tanino, K.; Ohshita, J.; Kunai, A. *Chem. Commun.* **2005**, 5678-5680.

(128) Yao, T.; Ren, B.; Wang, B.; Zhao, Y. *Org. Lett.* **2017**.

(129) Aly, A. A.; Hassan, A. A.; El-Shaieb, K. M.; El-Emary, T. I. *J. Heterocycl. Chem.* **2010,** *47*, 1079-1083.

(130) Dutt, M.; Fravel, B.; Ford, G. P.; Biehl, E. R. *J. Org. Chem.* **1994,** *59*, 497-499.

(131) Sha, F.; Huang, X. *Angew. Chem. Int. Ed.* **2009,** *48*, 3458-3461.

(132) Sha, F.; Wu, L.; Huang, X. *J. Org. Chem.* **2012,** *77*, 3754-3765.

(133) Dennis, N.; Katritzky, A. R.; Parton, S. K. *J. Chem. Soc., Chem. Commun.* **1972**, 1237-1238.

(134) Dennis, N.; Katritzky, A. R.; Ramaiah, M. *J. Chem. Soc., Perkin Trans. 1* **1975**, 1506-1514.

(135) (a) Dennis, N.; Katritzky, A. R.; Matsuo, T.; Parton, S. K.; Takeuchi, Y. *J. Chem. Soc., Perkin Trans. 1* **1974**, 746-750. (b) Dennis, N.; Katritzky, A. R.; Parton, S. K. *J. Chem. Soc., Perkin Trans. 1* **1976**, 2285-2288.

(136) Liu, Z.; Larock, R. C. *J. Org. Chem.* **2006,** *71*, 3198-3209.

(137) Lee, Y.-H.; Chen, Y.-C.; Hsieh, J.-C. *Eur. J. Org. Chem.* **2012,** *2012*, 247-250.

(138) Wang, A.; Tandel, S.; Zhang, H.; Holdeman, T. C.; Biehl, E. R. *Tetrahedron* **1998,** *54*, 15113-15120.

(139) Kranthikumar, R.; Chegondi, R.; Chandrasekhar, S. *J. Org. Chem.* **2016,** *81*, 2451-2459.

(140) Sibbel, F.; Daniliuc, C. G.; Studer, A. *Eur. J. Org. Chem.* **2015,** *2015*, 4635-4644.

(141) Liu, Z.; Larock, R. C. *Tetrahedron* **2007,** *63*, 347-355.

(142) Yoshida, H.; Fukushima, H.; Morishita, T.; Ohshita, J.; Kunai, A. *Tetrahedron* **2007,** *63*, 4793-4805.

(143) Tang, C.-Y.; Wang, G.; Yang, X.-Y.; Wu, X.-Y.; Sha, F. *Tetrahedron Lett.* **2014,** *55*, 6447-6450.

(144) Dhokale, R. A.; Thakare, P. R.; Mhaske, S. B. *Org. Lett.* **2012,** *14*, 3994-3997.

(145) Ni, C.; Zhang, L.; Hu, J. *J. Org. Chem.* **2008,** *73*, 5699-5713.

(146) Yang, Y.-Y.; Shou, W.-G.; Wang, Y.-G. *Tetrahedron Lett.* **2007,** *48*, 8163-8165.

(147) Rogness, D. C.; Larock, R. C. *J. Org. Chem.* **2011,** *76*, 4980-4986.

(148) Sala, X.; García Suárez, E. J.; Freixa, Z.; Benet-Buchholz, J.; van Leeuwen, P. W. N. M. *Eur. J. Org. Chem.* **2008,** *2008*, 6197-6205.

(149) Rao, U. N.; Sathunuru, R.; Biehl, E. R. *Heterocycles* **2004,** *63*, 1067-1075.

(150) Vaidya, S. D.; Argade, N. P. *Org. Lett.* **2013,** *15*, 4006-4009.

(151) (a) Liu, Z.; Larock, R. C. *Org. Lett.* **2003,** *5*, 4673-4675. (b) Liu, Z.; Larock, R. C. *Org. Lett.* **2004,** *6*, 99-102.

(152) Taniguchi, T.; Curran, D. P. *Angew. Chem. Int. Ed.* **2014,** *53*, 13150-13154.

(153) Yoshida, H.; Terayama, T.; Ohshita, J.; Kunai, A. *Chem. Commun.* **2004**, 1980-1981.

(154) Lin, W.; Sapountzis, I.; Knochel, P. *Angew. Chem. Int. Ed.* **2005,** *44*, 4258-4261.

(155) Anbarasan, P.; Neumann, H.; Beller, M. *Chem. - Asian J.* **2010,** *5*, 1775-1778.

(156) Yoshida, H.; Mimura, Y.; Ohshita, J. *Chem. Lett.* **2009,** *38*, 1132-1133.

(157) Samineni, R.; Bandi, C. R.; Srihari, P.; Mehta, G. *Org. Lett.* **2016,** *18*, 6184-6187.

(158) Thangaraj, M.; Bhojgude, S. S.; Jain, S.; Gonnade, R. G.; Biju, A. T. *J. Org. Chem.* **2016,** *81*, 8604-8611.

(159) Wallbaum, J.; Jones, P. G.; Werz, D. B. *J. Org. Chem.* **2015,** *80*, 3730-3734.

(160) Okuma, K.; Okada, A.; Koga, Y.; Yokomori, Y. *J. Am. Chem. Soc.* **2001,** *123*, 7166-7167.

(161) Li, R.; Tang, H.; Fu, H.; Ren, H.; Wang, X.; Wu, C.; Wu, C.; Shi, F. *J. Org. Chem.* **2014,** *79*, 1344-1355.

(162) Lopez-Leonardo, C.; Raja, R.; López-Ortiz, F.; Ángel del Águila-Sánchez, M.; Alajarin, M. *Eur. J. Org. Chem.* **2014,** *2014*, 1084-1095.

(163) Dubrovskiy, A. V.; Larock, R. C. *Org. Lett.* **2010,** *12*, 3117-3119.

(164) Biswas, K.; Greaney, M. F. *Org. Lett.* **2011,** *13*, 4946-4949.

(165) Li, H. Y.; Xing, L. J.; Lou, M. M.; Wang, H.; Liu, R. H.; Wang, B. *Org. Lett.* **2015,** *17*, 1098-1101.

(166) Li, X.; Sun, Y.; Huang, X.; Zhang, L.; Kong, L.; Peng, B. *Org. Lett.* **2017,** *19*, 838-841.

(167) Qi, N.; Zhang, N.; Allu, S. R.; Gao, J.; Guo, J.; He, Y. *Org. Lett.* **2016,** *18*, 6204-6207.

(168) Holden, C. M.; Sohel, S. M.; Greaney, M. F. *Angew. Chem. Int. Ed.* **2016,** *55*, 2450-2453.

(169) Xue, J.; Wu, L. L.; Huang, X. *Chin. Chem. Lett.* **2008,** *19*, 631-633.

(170) Kim, J.; Stoltz, B. M. *Tetrahedron Lett.* **2012,** *53*, 4994-4996.

(171) Fang, Y.; Rogness, D. C.; Larock, R. C.; Shi, F. *J. Org. Chem.* **2012,** *77*, 6262-6270.

(172) (a) Garcia-Lopez, J. A.; Oliva-Madrid, M. J.; Saura-Llamas, I.; Bautista, D.; Vicente, J. *Chem. Commun.* **2012,** *48*, 6744-6746. (b) Oliva-Madrid, M.-J.; Garcı⊠a-López, J.-A.; Saura-Llamas, I.; Bautista, D.; Vicente, J. *Organometallics* **2012,** *31*, 3647-3660. (c) Oliva-Madrid, M. J.; Saura-Llamas, I.; Bautista, D.; Vicente, J. *Chem. Commun.* **2013,** *49*, 7997-7999.

(173) Rarig, R. A.; Tran, M. N.; Chenoweth, D. M. *J. Am. Chem. Soc.* **2013,** *135*, 9213-9219.

(174) Suh, S.-E.; Tran, M. N.; Chenoweth, D. M. *Manuscript in Preparation* **2017**.

(175) Yamada, S.; Iwama, S.; Kinoshita, K.; Yamazaki, T.; Kubota, T.; Yajima, T. *Tetrahedron* **2014,** *70*, 6749-6756.

(176) Chatani, N.; Kamitani, A.; Oshita, M.; Fukumoto, Y.; Murai, S. *J. Am. Chem. Soc.* **2001,** *123*, 12686-12687.

(177) Biju, A. T.; Glorius, F. *Angew. Chem. Int. Ed.* **2010,** *49*, 9761-9764.

(178) Rao, B.; Tang, J.; Wei, Y.; Zeng, X. *Chem. - Asian J.* **2016,** *11*, 991-995.

(179) Okuma, K.; Hirano, K.; Tanabe, Y.; Itoyama, R.; Miura, A.; Nagahora, N.; Shioji, K. *Chem. Lett.* **2014,** *43*, 492-494.

Chapter 2

Triple Aryne-Tetrazine Reaction Enabling Rapid Access to a New Class of Polyaromatic Heterocycles

Adapted from Suh, S.-E.; Barros, S. A.; Chenoweth, D. M. *Chem. Sci.* **2015,** *6,* 5128-5132. -

2.1 Introduction

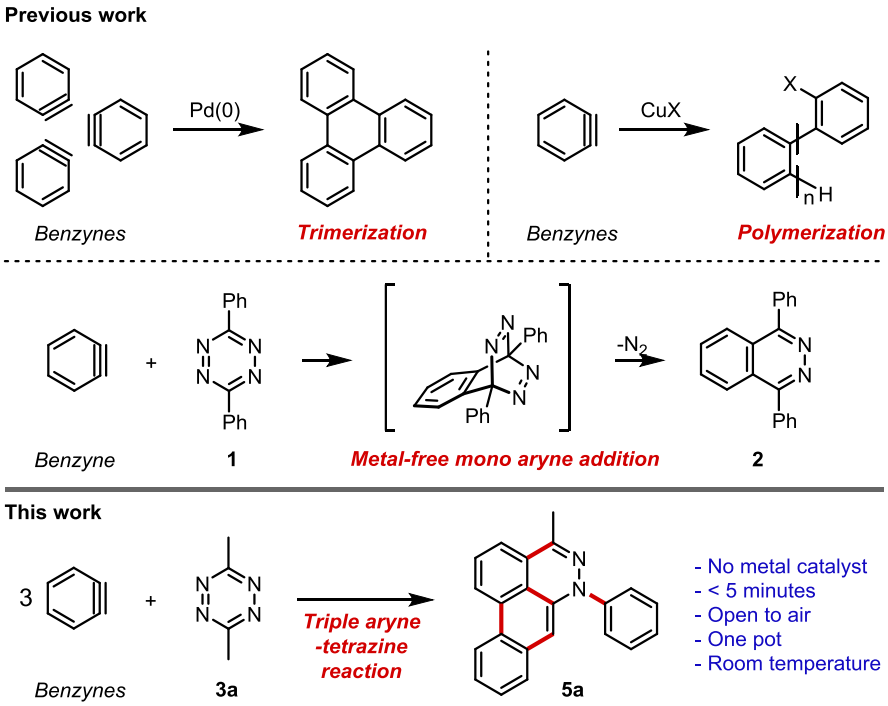

Figure 2.1. Triple aryne-retrazine reaction. Red bold lines represent new bonds formed during the course of the reaction.

New polyaromatic heterocycles are important for the discovery and development of lead bioactive molecules. Our interest in developing new chemical probes and selective nucleic acid modulators motivated us to explore direct methods for rapidly accessing novel polyaromatic systems.[1,2] Recent advances in benzyne/aryne chemistry have paved the way for use of these reactive intermediates in new synthetic methods,[3–12] complex natural product synthesis,[13–20] and aryne polymerizations (Figure 2.1).[21] In principal, multiple-consecutive aryne additions to a central core molecule could provide a novel and efficient approach for rapid access to new polyaromatic systems. Metal catalyzed methods have been reported for cyclotrimerization[22] and polymerization[21] of arynes. However, harnessing the reactivity of arynes for controlled multiple-

consecutive intermolecular reaction processes still remains a significant challenge. An alternative strategy for directly accessing higher order polyaromatic systems could be envisioned using arynes, such as benzyne, in combination with a reactive core molecule, such as a tetrazine, acting as a scaffold for iterative additions.

The reaction between benzyne and tetrazine **1** was reported approximately 50 years ago (Figure 2.1).[23] Tetrazine 1 proceeds through a Diels-Alder/retro-Diels-Alder process, producing phthalazine **2** as the terminal product. However, if phthalazine is thought of as an intermediate, one could envision further aryne additions, producing polyaromatic products. Here, we show that a simple change in the functionality on tetrazine (**3a**, Figure 2.1) can unveil latent reactivity in the presence of arynes, providing rapid and direct access to a new class of dibenzo[*de,g*]cinnoline polyaromatic heterocycles **5a**. This new class of dibenzo[*de,g*]cinnoline exhibits pH responsiveness resulting in dramatic shifts in photophysical properties upon protonation enabling tenability of these properties. These molecules have several potential applications as a new class of small molecule cellular imaging agents.

2.2 Results and Discussion

The reaction transforming tetrazines into dibenzocinnolines is operationally simple and requires less than 5 minutes from start to finish. Recently, important new methods have paved the way for the efficient synthesis of tetrazines, providing easy access to many substitution patterns.[24] A source of fluoride anion serves as a mild reagent to rapidly initiate the reaction via

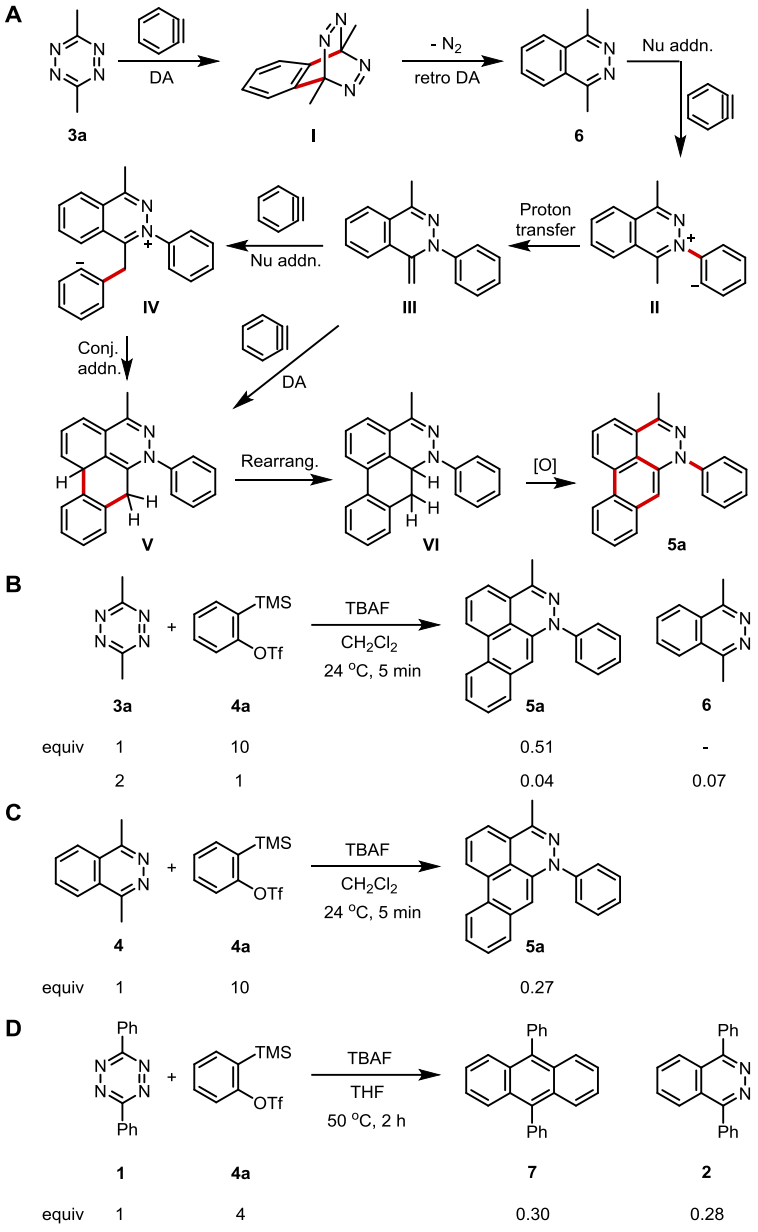

Figure 2.2. (A) Proposed mechanism of the reaction. DA, Diels-Alder; DA_{inv}, inverse electron demand Diels-Alder. (B) Reaction conditions trapping intermediate **6** (C) Resubjection of isolated intermediate 6 to the original reaction conditions. (D) Reaction of benzyne with diphenyltetrazine **1** to produce 9,10-diphenylanthracene **7**.

desilylation of a masked benzyne precursor,[25,26] obviating the necessity for a metal catalyst, external heat source, or inert gas. The reaction was performed in a vial, under air, charged with tetrazine and the benzyne precursor. After dropwise addition of a 1.0 M solution of tetrabutylammonium fluoride (TBAF) in THF at 24 °C, dibenzo[*de,g*]cinnoline **5a** was produced (Figure 2.1). The structure of dibenzocinnoline **5a** was confirmed using X-ray crystallography (Table 2.2 and SI). Dibenzo[*de,g*]cinnolines, which have not been previously reported, share significant structural homology to several natural products.[27,28]

A plausible mechanism for the reaction proceeding through six elementary steps is shown in Figure 2.2A. Aryne formation commences after addition of TBAF followed by formation of the initial [4+2] bicyclo intermediate **I** from **3a**. Cycloreversion with concomitant loss of nitrogen gas produces intermediate phthalazine heterocycle **6**.[23] Next, phthalazine **6** undergoes nucleophilic addition to benzyne, affording key intermediate **II** followed by proton transfer to produce *s-cis* diene intermediate **III**. A third aryne engages the newly formed diene through one of two possible mechanisms. This first possibility is a second [4+2] cycloaddition reaction, resulting in dihydrophenanthrene-like intermediate **V.** The alternate possibility is a non-concerted pathway where a third equivalent of benzyne is attacked by the nucleophilic enamine like intermediate **III** to produce iminium **IV**, followed by intramolecular conjugated addition to afford **V**.[29] Two mechanistic possibilities are envisioned for the final oxidation, where the first mechanism involves a direct 1,4-oxidation to yield **5a**. Although this mechanism is plausible, we favor a second possible pathway in which a base, such as fluoride, hydroxide, or water,[11] facilitates an initial 1,4- to 1,2-dihydro rearrangement of cross-conjugated intermediate **V** to restore aromaticity in the [*de*] ring leading to intermediate **VI**. This step is then followed by either direct oxidation or aryne promoted desaturation leading to the fully aromatized

dibenzocinnoline **5a.** The feasibility of the aryne promoted desaturation process was recently demonstrated in seminal studies by Hoye and coworkers.[12] To test the aryne desaturation pathway, we conducted the tandem reaction in the absence of air. The heterocyclic product was formed, providing support for the desaturation pathway.

Table 2.1. Selected Optimization Experiments of the Reaction.

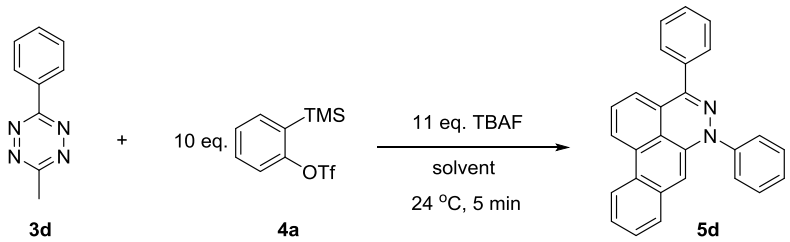

Entry	Solvent	Conc. (M)	Yield (%)[a]
1	THF	1	22
2	Et_2O	1	25
3	hexanes	1	14
4	xylenes	1	14
5	DMF	1	1
6	CH_3CN	1	25
7	CH_2Cl_2	1	26
8	CH_2Cl_2	0.1	6
9	CH_2Cl_2	0.5	7
10	CH_2Cl_2	1.5	10
11	CH_2Cl_2	2.0	13
12	-	-	19

[a] HPLC yield. 9.10-diphenylanthracene was used as an internal standard.

To trap intermediate pthalazine **6**, 2 equivalents of **3a** were used since **6** was not observed in the optimized condition shown in Table 2.1, entry 7. Using these conditions, **6** was obtained in 7% yield and was resubjected to the optimized reaction conditions (Figure 2.2B and 2C). The desired product **5a** was produced in 27% yield. Furthermore, we assumed that further

inverse Diels-Alder reaction between intermediate **6** and a benzyne might occur but no 9,10-dimethylanthracene was observed. However, when diphenyltetrazine **1** reacted with benzyne precursor **4a** and TBAF in THF at 50 °C for 2 hours, 9,10-diphenylanthracene **7** and 1,4-diphenylphthalazine **2** was obtained. This result was consistent with our hypothesis that a benzylic proton unveils masked reactivity at phthalazines and detoured to dibenzo[*de*,*g*]cinnolines to avoid anthracenes as further inverse Diels-Alder product.

Reaction optimization studies were conducted using nonvolatile tetrazine **3d** (Table 2.1). Among the several desilylating reagents used (see Table 2.5 in Section 2.4), TBAF afforded **5d** in 26% yield (Table 2.5, entry 1), while other fluoride anion sources, such as tetrabutylammonium difluorotriphenylsilicate (TBAT), CsF, HF, and KF, resulted in no reaction (Table 2.5, entries 2-12). In the presence of 18-crown-6, KF resulted in a low yield of product **5d** (Table 2.5, entry 13). As expected, the reaction did not occur when other additives including tetrabutylammonium chloride or tetrabutylammonium bromide were added in the absence of a fluoride source (Table 2.6 in Section 2.4).

The highest yields were obtained using CH_2Cl_2 as the solvent. However, several alternative solvents such as THF, Et_2O, xylene, hexane, and CH_3CN resulted in a reasonable yield of product **5d** (Table 2.1, entries 1-7). The reaction was sensitive to the concentration with the highest conversion to product achieved at a final concentration of 1.0 M (Table 2.1, entries 7-12). In addition, excess benzyne precursor and TBAF reagents were required to achieve optimal yields (Table 2.7 in Section 2.4). A decrease in the temperature and an increase in the reaction time resulted in decreased product yields (Table 2.8 in Section 2.4). The addition of TBAF to the reaction mixture over the course of 60 seconds resulted in the best yields. During

Table 2.2. Substrate Scope for the Synthesis of Dibenzo[*de,g*]cinnolines and X-Ray Crystal Structure of 5a.

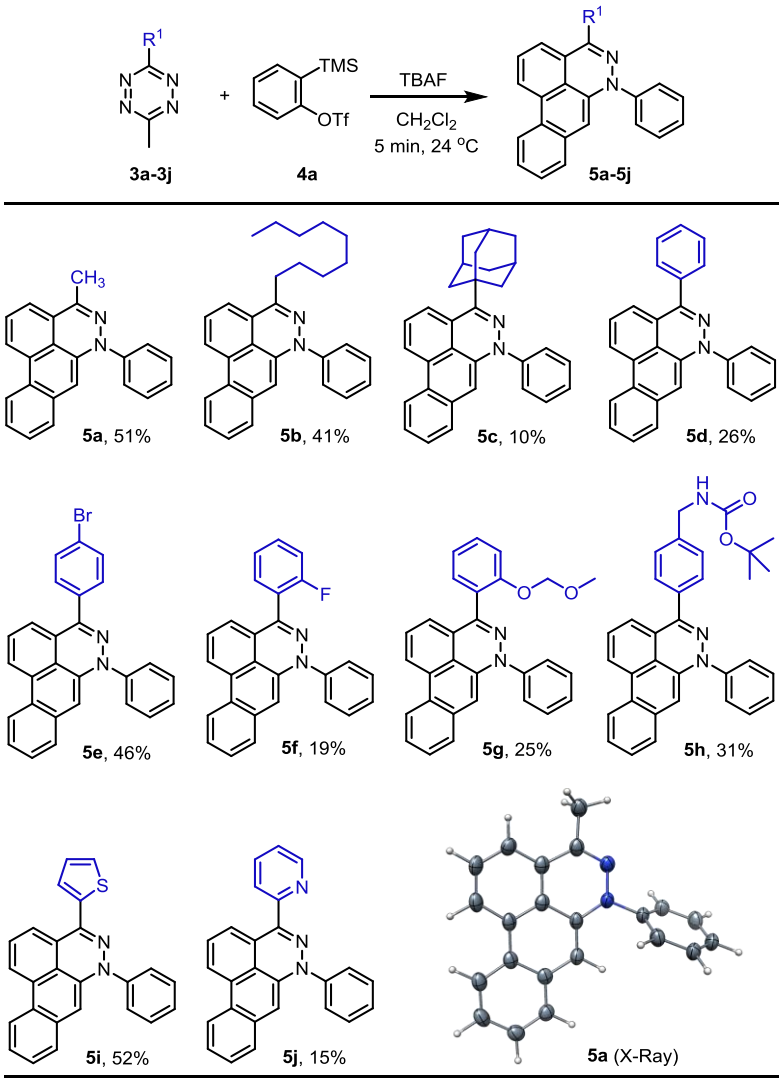

[a] Reactions were performed under the optimized condition shown in Table 1, entry 7.
[b] Isolated yield.

the TBAF addition, a steady increase in the internal temperature of the reaction mixture to a maximum of 51 °C after 70 seconds followed by a decrease to 24 °C was observed. After a total time of 300 seconds, the reaction was complete (see Figure 2.6 in Section 2.4).

Interestingly, **5d** was isolated in 27 % yield when **4a** was used as a limiting reagent, TBAF was added to **3d** over a period of 4 hours at 0 °C, and the solution was stirred for an additional 20 hours (entry 7, Table 2.8 in Section 2.4). Reduction in the amount of benzyne precursor used resulted in longer reaction times with unreacted tetrazine and required lower temperatures. Further optimization is currently underway in our group.

Using the optimized conditions described here, several dibenzocinnolines **5a**-**5j** were synthesized. Given that the reaction forms four new C-C bonds and one new C-N bond during the course of 6-8 steps, yields from 10-52% are quite reasonable. Alkyl, aryl, and heteroaryl substituents are tolerated in position R1. Differentially dialkylated tetrazines show selectivity for reaction at the least sterically hindered position. For example, 3-methyl-6-nonyl-1,2,4,5-tetrazine **3b** has two benzylic positions; however, only product **5b** (Table 2.2) was observed, consistent with nonyl group sterics dictating addition of the second benzyne to the least sterically hindered nitrogen atom (see intermediate **II** in Figure 2.2), which is much bulkier than the methyl group. In addition, isolated **5a** or **5b** did not react further with excess benzyne in CH_2Cl_2 or THF under refluxing conditions. This result is consistent with the nitrogen-benzyne adduct creating a sterically congested environment that precludes addition to the adjacent nitrogen atom, as seen from the crystal structure of **5a** in Table 2.2. To further test the infuence of steric hindrance, the bulky adamantyl tetrazine **3c** was used. The bulky adamantyl group was expected to shut down the Diels–Alder reaction, preventing appropriate alignment of the aryne with the central tetrazine carbon atoms. To our surprise, product **5c** was produced in 10% yield.

To broaden the scope of the reaction, difunctionalized tetrazines were explored. We found that the reaction is not limited to substitution at the R1 position. Difunctionalized tetrazines with substitution at R2 resulted in reasonable yields of dibenzocinnoline products **5k**-

5m (Table 2.3). Encouraged by these results, alternate benzyne precursors were tested with a set of tetrazines (Table 2.4). We found that addition of 4,5-dimethyl-*o*-benzyne to tetrazines afforded **5n-5p** in reasonable yields (24-31%; Table 2.4).

Table 2.3. Scope of Tetrazines for the Synthesis of Dibenzo[*de,g*]cinnolines.

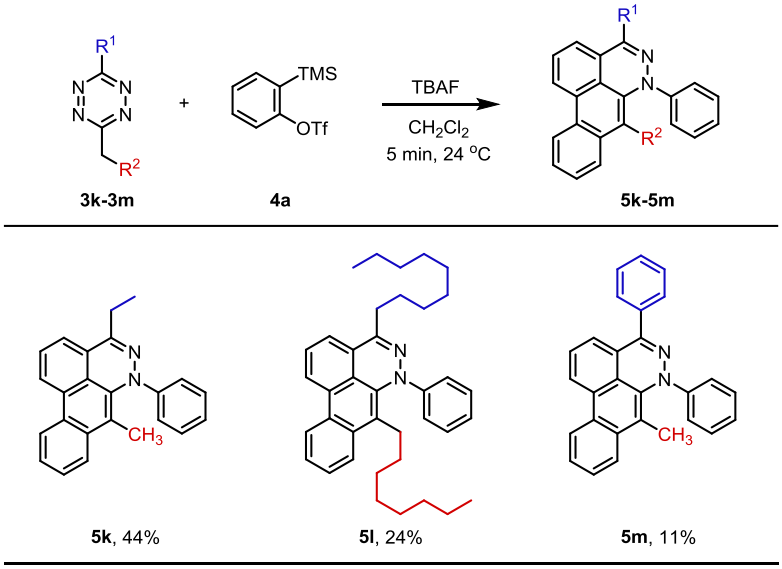

[a] Reactions were performed under the optimized conditions shown in Table 1, entry 7.
[b] Isolated yield.

Depending on the tetrazine used, we found that TBAF not only initiates the reaction but also decomposes the tetrazine starting materials in a competing but slower background reaction. For mono-substituted tetrazines, such as 3-methyl-1,2,4,5-tetrazine, decomposition was faster than the initial Diels-Alder reaction, resulting in neither the desired product nor the phthalazine intermediate. Additionally, 3-benzyl-6-methyl-1,2,4,5-tetrazine decomposed faster due to the increased acidity of the methylene accelerating the tetrazine decomposition. Also, the addition of dinaphthyne precursor to 3-methyl-6-phenyl-1,2,4,5-tetrazine **3d** led to dinaphthocinnoline **5q**.

Table 2.4. Addition of 4,5-Dimethyl-*o*-Benzyne.

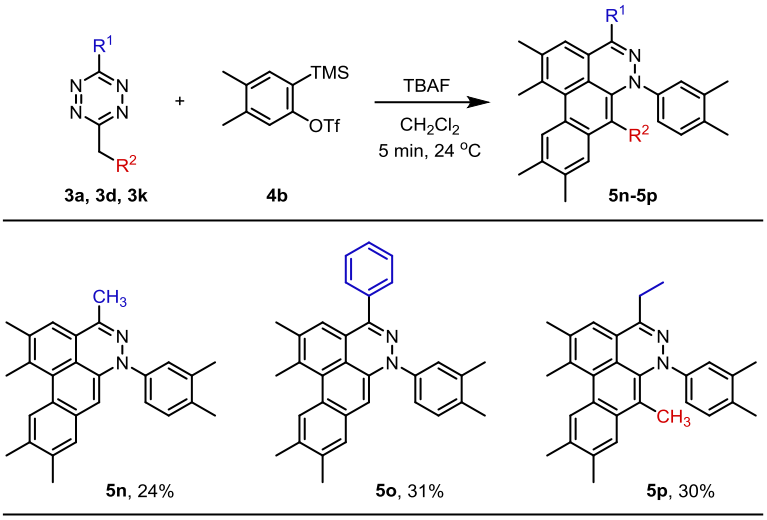

[a] Reactions were performed under the optimized condition shown in Table 1, entry 7.
[b] Isolated yield reported.

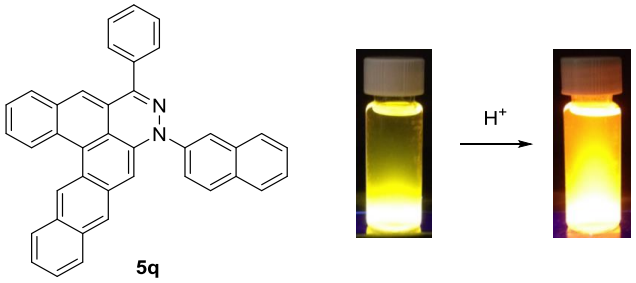

Figure 2.3. Structure of **5q**. Solutions of **5q** in CH_2Cl_2 (left) and in CH_2Cl_2/TFA (right) irradiated at 365 nm with a UV lamp (left).

Dibenzo[*de,g*]cinnolines exhibit interesting photophysical properties (Figure A1.77-90). Dibenzo[*de,g*]cinnolines **5b**, **5d**, and **5i** are emissive in the solid state and solution state under 365nm UV radiation. Additionally they exhibited hypsochromic emission response in the presence of acid. In contrast, dinaphthocinnoline **5q** exhibited a bathochromic emission shift in

the presence of acid unlike **5b**, **5d**, and **5i** (Figure 2.3). Taken together, these results show that the photophysical properties are tunable across a large window of the visible spectrum (Figure 2.4)

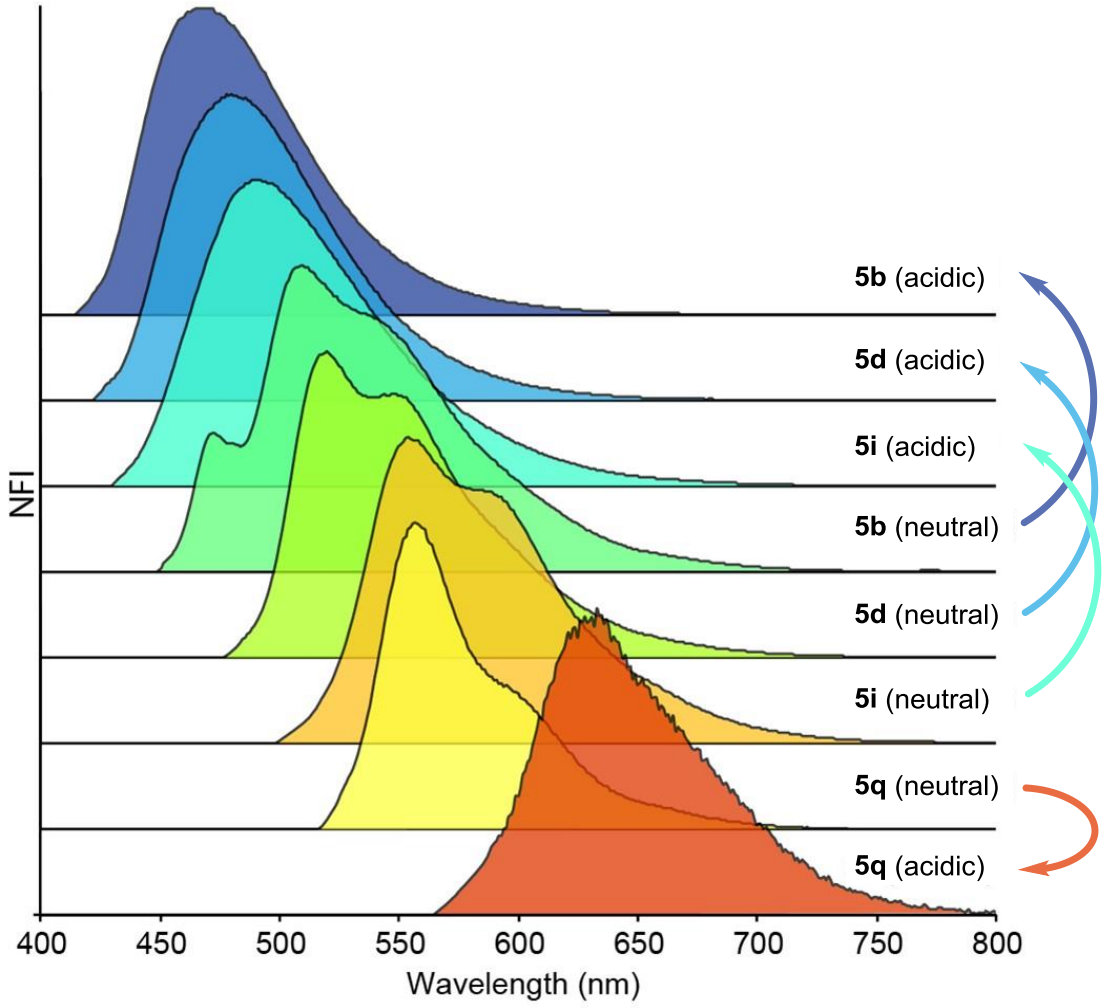

Figure 2.4. Emission spectra for the neutral and protonated forms of compounds **5b**, **5d**, **5i**, and **5q**.

and we expect even more interesting photophysical phenomena as we explore new derivatives for applications in materials, sensing, and imaging. Preliminary cellular imaging with **5e** shows that upon excitation of the acidic form at 405 nm, intracellular vesicles can be selectively stained

(Figure 2.5a). When paired with commonly used dyes, such as Hoechst and MitoTracker, we have the ability to differentiate different intracellular compartments (Figure 2.5b). The ability to tune the spectral properties of the dibenzocinnolines for selective imaging of subcellular structures makes this a promising new class of fluorescent probes for live cell imaging.

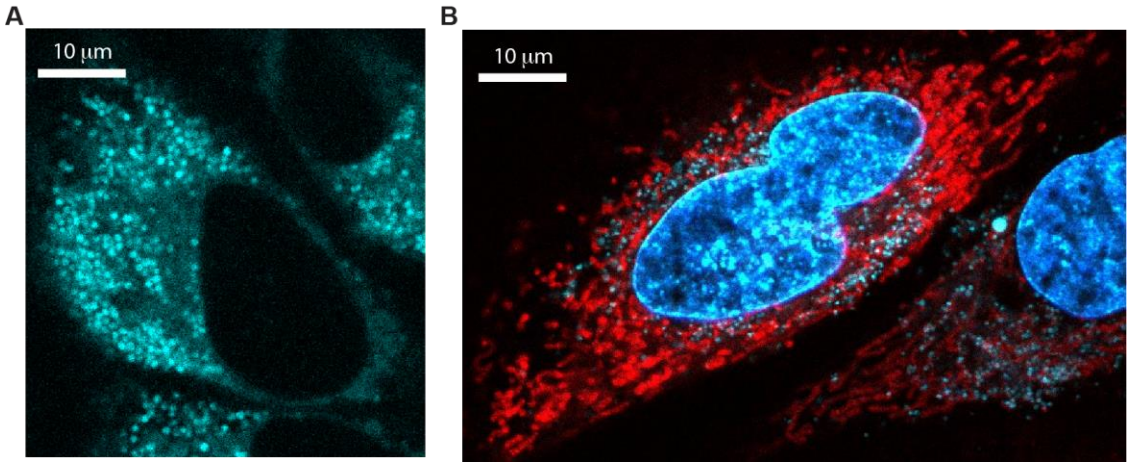

Figure 2.5. Live-cell imaging of HeLa cells in the presence of **5e**. (A) Cultured HeLa cells were incubated with **5e** for 2 hours and imaged using confocal microscopy. (B) Cells were incubated with **5e** for 2 hours, then counterstained with Hoechst 33342 and MitoTracker Red FM. Extranuclear cyan corresponds to compound **5e**. Using an excitation of 405 nm and emission from 450 to 500 nm allows for simultaneous visualization of **5e**, nuclear localized Hoechst 33342, and mitochondrial localized MitoTracker Red FM.

2.3 Conclusions

In summary, we have developed a new synthetic approach to rapidly access a structurally novel class of dibenzo[*de,g*]cinnolines using tetrazine and aryne precursors. The starting

materials are easily prepared, and the reaction is facile and simple, proceeding in less than 5 minutes. The photophysical properties of this new class of fluorophore are tunable and compatible with live-cell imaging. Efforts are currently underway to further probe the biological activity and to expand access to different structures via regioselective asymmetric aryne addition.[30]

2.4 Experimental Section

General information

Materials.

All commercial reagents and solvents were used as received. Zinc trifluoromethanesulfonate, hydrazine anhydrous, propionitrile, decanenitrile, 2-thiophenecarbonitrile, 2-pyridinecarbonitrile, 2-fluorobenzonitrile, adamantane-1-carbonitrile, 4-(aminomethyl)benzonitrile hydrochloride, di-*tert*-butyl dicarbonate and 1.0M tetrabutylammonium fluoride in THF were purchased from Aldrich. Acetonitrile and benzonitrile were purchased from Fisher Scientific, 4-bromobenzonitrile from Oakwood Products Inc, 3-(Trimethylsilyl)-2-naphthyl trifluoromethanesulfonate from TCI and methylene chloride-d_2 and chloroform-d from Cambridge Isotope Laboratories Inc. Flash column chromatography was performed using Silicycle silica gel (55–65 Å pore diameter). Thin-layer chromatography was performed on Sorbent Technologies silica plates (250 μm thickness). Dulbecco's Modified Eagle Medium (DMEM) and Alamar Blue were purchased

from Invitrogen. Fetal bovine serum (FBS) was purchased from Gibco, Life Technologies. L-glutamine and penicillin/streptomycin were purchased from Corning Cellgro.

General spectroscopic methods.

Proton nuclear magnetic resonance spectroscopy (^{1}H NMR) and Carbon nuclear magnetic resonance spectroscopy (^{13}C NMR) spectra were recorded on a Bruker UNI 500 NMR. Fluorine nuclear magnetic resonance spectroscopy (^{19}F NMR) was recorded on a Bruker DMX 360 NMR. High-resolution mass spectra were obtained by Dr. Rakesh Kohli at the University of Pennsylvania's Mass Spectrometry Service Center on a Micromass AutoSpec electrospray/chemical ionization spectrometer. X-ray diffraction data obtained and solved by Dr. Patrick Carroll at the University of Pennsylvania. Ultraviolet absorption spectrophotometry was performed on a JASCO V-650 spectrophotometer with a PAC-743R multichannel Peltier using quartz cells with a 1 cm cell path length. High performance liquid chromatography analysis was performed using a Jasco HPLC instrument equipped with a Phenomenex column (Luna 5u C18(2) 100A; 250 × 4.60 mm, 5 μm). Graph of time versus temperature was obtained using a Vernier Go-Link and temperature probe.

Cell culture and imaging.

HeLa cells were maintained in a humidified incubator at 37 °C in 5% CO_2. HeLa cells were cultured in DMEM supplemented with 10% fetal bovine serum (Giboc, Life Technologies) and penicillin and streptomycin (Corning Cellgro). For live cell imaging, cells

were plated in glass-bottom 35-mm dishes (MatTEK) 24 hours before experiments. 24 hours after plating, 1 μL of compounds (stock solution 10 mM) was added to 2 mL of media. Cells were incubated for 2 hours with compounds at 37 °C followed by washing with fresh media 2 times. During imaging, cells were maintained in DMEM without phenol red supplemented with 10% FBS.

A Leica TCS SP8 confocal microscope equipped with a 63x/1.4 NA oil immersion objecti ve lens was used. Compound **5e** was excited with 405 nm and emission was observed from 450-500 nm. To observe MitoTracker Red FM, an excitation of 552 nm and emission from 575-640 nm were used. Hoechst 33342 was observed by excitation with 405 nm and emission from 408-450 nm. Images were processed using Fiji ImageJ.

Additional optimization information.

The yield was determined by HPLC and 9,10-dipbhenylanthracene was used as an internal standard.

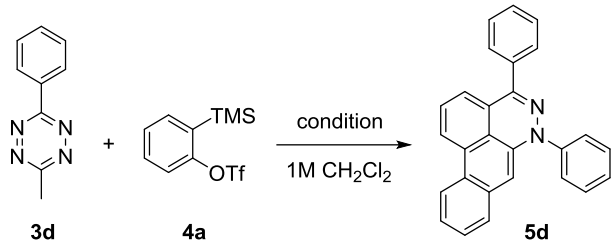

Table 2.5. Effect of Fluoride Anion Source and Combination with Additive.

Entry	F^-	Eq of F^-	Eq of Benz.	Additive[b]	Temp (^oC)	Time	Yield (%)[c]
1	TBAF[a]	10	11	-	24	1 h	-
2	TBAF[a]	10	11	TFA	24	1 h	-
3	TBAF[a]	10	11	NEt_3	24	1 h	-
4	TBAF	11	10	-	24	5 min	26 (23 [d])
5	TBAT	11	10	-	24	1 h	-
6	TBAT	11	10	TFA	24	1 h	-
7	TBAT	11	10	NEt_3	24	1 h	-
8	CsF	11	10	-	24	1 h	-
9	CsF	11	10	TFA	24	1 h	-
10	CsF	11	10	NEt_3	24	1 h	-
11	HF	11	10	-	24	1 h	-
12	KF	11	10	-	24	1 h	-
13	KF	11	10	18-crown-6	24	5 min	3

[a] 1 eq of TBAF was added to 1.1 eq of benzyne precursor and then 10 eq of stock solution from those mixture was added to tetrazine.
[b] 10 eq of additive was added.
[c] HPLC yield.
[d] Isolated yield.

Table 2.6. Effect of Additive without Fluoride Anion Source.

Entry	F^-	Eq of F^-	Eq of Benz.	Additive[a]	Temp (°C)	Time	Yield (%)[b]
1	-	-	10	Indole	24	1 h	-
2	-	-	10	Imidazole	24	1 h	-
3	-	-	10	TMG	24	1 h	-
4	-	-	10	DBU	24	1 h	-
5	-	-	10	t-BuOK/THF	24	1 h	-
6	-	-	10	2,6-lutidine	24	1 h	-
7	-	-	10	Pyridine	24	1 h	-
8	-	-	10	*t*-$BuNH_2$	24	1 h	-
9	-	-	10	TBAOH	24	1 h	-
10	-	-	10	TBABr	24	1 h	-
11	-	-	10	TBACl	24	1 h	-

[a] 10 eq of additive was added.
[b] HPLC yield.

Table 2.7. Effect of Equivalence of Benzyne Precursor and TBAF.

Entry	F^-	Eq of F^-	Eq of Benz.	Additive	Temp (°C)	Time	Yield (%)[a]
1	TBAF	11	10	-	24	5 min	26
2	TBAF	11	11	-	24	5 min	25
3	TBAF	8.8	8	-	24	5 min	19
4	TBAF	6.6	6	-	24	5 min	11
5	TBAF	4.4	4	-	24	5 min	6
6	TBAF	2.2	2	-	24	5 min	3
7	TBAF	1.1	1	-	24	5 min	1
8	TBAF	9	10	-	24	5 min	22
9	TBAF	7	10	-	24	5 min	14
10	TBAF	11	22	-	24	5 min	23

[a] HPLC yield.

Table 2.8. Effect of Temperature and Reaction Time.

Entry	F^-	Eq of F^-	Eq of Benz.	Additive	Temp (°C)	Time	Yield (%)[a]
1	TBAF	11	10	-	24	5 min	26
2	TBAF	11	10	-	0	5 min	6
3	TBAF	11	10	-	0 to 24[b]	35 min	7
4	TBAF	11	10	-	0 to 24[b]	65 min	10
5	TBAF	11	10	-	24	65 min	13
6	TBAF	3.3	3	-	0	24 h[c]	27[d]
7	TBAF	3.3	3	-	24	4 h[e]	5[d]

[a] HPLC yield except entry 6.

[b] TBAF was added dropwise for 5 min at 0 °C and then the reaction mixture was warmed to 24 °C for additional time.

[C] TBAF was added in period of 4 h at 0 °C and then was stirred for additional 20 h.

[d] Isolated yield based on the benzyne precursor as the starting material.

[e] TBAF was added in period of 4 h at 24 °C.

Real-time temperature study

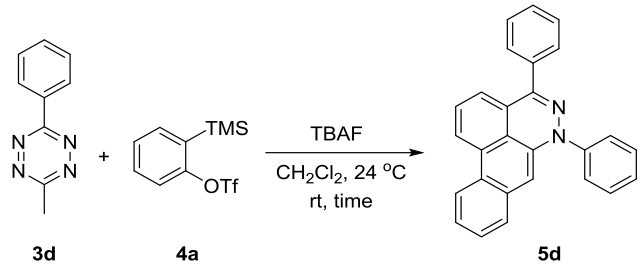

A vial was charged with 14.8 mg (0.086 mmol) of **3d** and 300 mg (0.86 mmol) of 3-(trimethylsilyl)-2-naphthyl trifluoromethanesulfonate in 0.09 mL of dichloromethane at 24˚C, and 1 M TBAF in THF (0.95 mL, 0.95 mmol) was slowly added to the solution over the course of 1 min (0 to 60 sec in Supplementary Figure 2.1). The highest temperature was 52 ˚C at 73 sec.

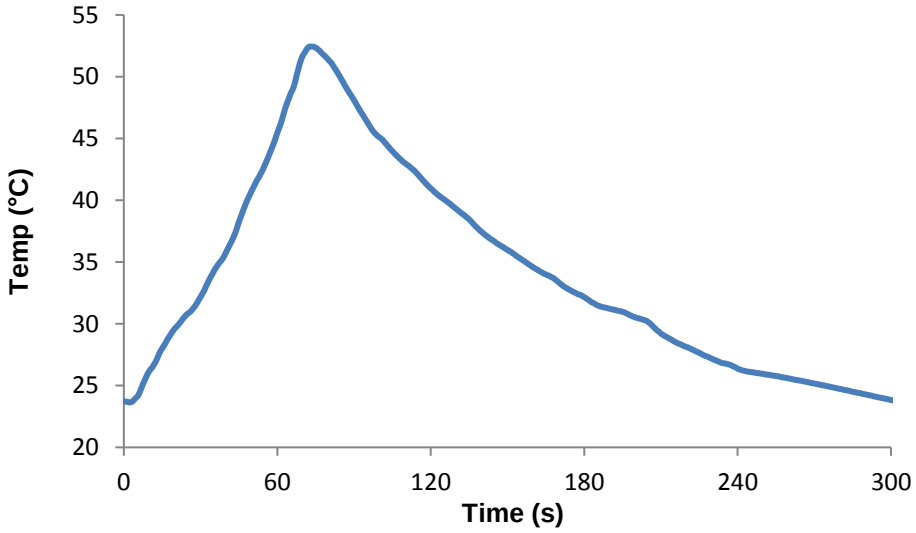

Figure 2.6. Graph of time vs. temperature of the reaction.

Experimental procedures

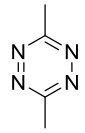

3a

3,6-dimethyl-1,2,4,5-tetrazine (3a): 3a was prepared according to the previously published procedure[24] from commercially available acetonitrile. The product was purified by flash column chromatography (ethyl acetate/hexane 1:4) to afford **3a**. The data for this compound was previously reported in the literature.[31-33]

Physical Property: Red crystal.

Isolated Yield: 30%

TLC: R_f = 0.29 (silica gel, ethyl acetate/hexane 1:4).

^{1}H NMR (500 MHz, $CDCl_3$) δ 2.96 (s, 6H).

^{13}C NMR (125 MHz, $CDCl_3$) δ 167.2, 21.0

IR (neat): 1636, 1412, 1350, 1292, 1270, 913, 873, and 734 cm^{-1}.

HRMS (ESI) calculated for $C_4H_7N_4$ $[M+H]^+$ 111.0660, no peak matched the calculated exact mass.[34]

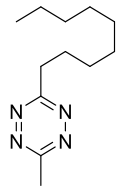

3b

3-methyl-6-nonyl-1,2,4,5-tetrazine (3b): 3b was prepared according to the previously published procedure[24] from commercially available acetonitrile and decanenitrile. The product was purified by flash column chromatography (ethyl acetate/hexane 1:16) to afford **3b**.

Physical Property: Purple crystal, m.p. = 33-34 °C.

Isolated Yield: 19%

TLC: R_f = 0.50 (silica gel, ethyl acetate/hexane 1:4).

^{1}H NMR (500 MHz, $CDCl_3$) δ 3.27 (t, 2H, J = 7.7 Hz), 3.02 (s, 3H), 1.96-1.88 (m, 2H), 1.46-1.19 (m, 12H), 0.90-0.84 (m, 3H).

^{13}C NMR (125 MHz, $CDCl_3$) δ 170.3, 167.4, 34.9, 32.0, 29.5, 29.39, 29.37, 29.27, 28.5, 22.8, 21.2, 14.2.

IR (neat): 2953, 2914, 2848, 2870, 1718, 1653, 1469, 1407, 1338, 1317, 1274, 1200, 891, 774, and 720 cm^{-1}.

HRMS (ESI) calculated for $C_{12}H_{23}N_4$ $[M+H]^+$ 223.1918, found 223.1922.

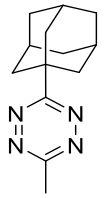

3c

3-((3r,5r,7r)-adamantan-1-yl)-6-methyl-1,2,4,5-tetrazine (3c): 3c was prepared according to the previously published procedure[24] from commercially available acetonitrile and adamantane-1-carbonitrile. The product was purified by flash column chromatography (ethyl acetate/hexane 1:12) to afford **3c**.

Physical Property: Red solid, m.p. = 55-56 °C.

Isolated Yield: 22%

TLC: R_f = 0.37 (silica gel, ethyl acetate/hexane 1:4).

^{1}H NMR (500 MHz, $CDCl_3$) δ 2.90 (s, 3H), 2.10-2.00 (m, 9H), 1.71 (bs, 6H).

^{13}C NMR (125 MHz, $CDCl_3$) δ 174.3, 166.6, 40.5, 39.2, 36.3, 28.2, 21.0.

IR (neat): 2905, 2850, 1453, 1398, 1353, 1312, 1088, 1046, 890, 736 cm^{-1}.

HRMS (ESI) calculated for $C_{13}H_{19}N_4$ $[M+H]^+$ 231.1605, found 231.1600.

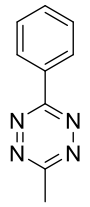

3d

3-methyl-6-phenyl-1,2,4,5-tetrazine (3d): 3d was prepared according to the previously published procedure[1] from commercially available acetonitrile and benzonitrile. The product was purified by flash column chromatography (ethyl acetate/hexane 1:10) to afford **3d**. The data for this compound was previously reported in the literature.[33,35]

Physical Property: Purple crystal.

Isolated Yield: 58%

TLC: R_f = 0.42 (silica gel, 25% ethyl acetate/hexane).

^{1}H NMR (500 MHz, $CDCl_3$) δ 8.51-8.45 (m, 2H), 7.56-7.46 (m, 3H), 3.01 (s, 3H).

^{13}C NMR (125 MHz, $CDCl_3$) δ 167.1, 163.9, 132.4, 131.8, 129.1, 127.8, 21.1.

IR (neat): 1473, 1401, 1362, 1176, 1089, 1022, 890, 760, 722, 692, and 675 cm^{-1}.

HRMS (ESI) calculated for $C_9H_9N_4$ $[M+H]^+$ 173.0822, found 173.0819.

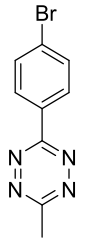

3e

3-(4-bromophenyl)-6-methyl-1,2,4,5-tetrazine (3e): 3e was prepared according to the previously published procedure[24] from commercially available acetonitrile and 4-bromobenzonitrile. The product was purified by flash column chromatography (ethyl acetate/hexane 1:10) to afford **3e**.

Physical Property: Purple crystal, m.p. = 151-152 °C.

Isolated Yield: 16%

TLC: R_f = 0.53 (silica gel, ethyl acetate/hexane 1:4).

^{1}H NMR (500 MHz, $CDCl_3$) δ 8.43-8.38 (m, 2H), 7.70-7.66 (m, 2H), 3.07 (s, 3H)

^{13}C NMR (125 MHz, $CDCl_3$) δ 167.5, 163.6, 132.6, 130.8, 129.4, 127.7, 21.3.

IR (neat): 1588, 1402, 1366, 1174, 1091, 1072, 1008, 890, 847, 798, and 633 cm^{-1}.

HRMS (ESI) calculated for $C_9H_8BrN_4$ $[M+H]^+$ 250.9922, no peak matched the calculated exact mass.

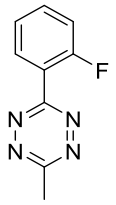

3f

3-(2-fluorophenyl)-6-methyl-1,2,4,5-tetrazine (3f): 3f was prepared according to the previously published procedure[24] from commercially available acetonitrile and 2-fluorobenzonitrile. The product was purified by flash column chromatography (ethyl acetate/hexane 1:8) to afford **3f**.

Physical Property: Red solid, m.p. = 50-51 ˚C.

Isolated Yield: 26%

TLC: R_f = 0.44 (silica gel, ethyl acetate/hexane 1:4).

^{1}H NMR (500 MHz, $CDCl_3$) δ 8.18 (td, 1H, J = 7.6, 1.8 Hz), 7.59-7.53 (m, 1H), 7.33 (td, 1H, J = 7.6, 1.0 Hz), 7.26 (dd, 1H, J = 10.8, 1.0 Hz), 3.08 (s, 3H).

^{13}C NMR (125 MHz, $CDCl_3$) δ 166.8, 163.9, 162.3, 160.2, 133.9, 133.8, 131.3, 124.74, 124.71, 120.7, 120.6, 117.32, 117.15, 21.2.

^{19}F NMR (338 MHz, $CDCl_3$) δ -112.8 to -112.9 (m, 1F).

IR (neat): 2129, 1614, 1586, 1497, 1466, 1400, 1364, 1253, 1216, 1114, 1087, 1028, 888, 821, 763, 736 cm^{-1}.

HRMS (ESI) calculated for $C_9H_8FN_4$ $[M+H]^+$ 191.0729, no peak matched the calculated exact mass.

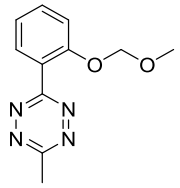

3g

3-(2-(methoxymethoxy)phenyl)-6-methyl-1,2,4,5-tetrazine (3g): A vial was charged with 80 mg (0.43 mmol) of **3n** and 0.44 mL (2.55 mmol) of *N,N*-diisopropylethylamine (DIPEA) in 1.00 mL of dichloromethane at 0 ˚C, and the solution was stirred for 20 min. To the resulting solution was added 0.01 mL (1.28 mmol) of chloromethylmethyl ether (MOMCl). After 20 min at 0 ˚C, the solution was warmed to 24 ˚C and stirred for another 12 h. The solution was quenched with saturated NH_4Cl solution, extracted with dichloromethane, and purified by column chromatography (ethyl acetate/hexane 1:4) to afford **3g** (54.1 mg).

Physical Property: Red oil.

Isolated Yield: 55%

TLC: R_f = 0.30 (silica gel, ethyl acetate/hexane 1:4).

^{1}H NMR (500 MHz, $CDCl_3$) δ 7.89 (dd, 1H, J = 7.7, 0.9 Hz), 7.53 (ddd, 1H, J = 8.4, 7.5, 1.7 Hz), 7.32 (d, 1H, J = 8.4 Hz), 7.20 (td, 1H, 7.5, 0.9 Hz), 5.23 (s, 2H), 3.47 (s, 3H), 3.10 (s, 3H).

^{13}C NMR (125 MHz, $CDCl_3$) δ 166.3, 165.9, 155.9, 132.9, 131.6, 123.3, 122.3, 116.1, 95.1, 56.4, 21.2.

IR (neat): 2923, 1603, 1496, 1461, 1399, 1154, 1080, 982, 756, 736 cm^{-1}.

HRMS (ESI) calculated for $C_{11}H_{13}N_4O_2$ $[M+H]^+$ 233.1034, found 233.1048.

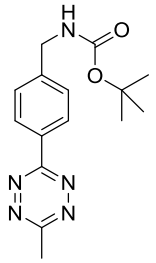

3h

***tert*-butyl (4-(6-methyl-1,2,4,5-tetrazin-3-yl)benzyl)carbamate (3h): 3h** was obtained according to the literature procedures and ^{1}H NMR was matched with the literature.[24]

^{1}H NMR (500 MHz, $CDCl_3$) δ 8.46 (d, 2H, J = 8.2 Hz), 7.44 (d, 2H, J = 8.2 Hz), 5.22 (bs, 1H), 4.38 (d, 2H, J = 5.7 Hz), 3.04 (s, 3H), 1.44 (s, 9H).

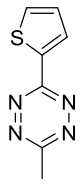

3i

3-methyl-6-(thiophen-2-yl)-1,2,4,5-tetrazine (3i): 3i was prepared according to the previously published procedure[24] from commercially available acetonitrile and thiophene-2-carbonitrile. The product was purified by flash column chromatography (ethyl acetate/hexane 1:10) to afford **3i**.

Physical Property: Orange-red crystal, m.p. = 132-133 °C.

Isolated Yield: 27%

TLC: R_f = 0.46 (silica gel, ethyl acetate/hexane 1:10).

^{1}H NMR (500 MHz, $CDCl_3$) δ 8.19 (dd, 1H, J = 3.7, 0.8 Hz), 7.62 (dd, 1H, J = 5.0, 0.8 Hz), 7.21-7.18 (m, 1H), 3.00 (s, 3H).

^{13}C NMR (125 MHz, $CDCl_3$) δ 166.7, 162.0, 135.8, 132.3, 131.0, 128.9, 21.2.

IR (neat): 1535, 1437, 1394, 1370, 1346, 1294, 1216, 1082, 1054, 991, 897, 854, 732, and 670 cm^{-1}.

HRMS (ESI) calculated for $C_7H_7N_4S$ $[M+H]^+$ 179.0386, found 179.0393.

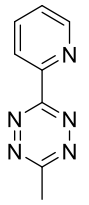

3j

3-methyl-6-(pyridin-2-yl)-1,2,4,5-tetrazine (3j): 3j was prepared according to the previously published procedure[24] from commercially available acetonitrile and 2-cyanopyridine. The product was purified by flash column chromatography (ethyl acetate/hexane 1:1) to afford **3j**.

Physical Property: Purple crystal, m.p. = 104-105 °C.

Isolated Yield: 11%

TLC: R_f = 0.06 (silica gel, ethyl acetate/hexane 1:4).

^{1}H NMR (500 MHz, $CDCl_3$) δ 8.70 (dd, 1H, J = 4.7, 0.7 Hz), 8.38 (d, 1H, J = 7.9 Hz), 7.76 (td, 1H, J = 7.8, 1.7 Hz), 7.34 (ddd, 1H, J = 7.6, 4.7, 1.0 Hz), 2.93 (s, 3H).

^{13}C NMR (125 MHz, $CDCl_3$) δ 167.7, 163.2, 150.5, 149.9, 137.1, 126.0, 123.5, 21.0.

IR (neat): 1641, 1584, 1567, 1400, 1364,1103, 1040, 992, 902, 778, 745, 736 cm^{-1}.

HRMS (ESI) calculated for $C_8H_8N_5$ $[M+H]^+$ 174.0775, found 174.0783.

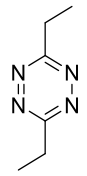

3k

3,6-diethyl-1,2,4,5-tetrazine (3k): 3k was prepared according to the previously published procedure[24] from commercially available propionitrile. The product was purified by flash column chromatography (ethyl acetate/hexane 1:20) to afford **3k**.

Physical Property: Red oil.

Isolated Yield: 38%

TLC: R_f = 0.60 (silica gel, ethyl acetate/hexane 1:4).

^{1}H NMR (500 MHz, $CDCl_3$) δ 3.22 (q, 4H, J = 7.6 Hz), 1.40 (t, 6H, J = 7.6 Hz).

^{13}C NMR (125 MHz, $CDCl_3$) δ 170.8, 28.2, 12.2.

IR (neat): 2983, 2942, 2884, 1688, 1464, 1399, 1266, 1056, 888, 737, 701, 652 cm^{-1}.

HRMS (ESI) calculated for $C_6H_{11}N_4$ $[M+H]^+$ 139.0973, no peak matched the calculated exact mass.

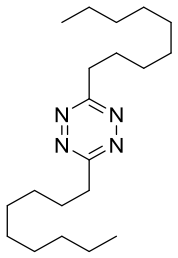

3l

3,6-dinonyl-1,2,4,5-tetrazine (3l): 3l was prepared according to the previously published procedure[24] from commercially available decanenitrile. The product was purified by flash column chromatography (ethyl acetate/hexane 1:20) to afford **3l**.

Physical Property: Red crystal, m.p. = 32-33 °C.

Isolated Yield: 40%

TLC: R_f = 0.75 (silica gel, ethyl acetate/hexane 1:4).

^{1}H NMR (500 MHz, $CDCl_3$) δ 3.27 (t, 4H, J = 7.7 Hz), 1.97-1.88 (m, 4H), 1.46-1.19 (m, 24H), 0.90-0.83 (m, 6H).

^{13}C NMR (125 MHz, $CDCl_3$) δ 170.2, 34.8, 31.9, 29.4, 29.3, 29.3, 29.2, 28.3, 22.7, 14.1.

IR (neat): 2928, 2856, 1458, 1395, 906, 731, 668 cm^{-1}.

HRMS (ESI) calculated for $C_{20}H_{39}N_4$ $[M+H]^+$ 335.3170, found 335.3180.

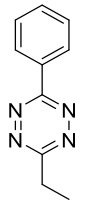

3m

3-ethyl-6-phenyl-1,2,4,5-tetrazine (3m): 3m was prepared according to the previously published procedure[24] from commercially available propionitrile and benzonitrile. The product was purified by flash column chromatography (ethyl acetate/hexane 1:12) to afford **3m**.

Physical Property: Red oil.

Isolated Yield: 69%

TLC: R_f = 0.57 (silica gel, ethyl acetate/hexane 1:4).

^{1}H NMR (500 MHz, $CDCl_3$) δ 8.57-8.53 (m, 2H), 7.58-7.52 (m, 3H), 3.36 (q, 2H, J = 7.6 Hz), 1.53 (t, 3H, J = 7.6 Hz).

^{13}C NMR (125 MHz, $CDCl_3$) δ 170.8, 164.2, 132.5, 131.9, 129.2, 127.9, 28.3, 12.3.

IR (neat): 1465, 1396, 1265, 1091, 898, 736, 692 cm^{-1}.

HRMS (ESI) calculated for $C_{10}H_{11}N_4$ $[M+H]^+$ 187.0980, no peak matched the calculated exact mass.

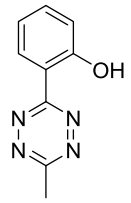

3n

2-(6-methyl-1,2,4,5-tetrazin-3-yl)phenol (3n): 3n was prepared according to the previously published procedure[24] from commercially available acetonitrile and 2-hydroxybenzonitrile. The product was purified by flash column chromatography (ethyl acetate/hexane 1:10) to afford **3n**.

Physical Property: Red crystal, m.p. = 63-64 °C.

Isolated Yield: 36%

TLC: R_f = 0.50 (silica gel, ethyl acetate/hexane 1:4).

^{1}H NMR (500 MHz, $CDCl_3$) δ 11.11 (bs, 1H), 8.64 (dd, 1H, J = 8.1, 1.7 Hz), 7.52 (ddd, 1H, J = 8.3, 7.2, 1.7 Hz), 7.14-7.05 (m, 2H), 3.12 (s, 3H).

^{13}C NMR (125 MHz, $CDCl_3$) δ 166.6, 164.9, 160.0, 135.1, 128.6, 120.3, 118.7, 114.1, 21.3.

IR (neat): 3053, 1618, 1585, 1484, 1402, 1265, 1234, 1085, 909, 759, 735 cm^{-1}.

HRMS (ESI) calculated for $C_9H_9N_4O$ $[M+H]^+$ 189.0772, no peak matched the calculated exact mass.

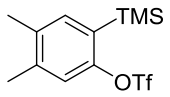

4b

4,5-dimethyl-2-(trimethylsilyl)phenyl trifluoromethanesulfonate (4b): 4b was obtained according to the literature procedures and ^{1}H NMR was matched with the literature.[36]

Isolated Yield: 82%.

^{1}H NMR (500 MHz, $CDCl_3$) δ 7.25 (s, 1H), 7.10 (s, 1H), 2.29 (s, 3H), 2.27 (s, 3H), 0.36 (s, 9H).

General procedure for the preparation of 4-nonyl-6-phenyl-6*H*-dibenzo[*de,g*]cinnoline (5a-5p): A vial was charged with 0.1 mmol of tetrazine **3a-3m** and 1 mmol of 2-(trimethylsilyl)phenyl trifluoromethanesulfonate **4a** (or 4,5-dimethyl-2-(trimethylsilyl)phenyl trifluoromethanesulfonate **4b**) in 0.1 mL of dichloromethane at 24˚C, and 1 M TBAF in THF (1.1 mmol) was slowly added to the solution over the course of 1 min. After the addition, the solution was concentrated in vacuo and purified by flash column chromatography to afford **5a-5p**.

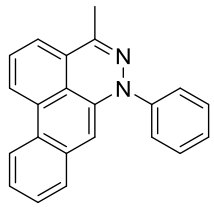

5a

4-methyl-6-phenyl-6*H*-dibenzo[*de,g*]cinnoline (5a): 5a was prepared according to the general procedure using **3a** and **4a**. The product was purified by flash column chromatography (ethyl acetate/hexane 1:20) to afford **5a**.

Physical Property: Yellow solid, m.p. = 145-146 °C.

Isolated Yield: 51%.

TLC: R_f = 0.60 (silica gel, ethyl acetate/hexane 1:4).

^{1}H NMR (500 MHz, CD_2Cl_2) δ 8.39 (d, 1H, J = 8.3 Hz), 8.34 (d, 1H, J = 8.2 Hz), 7.64-7.56 (m, 5H), 7.46-7.37 (m, 3H), 7.30 (ddd, 1H, J = 8.3, 6.2, 2.1 Hz), 7.26 (dd, 1H, J = 7.4, 0.9 Hz), 6.43 (s, 1H), 2.29 (s, 3H).

^{13}C NMR (125 MHz, CD_2Cl_2) δ 144.4, 142.6, 137.7, 134.3, 131.8, 130.3, 128.7, 127.9, 127.8, 127.1, 127.1, 126.3, 126.2, 124.3, 123.1, 123.0, 122.8, 118.2, 97.7, 19.1.

IR (neat): 3057, 2920, 2850, 1618, 1588, 1496, 1441, 1400, 1340, 1305, 1272, 1233, 1207, 1142, 1024, 807, 756, 744, 735, 699, and 644 cm^{-1}.

HRMS (ESI) calculated for $C_{22}H_{17}N_2$ $[M+H]^+$ 309.1387, found 309.1406.

Quantum Yield (Φ):

(a) 1.5 % of the neutral form.

(b) 27.7 % in the presence of 1073 equivalents of trifluoroacetic acid.

Extinction Coefficient (ε):

(a) 7362 ± 164 (417 nm), 16847 ± 348 (349 nm), 18285 ± 419 (269 nm), 34084 ± 214 (231 nm) for the neutral form.

(b) 7378 ± 181 (411 nm), 46894 ± 370 (230 nm) in the presence of of 1073 equivalents of trifluoroacetic acid.

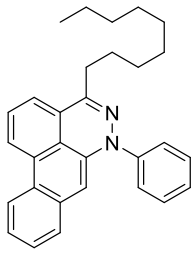

5b

4-nonyl-6-phenyl-6*H*-dibenzo[*de,g*]cinnoline (5b): 3b was prepared according to the general procedure using **3b** and **4a**. The product was purified by flash column chromatography (ethyl acetate/hexane 1:25) to afford **5b**.

Physical Property: Yellow solid, m.p. = 99-100 °C.

Isolated Yield: 41%.

TLC: R_f = 0.74 (silica gel, diethylether/hexane 1:4).

^{1}H NMR (500 MHz, CD_2Cl_2) δ 8.38 (d, 1H, J = 8.0 Hz), 8.34 (d, 1H, J = 8.1 Hz), 7.63-7.54 (m, 5H), 7.44-7.36 (m, 3H), 7.33-7.28 (m, 2H), 6.45 (s, 1H), 2.72-2.60 (m, 2H), 1.79-1.69 (m, 2H), 1.50-1.42 (m, 2H), 1.41-1.20 (m, 10H), 0.91-0.85 (m, 3H).

^{13}C NMR (125 MHz, CD_2Cl_2) δ 145.8, 144.5, 137.7, 134.3, 132.0, 130.3, 128.7, 127.8, 127.1, 127.0, 126.6, 125.7, 124.4, 123.1, 122.78, 122.76, 118.0, 97.6, 32.7, 32.3, 30.04, 30.01, 29.9, 29.8, 27.1, 23.1, 14.3.

IR (neat): 3050, 2925, 2852, 1616, 1588, 1496, 1461, 1442, 1399, 1338, 1301, 1264, 1232, 1206, 1142, 815, 738, 704, 668, and 649 cm^{-1}.

HRMS (ESI) calculated for $C_{30}H_{33}N_2$ $[M+H]^+$ 421.2639, found 421.2630.

Quantum Yield (Φ):

(a) 1.2% of the neutral form.

(b) 6.6% in the presence of 1048 equivalents of trifluoroacetic acid.

Extinction Coefficient (ε):

(a) 9205 ± 358 (419 nm), 15954 ± 109 (350 nm), 17336 ± 601 (269 nm), 34072 ± 342 (229 nm) for the neutral form.

(b) 7103 ± 16 (419 nm), 42445 ± 459 (229 nm) in the presence of 1048 equivalents of trifluoroacetic acid.

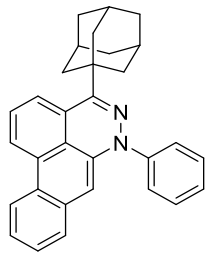

5c

4-((3*r*,5*r*,7*r*)-adamantan-1-yl)-6-phenyl-6*H*-dibenzo[*de*,*g*]cinnoline (5c): **5c** was prepared according to the general procedure using **1c** and **4a**. The product was purified by flash column chromatography (ethyl acetate/hexane 1:30) to afford **5c**.

Physical Property: Yellow oil.

Isolated Yield 10%.

TLC: R_f = 0.79 (silica gel, ethyl acetate/hexane 1:4).

^{1}H NMR (500 MHz, $CDCl_3$) δ 8.37 (m, 2H), 7.90 (d, 1H, J = 7.5 Hz), 7.66-7.52 (m, 5H), 7.44-7.36 (m, 3H), 7.31 (ddd, 1H, J = 8.3, 6.2, 1.7 Hz), 6.56 (s, 1H), 2.25-2.19 (m, 6H), 2.14 (bs, 3H), 1.90-1.80 (m, 6H).

^{13}C NMR (125 MHz, $CDCl_3$) δ 149.4, 144.3, 136.5, 133.5, 132.0, 129.6, 127.5, 127.30, 127.28, 126.9, 126.4, 125.7, 124.13, 123.9, 122.7, 122.3, 121.8, 120.1, 96.9, 40.5, 40.0, 37.0, 29.0.

IR (neat): 2903, 2848, 1612, 1584, 1494, 1440, 1392, 1339, 1288, 1233, 1144, 760, 736 cm^{-1}.

HRMS (ESI) calculated for $C_{31}H_{28}N_2$ $[M+H]^+$ 429.2326, found 429.2298.

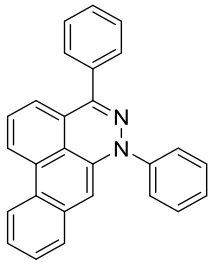

5d

4,6-diphenyl-6*H*-dibenzo[*de,g*]cinnoline (5d): 5d was prepared according to the general procedure using **3d** and **4a**. The product was purified by flash column chromatography (ethyl acetate/hexane 1:20) to afford **5d**.

Physical Property: Yellow solid, m.p. = 135-136 °C.

Isolated Yield 26%.

TLC: R_f = 0.53 (silica gel, diethylether/hexane 1:4).

^{1}H NMR (500 MHz, CD_2Cl_2) δ 8.37 (d, 1H, J = 8.0 Hz), 8.34 (d, 1H, J = 8.1 Hz), 7.65-7.60 (m, 4H), 7.59-7.54 (m, 2H), 7.53-7.37 (m, 7H), 7.33 (ddd, 1H, J = 8.2, 6.3, 2.1 Hz), 7.20 (dd, 1H, J = 7.5, 0.9 Hz), 6.45 (s, 1H).

^{13}C NMR (125 MHz, CD_2Cl_2) δ 146.0, 143.7, 137.2, 136.0, 133.8, 131.7, 129.9, 128.6, 128.53, 128.51, 128.1, 127.6, 127.5, 126.8, 126.4, 125.4, 124.2, 123.0, 122.6, 122.4, 119.4, 97.7.

IR (neat): 3052, 2918, 2848, 1614, 1586, 1492, 1458, 1441, 1398, 1320, 1237, 1145, 1129, 984, 816, 761, 735, and 698 cm^{-1}.

HRMS (ESI) calculated for $C_{27}H_{19}N_2$ $[M+H]^+$ 371.1543, found 371.1547.

Quantum Yield (Φ):

(a) 0.7% of the neutral form

(b) 8.1% in the presence of 1034 equivalents of trifluoroacetic acid.

Extinction Coefficient (ε):

(a) 4478 ± 140 (419 nm), 13669 ± 371 (357 nm), 18217 ± 536 (261 nm), 25145 ± 719 (242 nm) for the neutral form.

(b) 7346 ± 19 (417 nm), 25976 ± 371 (404 nm) in the presence of 1034 equivalents of trifluoroacetic acid.

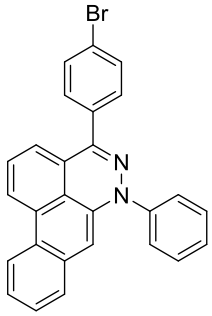

5e

4-(4-bromophenyl)-6-phenyl-6*H*-dibenzo[*de,g*]cinnoline (5e): 5e was prepared according to the general procedure using **3e** and **4a**. The product was purified by flash column chromatography (ethyl acetate/hexane 1:20) to afford **5e**.

Physical Property: Yellow solid, m.p. = 188-189 °C.

Isolated Yield 46%.

TLC: R_f = 0.59 (silica gel, diethylether/hexane 1:4).

^{1}H NMR (500 MHz, CD_2Cl_2) δ 8.37 (d, 1H, J = 8.3 Hz), 8.33 (d, 1H, J = 8.2 Hz), 7.65-7.38 (m, 12H), 7.33 (ddd, 1H, J = 8.1, 5.9, 2.4 Hz), 7.21 (dd, 1H, J = 7.4, 0.5 Hz), 6.45 (s, 1H).

^{13}C NMR (125 MHz, CD_2Cl_2) δ 144.8, 143.6, 137.1, 135.0, 133.7, 131.8, 131.7, 130.2, 129.9, 128.1, 127.7, 127.5, 126.92, 126.88, 126.5, 125.1, 124.2, 123.2, 122.7, 122.4, 122.4, 119.1, 98.0.

IR (neat): 3064, 2916, 2848, 2176, 1614, 1588, 1493, 1456, 1441, 1315, 1237, 1144, 1128, 1080, 1011, 984, 832, 757, 737, and 625 cm^{-1}.

HRMS (ESI) calculated for $C_{27}H_{18}BrN_2$ $[M+H]^+$ 449.0648, found 449.0643.

Quantum Yield (Φ):

(a) 0.5% of the neutral form.

(b) 6.9% in the presence of 1083 equivalents of trifluoroacetic acid.

Extinction Coefficient (ε):

(a) 5949 ± 130 (418 nm), 19021 ± 243 (358 nm), 34833 ± 827 (243 nm) for the neutral form.

(b) 7960 ± 63 (418 nm), 11769 ± 581 (356 nm), 40935 ± 701 (242 nm) in the presence of 1083 equivalents of trifluoroacetic acid.

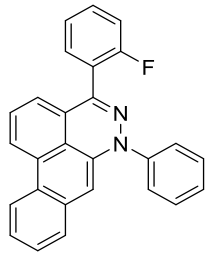

5f

4-(2-fluorophenyl)-6-phenyl-6*H*-dibenzo[*de,g*]cinnoline (5f): 5f was prepared according to the general procedure using **3f** and **4a**. The product was purified by flash column chromatography (ethyl acetate/hexane 1:20) to afford **5f**.

Physical Property: Yellow solid, m.p. = 80-81 °C.

Isolated Yield 19%.

TLC: R_f = 0.63 (silica gel, ethyl acetate/hexane 1:4).

^{1}H NMR (500 MHz, $CDCl_3$) δ 8.40-8.33 (m, 2H), 7.66-7.39 (m, 10H), 7.38-7.33 (m, 1H), 7.31 (td, 1H, J = 7.5, 1.2 Hz), 7.26-7.21 (m, 1H), 6.92 (ddd, 1H, J = 7.4, 2.9, 0.9 Hz).

^{13}C NMR (125 MHz, $CDCl_3$) δ 161.7, 159.7, 143.5, 141.7, 137.1, 133.7, 131.6, 131.43, 131.40, 130.73, 130.66, 130.0, 128.3, 127.8, 127.5, 126.9, 126.5, 125.5, 124.70, 124.67, 124.3, 123.7, 123.6, 123.2, 122.7, 122.4, 119.25, 119.23, 116.0, 115.8, 98.1.

^{19}F NMR (338 MHz, CD2Cl2) δ -113.3 to -113.4 (m, 1F).

IR (neat): 1738, 1373, 1238, 1045, 939, 918 cm^{-1}.

HRMS (ESI) calculated for $C_{27}H_{18}FN_2$ $[M+H]^+$ 389.1449, found 389.1454.

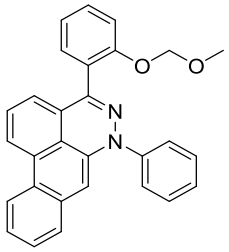

5g

4-(2-(methoxymethoxy)phenyl)-6-phenyl-6*H*-dibenzo[*de,g*]cinnoline (5g): 5g was prepared according to the general procedure using **3g** and **4a**. The product was purified by flash column chromatography (ethyl acetate/hexane 1:15) to afford **5g**.

Physical Property: Yellow oil.

Isolated Yield 25%.

TLC: R_f = 0.45 (silica gel, ethyl acetate/hexane 1:4).

^{1}H NMR (500 MHz, $CDCl_3$) δ 8.35 (dd, 2H, J = 8.6, 2.8 Hz), 7.66-7.61 (m, 2H), 7.60-7.54 (m, 2H), 7.51-7.38 (m, 6H), 7.33 (ddd, 1H, J = 8.3, 6.6, 1.7 Hz), 7.25 (d, 1H, J = 8.0 Hz), 7.14 (td, 1H, J = 7.6, 1.0 Hz), 6.84 (dd, 1H, J = 7.3, 0.7 Hz), 6.50 (s, 1H), 5.15 (m, 2H), 3.36 (s, 3H).

^{13}C NMR (125 MHz, $CDCl_3$) δ 155.6, 144.5, 143.7, 137.2, 133.8, 131.4, 130.9, 130.1, 129.8, 128.1, 127.5, 127.4, 126.8, 126.4, 126.3, 125.95, 125.90, 124.2, 123.0, 122.3, 122.2, 119.8, 114.8, 97.6, 94.7, 56.1.

IR (neat): 3053, 1587, 1493, 1453, 1440, 1398, 1319, 1264, 1234, 1153, 996, 735, 703 cm^{-1}.

HRMS (ESI) calculated for $C_{29}H_{23}N_2O_2$ $[M+H]^+$ 431.1755, found 431.1760.

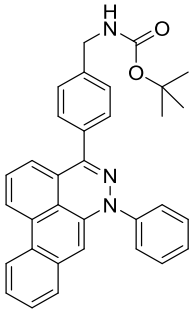

5h

***tert*-butyl (4-(6-phenyl-6*H*-dibenzo[*de,g*]cinnolin-4-yl)benzyl)carbamate (5h):** **5h** was prepared according to the general procedure using **3h** and **4a**. The product was purified by flash column chromatography (ethyl acetate/hexane 1:4) to afford **5h**.

Physical Property: Yellow solid, m.p. = 177-178 °C.

Isolated Yield: 31%.

TLC: R_f = 0.21 (silica gel, ethyl acetate/hexane 1:4).

^{1}H NMR (500 MHz, CD_2Cl_2) δ 8.40-8.25 (m, 2H), 7.67-7.56 (m, 5H), 7.55-7.49 (m, 1H), 7.48-7.38 (m, 5H), 7.34 (ddd, 1H, J = 8.3, 6.1, 2.2 Hz), 7.27 (d, 1H, J = 7.3 Hz), 6.47 (s, 1H), 5.03 (bs, 1H), 4.37 (d, 1H, J = 5.8 Hz), 1.48 (s, 9H).

^{13}C NMR (125 MHz, CD_2Cl_2) δ 155.8, 145.7, 143.7, 140.1, 137.2, 134.9, 133.8, 131.8, 129.9, 128.7, 128.1, 127.7, 127.5, 127.4, 126.9, 126.8, 126.5, 125.4, 124.2, 123.1, 122.6, 122.4, 119.5, 97.8, 79.2, 44.3, 28.1.

IR (neat): 3345, 2976, 1707, 1612, 1586, 1492, 1440, 1397, 1365, 1318, 1288, 1271, 1237, 1167, 1145, 1129,760, 737, 695 cm^{-1}.

HRMS (ESI) calculated for $C_{33}H_{30}N_3O_2$ $[M+H]^+$ 500.2333, found 500.2332.

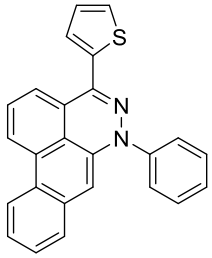

5i

6-phenyl-4-(thiophen-2-yl)-6*H*-dibenzo[*de,g*]cinnoline (5i): 5i was prepared according to the general procedure using **3i** and **4a**. The product was purified by flash column chromatography (ethyl acetate/hexane 1:20) to afford **5i**.

Physical Property: Red solid, m.p. = 139-140 °C.

Isolated Yield 52%.

TLC: R_f = 0.56 (silica gel, diethylether/hexane 1:4).

^{1}H NMR (500 MHz, CD_2Cl_2) δ 8.40 (d, 1H, J = 8.4 Hz), 8.35 (d, 1H, J = 8.1 Hz), 7.66 (dd, 1H, J = 7.5, 1.0 Hz), 7.64-7.53 (m, 6H), 7.48-7.38 (m, 4H), 7.34 (ddd, 1H, J = 8.2, 6.0, 2.2 Hz), 7.16 (dd, 1H, J = 5.1, 3.5 Hz), 6.47 (s, 1H).

^{13}C NMR (125 MHz, CD_2Cl_2) δ 143.9, 140.4, 138.8, 137.2, 134.1, 132.3, 130.4, 128.7, 128.3, 128.0, 127.5, 127.4, 127.3, 127.1, 126.9, 126.1, 125.4, 124.8, 123.8, 123.3, 122.9, 119.5, 98.8.

IR (neat): 3057, 2922, 2850, 1614, 1586, 1492, 1458, 1443, 1394, 1338, 1293, 1238, 1146, 1128, 947, 798, 752, 700, 694, and 674 cm^{-1}.

HRMS (ESI) calculated for $C_{25}H_{17}N_2S$ $[M+H]^+$ 377.1107, found 377.1099.

Quantum Yield (Φ):

(a) 0.6% of the neutral form.

(b) 1.5% in the presence of 1001 equivalents of trifluoroacetic acid.

Extinction Coefficient (ε):

(a) 4610 ± 20 (418 nm), 14238 ± 20 (362 nm), 27222 ± 192 (244 nm) for the neutral form.

(b) 6395 ± 318 (419 nm), 9607 ± 879 (360 nm), 31340 ± 27 (242 nm), 38234 ± 959 (228 nm) in the presence of 1001 equivalents of trifluoroacetic acid.

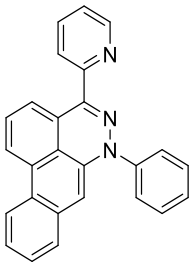

5j

6-phenyl-4-(pyridin-2-yl)-6*H*-dibenzo[*de,g*]cinnoline (5j): 5j was prepared according to the general procedure using **3j** and **4a**. The product was purified by flash column chromatography (ethyl acetate/hexane 1:4) to afford **5j**.

Physical Property: Orange solid, m.p. = 139-140 °C.

Isolated Yield 15%.

TLC: R_f = 0.12 (silica gel, diethylether/hexane 1:4).

^{1}H NMR (500 MHz, CD_2Cl_2) δ 8.70 (d, 1H, J = 4.5 Hz), 8.40 (d, 1H, J = 8.3 Hz), 8.37 (d, 1H, J = 8.2 Hz), 8.04 (d, 1H, J = 7.6 Hz), 7.81 (td, 1H, J = 7.7, 1.8 Hz), 7.76 (d, 1H, J = 7.9 Hz), 7.68-7.55 (m, 5H), 7.51-7.33 (m, 5H), 6.45 (s, 1H).

^{13}C NMR (125 MHz, CD_2Cl_2) δ 156.0, 148.8, 144.1, 143.8, 137.6, 137.3, 134.0, 132.1, 130.5, 128.6, 128.3, 127.9, 127.7, 127.3, 127.1, 125.01, 124.99, 123.74, 123.73, 123.6, 123.0, 122.8, 121.0, 98.7.

IR (neat): 3052, 2922, 1614, 1586, 1494, 1472, 1458, 1443, 1429, 1398, 1338, 1322, 1264, 1150, 1055, 997, 819, 736, 708, 698, and 645 cm^{-1}.

HRMS (ESI) calculated for $C_{26}H_{18}N_3$ $[M+H]^+$ 372.1496, found 372.1498.

Quantum Yield (Φ):

(a) 0.6% of the neutral form

(b) 0.0% in the presence of 1048 equivalents of trifluoroacetic acid.

Extinction Coefficient (ε):

(a) 1641 ± 46 (413 nm), 5306 ± 80 (361 nm), 17336 ± 601 (271 nm) for the neutral form.

(b) 1749 ± 100 (560 nm), 3857 ± 118 (365 nm), 26933 ± 133 (228 nm) in the presence of 1048 equivalents of trifluoroacetic acid.

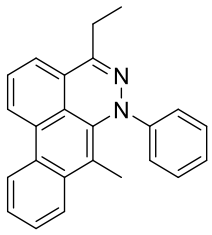

5k

4-ethyl-7-methyl-6-phenyl-6*H*-dibenzo[*de,g*]cinnoline (5k): 5k was prepared according to the general procedure using **3k** and **4a**. The product was purified by flash column chromatography (ethyl acetate/hexane 1:30) to afford **5k**.

Physical Property: Yellow solid, m.p. = 60-61 °C.

Isolated Yield: 44%.

TLC: R_f = 0.80 (silica gel, ethyl acetate/hexane 1:4).

^{1}H NMR (500 MHz, CD_2Cl_2) δ 8.53-8.48 (m, 2H), 7.87 (dd, 1H, J = 8.4, 0.6 Hz), 7.64-7.56 (m, 2H) 7.48 (ddd, 1H, J = 8.2, 7.0, 1.2 Hz), 7.40 (dd, 1H, J = 7.4, 0.8 Hz), 7.40-7.33 (m, 4H), 7.10 (tt, 1H, 6.8, 1.7 Hz), 2.82 (q, 2H, 7.4 Hz), 2.01 (s, 3H), 1.37 (t, 3H, 7.5 Hz)

^{13}C NMR (125 MHz, CD_2Cl_2) δ 149.7, 148.2, 134.3, 132.1, 129.6, 128.8, 127.3, 127.2, 126.9, 125.6, 123.5, 123.4, 122.9, 122.6, 121.2, 118.4, 109.2, 25.4, 16.9, 10.8.

IR (neat): 2916, 2849, 2360, 2342, 1587, 1485, 1446, 1388, 1372, 1335, 1283, 1265, 1231, 1212, 1138, 1032, 1012, 752, 737, 691, 668 cm^{-1}.

HRMS (ESI) calculated for $C_{24}H_{20}N_2$ $[M]^+$ 336.1621, found 336.1630.

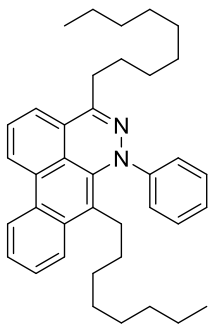

5l

4-nonyl-7-octyl-6-phenyl-6*H*-dibenzo[*de,g*]cinnoline (5l): 5l was prepared according to the general procedure using **3l** and **4a**. The product was purified by flash column chromatography (ethyl acetate/hexane 1:30) to afford **5l**.

Physical Property: Yellow oil.

Isolated Yield: 24%.

TLC: R_f = 0.80 (silica gel, ethyl acetate/hexane 1:4).

^{1}H NMR (500 MHz, CD_2Cl_2) δ 8.51 (d, 1H, J = 8.6 Hz), 8.48 (d, 1H, J = 8.2 Hz), 7.89 (d, 1H, J = 8.4 Hz), 7.63-7.58 (m, 1H), 7.55 (ddd, 1H, J = 8.5, 6.9, 1.3 Hz), 7.46 (ddd, 1H, J = 8.1, 6.9, 1.1 Hz), 7.43-7.38 (m, 3H), 7.36-7.30 (m, 2H), 7.10 (tt, 1H, J = 7.3, 1.1 Hz), 2.76 (t, 2H, J = 7.7 Hz), 2.59 (t, 2H, J = 7.6 Hz), 1.83-1.75 (m, 2H), 1.52-1.44 (m, 2H), 1.42-1.22 (m, 14H), 1.22-1.04 (m, 8H), 0.94-0.82 (m, 6H).

^{13}C NMR (125 MHz, CD_2Cl_2) δ 149.1, 148.9, 133.5, 132.1, 129.6, 129.0, 127.4, 127.0, 126.8, 126.2, 124.1, 123.89, 123.86, 123.4, 122.9, 122.8, 121.3, 118.5, 115.5, 32.2, 31.8, 31.8, 29.5, 29.5, 29.4, 29.32, 29.28, 29.19, 29.1, 28.2, 26.7, 22.67, 22.60, 13.84, 13.82.

IR (neat): 2954, 2924, 2853, 2361, 2340, 1586, 1490, 1438, 1386, 1332, 1281, 1264, 1228, 1211, 1136, 818, 755, 694, 612 cm^{-1}.

HRMS (ESI) calculated for $C_{38}H_{48}N_2$ $[M]^+$ 532.3812, found 532.3821.

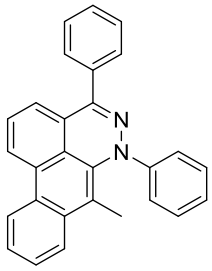

5m

7-methyl-4,6-diphenyl-6*H*-dibenzo[*de,g*]cinnoline (5m): 5m was prepared according to the general procedure using **3m** and **4a**. The product was purified by flash column chromatography (ethyl acetate/hexane 1:20) to afford **5m**.

Physical Property: Yellow oil.

Isolated Yield: 11%.

TLC: R_f = 0.61 (silica gel, ethyl acetate/hexane 1:4).

^{1}H NMR (500 MHz, CD_2Cl_2) δ 8.53-8.48 (m, 2H), 7.88 (dd, 1H, J = 8.3, 0.9 Hz), 7.68-7.63 (m, 2H), 7.59 (ddd, 1H, J = 8.3, 6.9, 1.3 Hz), 7.55-7.45 (m, 5H), 7.43-7.33 (m, 4H), 7.30 (dd, 1H, J = 7.5, 0.9 Hz), 7.13 (tt, 1H, 7.1, 1.5 Hz), 2.02 (s, 3H).

^{13}C NMR (125 MHz, CD_2Cl_2) δ 149.1, 148.1, 135.9, 134.5, 132.1, 129.8, 128.9, 128.82, 128.80, 128.5, 128.1, 127.5, 126.7, 125.7, 123.88, 123.86, 123.81, 123.6, 123.1, 122.7, 121.3, 120.6, 109.4, 16.8

IR (neat): 2916, 2849, 2348, 1594, 1489, 1460, 1445, 1372, 1138, 1031, 755, 696, 655, 644 cm^{-1}.

HRMS (ESI) calculated for $C_{28}H_{20}N_2$ $[M]^+$ 384.1621, found 384.1612.

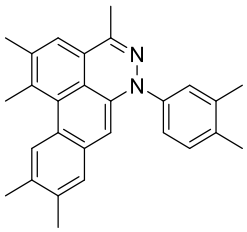

5n

6-(3,4-dimethylphenyl)-1,2,4,9,10-pentamethyl-6*H*-dibenzo[*de,g*]cinnoline (5n): **5n** was prepared according to the general procedure using **1a** and **4b**. The product was purified by flash column chromatography (ethyl acetate/hexane 1:20) to afford **5n**.

Physical Property: Yellow oil.

Isolated Yield: 24%.

TLC: R_f = 0.54 (silica gel, ethyl acetate/hexane 1:4).

^{1}H NMR (500 MHz, CD_2Cl_2) δ 8.20 (s, 1H), 7.33-7.25 (m, 2H), 7.25-7.20 (m, 1H), 7.16 (s, 1H), 7.12 (s, 1H), 6.21 (s, 1H), 2.85 (s, 3H), 2.54 (s, 3H), 2.41 (s, 3H), 2.36 (s, 3H), 2.34 (s, 3H), 2.33 (s, 3H), 2.27 (s, 3H).

^{13}C NMR (125 MHz, CD_2Cl_2) δ 142.0, 141.3, 138.5, 137.9, 137.0, 136.0, 135.8, 134.2, 133.7, 131.3, 130.7, 129.7, 128.2, 127.9, 126.3, 125.0, 124.0, 123.3, 123.0, 119.5, 96.7, 21.7, 21.6, 20.1, 19.6, 19.5, 19.22, 18.7.

IR (neat): 2916, 2857, 1606, 1502, 1449, 1372, 1300, 1235, 1194, 1170, 1086, 1014, 871, 803, 736 cm^{-1}.

HRMS (ESI) calculated for $C_{28}H_{28}N_2$ $[M]^+$ 392.2247, found 392.2252.

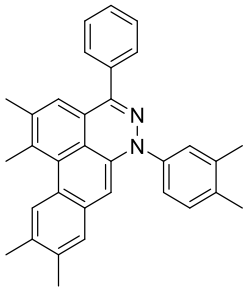

5o

6-(3,4-dimethylphenyl)-1,2,9,10-tetramethyl-4-phenyl-6*H*-dibenzo[*de,g*]cinnoline (5o): **5o** was prepared according to the general procedure using **3d** and **4b**. The product was purified by flash column chromatography (ethyl acetate/hexane 1:20) to afford **5o**.

Physical Property: Yellow oil.

Isolated Yield: 31%.

TLC: R_f = 0.59 (silica gel, ethyl acetate/hexane 1:4).

^{1}H NMR (500 MHz, CD_2Cl_2) δ 8.18 (s, 1H), 7.63-7.60 (m, 2H), 7.50-7.40 (m, 3H), 7.35-7.25 (m, 3H), 7.17 (s, 1H), 7.09 (s, 1H), 6.25 (s, 1H), 2.83 (s, 3H), 2.423 (s, 3H), 2.416 (s, 3H), 2.36 (s, 3H), 2.34 (s, 3H), 2.35-2.32 (m, 6H).

^{13}C NMR (125 MHz, CD_2Cl_2) δ 145.3, 141.8, 138.6, 137.9, 136.9, 136.4, 136.2, 136.0, 134.1, 133.9, 131.7, 130.7, 130.7, 130.1, 128.6, 128.5, 128.4, 128.2, 127.6, 126.4, 126.2, 123.8, 123.6, 122.4, 121.1, 29.7, 21.5, 20.1, 19.6, 19.4, 19.2.

IR (neat): 2921, 1603, 1500, 1418, 1300, 1264, 1227, 1141, 1068, 1005, 878, 831, 738, 687 cm^{-1}.

HRMS (ESI) calculated for $C_{33}H_{30}N_2$ $[M]^+$ 454.2404, found 454.2403.

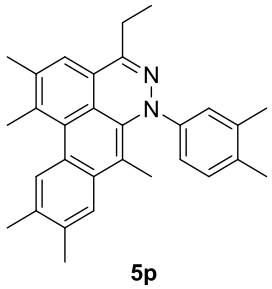

5p

6-(3,4-dimethylphenyl)-4-ethyl-1,2,7,9,10-pentamethyl-6*H*-dibenzo[*de,g*]cinnoline (5p): **5p** was prepared according to the general procedure using **3k** and **4b**. The product was purified by flash column chromatography (ethyl acetate/hexane 1:20) to afford **5p**.

Physical Property: Yellow oil.

Isolated Yield: 30%.

TLC: R_f = 0.69 (silica gel, ethyl acetate/hexane 1:4).

^{1}H NMR (500 MHz, CD_2Cl_2) δ 8.22 (s, 1H), 7.55 (s, 1H), 7.27 (s, 1H), 7.11 (d, 1H, J = 2.3 Hz), 7.04 (d, 1H, J = 8.2 Hz), 6.92 (dd, 1H, J = 8.2, 2.3 Hz), 2.85 (s, 3H), 2.79 (q, 2H, J = 7.4 Hz), 2.55 (s, 3H), 2.48 (s, 3H), 2.46 (s, 3H), 2.242 (s, 3H), 2.237 (s, 3H), 1.91 (s, 3H), 1.33 (3H, t, 7.4 Hz).

^{13}C NMR (125 MHz, CD_2Cl_2) δ 148.6, 146.6, 137.2, 136.7, 135.8, 134.9, 133.9, 131.8, 131.6, 130.4, 129.7, 129.5, 128.9, 126.8, 124.7, 123.0, 122.7, 120.7, 120.5, 118.7, 108.2, 25.5, 21.7, 21.6, 20.1, 20.0, 19.9, 19.0, 16.8, 11.3.

IR (neat): 2968, 2917, 1607, 1594, 1499, 1488, 1453, 1357, 1264, 1195, 1166, 1002, 865, 820, 737 cm^{-1}.

HRMS (ESI) calculated for $C_{30}H_{32}N_2$ $[M]^+$ 420.2560, found 420.2550.

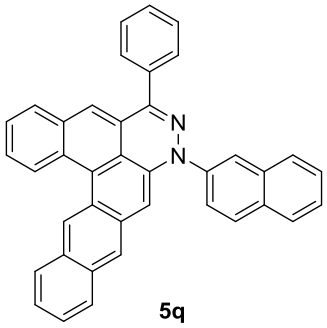

5q

8-(naphthalen-2-yl)-6-phenyl-8*H*-dinaphtho[3,2,1-*de*:2',3'-*g*]cinnoline (5q): A vial was charged with 14.8 mg (0.086 mmol) of **3d** and 300 mg (0.86 mmol) of 3-(trimethylsilyl)-2-naphthyl trifluoromethanesulfonate in 0.09 mL of dichloromethane at 24˚C, and 1 M TBAF in THF (0.95 mL, 0.95 mmol) was slowly added to the solution over the course of 1 min. After the addition, the solution was concentrated in vacuo, and fiterated on the silica gel, and purified by preparative TLC using ethyl acetate/hexane (1:10) as the eluent to give 0.61 mg of **5q**.

Physical Property: Red solid.

Isolated Yield: 1 %.

TLC: R_f = 0.50 (silica gel, ethyl acetate/hexane 1:4).

^{1}H NMR (500 MHz, CD_2Cl_2) δ 9.43 (s, 1H), 9.18 (d, 1H, J = 8.6 Hz), 8.21 (s, 1H), 8.15-7.94 (m, 6H), 7.90 (d, 1H, J = 8.0 Hz), 7.88-7.44 (m, 13H), 7.01 (s, 1H).

^{13}C NMR (125 MHz, CD_2Cl_2) δ 146.3, 141.9, 136.78, 136.73, 134.7, 134.6, 133.5, 133.1, 132.9, 131.3, 130.9, 130.2, 129.7, 129.4, 129.3, 129.2, 129.1, 128.7, 128.5, 128.31, 128.26, 128.0, 127.8, 127.4, 127.3, 127.1, 126.9, 126.8, 125.8, 125.5, 125.4, 124.8, 124.2, 124.0, 122.8, 122.0, 101.2.

HRMS (ESI) calculated for $C_{38}H_{48}N_2$ $[M]^+$ 520.1934, found 520.1930.

Quantum Yield (Φ):

(a) 6.7% of the neutral form.

(b) 2.0% in the presence of 1001 equivalents of trifluoroacetic acid.

Extinction Coefficient (ε):

(a) 2061 ± 339 (532 nm), 1850 ± 355 (501 nm), 9469 ± 57 (362 nm), 8663 ± 100 (340 nm), 23217 ± 698 (266 nm), 23141 ± 720 (257 nm) for the neutral form.

(b) 2290 ± 519 (524 nm), 15500 ± 793 (279 nm) in the presence of 1001 equivalents of trifluoroacetic acid.

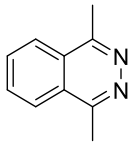

6

1,4-dimethylphthalazine (6): A vial was charged with 400 mg (4 mmol) of **1a** and 0.48 mL (2 mmol) of **2** in 2.0 mL of dichloromethane at 24 °C, and 1 M TBAF in THF (2.2 mmol, 1.1 mL) was slowly added to the solution over the course of 1 min. After the addition, the solution was concentrated in vacuo, and filtered on the silica gel, and purified by flash column chromatography (ethyl acetate = 100%) to afford 23 mg of **4**. The data for this compound was previously reported in the literature.[37]

Physical Property: White solid.

Isolated Yield: 7 %.

TLC: R_f = 0.10 (silica gel, 100% ethyl acetate).

^{1}H NMR (500 MHz, $CDCl_3$)

δ 8.03 (dd, 2H, J = 6.3, 3.3 Hz), 7.86 (dd, 2H, J = 6.3, 3.3 Hz), 2.93 (s, 6H).

^{13}C NMR (125 MHz, $CDCl_3$)

δ 156.26, 131.80, 125.85, 124.79, 19.76.

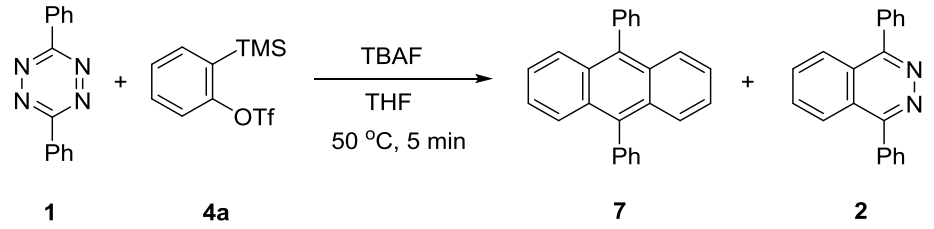

1 **4a** **7** **2**

9,10-diphenylanthracene (7) and 1,4-diphenylphthalazine (2): A vial was charged with 23.4 mg (0.1 mmol) of **1** and 298.4 mg (1 mmol) of **4a** in 0.1 mL of THF at 24 ˚C, and 1 M TBAF in THF (1.1 mmol, 1.1 mL) was added to the solution. After the addition, the solution was heated to 50 °C for 2 hours and athen was concentrated in vacuo, and filtered on the silica gel, and purified by flash column chromatography (ethyl acetate/hexane 1:4) to afford 10 mg of **7** and 8 mg of **2**. The data for these compounds were previously reported in the literature.[38,39]

9,10-diphenylanthracene (7)

Physical Property: White solid.

Isolated Yield: 30 %.

TLC: R_f = 0.79 (silica gel, ethyl acetate/hexane 1:4).

^{1}H NMR (500 MHz, $CDCl_3$)

δ 7.72-7.68 (m, 4H), 7.63-7.53 (m, 6H), 7.51-7.47 (m, 4H), 7.35-7.31 (m, 4H).

1,4-diphenylphthalazine (2)

Physical Property: White solid.

Isolated Yield: 28 %.

TLC: R_f = 0.11 (silica gel, silica gel, ethyl acetate/hexane 1:4).

^{1}H NMR (500 MHz, $CDCl_3$)

δ 8.17-8.12 (m, 4H), 7.87-7.79 (m, 6H), 7.62-7.54 (m, 6H).

2.5 Acknowledgments

This work was supported by funding from the University of Pennsylvania. We thank Pat Carroll for X-ray crystallographic assistance. Instruments supported by the National Science Foundation and the National Institutes of Health include HRMS (Grant NIH RR-023444) and X-ray diffractometer (Grant CHE-0840438).

2.6 References

(1) Rarig, R.-A. F.; Tran, M. N.; Chenoweth, D. M. *J. Am. Chem. Soc.*, **2013**, *135*, 9213–9219.

(2) Barros, S. A.; Chenoweth, D. M.; *Angew. Chemie Int. Ed.*, **2014**, *53*, 13746–13750.

(3) Tambar, U. K.; Stoltz, B. M. *J. Am. Chem. Soc.*, **2005**, *127*, 5340–5341.

(4) Gilmore, C. D.; Allan, K. M.; Stoltz, B. M. *J. Am. Chem. Soc.*, **2008**, *130*, 1558–1559.

(5) Tadross, P. M.; Gilmore, C. D.; Bugga, P.; Virgil, S. C.; Stoltz, B. M. *Org. Lett.*, **2010**, *12*, 1224–1227.

(6) Allan, K. M.; Gilmore, C. D.; Stoltz, B. M. *Angew. Chemie Int. Ed.*, **2011**, *50*, 4488–

4491.

(7) Bronner, S. M.; Bahnck, K. B.; Garg, N. K. *Org. Lett.*, **2009**, *11*, 1007–1010.

(8) Goetz, A. E.; Garg, N. K. *J. Org. Chem.*, **2014**, *79*, 846–851.

(9) Hoffmann, R. W.; Suzuki, K. *Angew. Chemie Int. Ed.*, **2013**, *52*, 2655–2656.

(10) Bhojgude, S. S.; Biju, A. T. *Angew. Chem. Int. Ed.*, **2012**, *51*, 1520–1522.

(11) Niu, D.; Willoughby, P. H.; Woods, B. P.; Baire, B.; Hoye, T. R. *Nature*, **2013**, *501*, 531–534.

(12) Niu, D.; Hoye, T. R. *Nat. Chem.*, **2014**, *6*, 34–40.

(13) Gampe, C. M.; Carreira, E. M. *Angew. Chem. Int. Ed.*, **2012**, *51*, 3766–3778.

(14) Bhunia, A.; Yetra, S. R.; Biju, A. T. *Chem. Soc. Rev.*, **2012**, *41*, 3140–3152.

(15) Dubrovskiy, A. V.; Markina, N. A.; Larock, R. C. *Org. Biomol. Chem.*, **2013**, *11*, 191–218.

(16) Allan, K. M.; Stoltz, B. M. *J. Am. Chem. Soc.*, **2008**, *130*, 17270–17271.

(17) Tadross, P. M.; Virgil, S. C.; Stoltz, B. M. *Org. Lett.*, **2010**, *12*, 1612–1614.

(18) Tadross, P. M.; Stoltz, B. M. *Chem. Rev.*, **2012**, *112*, 3550–3577.

(19) Goetz, A. E.; Silberstein, A. L.; Corsello, M. A.; Garg, N. K. *J. Am. Chem. Soc.*, **2015**, *136*, 3036–3039.

(20) Quasdorf, K. W.; Huters, A. D.; Lodewyk, M. W.; Tantillo, D. J.; Garg, N. K. *J. Am. Chem. Soc.*, **2012**, *134*, 1396–1399.

(21) Mizukoshi, Y.; Mikami, K.; Uchiyama, M. *J. Am. Chem. Soc.*, **2014**, *137*, 74–77.

(22) Peña, D.; Escudero, S.; Pérez, D.; Guitián, E.; Castedo, L. *Angew. Chem., Int. Ed.*, **1998**, *37*, 2659–2661.

(23) Sauer, J.; Heinrichs, G. *Tetrahedron Lett.*, **1966**, *7*, 4979–4984.

(24) Yang, J.; Karver, M. R.; Li, W.; Sahu, S.; Devaraj, N. K. *Angew. Chemie Int. Ed.*, **2012**, *51*, 5222–5225.

(25) Bronner, S. M.; Garg, N. K. *J. Org. Chem.*, **2009**, *74*, 8842–8843.

(26) Himeshima, Y.; Sonoda, T.; Kobayashi, H. *Chem. Lett.*, **1983**, 1211–1214.

(27) Choi, Y. L.; Kim, J. K.; Choi, S.-U.; Min, Y.-K.; Bae, M.-A.; Kim, B. T.; Heo, J.-N. *Bioorg. Med. Chem. Lett.*, **2009**, *19*, 3036–3040.

(28) Zhang, A.; Zhang, Y.; Branfman, A. R.; Baldessarini, R. J.; Neumeyer, J. L. *J. Med.*

Chem., **2007**, *50*, 171–181.

(29) Castedo, L.; Guitian, E.; Saá, C.; Suau, R.; Saá, J. M. *Tetrahedron Lett.*, **1983**, *24*, 2107–2108.

(30) Medina, J. M.; Mackey, J. L.; Garg, N. K.; Houk, K. N. **2014**, *136*, 15798–15805.

(31) Carboni, R. A.; Lindsey, R. V., Jr. *J. Am. Chem. Soc.* **1959**, *81*, 4342–4346.

(32) Skorianetz, W.; Kováts, E. Sz. *Helv. Chim. Acta* **1971**, *54*, 1922–1939.

(33) Counotte-Potman, A.; Van der Plas, H. C.; Van Veldhuizen, B. *J. Org. Chem.* **1981**, *46*, 2138–2141.

(34) Weininger, S. J.; Thornton, E. R. *J. Am. Chem. Soc.* **1967**, *89*, 2050–2054.

(35) Hu, W. X.; Xu, F. *J. Heterocycl. Chem.* **2008**, *45*, 1745–1750.

(36) Biju, A. T.; Glorius, F. *Angew. Chem. Int. Ed.* **2010**, *49*, 9761–9764.

(37) Bhattacharjee, D.; Popp, F. D. *J. Heterocycl. Chem.* **1980**, *17*, 433–437

(38) Yagodkin, E.; Douglas, C. J. *Tetrahedron Lett.* **2010**, *51*, 3037–3040.

(39) Li, J.; Gao, J.; Xiong, W.-W.; Zhang, Q. *Tetrahedron Lett.* **2014**, *55*, 4346–4349.

Appendix 1

NMR Spectra, Absorption, Emission, Exitation Spectra, X-Ray Structure Data Relevant to Chapter 2

Figure A1.1. ^{1}H NMR spectrum of **2** in $CDCl_3$ (500 MHz).

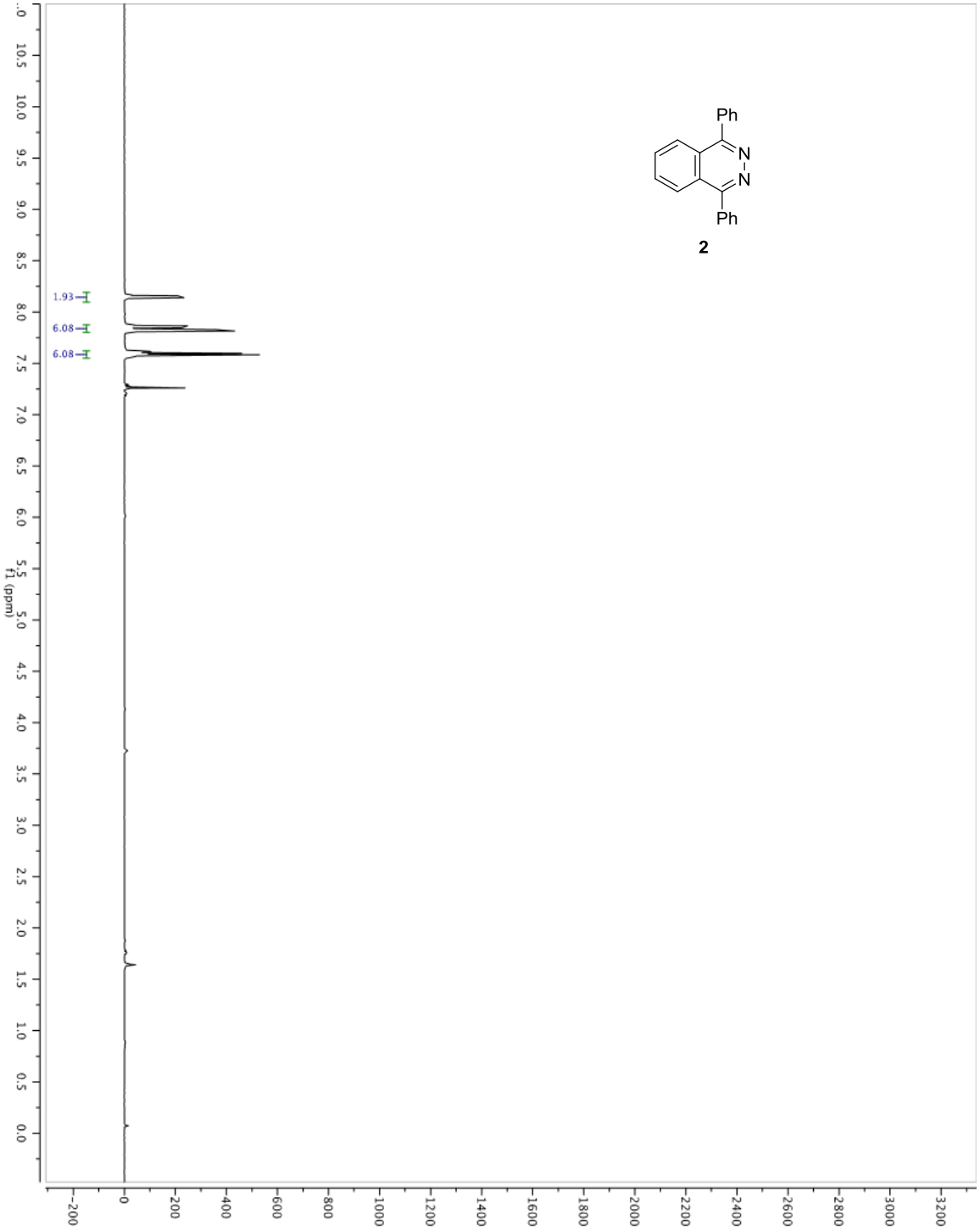

Figure A1.2. ^{1}H NMR spectrum of **3a** in $CDCl_3$ (500 MHz).

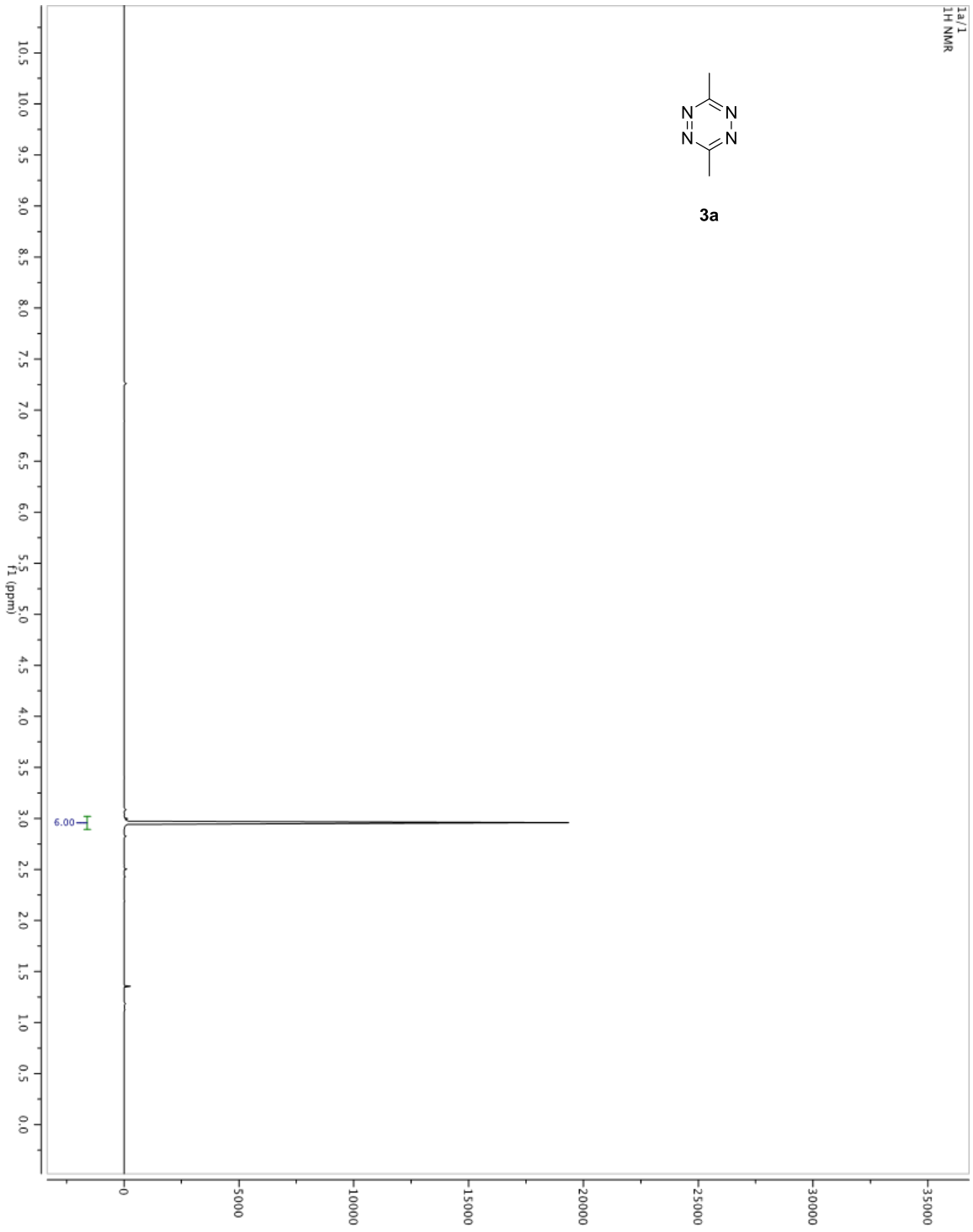

Figure A1.3. ^{13}C NMR spectrum of **3a** in $CDCl_3$ (125 MHz).

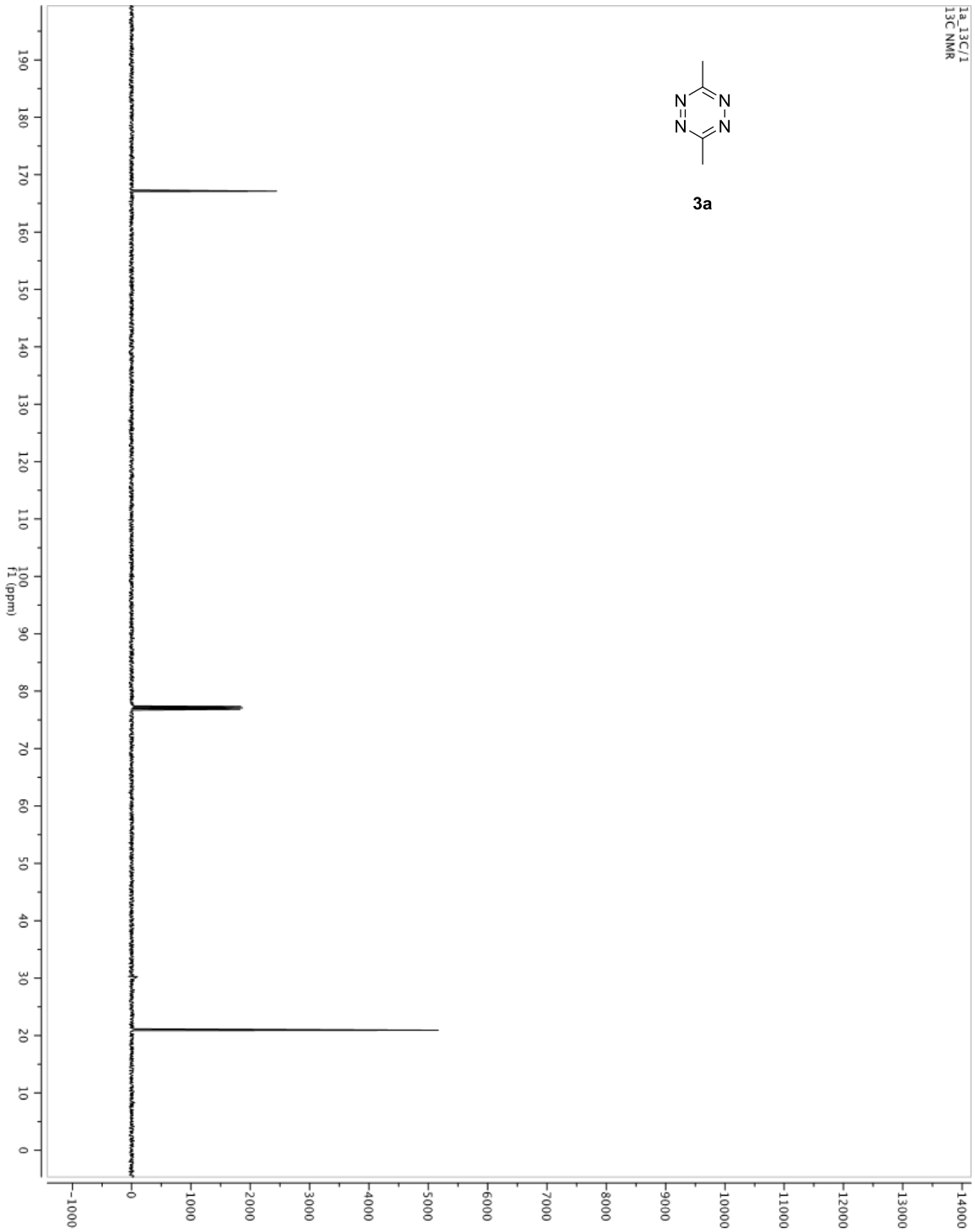

Figure A1.4. ^{1}H NMR spectrum of **3b** in $CDCl_3$ (500 MHz).

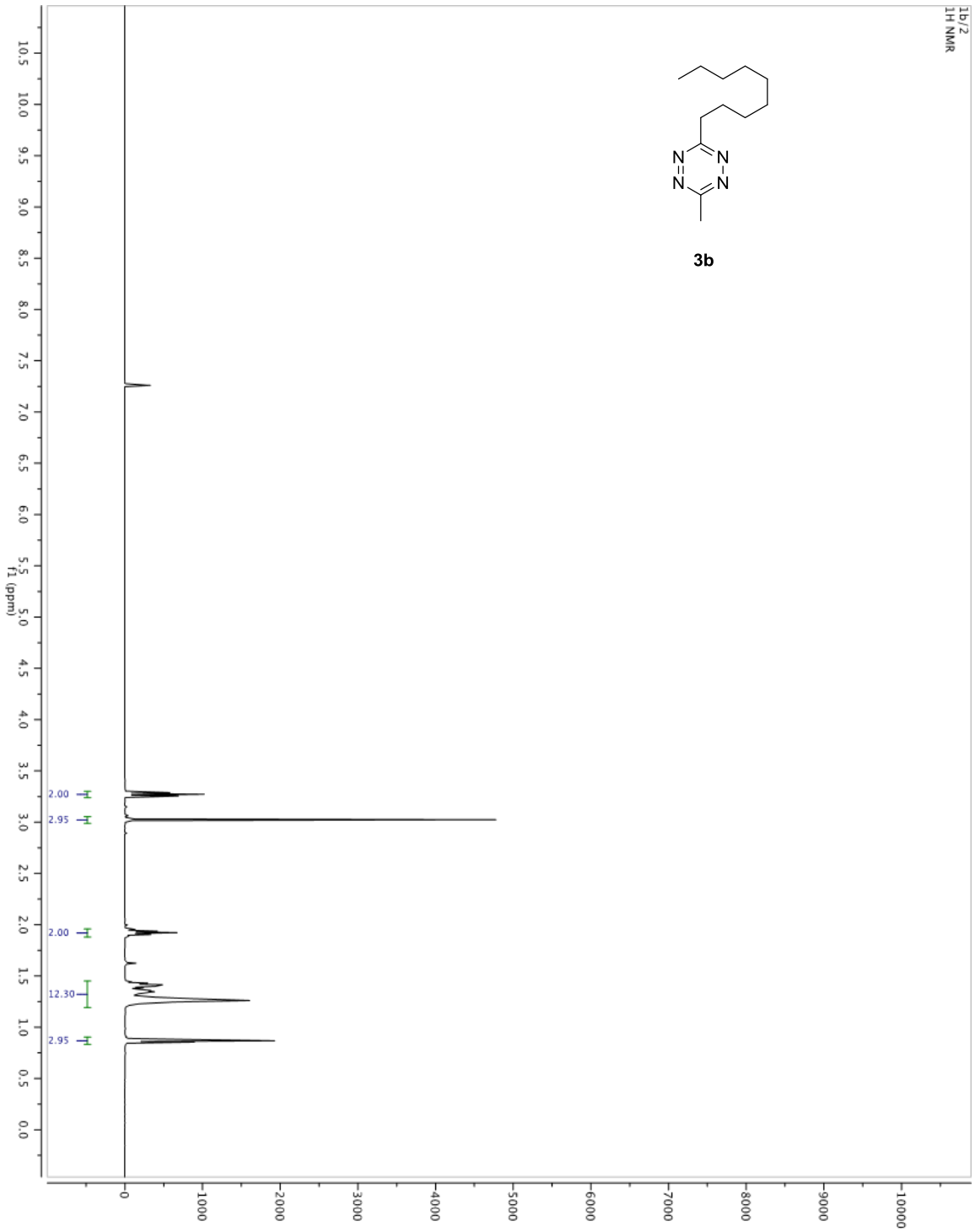

Figure A1.5. ^{13}C NMR spectrum of **3b** in $CDCl_3$ (125 MHz).

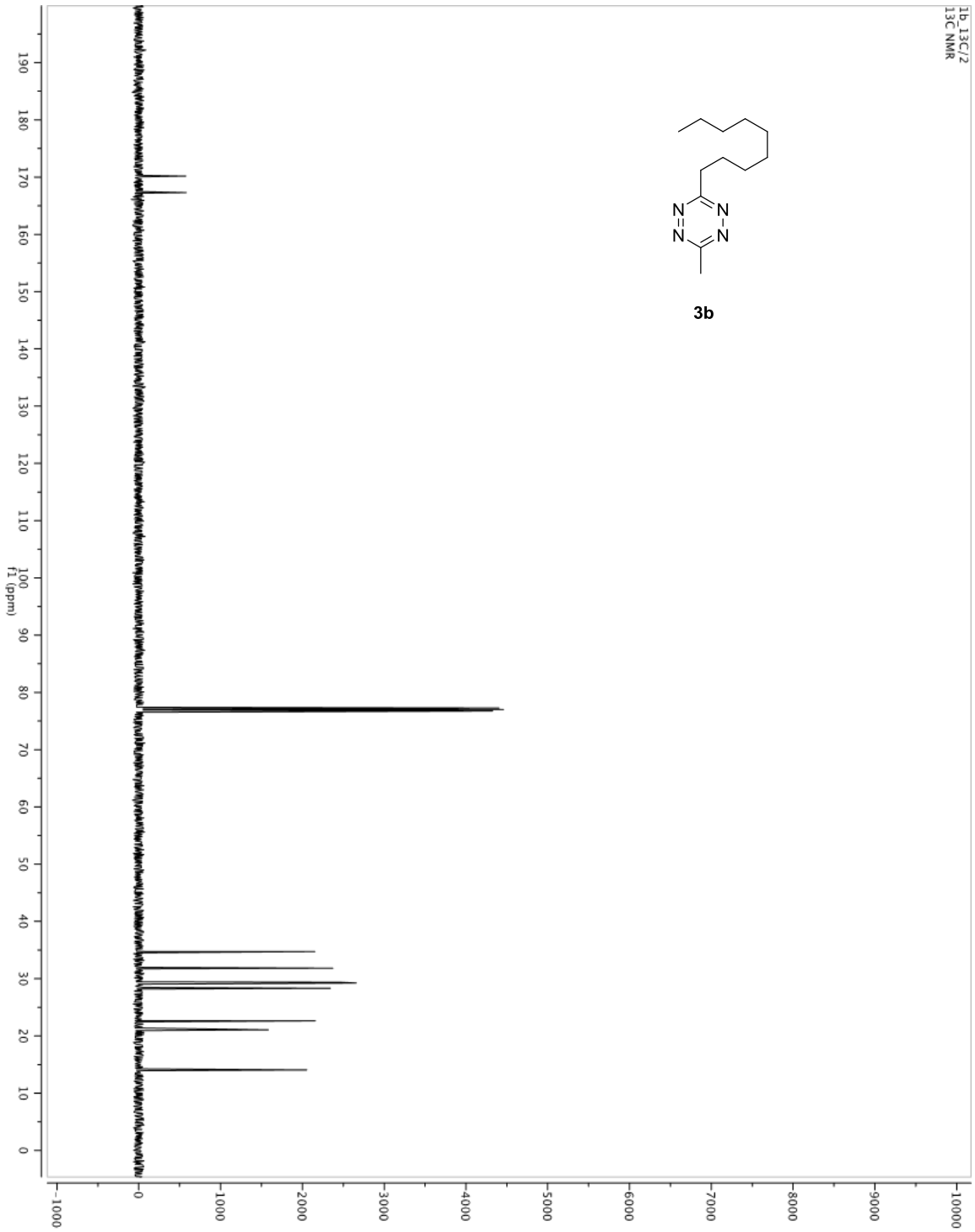

Figure A1.6. ^{1}H NMR spectrum of **3c** in $CDCl_3$ (500 MHz).

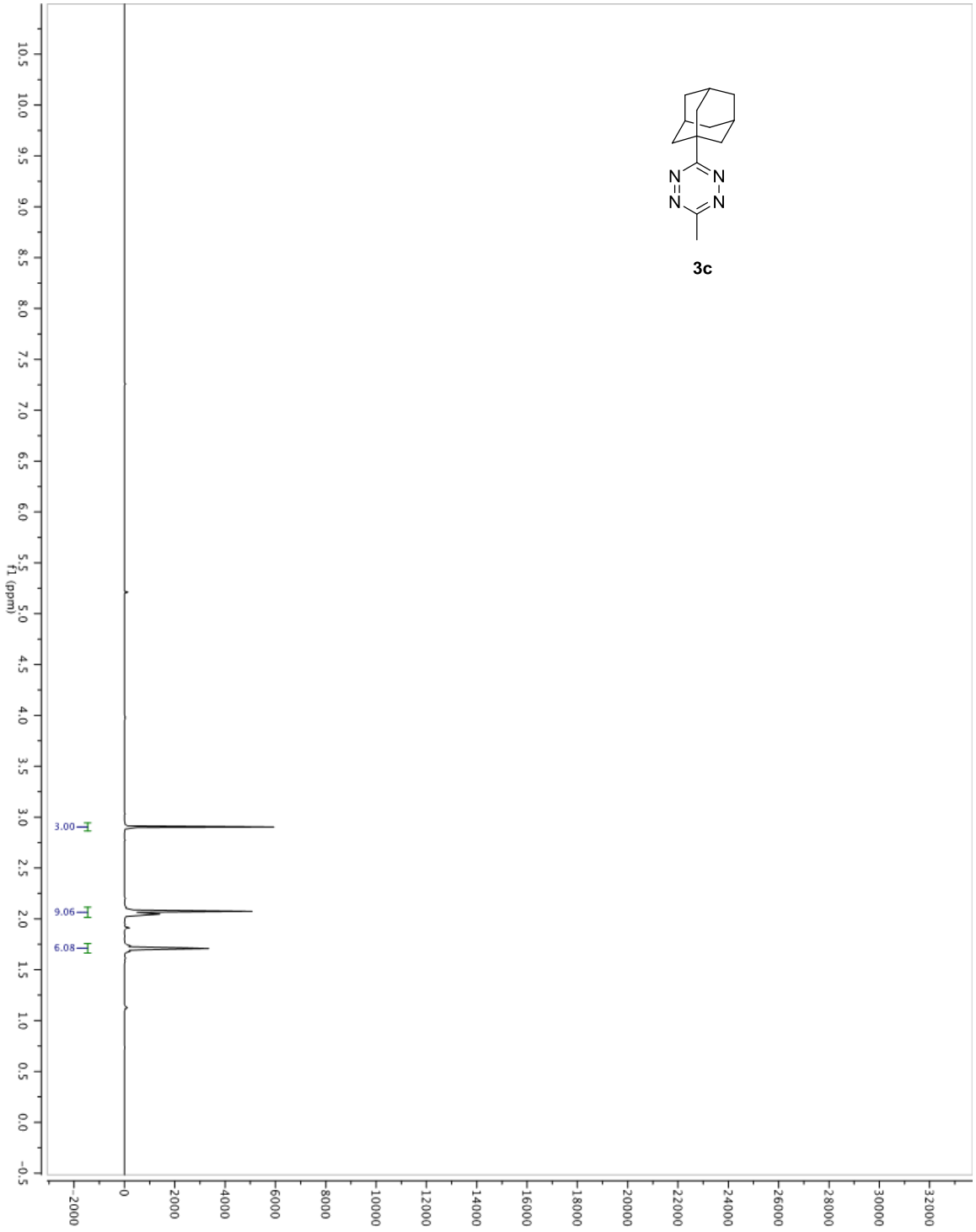

Figure A1.7. ^{13}C NMR spectrum of **3c** in $CDCl_3$ (125 MHz).

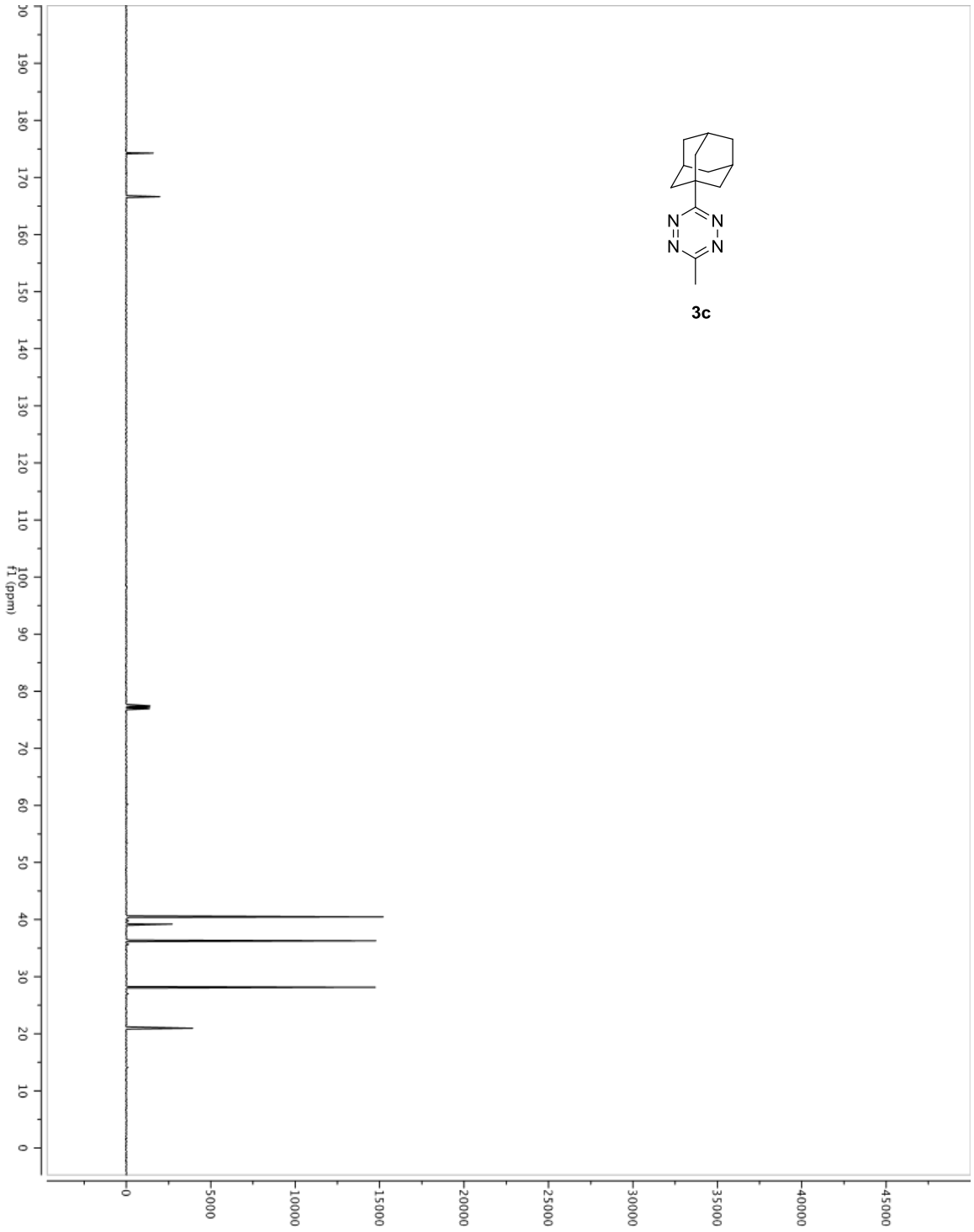

Figure A1.8. ^{1}H NMR spectrum of **3d** in $CDCl_3$ (500 MHz).

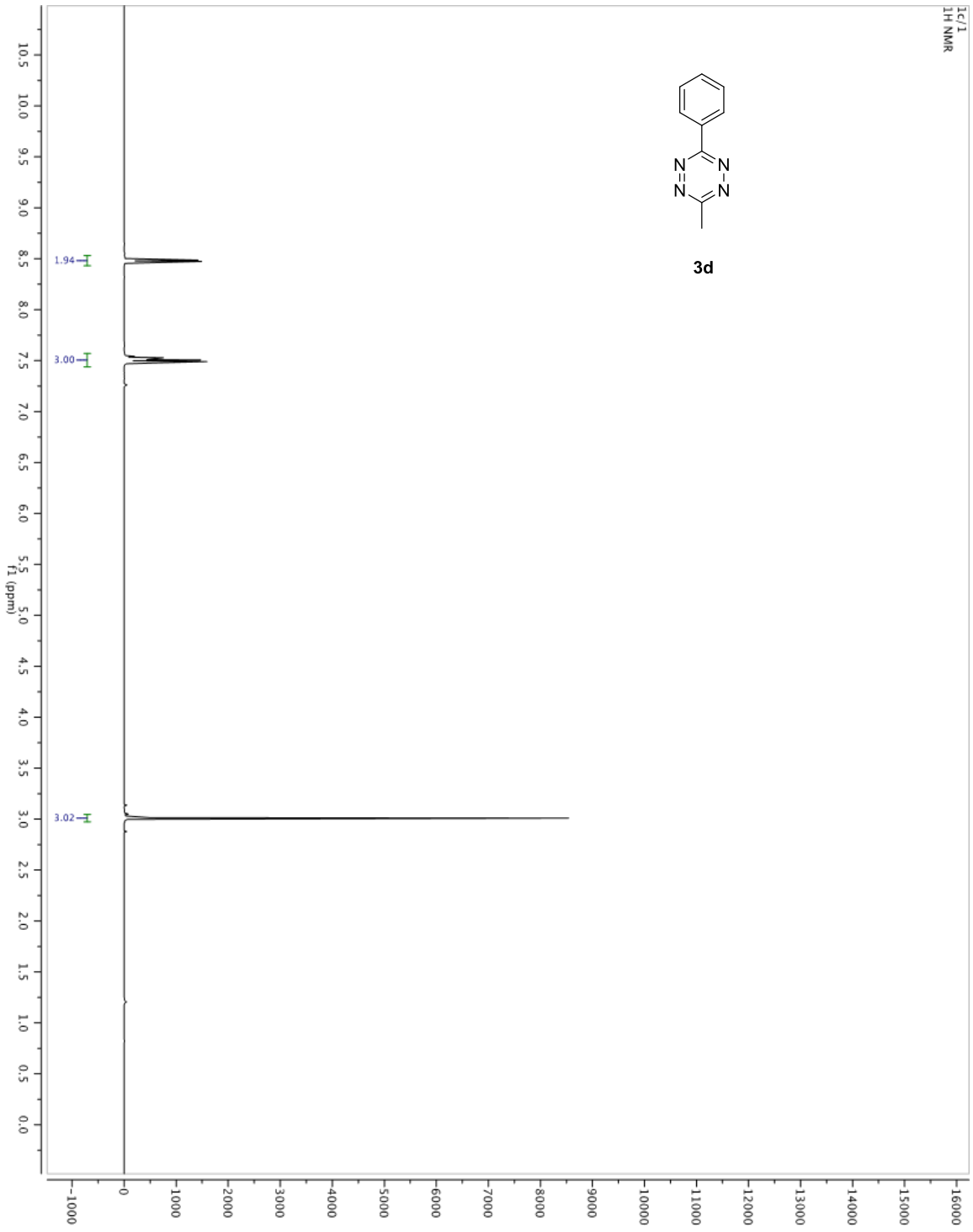

Figure A1.9. ^{13}C NMR spectrum of **3d** in $CDCl_3$ (125 MHz).

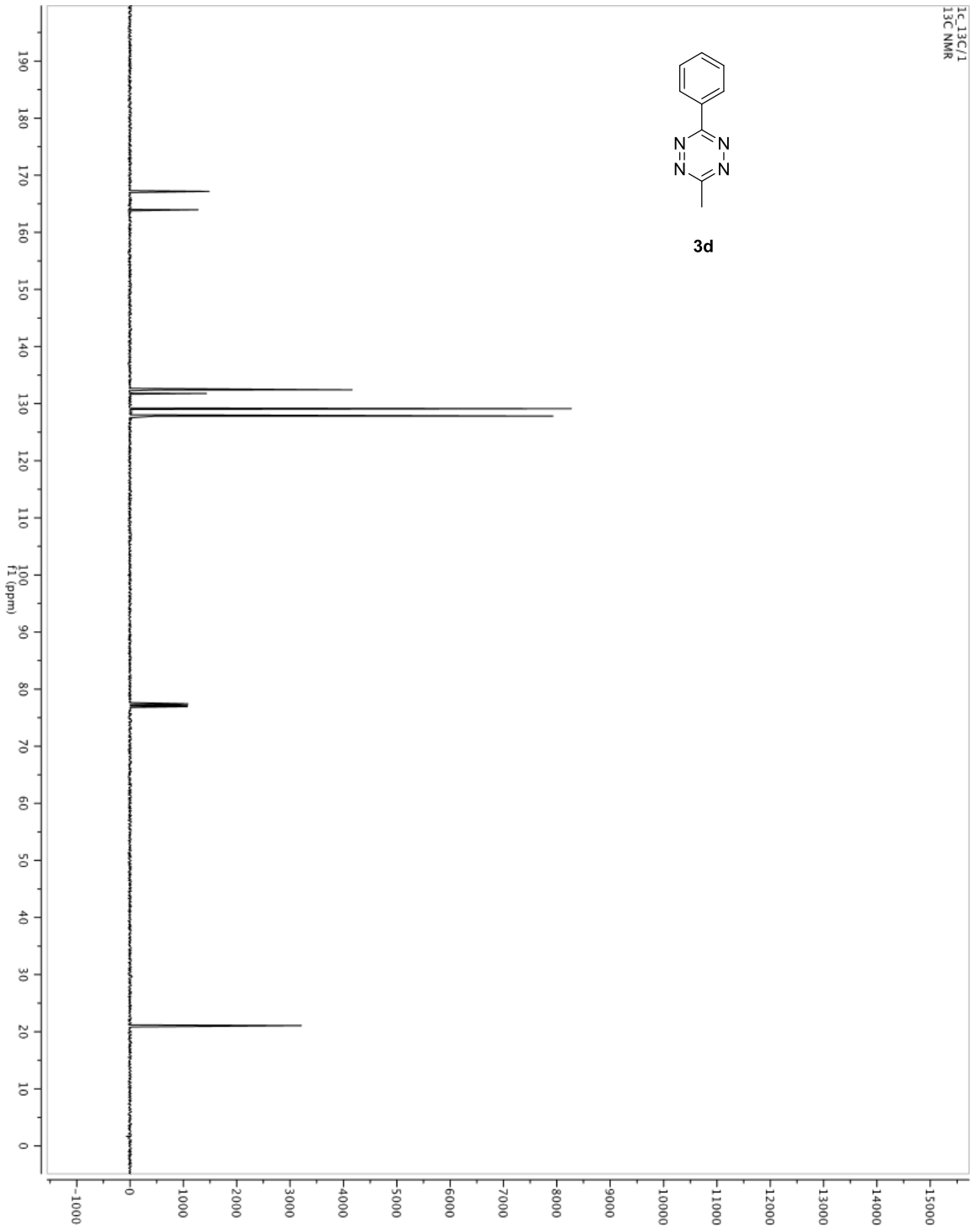

Figure A1.10. ^{1}H NMR spectrum of **3e** in $CDCl_3$ (500 MHz).

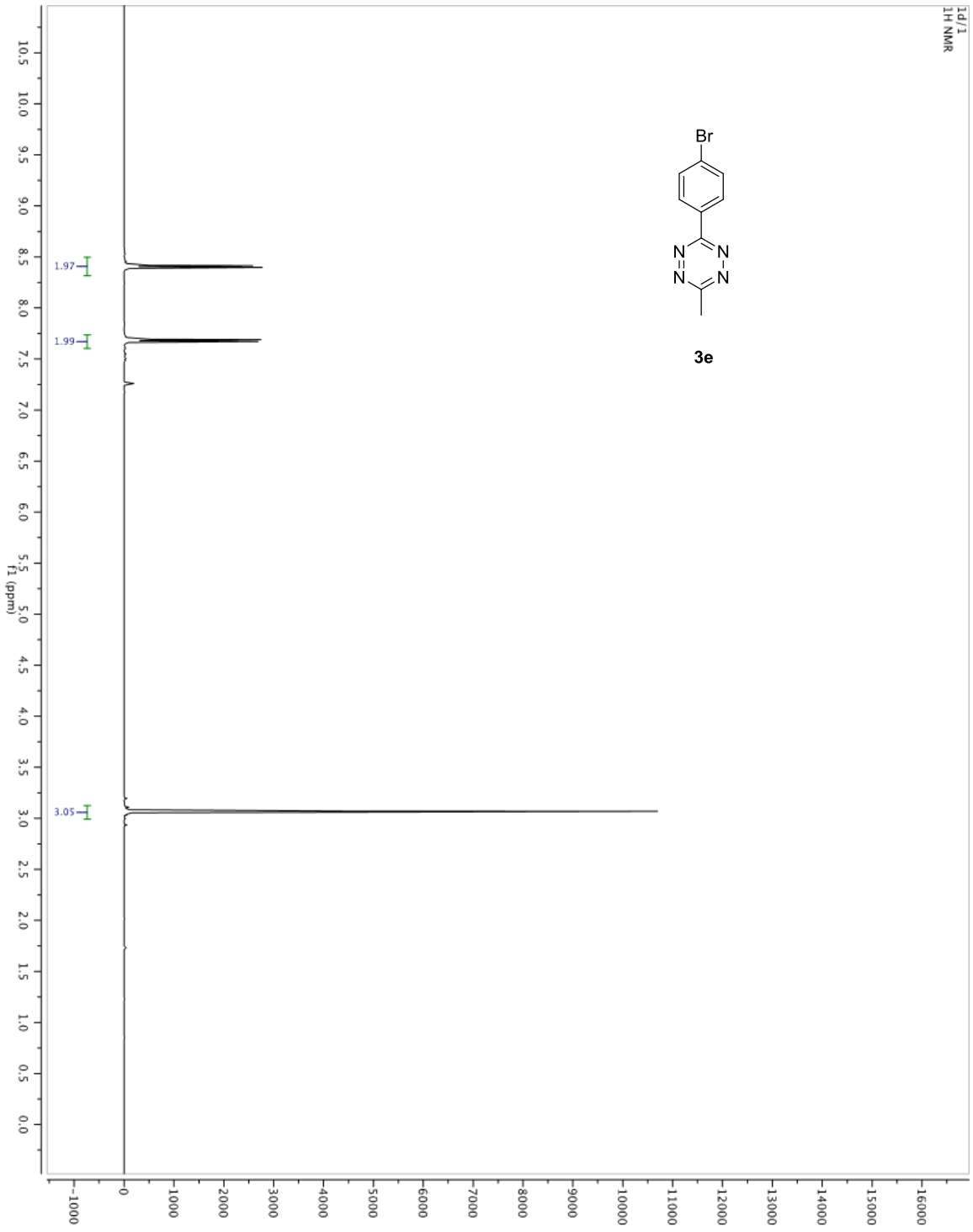

Figure A1.11. ^{13}C NMR spectrum of **3e** in $CDCl_3$ (125 MHz).

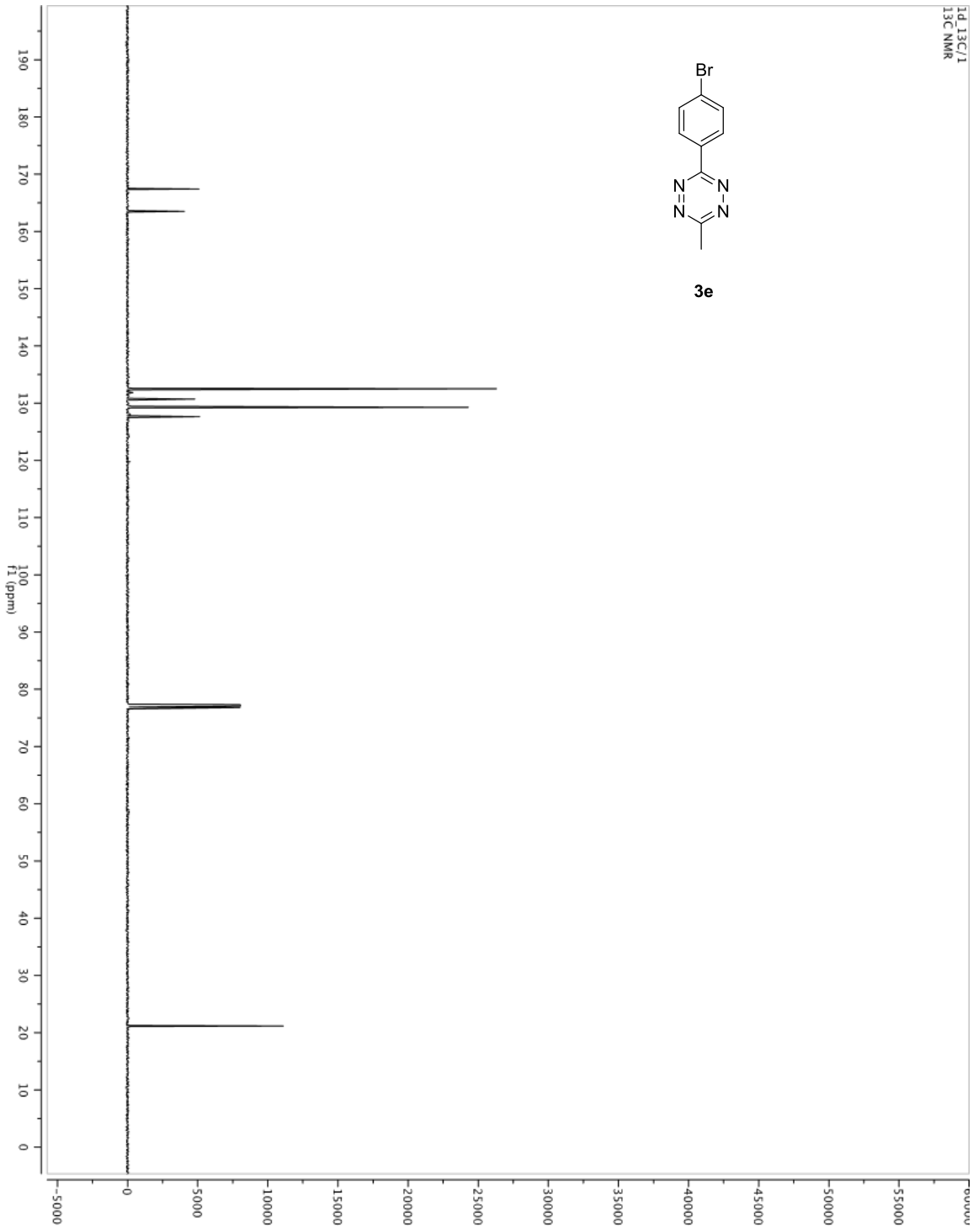

Figure A1.12. ^{1}H NMR spectrum of **3f** in $CDCl_3$ (500 MHz).

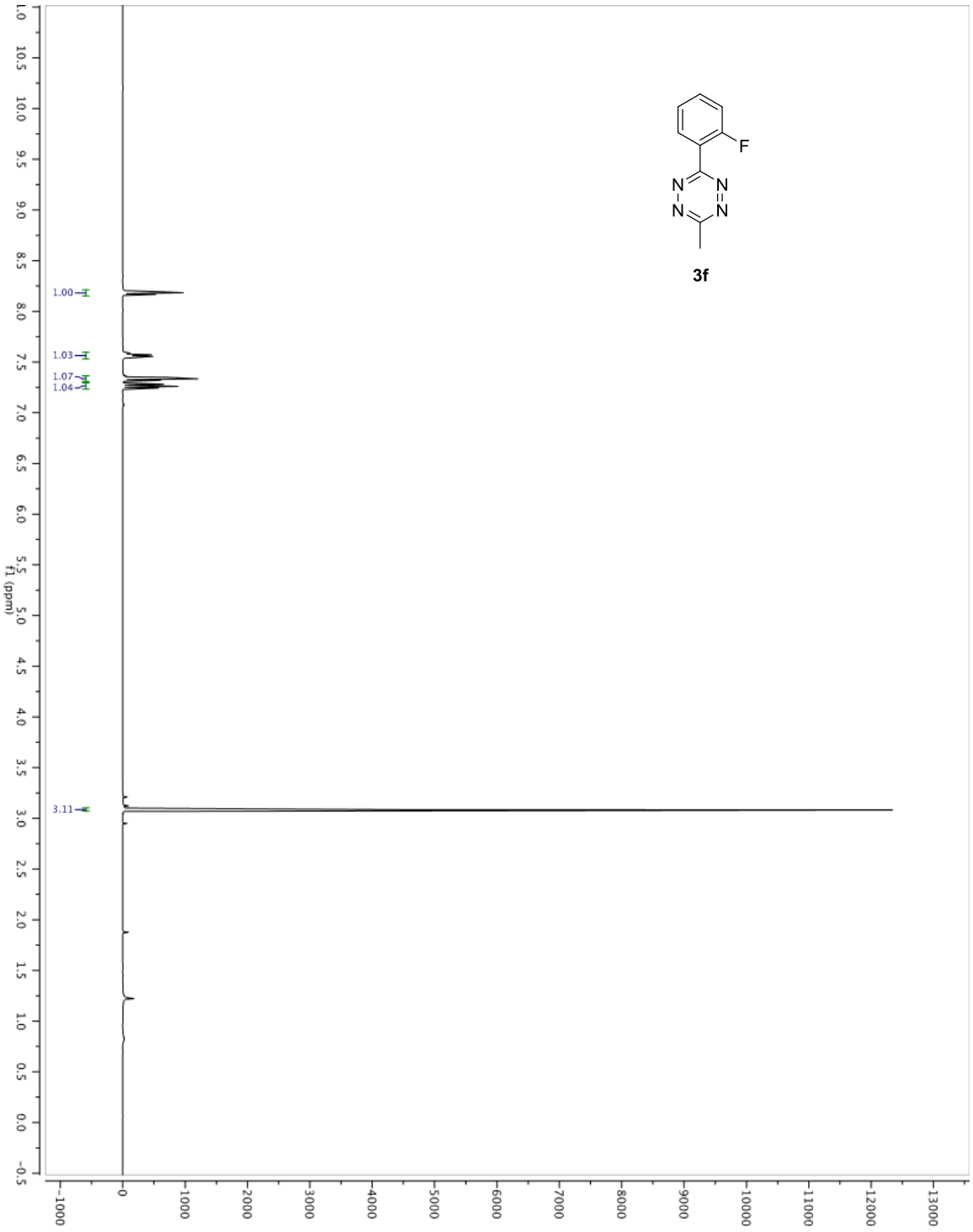

Figure A1.13. ^{13}C NMR spectrum of **3f** in $CDCl_3$ (125 MHz).

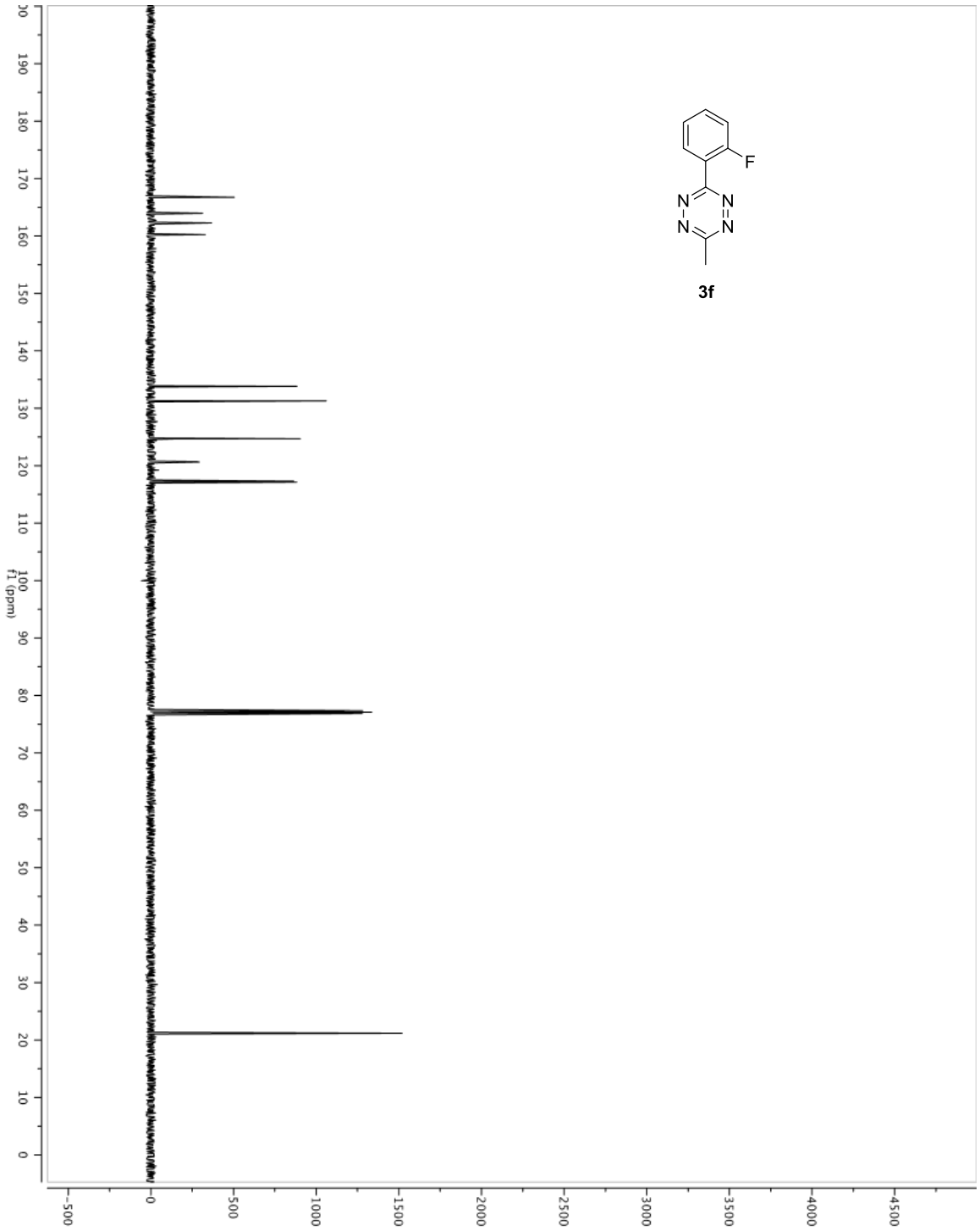

Figure A1.14. ^{19}F NMR spectrum of **3f** in $CDCl_3$ (338 MHz).

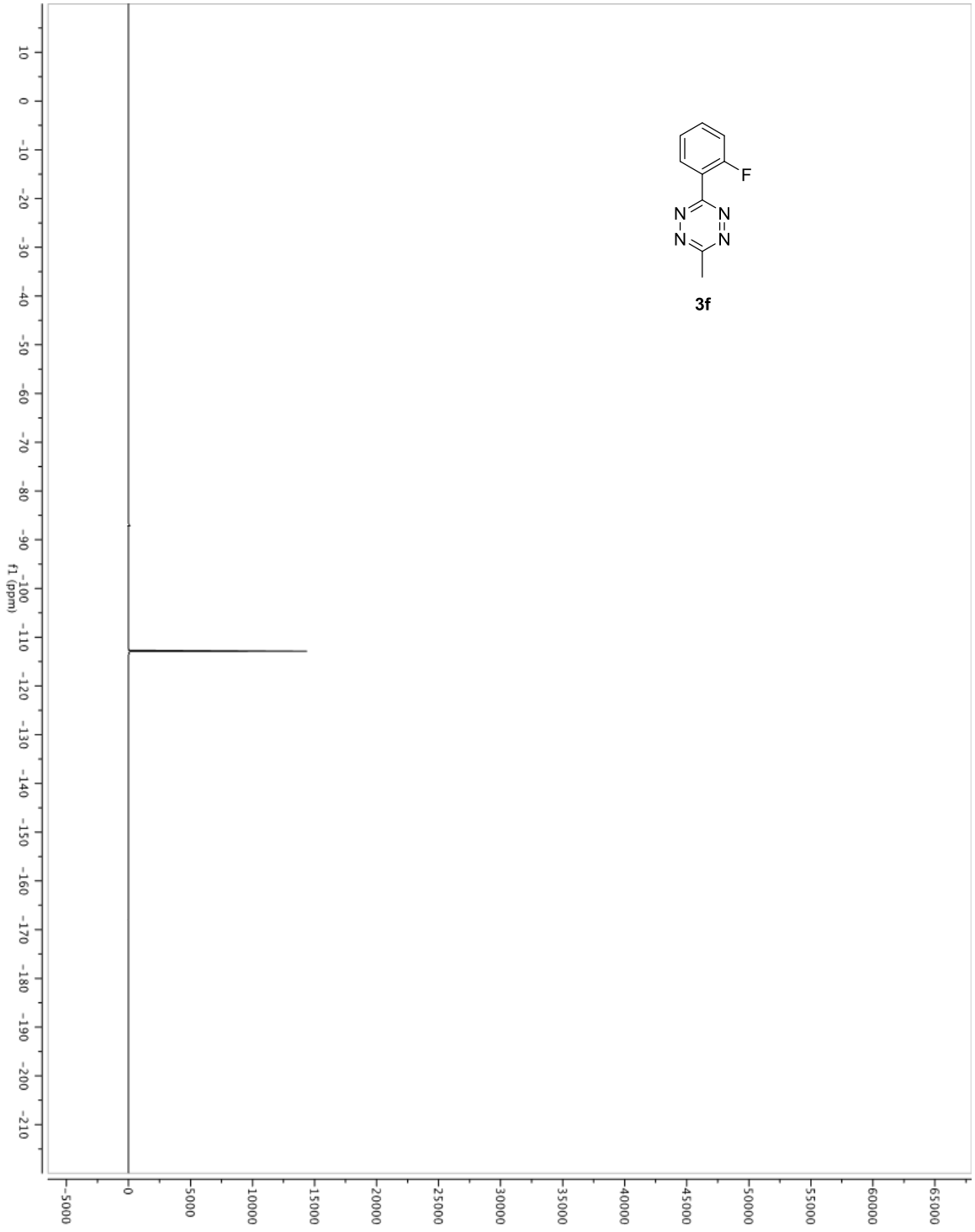

Figure A1.15. ^{1}H NMR spectrum of **3g** in $CDCl_3$ (500 MHz).

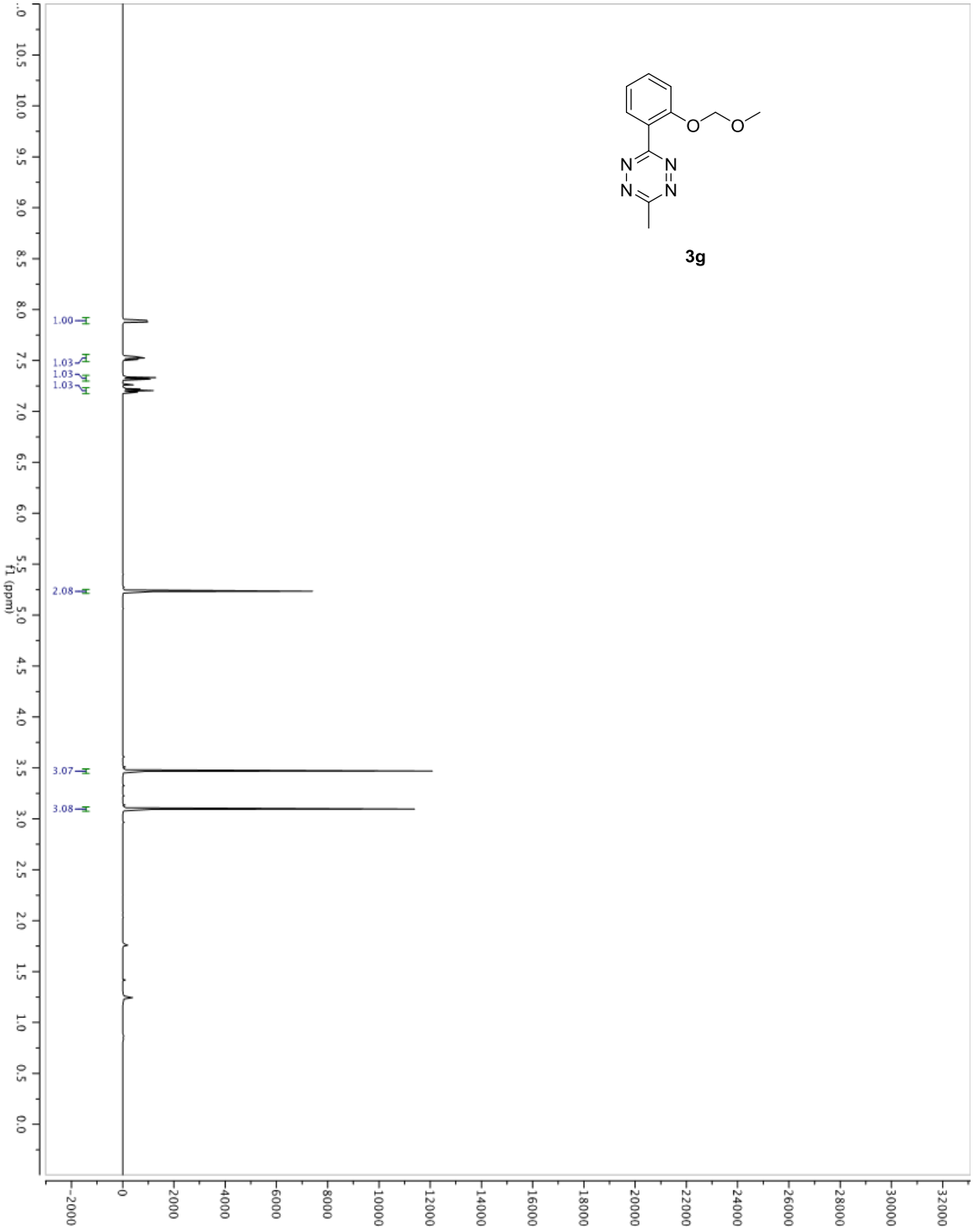

Figure A1.16. ^{13}C NMR spectrum of **3g** in $CDCl_3$ (125 MHz).

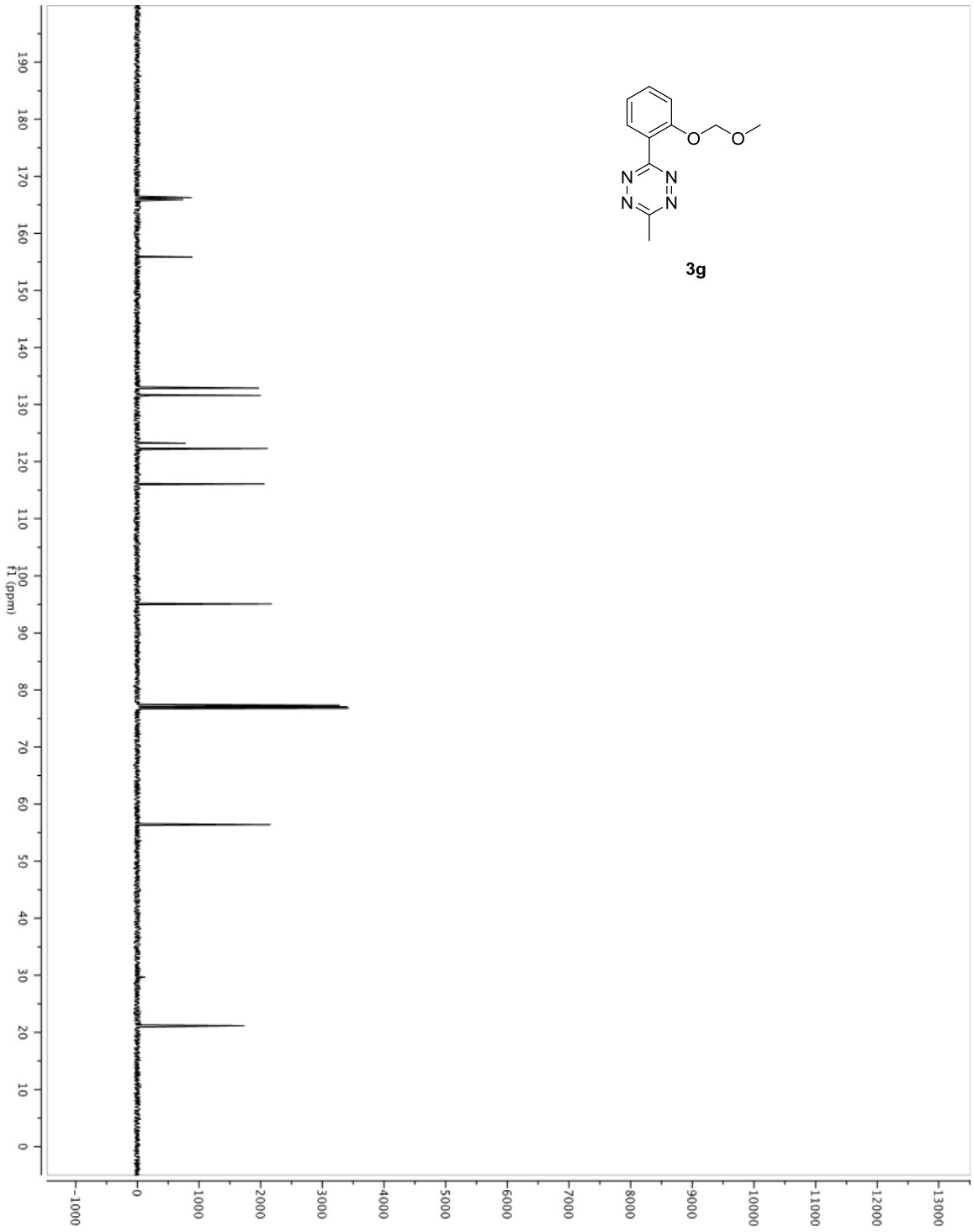

Figure A1.17. ^{1}H NMR spectrum of **3h** in $CDCl_3$ (500 MHz).

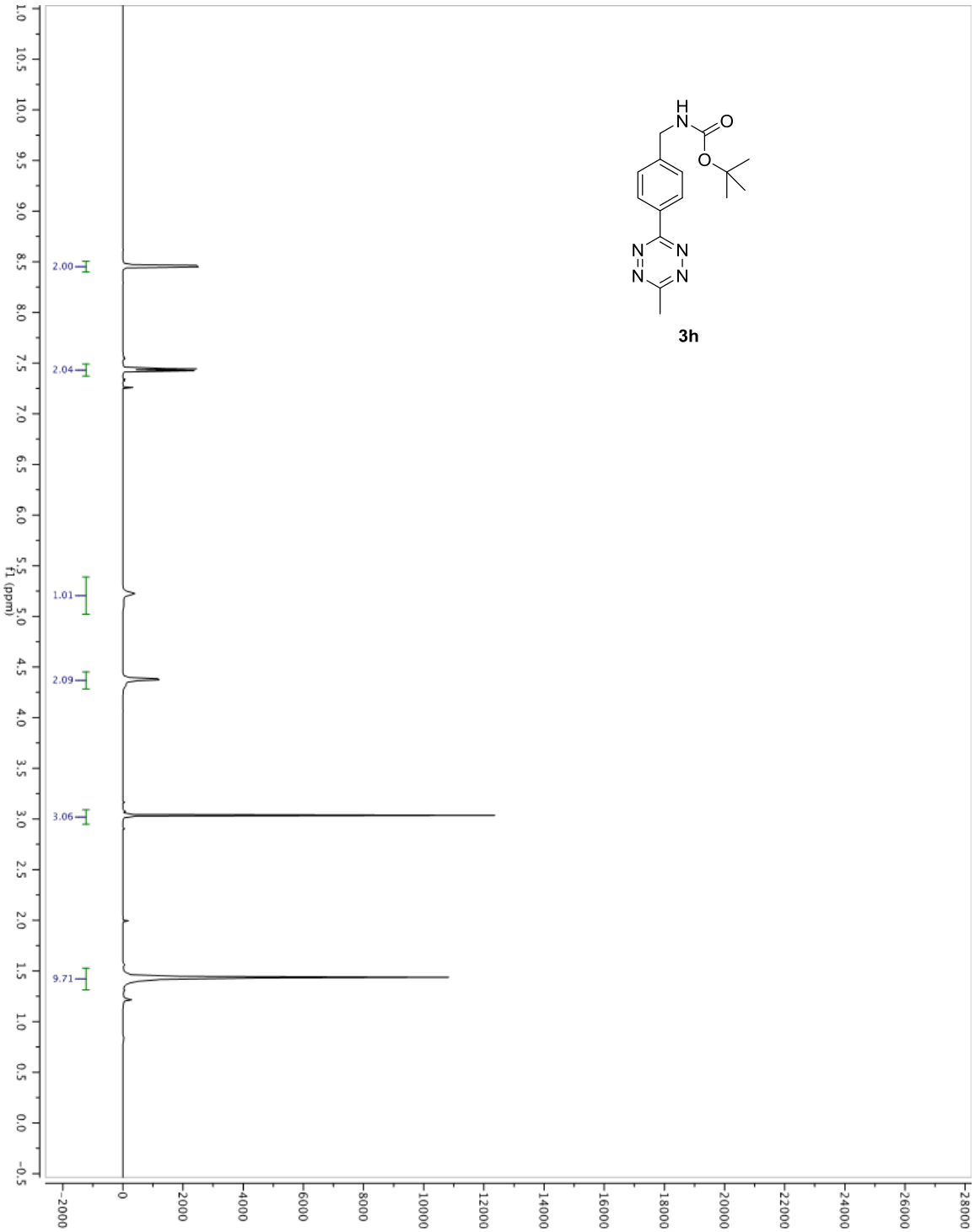

Figure A1.18. ^{1}H NMR spectrum of **3i** in $CDCl_3$ (500 MHz).

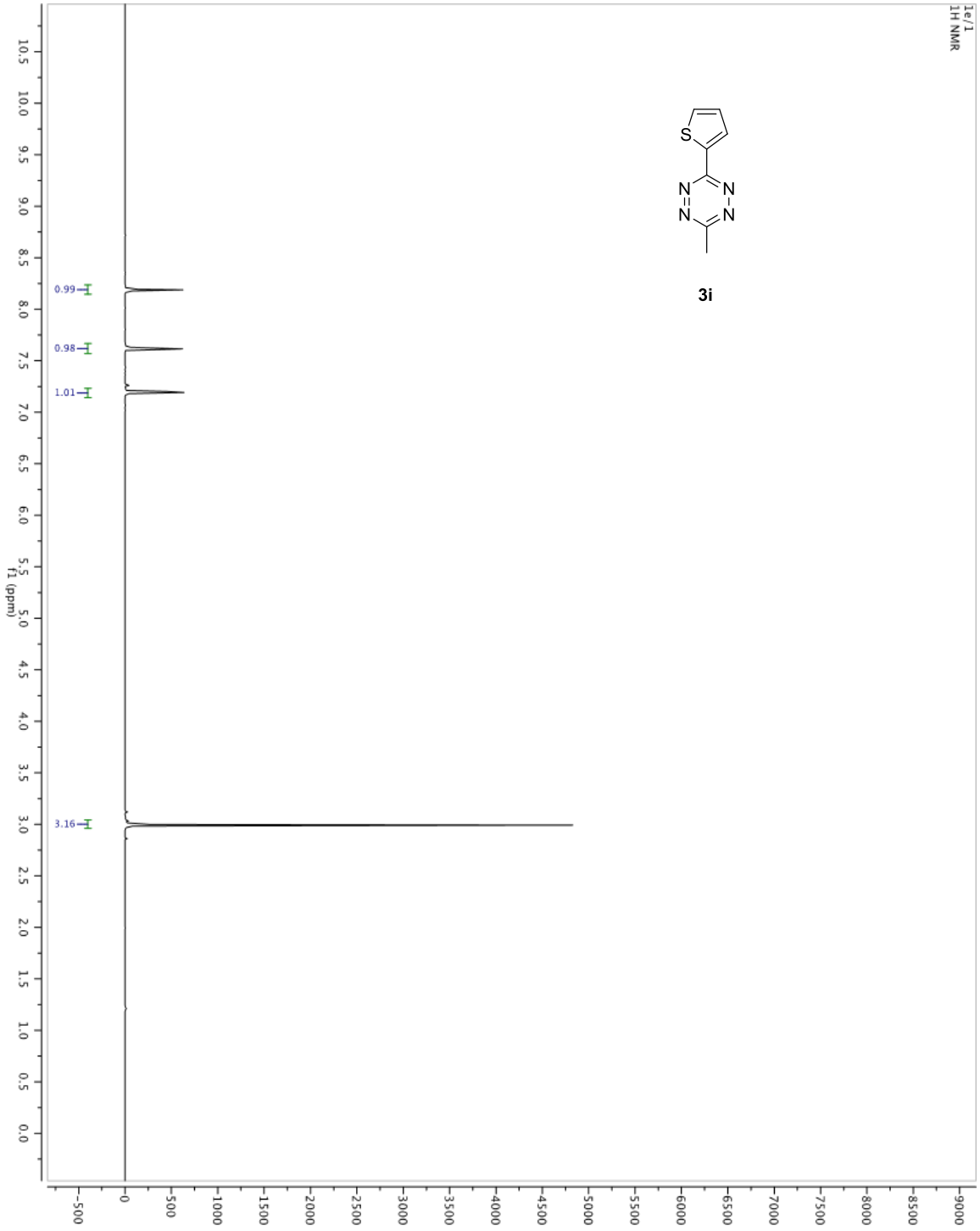

Figure A1.19. ^{13}C NMR spectrum of **3i** in $CDCl_3$ (125 MHz).

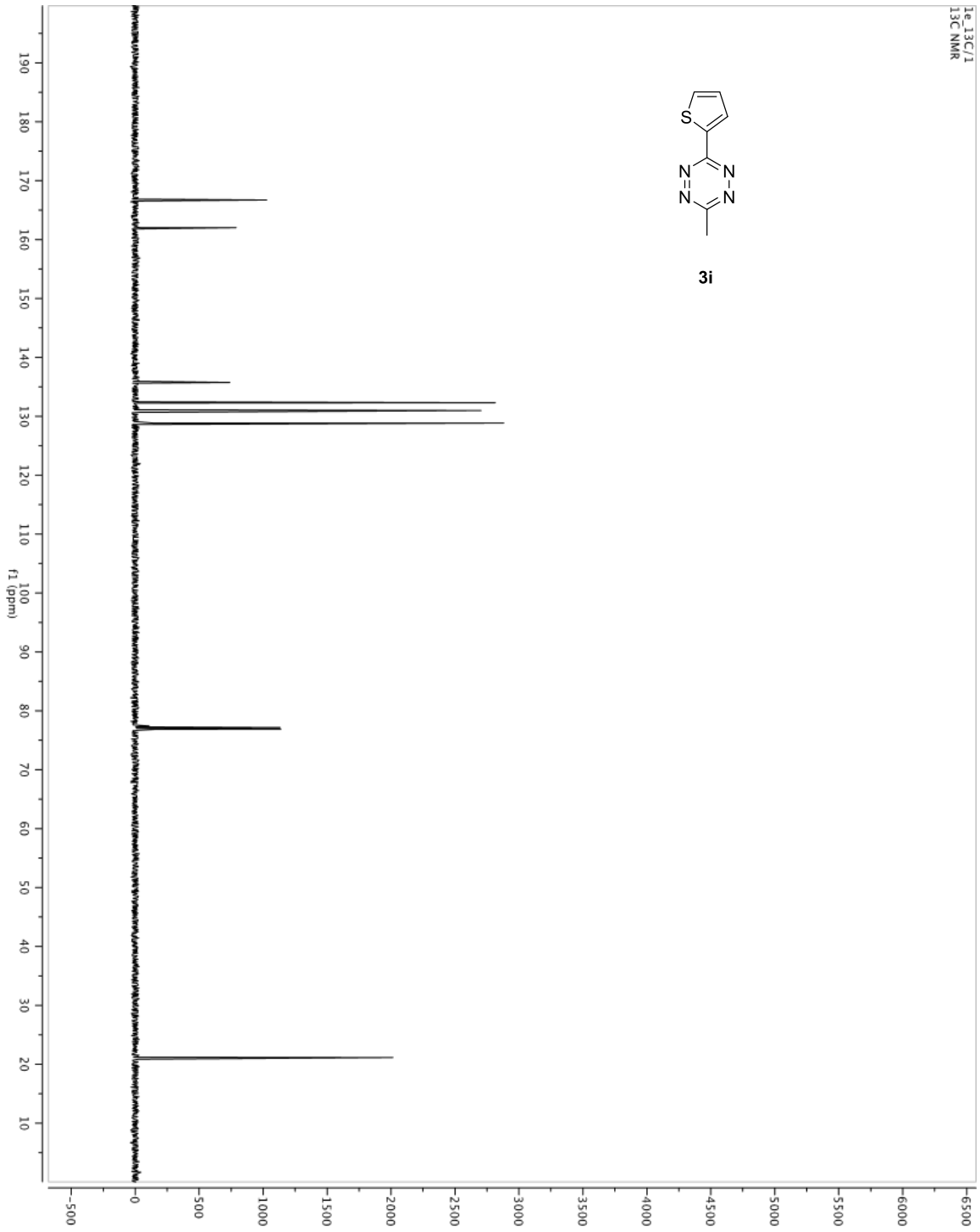

Figure A1.20. ^{1}H NMR spectrum of **3j** in $CDCl_3$ (500 MHz).

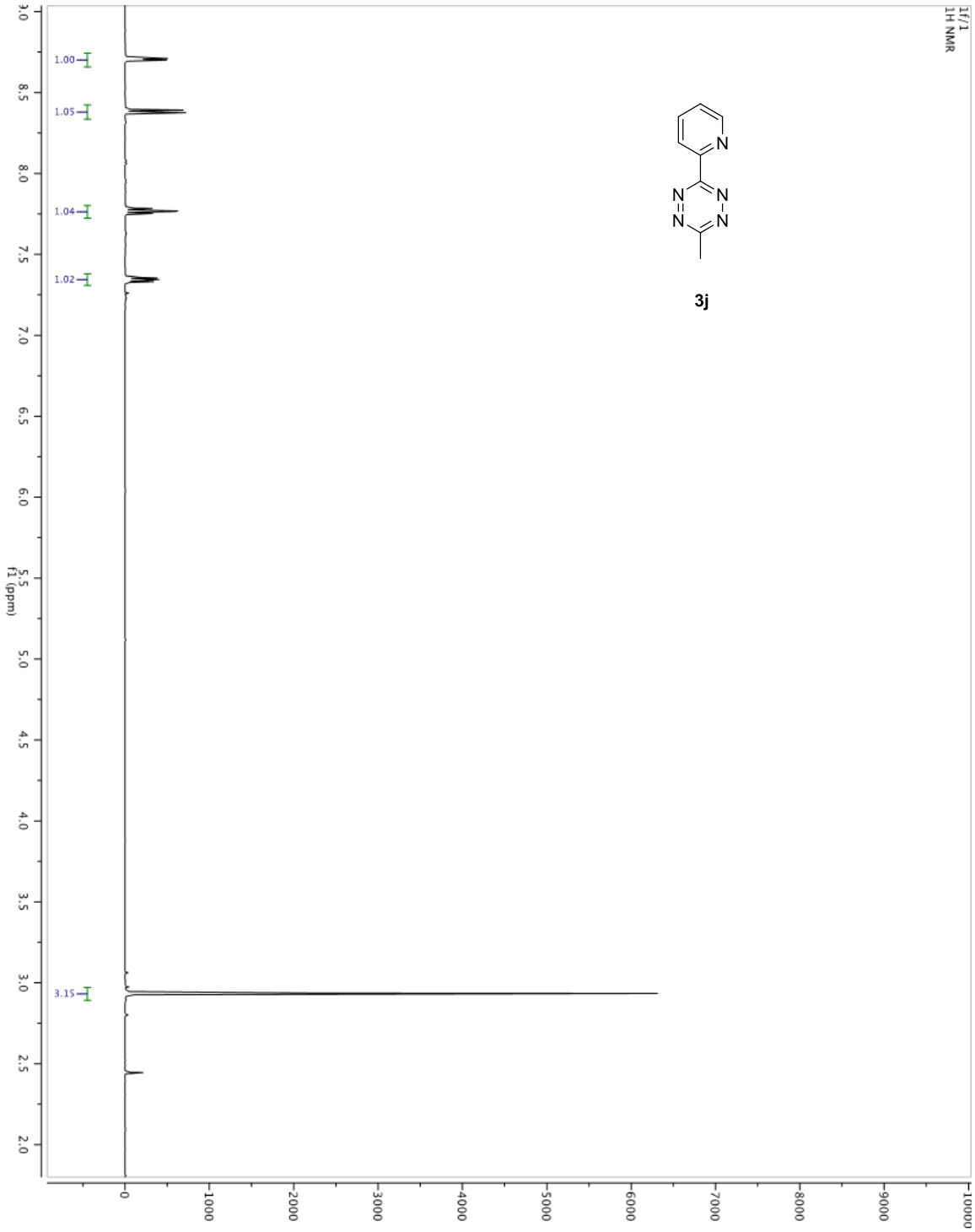

Figure A1.21. ^{13}C NMR spectrum of **3j** in $CDCl_3$ (125 MHz).

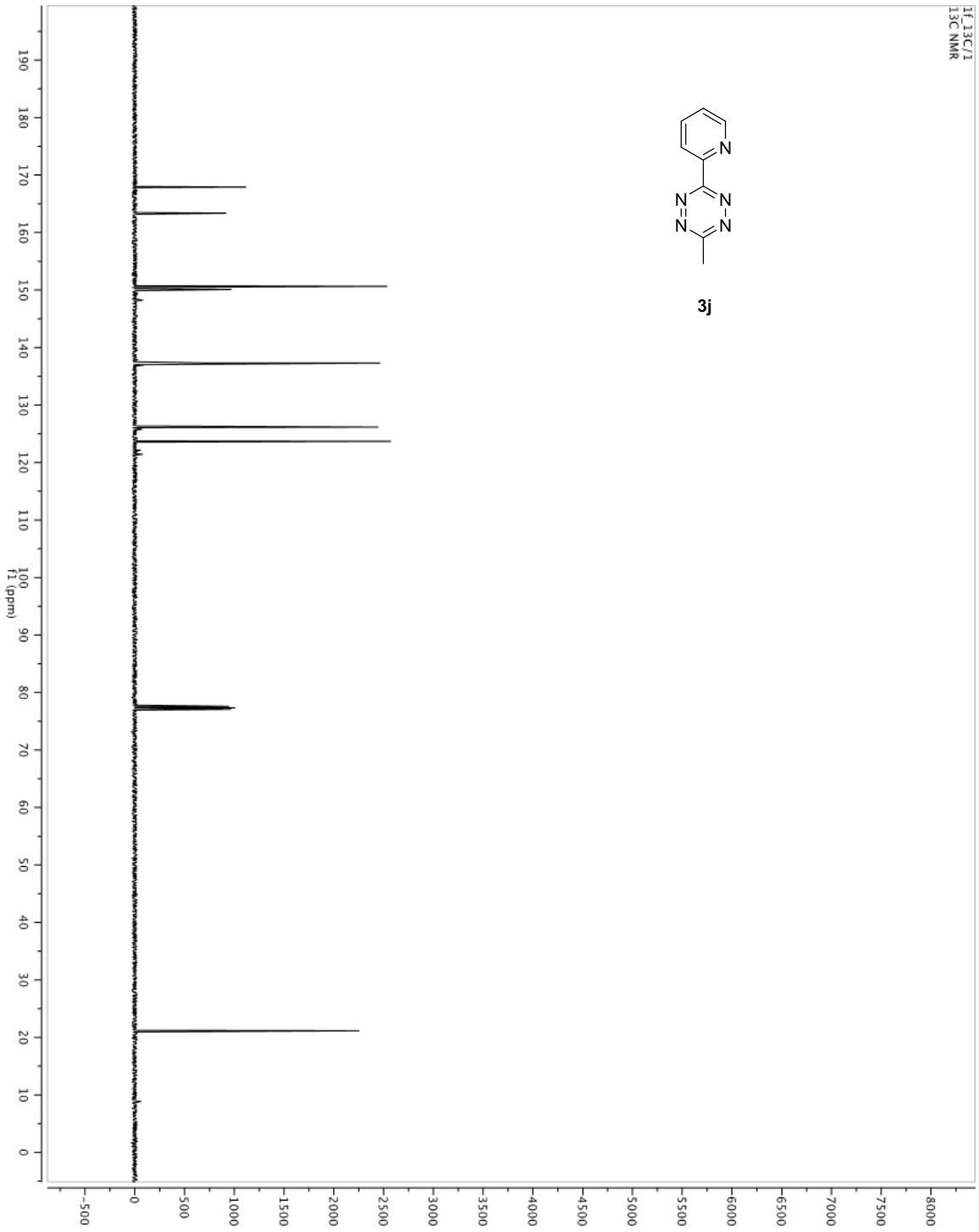

Figure A1.22. ^{1}H NMR spectrum of **3k** in $CDCl_3$ (500 MHz).

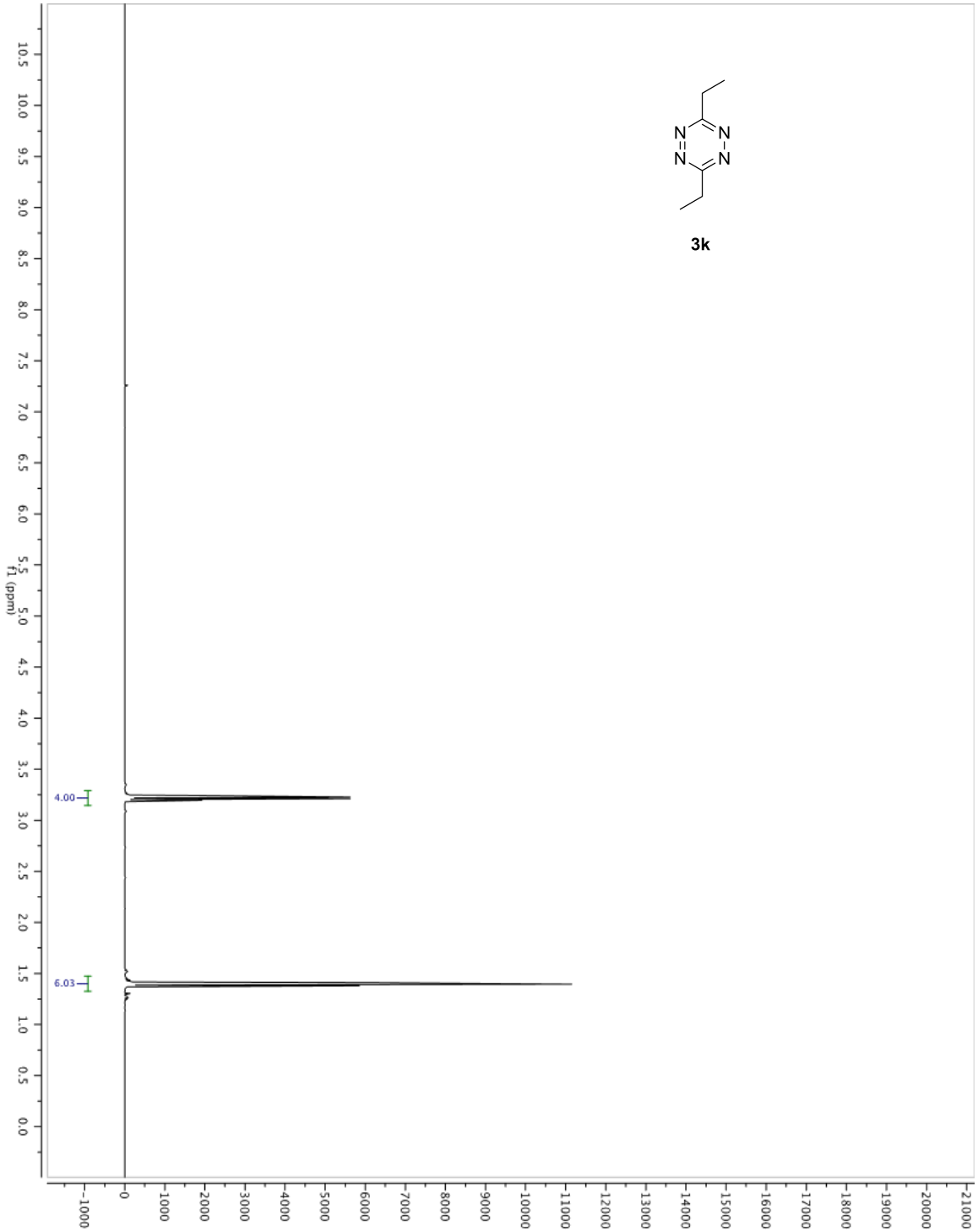

Figure A1.23. ^{13}C NMR spectrum of **3k** in $CDCl_3$ (125 MHz).

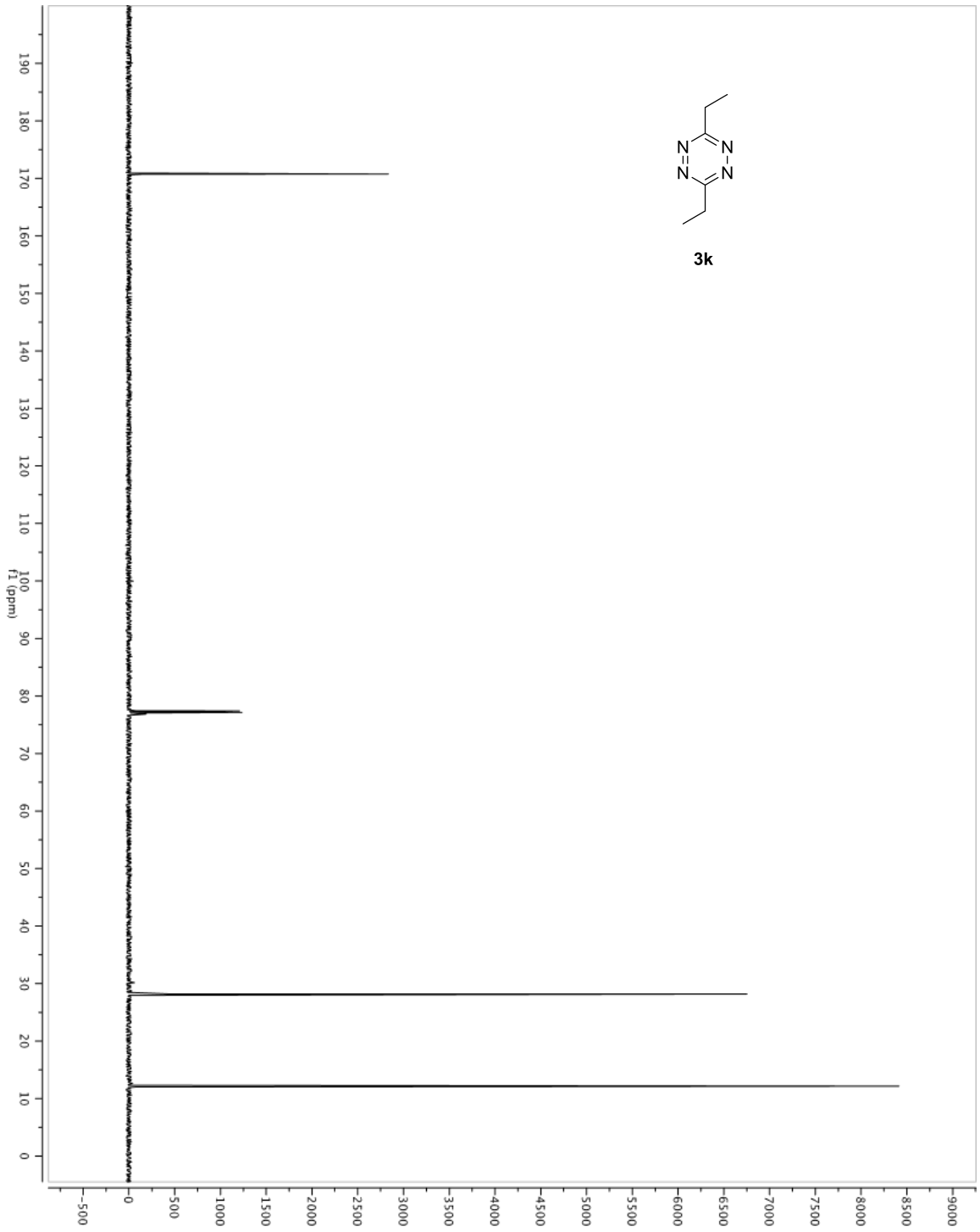

Figure A1.24. ^{1}H NMR spectrum of **3l** in $CDCl_3$ (500 MHz).

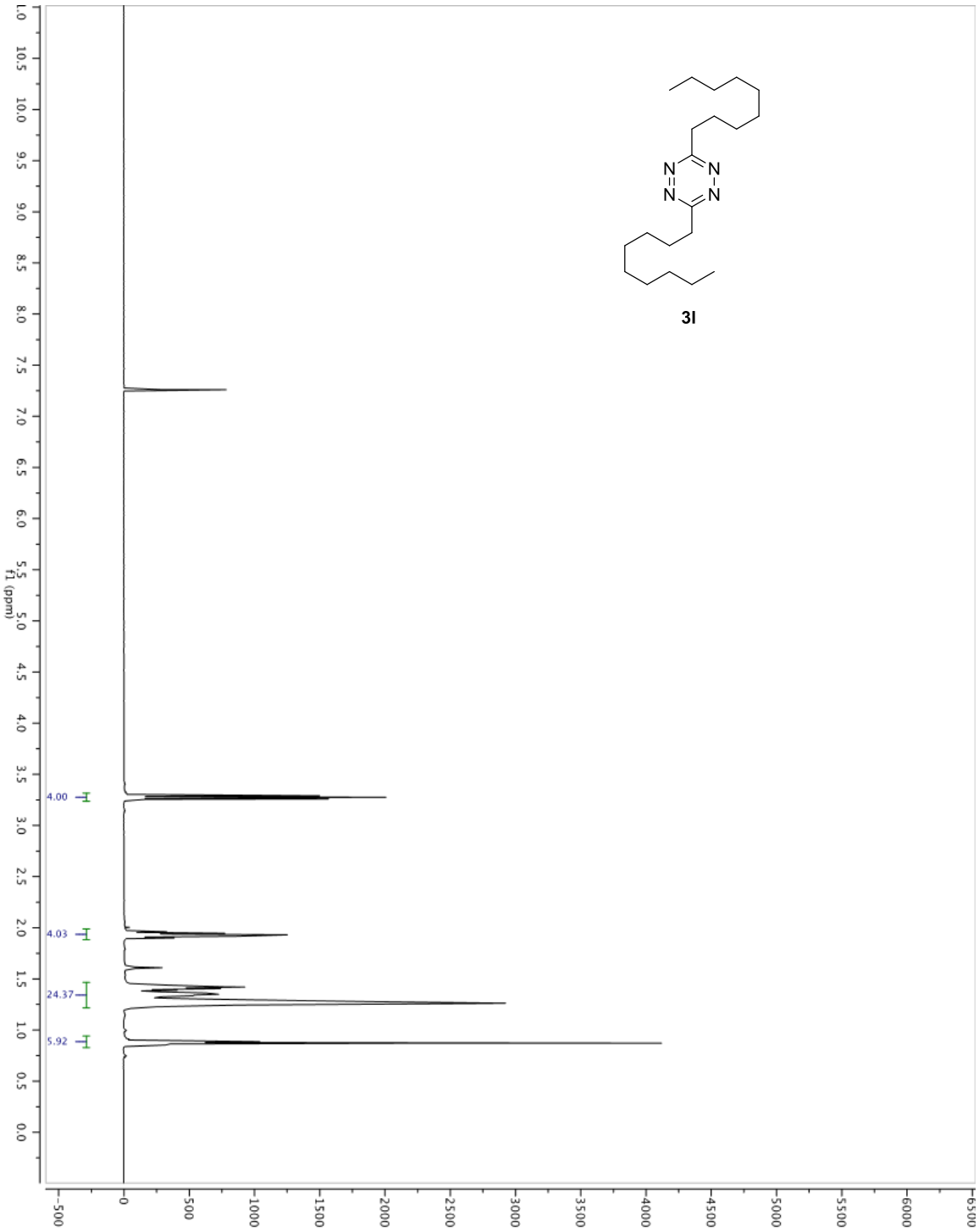

Figure A1.25. ^{13}C NMR spectrum of **3l** in $CDCl_3$ (125 MHz).

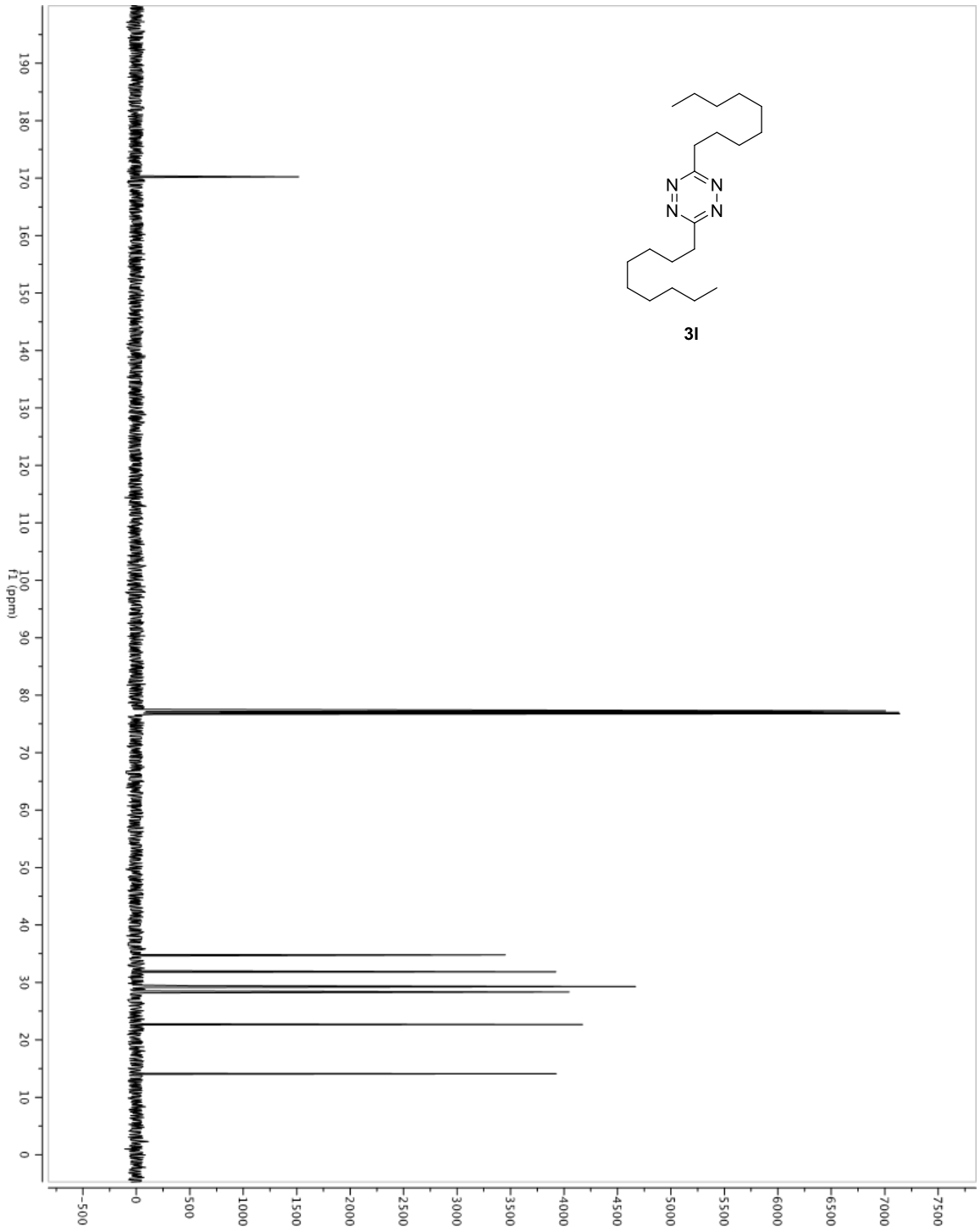

Figure A1.26. ^{1}H NMR spectrum of **3m** in $CDCl_3$ (500 MHz).

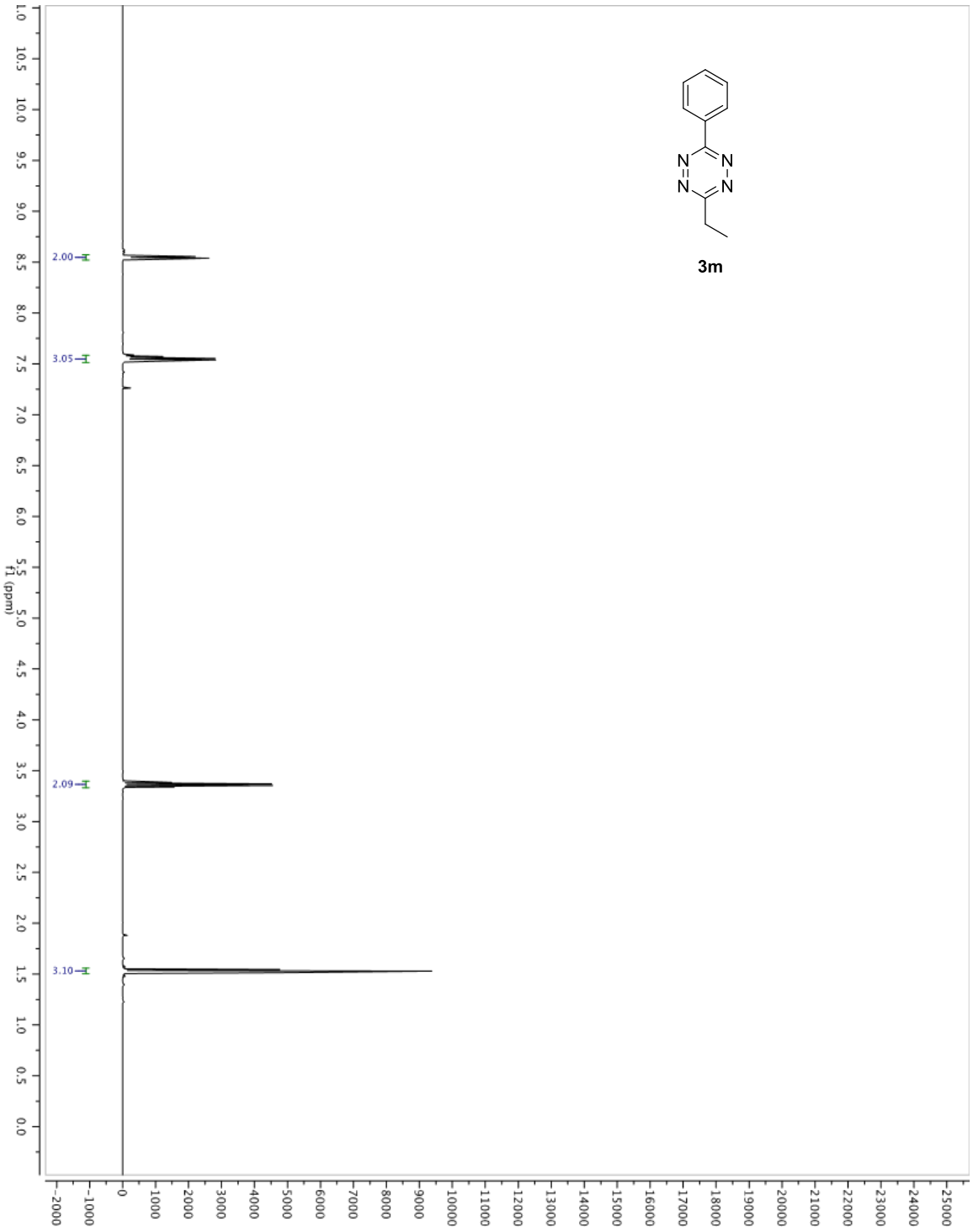

Figure A1.27. ^{13}C NMR spectrum of **3m** in $CDCl_3$ (125 MHz).

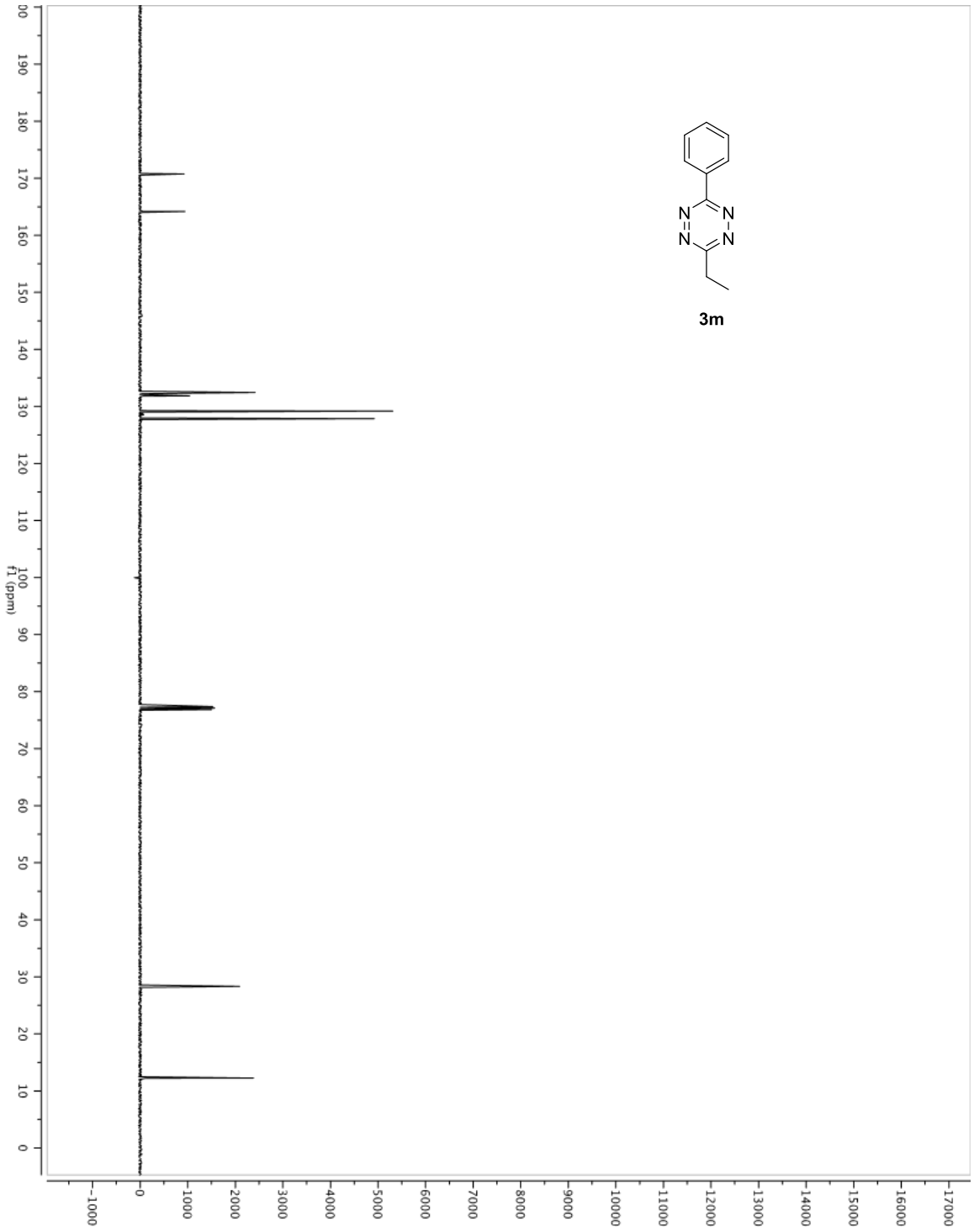

Figure A1.28. ^{1}H NMR spectrum of **3n** in $CDCl_3$ (500 MHz).

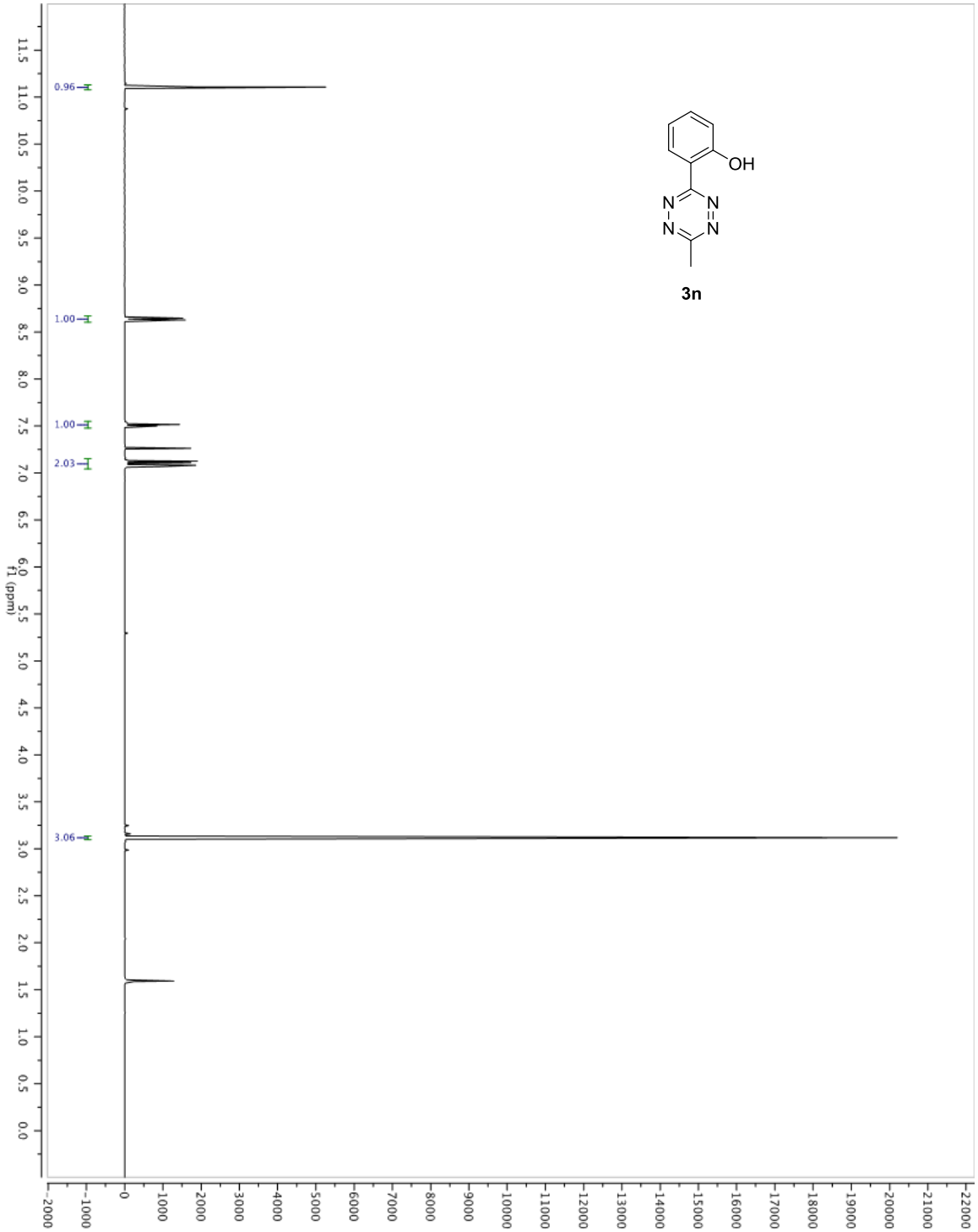

Figure A1.29. ^{13}C NMR spectrum of **3n** in $CDCl_3$ (125 MHz).

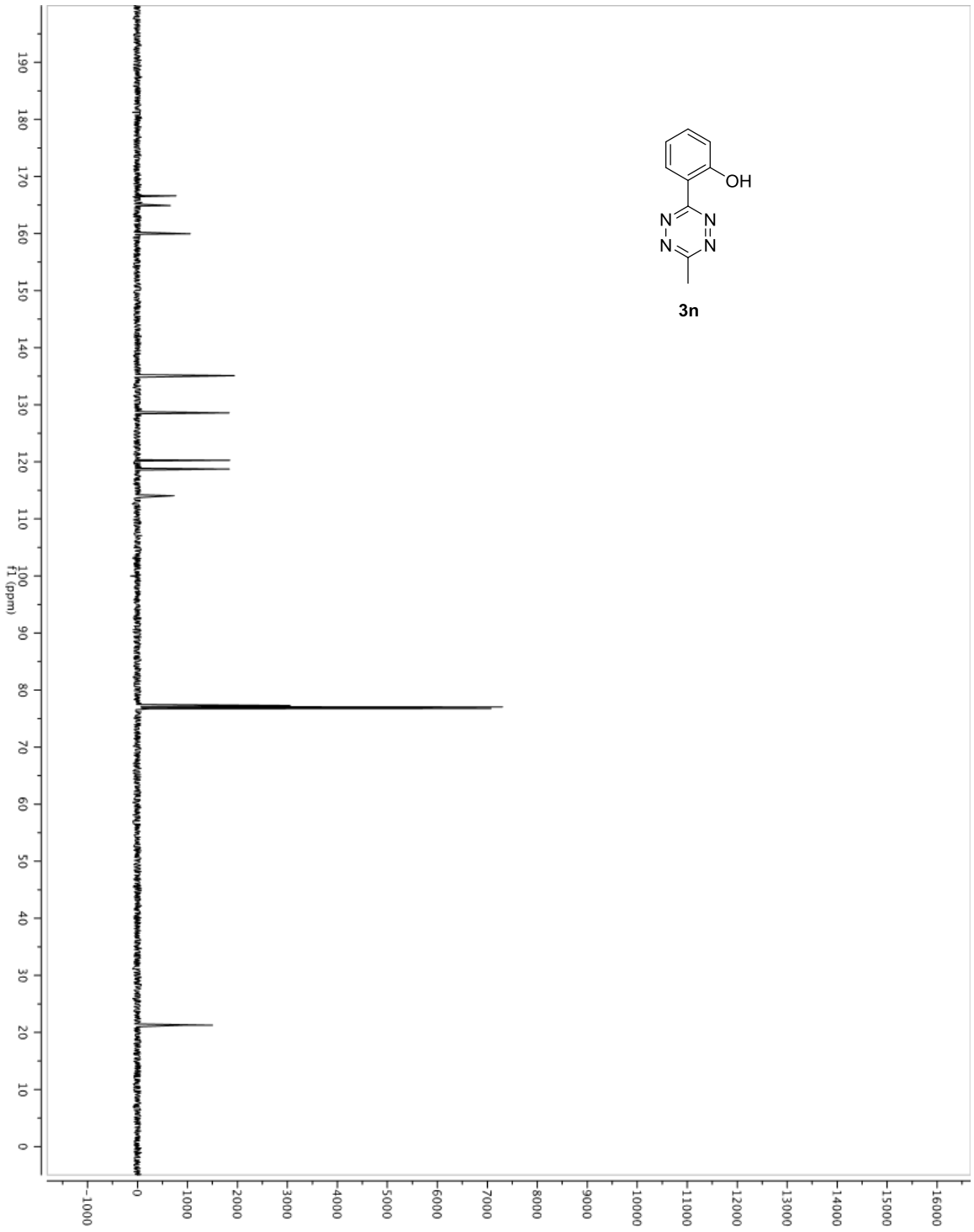

Figure A1.30. ^{1}H NMR spectrum of **4b** in $CDCl_3$ (500 MHz).

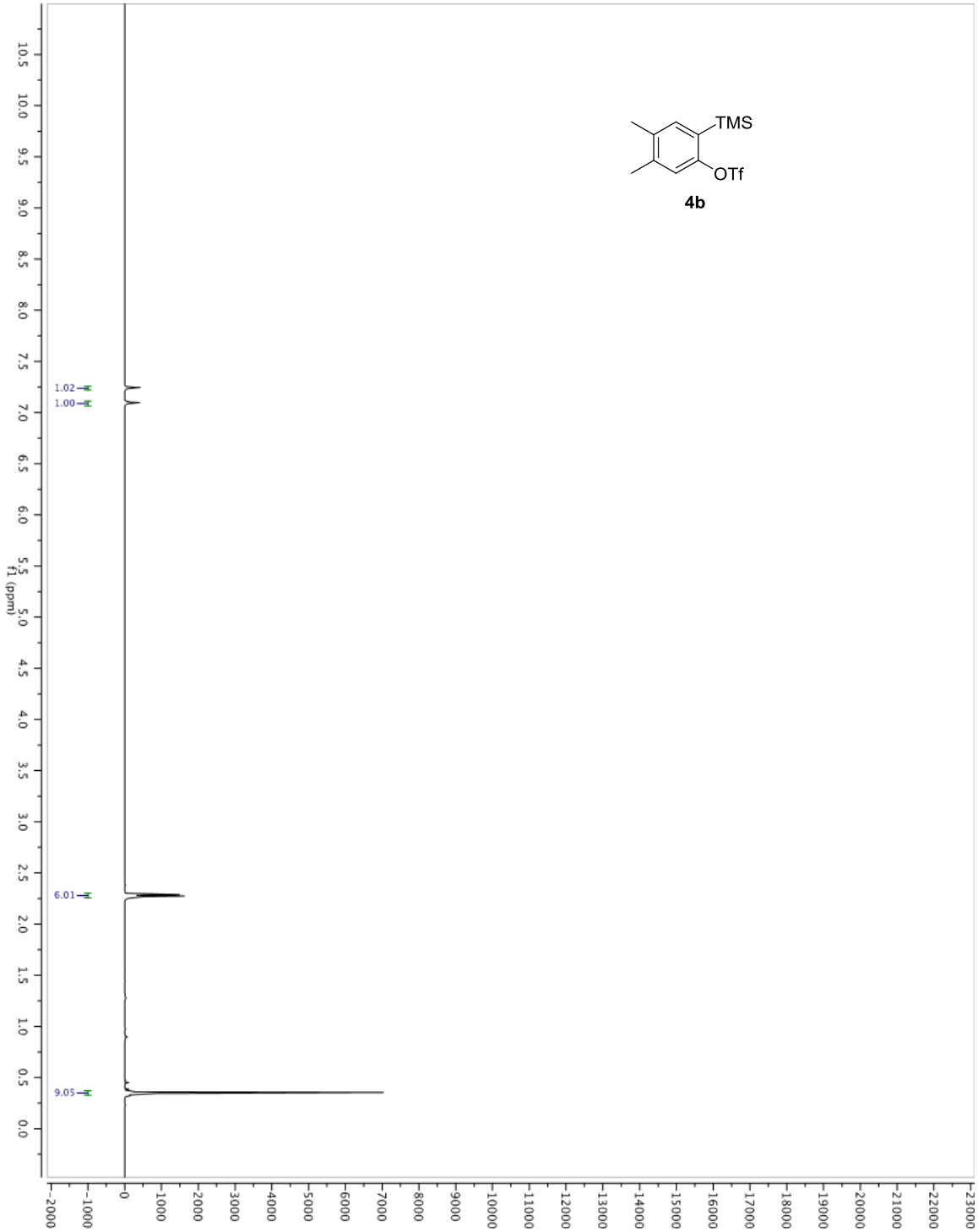

Figure A1.31. ^{1}H NMR spectrum of **5a** in CD_2Cl_2 (500 MHz).

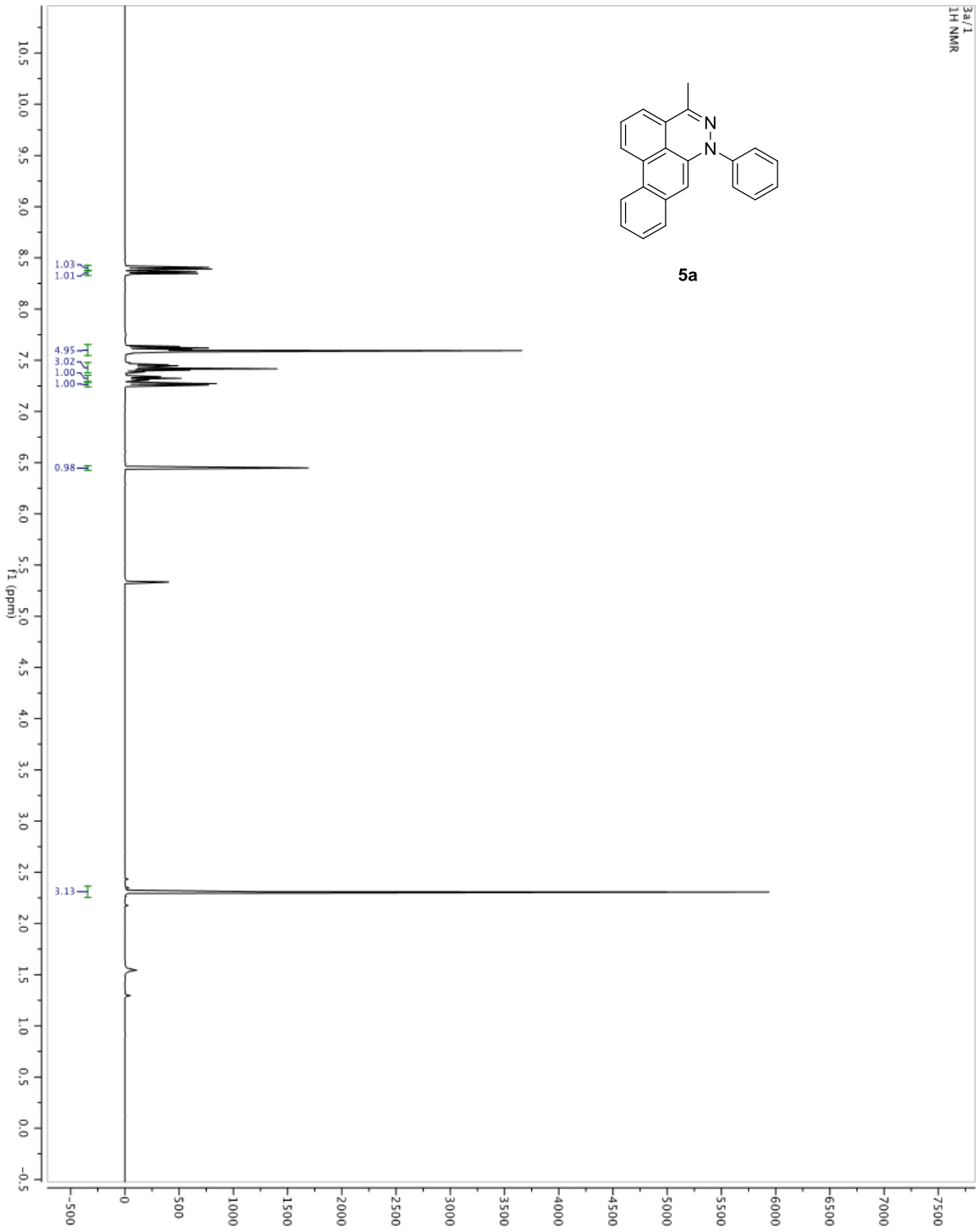

Figure A1.32. ^{13}C NMR spectrum of **5a** in CD_2Cl_2 (125 MHz).

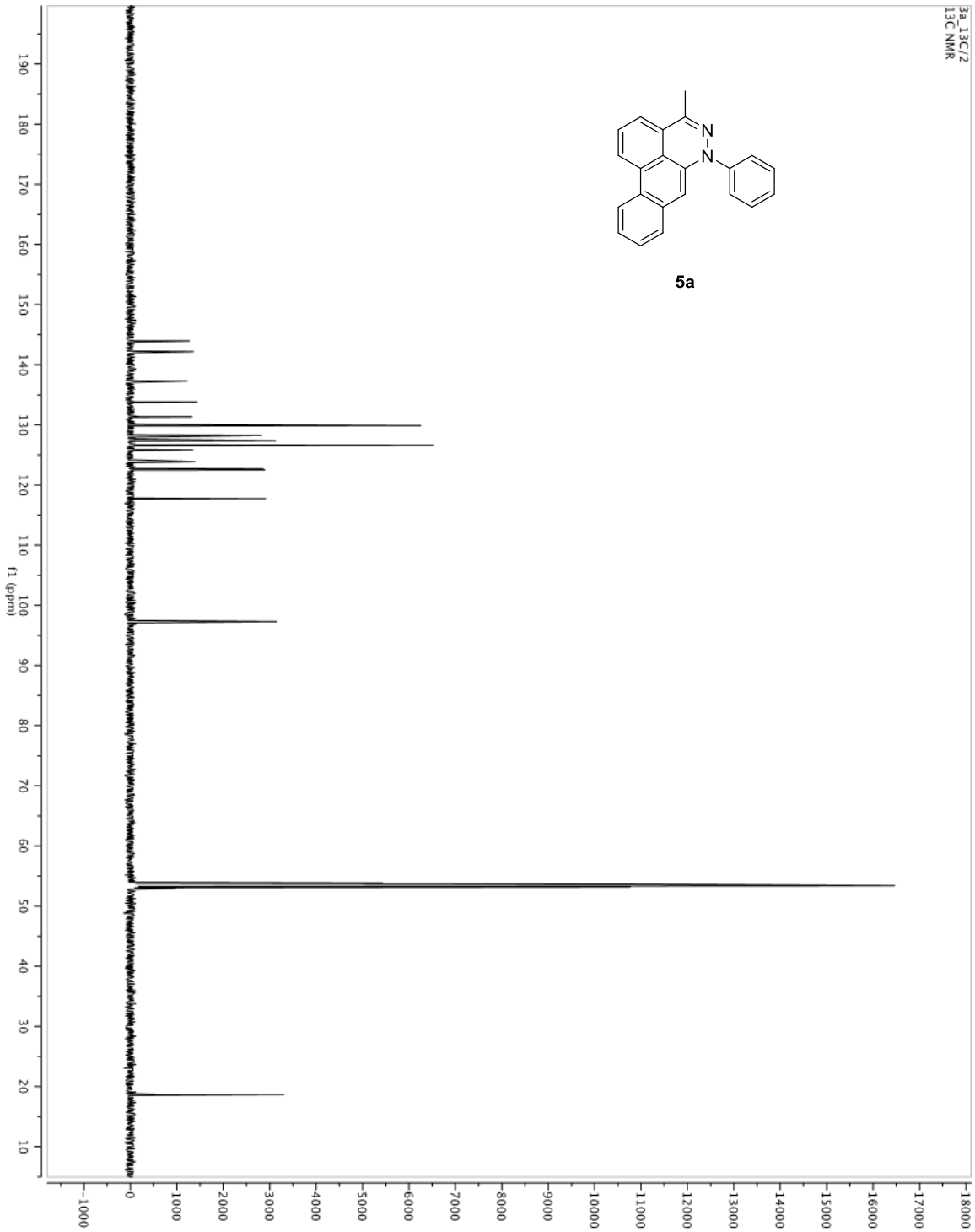

Figure A1.33. ^{1}H NMR spectrum of **5b** in CD_2Cl_2 (500 MHz).

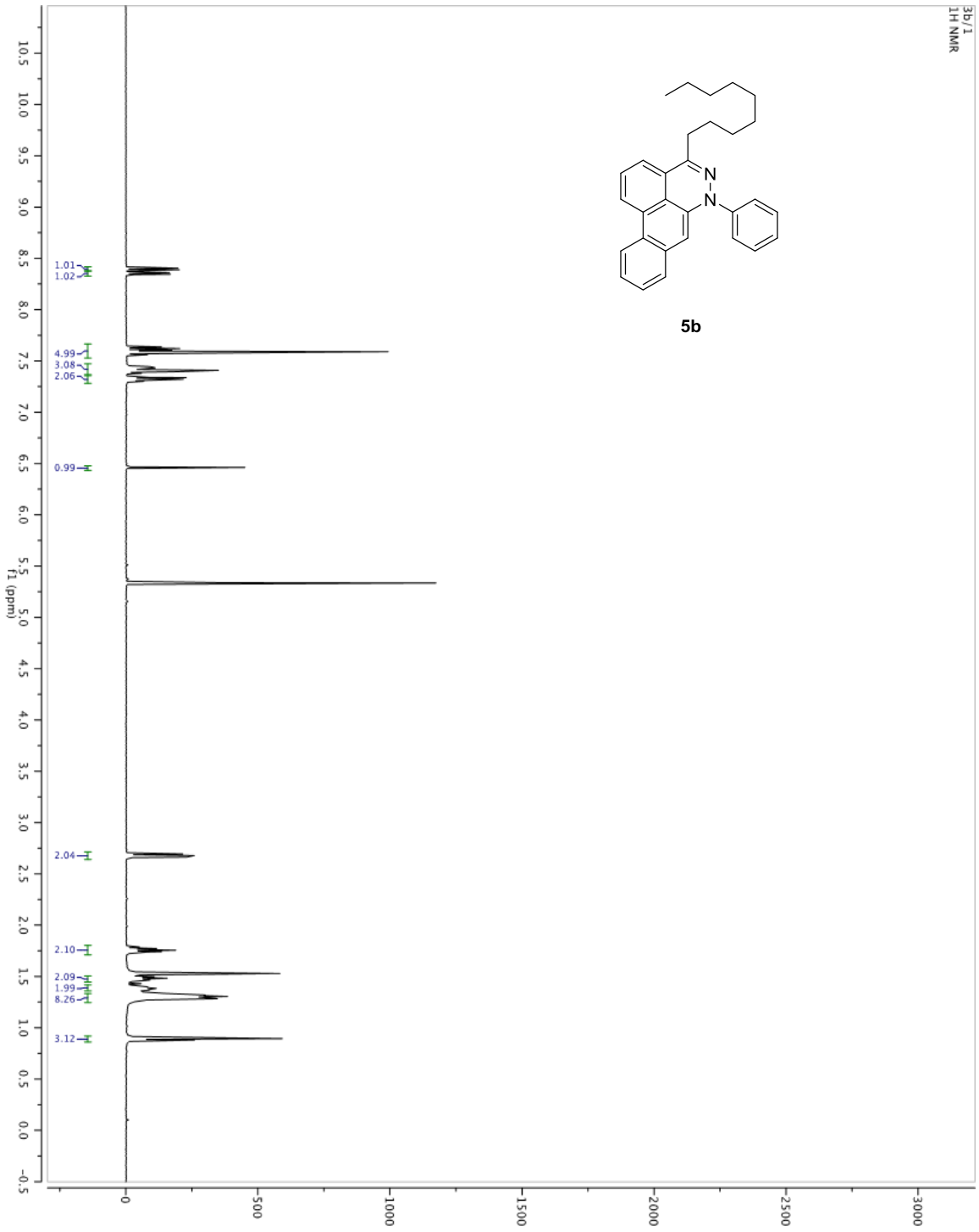

Figure A1.34. ^{13}C NMR spectrum of **5b** in CD_2Cl_2 (125 MHz).

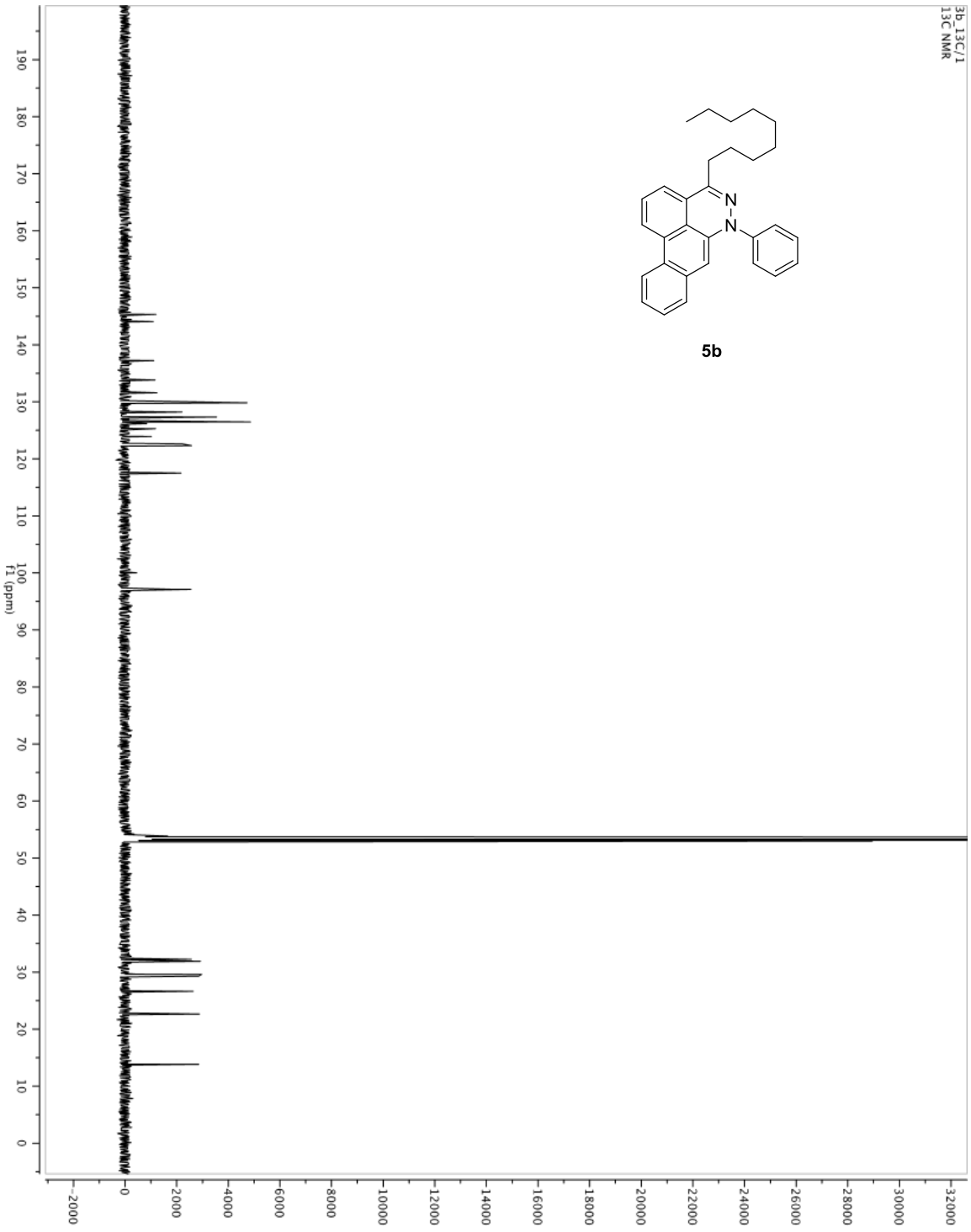

Figure A1.35. ^{1}H NMR spectrum of **5c** in CD_2Cl_2 (500 MHz).

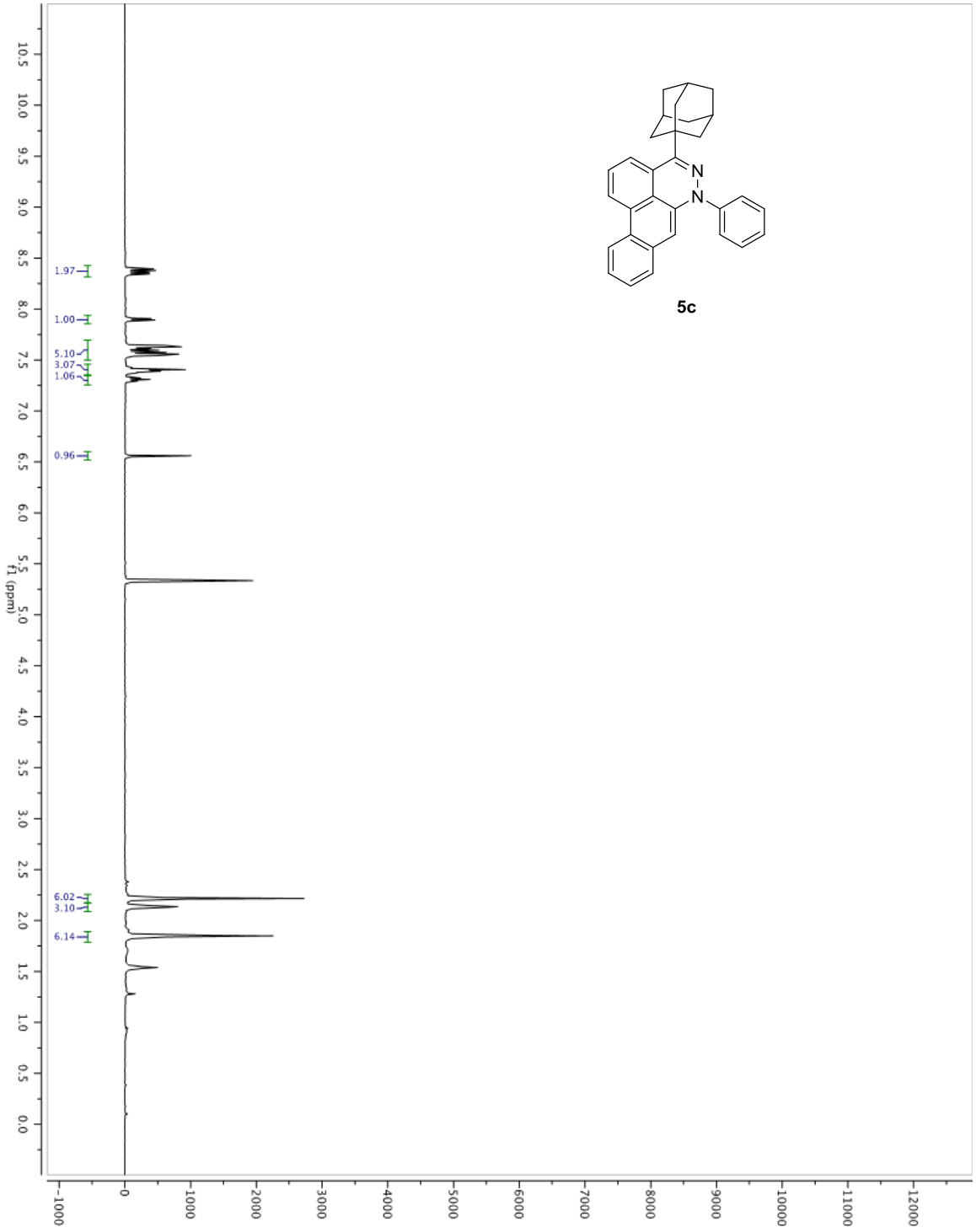

Figure A1.36. ^{13}C NMR spectrum of **5c** in CD_2Cl_2 (125 MHz).

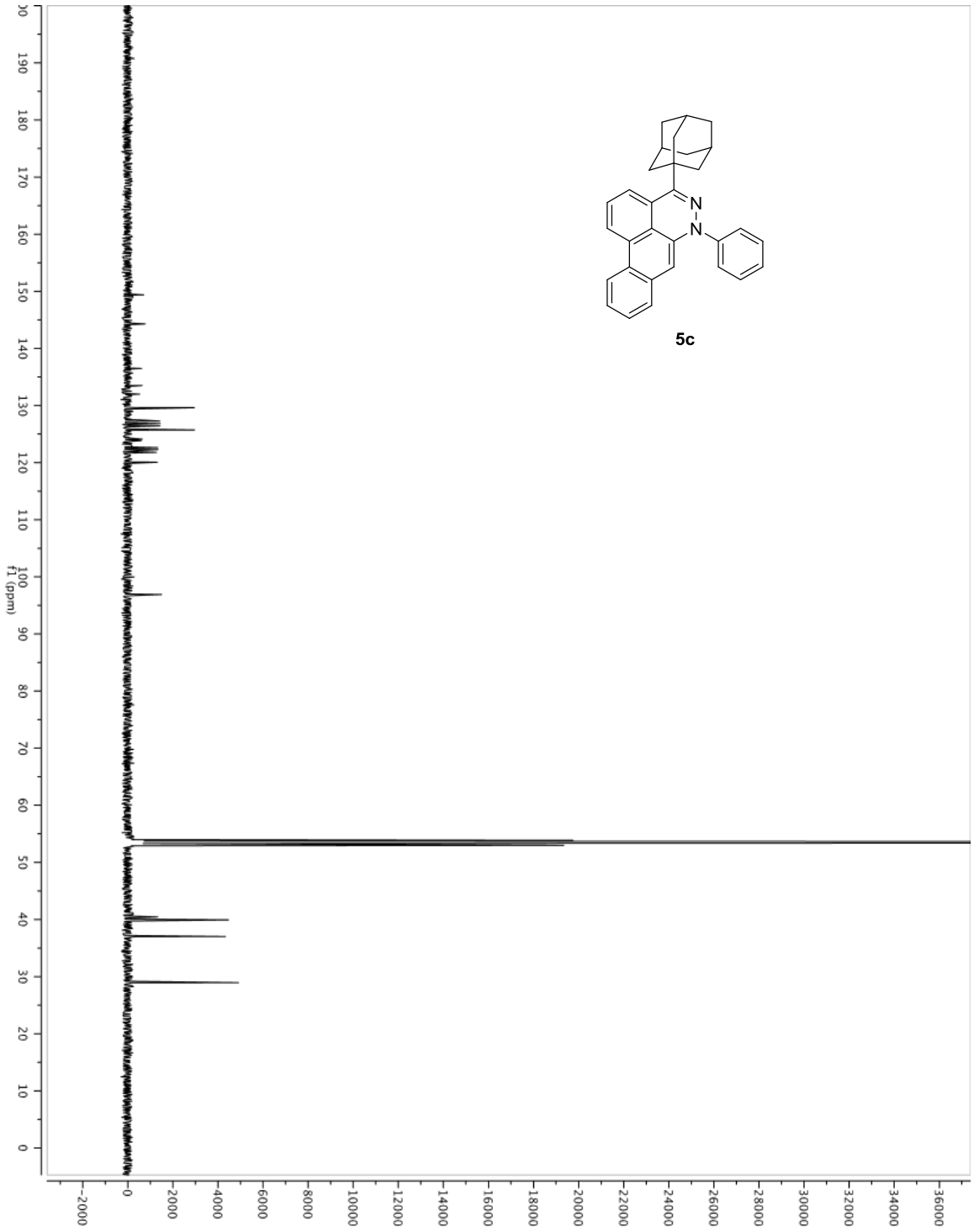

Figure A1.37. ^{1}H NMR spectrum of **5d** in CD_2Cl_2 (500 MHz).

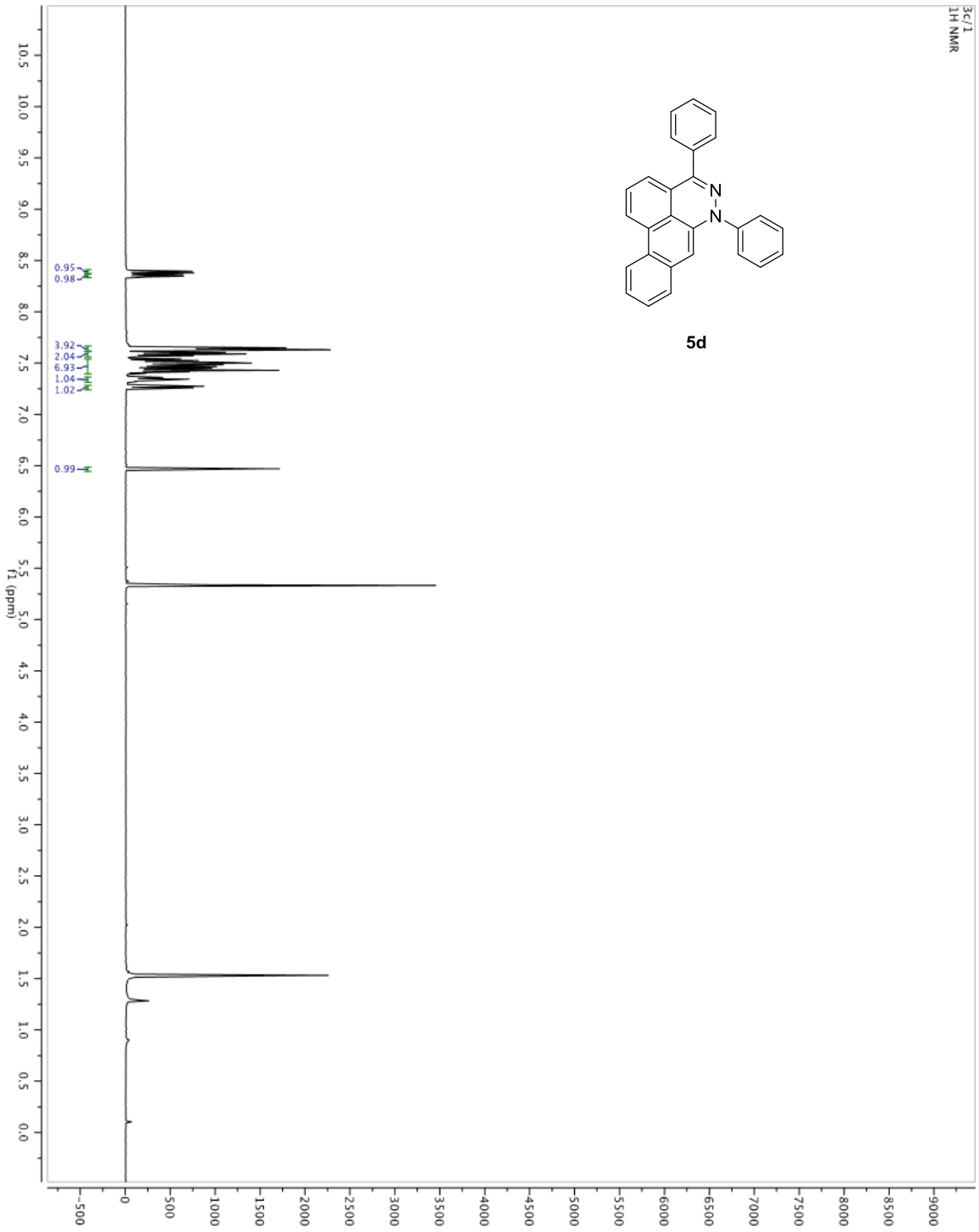

Figure A1.38. ^{13}C NMR spectrum of **5d** in CD_2Cl_2 (125 MHz).

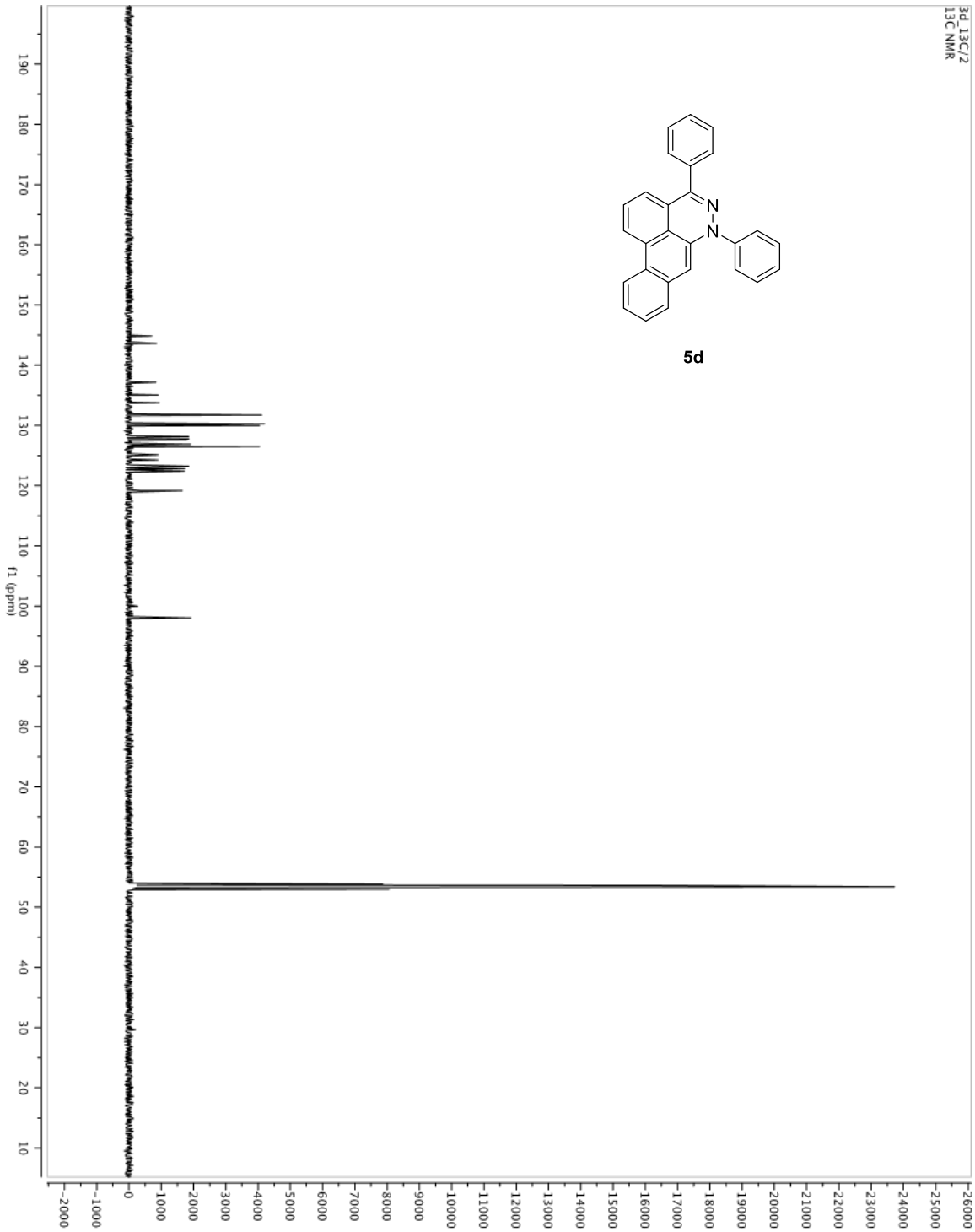

Figure A1.39. ^{1}H NMR spectrum of **5e** in CD_2Cl_2 (500 MHz).

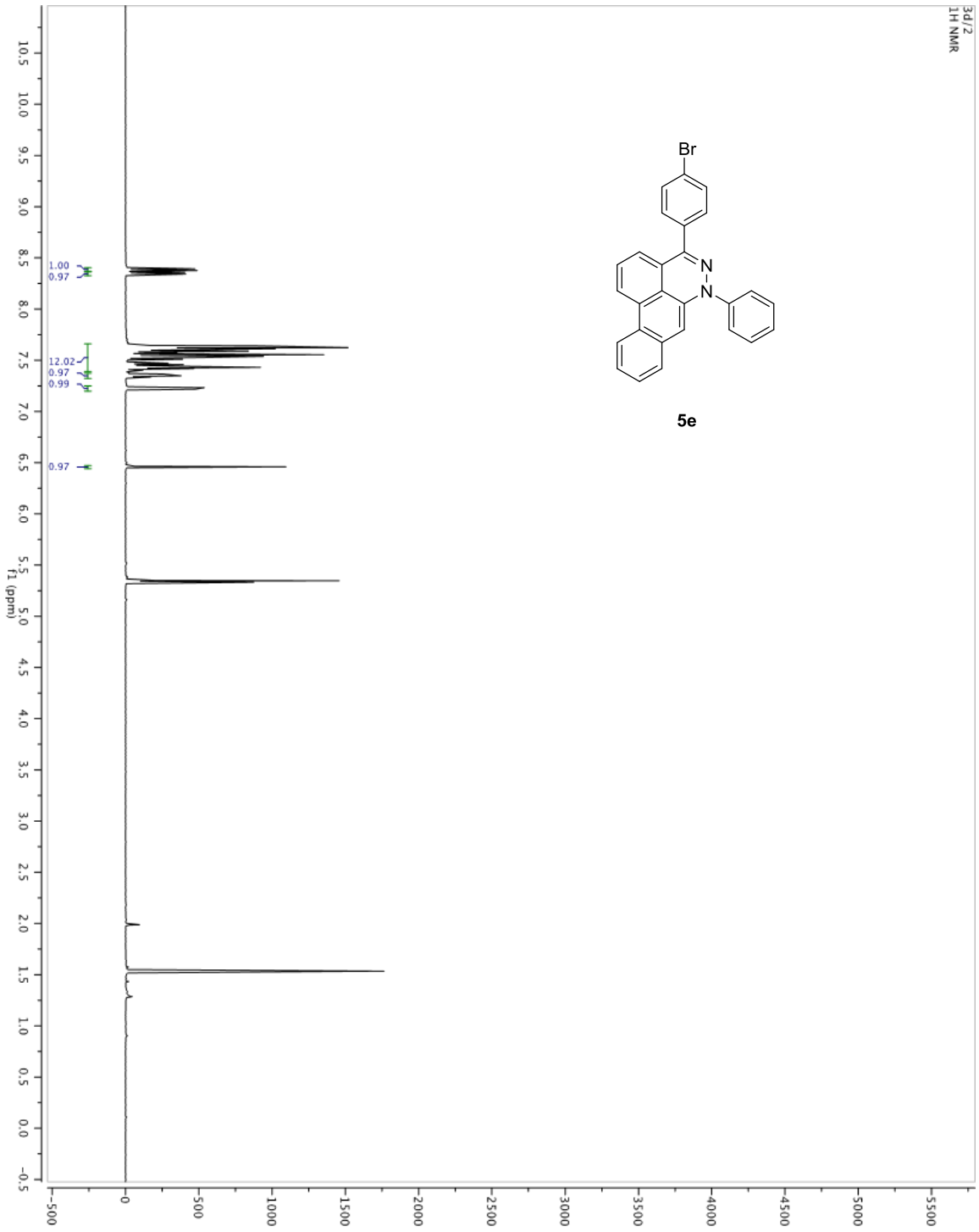

Figure A1.40. ^{13}C NMR spectrum of **5e** in CD_2Cl_2 (125 MHz).

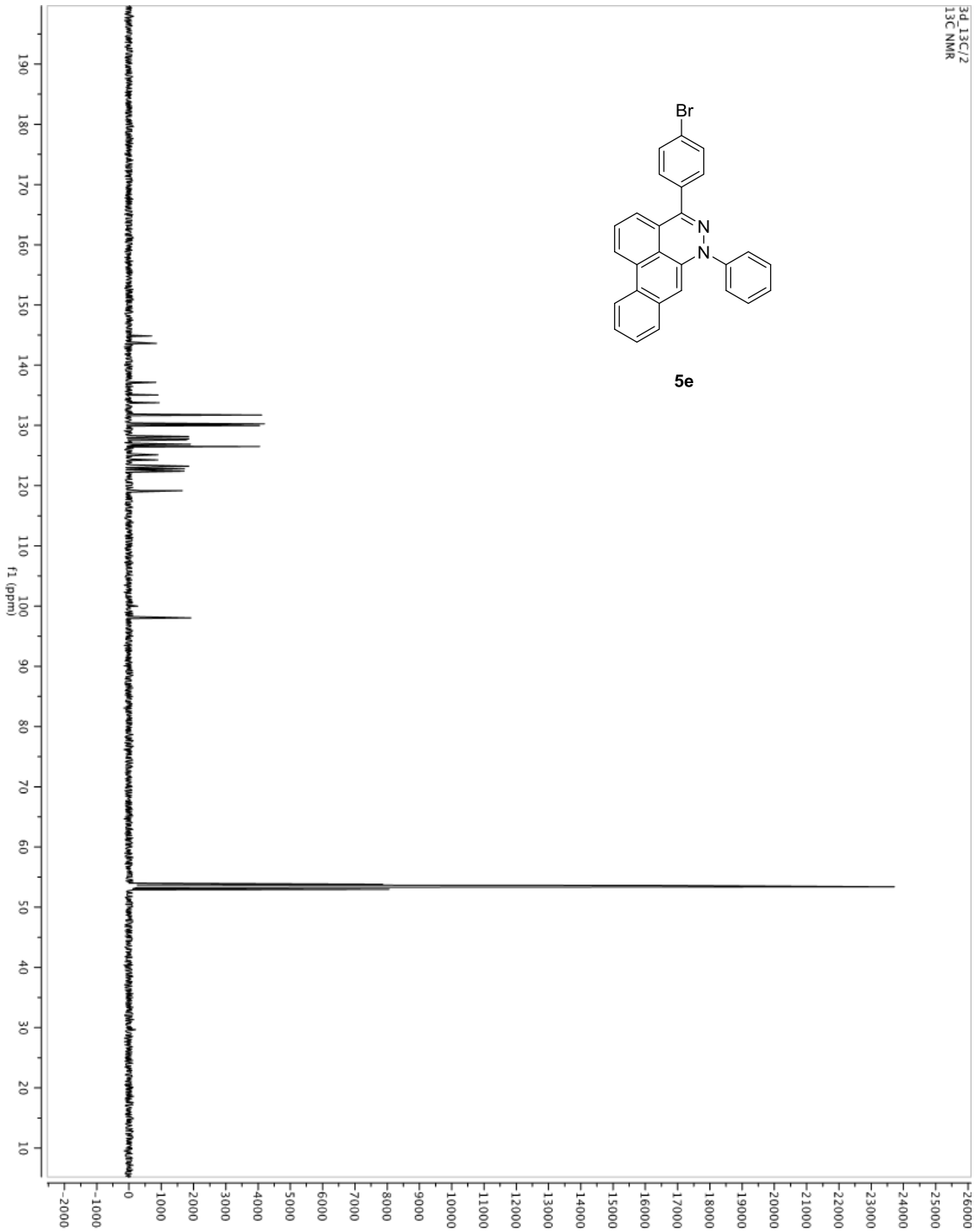

Figure A1.41. ^{1}H NMR spectrum of **5f** in CD_2Cl_2 (500 MHz).

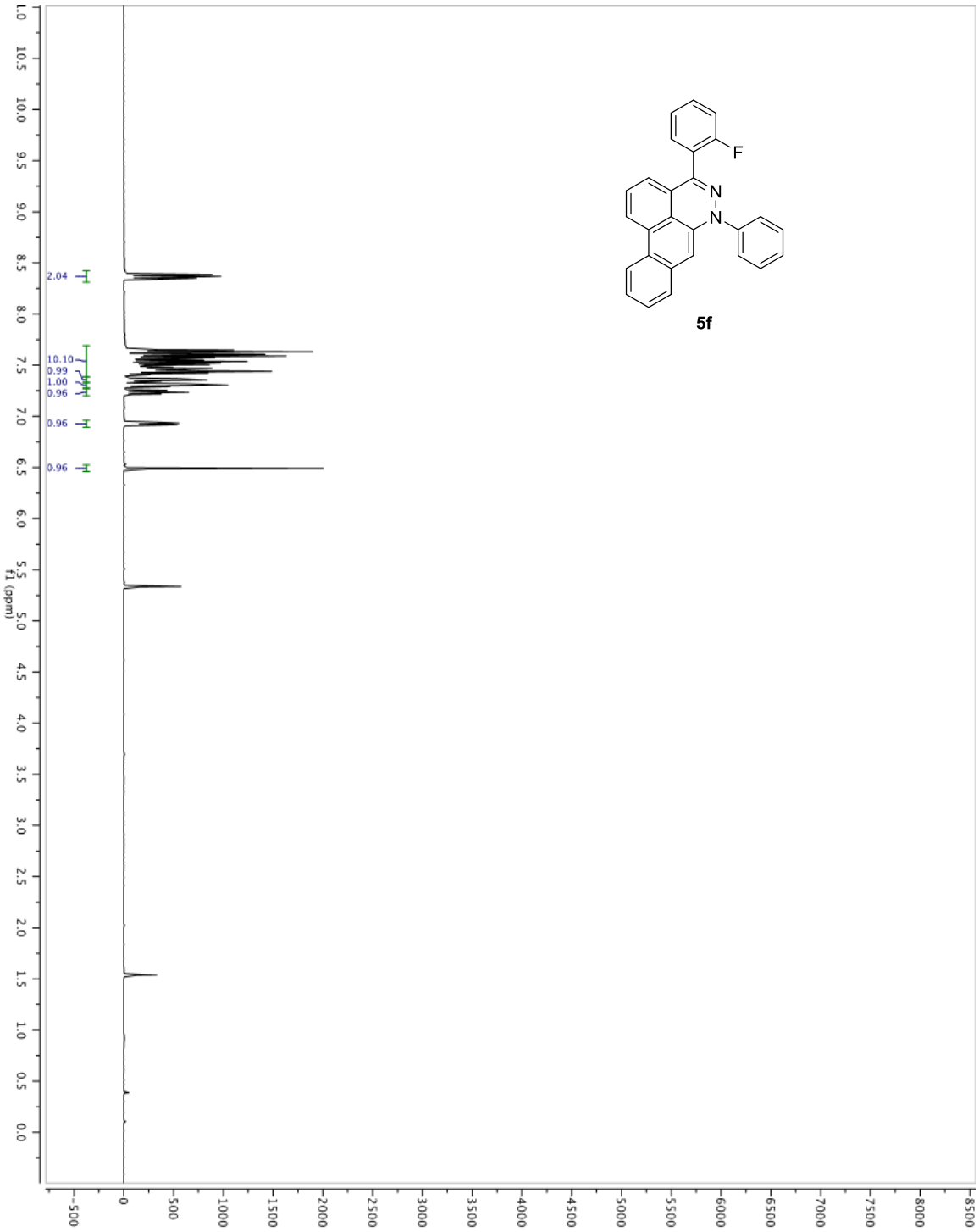

Figure A1.42. ^{13}C NMR spectrum of **5f** in CD_2Cl_2 (125 MHz).

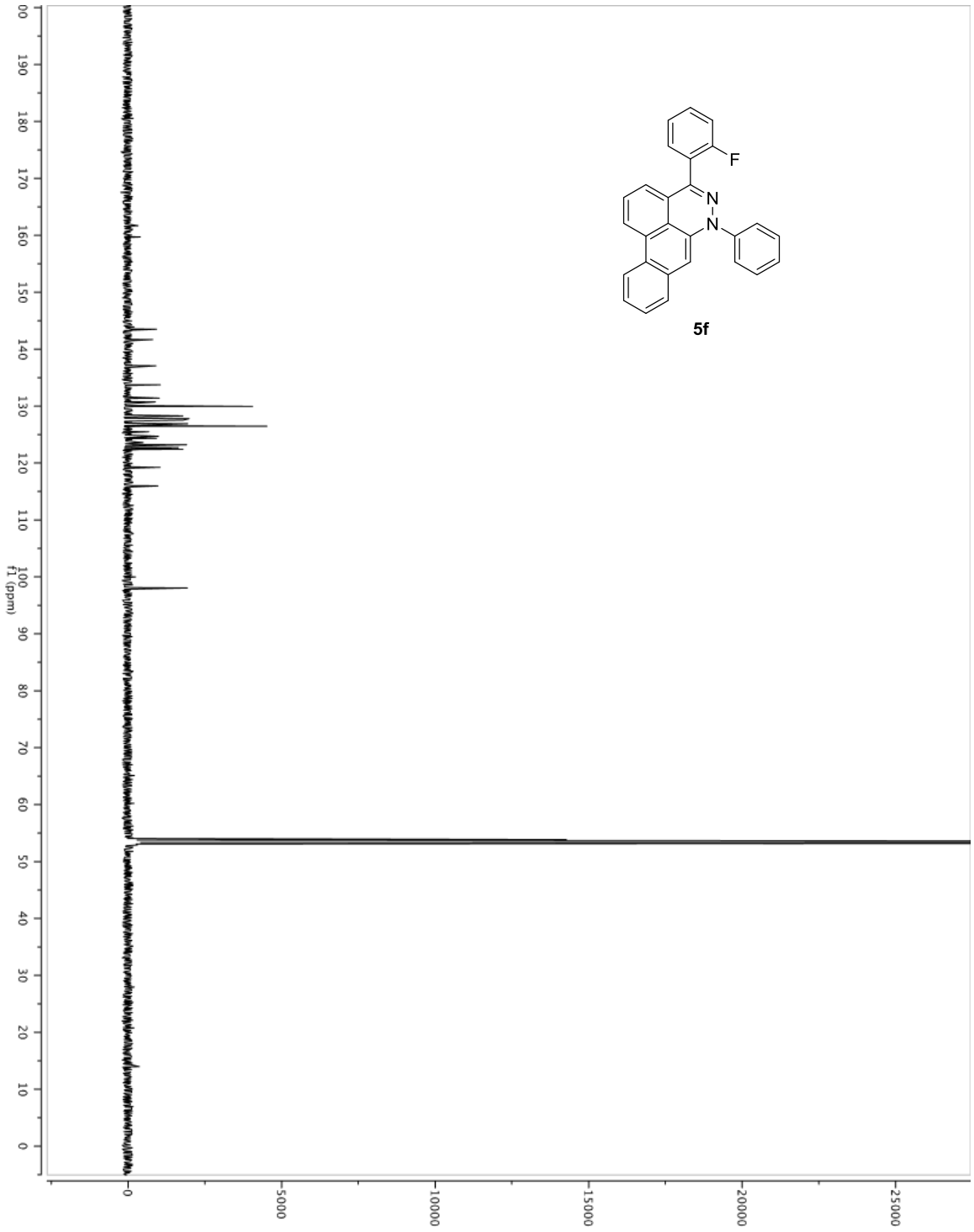

Figure A1.43. ^{19}F NMR spectrum of **5f** in CD_2Cl_2 (338 MHz).

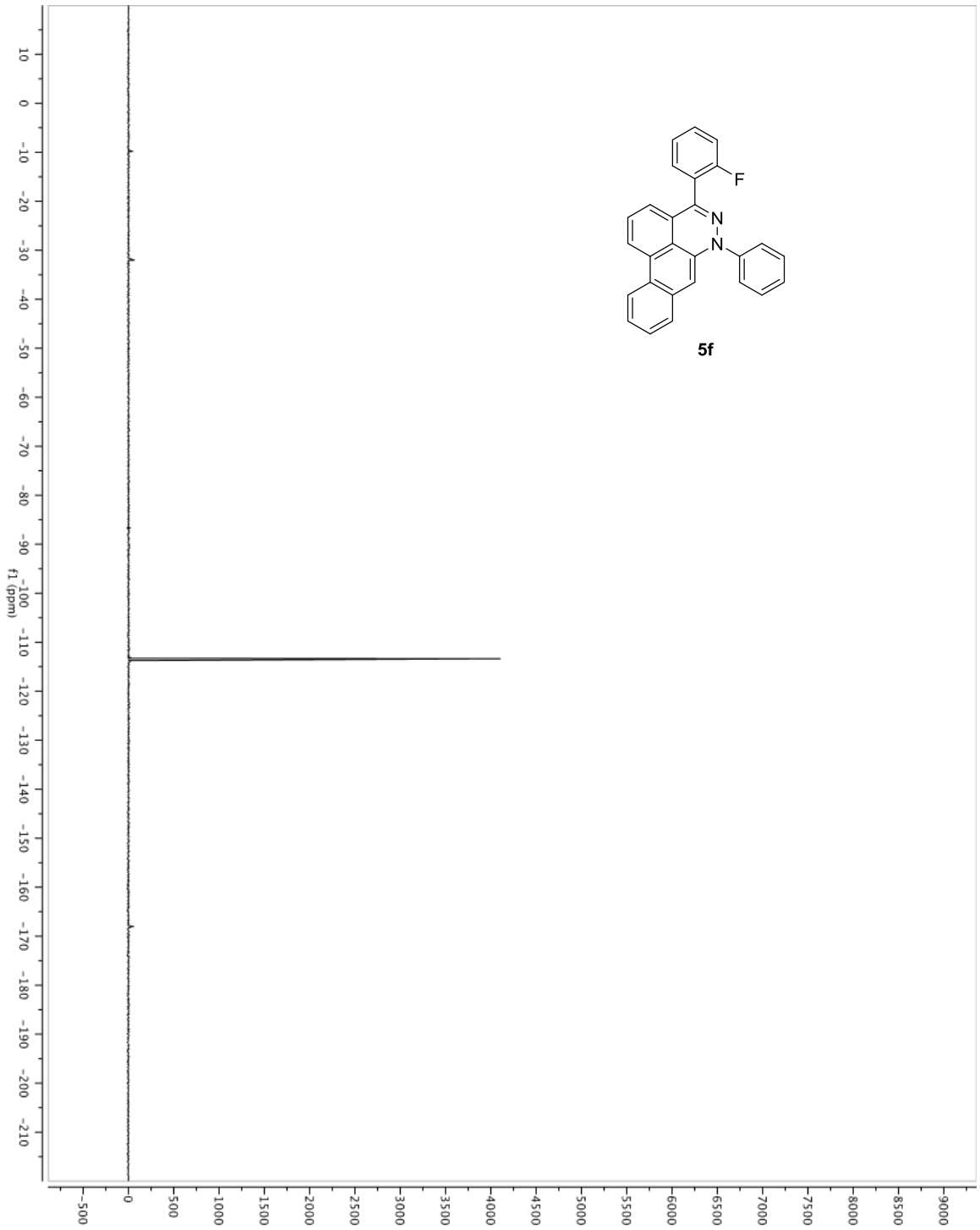

Figure A1.44. ^{1}H NMR spectrum of **5g** in CD_2Cl_2 (500 MHz).

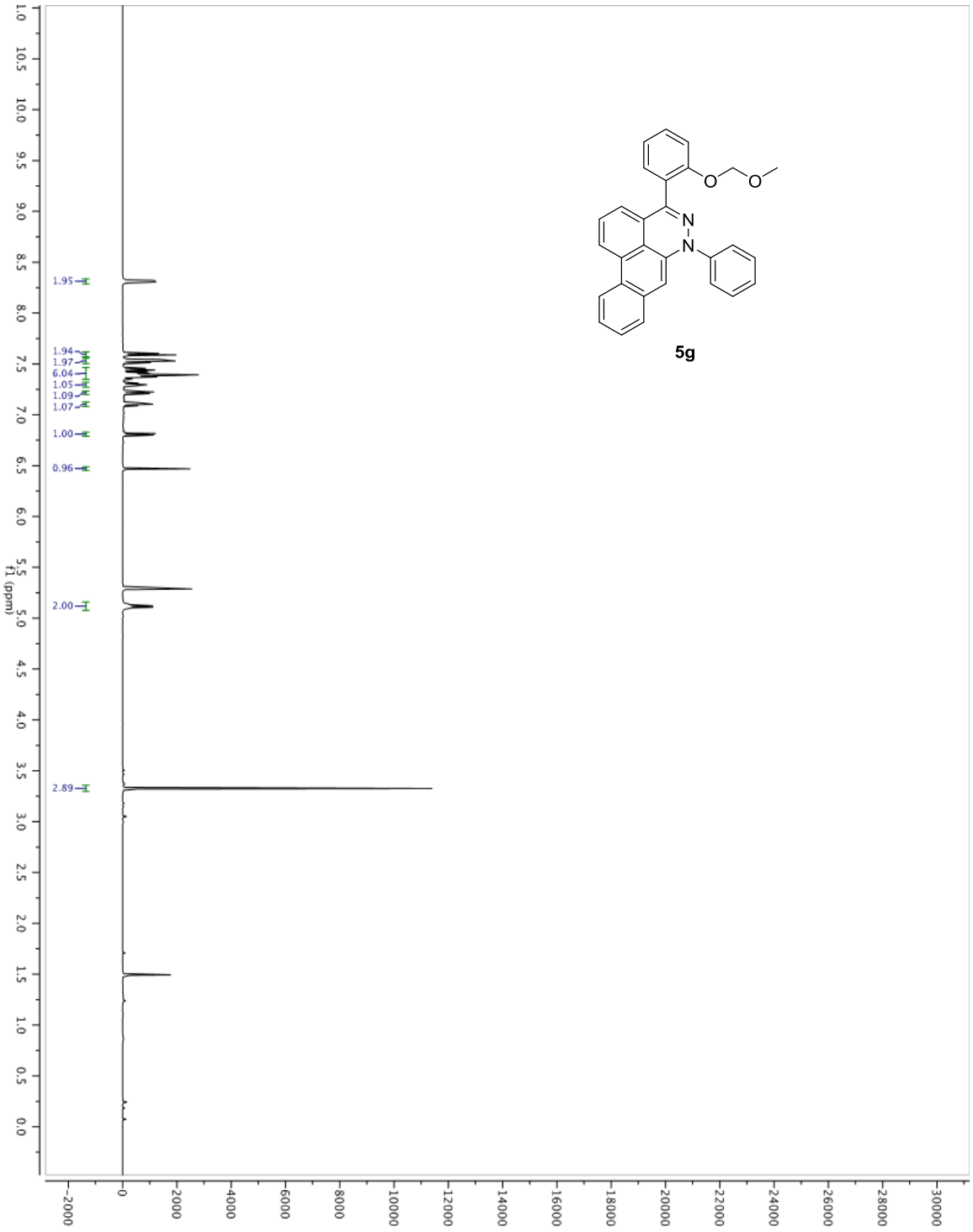

Figure A1.45. ^{13}C NMR spectrum of **5g** in CD_2Cl_2 (125 MHz).

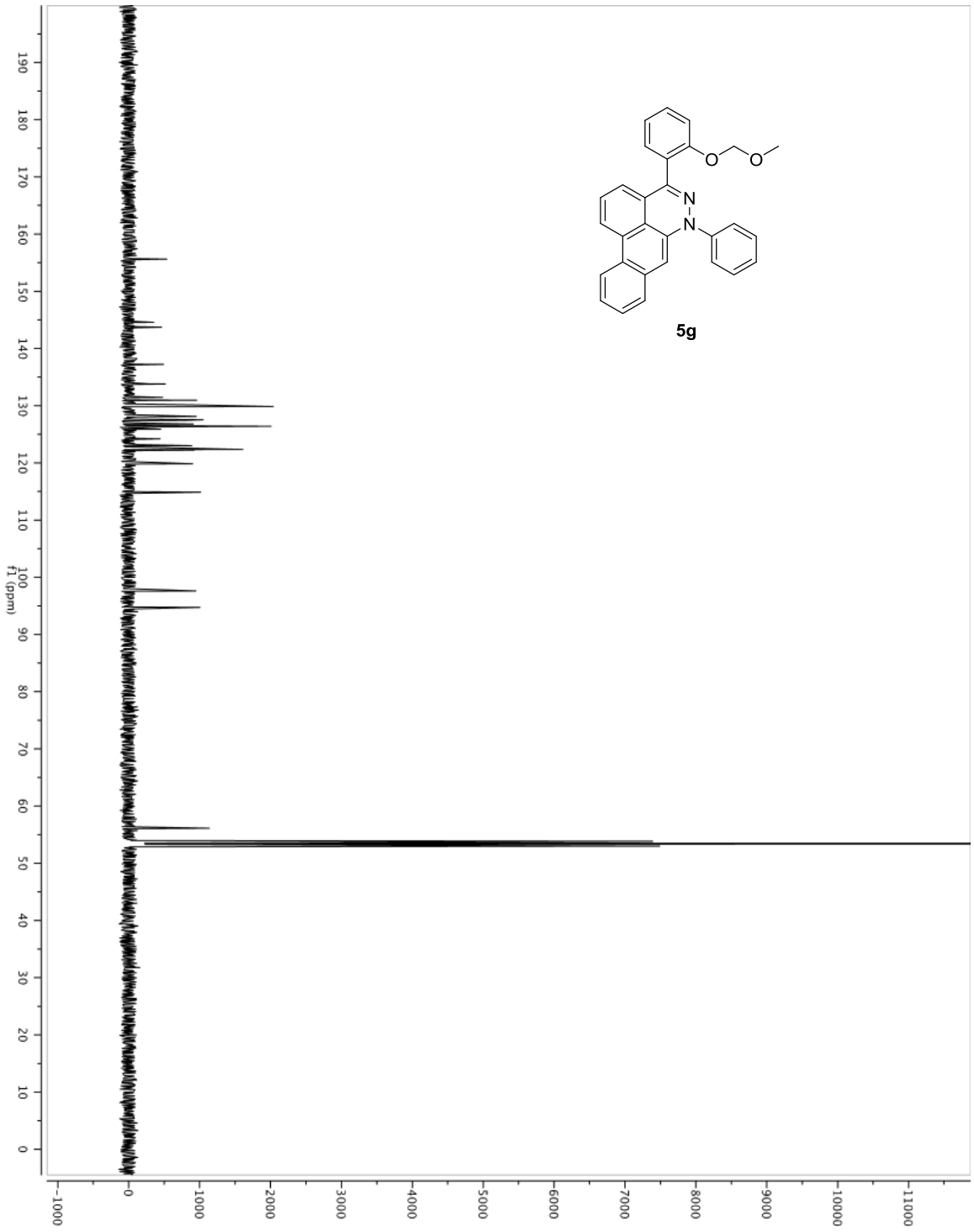

Figure A1.46. ^{1}H NMR spectrum of **5h** in CD_2Cl_2 (500 MHz).

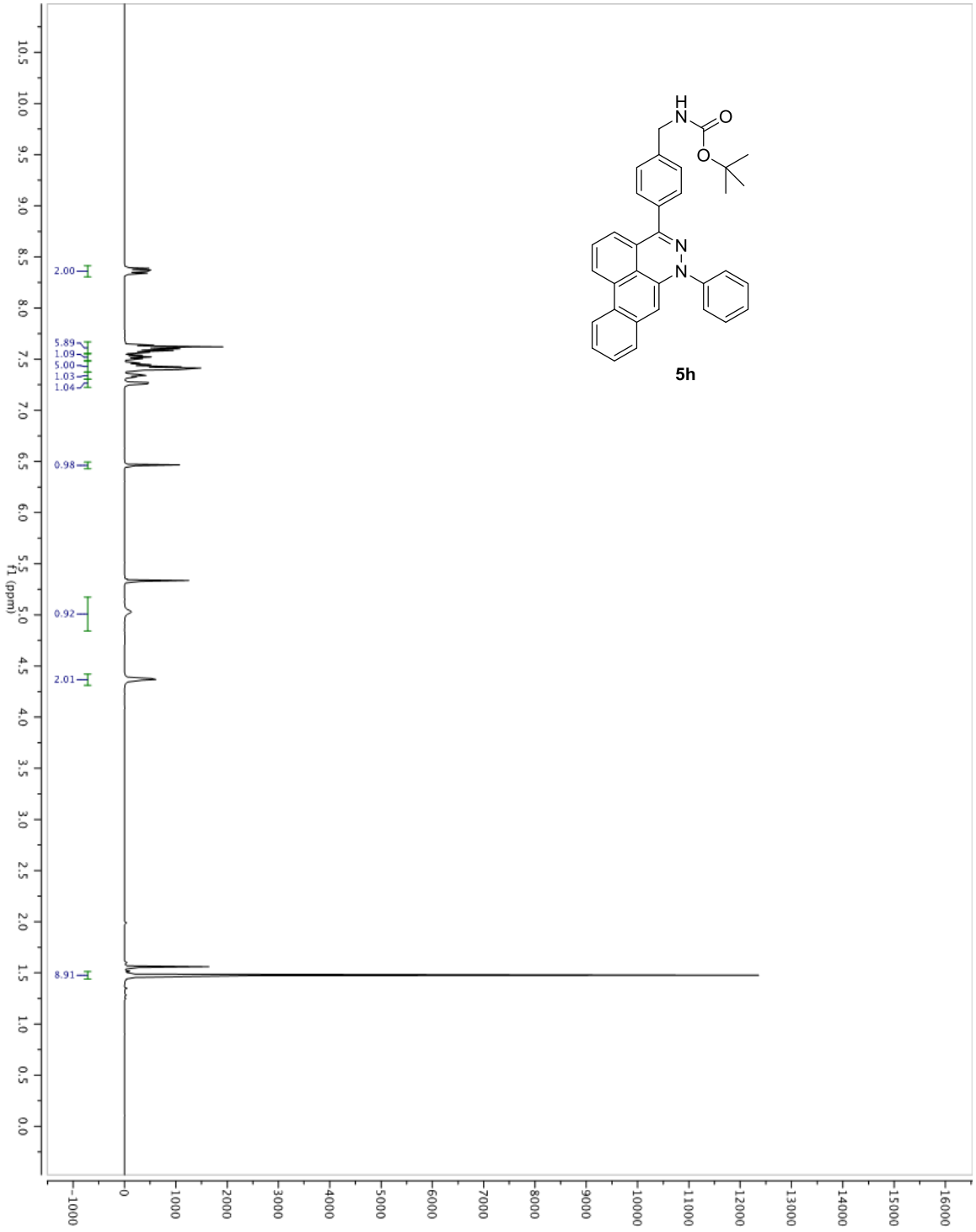

Figure A1.47. ^{13}C NMR spectrum of **5h** in CD_2Cl_2 (125 MHz).

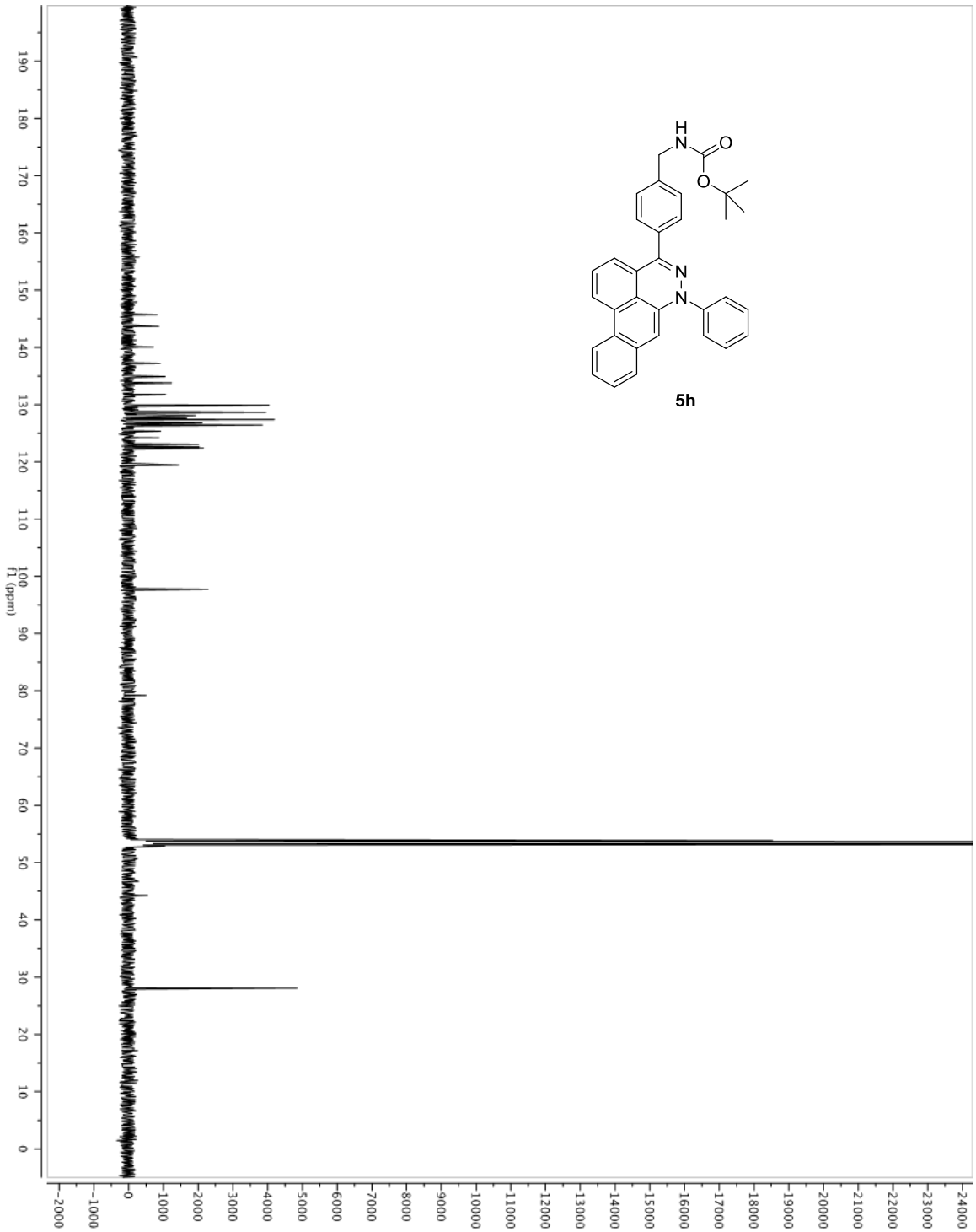

Figure A1.48. ^{1}H NMR spectrum of **5i** in CD_2Cl_2 (500 MHz).

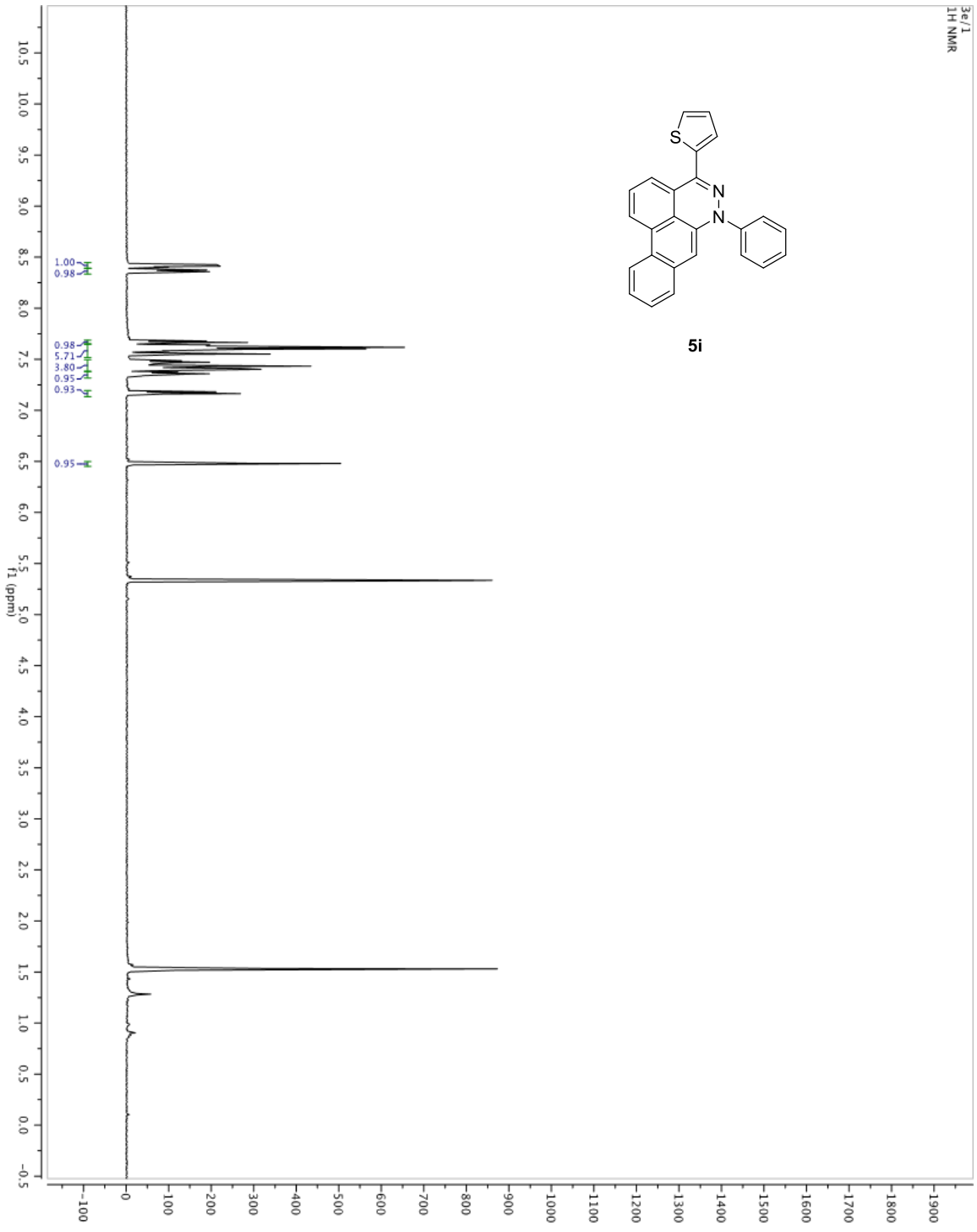

Figure A1.49. ^{13}C NMR spectrum of **5i** in CD_2Cl_2 (125 MHz).

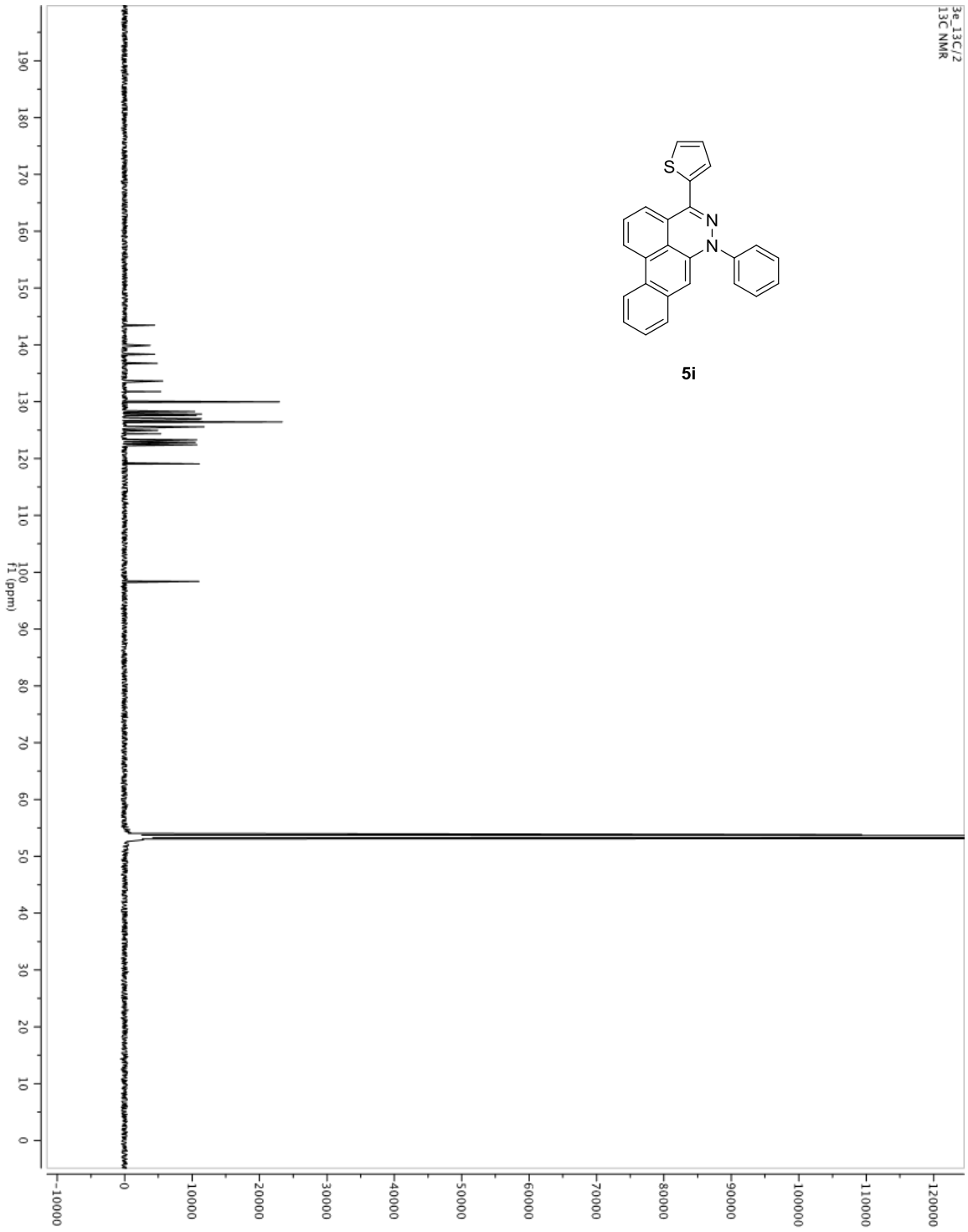

Figure A1.50. ^{1}H NMR spectrum of **5j** in CD_2Cl_2 (500 MHz).

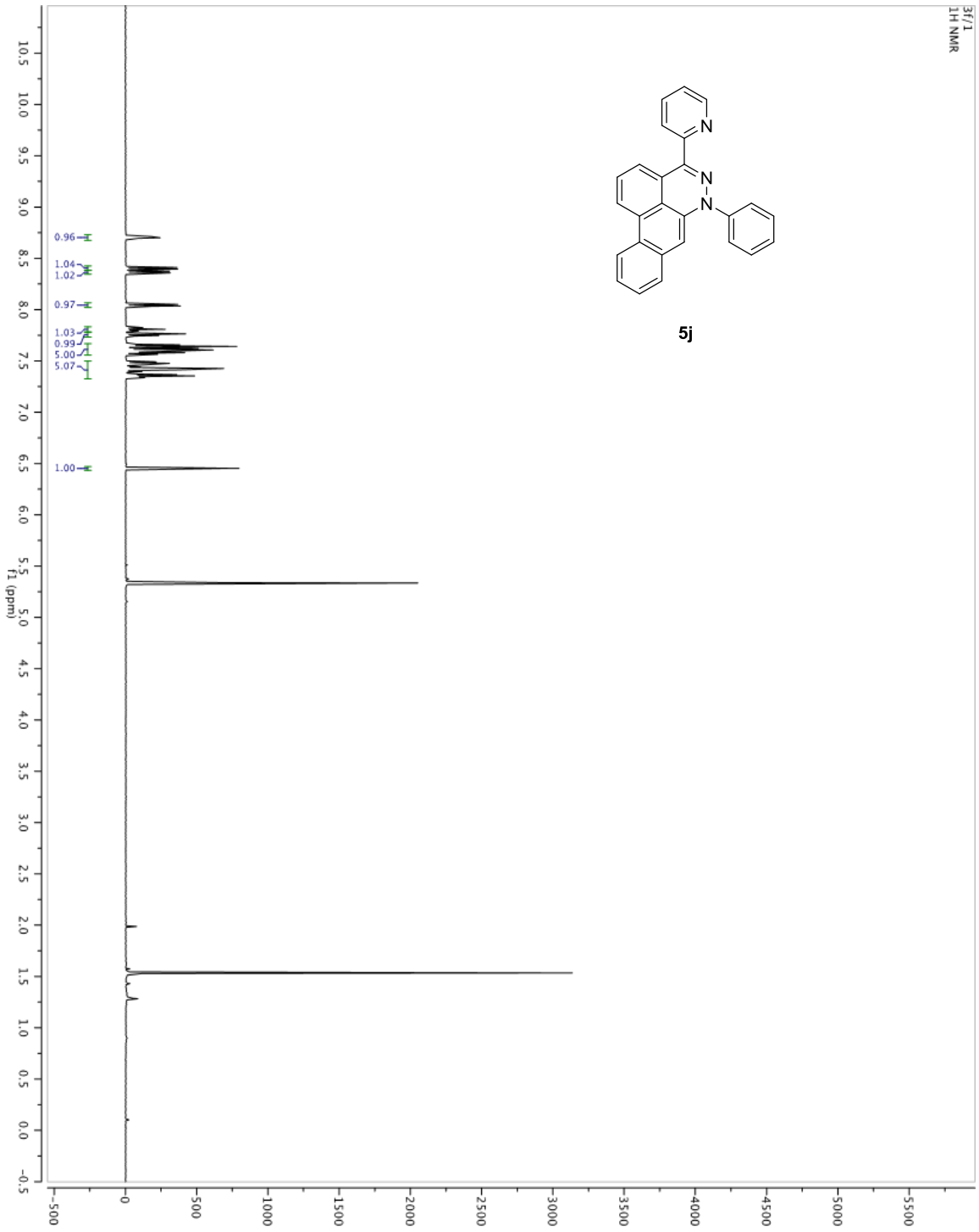

Figure A1.51. ^{13}C NMR spectrum of **5j** in CD_2Cl_2 (125 MHz).

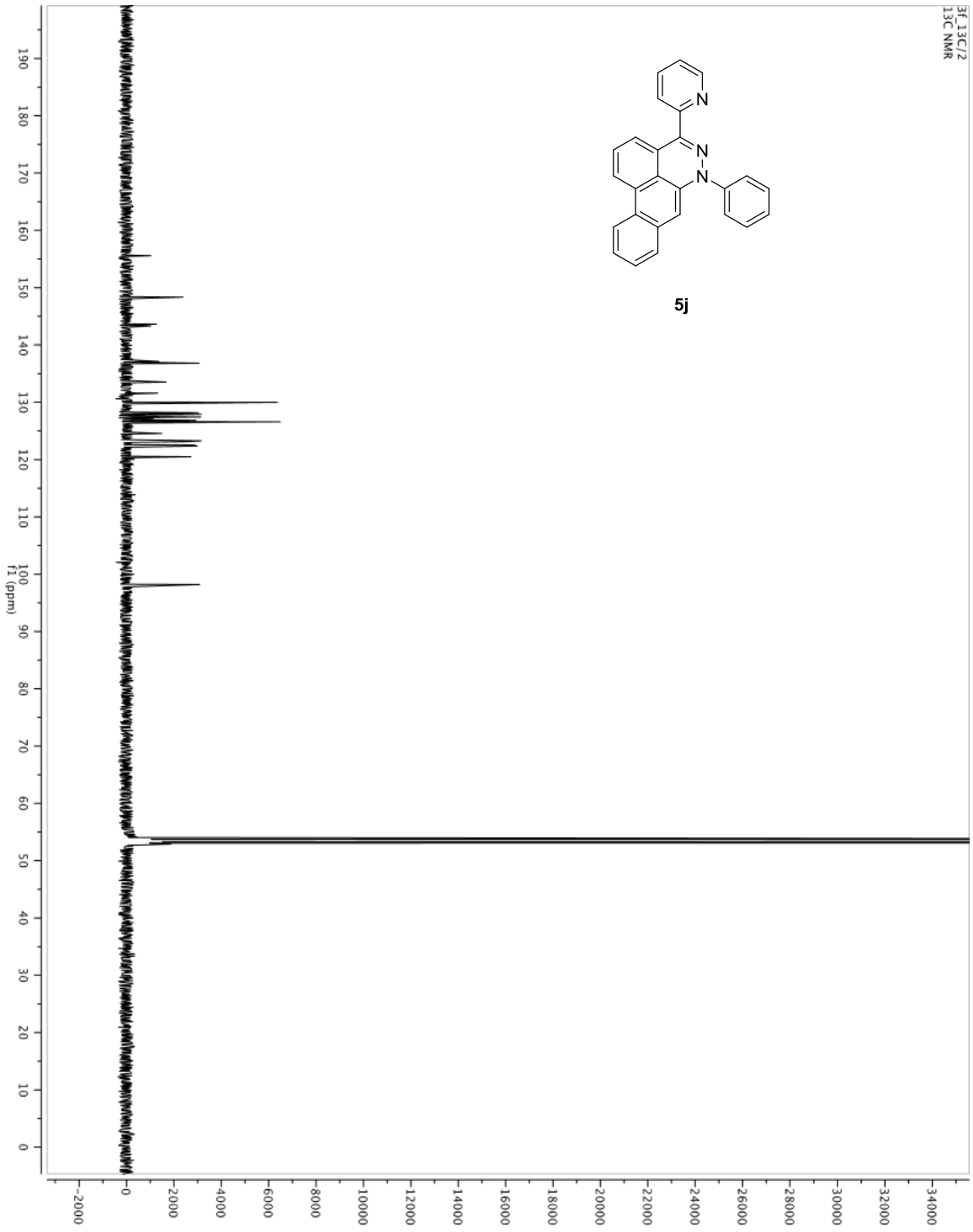

Figure A1.52. ^{1}H NMR spectrum of **5k** in CD_2Cl_2 (500 MHz).

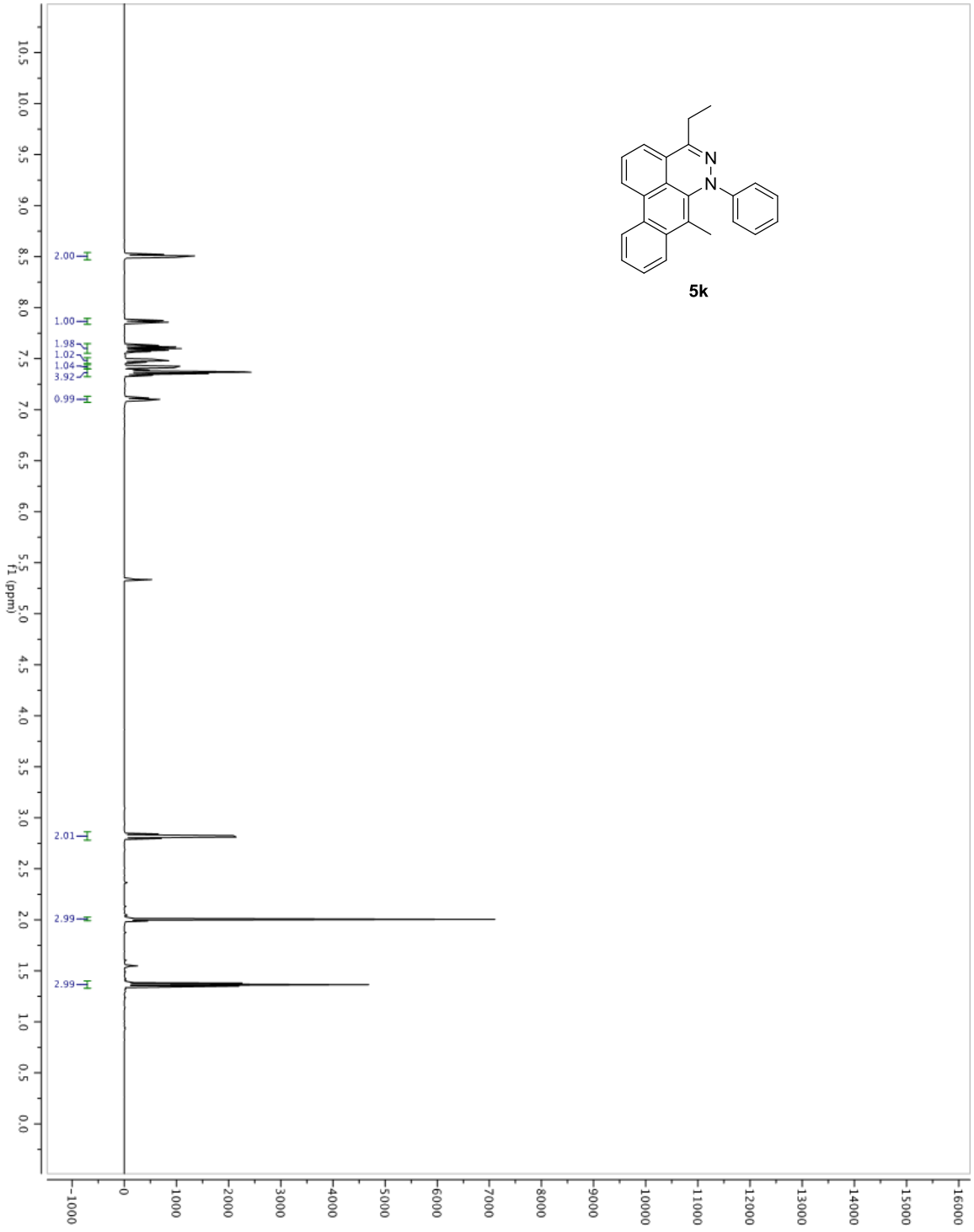

Figure A1.53. ^{13}C NMR spectrum of **5k** in CD_2Cl_2 (125 MHz).

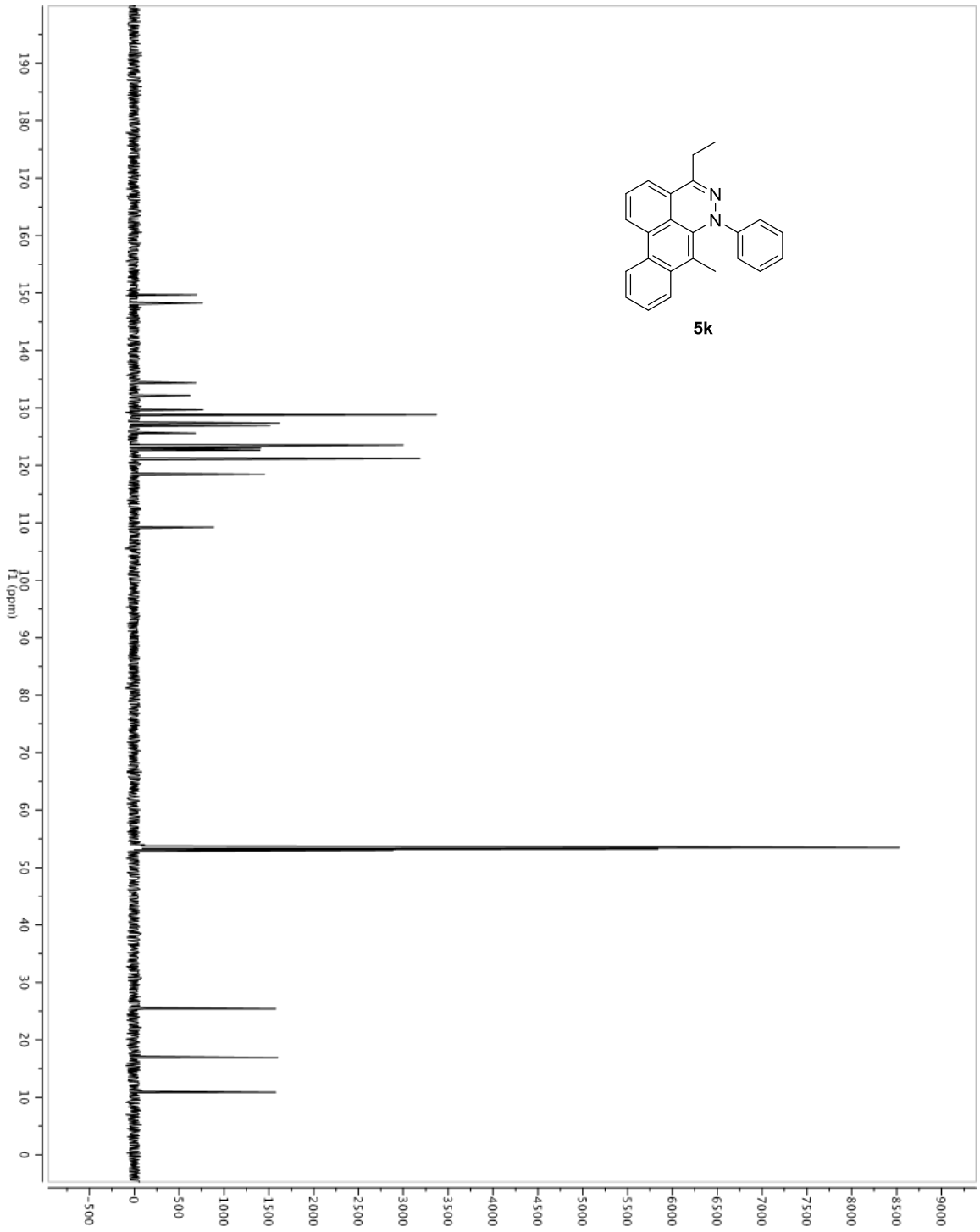

Figure A1.54. ^{1}H NMR spectrum of **5l** in CD_2Cl_2 (500 MHz).

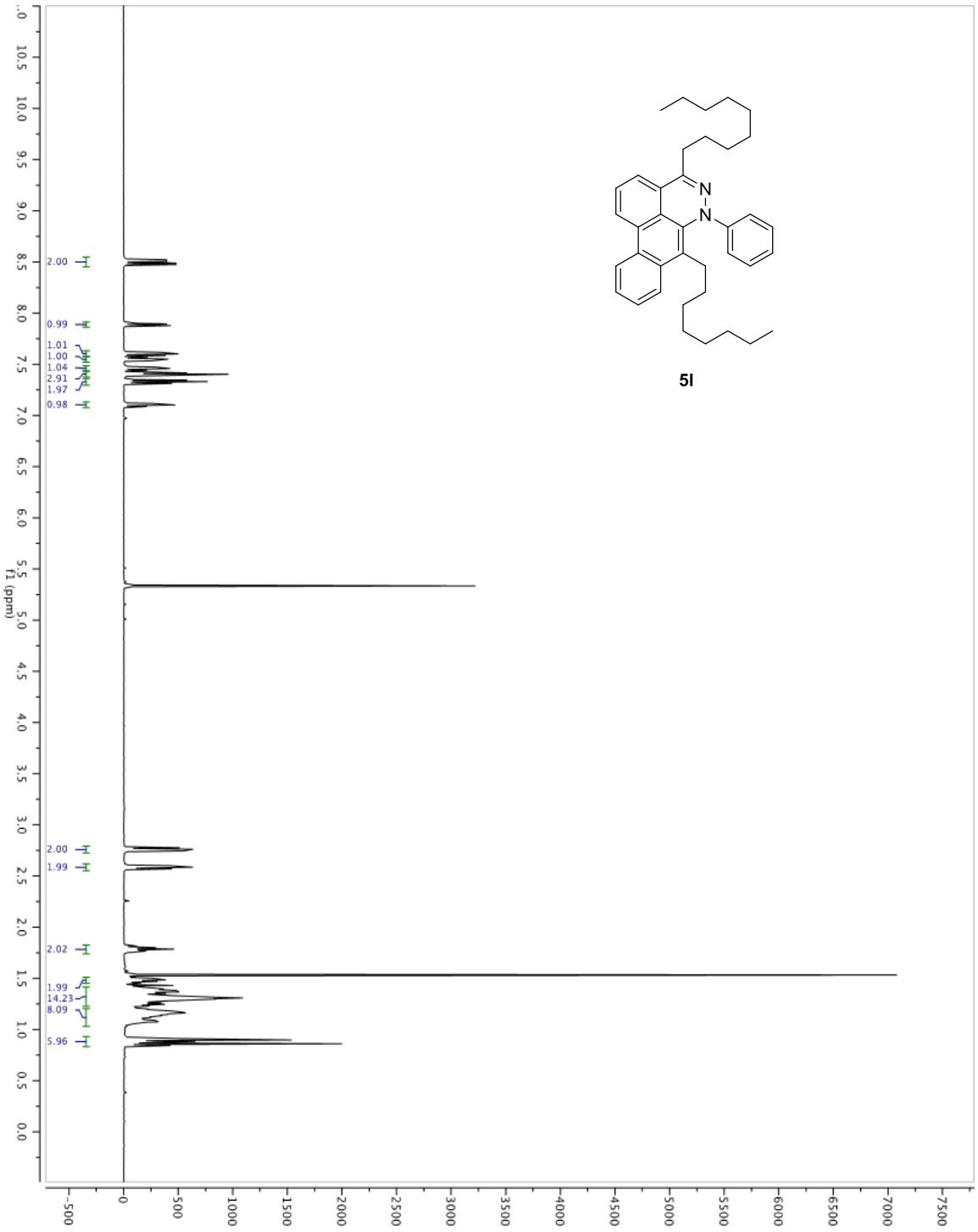

Figure A1.55. ^{13}C NMR spectrum of **5l** in CD_2Cl_2 (125 MHz).

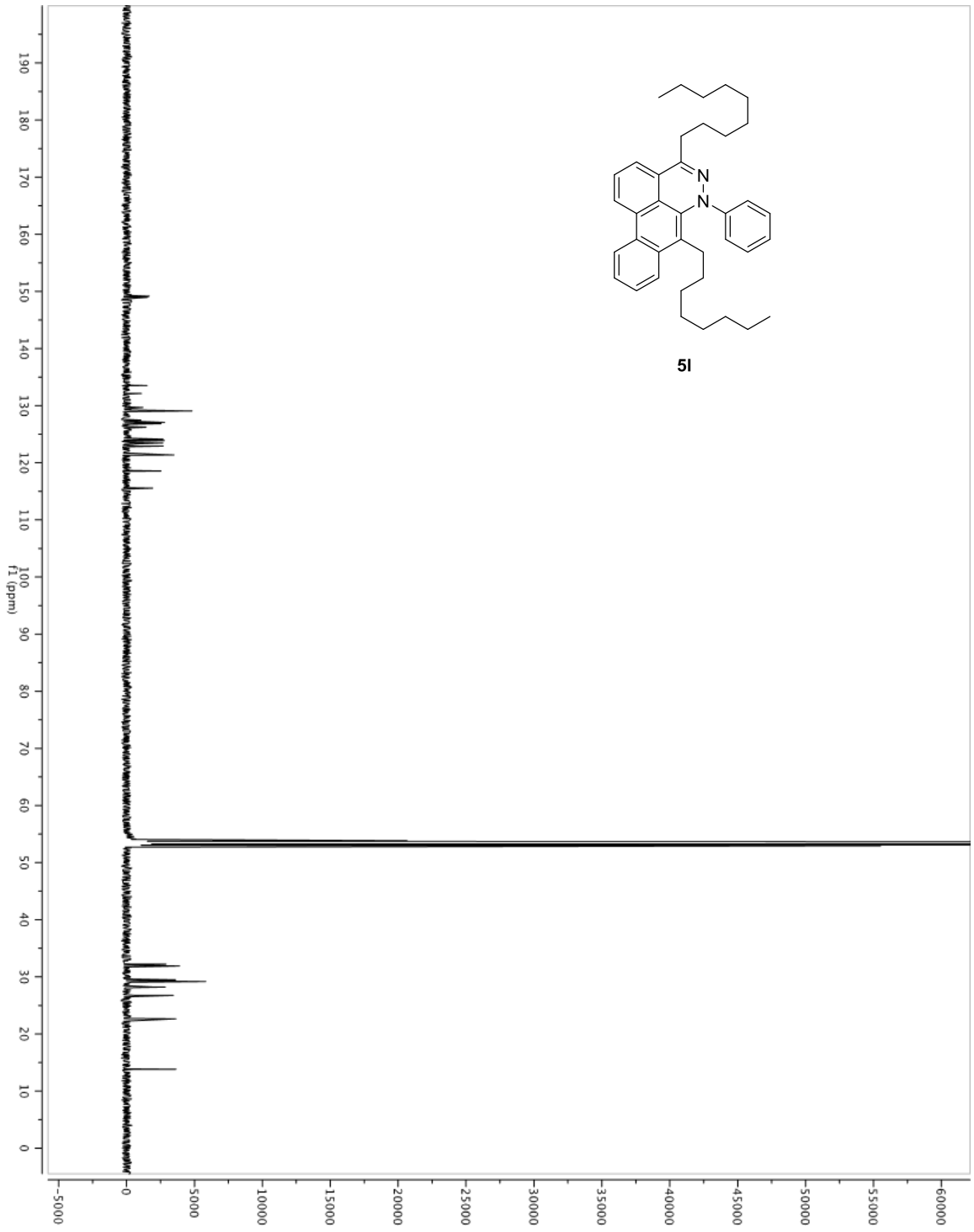

Figure A1.56. ^{1}H NMR spectrum of **5m** in CD_2Cl_2 (500 MHz).

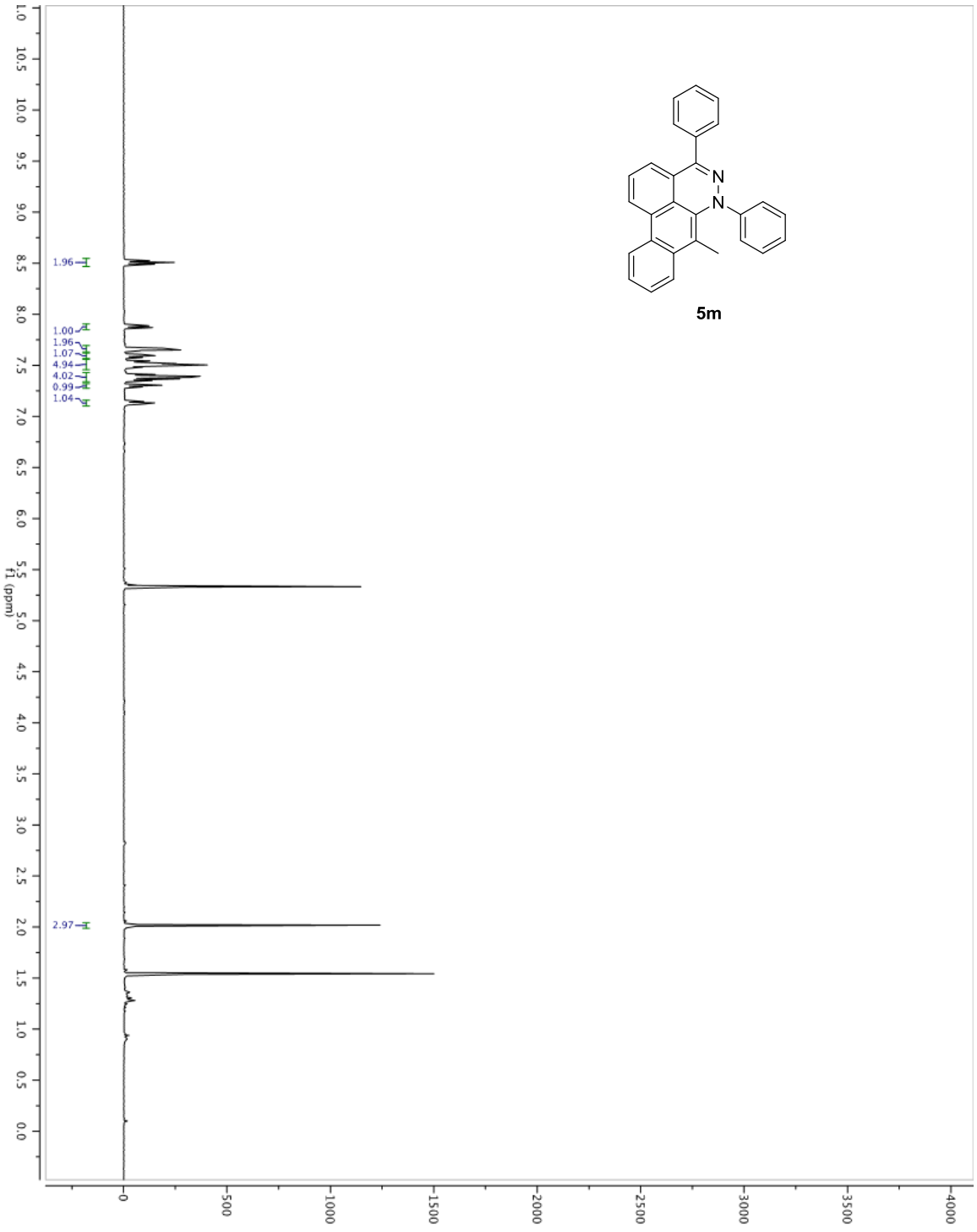

Figure A1.57. ^{13}C NMR spectrum of **5m** in CD_2Cl_2 (125 MHz).

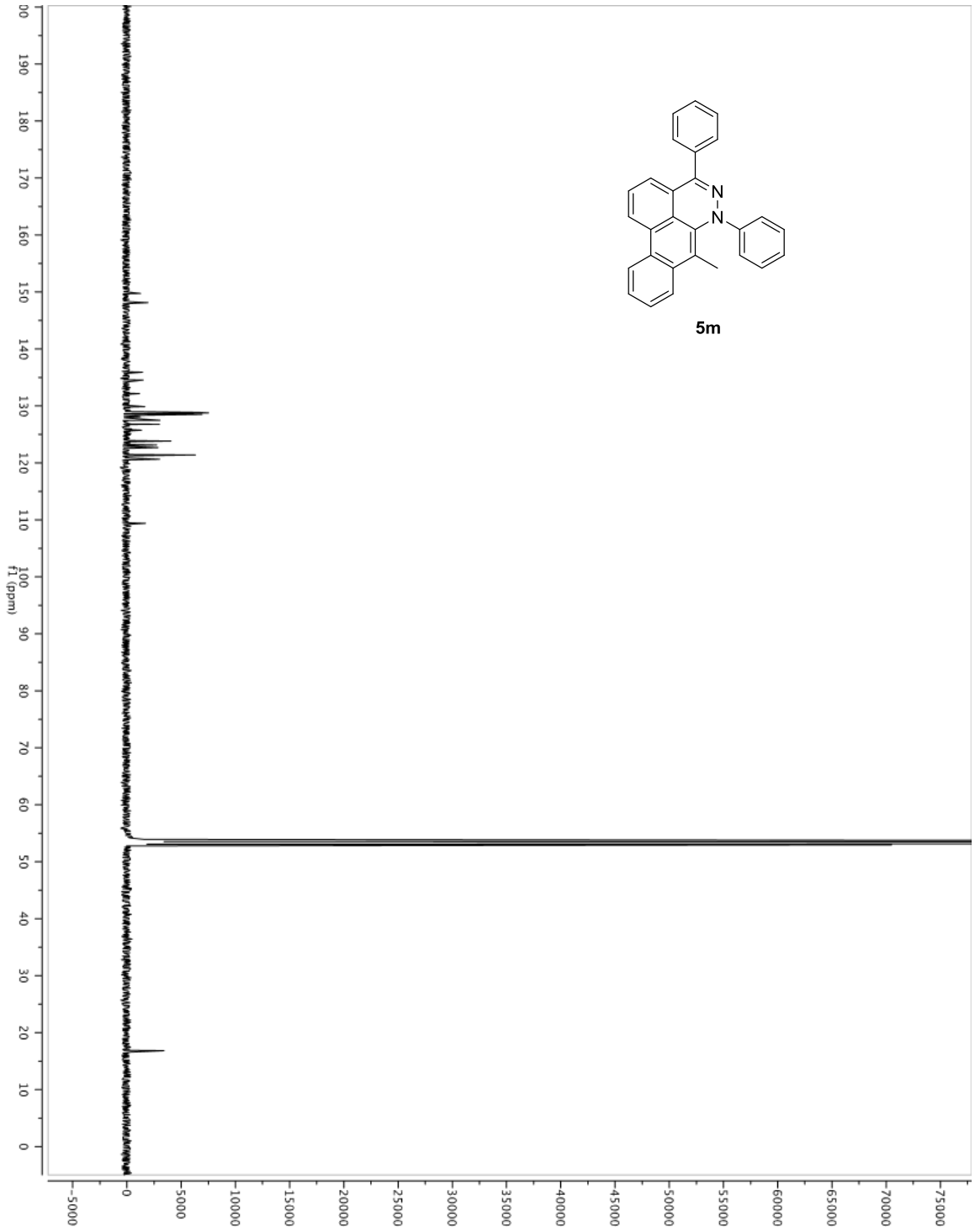

Figure A1.58. ^{1}H NMR spectrum of **5n** in CD_2Cl_2 (500 MHz).

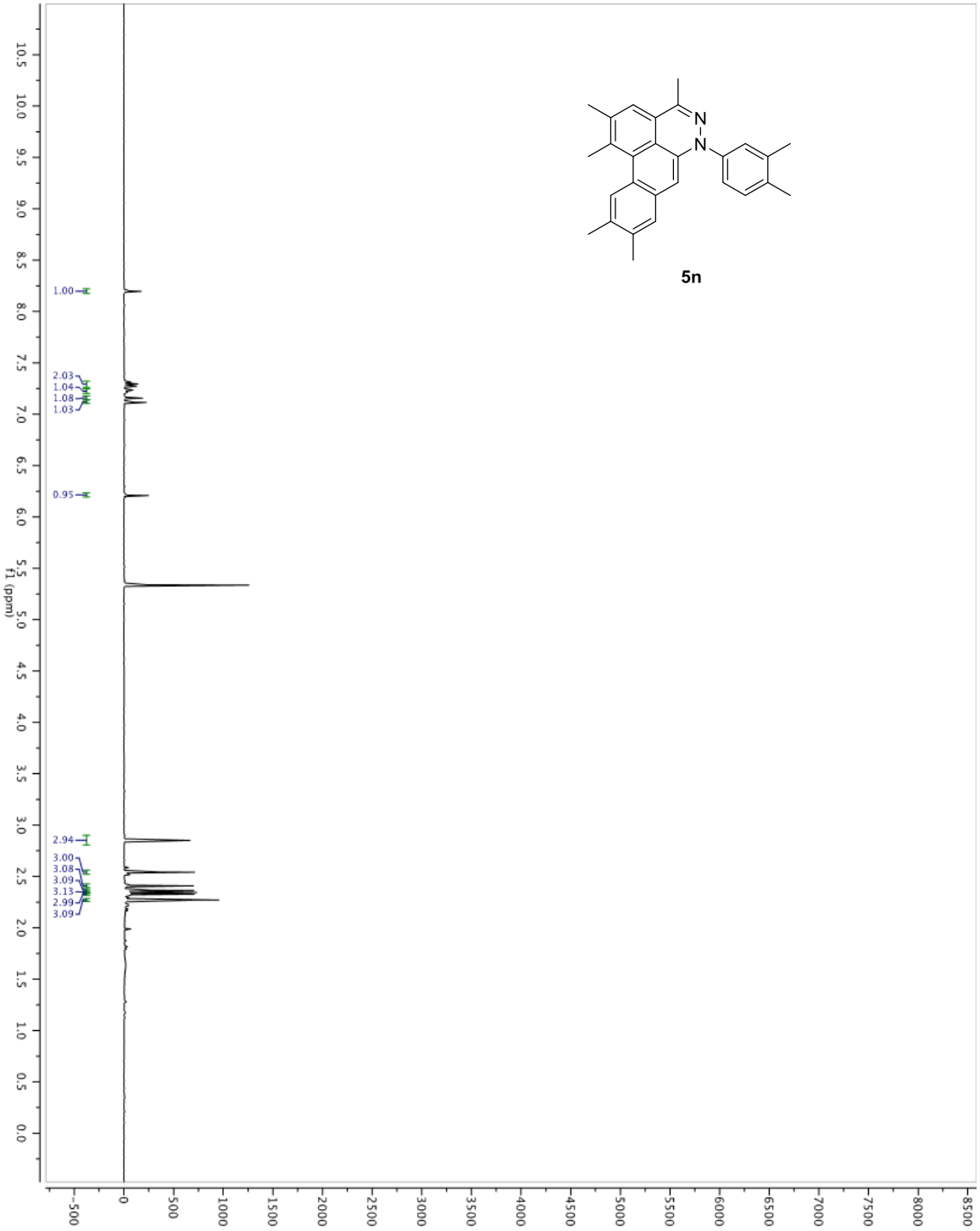

Figure A1.59. ^{13}C NMR spectrum of **5n** in CD_2Cl_2 (125 MHz).

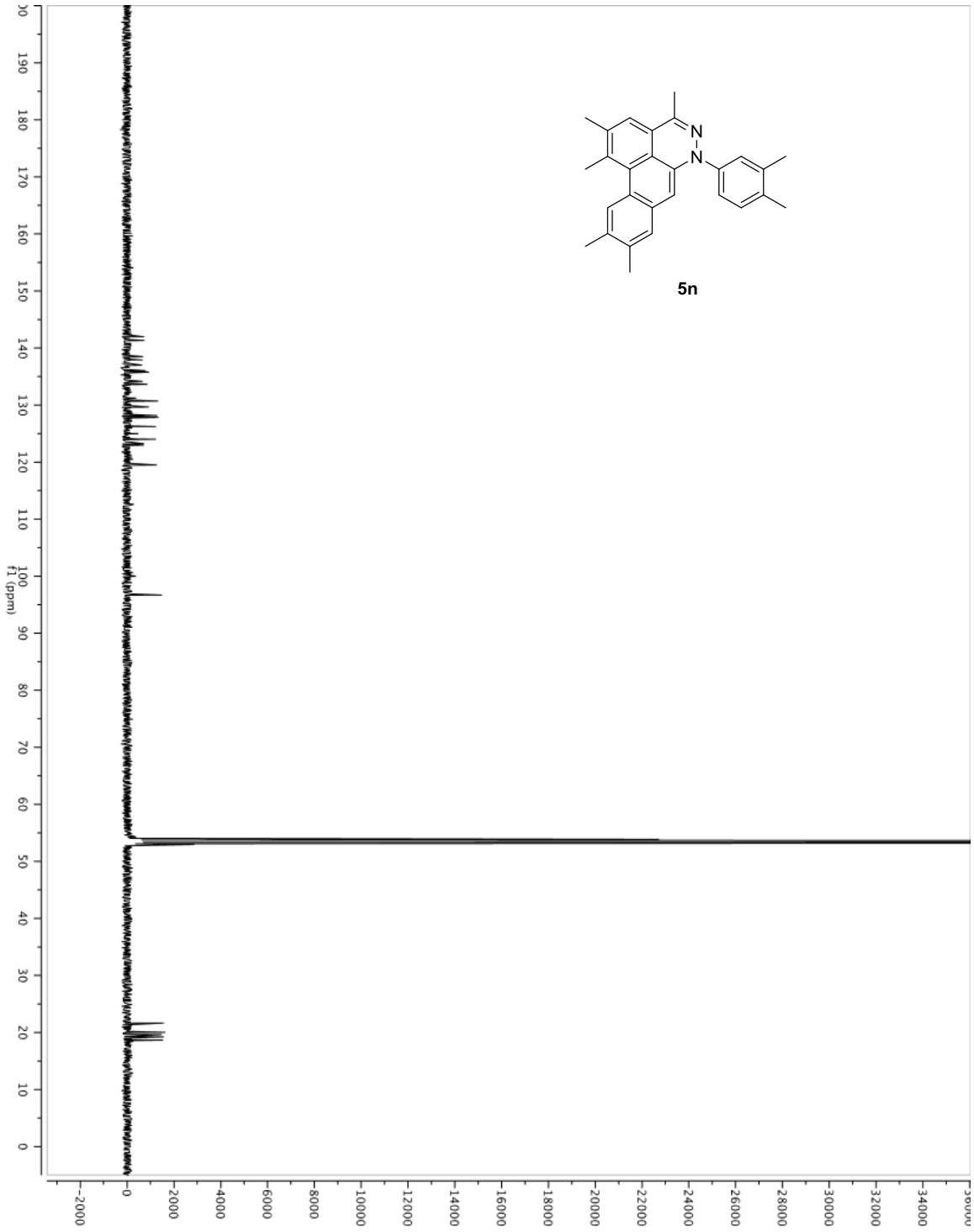

Figure A1.60. ^{1}H NMR spectrum of **5o** in CD_2Cl_2 (500 MHz).

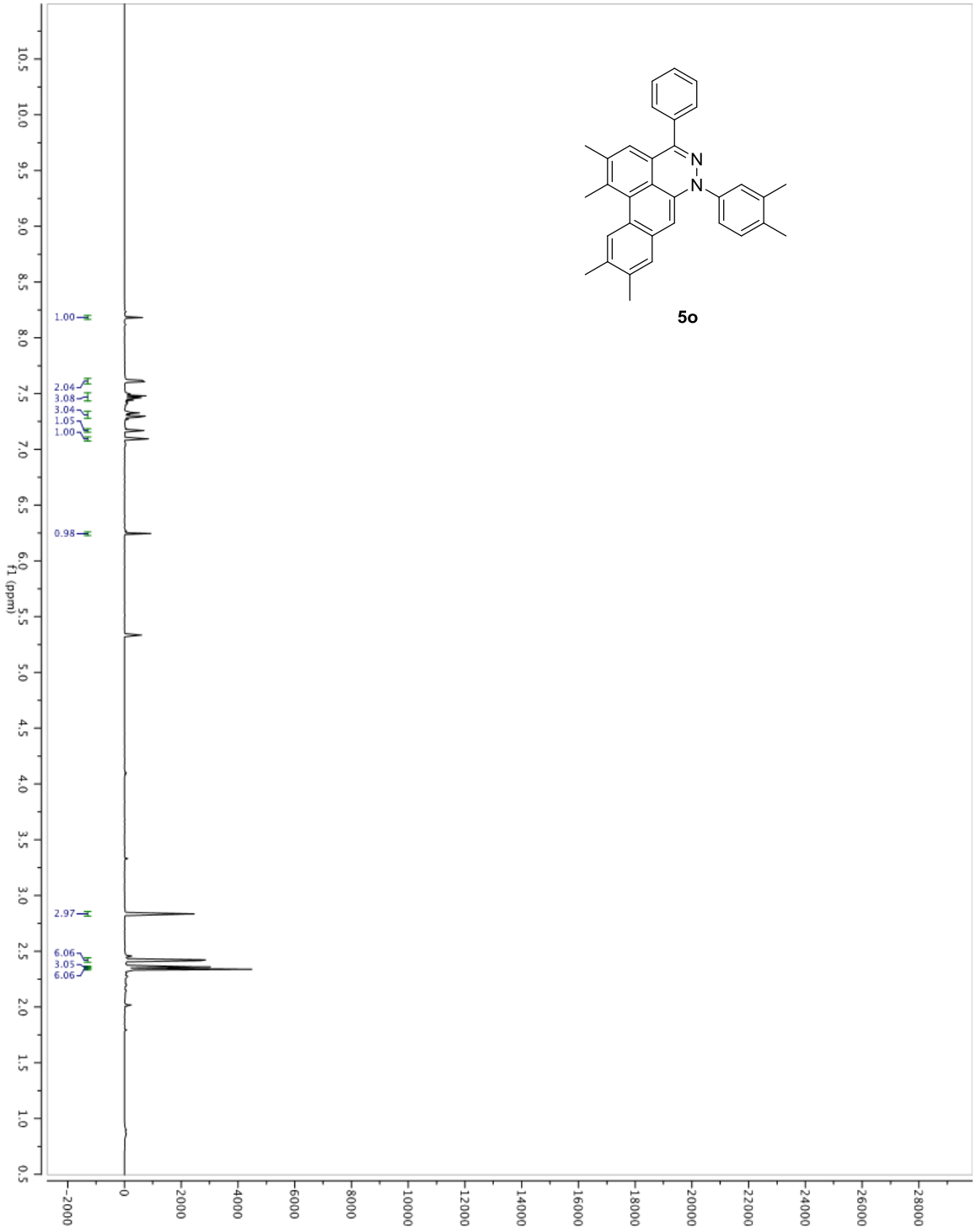

Figure A1.61. ^{13}C NMR spectrum of **5o** in CD_2Cl_2 (125 MHz).

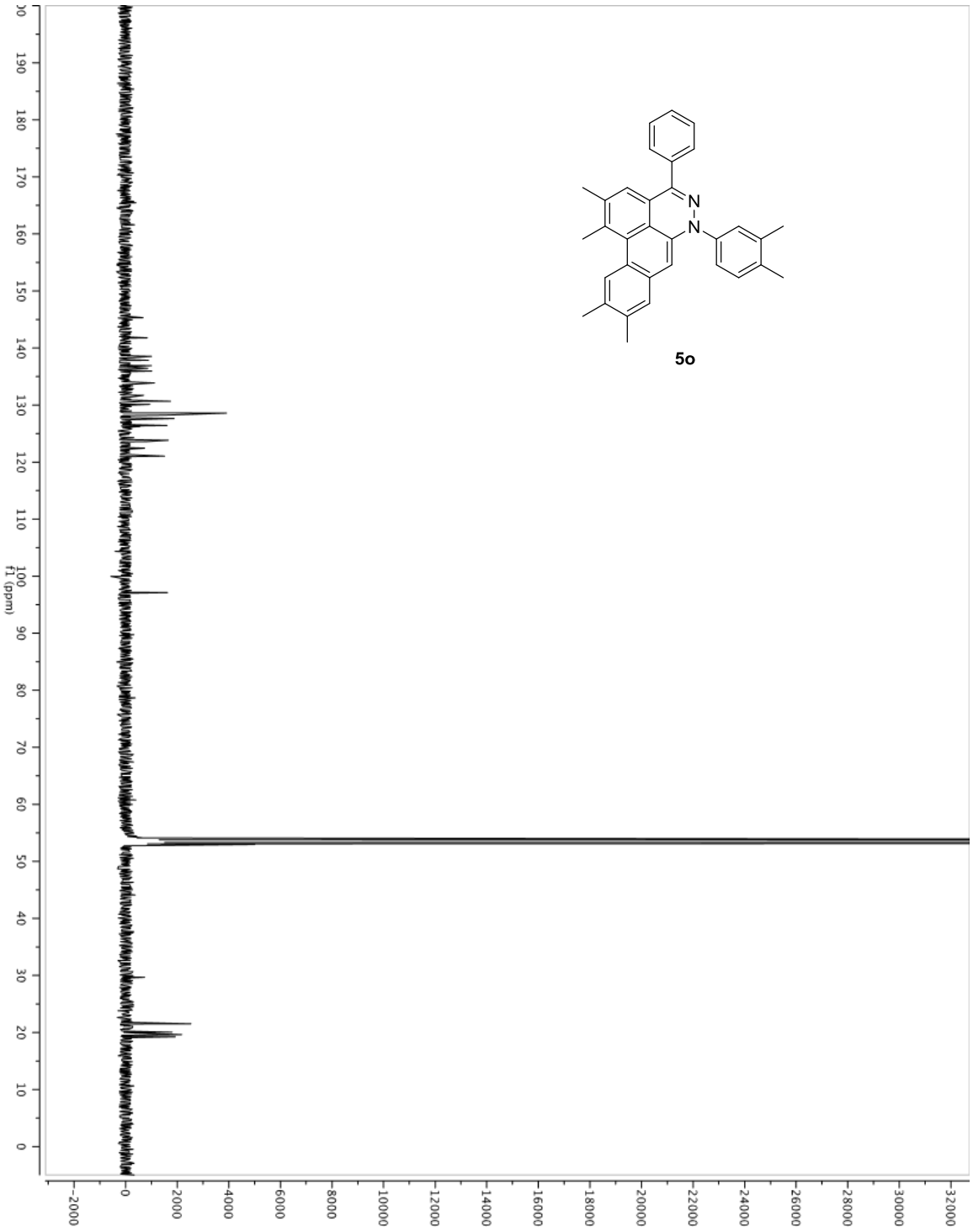

Figure A1.62. ^{1}H NMR spectrum of **5p** in CD_2Cl_2 (500 MHz).

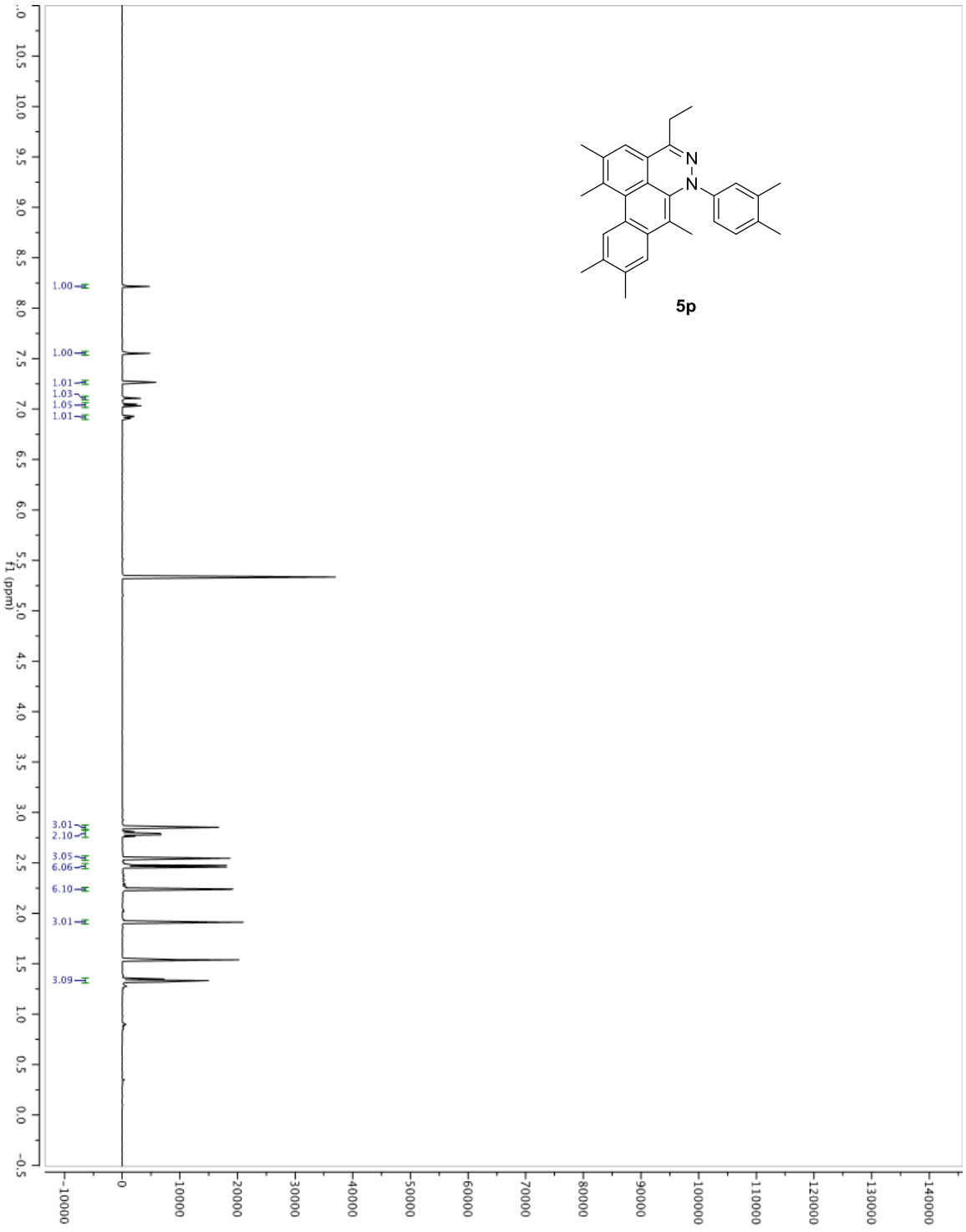

Figure A1.63. ^{13}C NMR spectrum of **5p** in CD_2Cl_2 (125 MHz).

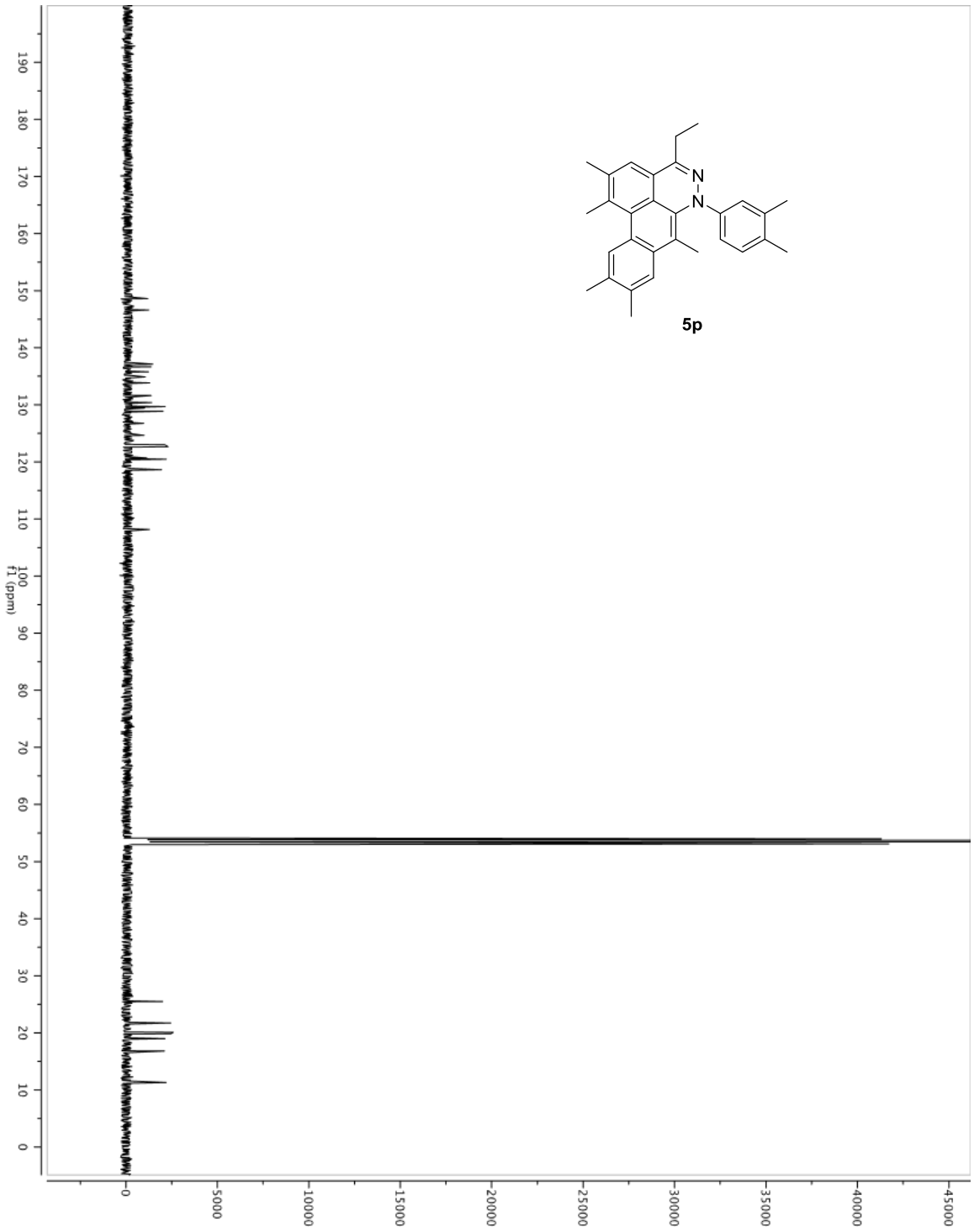

Figure A1.64. ^{1}H NMR spectrum of **5q** in CD_2Cl_2 (500 MHz).

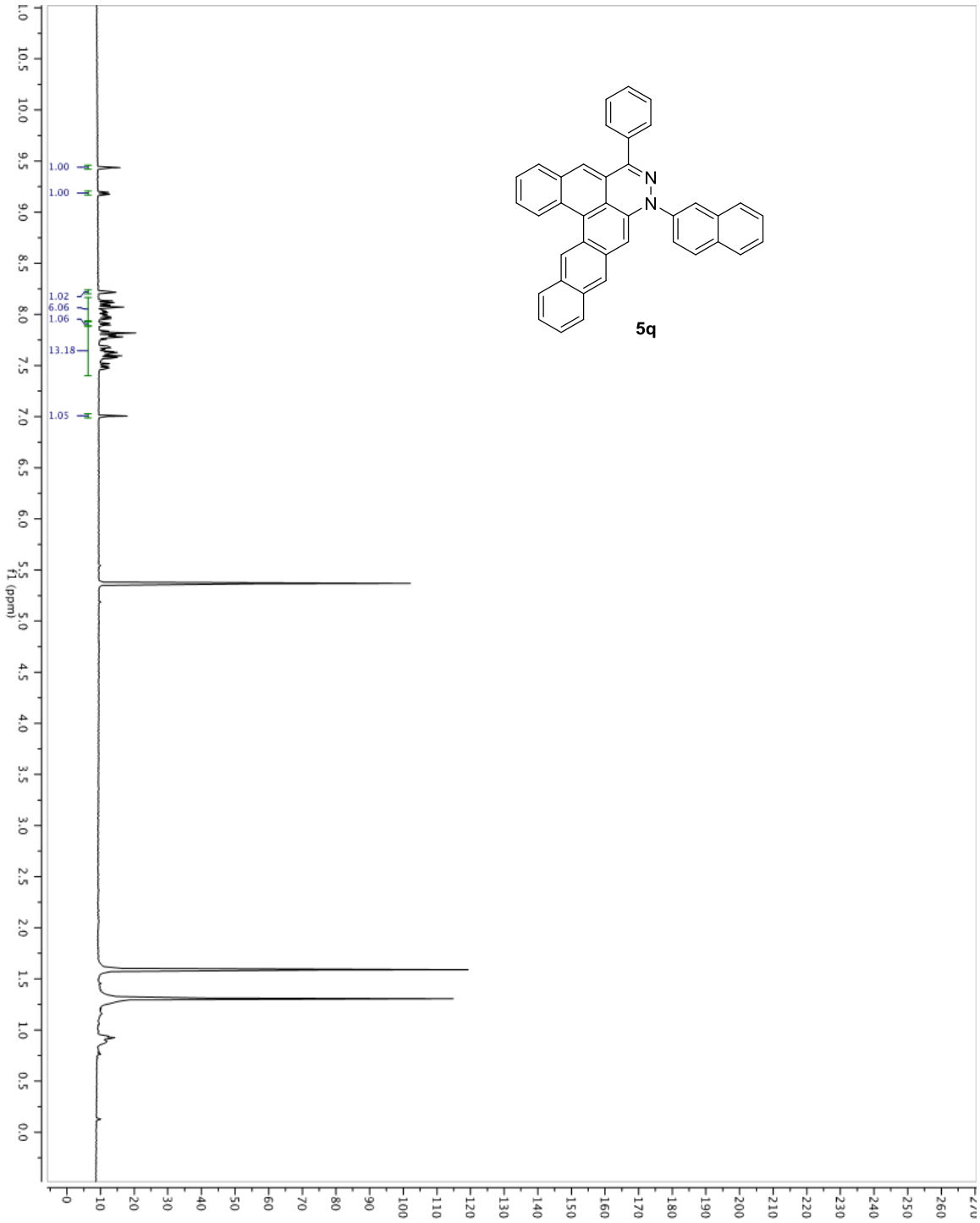

Figure A1.65. ^{13}C NMR spectrum of **5q** in CD_2Cl_2 (125 MHz).

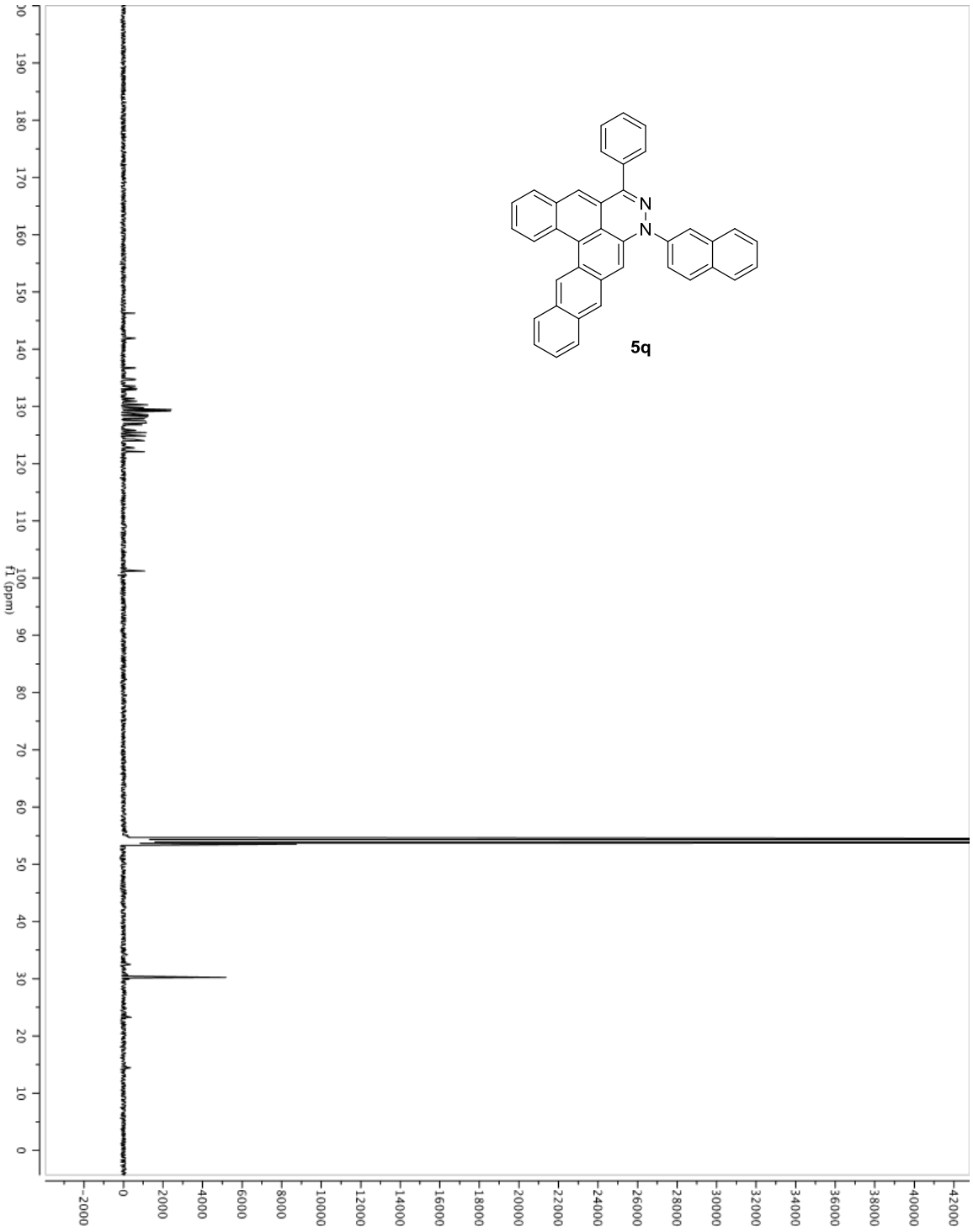

Figure A1.66. HSQC spectrum of **5q** in CD_2Cl_2.

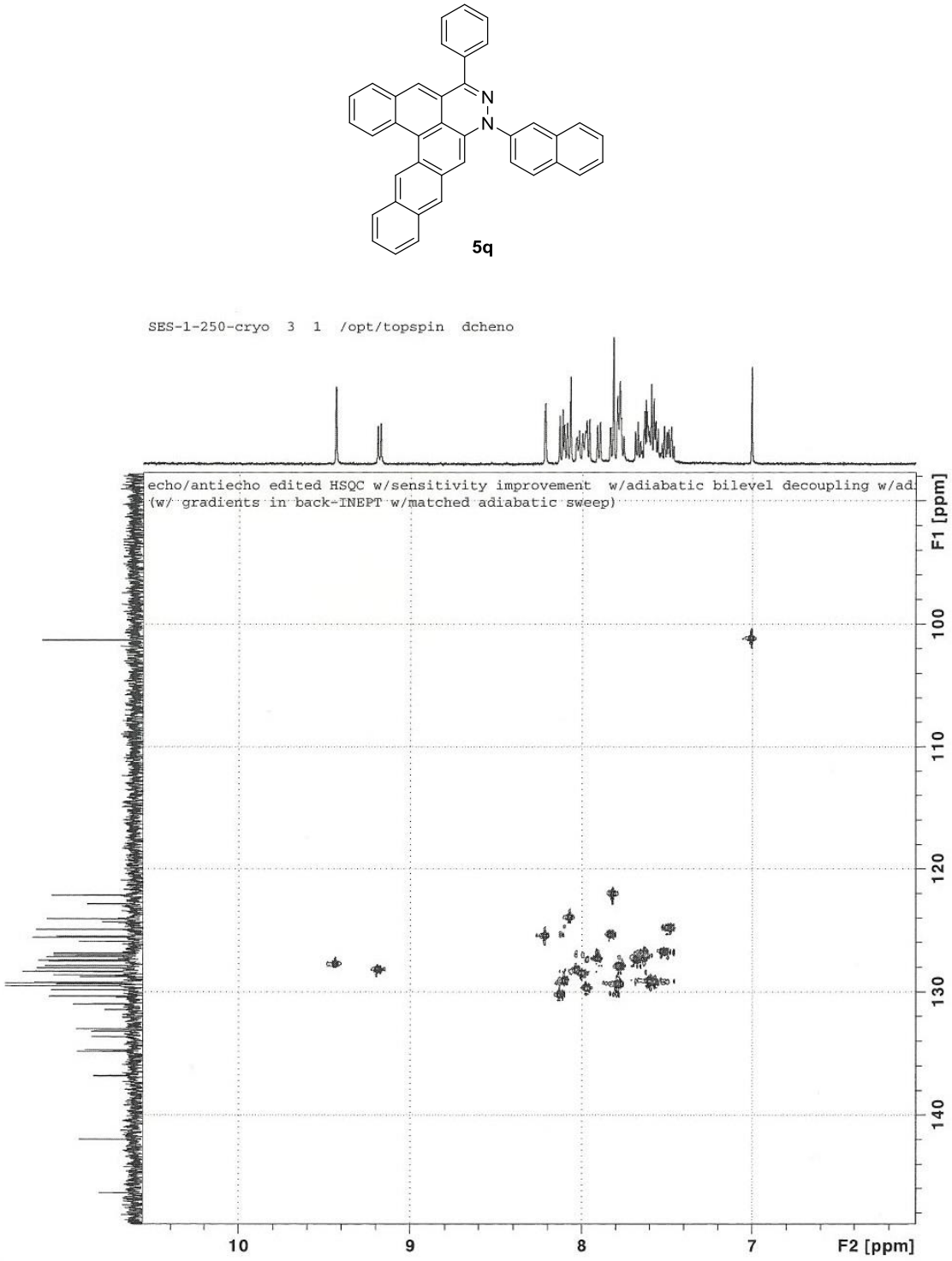

Figure A1.67. Expanded partial HSQC spectrum of **5q** in CD_2Cl_2.

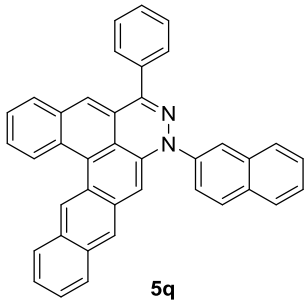

5q

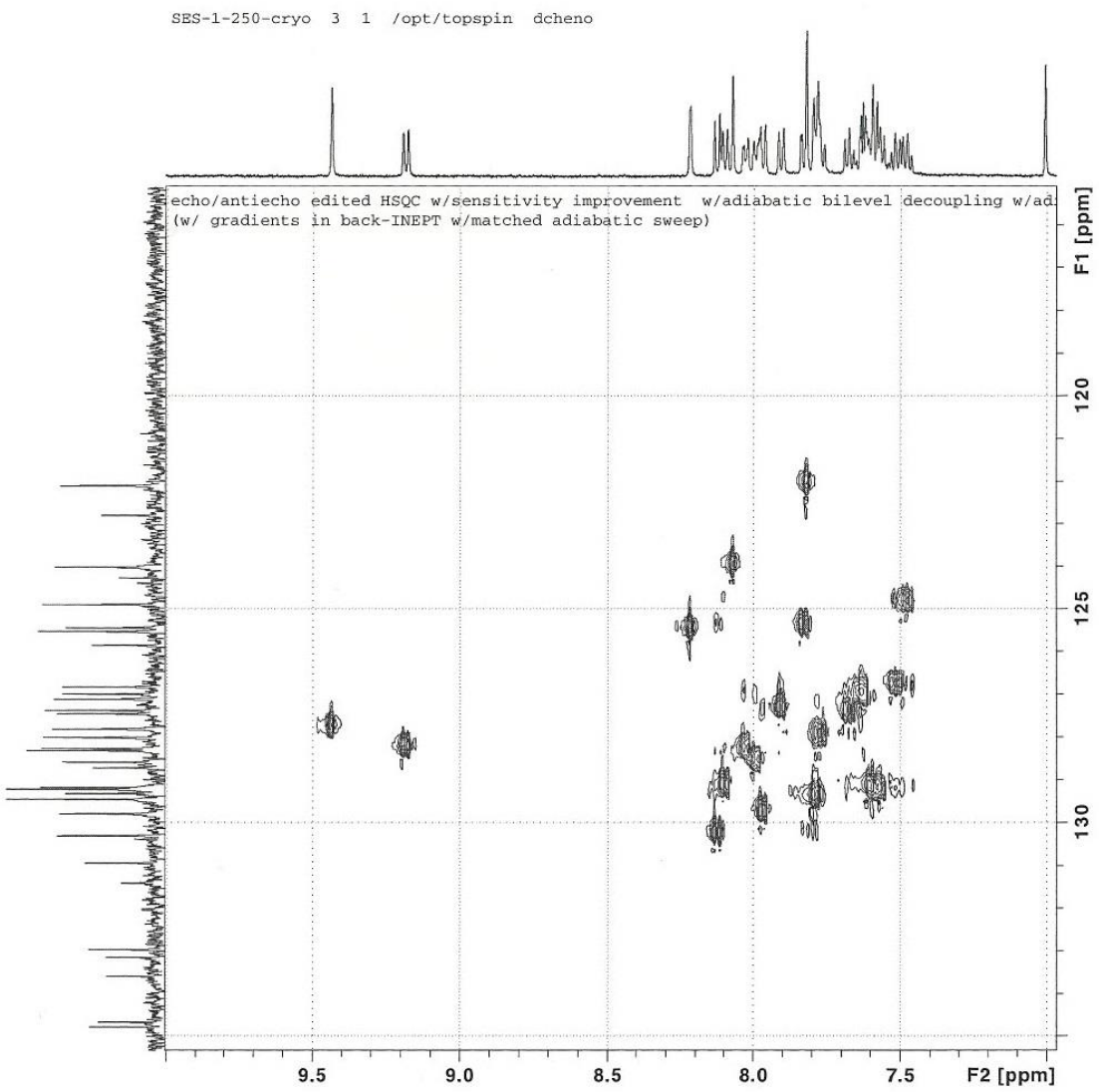

Figure A1.68. HMBC spectrum of **5q** in CD_2Cl_2.

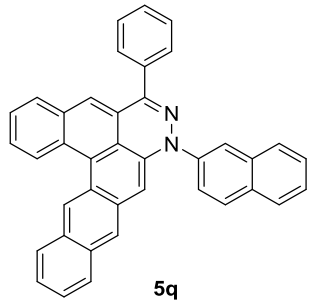

5q

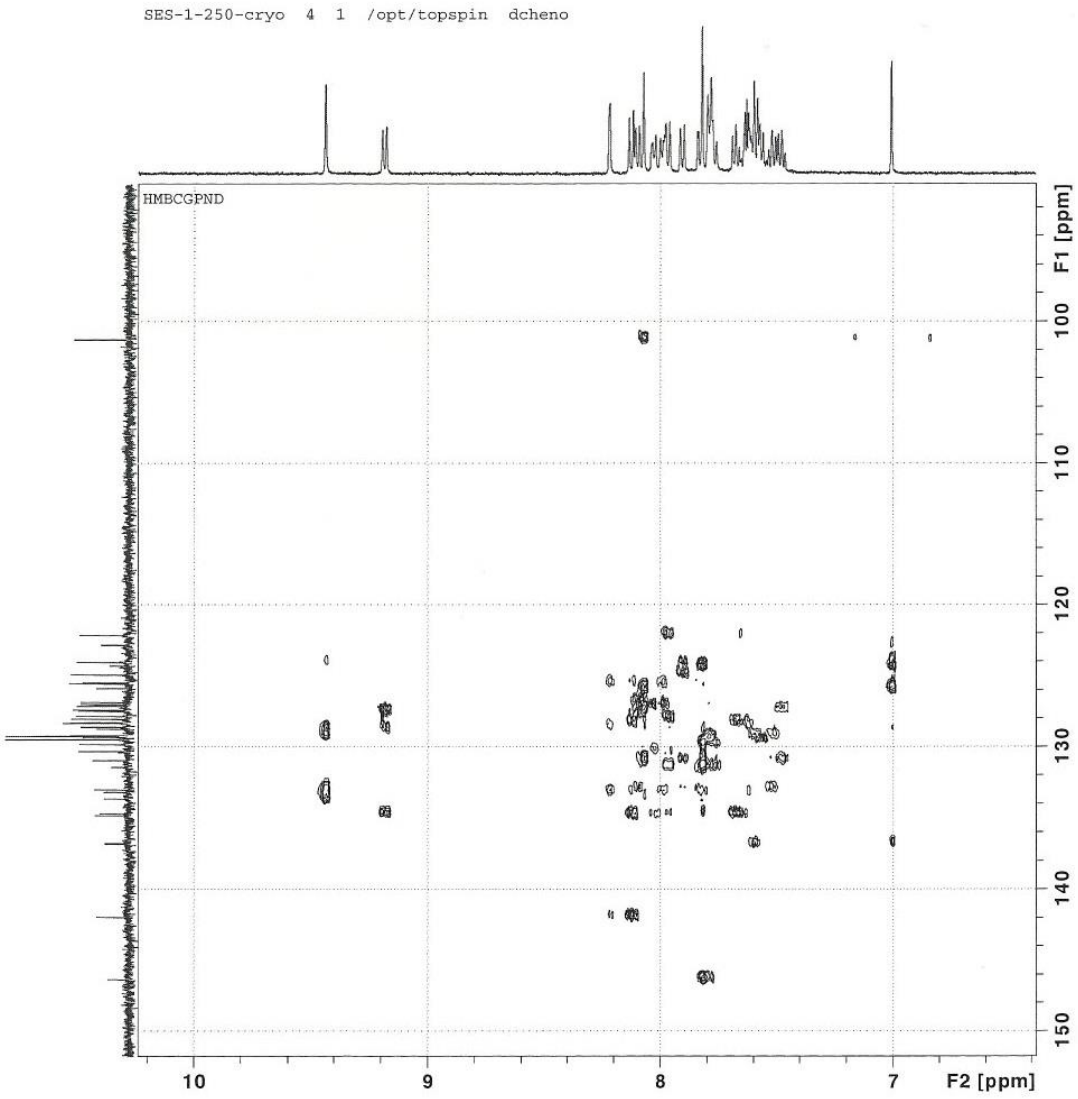

Figure A1.69. Expanded partial HMBC spectrum of **5q** in CD_2Cl_2.

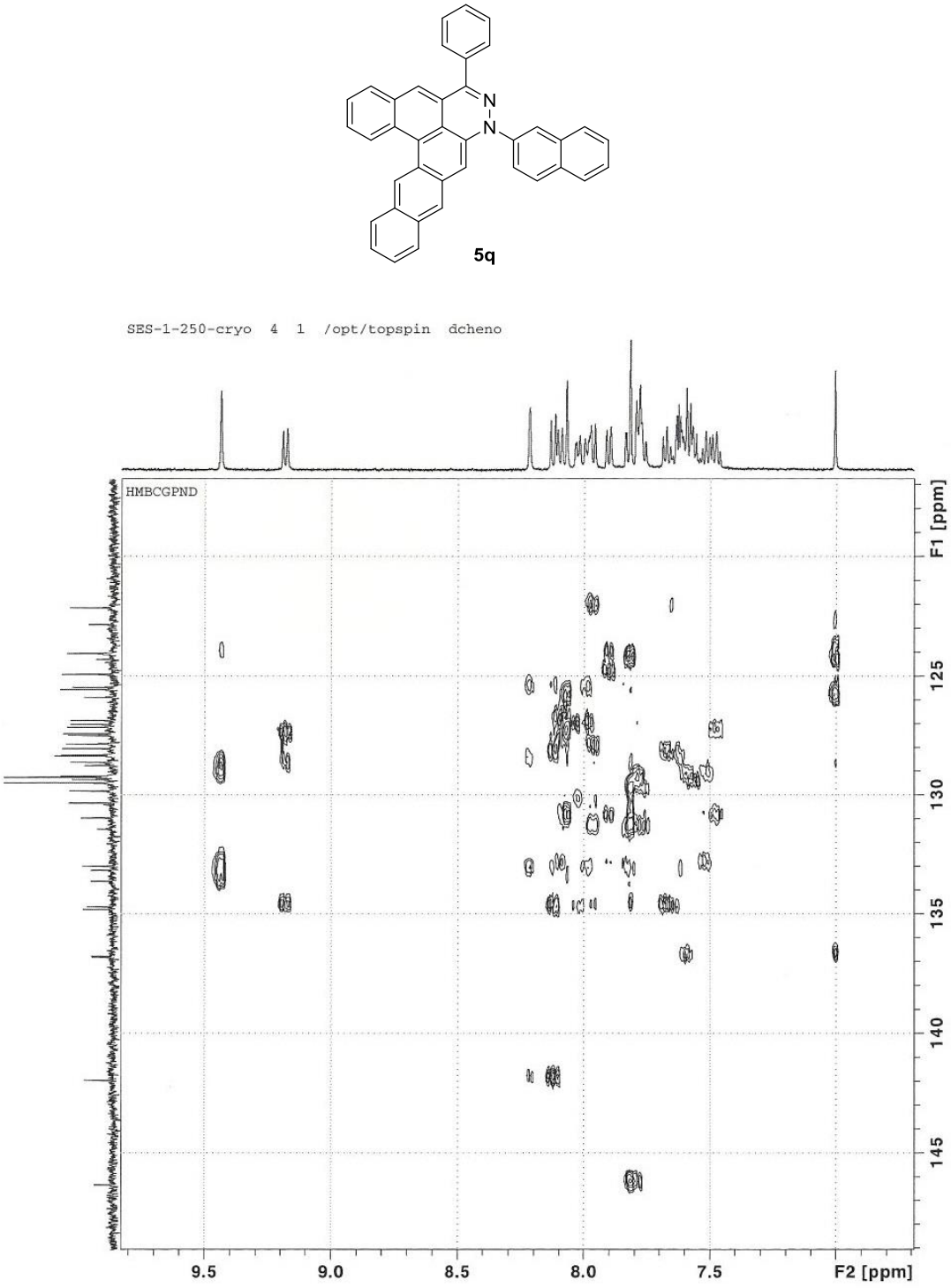

Figure A1.70. TOCSY spectrum of **5q** in CD_2Cl_2.

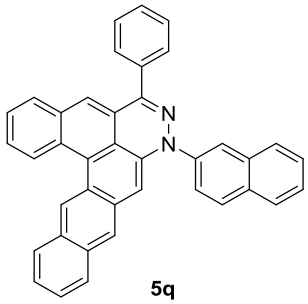

5q

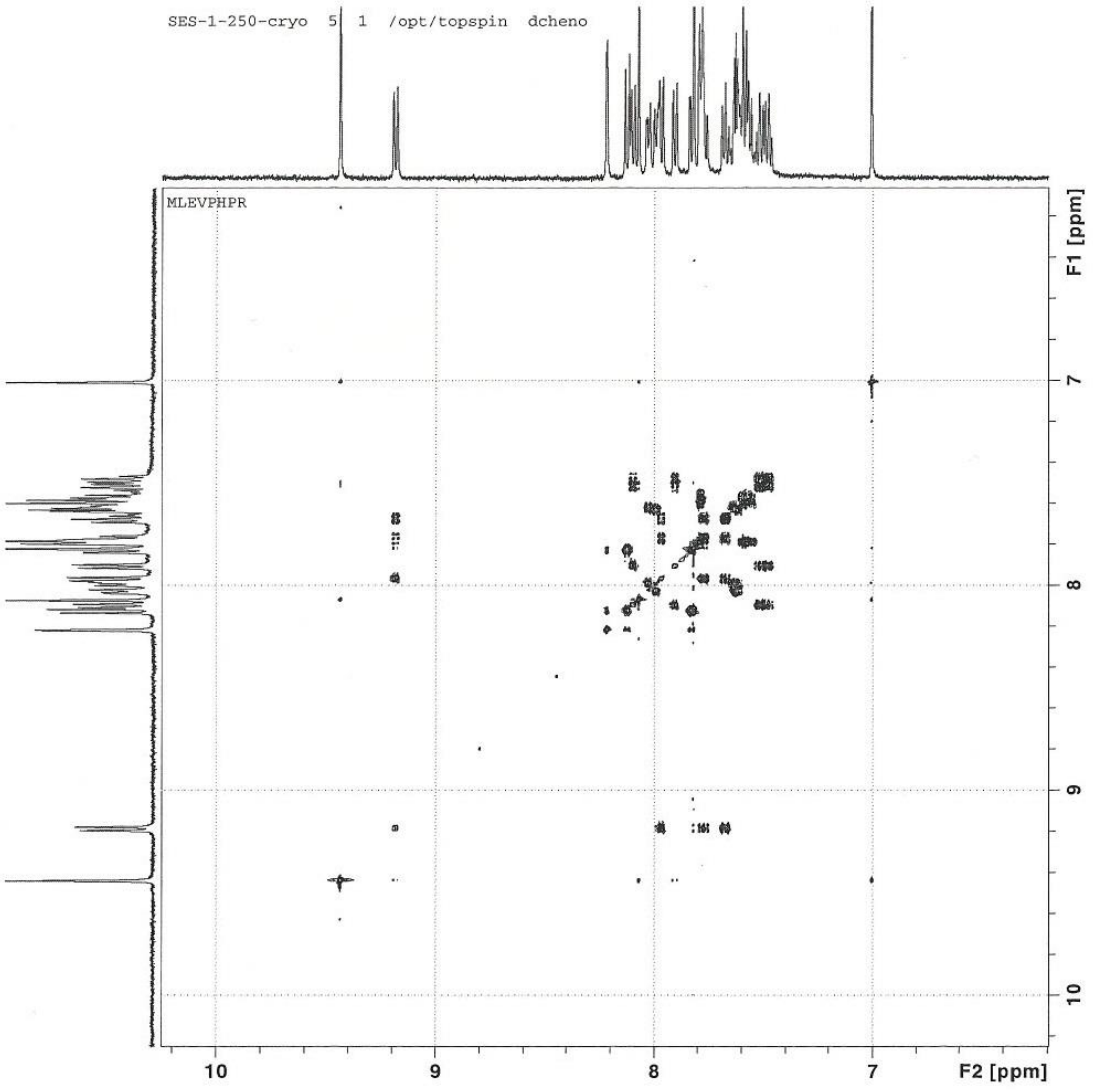

Figure A1.71. 1st Expanded partial TOCSY spectrum of **3m** in CD_2Cl_2.

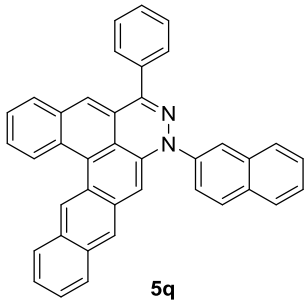

5q

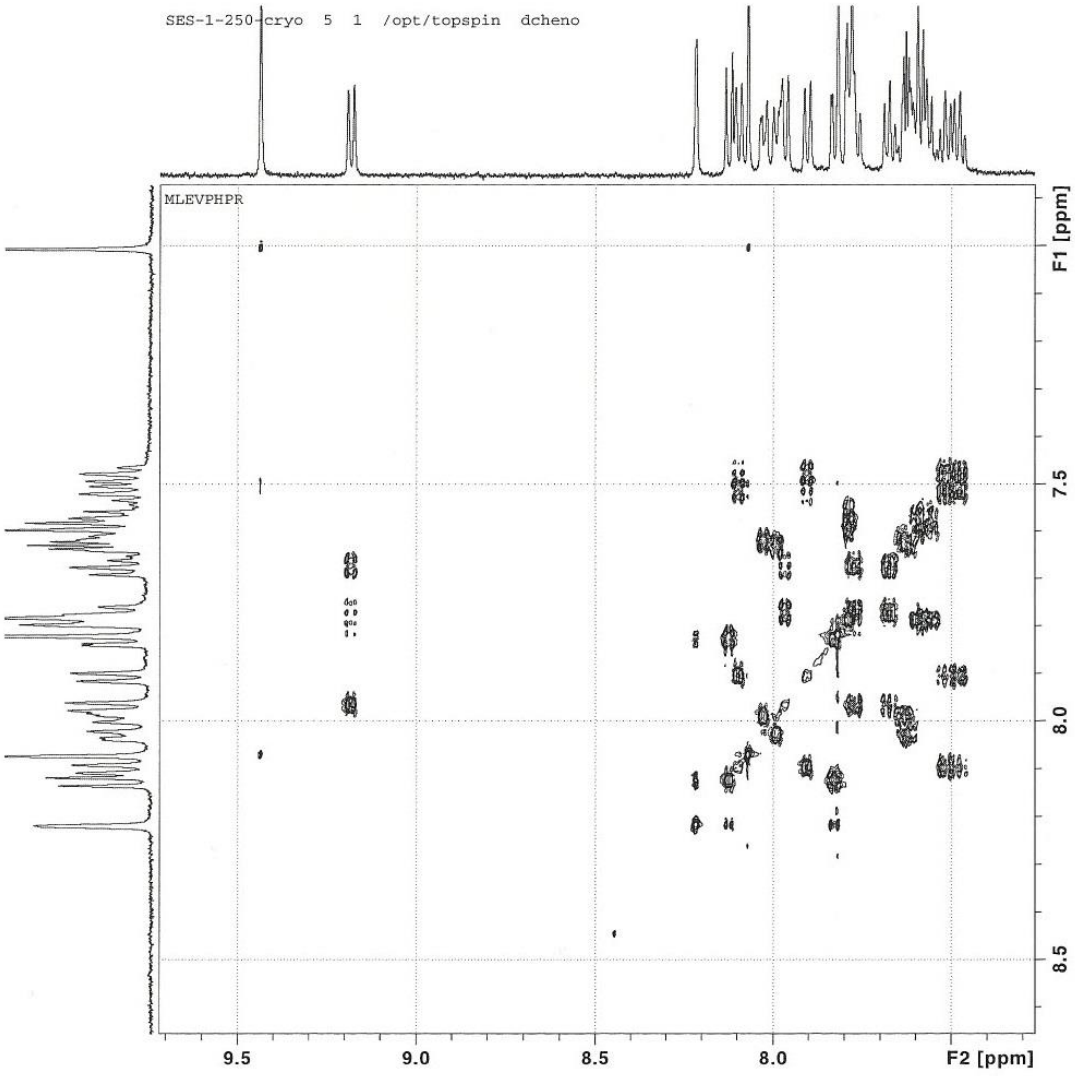

Figure A1.72. 2nd Expanded partial TOCSY spectrum of **3m** in CD_2Cl_2.

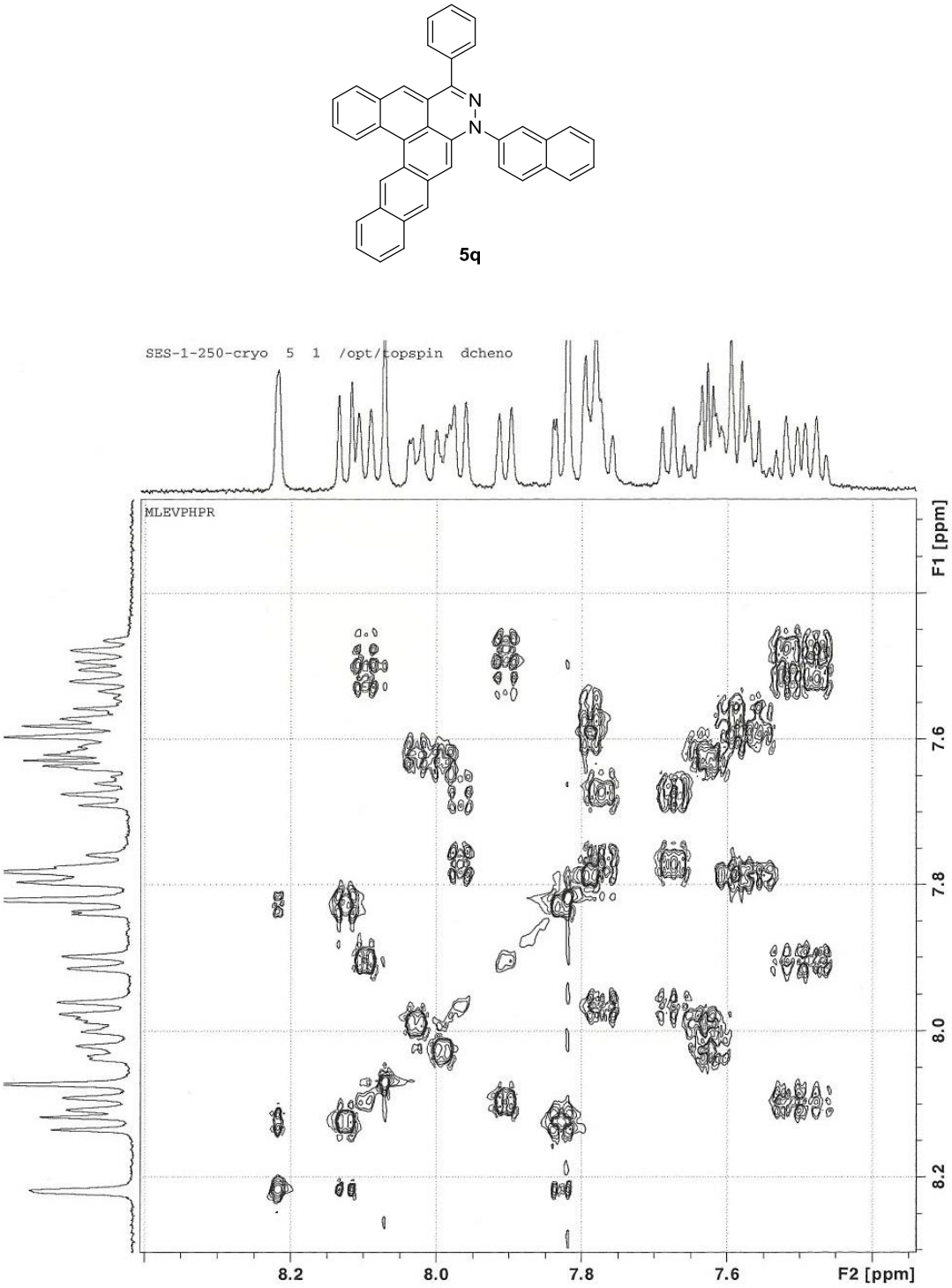

Figure A1.73. COSY spectrum of **3m** in CD_2Cl_2.

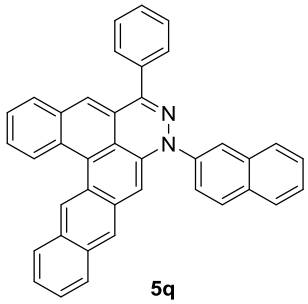

5q

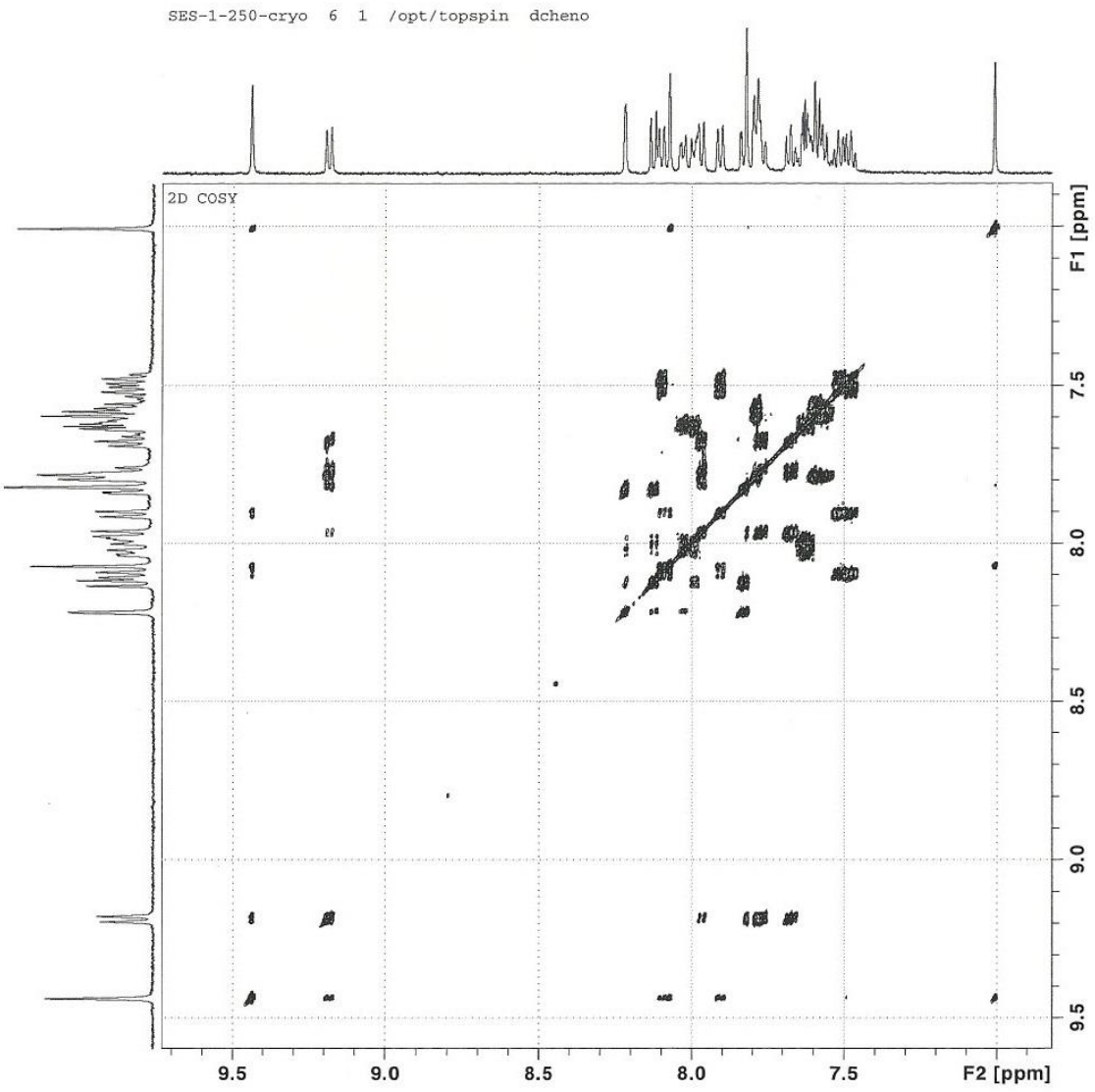

Figure A1.74. ^{1}H NMR spectrum of **6** in $CDCl_3$ (500 MHz).

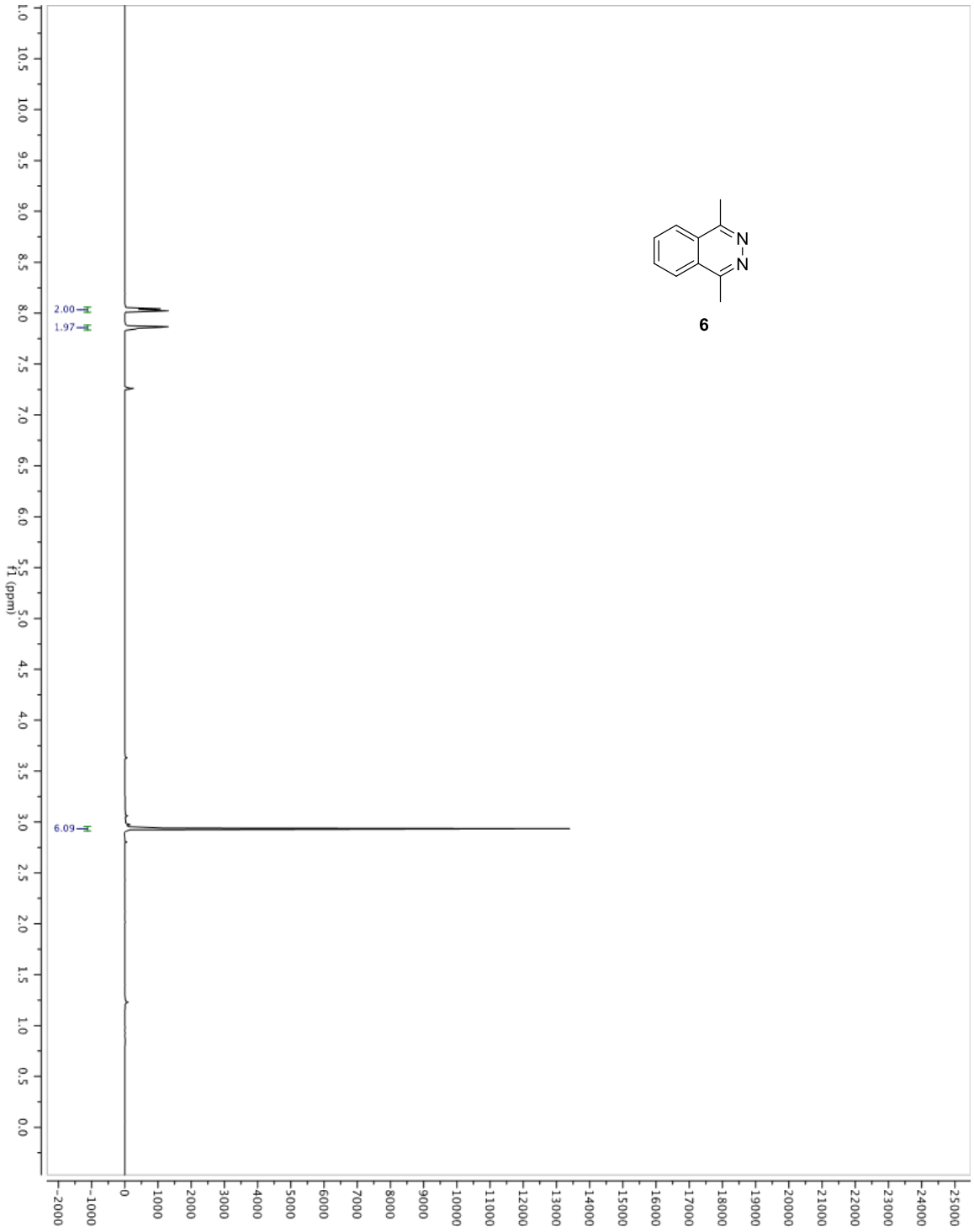

Figure A1.75. ^{13}C NMR spectrum of **6** in $CDCl_3$ (125 MHz).

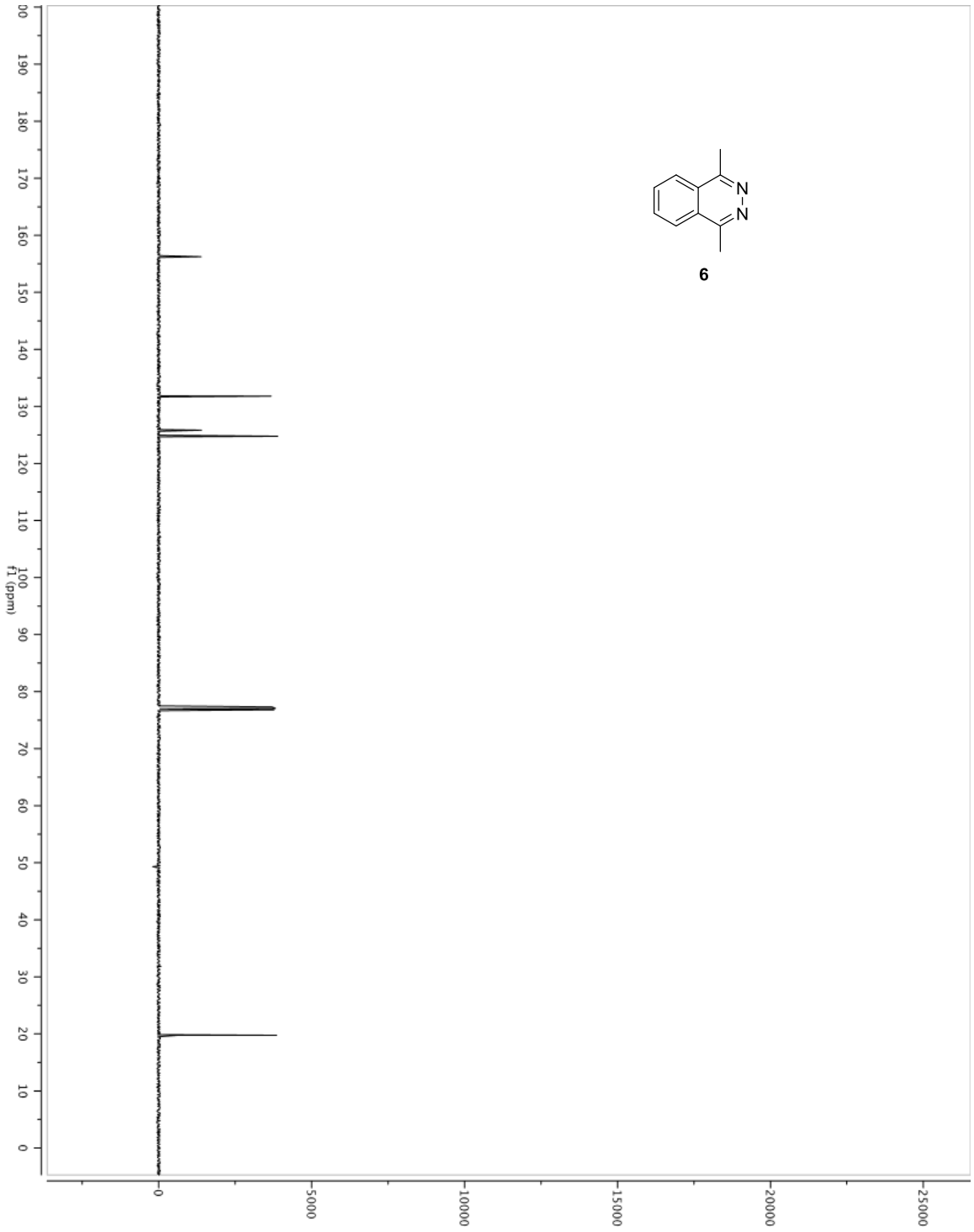

Figure A1.76. ^{1}H NMR spectrum of **7** in $CDCl_3$ (500 MHz).

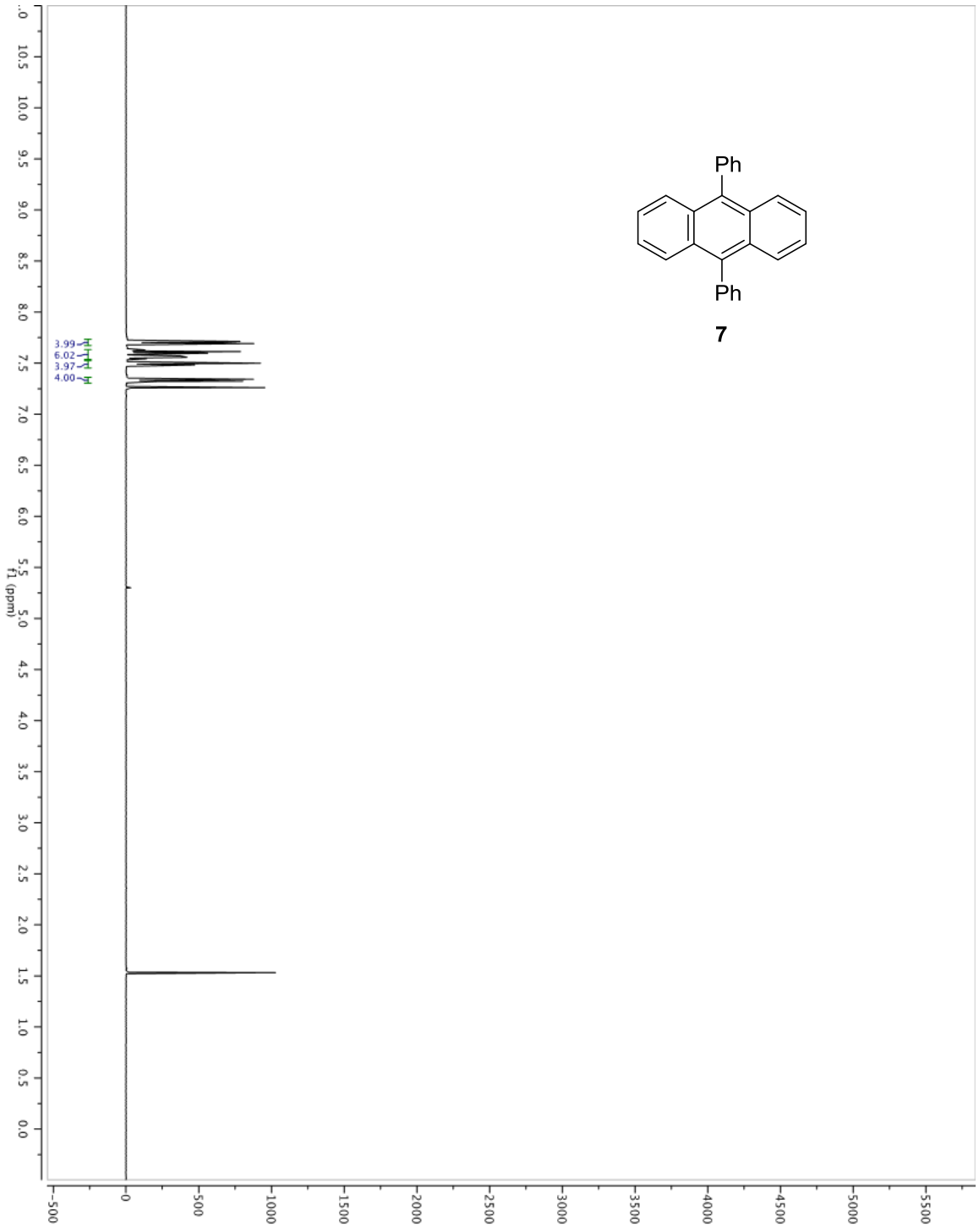

Figure A1.77. Absorption, emission, and exitation spectra of **5a** at 24 ˚C in CH_2Cl_2.

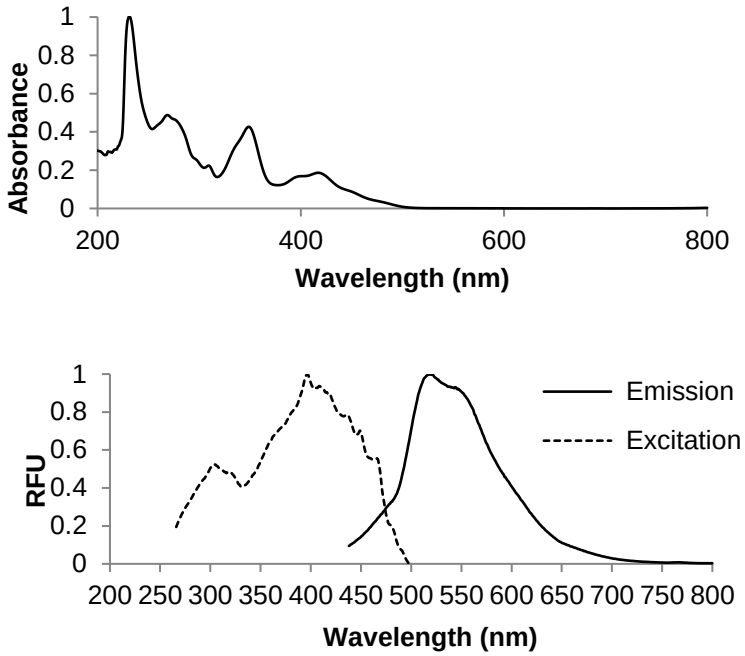

Figure A1.78. Absorption, emission, and excitation spectra of **5a** at 24 ˚C in CH_2Cl_2/TFA.

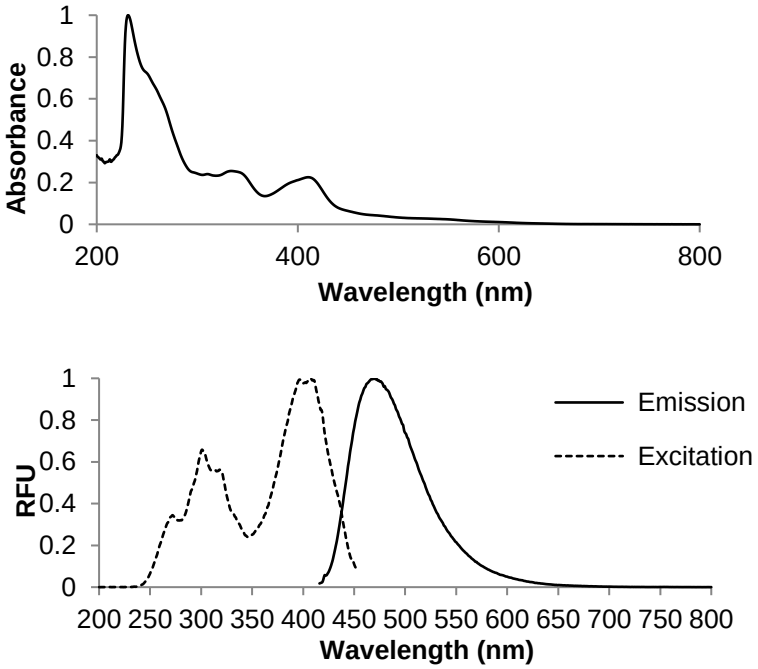

Figure A1.79. Absorption, emission, and excitation spectra of **5b** at 24 ˚C in CH_2Cl_2.

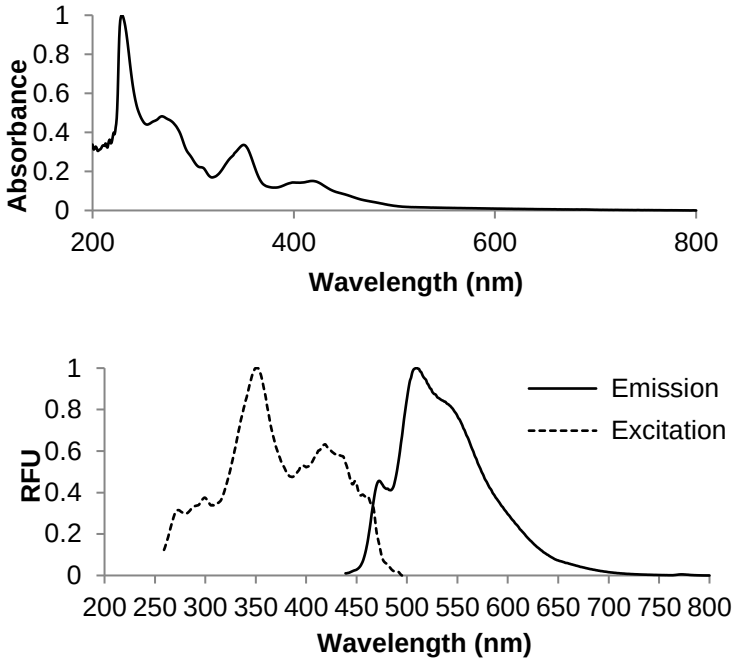

Figure A1.80. Absorption, emission, and excitation spectra of **5b** at 24 ˚C in CH_2Cl_2/TFA.

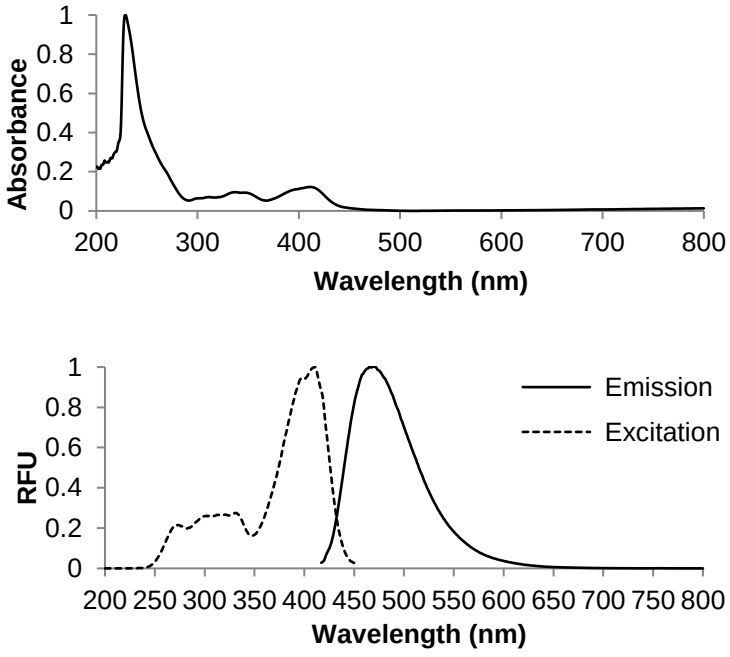

Figure A1.81. Absorption, emission, and excitation spectra of **5d** at 24 ˚C in CH_2Cl_2.

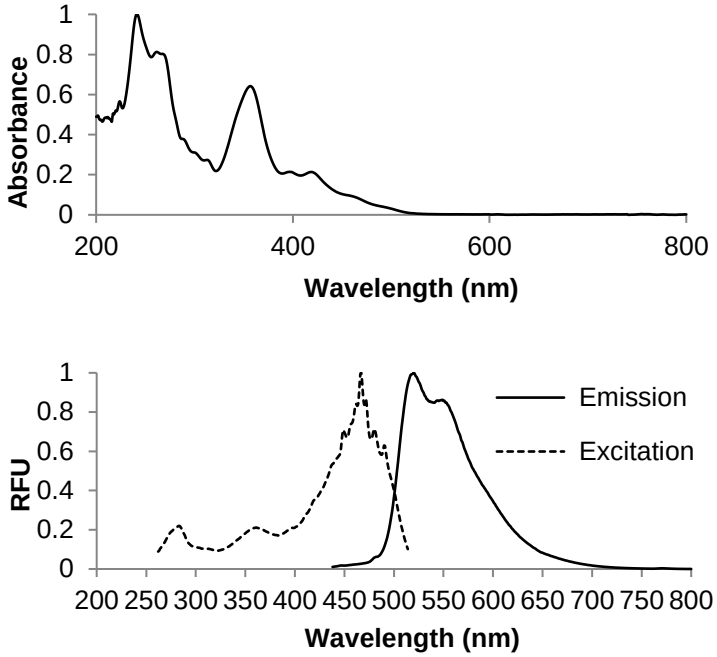

Figure A1.82. Absorption, emission, and excitation spectra of **5d** at 24 ˚C in CH_2Cl_2/TFA.

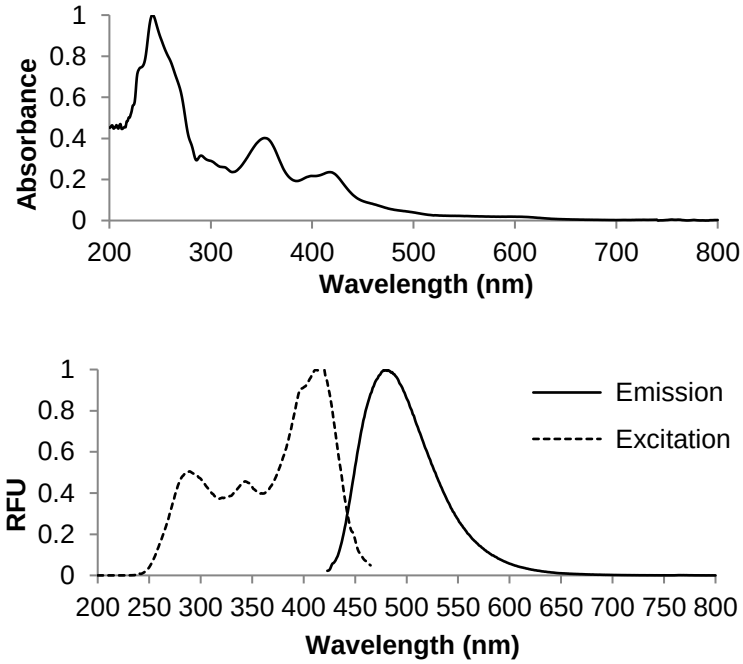

Figure A1.83. Absorption, emission, and excitation spectra of **5e** at 24 ˚C in CH_2Cl_2.

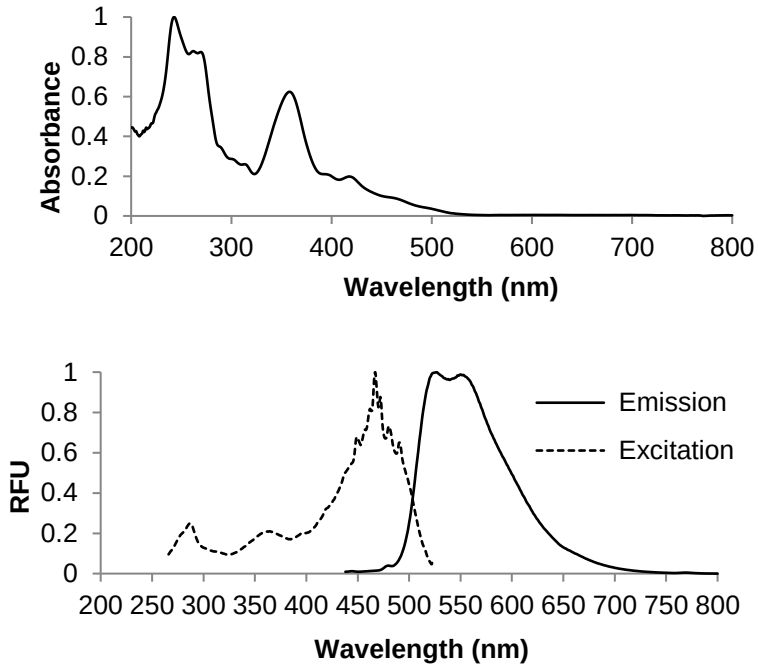

Figure A1.84. Absorption, emission, and excitation spectra of **5e** at 24 ˚C in CH_2Cl_2/TFA.

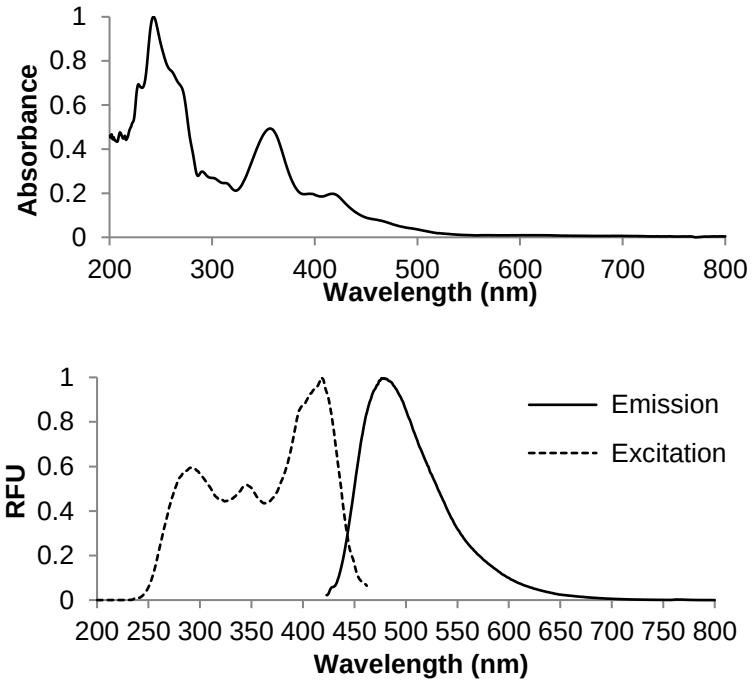

Figure A1.85. Absorption, emission, and excitation spectra of **5i** at 24 ˚C in CH_2Cl_2.

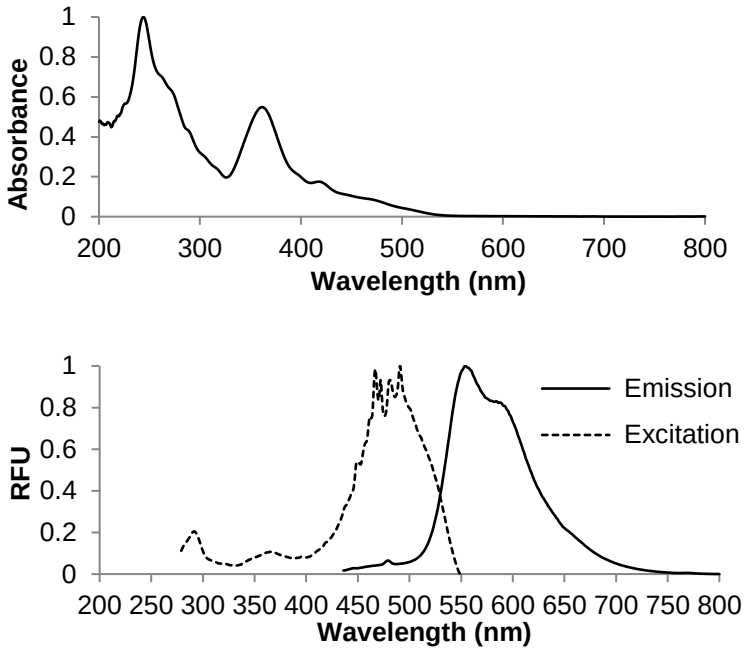

Figure A1.86. Absorption, emission, and excitation spectra of **5i** at 24 ˚C in CH_2Cl_2/TFA.

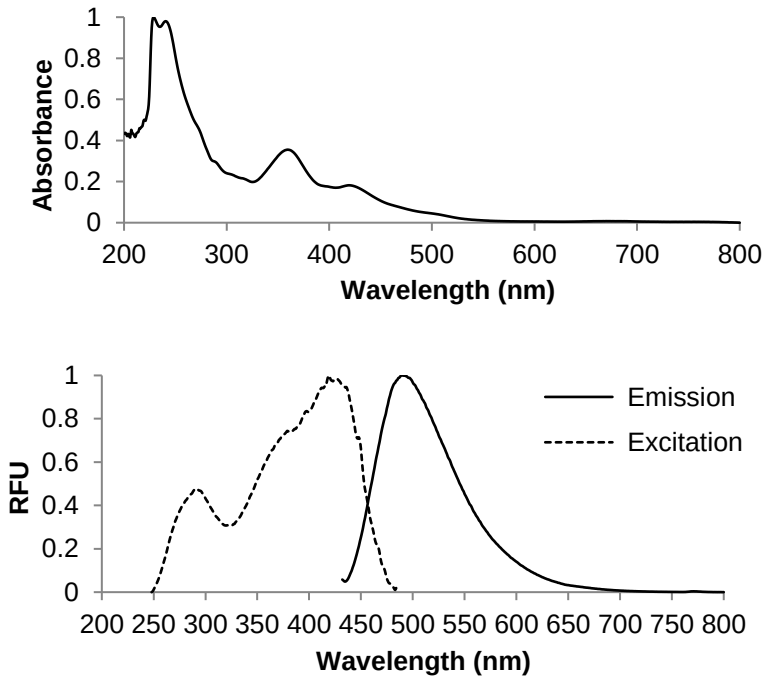

Figure A1.87. Absorption, emission, and excitation spectra of **5j** at 24 ˚C in CH_2Cl_2.

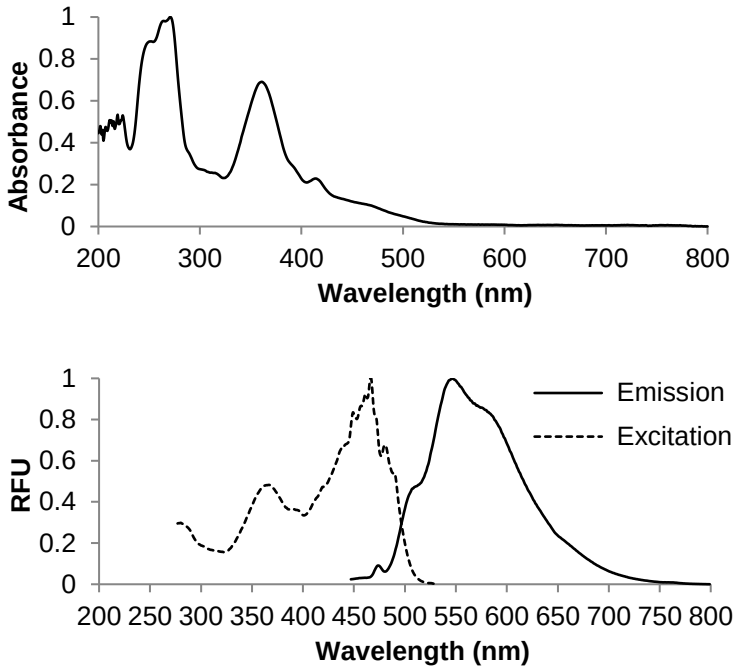

Figure A1.88. Absorption spectrum of **5j** at 24 ˚C in CH_2Cl_2/TFA.

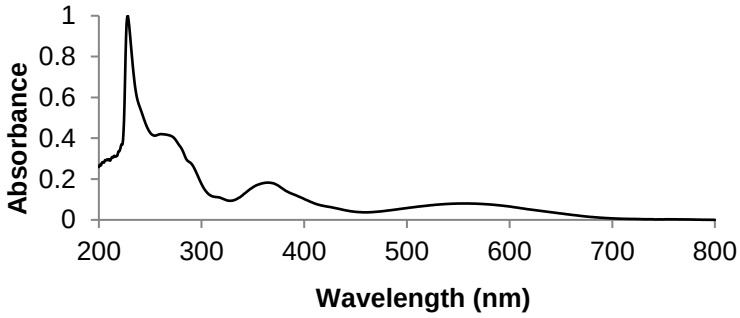

Figure A1.89. Absorption, emission, and excitation spectra of **5q** at 24 ˚C in CH_2Cl_2.

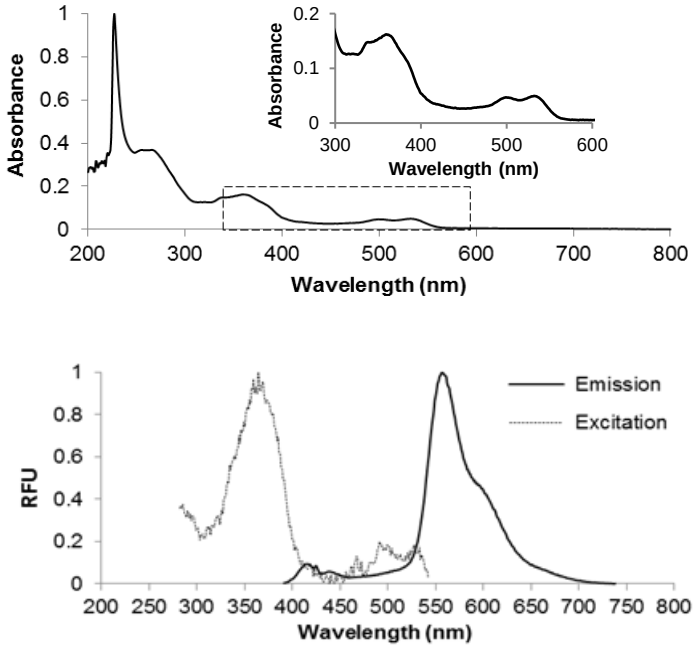

Figure A1.90. Absorption, emission, and excitation spectrum of **5q** at 24 ˚C in CH_2Cl_2/TFA.

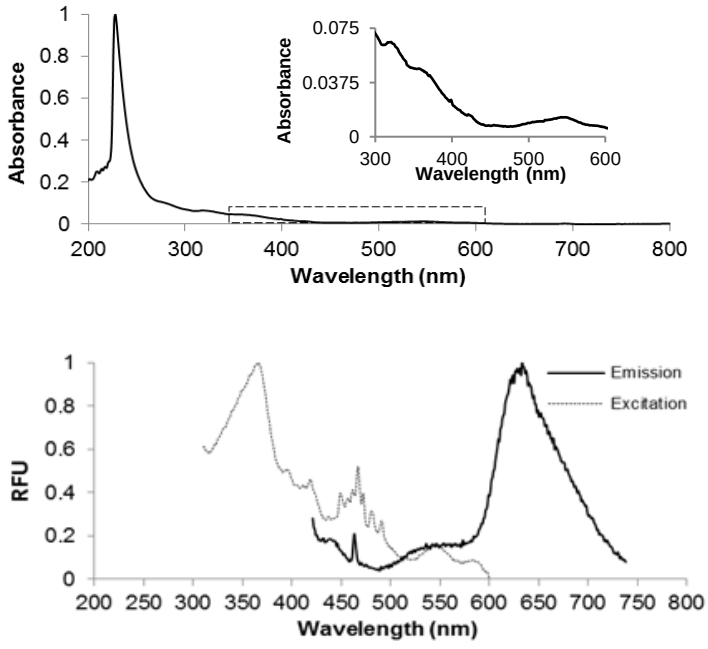

Table A1.1. Crystal Data and Structure Refinement for 5a.

Empirical formula	$C_{22}H_{16}N_2$
Formula weight	308.37
Temperature	100(1) K
Wavelength	0.71073 Å
Crystal system	monoclinic
Space group	$P2_1/c$
Cell constants:	
a	11.9993(9) Å
b	4.2453(3) Å
c	29.803(2) Å
b	100.261(4)°
Volume	1493.90(18) Å3
Z	4
Density (calculated)	1.371 Mg/m3
Absorption coefficient	0.081 mm-1
F(000)	648
Crystal size	0.48 x 0.12 x 0.04 mm3
Theta range for data collection	1.39 to 25.38°
Index ranges	$-14 \le h \le 14, -5 \le k \le 5, -35 \le l \le 35$
Reflections collected	32407
Independent reflections	2740 [R(int) = 0.0637]
Completeness to theta = 25.38°	99.9 %
Absorption correction	Semi-empirical from equivalents
Max. and min. transmission	0.7452 and 0.4717
Refinement method	Full-matrix least-squares on F2
Data / restraints / parameters	2740 / 0 / 219
Goodness-of-fit on F2	1.104
Final R indices [I>2sigma(I)]	R1 = 0.0541, wR2 = 0.1464
R indices (all data)	R1 = 0.0664, wR2 = 0.1579
Largest diff. peak and hole	0.308 and -0.270 e.Å-3

Chapter 3

Aryne Compatible Solvents are not Always Innocent

Adapted with permission from Suh, S.-E.; Chenoweth, D. M. *Org. Lett.* **2016,** *18,* 4080-4083.

3.1 Introduction

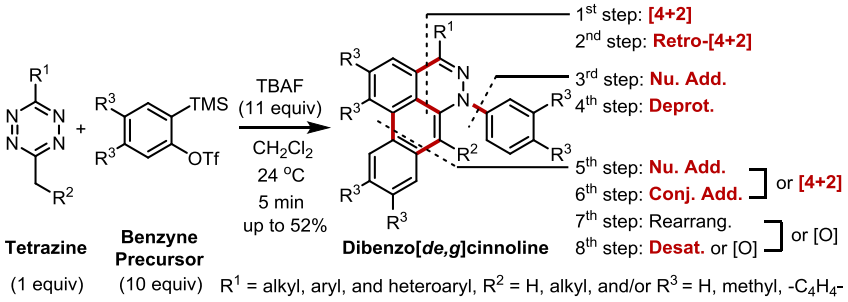

Figure 3.1. General Scheme of the TAT reaction and proposed mechanistic steps. Red bold lines represent newly formed bonds. Red bold fonts denote aryne-engaged steps.

Arynes have been utilized in a wide variety of transformations for the formation of multiple carbon-carbon, carbon-nitrogen, carbon-oxygen, and/or carbon-hydrogen bonds.[1–7] In comparison to an unstrained alkyne, arynes primarily exhibit high electrophilic reactivity due to LUMO lowering.[8] Several aryne-based reactions have been developed including sigma-bond insertions,[9–12] nucleophilic additions,[13-15] ene reactions,[1,16–18] desaturations,[19] cycloadditions, such as [4+2],[20–23] [3+2],[24–26] [2+2],[27,28] and [2+2+2][29–31] modes. Our laboratory is interested in new chemical tools and rapid access to new fluorescent probes.[32] Recently, we reported a new multistep aryne addition reaction referred to as the triple aryne-tetrazine (TAT) reaction.[32] The TAT reaction enables rapid access to a new class of polyaromatic heterocycles by coupling diverse reactivity modes between simple aryne and tetrazine[33] starting materials into a single multistep process (Figure 3.1). The TAT reaction provides a rapid route to several substituted dibenzo[*de,g*]cinnolines with unique fluorescent properties.

Aryne-based reactions are commonly performed in acetonitrile, dichloromethane or combinations of both.[34-38] A few notable studies by Hoye[19,39] and Coe[40] have described solvent effects on aryne-based reactions. However, reports describing the reactivity of common solvents used in aryne chemistry are limited to tetrahydrofuran,[41,42] acetonitrile,[43] and other alkylnitriles.[44] During recent investigtions into the TAT reaction we found that dichloromethane, as well as acetonitrile, are not innocent solvents and can result in byproduct formation when deprotonated by the resulting intermediate aryl anion formed after an initial aryne addition reaction. We discovered that these common aryne compatible solvents can contribute to low yields by reacting with key intermediates along the TAT reaction pathway to produce solvent adducts. Herein, we describe the formation of these solvent adducts in the context of the TAT reaction, providing insight into the reactivity of commonly used organic solvents in aryne-based reactions.

3.2 Results and Discussion

Scheme 3.1. Isolation of Phthalazine Intermediate 4.

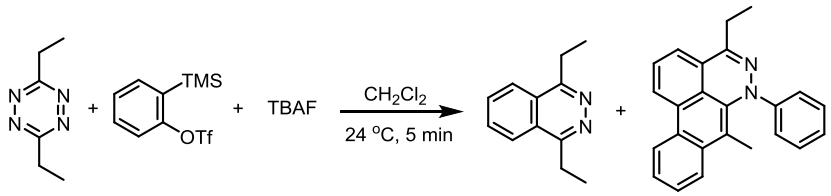

1	2		4	3
1 equiv	10 equiv	11 equiv	-	44%
2 equiv	1 equiv	1.1 equiv	37%	1%

During analysis of the TAT reaction, a phthalazine is the first isolable intermediate in the TAT reaction, following an initial Diels-Alder/retro-Diels-Alder reaction of benzyne with a tetrazine. Benzyne precursor **2**[45] was used as the limiting reagent in a reaction with tetrazine **1** to prepare phthalazine intermediate **4** in 37% yield. Intermediate **4** was isolated and characterized (Scheme 3.1) prior to use as the starting material under the TAT reaction conditions (Scheme 3.2, eq 1). Exposure of **4** to the TAT reaction conditions afforded desired product **3** in low yield (7%) (Scheme 3.2, eq 1), which is lower than the yield of **3** using the standard TAT reaction conditions (44%) (Scheme 3.1).[32] Interestingly, solvent adduct *rac*-**5a** was isolated from the complex reaction mixture (Scheme 3.2, eq 1). A trace amount of *rac*-**5a** was also observed in the standard TAT reaction. The crystal structure of **5a** (Figure 3.2) revealed that the dihydropyridazine ring is puckered with a dihedral angle (C1-N1-N2-C2 angle) of 28.2°. The N1-N2-C3-C4 dihedral angle between the dihydropyridazine plane and the N-phenyl plane was 54.9° due to the sterics imposed by the adjacent fully substituted carbon center.

A plausible mechanism leading to the formation of *rac*-**5a** involves nucleophilic addition of phthalazine **4** to benzyne, producing non-isolable zwitterionic intermediate **I.** The resulting zwitterion then deprotonates dichloromethane and the conjugate base attacks the hydrazonium species to afford solvent adduct *rac*-**5a**. To probe the reaction pathway from **4** to *rac*-**5a,** labeling experiments were performed using deuterated solvent. The reaction was conducted by addition of TBAF to **4b** and benzyne precursor **2,** using CD_2Cl_2 as the reaction solvent (Scheme 3.2, eq 2). The ^{1}H NMR analysis revealed a single deuterium (X^1 = D) on the *N*-phenyl group and a missing proton (X^2 = D) on the dichloromethyl substituent of *rac*-[D_2]-**5a**. The result supports

Scheme 3.2. Crossover Experiment for the Dichloromethane-Adduct Formation Reactions in CH_2Cl_2, CD_2Cl_2, 1:1 Mixture of CH_2Cl_2 and CD_2Cl_2, and CCl_4.

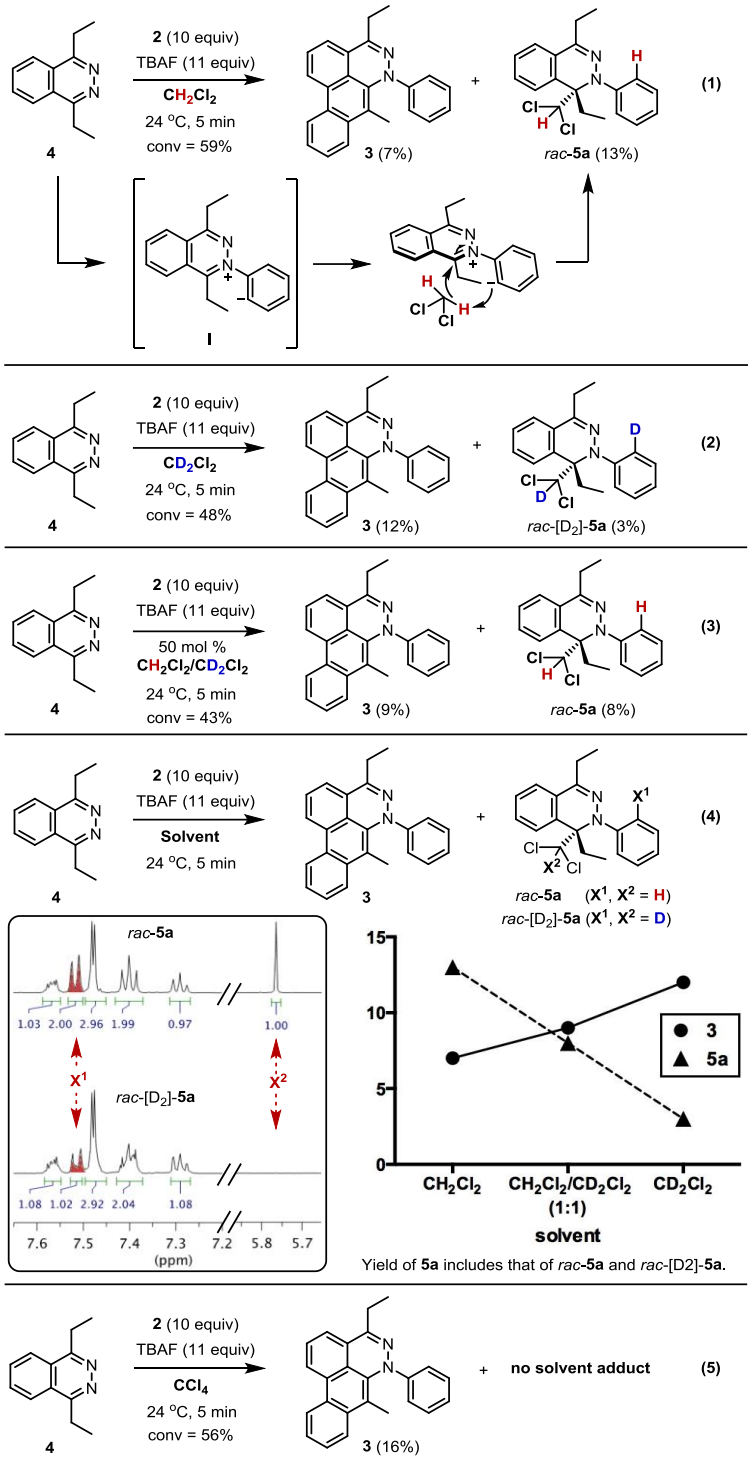

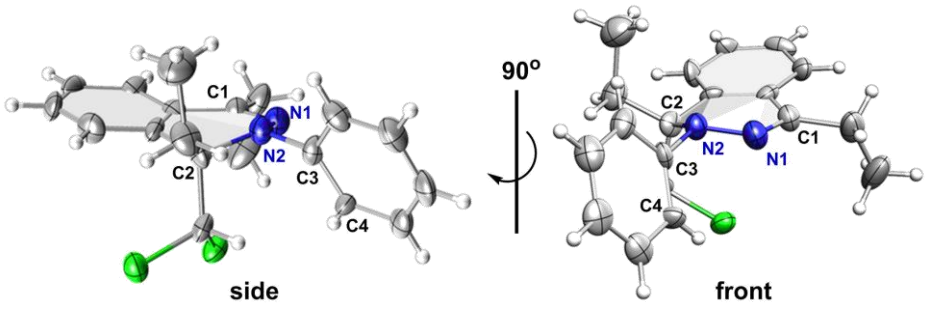

Figure 3.2. X-ray crystal structure of dichloromethane solvent adduct **5a**.

the idea that the formation of the solvent adduct is indeed initiated by deprotonation by the aryl zwitterion **I**.

By varying the concentration of deuterated to non-deuterated solvent, a significant kinetic isotope effect (KIE) was observed in dichloromethane. The yield of *rac*-**5a** reached 13% in CH_2Cl_2 (Scheme 3.2, eq 1) and the reaction in CD_2Cl_2 afforded the corresponding product *rac*-[D_2]-**5a** in only 3% yield (Scheme 3.2, eq 2). Although the ratio of *rac*-**5a**:*rac*-[D2]-**5a** was 4:1, *rac*-[D_2]-**5a** was not observed when the reaction was conducted in a 1:1 mixture of CH_2Cl_2 and CD_2Cl_2 (Scheme 3.2, eq 3). As the amount of CD_2Cl_2 was increased, the yield of **3** increased and the yield of the solvent adduct (*rac*-**5a** or *rac*-[D_2]-**5a**) decreased (Scheme 3.2, eq 4). Solvents such as CH_2Cl_2 appear to be acidic enough to be deprotonated under the reaction conditions and this leads to solvent adduct **5a**, as evidenced by the high KIE in CD_2Cl_2. Based on these results, we conducted the reaction in CCl_4 (Scheme 3.2, eq 5) and the yield of **3** was 16%. This was a higher yield of TAT reaction product than that obtained from the reaction in CH_2Cl_2, CD_2Cl_2, or a mixture of CH_2Cl_2/CD_2Cl_2 (Scheme 3.2, eq 4).

Scheme 3.3. Acetonitrile-Adduct Formation Reaction and Competitive Solvent Adduct Formation Using Different Ratios of CH_2Cl_2 and CH_3CN.

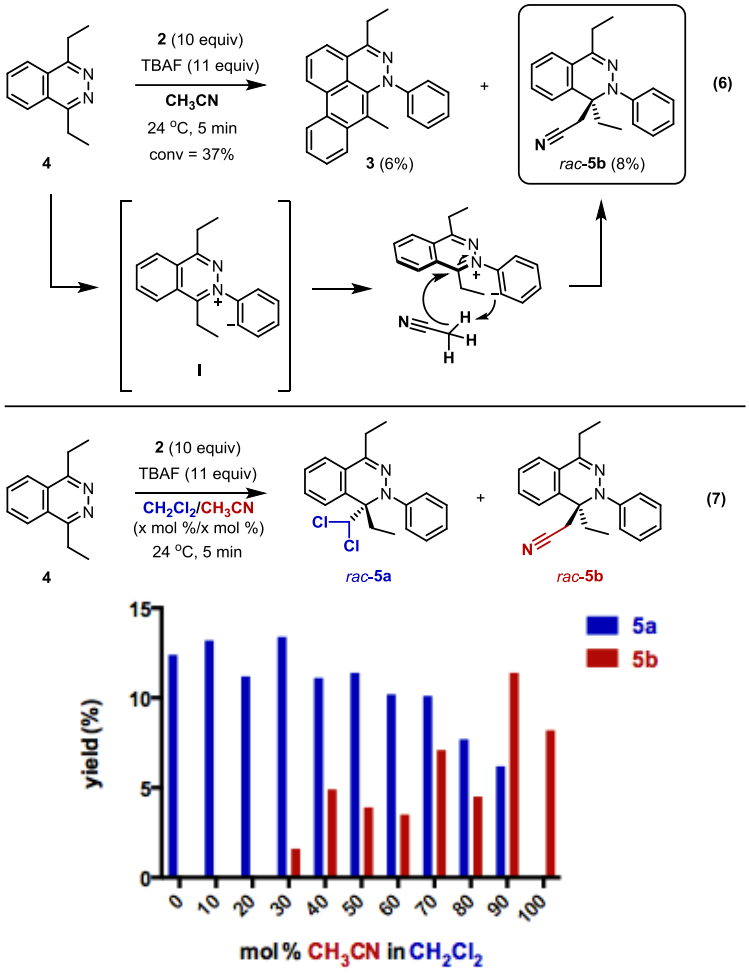

To determine if a solvent-trapped intermediate could be generated from other common organic solvents used in aryne chemistry, experiments were conducted in acetonitrile (Scheme 3.3, eq 6). This reaction afforded the acetonitrile adduct *rac*-**5b** in 8% yield. The zwitterion intermediate **I** also appears to be sufficiently basic enough to deprotonate acetonitrile. Note that the pKa of benzene is 43 in H_2O[48], and the pKa of acetonitrile has been reported to be 31.3 in DMSO.[49] Similar to the dichloromethane solvent adduct **5a,** the X-ray crystal structure of **5b**

exhibited a puckered conformation with a dihedral angle (C1-N1-N2-C2 angle) of 36.7° on dihydropyridazine ring (Figure 3.3). Consistent with the structure of **5a**, the biaryl ring torsional angle (N1-N2-C3-C4) between the dihydropyridazine plane and the N-phenyl plane was found to be twisted 50.0° away from coplanarity.

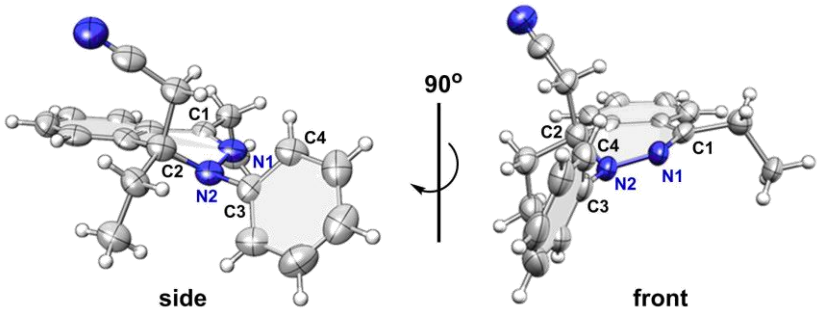

Figure 3.3. X-ray crystal structure of acetonitrile solvent adduct **5b**.

To gain insight into the relative reactivity of the two different solvents with benzyne, crossover experiments were conducted on a 10 μmol scale with several different ratios of CH_2Cl_2 and CH_3CN (Scheme 3.3, eq 7). Dichlromethane resulted in significant formation of the solvent adduct versus acetonitrile. When 1:1 CH_2Cl_2/CH_3CN was used as the solvent for the reaction, the yield of *rac*-**5a** was more than twice that of *rac*-**5b**.

Scheme 3.4. Solvent Adduct *rac*-7 from Intermediate 6.

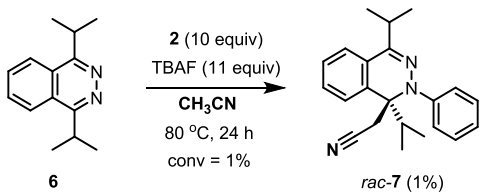

To probe steric effects on solvent adduct formation, phthalazine **6** was subjected to the TAT reaction conditions in dichloromethane and acetonitrile at 24 °C. None of the possible solvent adducts were observed and only starting material was recovered. Interestingly, when the reaction was conducted in acetonitrile at 80 °C for 24 hours the acetonitrile-adduct *rac*-**7** was produced in 1% yield (Scheme 3.4). This result indicates that the reaction is possible but strongly biased by the steric demands of the phthalazine substrate. The solvent adduct formation appears to be greatly influenced by the solvent pKa and the substrate sterics.

3.3 Conclusions

Herein, we reported participation of dichloromethane and acetonitrile in aryne reactions with phthalazines. Isolation of dichloromethane and acetonitrile solvent adducts (*rac*-**5a** and *rac*-**5b**) demonstrates that common solvents thought to be compatible with aryne chemistry are not always innocent bystanders. Deuterium labeling experiments not only confirmed non-interrupted bimolecular reaction pathways between the zwitterionic intermediate **I** and dichloromethane but also explained solvent-engaged side reaction leading to lower yields of desired product **3** in the course of TAT reaction. The crossover experiment of dichloromethane and acetonitrile highlighted that dichloromethane is more reactive than acetonitrile in the TAT reaction condition. As expected, the experiment with sterically bulky phthalazine **6** demonstrated that solvent adduct formation is affected by steric hinderance of the electrophile as well as pKa. The discovery of solvent participation in TAT reaction side product

formation provides insight into the reactivity of benzyne with two commonly used solvents. Similar side reactions may contribute to low yields in other aryne-based reactions. Additionally, these results could inspire new reactions for the construction of fully substituted carbon centers based on aryne addition/solvent capture reactions, as demonstrated in this report.

3.4 Experimental Section

General information

All commercial reagents and solvents were used as received. Flash column chromatography was performed using Silicycle silica gel (55–65 Å pore diameter). Thin-layer chromatography was performed on Sorbent Technologies silica plates (250 μm thickness). Proton nuclear magnetic resonance spectroscopy (^{1}H NMR) and Carbon nuclear magnetic resonance spectroscopy (^{13}C NMR) spectra were recorded on a Bruker DMX 500 ^{1}H NMR. High-resolution mass spectra were obtained by Dr. Rakesh Kohli at the University of Pennsylvania's Mass Spectrometry Service Center on a on a Waters LC-TOF mass spectrometer (model LCT-XE Premier) using electrospray ionization. X-ray diffraction data obtained and solved by Dr. Patrick Carroll at the University of Pennsylvania. High performance liquid chromatography analysis was performed using a Jasco HPLC instrument equipped with a Phenomenex column (Luna 5u C18(2) 100A; 250 × 4.60 mm, 5 μm).

Experimental procedures

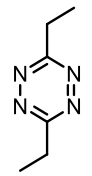

1

3,6-diethyl-1,2,4,5-tetrazine (1): Synthetic method and characterization data of **1** have been reported in our previous publication.[32a]

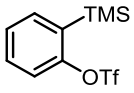

2

2-(trimethylsilyl)phenyl trifluoromethanesulfonate (2): 2 was prepared according to the literature procedure.[48]

^{1}H NMR (500 MHz, $CDCl_3$) δ 7.56-7.52 (m, 1H), 7.47-7.41 (m, 1H), 7.37-7.32 (m, 2H), 0.37 (s, 9H).

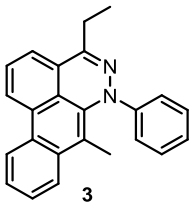

3

4-ethyl-7-methyl-6-phenyl-6H-dibenzo[de,g]cinnoline (3): Synthetic method and characterization data of **3** have been reported in our previous publication.[32a]

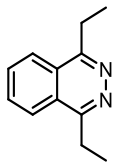

4

1,4-diethylphthalazine (4): A vial was charged with 8.0 mmol of **1** (1.10 g) and 4.0 mmol of **2** (0.97 mL) in 4.0 mL of dichloromethane at 24 °C, and 1 M TBAF in THF (4.4 mmol, 4.4 mL) was slowly added to the solution over the course of 20 minutes. After the addition, the solution was concentrated in vacuo, and filtered on the silica gel, and purified by flash column chromatography (hexanes/ethyl acetate 1:3) to afford **4** (0.27 g). The data for this compound was previously reported in the literature.[49,50]

Isolated Yield: 37 %.

Physical Property: White solid.

TLC: R_f = 0.17 (silica gel, 25% ethyl acetate/hexanes).

^{1}H NMR (500 MHz, $CDCl_3$)

δ 8.05 (dd, 2H, J = 6.3, 3.3 Hz), 7.80 (dd, 2H, J = 6.3, 3.3 Hz), 3.30 (q, 4H, 7.5 Hz), 1.44 (t, 6H, 7.5 Hz).

^{13}C NMR (125 MHz, $CDCl_3$)

δ 159.9, 131.5, 125.3, 124.5, 26.3, 13.1.

HRMS (ESI) calculated for $C_{12}H_{14}N_2Na^+$ $[M+Na]^+$ 209.1049, found 209.1064.

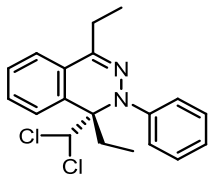

rac-**5a**

(*R*)- and (*S*)-1-(dichloromethyl)-1,4-diethyl-2-phenyl-1,2-dihydrophthalazine (*rac*-5a): A 4 mL vial was charged with 48 μmol of 1,4-diethylphthalazine **4** (9.0 mg), 480 μmol of 2-(trimethylsilyl)phenyl trifluoromethanesulfonate **2** (140 mg) in 50 μL of dichloromethane at 24 °C, 1 M TBAF in THF (530 μmol, 53 μL) was slowly added to the solution over the course of 5 minutes. After the addition, the solution was concentrated in vacuo, and filtered on the silica gel, and purified by flash column chromatography (ethyl acetate/hexanes 1:10) to afford *rac*-**5a** (2.2 mg).

Isolated Yield: 13 %

Physical Property: White solid, m.p. = 111-112 °C.

TLC: R_f = 0.70 (silica gel, ethyl acetate/hexanes 1:4).

^{1}H NMR (500 MHz, CD_2Cl_2)

δ 7.59-7.54 (m, 1H), 7.54-7.50 (m, 2H), 7.49-7.46 (m, 3H), 7.43-7.37 (m, 2H), 7.29 (tt, 1H, J = 7.4, 0.9 Hz), 5.77 (s, 1H), 2.79-2.55 (m, 3H), 2.04-1.95 (m, 1H), 1.22 (t, 3H, J = 7.5 Hz), 1.07 (t, 3H, J = 7.2 Hz).

^{13}C NMR (125 MHz, CD_2Cl_2)

δ 145.5, 142.4, 129.2, 128.6, 128.5, 127.9, 127.84, 127.80, 127.0, 126.3, 123.6, 122.7, 77.3, 69.8, 28.2, 25.4, 11.6, 9.9.

IR (neat): 2973, 2929, 2869, 1596, 1492, 1446, 1093, 1034, 753, 699 cm^{-1}.

HRMS (ESI) calculated for $C_{19}H_{21}N_2Cl_2^+$ $[M+H]^+$ 347.1076, found 347.1083.

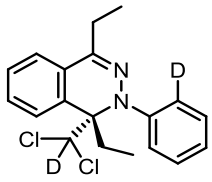

rac-[D_2]-**5a**

(*R*)- and (*S*)-1-(dichloromethyl-*d*)-1,4-diethyl-2-(phenyl-2-*d*)-1,2-dihydrophthalazine (*rac*-[D_2]-5a): A vial was charged with 19 mg (0.10 mmol) of **4** and 300 mg (1.0 mmol) of **2** in 100 μL of dichloromethane at 24 °C, and 1 M TBAF in THF (1.1 mmol, 1.1 mL) was slowly added to the solution over the course of 5 minutes. After the addition, the solution was concentrated in vacuo, and filtered on the silica gel, and purified by flash column chromatography (ethyl acetate/hexanes 1:10) to afford *rac*-[D_2]-**5a** (1.2 mg).

Isolated Yield: 3 %.

Physical Property: White solid, m.p. = 112-113 °C.

TLC: R_f = 0.70 (silica gel, ethyl acetate/hexanes 1:4).

^{1}H NMR (500 MHz, CD_2Cl_2)

δ 7.59-7.54 (m, 1H), 7.54-7.50 (m, 1H), 7.49-7.46 (m, 3H), 7.43-7.37 (m, 2H), 7.29 (tt, 1H, J = 7.4, 0.9 Hz), 2.79-2.55 (m, 3H), 2.04-1.95 (m, 1H), 1.22 (t, 3H, J = 7.5 Hz), 1.07 (t, 3H, J = 7.2 Hz).

HRMS (ESI) calculated for $C_{19}H_{18}D_2N_2Cl_2^+$ $[M+H]^+$ 349.1202, found 349.1204.

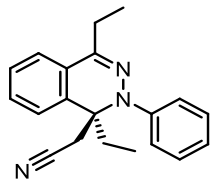

rac-**5b**

(*R*)- and (*S*)-2-(1,4-diethyl-2-phenyl-1,2-dihydrophthalazin-1-yl)acetonitrile (*rac*-5b), Procedure I (Scheme 3.2, eq 6): A 4 mL vial was charged with 48 μmol of 1,4-diethylphthalazine **4** (9.0 mg), 480 μmol of 2-(trimethylsilyl)phenyl trifluoromethanesulfonate **2** (140 mg) in 50 μL of dichloromethane at 24 °C, 1 M TBAF in THF (530 μmol, 530 μL) was slowly added to the solution over the course of 5 minutes. After the addition, the solution was concentrated in vacuo, and filtered on the silica gel, and purified by flash column chromatography (ethyl acetate/hexanes 1:10) to afford *rac*-**5b** (1.2 mg).

(*R*)- and (*S*)-2-(1,4-diethyl-2-phenyl-1,2-dihydrophthalazin-1-yl)acetonitrile (*rac*-5b), Procedure II: A 4.0 mL vial was charged with 48 μmol of 1,4-diethylphthalazine **4** (9.0 mg), 480 μmol of 2-(trimethylsilyl)phenyl trifluoromethanesulfonate **2** (140 mg), 530 μmol of anhydrous CsF (81 mg) in 50 μL of acetonitrile was heated to 80 °C. After 2 hours, the solution was cooled down, concentrated in vacuo and purified by flash column chromatography (ethyl acetate/hexanes 1:10) to afford *rac*-**5b** (3.6 mg).

Isolated Yield: 8% (Procedure I), 25 % (Procedure II).

Physical Property: Pale yellow solid, m.p. = 135-136 °C.

TLC: R_f = 0.38 (silica gel, ethyl acetate/hexanes 1:4).

^{1}H NMR (500 MHz, CD_2Cl_2)

δ 7.54-7.40 (m, 7H), 7.39-7.36 (m, 1H), 7.34-7.30 (m, 1H), 2.83-2.68 (m, 4H), 2.10-1.95 (m, 2H), 1.26 (t, 3H, J = 7.6 Hz), 0.97 (t, 3H, J = 7.3 Hz).

^{13}C NMR (125 MHz, CD_2Cl_2)

δ 146.1, 146.0, 132.9, 130.1, 128.6, 128.4, 128.2, 126.6, 125.2, 123.3, 117.6, 63.4, 27.7, 25.8, 25.4, 11.6, 8.9.

IR (neat): 2973, 2032, 2877, 1594, 1492, 1472, 1446, 1210, 1119, 756, 702 cm^{-1}.

HRMS (ESI) calculated for $C_{20}H_{22}N_3^+$ $[M+H]^+$ 304.1808, found 304.1808.

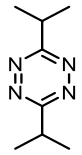

3,6-diisopropyl-1,2,4,5-tetrazine: 3,6-diisopropyl-1,2,4,5-tetrazine was prepared according to the literature procedure from commercially available isobutyronitrile.[33] The product was purified by flash column chromatography (ethyl acetate/hexanes = 6.25%).

Isolated Yield: 56 %.

Physical Property: Red oil.

TLC: R_f = 0.46 (silica gel, 25% ethyl acetate/hexanes).

^{1}H NMR (500 MHz, $CDCl_3$) δ 3.36 (sep, 2H, J = 7.0 Hz), 1.25 (d, 12H, J = 7.0 Hz).

^{13}C NMR (125 MHz, $CDCl_3$) δ 173.4, 33.9, 21.0.

IR (neat): 2973, 2934, 2877, 1472, 1461, 1383, 1365, 1336, 1286, 1250, 1072, 899, 883 cm^{-1}.

HRMS (ESI) calculated for $C_8H_{14}N_4^+$ $[M]^+$ 166.1213, found 166.1222.

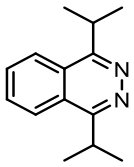

6

1,4-diisopropylphthalazine (6): A vial was charged with 0.117 mmol of 3,6-diisopropyl-1,2,4,5-tetrazine (19.5 mg) and 1.17 mmol of **2** (350 mg) in 0.1 mL of dichloromethane at 24 °C, and 1 M TBAF in THF (1.30 mmol, 1.30 mL) was slowly added to the solution over the course of 5 minutes. After the addition, the solution was concentrated in vacuo, and filtered on the silica gel, and purified by flash column chromatography (hexanes/ethyl acetate 1:3) to afford **6** (18.6 mg).

Isolated Yield: 74 %.

Physical Property: White solid, m.p. = 85-86 °C.

TLC: R_f = 0.19 (silica gel, ethyl acetate/hexanes 1:4).

^{1}H NMR (500 MHz, $CDCl_3$)

δ 8.18 (dd, 2H, J = 6.3, 3.3 Hz), 7.86 (dd, 2H, J = 6.3, 3.3 Hz), 3.86 (sep, 2H, 6.8 Hz), 1.53 (d, 12H, 6.8 Hz).

^{13}C NMR (125 MHz, $CDCl_3$)

δ 162.5, 131.3, 125.0, 124.3, 30.2, 22.0.

IR (neat): 2968, 2930, 2873, 1540, 1566, 1472, 1457, 1386, 1264, 1087, 1035, 991, 774, 735, 703, 668 cm^{-1}.

HRMS (ESI) calculated for $C_{22}H_{16}N_2^+$ $[M+H]^+$ 215.1543, found 215.1554.

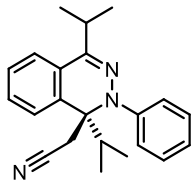

rac-**7**

(*R*)- and (*S*)-2-(1,4-diisopropyl-2-phenyl-1,2-dihydrophthalazin-1-yl)acetonitrile (*rac*-7): A 4 mL vial was charged with 0.13 mmol of 1,4-diisopropylphthalazine **6** (28 mg), 1.3 mmol of 2-(trimethylsilyl)phenyl trifluoromethanesulfonate **2** (390 mg), 1 M TBAF in THF (1.4 mmol, 1.4 mL) in 50 μL of dichloromethane was heated to 80 °C. After 2 hours, the solution was cooled down, concentrated in vacuo and purified by flash column chromatography (ethyl acetate/hexanes 1:10) to afford *rac*-**7** (0.60 mg).

Isolated Yield: 1 %.

Physical Property: White solid, m.p. = 140-141 °C.

TLC: R_f = 0.38 (silica gel, ethyl acetate/hexanes 1:4).

^{1}H NMR (500 MHz, CD_2Cl_2)

δ 7.60-7.40 (m, 7H), 7.35-7.28 (m, 1H), 7.24-7.18 (m, 1H), 3.37 (d, 1H, J = 17.6 Hz), 3.28-3.18 (m, 1H), 2.85 (d, 1H, J = 17.6 Hz), 2.19-2.09 (m, 1H), 1.25-1.21 (m, 6H), 0.90 (d, 3H, J = 6.8 Hz), 0.74 (d, 3H, J = 6.8 Hz).

^{13}C NMR (125 MHz, CD_2Cl_2)

δ 146.5, 146.2, 130.2, 129.4, 128.7, 128.5, 128.1, 126.4, 126.0, 125.7, 122.8, 118.1, 66.6, 37.0, 29.1, 27.6, 21.3, 19.7, 19.2, 17.6.

IR (neat): 2960, 2921, 2849, 1262, 1096, 1028, 803 cm^{-1}.

HRMS (ESI) calculated for $C_{22}H_{26}N_3^+$ $[M+H]^+$ 332.2121, found 332.2121.

Crossover Experiment in Scheme 3.2.

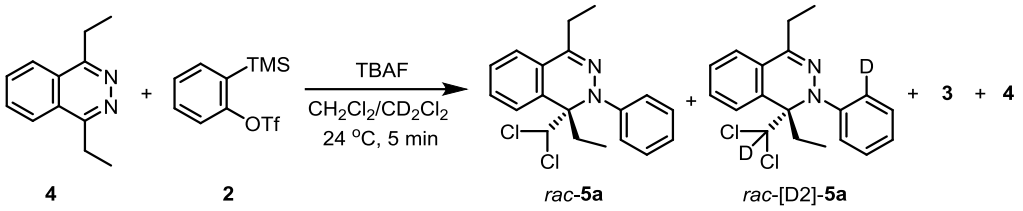

4 **2** *rac*-**5a** *rac*-[D2]-**5a**

Each vial was charged with 0.10 mmol of phthalazine **4** (19 mg) and 1.0 mmol of 2-(trimethylsilyl)phenyl trifluoromethanesulfonate **2** (300 mg) in 100 μL of CH_2Cl_2, CD_2Cl_2, CH_2Cl_2/CD_2Cl_2 (1:1), and CCl_4 at 24 °C, and 1 M TBAF in THF (1.1 mmol, 1.1 mL) was slowly added to the solution over the course of 5 minutes. After the addition, the solution was concentrated in vacuo, and filtered on the silica gel, and purified by flash column chromatography (ethyl acetate/hexanes 1:10 to straight ethyl acetate) to afford **3**, **4**, and *rac*-**5a** (or *rac*-[D_2]-**5a**).

Crossover Experiment in Scheme 3.3 (eq 7).

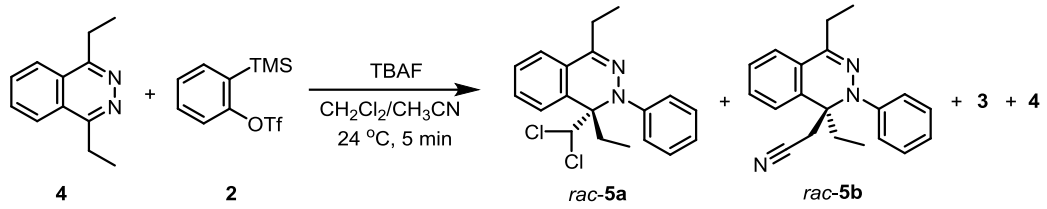

4 **2** *rac*-**5a** *rac*-**5b**

Each vial was charged with 10 μmol of phthalazine **4** (1.9 mg) and 100 μmol of 2-(trimethylsilyl)phenyl trifluoromethanesulfonate **2** (30 mg) in CH_3CN and CH_2Cl_2 in different molar ratios (total 5.0 mmol) at 24°C, and 1 M TBAF in THF (110 μmol, 110 μL) was slowly added to each solution over the course of 5 minutes. After the addition, the solutions and 9,10-diphenylanthracene as an internal standard were directly subjected to HPLC for analysis.

3.5 Acknowledgments

This work was supported by funding from the University of Pennsylvania. Instruments supported by the NSF and NIH including HRMS (NIH RR-023444). We thank Dr. George Furst, Dr. Rakesh Kohli, and Dr. Patrick Carroll, University of Pennsylvania for assistance in obtaining the high resolution NMR, mass spectral data, and single crystal X-ray analysis respectively.

3.6 References

(1) Niu, D.; Hoye, T. R. *Nat. Chem.* **2014**, *6*, 34.

(2) Gampe, C. M.; Carreira, E. M. *Angew. Chem. Int. Ed.* **2012**, *51*, 3766.

(3) Tadross, P. M.; Stoltz, B. M. *Chem. Rev.* **2012**, *112*, 3550.

(4) Dubrovskiy, A. V; Markina, N. a; Larock, R. C. *Org. Biomol. Chem.* **2013**, *11*, 191.

(5) Goetz, A. E.; Shah, T. K.; Garg, N. K. *Chem. Commun.* **2015**, *51*, 34.

(6) Wu, D.; Ge, H.; Liu, S. H.; Yin, J. *RSC Adv.* **2013**, *3*, 22727.

(7) Yeoman, J. T. S.; Reisman, S. E. *Nature* **2012**, *490*, 7.

(8) Hoffmann, R.; Imamura, A.; Hehre, W. J. *J. Am. Chem. Soc.* **1968**, *90*, 1499.

(9) Wallbaum, J.; Jones, P. G.; Werz, D. B. *J. Org. Chem.* **2015**, *80*, 3730.

(10) Peña, D.; Pérez, D.; Guitián, E. *Angew. Chem. Int. Ed.* **2006**, *45*, 3579.

(11) Tadross, P. M.; Virgil, S. C.; Stoltz, B. M. *Org. Lett.* **2010**, *12*, 1612.

(12) Allan, K. M.; Stoltz, B. M. *J. Am. Chem. Soc.* **2008**, *130*, 17270.

(13) Liu, Z.; Larock, R. C. *Org. Lett.* **2003**, *5*, 4673.

(14) Bentley, S. A.; Davies, S. G.; Lee, J. A.; Roberts, P. M.; Thomson, J. E. *Org. Lett.* **2011**, *13*, 2544.

(15) Ikawa, T.; Nishiyama, T.; Shigeta, T.; Mohri, S.; Morita, S.; Takayanagi, S.; Terauchi, Y.;

Morikawa, Y.; Takagi, A.; Ishikawa, Y.; Fujii, S.; Kita, Y.; Akai, S. *Angew. Chem. Int. Ed.* **2011**, *50*, 5674.

(16) Jayanth, T. T.; Jeganmohan, M.; Cheng, M.; Chu, S.; Cheng, C. *J. Am. Chem. Soc.* **2006**, *128*, 2232.

(17) Candito, D. A.; Dobrovolsky, D.; Lautens, M. *J. Am. Chem. Soc.* **2012**, *134*, 15572.

(18) Yun, S. Y.; Wang, K.-P.; Lee, N.-K.; Mamidipalli, P.; Lee, D. *J. Am. Chem. Soc.* **2013**, *135*, 4668.

(19) Hoye group reported aryne desaturation reaction with THF, 1,4-dioxane, cycloalkane, and norbornane. Niu, D.; Willoughby, P. H.; Woods, B. P.; Baire, B.; Hoye, T. R. *Nature* **2013**, *501*, 531.

(20) Dockendorff, C.; Sahli, S.; Olsen, M.; Milhau, L.; Lautens, M. *J. Am. Chem. Soc.* **2005**, *127*, 15028.

(21) Castillo, J.-C.; Quiroga, J.; Abonia, R.; Rodriguez, J.; Coquerel, Y. *Org. Lett.* **2015**, *17*, 3374.

(22) Castillo, J.-C.; Quiroga, J.; Abonia, R.; Rodriguez, J.; Coquerel, Y. *J. Org. Chem.* **2015**, *80*, 9767.

(23) Yanney, M.; Fronczek, F. R.; Sygula, A. *Org. Lett.* **2012**, *14*, 4942.

(24) Spiteri, C.; Keeling, S.; Moses, J. E. *Org. Lett.* **2010**, *12*, 3368.

(25) Shi, F.; Waldo, J. P.; Chen, Y.; Larock, R. C. *Org. Lett.* **2008**, *10*, 2409.

(26) McMahon, T. C.; Medina, J. M.; Yang, Y.-F.; Simmons, B. J.; Houk, K. N.; Garg, N. K. *J. Am. Chem. Soc.* **2015**, *137*, 4082.

(27) Chakrabarty, S.; Chatterjee, I.; Tebben, L.; Studer, A. *Angew. Chem. Int. Ed.* **2013**, *52*, 2968.

(28) Feltenberger, J. B.; Hayashi, R.; Tang, Y.; Babiash, E. S. C.; Hsung, R. P. *Org. Lett.* **2009**, *11*, 3666.

(29) Bachmann, W. E.; Clarke, H. T. *J. Am. Chem. Soc.* **1927**, *49*, 2089.

(30) Alonso, J. M.; Díaz-Álvarez, A. E.; Criado, A.; Pérez, D.; Peña, D.; Guitián, E. *Angew. Chem. Int. Ed.* **2012**, *51*, 173.

(31) Schuler, B.; Collazos, S.; Gross, L.; Meyer, G.; Pérez, D.; Guitián, E.; Peña, D. *Angew.*

Chem. Int. Ed. **2014**, *53*, 9004.

(32) (a). Suh, S.-E.; Barros, S. A.; Chenoweth, D. M. *Chem. Sci.* **2015**, *6*, 5128. (b) Rarig, R-A. F.; Tran, M. N.; Chenoweth, D. M. *J. Am. Chem. Soc.* **2013**, *135*, 9213-9219. (c) Tran, M. N.; Chenoweth, D. M. *Angew. Chem. Int. Ed.* **2015**, *54*, 6442-6446. (d) Tran, M. N.; Chenoweth, D. M. *Chem. Sci.* **2015**, *6*, 4508-4512. (e) Ballister, E. R.; Aonbangkhen, C.; Mayo, A. M.; Lampson, M. A.; Chenoweth, D. M. *Nat. Commun.* **2014**, *5*, 5475. (f) Ballister, E. R.; Ayloo, S.; Chenoweth, D. M.; Lampson, M. A.; Holzbaur, E. L.F. *Current Biology* **2015**, *10*, R407-R408. (g) Barros, S. A.; Chenoweth, D. M. *Angew. Chem. Int. Ed.* **2014**, *53*, 13746-13750. (h) Barros, S. A.; Chenoweth, D. M. *Chem. Sci.* **2015**, *6*, 4752-4755. (i) Yoon, I.; Suh, S-E.; Barros, S. A.; Chenoweth, D. M. *Org. Lett.* **2016**, *18*, 1096-1099. (j) Barros, S. A.; Yoon, I.; Suh, S-E.; Chenoweth, D. M. *Org. Lett.* **2016**, *18*, 2423-2426.

(33) Important new synthetic methods for accessing many new tetrazines in a straightforward and operationally simple manner have recently been developed by Devaraj and co-workers. See: Yang, J.; Karver, M. R.; Li, W.; Sahu, S.; Devaraj, N. K. *Angew. Chem., Int. Ed.*, **2012**, *51*, 5222.

(34) Li, J. B.; Zhao, Y. B.; Lu, J.; Li, G.; Zhang, J. P.; Zhao, Y.; Sun, X. W.; Zhang, Q. C. *J. Org. Chem.* **2015**, *80*, 109.

(35) Yanney, M.; Fronczek, F. R.; Sygula. A. *Org. Lett.*, **2012**, *14*, 4942.

(36) Alonso, J. M.; Díaz-Álvarez, A. D.; Criado, A.; Pérez, D.; Peña, D.; Guitián, E. *Angew. Chem., Int. Ed.* **2012**, *51*, 173.

(37) Im, G. Y. J.; Bronner, S. M.; Goetz, A. E.; Paton, R. S.; Cheong, P. H. Y.; Houk, K. N.; Garg, N. K. *J. Am. Chem. Soc.* **2010**, *132*, 17933.

(38) Cheong, P. H. Y.; Paton, R. S.; Bronner, S. M.; Im, G. Y. J.; Garg, N. K.; Houk, K. N. *J. Am. Chem. Soc.* **2010**, *132*, 1267.

(39) Hoye, T. R.; Baire, B.; Wang, T. *Chem. Sci.* **2014**, *5*, 545.

(40) Coe, J. W.; Wirtz, M. C.; Bashore, C. G.; Candler, J. *Org. Lett.* **2004**, *6*, 1589.

(41) Thangaraj, M.; Bhojgude, S. S.; Mane, M. V.; Biju, A. T. *Chem. Commun.* **2016**, *52*, 1665.

(42) Yoshida, H.; Yoshida, R.; Takaki, K. *Angew. Chem., Int. Ed.* **2013**, *52*, 8629.

(43) Stephens, D.; Zhang, Y.; Cormier, M.; Chavez, G.; Arman, H.; Larionov, O. V. *Chem. Commun.* **2013**, *49*, 6558.

(44) Gerfaud, T.; Neuville, L.; Zhu, J. *Angew. Chem., Int. Ed.* **2009**, *48*, 572.

(45) Himeshima, Y.; Sonoda, T.; Kobayashi, H. *Chem. Lett.* **1983**, 1211.

(46) Smith, M. B.; March, J. *March's Advanced Organic Chemistry: Reactions, Mechanisms, and Structure, 6th edition*; John Wiley & Sons: Hoboken, 2007.

(47) Matthews, W. S.; Bares, J. E.; Bartmess, J. E.; Bordwell, F. G.; Cornforth, F. J.; Drucker, G. E.; Margolin, Z.; McCallum, R. J.; McCollum, G. J.; Vanier, N. R. *J. Am. Chem. Soc.* **1975**, *97*, 7006.

(48) Shaibu, B. S.; Kawade, R. K.; Liu, R.-S. *Org. Biomol. Chem.* **2012**, *10*, 6834.

(49) Hayashi, E.; Iinuma, M.; Utsunomiya, I.; Iijima, C.; Oishi, E.; Higashino, T. *Chem. Pharm. Bull.* **1977**, *25*, 579.

(50) Stephenson, L.; Walker, T.; Warburton, W. K.; Webb, G. B. *J. Chem. Soc.* **1962**, 1282.

Appendix 2

NMR Spectra and X-Ray Structure Data Relevant to Chapter 3

Adapted with permission from Suh, S.-E.; Chenoweth, D. M. *Org. Lett.* **2016,** *18,* 4080-4083.

Figure A2.1. ^{1}H NMR spectrum of **2** in $CDCl_3$ (500 MHz).

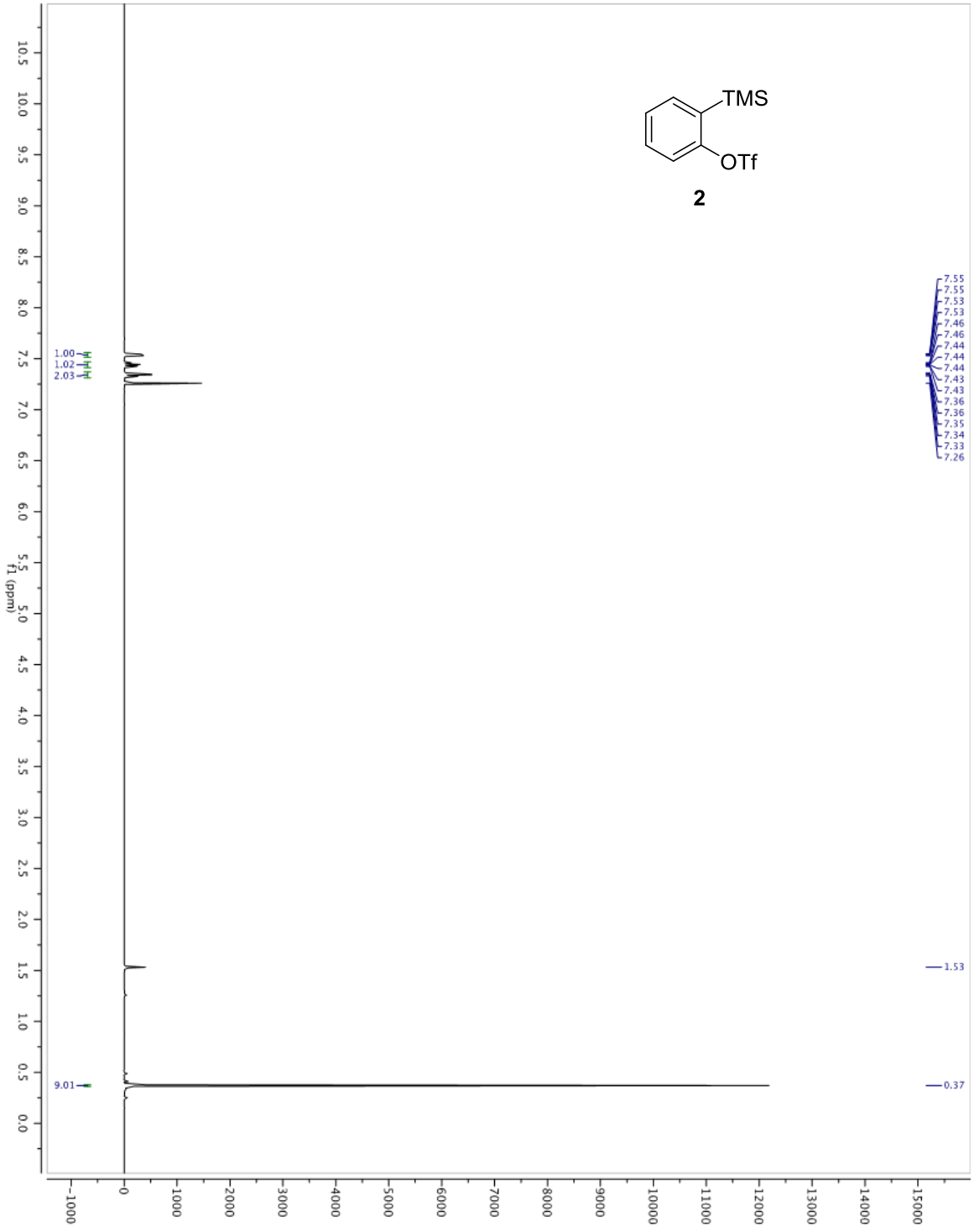

Figure A2.2. ^{1}H NMR spectrum of **4** in $CDCl_3$ (500 MHz).

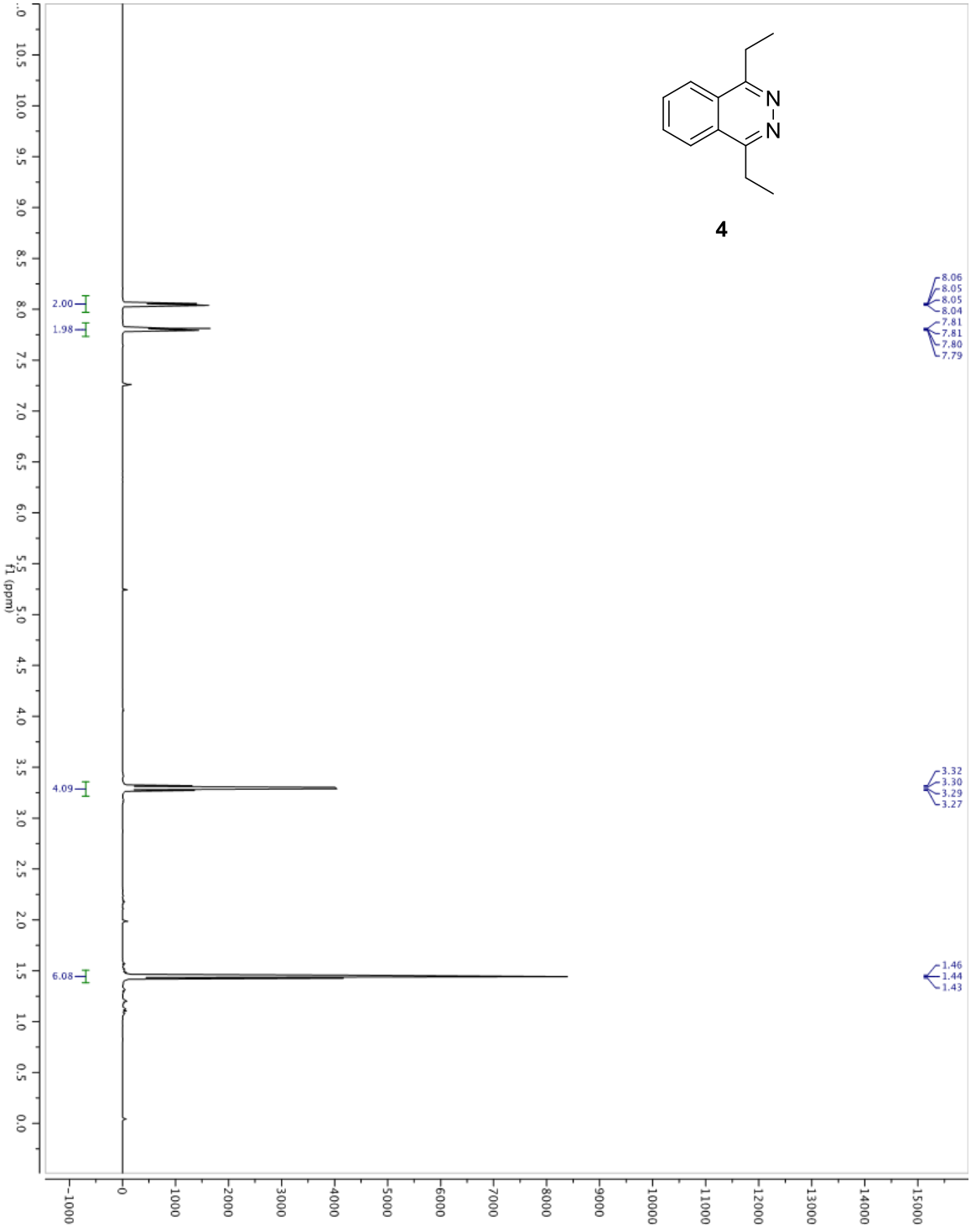

Figure A2.3. ^{13}C NMR spectrum of **4** in $CDCl_3$ (125 MHz).

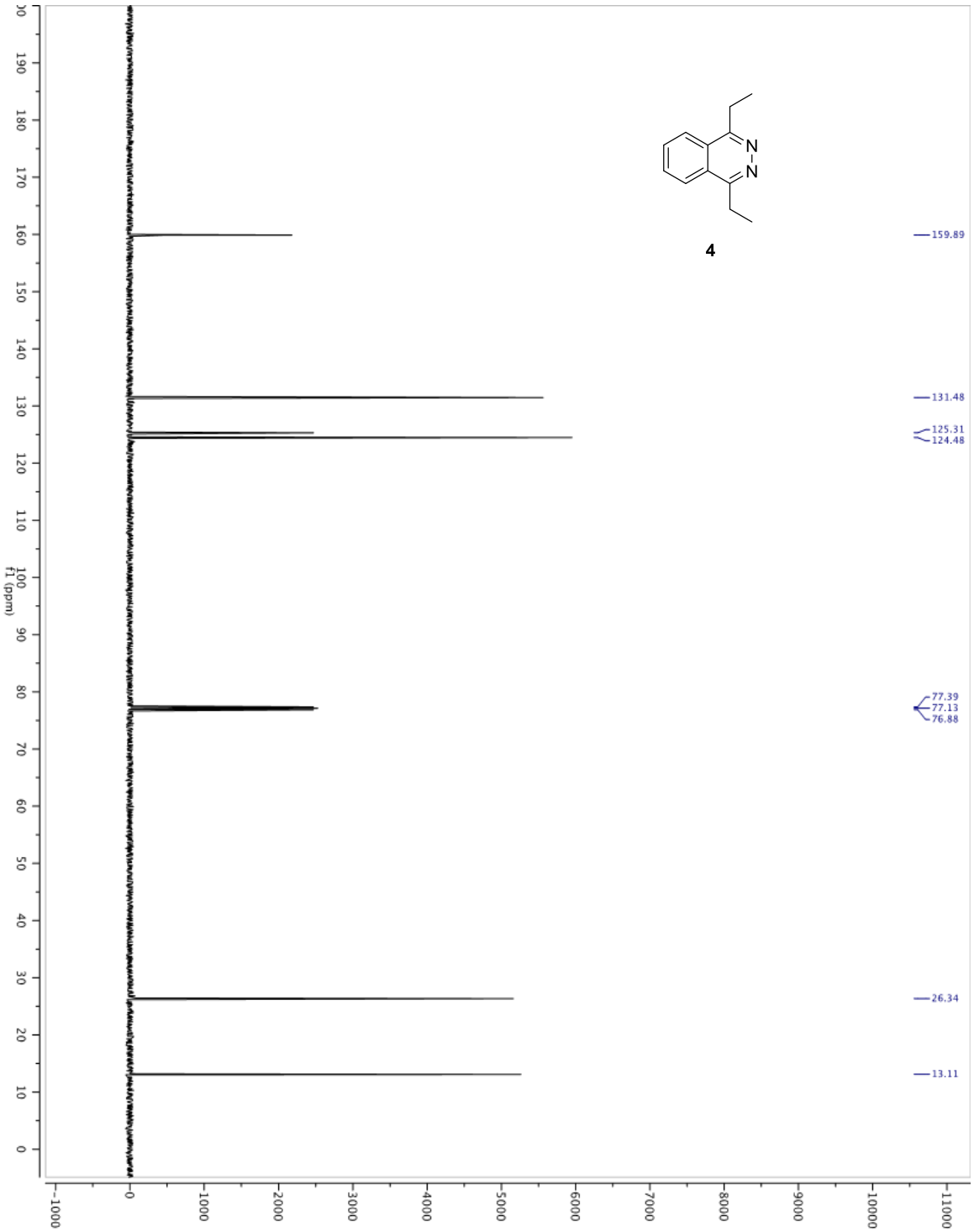

Figure A2.4. ^{1}H NMR spectrum of *rac*-**5a** in CD_2Cl_2 (500 MHz).

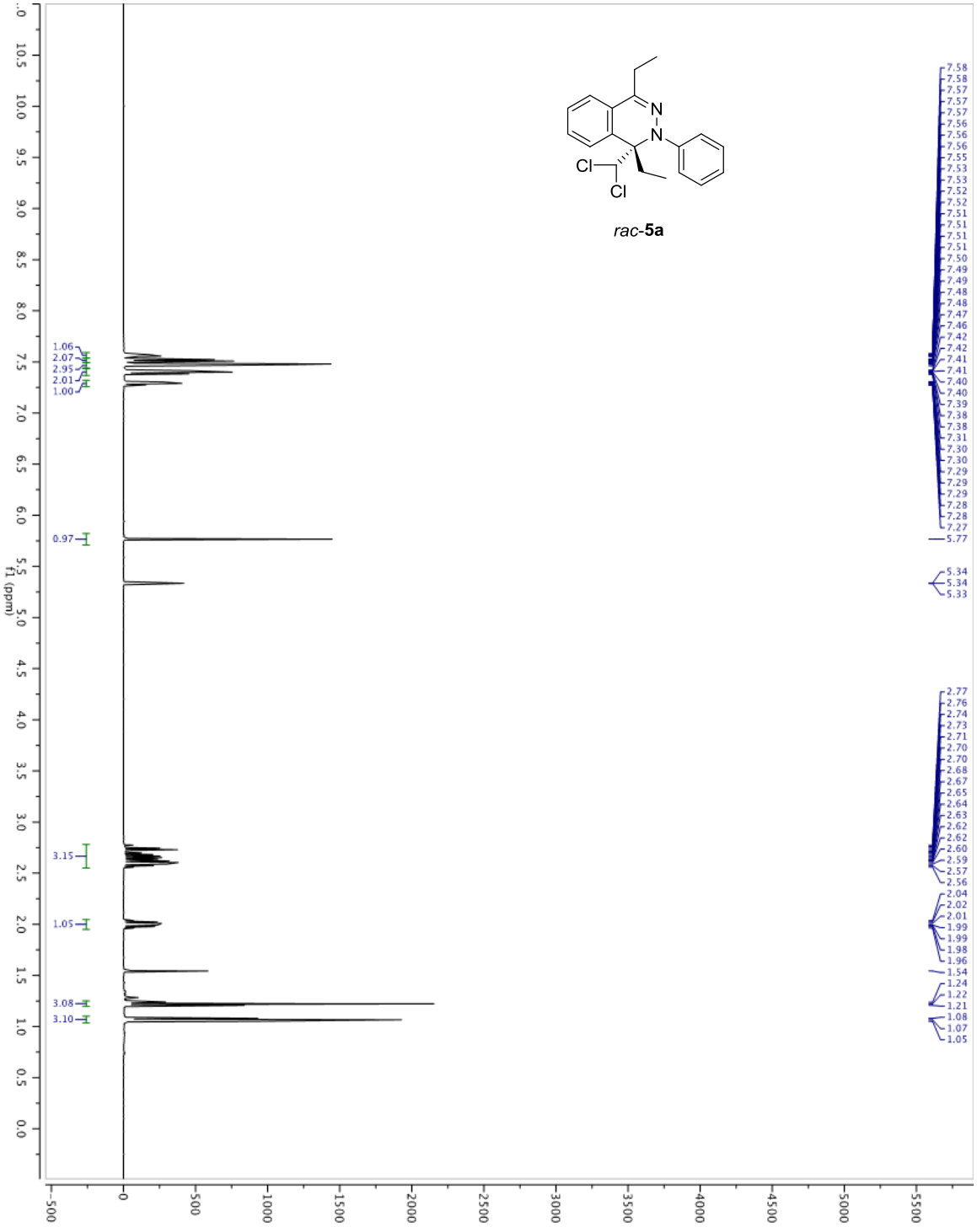

Figure A2.5. ^{13}C NMR spectrum of *rac*-**5a** in CD_2Cl_2 (125 MHz).

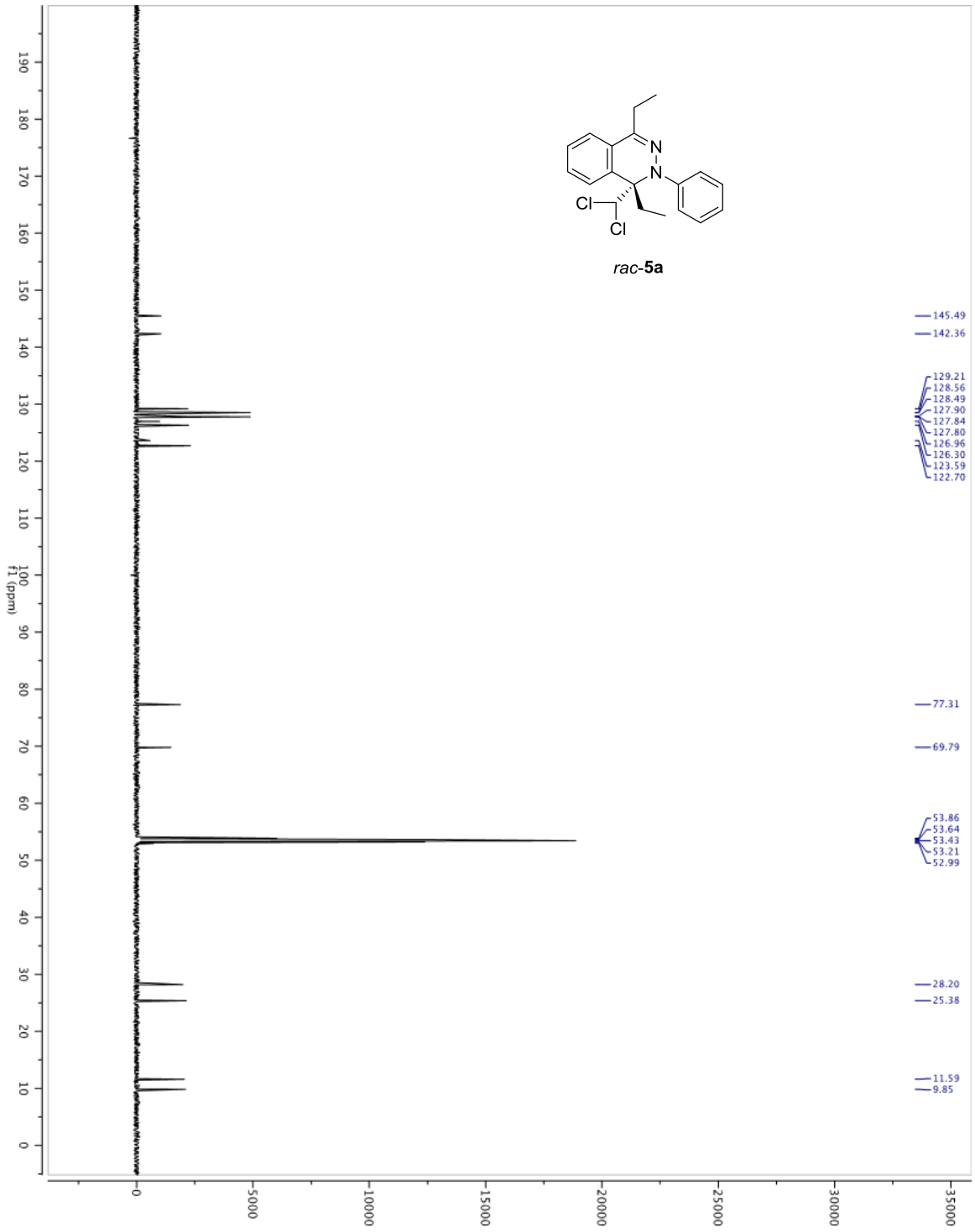

Figure A2.6. HSQC spectrum of *rac*-**5a** in CD_2Cl_2.

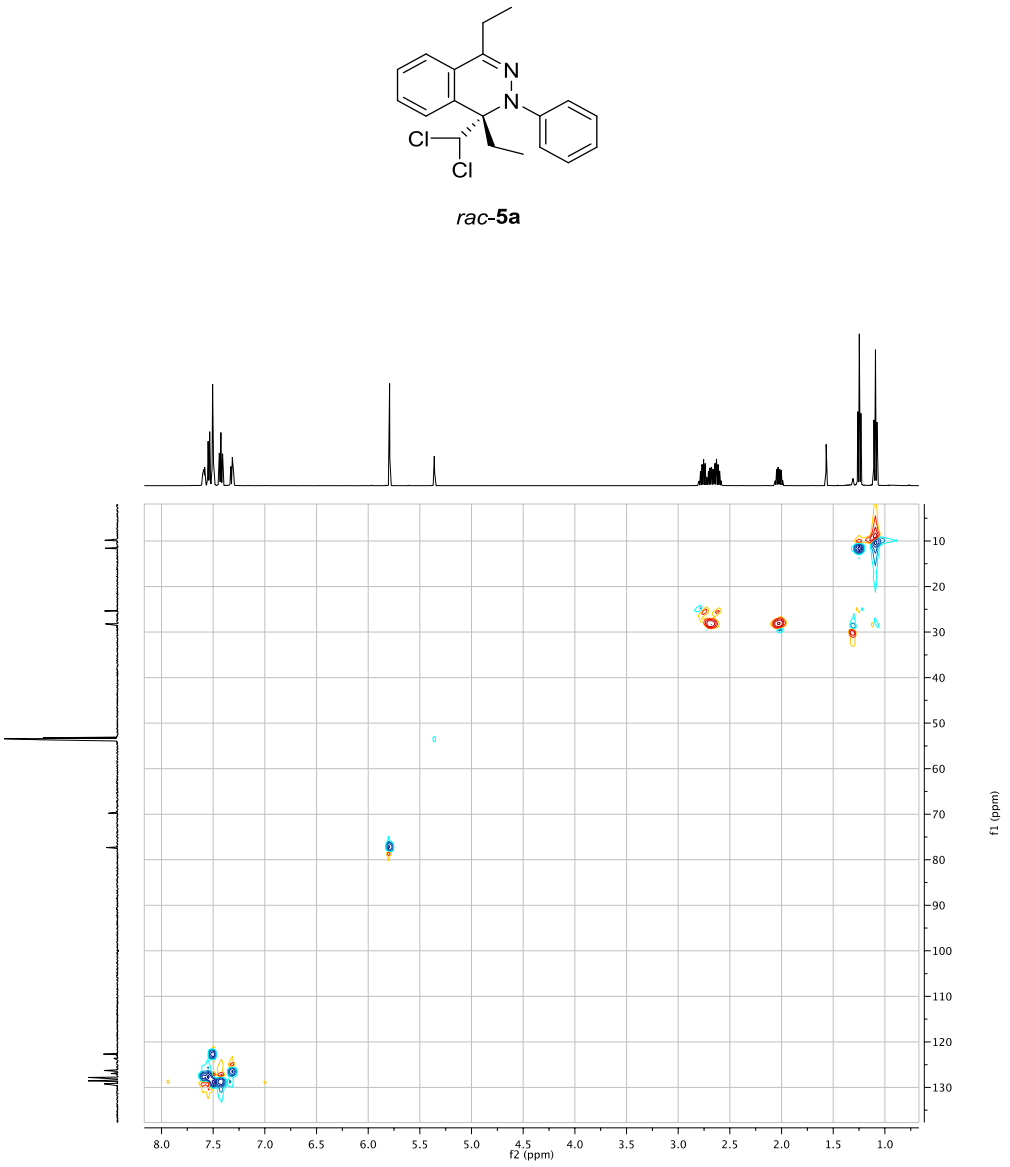

Figure A2.7. HMBC spectrum of *rac*-**5a** in CD_2Cl_2.

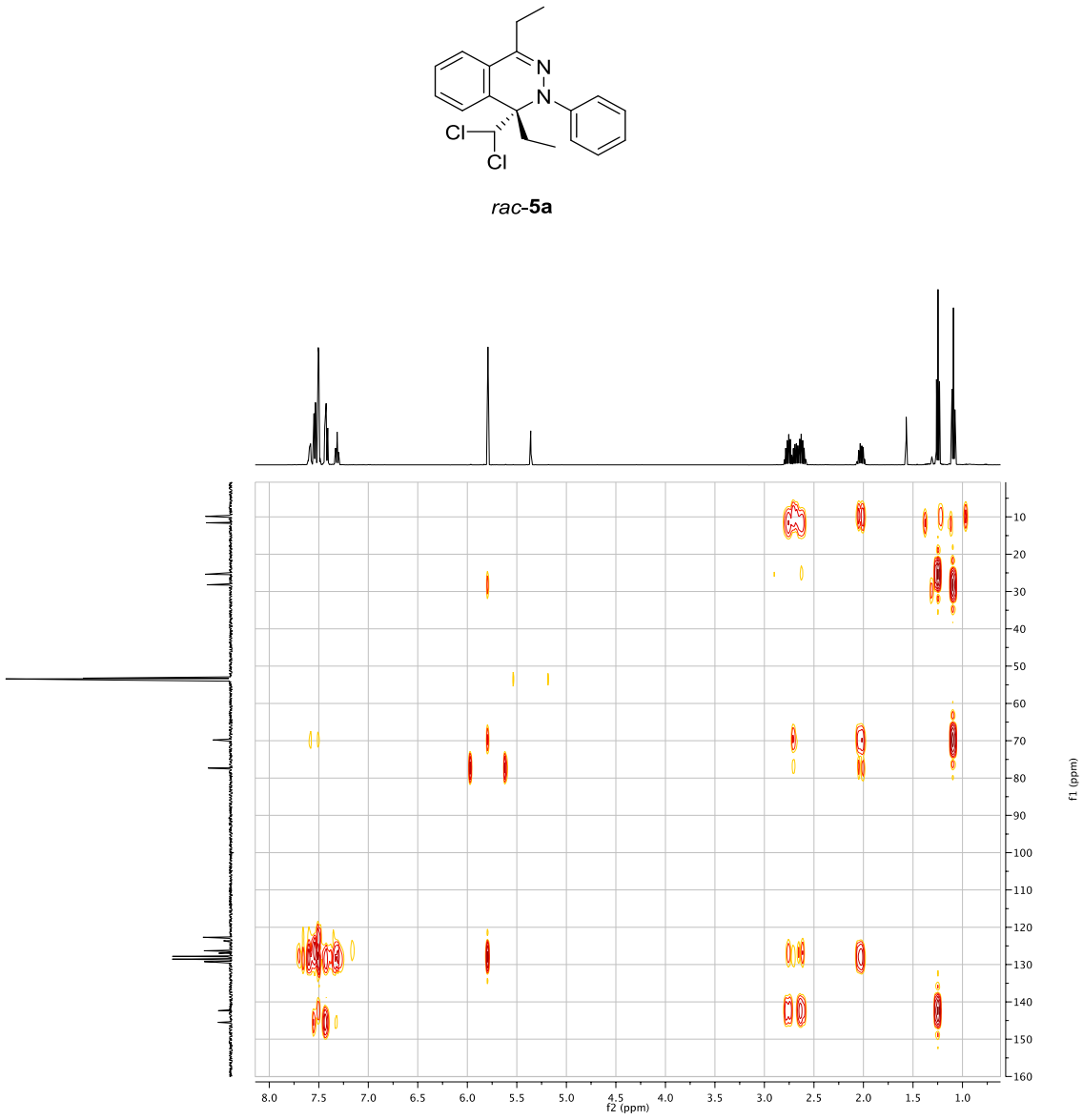

Figure A2.8. ^{1}H NMR spectrum of *rac*-[D_2]-**5a** in CD_2Cl_2 (500 MHz).

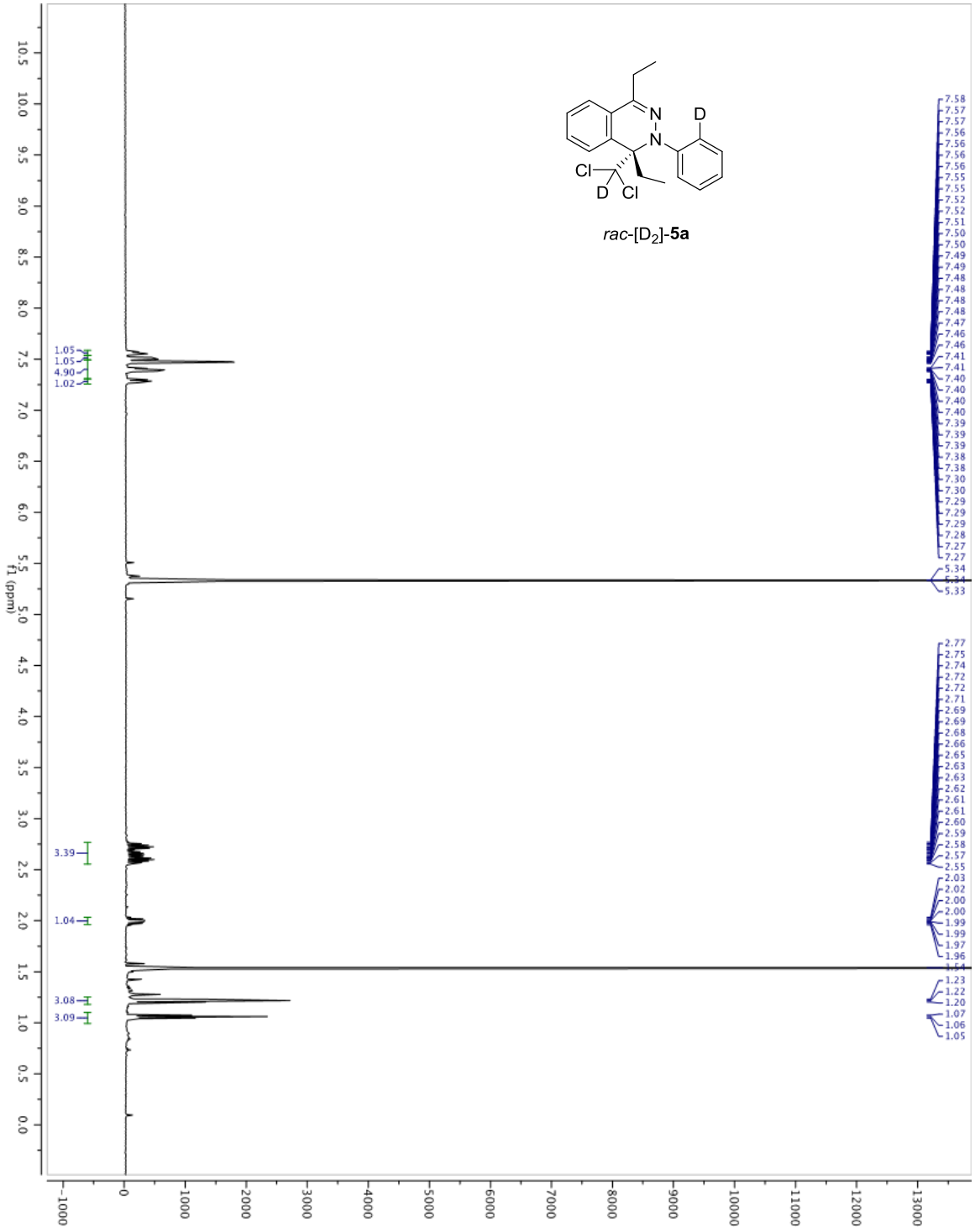

Figure A2.9. ^{1}H NMR spectrum of *rac*-**5b** in CD_2Cl_2 (500 MHz).

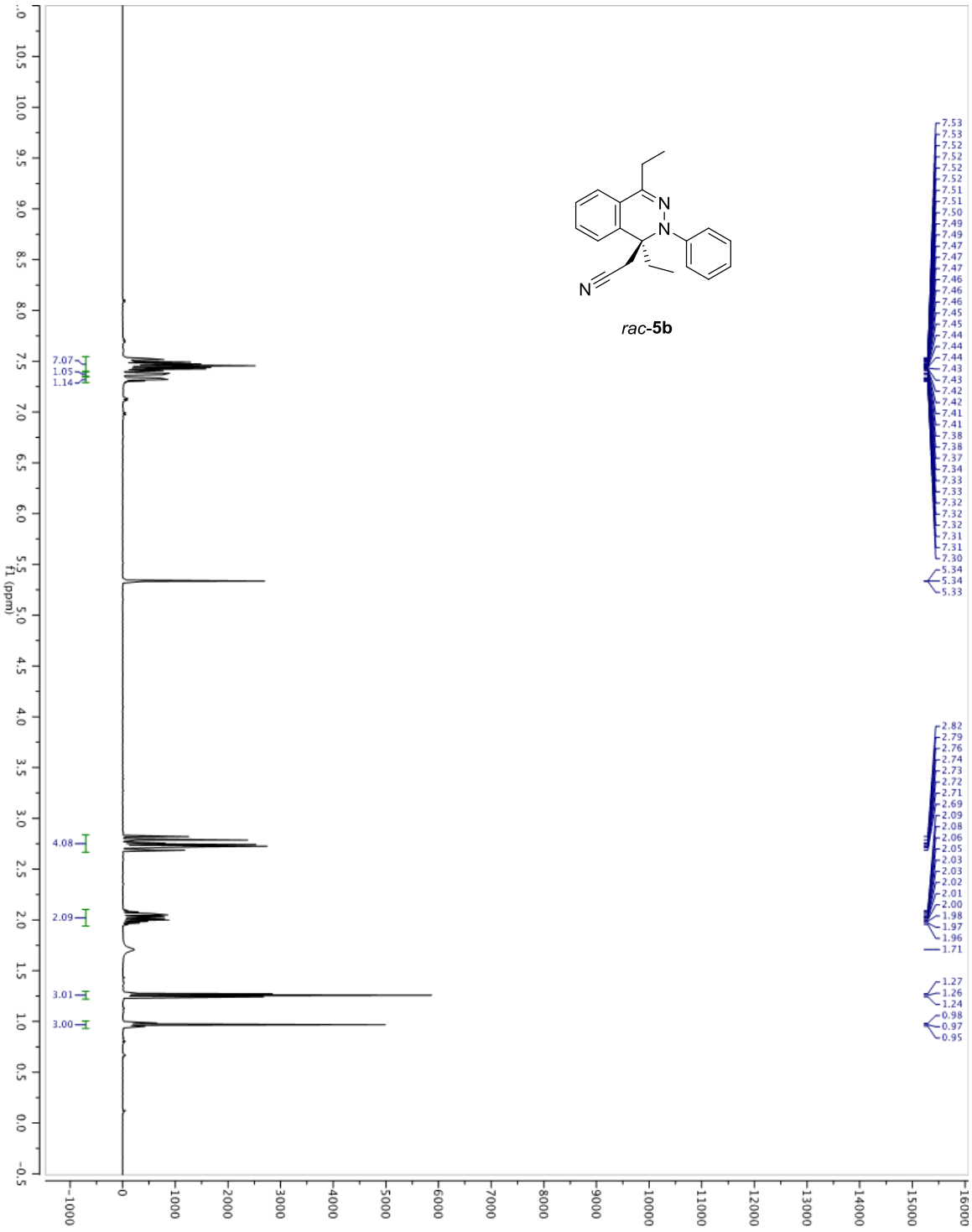

Figure A2.10. ^{13}C NMR spectrum of *rac*-**5b** in CD_2Cl_2 (125 MHz).

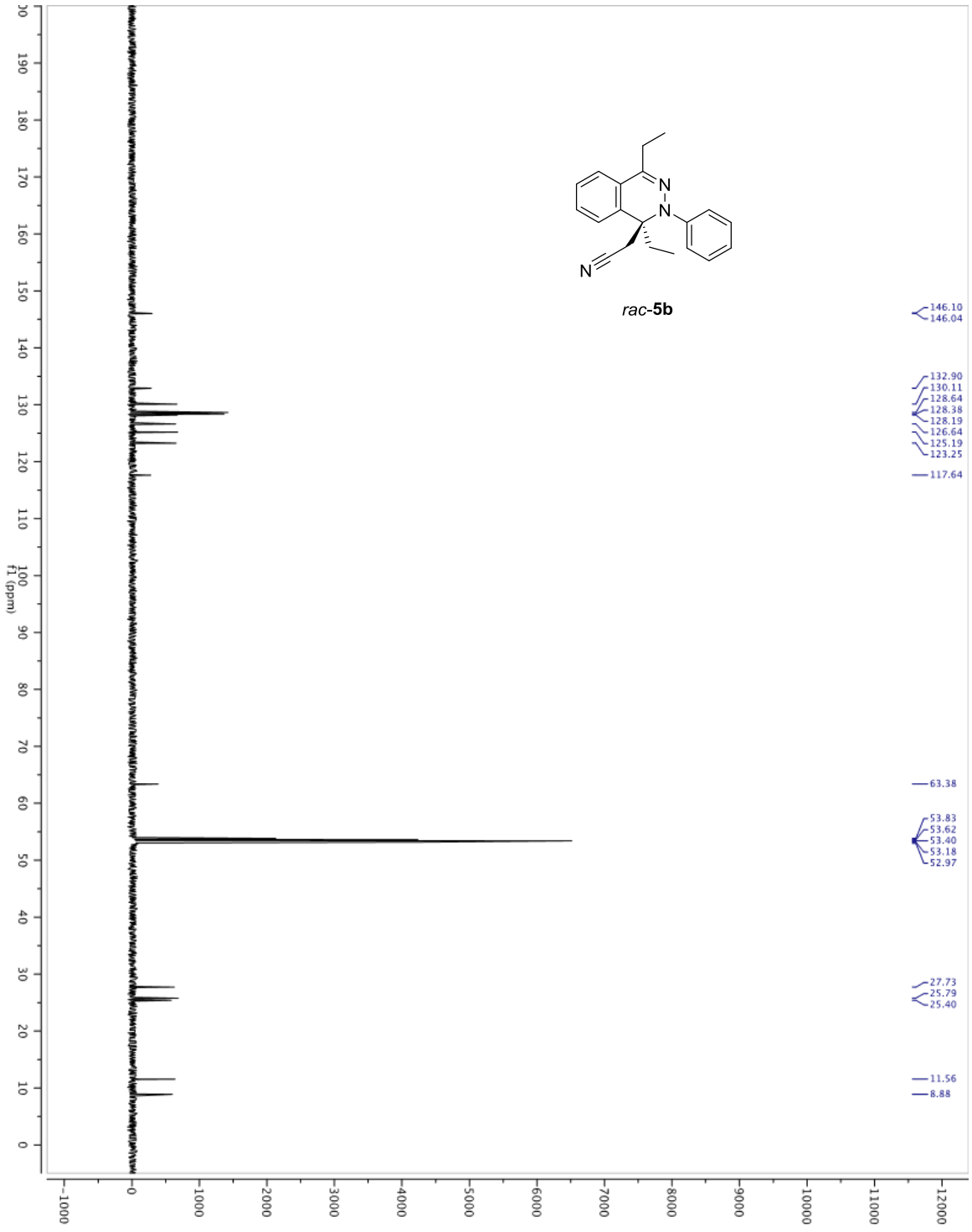

Figure A2.11. HMBC spectrum of *rac*-**5b** in CD_2Cl_2.

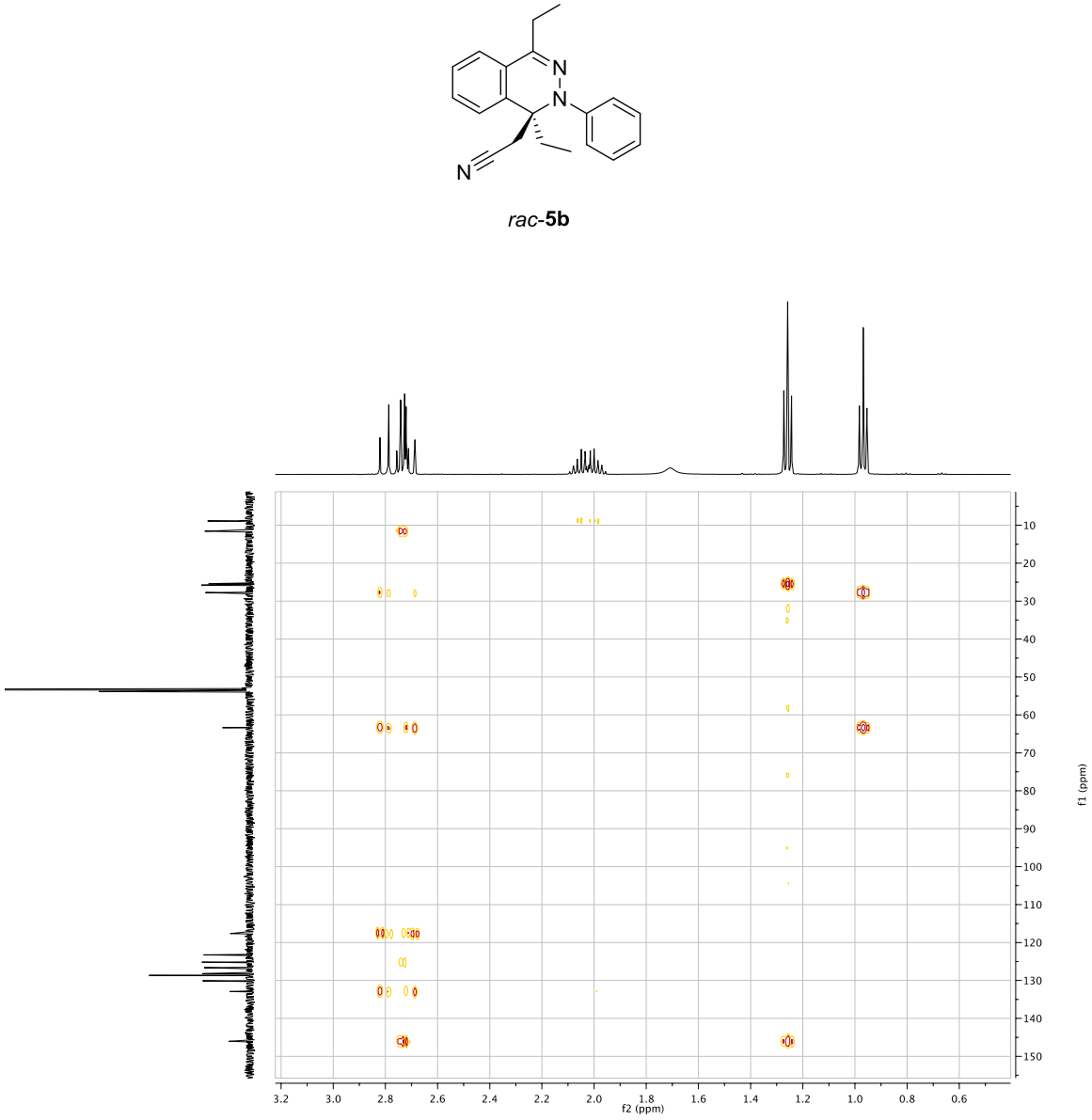

Figure A2.12. ^{1}H NMR spectrum of 3,6-diisopropyl-1,2,4,5-tetrazine in $CDCl_3$ (500 MHz).

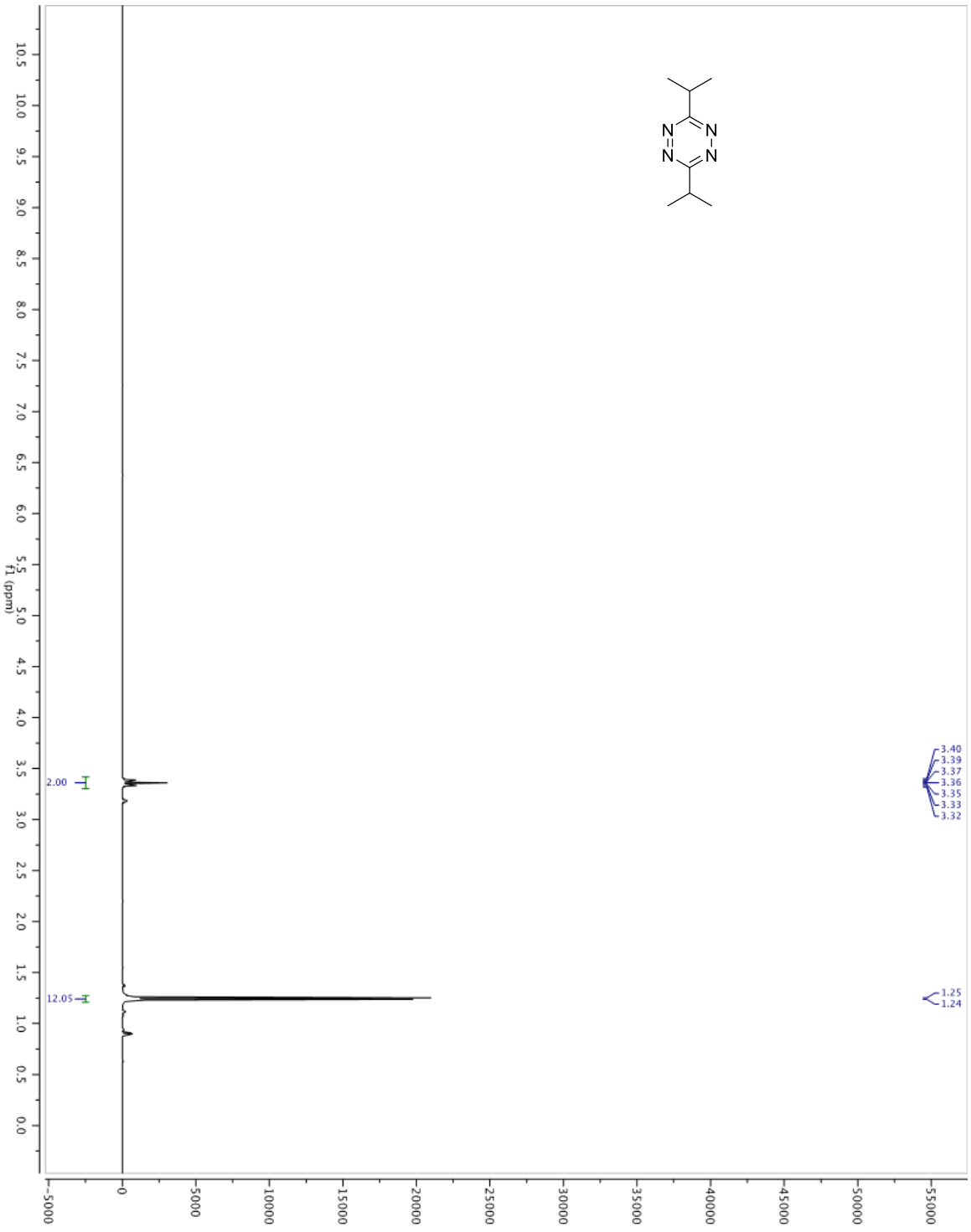

Figure A2.13. ^{13}C NMR spectrum of 3,6-diisopropyl-1,2,4,5-tetrazine in $CDCl_3$ (125 MHz).

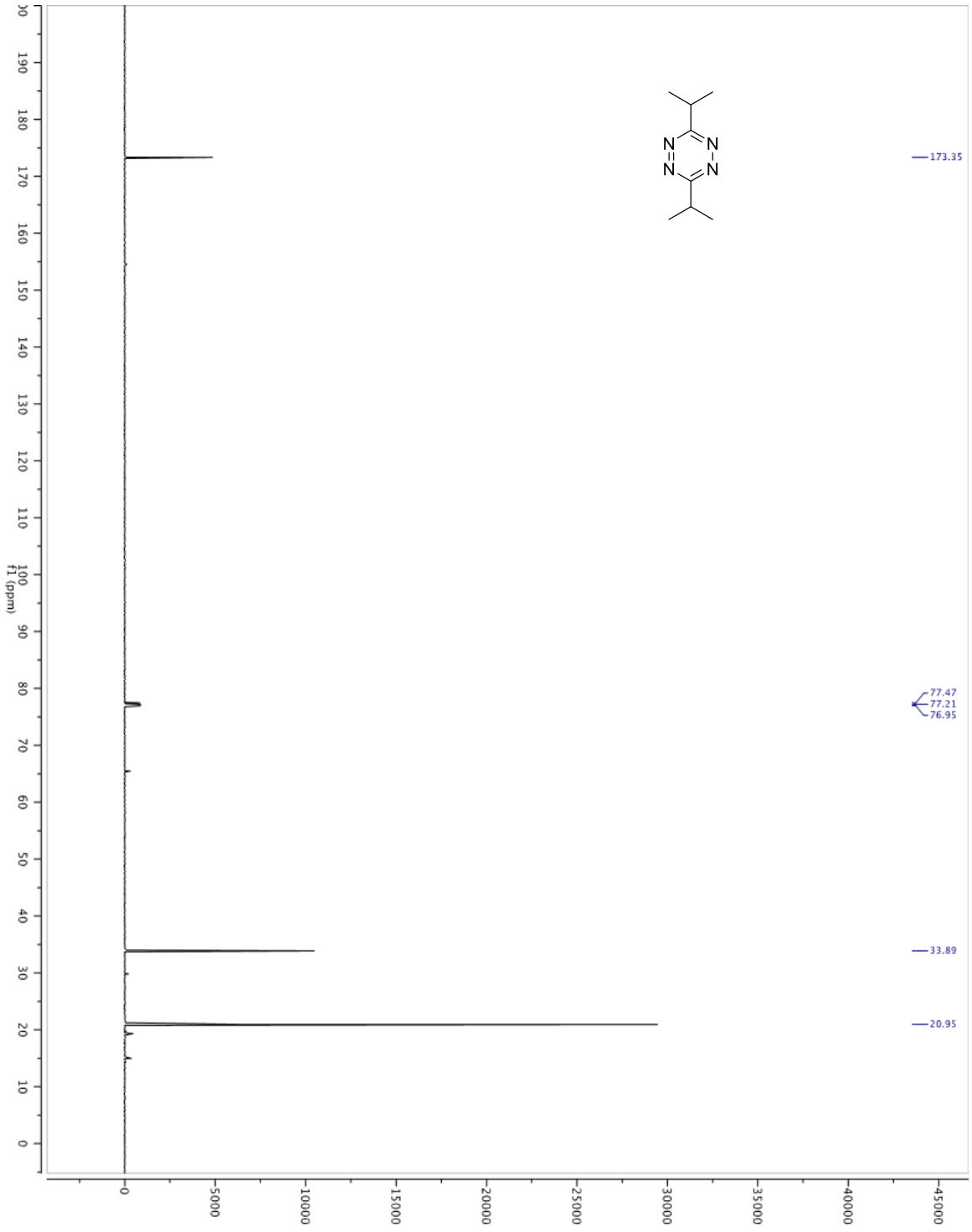

Figure A2.14. ^{1}H NMR spectrum of **6** in $CDCl_3$ (500 MHz).

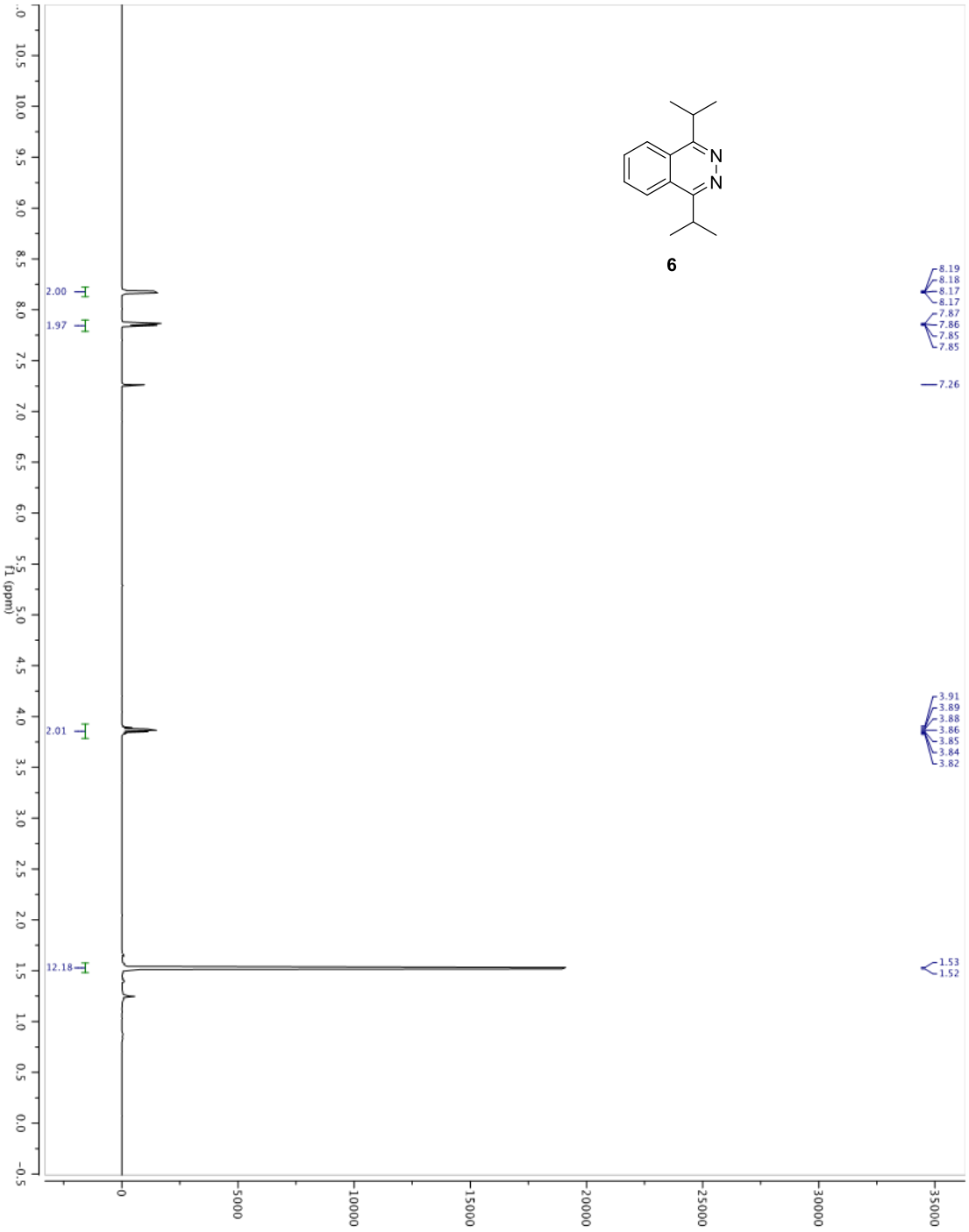

Figure A2.15. ^{13}C NMR spectrum of **6** in $CDCl_3$ (125 MHz).

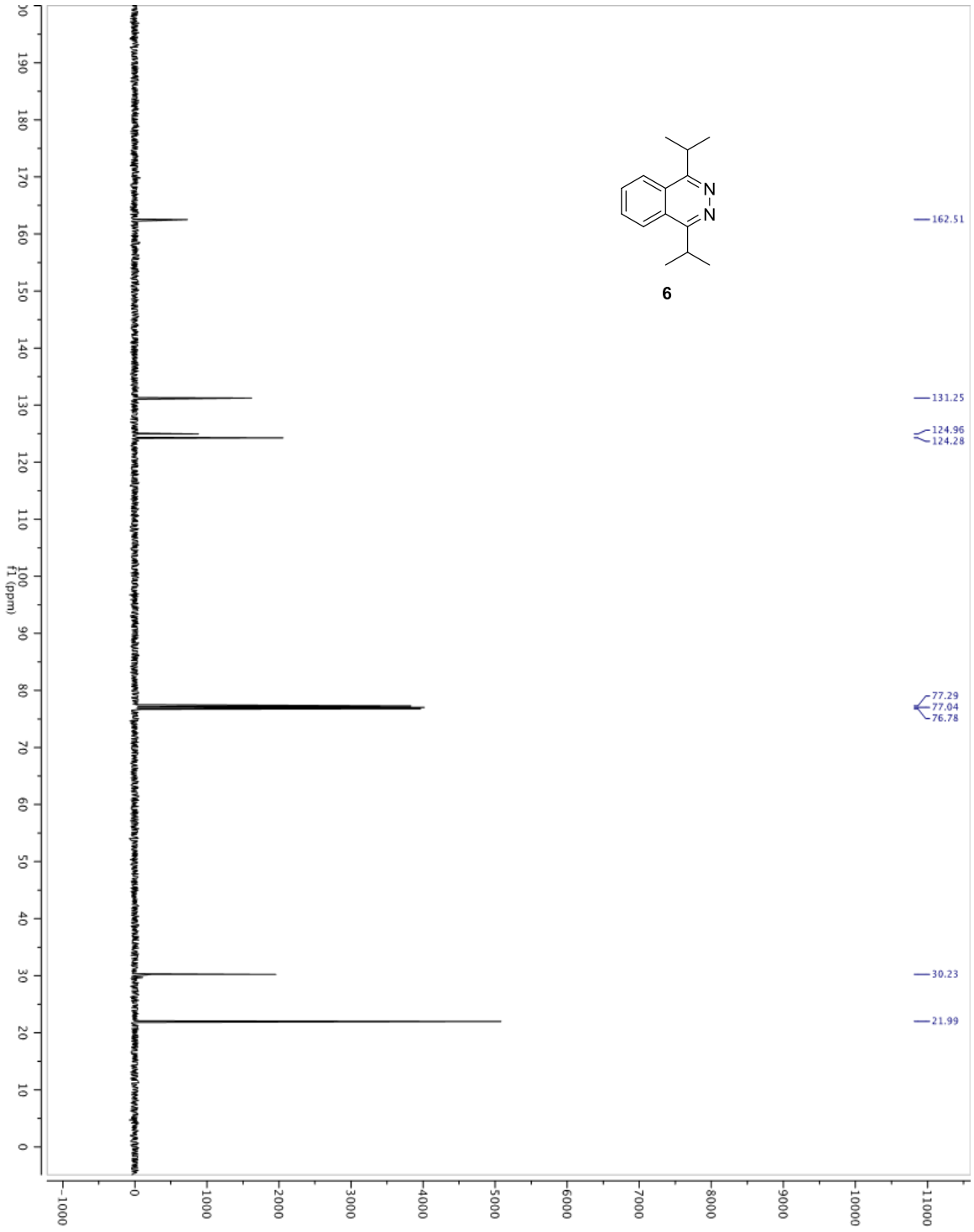

Figure A2.16. ^{1}H NMR spectrum of *rac*-**7** in CD_2Cl_2 (500 MHz).

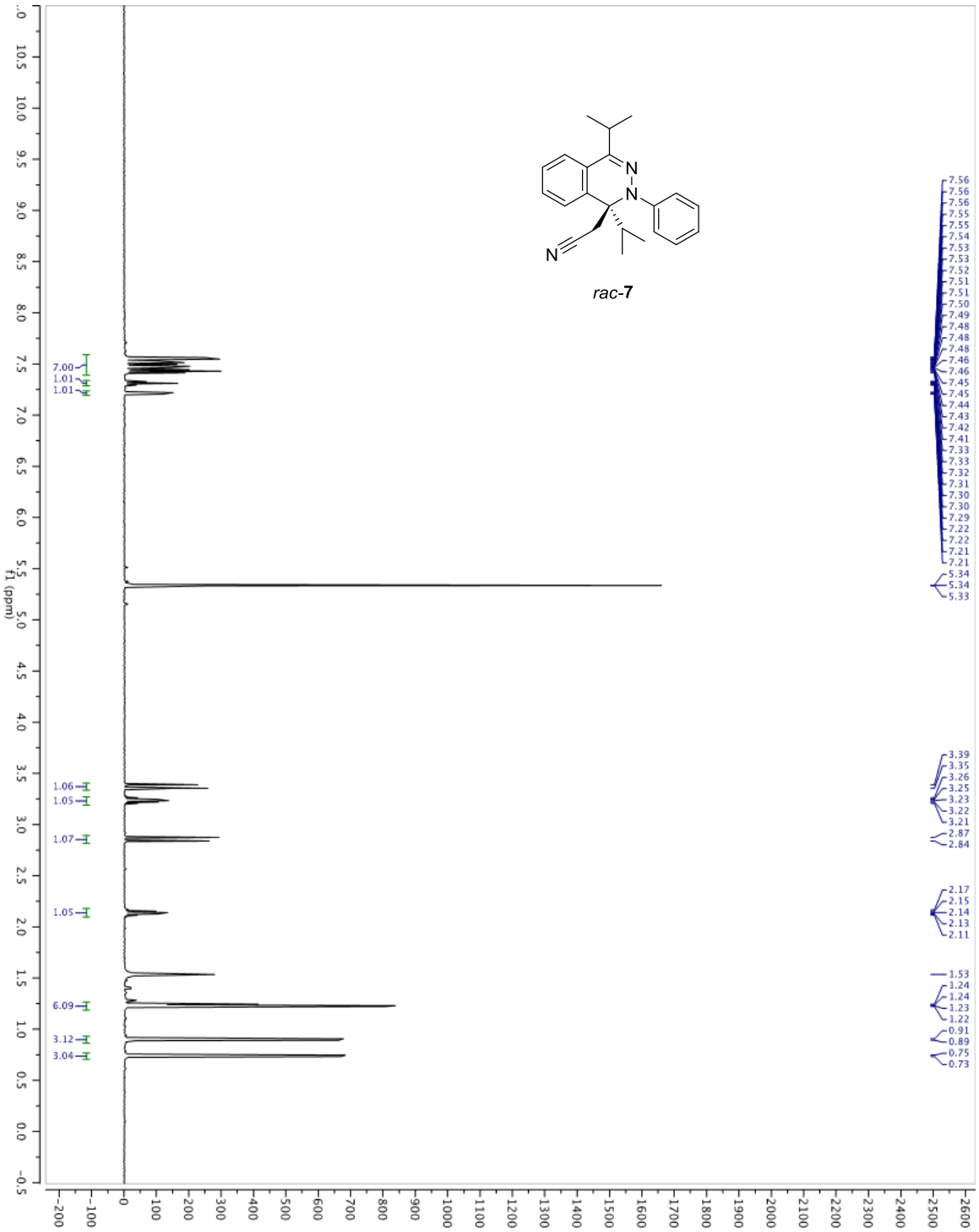

Figure A2.17. ^{13}C NMR spectrum of *rac*-**7** in CD_2Cl_2 (125 MHz).

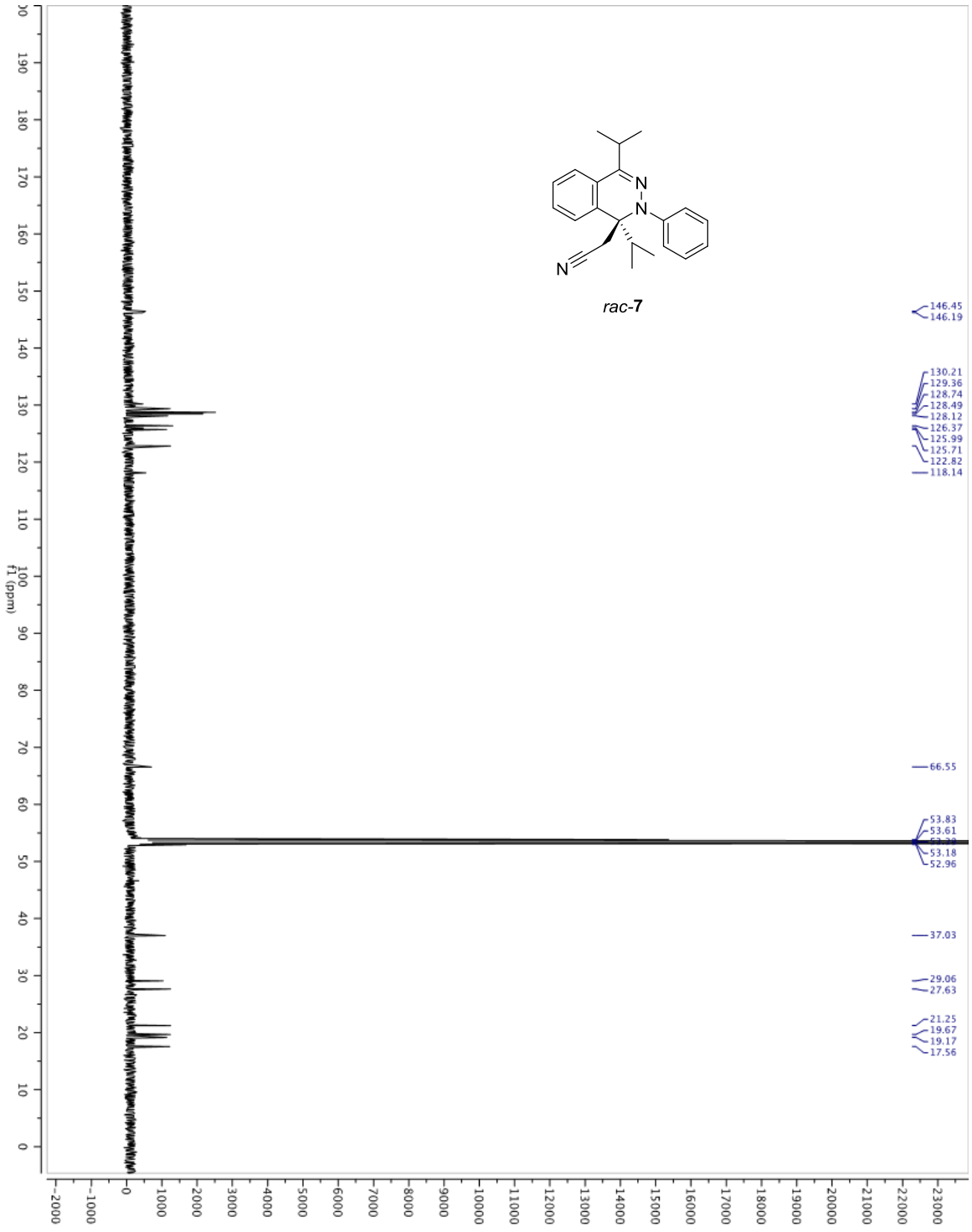

Table A2.1. Crystal Data and Structure Refinement for 5a.

Empirical formula	$C_{19}H_{20}N_2Cl_2$
Formula weight	347.27
Temperature	100(1) K
Wavelength	0.71073 Å
Crystal system	orthorhombic
Space group	$P2_12_12_1$
Cell constants:	
a	8.5618(10) Å
b	8.6657(9) Å
c	22.783(3) Å
Volume	1690.4(3) $Å^3$
Z	4
Density (calculated)	1.365 Mg/m^3
Absorption coefficient	0.385 mm^{-1}
F(000)	728
Crystal size	0.32 x 0.22 x 0.12 mm^3
Theta range for data collection	2.51 to 25.39°
Index ranges	$-10 \leq h \leq 10$, $-10 \leq k \leq 10$, $-27 \leq l \leq 27$
Reflections collected	22569
Independent reflections	3110 [R(int) = 0.0433]
Completeness to theta = 25.39°	99.8 %
Absorption correction	Semi-empirical from equivalents
Max. and min. transmission	0.7452 and 0.4705
Refinement method	Full-matrix least-squares on F^2
Data / restraints / parameters	3110 / 67 / 275
Goodness-of-fit on F^2	1.237
Final R indices [I>2sigma(I)]	R1 = 0.0764, wR2 = 0.1911
R indices (all data)	R1 = 0.0769, wR2 = 0.1913
Absolute structure parameter	0.49(19)
Largest diff. peak and hole	0.600 and -0.640 $e.Å^{-3}$

Table A2.2. Crystal Data and Structure Refinement for 5b.

Empirical formula	$C_{20}H_{21}N_3$
Formula weight	303.40
Temperature	100(1) K
Wavelength	0.71073 Å
Crystal system	monoclinic
Space group	$P2_1$
Cell constants:	
a	7.1149(3) Å
b	26.5631(11) Å
c	8.5150(4) Å
β	90.955(3)°
Volume	1609.06(12) $Å^3$
Z	4
Density (calculated)	1.252 Mg/m^3
Absorption coefficient	0.075 mm^{-1}
F(000)	648
Crystal size	0.12 x 0.12 x 0.05 mm^3
Theta range for data collection	1.53 to 25.48°
Index ranges	$-8 \leq h \leq 8$, $-31 \leq k \leq 32$, $-10 \leq l \leq 10$
Reflections collected	29916
Independent reflections	5858 [R(int) = 0.0402]
Completeness to theta = 25.48°	99.5 %
Absorption correction	Semi-empirical from equivalents
Max. and min. transmission	0.7452 and 0.6245
Refinement method	Full-matrix least-squares on F^2
Data / restraints / parameters	5858 / 1 / 420
Goodness-of-fit on F^2	1.080
Final R indices [I>2sigma(I)]	R1 = 0.0632, wR2 = 0.1647
R indices (all data)	R1 = 0.0748, wR2 = 0.1719
Absolute structure parameter	2(3)
Largest diff. peak and hole	0.485 and -0.238 $e.Å^{-3}$

Chapter 4

Mechanistic Study of the Triple Aryne–Tetrazine Reaction

This work was performed in collaboration with Dr. Kendall N. Houk and Dr. Shuming Chen at the University of California, Los Angeles.

4.1 Introduction

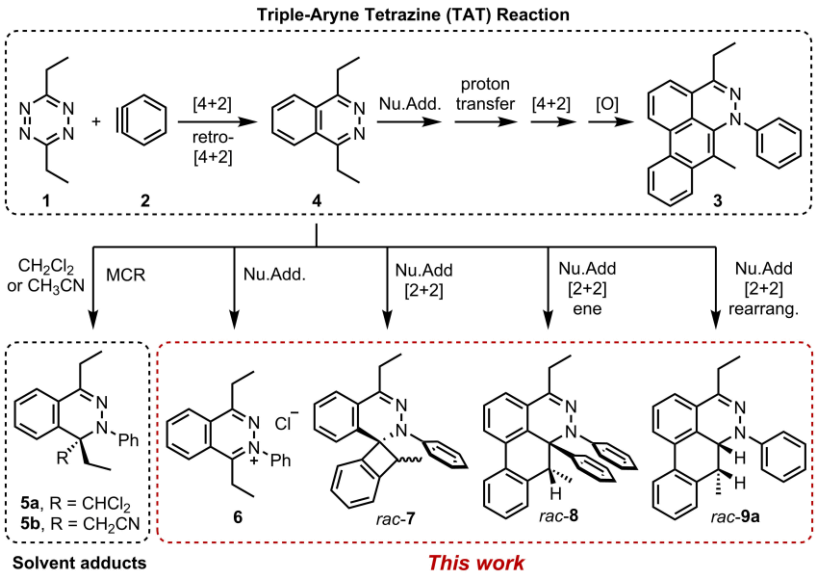

Figure 4.1. Reactivity modes of 1,2,4,5-tetrazine and arynes.

Recently, we reported a new multistep process termed the triple aryne-tetrazine (TAT) reaction.[1] The reaction coupled diverse reactivity modes between simple 1,2,4,5-tetrazine **1** (henceforth referred to as "tetrazine") starting materials[2] and aryne **2** into a single multistep process, resulting in the addition of three aryne equivalents to a tetrazine core. In the TAT reaction, dibenzocinnoline **3** and cycloaddition intermediate **4** were isolated. In addition, we reported solvent participation in aryne reactions with two solvent-trapped intermediates **5a** and **5b** (Scheme 4.1).[3] Detailed investigation of these side reactions can yield valuable insight into aryne chemistry[4] and provide access to new heterocyclic scaffolds.[5] Here we report new mechanistic aspects of the reaction between a tetrazines and arynes, elucidating unique divergent pathways to alternative products that arise during the reaction course. The reaction

mechanism consists of six consecutive elementary steps. As many as five steps can directly engage the aryne.[6] Using a combination of experimental and computational methods, we elucidate the unique competing pathways that are operational throughout the course of the reaction to yield products **6**, *rac*-**7**, *rac*-**8**, and *rac*-**9a.**

4.2 Results and Discussion

In the TAT reaction, it was observed that **1** undergoes [4+2] cycloaddition with **2** to afford phthalazine intermediate **4**[7] followed by several further mechanistic steps to give dibenzocinnoline **3** (Figure 4.2A). In the TAT reaction, anthracene **10** was not observed,[8] indicating that the phthalazine intermediate **4** does not undergo a further [4+2] cycloaddition. Instead, **4** is observed to undergo a nucleophilic addition to another equivalent of **2**. To compare the energy profiles of the competing [4+2] versus nucleophilic addition reaction pathways, density functional theory (DFT) calculations were performed on analogous structures with the ethyl substituents on phthalazine **4** simplified into methyl groups (Figure 4.2B). The optimized transition state and product structures for the nucleophilic addition of phthalazine **11** to aryne is shown in Figure 4.2C, with a Gibbs free energy of activation of 9.4 kcal/mol.[9] A very small C–N–C–C dihedral angle of approach (0.7°) indicate little distortion of planarity in the forming conjugated π system in the transition state. In contrast, the zwitterionic product **I** exhibits a C–N–C–C dihedral angle of 36.0°, indicating compromised planarity of the conjugated π system due to the alkyl substituent on the phthalazine fragment. The reaction is overall slightly

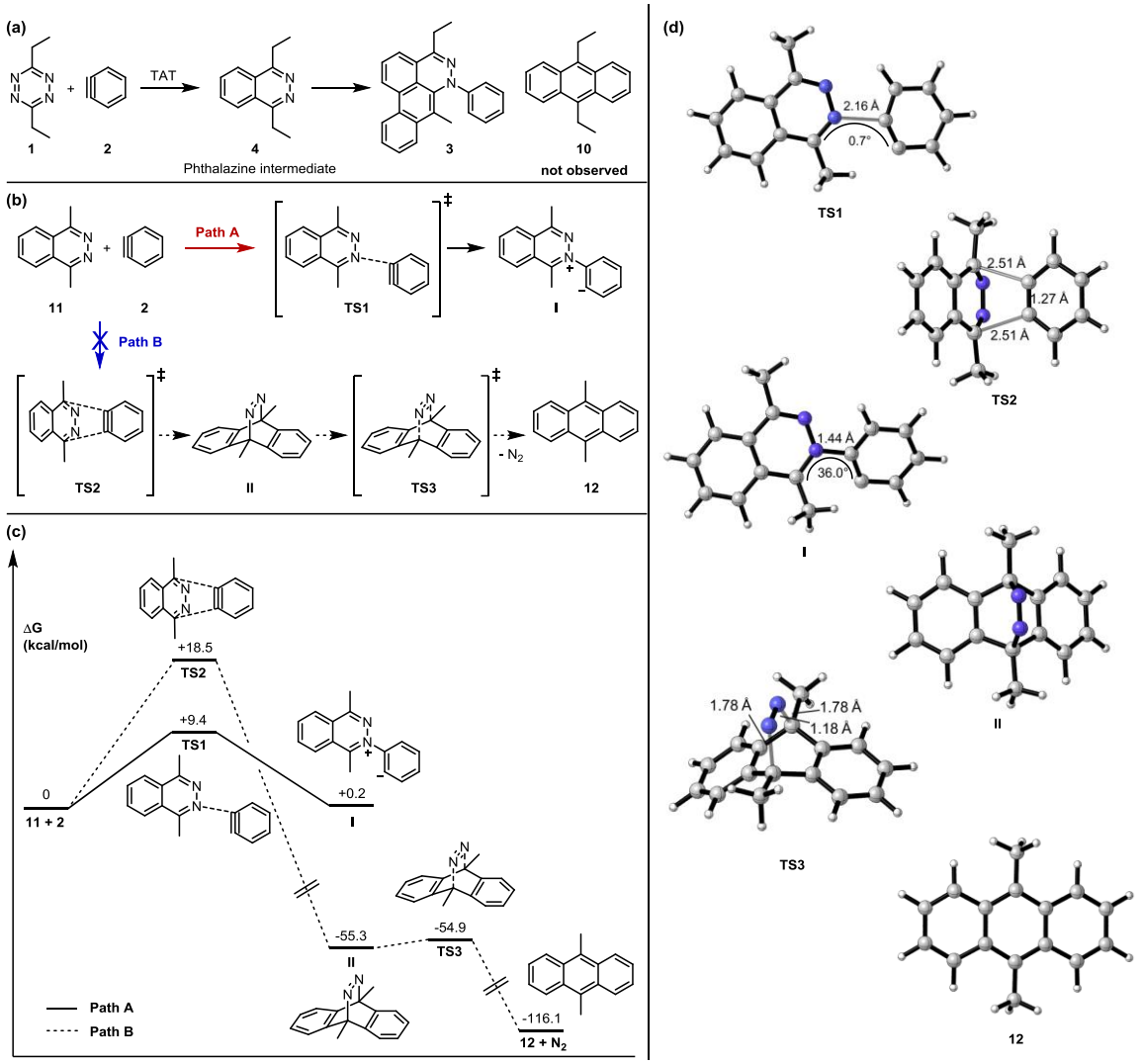

Figure 4.2. Two Possible Reaction Pathways. (a) The reported TAT reaction and isolated phthalazine intermediate **4**. (b) Nucleophilic addition reaction vs. Diels-Alder reaction. (c) Transition states and product structures for the nucleophilic addition and Diels-Alder/retro-Diels-Alder reaction pathway (B3LYP/6-31G(d)//B3LYP/6-311+G(d,p)/CPCM (CH_2Cl_2)). The Gibbs free energies of activation (ΔG‡) are reported in kcal/mol. (d) Optimized geometries of intermediates and transition states in the pathway 1 and 2.

endergonic. The Diels-Alder reaction between phthalazine **11** and aryne was calculated to have a Gibbs free energy of activation of 18.5 kcal/mol (**TS2**), 9.1 kcal/mol higher than the nucleophilic addition pathway (**TS1**). Although the Diels-Alder reaction is overall strongly exergonic, the significantly higher kinetic activation barrier renders it unfavorable compared to the nucleophilic addition pathway. Structures and energies were also calculated for the possible retro-Diels Alder reaction of adduct **II**. The retro-Diels Alder reaction was found to have a low activation barrier (0.4 kcal/mol, **TS3**), indicating facile extrusion of dinitrogen to give the dimethylanthracene **12**.[11]

The standard TAT reaction is conducted with **1**, tetrabutylammonium fluoride (TBAF) in THF, and benzyne precursor **13** in CH_2Cl_2 at 24 °C, to produce product **3** within 5 minutes. The intermediate **4** is isolable from the TAT reaction when conducted with an excess of tetrazine **1**. The reaction between **13** and intermediate **4** under standard TAT reaction conditions afforded the desired product **3** in 7% yield. Here, using anhydrous CsF instead of TBAF, which has a low concentration of water and is considered a wet fluoride source, we conducted the reaction in CH_3CN under reflux. Higher conversion and higher yield of the dibenzo[*de,g*]cinnoline **3** was observed (Figure 4.3A). To discriminate between an intra- versus intermolecular proton transfer pathway, the reaction was performed in CD_3CN and D_2O under reflux (Figure 4.3B). Only deuterated dibenzo[*de,g*]cinnoline [D]-**3** was isolated (11% yield), as analyzed by ^1H NMR. The result indicates that intermediate **III** most likely did not proceed through an intramolecular pathway but instead through an intermolecular proton transfer pathway, assisted by a fluoride, a hydroxide, conjugate base of CH_3CN, or a phenyl anion of another benzyne adduct. To further probe solvent participation in the proton transfer step,

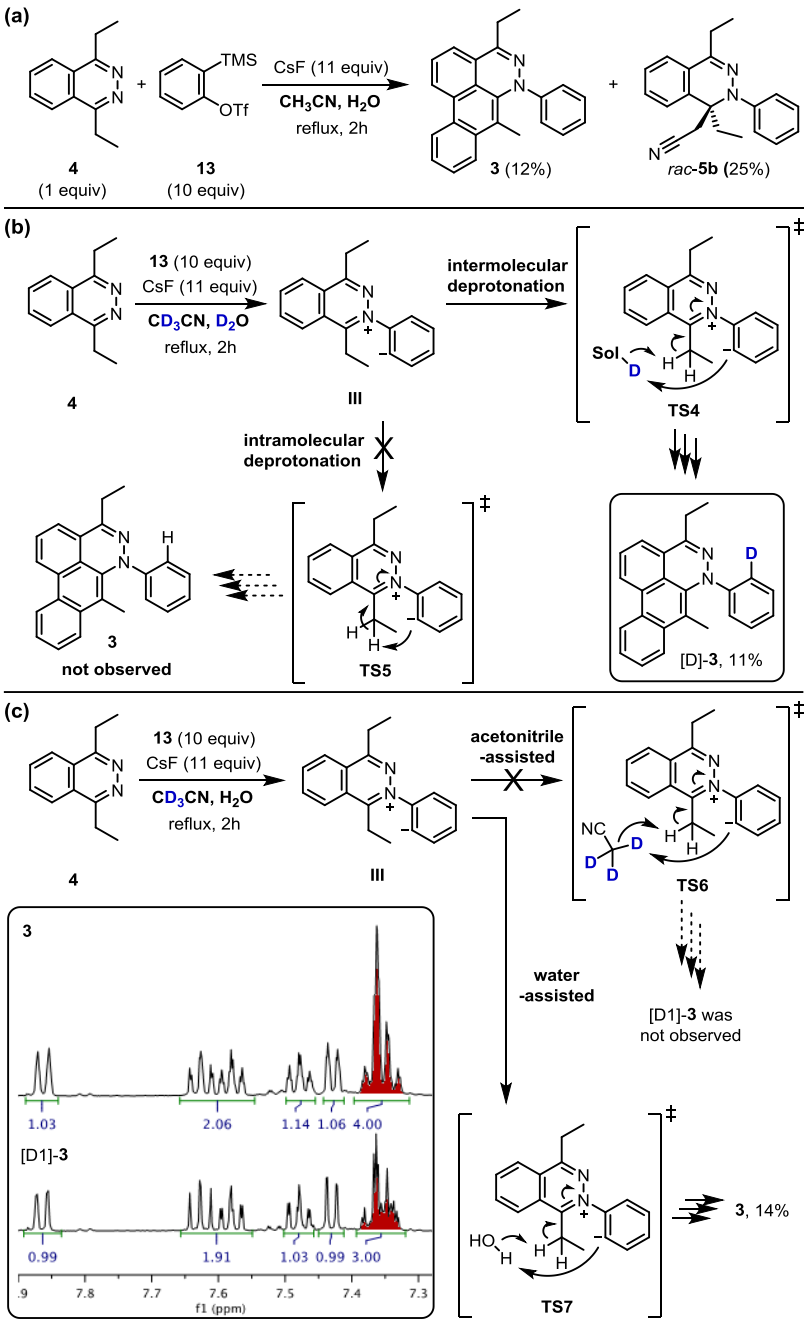

Figure 4.3. Crossover experiment to determine intra-, acetonitrile-assisted inter-, or water-assisted intermolecular proton transfer. (a) The reaction was conducted in the mixture of 1:1 ratio of CH_3CN/H_2O. (b) The mixture of 1:1 ratio of CD_3CN/D_2O. (c) The mixture of 1:1 ratio of CD_3CN/H_2O. (d) Importance of water in the previous crossover experiment.[3]

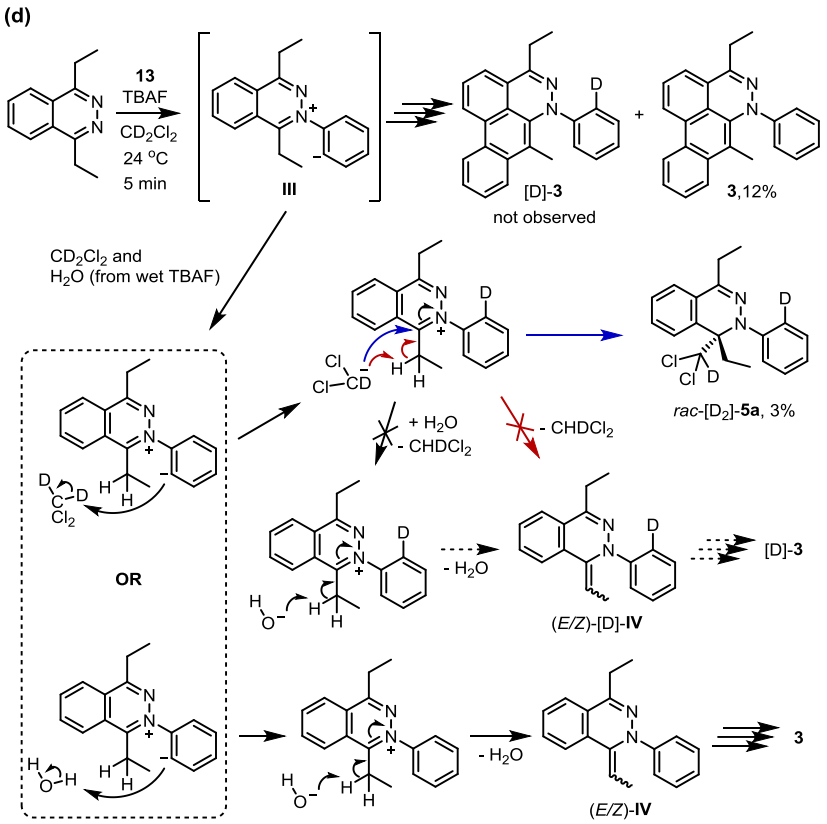

Figure 4.3. Continued.

experiments were conducted in CD_3CN and H_2O (Figure 4.3C). According to the result shown in Figure 4.3B, the intramolecular pathway is unlikely to be favored. Two possibilities arise for the intermolecular pathway, a water-mediated or CH_3CN-mediated proton transfer, assuming H_2O can only serve as the proton source and CD_3CN can only provide deuterium during the proton transfer step. After this reaction, only non-deuterated **3** was observed in 14% yield, which ruled out proton transfer with the conjugate base of CH_3CN, supporting a water-mediated proton transfer pathway. These results account for why only **3** and *rac*-[D_2]-**5a** were found and [D]-**3** was not observed in our previous crossover experiments performed in CD_2Cl_2 (Figure

4.3D).[3] When it comes to the stepwise mechanism in Figure 4.3D, after deuterium transfer from CD_2Cl_2 to the intermediate **III**, the deuterated cationic intermediate is formed. According to the isolation of **3** and *rac*-[D_2]-**5a,** the cationic intermediate may only react with dichloromethanide-*d* via 1,2-addition to provide *rac*-[D_2]-**5a.** but may not undergo further deprotonation assisted by either dichloromethanide-*d* or hydroxide to afford (*E/Z*)-[D]-**IV** because [D]-**3** was not detected. A plausible pathway to account for formation of **3** may involve a water-mediated proton transfer to give (*E/Z*)-**IV**. As shown above, water is an important proton source for the TAT reaction, and this result is consistent with the observation that no desired product from the TAT reaction is observed with anhydrous tetrabutylammonium difluorotriphenylsilicate (TBAT).[1]

The transition state structure (**TS8**) for a concerted water-assisted proton transfer is shown in Figure 4.4. The negative Gibbs free energy of activation indicates strongly favorable interactions between the water molecule and the zwitterionic substrate **I** to yield intermediate **14**. The transition state for the direct intramolecular transfer of proton could not be located. It is possible that due to the requirement that the σ C–H bond being broken must be in plane with the π system of the N=C bond, only a hydrogen abstraction from the top or bottom face of the molecule would have been favorable. Due to the geometrical constraints of the molecule, such a top- or bottom-face hydrogen abstraction by the anionic carbon is geometrically precluded.

To isolate non-isolable alkylidene intermediate, another starting material, 3-methyl-6-phenyl-1,2,4,5-tetrazine (**15**), was employed (Figure 4.5, middle). A phenyl group on 6-position was supposed to stabilize a tetrazine ring and a methyl group on 3-position was expected to afford a single methylidene intermediate **16** while 3,6-diethyltetrazine (**1**) may afford (*E/Z*)-**IV**

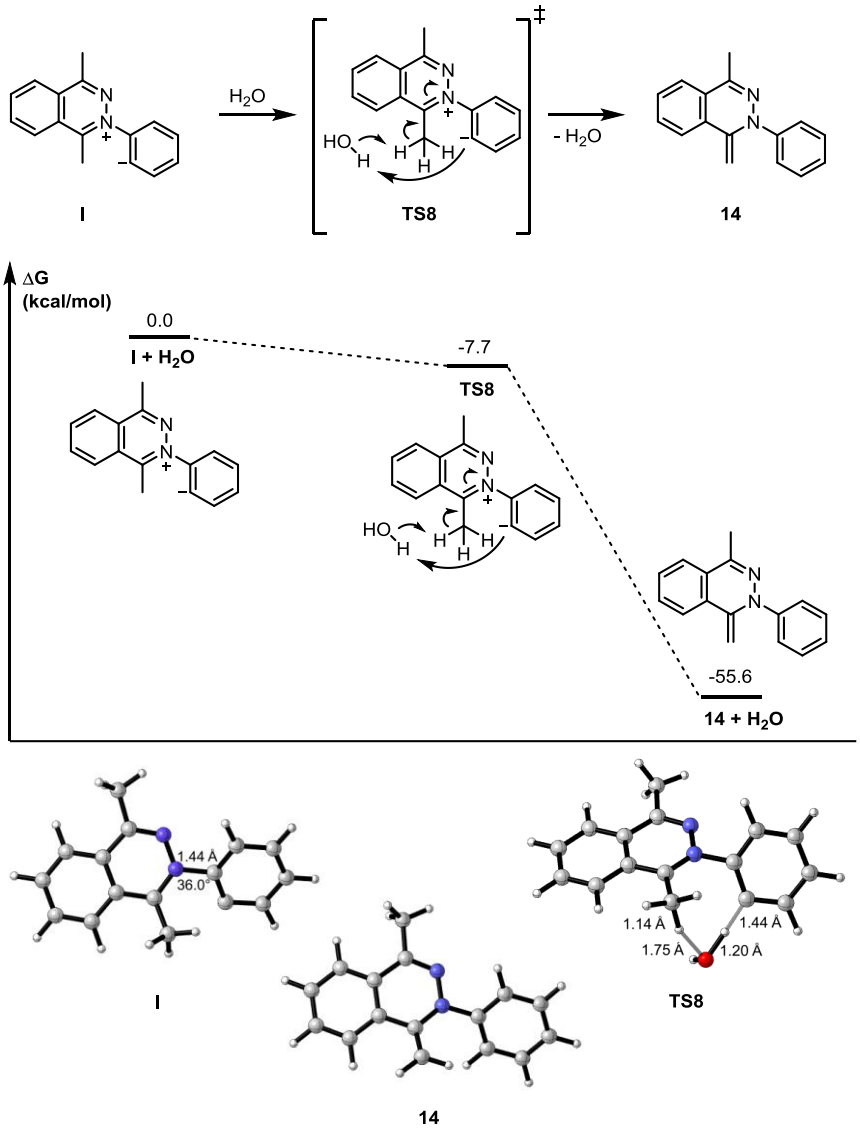

Figure 4.4. Optimized geometries of intermediates, product, and transition states for water-assisted proton transfer pathway (B3LYP/6-31G(d)//B3LYP/6-311+G(d,p)/CPCM (CH_2Cl_2)). The Gibbs free energies of activation (ΔG‡) are reported in kcal/mol.

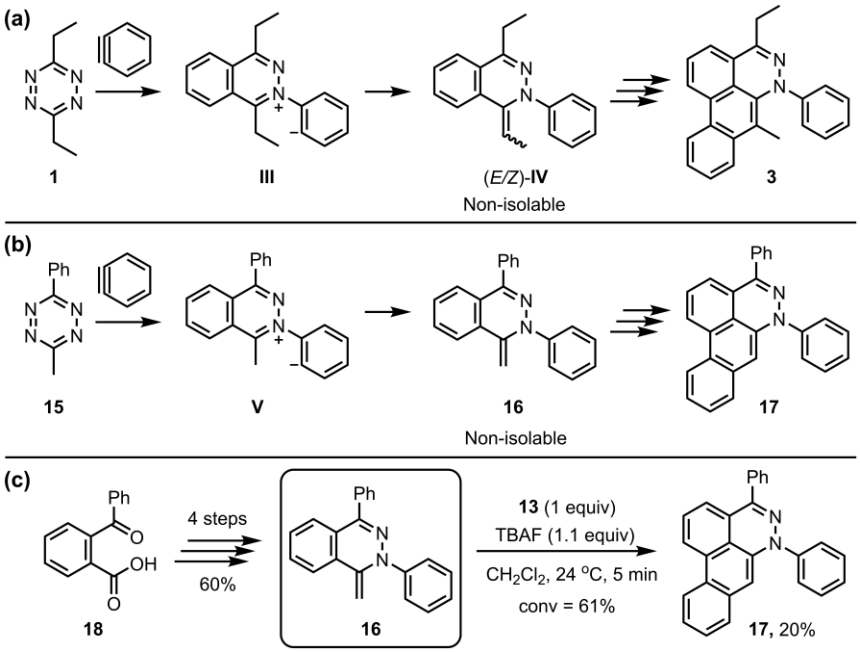

Figure 4.5. Alternative probe **16** to non-isolable intermediate (*E*/*Z*)-**IV** of the TAT reaction.

as two isomers (Figure 4.5, top). However, the aryne reaction of newly employed tetrazine **15** also didn't stop at the intermediate **16** but afforded the dibenzo[*de,g*]cinnoline **17**. Even if **16** was not isolated, we synthesized **16** through another synthetic route (Figure 4.5, bottom).[12] TBAF (1.1 equiv) was subjected to a solution containing **16** (1.0 equiv) and **13** (1.0 equiv) in CH_2Cl_2, which afforded the desired product **17** in 20% yield. This result supports the notion that a methylidene intermediate, such as **16** or (*E*/*Z*)-**IV**, might be a key intermediate in the third benzyne addition step of the TAT reaction.

Interestingly, the reaction between **4** and **13** with CsF in THF at 60 °C for 2 hours followed by treatment with saturated brine solution afforded the trapped intermediate **6** in 9% yield (Figure 4.6A). There are two possibilities that would lead to the formation of **6**. One possibility is that the intermediate **III** is simply quenched by an environmental proton source

such as solvent. The other possibility is that the intermediate **III** deprotonates itself through an intermolecular process to yield a neutral intermediate (*E/Z*)-**IV**, followed by tautomerization to hydrazonium salt **6**. The intermolecular pathway was ruled out in Figure 4.3B. Under the same reaction conditions as those employed in Figure 4.6A, the [2+2] cycloaddition product *rac*-**7** was observed as a mixture of inseparable diastereomers in 7% yield.[13] The relatively smaller amounts of the [2+2] cycloaddition product compared to [4+2] product **3** indicate that the [4+2] mode is experimentally more favorable than the [2+2] mode. Calculations support the idea that intermediate **14** can react with another equivalent of benzyne in either a formal [2+2] or [4+2] cucloaddition to give **VII** and **VIII**, respectively (Figure 4.6B). We located the common diradical intermediate **VI** expected on stepwise pathways of both the formal [2+2] and [4+2] cycloadditions between **14** and benzyne, with a free energy of -14.8 kcal/mol. Transition states for concerted [2+2] or [4+2] cycloadditions were not found for this system.

During the analysis of the standard TAT reaction in Scheme 4.1, 8% of *rac*-**8** was isolated and characterized by HMBC NMR experiments, and its relative stereochemistry was determined by NOESY NMR experiments (Figure 4.7). We propose two possible mechanisms for the synthesis of *rac*-**8** consisting of a concerted ene-reaction or stepwise ene-type reaction of *rac*-**IX**.[14] In both mechanisms, the two possible pathways support the existence of a currently non-isolable intermediate *rac*-**IX**.

Further observation of the rearranged intermediate *rac*-**9a** indirectly supports that the intermediate rac-**IX** is in the course of the TAT reaction. The structure of *rac*-**9a** was characterized by ^{1}H NMR and HRMS spectroscopy. The J coupling constant of two vicinal

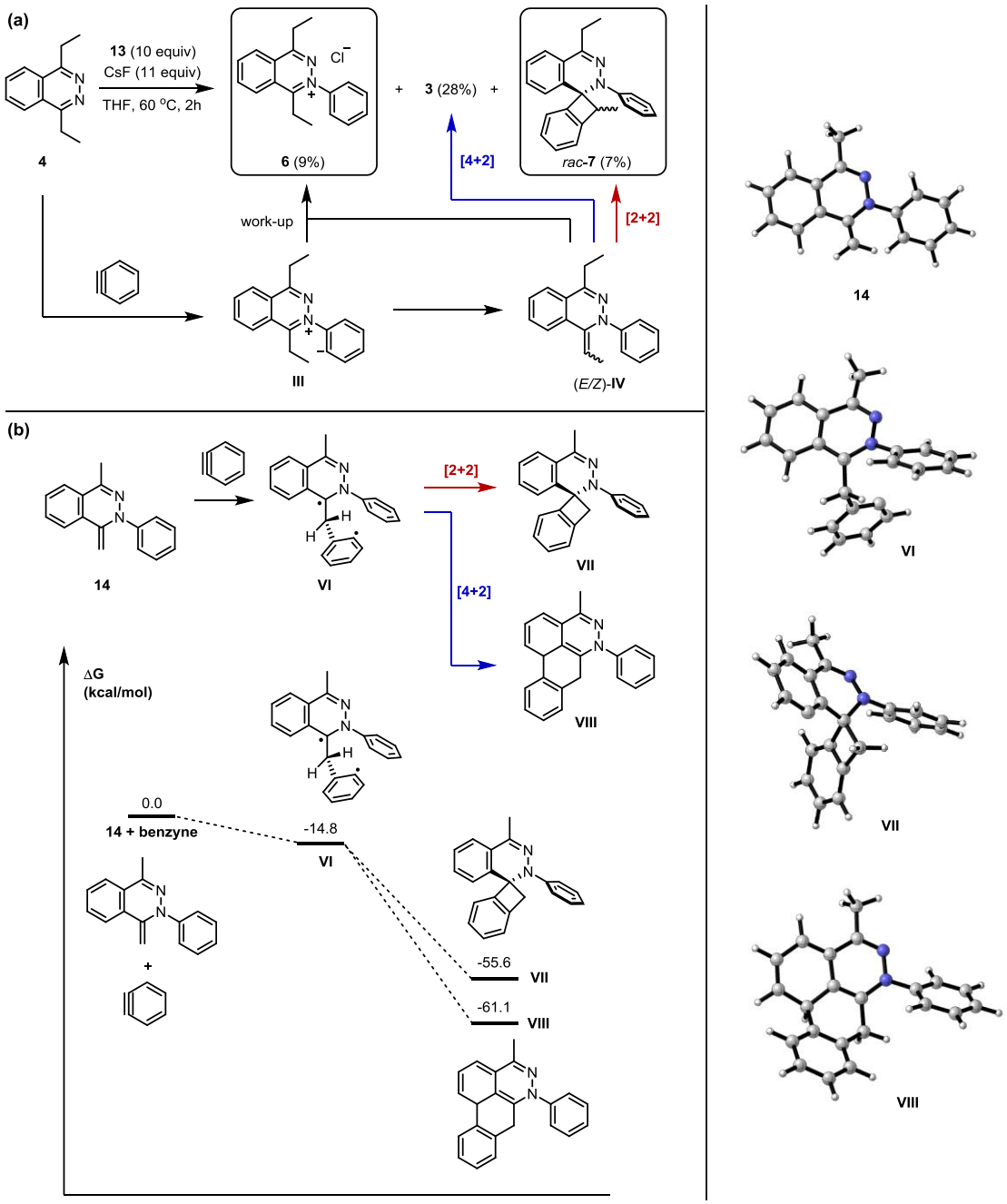

Figure 4.6. (a) Trapped intermediate salt **6** and competitive cycloaddition between [2+2] and [4+2]. (b) Optimized geometries of intermediates and product structures for [2+2] and [4+2] cycloaddition reaction pathways (B3LYP/6-31G(d)//B3LYP/6-311+G(d,p)/CPCM (CH_2Cl_2)). The Gibbs free energies of activation (ΔG‡) are reported in kcal/mol.

protons (J_A) was determined to be 5.5 Hz (Figure 4.8). Based on the results from the HF/6-31G (d) calculations, cis isomer *rac*-**9a** possessed 64 degree dihedral angles and a J coupling of 4.8 Hz between the two vicinal protons. This coupling constant differed from that observed for J_A by 0.7 Hz. Larger dihedral angles of 160 degrees for the trans isomer (*rac*-**9b**) resulted in a J_C of 12.9 Hz, which is quite different from the observed value.

Scheme 4.1. Ene or Stepwise Ene-Type Reaction and Rearrangement of the Intermediate *rac*-IX.

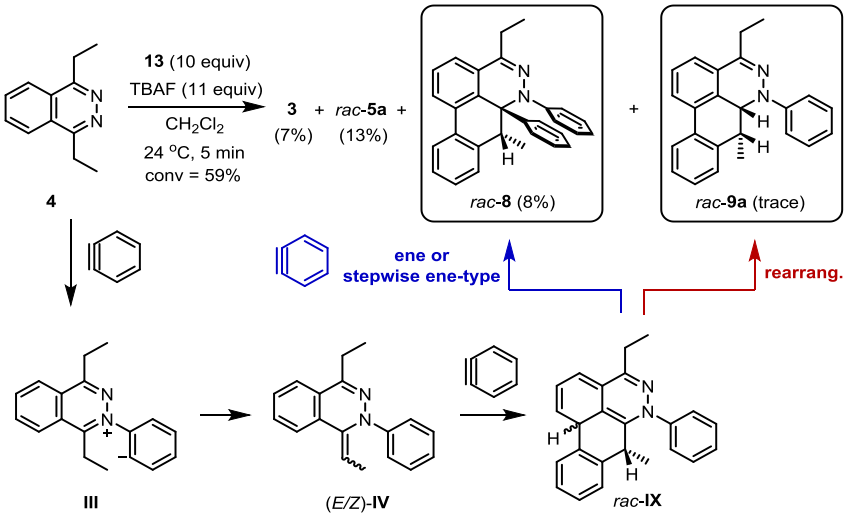

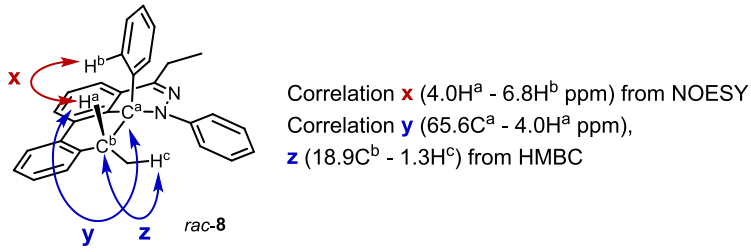

Figure 4.7. Representative NMR correlation assignments of *rac*-**8**.

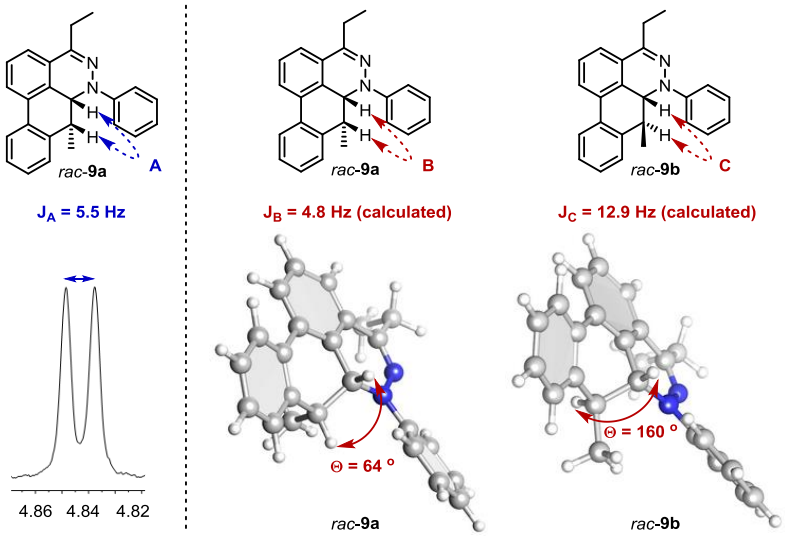

Figure 4.8. Determination of stereochemistry of *rac*-**9a**. J coupling constant of A from ^{1}H NMR spectrum (left) and calculated J coupling constant and degree between two protons on cis intermediate *rac*-**9a** and trans intermediate *rac*-**9b** (right).

4.3 Conclusions

Herein, we provide the first mechanistic insight into the reactivity between a tetrazine and arynes. During the course of the reaction, three aryne addition steps occur consecutively with each step displaying a distinct reactivity mode with benzyne. By isolating and trapping the key intermediates, each of these distinct aryne reactivity modes as well as alternative side product pathways were elucidated. DFT calculations of transition states of two competitive reactions, further [4+2] cycloaddition and nucleophilic addition, support the assertion that [4+2] cycloaddition has higher activation energy barrier, thus, the formation of anthracene is supposed to be unfavorable. The computational and experimental study for three plausible

proton transfer pathways were performed. This anaylsis showed that the water-assisted proton transfer is most favorable fashion. The dibenzocinnoline **17** was observed during the reaction of an alternative intermediate **16** with an aryne via [4+2] cycloaddition. The intermediate **III** undergoes further formal [2+2] and [4+2] cycloaddition, with both the [2+2] cycloaddition product *rac*-**7** and the [4+2] product **3** being observed. In addition, the plausibility of non-isolable intermediates *rac*-**IX** was confirmed by the isolation and characterization of the ene or the stepwise ene-type product *rac*-**8** and rearranged product *rac*-**9a**. The observed intermediates and byproducts are consistent with the overall proposed mechanism for the TAT reaction. We anticipate that the study of arynes-tetrazine-engaged reactivity modes will serve as guidance for future explorations of aryne chemistry, and especially in the context of intermolecular multiple consecutive aryne addition reactions.

4.4 Experimental Section

General information

All commercial reagents and solvents were used as received. Flash column chromatography was performed using Silicycle silica gel (55–65 Å pore diameter). Thin-layer chromatography was performed on Sorbent Technologies silica plates (250 μm thickness). Proton nuclear magnetic resonance spectroscopy (^{1}H NMR) and Carbon nuclear magnetic resonance spectroscopy (^{13}C NMR) spectra were recorded on a Bruker DMX 500 ^{1}H NMR. High-resolution mass spectra were obtained by Dr. Rakesh Kohli at the University of

Pennsylvania's Mass Spectrometry Service Center on a on a Waters LC-TOF mass spectrometer (model LCT-XE Premier) using electrospray ionization. X-ray diffraction data obtained and solved by Dr. Patrick Carroll at the University of Pennsylvania. High performance liquid chromatography analysis was performed using a Jasco HPLC instrument equipped with a Phenomenex column (Luna 5u C18(2) 100A; 250 × 4.60 mm, 5 μm).

Computational methods

For **2**, **11**, **12**, **14**, **I**, **II**, **VI**, **VII**, **VIII**, **TS1**, **TS2**, **TS3**, and **TS8**, all quantum chemical calculations were performed with Gaussian 09.[12] Geometry optimizations and frequencies were calculated with the B3LYP density functional with the 6-31G(d) basis set in conjunction with the CPCM implicit solvation model. Optimized geometries were verified by frequency calculations as minima (zero imaginary frequencies) or transition structures (a single imaginary frequency). Structure graphics were generated using CYLView.[13]

For *rac*-**9a** and *rac*-**9b**, all calculations were performed using Gaussian 09.[12] All local minima were optimized in the gas phase using Hartree-Fock methods with the 6-31G(d) basis set; calculation of total nuclear spin-spin coupling J (Hz) constant values were performed with the same basis set. Post processing was performed using UCSF Chimera.[14]

Experimental procedures

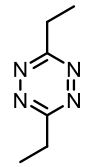

1

3,6-diethyl-1,2,4,5-tetrazine (1): Synthetic method and characterization data of **1** have been reported in our previous publication.[1]

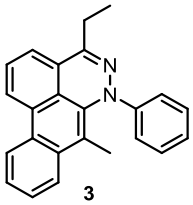

3

4-ethyl-7-methyl-6-phenyl-6H-dibenzo[de,g]cinnoline (3): Synthetic method and characterization data of **3** have been reported in our previous publication.[1]

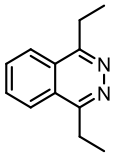

4

1,4-diethylphthalazine (4): Synthetic method and characterization data of **4** have been reported in our previous publication.[3]

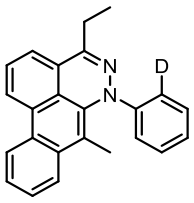

[D]-**3**

4-ethyl-7-methyl-6-(phenyl-2-*d*)-6*H*-dibenzo[*de,g*]cinnoline ([D]-3): A 10 mL round-bottom flask was charged with 43 μmol of phthalazine **4** (8.0 mg), 430 μmol of 2-(trimethylsilyl)phenyl trifluoromethanesulfonate **13** (128 mg), 470 μmol of anhydrous CsF (72 mg) in 40 μL of CD_3CN and 40 μL of D_2O and was heated under reflux. After 2 hours, the solution was cooled down, concentrated in vacuo and purified by flash column chromatography (ethyl acetate/hexane 1:30) to afford [D]-**3** (1.6 mg).

Isolated Yield: 11 %.

Physical Property: Yellow solid, m.p. = 59-60 °C.

TLC: R_f = 0.81 (silica gel, ethyl acetate/hexanes 1:4).

^{1}H NMR (500 MHz, CD_2Cl_2) δ 8.53-8.49 (m, 2H), 7.86 (dd, 1H, J = 8.2, 1.3 Hz), 7.63 (dd, 1H, J = 8.2, 7.4 Hz), 7.58 (ddd, 1H, J = 8.2, 6.9 1.3 Hz), 7.48 (ddd, 1H, J = 8.2, 6.9, 1.3 Hz), 7.43 (dd, 1H, J = 7.4, 1.0 Hz), 7.39-7.33 (m, 3H), 7.12-7.07 (m, 1H), 2.82 (q, 2H, J = 7.3 Hz), 2.00 (s, 3H), 1.36 (t, 3H, J = 7.3 Hz)

HRMS (ESI) calculated for $C_{24}H_{19}DN_2^+$ $[M]^+$ 337.1684, found 337.1689.

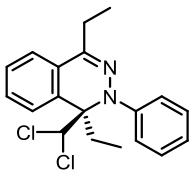

rac-**5a**

(*R*)- and (*S*)-1-(dichloromethyl)-1,4-diethyl-2-phenyl-1,2-dihydrophthalazine (*rac*-5a): Synthetic method and characterization data of *rac*-**5a** have been reported in our previous publication.[3]

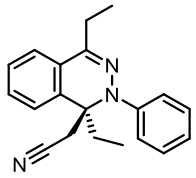

rac-**5b**

(*R*)- and (*S*)-2-(1,4-diethyl-2-phenyl-1,2-dihydrophthalazin-1-yl)acetonitrile (*rac*-5b): Synthetic method and characterization data of *rac*-**5b** have been reported in our previous publication.[3]

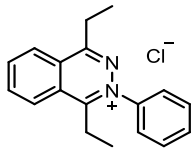

6

1,4-diethyl-2-phenylphthalazin-2-ium chloride (6): A 4 mL vial was charged with 48 μmol of 1,4-diethylphthalazine **4** (9.0 mg), 480 μmol of 2-(trimethylsilyl)phenyl trifluoromethanesulfonate **13** (144 mg), 530 μmol of anhydrous CsF (81 mg) in 0.05 mL of THF was heated to 60 °C. After 2 hours, the solution was cooled down, concentrated in vacuo and purified by reversed phase column chromatography using water containing 0.1% trifluoroacetic acid. Trifluoroacetate ion was replaced with chloride ion by the addition of a drop of brine to the resulting solid followed by co-evaporation under high-vacuum condition. The

solid was filtered with HPLC grade dichloromethane and the filtrate was dried in vacuo for 12 hours to afford **6** (1.3 mg).

Isolated Yield: 9 %.

Physical Property: Colorless semi-solid.

^{1}H NMR (500 MHz, CD_2Cl_2)

δ 8.74 (d, 1H, J = 8.3 Hz), 8.55 (d, 1H, J = 8.3 Hz), 8.48 (ddd, 1H, J = 8.3, 7.2, 1.1 Hz), 8.40 (ddd, 1H, J = 8.3, 7.2, 1.1 Hz), 7.80-7.72 (m, 3H), 7.68-7.63 (m, 2H), 3.56-3.48 (m, 4H), 1.50 (t, 3H, J = 7.4 Hz), 1.45 (t, 3H, J = 7.7 Hz).

^{13}C NMR (125 MHz, CD_2Cl_2)

δ 165.7, 164.6, 142.6, 139.1, 136.0, 131.5, 130.3, 129.3, 127.5, 127.2, 126.4, 125.1, 26.3, 25.1, 14.1, 11.5.

IR (neat): 2917, 2849, 1265, 1154, 1031, 638 cm^{-1}.

HRMS (ESI) calculated for $C_{18}H_{19}N_2^+$ [M] 263.1543, found 263.1544.

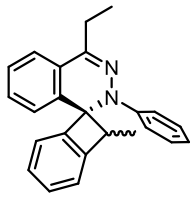

rac-**7**

(7R,8R)-, (7S,8S)-, (7R,8S)-, and (7S,8R)-4'-ethyl-8-methyl-2'-phenyl-2'H-spiro[bicyclo[4.2.0]octane-7,1'-phthalazine]-1(6),2,4-triene (*rac*-7): A 4 mL vial was charged with 48 μmol of 1,4-diethylphthalazine **4** (9.0 mg), 480 μmol of 2-(trimethylsilyl)phenyl trifluoromethanesulfonate **13** (144 mg), 530 μmol of anhydrous CsF (81 mg) in 50 μL of THF was heated to 60 °C. After 2 hours, the solution was cooled down, concentrated in vacuo and

purified by reversed phase column chromatography using water containing 0.1% trifluoroacetic acid to afford 1.1 mg of *rac*-**7**.

Isolated Yield: 7 % (overall).

Physical Property: White solid.

TLC: R_f = 0.30 (silica gel, ethyl acetate/hexanes 1:4).

^{1}H NMR (500 MHz, $CDCl_3$)

δ 7.71-7.67 (m, Major 1H), 7.44-6.96 (m, 10H Major, 11H Minor), 6.84 (td, Major 1H, J = 7.4, 0.9 Hz), 6.82 (td, Minor 1H, J = 7.4, 0.9 Hz), 6.66 (d, Minor 1H, J = 7.8 Hz), 6.54 (d, Major 1H, J = 7.8 Hz), 3.87 (q, Major 1H, J = 7.0 Hz), 3.53 (q, Minor 1H, J = 7.3 Hz), 2.82-2.62 (m, 2H Major, 2H Minor), 1.30 (t, 3H Minor, J = 7.4 Hz), 1.24 (t, 3H Major, J = 7.4 Hz), 1.05 (d, 3H Minor, J = 7.3 Hz), 0.94 (d, 3H Major, J = 7.0 Hz).

IR (neat): 2963, 2921, 2851, 1723, 1596, 1495, 1477, 1459, 1093, 1070, 1044, 800, 743, 699 cm^{-1}.

HRMS (ESI) calculated for $C_{24}H_{23}N_2^+$ $[M+H]^+$ 339.1856, found 339.1864.

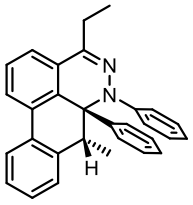

rac-**8**

(6a*S*,7*R*)- and (6a*R*,7*S*)-4-ethyl-7-methyl-6,6a-diphenyl-6a,7-dihydro-6*H*-dibenzo[*de,g*]cinnoline (*rac*-8): A 4 mL vial was charged with 48 μmol of 1,4-diethylphthalazine **4** (9.0 mg), 0.483 mmol of 2-(trimethylsilyl)phenyl trifluoromethanesulfonate **5**13(144 mg) in 50 μL of dichloromethane at 24 °C, 1.0 M TBAF in THF (530 μmol, 530 μL) was slowly added

to the solution over the course of 5 min. After the addition, the solution was concentrated in vacuo, and filtered on the silica gel, and purified by flash column chromatography (ethyl acetate/hexanes 1:20) to afford *rac*-**8** (1.6 mg).

Isolated Yield: 8 %.

Physical Property: Colorless oil.

TLC: R_f = 0.62 (silica gel, ethyl acetate/hexanes 1:4).

^{1}H NMR (500 MHz, $CDCl_3$)

δ 7.80-7.75 (m, 1H), 7.59-7.56 (m, 1H), 7.52-7.49 (m, 2H), 7.26-7.22 (m, 1H), 7.22-7.15 (m, 4H), 7.14-7.08 (m, 1H), 7.02-6.92 (m, 5H), 6.83-6.79 (m, 2H), 4.01 (q, 1H, J = 6.7 Hz), 2.90-2.68 (m, 2H), 1.48 (t, 3H, J = 6.7 Hz), 1.30 (t, 3H, J = 7.5 Hz).

^{13}C NMR (125 MHz, $CDCl_3$)

δ 147.2, 142.8, 140.9, 140.6, 132.1, 131.8, 130.6, 128.5, 128.2, 128.1, 127.8, 127.6, 127.1, 127.0, 126.9, 126.1, 125.8, 125.3, 124.7, 123.7, 122.4, 65.6, 40.7, 25.7, 18.9, 11.8.

IR (neat): 2963, 2919, 2849, 1259, 1085, 1018, 795, 704 cm^{-1}.

HRMS (ESI) calculated for $C_{30}H_{27}N_2^+$ $[M+H]^+$ 415.2169, found 415.2174.

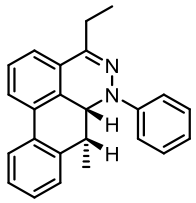

rac-**9a**

(6a*R*,7*R*)- and (6a*S*,7*S*)-4-ethyl-7-methyl-6-phenyl-6a,7-dihydro-6*H*-dibenzo[*de,g*]cinnoline (*rac*-9a): A 4 mL vial was charged with 48 μmol of 1,4-diethylphthalazine **4** (9.0 mg), 480 mmol of 2-(trimethylsilyl)phenyl trifluoromethanesulfonate **13** (144 mg) in 50 μL of dichloromethane

at 24 °C, 1.0 M TBAF in THF (530 μmol, 530 μL) was slowly added to the solution over the course of 5 min. After the addition, the solution was concentrated in vacuo, and filtered on the silica gel, and purified by flash column chromatography (ethyl acetate/hexanes 1:20) to afford *rac*-**9a** (0.1 mg). The extremely low stability and yield precluded the ^{13}C NMR characterization.

Isolated Yield: Less than 1 %.

Physical Property: White semi-solid.

TLC: R_f = 0.56 (silica gel, ethyl acetate/hexanes 1:4).

^{1}H NMR (500 MHz, $CDCl_3$)

δ 7.70 (d, 1H, J = 7.9 Hz), 7.50-7.23 (m, 11H), 4.84 (d, 1H, J = 5.5 Hz), 3.54-3.46 (m, 1H), 2.52-2.41 (m, 2H), 1.35 (d, 3H, J = 7.5 Hz), 0.95 (t, 3H, J = 7.4 Hz).

IR (neat): 2968, 2926, 2854, 1259, 1096, 1026, 800 cm^{-1}.

HRMS (ESI) calculated for $C_{24}H_{23}N_2^+$ $[M+H]^+$ 339.1856, found 339.1865.

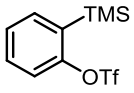

13

2-(trimethylsilyl)phenyl trifluoromethanesulfonate (13): 13 was prepared according to the literature procedure[15] and characterization data of **13** has been reported in our previous publication.[3]

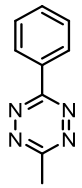

15

3-methyl-6-phenyl-1,2,4,5-tetrazine (15): Synthetic method and characterization data of **15** have been reported in our previous publication.[1]

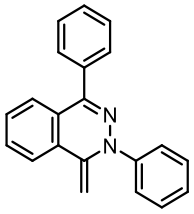

16

1-methylene-2,4-diphenyl-1,2-dihydrophthalazine (16): 3.0 M methylmagnesium bromide solution (0.3 mmol, 0.3 mL) in diethyl ether was slowly added to 0.1 mmol of 2,4-diphenyl-1(2*H*)-phthalazinone[16] (30 mg) in 0.3 mL of benzene at 24 °C. After 10 hours, 1M HCl solution was added.[9] Then, K_2CO_3 was added until the pH of the solution became 7. The organic layer was extracted with dichloromethane and water, was washed with brine solution, and was purified by flash column chromatography (ethyl acetate/hexanes 1:1 to 9:1) to afford **16** (23 mg).

Isolated Yield: 77 %

Physical Property: Green oil.

TLC: R_f = 0.30 (silica gel, ethyl acetate/hexanes 1:4).

^{1}H NMR (500 MHz, $CDCl_3$)

δ 7.77 (d, 1H, J = 7.9 Hz), 7.64-7.58 (m, 4H), 7.54-7.44 (m, 6H), 7.427.37 (m, 2H), 7.31 (t, 1H, J = 7.4 Hz), 4.52 (s, 1H), 4.17 (s, 1H).

^{13}C NMR (125 MHz, $CDCl_3$)

δ 145.3, 144.1, 142.4, 136.1, 131.9, 131.0, 129.3, 129.11, 129.09, 128.4, 128.3, 126.2, 125.8, 125.5, 124.7, 123.9, 81.6.

IR (neat): 2965, 2921, 2848, 1661, 1594, 1492, 1443, 1259, 1096, 1021, 797, 696 cm^{-1}.

HRMS (ESI) calculated for $C_{21}H_{17}N_2^+$ $[M+H]^+$ 297.1386, found 297.1404.

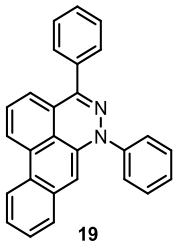

19

4,6-diphenyl-6*H*-dibenzo[*de*,g]cinnoline (19): A vial was charged with 24 μmol of **16** (7.0 mg), 24 μmol of 2-(trimethylsilyl)phenyl trifluoromethanesulfonate **13** (7.2 mg) in 30 μL of dichloromethane at 24°C, and 1.0 M TBAF in THF (26 μmol, 26 μL) was slowly added to the solution over the course of 1 min. After the addition, the solution was concentrated in vacuo and purified by flash column chromatography (ethyl acetate/hexane 1:30) to afford **19** (1.8 mg) in 20% yield. Characterization data of **19** have been reported in our previous publication.[1]

Deuterium Labeling Experiment in Figure 4.**3b** and **3c.**

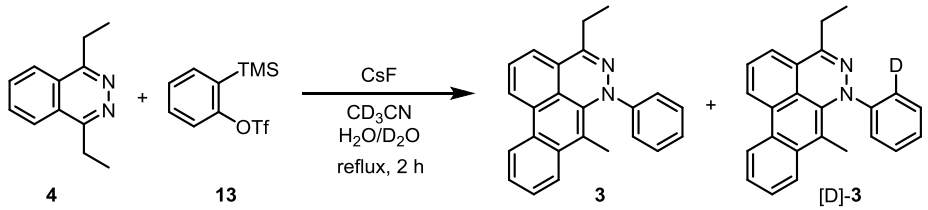

4 **13** **3** [D]-**3**

Each 10 mL round-bottom flask was charged with 43 μmol of phthalazine **4** (8.0 mg), 430 μmol of 2-(trimethylsilyl)phenyl trifluoromethanesulfonate **13** (128 mg), 470 μmol of anhydrous CsF (72 mg) in 40 μL of CD_3CN and 40 μL of D_2O (or 40 μL of CD_3CN and 40 μL of H_2O) and was heated under reflux. After 2 hours, the solution was cooled down, concentrated in vacuo and purified by flash column chromatography (ethyl acetate/hexane 1:30) to afford **3** (or [D]-**3**).

4.5 Acknowledgments

This work was supported by funding from the University of Pennsylvania. Instruments supported by the NSF and NIH including HRMS (NIH RR-023444). We thank Dr. George Furst and Dr. Rakesh Kohli for assistance in obtaining the high resolution NMR and mass spectral data, respectively. We are grateful to Dr. Patrick Carroll for X-ray crystallographic assistance.

4.6 References

(1) Suh, S.-E.; Barros, S. A.; Chenoweth, D. M. *Chem. Sci.* **2015,** *6*, 5128-5132.

(2) Yang, J.; Karver, M. R.; Li, W.; Sahu, S.; Devaraj, N. K. *Angew. Chem., Int. Ed.*, **2012**, *51*, 5222-5225.

(3) Suh, S.-E.; Chenoweth, D. M. *Org. Lett.* **2016,** *18*, 4080-4083.

(4) (a) Gampe, C. M.; Carreira, E. M. *Angew. Chem. Int. Ed.* **2012,** *51*, 3766-3778. (b) Sanz, R. *Org. Prep. Proced. Int.* **2008,** *40*, 215-291. (c) Tadross, P. M.; Stoltz, B. M. *Chem. Rev.* **2012,** *112*, 3550-3577. (d) Wu, C.; Shi, F. *Asian J. Org. Chem.* **2013,** *2*, 116-125. (e) Yoshida, H. *Compr. Org. Synth. (2nd Ed.)* **2014,** *4*, 517-579. (f) Yoshida, S.; Hosoya, T. *Chem. Lett.* **2015,** *44*, 1450-1460. (g) Garcia-Lopez, J. A.; Greaney, M. F. *Chem. Soc. Rev.* **2016,** *45*, 6766-6798.

(5) (a) Dubrovskiy, A. V.; Markina, N. A.; Larock, R. C. *Org. Biomol. Chem.* **2013,** *11*, 191-218. (b) Okuma, K. *Heterocycles* **2012,** *85*, 515-544.

(6) (a) Bhojgude, S. S.; Bhunia, A.; Biju, A. T. *Acc. Chem. Res.* **2016,** *49*, 1658-1670. (b) Bhojgude, S. S.; Biju, A. T. *Angew. Chem. Int. Ed.* **2012,** *51*, 1520-1522. (c) Biju, A.; Bhunia, A. *Synlett* **2014,** *25*, 608-614. (d) Yoshida, H.; Takaki, K. *Heterocycles* **2012,** *85*, 1333-1349.

(7) Sauer, J.; Heinrichs, G. *Tetrahedron Lett.*, **1966**, *7*, 4979–4984.

(8) Seitz, G.; Hoferichter, R.; Mohr, R. *Angew. Chem. Int. Ed.* **1987,** *26*, 332-334.

(9) Ovchinnikova, I. G.; Samartseva, I. V.; Pavlova, E. A. *Zh. Org. Khim.* **1984**, *20*, 2248.

(10) Castedo, L.; Guitian, E.; Saá, C.; Suau, R.; Saá, J. M. *Tetrahedron Lett.* **1983**, *24*, 2107.

(11) Siyang, H. X.; Wu, X. R.; Liu, H. L.; Wu, X. Y.; Liu, P. N. *J. Org. Chem.* **2014**, *79*, 1505.

(12) Frisch, M. J.; Trucks, G. W.; Schlegel, H. B.; Scuseria, G. E.; Robb, M. A.; Cheeseman, J. R.; Scalmani, G.; Barone, V.; Mennucci, B.; Petersson, G. A.; Nakatsuj, H.; Caricato, M.; Li, X.; Hratchian, H. P.; Izmaylov, A. F.; Bloino, J.; Zheng, G.; Sonnenberg, J. L.; Hada, M.; Ehara, M.; Toyota, K.; Fukuda, R.; Hasegawa, J.; Ishida, M.; Nakajima, T.; Honda, Y.; Kitao, O.; Nakai, H.; Vreven, T.; J. A. Montgomery, J.; Peralta, J. E.; Ogliaro, F.; Bearpark, M.; Heyd, J. J.; Brothers, E.; Kudin, K. N.; Staroverov, V. N.; Kobayashi, R.; Normand, J.; Raghavachari, K.; Rendell, A.; Burant, J. C.; Iyengar, S. S.; Tomasi, J.; Cossi, M.; Rega, N.; Millam, J. M.; Klene, M.; Knox, J. E.; Cross, J. B.; Bakken, V.; Adamo, C.; Jaramillo, J.; Gomperts, R.; Stratmann, R. E.; Yazyev, O.; Austin, A. J.; Cammi, R.; Pomelli, C.; Ochterski, J. W.; Martin, R. L.; Morokuma, K.; Zakrzewski, V. G.; Voth, G. A.; Salvador, P.; Dannenberg, J. J.; Dapprich, S.; Daniels, A. D.; Farkas, Ö.; Foresman, J. B.; Ortiz, J. V.; Cioslowski, J.; Fox, D. J. Gaussian 09, Revision B.01.; Gaussian, Inc.: Wallingford, CT, **2009**.

(13) Legault, C.Y.; CYLview, 1.0b, Université de Sherbrooke, 2009 (http://www.cylview.org).

(14) Pettersen, E. F.; Goddard, T. D.; Huang, C. C.; Couch, G. S.; Greenblatt, D. M.; Meng, E. C.; Ferrin, T. E. *J. Comput. Chem.,* **2004**, *25*, 1605.

(15) Shaibu, B. S.; Kawade, R. K.; Liu, R.-S. *Org. Biomol. Chem.* **2012**, *10*, 6834.

(16) Suresh, A. S.; Baburajan, P.; Ahmed, M. *Tetrahedron Lett.* **2014**, *55*, 3482.

Appendix 3

NMR Spectra and Computational Results Relevant to Chapter 4

This work was performed in collaboration with Dr. Kendall N. Houk and Dr. Shuming Chen at the University of California, Los Angeles.

Figure A3.1. ^{1}H NMR spectrum of *rac*-[D_1]-**3b** in CD_2Cl_2 (500 MHz).

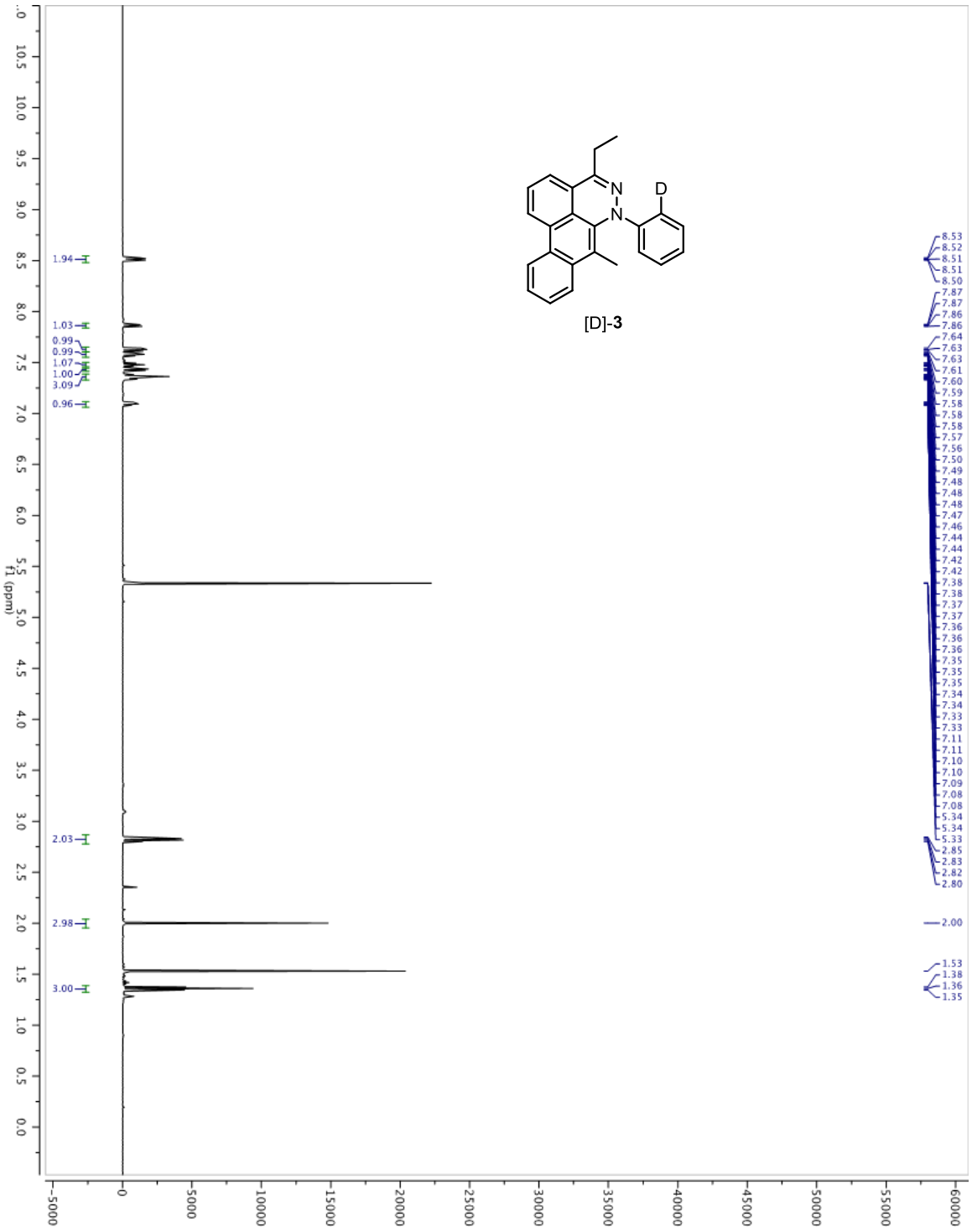

Figure A3.2. ^{1}H NMR spectrum of **6** in CD_2Cl_2 (500 MHz).

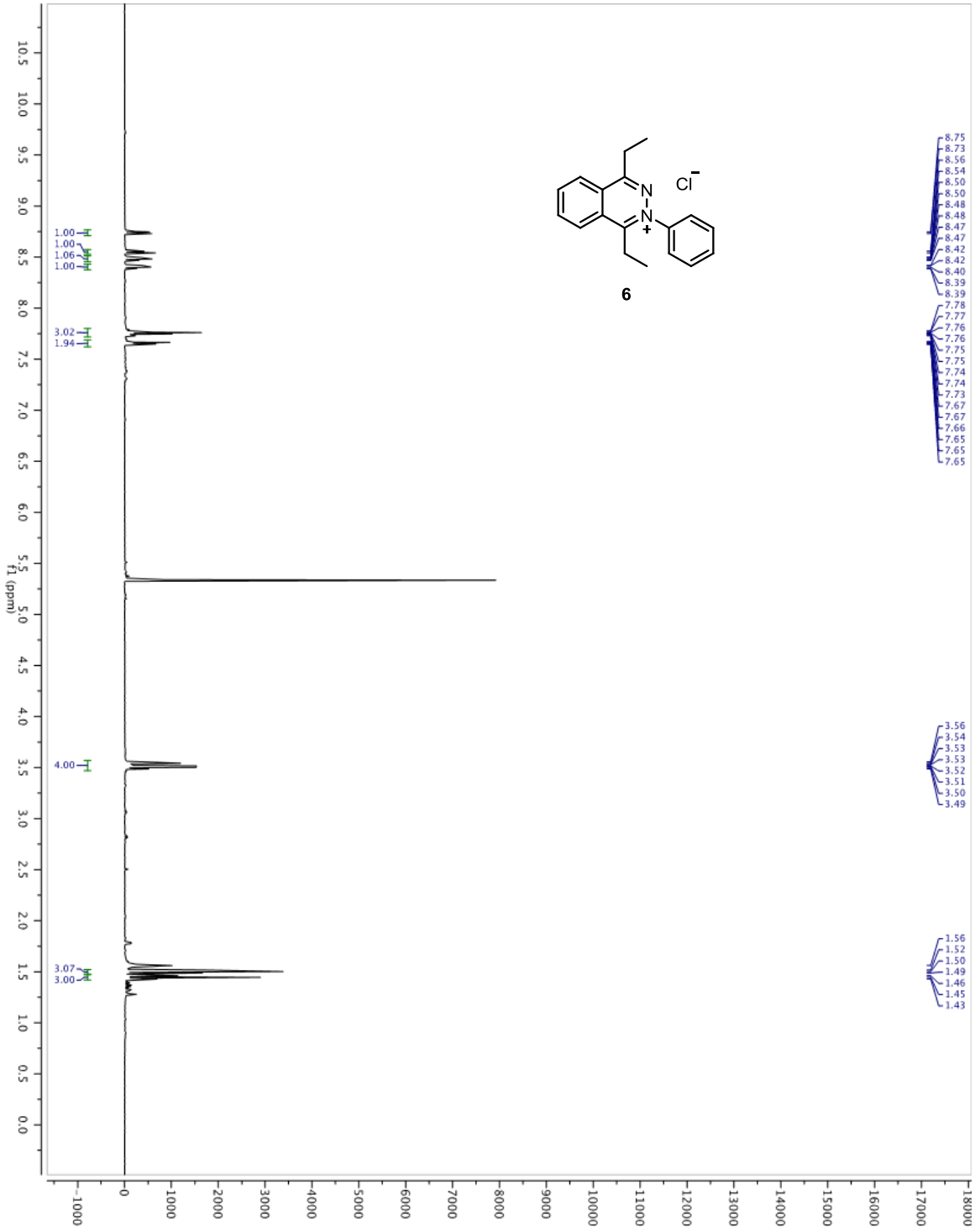

Figure A3.3. ^{13}C NMR spectrum of **6** in CD_2Cl_2 (125 MHz).

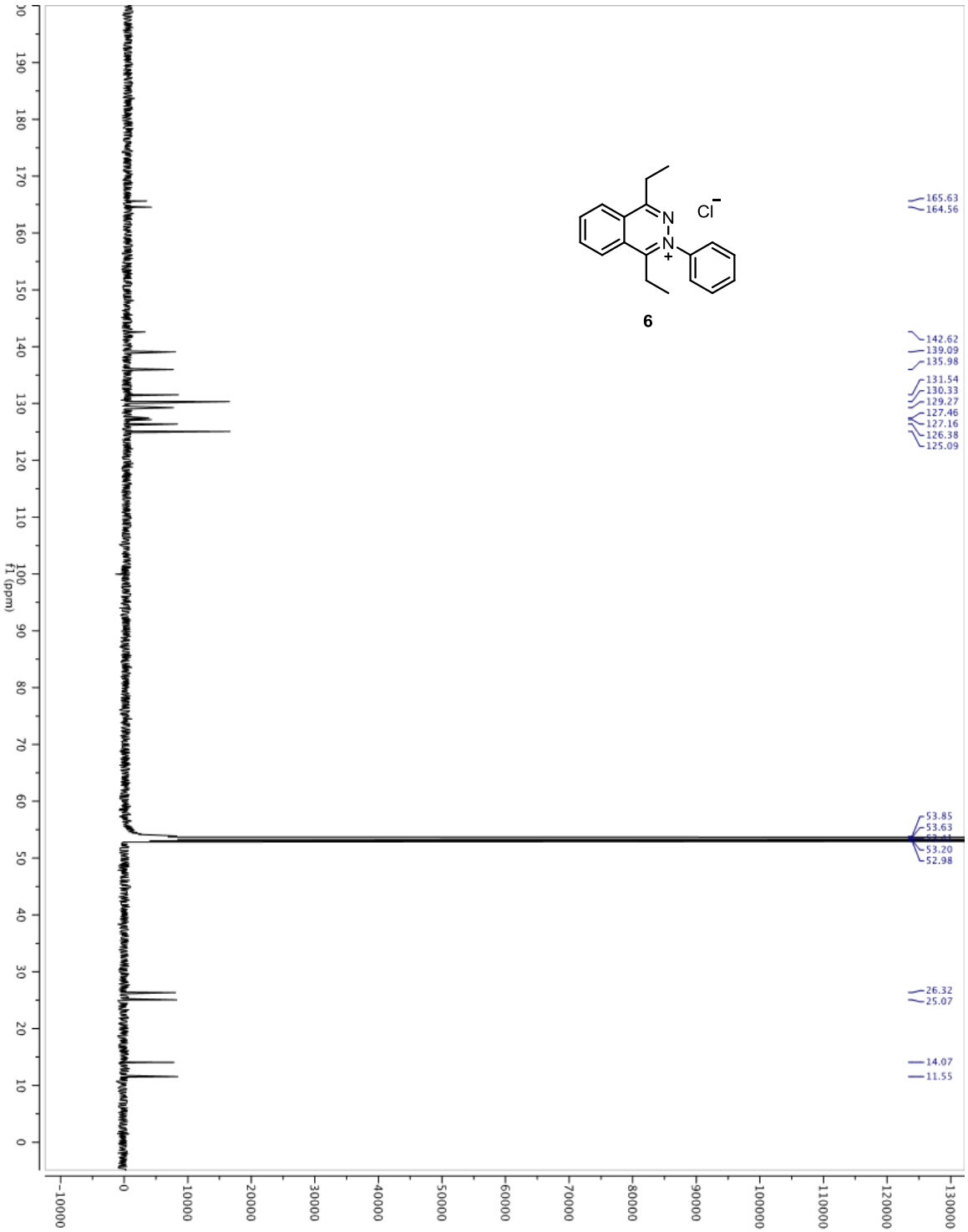

Figure A3.4. ^{1}H NMR spectrum of mixture *rac*-**7** in CD_2Cl_2 (500 MHz).

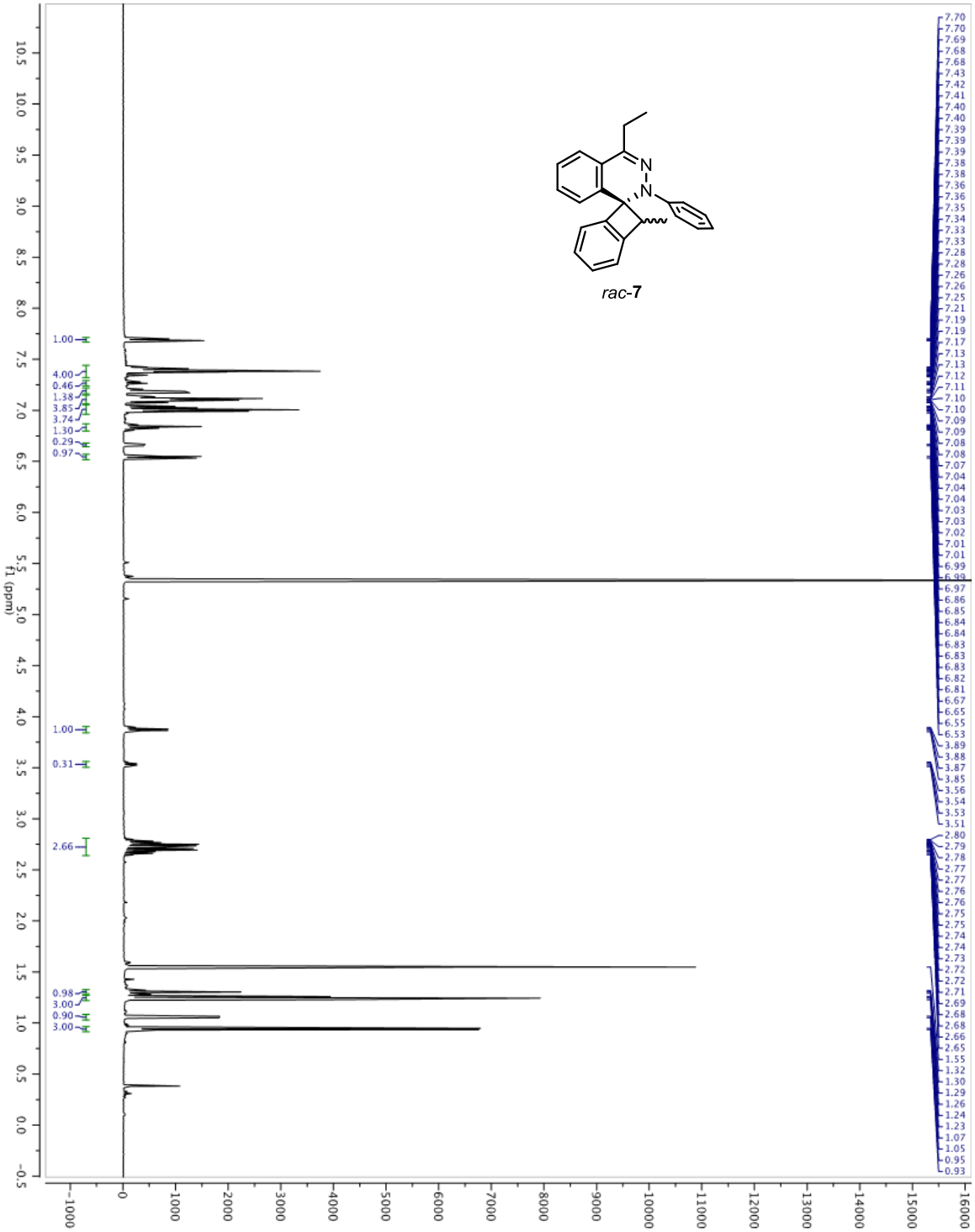

Figure A3.5. 1st expanded ^{1}H NMR spectrum of mixture *rac*-**7** in CD_2Cl_2 (500 MHz).

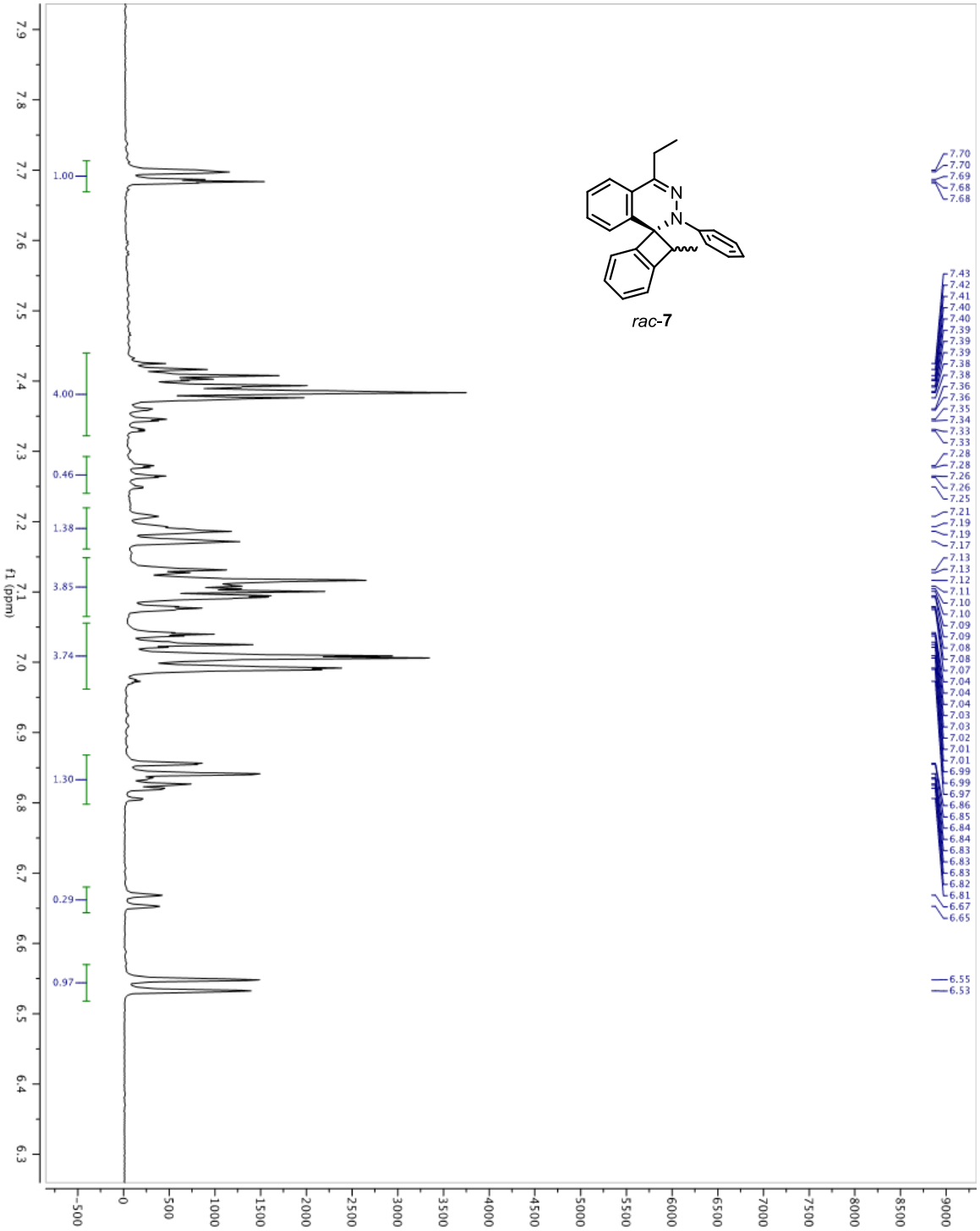

Figure A3.6. 2nd expanded ^{1}H NMR spectrum of mixture *rac*-**7** in CD_2Cl_2 (500 MHz).

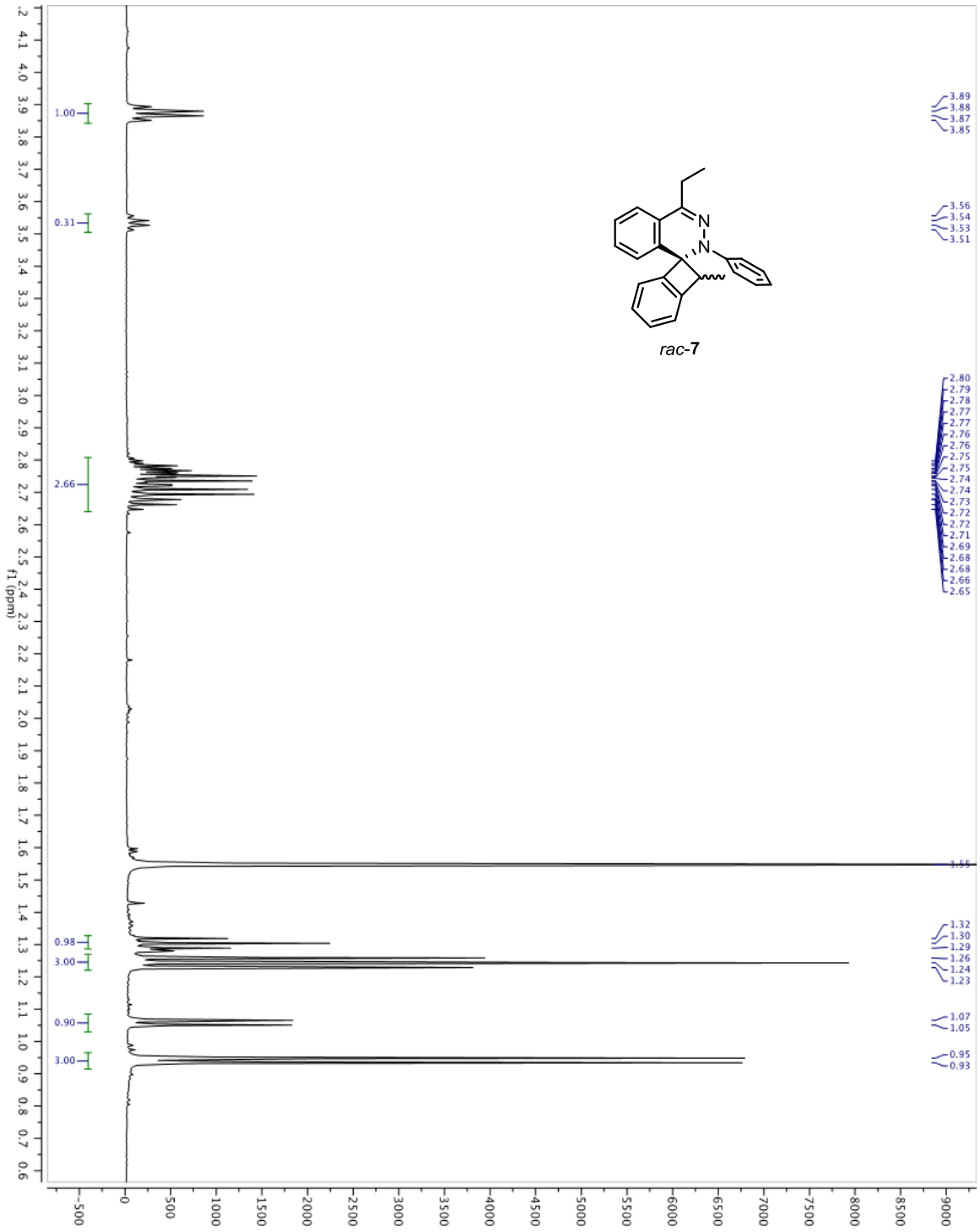

Figure A3.7. ^{1}H NMR spectrum of *rac*-**8** in CD_2Cl_2 (500 MHz).

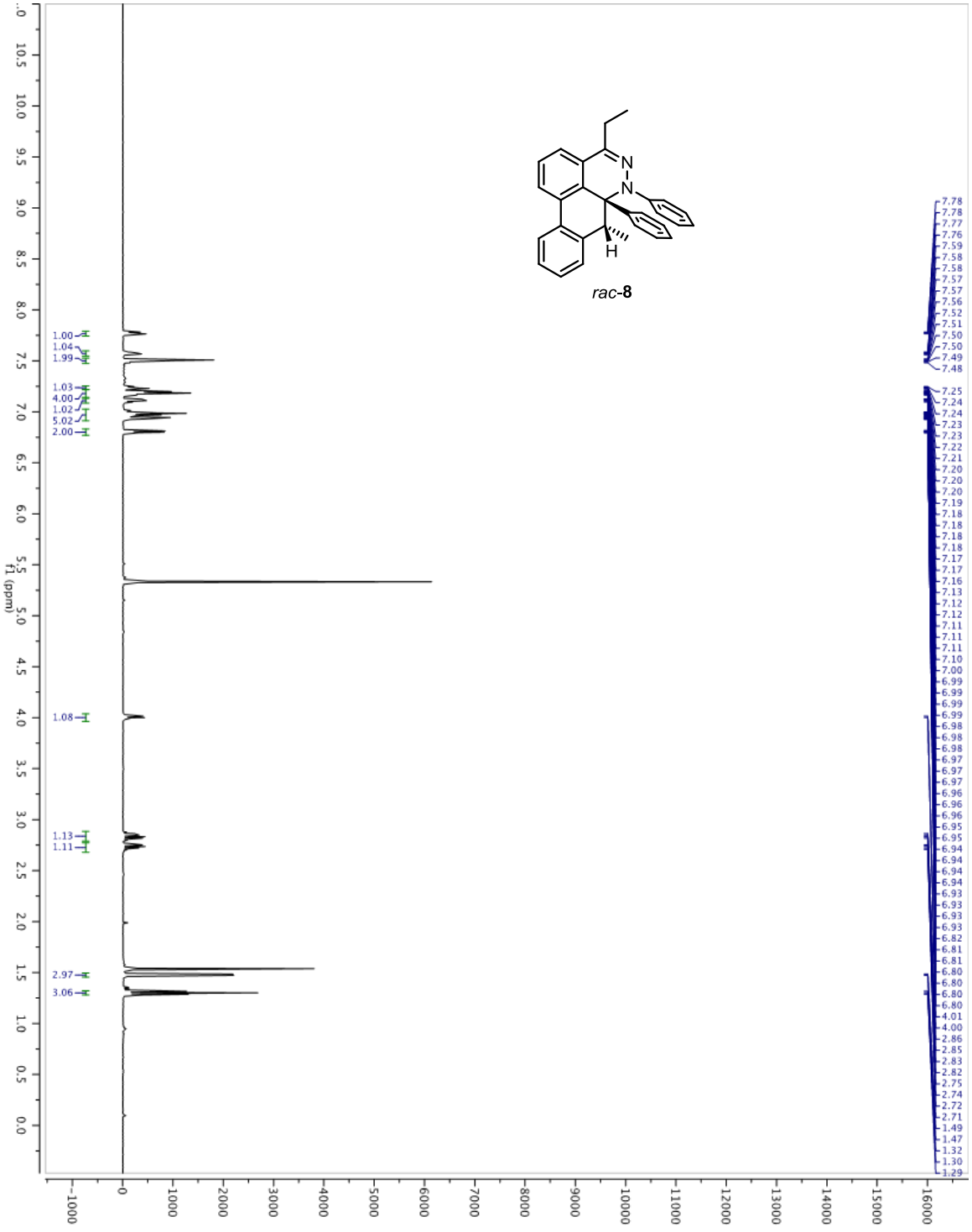

Figure A3.8. ^{13}C NMR spectrum of *rac*-**8** in CD_2Cl_2 (125 MHz).

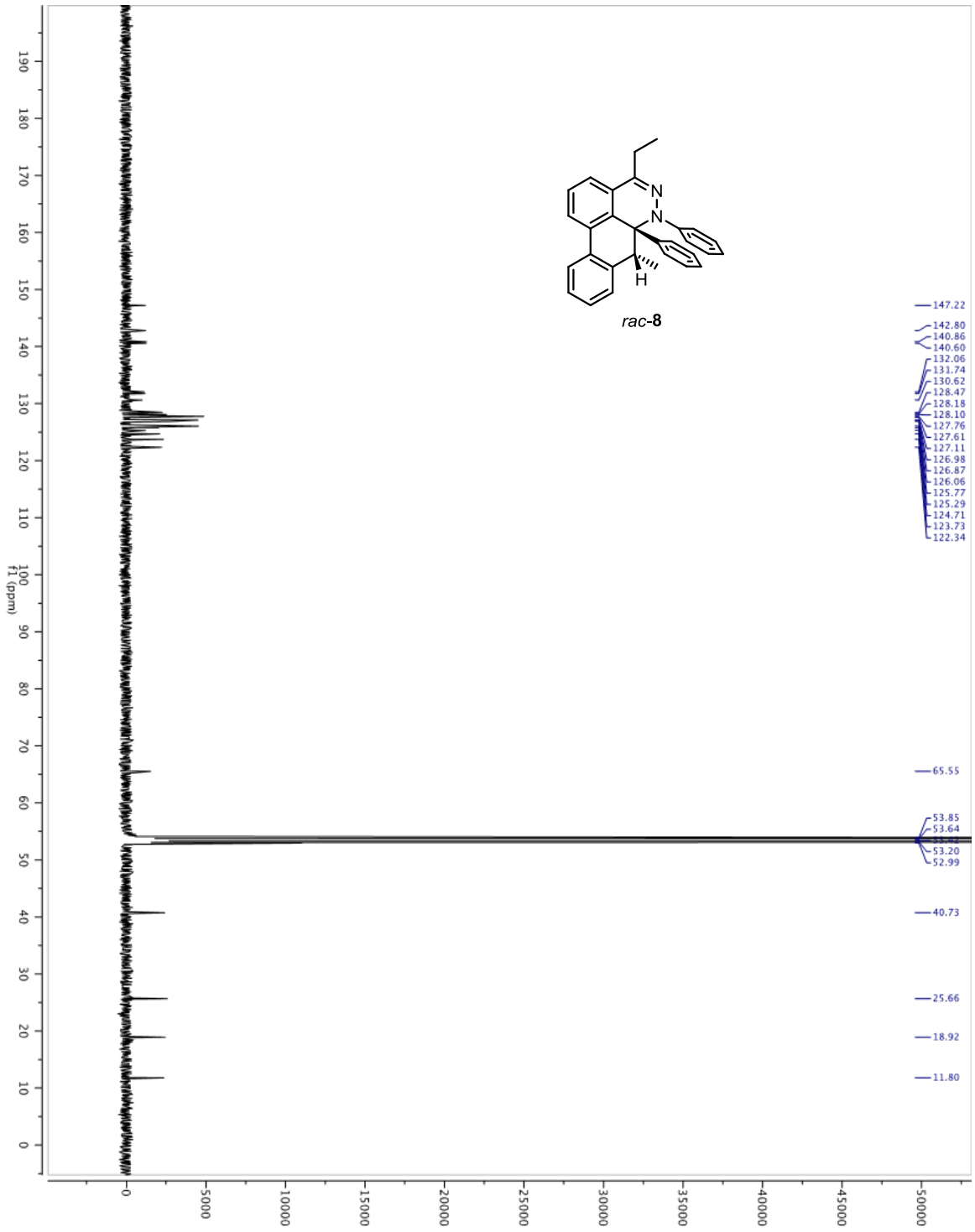

Figure A3.9. HMBC spectrum of *rac*-**8** in CD_2Cl_2.

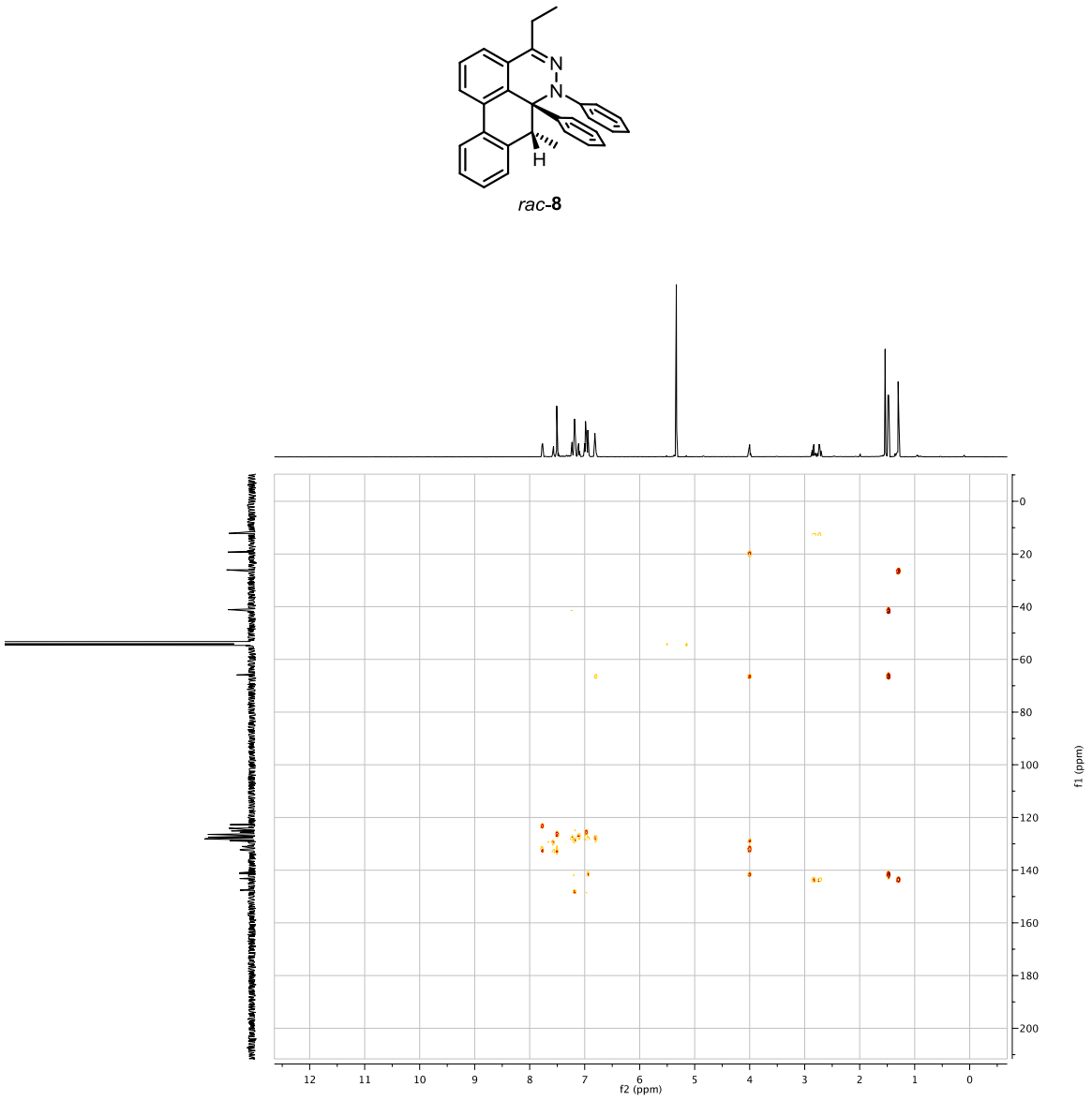

Figure A3.10. Expanded partial HMBC spectrum of *rac*-**8** in CD_2Cl_2.

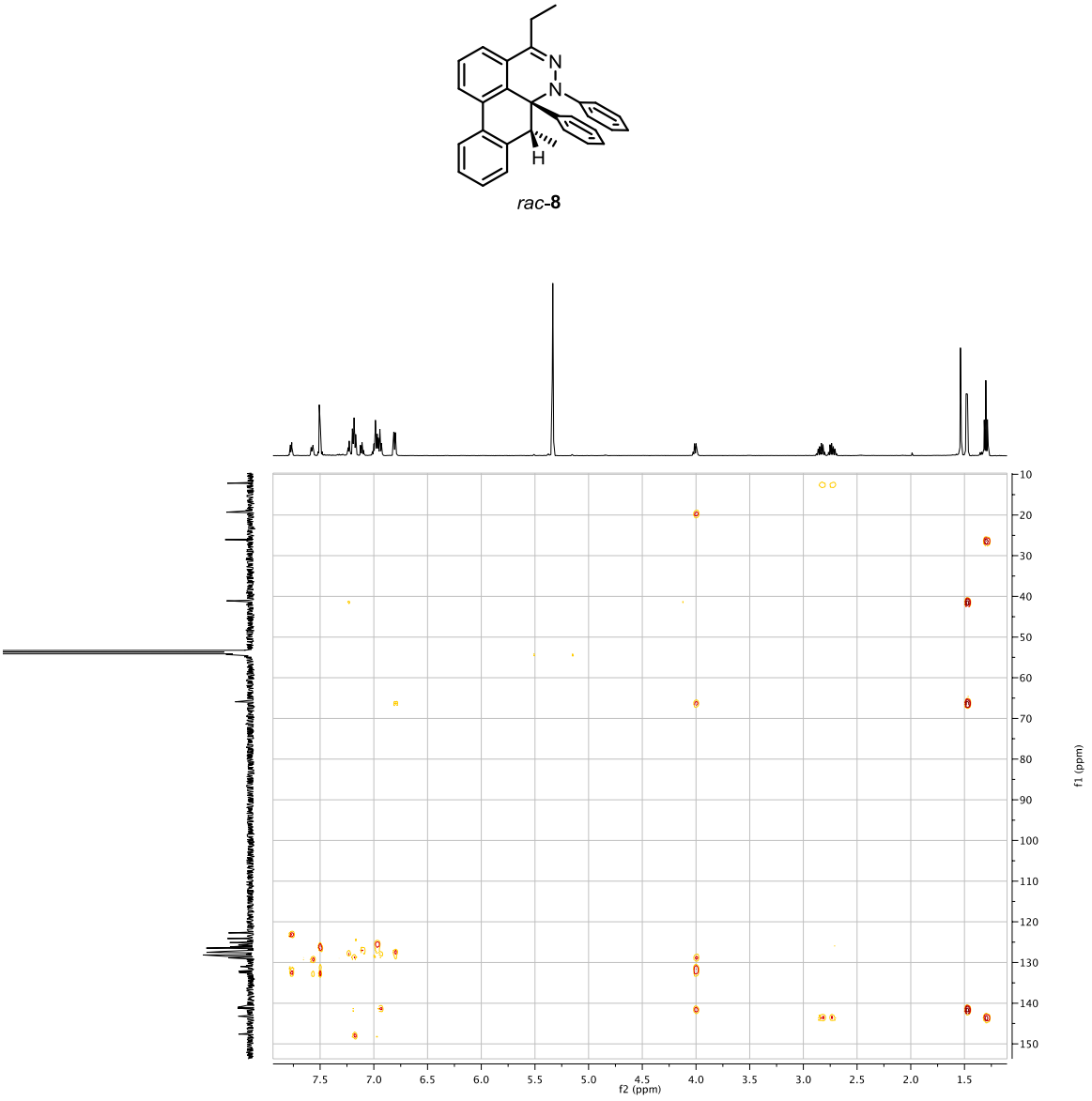

Figure A3.11. NOESY spectrum of *rac*-**8** in CD_2Cl_2.

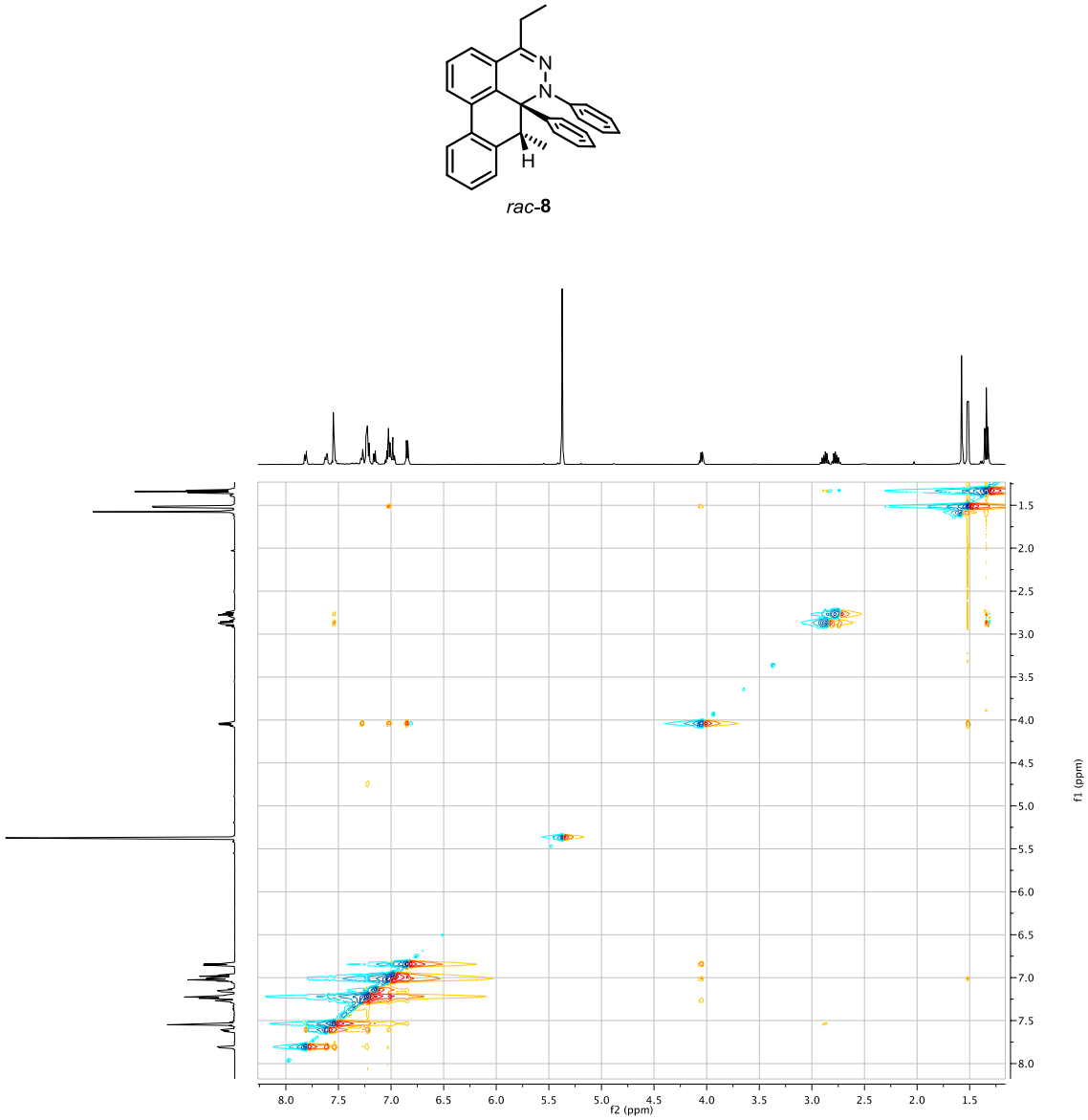

rac-**8**

Figure A3.12. ^{1}H NMR spectrum of *rac*-**9a** in CD_2Cl_2 (500 MHz).

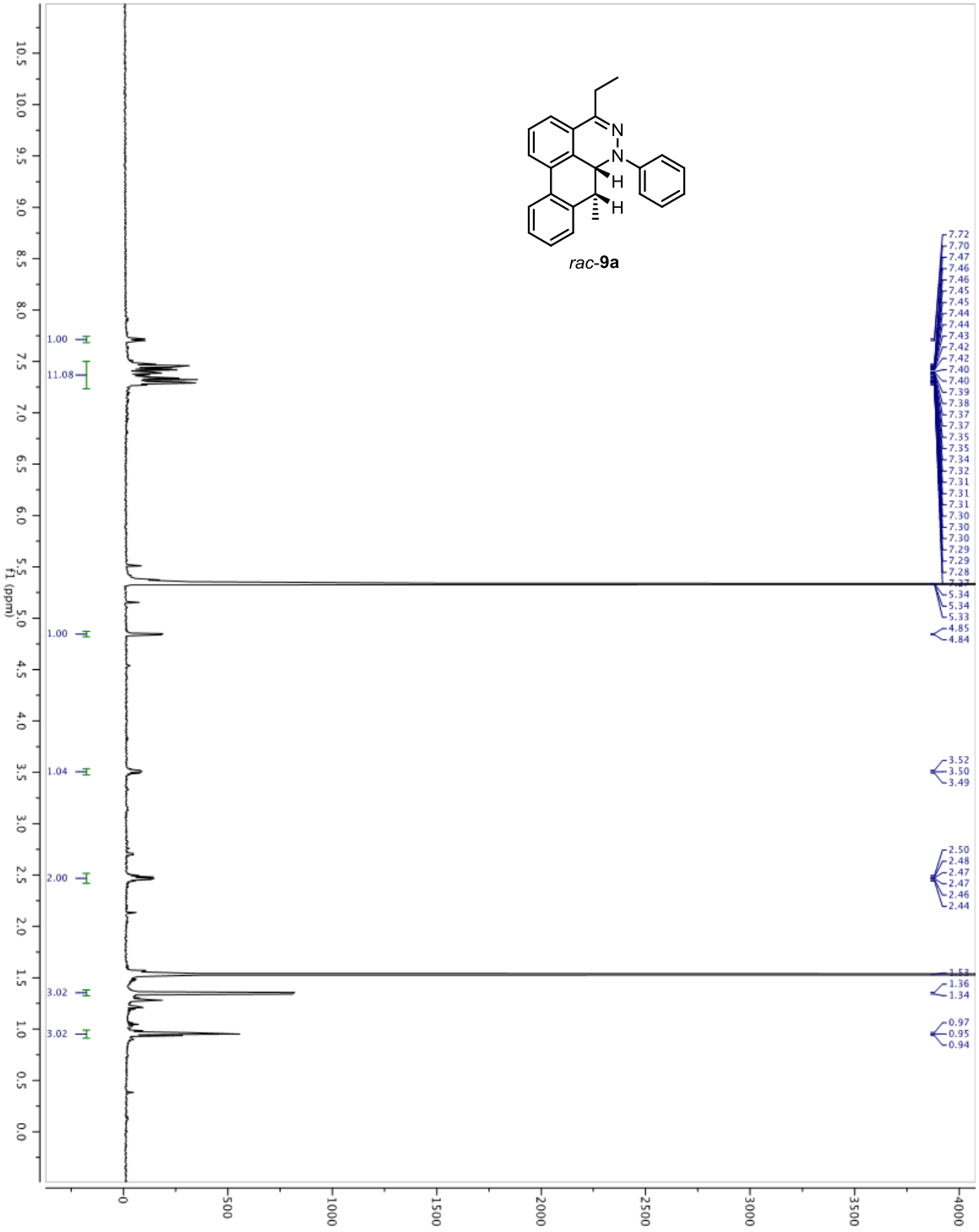

Figure A3.13. ^{1}H NMR spectrum of **16** in CD_2Cl_2 (500 MHz).

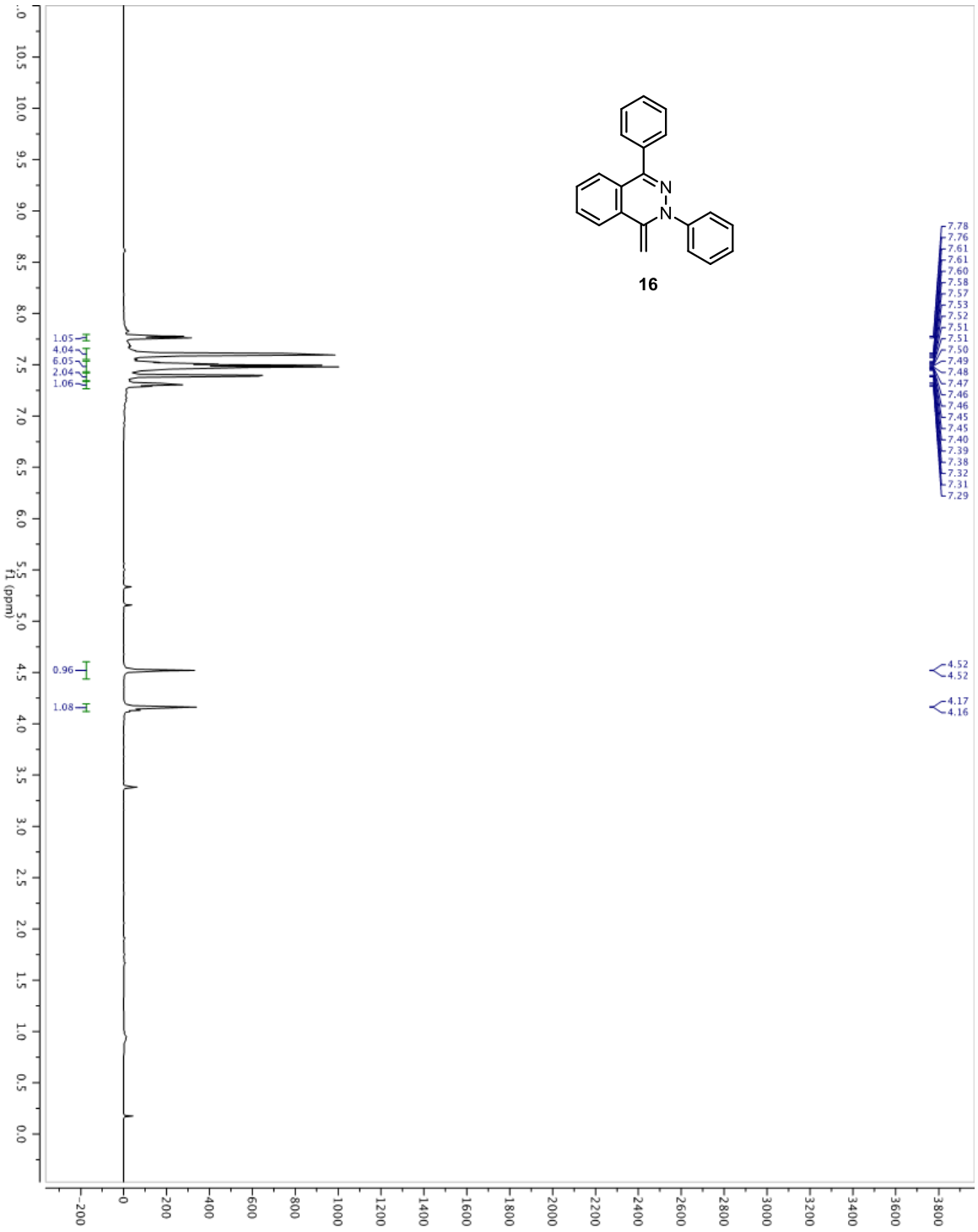

Figure A3.14. ^{13}C NMR spectrum of **16** in CD_2Cl_2 (125 MHz).

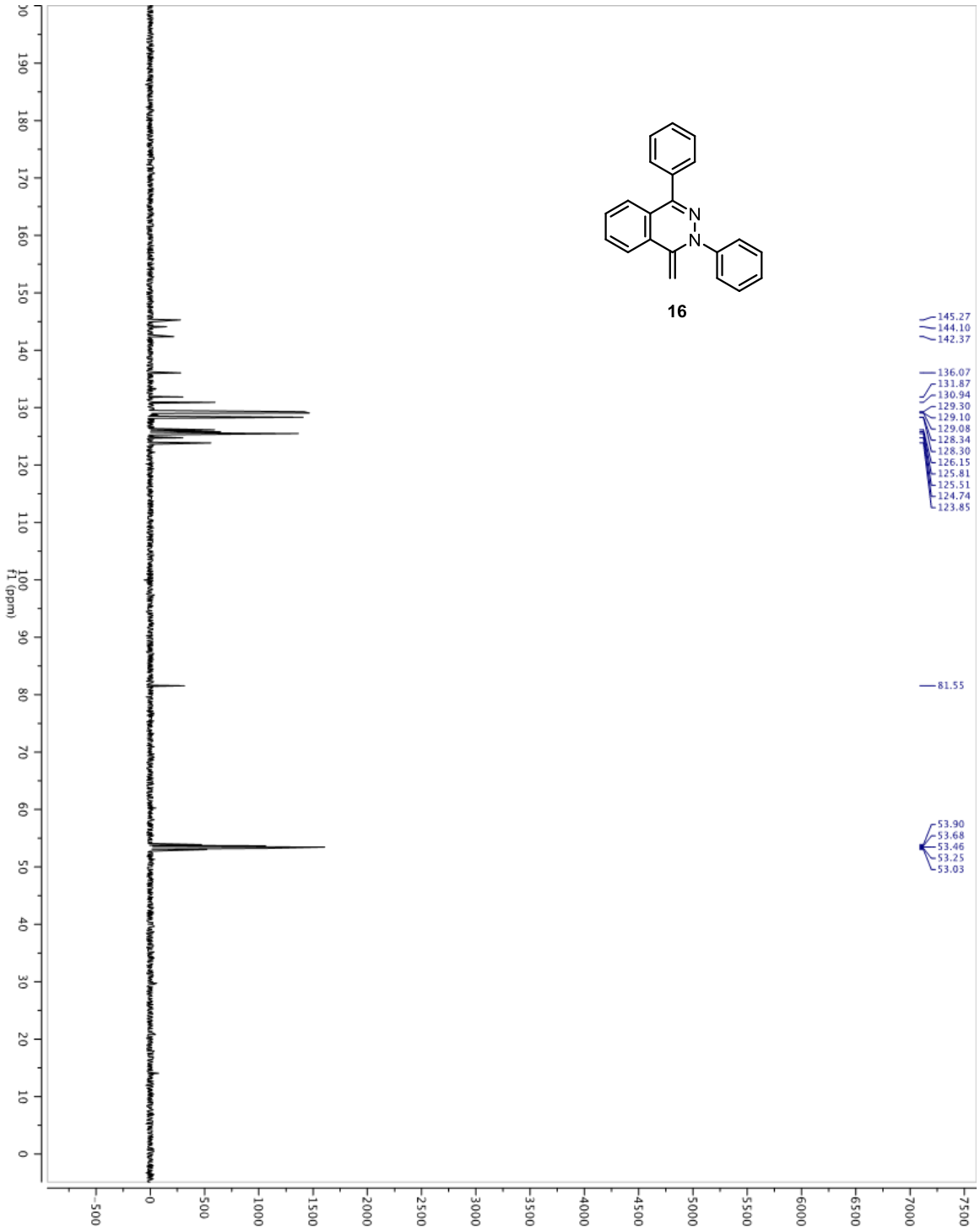

Table A3.1. Cartesian Coordinates of the Optimized Structures of 2, 11, 12, 14, I, II, VI, VII, VIII, TS1, TS2, TS3, and TS8.

2

C	0.000000	1.058663	0.703548	**C**	0.000000	1.058663	-0.703548
C	0.000000	-0.133780	1.461354	**H**	0.000000	2.010866	1.229771
C	0.000000	-1.237588	0.625468	**H**	0.000000	-0.134635	2.546586
C	0.000000	-1.237588	-0.625468	**H**	0.000000	-0.134635	-2.546586
C	0.000000	-0.133780	-1.461354	**H**	0.000000	2.010866	-1.229771

11

N	0.658688	1.187755	0.000049	**H**	3.165422	0.531002	-0.882339
C	1.288338	-0.005327	0.000047	**H**	3.165529	0.533035	0.881006
C	-1.288338	-0.005326	-0.000049	**C**	-2.787534	0.003387	-0.000012
N	-0.658687	1.187756	-0.000019	**H**	-3.165445	0.531078	0.882245
N	-0.662806	-1.192306	-0.000014	**H**	-3.165417	-1.020549	-0.001030
N	0.662804	-1.192306	0.000043	**H**	-3.165505	0.532960	-0.881101
C	2.787534	0.003386	-0.000027	**H**	3.165418	-1.020549	0.001063

12

C	-3.672435	-0.689608	-0.088057	**H**	-4.615664	-1.227211	-0.135912
C	-2.490962	-1.379009	-0.029894	**H**	-2.516043	-2.462270	-0.046014
C	-1.222837	-0.711712	0.022938	**H**	-2.502943	2.494513	-0.072617
C	-1.214596	0.737777	0.019681	**H**	-4.603815	1.275673	-0.150426
C	-2.479304	1.411846	-0.042387	**H**	4.603816	-1.275673	-0.150425
C	-3.665566	0.730075	-0.095512	**H**	4.615664	1.227211	-0.135913
C	-0.011821	-1.438769	0.065144	**H**	2.516043	2.462270	-0.046014
C	0.011821	1.438769	0.065144	**C**	0.052105	2.951698	0.135853
C	1.222838	0.711712	0.022938	**H**	0.828384	3.294387	0.826381

C	1.214596	-0.737778	0.019681	**H**	0.265296	3.404334	-0.842267
C	2.479305	-1.411846	-0.042386	**H**	-0.886189	3.375837	0.494261
H	2.502944	-2.494512	-0.072617	**C**	-0.052106	-2.951698	0.135852
C	3.665566	-0.730075	-0.095512	**H**	-0.828381	-3.294386	0.826386
C	3.672435	0.689608	-0.088058	**H**	-0.265305	-3.404332	-0.842267
C	2.490962	1.379009	-0.029894	**H**	0.886189	-3.375840	0.494254

14

C	4.411359	-0.272021	0.297656	**H**	2.119817	3.293972	1.007325
C	3.513223	0.787468	0.238043	**H**	2.208633	3.353772	-0.756839
C	2.143151	0.553703	0.029430	**H**	0.670448	3.704263	0.066566
C	1.678685	-0.769449	-0.135655	**C**	-1.999451	0.003262	0.030364
C	2.593252	-1.828375	-0.048738	**C**	-2.813003	0.958947	-0.589000
C	3.946974	-1.584452	0.162694	**C**	-2.585793	-1.028732	0.774971
H	5.468172	-0.079618	0.460336	**C**	-4.199640	0.877021	-0.465988
H	3.871469	1.804660	0.359781	**H**	-2.349124	1.764398	-1.146241
C	1.154061	1.628485	0.014916	**C**	-3.972560	-1.107310	0.883863
C	0.245764	-0.985660	-0.427767	**H**	-1.954054	-1.761868	1.265382
H	2.239016	-2.850649	-0.130738	**C**	-4.787444	-0.156406	0.264884
H	4.640579	-2.418145	0.228354	**H**	-4.822153	1.624341	-0.950997
N	-0.120388	1.393439	0.008147	**H**	-4.416283	-1.909946	1.466992
N	-0.577165	0.108751	-0.051778	**H**	-5.868298	-0.219177	0.354791
C	-0.236833	-2.100297	-1.014413	**H**	-1.288514	-2.234016	-1.228625
C	1.563366	3.076121	0.086364	**H**	0.432489	-2.901150	-1.300412

I

C	-4.366835	-0.272889	-0.274897	**H**	0.337356	-3.002180	-0.053225
C	-3.492590	0.800592	-0.265228	**H**	1.316818	-2.178609	1.132182
C	-2.111514	0.588503	-0.078586	**C**	-1.549992	3.102824	-0.096496
C	-1.613975	-0.731017	0.097063	**H**	-2.056656	3.324726	-1.043630

C	-2.529574	-1.811544	0.090094	**H**	-2.238424	3.366024	0.715277
C	-3.880718	-1.581806	-0.098098	**H**	-0.659420	3.729179	-0.023630
H	-5.430106	-0.105607	-0.419967	**C**	2.026524	0.016461	0.019463
H	-3.868093	1.809433	-0.399806	**C**	2.836957	1.020102	0.583684
C	-1.147659	1.654204	-0.021709	**C**	2.463422	-1.090498	-0.729671
C	-0.203503	-0.932221	0.269800	**C**	4.206790	0.923302	0.383968
H	-2.166385	-2.825866	0.204135	**H**	2.413357	1.831350	1.169151
H	-4.571390	-2.419871	-0.115239	**C**	3.869508	-1.155983	-0.830061
N	0.136335	1.428255	0.075347	**C**	4.723821	-0.166102	-0.336508
N	0.594198	0.152079	0.151545	**H**	4.871767	1.677169	0.797648
C	0.300638	-2.265597	0.751086	**H**	4.325239	-1.994891	-1.362514
H	-0.373601	-2.635677	1.538777	**H**	5.798004	-0.227497	-0.510828

II

C	3.361839	-0.698275	-1.153594	**H**	2.306171	-2.490396	-0.583378
C	2.294988	-1.404543	-0.590440	**H**	2.306846	2.490174	-0.582738
C	1.219743	-0.702266	-0.049487	**H**	4.196446	1.240790	-1.588974
C	1.219837	0.702209	-0.049466	**H**	-4.196300	-1.241045	-1.589089
C	2.295343	1.404322	-0.590110	**H**	-4.196170	1.240958	-1.589403
C	3.362043	0.697915	-1.153369	**H**	-2.306388	2.490256	-0.583264
C	-0.000028	-1.293439	0.623934	**C**	-0.000016	-2.795105	0.840507
C	0.000073	1.293468	0.623934	**H**	-0.000187	-3.334817	-0.112300
C	-1.219786	0.702184	-0.049532	**H**	0.884123	-3.096053	1.409898
C	-1.219808	-0.702267	-0.049435	**H**	-0.883982	-3.096068	1.410169
C	-2.295228	-1.404461	-0.590145	**C**	-0.000013	2.795236	0.839957
H	-2.306682	-2.490314	-0.582797	**H**	0.000128	3.334477	-0.113097
C	-3.361974	-0.698111	-1.153407	**H**	-0.884148	3.096365	1.409258
C	-3.361899	0.698066	-1.153567	**H**	0.883930	3.096524	1.409496
C	-2.295088	1.404414	-0.590391	**N**	0.000075	0.610802	2.052985
H	4.196030	-1.241245	-1.589486	**N**	-0.000072	-0.610186	2.053211

VI

C	-4.399150	-1.363393	-0.469632	**H**	2.502314	-0.837417	1.894386
C	-3.441133	-1.913541	0.381244	**C**	3.847176	-1.281405	-1.714593
C	-2.097321	-1.536601	0.290397	**H**	1.771530	-1.275058	-2.311171
C	-1.675371	-0.582201	-0.691484	**C**	4.744844	-1.222299	-0.648607
C	-2.678679	-0.013738	-1.525790	**H**	4.947542	-1.024890	1.491089
C	-4.002809	-0.405552	-1.415179	**H**	4.211213	-1.420263	-2.729125
H	-5.439552	-1.663452	-0.391800	**H**	5.813488	-1.299952	-0.827409
H	-3.744170	-2.634508	1.134114	**C**	0.846486	2.253722	0.740857
C	-1.077727	-2.028998	1.206558	**C**	0.833628	3.271285	1.668317
C	-0.302081	-0.240556	-0.775238	**C**	0.107232	2.210322	-0.422617
H	-4.743955	0.038980	-2.074798	**C**	-0.032617	4.350353	1.423046
N	0.183142	-1.746991	1.086620	**H**	1.457635	3.250302	2.558806
N	0.587294	-0.924830	0.062482	**C**	-0.739191	3.310056	-0.653020
C	-1.433916	-2.924457	2.364156	**C**	-0.809440	4.363421	0.263178
H	-2.145523	-2.435018	3.040358	**H**	-0.094807	5.169962	2.135390
H	-1.901009	-3.854476	2.016569	**H**	-1.338897	3.343344	-1.561482
H	-0.529412	-3.174496	2.921742	**H**	-1.473582	5.200814	0.065979
C	1.991898	-1.007581	-0.184493	**C**	0.184599	1.038829	-1.407145
C	2.890069	-0.959073	0.889686	**H**	1.215246	0.938703	-1.755058
C	2.473610	-1.186281	-1.487666	**H**	-0.415494	1.274228	-2.289780
C	4.256890	-1.068648	0.653205	**H**	-2.407609	0.723962	-2.272611

VII

C	-4.576084	-0.394838	-0.611979	**H**	2.033044	-0.744093	1.809091
C	-3.752915	-1.210513	0.158551	**C**	3.819943	-1.628701	-1.515887
C	-2.360536	-1.026601	0.160864	**H**	1.828022	-1.721870	-2.355894
C	-1.791135	-0.009132	-0.632266	**C**	4.574052	-1.414769	-0.361209
C	-2.630256	0.813372	-1.387523	**H**	4.510972	-0.938207	1.741771
C	-4.012625	0.621642	-1.384694	**H**	4.311095	-1.893740	-2.448416

H	-5.651922	-0.547095	-0.605736	**H**	5.656643	-1.503999	-0.391832
H	-4.190755	-1.999789	0.761701	**C**	0.078566	1.394479	0.424783
C	-1.457073	-1.878330	0.939417	**C**	0.008226	1.860542	1.731178
C	-0.289968	0.215138	-0.514016	**C**	0.602169	2.156703	-0.615351
H	-4.647009	1.272765	-1.979912	**C**	0.504278	3.155124	1.946843
N	-0.180436	-1.899075	0.727609	**H**	-0.405118	1.275843	2.548533
N	0.347370	-1.095353	-0.259335	**C**	1.084980	3.443084	-0.418103
C	-1.980809	-2.835800	1.978335	**C**	1.026687	3.927218	0.897934
H	-2.561597	-2.317285	2.751855	**H**	0.480677	3.576322	2.948853
H	-2.638493	-3.595047	1.534310	**H**	1.493042	4.054108	-1.219297
H	-1.139302	-3.346896	2.450838	**H**	1.395184	4.926838	1.114579
C	1.784327	-1.184314	-0.278795	**C**	0.388886	1.078052	-1.663464
C	2.541274	-0.980190	0.880416	**H**	1.308406	0.635481	-2.050915
C	2.428505	-1.523817	-1.472801	**H**	-0.258494	1.315577	-2.512460
C	3.929964	-1.097732	0.837165	**H**	-2.215661	1.628393	-1.971375

VIII

C	3.197695	2.616198	-0.130894	**H**	-3.754344	1.165378	1.208448
C	1.865995	3.144717	-0.337755	**C**	-3.728199	-2.127944	-0.836916
C	0.781201	2.339833	-0.122324	**H**	-1.667197	-1.651278	-1.268090
C	0.943278	0.976775	0.334116	**C**	-4.902638	-1.719468	-0.203407
C	2.313542	0.438657	0.752307	**H**	-5.825273	-0.199802	1.019283
C	3.428880	1.377642	0.348059	**H**	-3.714602	-3.039911	-1.427583
H	4.042898	3.261939	-0.360482	**H**	-5.805262	-2.318054	-0.287270
H	1.747198	4.169879	-0.669692	**C**	2.455449	-1.014223	0.280440
C	-0.608712	2.751250	-0.296701	**C**	3.613431	-1.549551	-0.285683
C	-0.136770	0.156386	0.444067	**C**	1.332353	-1.841294	0.452321
H	4.447832	1.046494	0.527950	**C**	3.665210	-2.895223	-0.659575
N	-1.624231	1.947171	-0.184495	**H**	4.478192	-0.915368	-0.452848
N	-1.405014	0.628934	0.120032	**C**	1.386090	-3.183834	0.074974
C	-0.940600	4.177440	-0.641022	**C**	2.554064	-3.716497	-0.475273

H	-0.551623	4.864307	0.120934	**H**	4.573506	-3.296526	-1.101515
H	-0.480336	4.462179	-1.595672	**H**	0.510501	-3.815533	0.209393
H	-2.022581	4.300347	-0.718303	**H**	2.589704	-4.762603	-0.767429
C	-2.577292	-0.180190	0.019209	**C**	0.077137	-1.220115	1.035406
C	-3.756781	0.238158	0.646154	**H**	-0.781991	-1.877897	0.907586
C	-2.569291	-1.356862	-0.740072	**H**	2.324718	0.371744	1.862102
C	-4.913221	-0.529596	0.529238	**H**	0.208457	-1.091585	2.124406

TS1

C	-4.609661	-0.089678	-0.041643	**H**	1.148405	-2.430970	0.036955
C	-3.669966	0.921442	-0.033311	**H**	-0.281549	-2.946984	0.971889
C	-2.290305	0.607765	-0.007252	**C**	-1.549392	3.071264	-0.007934
C	-1.882505	-0.750406	0.008909	**H**	-2.113293	3.356240	-0.904378
C	-2.863953	-1.770317	0.000748	**H**	-2.145887	3.366239	0.863842
C	-4.204455	-1.441981	-0.024101	**H**	-0.610078	3.626696	0.006051
H	-5.668132	0.153815	-0.061502	**C**	2.553161	-0.152163	0.006849
H	-3.986847	1.959043	-0.046410	**C**	2.980671	1.152448	0.043042
C	-1.249246	1.595617	0.005721	**C**	3.120440	-1.308246	-0.042937
C	-0.469170	-1.022871	0.036198	**C**	4.386722	1.200539	0.015587
H	-2.558274	-2.810687	0.014910	**H**	2.350208	2.031091	0.083768
H	-4.954659	-2.227547	-0.030199	**C**	4.530758	-1.240776	-0.071042
N	0.023042	1.266710	0.030167	**C**	5.146670	0.019851	-0.040688
N	0.400334	-0.032128	0.045249	**H**	4.883065	2.168141	0.038380
C	0.055685	-2.432837	0.063219	**H**	5.152140	-2.136677	-0.114192
H	-0.324384	-3.000195	-0.794873	**H**	6.232928	0.091820	-0.060343

TS2

C	2.898836	0.704697	-1.828732	**H**	1.418491	-3.303474	1.393131
C	2.148072	1.404715	-0.901746	**H**	-0.244868	-3.087460	1.970188
C	1.384431	0.707542	0.059406	**C**	0.450027	2.838847	1.165316

C	1.384423	-0.707537	0.059543	**H**	1.418534	3.303739	1.392477
C	2.148056	-1.404906	-0.901473	**H**	0.087539	3.270620	0.226961
C	2.898828	-0.705078	-1.828595	**H**	-0.244818	3.087852	1.969605
H	3.491560	1.242669	-2.563412	**C**	-3.578865	0.701960	-1.164673
H	2.150685	2.490057	-0.907038	**C**	-2.535447	1.446483	-0.574736
C	0.582214	1.340690	1.076495	**C**	-1.562070	0.636399	-0.016557
C	0.582196	-1.340479	1.076753	**C**	-1.562073	-0.636386	-0.016427
H	2.150656	-2.490249	-0.906551	**C**	-2.535454	-1.446580	-0.574438
H	3.491546	-1.243200	-2.563170	**C**	-3.578868	-0.702175	-1.164528
N	0.188442	0.662144	2.169970	**H**	-4.407835	1.231948	-1.628709
N	0.188434	-0.661718	2.170097	**H**	-2.537538	2.533136	-0.576211
C	0.449993	-2.838618	1.165862	**H**	-2.537550	-2.533234	-0.575689
H	0.087518	-3.270569	0.227584	**H**	-4.407841	-1.232254	-1.628455

TS3

C	-3.466985	0.700253	-1.009464	**H**	-2.369819	2.487539	-0.536172
C	-2.358323	1.401776	-0.544310	**H**	-2.369820	-2.487539	-0.536170
C	-1.222036	0.706194	-0.110284	**H**	-4.336356	-1.242937	-1.370631
C	-1.222037	-0.706194	-0.110285	**H**	4.336356	1.242936	-1.370631
C	-2.358324	-1.401776	-0.544309	**H**	4.336355	-1.242937	-1.370632
C	-3.466986	-0.700253	-1.009463	**H**	2.369819	-2.487539	-0.536171
C	0.000000	1.327411	0.454881	**C**	0.000000	2.818426	0.702998
C	0.000000	-1.327411	0.454881	**H**	0.000002	3.380327	-0.238499
C	1.222037	-0.706194	-0.110284	**H**	-0.883413	3.111054	1.277315
C	1.222037	0.706194	-0.110283	**H**	0.883411	3.111053	1.277319
C	2.358324	1.401776	-0.544309	**C**	0.000000	-2.818426	0.702997
H	2.369821	2.487539	-0.536170	**H**	-0.000008	-3.380326	-0.238500
C	3.466986	0.700252	-1.009463	**H**	0.883417	-3.111055	1.277310
C	3.466986	-0.700253	-1.009463	**H**	-0.883408	-3.111053	1.277323
C	2.358323	-1.401776	-0.544309	**N**	-0.000001	-0.592425	2.074125
H	-4.336355	1.242937	-1.370632	**N**	-0.000001	0.592424	2.074125

TS8

C	4.508189	-0.243863	0.056127	**C**	1.764839	3.123144	0.719554
C	3.658886	0.823741	0.279179	**H**	2.305533	3.107782	1.673244
C	2.268072	0.673038	0.095757	**H**	2.431664	3.560867	-0.032560
C	1.739811	-0.574171	-0.326215	**H**	0.885793	3.760491	0.827384
C	2.629618	-1.653793	-0.541907	**C**	-1.921324	0.310286	-0.139860
C	3.988106	-1.488026	-0.350183	**C**	-2.565303	1.400700	-0.747175
H	5.578293	-0.125802	0.199077	**C**	-2.559493	-0.742247	0.521606
H	4.058601	1.779645	0.600060	**C**	-3.952992	1.444627	-0.711483
C	1.328095	1.738706	0.320244	**H**	-1.994896	2.188063	-1.231220
C	0.314965	-0.705094	-0.511744	**C**	-3.965186	-0.637939	0.527165
H	2.244996	-2.622558	-0.834828	**C**	-4.656526	0.419132	-0.064651
H	4.659356	-2.326515	-0.510152	**H**	-4.482308	2.269261	-1.181615
N	0.039900	1.564156	0.213220	**H**	-4.538756	-1.422484	1.021702
N	-0.450473	0.344720	-0.160057	**H**	-5.744156	0.454162	-0.030079
C	-0.293379	-1.949846	-1.012018	**O**	-1.492075	-3.003709	1.327392
H	0.392827	-2.493974	-1.663159	**H**	-1.973653	-1.941358	1.060128
H	-0.599715	-2.587909	-0.114222	**H**	-0.901055	-2.810480	2.075186
H	-1.230172	-1.752032	-1.536604				

Table A3.2. Cartesian Coordinates of the Hartree-Fock Stationary Points of *rac*-9a.

C	2.20696	0.76325	-0.3341	**C**	1.11612	3.31742	-0.46768
C	0.82603	0.94612	-0.35276	**H**	0.7082	4.30516	-0.50629
C	0.27449	2.2133	-0.38958	**C**	2.48478	3.14686	-0.47866
C	2.74129	-0.61423	-0.1653	**H**	3.12928	4.0015	-0.52877
C	1.92432	-1.57456	0.43809	**C**	3.0297	1.87896	-0.393
C	0.49591	-1.21113	0.81193	**H**	4.09302	1.7639	-0.34537
C	-0.03764	-0.30094	-0.32033	**C**	4.02651	-0.96582	-0.55972
N	-1.45794	0.02697	-0.16176	**H**	4.64618	-0.24916	-1.05983
N	-1.95829	1.32841	-0.19055	**C**	4.51144	-2.23995	-0.33333
C	-1.19419	2.32991	-0.30283	**H**	5.50379	-2.49675	-0.64628
C	-2.45495	-0.96249	-0.24275	**C**	3.71119	-3.18123	0.28805
H	0.1114	-0.82195	-1.26367	**H**	4.0815	-4.17109	0.46669
H	-0.09384	-2.11601	0.84248	**C**	2.42247	-2.84629	0.66332
C	0.41677	-0.5287	2.18898	**H**	1.7946	-3.58111	1.1292
H	0.75732	-1.21188	2.95825	**C**	-2.18446	-2.22809	-0.75263
H	1.03793	0.35618	2.21766	**H**	-1.21196	-2.47118	-1.12343
H	-0.60637	-0.24707	2.40557	**C**	-3.17561	-3.19447	-0.8074
C	-1.78047	4.33937	1.11752	**H**	-2.93794	-4.16064	-1.20754
H	-2.25432	5.31479	1.11156	**C**	-4.45338	-2.92204	-0.3661
H	-2.29545	3.71083	1.83356	**H**	-5.21803	-3.67112	-0.40973
H	-0.75544	4.45835	1.44599	**C**	-4.73074	-1.65756	0.13039
C	-1.85504	3.69097	-0.28521	**H**	-5.71875	-1.42265	0.4749
H	-2.8928	3.54707	-0.5516	**C**	-3.75204	-0.69026	0.19383
H	-1.40829	4.34049	-1.02783	**H**	-3.9733	0.28421	0.56633

Table A3.3. Total Nuclear Spin-Spin Coupling J (Hz) of r*ac*-9a.

	1	**2**	**3**	**4**	**5**
1	0.000000D+00				
2	0.853201D+02	0.000000D+00			
3	0.142999D+02	0.668013D+02	0.000000D+00		
4	0.554313D+02	0.282370D+01	0.644484D+01	0.000000D+00	
5	0.156293D+02	-0.380570D+01	-0.638945D+01	0.178973D+02	0.000000D+00
6	-0.804260D+00	-0.716853D+01	0.104092D+01	0.104709D+02	0.503339D+02
7	-0.305024D+01	0.673358D+02	-0.150453D+01	-0.532962D+01	0.400108D+01
8	0.701566D+01	-0.694195D+01	0.692185D+01	0.157938D+01	-0.474420D+00

9	0.408250D+02	-0.412005D+02	0.322391D+02	0.126638D+02	-0.190798D+02
10	-0.986843D+02	0.100143D+03	-0.130296D+02	-0.308980D+02	0.474395D+02
11	0.490428D+01	-0.231699D+01	0.296101D+01	0.143102D+01	-0.254627D+01
12	0.637506D+01	-0.141815D+02	-0.153961D+01	0.142871D+01	-0.160335D+00
13	0.423943D+00	0.682231D+01	-0.101184D+00	-0.693798D+00	-0.560225D+01
14	0.282360D+01	0.979302D+00	-0.150963D+01	-0.895230D+01	0.253450D+01
15	-0.261765D+00	-0.269791D+00	0.237411D+00	0.795186D+00	0.139135D+01
16	0.113238D+00	0.173067D+00	0.507249D+00	0.100774D+01	0.164803D+01
17	0.747255D+00	-0.535242D+00	-0.374905D-01	-0.195778D+01	0.107416D+02
18	-0.190678D+02	0.193673D+02	-0.146322D+02	-0.581611D+01	0.913850D+01
19	-0.206132D+01	0.203174D+01	-0.186687D+01	-0.637601D+00	0.917674D+00
20	0.171554D+01	-0.182113D+01	0.124677D+01	0.624642D+00	-0.101528D+01
21	0.239139D+01	-0.240588D+01	0.185255D+01	0.605559D+00	-0.108204D+01
22	0.198123D+02	-0.181458D+02	0.176158D+02	0.590214D+01	-0.931939D+01
23	-0.752692D+01	0.832443D+01	-0.165225D+01	-0.230595D+01	0.362438D+01
24	-0.165698D+02	0.167397D+02	-0.117933D+02	-0.503533D+01	0.791419D+01
25	0.578862D+01	0.455902D+01	0.651546D+02	0.202694D+01	-0.342355D+01
26	-0.153647D+01	0.227506D+01	0.492892D+01	-0.126899D+01	0.151833D+01
27	-0.762981D+01	0.461599D+01	0.161020D+02	0.133083D+00	0.484133D+01
28	0.101663D+02	-0.306381D+01	-0.874444D+00	0.189787D+01	-0.205957D+01
29	0.899149D+02	0.267524D+01	-0.148027D+02	0.400754D+01	-0.469432D+01
30	-0.645239D+01	0.306551D+01	0.775118D+01	0.123350D+01	0.212871D+01
31	0.158549D+02	-0.276263D+01	-0.595922D+01	0.227856D+02	0.628211D+02
32	-0.459774D+01	0.212822D+01	0.297433D+01	0.206982D+02	-0.220301D+02
33	-0.149313D+02	0.603722D+01	0.715030D+01	0.613232D+02	-0.577447D+02
34	0.910055D+01	-0.256986D+01	-0.344535D+01	-0.201071D+02	0.244676D+02
35	0.173626D+02	-0.574331D+01	-0.683916D+01	-0.577044D+02	0.617504D+02
36	-0.795660D+01	0.248072D+01	0.308913D+01	0.248395D+02	-0.209318D+02
37	-0.154339D+02	0.544868D+01	0.708886D+01	0.621307D+02	0.261983D+02
38	0.926091D+01	-0.274185D+01	-0.350097D+01	-0.209217D+02	0.204700D+02
39	-0.823889D+01	0.852772D+01	-0.636058D+01	-0.255571D+01	0.431011D+01
40	0.342488D+01	-0.356780D+01	0.253395D+01	0.116367D+01	-0.158784D+01
41	0.883836D+01	-0.916111D+01	0.680442D+01	0.276608D+01	-0.455652D+01
42	-0.398713D+01	0.406984D+01	-0.302845D+01	-0.122776D+01	0.209467D+01
43	-0.861259D+01	0.887474D+01	-0.662608D+01	-0.269750D+01	0.444170D+01
44	0.366497D+01	-0.386882D+01	0.272227D+01	0.107587D+01	-0.197060D+01
45	0.856156D+01	-0.872757D+01	0.660851D+01	0.266909D+01	-0.443716D+01
46	-0.391713D+01	0.401133D+01	-0.299352D+01	-0.130182D+01	0.205138D+01
47	-0.888130D+01	0.939722D+01	-0.683017D+01	-0.279915D+01	0.459061D+01
48	0.324427D+01	-0.348181D+01	0.246017D+01	0.944801D+00	-0.180077D+01

	6	**7**	**8**	**9**	**10**
6	0.000000D+00				

7	0.699687D+02	0.000000D+00			
8	0.110172D+01	0.217773D+02	0.000000D+00		
9	-0.103909D+01	0.547412D+01	-0.689192D+01	0.000000D+00	
10	0.264707D+01	-0.161983D+02	0.559465D+01	0.527854D+02	0.000000D+00
11	-0.916054D+00	0.122732D+01	0.206367D+02	0.232449D+01	0.857413D+01
12	-0.580408D+01	0.188006D+03	-0.256954D+01	-0.124327D+02	0.318521D+02
13	0.173520D+03	-0.103763D+02	0.488645D+00	-0.137482D+01	0.324807D+01
14	0.539581D+02	-0.499265D+01	-0.360865D-01	-0.347794D+01	0.894712D+01
15	-0.793365D+01	0.962368D+01	-0.206526D+00	0.243476D+00	-0.798349D+00
16	-0.902724D+01	0.258794D+01	-0.898960D-01	0.583563D-01	-0.161237D+00
17	-0.101962D+02	0.297015D+01	-0.202531D+00	-0.848000D+00	0.240416D+01
18	0.572513D+00	-0.410349D+01	0.149447D+01	0.912549D+01	-0.274972D+02
19	0.161535D-01	-0.536096D+00	0.286721D+00	0.950063D+00	0.826882D+01
20	-0.587346D-01	0.441693D+00	-0.690111D-01	-0.921088D+00	0.443057D+01
21	-0.941146D-01	0.515981D+00	-0.172040D+00	-0.115983D+01	0.531027D+01
22	-0.513274D+00	0.403777D+01	0.155433D+01	-0.478408D+01	0.915655D+02
23	0.218716D+00	-0.162412D+01	0.294155D+00	0.481907D+01	-0.209977D+02
24	0.370807D+00	-0.356713D+01	0.199745D+01	0.102310D+02	-0.266335D+02
25	-0.337178D-01	0.411329D+01	-0.617877D+01	-0.409050D+02	0.103231D+03
26	-0.311247D+00	0.299843D-01	0.204913D+01	0.159739D+02	-0.392980D+02
27	0.560467D+00	-0.380462D+01	0.668897D+01	0.444435D+02	-0.106815D+03
28	-0.630755D+00	0.211756D+01	-0.244182D+01	-0.180693D+02	0.480035D+02
29	0.370504D+00	0.478513D+01	-0.624142D+01	-0.419410D+02	0.104084D+03
30	-0.429508D+00	0.226692D+00	0.218950D+01	0.161161D+02	-0.424147D+02
31	-0.103212D+02	0.764503D+01	-0.258411D+01	-0.189722D+02	0.475222D+02
32	0.689638D+01	-0.387858D+01	0.880939D+00	0.758520D+01	-0.201752D+02
33	0.116058D+02	-0.789707D+01	0.293923D+01	0.214550D+02	-0.536966D+02
34	-0.559186D+01	0.366889D+01	-0.115262D+01	-0.911648D+01	0.235810D+02
35	-0.910190D+01	0.829019D+01	-0.270820D+01	-0.205811D+02	0.515935D+02
36	0.650624D+01	-0.376369D+01	0.105081D+01	0.824554D+01	-0.214500D+02
37	0.973119D+01	-0.488635D+01	0.308134D+01	0.217044D+02	-0.542957D+02
38	-0.192684D+01	0.352109D+01	-0.106868D+01	-0.889001D+01	0.233443D+02
39	0.200692D+01	0.141257D+01	-0.106514D+01	0.369870D+01	-0.943779D+01
40	0.241716D+00	0.123219D+00	0.702061D+00	-0.114688D+01	0.395222D+01
41	-0.731897D+00	-0.122916D+00	0.204307D+01	-0.280216D+01	0.109625D+02
42	0.338139D+00	0.539193D-03	0.182868D+00	0.125067D+01	-0.465530D+01
43	0.856516D+00	0.196944D+00	-0.835245D+00	0.291414D+01	-0.104707D+02
44	-0.462353D+00	-0.979631D-01	0.809789D-01	-0.109962D+01	0.431203D+01
45	-0.728377D+00	-0.148787D+00	0.198620D+01	-0.266335D+01	0.104587D+02
46	0.257207D+00	0.338007D+00	0.673262D-01	0.109809D+01	-0.470969D+01
47	0.727584D+00	0.191579D+01	-0.170769D+01	0.497320D+01	-0.107818D+02
48	-0.387628D+00	-0.566331D+00	0.908002D+00	-0.116320D+01	0.383635D+01

	11	12	13	14	15
11	0.000000D+00				
12	0.196104D+01	0.000000D+00			
13	-0.844874D-01	0.484993D+01	0.000000D+00		
14	-0.660327D+00	0.583082D+01	-0.857473D+01	0.000000D+00	
15	0.347765D-01	0.226073D+00	0.556904D+01	0.153823D+03	0.000000D+00
16	-0.934459D-01	-0.143551D+01	0.143023D+02	0.155645D+03	-0.301534D+02
17	0.169592D+00	-0.155795D+01	0.477094D+01	0.154597D+03	-0.303750D+02
18	0.119390D+01	0.693220D+01	0.669947D+00	0.185675D+01	-0.238362D+00
19	0.112932D+00	0.435142D+00	-0.158070D+00	0.168204D+00	-0.252069D+00
20	-0.135302D+00	-0.995745D+00	-0.153676D+00	-0.154382D+00	-0.950355D-02
21	-0.207986D+00	-0.116390D+01	-0.266400D+00	-0.214645D+00	-0.485049D-01
22	-0.153908D+01	-0.747489D+01	-0.828317D+00	-0.195605D+01	0.178273D+00
23	0.471140D+00	0.257973D+01	0.760342D-01	0.717272D+00	-0.335525D+00
24	0.771277D+00	0.620167D+01	0.383917D+00	0.160647D+01	-0.478522D+00
25	-0.490153D+01	-0.301497D+01	0.150544D+00	-0.415761D+00	-0.827788D-01
26	0.188355D+01	0.490764D+00	-0.212070D+00	0.180814D+00	-0.315452D+00
27	0.510283D+01	0.505823D+01	0.380954D-01	0.681567D+00	-0.665972D-01
28	-0.233051D+01	-0.367565D+01	-0.552726D+00	-0.412280D+00	-0.266829D+00
29	-0.475731D+01	-0.390313D+01	-0.568021D+00	-0.119446D+01	0.277798D-01
30	0.209989D+01	0.607469D+00	-0.246753D+00	0.331206D+00	-0.250843D+00
31	-0.220880D+01	-0.262907D+01	0.499658D+01	0.966064D+01	-0.969635D+00
32	0.893391D+00	0.130191D+01	-0.229104D+01	-0.480535D+01	0.216278D+00
33	0.246311D+01	0.294791D+01	-0.477047D+01	-0.908798D+01	0.857056D+00
34	-0.126040D+01	-0.166864D+01	0.172686D+01	0.397611D+01	-0.698154D+00
35	-0.240120D+01	-0.298593D+01	0.471115D+01	0.942597D+01	-0.927902D+00
36	0.948784D+00	0.131302D+01	-0.268588D+01	-0.469293D+01	0.359356D+00
37	0.259053D+01	0.268511D+01	-0.115893D+00	-0.817508D+01	0.684934D+00
38	-0.109207D+01	-0.151634D+01	0.233744D+01	0.383245D+01	-0.119922D-01
39	0.259961D+02	-0.518659D+00	0.529765D+00	0.877993D+00	-0.692805D-01
40	0.211662D+02	0.898434D+00	0.643225D+00	-0.416529D+00	0.565934D-02
41	0.705939D+02	0.665278D+00	-0.209896D+00	-0.100944D+01	0.893274D-01
42	-0.228581D+02	-0.283100D+00	0.456224D+00	0.462288D+00	-0.170087D+00
43	-0.667500D+02	-0.701990D+00	0.398378D+00	0.981632D+00	-0.113281D+00
44	0.280767D+02	0.101797D+00	-0.193559D+00	-0.513253D+00	-0.124514D+00
45	0.703708D+02	0.775680D+00	-0.422626D+00	-0.984163D+00	0.707920D-01
46	-0.216259D+02	-0.740666D+00	0.507399D-01	0.448784D+00	-0.225072D+00
47	0.241132D+02	-0.108799D+01	0.493611D+00	0.102501D+01	-0.105183D+00
48	0.216557D+02	0.192080D+00	-0.353564D+00	-0.435180D+00	-0.930245D-01

	16	17	18	19	20
16	0.000000D+00				
17	-0.296909D+02	0.000000D+00			

18	-0.475723D-01	0.463067D+00	0.000000D+00		
19	-0.117678D+00	-0.467261D-01	0.150914D+03	0.000000D+00	
20	0.234177D+00	0.408977D+00	0.157668D+03	-0.302788D+02	0.000000D+00
21	0.391510D+00	0.145210D+00	0.153220D+03	-0.298929D+02	-0.302484D+02
22	0.119811D+00	-0.395851D+00	0.601605D+02	-0.827348D+01	-0.100645D+02
23	-0.206029D+00	0.166503D+00	-0.124984D+02	0.420368D+01	0.638756D+01
24	-0.199889D+00	0.191964D+00	-0.138416D+02	0.469110D+01	0.155849D+02
25	0.728824D-01	-0.281971D+00	0.200350D+02	0.197106D+01	-0.197084D+01
26	0.331159D-02	-0.119706D+00	-0.870751D+01	-0.770522D+00	0.735824D+00
27	0.147670D+00	0.318451D+00	-0.209318D+02	-0.225021D+01	0.192977D+01
28	-0.114567D+00	-0.398566D+00	0.100229D+02	0.102562D+01	-0.132973D+01
29	0.260869D+00	-0.472108D+00	0.199863D+02	0.204838D+01	-0.191613D+01
30	0.604600D-01	-0.266872D+00	-0.917681D+01	-0.129037D+01	0.802977D+00
31	-0.105574D+01	0.171243D+01	0.926148D+01	0.936860D+00	-0.106861D+01
32	0.431536D+00	-0.119388D+01	-0.438233D+01	-0.668041D+00	0.352108D+00
33	0.104927D+01	-0.158521D+01	-0.104767D+02	-0.114180D+01	0.113835D+01
34	-0.729133D+00	0.347822D+00	0.497075D+01	0.397225D+00	-0.744141D+00
35	-0.114818D+01	0.164928D+01	0.101059D+02	0.103102D+01	-0.116334D+01
36	0.279524D+00	-0.116657D+01	-0.456242D+01	-0.641155D+00	0.336310D+00
37	0.872059D+00	-0.188954D+01	-0.105644D+02	-0.114955D+01	0.115654D+01
38	-0.729339D+00	0.630558D+00	0.499651D+01	0.433922D+00	-0.635887D+00
39	0.101517D+00	0.173228D+00	-0.230348D+01	-0.371657D+00	0.214666D+00
40	-0.122386D+00	-0.366405D-01	0.105229D+01	-0.632072D-01	-0.276635D+00
41	-0.784059D-01	-0.736916D-01	0.250170D+01	0.298163D+00	-0.288160D+00
42	-0.245159D+00	-0.643079D-01	-0.126083D+01	-0.363163D+00	-0.214588D-01
43	-0.115478D-01	0.885083D-01	-0.245761D+01	-0.379006D+00	0.231041D+00
44	-0.276338D+00	-0.226965D+00	0.110408D+01	0.276404D-02	-0.214959D+00
45	-0.875450D-01	-0.350151D-01	0.242466D+01	0.307135D+00	-0.234775D+00
46	-0.188524D+00	0.512215D-01	-0.122226D+01	-0.257975D+00	0.213498D+00
47	0.186861D-01	0.216846D+00	-0.249926D+01	-0.376385D+00	0.289652D+00
48	-0.810133D-01	0.363568D+00	0.111647D+01	0.166141D+00	0.451835D+00

	21	**22**	**23**	**24**	**25**
21	0.000000D+00				
22	-0.101863D+02	0.000000D+00			
23	0.162771D+02	0.169876D+03	0.000000D+00		
24	0.471921D+01	0.167946D+03	-0.314545D+02	0.000000D+00	
25	-0.238076D+01	-0.196426D+02	0.820029D+01	0.174884D+02	0.000000D+00
26	0.201257D+01	0.966149D+01	-0.425352D+01	-0.733912D+01	0.157202D+03
27	0.273263D+01	0.213564D+02	-0.850489D+01	-0.181289D+02	0.939487D+02
28	-0.123346D+01	-0.107503D+02	0.395765D+01	0.913636D+01	-0.788961D+01
29	-0.252672D+01	-0.204548D+02	0.798378D+01	0.172566D+02	0.199838D+00
30	0.106818D+01	0.956917D+01	-0.385537D+01	-0.847497D+01	0.475793D+01

31	-0.107594D+01	-0.944086D+01	0.363934D+01	0.805327D+01	-0.350653D+01
32	0.516445D+00	0.457480D+01	-0.203047D+01	-0.406072D+01	0.138266D+01
33	0.117877D+01	0.106843D+02	-0.422271D+01	-0.917302D+01	0.385763D+01
34	-0.778586D+00	-0.536654D+01	0.176848D+01	0.442028D+01	-0.178468D+01
35	-0.120094D+01	-0.103624D+02	0.399181D+01	0.881067D+01	-0.369521D+01
36	0.483154D+00	0.471736D+01	-0.207510D+01	-0.418594D+01	0.142187D+01
37	0.119929D+01	0.107800D+02	-0.424286D+01	-0.925888D+01	0.385664D+01
38	-0.759454D+00	-0.534944D+01	0.196635D+01	0.438696D+01	-0.173451D+01
39	0.243281D+00	0.239637D+01	-0.945514D+00	-0.159670D+01	0.861026D+01
40	-0.275680D+00	-0.113942D+01	0.225637D+00	0.627811D+00	-0.361853D+01
41	-0.356184D+00	-0.251078D+01	0.951145D+00	0.181066D+01	-0.929444D+01
42	-0.268185D-01	0.119584D+01	-0.669487D+00	-0.106764D+01	0.410560D+01
43	0.257601D+00	0.242922D+01	-0.985159D+00	-0.184101D+01	0.901379D+01
44	-0.325980D+00	-0.117825D+01	0.345788D+00	0.634003D+00	-0.393046D+01
45	-0.337851D+00	-0.242458D+01	0.978976D+00	0.170867D+01	-0.898942D+01
46	-0.168815D-01	0.118933D+01	-0.373673D+00	-0.106351D+01	0.406093D+01
47	0.268867D+00	0.246398D+01	-0.944177D+00	-0.189503D+01	0.937925D+01
48	-0.179269D+00	-0.985078D+00	0.103423D+01	0.645008D+00	-0.349222D+01

	26	**27**	**28**	**29**	**30**
26	0.000000D+00				
27	-0.682129D+01	0.000000D+00			
28	0.978095D+01	0.163872D+03	0.000000D+00		
29	0.520501D+01	0.951142D+02	-0.889695D+01	0.000000D+00	
30	0.130966D+01	-0.713058D+01	0.988199D+01	0.158502D+03	0.000000D+00
31	0.160693D+01	0.476604D+01	-0.232453D+01	-0.574154D+01	0.240701D+01
32	-0.977575D+00	-0.210856D+01	0.120929D+01	0.318621D+01	-0.552609D+00
33	-0.191866D+01	-0.545239D+01	0.246126D+01	0.795599D+01	-0.277295D+01
34	0.658676D+00	0.240225D+01	-0.138845D+01	-0.391601D+01	0.148083D+01
35	0.169718D+01	0.517967D+01	-0.248702D+01	-0.777290D+01	0.258571D+01
36	-0.114543D+01	-0.226456D+01	0.832107D+00	0.336107D+01	-0.137467D+01
37	-0.192866D+01	-0.533125D+01	0.246280D+01	0.836281D+01	-0.279694D+01
38	0.570540D+00	0.235893D+01	-0.157094D+01	-0.357686D+01	0.986761D+00
39	-0.369960D+01	-0.911951D+01	0.408698D+01	0.864853D+01	-0.370761D+01
40	0.144895D+01	0.374437D+01	-0.202711D+01	-0.363116D+01	0.170381D+01
41	0.385773D+01	0.980699D+01	-0.453338D+01	-0.934039D+01	0.395775D+01
42	-0.228882D+01	-0.444908D+01	0.197469D+01	0.418887D+01	-0.205341D+01
43	-0.388269D+01	-0.955588D+01	0.432880D+01	0.906174D+01	-0.394929D+01
44	0.154520D+01	0.405376D+01	-0.228488D+01	-0.399165D+01	0.160985D+01
45	0.375385D+01	0.948933D+01	-0.437755D+01	-0.903069D+01	0.380265D+01
46	-0.202137D+01	-0.438112D+01	0.187343D+01	0.408990D+01	-0.220282D+01
47	-0.395716D+01	-0.994540D+01	0.444636D+01	0.945973D+01	-0.404715D+01
48	0.194617D+01	0.365748D+01	-0.201093D+01	-0.362094D+01	0.138413D+01

	31	32	33	34	35
31	0.000000D+00				
32	0.131498D+03	0.000000D+00			
33	0.299736D+02	0.192125D+02	0.000000D+00		
34	0.200108D+02	-0.281998D+01	0.134378D+03	0.000000D+00	
35	0.604134D+02	-0.196256D+02	0.272252D+02	0.197813D+02	0.000000D+00
36	-0.201501D+02	0.126590D+02	0.201386D+02	-0.339065D+01	0.133105D+03
37	-0.574325D+02	0.241172D+02	0.586770D+02	-0.193009D+02	0.282983D+02
38	0.239438D+02	-0.128521D+02	-0.188969D+02	0.123264D+02	0.197863D+02
39	0.394820D+01	-0.179322D+01	-0.448136D+01	0.204951D+01	0.430608D+01
40	-0.168204D+01	0.759743D+00	0.194568D+01	-0.107835D+01	-0.181109D+01
41	-0.427018D+01	0.186847D+01	0.481859D+01	-0.232671D+01	-0.464978D+01
42	0.194018D+01	-0.106859D+01	-0.222098D+01	0.974111D+00	0.213978D+01
43	0.414511D+01	-0.190500D+01	-0.470501D+01	0.220020D+01	0.452218D+01
44	-0.183749D+01	0.737264D+00	0.199825D+01	-0.114097D+01	-0.199370D+01
45	-0.413170D+01	0.179442D+01	0.465290D+01	-0.225045D+01	-0.450080D+01
46	0.194533D+01	-0.108933D+01	-0.227449D+01	0.946642D+00	0.212003D+01
47	0.428790D+01	-0.195350D+01	-0.487044D+01	0.224097D+01	0.467368D+01
48	-0.168389D+01	0.607701D+00	0.180189D+01	-0.110779D+01	-0.182219D+01

	36	37	38	39	40
36	0.000000D+00				
37	0.203216D+02	0.000000D+00			
38	-0.324737D+01	0.133682D+03	0.000000D+00		
39	-0.185959D+01	-0.462429D+01	0.211889D+01	0.000000D+00	
40	0.851172D+00	0.211396D+01	-0.466257D+00	0.128518D+03	0.000000D+00
41	0.196911D+01	0.499051D+01	-0.217840D+01	0.175865D+02	0.237931D+02
42	-0.104368D+01	-0.226031D+01	0.127281D+01	0.264300D+02	-0.503083D+01
43	-0.196891D+01	-0.485753D+01	0.218495D+01	0.727269D+02	-0.254755D+02
44	0.794151D+00	0.207027D+01	-0.109797D+01	-0.255844D+02	0.149339D+02
45	0.189194D+01	0.481402D+01	-0.215729D+01	-0.695358D+02	0.293435D+02
46	-0.109185D+01	-0.234876D+01	0.931981D+00	0.289963D+02	-0.155080D+02
47	-0.202869D+01	-0.502825D+01	0.223028D+01	0.749287D+02	-0.272220D+02
48	0.830445D+00	0.187203D+01	-0.102304D+01	-0.288102D+02	0.169275D+02

	41	42	43	44	45
41	0.000000D+00				
42	0.126838D+03	0.000000D+00			
43	0.130826D+02	0.258680D+02	0.000000D+00		
44	0.268575D+02	-0.634390D+01	0.127882D+03	0.000000D+00	
45	0.726286D+02	-0.247229D+02	0.112046D+02	0.271451D+02	0.000000D+00
46	-0.246690D+02	0.155635D+02	0.260631D+02	-0.659593D+01	0.127525D+03

47	-0.715656D+02	0.300863D+02	0.739726D+02	-0.267091D+02	0.181295D+02
48	0.313233D+02	-0.165923D+02	-0.263969D+02	0.159346D+02	0.254063D+02

	46	**47**	**48**
46	0.000000D+00		
47	0.256107D+02	0.000000D+00	
48	-0.475260D+01	0.133144D+03	0.000000D+00

Table A3.4. Cartesian Coordinates of the Hartree-Fock Stationary Points of *rac*-9b.

C	2.23216	0.75707	-0.42786	**H**	4.03137	-4.13814	0.66281
C	0.85975	0.9708	-0.33829	**C**	2.46571	-2.71913	0.94127
C	0.33338	2.24727	-0.36286	**H**	1.90595	-3.37382	1.57551
C	2.73745	-0.61824	-0.18306	**C**	-3.76885	-0.53303	0.10522
C	1.97682	-1.45929	0.64465	**H**	-3.97231	0.41415	0.54997
C	0.6204	-0.94524	1.14313	**C**	-4.78591	-1.43531	-0.11952
C	-0.00577	-0.25476	-0.11081	**H**	-5.78457	-1.17684	0.1738
N	-1.42412	0.09681	-0.01901	**C**	-4.53432	-2.66181	-0.7132
N	-1.8863	1.41514	0.07106	**H**	-5.32869	-3.35982	-0.88475
C	-1.10939	2.39903	-0.09592	**C**	-3.23967	-2.96315	-1.08151
C	-2.45545	-0.83491	-0.25854	**H**	-3.01728	-3.90176	-1.55028
H	0.7975	-0.16119	1.87436	**C**	-2.20966	-2.06413	-0.86119
H	0.13613	-0.91524	-0.9566	**H**	-1.224	-2.33835	-1.16716
C	1.18493	3.32464	-0.58548	**C**	-0.24948	-2.01975	1.80827
H	0.79652	4.32045	-0.62367	**H**	-1.21255	-1.60186	2.06502
C	2.5404	3.11832	-0.73844	**H**	-0.41001	-2.87123	1.16158
H	3.19192	3.95295	-0.90331	**H**	0.22093	-2.36078	2.72391
C	3.06837	1.84337	-0.63335	**C**	-1.41307	4.40095	1.42073
H	4.12915	1.70248	-0.67741	**H**	-1.85476	5.38826	1.49793
C	3.93641	-1.07044	-0.712	**H**	-1.82933	3.77613	2.20142
H	4.49746	-0.43961	-1.37216	**H**	-0.34667	4.48867	1.58741
C	4.4072	-2.33583	-0.41119	**C**	-1.72014	3.77634	0.03922
H	5.33367	-2.67586	-0.82901	**H**	-2.78982	3.66414	-0.06882
C	3.67441	-3.15634	0.42245	**H**	-1.37173	4.42515	-0.75509

Table A3.5. Total Nuclear Spin-Spin Coupling J (Hz) of *rac*-9b.

	1	2	3	4	5
1	0.000000D+00				
2	0.813947D+02	0.000000D+00			
3	0.165516D+02	0.648508D+02	0.000000D+00		
4	0.553559D+02	0.210383D+01	0.690854D+01	0.000000D+00	
5	0.144759D+02	-0.366909D+01	-0.719958D+01	0.134437D+02	0.000000D+00
6	0.155643D+00	-0.784429D+01	0.689118D+00	0.108690D+02	0.518446D+02
7	-0.153124D+01	0.672640D+02	-0.170035D+01	-0.843788D+01	0.587909D+01
8	0.613962D+01	-0.603145D+01	0.620754D+01	0.939212D+00	0.270666D+00
9	0.400809D+02	-0.398766D+02	0.315549D+02	0.112852D+02	-0.175758D+02
10	-0.955094D+02	0.954894D+02	-0.109253D+02	-0.277017D+02	0.438017D+02
11	0.366579D+01	-0.159387D+01	0.201629D+01	0.942689D+00	-0.147664D+01
12	0.426282D+01	0.481123D+01	-0.221678D+01	-0.150239D+02	0.590049D+01
13	0.330450D+01	-0.119029D+02	-0.298120D+01	0.613560D+00	0.290431D+01
14	0.317553D+01	0.732660D+01	0.628368D+02	0.114480D+01	-0.213388D+01
15	-0.394121D+00	0.110100D+01	0.592219D+01	-0.909030D+00	0.980574D+00
16	-0.463998D+01	0.133385D+01	0.185745D+02	0.117262D+01	0.334738D+01
17	0.884245D+01	-0.159835D+01	-0.190350D+01	0.153325D+01	-0.146716D+01
18	0.868256D+02	0.584676D+01	-0.171183D+02	0.349307D+01	-0.383610D+01
19	-0.538804D+01	0.181517D+01	0.868577D+01	0.154020D+01	0.158957D+01
20	0.142007D+02	-0.178843D+01	-0.646106D+01	0.228529D+02	0.647751D+02
21	-0.375488D+01	0.172869D+01	0.319462D+01	0.207672D+02	-0.226507D+02
22	-0.132038D+02	0.495638D+01	0.798563D+01	0.623260D+02	-0.598063D+02
23	0.841972D+01	-0.215720D+01	-0.382504D+01	-0.207061D+02	0.253216D+02
24	0.159337D+02	-0.475698D+01	-0.769581D+01	-0.589207D+02	0.640791D+02
25	-0.741156D+01	0.208437D+01	0.344163D+01	0.254494D+02	-0.221054D+02
26	-0.136350D+02	0.433464D+01	0.798855D+01	0.627467D+02	0.255847D+02
27	0.859451D+01	-0.230080D+01	-0.384586D+01	-0.210127D+02	0.203931D+02
28	-0.608082D+01	0.663955D+01	-0.458474D+01	-0.172519D+01	0.267037D+01
29	0.204564D+01	-0.227661D+01	0.154819D+01	0.639051D+00	-0.108131D+01
30	0.590059D+01	-0.602819D+01	0.451065D+01	0.166925D+01	-0.257642D+01
31	-0.284758D+01	0.289204D+01	-0.215677D+01	-0.911530D+00	0.126811D+01
32	-0.602479D+01	0.625174D+01	-0.457965D+01	-0.172244D+01	0.261497D+01
33	0.256259D+01	-0.273679D+01	0.185963D+01	0.696166D+00	-0.117846D+01
34	0.622396D+01	-0.650497D+01	0.473524D+01	0.177463D+01	-0.270524D+01
35	-0.276309D+01	0.282603D+01	-0.209231D+01	-0.828371D+00	0.127232D+01
36	-0.572476D+01	0.611983D+01	-0.435093D+01	-0.161554D+01	0.251072D+01
37	0.254189D+01	-0.259307D+01	0.185382D+01	0.860771D+00	-0.949736D+00
38	0.144385D-01	0.417403D+01	-0.357408D+00	0.101763D+01	-0.276790D+01
39	-0.164451D+00	-0.523218D+00	0.101892D+00	0.110741D+01	0.886376D+01

40	-0.186192D+00	-0.526385D+00	0.528324D-01	0.229740D+00	0.171889D+01
41	-0.201937D+00	0.163638D+00	0.102570D+00	0.139682D+00	0.109565D+01
42	-0.182177D+02	0.181546D+02	-0.138669D+02	-0.524762D+01	0.840558D+01
43	-0.182578D+01	0.171779D+01	-0.166712D+01	-0.533374D+00	0.768865D+00
44	0.162352D+01	-0.168172D+01	0.117577D+01	0.586959D+00	-0.950866D+00
45	0.229430D+01	-0.224813D+01	0.178614D+01	0.532146D+00	-0.973612D+00
46	0.191817D+02	-0.171696D+02	0.169462D+02	0.538847D+01	-0.869834D+01
47	-0.662874D+01	0.734187D+01	-0.850384D+00	-0.190036D+01	0.305005D+01
48	-0.177148D+02	0.174969D+02	-0.126167D+02	-0.506205D+01	0.813641D+01

	6	**7**	**8**	**9**	**10**
6	0.000000D+00				
7	0.693095D+02	0.000000D+00			
8	0.138700D+01	0.199164D+02	0.000000D+00		
9	-0.333293D+01	0.427252D+01	-0.685355D+01	0.000000D+00	
10	0.845282D+01	-0.133659D+02	0.430672D+01	0.520905D+02	0.000000D+00
11	0.454552D+00	0.296312D+00	0.212379D+02	0.265004D+01	0.725470D+01
12	0.176799D+03	-0.799900D+01	-0.482083D+00	-0.507664D+01	0.130097D+02
13	-0.557871D+01	0.189589D+03	-0.234727D+01	-0.945206D+01	0.236168D+02
14	-0.108999D+01	0.380466D+01	-0.528057D+01	-0.406181D+02	0.101161D+03
15	0.846025D-01	0.224001D+00	0.177749D+01	0.158854D+02	-0.385453D+02
16	0.196634D+01	-0.324233D+01	0.569031D+01	0.438887D+02	-0.103955D+03
17	-0.136516D+01	0.181764D+01	-0.205122D+01	-0.178518D+02	0.468373D+02
18	-0.760209D+00	0.400459D+01	-0.533443D+01	-0.412454D+02	0.100865D+03
19	-0.657622D-02	0.438547D+00	0.190370D+01	0.159833D+02	-0.413825D+02
20	-0.110105D+02	0.105381D+02	-0.171770D+01	-0.168525D+02	0.422231D+02
21	0.708731D+01	-0.528209D+01	0.588428D+00	0.688625D+01	-0.182308D+02
22	0.122293D+02	-0.106129D+02	0.201318D+01	0.195611D+02	-0.490411D+02
23	-0.590365D+01	0.493128D+01	-0.916688D+00	-0.872809D+01	0.221607D+02
24	-0.102811D+02	0.110055D+02	-0.183023D+01	-0.189416D+02	0.475199D+02
25	0.684809D+01	-0.523560D+01	0.841420D+00	0.788242D+01	-0.201275D+02
26	0.103416D+02	-0.838689D+01	0.219694D+01	0.198178D+02	-0.496555D+02
27	-0.330306D+01	0.450784D+01	-0.752724D+00	-0.823668D+01	0.214988D+02
28	-0.119787D+01	0.275893D+01	-0.223721D+01	0.375456D+01	-0.784496D+01
29	0.588725D+00	-0.914758D+00	0.106463D+01	-0.688469D+00	0.272502D+01
30	0.117149D+01	-0.864925D+00	0.246262D+01	-0.131603D+01	0.773131D+01
31	-0.626442D+00	0.701933D+00	-0.135239D+00	0.565177D+00	-0.366551D+01
32	-0.115620D+01	0.914946D+00	-0.134245D+01	0.165378D+01	-0.781556D+01
33	0.474458D+00	-0.416508D+00	0.276992D+00	-0.558382D+00	0.319395D+01
34	0.114306D+01	-0.772471D+00	0.257200D+01	-0.154652D+01	0.826778D+01
35	-0.587828D+00	0.380028D+00	-0.312313D-01	0.666097D+00	-0.352595D+01
36	-0.107217D+01	0.234784D+01	-0.158871D+01	0.242296D+01	-0.689809D+01
37	0.424458D+00	-0.319818D+00	0.948465D+00	-0.666645D+00	0.302393D+01

38	0.605878D+02	-0.395958D+01	0.336440D+00	-0.843491D+00	0.205659D+01
39	-0.976552D+01	0.264267D+01	-0.661189D-01	0.169258D+00	-0.398591D+00
40	-0.918100D+01	0.184877D+01	-0.626075D-01	0.185579D+00	-0.631863D+00
41	-0.978898D+01	0.988721D+01	-0.237029D+00	-0.817361D-01	0.960138D-01
42	0.181106D+01	-0.338502D+01	0.126880D+01	0.888609D+01	-0.265921D+02
43	0.148012D+00	-0.421994D+00	0.259846D+00	0.850353D+00	0.842185D+01
44	-0.172392D+00	0.370912D+00	-0.205796D-01	-0.865791D+00	0.432614D+01
45	-0.241979D+00	0.432389D+00	-0.176597D+00	-0.119020D+01	0.527288D+01
46	-0.190307D+01	0.335219D+01	0.184902D+01	-0.456500D+01	0.905896D+02
47	0.635547D+00	-0.119832D+01	0.182423D+00	0.445408D+01	-0.200194D+02
48	0.160403D+01	-0.336503D+01	0.192870D+01	0.110305D+02	-0.278287D+02

	11	**12**	**13**	**14**	**15**
11	0.000000D+00				
12	-0.726866D+00	0.000000D+00			
13	0.311918D+01	0.129217D+02	0.000000D+00		
14	-0.374123D+01	-0.333539D+00	0.985698D-01	0.000000D+00	
15	0.149918D+01	0.166536D+00	-0.849164D+00	0.156243D+03	0.000000D+00
16	0.385375D+01	0.771485D+00	0.127942D+01	0.913556D+02	-0.567610D+01
17	-0.180305D+01	-0.621530D+00	-0.171783D+01	-0.672119D+01	0.926067D+01
18	-0.359537D+01	-0.167479D+01	-0.492599D+00	0.292683D+01	0.406517D+01
19	0.172776D+01	0.332202D+00	-0.821935D+00	0.361791D+01	0.181998D+01
20	-0.154866D+01	0.159092D+02	-0.973537D+00	-0.211178D+01	0.992534D+00
21	0.657524D+00	-0.842944D+01	0.576799D+00	0.800340D+00	-0.701396D+00
22	0.174911D+01	-0.153552D+02	0.112683D+01	0.233412D+01	-0.126810D+01
23	-0.101919D+01	0.664743D+01	-0.754281D+00	-0.111780D+01	0.341675D+00
24	-0.173766D+01	0.157057D+02	-0.115392D+01	-0.226227D+01	0.108550D+01
25	0.748254D+00	-0.841283D+01	0.538943D+00	0.835695D+00	-0.837375D+00
26	0.178729D+01	-0.133609D+02	0.104771D+01	0.227425D+01	-0.125603D+01
27	-0.829037D+00	0.605869D+01	-0.608098D+00	-0.106605D+01	0.264571D+00
28	0.243515D+02	0.105288D+01	-0.211107D+01	0.656484D+01	-0.280449D+01
29	0.215311D+02	-0.462379D+00	0.606566D+00	-0.231197D+01	0.139076D+01
30	0.702852D+02	-0.107246D+01	0.175024D+01	-0.632052D+01	0.265721D+01
31	-0.215567D+02	0.318515D+00	-0.120167D+01	0.296235D+01	-0.148750D+01
32	-0.666244D+02	0.979005D+00	-0.171254D+01	0.642012D+01	-0.280134D+01
33	0.279886D+02	-0.739964D+00	0.582286D+00	-0.280234D+01	0.106096D+01
34	0.705159D+02	-0.113001D+01	0.164269D+01	-0.666894D+01	0.277947D+01
35	-0.226866D+02	0.250555D+00	-0.739119D+00	0.288880D+01	-0.168207D+01
36	0.267022D+02	0.107267D+01	-0.173559D+01	0.608889D+01	-0.262880D+01
37	0.211160D+02	-0.647407D+00	0.169785D+01	-0.267360D+01	0.990001D+00
38	-0.363946D+00	-0.881341D+01	0.996638D+00	0.306781D+00	-0.108788D+00
39	0.934411D+00	0.425600D+01	-0.617196D+00	-0.813150D-01	-0.245880D+00
40	0.125460D+00	0.146974D+02	0.166079D+00	-0.106633D+00	-0.284647D+00

41	0.462553D+00	0.627977D+01	-0.168371D+01	0.286393D-01	-0.276053D+00
42	0.928867D+00	0.263423D+01	0.496687D+01	0.192503D+02	-0.835699D+01
43	0.594373D-01	0.171635D+00	0.174476D+00	0.172608D+01	-0.672099D+00
44	-0.112392D+00	0.371353D-01	-0.786148D+00	-0.189186D+01	0.699607D+00
45	-0.184137D+00	-0.356668D-01	-0.917834D+00	-0.229283D+01	0.194784D+01
46	-0.133389D+01	-0.274967D+01	-0.537394D+01	-0.191666D+02	0.940070D+01
47	0.318613D+00	0.858754D+00	0.159899D+01	0.731126D+01	-0.384599D+01
48	0.724545D+00	0.246148D+01	0.500789D+01	0.187905D+02	-0.791752D+01

	16	**17**	**18**	**19**	**20**
16	0.000000D+00				
17	0.162654D+03	0.000000D+00			
18	0.915419D+02	-0.749229D+01	0.000000D+00		
19	-0.563808D+01	0.913718D+01	0.157613D+03	0.000000D+00	
20	0.309878D+01	-0.163249D+01	-0.475235D+01	0.178472D+01	0.000000D+00
21	-0.141256D+01	0.840691D+00	0.267178D+01	-0.277919D+00	0.131704D+03
22	-0.370131D+01	0.172099D+01	0.659651D+01	-0.210018D+01	0.283018D+02
23	0.163137D+01	-0.103814D+01	-0.338866D+01	0.110764D+01	0.205357D+02
24	0.353647D+01	-0.178588D+01	-0.657315D+01	0.197474D+01	0.611966D+02
25	-0.158046D+01	0.519258D+00	0.289636D+01	-0.109098D+01	-0.203570D+02
26	-0.352253D+01	0.170236D+01	0.700276D+01	-0.211527D+01	-0.577218D+02
27	0.158751D+01	-0.117731D+01	-0.303481D+01	0.678347D+00	0.241614D+02
28	-0.690834D+01	0.308187D+01	0.657125D+01	-0.289495D+01	0.268823D+01
29	0.236876D+01	-0.142443D+01	-0.237320D+01	0.847232D+00	-0.113206D+01
30	0.661364D+01	-0.305876D+01	-0.628354D+01	0.271243D+01	-0.263184D+01
31	-0.320336D+01	0.129118D+01	0.295823D+01	-0.163005D+01	0.131300D+01
32	-0.675668D+01	0.304000D+01	0.638791D+01	-0.287309D+01	0.267275D+01
33	0.284782D+01	-0.166755D+01	-0.282624D+01	0.109229D+01	-0.121595D+01
34	0.697928D+01	-0.322926D+01	-0.663779D+01	0.287626D+01	-0.277653D+01
35	-0.312587D+01	0.134065D+01	0.291275D+01	-0.148700D+01	0.130131D+01
36	-0.639362D+01	0.280490D+01	0.604577D+01	-0.264060D+01	0.250638D+01
37	0.274334D+01	-0.150378D+01	-0.265564D+01	0.121150D+01	-0.113168D+01
38	-0.774789D-01	-0.795110D-01	-0.278145D-01	-0.110103D+00	0.156296D+01
39	-0.493926D-01	-0.258766D+00	-0.243062D-02	-0.262157D+00	-0.482196D+00
40	-0.661895D-01	-0.314141D+00	-0.213862D-01	-0.222520D+00	-0.698486D+00
41	-0.746702D-01	-0.254282D+00	0.444823D-01	-0.262558D+00	-0.654806D+00
42	-0.200577D+02	0.954275D+01	0.190623D+02	-0.876591D+01	0.821750D+01
43	-0.198482D+01	0.874643D+00	0.178930D+01	-0.116249D+01	0.755677D+00
44	0.183719D+01	-0.129585D+01	-0.181111D+01	0.752519D+00	-0.971845D+00
45	0.263422D+01	-0.118584D+01	-0.240339D+01	0.104378D+01	-0.946179D+00
46	0.207287D+02	-0.104043D+02	-0.197740D+02	0.928127D+01	-0.848929D+01
47	-0.755201D+01	0.346135D+01	0.703494D+01	-0.343370D+01	0.294491D+01
48	-0.194177D+02	0.973913D+01	0.184124D+02	-0.902553D+01	0.798331D+01

	21	22	23	24	25
21	0.000000D+00				
22	0.197010D+02	0.000000D+00			
23	-0.317744D+01	0.133761D+03	0.000000D+00		
24	-0.199731D+02	0.269240D+02	0.201114D+02	0.000000D+00	
25	0.128794D+02	0.204053D+02	-0.348323D+01	0.132897D+03	0.000000D+00
26	0.241933D+02	0.591784D+02	-0.195661D+02	0.272038D+02	0.212436D+02
27	-0.129271D+02	-0.192957D+02	0.124095D+02	0.199026D+02	-0.331248D+01
28	-0.129272D+01	-0.313319D+01	0.153080D+01	0.303787D+01	-0.141455D+01
29	0.340583D+00	0.122352D+01	-0.803005D+00	-0.126988D+01	0.507751D+00
30	0.116797D+01	0.302682D+01	-0.157865D+01	-0.296836D+01	0.130384D+01
31	-0.798018D+00	-0.160095D+01	0.596072D+00	0.148185D+01	-0.814908D+00
32	-0.128264D+01	-0.311124D+01	0.153517D+01	0.302179D+01	-0.139121D+01
33	0.450163D+00	0.134030D+01	-0.824688D+00	-0.136435D+01	0.521514D+00
34	0.124873D+01	0.320684D+01	-0.165400D+01	-0.313049D+01	0.139073D+01
35	-0.738183D+00	-0.152107D+01	0.657947D+00	0.148805D+01	-0.727861D+00
36	-0.117406D+01	-0.291050D+01	0.140333D+01	0.283122D+01	-0.129289D+01
37	0.567227D+00	0.140994D+01	-0.737064D+00	-0.127030D+01	0.621598D+00
38	-0.588094D+00	-0.143298D+01	0.651319D+00	0.180224D+01	-0.890459D+00
39	0.196363D+00	0.791055D+00	-0.738226D+00	-0.944678D+00	0.120664D+00
40	0.622151D-01	0.628733D+00	-0.538790D+00	-0.679874D+00	0.314062D+00
41	-0.451928D-01	0.542988D+00	-0.527602D+00	-0.610243D+00	0.260089D+00
42	-0.390705D+01	-0.956191D+01	0.452707D+01	0.928780D+01	-0.420110D+01
43	-0.581946D+00	-0.962424D+00	0.296708D+00	0.862539D+00	-0.568718D+00
44	0.311113D+00	0.106720D+01	-0.681136D+00	-0.109659D+01	0.307797D+00
45	0.457980D+00	0.106552D+01	-0.730394D+00	-0.109627D+01	0.440698D+00
46	0.414118D+01	0.988430D+01	-0.496232D+01	-0.965608D+01	0.439538D+01
47	-0.170918D+01	-0.353779D+01	0.145385D+01	0.335363D+01	-0.180313D+01
48	-0.406563D+01	-0.936263D+01	0.448657D+01	0.905360D+01	-0.431353D+01

	26	27	28	29	30
26	0.000000D+00				
27	0.133695D+03	0.000000D+00			
28	-0.318702D+01	0.146828D+01	0.000000D+00		
29	0.124053D+01	-0.730302D+00	0.133764D+03	0.000000D+00	
30	0.307933D+01	-0.144552D+01	0.185336D+02	0.251984D+02	0.000000D+00
31	-0.162340D+01	0.594651D+00	0.255898D+02	-0.464557D+01	0.127674D+03
32	-0.315958D+01	0.146192D+01	0.734190D+02	-0.261728D+02	0.118432D+02
33	0.136201D+01	-0.797183D+00	-0.265234D+02	0.158435D+02	0.269131D+02
34	0.326967D+01	-0.148536D+01	-0.710212D+02	0.311192D+02	0.720385D+02
35	-0.151667D+01	0.824810D+00	0.298775D+02	-0.164862D+02	-0.244726D+02
36	-0.294209D+01	0.138487D+01	0.748691D+02	-0.288246D+02	-0.694839D+02

37	0.152463D+01	-0.351043D+00	-0.272434D+02	0.169896D+02	0.293045D+02
38	0.141756D+01	0.111140D+01	0.766116D+00	-0.383095D+00	-0.739348D+00
39	0.153817D+01	-0.104321D+01	-0.247664D+00	0.497850D+00	0.570598D+00
40	0.774843D+00	0.130763D+00	0.862839D-01	-0.210250D+00	-0.380475D-01
41	0.808550D+00	0.171328D+00	-0.421202D+00	-0.140936D-01	0.405809D+00
42	-0.966402D+01	0.453347D+01	-0.178273D+01	0.786354D+00	0.173482D+01
43	-0.969925D+00	0.340355D+00	-0.275414D+00	0.114120D+00	0.211881D+00
44	0.109063D+01	-0.578594D+00	0.189803D+00	0.341737D+00	-0.164335D+00
45	0.109128D+01	-0.688817D+00	0.188914D+00	-0.162104D+00	-0.263917D+00
46	0.999714D+01	-0.493921D+01	0.177587D+01	-0.670570D+00	-0.177064D+01
47	-0.356409D+01	0.161766D+01	-0.595813D+00	0.952335D+00	0.649749D+00
48	-0.947402D+01	0.446041D+01	-0.144640D+01	0.476535D+00	0.128521D+01

	31	**32**	**33**	**34**	**35**
31	0.000000D+00				
32	0.258196D+02	0.000000D+00			
33	-0.649633D+01	0.128093D+03	0.000000D+00		
34	-0.244137D+02	0.133728D+02	0.267384D+02	0.000000D+00	
35	0.154822D+02	0.256515D+02	-0.629424D+01	0.127010D+03	0.000000D+00
36	0.289905D+02	0.727117D+02	-0.256298D+02	0.180737D+02	0.264011D+02
37	-0.155026D+02	-0.254301D+02	0.148903D+02	0.235408D+02	-0.485286D+01
38	0.315378D+00	0.741989D+00	-0.399206D+00	-0.746022D+00	0.327127D+00
39	-0.195323D+00	-0.429839D+00	-0.236392D-01	0.576956D+00	-0.305576D+00
40	-0.265688D+00	0.918384D-01	-0.600773D-01	0.172783D+00	0.252740D+00
41	-0.461252D+00	-0.434004D+00	-0.441418D-01	0.449389D+00	-0.428329D+00
42	-0.899903D+00	-0.177966D+01	0.784153D+00	0.182103D+01	-0.917549D+00
43	-0.214700D+00	-0.283385D+00	-0.433640D-01	0.202461D+00	-0.314871D+00
44	0.125713D+00	0.148518D+00	-0.196850D+00	-0.210293D+00	-0.562165D-01
45	-0.642490D-01	0.181581D+00	-0.290846D+00	-0.281608D+00	-0.736419D-01
46	0.876207D+00	0.178522D+01	-0.874717D+00	-0.186699D+01	0.865033D+00
47	-0.201123D+00	-0.656858D+00	0.194925D+00	0.619666D+00	-0.506158D+00
48	-0.836811D+00	-0.142251D+01	0.448408D+00	0.140473D+01	-0.849658D+00

	36	**37**	**38**	**39**	**40**
36	0.000000D+00				
37	0.127522D+03	0.000000D+00			
38	0.124073D+01	0.808368D-01	0.000000D+00		
39	-0.223046D+00	0.241667D+00	0.157860D+03	0.000000D+00	
40	0.546264D+00	0.996378D+00	0.157904D+03	-0.305444D+02	0.000000D+00
41	-0.140598D+00	0.227814D+00	0.153278D+03	-0.308813D+02	-0.293509D+02
42	-0.163117D+01	0.760453D+00	0.428339D+00	-0.903924D-01	-0.142280D+00
43	-0.278649D+00	-0.997010D-01	0.361945D-02	-0.111183D+00	-0.232918D+00
44	0.131653D+00	-0.230970D+00	-0.301723D-01	0.255691D+00	-0.905617D-01

45	0.170652D+00	-0.231394D+00	-0.705734D-01	0.174815D-01	-0.155483D+00
46	0.175778D+01	-0.852207D+00	-0.487629D+00	0.101382D+00	0.588933D-01
47	-0.625132D+00	0.778993D-01	0.128696D+00	-0.393489D-01	-0.235229D+00
48	-0.114836D+01	0.433168D+00	0.397705D+00	-0.267487D+00	-0.336626D+00

	41	**42**	**43**	**44**	**45**
41	0.000000D+00				
42	-0.127842D-01	0.000000D+00			
43	-0.174853D+00	0.151130D+03	0.000000D+00		
44	0.149604D-01	0.157367D+03	-0.303452D+02	0.000000D+00	
45	-0.651258D-01	0.153271D+03	-0.299869D+02	-0.301845D+02	0.000000D+00
46	-0.582480D-01	0.599358D+02	-0.838052D+01	-0.100035D+02	-0.102002D+02
47	-0.190357D+00	-0.121384D+02	0.425063D+01	0.626179D+01	0.162194D+02
48	-0.225845D+00	-0.141530D+02	0.474729D+01	0.157000D+02	0.480761D+01

	46	**47**	**48**
46	0.000000D+00		
47	0.169704D+03	0.000000D+00	
48	0.168049D+03	-0.314031D+02	0.000000D+00

Chapter 5

Two-Step Synthesis of the Reported Structure of Xylopyridine A, Precursor to New Fluorescent Probes

This work was performed in collaboration with Dr. Mai N. Tran, a previous graduate student in the Chenoweth group at the University of Pennsylvania.

5.1 Introduction

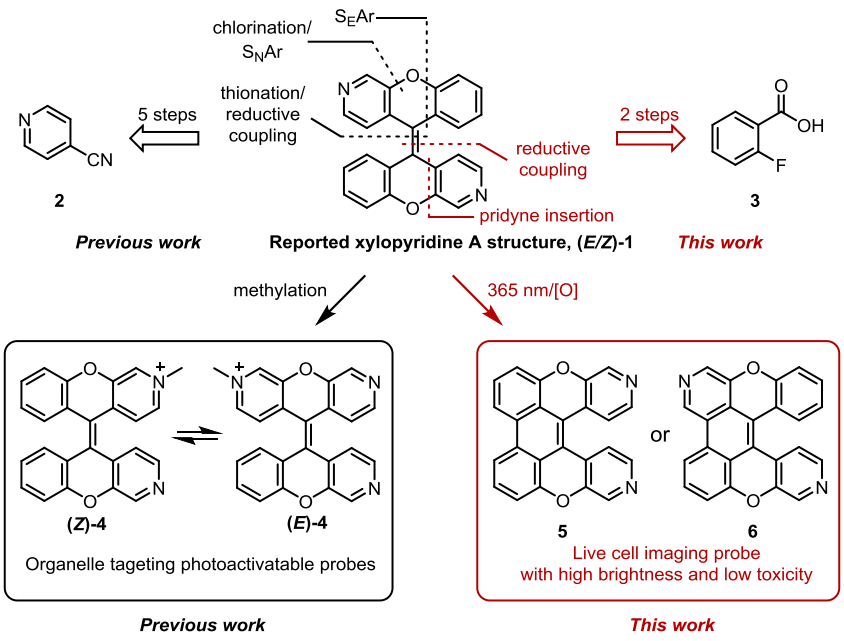

Figure 5.1. New route for the synthesis of the reported structure of xylopyridine A, **(*E*/*Z*)-1** and applications of the derivatives.

Recently, we synthesized the reported structure of the natural product xylopyridine A **(*E*/*Z*)-1** in five steps from 4-cyanopyridine **2** (Fig. 5.1). To our surprise, the reported structure of xylopyridine A was inconsistent with all characterization data obtained for the originally proposed 2,2'-diazaxanthilidene structure (***E*-1**).[1] Despite this unexpected finding, we discovered that the 2,2'-diazaxanthilidene scaffold has fascinating potential for applications in structure-specific nucleic acid binding[1] and in the development of photoactivatable fluorophores[2] for live cell optical imaging applications (Fig. 5.1). Fluorescent dyes have been developed for many in vivo or in vitro labeling and tracking applications over the last 10

decades.[3] For certain applications, small molecule organic dyes can be advantageous over biological fluorophores and quantum dots due to their low molecular weight and potential for live cell, tissue, and whole organism imaging without genetic manipulation even though toxicity can be a major issue.[3,4] As a result, photostability and live cell imaging compatibility have become some of the most desirable properties of small-molecule fluorescent dyes for optical imaging applications in biology. Herein, we report a two-step synthesis of (*E/Z*)-**1** using a commercially available pyridyne precursor **7** and 2-fluorobenzoic acid **3**. We show that (*E/Z*)-**1** can be efficiently converted into two photoproducts **5** and **6** using a photoelectrocyclization/oxidation reaction. Furthermore, we show that photoproducts **5** and **6** are photostable, cell-permeability, non-cytotoxic, and compatible with live cell imaging studies.

5.2 Results and Discussion

Scheme 5.1. Two-step synthesis of (*E/Z*)-1.

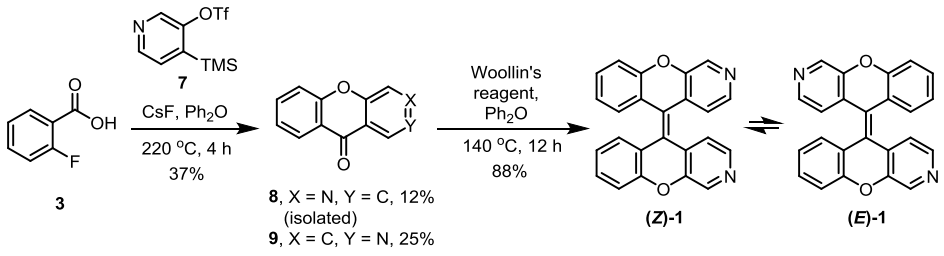

In an effort to minimize the number of chemical steps and allow rapid access to (*E/Z*)-**1**, we envisioned the retrosynthesis outlined in Fig. 1. In the first step of the synthesis, 3,4-pyridyne precursor **7** was chosen to react with 2-fluorobenzoic acid **3**. Pyridyne precursor **7** is

commercially available or can be prepared in a straightforward fashion.[5] A pyridyne insertion reaction with **3** resulted in the desired azaxanthone **8** and its isomer **9**. The resulting azaxanthone **8** underwent a tandem selenation/reductive coupling reaction to give (*E/Z*)-**1**. In our recently reported study on the structure of xylopyridine A, we developed a three-step synthesis of the key intermediate 3-azaxanthone **8** from 4-cyanopyridine **2**.[1] In our current one step protocol we produce not only our desired 3-azaxanthone **8** but also the 2-azaxanthone isomer **9.** Azaxanthone isomer **9** is an important substructure that is embedded in several natural products such as SB236049, diaporphasine A-D, and 7-hydroxy-8-methoxy-3-methyl-10-oxo-10*H*-chromeno[3,2-*c*]pyridine-9-carboxylic acid (Fig. 5.6).[6] Among the several known synthesis of 2-azaxanthone **9**,[7] the three step synthesis from 4-fluoropyridine is one of the most efficient.[7a] Here, we describe a new directsynthesis of azaxanthone **8** and **9** by pyridyne insertion into 2-fluorobenzoic acid **3**. We conducted a thorough reaction optimization study in an effort to define conditions for the pyridyne insertion reaction (Table 5.2). Rather than **3**, all alternative 2-halobenzoic acids were examined for optimization but no other halogen substituents resulted in improved yields over the fluorine substituent, as expected based on the inverse element effect observed in S_NAr chemistry (entry 1-7, Table 5.2). Common fluoride sources such as tetra-*n*-butylammonium fluoride (TBAF) and CsF were tested for pyridyne insertion reaction, and CsF afforded the desired product **8** in relatively higher yield (entry 7-9, Table 5.2). Cs_2CO_3 as a basic additive for a deprotonation step made the total yield of **8** and **9** drop (entry 1, 2, 4, and 6, Table S1) even if the ratio of the two isomers was changed in some case (entry 4, Table 5.2). Most of the reaction conditions consistently gave **9** as a major product. Due to the required high reaction temperature (i.e., above 140 °C) for the completion of the reaction, *o*-Xylene and Ph_2O

wereemployed as the solvents. At identical temperatures (140 °C), Ph_2O resulted in higher yields than *o*-xylene (entries 10 and 11, Table 5.2). As a limiting reagent, **3** was chosen rather than **7** but the yield of **8** did not improve (entries 12-15, Table 5.2). Recently, the Daugulis group reported a new benzyne precursor that possesses a silylaryl halide scaffold and allows for the use of mild conditions to generate benzyne.[8] Based on their studies, we prepared silylpyridyl bromide and performed the pyridine insertion reaction. However, no improvement in the yield of **8** was observed (Entries 16 and 17, Table 5.2). Rather than the insertion to benzoic acid, a reaction with methyl 2-hydroxybenzoate was also conducted but did not increase the yield of **8** (entries 18-22, Table 5.2). The best yield of the desired product **8** was achieved by employing the reaction of **3** and **7** with CsF in Ph_2O at 220 °C for 4 hours (entry 7, Table 5.2).

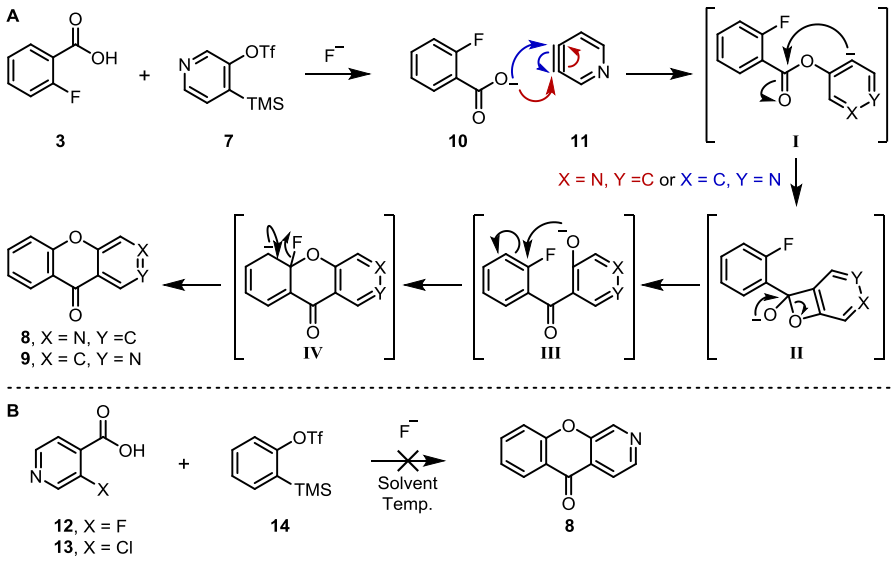

Figure 5.2. A. Proposed mechanism of pyridine insertion reaction. B. Attempt to synthesize **8** via benzyne insertion reaction.

A plausible pyridyne insertion mechanism is described in Fig. 5.2A. The fluoride anion has a dual role in the first mechanistic step. First, after this anion deprotonation of the carboxylic group of benzoic acid **3** and generation of pyridine **11**, Carboxylate **10** undergoes nucleophilic addition to pyridyne **11**. The resulting *p*- or *m*-pyridinide anion on intermediate **I** is added to the ester carbon to form four-membered intermediate **II**. After rearrangement, a phenoxide anion on **III** attacks the carbon adjacent to the leaving group to form the *ipso*- carbon-bearing intermediate **IV**. To restore the aromaticity, elimination occurs to afford the desired 3- and 2-azaxanthone **8** and **9**. Larock et al. reported a benzyne insertion reaction to 2-fluorobenzoic acid to afford acridone.[9] Furthermore, they successfully synthesized 4-azaxanthone from 2-chloronicotinic acid in 22% yield. However, synthesis of 3-azaxanthone **8** has not been achieved

Table 5.1. Optimization of Reductive Coupling Reaction of 8.

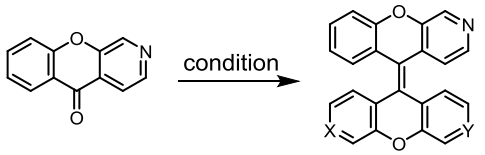

8 **(*E*/*Z*)-1** (X or Y = N)

entry	condition (eq)	solvent	conc. (M)	temp (°C)	time (h)	yield (%)[c]
1	Woollins' (1.0), **8** (2.2)[a]	toluene	0.05	100	12	35
2	Woollins' (1.0), **8** (2.2)[a]	*o*-xylene	0.05	100	12	25
3	Woollins' (1.0), **8** (2.2)[a]	Ph_2O	0.05	100	12	65
4	Woollins' (1.0), **8** (2.2)[a]	toluene	0.05	140[b]	12	32
5	Woollins' (1.0), **8** (2.2)[a]	*o*-xylene	0.05	140	12	73
6	**Woollins' (1.0), 8 (2.2)[a]**	**Ph_2O**	**0.05**	**140**	**12**	**88**
7	Woollins' (1.0), **8** (2.2)[a]	Ph_2O	0.05	170	12	85
8	Zn (1.8), HCl (0.01)	AcOH	0.05	140	18	trace
9	$TiCl_4$ (5.0), Zn (10.0), pyridine (2.5)	THF	0.2	65	12	0

[a] Woollins' reagent was used as a limiting reagent. [b] Reaction was conducted in a sealed tube.
[c] Isolated yield.

utilizing this method. We surveyed various fluoride sources (TBAF, KF/18-crown-6, and CsF), two different isonicotinic acids (**12** and **13**), common solvents (THF, CH_3CN, toluene, and Ph_2O), and various temperatures ranging from 60 °C to 220 °C. However, no azaxanthone **8** was observed (Fig. 5.2B). After optimization, our best set of reaction conditions for pyridyne insertion, the reaction of **3** and **7** with CsF in Ph_2O at 220 °C within 4 hours, afforded the desired azaxanthone **8** in 12% yield and isomer **9** in 25% yield (Scheme 5.1).

Next, wee focused the optimization of a single step reductive coupling reaction to conclude our 2-step approach. In our previous report, the two discrete synthetic steps involving thionation of azaxanthone **8** followed by copper reductive coupling yielded (*E/Z*)-**1** in 73% over the two steps. We envisioned the possibility of a one-step homodimerization approach by utilizing Woollins' reagent, the selenium analog of Lawesson's reagent. The standard solvent often utilized for ketone-ketone homocoupling using Woollins' reagent is toluene at a temperature of approximately 100 °C.[10] A single example of a homo xanthone coupling has been reported using these standard conditions.[10] However, the results of our solvent screen clearly indicated that toluene was not the best solvent for the azaxanthone coupling reaction. Interestingly, the reaction in Ph_2O afforded a much higher yield of (*E/Z*)-**1** than that in toluene or xylene at 100 or 140 °C (entries 1-6, Table 5.1). To investigate the effect of the reaction temperature, the reaction was conducted in Ph_2O at 100, 140, and 170 °C (entries 3, 6, and 7, Table 5.1), and the best yield was obtained at 140 °C. In addition to the Woollins' reaction, two known homo ketone reductive coupling conditions including McMurry coupling were tested. However, only a trace amount of the desired product was obtained from Zn/HCl reductive

coupling (entries 8 and 9, Table 5.1). The best yield of **(*E/Z*)-1** was 88% utilizing our new Woollins' reagent homodimerization approach in Ph_2O at 140 °C for 12 hours.

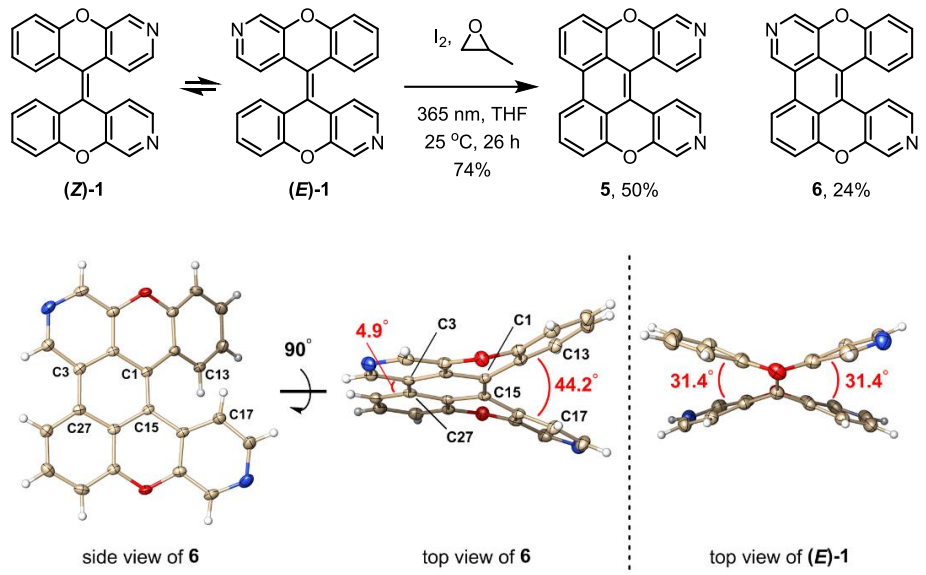

Figure 5.3. Photocyclization of (*E/Z*)-**1** and X-ray crystal structure of **6** and (*E*)-**1**. Thermal ellipsoids are drawn at the 50% probability level. Chloroform was omitted for clarity of the structure of **6**.

After successfully developing a rapid 2-step synthetic approach to access **(*E/Z*)-1**, we focused on optimization of the photocyclization reaction of **1** in an effort to rapidly access our newly discovered class of fluorescent dyes. Applying Katz's condition reported in 1991 for stilbene photocyclization,[11] a catalytic amount of iodine and excess methyloxirane were added to the solution of **(*E/Z*)-1** upon exposure to a 365 nm UV light from a Rayonet photoreactor (Fig. 5.3). The reaction successfully gave the two desired products in 74% yield with a 2:1 ratio of **5** and **6**. Based on a comparison of the x-ray structures of **1** and **6**, the red shifts in the absorption spectra (i.e., 76 nm) and emission spectra (39 nm) of **6** were due to the larger conjugated system

and an increase in planarity within the scaffold, which allows for greater electron delocalization throughout the extended π-system. The crystal structure of **6** revealed that the dihedral angle (C13-C1-C15-C17 angle) of 44.2° is much greater than that of 31.4° for **1**[1] (Fig. 5.3). However, on the opposite side, the dihedral angle (C3-C1-C15-C27 angle) of 4.9° is much less than that of 31.4° for **1**. Similar bathochromic shifts were also observed in **5**. The higher rigidity also reduces non-radiative bond rotation and remarkably improves quantum yield (Fig. 5.4). Both photoproducts have higher quantum yields than most of the well-known fluorophores, such as quinine, DAPI, Hoechst, Cy3n, and Cy5.[12,13] The photoconversion of **(*E*/*Z*)-1** into **5** and **6** was conducted in one pot. However, this conversion was composed of two mechanistic steps including photocyclization of **(*E*)-1** and **(*Z*)-1** to intermediates **5Int** and **6Int** bearing dihydrophenanthrene (for **5Int**) and dihydrobenzoisoquinoline (for **6Int**) followed by air oxidation to afford **5** and **6**. According to the relative ground-state free energy diagram obtained using the TD-B3LYP 6-31G(d) method on the center of Fig. 5.4, **5Int** and **6Int** (38.3 and 37.5 kcal/mol) are highly unstable compared to **(*E*/*Z*)-1**, **5**, and **6** (0.0, -0.6, -21.7, and -21.6 kcal/mol). The instability of **5Int** and **6Int** may prevent isolation during the reaction. By comparing the HOMO and LUMO levels of each molecule, the HOMO-LUMO gap of cyclized intermediates **5Int** and **6Int** (2.50 and 2.54 eV) was much narrower than those of pre- cyclized forms **(*Z*)-1** and **(*E*)-1** (3.70 and 3.71 eV) or post-oxidized forms **5** and **6** (3.14 and 3.18 eV).

To predict the UV/vis spectra of non-isolable intermediates **5Int** and **6Int**, the same basis set [TD-B3LYP 6-31G(d)] was employed (middle-left, -right, and bottom, Fig. 5.4). This method successfully predicted the wavelength at maximum absorption for **5** and **6** (454 and 451 nm from the experiment, 450 and 443 nm in theory) as well as **(*Z*)-1** and **(*E*)-1** (375 nm from

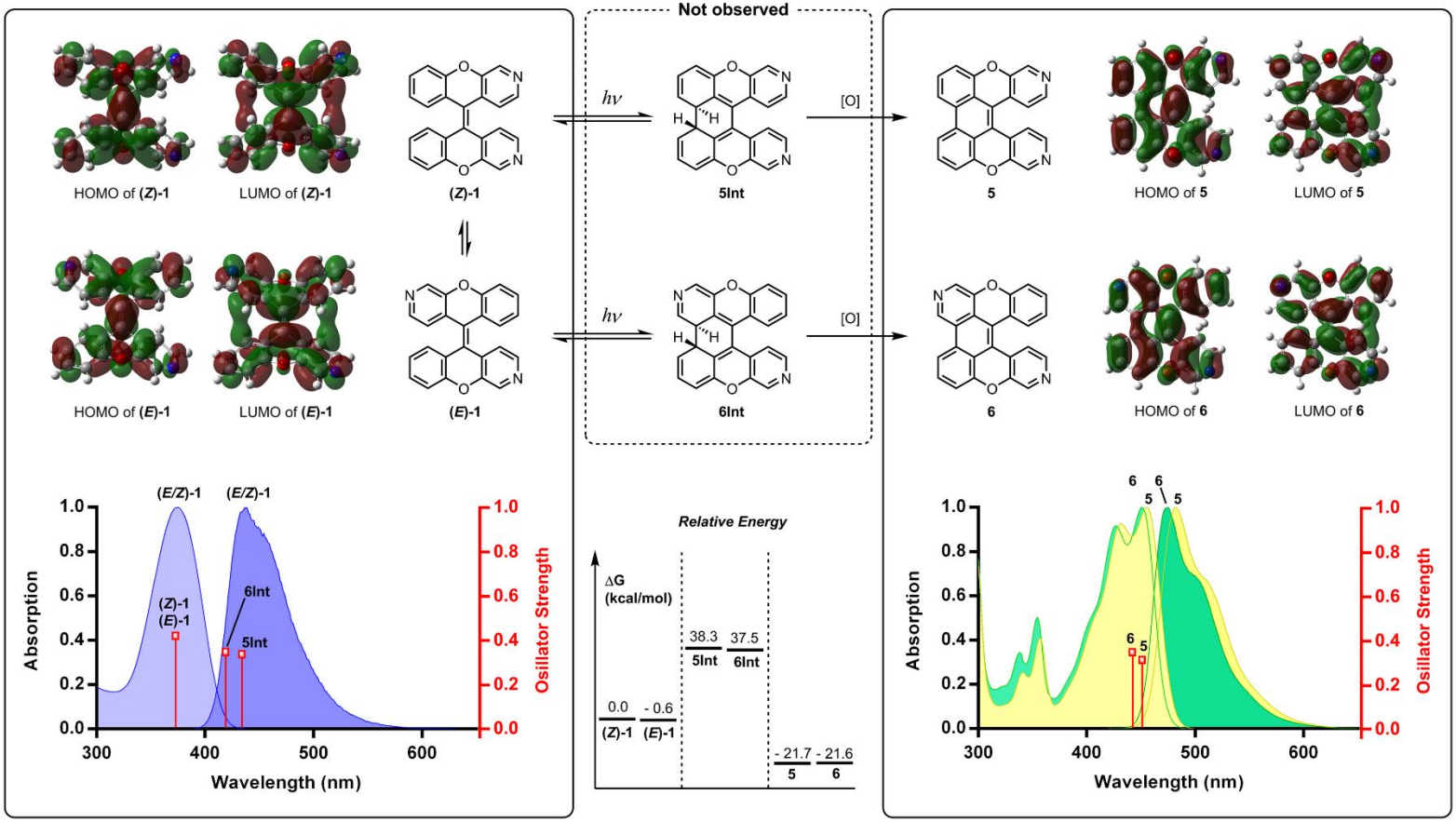

	Abs λ_{max} (nm)	Em λ_{max} (nm)	Abs λ_{calcd} (nm)[b]	f [a,b]	Excitation energy (eV)[b]	HOMO (eV)[b]	LUMO (eV)[b]	HOMO-LUMO energy gap (eV)[b]	Relative energy (kcal/mol)[c]	ε ($M^{-1}cm^{-1}$)	Φ_f	ε Φ_f ($M^{-1}cm^{-1}$)
(*Z*)-1	375	438	385	0.4432	3.30	- 5.74	- 2.04	3.70	0.0	16700	0.09	1500
5Int	-	-	434	0.3638	2.86	- 4.92	- 2.42	2.50	38.3	-	-	-
5	454	484	450	0.3573	2.76	- 5.35	- 2.21	3.14	- 21.7[d]	5000	0.73	3700
(*E*)-1	375	438	384	0.4545	3.23	- 5.74	- 2.03	3.71	- 0.6	16700	0.09	1500
6Int	-	-	418	0.3870	2.96	- 4.97	- 2.43	2.54	37.5	-	-	-
6	451	477	443	0.3748	2.80	- 5.37	- 2.19	3.18	- 21.6[d]	18100	0.80	14500

Figure 5.4 Overall photophysical properties and relative energy diagram of (*E*/*Z*)-**1**, **5**, and **6**. Frontier molecular orbitals of HOMO and LUMO of (*E*)-**1** and (*Z*)-**1** (upper-left corner) as well as **5** and **6** (upper-right corner) were depicted. Observed absorption and emission spectra of (*E*)-**1** and (*Z*)-**1** (middle-left corner) as well as **5** and **6** (middle-right corner) were shown. The height of each red marker represents the oscillator strength at each level of theory. Relative Gibbs free energy diagram describing each energy level of (*E*)-**1**, (*Z*)-**1**, **5Int**, **6Int**, **5**, and **6** was depicted on the center. Photophysical property of each molecule was depicted in the bottom. [a] Maximum oscillator strength in the range between 300 and 800 nm. [b] Calculations were performed with TD-B3LYP method and 6-31G(d) basis set in chloroform. [c] Geometrically obtimized at DFT B3LYP/6-311G+(2d,p) level. [d] Ground state energy of two hydrogen atoms were added to the calculated energy of **5** and **6**.

the experiment, 385 and 384 nm in theory). Encouraged by these results, the predicted maximum absorption wavelengths of **5Int** and **6Int** were observed at 434 and 418 nm. These molecules were expected to have longer absorption wavelengths than **5** and **6** due to their smaller HOMO-LUMO gaps. This result may be explained by predicting the set of excitation transitions for each molecule. The transition of an electron from the HOMO to the LUMO of ground-state **5** or **6** (MO = 93 to 94, Figure A4.11) is predominant among the other transitions to higher excited states. However, a combination of two or three different transitions of **5Int** or **6Int** including one major transition from HOMO to a higher excited state than LUMO (MO = 94 to 96, Figure A4.11) affects the excitation energy and results in a higher energy and shorter wavelengths compared to the expected result.

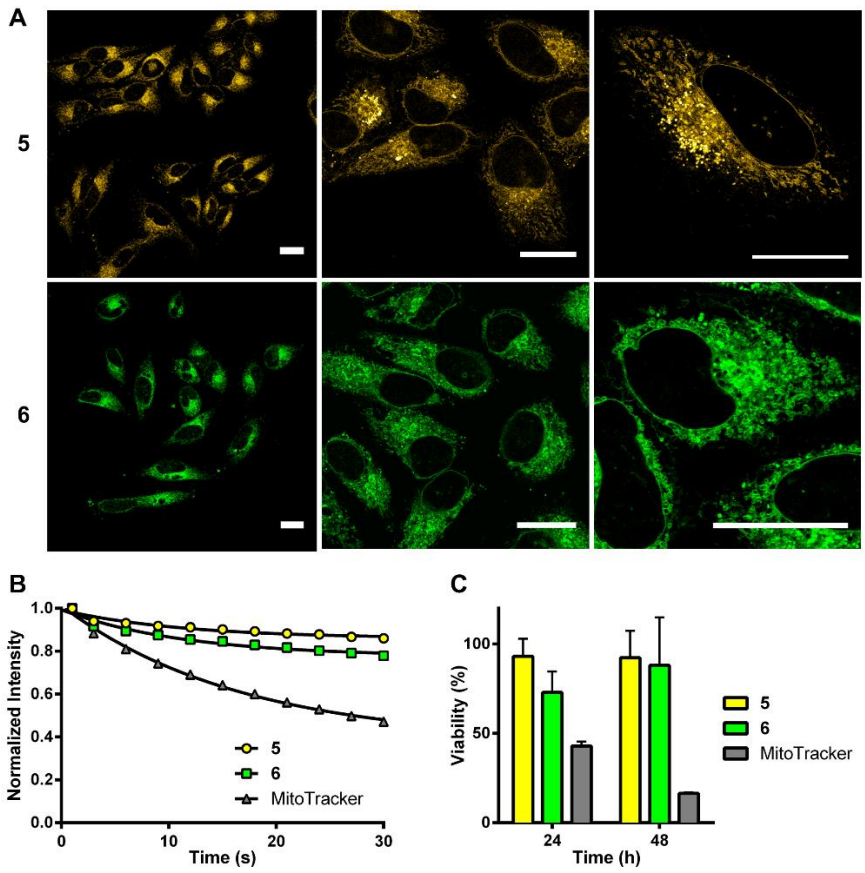

Figure 5.5. A. Fluorescence images of live HeLa cells stained with **5** (upper panels) and **6** (lower panels). A 488/495 channel was used to observed **5** and **6** in live HeLa cells. Scale bar = 25 μm. B. Normalized plot of the average intensity of **5**, **6**, and Mitotracker Red FM over 100 laser pulses (300 ms/scan). The 444/525 channel was used to observe **5** and **6**, and the 594/632 channel was used to observe MitoTracker Red FM. C. Viabililty assays of HeLa cells incubated with **5** (5 μM), **6** (5 μM), and MitoTracker Red FM (1 μM) at 37 °C in a humidified atmosphere with 5% CO_2 over 24 and 48 hours.

Based on confocal microscopy, both **5** and **6** were cell permeable and localized primarily in tubular networks in the cytoplasm of live HeLa cells (Fig. 5.5A). The 458/500 channel was

used to observe the two photoproducts **5** and **6**. A high fluorescent contrast was still observed. To investigate the photostability of **5** and **6**, time-lapse microscopy experiments using the 444/495 channel were carried out. After 100 scans (300 ms/scan), only a slight decrease in the intensity (10 to 20%) was detected for both **5** and **6**, indicating high resistance to photobleaching (Fig. 5.5B). In comparison, a similar experiment was performed using the 594/632 channel to observe MitoTracker Red FM[14], a commonly used commercially available mitochondrial stain. The dye was quite stable but only approximately 60% of the intensity remained at the end of the experiment. Cell viability assays in HeLa cells confirmed that both **5** and **6** exhibited very low cytotoxicities. The percent viabilities were close to 90% after 48 hours (Fig. 5.5C). These dyes provide a starting point for a new class of helicene-based fluorescent dye with low toxicity and many potential uses for live cell imaging.

5.3 Conclusions

In conclusion, the two-step synthesis of (*E/Z*)-**1**, which is the precursor for photoproducts **5** and **6**, was successfully performed. Using CsF as a fluoride ion source and Ph_2O as the solvent, the pyridyne insertion into 2-fluorobenzoic acid **3** was conducted at 220 °C for 4 hours, to afford both 3- and 2-azaxanthone (**8** and **9**). Employing the Woollin's reductive coupling reaction of **8**, the reported xylopyridine A structure (*E/Z*)-**1** was obtained in good yield. Photocylization of (*E/Z*)-**1** resulted in the two isomeric fluorescent molecules **5** and **6** which were found to be non-cytotoxic, cell-permeable, and photostable with high quantum

yields and are well-suited as a new scaffold for the development of fluorescent live cell imaging probes. Further investigations into the versatility of diazaxanthilidene scaffolds as new chemical tools for imaging and sensing are ongoing in our laboratory.

5.4 Experimental Section

General information:

Materials and spectroscopic methods.

The reagents for the syntheses were purchased from Sigma Aldrich or Acros and used without further purification. The solvents were purchased from Fisher Scientific or Sigma Aldrich. The anhydrous solvents were purchased from Fisher Scientific and dried by passing through an alumina column in a solvent purification system. The silica gel (230-400 mesh) that was used for column chromatography was purchased from Silicycle. Thin layer chromatography plates (250 μm thickness) were purchased from Sorbent Technologies or Merck. Reverse-phase column chromatography was performed using a Teledyne Isco CombiFlash Rf system equipped with a RediSep Rf Gold C18 column. High-performance liquid chromatography (HPLC) was performed on a Jasco HPLC system using a Phenomenex column (Luna 5u C18(2) 100A; 250 x 4.60 mm, 5 micron). The UV absorption spectra were recorded on a Jasco V-650 spectrophotometer using a 1 cm path length quartz cuvette. The fluorescence emission spectra were recorded on a Horiba Jobin-Yvon FluoroLog using a 1 cm path length fluorescence quartz cuvette. The ^{1}H NMR and ^{13}C NMR spectra were recorded on either a Bruker DMX 500 (500

MHz) or a Bruker AVII 500 (500 MHz). High-resolution mass spectrometry was performed by Dr. Rakesh Kohli at the University of Pennsylvania using a Waters LCT Premier XE Mass Spectrometer (model KE 332). X-Ray chromatography was performed by Dr. Pattrick Carroll at the University of Pennsylvania using a Bruker APEX2-DUO CCD X-Ray Diffractometer. The photoreactions were carried out in a Rayonet Photochemical Reactor (model RPR-100). The quantum yield was determined using the serial dilution method with fluorescein (in NaOH 0.1 M, $\Phi = 0.95$) as a reference.[12]

Cell imaging

For live cell imaging, HeLa cells (purchased from ATCC) were used. The cells were cultured in a 60 mm culture dish or a 75 cm^2 culture flask using Life Technologies Dulbecco's Modified Eagle Medium (DMEM) media with phenol red, 10% fetal bovine serum and 1% penicillin-streptomycin at 37 °C in a humidified atmosphere with 5% CO_2. The cells were detached with 0.05% trypsin-EDTA and transferred to a 35 mm glass-bottom poly-D-lysine coated dish 2 days prior to imaging with approximately 2 mL of the previously mentioned media. Four microliters of a 1.5 mM solution of **5** and **6** in MiliQ water was mixed with 2 mL of new media and added to the cells after the old media was removed. After incubation for 12 hours, the excess dyes were washed twice with DMEM without phenol red prior to imaging. The cells were maintained in 1 mL of non-phenol red DMEM during imaging. A Leica DMI 6000B inverted microscope equipped with a 100x oil immersion HCX PL APO (1.46 NA; correction collar), 63x oil immersion HCX PL APO CS (1.40-0.60 NA; variable iris), and 20x dry HC PLAN APO (0.70 NA) was used to record the images shown in Fig. 4. A Leica DM4000

spinning disk confocal microscope equipped with a 100x/1.4 NA oil immersion objective was used to obtain the images shown in Figs. S1-S3. All image processing was performed by using Fiji.

Cytotoxicity studies

In a 96-well plate, HeLa cells were plated at 5,000 cells/well in the previously mentioned culture media (50 μL/well) and incubated at 37 °C in a humidified atmosphere with 5% CO_2. After 24 hours, the cells were treated with **5** and **6** (final concentration of 5 μM) as well as MitoTracker Red FM[14] (final concentration 1 μM) and DMSO (vehicle control for MitoTracker). For wells treated with MitoTracker and DMSO, the DMSO concentration was maintained at 1%. Untreated cells were used as a vehicle control for **5** and **6**. The final volumes were 100 μL/well. The cells were incubated at 37 °C in 5% CO_2 for 24 or 48 hours. Alamar Blue (10 μL) was added 2 hours prior to the fluorescence measurement. Fluorescence was measured at an excitation wavelength of 560 nm and an emission wavelength of 590 nm. The vehicle control was taken as 100% cell viability.

Computational details

All theoretical calculations were performed using Gaussian09.[15] The optimized structures of **(*E*)-1** and **(*Z*)-1** [B3LYP/6-311+G(2d,p)] were taken from our previous publication.[1] All other structures (**5Int**, **6Int**, **5**, and **6**) were optimized at the B3LYP method

with the 6-311+G(2d,p) basis sets. The TD-DFT calculations of **(*E*)-1**, **(Z)-1**, **5Int**, **6Int**, **5**, and **6** were performed at the B3LYP/6-31G(d) level in chloroform.

Experimental procedures

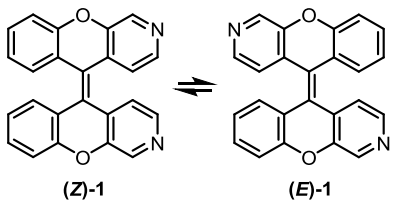

(*E/Z*)-3,3′-Diazaxanthylidene (1): A 4 mL vial was charged with 42 μmol of **8** (8.3 mg) from the stock solution of **8**. 19 μmol of Woollins' reagent (10.1 mg) and 840 uL of Ph_2O was added to the vial inside the glovebox. Outside the glovebox, the resulting mixture was heated to 140 °C in a dark room. After 12 hours, the solution was cooled and purified using flash column chromatography (50% acetate/hexane to 100% acetone) to afford **1** (6.1 mg, 88%). The characterization data for **1** was reported in our previous publication.[1]

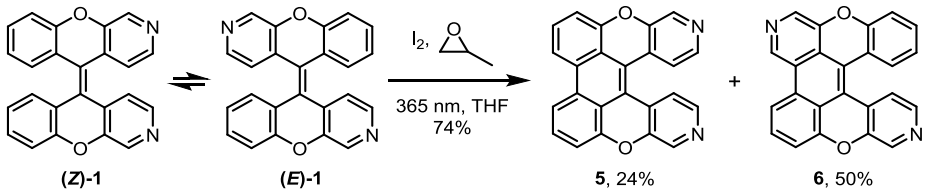

The photolysis of **1** was performed using a modified version of a procedure reported by Katz et al.[11] An oven-dried 25 mL vial was charged with a solution of ***(E)*-1/*(Z)*-1** (96.0 mg, 265 μmol) in 20 mL of THF and 1 mL of methyloxirane. A very small amount of iodine (sub-stoichiometric) was added to the solution before capping and irradiating the vial with 365 nm light in a Rayonet photoreactor for 26 h. The crude mixture was rotary evaporated to dryness on

Celite. Reverse-phase chromatography was used with acetonitrile and 0.1% TFA as the eluents to separate a mixture of protonated **5** and **6** from protonated **1**. The protonated mixture of **5** and **6** was transferred to a separatory funnel, treated with saturated sodium bicarbonate, and extracted with chloroform. Then, the mixture was separated on normal-phase silica gel using 50% dichloromethane/ethyl acetate to afford **5** (48.0 mg, 50%) and **6** (23.0 mg, 24%). Basification and chloroform extraction of the protonated **1** solution provided 9.7 mg of pure recovered **1** (10 mg, 10%).

For **5**:

^{1}H NMR (500 MHz, $CDCl_3/CD_2Cl_2$): δ (ppm) 8.65 (s, 2H), 8.21 (d, 2H, J = 5.3 Hz), 8.13 (d, 2H, J = 7.8 Hz), 7.73 (d, 2H, J = 5.3 Hz), 7.62 (t, 2H, J = 8.0 Hz), 7.31 (dd, 2H, J = 8.0, 0.9 Hz).

^{13}C NMR (125 MHz, $CDCl_3$): δ (ppm) 150.4, 149.0, 143.6, 141.3, 130.4, 128.8, 127.6, 121.4, 119.8, 117.7, 117.5, 113.0.

IR (neat): 3042, 2921, 1588, 1487, 1459, 1420, 1412, 1292, 781, 759 cm^{-1}.

HRMS (m/z): $[M+H]^+$ calcd for $C_{24}H_{13}N_2O_2^+$, 361.0972; found, 361.0975.

Meting point 275-278 °C.

Extinction coefficient (ε) = 4986 $M^{-1}.cm^{-1}$ (solvent: chloroform).

Quantum yield (Φ) = 0.734 (solvent: chloroform, standard: fluorescein in NaOH 0.1 M).

For **6**:

^{1}H NMR (500 MHz, $CDCl_3$): δ (ppm) 9.41 (s, 1H), 8.62 (s, 1H), 8.55 (s, 1H), 8.23-8.17 (m, 2H), 7.90 (dd, 1H, J = 8.0, 1.5 Hz), 7.81 (d, 1H, J = 5.3 Hz), 7.63 (t, 1H, J = 8.0 Hz), 7.42-7.37 (m, 1H), 7.32 (dd, 1H, J = 7.9, 1.0 Hz), 7.29 (dd, 1H, J = 8.3, 1.3 Hz), 7.05-7.00 (m, 1H).

^{13}C NMR (125 MHz, $CDCl_3$): δ (ppm) 152.9, 150.5, 149.2, 146.4, 143.6, 141.3, 140.0, 132.8, 131.5, 129.0, 128.3, 127.9, 127.2, 125.8, 124.1, 123.4, 122.2, 120.1, 119.7, 119.0, 118.5, 118.4, 117.0, 113.7.

IR (neat): 2921, 1733, 1452, 1417, 1275, 1198, 813, 765, 605 cm^{-1}.

HRMS (m/z): $[M+H]^+$ calcd for $C_{24}H_{13}N_2O_2^+$, 361.0972; found, 361.0985.

Meting point 280-283 °C.

Extinction coefficient (ε) = 18085 $M^{-1}.cm^{-1}$ (solvent: chloroform).

Quantum yield (Φ) = 0.796 (solvent: chloroform, standard: fluorescein in NaOH 0.1 M).

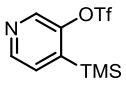

7

4-(trimethylsilyl)pyridin-3-yl trifluoromethanesulfonate (7): 7 was prepared according to the literature procedure.[5]

^{1}H NMR (500 MHz, $CDCl_3$): δ (ppm) 8.57 (s, 1H), 8.53 (d, 1H, J = 4.7 Hz), 7.44 (dd, 1H, J = 4.7, 0.4 Hz), 0.37 (s, 9H).

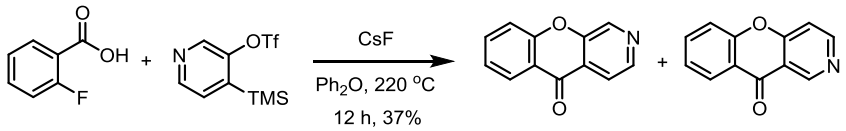

3 **7** **8**, 12% **9**, 25%

A 10 mL round-bottom flask was charged with 0.66 mmol of **3** (92.5 mg), 0.15 mmol of **7** (45.0 mg), and 1.16 mmol of CsF (176 mg) in 2.0 mL of Ph_2O and heated to 220 °C. After 12 hours, the solution was cooled and purified by flash column chromatography (100% hexane to 30% ethyl acetate/hexane) to afford **8** (3.5 mg, 12% yield) and **9** (7.3 mg, 25% yield).

For **8**:

The characterization data of **8** was reported in our previous publication.[1]

For **9**:

The characterization data of **9** have been previously reported in the literature.[16]

^{1}H NMR (500 MHz, $CDCl_3$): δ (ppm) 9.52 (s, 1H), 8.81 (d, 1H, J = 5.9 Hz), 8.35 (dd, 1H, J = 7.9, 1.6 Hz), 7.78 (ddd, 1H, J = 8.6, 7.4, 1.6 Hz), 7.53 (d, 1H, J = 8.4 Hz), 7.45 (d, 1H, J = 7.4 Hz), 7.39 (d, 1H, J = 5.9 Hz).

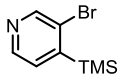

S1

3-bromo-4-(trimethylsilyl)pyridine (S1): S1 was prepared according to the literature procedure.[17]

^{1}H NMR (500 MHz, $CDCl_3$): δ (ppm) 8.64 (d, 1H, J = 0.6 Hz), 8.46 (d, 1H, J = 4.7 Hz), 7.31 (dd, 1H, J = 4.7, 0.6 Hz), 0.41 (s, 9H).

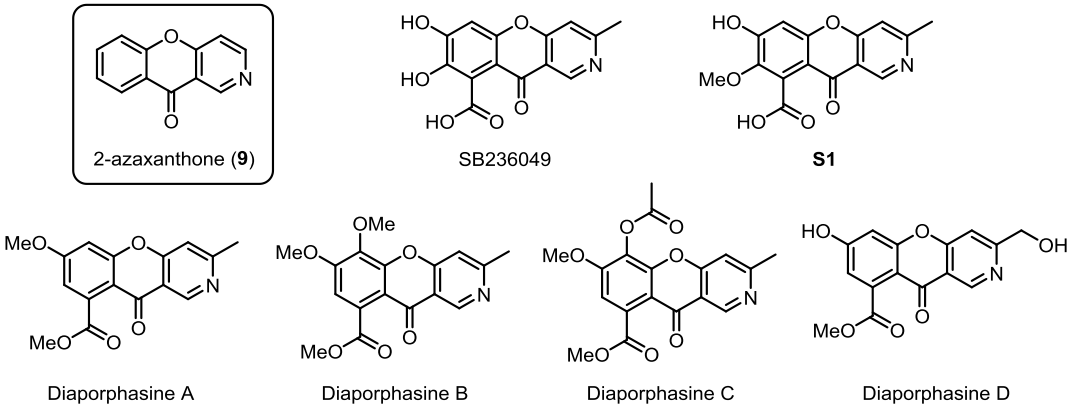

Figure 5.6. Structures of the natural product bearing a 2-azaxanthone (**9**) moiety.[6] **S1**, 7-hydroxy-8-methoxy-3-methyl-10-oxo-10*H*-chromeno[3,2-c]pyridine-9-carboxylic acid.

Table 5.2. Optimization of the Pyridyne Insertion Reaction[a].

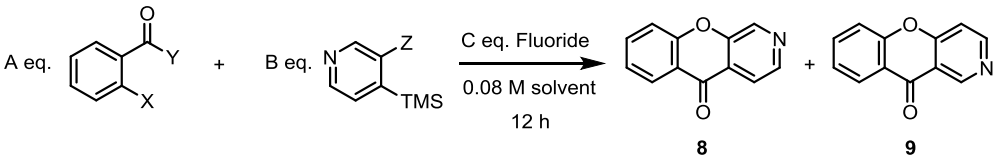

entry	A	B	C	X	Y	Z	additive	solvent	Fluoride	temp (°C)	**8** (%)[g]	**9** (%)[g]
1	4.4	1.0	7.7	I	OH	OTf	Cs_2CO_3	Ph_2O	CsF	220	5	14
2	4.4	1.0	7.7	Br	OH	OTf	Cs_2CO_3	Ph_2O	CsF	220	5	12
3	4.4	1.0	7.7	Br	OH	OTf	-	Ph_2O	CsF	220	6	19
4	4.4	1.0	7.7	Cl	OH	OTf	Cs_2CO_3	Ph_2O	CsF	220	4	2
5	4.4	1.0	7.7	Cl	OH	OTf	-	Ph_2O	CsF	220	8	25
6	4.4	1.0	7.7	F	OH	OTf	Cs_2CO_3	Ph_2O	CsF	220	5	8
7	4.4	1.0	7.7	F	OH	OTf	-	Ph_2O	CsF	220	(12)[h] 13	(25)[h] 25
8	4.4	1.0	7.7	F	OH	OTf	-	Ph_2O	TBAF	220[d]	1	2
9	4.4	1.0	7.7	F	OH	OTf	-	Ph_2O	TBAF	220[e]	1	3
10	4.4	1.0	7.7	F	OH	OTf	-	Ph_2O	CsF	140	4	15
11	4.4	1.0	7.7	F	OH	OTf	-	*o*-xylene	CsF	140	1	5
12	1.0	3.0	6.0	F	OH	OTf	-	Ph_2O	CsF	160	4	16
13	1.0	3.0	6.0	F	OH	OTf	-	Ph_2O	CsF	220	6	24
14	1.0	3.0	6.0	F	OH	OTf	Cs_2CO_3[c]	Ph_2O	CsF	220	4	19
15	1.0	3.0	6.0	F	OH	OTf	-	Ph_2O	CsF	80 to 220[f]	7	26
16	4.4	1.0	7.7	F	OH	Br	-	*o*-xylene	CsF	140	4	11
17	4.4	1.0	7.7	F	OH	Br	-	Ph_2O	CsF	220	2	5
18	1.0	1.1	4.0	OH	OCH_3	Br	-	THF	CsF	60	4	7
19	1.0	1.1	4.0	OH	OCH_3	Br	-	Ph_2O	CsF	220	2	1
20	1.0	1.1	4.0	OH	OCH_3	OTf	-	THF	CsF	60	0	1
21	1.0	5.0	4.0	OH	OCH_3	Br	-	THF	CsF	60	5	11
22	1.0	5.0[b]	4.0	OH	OCH_3	Br	-	THF	CsF	60	8	20

[a]All reactions were consistently performed on 0.15 mmol scale. [b] pyridyne precursor was added dropwise at 60 °C for 10 h. [c] 2-fluorobenzoic acid and Cs_2CO_3 were stirred in Ph_2O at 25 °C for 1 h. [d] TBAF was added dropwise at 25 °C. [e] TBAF was added dropwise at 220 °C. [f] After 12 h at 80 °C, the reaction temperature was raised to 220 °C for 12 h. [g] HPLC yield. [h] Isolated yield.

5.5 Acknowledgments

The authors gratefully acknowledge the support of the Vietnam Education Foundation for funding (VEF Fellowship to Mai N. Tran) and the NSF and NIH including HRMS (NIH RR-023444). We wish to thank Dr. Patrick Carroll for X-ray crystallographic assistance, Dr. Robert-André F. Rarig for his contribution to one of the initial studies, and Sergei Tcyrulnikov for helpful discussions on the computational studies.

5.6 References

(1) Rarig, R. F.; Tran, M. N.; Chenoweth, D. M. *J. Am. Chem. Soc.*, **2013**, *135*, 9213–9219.

(2) Tran, M. N.; Rarig, R. F.; Chenoweth, D. M. *Chemical Science*, **2015**, *6*, 4508–4512.

(3) Zhu, H.; Fan, J.; Du, J.; Peng, X. *Acc. Chem. Res.* **2016**, *49*, 2115–2126.

(4) Resch-Genger, U.; Grabolle, M.; Cavaliere-Jaricot, S.; Nitschke, R.; Nann, T. *Nat. Meth ods*, **2008**, *5*, 763–775.

(5) Goetz, A. E.; Garg, N. K. *Nat. Chem.*, **2013**, *5*, 54–60.

(6) (a) Payne, D. J.; Hueso-Rodríguez, J. A.; Boyd, H.; Concha, N. O.; Janson, C. A.; Gilpin, M.; Bateson, J. H.; Cheever, C.; Niconovich, N. L.; Pearson, S. *Antimicrob. Agents Che mother.* **2002**, *46*, 1880–1886. (b) Gan, M.; Liu, Y.; Bai, Y.; Guan, Y.; Li, L.; Gao, R.; He , W.; You, X.; Li, Y.; Yu, L.; Xiao, C. *J. Nat. Prod.*, **2013**, *76*, 1535–1540. (c) Cui, H.; Yu, J.; Chen, S.; Ding, M.; Huang, X.; Yuan, J.; She, Z. *Bioorg. Med. Chem. Lett.*, **2017**, *27*, 8 03–807.

(7) (a) Marsais, F.; Trécourt, F.; Bréant, P.; Quéguiner, G. *J. Heterocyclic Chem.*, **1988**, *25*, 81–87. (b) Ghosh, C. K.; Pal, C.; Maiti, J.; Sarkar, M. *J. Chem. Soc., Perkin Trans. 1*, **19 88**, 1489–1493. (c) Villani, F. J.; Mann, T. A.; Wefer, E. A.; Hannon, J.; Larca, L. L.; Lan

don, M. J.; Spivak, W.; Vashi, D.; Tozzi, S. *J. Med. Chem.*, **1975**, *18*, 1–8. (d) Marquise, N.; Harford, P. J.; Chevallier, F.; Roisnel, T.; Dorcet, V.; Gagez, A.-L.; Sablé, S.; Picot, L. ; Thiéry, V.; Wheatley, A. E. H.; Gros, P. C.; Mongin, F. *Tetrahedron*, **2013**, *69*, 10123–10133. (e) Familoni, O. B.; Ionica, I.; Bower, J. F.; Snieckus, V. *Synlett*, **1997**, 1081–1083. (f) Cordonnier, G.; Sliwa, H. *J. Heterocyclic Chem.*, **1987**, *24*, 111–115.

(8) Mesgar, M.; Daugulis, O. *Org. Lett.*, **2016**, *18*, 3910–3913.

(9) Dubrovskiy, A. V.; Larock, R. C. *Tetrahedron*, **2013**, *69*, 2789–2798.

(10) Hua, G.; Li, Y.; Slawin, A. M. Z.; Woollins, J. D. *Dalton Trans.*, **2007**, 1477–1480.

(11) Liu, L.; Yang, B.; Katz, T. J.; Poindexter, M. K. *J. Org. Chem.*, **1991**, *56*, 3769–3775.

(12) Brouwer, A. M. *Pure Appl. Chem.*, **2011**, *83*, 2213–2228.

(13) Lavis, L. D.; Raines, R. T. *ACS Chem. Biol.*, **2008**, *3*, 142–155.

(14) Wood, E. J. *Biochem. Educ.*, **1994**, *22*, 83–83.

(15) Frisch, M. J.; Trucks, G. W.; Schlegel, H. B.; Scuseria, G. E.; Robb, M. A.; Cheeseman, J. R.; Scalmani, G.; Barone, V.; Mennucci, B.; Petersson, G. A.; Nakatsuj, H.; Caricato, M.; Li, X.; Hratchian, H. P.; Izmaylov, A. F.; Bloino, J.; Zheng, G.; Sonnenberg, J. L.; Hada, M.; Ehara, M.; Toyota, K.; Fukuda, R.; Hasegawa, J.; Ishida, M.; Nakajima, T.; Honda, Y.; Kitao, O.; Nakai, H.; Vreven, T. Montgomery, J. A.Jr.; Peralta, J. E.; Ogliaro, F.; Bear park, M.; Heyd, J. J.; Brothers, E.; Kudin, K. N.; Staroverov, V. N.; Kobayashi, R.; Norm and, J.; Raghavachari, K.; Rendell, A.; Burant, J. C.; Iyengar, S. S.; Tomasi, J.; Cossi, M.; Rega, N.; Millam, J. M.; Klene, M.; Knox, J. E.; Cross, J. B.; Bakken, V.; Adamo, C.; Jara millo, J.; Gomperts, R.; Stratmann, R. E.; Yazyev, O.; Austin, A. J., Cammi, R.; Pomelli, C.; Ochterski, J. W.; Martin, R. L.; Morokuma, K.; Zakrzewski, V. G.; Voth, G. A.; Salva dor, P.; Dannenberg, J. J.; Dapprich, S.; Daniels, A. D.; Farkas, Ö.; Foresman, J. B.; Ortiz , J. V.; Cioslowski, J.; Fox, D. J. Gaussian 09, revision B.01; Gaussian, Inc.: Wallingford, CT, **2010**.

(16) Cordonnier, G.; Sliwa, H. J. *Heterocyclic Chem.* **1987**, *24*, 111-115.

(17) Le Nôtre, J.; Firet, J. J.; Sliedregt, L. A. J. M.; Van Steen, B. J.; Van Koten, G.; Klein Geb bink, R. J. M. *Org. Lett.* **2005**, *7*, 363-366.

Appendix 4

NMR Spectra, Cell Images, Computational Results, and X-Ray Structure Data Relevant to Chapter 5

This work was performed in collaboration with Dr. Mai N. Tran, a previous graduate student in the Chenoweth group at the University of Pennsylvania.

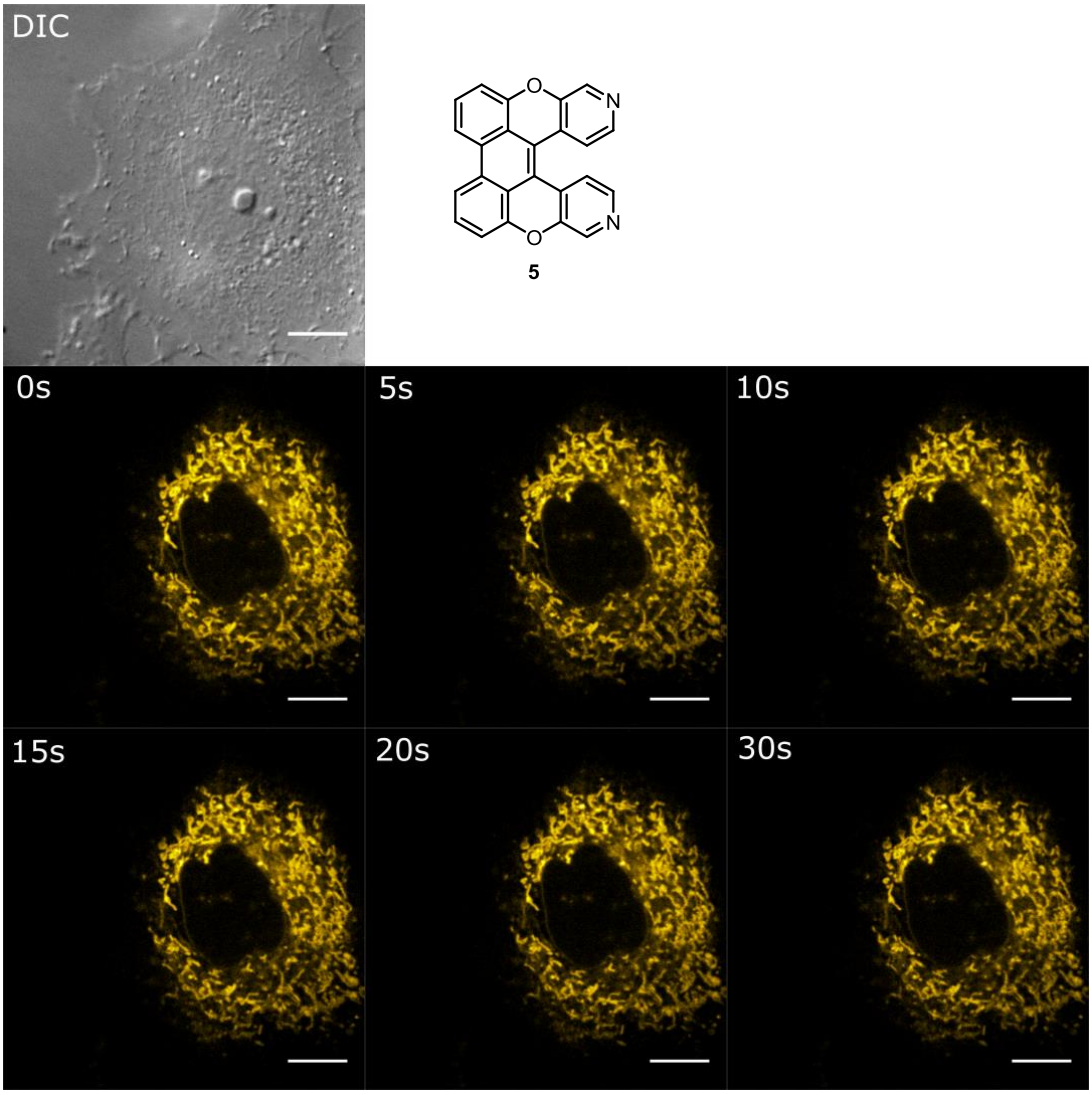

Figure A4.1. Time-lapse experiment for HeLa cells incubated with **5**. Continuous irradiation was performed using the 444/495 channel for 30 seconds. Scale bar = 10 μm.

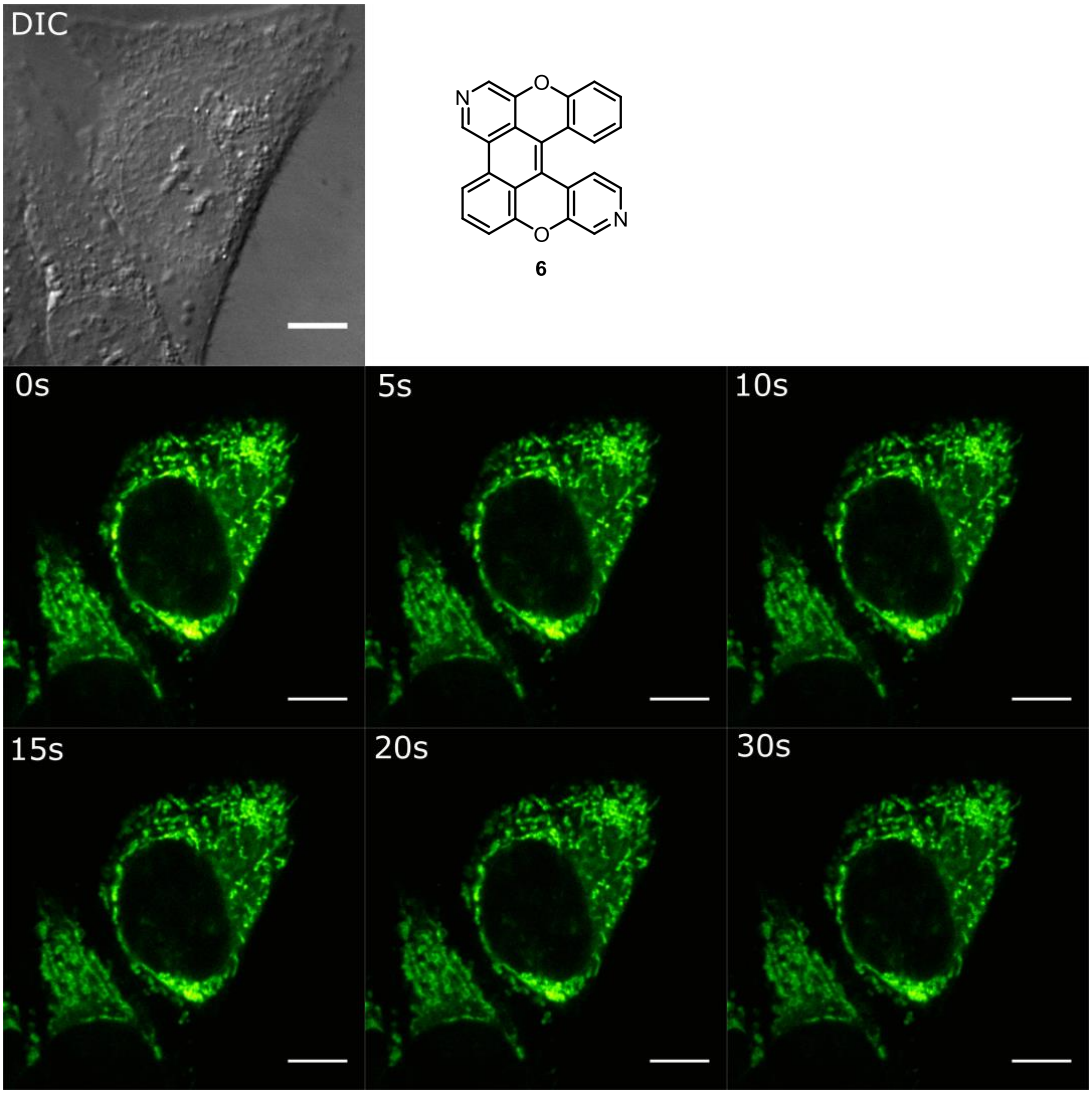

Figure A4.2. Time-lapse experiment for HeLa cells incubated with **6**. Continuous irradiation was performed using the 444/495 channel for 30 seconds. Scale bar = 10 μm.

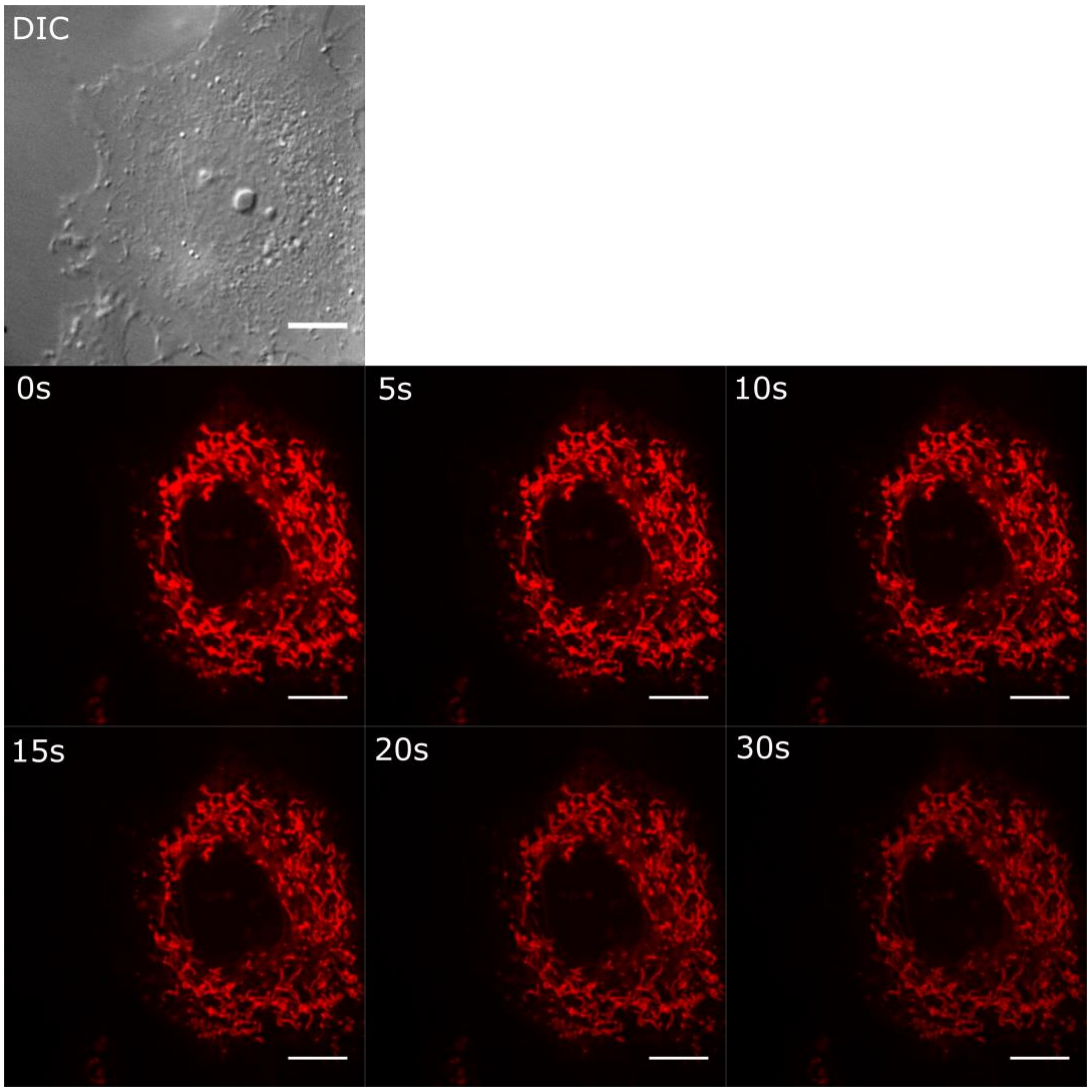

Figure A4.3. Time-lapse experiment for HeLa cells incubated with MitoTracker Red FM. Continuous irradiation was performed using the 594/632 channel for 30 seconds. Scale bar = 10 μm.

Figure A4.4. ^{1}H NMR spectrum of **5** in $CD_2Cl_2/CDCl_3$ (500 MHz).

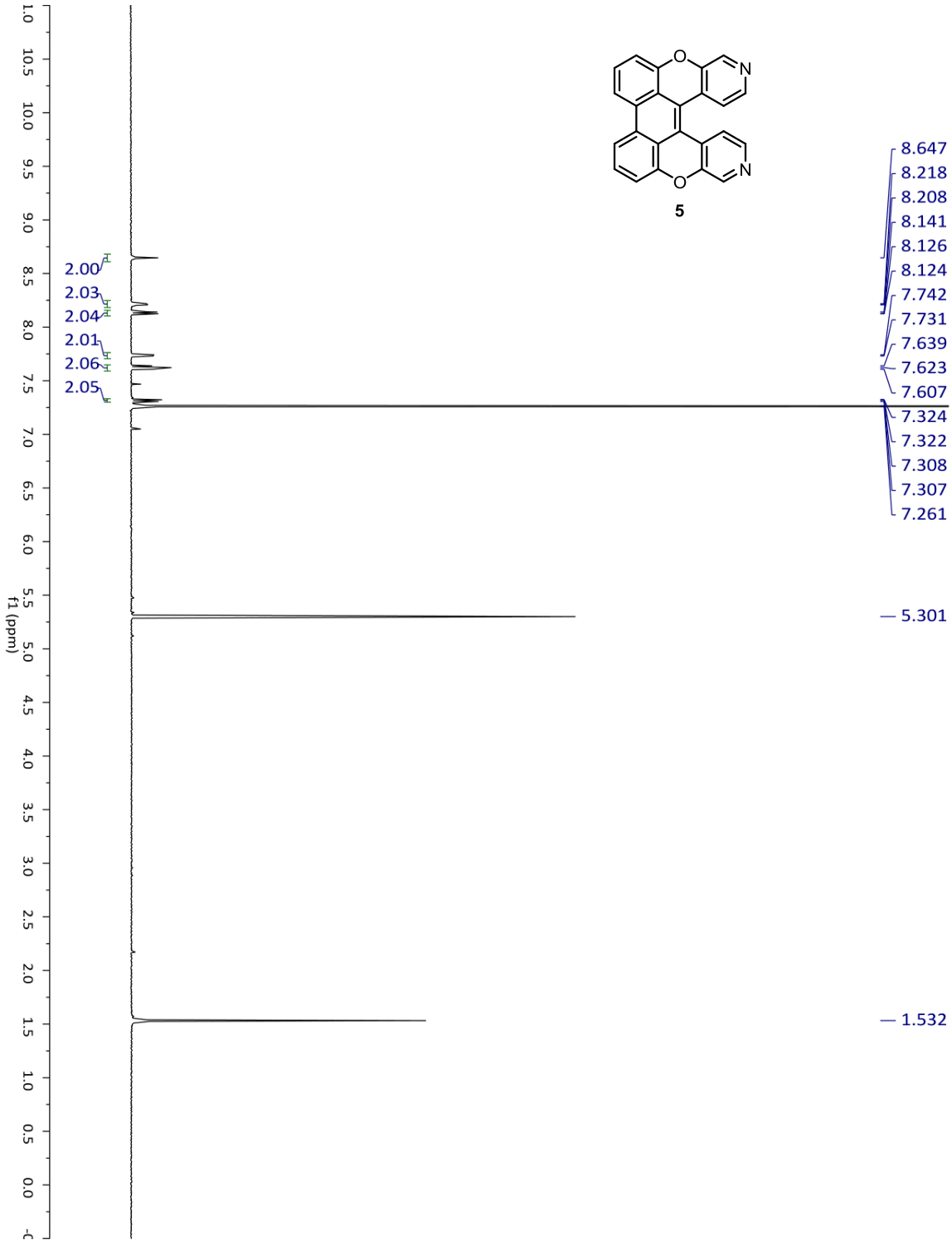

Figure A4.5. ^{13}C NMR spectrum of **5** in $CDCl_3$ (125 MHz).

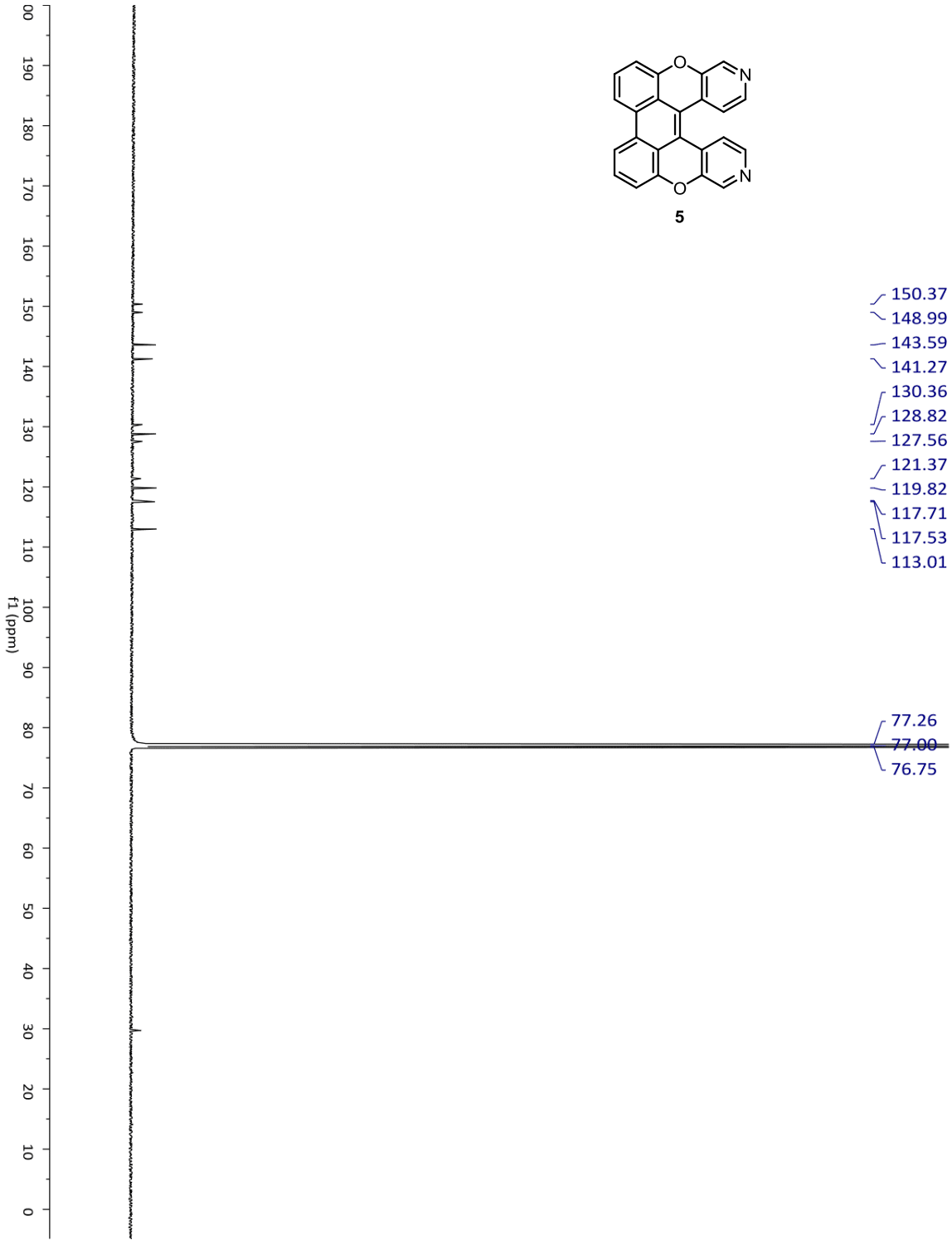

Figure A4.6. ^{1}H NMR spectrum of **6** in $CDCl_3$ (500 MHz).

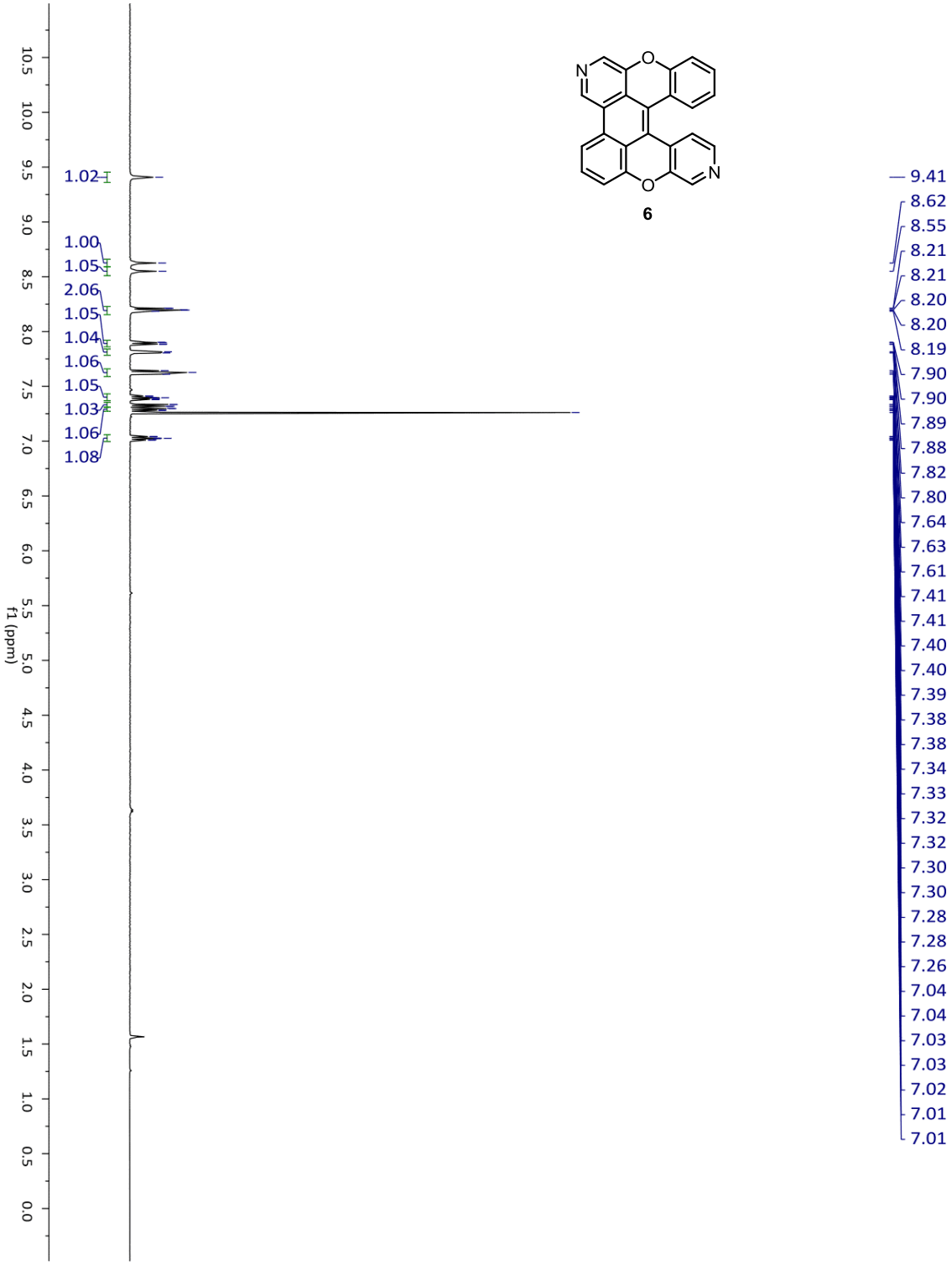

Figure A4.7. ^{13}C NMR spectrum of **6** in $CDCl_3$ (125 MHz).

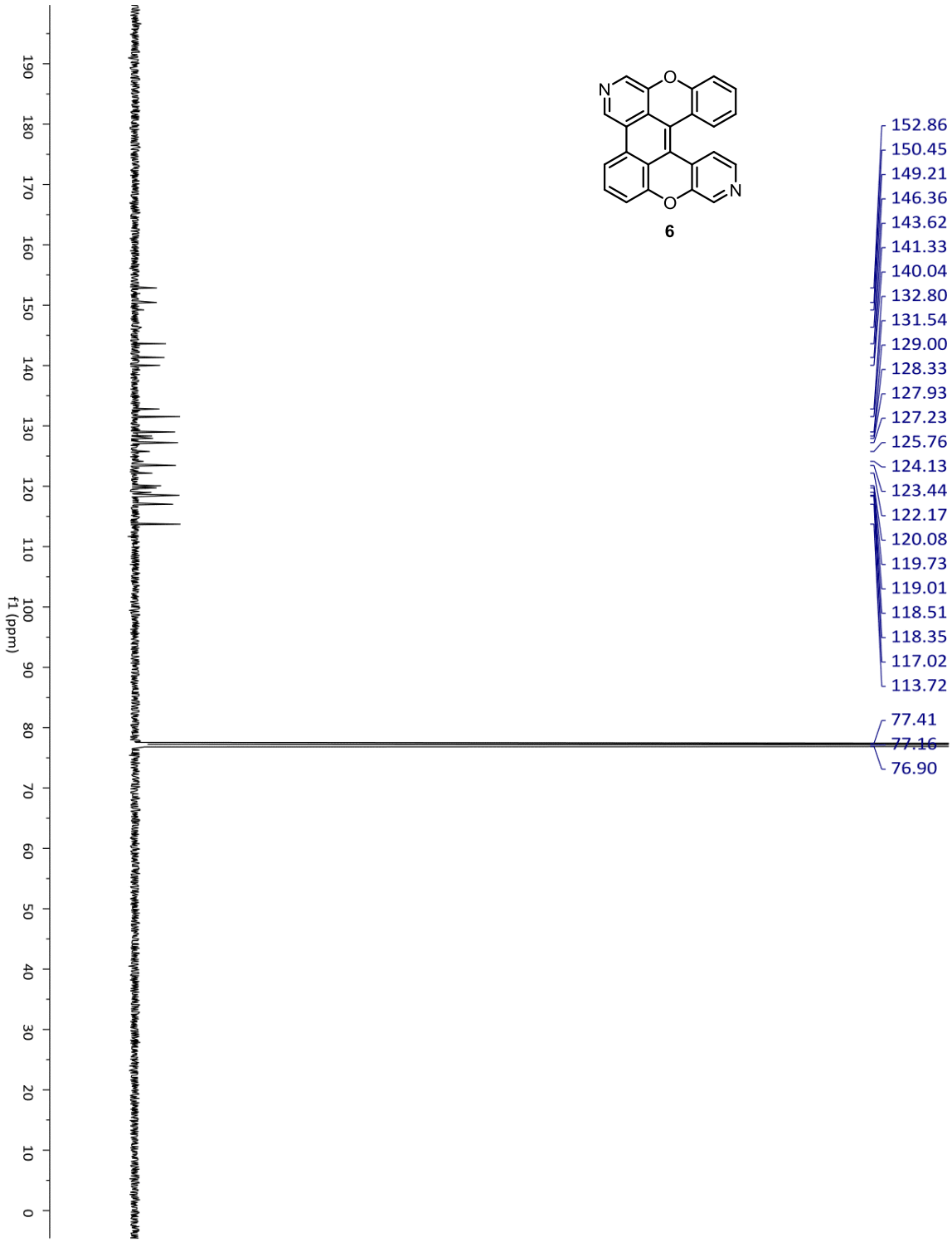

Figure A4.8. ^{1}H NMR spectrum of **7** in $CDCl_3$ (500 MHz).

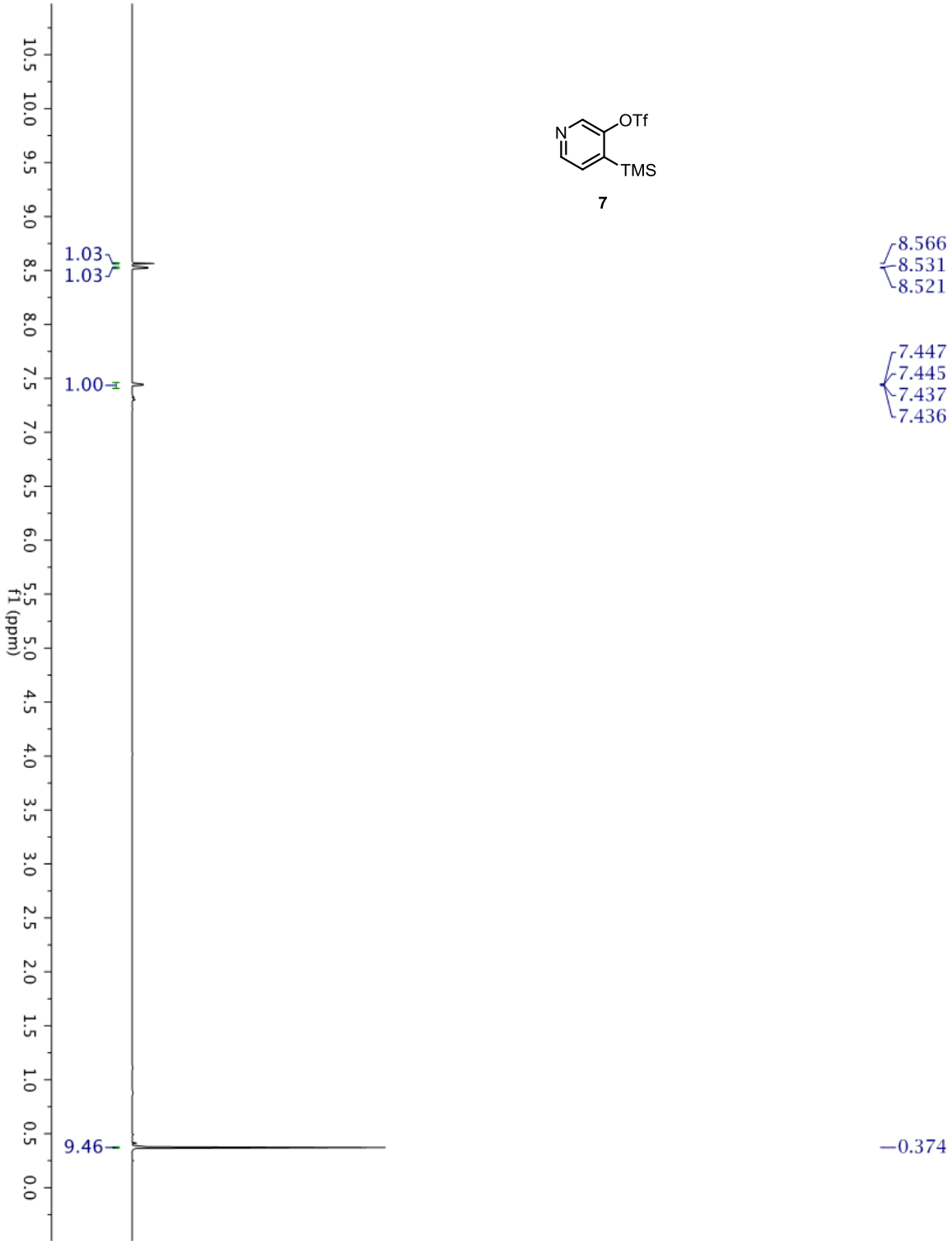

Figure A4.9. ^{1}H NMR spectrum of **9** in $CDCl_3$ (500 MHz).

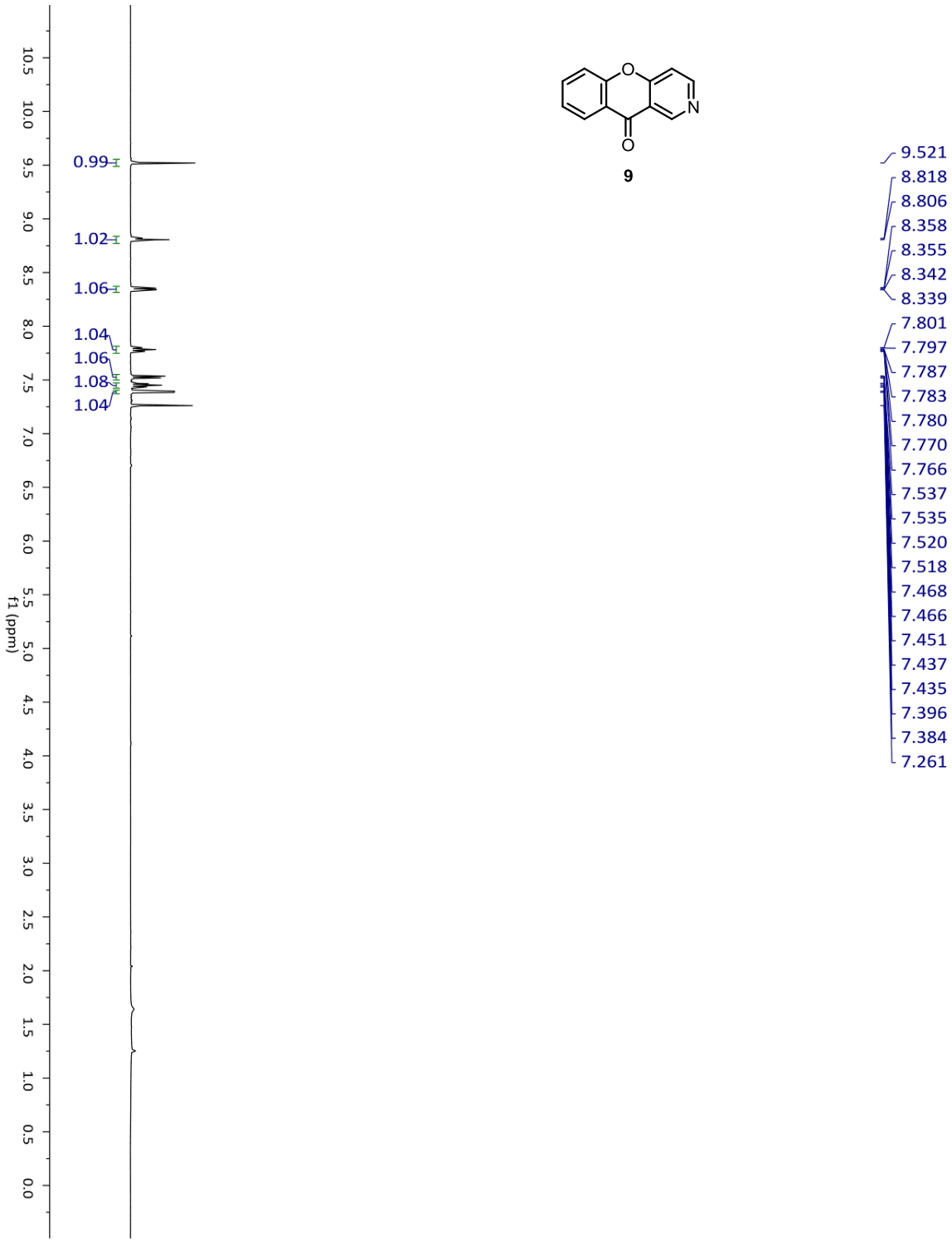

Figure A4.10. ^{1}H NMR spectrum of **S1** in $CDCl_3$ (500 MHz).

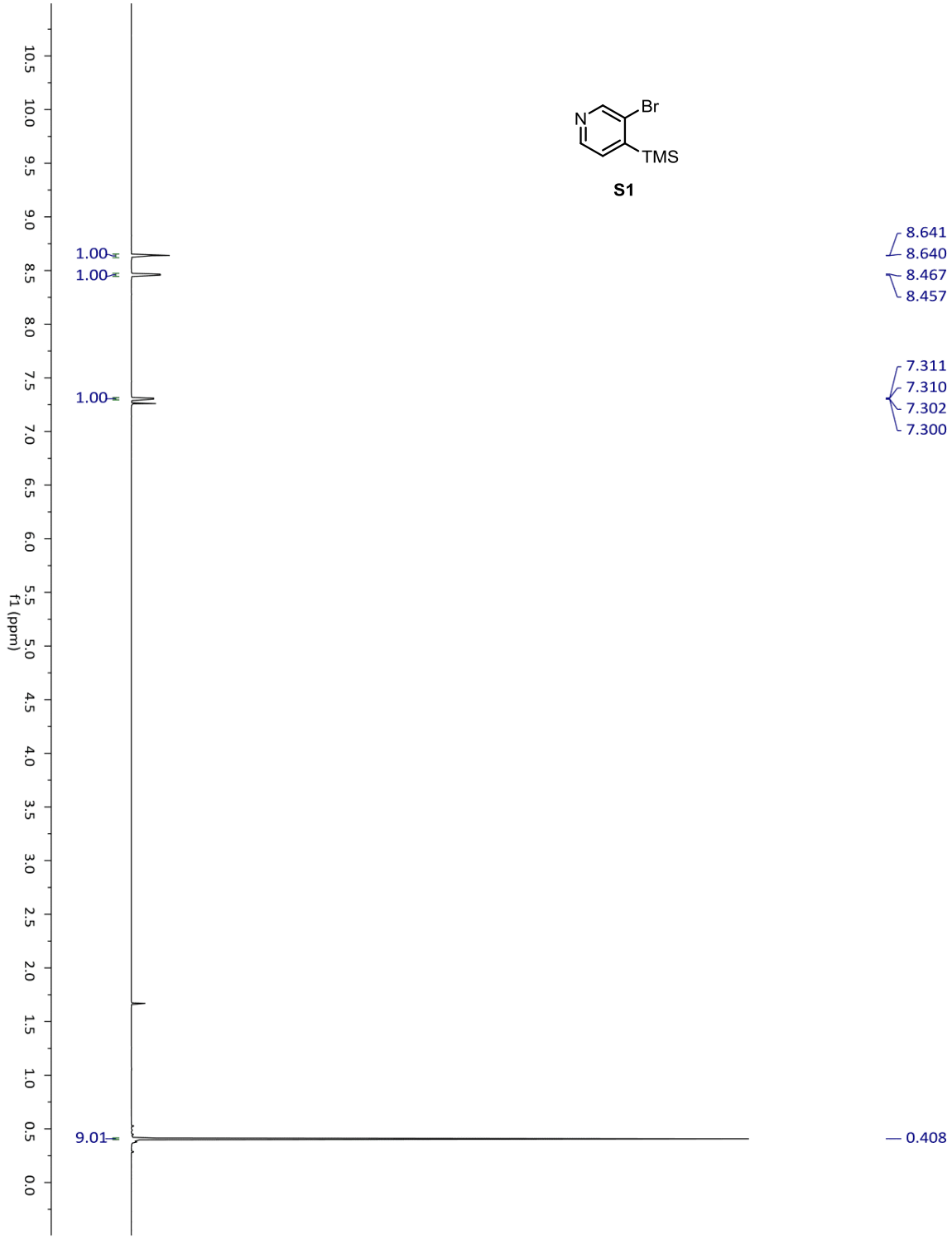

Table A4.1. Summary of Structure Determination of 3.

Empirical formula	$C_{25}H_{13}N_2O_2Cl_3$
Formula weight	479.72
Temperature	143(1) K
Wavelength	0.71073 Å
Crystal system	monoclinic
Space group	C2/c
Cell constants:	
a	26.245(5) Å
b	10.808(2) Å
c	28.103(5) Å
b	91.015(10)°
Volume	7970(3) $Å^3$
Z	16
Density (calculated)	1.599 Mg/m^3
Absorption coefficient	0.489 mm^{-1}
F(000)	3904
Crystal size	0.45 x 0.22 x 0.01 mm^3
Theta range for data collection	1.45 to 25.48°
Index ranges	$-29 \leq h \leq 31$, $-12 \leq k \leq 13$, $-33 \leq l \leq 33$
Reflections collected	73138
Independent reflections	7329 [R(int) = 0.0464]
Completeness to theta = 25.48°	99.0 %
Absorption correction	Semi-empirical from equivalents
Max. and min. transmission	0.7452 and 0.6513
Refinement method	Full-matrix least-squares on F^2
Data / restraints / parameters	7329 / 0 / 578
Goodness-of-fit on F^2	1.068
Final R indices [I>2sigma(I)]	R1 = 0.0456, wR2 = 0.1040
R indices (all data)	R1 = 0.0636, wR2 = 0.1130
Largest diff. peak and hole	0.522 and -0.466 $e.Å^{-3}$

DFT Calculations

Figure A4.11. Calculated transition molecular orbitals of (*Z*)-**1**, (*E*)-**1**, **5Int**, **6Int**, **5**, and **6** contributing to each excitation.

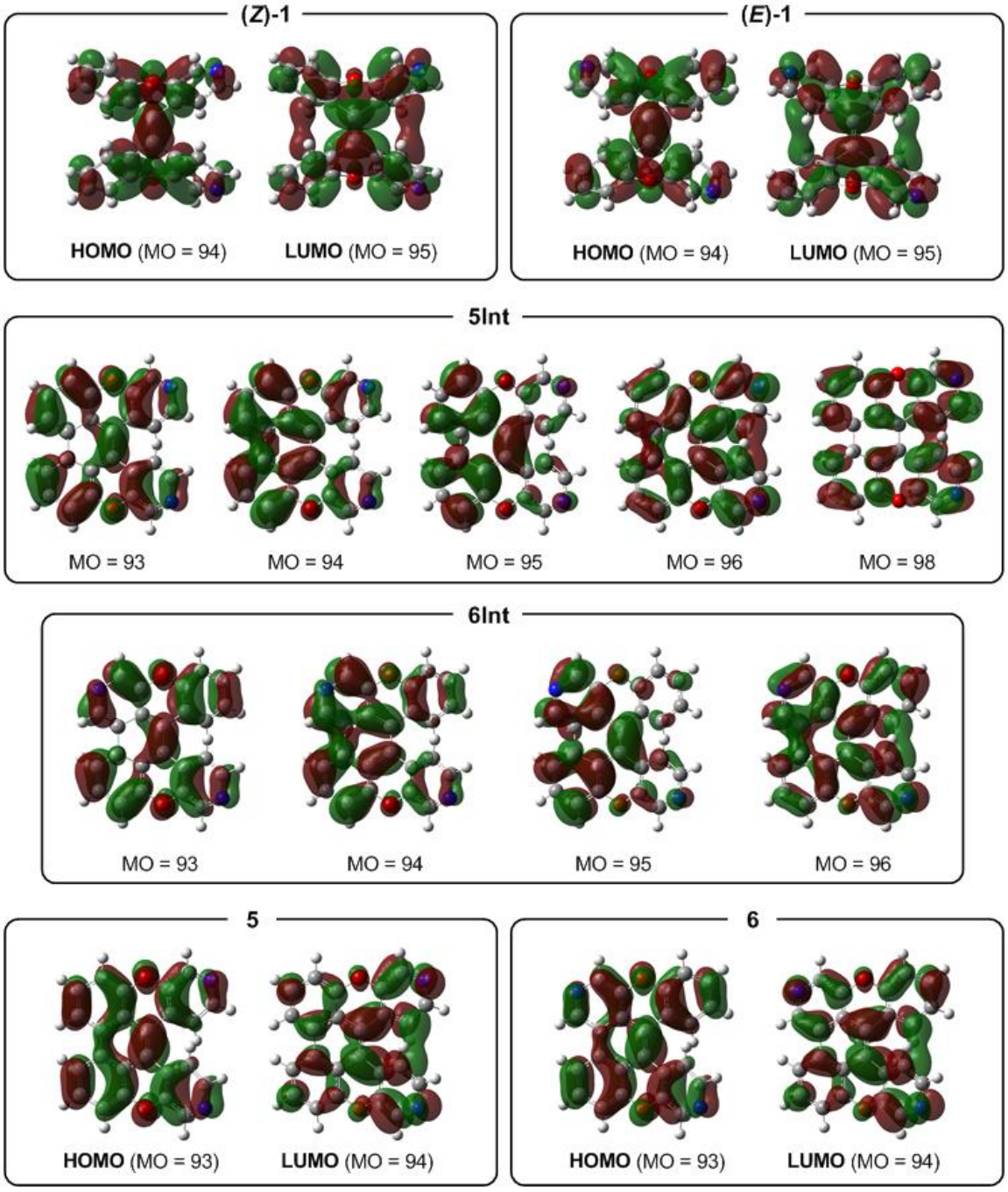

Table A4.2. Coordinates of the B3LYP/6-311+G(2d,p) Stationary Point for 5.

C	0.69146	-0.10168	-0.02632	**H**	-0.15332	-2.55433	1.31247
C	1.38958	1.15148	0.14600	**C**	-2.10264	-3.41451	1.24516
C	0.71296	2.39796	0.13805	**H**	-1.80141	-4.32064	1.75964
C	1.43872	3.57226	0.40029	**C**	-3.79263	-2.21015	0.31311
H	0.93175	4.52636	0.42356	**H**	-4.84209	-2.11424	0.05304
C	3.47481	2.30827	0.67130	**C**	-2.92674	-1.15288	0.03721
H	4.53374	2.24942	0.88604	**O**	-3.48412	-0.02521	-0.49580
C	2.77498	1.14808	0.41583	**C**	-2.77495	1.14799	-0.41603
O	3.48432	-0.02503	0.49520	**C**	-3.47484	2.30819	-0.67131
C	2.92683	-1.15280	-0.03742	**H**	-4.53375	2.24935	-0.88617
C	3.79267	-2.21014	-0.31324	**C**	-1.43883	3.57226	-0.40008
H	4.84216	-2.11426	-0.05327	**H**	-0.93196	4.52640	-0.42322
C	2.10258	-3.41468	-1.24486	**C**	-0.71300	2.39796	-0.13797
H	1.80135	-4.32094	-1.75910	**C**	-1.38958	1.15145	-0.14611
C	1.17478	-2.42148	-0.98724	**C**	2.79384	3.52564	0.66103
H	0.15321	-2.55453	-1.31199	**H**	3.33513	4.44047	0.86850
C	1.56130	-1.25191	-0.31505	**C**	-2.79392	3.52556	-0.66084
C	-0.69142	-0.10168	0.02622	**H**	-3.33530	4.44038	-0.86816
C	-1.56124	-1.25189	0.31506	**N**	3.39342	-3.33316	-0.89430
C	-1.17482	-2.42134	0.98751	**N**	-3.39347	-3.33304	0.89455

Table A4.3. Coordinates of the B3LYP/6-311+G(2d,p) Stationary Point for 6.

C	-0.70047	-0.06823	0.03724	**C**	0.68171	-0.13888	-0.01830
C	-1.31193	1.22430	-0.14045	**C**	1.49051	-1.33353	-0.30721
C	-0.57428	2.42839	-0.13275	**C**	1.04025	-2.48176	-0.97653
C	-1.26735	3.62217	-0.40301	**H**	0.01092	-2.56157	-1.29384
H	-0.73602	4.56610	-0.43292	**C**	1.91403	-3.52163	-1.23832
N	-2.56494	3.68602	-0.65717	**H**	1.56384	-4.41067	-1.75163
C	-3.26846	2.54672	-0.66440	**N**	3.20857	-3.50838	-0.89203
H	-4.32868	2.60690	-0.88420	**C**	3.66796	-2.40856	-0.31103
C	-2.68541	1.31919	-0.41817	**H**	4.72168	-2.36829	-0.05363
O	-3.47792	0.20779	-0.51091	**C**	2.85983	-1.30710	-0.03223
C	-3.00812	-0.96848	0.01669	**O**	3.47762	-0.21159	0.50153
C	-3.96452	-1.94937	0.25770	**C**	2.83301	0.99842	0.41862
H	-4.99269	-1.75078	-0.01628	**C**	3.59618	2.12019	0.66647
C	-3.58751	-3.13451	0.86549	**H**	4.65074	2.00332	0.87907
H	-4.32883	-3.89919	1.06170	**C**	2.98596	3.37454	0.65029
C	-2.26079	-3.32057	1.25597	**H**	3.57928	4.25809	0.85045
H	-1.96724	-4.22349	1.77640	**C**	1.63497	3.49650	0.39212
C	-1.31638	-2.34530	0.98889	**H**	1.18023	4.47683	0.40839
H	-0.29726	-2.49678	1.31413	**C**	0.84743	2.36141	0.13888
C	-1.64963	-1.15936	0.31288	**C**	1.44983	1.07652	0.15144

Table A4.4. Coordinates of the B3LYP/6-311+G(2d,p) Stationary Point for Int5.

C	-0.72995	-0.10492	-0.00482	**C**	2.05863	-3.40980	-1.33588
C	-1.40861	1.07942	-0.15682	**H**	1.72930	-4.30243	-1.85715
C	-0.75884	2.42786	0.08836	**C**	3.78961	-2.23789	-0.43709
C	-1.43281	3.55913	-0.63609	**H**	4.84891	-2.15698	-0.21524
H	-0.86801	4.46222	-0.82966	**C**	2.94322	-1.18855	-0.09898
C	-3.46764	2.24426	-0.76678	**O**	3.51289	-0.07944	0.46393
H	-4.51799	2.18894	-1.02121	**C**	2.81608	1.10348	0.40897
C	-2.81624	1.10305	-0.40895	**C**	3.46721	2.24476	0.76709
O	-3.51278	-0.08005	-0.46422	**H**	4.51753	2.18956	1.02168
C	-2.94299	-1.18902	0.09888	**C**	1.43221	3.55935	0.63602
C	-3.78924	-2.23842	0.43712	**H**	0.86730	4.46241	0.82937
H	-4.84857	-2.15762	0.21536	**C**	0.75847	2.42798	-0.08848
C	-2.05811	-3.41002	1.33600	**C**	1.40847	1.07965	0.15667
H	-1.72866	-4.30253	1.85739	**C**	-2.73130	3.46417	-0.96747
C	-1.14385	-2.41612	1.01858	**H**	-3.24145	4.29924	-1.43316
H	-0.11064	-2.53792	1.30804	**C**	2.73065	3.46456	0.96768
C	-1.56622	-1.26928	0.33341	**H**	3.24057	4.29969	1.43352
C	0.73002	-0.10479	0.00467	**N**	-3.35833	-3.34578	1.03462
C	1.56647	-1.26903	-0.33351	**N**	3.35882	-3.34540	-1.03441
C	1.14425	-2.41599	-1.01857	**H**	-0.95728	2.59223	1.17051
H	0.11103	-2.53796	-1.30798	**H**	0.95681	2.59245	-1.17064

Table A4.5. Coordinates of the B3LYP/6-311+G(2d,p) Stationary Point for Int6.

C	0.74033	-0.07355	-0.00120	**C**	-1.50866	-1.33495	0.33106
C	1.34663	1.14422	0.15476	**C**	-1.04136	-2.45592	1.02981
C	0.64300	2.45989	-0.07624	**H**	-0.00500	-2.52942	1.32438
C	1.28495	3.56723	0.72020	**C**	-1.91411	-3.48523	1.35068
H	0.67622	4.41731	1.02208	**H**	-1.55018	-4.35756	1.88322
N	2.52693	3.57423	1.03330	**N**	-3.21373	-3.48088	1.03952
C	3.29926	2.45852	0.74262	**C**	-3.68812	-2.39908	0.42817
H	4.35553	2.52743	0.96730	**H**	-4.74821	-2.36682	0.19787
C	2.74517	1.26300	0.38996	**C**	-2.88570	-1.31713	0.08598
O	3.52326	0.13577	0.43381	**O**	-3.49797	-0.23860	-0.49247
C	3.02024	-1.02398	-0.09808	**C**	-2.85702	0.97511	-0.43030
C	3.94778	-2.00978	-0.40697	**C**	-3.55810	2.08604	-0.79164
H	4.99224	-1.82770	-0.18865	**H**	-4.60286	1.98130	-1.05359
C	3.52124	-3.18450	-1.00819	**C**	-2.88153	3.34129	-0.98194
H	4.24087	-3.95585	-1.25317	**H**	-3.42911	4.15310	-1.44609
C	2.17482	-3.35067	-1.32271	**C**	-1.59145	3.49759	-0.64002
H	1.83939	-4.24596	-1.83091	**H**	-1.06772	4.42788	-0.82165
C	1.25601	-2.36651	-0.99064	**C**	-0.87150	2.39573	0.08311
H	0.21981	-2.50612	-1.26061	**C**	-1.45214	1.01512	-0.16772
C	1.64326	-1.19398	-0.32334	**H**	0.86175	2.68880	-1.14171
C	-0.72077	-0.13849	-0.01118	**H**	-1.09078	2.54300	1.16393

Table A4.6. Excitation Energies and Oscillator Strengths of (*Z*)-1 Using the TD-B3LYP Method with 6-31G(d) Basis Sets in Chloroform.

Excited State 1: Singlet-B 3.2192 eV 385.14 nm f=0.4432 <S**2>=0.000
94 -> 95 0.70248
This state for optimization and/or second-order correction.
Total Energy, E(TD-HF/TD-KS) = -1182.79895077
Copying the excited state density for this state as the 1-particle RhoCI density.

Excited State 2: Singlet-A 3.8928 eV 318.50 nm f=0.0044 <S**2>=0.000
93 -> 95 0.69759

Excited State 3: Singlet-B 3.8946 eV 318.35 nm f=0.0172 <S**2>=0.000
92 -> 95 0.70011

Excited State 4: Singlet-B 4.2969 eV 288.54 nm f=0.0013 <S**2>=0.000
87 -> 95 0.11755
89 -> 95 0.20426
91 -> 95 0.62454
94 -> 97 -0.17168

Excited State 5: Singlet-A 4.3567 eV 284.58 nm f=0.0061 <S**2>=0.000
88 -> 95 0.40095
90 -> 95 0.28697
94 -> 96 0.47759

Excited State 6: Singlet-B 4.4062 eV 281.38 nm f=0.0052 <S**2>=0.000
89 -> 95 0.25523
94 -> 97 0.64419

Excited State 7: Singlet-A 4.4168 eV 280.71 nm f=0.0004 <S**2>=0.000
88 -> 95 -0.31113
90 -> 95 -0.35253
94 -> 96 0.49476

Excited State 8: Singlet-B 4.5063 eV 275.13 nm f=0.0120 <S**2>=0.000
87 -> 95 0.19722
89 -> 95 0.50483
91 -> 95 -0.26876
94 -> 97 -0.19382
94 -> 98 -0.25609

Excited State 9: Singlet-A 4.5573 eV 272.05 nm f=0.1213 <S**2>=0.000

88 -> 95 -0.45569
90 -> 95 0.49987
94 -> 99 0.12016

Excited State 10: Singlet-B 4.6216 eV 268.27 nm f=0.0093 <S**2>=0.000
87 -> 95 0.58151
91 -> 95 -0.10008
92 -> 97 -0.11386
94 -> 98 0.32774

Excited State 11: Singlet-B 4.6708 eV 265.45 nm f=0.0172 <S**2>=0.000
87 -> 95 -0.28357
89 -> 95 0.31781
94 -> 98 0.53066
94 ->100 0.10912

Excited State 12: Singlet-A 4.7956 eV 258.54 nm f=0.0011 <S**2>=0.000
86 -> 95 0.17339
94 -> 99 0.64561

Excited State 13: Singlet-A 4.8336 eV 256.51 nm f=0.0065 <S**2>=0.000
86 -> 95 0.60982
94 -> 99 -0.16710
94 ->101 -0.27298

Excited State 14: Singlet-B 4.8708 eV 254.54 nm f=0.1098 <S**2>=0.000
94 -> 98 -0.14394
94 ->100 0.65428

Excited State 15: Singlet-A 5.0452 eV 245.75 nm f=0.0195 <S**2>=0.000
86 -> 95 0.26494
92 -> 96 -0.21384
92 -> 99 0.13402
93 -> 97 -0.18267
93 -> 98 -0.14336
94 ->101 0.54042

Excited State 16: Singlet-B 5.2482 eV 236.24 nm f=0.0061 <S**2>=0.000
92 -> 97 0.23652
93 -> 96 0.62210
94 -> 98 0.10548

Excited State 17: Singlet-A 5.3005 eV 233.91 nm f=0.1437 <S**2>=0.000

85 -> 95 -0.13720
92 -> 96 0.58854
94 ->101 0.19800
94 ->102 -0.18217

Excited State 18: Singlet-A 5.3314 eV 232.56 nm f=0.1948 <S**2>=0.000
88 -> 97 -0.17140
91 -> 96 0.12080
93 -> 97 0.46736
94 ->101 0.18683
94 ->102 0.36980

Excited State 19: Singlet-B 5.3472 eV 231.87 nm f=0.0062 <S**2>=0.000
91 -> 97 0.13337
92 -> 97 0.55918
93 -> 96 -0.27149
93 -> 99 -0.14789
94 ->100 0.12327

Excited State 20: Singlet-A 5.4015 eV 229.53 nm f=0.0262 <S**2>=0.000
92 -> 96 0.22133
93 -> 97 -0.38281
93 -> 98 0.15575
94 ->102 0.46859

Excited State 21: Singlet-B 5.4658 eV 226.84 nm f=0.0018 <S**2>=0.000
87 -> 97 0.16607
88 -> 96 -0.19109
88 -> 99 0.12860
88 ->101 0.11747
89 -> 97 0.25965
89 -> 98 -0.11342
90 -> 99 0.13893
91 -> 97 0.32776
91 -> 98 -0.12375
92 -> 97 -0.17767
92 -> 98 -0.26227
92 ->100 0.10002

Excited State 22: Singlet-A 5.4889 eV 225.88 nm f=0.0382 <S**2>=0.000
85 -> 95 -0.10874
88 -> 97 0.30029
88 -> 98 -0.13583

89 -> 96 -0.13012
89 -> 99 0.10936
90 -> 97 0.26590
90 ->100 0.10449
91 -> 96 -0.15258
91 -> 99 0.14996
92 -> 99 0.11019
93 -> 97 0.20535
93 -> 98 0.28295
94 ->101 0.13224

Excited State 23: Singlet-A 5.5625 eV 222.89 nm f=0.0080 <S**2>=0.000
85 -> 95 0.18376
87 -> 96 0.10359
88 -> 98 -0.12510
89 -> 96 0.18638
90 -> 97 -0.13014
91 -> 96 0.36271
93 -> 98 0.41139
94 ->102 -0.18624

Excited State 24: Singlet-B 5.5765 eV 222.33 nm f=0.0000 <S**2>=0.000
87 -> 95 -0.10948
87 -> 98 0.10903
88 -> 96 -0.36101
90 -> 96 -0.27424
91 -> 97 0.10238
91 -> 98 0.12591
92 -> 98 0.41004
93 -> 99 0.11252

Excited State 25: Singlet-A 5.6064 eV 221.15 nm f=0.1022 <S**2>=0.000
85 -> 95 0.32986
87 -> 96 -0.24154
88 -> 95 -0.10497
88 -> 98 0.19448
89 -> 96 -0.20766
90 -> 98 0.14251
91 -> 96 -0.18194
92 -> 99 -0.22450
93 -> 98 0.19101
93 ->100 0.10580
94 ->101 0.10075

94 ->102 -0.13977

Excited State 26: Singlet-B 5.6137 eV 220.86 nm f=0.0210 <S**2>=0.000
92 -> 97 0.21246
92 ->100 0.31285
93 -> 99 0.53469

Excited State 27: Singlet-A 5.6273 eV 220.33 nm f=0.0825 <S**2>=0.000
85 -> 95 0.43694
87 -> 96 -0.13143
88 -> 97 0.13490
90 -> 97 0.12537
90 -> 98 -0.10945
91 -> 96 0.24025
92 -> 96 0.14167
93 -> 97 0.12639
93 -> 98 -0.31876

Excited State 28: Singlet-B 5.6749 eV 218.48 nm f=0.0029 <S**2>=0.000
87 -> 97 0.10559
87 -> 98 -0.12883
88 -> 96 0.20747
88 ->101 0.11003
89 -> 97 0.12473
89 -> 98 -0.17232
90 -> 96 0.20941
90 -> 99 0.11809
91 -> 98 -0.18927
92 -> 98 0.45711

Excited State 29: Singlet-A 5.7092 eV 217.17 nm f=0.0257 <S**2>=0.000
85 -> 95 0.16936
88 -> 98 0.12899
89 -> 99 -0.11211
90 ->100 -0.11246
92 -> 99 0.43292
93 -> 98 0.17738
93 ->100 -0.38305

Excited State 30: Singlet-B 5.7689 eV 214.92 nm f=0.1010 <S**2>=0.000
89 -> 98 0.16540
90 -> 96 -0.13309
91 -> 97 -0.13921

92 -> 98 0.10668
92 ->100 0.50715
93 -> 99 -0.34537
93 ->101 -0.12081

Excited State 31: Singlet-A 5.7913 eV 214.09 nm f=0.2651 <S**2>=0.000
89 -> 96 -0.22786
92 -> 99 0.36484
93 ->100 0.49857

Excited State 32: Singlet-B 5.8301 eV 212.66 nm f=0.0088 <S**2>=0.000
86 -> 96 -0.14758
87 -> 97 -0.22269
87 -> 98 0.16735
88 -> 96 -0.11444
89 -> 97 -0.20995
90 -> 96 0.29349
91 -> 97 0.37709
92 ->100 0.21932
93 ->101 -0.11528

Excited State 33: Singlet-A 5.8656 eV 211.37 nm f=0.0000 <S**2>=0.000
85 -> 95 0.14648
87 ->101 -0.10566
88 -> 98 0.11998
89 -> 96 0.40720
89 ->101 0.10645
90 -> 98 -0.28449
91 -> 96 -0.28803
91 -> 99 0.11148
93 ->100 0.21674

Excited State 34: Singlet-B 5.9778 eV 207.41 nm f=0.0137 <S**2>=0.000
89 -> 97 0.10867
91 ->100 -0.17249
92 ->100 0.18769
93 ->101 0.60465

Excited State 35: Singlet-B 5.9971 eV 206.74 nm f=0.0367 <S**2>=0.000
88 -> 96 0.39734
89 -> 98 -0.10259
90 -> 96 -0.36278
91 -> 97 0.25307

91 -> 98 0.23614
93 -> 99 0.10141
93 ->101 -0.11835
94 ->103 -0.13494

Excited State 36: Singlet-A 6.0339 eV 205.48 nm f=0.0001 <S**2>=0.000
86 ->100 0.12119
87 -> 96 0.11914
88 -> 98 -0.12730
88 ->100 -0.10321
90 -> 98 0.11084
90 ->100 0.21997
91 -> 96 -0.14328
92 -> 99 0.11959
92 ->101 0.47344
92 ->102 0.24805

Excited State 37: Singlet-A 6.0690 eV 204.29 nm f=0.0007 <S**2>=0.000
86 -> 97 0.17990
88 -> 97 0.23105
88 -> 98 0.15030
89 -> 96 -0.13007
89 -> 99 -0.12372
90 -> 97 -0.25501
91 -> 96 0.12281
91 -> 99 0.18291
92 -> 99 -0.10414
92 ->101 0.39653
92 ->102 -0.17022

Excited State 38: Singlet-B 6.1010 eV 203.22 nm f=0.0028 <S**2>=0.000
87 -> 97 -0.22446
89 -> 97 0.44284
90 -> 96 0.20183
91 -> 98 0.32157
91 ->100 0.13330
93 ->102 0.22264

Excited State 39: Singlet-B 6.1314 eV 202.21 nm f=0.0134 <S**2>=0.000
86 -> 96 -0.25234
87 -> 97 -0.23213
88 -> 96 -0.10926
89 -> 98 -0.26033

90 -> 96 -0.20802
91 -> 97 -0.21009
91 -> 98 -0.22984
91 ->100 0.10886
93 ->102 0.33057
94 ->103 -0.11557

Excited State 40: Singlet-A 6.1579 eV 201.34 nm f=0.2250 <S**2>=0.000
86 -> 97 0.18152
87 -> 96 -0.27365
88 -> 98 0.13322
89 -> 96 0.25639
90 -> 97 0.33961
90 -> 98 0.26637
91 -> 96 0.17965
92 ->101 0.12919
92 ->102 0.13684

Excited State 41: Singlet-B 6.1676 eV 201.03 nm f=0.0130 <S**2>=0.000
84 -> 95 0.47753
94 ->103 0.48074

Excited State 42: Singlet-A 6.1718 eV 200.89 nm f=0.0133 <S**2>=0.000
86 -> 97 0.12226
86 -> 98 0.12270
87 -> 96 0.31757
87 -> 99 0.11777
88 -> 97 -0.18417
88 -> 98 0.14847
89 -> 96 -0.15018
89 -> 99 -0.17718
90 -> 97 0.37989
90 -> 98 -0.13694
92 -> 99 -0.10586
92 ->101 0.12545

Excited State 43: Singlet-A 6.2098 eV 199.66 nm f=0.0528 <S**2>=0.000
87 -> 96 0.37555
88 -> 97 0.43628
88 -> 98 0.26691
89 -> 96 0.10563
90 -> 98 0.15062

Excited State 44: Singlet-B 6.2415 eV 198.65 nm f=0.0505 <S**2>=0.000
86 -> 96 0.16289
87 -> 97 0.26608
87 -> 98 0.26557
87 ->100 0.15095
89 ->100 -0.14181
90 -> 99 -0.11248
91 ->100 -0.23441
93 ->102 0.37517
94 ->103 0.12871

Excited State 45: Singlet-B 6.2690 eV 197.77 nm f=0.0862 <S**2>=0.000
86 -> 96 -0.14955
87 -> 97 0.24342
87 -> 98 0.18956
87 ->100 -0.13545
88 -> 96 0.18999
88 -> 99 -0.21005
89 -> 98 0.29611
90 -> 99 0.11000
91 -> 97 0.11327
91 -> 98 -0.18455
91 ->100 0.26213
93 ->101 0.11365
93 ->102 0.11994

Excited State 46: Singlet-A 6.2699 eV 197.75 nm f=0.0517 <S**2>=0.000
86 -> 97 0.35390
86 ->100 -0.12918
89 -> 96 -0.14058
90 -> 98 -0.12350
91 -> 99 0.18862
92 ->101 -0.11624
92 ->102 0.49293

Excited State 47: Singlet-B 6.2868 eV 197.21 nm f=0.1963 <S**2>=0.000
82 -> 95 0.10258
84 -> 95 0.25747
86 -> 96 0.34616
87 -> 97 -0.19568
87 -> 98 -0.20217
89 -> 98 0.15425
91 -> 97 0.11471

91 -> 98 -0.29349
91 ->100 -0.15521
93 ->102 0.15628
94 ->103 -0.13568

Excited State 48: Singlet-B 6.3060 eV 196.61 nm f=0.0827 <S**2>=0.000
86 -> 96 0.35732
89 -> 97 -0.24192
89 -> 98 -0.14002
90 -> 99 0.21872
91 -> 98 0.16591
91 ->100 0.39011
93 ->101 0.11223
93 ->102 0.12629

Excited State 49: Singlet-A 6.3067 eV 196.59 nm f=0.0025 <S**2>=0.000
86 -> 97 -0.29110
88 -> 97 -0.13480
88 -> 98 0.12685
90 -> 98 0.19991
91 -> 99 0.55512

Excited State 50: Singlet-B 6.3665 eV 194.74 nm f=0.0523 <S**2>=0.000
82 -> 95 0.24290
84 -> 95 0.29672
86 -> 96 -0.12964
86 -> 99 0.10324
87 -> 97 0.17491
88 -> 96 -0.10041
88 -> 99 0.12318
90 -> 96 0.10332
90 -> 99 0.25263
91 -> 97 -0.13751
91 -> 98 0.18130
91 ->100 -0.16359
94 ->103 -0.25385

Excited State 51: Singlet-A 6.3681 eV 194.70 nm f=0.1710 <S**2>=0.000
83 -> 95 0.30020
87 -> 99 -0.13269
88 -> 98 0.30337
89 -> 99 0.19601
89 ->101 -0.12032

90 -> 98 -0.19273
90 ->100 0.33419
91 -> 96 0.13751

Excited State 52: Singlet-A 6.4185 eV 193.17 nm f=0.0344 <S**2>=0.000
83 -> 95 0.43611
86 -> 97 -0.21824
88 -> 98 -0.10865
88 ->100 -0.13749
89 -> 99 -0.37580
92 ->102 0.13060

Excited State 53: Singlet-B 6.4302 eV 192.81 nm f=0.0855 <S**2>=0.000
82 -> 95 -0.14953
87 -> 97 -0.18598
87 -> 98 0.11308
88 -> 99 0.43380
89 -> 98 0.31790
89 ->100 -0.20188
90 -> 99 0.22161

Excited State 54: Singlet-B 6.4460 eV 192.34 nm f=0.0190 <S**2>=0.000
82 -> 95 0.16657
86 -> 96 0.20813
87 -> 97 -0.13302
87 -> 98 0.37545
87 ->100 -0.20671
88 -> 99 0.14359
89 ->100 0.38841

Excited State 55: Singlet-A 6.4569 eV 192.02 nm f=0.0309 <S**2>=0.000
83 -> 95 0.37524
86 -> 98 0.14188
87 -> 99 0.33790
88 ->100 0.10993
89 -> 99 0.20376
89 ->101 0.14574
90 -> 98 0.23909
91 ->101 0.16219

Excited State 56: Singlet-B 6.4608 eV 191.90 nm f=0.0296 <S**2>=0.000
82 -> 95 -0.11219
87 ->100 -0.18175

88 -> 99 -0.24615
88 ->101 0.10609
89 -> 98 -0.10999
89 ->100 -0.23518
90 -> 99 0.42174
91 ->100 -0.25741

Excited State 57: Singlet-A 6.4838 eV 191.22 nm f=0.0633 <S**2>=0.000
83 -> 95 0.10681
87 -> 99 -0.21406
88 ->100 0.58471
90 ->100 0.11695
91 ->101 -0.23197

Excited State 58: Singlet-B 6.5023 eV 190.68 nm f=0.0310 <S**2>=0.000
82 -> 95 0.16695
86 -> 99 0.30584
87 -> 98 0.21488
87 ->100 0.22802
89 -> 97 0.18026
89 -> 98 -0.11348
89 ->100 -0.21940
90 ->101 -0.15713
93 ->102 -0.30326

Excited State 59: Singlet-A 6.5181 eV 190.21 nm f=0.0345 <S**2>=0.000
83 -> 95 -0.16550
86 -> 98 -0.11867
86 ->100 -0.24272
87 -> 99 0.28506
88 -> 98 0.14949
88 ->100 0.14816
89 -> 99 -0.25187
90 ->100 0.32199
91 ->101 0.23350

Excited State 60: Singlet-B 6.5469 eV 189.38 nm f=0.0961 <S**2>=0.000
82 -> 95 -0.22521
87 ->100 0.46377
88 -> 99 -0.20947
89 -> 98 0.10182
89 ->100 0.32370
90 -> 99 0.15197

90 ->102 0.10612

Excited State 61: Singlet-A 6.5754 eV 188.56 nm f=0.0142 <S**2>=0.000
86 -> 97 -0.12075
86 -> 98 0.43182
87 -> 99 -0.30244
89 -> 99 -0.10120
91 ->101 0.40758

Excited State 62: Singlet-A 6.6342 eV 186.89 nm f=0.0367 <S**2>=0.000
86 -> 97 -0.16824
87 -> 99 0.14041
87 ->101 0.31131
88 -> 98 0.18047
88 ->100 0.11514
89 ->101 -0.29159
90 -> 98 -0.18851
90 ->100 -0.31152
91 -> 99 -0.11469
91 ->102 0.12022
92 ->102 0.10812

Excited State 63: Singlet-B 6.6587 eV 186.20 nm f=0.0292 <S**2>=0.000
86 -> 99 0.37209
87 ->100 -0.14504
88 -> 99 -0.14007
88 ->101 -0.19927
89 -> 98 0.10818
89 ->100 0.10644
90 ->101 0.45100

Excited State 64: Singlet-A 6.6979 eV 185.11 nm f=0.1929 <S**2>=0.000
85 -> 97 0.17414
86 -> 98 0.37145
86 ->100 -0.36146
87 ->101 -0.11219
88 ->100 -0.11843
90 ->100 0.11702
91 ->101 -0.33825

Excited State 65: Singlet-B 6.7080 eV 184.83 nm f=0.0266 <S**2>=0.000
79 -> 95 0.11587
81 -> 95 -0.21444

82 -> 95 0.43760
84 -> 95 -0.16048
85 -> 96 0.10013
86 -> 99 -0.14723
86 ->101 -0.11428
87 ->100 0.15903
88 ->101 -0.12778
90 ->101 0.15667
90 ->102 0.16567
94 ->103 0.19209

Excited State 66: Singlet-B 6.7215 eV 184.46 nm f=0.0021 <S**2>=0.000
87 -> 98 0.15149
88 -> 99 -0.17143
88 ->101 0.51622
89 -> 98 0.10234
90 -> 99 -0.15692
90 ->101 0.30660
90 ->102 0.11623

Excited State 67: Singlet-A 6.7382 eV 184.00 nm f=0.0081 <S**2>=0.000
86 -> 98 -0.14430
86 ->100 -0.27518
87 -> 99 -0.17560
87 ->101 0.21944
89 ->101 0.42223
89 ->102 0.12421
91 ->102 0.29014

Excited State 68: Singlet-A 6.8249 eV 181.66 nm f=0.0850 <S**2>=0.000
85 -> 97 -0.26748
87 ->101 -0.24941
87 ->102 -0.12757
89 ->101 -0.19394
91 ->102 0.51974

Excited State 69: Singlet-B 6.8766 eV 180.30 nm f=0.0532 <S**2>=0.000
81 -> 95 0.40666
85 -> 96 -0.19304
86 -> 99 -0.26823
88 ->101 -0.24434
89 ->100 -0.11949
90 ->101 0.15706

90 ->102 0.20770
92 ->103 0.15867
93 ->102 -0.11294

Excited State 70: Singlet-A 6.8895 eV 179.96 nm f=0.1148 <S**2>=0.000
85 -> 98 -0.11564
86 -> 97 0.10265
86 -> 98 0.14957
86 ->100 0.22291
87 -> 99 0.10337
87 ->101 0.28509
87 ->102 0.18316
89 -> 99 -0.20570
89 ->102 -0.20199
91 ->102 0.20611
92 ->101 -0.10566
93 ->103 0.27417

Excited State 71: Singlet-B 6.9560 eV 178.24 nm f=0.0029 <S**2>=0.000
86 -> 99 0.20570
86 ->101 0.31688
88 ->102 -0.36890
90 ->102 0.38347
92 ->103 -0.20768

Excited State 72: Singlet-B 6.9690 eV 177.91 nm f=0.0012 <S**2>=0.000
81 -> 95 0.45399
82 -> 95 0.12780
85 -> 96 0.19711
86 -> 99 0.13247
86 ->102 0.12251
88 ->102 0.17266
92 ->103 -0.34305

Excited State 73: Singlet-A 6.9886 eV 177.41 nm f=0.0001 <S**2>=0.000
80 -> 95 0.14032
86 ->100 0.21212
87 ->101 -0.20878
89 ->102 0.53523
93 ->103 0.18052

Excited State 74: Singlet-B 6.9996 eV 177.13 nm f=0.0034 <S**2>=0.000
81 -> 95 -0.12654

86 ->101 0.13576
88 ->101 -0.14110
88 ->102 0.50584
90 ->102 0.37513

Excited State 75: Singlet-A 7.0200 eV 176.62 nm f=0.1210 <S**2>=0.000
80 -> 95 -0.32608
85 -> 97 -0.11407
86 -> 97 0.10015
87 ->101 0.16676
87 ->102 -0.32142
89 ->102 0.17855
91 ->102 -0.11063
93 ->103 0.38464

Excited State 76: Singlet-A 7.0442 eV 176.01 nm f=0.0007 <S**2>=0.000
80 -> 95 0.45650
85 -> 98 0.15084
87 ->102 -0.37151
89 ->101 0.14750
89 ->102 -0.16399
93 ->103 0.18713

Excited State 77: Singlet-B 7.0801 eV 175.12 nm f=0.0275 <S**2>=0.000
85 -> 96 0.40228
86 ->101 0.35486
86 ->102 0.21727
90 ->102 -0.11723
92 ->103 0.33246

Excited State 78: Singlet-A 7.1750 eV 172.80 nm f=0.0788 <S**2>=0.000
80 -> 95 0.15618
85 -> 97 -0.34793
85 ->100 -0.10949
86 ->100 -0.18924
87 ->102 0.37233
89 -> 99 0.11135
92 ->101 0.10398
93 ->103 0.23414

Excited State 79: Singlet-A 7.2123 eV 171.91 nm f=0.2528 <S**2>=0.000
78 -> 95 0.12709
80 -> 95 -0.11625

85 -> 97 0.37920
85 -> 98 0.16302
85 ->100 -0.23579
86 -> 98 -0.12623
87 ->101 -0.12306
89 ->102 -0.16814
90 ->100 -0.10878
93 ->103 0.29714

Excited State 80: Singlet-B 7.2162 eV 171.81 nm f=0.0922 <S**2>=0.000
79 -> 95 -0.27432
85 -> 96 -0.29141
85 -> 99 -0.12717
86 ->101 0.33638
86 ->102 0.19466
88 ->102 0.12779
90 ->102 -0.20304
92 ->103 -0.19041

Excited State 81: Singlet-B 7.2327 eV 171.42 nm f=0.0356 <S**2>=0.000
79 -> 95 0.46493
85 -> 96 -0.24763
86 ->102 0.38954

Excited State 82: Singlet-A 7.2811 eV 170.28 nm f=0.0493 <S**2>=0.000
78 -> 95 0.44445
80 -> 95 0.16303
85 -> 97 0.10468
86 -> 97 0.14707
87 ->101 0.16745
89 ->101 -0.17262
89 ->102 0.13671
90 -> 98 0.11528
92 ->102 -0.12134
93 ->103 -0.12288

Excited State 83: Singlet-B 7.2911 eV 170.05 nm f=0.0248 <S**2>=0.000
77 -> 95 0.54319
79 -> 95 0.17993
83 -> 96 -0.11151
85 -> 99 -0.15517
86 ->102 -0.15619
92 ->103 -0.16303

Excited State 84: Singlet-B 7.3098 eV 169.61 nm f=0.2778 <S**2>=0.000
77 -> 95 -0.30804
79 -> 95 0.34994
86 ->101 0.23255
86 ->102 -0.32717
90 ->102 -0.10270
92 ->103 -0.15898

Excited State 85: Singlet-A 7.3661 eV 168.32 nm f=0.0637 <S**2>=0.000
76 -> 95 -0.14933
78 -> 95 0.20986
80 -> 95 -0.21903
85 -> 97 -0.12925
85 -> 98 0.41184
85 ->100 0.28066
94 ->104 -0.17162

Excited State 86: Singlet-A 7.3926 eV 167.71 nm f=0.0206 <S**2>=0.000
78 -> 95 0.21034
85 ->100 0.26064
94 ->104 0.58394

Excited State 87: Singlet-B 7.4147 eV 167.21 nm f=0.1140 <S**2>=0.000
77 -> 95 0.18396
85 -> 96 -0.11989
85 -> 99 0.44887
86 ->101 0.12214
86 ->102 -0.19235
87 ->103 -0.12282
91 ->103 0.16895
92 ->103 0.11218
94 ->103 0.11024
94 ->105 0.20662

Excited State 88: Singlet-A 7.4335 eV 166.79 nm f=0.0624 <S**2>=0.000
76 -> 95 -0.11946
78 -> 95 -0.35999
80 -> 95 0.12366
84 -> 96 -0.13966
85 -> 98 0.37697
86 -> 97 0.10472
87 ->101 0.10823

89 ->101 -0.10114
94 ->104 0.23472

Excited State 89: Singlet-A 7.4773 eV 165.81 nm f=0.0026 <S**2>=0.000
76 -> 95 0.60748
83 -> 97 0.13818
84 -> 96 -0.11449
85 -> 98 0.20838

Excited State 90: Singlet-B 7.4805 eV 165.74 nm f=0.0410 <S**2>=0.000
85 -> 99 -0.21864
94 ->105 0.62445

Excited State 91: Singlet-A 7.5476 eV 164.27 nm f=0.0001 <S**2>=0.000
80 -> 95 0.10905
83 ->100 -0.13014
84 -> 96 -0.24547
85 -> 97 0.12873
85 -> 98 -0.13584
85 ->100 0.43595
86 -> 98 -0.10129
91 ->101 0.10019
93 ->103 0.16399
94 ->104 -0.18899

Excited State 92: Singlet-B 7.5514 eV 164.19 nm f=0.1197 <S**2>=0.000
85 -> 96 0.12409
85 -> 99 0.36169
86 -> 99 -0.11234
90 ->101 0.12324
91 ->103 -0.32535
92 ->103 -0.21197
94 ->105 0.15325

Excited State 93: Singlet-B 7.6185 eV 162.74 nm f=0.0129 <S**2>=0.000
83 -> 96 -0.13068
84 -> 97 0.26927
84 -> 98 -0.10039
85 -> 99 0.11830
85 ->101 -0.26126
86 ->102 0.10508
91 ->103 0.42637
92 ->103 -0.11114

Excited State 94: Singlet-B 7.6704 eV 161.64 nm f=0.0613 <S**2>=0.000
77 -> 95 -0.13988
82 -> 97 0.15272
83 -> 96 -0.23565
83 -> 99 0.15044
84 -> 97 0.43368
84 -> 98 0.14708
85 ->101 0.22802
91 ->103 -0.13806

Excited State 95: Singlet-A 7.7010 eV 161.00 nm f=0.0176 <S**2>=0.000
76 -> 95 -0.19593
78 -> 95 0.13066
83 -> 97 0.39181
84 -> 96 -0.37947
84 -> 99 0.17653
85 ->100 -0.20492

Excited State 96: Singlet-B 7.7488 eV 160.00 nm f=0.0092 <S**2>=0.000
75 -> 95 -0.13039
82 ->100 0.10897
84 ->100 0.20012
85 ->101 0.44048
85 ->102 -0.11606
89 ->103 0.18425
91 ->103 0.32840

Excited State 97: Singlet-A 7.7623 eV 159.73 nm f=0.0415 <S**2>=0.000
83 -> 97 0.12193
88 ->103 -0.17996
90 ->103 0.61956

Excited State 98: Singlet-B 7.8076 eV 158.80 nm f=0.0043 <S**2>=0.000
83 -> 96 -0.12866
85 ->101 -0.14695
89 ->103 0.50560
94 ->106 -0.39586

Excited State 99: Singlet-A 7.8201 eV 158.54 nm f=0.0001 <S**2>=0.000
74 -> 95 0.14306
84 -> 96 0.16455
84 -> 99 0.15426

88 ->103 0.59375
90 ->103 0.12365

Excited State 100: Singlet-B 7.8405 eV 158.13 nm f=0.0113 <S**2>=0.000
83 -> 96 -0.18746
84 -> 97 -0.15372
89 ->103 0.30095
94 ->106 0.53207

Table A4.7. Excitation Energies and Oscillator Strengths of (*E*)-1 Using the TD-B3LYP Method with 6-31G(d) Basis Sets in Chloroform.

Excited State 1: Singlet-A 3.2255 eV 384.39 nm f=0.4545 <S**2>=0.000
94 -> 95 0.70236
This state for optimization and/or second-order correction.
Total Energy, E(TD-HF/TD-KS) = -1182.79889761
Copying the excited state density for this state as the 1-particle RhoCI density.

Excited State 2: Singlet-A 3.8889 eV 318.82 nm f=0.0000 <S**2>=0.000
93 -> 95 0.69695

Excited State 3: Singlet-A 3.9347 eV 315.10 nm f=0.0222 <S**2>=0.000
92 -> 95 0.70048

Excited State 4: Singlet-A 4.2221 eV 293.66 nm f=0.0000 <S**2>=0.000
88 -> 95 -0.14342
91 -> 95 0.62071
94 -> 96 0.27200

Excited State 5: Singlet-A 4.3171 eV 287.19 nm f=0.0000 <S**2>=0.000
91 -> 95 -0.26201
94 -> 96 0.63897

Excited State 6: Singlet-A 4.4032 eV 281.58 nm f=0.0117 <S**2>=0.000
87 -> 95 -0.10724
88 -> 96 0.13012
89 -> 95 0.65705
94 -> 97 -0.11585

Excited State 7: Singlet-A 4.4689 eV 277.44 nm f=0.0000 <S**2>=0.000
88 -> 95 0.49166
89 -> 96 0.10745

90 -> 95 -0.37067
91 -> 95 0.15874
94 -> 98 0.24987

Excited State 8: Singlet-A 4.5254 eV 273.97 nm f=0.0038 <S**2>=0.000
87 -> 95 -0.22929
94 -> 97 0.65462

Excited State 9: Singlet-A 4.5323 eV 273.56 nm f=0.0000 <S**2>=0.000
88 -> 95 0.44581
90 -> 95 0.39301
94 -> 98 -0.32795

Excited State 10: Singlet-A 4.6411 eV 267.14 nm f=0.1045 <S**2>=0.000
87 -> 95 0.63129
89 -> 95 0.15120
93 -> 96 -0.11180
94 -> 97 0.19466

Excited State 11: Singlet-A 4.6454 eV 266.90 nm f=0.0002 <S**2>=0.000
90 -> 95 0.42294
94 -> 98 0.55134

Excited State 12: Singlet-A 4.8136 eV 257.57 nm f=0.0000 <S**2>=0.000
85 -> 95 -0.10368
94 ->100 0.65805

Excited State 13: Singlet-A 4.8687 eV 254.66 nm f=0.1107 <S**2>=0.000
94 -> 99 0.66421
94 ->101 0.10013

Excited State 14: Singlet-A 4.9349 eV 251.24 nm f=0.0202 <S**2>=0.000
86 -> 95 0.57372
94 ->101 0.37318

Excited State 15: Singlet-A 5.0577 eV 245.14 nm f=0.0238 <S**2>=0.000
86 -> 95 -0.33964
92 -> 97 -0.20348
93 -> 96 -0.26498
93 ->100 -0.12076
94 ->101 0.47651

Excited State 16: Singlet-A 5.2256 eV 237.26 nm f=0.0000 <S**2>=0.000

85 -> 95 0.10609
92 -> 96 0.64381
93 -> 97 0.15599

Excited State 17: Singlet-A 5.2442 eV 236.42 nm f=0.2365 <S**2>=0.000
86 -> 95 -0.14336
93 -> 96 0.61357
94 ->101 0.20613

Excited State 18: Singlet-A 5.3375 eV 232.29 nm f=0.0000 <S**2>=0.000
85 -> 95 -0.12193
88 -> 97 0.10092
89 -> 96 0.13422
91 -> 97 -0.10136
92 ->100 0.12021
93 -> 97 0.32008
94 ->102 0.52006

Excited State 19: Singlet-A 5.4264 eV 228.48 nm f=0.0609 <S**2>=0.000
88 -> 96 -0.17726
88 -> 98 -0.14859
89 -> 97 -0.26850
89 -> 99 0.13149
90 -> 96 0.10507
91 -> 96 0.35024
91 -> 98 0.17816
92 -> 97 -0.11294
93 -> 98 -0.33602

Excited State 20: Singlet-A 5.4435 eV 227.76 nm f=0.0000 <S**2>=0.000
87 -> 96 -0.13925
88 -> 97 0.11927
89 -> 96 0.13749
89 -> 98 0.12407
91 -> 97 -0.10874
92 -> 96 -0.17903
92 -> 98 0.12045
93 -> 97 0.42484
94 ->102 -0.37749

Excited State 21: Singlet-A 5.4929 eV 225.72 nm f=0.0044 <S**2>=0.000
88 -> 96 -0.12822
91 -> 96 0.20783

92 -> 97 -0.37493
93 -> 96 0.10335
93 -> 98 0.48141
94 ->101 -0.12690

Excited State 22: Singlet-A 5.5034 eV 225.28 nm f=0.0000 <S**2>=0.000
88 -> 97 0.24289
89 -> 96 0.34344
89 -> 98 0.18275
90 -> 97 -0.10682
91 -> 97 -0.22575
91 -> 99 0.12713
93 -> 97 -0.33125
93 -> 99 -0.14927

Excited State 23: Singlet-A 5.5199 eV 224.61 nm f=0.0000 <S**2>=0.000
85 -> 95 0.59537
91 -> 97 0.16644
92 -> 96 -0.12282
92 ->100 -0.12755
93 -> 97 0.10919
94 ->102 0.14958

Excited State 24: Singlet-A 5.5621 eV 222.91 nm f=0.4174 <S**2>=0.000
86 -> 95 -0.10607
88 -> 96 -0.25428
88 -> 98 0.13028
89 -> 95 0.13144
89 -> 99 -0.14362
91 -> 96 0.27282
91 -> 98 -0.10013
92 -> 97 0.42227
93 -> 98 0.13365
94 ->101 0.16896

Excited State 25: Singlet-A 5.5826 eV 222.09 nm f=0.0847 <S**2>=0.000
88 -> 96 -0.16064
88 -> 98 -0.25575
89 -> 97 -0.16825
89 -> 99 0.16078
89 ->101 0.12560
91 -> 96 -0.26732
91 -> 98 0.10919

92 -> 99 0.20969
93 -> 98 0.13038
93 ->100 0.33450
94 ->101 0.13712

Excited State 26: Singlet-A 5.5923 eV 221.71 nm f=0.0000 <S**2>=0.000
85 -> 95 0.14218
88 -> 95 0.12267
88 -> 99 -0.12290
89 -> 96 -0.25698
89 -> 98 0.23098
91 -> 99 0.14183
92 -> 98 0.47767
93 -> 97 -0.12738
93 -> 99 -0.15848

Excited State 27: Singlet-A 5.6527 eV 219.34 nm f=0.0000 <S**2>=0.000
87 -> 96 -0.14165
88 -> 99 0.13736
88 ->101 0.10988
89 -> 96 0.27033
89 -> 98 -0.24704
91 -> 99 -0.11354
92 -> 98 0.42483
93 -> 97 -0.13108
93 -> 99 0.20841
93 ->101 0.12175

Excited State 28: Singlet-A 5.6566 eV 219.18 nm f=0.1039 <S**2>=0.000
88 -> 98 -0.11671
89 -> 99 0.12714
90 -> 96 -0.15331
90 -> 98 0.15331
91 -> 98 0.33327
92 -> 97 0.24542
92 -> 99 -0.18151
93 -> 98 0.27014
93 ->100 -0.30378

Excited State 29: Singlet-A 5.7423 eV 215.91 nm f=0.0000 <S**2>=0.000
88 -> 99 -0.10498
89 -> 98 0.19132
90 -> 97 -0.12492

91 -> 97 0.10083
91 -> 99 0.11470
92 ->100 -0.19623
93 -> 99 0.56874

Excited State 30: Singlet-A 5.7542 eV 215.47 nm f=0.0773 <S**2>=0.000
88 -> 96 0.27977
89 -> 97 0.11364
90 -> 96 -0.22086
91 -> 96 0.28114
91 -> 98 0.10270
92 -> 99 0.47889

Excited State 31: Singlet-A 5.7985 eV 213.82 nm f=0.0797 <S**2>=0.000
88 -> 96 0.12830
90 -> 96 -0.26644
90 ->100 -0.11027
91 -> 96 0.17032
92 -> 99 -0.35406
93 ->100 0.43563

Excited State 32: Singlet-A 5.8166 eV 213.16 nm f=0.0000 <S**2>=0.000
85 -> 95 0.12874
87 -> 98 -0.13454
91 ->101 0.12342
92 -> 98 -0.11331
92 ->100 0.58929
93 -> 99 0.10945

Excited State 33: Singlet-A 5.8925 eV 210.41 nm f=0.1229 <S**2>=0.000
88 -> 96 0.33098
88 -> 98 -0.26026
89 -> 99 0.11521
90 -> 96 0.38701
91 -> 96 0.16959
91 -> 98 -0.20472
92 -> 97 0.14536
92 -> 99 -0.11449

Excited State 34: Singlet-A 5.8955 eV 210.30 nm f=0.0003 <S**2>=0.000
86 -> 96 0.10841
87 -> 96 0.35440
87 -> 98 -0.27672

87 ->100 0.12281
90 -> 97 0.20880
90 ->101 0.12345
91 -> 97 -0.30948
91 ->101 0.13985
93 -> 99 0.14866

Excited State 35: Singlet-A 5.9699 eV 207.68 nm f=0.0000 <S**2>=0.000
88 -> 99 -0.10415
89 -> 98 0.11229
91 -> 99 -0.24654
92 ->100 -0.11834
93 ->101 0.59518

Excited State 36: Singlet-A 6.0314 eV 205.56 nm f=0.0722 <S**2>=0.000
87 -> 97 -0.24807
88 -> 98 0.19098
90 -> 96 0.33302
90 ->100 -0.19608
91 -> 98 0.38795
93 ->100 0.16171
93 ->102 -0.15320

Excited State 37: Singlet-A 6.0633 eV 204.48 nm f=0.0000 <S**2>=0.000
86 -> 96 0.11911
89 -> 96 0.24878
89 -> 98 0.10794
90 -> 97 0.22509
91 -> 97 0.45067
91 -> 99 -0.10480
92 ->100 -0.11492
92 ->102 0.19355
93 ->101 -0.11237

Excited State 38: Singlet-A 6.0755 eV 204.07 nm f=0.0000 <S**2>=0.000
87 -> 96 0.39121
87 ->100 -0.20034
88 -> 97 -0.11216
89 -> 96 0.17628
90 -> 97 -0.24999
91 -> 97 0.16168
91 -> 99 0.29197
93 ->101 0.16046

Excited State 39: Singlet-A 6.0982 eV 203.31 nm f=0.0292 <S**2>=0.000
86 -> 99 0.10182
90 ->100 -0.10262
91 -> 98 -0.14600
92 ->101 0.64326

Excited State 40: Singlet-A 6.1598 eV 201.28 nm f=0.0397 <S**2>=0.000
84 -> 95 0.10754
87 -> 97 -0.16423
90 -> 98 -0.38324
93 ->102 0.46477
94 ->103 -0.21996

Excited State 41: Singlet-A 6.1868 eV 200.40 nm f=0.0653 <S**2>=0.000
84 -> 95 -0.30347
87 -> 97 0.13482
89 -> 97 0.11541
90 -> 98 -0.18661
91 ->100 0.12600
93 ->102 0.15174
94 ->103 0.51242

Excited State 42: Singlet-A 6.1946 eV 200.15 nm f=0.0000 <S**2>=0.000
86 -> 96 0.13041
87 -> 96 -0.31458
87 -> 98 -0.17885
89 -> 98 -0.12039
90 -> 97 0.13368
90 -> 99 0.17140
91 -> 99 0.40279
92 ->102 0.23344
93 ->101 0.19773

Excited State 43: Singlet-A 6.2353 eV 198.84 nm f=0.1514 <S**2>=0.000
84 -> 95 0.13831
87 -> 99 0.16385
89 -> 97 0.11470
90 -> 98 0.18346
91 ->100 0.59865

Excited State 44: Singlet-A 6.2433 eV 198.59 nm f=0.0232 <S**2>=0.000
84 -> 95 0.11939

88 -> 96 -0.29201
88 -> 98 -0.18588
89 -> 97 0.53200
91 ->100 -0.14789

Excited State 45: Singlet-A 6.2588 eV 198.09 nm f=0.0000 <S**2>=0.000
83 -> 95 0.10466
86 -> 96 -0.35666
87 -> 96 0.11756
88 -> 97 0.11892
90 -> 97 -0.14702
90 -> 99 -0.15578
92 ->102 0.48814

Excited State 46: Singlet-A 6.2869 eV 197.21 nm f=0.0000 <S**2>=0.000
86 -> 96 0.26429
88 -> 97 0.53529
89 -> 96 -0.24901
89 -> 98 -0.18163

Excited State 47: Singlet-A 6.3106 eV 196.47 nm f=0.1081 <S**2>=0.000
84 -> 95 0.33522
87 -> 97 0.41392
87 -> 99 0.10818
90 -> 98 -0.30335
90 ->100 -0.17198
93 ->102 -0.18480

Excited State 48: Singlet-A 6.3162 eV 196.29 nm f=0.0000 <S**2>=0.000
83 -> 95 0.22712
86 -> 96 -0.29706
87 -> 98 0.10294
87 ->100 -0.22128
88 -> 97 0.16218
90 -> 97 0.42406
90 -> 99 -0.11099
92 ->102 -0.17479

Excited State 49: Singlet-A 6.3499 eV 195.25 nm f=0.4399 <S**2>=0.000
86 ->101 -0.11982
87 -> 97 0.19689
87 ->101 0.10908
88 -> 96 0.12047

88 -> 98 0.19895
88 ->100 0.10960
89 -> 99 -0.11318
90 -> 96 0.12029
90 -> 98 0.11938
90 ->100 0.35806
91 -> 98 0.20313
91 ->102 -0.26609
92 -> 99 -0.10599
92 ->101 0.12072
93 ->102 0.13055

Excited State 50: Singlet-A 6.3629 eV 194.85 nm f=0.0002 <S**2>=0.000
83 -> 95 0.35153
87 -> 98 0.29972
87 ->100 0.23915
90 -> 97 -0.11361
90 -> 99 0.24093
91 ->101 0.31903

Excited State 51: Singlet-A 6.3867 eV 194.13 nm f=0.0000 <S**2>=0.000
83 -> 95 0.48667
87 -> 98 -0.33318
88 -> 97 -0.10151
90 -> 97 -0.10315
91 -> 99 -0.19314
91 ->101 -0.20983

Excited State 52: Singlet-A 6.4192 eV 193.15 nm f=0.0244 <S**2>=0.000
82 -> 95 0.14272
84 -> 95 0.27952
87 -> 97 -0.31183
87 -> 99 0.10146
89 -> 99 0.15775
90 -> 98 -0.15224
90 ->100 0.38241
93 ->102 -0.17806
94 ->103 0.19556

Excited State 53: Singlet-A 6.4340 eV 192.70 nm f=0.0389 <S**2>=0.000
84 -> 95 0.14588
86 -> 97 -0.25672
88 -> 98 0.24137

88 ->100 0.22461
89 -> 99 0.35192
90 ->100 -0.17181
91 ->100 -0.11101
93 ->102 0.24210
94 ->103 0.13191

Excited State 54: Singlet-A 6.4421 eV 192.46 nm f=0.0000 <S**2>=0.000
87 ->100 -0.17764
88 -> 99 0.48733
89 -> 98 0.27789
89 ->100 -0.14437
90 -> 99 0.19080
91 -> 99 -0.13495
92 ->102 0.15377

Excited State 55: Singlet-A 6.4598 eV 191.93 nm f=0.0127 <S**2>=0.000
84 -> 95 -0.18064
86 -> 97 0.36533
88 -> 98 0.26568
89 -> 99 0.40645
90 -> 98 -0.11787
91 ->102 -0.11823
93 ->102 -0.14462
94 ->103 -0.12151

Excited State 56: Singlet-A 6.4650 eV 191.78 nm f=0.0000 <S**2>=0.000
83 -> 95 -0.12884
86 -> 96 -0.17481
88 -> 99 -0.25904
89 -> 98 -0.22366
89 ->100 -0.30243
90 -> 99 0.43936

Excited State 57: Singlet-A 6.4801 eV 191.33 nm f=0.0000 <S**2>=0.000
86 -> 96 -0.10138
87 ->100 -0.22355
89 ->100 0.59891
90 -> 99 0.22944

Excited State 58: Singlet-A 6.4903 eV 191.03 nm f=0.0270 <S**2>=0.000
86 -> 97 0.15448
87 -> 99 0.42523

88 -> 98 -0.10382
88 ->100 0.47810

Excited State 59: Singlet-A 6.5594 eV 189.02 nm f=0.0000 <S**2>=0.000
86 -> 98 -0.22207
86 ->100 0.14382
87 -> 98 -0.21365
88 ->101 -0.18470
89 -> 98 -0.17137
90 -> 99 -0.14224
90 ->101 -0.16873
91 ->101 0.46520

Excited State 60: Singlet-A 6.5761 eV 188.54 nm f=0.2850 <S**2>=0.000
82 -> 95 -0.11669
85 -> 96 0.11311
86 -> 97 -0.18574
87 -> 99 0.44533
88 ->100 -0.38673
91 ->100 -0.14629

Excited State 61: Singlet-A 6.6328 eV 186.93 nm f=0.0742 <S**2>=0.000
82 -> 95 0.33567
84 -> 95 0.13224
86 -> 97 0.32831
87 ->101 0.29464
88 ->100 -0.16600
89 ->101 0.19315
90 -> 98 0.16117
90 ->100 -0.13027

Excited State 62: Singlet-A 6.6431 eV 186.64 nm f=0.0000 <S**2>=0.000
83 -> 95 0.11364
86 -> 96 0.19361
86 -> 98 -0.33850
87 -> 98 0.18150
87 ->100 -0.28590
88 -> 99 -0.15067
90 ->101 0.35981

Excited State 63: Singlet-A 6.6941 eV 185.21 nm f=0.0252 <S**2>=0.000
85 -> 96 0.10716
86 -> 99 -0.13263

87 ->101 -0.20779
88 -> 98 0.12099
88 ->102 0.11412
89 -> 99 -0.12981
89 ->101 0.48565
90 -> 98 -0.11513
91 ->102 -0.31600

Excited State 64: Singlet-A 6.7004 eV 185.04 nm f=0.0001 <S**2>=0.000
81 -> 95 -0.17204
86 -> 98 0.40307
86 ->100 0.19680
87 ->100 -0.15907
88 ->101 -0.22938
89 ->102 -0.10232
90 ->101 0.35420

Excited State 65: Singlet-A 6.7495 eV 183.69 nm f=0.1616 <S**2>=0.000
82 -> 95 -0.23947
85 -> 96 -0.19621
86 -> 99 0.10984
88 -> 98 0.13621
89 ->101 0.35915
90 ->100 0.10996
91 ->102 0.43649

Excited State 66: Singlet-A 6.7532 eV 183.59 nm f=0.0015 <S**2>=0.000
81 -> 95 -0.35441
86 ->100 0.30488
88 ->101 0.45383
89 -> 98 0.11480

Excited State 67: Singlet-A 6.8040 eV 182.22 nm f=0.0121 <S**2>=0.000
82 -> 95 0.31795
85 -> 96 0.23822
86 -> 97 -0.11409
86 -> 99 0.48054
87 ->101 -0.10161
89 ->101 0.10374
91 ->102 0.11317
94 ->103 -0.10214

Excited State 68: Singlet-A 6.8065 eV 182.16 nm f=0.0000 <S**2>=0.000

80 -> 95 -0.16752
81 -> 95 0.51596
86 -> 98 0.11375
86 ->100 0.20435
87 ->102 -0.10854
88 ->101 0.25226

Excited State 69: Singlet-A 6.8374 eV 181.33 nm f=0.0228 <S**2>=0.000
82 -> 95 -0.25812
85 -> 96 0.24196
86 -> 99 0.12294
87 -> 99 -0.11702
87 ->101 0.45046
90 ->100 -0.10530
90 ->102 0.23810

Excited State 70: Singlet-A 6.9109 eV 179.40 nm f=0.0000 <S**2>=0.000
80 -> 95 0.11598
85 -> 97 0.15372
85 -> 99 -0.10603
86 -> 98 -0.18735
86 ->100 0.37207
87 ->100 0.17602
87 ->102 -0.20250
88 -> 99 0.10580
89 ->102 -0.28286
91 ->101 -0.13745
93 ->103 -0.20174

Excited State 71: Singlet-A 6.9370 eV 178.73 nm f=0.0854 <S**2>=0.000
82 -> 95 -0.18338
85 -> 96 -0.11857
86 -> 99 0.30410
88 ->102 0.45775
89 ->101 -0.14249
90 ->102 -0.10330
91 ->102 -0.13650
92 ->103 -0.19553
94 ->103 0.10298

Excited State 72: Singlet-A 6.9453 eV 178.51 nm f=0.0001 <S**2>=0.000
86 ->100 0.19611
87 ->102 -0.13839

88 -> 99 -0.10400
88 ->101 -0.22551
89 ->102 0.58289
93 ->103 -0.10931

Excited State 73: Singlet-A 6.9595 eV 178.15 nm f=0.0795 <S**2>=0.000
85 ->100 0.12511
86 -> 97 0.12878
87 ->101 -0.13178
90 ->102 0.55088
92 ->103 -0.27508

Excited State 74: Singlet-A 7.0036 eV 177.03 nm f=0.0000 <S**2>=0.000
80 -> 95 0.16159
85 -> 97 0.26366
86 -> 96 -0.12475
87 ->102 0.50431
90 ->101 0.19316
92 ->102 -0.10426

Excited State 75: Singlet-A 7.0125 eV 176.81 nm f=0.0259 <S**2>=0.000
82 -> 95 0.11440
85 -> 98 -0.29294
86 -> 99 -0.15523
86 ->101 -0.24207
87 ->101 0.15086
88 ->102 0.38369
90 ->102 0.11805
92 ->103 0.28966

Excited State 76: Singlet-A 7.0433 eV 176.03 nm f=0.0000 <S**2>=0.000
80 -> 95 0.18484
85 -> 97 0.15299
86 -> 98 -0.12502
86 ->100 -0.14106
87 ->102 -0.31545
93 ->103 0.50771

Excited State 77: Singlet-A 7.0498 eV 175.87 nm f=0.5257 <S**2>=0.000
79 -> 95 0.22300
85 -> 96 0.45195
86 -> 99 -0.15205
88 ->102 0.19310

90 ->100 0.12795
90 ->102 -0.18294
91 ->102 0.16300
92 ->103 -0.10711

Excited State 78: Singlet-A 7.1055 eV 174.49 nm f=0.0000 <S**2>=0.000
80 -> 95 0.49933
81 -> 95 0.11784
85 -> 97 -0.24938
85 -> 99 0.15871
86 ->100 -0.16146
90 ->101 0.12912
93 ->103 -0.21927

Excited State 79: Singlet-A 7.1451 eV 173.52 nm f=0.1486 <S**2>=0.000
79 -> 95 0.59639
85 -> 96 -0.17927
85 ->100 0.18774
90 ->102 0.10957

Excited State 80: Singlet-A 7.1985 eV 172.24 nm f=0.0373 <S**2>=0.000
77 -> 95 -0.11167
79 -> 95 -0.10506
85 -> 98 0.47213
85 ->100 0.18985
88 ->102 0.13992
92 ->103 0.35468

Excited State 81: Singlet-A 7.2055 eV 172.07 nm f=0.0000 <S**2>=0.000
78 -> 95 0.10088
85 -> 97 0.41131
85 -> 99 0.38528
86 ->100 -0.12861
87 ->102 -0.14104
91 ->103 -0.16039
93 ->103 -0.17051

Excited State 82: Singlet-A 7.2514 eV 170.98 nm f=0.3359 <S**2>=0.000
79 -> 95 -0.12246
85 -> 98 -0.25420
85 ->100 0.20122
85 ->102 -0.12650
86 ->101 0.54494

Excited State 83: Singlet-A 7.2882 eV 170.12 nm f=0.0458 <S**2>=0.000
76 -> 95 0.17858
77 -> 95 0.38371
79 -> 95 -0.13664
83 -> 96 -0.13247
85 -> 98 -0.12561
85 ->100 0.36551
86 ->101 -0.15406
92 ->103 0.11282

Excited State 84: Singlet-A 7.2919 eV 170.03 nm f=0.0007 <S**2>=0.000
78 -> 95 0.42435
80 -> 95 -0.20026
84 -> 96 0.17638
85 -> 97 -0.16217
85 -> 99 -0.15427
86 ->102 0.25833
90 ->101 0.13809
93 ->103 -0.12541

Excited State 85: Singlet-A 7.3212 eV 169.35 nm f=0.0000 <S**2>=0.000
78 -> 95 0.48660
80 -> 95 0.10733
86 ->100 0.10621
86 ->102 -0.28416
90 ->101 -0.13057
93 ->103 0.11285
94 ->104 -0.15068

Excited State 86: Singlet-A 7.3423 eV 168.86 nm f=0.0000 <S**2>=0.000
80 -> 95 0.15702
85 -> 99 0.15463
86 -> 96 0.10553
86 ->102 0.52209
87 ->100 -0.10674
90 ->101 -0.15724
91 ->103 0.11061

Excited State 87: Singlet-A 7.3896 eV 167.78 nm f=0.0785 <S**2>=0.000
77 -> 95 0.24744
80 -> 95 0.11697
85 -> 99 -0.12776

85 ->100 -0.21550
94 ->104 0.50543

Excited State 88: Singlet-A 7.3900 eV 167.77 nm f=0.1872 <S**2>=0.000
77 -> 95 0.38723
85 ->100 -0.33773
86 ->101 0.13963
94 ->104 -0.32679

Excited State 89: Singlet-A 7.4952 eV 165.42 nm f=0.0086 <S**2>=0.000
93 ->104 0.10877
94 ->105 0.66464

Excited State 90: Singlet-A 7.5070 eV 165.16 nm f=0.0000 <S**2>=0.000
80 -> 95 -0.10360
83 -> 99 -0.10010
84 -> 96 0.11216
85 -> 97 -0.21430
85 -> 99 0.33907
85 ->101 -0.10137
86 -> 98 -0.10609
90 ->103 -0.10687
91 ->101 -0.13316
91 ->103 -0.21281
93 ->103 0.19364
94 ->104 0.26368

Excited State 91: Singlet-A 7.5183 eV 164.91 nm f=0.0713 <S**2>=0.000
76 -> 95 0.46210
77 -> 95 -0.24614
79 -> 95 0.10050
85 -> 98 -0.13568
85 ->100 -0.20319
87 ->101 -0.13446
92 ->103 0.15008
94 ->105 0.11872

Excited State 92: Singlet-A 7.5196 eV 164.88 nm f=0.0001 <S**2>=0.000
84 -> 96 0.10649
85 ->101 -0.29167
91 ->103 0.55100

Excited State 93: Singlet-A 7.6246 eV 162.61 nm f=0.0563 <S**2>=0.000

74 -> 95 -0.11061
76 -> 95 0.36859
82 -> 95 0.13677
82 -> 97 0.10029
83 -> 96 -0.16501
83 -> 98 -0.11277
84 -> 95 -0.13416
85 -> 96 -0.10655
85 -> 98 0.14785
86 -> 97 -0.12600
87 ->101 0.16239
87 ->103 0.12468
92 ->103 -0.23657
94 ->103 -0.13327

Excited State 94: Singlet-A 7.6286 eV 162.53 nm f=0.0000 <S**2>=0.000
85 -> 99 0.21778
85 ->101 0.52719
90 ->103 0.16742
91 ->103 0.26752

Excited State 95: Singlet-A 7.6854 eV 161.32 nm f=0.0420 <S**2>=0.000
76 -> 95 0.22828
77 -> 95 0.12323
83 -> 96 0.49907
83 -> 98 0.17680
84 -> 97 -0.22303
84 -> 99 -0.12074
85 ->102 -0.13627

Excited State 96: Singlet-A 7.7033 eV 160.95 nm f=0.0000 <S**2>=0.000
75 -> 95 -0.13126
78 -> 95 -0.16413
83 -> 97 -0.32327
84 -> 96 0.48354
85 -> 99 -0.11605

Excited State 97: Singlet-A 7.7815 eV 159.33 nm f=0.0000 <S**2>=0.000
85 ->101 -0.13191
90 ->103 0.48988
94 ->106 -0.43549

Excited State 98: Singlet-A 7.8116 eV 158.72 nm f=0.1502 <S**2>=0.000

84 -> 97 -0.19361
85 ->102 0.25733
87 ->103 0.10828
89 ->103 0.57176

Excited State 99: Singlet-A 7.8228 eV 158.49 nm f=0.0001 <S**2>=0.000
85 ->101 -0.12200
88 ->103 -0.17031
90 ->103 0.39442
94 ->106 0.50310

Excited State 100: Singlet-A 7.8525 eV 157.89 nm f=0.0354 <S**2>=0.000
74 -> 95 0.11119
83 -> 96 -0.15080
84 -> 97 -0.11894
85 ->102 -0.33850
87 ->103 0.51771

Table A4.8. Excitation Energies and Oscillator Strengths of 5Int Using the TD-B3LYP Method with 6-31G(d) Basis Sets in Chloroform.

Excited State 1: Singlet-A 2.1453 eV 577.94 nm f=0.1147 <S**2>=0.000
94 -> 95 0.70768
This state for optimization and/or second-order correction.
Total Energy, E(TD-HF/TD-KS) = -1182.77834307
Copying the excited state density for this state as the 1-particle RhoCI density.

Excited State 2: Singlet-A 2.5489 eV 486.42 nm f=0.0107 <S**2>=0.000
93 -> 95 0.60410
94 -> 96 0.35631

Excited State 3: Singlet-A 2.8565 eV 434.04 nm f=0.3638 <S**2>=0.000
93 -> 95 -0.34094
94 -> 96 0.60214
94 -> 98 -0.10378

Excited State 4: Singlet-A 3.3170 eV 373.78 nm f=0.1240 <S**2>=0.000
93 -> 96 0.67344
94 -> 97 0.19233

Excited State 5: Singlet-A 3.5266 eV 351.57 nm f=0.0177 <S**2>=0.000
93 -> 96 -0.20030

94 -> 97 0.66474

Excited State 6: Singlet-A 3.7838 eV 327.67 nm f=0.0995 <S**2>=0.000
91 -> 95 -0.22542
94 -> 98 0.64631

Excited State 7: Singlet-A 3.9228 eV 316.06 nm f=0.0145 <S**2>=0.000
92 -> 95 0.68962

Excited State 8: Singlet-A 3.9915 eV 310.62 nm f=0.0874 <S**2>=0.000
90 -> 95 0.10279
91 -> 95 0.64067
93 -> 97 0.14368
94 -> 98 0.20653

Excited State 9: Singlet-A 4.1093 eV 301.72 nm f=0.0002 <S**2>=0.000
87 -> 95 -0.16977
90 -> 95 0.46945
94 -> 98 -0.10850
94 -> 99 -0.45763

Excited State 10: Singlet-A 4.1429 eV 299.27 nm f=0.0506 <S**2>=0.000
88 -> 95 0.14010
93 -> 98 -0.11853
94 ->100 0.65584

Excited State 11: Singlet-A 4.1620 eV 297.90 nm f=0.0018 <S**2>=0.000
90 -> 95 -0.39310
93 -> 97 0.41703
94 -> 99 -0.37099

Excited State 12: Singlet-A 4.1743 eV 297.02 nm f=0.0074 <S**2>=0.000
89 -> 95 0.66033
90 -> 96 0.18194

Excited State 13: Singlet-A 4.2382 eV 292.54 nm f=0.1621 <S**2>=0.000
87 -> 95 0.15802
89 -> 96 0.10812
90 -> 95 0.25275
91 -> 95 -0.12631
93 -> 97 0.52907
94 -> 99 0.28476

Excited State 14: Singlet-A 4.3326 eV 286.17 nm f=0.0009 <S**2>=0.000
88 -> 95 0.52503
93 -> 98 -0.38958
93 -> 99 0.10337
94 ->100 -0.20291

Excited State 15: Singlet-A 4.4097 eV 281.17 nm f=0.0039 <S**2>=0.000
88 -> 95 0.38355
91 -> 96 0.10759
93 -> 98 0.55086
94 ->101 0.15708

Excited State 16: Singlet-A 4.4737 eV 277.14 nm f=0.0023 <S**2>=0.000
87 -> 95 0.63469
89 -> 96 0.13361
94 -> 99 -0.21099

Excited State 17: Singlet-A 4.6451 eV 266.91 nm f=0.0112 <S**2>=0.000
89 -> 96 0.21575
90 -> 95 -0.11969
92 -> 96 0.58685
93 ->100 -0.24644

Excited State 18: Singlet-A 4.6659 eV 265.72 nm f=0.0038 <S**2>=0.000
89 -> 95 -0.17425
90 -> 96 0.30358
91 -> 96 0.54590
93 -> 98 -0.11683
94 ->101 0.16221

Excited State 19: Singlet-A 4.7593 eV 260.51 nm f=0.0137 <S**2>=0.000
87 -> 96 0.10543
89 -> 95 -0.13191
90 -> 96 0.54010
91 -> 96 -0.25255
93 -> 99 -0.13233
94 ->101 -0.20636

Excited State 20: Singlet-A 4.7658 eV 260.16 nm f=0.0003 <S**2>=0.000
87 -> 95 -0.12369
89 -> 96 0.55068
90 -> 95 -0.14537
90 -> 97 -0.10079

92 -> 96 -0.10578
93 ->100 0.31661

Excited State 21: Singlet-A 4.7825 eV 259.25 nm f=0.0103 <S**2>=0.000
91 -> 96 -0.15205
93 -> 99 -0.37305
94 ->101 0.55303

Excited State 22: Singlet-A 4.8180 eV 257.34 nm f=0.1301 <S**2>=0.000
89 -> 96 -0.21681
92 -> 96 0.32291
93 ->100 0.55159

Excited State 23: Singlet-A 4.9177 eV 252.12 nm f=0.1210 <S**2>=0.000
88 -> 95 -0.14476
90 -> 96 0.15101
91 -> 96 -0.27427
93 -> 99 0.53165
94 ->101 0.23241

Excited State 24: Singlet-A 5.1280 eV 241.78 nm f=0.0075 <S**2>=0.000
88 -> 96 0.67432
91 -> 97 0.10308
92 -> 98 -0.11817

Excited State 25: Singlet-A 5.2015 eV 238.36 nm f=0.0070 <S**2>=0.000
87 -> 96 0.64768
91 -> 98 -0.13330
92 -> 97 0.14828

Excited State 26: Singlet-A 5.3473 eV 231.86 nm f=0.0085 <S**2>=0.000
83 -> 95 0.20517
85 -> 95 0.15008
86 -> 95 0.64942

Excited State 27: Singlet-A 5.4294 eV 228.36 nm f=0.0005 <S**2>=0.000
84 -> 95 -0.11949
89 -> 98 0.25075
89 -> 99 0.10187
90 -> 97 0.15686
90 -> 98 0.10122
90 ->100 0.11668
91 -> 97 0.23754

93 ->101 0.49905

Excited State 28: Singlet-A 5.4406 eV 227.89 nm f=0.0097 <S**2>=0.000
87 -> 98 0.10314
89 -> 97 0.29541
89 ->100 0.17774
89 ->101 -0.11918
90 -> 98 0.37589
90 -> 99 0.13914
91 -> 98 0.13673
92 -> 97 0.30803
93 ->101 -0.17763

Excited State 29: Singlet-A 5.4634 eV 226.94 nm f=0.0005 <S**2>=0.000
84 -> 95 0.11863
89 -> 98 0.35427
89 -> 99 0.13156
90 -> 97 0.34039
90 ->100 0.15705
90 ->101 -0.10581
92 -> 98 0.18414
93 ->101 -0.33679

Excited State 30: Singlet-A 5.5007 eV 225.40 nm f=0.0128 <S**2>=0.000
83 -> 95 0.32837
85 -> 95 0.53717
86 -> 95 -0.22210
90 -> 98 -0.12740

Excited State 31: Singlet-A 5.5619 eV 222.92 nm f=0.0570 <S**2>=0.000
85 -> 95 -0.12638
87 -> 96 -0.14738
89 -> 97 -0.17761
90 -> 98 -0.17933
90 -> 99 -0.10341
92 -> 97 0.57911

Excited State 32: Singlet-A 5.6407 eV 219.80 nm f=0.1004 <S**2>=0.000
84 -> 95 -0.23604
88 -> 96 -0.10084
91 -> 97 0.49388
93 ->101 -0.22525
94 ->102 0.26888

Excited State 33: Singlet-A 5.6785 eV 218.34 nm f=0.0432 <S**2>=0.000
84 -> 95 0.37243
89 -> 98 -0.15151
89 -> 99 -0.14079
90 -> 97 0.11969
90 ->100 -0.13639
91 -> 97 0.30974
94 ->102 -0.37074

Excited State 34: Singlet-A 5.7164 eV 216.89 nm f=0.1596 <S**2>=0.000
83 -> 95 0.56622
85 -> 95 -0.34778
88 -> 97 0.10481

Excited State 35: Singlet-A 5.7568 eV 215.37 nm f=0.0072 <S**2>=0.000
84 -> 95 -0.13385
89 -> 96 0.10674
89 -> 97 0.32732
89 -> 99 -0.15141
89 ->100 -0.18559
90 -> 96 0.11507
90 -> 97 0.36237
90 -> 99 -0.18926
90 ->100 -0.17265
91 -> 97 -0.13635
92 -> 98 -0.13273

Excited State 36: Singlet-A 5.7598 eV 215.26 nm f=0.0069 <S**2>=0.000
84 -> 95 0.12313
89 -> 96 -0.10751
89 -> 97 0.37646
89 -> 99 0.11008
89 ->100 -0.24282
90 -> 96 0.11455
90 -> 97 -0.31643
90 -> 99 -0.15390
90 ->100 0.18366
91 -> 97 0.12112
92 -> 98 0.12071

Excited State 37: Singlet-A 5.8239 eV 212.89 nm f=0.2356 <S**2>=0.000
84 -> 95 0.18528

88 -> 96 0.11896
88 -> 98 -0.12680
89 -> 98 -0.11597
90 ->100 -0.14367
92 -> 98 0.44651
94 ->102 0.38803

Excited State 38: Singlet-A 5.8830 eV 210.75 nm f=0.0914 <S**2>=0.000
82 -> 95 -0.12133
84 -> 95 -0.37770
87 -> 97 -0.23812
89 -> 98 -0.12047
92 -> 98 0.40058
94 ->102 -0.25754
94 ->103 0.10806

Excited State 39: Singlet-A 5.9161 eV 209.57 nm f=0.0228 <S**2>=0.000
87 -> 98 -0.13938
88 ->100 0.10147
90 -> 98 -0.12540
91 -> 98 0.59818
92 ->100 0.13428

Excited State 40: Singlet-A 5.9427 eV 208.63 nm f=0.0239 <S**2>=0.000
82 -> 95 0.66212
94 ->102 -0.11691

Excited State 41: Singlet-A 6.0984 eV 203.30 nm f=0.0981 <S**2>=0.000
88 -> 97 0.62969
90 -> 98 -0.10413
92 ->100 0.14253
93 ->102 0.16953

Excited State 42: Singlet-A 6.1020 eV 203.19 nm f=0.0055 <S**2>=0.000
83 -> 96 0.10680
85 -> 96 0.11260
86 -> 96 0.46691
87 -> 97 0.35840
87 ->100 -0.10324
90 -> 97 -0.10562
91 ->100 0.18237
92 -> 99 0.10537
94 ->103 0.13498

Excited State 43: Singlet-A 6.1605 eV 201.26 nm f=0.0012 <S**2>=0.000
88 -> 98 -0.13113
89 -> 98 -0.16540
90 -> 97 0.12458
91 -> 99 0.18733
91 ->100 0.21629
92 -> 99 0.53238
92 ->100 0.18277

Excited State 44: Singlet-A 6.1621 eV 201.20 nm f=0.0004 <S**2>=0.000
89 -> 97 0.14053
90 -> 98 -0.16560
91 -> 98 -0.10474
91 -> 99 0.31702
91 ->100 -0.16676
92 -> 99 -0.20368
92 ->100 0.47827

Excited State 45: Singlet-A 6.2171 eV 199.42 nm f=0.0011 <S**2>=0.000
85 -> 96 -0.16782
86 -> 96 0.31935
87 -> 97 -0.20479
88 -> 99 0.11628
89 -> 98 -0.28438
89 -> 99 0.15159
90 -> 97 0.17920
90 ->100 0.30428
92 -> 99 -0.10572

Excited State 46: Singlet-A 6.2209 eV 199.30 nm f=0.0077 <S**2>=0.000
87 -> 98 -0.15522
89 -> 97 -0.17080
89 ->100 -0.26511
90 -> 98 0.40492
90 -> 99 -0.24399
91 -> 99 -0.13527
92 ->100 0.23730

Excited State 47: Singlet-A 6.2741 eV 197.61 nm f=0.0317 <S**2>=0.000
81 -> 95 -0.17541
83 -> 96 -0.26750
86 -> 96 -0.15639

87 -> 97 0.39329
89 -> 98 -0.27455
89 -> 99 0.14476
90 ->100 0.13257
91 ->100 0.16670
92 -> 99 -0.19441

Excited State 48: Singlet-A 6.2926 eV 197.03 nm f=0.0001 <S**2>=0.000
81 -> 95 0.16008
83 -> 96 0.26186
85 -> 96 0.49075
86 -> 96 -0.13421
89 -> 98 -0.17317
89 -> 99 0.11278
90 ->100 0.16970
91 ->100 -0.11888
94 ->103 -0.12020

Excited State 49: Singlet-A 6.3074 eV 196.57 nm f=0.1660 <S**2>=0.000
87 -> 98 0.21723
89 -> 97 -0.11052
89 ->100 -0.22698
90 -> 98 0.12747
90 -> 99 -0.13174
91 -> 98 0.10743
91 -> 99 0.51535
92 ->100 -0.19585

Excited State 50: Singlet-A 6.3692 eV 194.66 nm f=0.0160 <S**2>=0.000
87 -> 98 -0.33972
88 -> 98 0.17593
89 ->100 0.10012
92 ->100 -0.15953
93 ->102 0.46014
94 ->103 -0.11163
94 ->104 -0.12942

Excited State 51: Singlet-A 6.3702 eV 194.63 nm f=0.0176 <S**2>=0.000
83 -> 96 -0.12159
85 -> 96 -0.13180
86 -> 96 0.13056
87 -> 98 0.12938
88 -> 98 0.45343

91 ->100 -0.17653
92 -> 99 0.16612
93 ->102 -0.17892
94 ->103 -0.28809

Excited State 52: Singlet-A 6.4378 eV 192.59 nm f=0.0476 <S**2>=0.000
83 -> 96 0.13966
86 -> 98 0.10334
87 -> 97 -0.11165
88 -> 98 0.17974
89 -> 99 -0.19366
91 ->100 0.47047
92 -> 99 -0.19495
94 ->103 -0.26910

Excited State 53: Singlet-A 6.4447 eV 192.38 nm f=0.0052 <S**2>=0.000
81 -> 95 0.21565
83 -> 96 0.26865
85 -> 96 -0.21407
86 -> 96 -0.14435
87 ->100 0.16357
88 -> 98 0.25191
89 -> 99 0.15791
90 ->100 -0.15688
94 ->103 0.36459

Excited State 54: Singlet-A 6.4690 eV 191.66 nm f=0.0766 <S**2>=0.000
84 -> 96 0.38935
87 -> 98 0.30143
88 -> 97 -0.15103
89 ->100 0.19524
90 -> 99 -0.29548
91 -> 98 0.10199
92 ->101 -0.12866
93 ->102 0.16598

Excited State 55: Singlet-A 6.5038 eV 190.63 nm f=0.0536 <S**2>=0.000
84 -> 96 0.30153
87 -> 98 0.15881
89 ->100 -0.32614
90 -> 99 0.42832
93 ->102 0.17140
94 ->104 0.17795

Excited State 56: Singlet-A 6.5131 eV 190.36 nm f=0.0079 <S**2>=0.000
84 -> 96 -0.10131
89 ->100 0.11694
90 -> 99 -0.15985
93 ->102 0.18775
94 ->104 0.60972

Excited State 57: Singlet-A 6.5431 eV 189.49 nm f=0.1093 <S**2>=0.000
88 -> 98 -0.10277
89 -> 99 0.49701
90 ->100 -0.37841
91 ->100 0.10125
91 ->101 0.10967
94 ->103 -0.14727

Excited State 58: Singlet-A 6.6021 eV 187.80 nm f=0.0010 <S**2>=0.000
83 -> 96 -0.20852
85 -> 96 0.22826
87 -> 97 -0.12315
88 -> 98 0.20601
88 -> 99 0.50388
91 ->100 0.10866
94 ->103 0.20309

Excited State 59: Singlet-A 6.6337 eV 186.90 nm f=0.0237 <S**2>=0.000
82 -> 96 -0.13563
86 -> 97 -0.14872
87 -> 98 0.13315
87 -> 99 -0.31468
88 ->100 0.47475
92 ->101 0.24491

Excited State 60: Singlet-A 6.6608 eV 186.14 nm f=0.3788 <S**2>=0.000
78 -> 95 0.11984
80 -> 95 0.16442
82 -> 96 -0.14565
84 -> 96 0.35346
86 -> 97 0.11791
87 -> 98 -0.28622
88 -> 97 0.11856
91 -> 99 0.11405
92 ->100 -0.10486

92 ->101 -0.10875
93 ->102 -0.26482
94 ->106 -0.19174

Excited State 61: Singlet-A 6.6936 eV 185.23 nm f=0.0927 <S**2>=0.000
81 -> 95 0.26763
83 -> 96 -0.32422
85 -> 96 0.11387
86 -> 96 0.10994
87 ->100 0.20378
88 -> 99 -0.25241
91 -> 97 0.10467
91 ->101 0.35597

Excited State 62: Singlet-A 6.7075 eV 184.84 nm f=0.0748 <S**2>=0.000
78 -> 95 -0.33113
80 -> 95 -0.16452
82 -> 96 0.45593
84 -> 96 0.21977
87 -> 99 -0.14015
92 ->101 0.18163

Excited State 63: Singlet-A 6.7224 eV 184.43 nm f=0.0447 <S**2>=0.000
81 -> 95 0.50121
83 -> 96 -0.22129
86 -> 96 -0.10504
87 ->100 -0.31360
91 ->101 -0.20551

Excited State 64: Singlet-A 6.7629 eV 183.33 nm f=0.0004 <S**2>=0.000
87 -> 99 0.54229
88 ->100 0.37099
94 ->106 -0.14414

Excited State 65: Singlet-A 6.8024 eV 182.26 nm f=0.0026 <S**2>=0.000
87 ->100 -0.18780
88 -> 99 -0.10306
93 ->104 -0.23016
94 ->105 0.61306

Excited State 66: Singlet-A 6.8154 eV 181.92 nm f=0.0109 <S**2>=0.000
78 -> 95 -0.17485
80 -> 95 0.60790

81 -> 96 0.14219
82 -> 96 0.15865

Excited State 67: Singlet-A 6.8555 eV 180.85 nm f=0.0215 <S**2>=0.000
78 -> 95 0.20401
86 -> 97 0.20846
87 -> 99 0.11261
88 ->100 -0.17860
92 ->101 0.56132

Excited State 68: Singlet-A 6.9101 eV 179.43 nm f=0.0279 <S**2>=0.000
81 -> 95 0.16336
84 -> 95 -0.10068
87 ->100 0.44832
88 -> 98 -0.15264
88 -> 99 0.22418
91 ->101 -0.12307
93 ->104 -0.10632
94 ->103 -0.18375
94 ->105 0.17760

Excited State 69: Singlet-A 6.9573 eV 178.21 nm f=0.0265 <S**2>=0.000
78 -> 95 0.50708
82 -> 96 0.40370
86 -> 97 -0.15918
92 ->101 -0.10643

Excited State 70: Singlet-A 6.9758 eV 177.73 nm f=0.3676 <S**2>=0.000
79 -> 95 0.43616
86 -> 98 0.12470
87 ->100 0.10638
88 -> 99 -0.12084
90 ->101 -0.20038
91 ->101 -0.39054

Excited State 71: Singlet-A 7.0322 eV 176.31 nm f=0.0645 <S**2>=0.000
82 -> 96 -0.11258
85 -> 97 0.28461
86 -> 97 -0.14737
88 ->101 0.10295
89 ->101 0.25697
93 ->103 0.44129
94 ->106 -0.20275

Excited State 72: Singlet-A 7.0447 eV 176.00 nm f=0.0008 <S**2>=0.000
77 -> 95 0.11268
79 -> 95 0.29533
90 ->101 0.58851

Excited State 73: Singlet-A 7.0774 eV 175.18 nm f=0.0173 <S**2>=0.000
89 ->101 0.61139
93 ->103 -0.23366

Excited State 74: Singlet-A 7.1126 eV 174.32 nm f=0.0585 <S**2>=0.000
77 -> 95 -0.12703
79 -> 95 -0.32807
86 -> 98 0.38017
88 -> 99 -0.10559
90 ->101 0.24992
91 ->101 -0.28624

Excited State 75: Singlet-A 7.1392 eV 173.67 nm f=0.0211 <S**2>=0.000
83 -> 97 0.17062
86 -> 97 0.26170
88 ->100 0.12408
88 ->101 -0.10567
93 ->103 0.34093
94 ->104 0.10485
94 ->106 0.42162

Excited State 76: Singlet-A 7.1742 eV 172.82 nm f=0.1152 <S**2>=0.000
80 -> 95 0.15145
83 -> 97 0.27019
85 -> 97 0.24123
86 -> 97 0.37512
88 ->101 0.14010
89 ->101 -0.10868
93 ->103 -0.16580
94 ->106 -0.25927

Excited State 77: Singlet-A 7.1827 eV 172.61 nm f=0.0114 <S**2>=0.000
74 -> 95 0.10462
77 -> 95 0.57911
79 -> 95 -0.11960
80 -> 96 -0.10992
83 -> 98 0.10672

85 -> 98 0.12542
86 -> 98 0.12000
93 ->104 0.14803

Excited State 78: Singlet-A 7.2214 eV 171.69 nm f=0.0003 <S**2>=0.000
77 -> 95 -0.18628
84 -> 97 0.14036
86 -> 98 -0.10927
93 ->104 0.57531
94 ->105 0.22304
94 ->109 0.10771

Excited State 79: Singlet-A 7.2401 eV 171.25 nm f=0.0038 <S**2>=0.000
83 -> 97 -0.18965
85 -> 97 -0.35452
86 -> 97 0.22280
88 ->101 0.45542
93 ->103 0.17467

Excited State 80: Singlet-A 7.3094 eV 169.62 nm f=0.0358 <S**2>=0.000
74 -> 95 -0.11474
77 -> 95 -0.15657
80 -> 96 -0.16024
83 -> 98 0.22888
84 -> 97 0.17882
85 -> 98 0.32838
85 -> 99 -0.10445
86 -> 98 0.11953
87 ->101 0.36544
93 ->104 -0.10630

Excited State 81: Singlet-A 7.3521 eV 168.64 nm f=0.0013 <S**2>=0.000
84 -> 97 0.29723
86 -> 98 -0.26597
87 ->101 -0.14749
91 ->101 -0.10993
93 ->106 0.22032
94 ->108 0.34777
94 ->109 -0.21906

Excited State 82: Singlet-A 7.3702 eV 168.22 nm f=0.0548 <S**2>=0.000
83 -> 97 0.14969
86 -> 97 -0.11285

88 ->101 0.26095
93 ->103 -0.11672
93 ->105 -0.15498
94 ->106 0.16990
94 ->107 0.52319

Excited State 83: Singlet-A 7.3811 eV 167.98 nm f=0.0375 <S**2>=0.000
81 -> 96 0.53460
85 -> 97 0.15693
88 ->101 0.23445
94 ->107 -0.24433

Excited State 84: Singlet-A 7.4067 eV 167.40 nm f=0.0091 <S**2>=0.000
74 -> 95 0.13717
75 -> 95 0.19214
77 -> 95 0.11259
80 -> 96 0.22538
83 -> 98 -0.19394
84 -> 97 0.11758
86 -> 98 -0.11780
86 -> 99 0.11173
87 ->101 0.46545
94 ->108 -0.14163

Excited State 85: Singlet-A 7.4131 eV 167.25 nm f=0.1253 <S**2>=0.000
79 -> 96 -0.11174
81 -> 96 0.33737
83 -> 97 -0.29949
86 -> 97 0.20414
88 ->101 -0.26982
93 ->105 -0.10691
94 ->107 0.26400

Excited State 86: Singlet-A 7.4761 eV 165.84 nm f=0.0000 <S**2>=0.000
75 -> 95 0.14958
80 -> 96 0.17523
84 -> 97 -0.18752
86 -> 98 0.19865
93 ->104 0.10833
94 ->108 0.49140

Excited State 87: Singlet-A 7.4888 eV 165.56 nm f=0.0403 <S**2>=0.000
76 -> 95 0.26031

81 -> 96 0.17357
83 -> 97 0.39604
85 -> 97 -0.34176
88 ->101 -0.13361
93 ->103 0.10473
94 ->106 -0.10434
94 ->110 0.10267

Excited State 88: Singlet-A 7.5161 eV 164.96 nm f=0.0071 <S**2>=0.000
74 -> 95 0.29874
75 -> 95 0.22502
77 -> 95 -0.10346
80 -> 96 0.21584
82 -> 97 -0.13499
83 -> 98 0.23955
85 -> 98 0.24382
86 -> 99 -0.16313
87 ->101 -0.21007
94 ->108 -0.15557

Excited State 89: Singlet-A 7.5508 eV 164.20 nm f=0.0722 <S**2>=0.000
72 -> 95 0.13238
73 -> 95 -0.15403
76 -> 95 0.59276
83 -> 97 -0.11788
85 -> 97 0.16743

Excited State 90: Singlet-A 7.5622 eV 163.95 nm f=0.0264 <S**2>=0.000
84 -> 97 0.45675
85 -> 98 -0.37417
86 -> 98 0.23350
86 -> 99 -0.17971

Excited State 91: Singlet-A 7.6068 eV 162.99 nm f=0.0098 <S**2>=0.000
93 ->105 0.62127
94 ->106 -0.14660
94 ->107 0.22445

Excited State 92: Singlet-A 7.6426 eV 162.23 nm f=0.0002 <S**2>=0.000
74 -> 95 0.10000
75 -> 95 0.17780
80 -> 96 -0.12580
82 -> 97 -0.13000

83 -> 98 0.39636
83 -> 99 -0.10473
85 -> 98 -0.23257
86 -> 98 -0.10822
86 -> 99 0.24617
93 ->106 -0.21097
94 ->108 0.12412
94 ->109 0.12043

Excited State 93: Singlet-A 7.6550 eV 161.97 nm f=0.1719 <S**2>=0.000
73 -> 95 0.10222
79 -> 96 -0.14454
84 -> 98 -0.32996
86 ->100 0.53118
93 ->105 -0.12147

Excited State 94: Singlet-A 7.6609 eV 161.84 nm f=0.0243 <S**2>=0.000
74 -> 95 -0.26138
75 -> 95 0.13345
77 -> 95 0.10218
78 -> 96 -0.22388
80 -> 96 0.20086
82 -> 97 0.34018
83 -> 98 0.16518
85 -> 98 -0.12076
86 -> 98 0.10057
86 -> 99 0.18685
93 ->106 0.17576
94 ->108 -0.12031

Excited State 95: Singlet-A 7.6776 eV 161.49 nm f=0.0168 <S**2>=0.000
73 -> 95 0.40060
76 -> 95 0.12818
77 -> 96 0.13916
79 -> 96 -0.13297
84 -> 98 0.22987
94 ->110 -0.36823
94 ->111 -0.14677

Excited State 96: Singlet-A 7.6946 eV 161.13 nm f=0.0013 <S**2>=0.000
74 -> 95 0.21306
75 -> 95 0.34582
78 -> 96 0.13059

80 -> 96 -0.34087
82 -> 97 0.20136
83 -> 98 -0.15464
85 -> 99 -0.17940
93 ->106 0.17273
94 ->109 -0.10427

Excited State 97: Singlet-A 7.7355 eV 160.28 nm f=0.0021 <S**2>=0.000
74 -> 95 0.42460
75 -> 95 -0.35179
78 -> 96 -0.20137
82 -> 97 0.27447
85 -> 99 -0.14381

Excited State 98: Singlet-A 7.7389 eV 160.21 nm f=0.0020 <S**2>=0.000
86 -> 99 0.25274
93 ->104 -0.12668
93 ->106 0.26018
94 ->109 0.50899

Excited State 99: Singlet-A 7.7486 eV 160.01 nm f=0.0841 <S**2>=0.000
73 -> 95 -0.29551
77 -> 96 -0.10994
79 -> 96 0.32742
84 -> 98 0.22221
85 ->100 0.17726
86 ->100 0.24734
94 ->110 -0.31049

Excited State 100: Singlet-A 7.7587 eV 159.80 nm f=0.0092 <S**2>=0.000
72 -> 95 -0.14719
73 -> 95 0.10776
79 -> 96 0.27364
82 -> 98 0.10720
84 -> 98 -0.24209
85 ->100 -0.15809
91 ->102 0.40321
94 ->110 -0.23350

Table A4.9. Excitation Energies and Oscillator Strengths of 6Int Using the TD-B3LYP Method with 6-31G(d) Basis Sets in Chloroform.

Excited State 1: Singlet-A 2.1993 eV 563.75 nm f=0.1155 <S**2>=0.000
94 -> 95 0.70758
This state for optimization and/or second-order correction.
Total Energy, E(TD-HF/TD-KS) = -1182.77816052
Copying the excited state density for this state as the 1-particle RhoCI density.

Excited State 2: Singlet-A 2.5655 eV 483.28 nm f=0.0305 <S**2>=0.000
93 -> 95 0.63472
94 -> 96 -0.29816

Excited State 3: Singlet-A 2.9616 eV 418.64 nm f=0.3870 <S**2>=0.000
93 -> 95 0.28351
94 -> 96 0.62939

Excited State 4: Singlet-A 3.4035 eV 364.28 nm f=0.1360 <S**2>=0.000
93 -> 96 0.68317
94 -> 97 -0.11709

Excited State 5: Singlet-A 3.5915 eV 345.22 nm f=0.0131 <S**2>=0.000
90 -> 95 -0.18823
92 -> 95 0.52969
93 -> 96 -0.14542
94 -> 97 -0.37233

Excited State 6: Singlet-A 3.6598 eV 338.78 nm f=0.0513 <S**2>=0.000
90 -> 95 -0.26644
92 -> 95 0.30584
94 -> 97 0.52930
94 -> 98 0.14060

Excited State 7: Singlet-A 3.8192 eV 324.64 nm f=0.0708 <S**2>=0.000
88 -> 95 -0.12652
90 -> 95 0.14218
91 -> 95 -0.16227
94 -> 97 -0.13305
94 -> 98 0.62860

Excited State 8: Singlet-A 3.8573 eV 321.43 nm f=0.0210 <S**2>=0.000
90 -> 95 0.57308
90 -> 96 -0.10680

92 -> 95 0.31811
94 -> 97 0.14471

Excited State 9: Singlet-A 3.9437 eV 314.39 nm f=0.0904 <S**2>=0.000
91 -> 95 0.66120
94 -> 98 0.15814
94 -> 99 0.11033

Excited State 10: Singlet-A 4.1535 eV 298.51 nm f=0.0110 <S**2>=0.000
88 -> 95 0.11431
89 -> 95 0.55208
89 -> 96 0.13341
94 -> 99 -0.34111

Excited State 11: Singlet-A 4.1622 eV 297.88 nm f=0.0081 <S**2>=0.000
89 -> 95 0.33524
92 -> 96 0.10061
93 -> 97 0.13445
94 -> 99 0.56619

Excited State 12: Singlet-A 4.2494 eV 291.77 nm f=0.0663 <S**2>=0.000
88 -> 95 0.26522
89 -> 95 -0.11980
93 -> 97 0.55898
94 ->100 0.24310

Excited State 13: Singlet-A 4.3183 eV 287.11 nm f=0.0358 <S**2>=0.000
87 -> 95 -0.10433
92 -> 96 -0.16374
93 -> 97 -0.31688
93 -> 98 -0.21148
94 -> 99 0.12101
94 ->100 0.52435

Excited State 14: Singlet-A 4.3638 eV 284.12 nm f=0.0021 <S**2>=0.000
87 -> 95 0.31172
88 -> 95 0.10495
93 -> 98 0.54822
94 ->100 0.22874

Excited State 15: Singlet-A 4.4216 eV 280.40 nm f=0.0097 <S**2>=0.000
87 -> 95 -0.30057
88 -> 95 0.42076

92 -> 96 0.33107
93 -> 97 -0.16126
93 -> 99 -0.11019
94 ->100 -0.12293
94 ->101 -0.13326

Excited State 16: Singlet-A 4.4715 eV 277.28 nm f=0.0540 <S**2>=0.000
87 -> 95 0.47282
88 -> 95 0.34146
93 -> 98 -0.29770
94 ->100 -0.16052

Excited State 17: Singlet-A 4.5036 eV 275.30 nm f=0.0144 <S**2>=0.000
87 -> 95 0.17898
88 -> 95 -0.19560
90 -> 96 -0.12116
92 -> 96 0.52806
93 -> 98 -0.20933
94 ->100 0.21068

Excited State 18: Singlet-A 4.7114 eV 263.16 nm f=0.0056 <S**2>=0.000
90 -> 96 0.43305
91 -> 96 -0.32182
92 -> 98 0.10262
93 -> 99 -0.34992

Excited State 19: Singlet-A 4.7379 eV 261.69 nm f=0.0174 <S**2>=0.000
89 -> 96 0.12449
90 -> 96 0.40947
91 -> 96 0.36743
92 -> 96 0.11470
92 -> 98 0.10323
93 -> 99 0.27147
93 ->100 0.18028

Excited State 20: Singlet-A 4.7950 eV 258.57 nm f=0.0252 <S**2>=0.000
89 -> 95 -0.12496
89 -> 96 0.38023
91 -> 96 -0.25464
93 -> 99 0.30086
94 ->101 -0.37896

Excited State 21: Singlet-A 4.8124 eV 257.63 nm f=0.0108 <S**2>=0.000

89 -> 95 -0.13669
89 -> 96 0.48791
93 -> 99 -0.21688
94 ->101 0.36800

Excited State 22: Singlet-A 4.8913 eV 253.48 nm f=0.0773 <S**2>=0.000
91 -> 96 0.39118
93 -> 99 -0.28017
93 ->100 -0.26497
94 ->101 -0.37807

Excited State 23: Singlet-A 4.9326 eV 251.35 nm f=0.0804 <S**2>=0.000
90 -> 96 -0.17233
92 -> 96 -0.11627
92 -> 98 0.10187
93 -> 99 -0.21332
93 ->100 0.58312
94 ->101 -0.10920

Excited State 24: Singlet-A 5.1474 eV 240.87 nm f=0.0496 <S**2>=0.000
84 -> 95 0.10984
86 -> 95 0.67684

Excited State 25: Singlet-A 5.1981 eV 238.52 nm f=0.0010 <S**2>=0.000
88 -> 96 0.64909
90 -> 98 -0.12239
91 -> 97 -0.10976

Excited State 26: Singlet-A 5.2455 eV 236.36 nm f=0.0023 <S**2>=0.000
87 -> 96 0.64633
91 -> 97 0.13927
92 -> 98 -0.15219

Excited State 27: Singlet-A 5.3703 eV 230.87 nm f=0.0399 <S**2>=0.000
89 -> 97 0.13458
89 -> 98 -0.11964
89 -> 99 0.10039
90 -> 96 -0.15697
90 -> 97 -0.13790
90 -> 98 -0.23663
92 -> 97 0.48846
92 -> 98 0.16218
93 ->101 0.18981

Excited State 28: Singlet-A 5.4403 eV 227.90 nm f=0.0428 <S**2>=0.000
89 -> 97 0.26225
89 -> 99 0.18689
90 -> 96 0.12080
90 -> 97 0.12480
90 -> 98 0.27387
92 -> 98 -0.33022
93 ->101 0.33962

Excited State 29: Singlet-A 5.4578 eV 227.17 nm f=0.0048 <S**2>=0.000
85 -> 95 0.13523
89 -> 97 -0.26904
89 -> 99 -0.15671
91 -> 97 -0.10037
92 -> 97 -0.16561
92 -> 98 0.14007
93 ->101 0.51651

Excited State 30: Singlet-A 5.5560 eV 223.15 nm f=0.0091 <S**2>=0.000
89 -> 97 -0.30932
89 -> 98 0.16013
89 -> 99 -0.21717
90 -> 97 0.15652
90 -> 98 0.11572
91 -> 97 0.10095
92 -> 97 0.41388
92 -> 98 -0.17667
92 -> 99 -0.12747

Excited State 31: Singlet-A 5.6145 eV 220.83 nm f=0.0136 <S**2>=0.000
84 -> 95 -0.36465
85 -> 95 0.51728
92 -> 98 -0.12937
94 ->102 -0.11561

Excited State 32: Singlet-A 5.6616 eV 218.99 nm f=0.0244 <S**2>=0.000
84 -> 95 0.42712
85 -> 95 0.11635
86 -> 96 -0.10945
91 -> 97 -0.26944
93 ->101 -0.12813
94 ->102 -0.40506

Excited State 33: Singlet-A 5.6664 eV 218.81 nm f=0.0873 <S**2>=0.000
84 -> 95 0.12605
85 -> 95 0.23895
88 -> 96 0.15867
90 -> 97 0.20956
90 -> 98 0.18967
91 -> 97 0.40845
92 -> 98 0.26330
94 ->102 -0.15678

Excited State 34: Singlet-A 5.7493 eV 215.65 nm f=0.3662 <S**2>=0.000
87 -> 96 -0.20622
90 -> 97 -0.20543
90 -> 98 -0.13695
91 -> 97 0.33116
92 -> 98 -0.27843
93 ->100 0.11260
94 ->102 -0.32157

Excited State 35: Singlet-A 5.8238 eV 212.89 nm f=0.0359 <S**2>=0.000
84 -> 95 -0.26644
85 -> 95 -0.20977
89 -> 97 -0.10665
89 -> 99 0.13947
90 -> 97 0.38634
92 -> 99 0.25887
94 ->102 -0.25738

Excited State 36: Singlet-A 5.8506 eV 211.92 nm f=0.0117 <S**2>=0.000
84 -> 95 0.14963
85 -> 95 0.10560
88 -> 97 0.11286
89 -> 96 -0.12455
89 -> 97 -0.23528
89 -> 99 0.19482
91 -> 98 0.15829
92 -> 99 0.45395
92 ->100 0.10425
94 ->102 0.19040

Excited State 37: Singlet-A 5.8914 eV 210.45 nm f=0.0859 <S**2>=0.000
89 -> 99 -0.11683

91 -> 98 0.64086

Excited State 38: Singlet-A 5.9246 eV 209.27 nm f=0.0325 <S**2>=0.000
84 -> 95 0.13301
85 -> 95 0.12482
86 -> 96 0.12660
89 -> 97 0.13293
89 -> 99 -0.12883
90 -> 97 0.40860
90 -> 98 -0.37408
92 -> 98 -0.15624
94 ->102 0.11466

Excited State 39: Singlet-A 5.9633 eV 207.91 nm f=0.0128 <S**2>=0.000
86 -> 96 -0.20349
89 -> 96 -0.11494
89 -> 97 -0.18003
89 -> 99 0.40069
89 ->100 0.14213
90 -> 98 -0.14013
90 -> 99 -0.11788
91 -> 98 0.11345
92 -> 99 -0.36104

Excited State 40: Singlet-A 6.0089 eV 206.34 nm f=0.0583 <S**2>=0.000
82 -> 95 -0.11515
83 -> 95 0.34287
86 -> 96 0.50335
88 -> 97 -0.11044
92 -> 99 -0.12060
92 ->100 0.15343

Excited State 41: Singlet-A 6.0650 eV 204.43 nm f=0.0530 <S**2>=0.000
81 -> 95 0.10667
83 -> 95 0.52835
84 -> 96 -0.11372
86 -> 96 -0.18688
88 -> 97 0.11401
89 -> 97 0.11175
89 -> 99 -0.12393
92 -> 99 0.11649
94 ->102 0.12213

Excited State 42: Singlet-A 6.1814 eV 200.58 nm f=0.0281 <S**2>=0.000
86 -> 96 -0.13086
87 -> 97 -0.27493
88 -> 97 -0.14797
88 -> 98 -0.15732
89 -> 98 -0.24519
91 -> 99 0.20820
92 ->100 0.41584
93 ->102 0.10893

Excited State 43: Singlet-A 6.2144 eV 199.51 nm f=0.0134 <S**2>=0.000
87 -> 97 -0.13682
87 -> 98 -0.10837
89 -> 97 0.19940
89 -> 98 0.47092
91 -> 99 -0.19199
91 ->100 0.20176
92 ->100 0.28040

Excited State 44: Singlet-A 6.2237 eV 199.21 nm f=0.0174 <S**2>=0.000
82 -> 95 -0.13753
87 -> 97 -0.25602
88 -> 99 -0.10069
89 -> 98 0.25362
91 -> 99 0.43570
91 ->100 -0.21996
92 ->100 -0.17204
93 ->102 0.10590

Excited State 45: Singlet-A 6.2654 eV 197.89 nm f=0.0353 <S**2>=0.000
82 -> 95 -0.22944
87 -> 97 0.29590
88 -> 97 0.38113
88 -> 98 -0.23107
91 -> 99 0.15683
92 ->100 0.19239
93 ->102 -0.12433
94 ->103 0.12876

Excited State 46: Singlet-A 6.2800 eV 197.43 nm f=0.0836 <S**2>=0.000
82 -> 95 -0.29709
84 -> 96 0.10085
87 -> 97 -0.29744

88 -> 97 0.10679
88 -> 98 0.10584
89 -> 98 -0.18706
91 -> 99 -0.17517
91 ->100 0.31211
92 ->100 -0.12950
93 ->102 0.18987
94 ->103 0.19005

Excited State 47: Singlet-A 6.2911 eV 197.08 nm f=0.0138 <S**2>=0.000
82 -> 95 0.25649
86 -> 96 0.14595
88 -> 97 0.31944
90 -> 98 0.10596
90 -> 99 -0.16199
91 ->100 -0.10309
92 ->101 -0.19714
93 ->102 0.36165

Excited State 48: Singlet-A 6.3140 eV 196.36 nm f=0.0008 <S**2>=0.000
82 -> 95 0.11512
87 -> 98 -0.10771
88 -> 98 0.10562
89 -> 98 -0.12397
90 -> 98 -0.16131
90 -> 99 0.58873

Excited State 49: Singlet-A 6.3348 eV 195.72 nm f=0.0034 <S**2>=0.000
87 -> 98 -0.32433
88 -> 97 0.20565
88 -> 98 0.34498
90 -> 99 -0.16640
90 ->100 -0.13338
91 ->100 -0.18604
92 ->100 0.15393
93 ->102 -0.19679

Excited State 50: Singlet-A 6.3750 eV 194.49 nm f=0.0322 <S**2>=0.000
82 -> 95 0.27185
86 -> 96 0.11591
88 -> 97 0.10789
88 -> 98 0.18603
91 -> 99 0.26886

91 ->100 0.38102
93 ->102 -0.25782

Excited State 51: Singlet-A 6.4386 eV 192.56 nm f=0.0407 <S**2>=0.000
81 -> 95 0.20632
83 -> 96 0.11371
85 -> 96 0.15664
87 -> 97 -0.13993
87 -> 98 -0.12245
88 -> 98 -0.11586
90 -> 99 0.11783
90 ->100 0.31472
91 ->100 -0.12893
92 ->101 -0.18767
93 ->102 -0.15485
94 ->103 0.33264

Excited State 52: Singlet-A 6.4622 eV 191.86 nm f=0.0022 <S**2>=0.000
82 -> 95 0.14942
87 -> 98 0.21142
90 ->100 -0.34530
92 ->101 0.22085
94 ->103 0.41271

Excited State 53: Singlet-A 6.4815 eV 191.29 nm f=0.0993 <S**2>=0.000
82 -> 95 -0.10961
85 -> 95 -0.10453
85 -> 96 0.43183
87 -> 97 -0.17414
87 -> 98 0.21309
88 -> 97 0.11812
88 -> 98 -0.24426
92 ->101 0.15211
93 ->102 -0.16063
94 ->103 -0.19161

Excited State 54: Singlet-A 6.4863 eV 191.15 nm f=0.0193 <S**2>=0.000
81 -> 95 -0.23033
84 -> 96 0.16256
87 -> 98 0.35243
87 -> 99 0.19178
88 -> 98 0.20497
88 -> 99 0.10195

88 ->100 -0.15310
91 ->100 -0.17761
92 ->100 0.11450
92 ->101 -0.24597

Excited State 55: Singlet-A 6.5289 eV 189.90 nm f=0.1505 <S**2>=0.000
82 -> 95 0.22008
84 -> 96 0.28434
85 -> 96 -0.26727
86 -> 97 0.10506
87 -> 97 -0.10515
88 -> 98 -0.13909
88 -> 99 -0.14583
91 -> 99 -0.12974
92 ->101 0.15636
93 ->102 -0.16184
94 ->104 -0.27007

Excited State 56: Singlet-A 6.5843 eV 188.30 nm f=0.0260 <S**2>=0.000
81 -> 95 -0.15401
84 -> 96 0.14975
87 ->100 0.10944
90 ->100 0.17003
92 ->101 0.22515
94 ->104 0.50958

Excited State 57: Singlet-A 6.5934 eV 188.04 nm f=0.0448 <S**2>=0.000
81 -> 95 -0.17214
84 -> 96 -0.13566
87 -> 99 -0.10591
88 -> 99 0.43319
90 ->100 0.21114
92 ->101 0.21119
94 ->104 -0.21877

Excited State 58: Singlet-A 6.6145 eV 187.44 nm f=0.1491 <S**2>=0.000
80 -> 95 0.11340
81 -> 95 -0.13164
84 -> 96 -0.27958
88 -> 98 0.15233
88 -> 99 -0.22355
89 -> 99 -0.11695
89 ->100 0.29844

90 ->100 0.24492
91 ->101 0.20202

Excited State 59: Singlet-A 6.6494 eV 186.46 nm f=0.0554 <S**2>=0.000
84 -> 96 0.15387
87 -> 99 -0.10610
88 -> 99 0.17481
89 -> 99 -0.16917
89 ->100 0.57253
91 ->101 -0.18420

Excited State 60: Singlet-A 6.6816 eV 185.56 nm f=0.1895 <S**2>=0.000
84 -> 96 0.32966
85 -> 96 0.33460
86 -> 97 -0.16621
87 -> 97 0.15440
87 -> 99 0.12518
88 -> 99 -0.11028
91 ->101 -0.10040
93 ->102 0.13895
94 ->103 0.12202
94 ->104 -0.17849
94 ->106 -0.15175

Excited State 61: Singlet-A 6.7159 eV 184.61 nm f=0.0630 <S**2>=0.000
79 -> 95 0.13501
80 -> 95 -0.13705
81 -> 95 0.29969
87 -> 99 0.38018
87 ->100 0.11948
88 -> 99 0.20718
90 ->101 -0.18753
91 ->101 0.14401
92 ->101 0.13576
94 ->103 -0.11351

Excited State 62: Singlet-A 6.7443 eV 183.83 nm f=0.0487 <S**2>=0.000
79 -> 95 -0.12606
81 -> 95 -0.27055
84 -> 96 -0.13673
87 -> 98 -0.19893
87 -> 99 0.35667
87 ->100 -0.21709

90 ->100 -0.20143
90 ->101 -0.15822
92 ->100 -0.13388

Excited State 63: Singlet-A 6.8032 eV 182.24 nm f=0.0525 <S**2>=0.000
86 -> 97 0.14056
87 -> 99 0.22971
87 ->100 0.18090
88 -> 99 0.14041
88 ->100 0.37975
90 -> 99 0.10210
90 ->101 0.32091
91 ->101 -0.22420
92 ->101 -0.13358

Excited State 64: Singlet-A 6.8594 eV 180.75 nm f=0.0388 <S**2>=0.000
78 -> 95 -0.22500
79 -> 95 0.37995
80 -> 95 -0.28883
81 -> 95 -0.11061
86 -> 97 -0.19638
87 ->100 -0.12270
88 ->100 0.14153
91 ->101 0.14755
94 ->105 0.18344

Excited State 65: Singlet-A 6.8744 eV 180.36 nm f=0.0479 <S**2>=0.000
79 -> 95 -0.30165
86 -> 97 -0.17103
87 ->100 0.10405
88 -> 99 0.17296
90 ->101 0.32532
91 ->101 0.36072
93 ->103 -0.10733
94 ->105 0.10151

Excited State 66: Singlet-A 6.8938 eV 179.85 nm f=0.0614 <S**2>=0.000
78 -> 95 -0.35537
79 -> 95 0.14480
80 -> 95 0.41827
81 -> 95 0.14099
83 -> 96 -0.12107
87 ->100 -0.12707

90 ->101 0.12608
94 ->103 -0.10455
94 ->105 -0.10742

Excited State 67: Singlet-A 6.9045 eV 179.57 nm f=0.0018 <S**2>=0.000
79 -> 95 -0.12697
83 -> 96 -0.10773
86 -> 97 -0.13646
87 ->100 -0.30235
88 ->100 0.22354
91 ->101 0.12305
93 ->103 0.16021
93 ->104 0.16258
94 ->105 -0.29926
94 ->106 0.30805

Excited State 68: Singlet-A 6.9324 eV 178.85 nm f=0.0198 <S**2>=0.000
79 -> 95 0.14937
80 -> 95 0.13169
81 -> 95 -0.21791
83 -> 96 0.39733
86 -> 97 -0.17555
87 ->100 0.19090
91 ->101 0.14855
94 ->105 -0.30500

Excited State 69: Singlet-A 6.9475 eV 178.46 nm f=0.0126 <S**2>=0.000
78 -> 95 0.38345
79 -> 95 0.17105
80 -> 95 0.25739
86 -> 97 -0.10011
86 -> 98 0.16212
87 ->100 -0.16000
88 ->100 0.12259
91 ->101 0.16047
93 ->104 -0.10418
94 ->105 0.27515

Excited State 70: Singlet-A 6.9783 eV 177.67 nm f=0.1630 <S**2>=0.000
78 -> 95 -0.18205
83 -> 96 -0.11552
86 -> 97 0.14284
86 -> 98 0.43897

88 ->100 0.13237
89 ->101 -0.10618
90 ->101 -0.25467
91 ->101 0.16403
92 ->101 -0.14459

Excited State 71: Singlet-A 7.0089 eV 176.89 nm f=0.0579 <S**2>=0.000
76 -> 95 -0.11649
77 -> 95 -0.20860
78 -> 95 -0.22379
79 -> 95 -0.21852
83 -> 96 0.34155
86 -> 97 -0.15934
88 ->100 0.21597
90 ->101 -0.14068
94 ->105 0.14592

Excited State 72: Singlet-A 7.0324 eV 176.30 nm f=0.0401 <S**2>=0.000
80 -> 95 0.10212
82 -> 96 -0.12278
83 -> 96 -0.10504
85 -> 97 -0.12076
86 -> 97 -0.17317
87 ->100 0.18261
88 ->100 -0.20142
89 ->101 -0.23655
93 ->103 0.29161
94 ->105 0.18669
94 ->106 0.27202

Excited State 73: Singlet-A 7.0651 eV 175.49 nm f=0.0148 <S**2>=0.000
86 -> 98 0.14018
89 ->101 0.61564
93 ->103 0.11106

Excited State 74: Singlet-A 7.0798 eV 175.12 nm f=0.0891 <S**2>=0.000
76 -> 95 -0.13153
77 -> 95 0.25164
78 -> 95 -0.13033
80 -> 95 0.11552
83 -> 96 0.18010
84 -> 97 0.12690
85 -> 97 -0.13563

86 -> 97 0.30761
87 ->100 -0.15203
93 ->103 0.26308

Excited State 75: Singlet-A 7.1171 eV 174.21 nm f=0.0433 <S**2>=0.000
76 -> 95 0.15918
93 ->103 0.45802
93 ->104 -0.20896
94 ->104 0.13722
94 ->105 -0.10941
94 ->106 -0.33821

Excited State 76: Singlet-A 7.1691 eV 172.94 nm f=0.0633 <S**2>=0.000
76 -> 95 0.26557
77 -> 95 -0.27449
81 -> 96 0.10573
82 -> 96 0.41503
83 -> 96 0.16815
87 ->101 0.11592
88 ->100 -0.10137
90 ->101 0.11235
94 ->106 0.11706

Excited State 77: Singlet-A 7.2114 eV 171.93 nm f=0.0436 <S**2>=0.000
76 -> 95 0.49877
77 -> 95 0.11929
78 -> 96 -0.10305
79 -> 95 -0.19625
82 -> 96 -0.32778

Excited State 78: Singlet-A 7.2411 eV 171.22 nm f=0.0197 <S**2>=0.000
77 -> 95 0.40743
82 -> 96 0.17747
86 -> 97 -0.16058
86 -> 99 0.15053
86 ->100 -0.13505
91 ->101 -0.11423
93 ->104 -0.29379
94 ->106 0.12783

Excited State 79: Singlet-A 7.2491 eV 171.03 nm f=0.0205 <S**2>=0.000
77 -> 95 0.18468
82 -> 96 0.24139

85 -> 97 0.18237
86 -> 98 -0.10143
87 ->101 0.10512
88 ->101 0.13439
93 ->103 0.10946
93 ->104 0.44385
94 ->105 0.18527
94 ->106 -0.13835

Excited State 80: Singlet-A 7.2711 eV 170.52 nm f=0.2062 <S**2>=0.000
76 -> 95 -0.19516
84 -> 98 0.17133
85 -> 97 0.23053
86 -> 98 0.31855
86 -> 99 0.13586
87 ->100 -0.11598
88 ->100 -0.13910
88 ->101 -0.19460
90 ->101 0.13447
91 ->101 -0.12590
92 ->101 0.12271
92 ->102 -0.12944
94 ->106 -0.12673

Excited State 81: Singlet-A 7.3276 eV 169.20 nm f=0.0043 <S**2>=0.000
81 -> 96 -0.11478
84 -> 97 -0.12779
84 -> 98 -0.12874
85 -> 97 0.24906
87 ->101 0.44475
88 ->101 -0.30657
93 ->104 -0.12716

Excited State 82: Singlet-A 7.3629 eV 168.39 nm f=0.0242 <S**2>=0.000
81 -> 96 -0.16640
86 -> 98 0.12297
86 -> 99 0.22884
87 ->101 0.26503
88 ->101 0.45441
94 ->107 0.11299

Excited State 83: Singlet-A 7.4139 eV 167.23 nm f=0.0142 <S**2>=0.000
81 -> 96 0.18114

85 -> 97 0.19785
87 ->101 -0.20167
92 ->102 -0.11134
93 ->105 -0.27098
93 ->107 0.10125
94 ->107 0.42350
94 ->110 -0.13587

Excited State 84: Singlet-A 7.4413 eV 166.62 nm f=0.0271 <S**2>=0.000
74 -> 95 -0.10704
84 -> 97 0.27889
84 -> 98 0.21914
87 ->101 0.13082
90 ->102 -0.11584
92 ->102 0.41425
94 ->107 0.22376

Excited State 85: Singlet-A 7.4643 eV 166.10 nm f=0.1213 <S**2>=0.000
81 -> 96 -0.11328
84 -> 97 -0.22675
86 -> 99 0.17602
86 ->100 0.18073
87 ->101 -0.24591
90 ->102 -0.14156
92 ->102 0.39414
94 ->108 -0.12110

Excited State 86: Singlet-A 7.4822 eV 165.71 nm f=0.0044 <S**2>=0.000
74 -> 95 0.32184
81 -> 96 0.24764
84 -> 97 0.19398
85 -> 97 0.17436
86 -> 99 0.13633
92 ->102 0.10361
93 ->105 -0.11798
93 ->106 -0.13011
94 ->107 -0.28020
94 ->109 0.13316

Excited State 87: Singlet-A 7.4923 eV 165.48 nm f=0.0162 <S**2>=0.000
74 -> 95 0.45791
75 -> 95 -0.13939
78 -> 96 0.13738

84 -> 97 -0.11203
84 -> 98 -0.10398
86 -> 99 -0.22197
92 ->102 0.12592
94 ->107 0.24208

Excited State 88: Singlet-A 7.5222 eV 164.82 nm f=0.0075 <S**2>=0.000
74 -> 95 -0.23741
80 -> 96 -0.12230
81 -> 96 0.41657
84 -> 97 -0.18318
84 -> 98 -0.13622
85 -> 98 0.10295
86 -> 99 -0.16465
88 ->101 0.11594
92 ->102 0.12709
94 ->107 -0.13329
94 ->108 0.13693

Excited State 89: Singlet-A 7.5515 eV 164.18 nm f=0.0229 <S**2>=0.000
81 -> 96 -0.11845
84 -> 97 -0.18903
84 -> 98 0.36355
85 -> 98 -0.23401
86 -> 99 -0.30523
86 ->100 0.10015
88 ->101 0.15489

Excited State 90: Singlet-A 7.5582 eV 164.04 nm f=0.0023 <S**2>=0.000
81 -> 96 0.13572
85 -> 97 0.12343
93 ->105 0.56166
93 ->106 -0.18785
94 ->107 0.14723
94 ->108 -0.10103
94 ->110 -0.10421

Excited State 91: Singlet-A 7.5813 eV 163.54 nm f=0.1167 <S**2>=0.000
78 -> 96 0.10453
84 -> 97 0.15029
84 ->100 0.11005
86 ->100 0.49577
90 ->102 0.16221

91 ->102 -0.11009
94 ->109 -0.16427

Excited State 92: Singlet-A 7.6108 eV 162.91 nm f=0.0218 <S**2>=0.000
79 -> 96 0.12832
81 -> 96 0.12204
84 -> 97 -0.16880
85 -> 97 -0.19990
85 -> 98 -0.22579
86 -> 99 0.18115
86 ->100 0.14503
93 ->106 0.12169
94 ->108 0.36488

Excited State 93: Singlet-A 7.6395 eV 162.29 nm f=0.0108 <S**2>=0.000
75 -> 95 0.45596
79 -> 96 0.19870
80 -> 96 -0.10409
84 -> 97 0.11292
93 ->106 0.23553
94 ->108 -0.18827
94 ->110 0.13847

Excited State 94: Singlet-A 7.6665 eV 161.72 nm f=0.0134 <S**2>=0.000
79 -> 96 -0.12018
80 -> 96 -0.14242
85 -> 97 0.12008
85 -> 98 0.16295
90 ->102 0.15511
93 ->106 0.12225
94 ->108 0.20222
94 ->109 0.46907
94 ->110 -0.10148

Excited State 95: Singlet-A 7.6686 eV 161.68 nm f=0.0228 <S**2>=0.000
73 -> 95 0.16572
75 -> 95 0.16354
83 -> 97 0.10163
85 -> 97 0.17964
85 -> 98 0.26575
91 ->102 0.14271
94 ->108 0.35896
94 ->109 -0.28936

Excited State 96: Singlet-A 7.6872 eV 161.29 nm f=0.0310 <S**2>=0.000
74 -> 95 -0.15547
75 -> 95 -0.15779
78 -> 96 0.11562
79 -> 96 0.39374
80 -> 96 0.34985
84 -> 98 0.10125
85 -> 98 0.18383
91 ->102 0.17465

Excited State 97: Singlet-A 7.7128 eV 160.75 nm f=0.0146 <S**2>=0.000
73 -> 95 -0.11638
75 -> 95 0.29254
78 -> 96 0.17384
79 -> 96 -0.13644
80 -> 96 0.33451
83 -> 97 -0.13207
84 -> 98 -0.14752
85 -> 98 -0.24533
91 ->102 0.14326
93 ->106 -0.12025
94 ->108 0.11479

Excited State 98: Singlet-A 7.7252 eV 160.49 nm f=0.0385 <S**2>=0.000
73 -> 95 0.15397
78 -> 96 0.10771
79 -> 96 -0.24680
80 -> 96 0.15587
83 -> 98 -0.10452
84 -> 98 0.11169
86 ->100 0.11313
90 ->102 -0.26770
92 ->102 -0.11257
93 ->106 0.34051

Excited State 99: Singlet-A 7.7449 eV 160.09 nm f=0.0037 <S**2>=0.000
73 -> 95 0.16790
74 -> 95 -0.10996
78 -> 96 0.28388
79 -> 96 0.18661
80 -> 96 -0.20103
83 -> 97 0.18180

84 -> 99 -0.12695
84 ->100 0.10697
85 -> 98 -0.26182
85 -> 99 0.11878
90 ->102 -0.19801
94 ->108 0.11232

Excited State 100: Singlet-A 7.7541 eV 159.90 nm f=0.0246 <S**2>=0.000
73 -> 95 0.12927
78 -> 96 0.13429
79 -> 96 -0.15482
83 -> 97 0.13153
85 -> 98 -0.10729
85 -> 99 0.17392
90 ->102 0.33052
91 ->102 0.34183
93 ->106 0.17396
94 ->108 -0.14156
94 ->109 -0.11600

Table A4.10. Excitation Energies and Oscillator Strengths of 5 Using the TD-B3LYP Method with 6-31G(d) Basis Set in Chloroform.

Excited State 1: Singlet-A 2.7546 eV 450.09 nm f=0.3573 <S**2>=0.000
93 -> 94 0.70025
This state for optimization and/or second-order correction.
Total Energy, E(TD-HF/TD-KS) = -1181.65767030
Copying the excited state density for this state as the 1-particle RhoCI density.

Excited State 2: Singlet-A 3.2425 eV 382.37 nm f=0.0027 <S**2>=0.000
92 -> 94 0.68058
93 -> 95 -0.17125

Excited State 3: Singlet-A 3.5452 eV 349.73 nm f=0.1165 <S**2>=0.000
92 -> 94 0.15916
93 -> 95 0.63836
93 -> 96 0.20455

Excited State 4: Singlet-A 3.7749 eV 328.44 nm f=0.0068 <S**2>=0.000
93 -> 95 -0.17847
93 -> 96 0.66807

Excited State 5: Singlet-A 3.9781 eV 311.66 nm f=0.0069 <S**2>=0.000
91 -> 94 -0.31547
93 -> 97 0.62586

Excited State 6: Singlet-A 4.1174 eV 301.13 nm f=0.0038 <S**2>=0.000
89 -> 94 -0.22362
91 -> 94 0.57558
93 -> 97 0.30609

Excited State 7: Singlet-A 4.2110 eV 294.43 nm f=0.0080 <S**2>=0.000
88 -> 94 0.55295
89 -> 94 0.11246
90 -> 94 -0.37844

Excited State 8: Singlet-A 4.2146 eV 294.18 nm f=0.0051 <S**2>=0.000
88 -> 94 -0.10339
89 -> 94 0.63092
91 -> 94 0.19891
92 -> 95 0.12020

Excited State 9: Singlet-A 4.3605 eV 284.33 nm f=0.1500 <S**2>=0.000
91 -> 94 -0.12233
92 -> 95 0.59150
92 -> 96 0.22933
93 -> 98 -0.23647

Excited State 10: Singlet-A 4.3697 eV 283.73 nm f=0.0403 <S**2>=0.000
88 -> 94 0.38105
90 -> 94 0.52671
93 -> 99 -0.17825
93 ->100 -0.11138

Excited State 11: Singlet-A 4.4569 eV 278.19 nm f=0.0578 <S**2>=0.000
90 -> 95 0.10356
92 -> 95 0.10364
92 -> 96 0.34458
93 -> 98 0.56851

Excited State 12: Singlet-A 4.4828 eV 276.58 nm f=0.1011 <S**2>=0.000
87 -> 94 -0.14611
90 -> 94 0.17825
93 -> 99 0.64136

Excited State 13: Singlet-A 4.6106 eV 268.91 nm f=0.0284 <S**2>=0.000
87 -> 94 0.64847
92 -> 97 -0.18344
93 -> 99 0.16713

Excited State 14: Singlet-A 4.6600 eV 266.06 nm f=0.2166 <S**2>=0.000
86 -> 94 0.29973
92 -> 95 -0.26717
92 -> 96 0.49724
93 -> 98 -0.27679

Excited State 15: Singlet-A 4.8562 eV 255.31 nm f=0.0294 <S**2>=0.000
86 -> 94 0.61681
92 -> 95 0.15828
92 -> 96 -0.24172

Excited State 16: Singlet-A 4.9621 eV 249.86 nm f=0.4053 <S**2>=0.000
87 -> 94 0.17677
91 -> 95 -0.17187
92 -> 97 0.62864
93 -> 95 0.11575

Excited State 17: Singlet-A 5.1495 eV 240.77 nm f=0.0986 <S**2>=0.000
85 -> 94 0.63587
87 -> 95 -0.10786
92 -> 99 0.17186
93 ->101 0.14587

Excited State 18: Singlet-A 5.1799 eV 239.36 nm f=0.0538 <S**2>=0.000
91 -> 95 0.58735
92 -> 97 0.12650
92 -> 98 0.20234
93 ->100 0.28185

Excited State 19: Singlet-A 5.2010 eV 238.38 nm f=0.0005 <S**2>=0.000
84 -> 94 0.11706
91 -> 96 0.27164
92 -> 98 -0.39638
93 ->100 0.44373

Excited State 20: Singlet-A 5.2427 eV 236.49 nm f=0.0085 <S**2>=0.000
85 -> 94 -0.21900
87 -> 95 -0.12199

90 -> 96 -0.13174
92 -> 99 0.61743

Excited State 21: Singlet-A 5.2592 eV 235.75 nm f=0.1237 <S**2>=0.000
86 -> 95 -0.11335
91 -> 95 -0.31957
92 -> 98 0.48309
93 ->100 0.33104

Excited State 22: Singlet-A 5.3714 eV 230.82 nm f=0.0018 <S**2>=0.000
88 -> 95 0.18689
88 -> 96 0.28312
88 -> 97 -0.20119
89 -> 95 0.20597
89 -> 96 0.29661
89 -> 97 -0.29372
90 -> 95 -0.10467
90 -> 96 -0.18401
90 -> 97 0.10402

Excited State 23: Singlet-A 5.3748 eV 230.68 nm f=0.0015 <S**2>=0.000
88 -> 95 -0.16529
88 -> 96 -0.24779
88 -> 97 -0.24782
89 -> 95 0.24034
89 -> 96 0.34191
89 -> 97 0.24322
90 -> 96 0.15221
90 -> 97 0.11981

Excited State 24: Singlet-A 5.4189 eV 228.80 nm f=0.2050 <S**2>=0.000
90 -> 95 0.58662
90 -> 96 -0.18967
92 -> 99 -0.19000
92 ->100 -0.17454

Excited State 25: Singlet-A 5.4461 eV 227.66 nm f=0.3284 <S**2>=0.000
84 -> 94 0.22491
91 -> 96 0.56117
92 -> 98 0.13077
93 ->100 -0.24141

Excited State 26: Singlet-A 5.5400 eV 223.80 nm f=0.0242 <S**2>=0.000

87 -> 95 0.40801
88 -> 95 0.27219
88 -> 96 0.16715
90 -> 95 0.21901
90 -> 96 0.33115
92 -> 99 0.16275

Excited State 27: Singlet-A 5.5918 eV 221.72 nm f=0.0305 <S**2>=0.000
88 -> 97 0.25096
88 -> 98 0.17984
89 -> 95 0.54495
89 -> 99 -0.22486

Excited State 28: Singlet-A 5.5966 eV 221.54 nm f=0.0079 <S**2>=0.000
87 -> 95 0.18541
88 -> 95 0.12726
90 -> 95 -0.12854
91 -> 97 0.16012
93 ->101 0.58557

Excited State 29: Singlet-A 5.6153 eV 220.80 nm f=0.0157 <S**2>=0.000
87 -> 95 -0.17797
88 -> 95 0.47626
88 -> 99 -0.22231
89 -> 97 0.26208
89 -> 98 0.22994
93 ->101 -0.16043

Excited State 30: Singlet-A 5.6620 eV 218.98 nm f=0.0495 <S**2>=0.000
87 -> 95 -0.29791
88 -> 96 0.15604
90 -> 96 0.39382
91 -> 97 0.35476
91 -> 98 -0.10835
92 ->100 -0.21687

Excited State 31: Singlet-A 5.6694 eV 218.69 nm f=0.0679 <S**2>=0.000
84 -> 94 0.33728
88 -> 97 0.13129
88 -> 98 0.22358
89 -> 95 -0.25681
89 -> 96 0.33256
89 -> 99 -0.26380

90 -> 98 -0.10907
91 -> 96 -0.12727

Excited State 32: Singlet-A 5.7089 eV 217.18 nm f=0.0067 <S**2>=0.000
87 -> 95 0.10985
88 -> 95 -0.31296
88 -> 96 0.39490
88 -> 99 -0.26247
89 -> 97 0.11469
89 -> 98 0.25837
90 -> 96 -0.17448
90 -> 99 0.12810

Excited State 33: Singlet-A 5.7226 eV 216.66 nm f=0.0851 <S**2>=0.000
84 -> 94 0.42738
86 -> 95 -0.13819
88 -> 98 -0.11599
89 -> 96 -0.25957
89 -> 99 0.15134
90 -> 97 0.30411
91 -> 96 -0.22096

Excited State 34: Singlet-A 5.8057 eV 213.56 nm f=0.1696 <S**2>=0.000
84 -> 94 0.17424
86 -> 95 0.54788
88 -> 97 -0.11072
89 -> 96 -0.11679
89 -> 99 0.11492
90 -> 97 -0.24683

Excited State 35: Singlet-A 5.8103 eV 213.39 nm f=0.0867 <S**2>=0.000
87 -> 95 0.19685
87 -> 96 0.12380
88 -> 96 -0.19416
90 -> 96 -0.23094
91 -> 97 0.50323
93 ->101 -0.22198

Excited State 36: Singlet-A 5.9419 eV 208.66 nm f=0.0381 <S**2>=0.000
87 -> 95 0.18088
87 -> 96 0.48577
91 -> 97 -0.13232
92 ->100 -0.42044

93 ->102 0.12805

Excited State 37: Singlet-A 6.0292 eV 205.64 nm f=0.0136 <S**2>=0.000
83 -> 94 -0.10929
84 -> 94 -0.10516
85 -> 95 0.10882
86 -> 95 0.28240
86 -> 96 -0.19208
88 -> 97 0.19783
90 -> 97 0.47031
92 ->101 0.16842

Excited State 38: Singlet-A 6.0902 eV 203.58 nm f=0.1960 <S**2>=0.000
86 -> 97 0.20175
87 -> 95 -0.10608
87 -> 96 0.37474
89 -> 97 -0.18527
91 -> 98 -0.29667
92 ->100 0.34509
93 ->101 0.10708

Excited State 39: Singlet-A 6.1002 eV 203.25 nm f=0.0308 <S**2>=0.000
87 -> 96 0.18299
87 -> 99 -0.10237
89 -> 97 0.11561
90 -> 99 -0.16512
91 -> 98 0.55710
92 ->100 0.20569
93 ->101 0.10379

Excited State 40: Singlet-A 6.1057 eV 203.06 nm f=0.0206 <S**2>=0.000
83 -> 94 0.38806
85 -> 95 0.20229
86 -> 96 -0.28212
90 -> 98 -0.13918
91 -> 99 0.42151

Excited State 41: Singlet-A 6.1651 eV 201.11 nm f=0.0010 <S**2>=0.000
83 -> 94 0.21582
88 -> 97 0.40645
88 -> 98 -0.15563
89 -> 96 0.23592
89 -> 99 0.25958

90 -> 97 -0.13684
90 -> 98 0.22889
91 -> 99 -0.19604

Excited State 42: Singlet-A 6.1685 eV 200.99 nm f=0.1162 <S**2>=0.000
83 -> 94 0.14888
88 -> 96 0.23401
88 -> 97 -0.11111
88 -> 99 0.26050
89 -> 97 0.40369
89 -> 98 -0.26706
91 -> 98 -0.19839
91 -> 99 -0.10908

Excited State 43: Singlet-A 6.1687 eV 200.99 nm f=0.0335 <S**2>=0.000
83 -> 94 0.40643
88 -> 97 -0.18945
88 -> 98 0.15799
88 -> 99 -0.10482
89 -> 96 -0.10542
89 -> 97 -0.16407
89 -> 98 0.10626
89 -> 99 -0.17383
90 -> 98 0.16877
91 -> 99 -0.32252

Excited State 44: Singlet-A 6.1881 eV 200.36 nm f=0.0073 <S**2>=0.000
83 -> 94 -0.14484
85 -> 95 0.50269
85 -> 96 -0.12984
86 -> 95 -0.11099
87 -> 97 0.13666
90 -> 97 -0.10468
91 -> 99 -0.14374
92 ->101 0.32464

Excited State 45: Singlet-A 6.2813 eV 197.39 nm f=0.0993 <S**2>=0.000
83 -> 94 0.10756
86 -> 96 0.35860
86 -> 99 0.11611
87 -> 97 0.48418
87 -> 98 -0.18757
88 -> 97 0.15001

Excited State 46: Singlet-A 6.3198 eV 196.18 nm f=0.0052 <S**2>=0.000
82 -> 94 0.31038
88 -> 99 0.11773
90 -> 99 0.42426
93 ->102 -0.41543

Excited State 47: Singlet-A 6.3621 eV 194.88 nm f=0.0000 <S**2>=0.000
83 -> 94 -0.17318
84 -> 94 0.12634
85 -> 95 0.12849
85 -> 96 0.15436
86 -> 96 -0.31153
87 -> 97 0.35232
87 -> 98 0.13485
90 -> 98 0.23882
92 ->101 -0.27301

Excited State 48: Singlet-A 6.3836 eV 194.22 nm f=0.0026 <S**2>=0.000
82 -> 94 -0.28650
86 -> 97 -0.22555
89 -> 98 -0.13570
90 -> 99 0.42970
93 ->102 0.32612

Excited State 49: Singlet-A 6.3900 eV 194.03 nm f=0.0012 <S**2>=0.000
85 -> 96 -0.32183
87 -> 98 -0.14743
89 -> 99 -0.13310
90 -> 98 0.47907
91 -> 99 0.27103

Excited State 50: Singlet-A 6.4188 eV 193.16 nm f=0.0009 <S**2>=0.000
81 -> 94 -0.34181
82 -> 94 0.47312
86 -> 97 -0.13083
93 ->102 0.32903

Excited State 51: Singlet-A 6.4515 eV 192.18 nm f=0.4498 <S**2>=0.000
84 -> 97 -0.13593
85 -> 96 0.39431
86 -> 96 0.25770
86 -> 99 -0.15749

87 -> 98 0.16383
88 -> 98 0.16153
90 -> 98 0.22782
91 -> 99 0.12644
91 ->100 -0.15281
92 ->101 0.11864

Excited State 52: Singlet-A 6.4862 eV 191.15 nm f=0.0033 <S**2>=0.000
85 -> 97 0.10212
88 -> 99 0.47024
89 -> 98 0.48352

Excited State 53: Singlet-A 6.5020 eV 190.69 nm f=0.0031 <S**2>=0.000
85 -> 96 -0.13126
87 -> 98 -0.16065
88 -> 98 0.50516
89 -> 99 0.42335

Excited State 54: Singlet-A 6.5478 eV 189.35 nm f=0.0385 <S**2>=0.000
85 -> 95 -0.26555
85 -> 96 -0.20662
87 -> 97 0.20706
87 -> 98 0.40818
88 -> 98 0.10337
91 ->100 -0.14532
92 ->101 0.31736

Excited State 55: Singlet-A 6.5626 eV 188.93 nm f=0.3350 <S**2>=0.000
81 -> 94 -0.22537
84 -> 95 -0.17891
85 -> 97 -0.16778
86 -> 97 0.48365
87 -> 96 -0.13287
87 -> 99 -0.16839
88 -> 99 0.11528
90 -> 99 0.17253

Excited State 56: Singlet-A 6.5978 eV 187.92 nm f=0.0105 <S**2>=0.000
81 -> 94 -0.18254
84 -> 95 -0.14289
84 -> 96 -0.13725
85 -> 97 0.19726
86 -> 97 0.15010

86 -> 98 -0.27639
87 -> 99 0.48241

Excited State 57: Singlet-A 6.6939 eV 185.22 nm f=0.1474 <S**2>=0.000
81 -> 94 -0.21393
83 -> 95 0.11518
84 -> 95 0.60254
85 -> 97 -0.17455
87 -> 99 0.14060

Excited State 58: Singlet-A 6.7210 eV 184.47 nm f=0.0579 <S**2>=0.000
80 -> 94 0.14843
85 -> 95 -0.12569
85 -> 96 0.25847
86 -> 99 0.22941
91 ->100 0.50438
92 ->101 0.23035

Excited State 59: Singlet-A 6.7393 eV 183.97 nm f=0.0708 <S**2>=0.000
79 -> 94 -0.22153
81 -> 94 0.26541
82 -> 94 0.14634
83 -> 95 0.10255
84 -> 95 0.18150
85 -> 97 0.39664
86 -> 97 0.24573
86 -> 98 -0.12693
87 -> 99 -0.12082
93 ->102 0.13680

Excited State 60: Singlet-A 6.7849 eV 182.74 nm f=0.0098 <S**2>=0.000
79 -> 94 -0.16386
81 -> 94 0.22656
84 -> 96 -0.11838
85 -> 97 -0.10919
86 -> 98 0.46325
87 -> 99 0.33875
93 ->102 0.10192

Excited State 61: Singlet-A 6.7926 eV 182.53 nm f=0.0160 <S**2>=0.000
80 -> 94 0.54610
86 -> 99 -0.22427
87 -> 98 -0.28508

91 ->100 -0.15975

Excited State 62: Singlet-A 6.9008 eV 179.67 nm f=0.0014 <S**2>=0.000
79 -> 94 0.44367
84 -> 96 0.14978
85 -> 97 0.34479
86 -> 98 0.31530

Excited State 63: Singlet-A 6.9461 eV 178.49 nm f=0.0016 <S**2>=0.000
79 -> 94 -0.33095
81 -> 94 -0.16044
84 -> 96 0.47074
85 -> 97 0.10384
90 ->100 -0.25801

Excited State 64: Singlet-A 6.9519 eV 178.35 nm f=0.1394 <S**2>=0.000
80 -> 94 0.28357
85 -> 95 0.11551
86 -> 99 0.51022
87 -> 98 0.10056
90 ->101 -0.13724
91 ->100 -0.18916
92 ->101 -0.11167
92 ->102 0.15227

Excited State 65: Singlet-A 6.9897 eV 177.38 nm f=0.0145 <S**2>=0.000
79 -> 94 -0.18619
81 -> 94 -0.14143
85 -> 97 0.11796
90 ->100 0.59784

Excited State 66: Singlet-A 7.0214 eV 176.58 nm f=0.0402 <S**2>=0.000
85 -> 99 -0.14781
89 ->100 0.62646
92 ->102 0.13064

Excited State 67: Singlet-A 7.0798 eV 175.12 nm f=0.0206 <S**2>=0.000
83 -> 95 0.29061
84 -> 96 -0.16293
85 -> 98 -0.14184
88 ->100 0.56653

Excited State 68: Singlet-A 7.0860 eV 174.97 nm f=0.0039 <S**2>=0.000

80 -> 94 0.15124
85 -> 99 0.41852
89 ->100 0.24004
90 ->101 -0.16151
91 ->100 0.15078
92 ->102 -0.35093

Excited State 69: Singlet-A 7.0934 eV 174.79 nm f=0.0042 <S**2>=0.000
79 -> 94 0.10668
83 -> 95 0.55548
85 -> 98 -0.17480
88 ->100 -0.31250

Excited State 70: Singlet-A 7.1193 eV 174.15 nm f=0.0022 <S**2>=0.000
85 -> 99 0.12837
92 ->102 0.11336
92 ->103 -0.10806
93 ->104 0.65034

Excited State 71: Singlet-A 7.1393 eV 173.67 nm f=0.0066 <S**2>=0.000
78 -> 94 -0.16068
84 -> 97 -0.10846
85 -> 99 0.17868
86 -> 95 0.10259
86 -> 99 -0.15004
87 -> 98 0.14300
87 ->101 -0.16410
90 ->101 0.11387
91 ->100 0.14726
92 ->101 -0.11317
92 ->102 0.44920
93 ->104 -0.18867

Excited State 72: Singlet-A 7.1501 eV 173.40 nm f=0.0940 <S**2>=0.000
83 -> 95 0.20272
84 -> 99 0.10040
85 -> 98 0.57489
86 -> 98 -0.10935
87 ->100 -0.11884
93 ->103 -0.13595

Excited State 73: Singlet-A 7.1609 eV 173.14 nm f=0.0052 <S**2>=0.000
85 -> 98 0.11294

92 ->104 -0.11352
93 ->103 0.67475

Excited State 74: Singlet-A 7.1713 eV 172.89 nm f=0.0000 <S**2>=0.000
78 -> 94 0.53538
83 -> 97 -0.13137
84 -> 97 -0.32660
86 ->100 0.11100

Excited State 75: Singlet-A 7.1935 eV 172.36 nm f=0.0163 <S**2>=0.000
78 -> 94 0.32927
82 -> 95 -0.11778
84 -> 97 0.37981
85 -> 99 0.32737
86 ->100 -0.13141
92 ->101 0.10020
92 ->102 0.19712

Excited State 76: Singlet-A 7.2051 eV 172.08 nm f=0.0498 <S**2>=0.000
79 -> 94 0.17620
81 -> 94 0.15107
83 -> 96 0.18516
84 -> 96 0.29718
85 -> 97 -0.16022
85 -> 98 -0.12381
87 -> 99 0.10202
87 ->100 -0.11619
90 ->100 0.14899
91 ->101 0.38620

Excited State 77: Singlet-A 7.2369 eV 171.32 nm f=0.0033 <S**2>=0.000
81 -> 95 -0.29218
82 -> 95 0.59746
84 -> 97 0.12862

Excited State 78: Singlet-A 7.2613 eV 170.75 nm f=0.0043 <S**2>=0.000
83 -> 96 -0.11416
84 -> 96 -0.10561
85 -> 98 0.18386
87 ->100 0.45718
91 ->101 0.45395

Excited State 79: Singlet-A 7.3431 eV 168.85 nm f=0.1522 <S**2>=0.000

77 -> 94 0.10041
79 -> 94 0.10299
83 -> 96 0.26570
84 -> 99 0.15149
86 -> 98 -0.10688
87 ->100 0.46406
91 ->101 -0.30702

Excited State 80: Singlet-A 7.4178 eV 167.14 nm f=0.0085 <S**2>=0.000
80 -> 94 -0.10844
81 -> 95 -0.12996
82 -> 96 -0.10840
84 -> 97 -0.20196
84 -> 98 -0.12504
85 -> 99 0.28656
86 -> 99 0.11191
86 ->100 0.15388
87 -> 98 -0.12354
87 ->101 0.17303
90 ->101 0.36186
91 ->100 -0.15127
92 ->101 0.10137

Excited State 81: Singlet-A 7.4373 eV 166.71 nm f=0.0648 <S**2>=0.000
77 -> 94 0.33950
81 -> 94 -0.10500
83 -> 96 0.44649
84 -> 96 -0.21158
84 -> 99 -0.13918
91 ->101 0.11193

Excited State 82: Singlet-A 7.4814 eV 165.72 nm f=0.0684 <S**2>=0.000
78 -> 94 -0.14678
82 -> 96 -0.10245
83 -> 97 -0.19253
84 -> 97 -0.24677
84 -> 98 0.29990
85 ->100 -0.16891
86 ->100 -0.20061
87 -> 98 -0.11035
87 ->101 0.14646
90 ->101 -0.29954
92 ->102 0.11836

Excited State 83: Singlet-A 7.5555 eV 164.10 nm f=0.0236 <S**2>=0.000
77 -> 94 0.57616
83 -> 96 -0.34728

Excited State 84: Singlet-A 7.5954 eV 163.24 nm f=0.0025 <S**2>=0.000
81 -> 95 0.24486
82 -> 95 0.12984
84 -> 98 0.11793
85 ->100 -0.10107
86 ->100 0.53676

Excited State 85: Singlet-A 7.6091 eV 162.94 nm f=0.0003 <S**2>=0.000
76 -> 94 0.54119
81 -> 96 -0.11487
82 -> 96 0.11807
83 -> 97 0.24908
84 -> 97 -0.11952
86 ->100 0.10529
90 ->101 -0.13189

Excited State 86: Singlet-A 7.6271 eV 162.56 nm f=0.0028 <S**2>=0.000
89 ->101 -0.22408
92 ->104 -0.17121
93 ->105 0.60676

Excited State 87: Singlet-A 7.6461 eV 162.15 nm f=0.0003 <S**2>=0.000
89 ->101 0.64359
93 ->105 0.22655

Excited State 88: Singlet-A 7.6578 eV 161.91 nm f=0.0002 <S**2>=0.000
76 -> 94 -0.11258
81 -> 95 -0.23275
82 -> 96 0.18779
84 -> 98 -0.21406
87 ->101 0.11782
88 ->101 0.49575
90 ->101 -0.21619

Excited State 89: Singlet-A 7.6899 eV 161.23 nm f=0.1497 <S**2>=0.000
75 -> 94 0.13510
80 -> 95 -0.10682
84 -> 99 0.57125

86 ->101 -0.11188
89 ->101 -0.10432
91 ->102 0.17216

Excited State 90: Singlet-A 7.6933 eV 161.16 nm f=0.0012 <S**2>=0.000
76 -> 94 -0.39028
79 -> 96 0.12808
81 -> 95 -0.13863
81 -> 96 -0.13252
83 -> 97 0.41976
84 -> 98 0.11484
85 ->100 -0.12361
88 ->101 -0.18065

Excited State 91: Singlet-A 7.6988 eV 161.04 nm f=0.0088 <S**2>=0.000
81 -> 95 -0.29036
82 -> 95 -0.16349
82 -> 96 -0.12771
84 -> 98 0.17485
85 ->100 0.36944
86 ->100 0.17730
87 ->101 -0.27179
90 ->101 -0.19285

Excited State 92: Singlet-A 7.7203 eV 160.60 nm f=0.0002 <S**2>=0.000
81 -> 95 -0.13050
81 -> 96 -0.11289
82 -> 96 0.38532
83 -> 97 -0.23943
88 ->101 -0.27796
92 ->103 0.26416
93 ->106 0.22842

Excited State 93: Singlet-A 7.7269 eV 160.46 nm f=0.0026 <S**2>=0.000
81 -> 95 0.13266
82 -> 95 0.10007
84 -> 98 0.29097
87 ->101 -0.14550
88 ->101 0.32052
92 ->103 0.33688
93 ->106 0.23789

Excited State 94: Singlet-A 7.7537 eV 159.90 nm f=0.0174 <S**2>=0.000

81 -> 96 -0.10484
82 -> 96 0.32578
83 -> 97 -0.10477
84 -> 98 0.31903
90 ->101 0.19329
92 ->103 -0.22709
93 ->106 -0.28231

Excited State 95: Singlet-A 7.7669 eV 159.63 nm f=0.0056 <S**2>=0.000
79 -> 95 0.10943
81 -> 95 -0.26196
81 -> 96 0.19135
82 -> 95 -0.16726
82 -> 96 -0.15200
84 -> 97 0.14223
84 -> 98 0.14164
85 -> 99 -0.12723
85 ->100 -0.18787
87 ->101 0.27408
90 ->101 0.14503
92 ->103 0.18290
93 ->106 0.13982

Excited State 96: Singlet-A 7.7724 eV 159.52 nm f=0.0096 <S**2>=0.000
73 -> 94 0.41922
75 -> 94 0.46204
84 -> 99 -0.14068
92 ->104 -0.10770

Excited State 97: Singlet-A 7.8232 eV 158.48 nm f=0.0038 <S**2>=0.000
80 -> 95 0.48992
92 ->104 -0.41769
93 ->105 -0.10541
93 ->107 -0.14371

Excited State 98: Singlet-A 7.8428 eV 158.09 nm f=0.0006 <S**2>=0.000
80 -> 95 -0.16308
92 ->103 -0.40462
92 ->104 -0.17674
93 ->106 0.48013

Excited State 99: Singlet-A 7.8428 eV 158.09 nm f=0.0020 <S**2>=0.000
73 -> 94 0.16110

80 -> 95 0.39032
92 ->103 -0.17292
92 ->104 0.40896
93 ->105 0.16741
93 ->106 0.20385

Excited State 100: Singlet-A 7.8697 eV 157.55 nm f=0.0022 <S**2>=0.000
73 -> 94 -0.40044
75 -> 94 0.46200
80 -> 95 0.11634
82 -> 97 0.21955

Table A4.11. Excitation Energies and Oscillator Strengths of 6 Using the TD-B3LYP Method with 6-31G(d) Basis Set in Chloroform.

Excited State 1: Singlet-A 2.7982 eV 443.08 nm f=0.3748 <S**2>=0.000
93 -> 94 0.69958
This state for optimization and/or second-order correction.
Total Energy, E(TD-HF/TD-KS) = -1181.65604131
Copying the excited state density for this state as the 1-particle RhoCI density.

Excited State 2: Singlet-A 3.3212 eV 373.31 nm f=0.0010 <S**2>=0.000
92 -> 94 0.64220
93 -> 95 0.28035

Excited State 3: Singlet-A 3.5443 eV 349.81 nm f=0.1493 <S**2>=0.000
92 -> 94 -0.27703
93 -> 95 0.61818
93 -> 96 0.13684

Excited State 4: Singlet-A 3.8099 eV 325.42 nm f=0.0098 <S**2>=0.000
93 -> 95 -0.11775
93 -> 96 0.68547

Excited State 5: Singlet-A 3.9473 eV 314.10 nm f=0.0045 <S**2>=0.000
91 -> 94 0.49919
93 -> 97 0.48404

Excited State 6: Singlet-A 4.0195 eV 308.45 nm f=0.0116 <S**2>=0.000
91 -> 94 -0.47189
93 -> 97 0.50341

Excited State 7: Singlet-A 4.2272 eV 293.30 nm f=0.0015 <S**2>=0.000
88 -> 94 -0.39711
89 -> 94 0.52299
90 -> 94 0.11759
92 -> 95 0.12139

Excited State 8: Singlet-A 4.2992 eV 288.39 nm f=0.0026 <S**2>=0.000
88 -> 94 0.53051
89 -> 94 0.42937
89 -> 97 -0.10948

Excited State 9: Singlet-A 4.3512 eV 284.95 nm f=0.0933 <S**2>=0.000
87 -> 94 0.13714
88 -> 94 0.13282
90 -> 94 0.18504
92 -> 95 0.49430
92 -> 96 0.13294
93 -> 98 -0.37027

Excited State 10: Singlet-A 4.4016 eV 281.68 nm f=0.0736 <S**2>=0.000
90 -> 94 0.58142
92 -> 95 -0.29294
93 -> 98 -0.10121

Excited State 11: Singlet-A 4.4574 eV 278.15 nm f=0.1417 <S**2>=0.000
90 -> 94 0.24051
92 -> 95 0.24251
92 -> 96 0.24568
93 -> 98 0.52830

Excited State 12: Singlet-A 4.5961 eV 269.76 nm f=0.0318 <S**2>=0.000
90 -> 94 0.11895
91 -> 96 0.11890
92 -> 96 -0.14651
93 -> 99 0.63279

Excited State 13: Singlet-A 4.6470 eV 266.80 nm f=0.0501 <S**2>=0.000
86 -> 94 -0.16458
87 -> 94 0.49608
92 -> 96 -0.40087
93 -> 98 0.17385

Excited State 14: Singlet-A 4.7002 eV 263.78 nm f=0.0416 <S**2>=0.000

86 -> 94 0.58956
87 -> 94 0.22711
92 -> 97 0.26710

Excited State 15: Singlet-A 4.7986 eV 258.38 nm f=0.0478 <S**2>=0.000
86 -> 94 -0.19454
87 -> 94 0.37476
92 -> 95 -0.23464
92 -> 96 0.43977
93 -> 99 0.15626

Excited State 16: Singlet-A 4.8976 eV 253.15 nm f=0.0099 <S**2>=0.000
88 -> 95 0.22708
89 -> 95 0.55930
91 -> 95 0.30766

Excited State 17: Singlet-A 4.9773 eV 249.10 nm f=0.3189 <S**2>=0.000
86 -> 94 -0.21408
87 -> 95 0.11991
89 -> 95 0.13909
91 -> 95 -0.23633
92 -> 97 0.57068

Excited State 18: Singlet-A 5.0213 eV 246.92 nm f=0.1157 <S**2>=0.000
86 -> 94 -0.11045
88 -> 95 -0.11244
89 -> 95 -0.25034
91 -> 95 0.56875
92 -> 97 0.21553

Excited State 19: Singlet-A 5.1855 eV 239.10 nm f=0.0086 <S**2>=0.000
84 -> 94 0.13012
85 -> 94 -0.29584
91 -> 96 -0.27644
93 ->100 0.51888

Excited State 20: Singlet-A 5.2521 eV 236.07 nm f=0.0054 <S**2>=0.000
91 -> 96 -0.17878
92 -> 98 0.63424
93 ->100 -0.18238

Excited State 21: Singlet-A 5.2915 eV 234.31 nm f=0.1119 <S**2>=0.000
85 -> 94 0.45998

91 -> 96 0.16775
91 -> 97 -0.12025
92 -> 98 0.14556
92 -> 99 0.13628
93 ->100 0.33951
93 ->101 -0.17692

Excited State 22: Singlet-A 5.3685 eV 230.95 nm f=0.1195 <S**2>=0.000
85 -> 94 0.24558
88 -> 97 0.14861
89 -> 95 -0.13338
89 -> 96 -0.22999
89 -> 97 0.12009
90 -> 95 0.41858
90 -> 96 -0.17311
91 -> 96 -0.13220
91 -> 97 0.15553
92 -> 98 -0.10915
92 -> 99 -0.15580

Excited State 23: Singlet-A 5.3906 eV 230.00 nm f=0.0978 <S**2>=0.000
88 -> 95 -0.14769
88 -> 96 -0.19211
88 -> 97 -0.23167
88 -> 98 -0.12073
89 -> 96 0.30291
90 -> 95 0.41980
91 -> 96 0.12447
91 -> 97 0.13554
92 -> 98 0.11339

Excited State 24: Singlet-A 5.4155 eV 228.94 nm f=0.0141 <S**2>=0.000
88 -> 95 -0.19935
88 -> 96 -0.35602
88 -> 98 -0.13826
89 -> 96 -0.26828
89 -> 97 0.38166
90 -> 95 -0.13375
91 -> 97 0.10691

Excited State 25: Singlet-A 5.4284 eV 228.40 nm f=0.1052 <S**2>=0.000
85 -> 94 -0.22577
86 -> 95 -0.16513

88 -> 97 0.12311
89 -> 96 -0.18801
90 -> 95 0.24366
92 -> 99 0.46181

Excited State 26: Singlet-A 5.4905 eV 225.82 nm f=0.3789 <S**2>=0.000
84 -> 94 -0.17544
85 -> 94 -0.16149
87 -> 95 0.11166
88 -> 97 0.10330
88 -> 98 0.11131
90 -> 96 -0.10535
91 -> 96 0.45972
91 -> 97 0.20487
92 -> 98 0.15000
92 -> 99 -0.21787
93 ->100 0.10854

Excited State 27: Singlet-A 5.5337 eV 224.05 nm f=0.1509 <S**2>=0.000
84 -> 94 -0.19510
86 -> 95 0.16908
87 -> 95 0.29341
88 -> 95 -0.22222
88 -> 96 0.10002
89 -> 95 0.11629
90 -> 96 -0.18306
91 -> 96 -0.15706
91 -> 97 0.26121
92 -> 99 0.25590
93 ->101 -0.12412

Excited State 28: Singlet-A 5.5534 eV 223.26 nm f=0.0309 <S**2>=0.000
84 -> 94 -0.13952
88 -> 95 -0.27470
90 -> 96 -0.20897
91 -> 97 -0.36109
92 ->100 -0.11593
93 ->101 0.39554

Excited State 29: Singlet-A 5.5857 eV 221.97 nm f=0.0286 <S**2>=0.000
84 -> 94 -0.11445
86 -> 95 0.19004
88 -> 95 0.45472

88 -> 96 -0.18414
88 -> 97 -0.11640
89 -> 95 -0.17785
89 -> 96 0.12612
90 -> 96 -0.17447
92 -> 99 0.22716

Excited State 30: Singlet-A 5.6211 eV 220.57 nm f=0.1189 <S**2>=0.000
86 -> 95 0.44151
87 -> 95 -0.18951
88 -> 95 -0.10664
91 -> 96 0.10772
91 -> 97 -0.16060
92 ->100 -0.11216
93 ->101 -0.38152

Excited State 31: Singlet-A 5.6685 eV 218.73 nm f=0.1017 <S**2>=0.000
87 -> 95 0.45950
88 -> 98 -0.12640
90 -> 95 0.10604
90 -> 96 0.11062
90 -> 97 0.17108
91 -> 97 -0.27094
91 -> 98 0.12256
92 -> 99 -0.20290
93 ->101 -0.14750

Excited State 32: Singlet-A 5.7142 eV 216.98 nm f=0.0464 <S**2>=0.000
83 -> 94 -0.11178
84 -> 94 0.52122
87 -> 95 0.15759
90 -> 96 -0.15658
90 -> 97 0.23006
93 ->101 0.12849

Excited State 33: Singlet-A 5.7816 eV 214.45 nm f=0.0351 <S**2>=0.000
88 -> 94 0.12264
88 -> 96 -0.18179
88 -> 97 -0.15151
88 -> 98 0.45007
88 -> 99 0.16368
89 -> 96 0.11000
89 -> 97 0.11458

89 -> 98 -0.23121
90 -> 98 -0.11493
91 -> 97 -0.10508
91 -> 98 -0.17937

Excited State 34: Singlet-A 5.8192 eV 213.06 nm f=0.0467 <S**2>=0.000
86 -> 95 0.25632
90 -> 96 0.48799
91 -> 97 0.15938
92 ->100 -0.25343
93 ->101 0.19997

Excited State 35: Singlet-A 5.9251 eV 209.25 nm f=0.0977 <S**2>=0.000
88 -> 98 0.16562
89 -> 98 -0.11097
91 -> 98 0.61843

Excited State 36: Singlet-A 5.9496 eV 208.39 nm f=0.0016 <S**2>=0.000
88 -> 96 0.24777
88 -> 97 0.22745
89 -> 96 0.37182
89 -> 97 0.46690

Excited State 37: Singlet-A 5.9837 eV 207.20 nm f=0.0745 <S**2>=0.000
83 -> 94 0.10399
84 -> 94 -0.10906
86 -> 95 -0.14214
86 -> 96 -0.10761
86 -> 98 0.10312
87 -> 95 -0.18566
90 -> 97 0.50699
92 ->100 -0.23103

Excited State 38: Singlet-A 6.0246 eV 205.80 nm f=0.0209 <S**2>=0.000
86 -> 95 0.18584
86 -> 96 0.20406
87 -> 95 -0.11200
87 -> 96 0.11650
87 -> 97 -0.12850
88 -> 97 0.10299
90 -> 97 0.22182
92 ->100 0.48597
93 ->102 0.11827

Excited State 39: Singlet-A 6.0708 eV 204.23 nm f=0.0184 <S**2>=0.000
88 -> 96 -0.37256
88 -> 97 0.47839
89 -> 96 0.16954
89 -> 97 -0.17431
90 -> 97 -0.10714

Excited State 40: Singlet-A 6.1190 eV 202.62 nm f=0.0276 <S**2>=0.000
83 -> 94 -0.32236
85 -> 95 0.14696
86 -> 96 0.12275
87 -> 96 0.49052
88 -> 97 -0.14099
91 -> 99 -0.18966

Excited State 41: Singlet-A 6.1444 eV 201.78 nm f=0.1118 <S**2>=0.000
83 -> 94 0.30470
85 -> 95 -0.12824
86 -> 96 0.48503
87 -> 97 0.27797
92 ->100 -0.10437

Excited State 42: Singlet-A 6.1942 eV 200.16 nm f=0.0245 <S**2>=0.000
83 -> 94 -0.22442
85 -> 95 0.33672
86 -> 97 -0.13901
87 -> 96 -0.14111
87 -> 97 0.20848
91 -> 99 0.38069
92 ->101 0.23494

Excited State 43: Singlet-A 6.2045 eV 199.83 nm f=0.0031 <S**2>=0.000
83 -> 94 0.40245
84 -> 94 0.10235
85 -> 95 0.27468
86 -> 96 -0.17967
86 -> 97 0.26242
87 -> 96 0.23174
91 -> 99 0.13370
92 ->101 0.15824

Excited State 44: Singlet-A 6.2285 eV 199.06 nm f=0.0221 <S**2>=0.000

85 -> 95 -0.29793
86 -> 96 -0.14517
86 -> 97 0.13076
86 -> 98 0.13086
87 -> 96 0.23260
87 -> 97 0.18262
90 -> 98 0.20081
90 -> 99 -0.12470
91 -> 99 0.31649
92 ->101 -0.24603

Excited State 45: Singlet-A 6.3202 eV 196.17 nm f=0.1105 <S**2>=0.000
83 -> 94 -0.15429
85 -> 95 -0.13092
86 -> 96 0.17022
86 -> 97 0.34006
87 -> 97 -0.25257
91 -> 99 0.19092
92 ->100 -0.14196
92 ->101 0.12377
93 ->102 0.32123

Excited State 46: Singlet-A 6.3573 eV 195.03 nm f=0.0982 <S**2>=0.000
82 -> 94 0.16237
86 -> 97 -0.19477
87 -> 97 -0.12149
89 -> 98 -0.18869
90 -> 98 0.46638
93 ->102 0.32174

Excited State 47: Singlet-A 6.3780 eV 194.39 nm f=0.0028 <S**2>=0.000
86 -> 97 -0.14033
88 -> 98 0.24742
89 -> 98 0.54792
89 -> 99 -0.17191
93 ->102 0.13015

Excited State 48: Singlet-A 6.4003 eV 193.72 nm f=0.0957 <S**2>=0.000
82 -> 94 0.23320
84 -> 95 -0.10745
85 -> 96 0.10973
86 -> 96 -0.14507
87 -> 97 0.15885

90 -> 98 -0.33335
90 -> 99 0.25277
92 ->101 -0.18600
93 ->102 0.34066

Excited State 49: Singlet-A 6.4127 eV 193.34 nm f=0.0787 <S**2>=0.000
84 -> 95 -0.19406
86 -> 97 0.23928
87 -> 97 0.32300
87 -> 98 -0.23438
87 -> 99 0.14885
88 -> 98 0.11995
89 -> 98 0.13141
90 -> 98 0.12953
91 -> 99 -0.16486
91 ->100 -0.21512
92 ->101 0.12989

Excited State 50: Singlet-A 6.4899 eV 191.04 nm f=0.0247 <S**2>=0.000
85 -> 95 -0.13117
85 -> 96 -0.23569
86 -> 97 0.16935
86 -> 98 0.20742
87 -> 98 -0.10689
87 -> 99 -0.15643
89 -> 99 -0.15952
90 -> 99 0.32189
91 ->100 0.28933
92 ->101 0.17155

Excited State 51: Singlet-A 6.5166 eV 190.26 nm f=0.0842 <S**2>=0.000
82 -> 94 0.34787
84 -> 95 0.17361
84 -> 96 -0.16041
85 -> 96 -0.13618
86 -> 98 0.23469
87 -> 98 -0.23136
90 -> 99 -0.32094

Excited State 52: Singlet-A 6.5470 eV 189.38 nm f=0.0994 <S**2>=0.000
84 -> 95 0.32909
85 -> 95 -0.13365
85 -> 96 -0.11539

85 -> 97 0.14070
86 -> 97 -0.11267
86 -> 98 -0.14412
87 -> 99 0.13566
89 -> 99 0.25261
90 -> 99 0.22866
91 ->100 -0.22206
92 ->101 0.16076

Excited State 53: Singlet-A 6.5786 eV 188.47 nm f=0.0427 <S**2>=0.000
84 -> 95 -0.14855
85 -> 97 -0.11151
86 -> 98 0.14068
88 -> 98 0.17334
89 -> 99 0.56374
91 ->100 0.15606

Excited State 54: Singlet-A 6.6256 eV 187.13 nm f=0.0134 <S**2>=0.000
82 -> 94 0.19852
84 -> 95 -0.15781
85 -> 96 -0.16560
87 -> 98 0.26539
88 -> 99 0.38710
89 -> 99 0.15997
90 -> 99 -0.14067
90 ->100 0.11802

Excited State 55: Singlet-A 6.6472 eV 186.52 nm f=0.1748 <S**2>=0.000
82 -> 94 -0.13778
84 -> 95 0.27728
85 -> 96 0.29094
86 -> 98 -0.11179
87 -> 98 -0.19273
88 -> 99 0.35038
89 -> 99 0.10176
90 -> 99 -0.10326
91 ->100 0.20254
93 ->102 0.11714

Excited State 56: Singlet-A 6.6642 eV 186.04 nm f=0.1509 <S**2>=0.000
82 -> 94 -0.12730
84 -> 96 -0.10388
85 -> 96 -0.19515

85 -> 97 -0.10553
86 -> 98 0.18380
86 -> 99 0.10696
87 -> 98 -0.11744
87 -> 99 0.18012
88 -> 99 0.38710
90 -> 99 0.15282
90 ->100 -0.11507
91 ->100 -0.20732
92 ->101 -0.11821

Excited State 57: Singlet-A 6.6698 eV 185.89 nm f=0.0386 <S**2>=0.000
84 -> 95 -0.25373
84 -> 96 -0.11835
85 -> 95 -0.20913
85 -> 96 0.11916
86 -> 97 -0.17923
86 -> 98 -0.21287
86 -> 99 0.20331
87 -> 98 -0.15080
91 -> 99 0.10369
91 ->100 0.16058
92 ->101 0.27791

Excited State 58: Singlet-A 6.6944 eV 185.21 nm f=0.1465 <S**2>=0.000
79 -> 94 -0.21990
80 -> 94 0.28244
81 -> 94 0.28237
82 -> 94 0.21709
85 -> 95 0.10457
85 -> 96 0.13586
86 -> 96 0.11351
87 -> 97 -0.11653
87 -> 98 -0.14702
90 -> 99 0.16309
92 ->101 -0.12679
93 ->102 -0.19197

Excited State 59: Singlet-A 6.7172 eV 184.58 nm f=0.0470 <S**2>=0.000
81 -> 94 0.40798
82 -> 94 -0.10115
85 -> 96 0.10948
85 -> 97 -0.24419

86 -> 98 0.19904
87 -> 98 0.28524
87 -> 99 0.22647
91 ->100 0.10382

Excited State 60: Singlet-A 6.7305 eV 184.21 nm f=0.1465 <S**2>=0.000
81 -> 94 0.42082
82 -> 94 -0.10463
84 -> 95 -0.13578
85 -> 96 -0.27670
86 -> 98 -0.17277
87 -> 98 -0.22420
87 -> 99 -0.21415
90 -> 99 -0.11347

Excited State 61: Singlet-A 6.8467 eV 181.09 nm f=0.0181 <S**2>=0.000
79 -> 94 0.15651
80 -> 94 -0.25906
81 -> 94 0.13339
84 -> 95 -0.10076
85 -> 96 0.17357
85 -> 97 0.46251
86 -> 98 0.21710
89 ->100 0.11622

Excited State 62: Singlet-A 6.9137 eV 179.33 nm f=0.0425 <S**2>=0.000
80 -> 94 0.17703
84 -> 96 -0.10233
86 -> 99 0.49819
87 -> 98 0.10764
87 -> 99 -0.26395
90 ->100 -0.14928
91 ->101 0.11445

Excited State 63: Singlet-A 6.9345 eV 178.79 nm f=0.0220 <S**2>=0.000
79 -> 94 0.20024
80 -> 94 -0.13767
82 -> 94 0.15793
84 -> 96 0.39673
85 -> 96 -0.10529
85 -> 97 -0.12415
86 -> 99 0.24058
89 ->100 0.28562

90 ->100 -0.12815
91 ->100 0.10160

Excited State 64: Singlet-A 6.9606 eV 178.12 nm f=0.0210 <S**2>=0.000
80 -> 94 0.30651
82 -> 94 -0.13226
84 -> 96 -0.11203
85 -> 97 0.14309
87 -> 99 0.11898
89 ->100 0.45612
89 ->101 -0.10260
91 ->101 -0.19473

Excited State 65: Singlet-A 6.9916 eV 177.33 nm f=0.0233 <S**2>=0.000
79 -> 94 0.14464
83 -> 95 -0.12604
84 -> 96 -0.24522
85 -> 97 -0.15569
89 ->100 0.18363
90 ->100 0.47241
91 ->101 0.21748

Excited State 66: Singlet-A 7.0223 eV 176.56 nm f=0.0204 <S**2>=0.000
79 -> 94 0.43936
80 -> 94 0.23492
85 -> 97 0.11863
87 -> 99 0.17470
88 ->100 -0.13862
89 ->100 -0.27666
90 ->100 0.10830
91 ->100 0.11681
93 ->103 0.10032

Excited State 67: Singlet-A 7.0416 eV 176.07 nm f=0.0028 <S**2>=0.000
79 -> 94 0.15718
80 -> 94 0.10696
83 -> 95 0.12476
88 ->100 0.55707
93 ->103 -0.28161

Excited State 68: Singlet-A 7.0565 eV 175.70 nm f=0.0251 <S**2>=0.000
83 -> 95 -0.30341
84 -> 97 -0.10311

88 ->100 0.28819
89 ->101 -0.12336
91 ->101 -0.25101
93 ->103 0.41699

Excited State 69: Singlet-A 7.0574 eV 175.68 nm f=0.0092 <S**2>=0.000
83 -> 95 0.35034
84 -> 96 -0.13509
84 -> 97 0.11322
88 ->100 0.12268
89 ->100 0.10049
90 ->100 -0.14476
91 ->101 0.23470
93 ->103 0.44647

Excited State 70: Singlet-A 7.0695 eV 175.38 nm f=0.0309 <S**2>=0.000
83 -> 95 0.41942
84 -> 95 0.11395
84 -> 96 0.18970
85 -> 98 -0.12149
86 -> 99 0.15831
89 ->100 -0.10056
90 ->100 0.30471
91 ->101 -0.22083

Excited State 71: Singlet-A 7.1350 eV 173.77 nm f=0.0114 <S**2>=0.000
79 -> 94 0.10435
80 -> 94 -0.10325
82 -> 94 0.12640
83 -> 95 0.10912
84 -> 96 -0.17580
85 -> 98 0.40483
85 -> 99 0.10885
86 -> 98 -0.10143
89 ->101 -0.20741
91 ->101 -0.27062
92 ->102 -0.10689

Excited State 72: Singlet-A 7.1388 eV 173.68 nm f=0.0281 <S**2>=0.000
84 -> 96 -0.18124
84 -> 97 0.39581
85 -> 98 -0.26848
85 -> 99 0.10672

86 -> 99 0.10454
87 ->100 0.18010
90 ->101 0.11166
91 ->101 -0.18460
92 ->101 -0.12100

Excited State 73: Singlet-A 7.1623 eV 173.11 nm f=0.0008 <S**2>=0.000
78 -> 94 0.10872
82 -> 95 -0.13455
88 ->101 -0.13782
89 ->100 -0.10200
89 ->101 -0.42060
91 ->101 0.11997
92 ->102 0.44958

Excited State 74: Singlet-A 7.1938 eV 172.35 nm f=0.0246 <S**2>=0.000
78 -> 94 0.11414
84 -> 97 -0.10315
85 -> 98 0.22255
88 ->100 0.12921
88 ->101 0.13360
89 ->101 0.33270
90 ->101 0.10857
92 ->102 0.34949
93 ->104 0.20679

Excited State 75: Singlet-A 7.2122 eV 171.91 nm f=0.0032 <S**2>=0.000
77 -> 94 0.38794
78 -> 94 0.25569
80 -> 94 0.10473
83 -> 97 -0.12516
84 -> 97 0.10760
92 ->102 -0.23004
93 ->104 0.32813

Excited State 76: Singlet-A 7.2245 eV 171.62 nm f=0.0045 <S**2>=0.000
77 -> 94 -0.22595
78 -> 94 -0.27406
93 ->104 0.54834

Excited State 77: Singlet-A 7.2494 eV 171.03 nm f=0.0143 <S**2>=0.000
77 -> 94 -0.39906
78 -> 94 0.49035

86 ->100 0.10081

Excited State 78: Singlet-A 7.3187 eV 169.41 nm f=0.0644 <S**2>=0.000
78 -> 94 -0.17444
79 -> 94 -0.19154
80 -> 94 -0.10722
82 -> 94 -0.10978
84 -> 97 0.14744
84 -> 98 0.15775
85 -> 97 0.10015
85 -> 98 0.29447
86 -> 99 0.10597
86 ->100 0.25559
87 -> 99 0.13846
89 ->101 -0.12578
91 ->100 0.10900
91 ->101 0.14519

Excited State 79: Singlet-A 7.3417 eV 168.88 nm f=0.1240 <S**2>=0.000
77 -> 94 -0.21200
80 -> 94 0.10480
84 -> 97 0.36367
85 -> 98 0.13638
85 -> 99 -0.24250
86 ->100 -0.21450
87 ->100 -0.29280
91 ->100 -0.11007

Excited State 80: Singlet-A 7.3980 eV 167.59 nm f=0.0690 <S**2>=0.000
83 -> 96 0.10113
84 -> 98 -0.25568
85 -> 98 -0.11611
86 ->100 0.40820
87 ->100 -0.21060
90 ->101 0.37121

Excited State 81: Singlet-A 7.4149 eV 167.21 nm f=0.0255 <S**2>=0.000
75 -> 94 -0.15547
76 -> 94 -0.15610
81 -> 97 -0.11001
83 -> 96 0.48876
84 -> 98 0.10600
85 -> 99 -0.16240

86 ->100 -0.16848
87 ->100 -0.18113

Excited State 82: Singlet-A 7.4498 eV 166.43 nm f=0.0500 <S**2>=0.000
75 -> 94 -0.12218
76 -> 94 -0.14722
80 -> 94 0.10451
83 -> 96 0.21253
84 -> 96 0.11238
84 -> 97 0.11255
85 -> 98 0.11701
85 -> 99 0.11406
86 -> 98 0.10333
86 ->100 0.28865
86 ->101 0.14784
87 -> 99 -0.14666
87 ->100 0.16079
90 ->101 -0.23129
91 ->100 -0.11595

Excited State 83: Singlet-A 7.4878 eV 165.58 nm f=0.0819 <S**2>=0.000
79 -> 95 -0.13052
81 -> 95 0.10906
82 -> 95 0.43627
85 -> 99 0.36672
86 ->101 0.12405
87 ->100 -0.22462
91 ->102 -0.10170

Excited State 84: Singlet-A 7.5199 eV 164.87 nm f=0.0845 <S**2>=0.000
75 -> 94 -0.19298
79 -> 95 -0.13705
81 -> 95 0.10320
82 -> 95 0.29735
83 -> 97 0.11407
85 -> 99 -0.26551
87 ->100 0.31820
90 ->101 0.26695

Excited State 85: Singlet-A 7.5332 eV 164.58 nm f=0.0184 <S**2>=0.000
75 -> 94 0.11650
76 -> 94 0.11594
77 -> 94 0.10902

82 -> 95 0.21000
84 -> 98 0.30822
84 -> 99 -0.16708
85 -> 99 -0.21928
86 ->100 0.18750
87 ->100 -0.19480
87 ->101 0.14405
90 ->101 -0.12535

Excited State 86: Singlet-A 7.5601 eV 164.00 nm f=0.0096 <S**2>=0.000
75 -> 94 0.33051
76 -> 94 0.41880
83 -> 96 0.29368
83 -> 97 -0.17140
87 ->100 0.10687
90 ->101 0.11198

Excited State 87: Singlet-A 7.6336 eV 162.42 nm f=0.0002 <S**2>=0.000
76 -> 94 -0.19158
81 -> 95 0.21096
81 -> 96 0.11424
83 -> 96 -0.12027
83 -> 97 -0.25296
84 -> 98 0.10350
88 ->101 -0.28356
90 ->101 0.12834
93 ->105 0.37904

Excited State 88: Singlet-A 7.6340 eV 162.41 nm f=0.0115 <S**2>=0.000
75 -> 94 0.19384
81 -> 96 -0.10463
83 -> 97 0.24538
84 -> 98 -0.16240
84 -> 99 0.21949
90 ->101 -0.12685
93 ->105 0.45986

Excited State 89: Singlet-A 7.6527 eV 162.01 nm f=0.0066 <S**2>=0.000
75 -> 94 -0.11663
81 -> 95 0.10477
83 -> 97 -0.12449
84 -> 98 0.10260
84 -> 99 -0.12994

88 ->101 0.55608
89 ->101 -0.21015
93 ->105 0.21718

Excited State 90: Singlet-A 7.6579 eV 161.90 nm f=0.0149 <S**2>=0.000
75 -> 94 0.23189
76 -> 94 -0.16744
79 -> 95 -0.16801
80 -> 95 0.17537
81 -> 95 0.30557
83 -> 97 -0.10630
84 -> 99 0.18507
88 ->101 0.11890
90 ->101 -0.16916
91 ->102 0.14964
93 ->105 -0.22378

Excited State 91: Singlet-A 7.6944 eV 161.14 nm f=0.0912 <S**2>=0.000
79 -> 95 0.10788
84 -> 98 0.29763
84 -> 99 0.49604
87 ->101 0.12009
90 ->101 0.16813
91 ->102 0.11963

Excited State 92: Singlet-A 7.6996 eV 161.03 nm f=0.0040 <S**2>=0.000
81 -> 95 0.38625
81 -> 96 -0.11547
82 -> 95 -0.22911
82 -> 96 0.13403
83 -> 97 0.34667
84 -> 98 0.14222
86 ->101 -0.10034

Excited State 93: Singlet-A 7.7228 eV 160.54 nm f=0.0049 <S**2>=0.000
75 -> 94 0.36330
76 -> 94 -0.35165
83 -> 97 0.11059
84 -> 99 -0.21186
87 ->101 0.19710
90 ->101 0.13958

Excited State 94: Singlet-A 7.7589 eV 159.80 nm f=0.0037 <S**2>=0.000

80 -> 95 -0.10457
84 -> 98 0.11251
85 ->100 0.28511
86 ->101 0.39901
87 ->101 -0.36239
91 ->102 0.17034

Excited State 95: Singlet-A 7.8026 eV 158.90 nm f=0.0075 <S**2>=0.000
78 -> 95 0.13170
79 -> 95 -0.29463
80 -> 95 0.33383
81 -> 95 -0.23963
82 -> 95 -0.13592
84 -> 98 0.10058
85 ->100 0.14113
87 ->101 0.11570
92 ->103 0.23187
92 ->104 0.15883

Excited State 96: Singlet-A 7.8140 eV 158.67 nm f=0.0069 <S**2>=0.000
79 -> 95 0.15508
80 -> 95 -0.14211
81 -> 95 0.13399
92 ->103 0.47638
92 ->104 0.32168
93 ->104 0.12626
93 ->107 0.12443

Excited State 97: Singlet-A 7.8467 eV 158.01 nm f=0.0654 <S**2>=0.000
81 -> 95 0.11569
85 ->100 0.26072
86 ->101 0.25611
87 ->101 0.40719
91 ->102 -0.22858

Excited State 98: Singlet-A 7.8956 eV 157.03 nm f=0.0173 <S**2>=0.000
74 -> 94 0.11229
75 -> 94 0.12287
79 -> 96 -0.12069
81 -> 96 0.16829
82 -> 96 0.39271
87 ->101 -0.12956
91 ->102 -0.35839

93 ->106 0.10247

Excited State 99: Singlet-A 7.9078 eV 156.79 nm f=0.0069 <S**2>=0.000
73 -> 94 0.44190
74 -> 94 -0.42420
81 -> 97 0.10105

Excited State 100: Singlet-A 7.9380 eV 156.19 nm f=0.0107 <S**2>=0.000
79 -> 95 0.13147
80 -> 95 0.14729
91 ->102 0.16700
91 ->103 -0.13381
92 ->103 0.16754
92 ->104 -0.30324
93 ->106 0.41706
93 ->107 0.19349

Chapter 6

Diazaxanthylidene-based Novel Molecular Tools for Nuclear Staining of Neuronal Subpopulations and Populations

This work was performed in collaboration with Dr. J. Nicholas Betley and Elen Hernandez in the Betley group and Dr. Mai N. Tran, a previous graduate student in the Chenoweth group at the University of Pennsylvania.

6.1 Introduction

Fluorescent microscopic imaging has been a critical tool capable of visualizing cells and tissues in both the biology and medical fields.[1] Many fluorophores have been developed to meet requirements for various imaging experiments.[2] In our previous reports, we have provided the synthesis of diazaxanthylidene derivatives and introduced their unique photophysical properties.[3] *N*-methylated diazaxanthylidenes bearing a positive charge undergo tandem photocylization-oxidation reactions that makes original absorption and emission wavelength shifted to the red end of spectrum. Accompanying with high quantum yield, low toxicity, and specific sub-cellular localization of photoactivated diazaxanthylidenes, photocylization/oxidation mechanism is especially useful to enable intracellular photoconversion.

Inspired by cell imaging data that demonstrated the staining potential of diazaxanthylidene derivatives to be used as fluorescent markers, we report post-photocyclization/oxidation/methylation diazaxanthylidenes that can be used as nuclei-specific fluorescent probes for both live and fixed brain tissue imaging. Incubation of mouse brain tissue slices with these probes resulted in nuclear staining of neurons within the hippocampal region[4] as well as the Islands of Calleja (IC).[5] Low toxicity was evaluated and shown through intracranial injections and live imaging. As a result of intracranial injections, potential retrograding properties were demonstrated. These fluorophores were evaluated for degradation and found to be stable after the incubation of fluorescent antibodies by using immunohistochemical protocols.

6.2 Results and Discussion

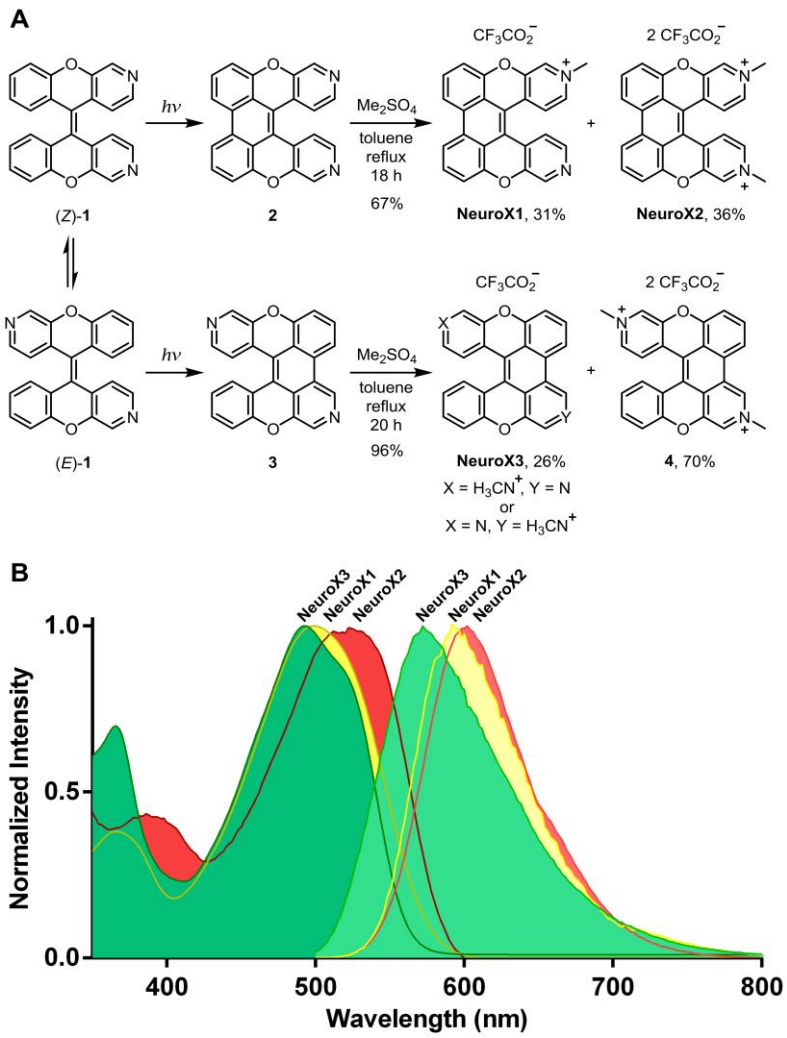

Figure 6.1. Preparation and photophysical properties of **NeuroX1-X3**. (A) Synthesis of **NeuroX1-X3**. (B) Absorption and emission spectra of **NeuroX1-X3**. **NeuroX1** (Abs l_{max} = 499 nm, Em l_{max} = 592 nm, ε = 10437 $M^{-1}cm^{-1}$, Φ = 0.101) and **NeuroX2** (Abs l_{max} = 521 nm, Em l_{max} = 602 nm, ε = 9240 $M^{-1}cm^{-1}$, Φ = 0.133) in water. **NeuroX3** (Abs l_{max} = 493 nm, Em l_{max} = 572 nm, ε = 6385 $M^{-1}cm^{-1}$, Φ = 0.217).

Due to the low isomerization barrier of (*E*)-**1** to (*Z*)-**1**, as an isomeric form of (*E*)-**1**, four final photoproducts (**NeuroX1**-**X3** and **8**) were able to be prepared advantageously from only a single starting material during the two-step synthesis that proceeded via photocyclization/oxidation and *N*-methylation (Figure 6.1A). We applied Katz's condition,[6] which has been often used for stilbenes photocyclization, to (*E*/*Z*)-**1** which bears stilbene scaffold. With propylene oxide, as a scavenger, and a catalytic amount of iodine, the photocyclization of (*E*/*Z*)-**1** gave 2:3 ratio of **2** and **3**.[3b] To utilize the resulting photoproducts as water-soluble fluorescent probes in cells and tissues, **2** and **3** were methylated. Using dimethylsulfate, **2** provided only mono-*N*-methylated photoproduct, **NeuroX1**, and di-*N*-methylated one, **NeuroX2** in nearly 1:1 ratio. In the case of **3**, the methylation reaction gave **NeuroX3**, a mixture of two regioisomers resulting from asymmetricity of **3**, as well as dimethylated photoproduct **4**. In comparing the ratio from the former case, interestingly, **NeuroX3** is to around one of third to **4**. The resulting photoproducts were purified in gradient elution with 0.1% trifluoroacetic acid in water and acetonitrile on high-performance liquid chromatography. We have found both mono- and di-*N*-methylated products to show large Stokes shifts (80-100 nm). All absorption and emission wavelengths of the methylated photoproducts fell into the same range in the visible light spectrum with the dimethylated compound slightly more red-shifted than the corresponding monomethylated derivatives. Water solubility is also a benefit for biological applications.

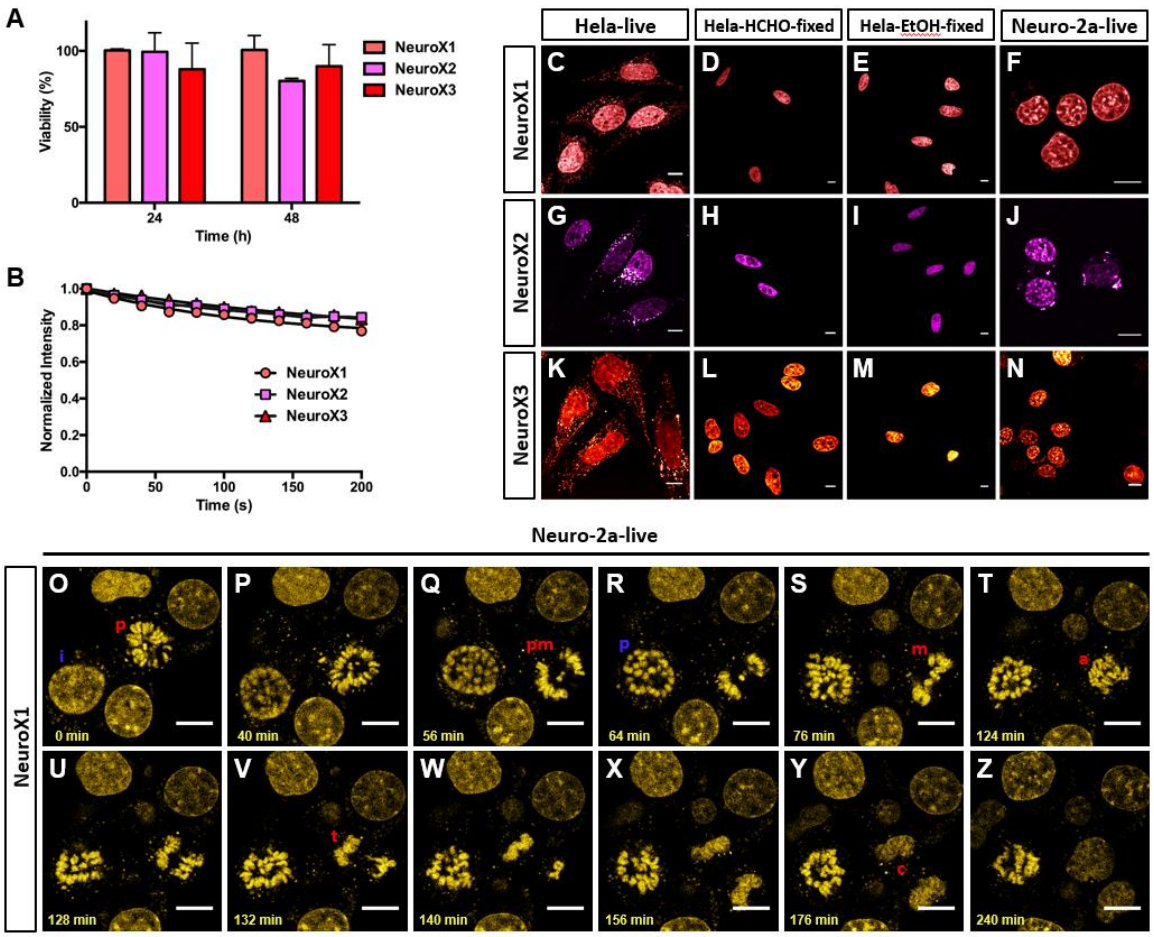

Figure 6.2. (A) Viability assays of HeLa cells incubated with **NeuroX1-X3** (5 μM) at 37 °C in a humidified atmosphere with 5% CO_2 over 24 and 48 hours. (B) A normalized plot of the average intensity of **NeuroX1-X3** over 200 seconds of continuous irradiation. (C-N) Confocal images of live HeLa cells, formaldehyde-fixed HeLa cells, ethanol-fixed HeLa cells, and live Neuro-2a cells stained with **NeuroX1-X3**. A 488/600 channel was used to observe **NeuroX1** and **NeuroX3**, while a 552/600 channel was used for **NeuroX2**, scale bar = 10 μm. (O-Z) Confocal time-lapse microscopy of division of live Neuro 2a cells stained with **NeuroX1**, scale bar = 10 μm. i, interphase; p, prophase; pm, prometaphase; m, metaphase; a, anaphase; t, telophase; c, cytokinesis.

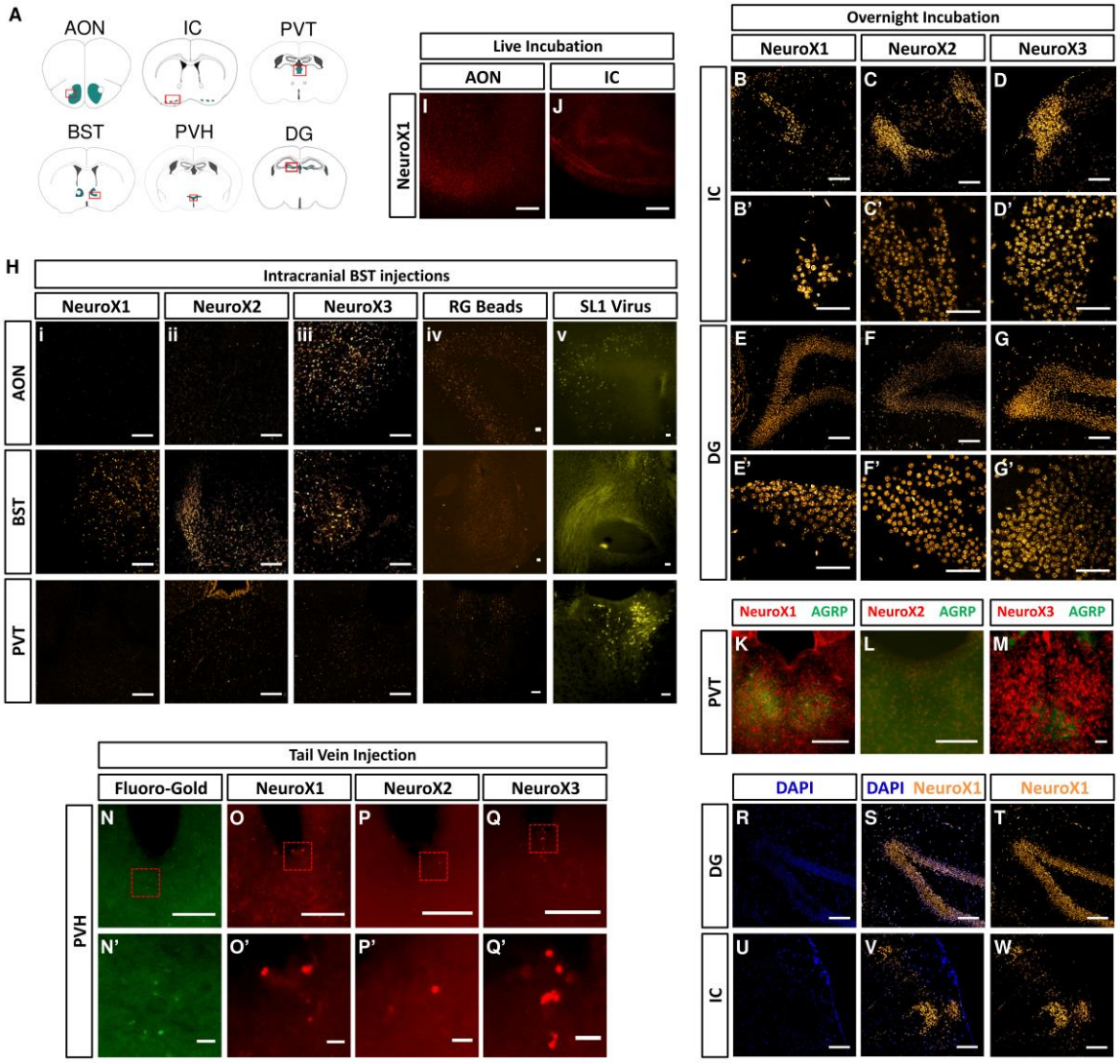

Figure 6.3. (A) Red and box indicate region imaged. (B-D) Representative confocal imaging of overnight incubation of **NeuroX1**-**X3** at 1.0 μM concentration located in the islands of Calleja (IC) imaged on confocal microscope with 20x objective, scale bar 100 μm. (B'-D') with 63x objective, scale bar 50 μm. (E-G) in dentate gyrus (DG), scale bar = 100 μm. (E'-G') with 63x objective, scale bar = 50 μm. (H) Representative confocal imaging of retrograde labeling of probes using intracranial bed nucleus stria terminalis (BST) injections, scale bar = 100 μm. (i) **NeuroX1**. (ii) **NeuroX2**. (iii) **NeuroX3**. (iv) RG Bead (v) SL1 Virus staining of neurons in

anterior olfactory nucleus (AON), BST, and paraventricular nucleus of thalamus (PVT). (I, J) Live tissue incubation of 1.0 μM of **NeuroX1** in AON in IC, scale bar = 100 μm. (K-M) Expression of agouti-related peptide (AGRP) antibody (green) and **NeuroX1-3** (red) in PVT of C57blk/6 mice, scale bar = 100 μm. **NeuroX1** had minimal degradation after incubation with fluorescent antibody in the PVT. **NeuroX2** degraded AGRP expression in the PVT. **NeuroX3** incubated after AGRP staining and had no degradation of either fluorescence. (N-Q) Tail vein injections of either fluorogold or **NeuroX1-3** to paraventricular nucleus of the hypothalamus (PVH), scale bar = 100 μm. **NeuroX1** expression in the PVH following tail vein injection of 1.5 mM concentration. Minimal expression of **NeuroX2** in the PVH using 2.0 mM. Staining of **NeuroX3** in the PVH using 2.0 mM. (N'-Q') Zoomed-in images from the red dashed box in N-Q, scale bar = 10 μm. (R-W) NeuroX1 expression with DAPI Counterstaining in DG and IC, scale bar = 100 μm.

Cell imaging experiments were performed using HeLa cells and neuro-2a cells. All methylated products were water-soluble, cell-permeable, and primarily localized in the nuclei, except for **4**, which accumulated in vesicles within the cytoplasm of HeLa cells. To assess the photostability of **NeuroX1-X3**, timelapse experiments were performed with a 488/600 channel for the monomethylated derivatives **NeuroX1** and **NeuroX3**, and a 552/600 channel for the dimethylated derivatives **NeuroX2** (Figure 6.2A). After 200 seconds of continuous irradiation, around 80% or more of the average fluorescent intensity still remained, indicating high resistance to photobleaching. Viability assay showed low cytotoxicity for most methylated derivatives with more than 80% viability after 48 hours. Compound **4** had the lowest viability,

but more than 60% of the cells still survived after 48 hours. In formaldehyde-treated and ethanol-treated HeLa cells, all methylated photoproducts became much more selective nuclear stains (Figure 6.2B). Similar localization patterns were also seen in neuro-2a cell line. Furthermore, time-lapse experiment was performed for watching division of Neuro-2a cells (Figure 6.2O-2Z). On confocal microscope, the cells were incubated for 4 hours. A cell cycle from interphase to prophase and another cell cycle from prophase to cytokinesis were observed independently with no degradation or photobleaching.

To examine the toxicity of these derivatives in tissues, we implemented strategies for incubations conducting intracranial injections (Figure 6.3H). A C57blk/6 WT mouse was used for live imaging of the derivatives to observe the toxicity against live neurons. Coronal sections with a thickness of 200 μm were incubated with a probe and imaged for staining. As a representative, **NeuroX1** was used in the incubation with live slices prior to intracranial injections. **NeuroX1** was uptaken by live neurons within the anterior olfactory nucleus and IC (Figure 6.3I and 3J). These results demonstrate the low toxicity of these probes towards live cell imaging. There were no staining differences of the probes between live and fixed cells (Figure 6.2C-2N). As a result of low toxicity in live imaging, intracranial injections of each probe was performed in C57blk/6 WT mice. The target region for injection site was the bed nucleus stria terminalis (BST) for each probe. Probes stained live neurons within the bed nucleus stria terminalis post-surgery (Figure 6.3H).

To determine the staining properties of these diazaxanthylidene derivatives, **NeuroX1-X3** (Figure 6.3B-3G'), we incubated coronal brain slices from a C57blk/6 WT mouse with a molecule overnight. A range of molarities were tested to determine the optimal concentration of

each probe. These derivatives demonstrated similar nuclear staining of neurons is several regions within fixed brain slices. **NeuroX1** resulted in nuclear staining of neurons within IC (3B and 3B') and dentate gyrus (DG) of the hippocampus (Figure 6.3E and 3E'). The staining for **NeuroX1** was used at 1 μM as determined by the intensity (See Supplemental information). Both **NeuroX2** and **NeuroX3** stained neurons within the IC (Figure 6.3C, 3C', 3D, and 3D') and DG (Figure 6.3F, 3F', 3G, and 3G'). The optimal concentration used for both these compounds was 2 μM. Expression of neuropeptide Y (NPY) neuron from transgenic mouse was not overlapped with nucleus (Red) co-stained with **NeuroX1** (Figure 6.4).

To directly examine whether these probes can be used with immunohistochemistry, fixed coronal slices were incubated with AGRP primary antibody and probes (Figure 6.3K-3M). **NeuroX1** was incubated first overnight then applied AGRP antibody. Post- incubation of antibody resulted in minimal probe degradation (Figure 6.3K). **NeuroX2** was incubated after AGRP antibody staining and resulted in antibody degradation (Figure 6.3L). **NeuroX3** was incubated after AGRP antibody staining and resulted in no degradation of the probe (Figure 6.3M).

To determine whether these probes have the potential to cross blood brain barrier, tail vein injections were performed (Figure 6.3N-3Q'). Using the tail vein protocol adapted from SWANSON (insert citation), each probe was diluted and injected into the tail vein of C57blk/6 WT mice. Fluorogold was used as a control as it was previously shown to stain neurons located in the paraventricular hypothalamus (PVH) (Figure 6.3N and 3N'). Fluorogold resulted in an absence of neuron labeling within the PVH. **NeuroX1** and **NeuroX3** demonstrated minimal

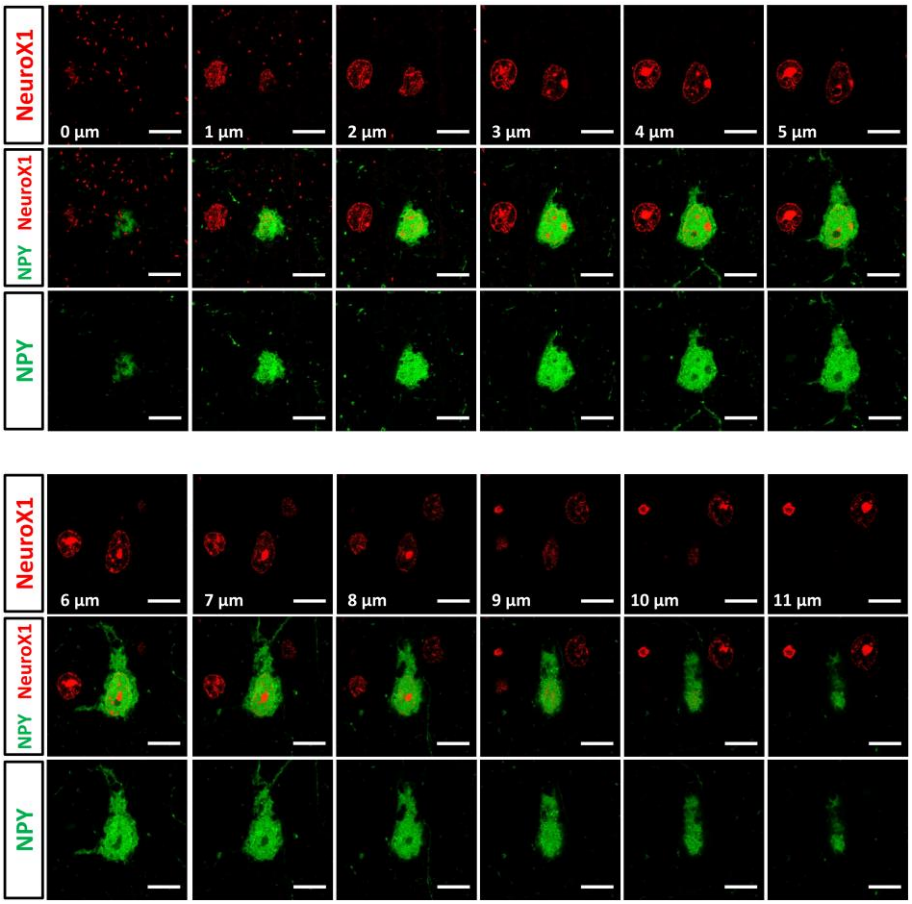

Figure 6.4. Snapshots of reconstructed NPY neuron (green) with nucleus (Red) stained with **NeuroX1** on confocal microscope with 100x objective, scale bar = 10 µm, each step 1.0 µm (total Z-stack size = 14.0 µm).

staining located in the paraventricular hypothalamus (Figure 6.3O, 3O', 3Q, and 3Q'). **NeuroX2** resulted in no staining of neurons with the PVH (Figure 6.3P and 3P').

To investigate potential retrograde labeling of these probes, intracranial injections to the BNST were performed for each probe. C57blk/6 WT mice were injected unilaterally with a probe to the BNST and recovered for two weeks. Mice were then perfused and coronal sections

were images for potential retrograde labeling. **NeuroX1** resulted in minimal retrograde labeling in the anterior olfactory nucleus (AON) (top, Figure 6.3Hi). Injection site of the BNST demonstrated local staining of neurons as a result of each probe (middle, Figure 6.3Hi). Retrograde labeling of **NeuroX1** was visible within the paraventricular thalamus (PVT) (bottom, Figure 6.3Hi). The concentration for **NeuroX1** intracranial injection was 3 μM. As a result of minimal retrograde labeling, a higher concentration of probes was prepared for injections. **NeuroX2** was injected at a concentration of 30 μM. As a result of a higher concentration, retrograde labeling in the AON and PVT was easily detectable (top and bottom, Figure 6.3ii). **NeuroX3** was injected at a concentration of 30 μM and resulted in a higher retrograde labeling in AON in comparison to **NeuroX1** and **NeuroX2** (top, Figure 6.3iii). Retrograde labeling in the PVT was less than **NeuroX2**, but more visible than **NeuroX1** (bottom, Figure 6.3iii). Comparing retrograde tracing ability, retrograde (RG) beads were injected (Figure 6.3iv).[7] The minimal expression was shown in the PVT and more visible in the BST and AON. When SL1 virus was employed for tracing, competitive expression was shown in the AON, BST, and PVT (Figure 6.3v).

6.3 Conclusions

We have generated a set of photocyclized diazaxanthylidene dyes which exist as trifluoroacetate salt form. Taken the advantage of isomerization of the starting material (*E/Z*)-**1**, we have synthesized the three fluorescent compounds **NeuroX1**-**X3** from a single compound in

two steps. We have examined the fluorescent properties of these dyes as tools for staining several types of cell populations. According to the live and fixed cell imaging experiments, all three dyes were found to be competitive probes for the nucleus. Encouraged by these results, we have extended the research into the mice brain tissue imaging. Incubation of these molecules in brain tissue slices revealed nuclear staining of neurons in both the IC and DG. The IC are small clusters of granule cells placed in the olfactory tubercle and have been associated with dopamine 1 and 3 receptors.[5] DG is a cortical region located in the hippocampus related with pattern separation and environmental representation.[4] The DG is consisted of glutamatergic and GABAergic granule cells. Both regions are associated with different functions and neuronal types, however, are selectively labeled by these fluorescent probes.

As an alternative to viral and dye labeling of neurons, these fluorescents probes can be used to stain specific neuronal populations through incubation. The unique uptaking of these derivatives allows for a clear visualization of a neuronal nucleus within different regions such as IC and DG. Low toxicity of these probes in incubation of live or fixed tissues allows for multiple implications of these novel tools. The stability of these probes demonstrated minimal to no photobleaching of the samples in cell and tissue imaging, especially overtime. Probes had little to no degradation after incubation of fluorescent antibodies. Overlaying all of these studies, **NeuroX1-X3** as new nuclear staining dyes targeting to neuronal tissues, as well as either live or fixed cells, will enable research in neurobiology and chemical biology, which requires low toxic and slow photobleaching dyes.

6.4 Experimental Section

General information

Materials and spectroscopic methods

Reagents for synthesis were purchased from Sigma Aldrich or Acros and used without further purification. Solvents were purchased from Fisher Scientific or Sigma Aldrich. Anhydrous solvents was purchased from Fisher Scientific and dried by passing through an alumina column of a solvent purification system. Silica gel (230-400 mesh) used for column chromatography was purchased from Silicycle. Thin layer chromatography plates (250 μm thickness) were purchased from Sorbent Technologies or Merck. Revered-phase column chromatography was done using a RediSep Rf Gold C18 column on a Teledyne Isco CombiFlash Rf system. High-performance liquid chromatography (HPLC) was performed on a Jasco HPLC system using a Phenomenex column (Luna 5u C18(2) 100A; 250 x 4.60 mm, 5 micron). UV absorption spectra were obtained on a Jasco V-650 spectrophotometer using a 1 cm path length quartz cuvette. Fluorescence emission spectra were taken on a Horiba Jobin-Yvon FluoroLog using a 1 cm path length fluorescence quartz cuvette. ^{1}H NMR and ^{13}C NMR were recorded on either a Bruker DMX 500 (500 MHz) or a Bruker AVII 500 (500 MHz). High-resolution mass spectrometry was performed by Dr. Rakesh Kohli at the University of Pennsylvania using a Waters LCT Premier XE Mass Spectrometer (model KE 332). X-Ray chromatography was performed by Dr. Pattrick Carroll at the University of Pennsylvania using a Bruker APEX2-DUO CCD X-Ray Diffractometer. Photoreactions were carried out in a Rayonet

Photochemical Reactor (model RPR-100). Quantum yield was determined by serial dilution method using fluorescein (in NaOH 0.1 M, $\Phi = 0.95$) as reference.[8]

Cell imaging

For live cell imaging, HeLa cells and neuro-2a cells (purchased from ATCC) were used. Cells were cultured in a 60 mm culture dish or a 75 cm^2 culture flask using Life Technologies Dulbecco's Modified Eagle Medium (DMEM) media with phenol red, 10% Fetal Bovine Serum and 1% penicillin-streptomycin at 37 °C in a humidified atmosphere with 5% CO_2. The cells were detached with 0.05% trypsin-EDTA and transferred to a 35 mm glass bottom poly-D-lysine coated dish 2 days before imaging with about 2 mL of the above-mentioned media. One microliter of a 5 mM solution of **NeuroX1-X3**, or **4** in MiliQ water was mixed with 2 mL new media and added to the cells after the old media was removed. After incubation (3 hours to overnight for **NeuroX1-X3**, and **4**), the excess dyes were washed twice with non-phenol red DMEM before imaging. The cells were kept in 1 mL non-phenol red DMEM during imaging. A Leica DM4000 spinning disk confocal microscope equipped with a 100x/1.4 NA oil immersion objective was used in Figure 6.2C-2N. A Leica TCS SP8 confocal microscope equipped with a 63x/1.4 NA oil immersion objective lens was used in Figure 6.2O-2Z. All image processing was done using Fiji.

Formaldehyde fixation

After achieving the desired cell confluency (70-90%), media was removed and the cells were washed once with prewarmed PBS buffer and once with a prewarmed 4% formaldehyde solution. The cells were kept in 4% formaldehyde at room temperature for 20 minutes before the formaldehyde solution was removed and the dish was washed twice with PBS buffer. The sample can be kept in PBS buffer at 2-8 °C until needed.

Ethanol fixation

After achieving the desired cell confluency, media was removed and the cells were washed with PBS buffer, cold ethanol (- 20 °C), then kept in ethanol at - 20 °C. After 10 minutes, ethanol was removed and the dish was washed twice with PBS buffer and stored in PBS buffer at 2-8 °C until needed.

Cytotoxicity studies

In a 96-well plate, HeLa cells were plated at 5,000 cells/well in culture media mentioned above (50 µL/well) and incubated at 37 °C in a humidified atmosphere with 5% CO_2. After 24 hours, cells were treated with **NeuroX1-X3** and **4** (final concentration 5 µM), and MitoTracker Red FM[24] (final concentration 1 µM), and DMSO (vehicle control for MitoTracker). For wells treated with MitoTracker and DMSO, DMSO concentration was kept at 1%. Untreated cells were used as vehicle control for **NeuroX1-X3** and **4**. Final volumes were 100 µL/well. Cells were

incubated at 37 °C in 5% CO_2 for 24 or 48 hours. Alamar Blue (10 μL) was added 2 hours prior to fluorescence measurement. Fluorescence was measured at 560 nm excitation and 590 nm emission. Vehicle control was taken as 100% cell viability.

Intracranial injections of derivatives

Mice were anesthetized with 2% isoflurane and were placed into a stereotaxic apparatus (Stoelting Instruments). The skull was exposed through a small incision and a small hole was drilled for injection. Mice were injected with a probe unilaterally at the targeted brain region. A pulled glass pipette with 40–60-μm tip diameter was inserted into the brain and a unilateral injection (150 nl) of the probe was performed at coordinates around the BNST (bregma, +1.0 mm; midline, -0.83 mm; dorsal surface, –4.25 mm). A micromanipulator was used to control the injection speed (10 nl min^{-1}) and the pipette was withdrawn 2 minutes after injection of a probe. The incision was closed using sutures (Ethicon) and mice were returned to their home cage for a recovery period of two weeks.

Live Tissue Imaging

Mice were deeply anesthetized and killed by decapitation. Brains were dissected and immediately sectioned at 200μm using vibratome (Campden Instruments) submerged in a 95 % O_2 / 5% CO_2 bubbled ACSF bath. Coronal slices were incubated for 2 hours with a probe diluted in bubbled ACSF. Slices were mounted on glass slides using VECTASHIELD mounting

medium with DAPI, and cover-slipped for imaging. Tissue images were obtained using stereomicroscope (Leica).

Immunohistochemistry

Mice were deeply anesthetized and then killed by perfusion with phosphate buffered saline (PBS) followed by 4% paraformaldehyde in PBS. Brains were dissected and fixed overnight in 4% paraformaldehyde and transferred to PBS. Brain slices (100 μm) were cut by vibratome sectioning (Leica) and incubated overnight with a probe. Slices were mounted on glass slides using VECTASHIELD mounting medium with DAPI, and coverslipped for imaging. Tissue images were obtained using either a stereomicroscope (Leica) or deconvolution microscope (Leica). Neuronal images were collected using a confocal microscope (Leica).

Statistical Analysis

Values are reported as means and linear fitting was conducted using excel and SigmaPlot. Correlations and R values were obtained using SigmaPlot software.

Experimental procedures

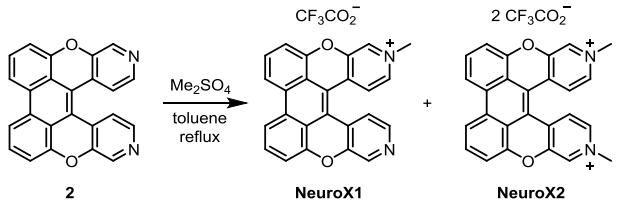

In a round bottom flask, **2**[3b] (6.6 mg, 0.018 mmol) was dissolved in toluene (7 mL). Dimethyl sulfate 1% v/v in toluene (0.55 mL, 0.058 mmol) was added and the reaction mixture was refluxed under argon. After 18 hours, the reaction mixture was allowed to cool down to room temperature. The reaction mixture was filtered. The red residue was washed with toluene and diethyl ether before being re-dissolved in methanol and dry-loaded to a reversed phase automated column using 0.1% TFA water and acetonitrile as eluents to obtain **NeuroX1**[3d] (2.8 mg, 0.0057 mmol, 31%), and **NeuroX2** (4.1 mg, 0.0067 mmol, 36%), both as orange-red solides. The starting material **2** was also recovered after column chromatography (1.4 mg, 0.0038 mmol, 21%).

For **NeuroX1**: Characterization data of **NeuroX1** have been published in our previous publication.[3d]

For **NeuroX2**: ^{1}H NMR (500 MHz, D_2O): δ (ppm) 8.89 (d, 2H, J = 1.4 Hz), 8.32 (dd, 2H, J = 6.6, 1.5 Hz), 8.23 (d, 2H, J = 6.6 Hz), 7.87 (d, 2H, J = 8.2 Hz), 7.75 (t, 2H, J = 8.1 Hz), 7.27 (d, 2H, J = 7.9 Hz), 4.40 (s, 3H). ^{13}C NMR (125 MHz, D_2O): δ (ppm) 151.6, 148.8, 139.3, 136.7, 134.9, 130.9, 129.9, 123.7, 119.5, 118.7, 118.3, 114.0, 48.2. IR (neat): 2924, 1682, 1207, 1133, 801, 723 cm^{-1}. HRMS (m/z): $[M/2]^+$ calcd for $C_{13}H_9NO^+$, 195.0679; found, 195.0687.

Meting point 200-203 °C. Extinction coefficient ε = 9240 $M^{-1}.cm^{-1}$ (solvent: water). Quantum yield Φ = 0.133 (solvent: water, standard: fluorescein in NaOH 0.1 M).

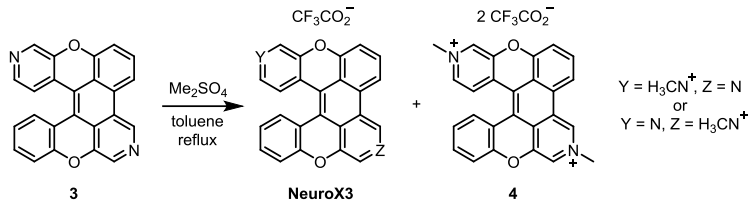

In a round-bottom flask, compound **3**[3b] (8.2 mg, 0.023 mmol) was dissolved in toluene (8 mL) and a 1% (v/v) solution of dimethyl sulfate in toluene (0.6 mL, 0.068 mmol) was added. The reaction mixture was heat under reflux under argon for 20 hours before allowed to cool down to room temperature. Solvent was removed and the residue was washed with 15 mL diethyl ether and dried under vacuum. The residue was dissolved in methanol and dry-loaded in celite to a C18 column for a reverse phase chromatography using acetonitrile and 0.1% TFA water as eluents. A mixture of **NeuroX3** (3.2 mg, 0.006 mmol, 26%) and pure **4** (10.4 mg, 0.016 mmol, 70%) were obtained as orange-red solid.

For **NeuroX3**: ^{1}H NMR (500 MHz, D_2O): δ (ppm) 9.53 (s, 1H Major), 9.34 (s, 1H Minor), 8.81 (s, 1H Minor), 8.72 (s, 1H Major), 8.67 (s, 1H Major), 8.54 (s, 1H Minor), 8.33 (d, 1H Major, J = 6.3 Hz), 8.26 (d, 1H Minor, J = 6.6 Hz), 8.24-8.20 (m, 1H Major and 1H Minor), 8.18 (d, 1H Major, J = 8.2 Hz), 8.14 (d, 1H Minor, J = 8.3 Hz), 7.85-7.77 (m, 1H Major and 1H Minor), 7.69-7.64 (m, 1H Major and 1H Minor), 7.58 (d, 1H Major, J = 7.9 Hz), 7.55 (d, 1H Minor, J = 8.1 Hz), 7.53-7.48 (m, 2H Major and 1H Minor), 7.45 (d, 1H Minor, J = 8.3 Hz), 7.19-7.13 (m, 1H Major and 1H Minor), 4.57 (s, 3H Major), 4.36 (s, 3H Minor). HRMS (m/z): $[M]^+$ calcd for $C_{25}H_{15}N_2O_2^+$, 375.1128; found, 375.1127. Extinction coefficient ε = 6385

$M^{-1}.cm^{-1}$ (solvent: water). Quantum yield Φ = 0.217 (solvent: water, standard: fluorescein in NaOH 0.1 M).

For **4**: ^1H NMR (500 MHz, D_2O): δ (ppm) 9.64 (s, 1H), 8.78 (s, 1H), 8.68 (s, 1H), 8.29 (dd, 1H, J = 6.7, 2.1 Hz), 8.21 (d, 1H, J = 6.7 Hz), 8.12 (d, 1H, J = 8.1 Hz), 7.79 (td, 1H, J = 7.9, 2.1 Hz), 7.70 (t, 1H, J = 7.9 Hz), 7.56-7.50 (m, 2H), 7.46 (dd, 1H, J = 8.0, 2.1 Hz), 7.17 (t, 1H, J = 7.7 Hz), 4.55 (s, 3H), 4.32 (s, 3H). IR (neat): 2925, 1682, 1204, 1127, 801, 722 cm^{-1}. HRMS (m/z): $[M/2]^+$ calcd for $C_{16}H_9NO^+$, 195.0679; found, 195.0683. Meting point 194-197 °C. Extinction coefficient ε = 13326 $M^{-1}.cm^{-1}$ (solvent: water). Quantum yield Φ = 0.343 (solvent: water, standard: fluorescein in NaOH 0.1 M).

6.5 Acknowledgments

This work was supported by funding from the University of Pennsylvania. We thank the support of the Vietnam Education Foundation for funding (VEF Fellowship to Mai N. Tran) and the NSF and NIH including HRMS (NIH RR-023444). We wish to thank Dr. Patrick Carroll for X-ray crystallographic assistance.

6.6 References

(1) (a) Bullen, A. *Nat. Rev. Drug. Discov.* **2008,** *7,* 54-67. (b) Ji, N. *Nat. Methods.* **2017,** *14,* 374-380. (c) Lichtman, J. W.; Conchello, J. A. *Nat. Methods.* **2005,** *2,* 910-919. (d) Sauer, M.; H

eilemann, M. *Chem. Rev.* **2017,** *117*, 7478-7509. (e) Shechtman, Y.; Weiss, L. E.; Backer, A. S.; Lee, M. Y.; Moerner, W. E. *Nat. Photonics.* **2016,** *10*, 590-594. (f) Yang, Z.; Sharma, A.; Qi, J.; P eng, X.; Lee, D. Y.; Hu, R.; Lin, D.; Qu, J.; Kim, J. S. *Chem. Soc. Rev.* **2016,** *45*, 4651-4667.

(2) (a) Kim, E.; Lee, Y.; Lee, S.; Park, S. B. *Acc. Chem. Res.* **2015,** *48*, 538-547. (b) de Moli ner, F.; Kielland, N.; Lavilla, R.; Vendrell, M. *Angew. Chem. Int. Ed.* **2017,** *56*, 3758-3769. (c) L ukinavicius, G.; Johnsson, K. *Nat. Chem.* **2014,** *6*, 663-664. (d) Zheng, Q.; Lavis, L. D. *Curr. Opi n. Chem. Biol.* **2017,** *39*, 32-38.

(3) (a) Rarig, R. A.; Tran, M. N.; Chenoweth, D. M. *J. Am. Chem. Soc.* **2013,** *135*, 9213-921 9. (b) Suh, S.-E.; Tran, M. N.; Chenoweth, D. M. *Manuscript in Preparation* **2017**. (c) Tran, M. N.; Chenoweth, D. M. *Angew. Chem. Int. Ed.* **2015,** *54*, 6442-6446. (d) Tran, M. N.; Rarig, R. F. ; Chenoweth, D. M. *Chem. Sci.* **2015,** *6*, 4508-4512.

(4) Ito, R.; Lee, A. C. *Behavioural brain research* **2016,** *313*, 345-357.

(5) de Vente, J.; Hani, L.; Steinbusch, H. E.; Steinbusch, H. W. M. *Neuroreport* **2001,** *12*, 56 5-568.

(6) Liu, L.; Yang, B.; Katz, T. J.; Poindexter, M. K. *J. Org. Chem.* **1991,** *56*, 3769-3775.

(7) KATZ, L. C.; BURKHALTER, A.; DREYER, W. J. *Nature* **1984,** *310*, 498-500.

(8) Brouwer, A. M. *Pure Appl. Chem.* **2011***, 12,* 2213-2228.

Appendix 5
NMR Spectra, Cell Images, and HPLC Diagrams Relevant to Chapter 6

This work was performed in collaboration with Dr. J. Nicholas Betley and Elen Hernandez in the Betley group and Dr. Mai N. Tran, a previous graduate student in the Chenoweth group at the University of Pennsylvania.

Figure A5.1. ^{1}H NMR spectrum of **NeuroX2** in D_2O.

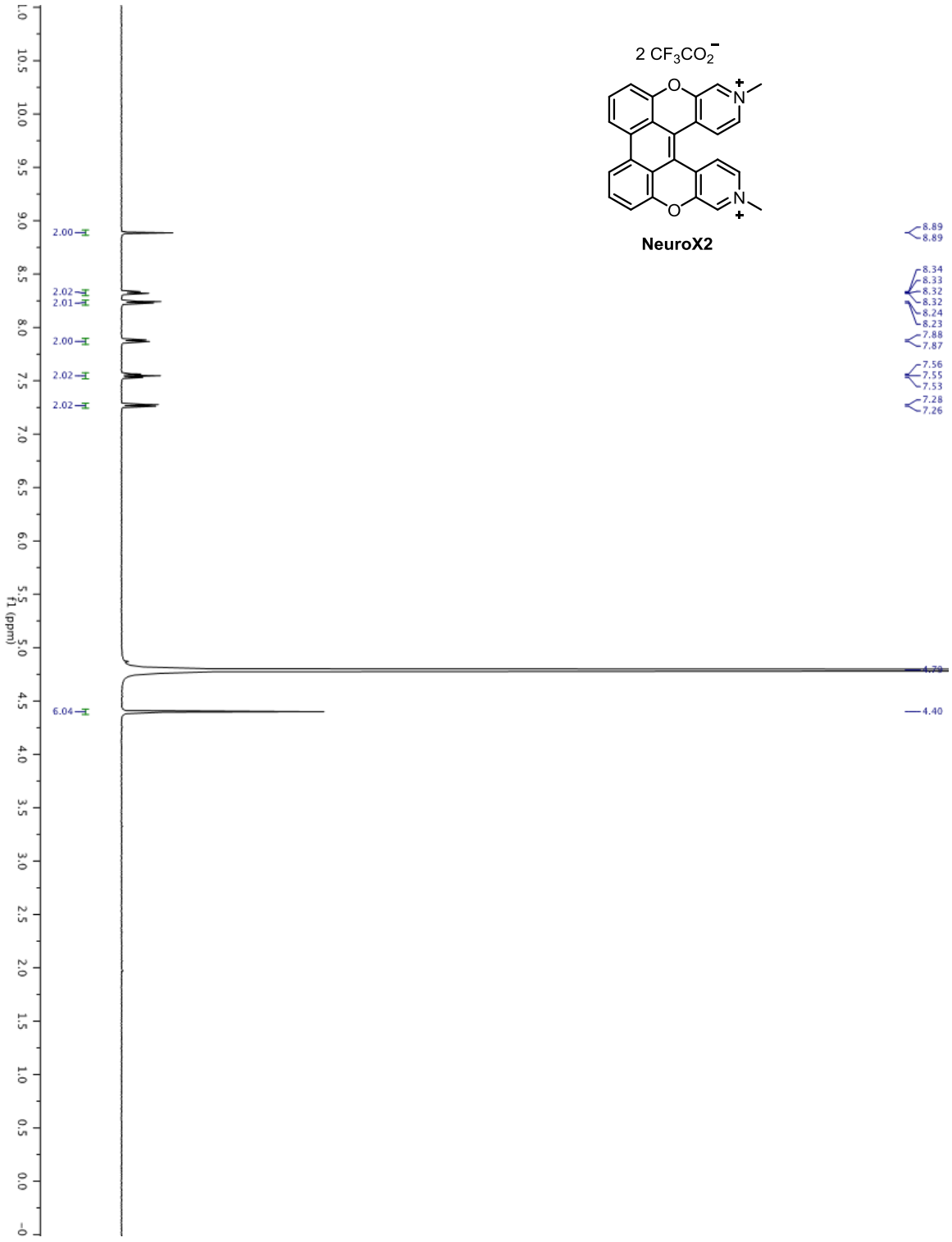

Figure A5.2. ^{13}C NMR spectrum of **NeuroX2** in D_2O.

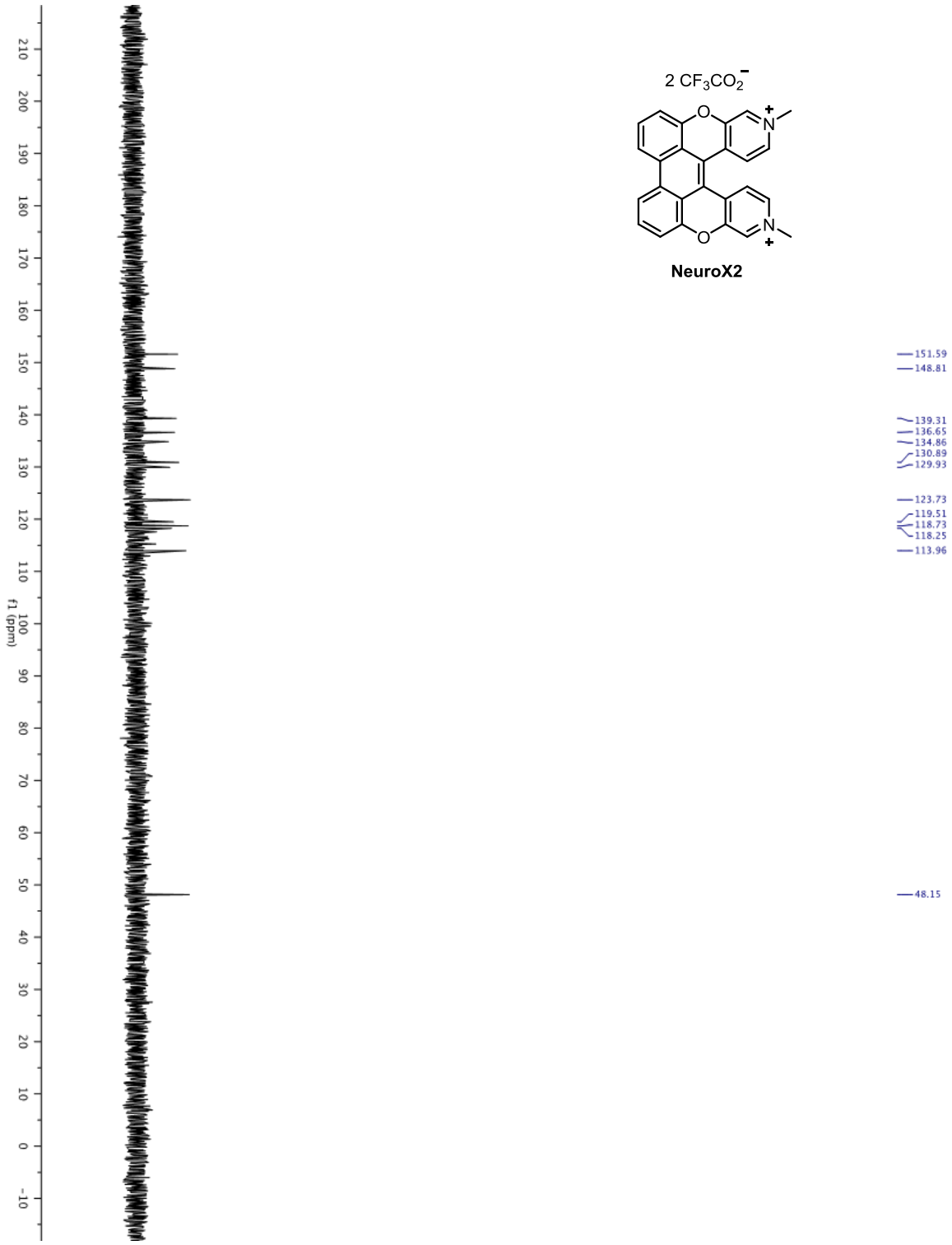

Figure A5.3. ^{1}H NMR spectrum of **NeuroX3** in D_2O.

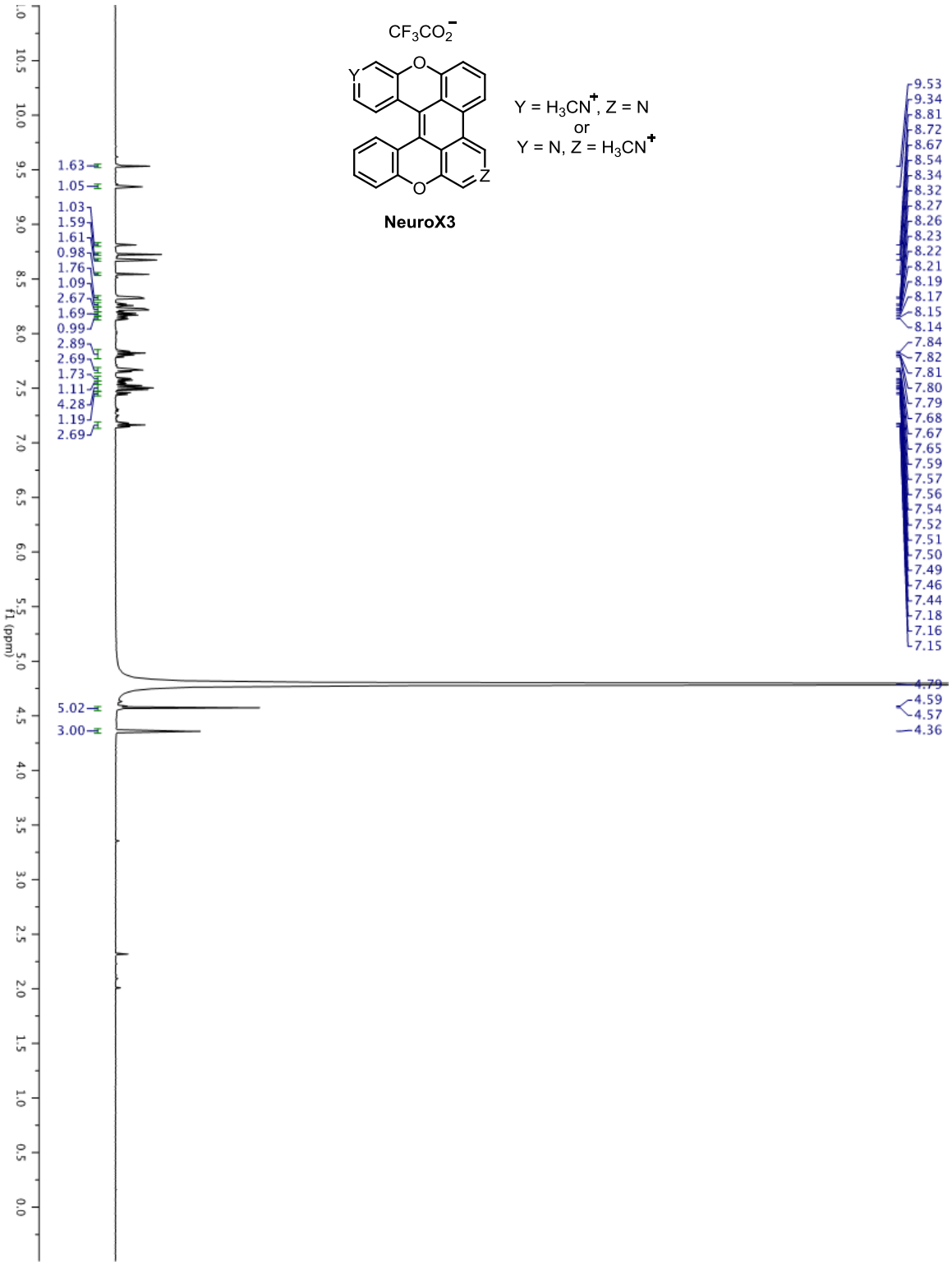

Figure A5.4. Expanded ^{1}H NMR spectrum of **NeuroX3** in D_2O.

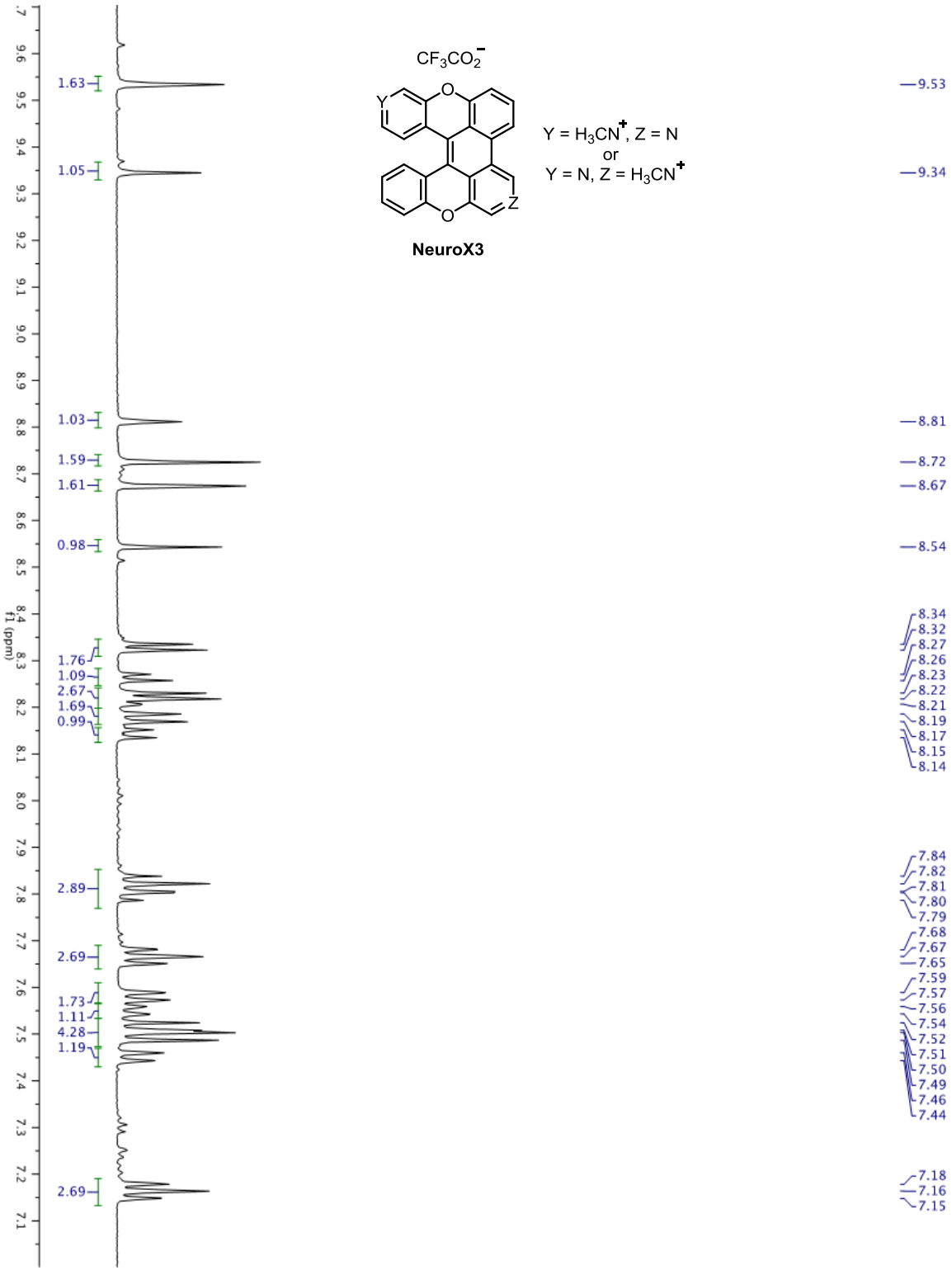

Figure A5.5. Expanded ^{1}H NMR spectrum of **NeuroX3** in D_2O.

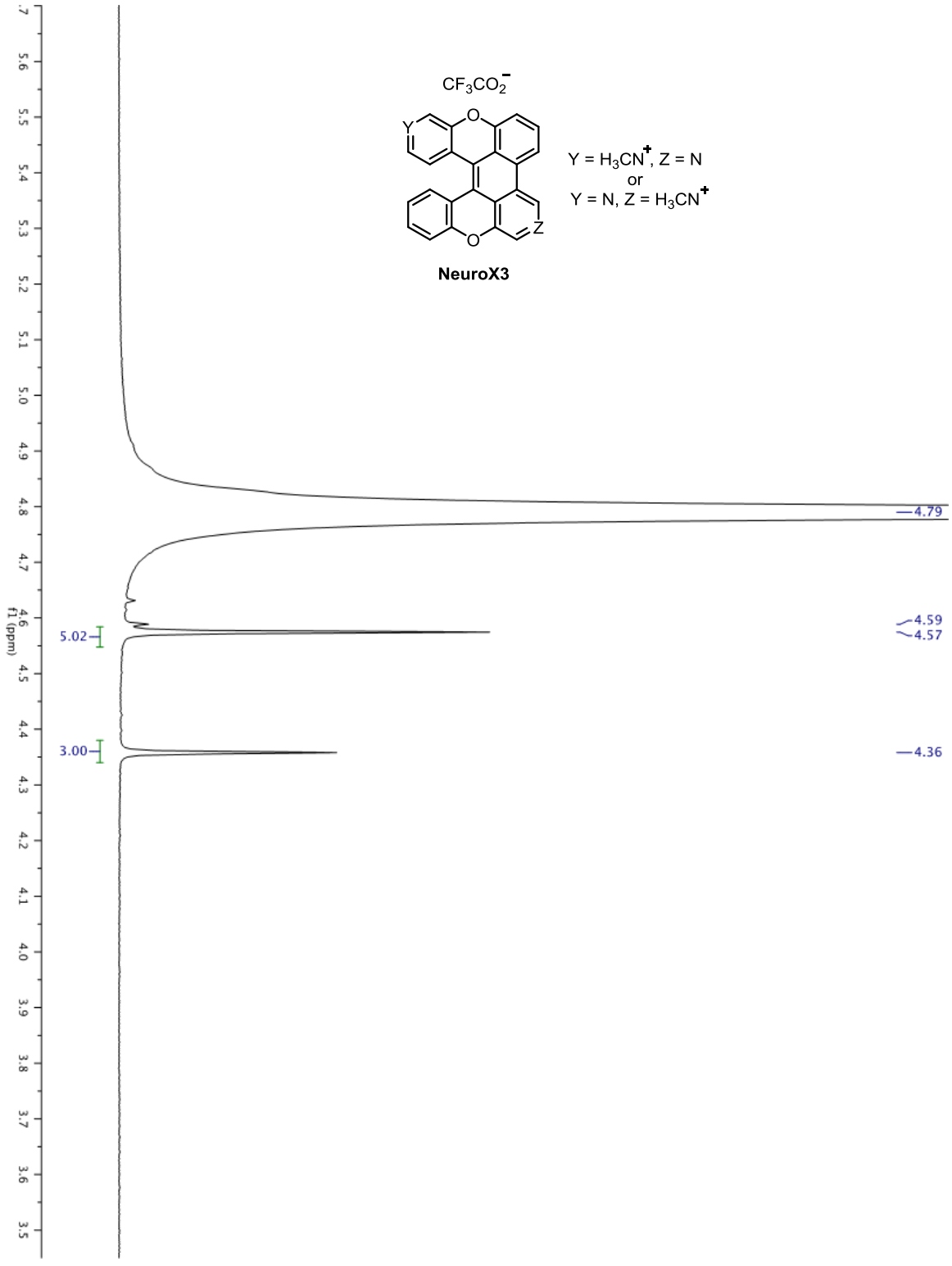

Figure A5.6. ^{1}H NMR spectrum of **4** in D_2O.

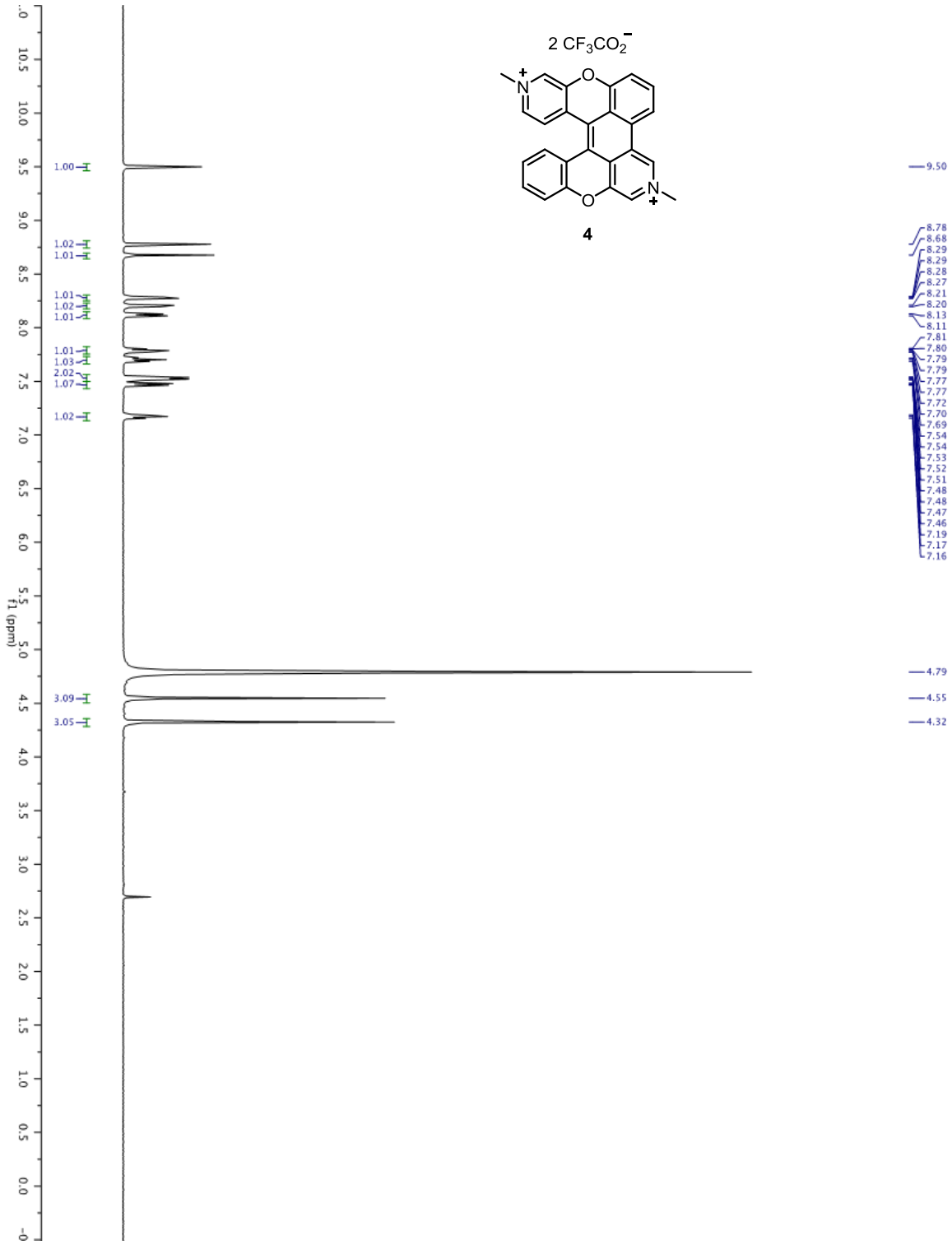

Figure A5.7. ^{13}C NMR spectrum of **4** in D_2O.

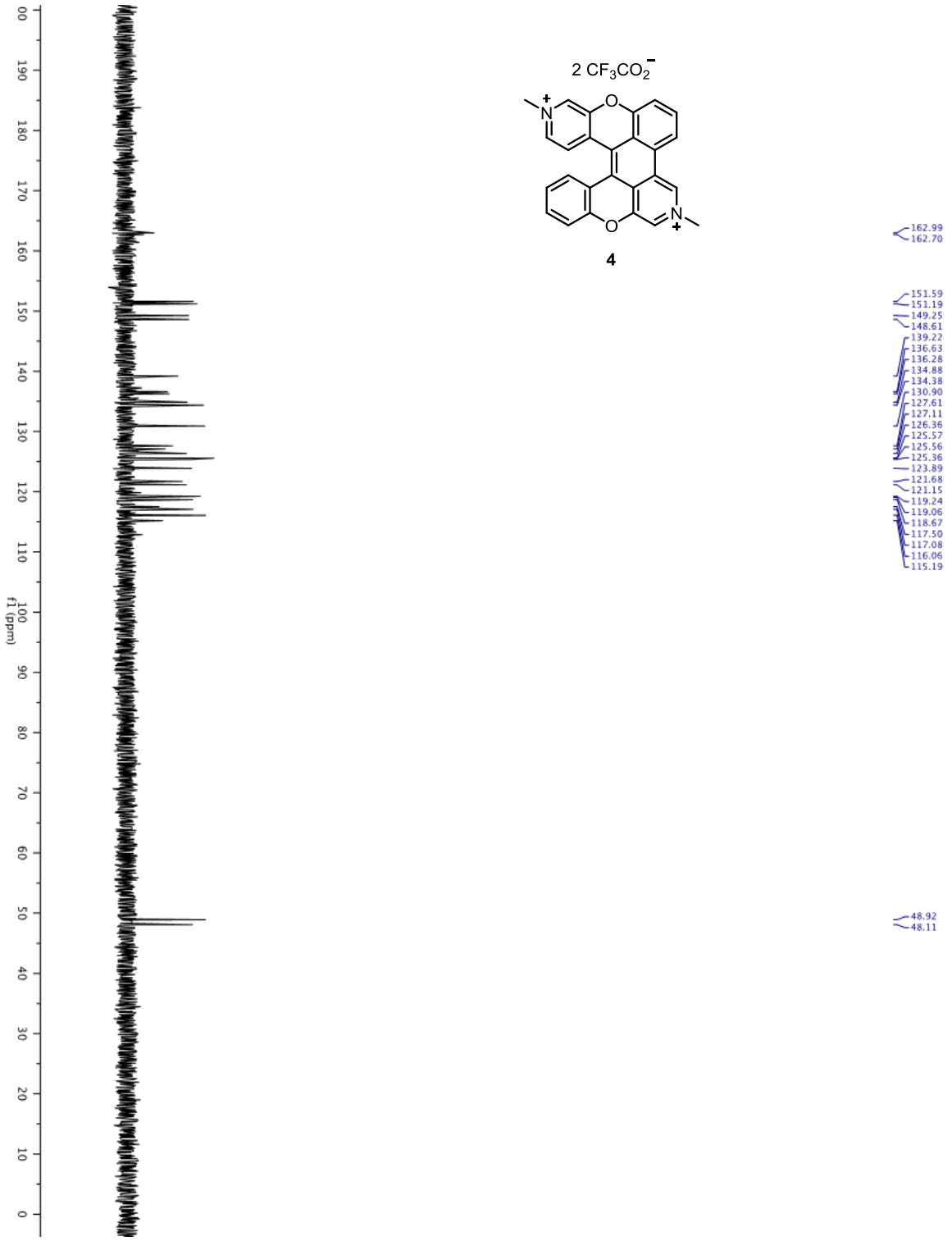

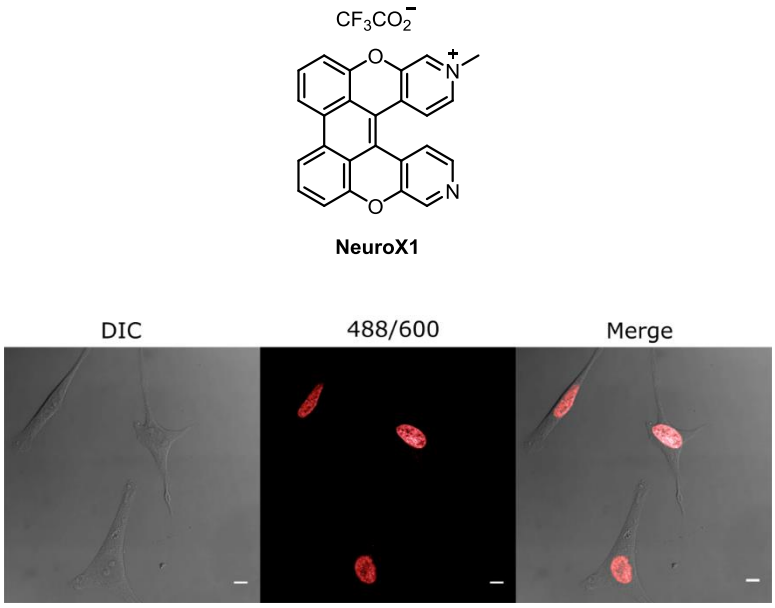

Figure A5.8. Confocal microscopy images of paraformaldehyde-fixed HeLa cells incubated with **NeuroX1**. The fluorescence image was observed using the 488/600 channel. Scale bar = 10 μm.

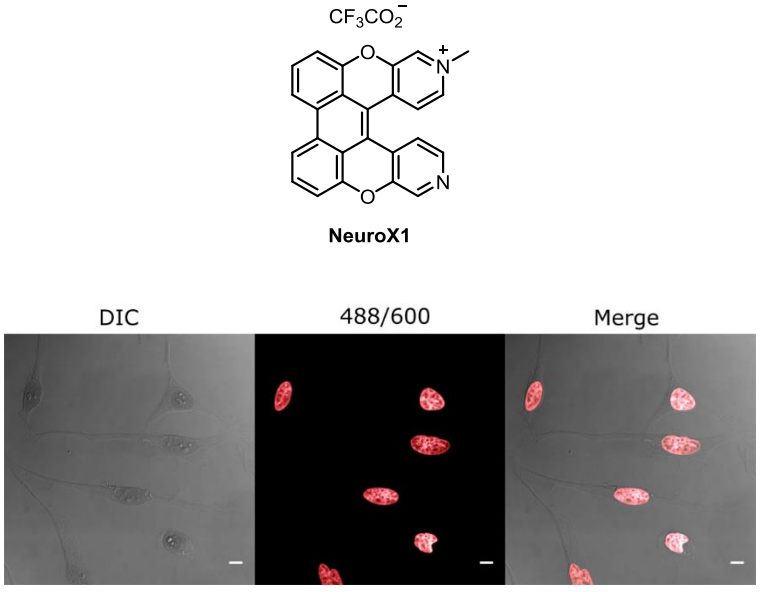

Figure A5.9. Confocal microscopy images of EtOH-fixed HeLa cells incubated with **NeuroX1**. The fluorescence image was observed using the 488/600 channel. Scale bar = 10 μm.

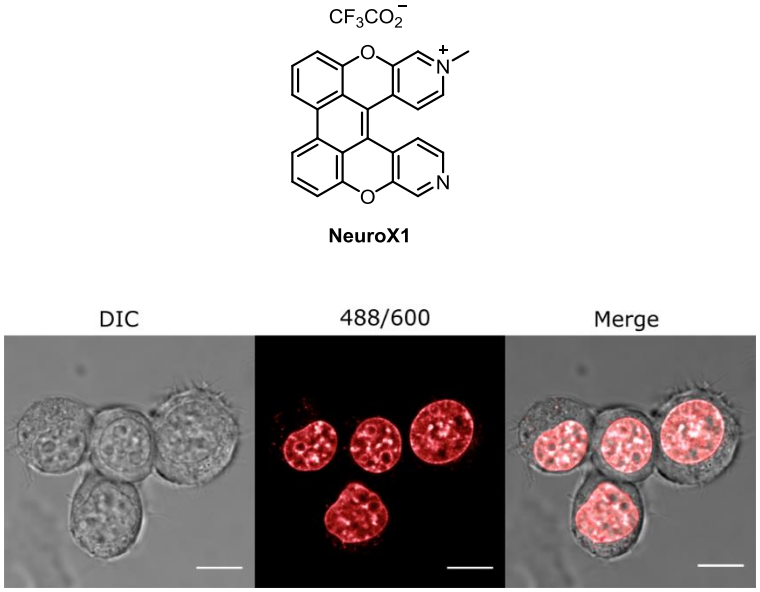

Figure A5.10. Confocal microscopy images of live neuro-2a cells incubated with **NeuroX1**. The fluorescence image was observed using the 488/600 channel. Scale bar = 10 μm.

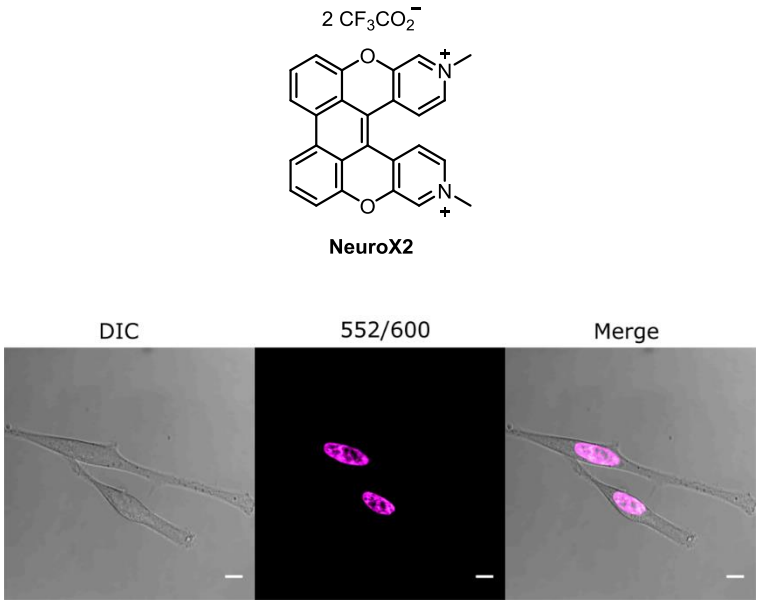

Figure A5.11. Confocal microscopy images of paraformaldehyde-fixed HeLa cells incubated with **NeuroX2**. The fluorescence image was observed using the 552/600 channel. Scale bar = 10 μm.

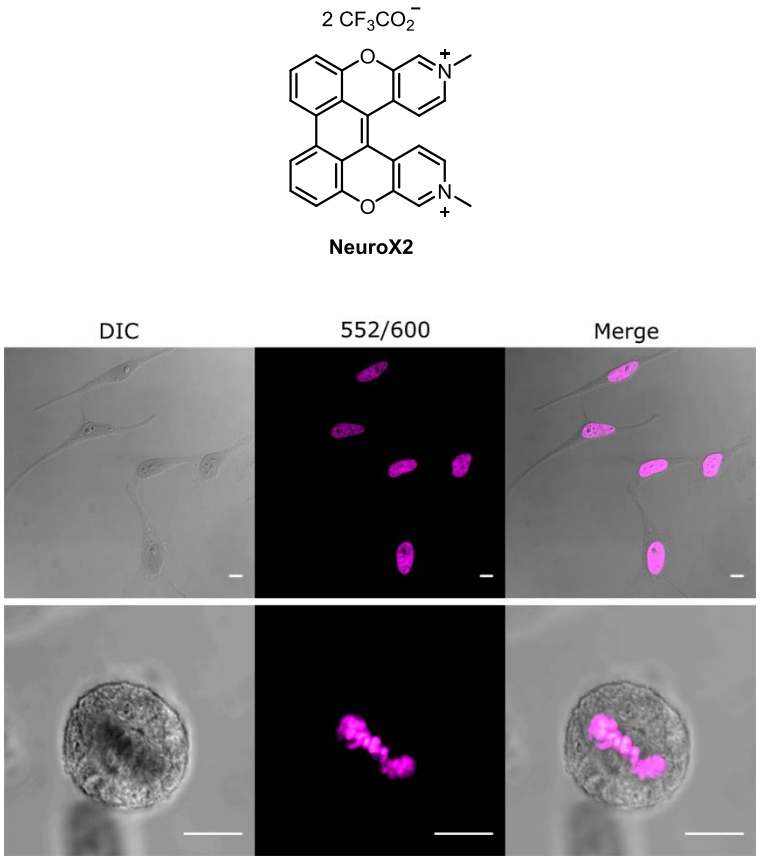

Figure A5.12. Confocal microscopy images of EtOH-fixed HeLa cells incubated with **NeuroX2**.

The fluorescence image was observed using the 552/600 channel. Scale bar = 10 μm.

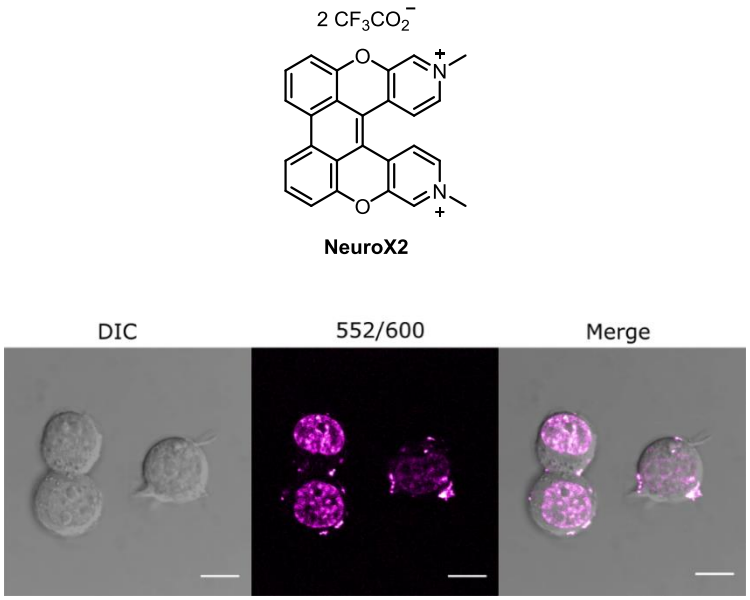

Figure A5.13. Confocal microscopy images of live neuro-2a cells incubated with **NeuroX2**. The fluorescence image was observed using the 552/600 channel. Scale bar = 10 μm.

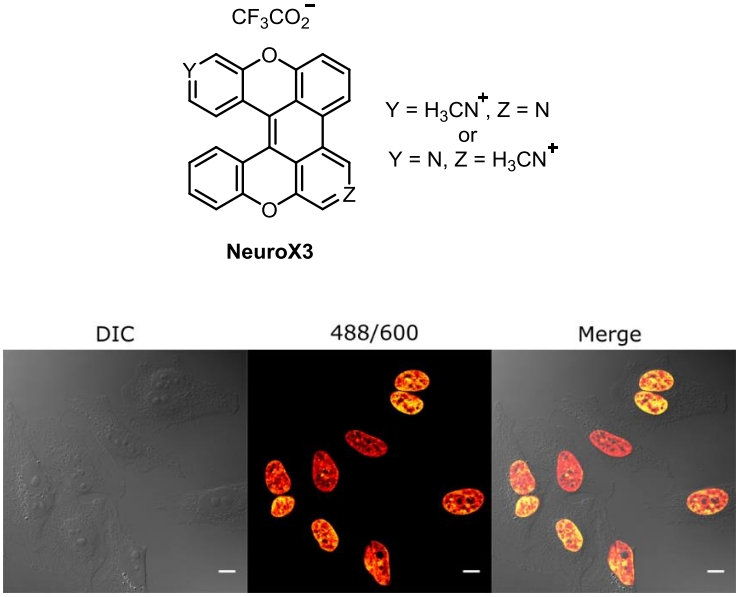

Figure A5.14. Confocal microscopy images of paraformaldehyde-fixed HeLa cells incubated with **NeuroX3**. The fluorescence image was observed using the 488/600 channel. Scale bar = 10 μm.

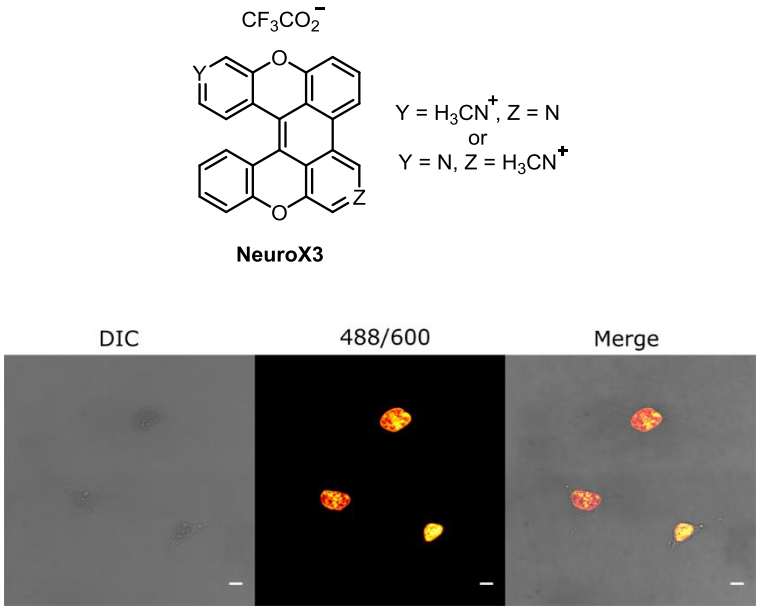

Figure A5.15. Confocal microscopy images of EtOH-fixed HeLa cells incubated with **NeuroX3**. The fluorescence image was observed using the 488/600 channel. Scale bar = 10 μm.

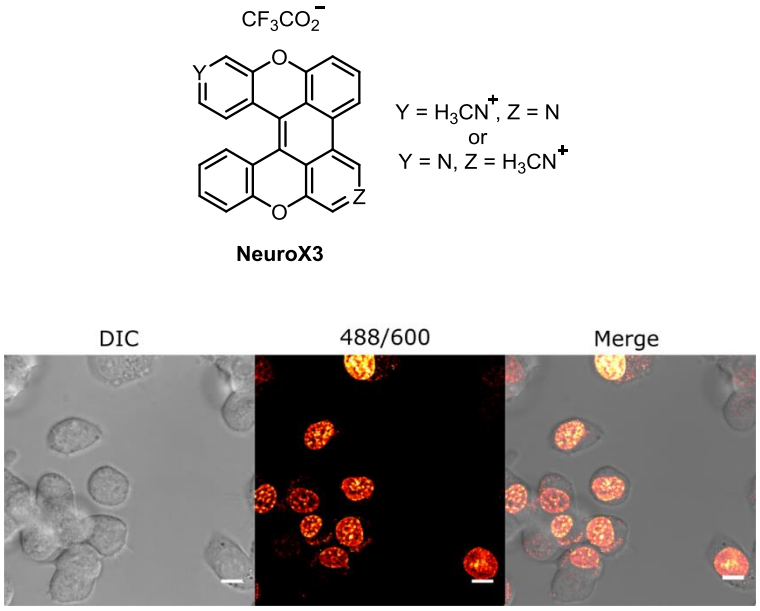

Figure A5.16. Confocal microscopy images of live neuro-2a cells incubated with **NeuroX3**. The fluorescence image was observed using the 488/600 channel. Scale bar = 10 μm.

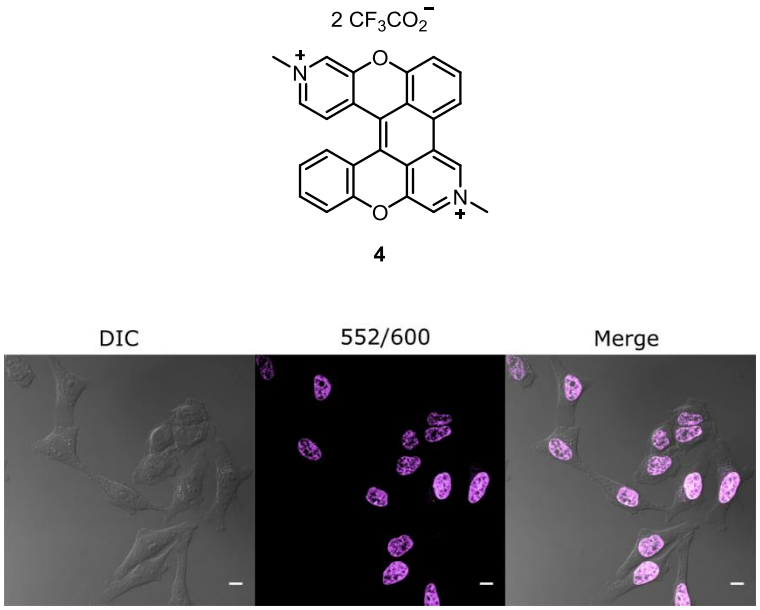

Figure A5.17. Confocal microscopy images of paraformaldehyde-fixed HeLa cells incubated with **4**. The fluorescence image was observed using the 552/600 channel. Scale bar = 10 μm.

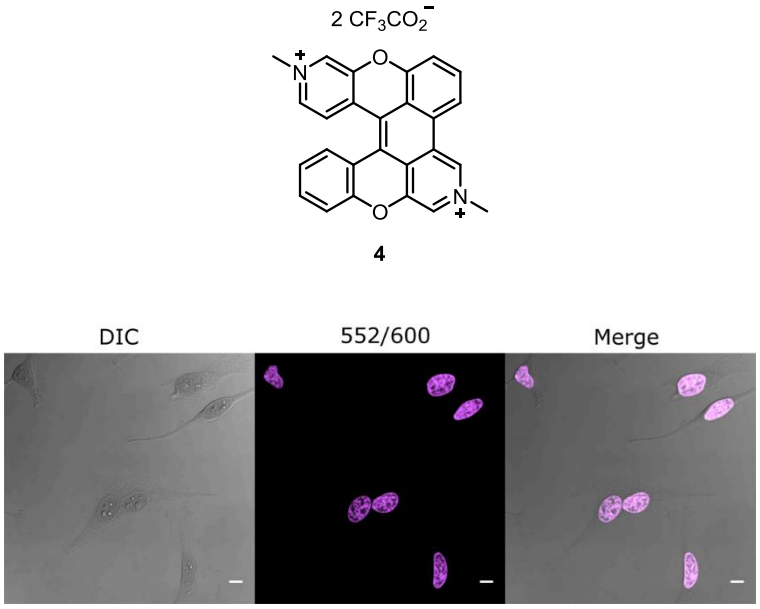

Figure A5.18. Confocal microscopy images of EtOH-fixed HeLa cells incubated with **4**. The fluorescence image was observed using the 552/600 channel. Scale bar = 10 μm.

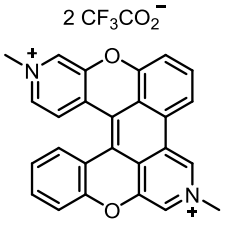

4

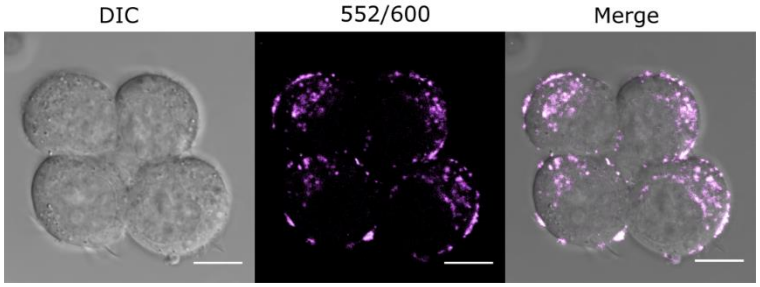

Figure A5.19. Confocal microscopy images of live neuro-2a cells incubated with **4**. The fluorescence image was observed using the 552/600 channel. Scale bar = 10 μm.

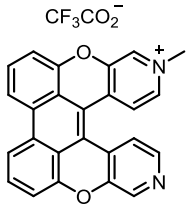

NeuroX1

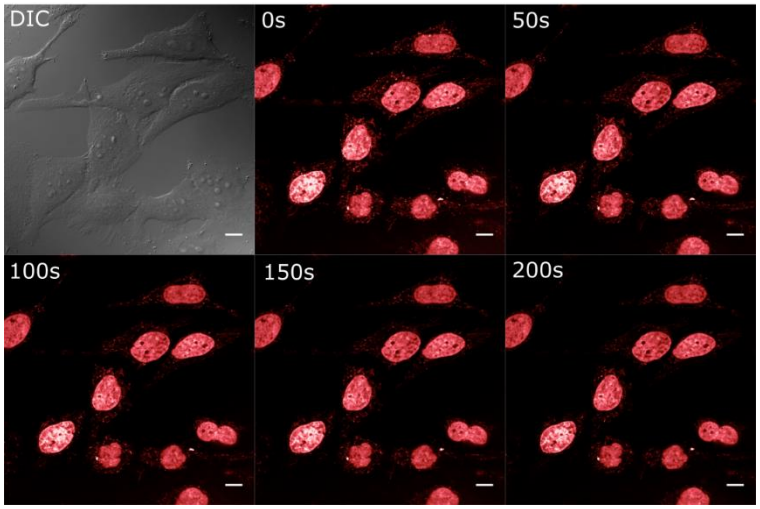

Figure A5.20. Timelapse experiment of HeLa cells incubated with **NeuroX1**. Continuous irradiation was perform using the 488/600 channel for 200 seconds. Scale bar = 10 μm.

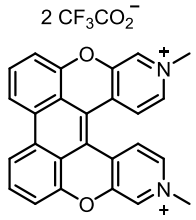

NeuroX2

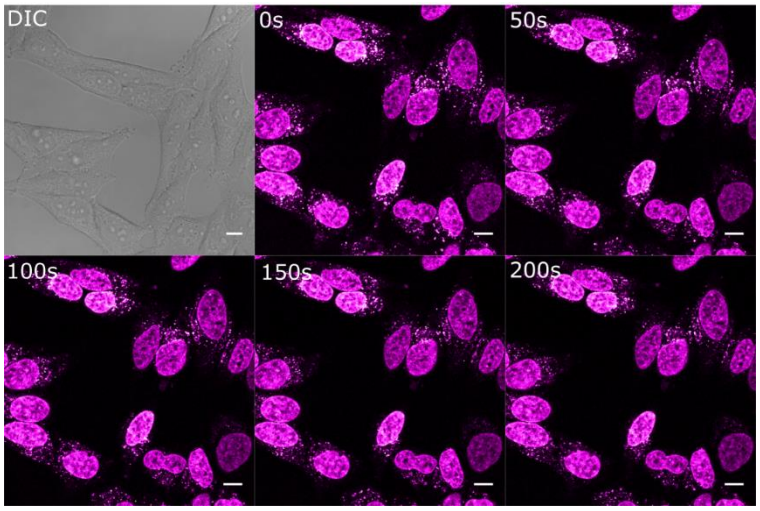

Figure A5.21. Timelapse experiment of HeLa cells incubated with **NeuroX2**. Continuous irradiation was perform using the 552/600 channel for 200 seconds. Scale bar = 10 μm.

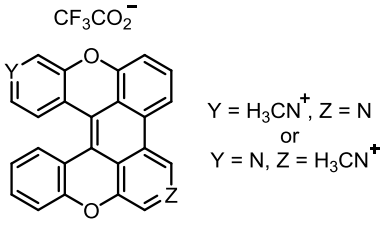

NeuroX3

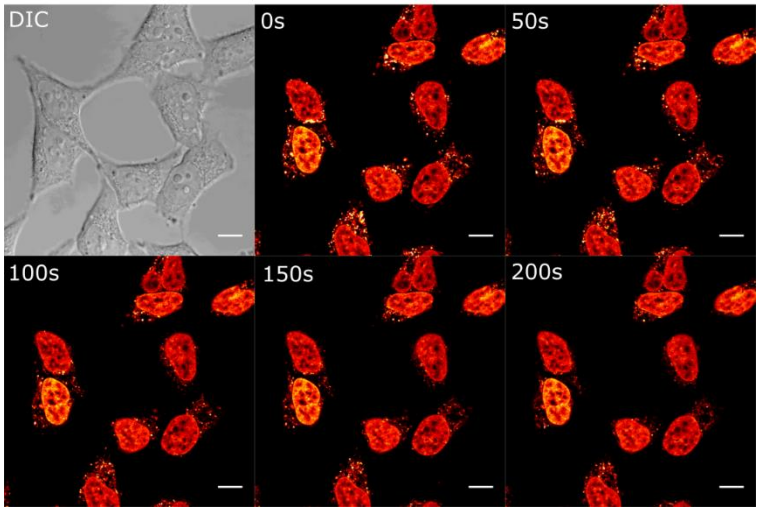

Figure A5.22. Timelapse experiment of HeLa cells incubated with **NeuroX3**. Continuous irradiation was perform using the 488/600 channel for 200 seconds. Scale bar = 10 μm.

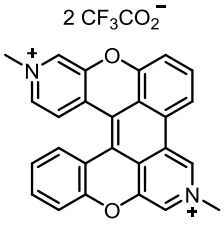

4

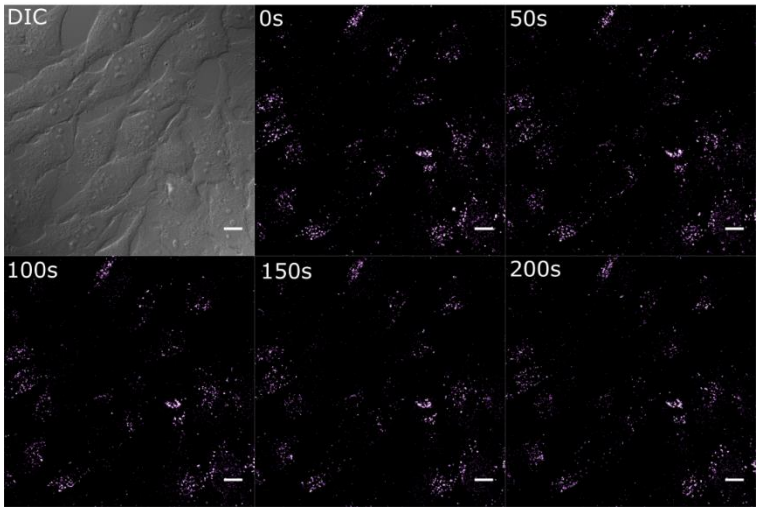

Figure A5.23. Timelapse experiment of HeLa cells incubated with **4**. Continuous irradiation was perform using the 552/600 channel for 200 seconds. Scale bar = 10 μm.

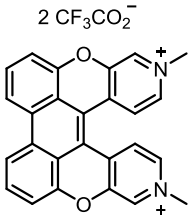

NeuroX2

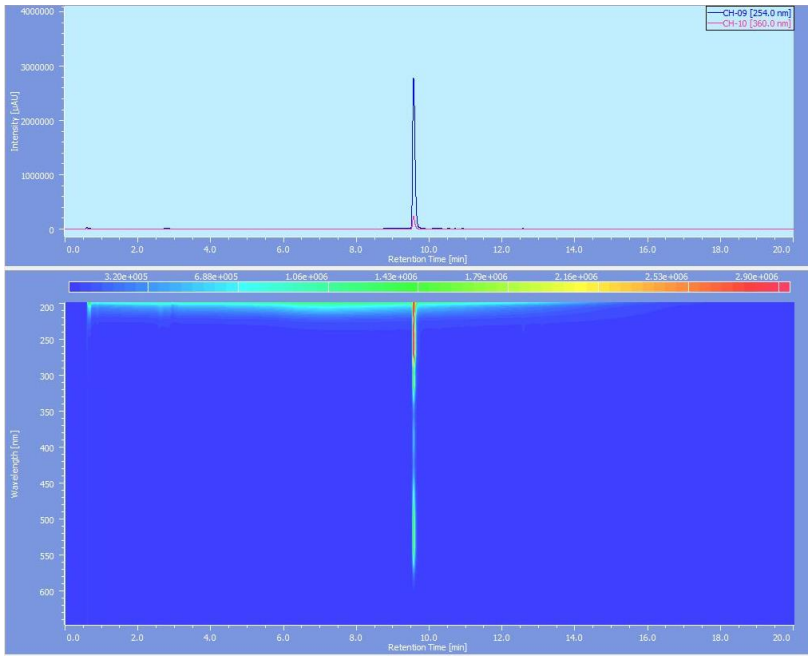

Figure A5.24. HPLC chromatogram of **NeuroX2**. Water containing 0.1% (v/v) trifluoroacetic acid and acetonitrile were used as eluents. Flow rate was 1 mL/min. Method time was 20 minutes.

Time (min)	% acetonitrile	Time (min)	% acetonitrile
0.00	0.0	17.80	100.0
1.00	0.0	18.00	0.0
12.00	100.0	20.00	0.0

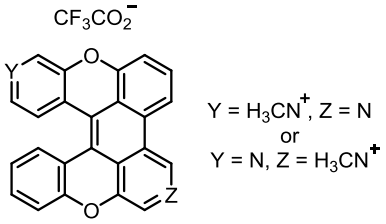

NeuroX3

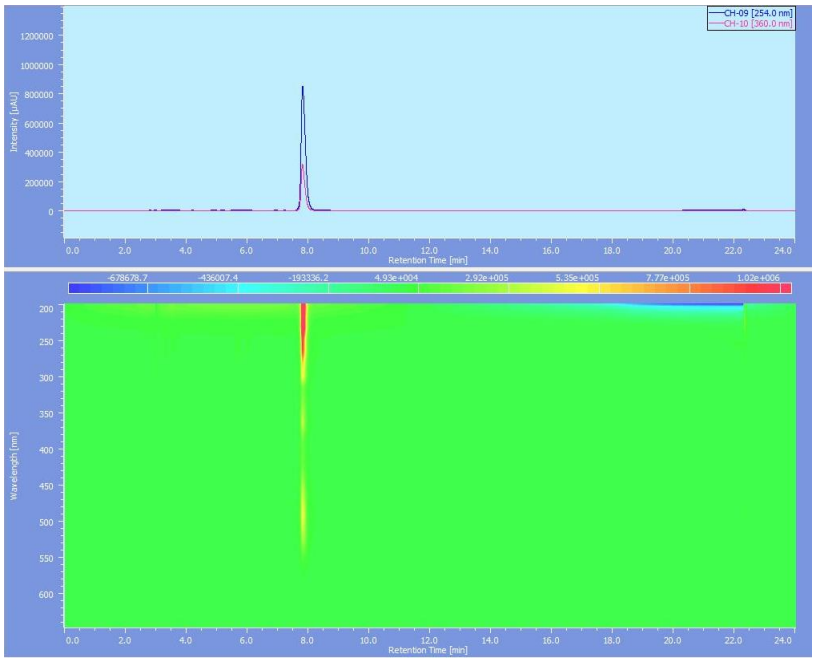

Figure A5.25. HPLC chromatogram of **NeuroX3**. Water containing 0.1% (v/v) trifluoroacetic acid and acetonitrile were used as eluents. Flow rate was 1 mL/min. Method time was 20 minutes.

Time (min)	% acetonitrile	Time (min)	% acetonitrile
0.00	30.0	15.50	100.0
1.00	30.0	18.80	100.0
15.00	80.0	19.00	30.0

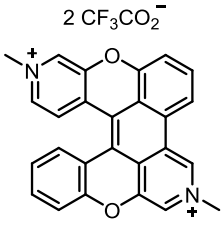

4

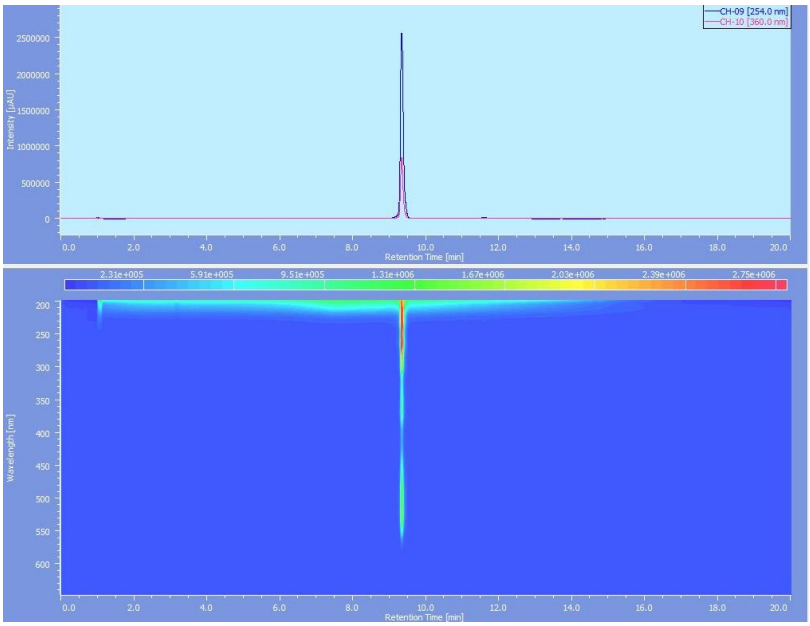

Figure A5.26. HPLC chromatogram of **4**. Water containing 0.1% (v/v) trifluoroacetic acid and acetonitrile were used as eluents. Flow rate was 1 mL/min. Method time was 20 minutes.

Time (min)	% acetonitrile	Time (min)	% acetonitrile
0.00	0.0	17.80	100.0
1.00	0.0	18.00	0.0
12.00	100.0	20.00	0.0

Chapter 7

Synthesis of 9-Substituted Triptycene Building Blocks for Solid-Phase Diversification and Nucleic Acid Junction Targeting

Adapted with permission from Yoon, I.;* Suh, S.-E.;* Barros, S. A.; Chenoweth, D. M. *Org. Lett.* **2016,** *18,* 1096-1099 (* Equally contributed).

7.1 Introduction

Nucleic acid junctions play important roles in many biological events. Three-way junctions (3WJs) have diverse architectures and are found in DNA and RNA, where they often serve as important structural elements.[1] Several small molecules are known to bind to nucleic acid junctions. However, these molecules often lack specificity, leading to binding of various structures.[2,3] Recently, we reported a new class of three-way junction stabilizers based on the triptycene scaffold.[4] The unique shape and 3-fold symmetry of triptycene allows for binding to nucleic acid three-way junctions. We also reported triptycene derivatives that bind to a d(CAG)·(CTG) trinucleotide repeat junction.[5]

Efficient strategies for triptycene diversification are needed to accelerate the discovery of new nucleic acid junction binders with enhanced specificity and binding properties. Triptycene building blocks that are amenable to immobilization on a solid support would allow for rapid diversification and compound library construction (Scheme 7.1).[6] To immobilize triptycene, we designed and synthesized a 9-substituted derivative that provides a point of attachment at the bridgehead, maintaining the C_3 symmetry.[7] Although triptycene has been extensively modified for use in materials chemistry applications,[8] functionalization at the C9-position of triptycene has rarely been reported.[9]

A carboxylic acid was chosen for functionalization at the C9 tertiary carbon of triptycene, due to its versatility of conversion into other functional groups, such as aldehyde, haloalkane, ester, and amide. The carboxyl group may also be removed via decarboxylation at a later stage. More importantly, the carboxyl group has been extensively employed for directed C-

H bond functionalization reactions, which could prove valuable during future triptycene diversification efforts.[10,11]

7.2 Results and Discussion

Scheme 7.1. Strategy for Triptycene Solid-Phase Diversification and Retrosynthesis of Key Building Block A.[a]

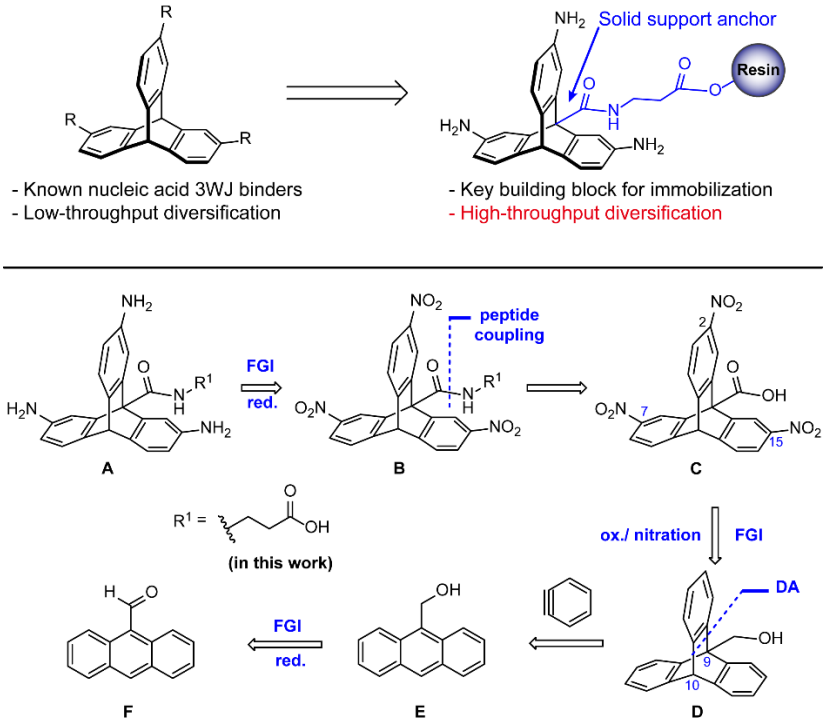

[a]FGI = functional group interconversion; ox. = oxidation; red. = reduction; DA = Diels-Alder reaction

Our synthetic plan (Scheme 7.1) relies on reduction of the nitro groups on precursor **B** to yield building block **A**. Further disconnection of the amide bond at the bridgehead position affords carboxylic acid **C**. A *β*-alanine ethyl ester was coupled to the carboxylic acid on **C**. O-

directed nitration was envisioned to regioselectively build three nitro groups onto triptycene **D**. In addition to nitration, simultaneous oxidation of the alcohol of **D** to the desired bridgehead carboxylic acid was anticipated. Next, disconnection at C9 and C10 affords benzyne and anthracene **E** precursors, which could be assembled via a Diels-Alder reaction. Precursor **E** was prepared by reduction of aldehyde **F**. Early-stage functionalization of triptycene at C9 would provide an efficient route to a triptycene building block suitable for solid-phase immobilization and further diversification.

Scheme 7.2. Approach Toward the Synthesis of 9-substituted Trifunctionalized Triptycene 6a-6c and X-ray Crystal Structure of 5a

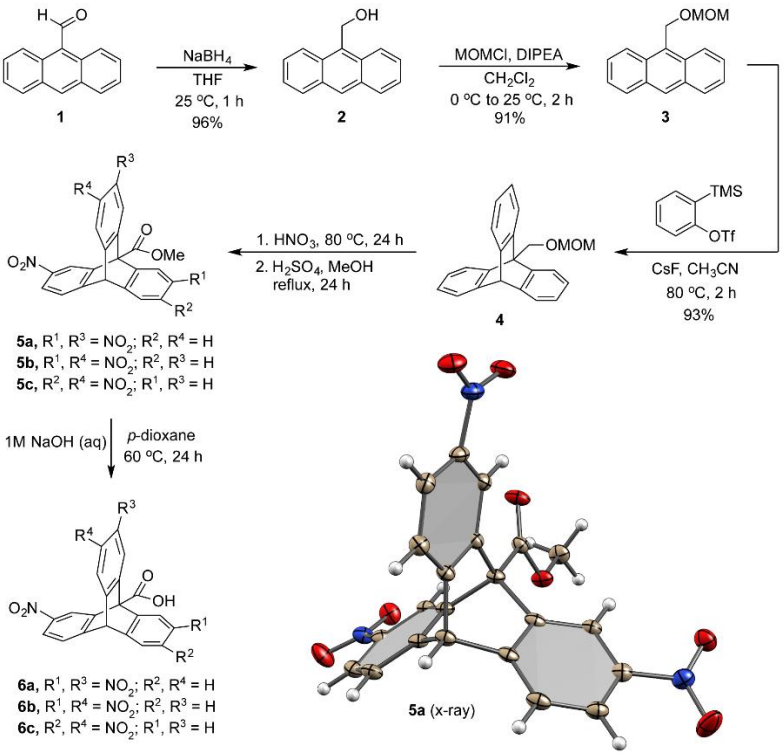

Commercially available anthracene-9-carbaldehyde **1** was employed as a starting material. Reduction of **1** using sodium borohydride afforded anthracen-9-ylmethanol **2** in 96% yield within one hour (Scheme 7.2). Prior to the addition of the Kobayashi benzyne precursor, the primary alcohol was protected with a MOM group to prevent electrophilic attack by benzyne. The Diels-Alder reaction between **3** and benzyne, which was generated *in situ* from 2-(trimethylsilyl)phenyltrifluoromethanesulfonate and cesium fluoride, led to the efficient formation of triptycene **4** in high yield.

Treatment of **4** with nitric acid resulted in nitration of the aromatic rings. During the nitration reaction the protecting group on the alcohol was simultaneously deprotected and oxidized to the carboxylic acid, providing **6a** along with two other isomers **6b** and **6c**. The nitrated triptycene isomers proved inseparable by silica gel chromatography. Acid-catalyzed esterification of the crude mixture provided ester isomers **5a**-**5c**, which were separated via silica gel chromatography. The structures of ester isomers **5a**-**5c** were confirmed by two-dimensional NMR spectroscopy, HMBC and HSQC. Single crystals of **5a** were grown in $CHCl_3/CH_2Cl_2/CH_3OH$, and the structure was determined by X-ray crystallography (Scheme 7.2). Following separation of each isomer, saponification was performed to convert the ester to a carboxylic acid for coupling to an amine linker. Nitration on the alpha-carbon was not observed due to its higher electronegativity compared to that of beta-carbons.[11]

To investigate the O-directing effect observed during nitration and to further reduce the number of undesired side products, compound **8**, containing a carboxylic acid at the C9 position, was prepared by deprotection of **4** followed by $KMnO_4$ oxidation (Scheme 7.3). Compounds **4**, **7**, and **8** were treated with excess nitric acid at 80 °C for 24 h, and the crude

mixtures were analyzed by HPLC using 9,10-diphenylanthrancene as an internal standard. HPLC analysis demonstrated that nitration of **8** led to fewer side products compared to nitration of **4** and **7** (Figure A6.36-40 in Appendix 6).

Scheme 7.3. Compositions of 6a-6c from the Nitration of Compounds 4, 7, and 8

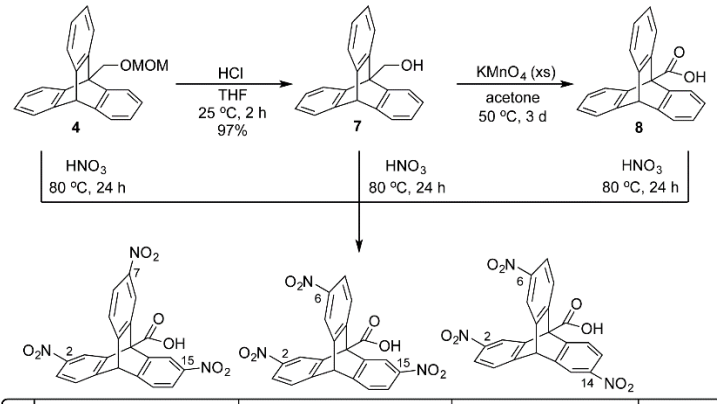

	6a	6b	6c	overall
4	16%	34%	22%	72%
7	0.8%	0.7%	0.9%	2.4%
8	30%	37%	13%	80%

Interestingly, nitration of **7** produced little of desired products **6a-6c**. The composition of **6a** and **6c** significantly changed compared to that from the nitration of **4** and **8**, and the overall yield increased for the nitration of **8**. Attempts were made to increase the proportion of **6a** over that of the other isomers. The highest ratio of **6a** to **6b** achieved using this nitration method was 0.33.[12] The introduction of a carboxylic acid at the C9 position of triptycene significantly increased the ratio of **6a** to **6b** to 0.81. These observations are consistent with the carboxylic acid functioning as a directing group during the nitration reaction.

Isomer **6a** was chosen for further elaboration due to its three-fold symmetry, which is complementary to that of nucleic acid 3WJs. To extend the length of the linker at the 9-position, several standard reaction conditions for amide bond formation were examined. However, the

Table 8.1. Reaction Conditions for Amide Bond Formation at the Linker Position.

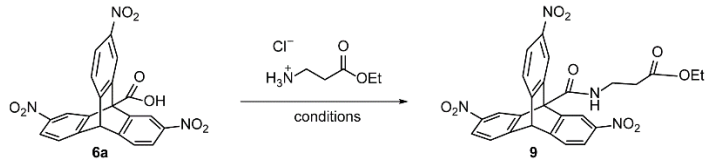

entry	conditions	yield (%) [a]
1	EDC (1.1 equiv), HOBt (1.1 equiv), Py (15 equiv), CH_2Cl_2, 25 °C, 24 h	–
2	$SOCl_2$ (3.0 equiv), Py (15 equiv), DCE, 25 °C, 24 h	–
3	$(COCl)_2$ (2.0 equiv), Py (15 equiv), CH_2Cl_2, 25 °C, 24 h	–
4	$(COCl)_2$ (2.0 equiv), Py (15 equiv), DMF, CH_2Cl_2, 25 °C, 24 h	–
5	MsCl (2.0 equiv), Py (4.0 equiv), CH_2Cl_2, 25 °C, 1 h	92
6	MsCl (1.2 equiv), Py (2.4 equiv), CH_2Cl_2, 25 °C, 1 h	61
7	MsCl (5.0 equiv), Et_3N (10 equiv), CH_2Cl_2, 25 °C, 1 h	48

[a] NMR yield. Durene was used as an internal standard.

amidation reaction proved recalcitrant and all attempted conditions resulted in unreacted starting material (Table 8.1, entries 2-4). The coupling of 9-triptycenecarboxylic acid derivatives with EDC has been previously reported.[13] However, this method was not reproducible using **6a** as the starting material (Table 8.1, entry 1). Our results suggested that the sterically hindered environment around the carboxylic acid prevents coupling of amines under standard conditions, possibly due in part to the bulky active ester intermediates. After a comprehensive literature search, we were inspired by Nicolaou's use of methanesulfonyl chloride (MsCl) in the total synthesis of the CP molecules to overcome limitations of a difficult Arndt-Eistert homologation on sterically encumbered carboxylic acids.[14] Triethylamine and MsCl were added to **6a** followed by addition of β-alanine ethyl ester hydrochloride, which was pre-treated with triethylamine at 0 °C. After warming to room temperature, **9** was synthesized in 48% yield (Table 8.1, entry 7). However, complete conversion of the starting material was not achieved under these conditions. To drive the reaction to completion, the base was changed to pyridine, which is less sterically

hindered and allows for access to the carboxylic acid near the bridge-head position. The solvent was also changed to dichloromethane due to solubility issues. These changes led to completion of the reaction within one hour after warming to room temperature and a substantial increase in the yield to 92% (Table 8.1, entry 5). A decrease in the equivalence of MsCl and pyridine decreased the yield to 61% (Table 8.1, entry 6). Among the various amide bond forming reaction conditions tested on triptycene **6a**, only the mesylation route afforded the desired product in high yield.

Scheme 7.4. Synthesis of SPPS Precursor 12 and Loading on 2-Chlorotrityl Chloride Resin.

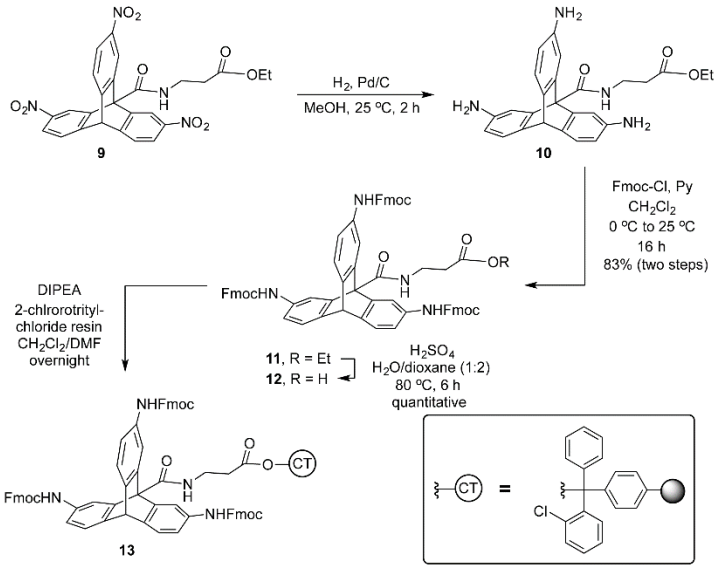

Pd/C-catalyzed hydrogenation of **9** led to reduction of the three nitro groups to afford triaminotriptycene **10**. Next, the free amines were protected with Fmoc groups by treatment with Fmoc-chloride and pyridine. The linker ester group was hydrolyzed in the presence of sulfuric acid and water to produce acid **12**. The free carboxylate of fully protected building block

Scheme 7.5. (a) Solid-Phase Peptide Synthesis of 9-substituted Triptycene on 2-Chlorotrityl Chloride Resin (b) Cleavage from the Resin to Generate Triptycene Derivatives 17-19.

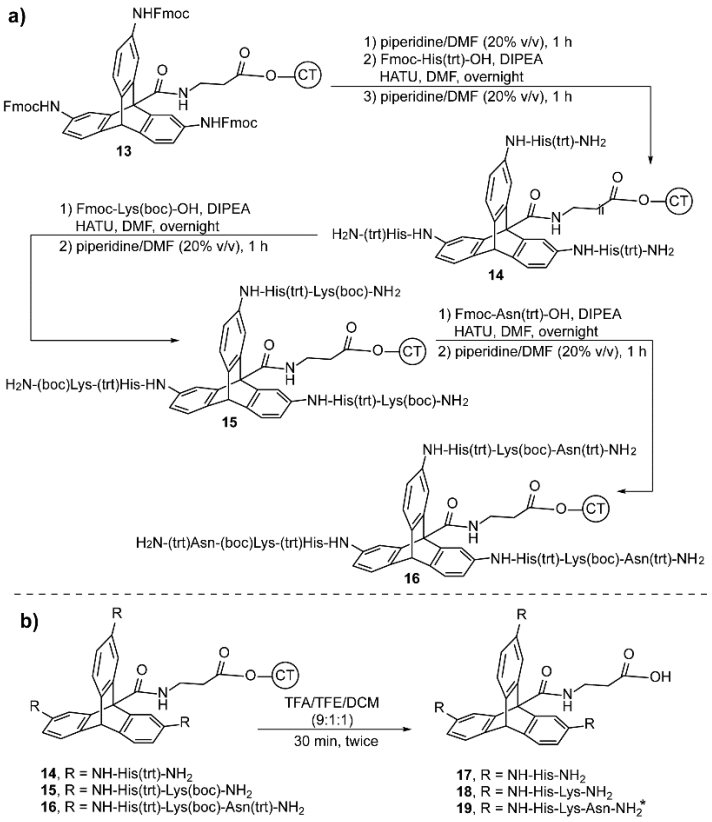

*Deprotection required 12 h for triptycene **19**. CT = 2-chlorotrityl chloride resin.

12 allowed for attachment to 2-chlorotrityl chloride resin, which is compatible with Fmoc deprotection chemistry (Scheme 7.4). After attachment to resin, the Fmoc groups were deprotected using 20% piperidine in dimethylformamide to generate the free amines. The corresponding Fmoc-protected amino acid was pre-activated with HATU and N,N-diisopropylethylamine (DIPEA) and added to the deprotected triptycene on resin. (L)-histidine, (L)-lysine, and (L)-asparagine were selected for attachment to the triptycene arms. The deprotection and coupling steps were repeated until the desired sequence of amino acids

was achieved (Scheme 7.5a). Once the desired peptide was synthesized on solid phase, the triptycene derivatives were cleaved from the resin with simultaneous deprotection of the amino acid side chain protecting groups by treatment with a cleavage solution (9:1:1 trifluoroacetic acid (TFA) : 2,2,2-trifluoroethanol (TFE) : dichloromethane). Asparagine, which was coupled at the N-terminus, required longer cleavage times due to the slow deprotection rate of the trityl group close to the amino group (Scheme 7.5b).[15] Each compound was purified by preparative reverse-phase HPLC and analyzed by analytical HPLC and MALDI-MS.

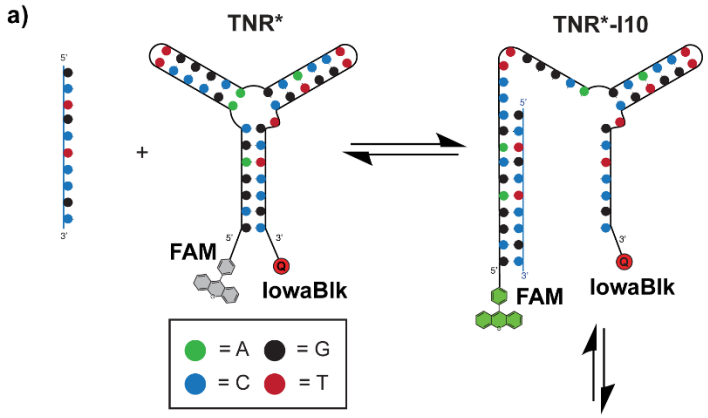

compound	K_d (μM)
17, Trip-(His)$_3$	8.38 ± 1.358
18, Trip-(His-Lys)$_3$	0.269 ± 0.055
19, Trip-(His-Lys-Asn)$_3$	0.460 ± 0.092
20, Trip-(His)$_3$*	1.76 ± 0.215

Figure 7.1. (a) Graphical representation of the fluorescence-quenching 3WJ assay. (b) Dissociation constants of triptycenes **17**-**20**. Note: Synthesis of triptycene **20** lacking a bridgehead substituent has been previously reported.[5]

Triptycenes **17**-**19** were evaluated for binding towards a d(CAG)·(CTG) trinucleotide repeat junction using a previously developed fluorescence-quenching experiment.[5] The binding of triptycenes **17**-**19** were compared to a previously reported triptycene that binds to the junction. The previously reported junction binder (**20**) is analogous to **17** but lacks the linker at the 9-position. A d(CAG)·(CTG) repeat junction was labelled with a fluorophore (FAM) and a quencher (IowaBlk). This labelled 3WJ was pre-incubated with a 10 bp inhibitor (I10) strand that is complementary to the junction. Hybridization of the inhibitor strand to the junction results in an open form, leading to an increase in fluorescence (Figure 7.1a). Triptycenes **17**-**20** were added to the pre-incubated fluorescent form. Binding of the triptycenes leads to displacement of I10 and reformation of the 3WJ, resulting in a decrease in fluorescence. The K_d value for triptycene **17** was determined to be 8.38 μM and exhibited a slight decrease in binding compared to that of triptycene **20** (i.e., K_d value of 1.76 μM). Triptycenes **18** and **19**, containing di- or tripeptides substituents, exhibited enhanced binding affinity toward the junction compared to that of **20** with K_d values of 0.27 μM and 0.46 μM, respectively (Figure 7.1b). The presence of lysine appears to play an important role in binding to the junction and will be investigated in future studies.

7.3 Conclusions

In summary, we have developed a synthetic approach for preparing new 9-substituted triptycene building blocks. This approach enables solid-phase diversification of triptycene.

During the synthesis, O-directed nitration was observed from the MOM protected primary alcohol (**4**), primary alcohol (**7**), and carboxylic acid (**8**) at the C9 position of triptycene. These results indicated that the carboxylic group increased the ratio of nitration on beta-carbons toward the linker position, pointing to a possible carboxylic acid directing effect. In addition, a key amide bond formation was achieved on a sterically hindered and geometrically fixed tertiary carboxylic acid using a unique MsCl activation strategy. This may be regarded as a general strategy toward functionalization of extremely sterically encumbered tertiary carboxylic acids. For diversification of the new triptycene building block, three amino acids were utilized including histidine, lysine, and asparagine to produce trisubstituted peptide **17**-**19**. The binding ability of the synthesized triptycene derivatives toward a d(CAG)·(CTG) trinucleotide repeat junction was evaluated and triptycene **18** and **19** exhibited better binding affinity to the junction compared to that of a previously reported triptycene with no linker (**20**). This new synthetic strategy provides rapid and efficient access to triptycene building blocks, enabling high-throughput diversification for rapid evaluation of potential junction binders and other medicinal chemistry targets.

7.4 Experimental Section

General information

All commercial reagents and solvents were used as received. 9-anthracenecarboxaldehyde, sodium borohydride, *N*,*N*-diisopropylethylamine, chloromethyl

methyl ether, beta-Alanine ethyl ester hydrochloride, Fmoc chloride, palladium on activated carbon, cesium fluoride, 2-(trimethylsilyl)phenyl trifluoromethanesulfonate, and nitric acid from Aldrich, 1-[bis(dimethylamino)methylene]-1H-1,2,3-triazolo[4,5-b]pyridinium3-oxide hexafluorophosphate (HATU) from Oakwood Products, Inc., 2-chlorotrityl chloride resin from Advanced ChemTech, chloroform-d, methylene chloride-d2, dimethylsulfoxide-d6, and acetone-d6 from Cambridge Isotope Laboratories Inc. were purchased. HPLC-purified TNR DNA 3WJ oligo modified with a 5'-FAM and a 3'-IowaBlack (5'-(FAM)-GCGGAGCAGCCCTTGGGCAGCACCTTGGTGCTGCTCCGC-(IowaBlk)-3') and DNA inhibitor 10 (5'-GCTGCTCCGC-3') were purchased from Integrated DNA Technologies (IDT).

Flash column chromatography was performed using Silicycle silica gel (55–65 Å pore diameter). Thin-layer chromatography was performed on Sorbent Technologies silica plates (250 μm thickness). Proton nuclear magnetic resonance spectra (^{1}H NMR) and Carbon nuclear magnetic resonance (^{13}C NMR) spectra were recorded on a Bruker DMX 500. High-resolution mass spectrometry analysis was obtained by Dr. Rakesh Kohli at the University of Pennsylvania's Mass Spectrometry Service Center on a Waters LC-TOF mass spectrometer (model LCT-XE Premier) using electrospray ionization. High-performance liquid chromatography (HPLC) chromatograms were recorded and triptycenes **17**-**19** was purified on JASCO HPLC (Easton, MD) equipped with a Phenomenx (Torrance, CA) column (Analytical: Luna 5μ C18(2) 100A; 250 x 4.60 mm, 5 μm Semi-prep: 5μ C18(2) 100A; 250 x 10.00 mm, 5 μm) using aqueous (H_2O + 0.1% CF_3CO_2H) and organic (CH_3CN) phases. Matrix-assisted laser desorption ionization

(MALDI) mass spectra were recorded on a Bruker Ultraflex III MALDI-TOF-TOF mass spectrometer (Billerica, MA) using α-cyano-4-hydroxycinnamic acid (CHCA). Fluorescence measurements were obtained on a Tecan M1000 plate reader (Mannedorf, Switzerland).

Experimental procedures

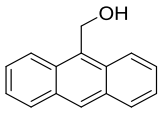

2

anthracen-9-ylmethanol (2): To 4.9 g (23.76 mmol) of anthracene-9-carbaldehyde (**1**) in THF (50 mL) was added 1.35g (35.64 mmol) of $NaBH_4$. The mixture was stirred for 1 h at 25 ˚C. The mixture was poured into water (400 mL) resulting in a yellow precipitate. The yellow solid was filtered off, washed thoroughly with water, and dried. (4.7 g, 96 % isolated yield).[16]

^{1}H NMR (500 MHz, $CDCl_3$) δ 8.46 (s, 1H), 8.40 (d, 2H, J = 8.8 Hz), 8.02 (d, 2H, J = 8.4 Hz), 7.59-7.53 (m, 2H), 7.52-7.46 (m, 2H), 5.65 (s, 2H).

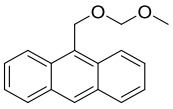

3

9-((methoxymethoxy)methyl)anthracene (3): To 354 mg (1.7 mmol) of anthracen-9-ylmethanol **2** in CH_2Cl_2 was added 1.76 mL (10.2 mmol) of *N,N*-diisopropylethylamine at 0 ˚C. After stirring for 30 min, 0.4 mL (5.1 mmol) of chloromethylmethyl ether was added to this solution at 0 ˚C. The mixture was stirred for 10 min, warmed to 25 ˚C, and stirred for 18 h. Saturated NH_4Cl (aq) solution was added to the reaction. The organic layer was extracted from

the solution, dried with anhydrous sodium sulfate, concentrated in vacuo, and purified by column chromatography using ethyl acetate/hexanes (4%) as the eluent to give 391 mg of **3** (391 mg, 91 % isolated yield).

Physical Property: Pale yellow solid, m.p. = 80-81 ˚C.

TLC: R_f = 0.52 (silica gel, 25% ethyl acetate/hexanes).

^{1}H NMR (500 MHz, $CDCl_3$) δ 8.53 (d, 2H, J = 8.8 Hz), 8.47 (s, 1H), 8.04 (d, 2H, J = 8.4 Hz), 7.68-7.62 (m, 2H), 7.58-7.51 (m, 2H), 5.67 (s, 2H), 4.90 (s, 2H), 3.61 (s, 3H).

^{13}C NMR (125 MHz, $CDCl_3$) δ 131.6, 131.3, 129.2, 128.7, 128.4, 126.4, 125.1, 124.4, 95.7, 61.1, 55.8.

IR (neat): 1733, 1446, 1265, 1147, 1093, 1061, 1029, 934, 914, 891, 731, 703, 640 cm^{-1}.

HRMS (ESI) calculated for $C_{17}H_{16}NaO_2^+$ $[M+Na]^+$ 275.1043, found 275.1055.

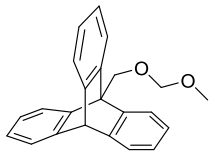

4

9-((methoxymethoxy)methyl)-9,10-dihydro-9,10-[1,2]benzenoanthracene (4): To a vial was added 384 mg (1.52 mmol) of **3**, 907 mg (3.04 mmol) of 2-(trimethylsilyl)phenyl trifluoromethanesulfonate, 693 mg (4.56 mmol) of CsF, and 2.5 mL of acetonitrile at 25 ˚C. The solution was heated to 80 ˚C and stirred for 2 h under Argon gas. After the reaction was completed, Saturated NH_4Cl (aq) solution and ethyl acetate were added to the reaction mixture. The organic layer was extracted from the solution, dried with anhydrous sodium sulfate,

concentrated in vacuo, and washed with hexanes. The crude mixture was then purified by column chromatography using dichloromethane (100%) as the eluent to give **4** (464 mg, 93 % isolated yield).

Physical Property: Pale yellow solid, m.p. = 197-198 ˚C.

TLC: R_f = 0.39 (silica gel, 25% ethyl acetate/hexanes).

^{1}H NMR (500 MHz, $CDCl_3$) δ 7.62-7.46 (m, 6H), 7.18-7.09 (m, 6H), 5.52 (s, 1H), 5.27 (s, 2H), 5.22 (s, 2H), 3.80 (s, 3H).

^{13}C NMR (125 MHz, $CDCl_3$) δ 146.7, 144.8, 125.3, 125.2, 123.6, 122.4, 98.3, 67.0, 56.8, 54.5, 53.2.

IR (neat): 1375, 1337, 1265, 1183, 1035, 951, 945, 824, 736, 647, 634 cm^{-1}.

HRMS (ESI) calculated for $C_{23}H_{20}NaO_2^+$ $[M+Na]^+$ 351.1356, found 351.1356.

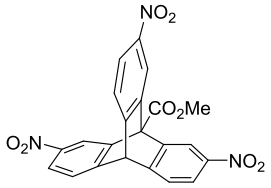

5a

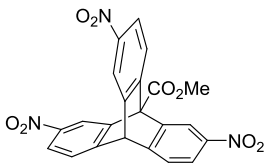

5b

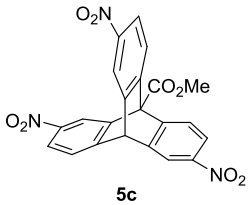

5c

methyl trinitro-9,10-[1,2]benzenoanthracene-9(10*H*)-carboxylate (5a-5c): To a round bottom flask was added 3.97 g (12.1 mmol) of **4** and 50 mL of concentrated nitric acid at 25 ˚C. The solution was heated to 80 ˚C and stirred for 24 h. After the reaction was complete, water was added to the solution. The solution was neutralized with K_2CO_3 and re-acidified with 1M HCl. Ethyl acetate was added to the solution and the organic layer was extracted from the solution. The combined organic solution was dried with anhydrous sodium sulfate, and concentrated in

vacuo. To the crude mixture was added 40 mg of H_2SO_4 and 100 mL of anhydrous methanol. The solution was stirred under reflux for 24 h. After the reaction was completed, the solution was cooled, extracted with ethyl acetate, dried with anhydrous sodium sulfate, and then concentrated in vacuo. The crude mixture of **5a**-**5c** was then purified using column chromatography. The composition of each isomer was determined by HPLC analysis.

methyl 2,7,15-trinitro-9,10-[1,2]benzenoanthracene-9(10*H*)-carboxylate (5a):

Physical Property: White solid, m.p. = 282-283 ˚C.

TLC: R_f = 0.41 (silica gel, 50% ethyl acetate/hexanes).

^{1}H NMR (500 MHz, $CDCl_3$) δ 8.64 (d, 3H, J = 2.1 Hz), 8.08 (dd, 3H, J = 8.2, 2.2 Hz), 7.64 (d, 3H, J = 8.2 Hz), 5.77 (s, 1H), 4.43 (s, 3H).

^{13}C NMR (125 MHz, $CDCl_3$) δ .167.9, 148.9, 146.3, 143.1, 124.9, 122.9, 120.1, 61.4, 53.8, 53.6.

IR (neat): 2924, 1746, 1522, 1455, 1340, 1301, 1274, 1250, 1214, 1166, 1025, 903 cm^{-1}.

HRMS (ESI) calculated for $C_{22}H_{14}N_3O_8^+$ $[M+H]^+$, no peak matched the calculated exact mass. Hydrolysis of the ester to carboxylic acid **6a** was required to obtain the HRMS. See next page for HRMS data on acid **6a**.

methyl (9s,10r)-2,6,15-trinitro-9,10-[1,2]benzenoanthracene-9(10*H*)-carboxylate (5b):

Physical Property: White Solid, m.p. = 163-164 ˚C.

TLC: R_f = 0.73 (silica gel, 50% ethyl acetate/hexanes).

^{1}H NMR (500 MHz, $CDCl_3$) δ 8.63 (d, 2H, J = 2.0 Hz), 8.33 (d, 1H, J = 2.0 Hz), 8.04 (dd, 2H, J = 8.1, 2.0 Hz), 7.99 (dd, 1H, J = 8.5, 2.0 Hz), 7.89 (d, 1H , J = 8.5 Hz), 7.70 (d, 2H, J = 8.1 Hz), 5.89 (s, 1H), 4.40 (s, 3H).

^{13}C NMR (125 MHz, $CDCl_3$) δ 168.1, 149.6, 147.9, 146.2, 144.4, 142.7, 125.4, 125.1, 122.9, 122.1, 120.1, 119.4, 61.6, 53.5, 53.4.

IR (neat): 2924, 1743, 1519, 1455, 1341, 1297, 1214, 1165, 1071, 1024, 892 cm^{-1}.

HRMS (ESI) calculated for $C_{22}H_{14}N_3O_8^+$ $[M+H]^+$, no peak matched the calculated exact mass. Hydrolysis of the ester to carboxylic acid **6b** was required to obtain the HRMS. See next page for HRMS data on acid **6b**.

methyl (9r,10s)-2,6,14-trinitro-9,10-[1,2]benzenoanthracene-9(10*H*)-carboxylate (5c):

Physical Property: White Solid, m.p. = 161-162 °C.

TLC: R_f = 0.81 (silica gel, 50% ethyl acetate/hexanes).

^{1}H NMR (500 MHz, $CDCl_3$) δ 8.65 (d, 1H, J = 2.2 Hz), 8.33 (d, 2H, J = 2.3 Hz), 8.09 (dd, 1H, J = 8.2, 2.2 Hz), 8.05 (dd, 2H, J = 8.6, 2.3 Hz), 7.93 (d, 2H, J = 8.6 Hz), 7.67 (d, 1H, J = 8.2 Hz), 5.80 (s, 1H), 4.37 (s, 3H).

^{13}C NMR (125 MHz, $CDCl_3$) δ 168.1, 149.8, 147.4, 146.24, 146.21, 144.7, 142.3, 125.5, 124.9, 122.9, 122.1, 120.3, 119.3, 61.9, 53.4, 53.3.

IR (neat): 2924, 1744, 1598, 1458, 1438, 1342, 1254, 1165, 1023 cm^{-1}.

HRMS (ESI) calculated for $C_{22}H_{14}N_3O_8^+$ $[M+H]^+$, no peak matched the calculated exact mass. Hydrolysis of the ester to carboxylic acid **6c** was required to obtain the HRMS. See next page for HRMS data on acid **6c**.

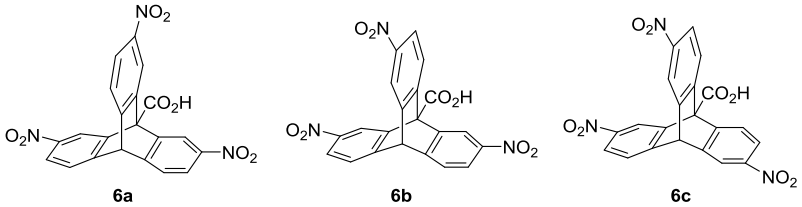

General procedure for preparation of trinitro-9,10-[1,2]benzenoanthracene-9(10*H*)-carboxylic acid (6a-6c): To 1 eq of **5a** (or **5b**, **5c**) dissolved in *p*-dioxane was added 3 eq of 1M NaOH (aq) and heated to 60 ˚C for 24 h. After the reaction was completed, the solution was neutralized and acidified with 1N HCl. Ethyl acetate was added to the solution and the organic layer was extracted from the solution. The combined organic layer was washed with NH_4Cl (aq) and brine. The organic layer was dried with anhydrous sodium sulfate, and concentrated in vacuo to give **6a** (or **6b**, **6c**) in quantitative yield.

2,7,15-trinitro-9,10-[1,2]benzenoanthracene-9(10*H*)-carboxylic acid (6a):

Physical Property: Pale yellow solid, m.p. = 358-359 ˚C.

TLC: R_f = 0.43 (silica gel, 100% ethyl acetate).

^{1}H NMR (500 MHz, $(CD_3)_2CO$) δ 9.23 (s, 3H), 7.96 (dd, 3H, J = 8.1, 1.9 Hz), 7.74 (d, 3H, 8.1 Hz), 6.21 (s, 1H).

^{13}C NMR (125 MHz, $(CD_3)_2CO$) δ 171.3, 151.3, 147.5, 146.1, 124.6, 121.8, 121.4, 63.7, 53.4.

IR (neat): 2924, 1592, 1518, 1341, 1262, 1092, 1069, 1023, 903 cm^{-1}.

HRMS (ESI) calculated for $C_{21}H_{10}N_3O_8^-$ $[M-H]^-$ 432.0473, found 432.0457.

(9s,10r)-2,6,15-trinitro-9,10-[1,2]benzenoanthracene-9(10*H*)-carboxylic acid (6b):

Physical Property: Pale yellow solid, m.p. = 265-266 °C.

TLC: R_f = 0.23 (silica gel, 100% ethyl acetate).

^{1}H NMR (500 MHz, $(CD_3)_2CO$) δ 9.29 (d, 2H, J = 2.2 Hz), 8.54 (d, 1H, J = 8.3 Hz), 8.36 (d, 1H, J = 2.2 Hz), 8.01 (dd, 2H, J = 8.1, 2.2 Hz), 7.88 (d, 1H, J = 8.1 Hz), 7.81 (d, 2H, J = 8.1 Hz), 6.28 (s, 1H).

^{13}C NMR (125 MHz, $(CD_3)_2CO$) δ 171.2, 152.5, 151.7, 146.8, 146.0, 145.9, 145.5, 127.3, 124.6, 121.8, 121.4, 121.1, 118.6, 63.7, 53.1.

IR (neat): 2921, 1737, 1593, 1524, 1462, 1377, 1344, 1260, 1093 cm^{-1}.

HRMS (ESI) calculated for $C_{21}H_{10}N_3O_8^-$ $[M-H]^-$ 432.0473, found 432.0462.

(9r,10s)-2,6,14-trinitro-9,10-[1,2]benzenoanthracene-9(10*H*)-carboxylic acid (6c):

Physical Property: White solid, m.p. = 202-203 °C.

TLC: R_f = 0.03 (silica gel, 100% ethyl acetate).

^{1}H NMR (500 MHz, $(CD_3)_2CO$) δ 8.92 (s, 1H), 8.49 (s, 2H), 8.23 (d, 2H, J = 8.6 Hz), 8.15-8.06 (m, 3H), 7.95 (d, 1H, 8.2 Hz), 6.47 (s, 1H).

^{13}C NMR (125 MHz, $(CD_3)_2CO$) δ 168.6, 151.1, 148.2, 146.2, 146.1, 145.7, 142.9, 125.8, 125.53, 122.51, 121.7, 120.1, 119.5, 61.8, 52.5.

IR (neat): 2927, 1720, 1598, 1518, 1458, 1418, 1341, 1260, 1179, 1090, 902 cm^{-1}.

HRMS (ESI) calculated for $C_{21}H_{10}N_3O_8^-$ $[M-H]^-$ 432.0473, found 432.0466.

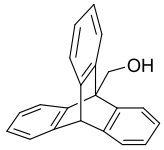

7

9,10-[1,2]benzenoanthracen-9(10*H*)-ylmethanol (7): To a vial was added 1.95 g (5.94 mmol) of **4**, 70 mL of 1M HCl, and 100 mL of THF. The solution was stirred at 25 °C. After 1 h, ethyl acetate was added to the solution. The organic layer was extracted from the solution, dried with anhydrous sodium sulfate, and concentrated in vacuo to give **7** (1.68 g, 99 % isolated yield).

Physical Property: Pale yellow solid.[17]

TLC: R_f = 0.31 (silica gel, 25% ethyl acetate/hexanes).

^{1}H NMR (500 MHz, $(CD_3)_2CO$) δ 7.65-7.44 (m, 6H), 7.04-6.97 (m, 6H), 5.58 (s, 1H), 5.30 (d, 2H, J = 3.6 Hz), 4.60 (t, 1H, J = 3.6 Hz).

^{13}C NMR (125 MHz, $(CD_3)_2CO$) δ 147.2, 145.6, 124.71, 124.66, 123.3, 122.9, 60.0, 54.2, 54.0.

IR (neat): 3308, 2962, 2918, 1579, 1458, 1261, 1071, 1035, 798, 740, 648, 629, 611, 481 cm^{-1}.

HRMS (ESI) calculated for $C_{21}H_{17}O^+$ $[M+H]^+$ 285.1274, found 285.1288.

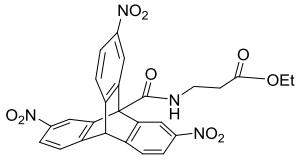

9

9,10-[1,2]benzenoanthracene-9(10*H*)-carboxylic acid (8): To a vial, 31.9 mg (0.11 mmol) of **7** was dissolved in acetone and heated to 50 °C. 88.6 mg (0.56 mmol) of $KMnO_4$ was added to the

solution. Whenever the solution turned to black or brown, an additional 88.6 mg (0.56 mmol) of $KMnO_4$ was added to the solution. After 3 days, sodium sulfite solution (aq) was added to the crude mixture and then extracted with ethyl acetate. The combined organic layer was dried with anhydrous sodium sulfate, and concentrated in vacuo to yield **8** (22.4 mg, 67 % isolated yield).

Physical Property: Pale yellow solid.[18]

TLC: R_f = 0.28 (silica gel, 100% ethyl acetate).

^{1}H NMR (500 MHz, $(CD_3)_2CO$) δ 8.09-8.01 (m, 3H), 7.46-7.42 (m, 3H), 7.02-6.97 (m, 6H), 5.57 (s, 1H)

^{13}C NMR (125 MHz, $(CD_3)_2CO$) δ 172.3, 146.4, 144.6, 125.1, 124.6, 124.6, 123.2, 62.4, 54.2.

IR (neat): 2925, 1712, 1458, 1448, 1386, 1261, 1213, 1171, 1085, 1032, 867, 801, 748, 735, 703, 685, 645, 624, 609, 478 cm^{-1}.

HRMS (ESI) calculated for $C_{21}H_{13}O_2^-$ $[M-H]^-$ 297.0921, found 297.0914.

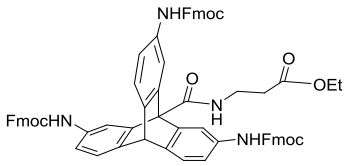

11

ethyl 3-(2,7,15-tris((((9H-fluoren-9-yl)methoxy)carbonyl)amino)-9,10-dihydro-9,10-[1,2]benzenoanthracene-9-carboxamido)propanoate (11): To a vial was charged 180 mg (0.338 mmol) of **9**, 3.6 mg (0.034 mmol) of Pd/C, 2 mL of MeOH under H_2 gas. After 24 h stirring at 25 ˚C, the solution was filtered and concentrated in vacuo to yield crude of **10**. To a round flask was added **10**, 0.27 mL (3.38 mmol) of pyridine, and 30 mL of CH_2Cl_2. The solution

was cooled and stirred for 30 minutes at 0 ˚C. 612.1 mg (2.37 mmol) of Fmoc-Cl in 3 mL of CH_2Cl_2 was added to the solution. The crude mixture was warmed to 25 ˚C and stirred for 16 h. The solution was washed with saturated NH_4Cl (aq), dried, and purified by column chromatography using ethyl acetate (100%) as the eluent to give **11** (310 mg, 83 % isolated yield).

Physical Property: White solid, m.p. = 157-158.3 ˚C.

TLC: R_f = 0.81 (silica gel, 50% ethyl acetate/hexanes).

^{1}H NMR (500 MHz, CD_2Cl_2) δ 7.98 (s, 3H), 7.78 (d, 6H, J = 7.5 Hz), 7.59 (d, 6H, J = 6.3 Hz), 7.39 (t, 6H, J = 7.5 Hz), 7.32-7.20 (m, 12H), 7.15 (s, 3H), 6.75 (bs, 1H), 5.28 (s, 1H), 4.40 (d, 6H, J = 6.7 Hz), 4.19 (t, 3H, J = 6.7 Hz), 4.06 (q, 2H, J = 7.1 Hz), 3.89 (q, 2H, J = 5.7 Hz), 2.80 (t, 2H, J = 5.7 Hz), 1.11 (t, 3H, J = 7.1 Hz).

^{13}C NMR (125 MHz, CD_2Cl_2) δ 173.1, 168.8, 153.4, 144.3, 143.9, 141.4, 141.3, 135.2, 127.7, 127.0, 125.0, 123.6, 119.9, 115.9, 66.7, 60.9, 60.5, 52.4, 47.1, 35.8, 34.1, 13.9.

IR (neat): 1715, 1604, 1526, 1464, 1450, 1409, 1322, 1297, 1260, 1213, 1155, 1055, 985, 804, 758, 737, 702, 621, 531, 501 cm^{-1}.

HRMS (ESI) calculated for $C_{71}H_{56}N_4NaO_9^+$ $[M+Na]^+$ 1131.3940, found 1131.3949.

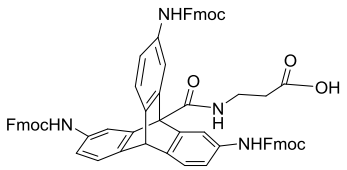

12

3-(2,7,15-tris((((9H-fluoren-9-yl)methoxy)carbonyl)amino)-9,10-dihydro-9,10-[1,2]benzenoanthracene-9-carboxamido)propanoic acid (12): To a vial was charged 30.0 mg (0.027 mmol) of **11**, 0.1 mL of H_2SO_4, 4 mL of 1,4-dioxane, and 2 mL of water. The solution was stirred at 80 ˚C. After 24 h, the solution was concentrated in vacuo and purified by column chromatography using ethyl acetate (100%) as the eluent to give **12** in quantitative yield.

Physical Property: White solid, m.p. = 188-189 ˚C.

TLC: R_f = 0.67 (silica gel, 100% ethyl acetate).

^{1}H NMR (500 MHz, $(CD_3)_2SO$) δ 9.83-9.53 (bs, 3H), 8.12-7.94 (bs, 4H), 7.87 (d, 6H, J = 7.5 Hz), 7.71 (d, 6H, J = 7.5 Hz), 7.39 (t, 6H, J = 7.5 Hz), 7.30 (t, 6H, J = 7.5 Hz), 7.28-7.07 (m, 6H), 5.36 (s, 1H), 4.39 (d, 6H, J = 6.8 Hz), 4.25 (t, 3H, J = 6.8 Hz), 3.78-3.68 (m, 2H), 2.78-2.62 (m, 2H).

IR (neat): 3324, 2924, 1719, 1604, 1536, 1464, 1299, 1216, 1052, 985 cm^{-1}.

HRMS (ESI) calculated for $C_{69}H_{51}N_4O_9^-$ $[M-H]^-$ 1079.3662, found 1079.3630.

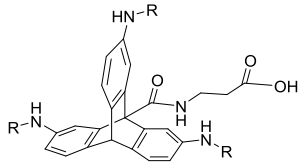

17 R = His-NH_2
18 R = His-Lys-NH_2
19 R = His-Lys-Asn-NH_2

General procedure for preparation of 17-19 (Solid-Phase Peptide Synthesis): To a SPPS reaction vessel was added 1 eq of 2-chlorotrityl chloride resin (100-200 mesh, substitution: 1.4 mmol/g). The resin was stirred in dry CH_2Cl_2 for 30 min and the solvent was removed by vacuum. 1.2 eq of **12** dissolved in dimethylformamide:CH_2Cl_2 (1:5 volume ratio) and 5 eq of N,N-diisopropylethylamine (DIPEA) were added to the resin. After stirring for 10 min, an additional 1.5 eq of DIPEA was added to the resin and stirred overnight (12 hours) at 25 ˚C. HPLC grade methanol was added and stirred for 20 min to cap the remaining reactive functional group on the resin. The solution was removed by vacuum and the resin was washed with CH_2Cl_2 (1 min, 3 times) and dimethylformamide (1 min, 3 times). 20 % (v/v) piperidine in dimethylformamide was added to the resin, stirred for 1 h, and then the solution was drained. The resin was washed with dimethylformamide (1 min, 3 times), CH_2Cl_2 (1 min, 3 times) and dimethylformamide (1 min, 3 times). 9.5 eq of corresponding Fmoc-protected amino acid (Fmoc-His(trt)-OH, Fmoc-Lys(boc)-OH, or Fmoc-Asn(trt)-OH) was pre-activated with 9 eq of HATU and 18 eq of DIPEA in dimethylformamide. The pre-activated solution was then added to the reaction vessel and stirred for ~12 hours overnight. The solution was removed by vacuum and the resin was washed with dimethylformamide (1 min, 3 times), CH_2Cl_2 (1 min, 3 times) and dimethylformamide (1 min, 3 times). 20 % (v/v) piperidine in dimethylformamide was added to the resin, stirred for 1 h, and then the solution was drained. The process of washing

the resin and the amino acid coupling was repeated until the desired sequence of peptide was achieved. When the peptide coupling is completed, the resin was washed with dimethylformamide (1 min, 4 times), CH_2Cl_2 (1 min, 4 times). The desired product was cleaved from the resin by treating a mixture of trifluoroacetic acid(TFA), 2,2,2-trifluoroethanol(TFE), and CH_2Cl_2 (9:1:1 volume ratio) for 30 min twice. For compound **19**, cleavage took 12 h. The cleavage solution was then collected and concentrated in vacuo. The crude mixture was dissolved in MilliQ water and purified by reverse-phase HPLC. Purified products (**17**-**19**) were analyzed by MALDI-MS and analytical reverse-phase HPLC for the purity.

Fluorescence-quenching experiment

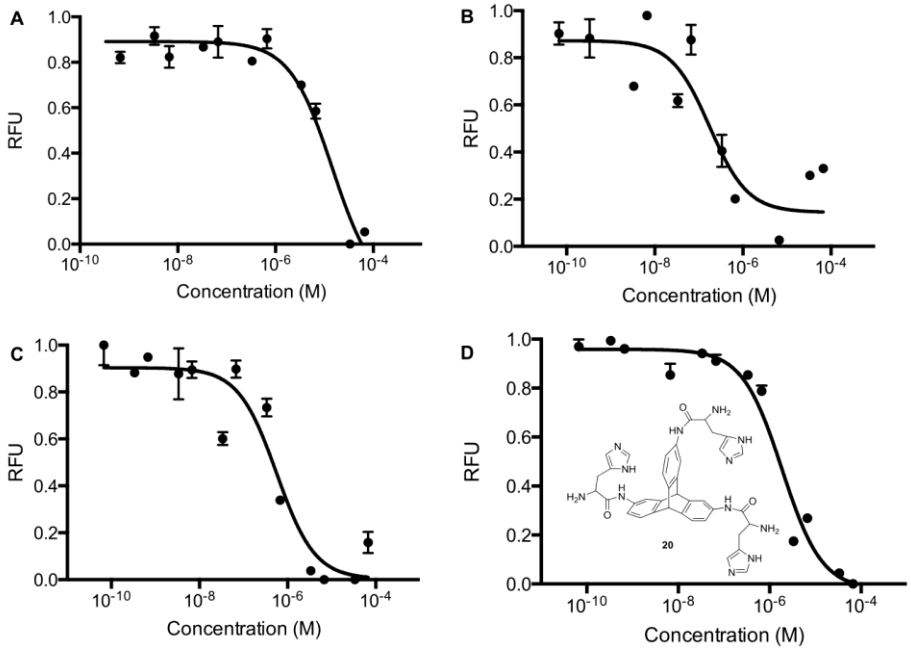

Figure 7.2. Fluorescence-quenching assay for triptycenes **17** (A), **18** (B), **19** (C), and **20*** (D)

*Triptycene **20** is an analogue of triptycene **17** lacking a linker at the C9 position.[5]

Fluorescence-quenching experiments were conducted in 50 mM sodium phosphate buffer, pH 7.2. Inhibitor (I10) strand binding curves were obtained by adding 1 μL of increasing concentrations of I10 to 19 μL of 120 nM FQ-TNR 3WJ. Samples were incubated for 2 hours and ran in triplicate. Inhibitor strand displacement curves with tripycenes were obtained by incubating 14 μL of 120 nM FQ-TNR 3WJ with 1 μL of 150 μM I10 for 2 hours a room temperature. To this complex, 1 μL of increasing concentrations of triptycene was added and incubated for 2 hours. Fluoresence measurements were conducted in a 384-well plate and were recorded with an excitation at 495 nm and emission at 520 nm using 5 nm bandwidths.

7.5 Acknowledgments

This work was supported by funding from the University of Pennsylvania. We thank Pat Carroll (University of Pennsylvania) for X-ray crystallographic assistance. The instruments were supported by the National Science Foundation and the National Institutes of Health including HRMS (Grant NIH RR-023444) and X-ray diffractometer (Grant CHE-0840438). I.Y. is grateful for support from a fellowship from the Kwanjeong Educational Foundation.

7.6 References

(1) (a) Duckett, D. R.; Lilley, D. M. J. *EMBO J.* **1990**, *9*, 1659-1664. (b) Shlyakhtenko, L. S.; Potaman, V. N.; Sinden, R. R.; Gall, A. A.; Lyubchenko, Y. L. *Nucleic Acids Res.* **2000**, *28*, 3472-3477. (c) Lilley, D. M. J. *Q. Rev. Biophisics* **2000**, *33*, 109-159.

(2) (a) Tor, Y. *ChemBioChem* **2003**, *4*, 998-1007. (b) Thomas, J. R.; Hergenrother, P. J. *Chem. Rev.* **2008**, *108*, 1171-1224. (c) Blond, A.; Ennifar, E.; Tisné, C.; Micouin, L. *ChemMedChem* **2014**, *9*, 1982-1996.

(3) Guan, L.; Disney, M. D. *ACS Chem. Biol.* **2012**, *7*, 73-86.

(4) Barros, S. A.; Chenoweth, D. M. *Angew. Chem. Int. Ed.* **2014**, *53*, 13746-13750.

(5) Barros, S. a; Chenoweth, D. M. *Chem. Sci.* **2015**, *6*, 4752-4755.

(6) (a)Boas, U.; Brask, J.; Jensen, K. J. *Chem. Rev.* **2009**, *109*, 2092-2118. (b) Guillier, F.; Orain, D.; Bradley, M. *Chem. Rev.* **2000**, *100*, 2091-2158.

(7) (a) Bartlett, P. D.; Cohen, S. G.; Cotman, J. D.; Kornblum, N.; Landry, J. R.; Lewis, E. S. *J. Am. Chem. Soc.* **1950**, *72*, 1003-1004. (b) Bartlett, P. D.; Lewis, E. S. *J. Am. Chem. Soc.* **1950**, *72*, 1005-1009.

(8) (a) Swager, T. M. *Acc. Chem. Res.* **2008**, *41*, 1181-1189. (b) Chong, J. H.; MacLachlan, M. J. *Chem. Soc. Rev.* **2009**, *38*, 3301-3315.

(9) Ng, K.-K. D.; Hart, H. *Tetrahedron* **1995**, *51*, 7883-7906.

(10) (a) Wang, D.; Mei, T.; Yu, J. *J. Am. Chem. Soc.* **2008**, *130*, 17676-17677. (b) Zhang, Y.; Zhao, H.; Zhang, M.; Su, W. *Angew. Chem. Int. Ed.* **2015**, *54*, 3817-3821. (c) Wang, D.-H.; Engle, K. M.; Shi, B.-F.; Yu, J.-Q. *Science* **2010**, *327*, 315-320.

(11) Harsanyi, M. C.; Norris, R. K.; Sze, G.; Witting, P. K. *Aust. J. Chem.* **1995**, *48*, 1949-1967.

(12) (a) Klanderman, B. H.; Perkins, W. C. *J. Org. Chem.* **1969**, *34*, 630-633. (b) Chong, J. H.; MacLachlan, M. J. *J. Org. Chem.* **2007**, *72*, 8683-8690. (c) Chong, J. H.; MacLachlan, M. J. *Inorg. Chem.* **2006**, *45*, 1442-1444. (d) Zhang, C.; Chen, C.-F. *J. Org. Chem.* **2006**, *71*, 6626-6629. (e) Ma, Y.-X.; Meng, Z.; Chen, C.-F. *Synlett* **2015**, *26*, 6-30.

(13) Xu, M.-L.; Huang, W. *Synth. Commun.* **2014**, *44*, 3435-3440.

(14) Nicolaou, K. C.; Baran, P. S.; Zhong, Y.-L.; Choi, H.-S.; Yoon, W. H.; He, Y.; Fong, K. C. *Angew. Chem. Int. Ed.* **1999**, *38*, 1669-1675.

(15) (a) Friede, M.; Denery, S.; Neimark, J.; Kieffer, S.; Gausepohl, H.; Briand, J. P. *Pept. Res.* **1992**, *5*, 145-147. (b) Quesnel, A.; Briand, J. P. *J. Pept. Res.* **1998**, *52*, 107-111.

(16) Fowelin, C.; Schüpbach, B.; Terfort, A. *Eur. J. Org. Chem.,* **2007**, 1013–1017.

(17) Kornfeld, E. C.; Barney, P.; Blankley, J.; Faul, W. *J. Med. Chem.,* **1965**, *8*, 342–347.

(18) Bartlett, P. D.; Greene, F. D. *J. Am. Chem. Soc.,* **1954**, *76*, 1088–1096.

Appendix 6

NMR Spectra, HPLC Diagram, MALDI Spectra, and X-Ray Structure Data Relevant to Chapter 7

Figure A6.1. ^{1}H NMR spectrum of **2** in $CDCl_3$ (500 MHz).

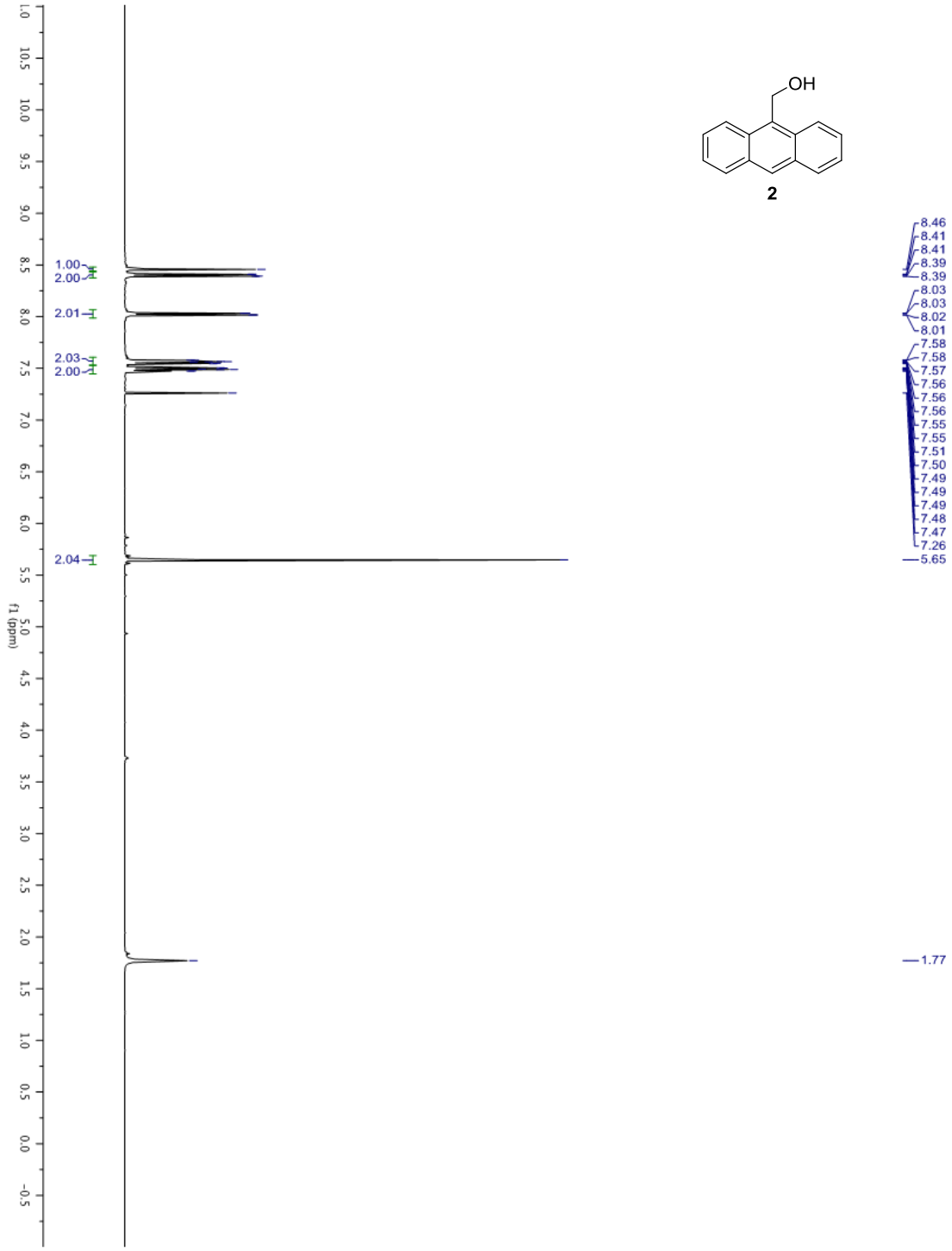

Figure A6.2. ^{1}H NMR spectrum of **3** in $CDCl_3$ (500 MHz).

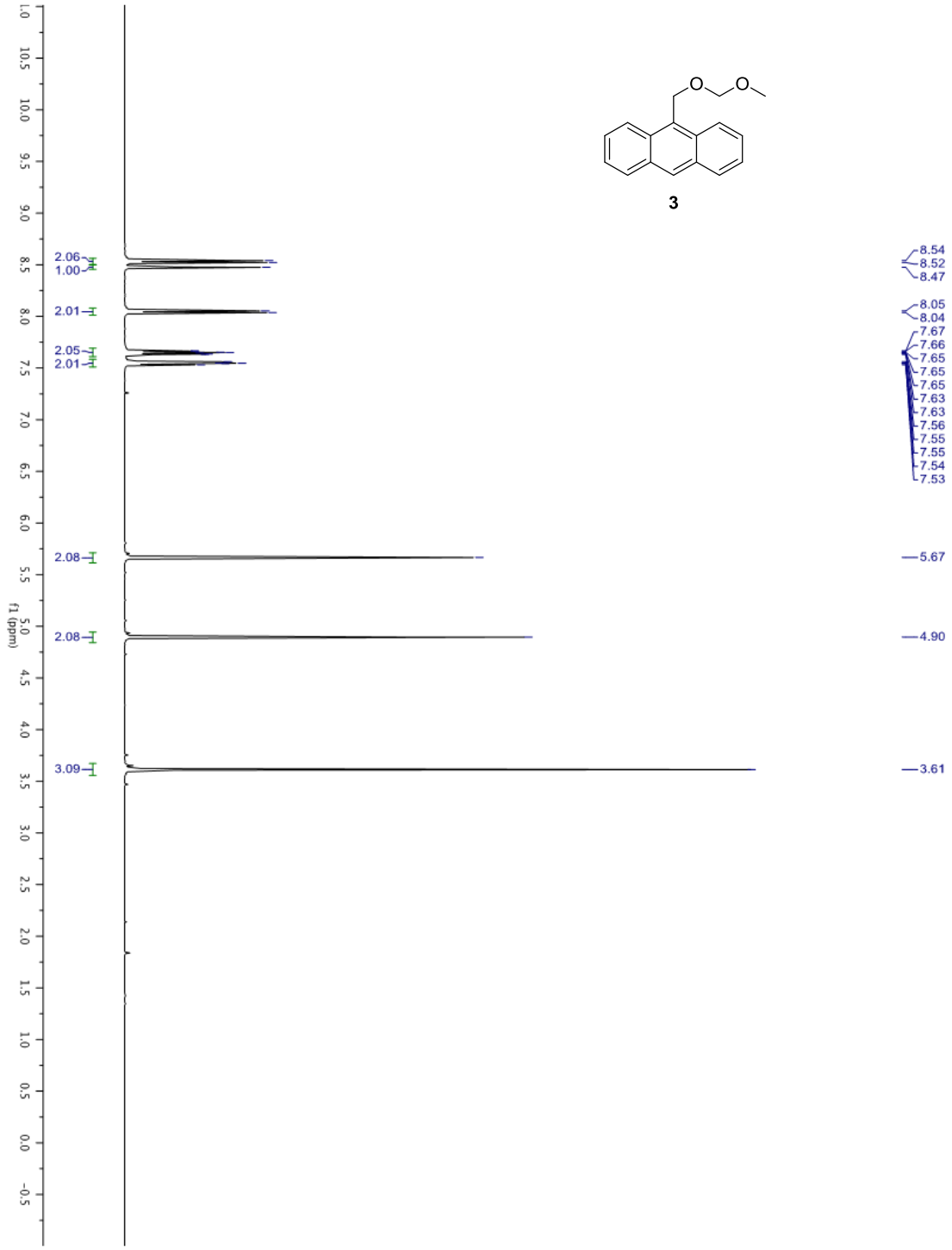

Figure A6.3. ^{13}C NMR spectrum of **3** in $CDCl_3$ (125 MHz).

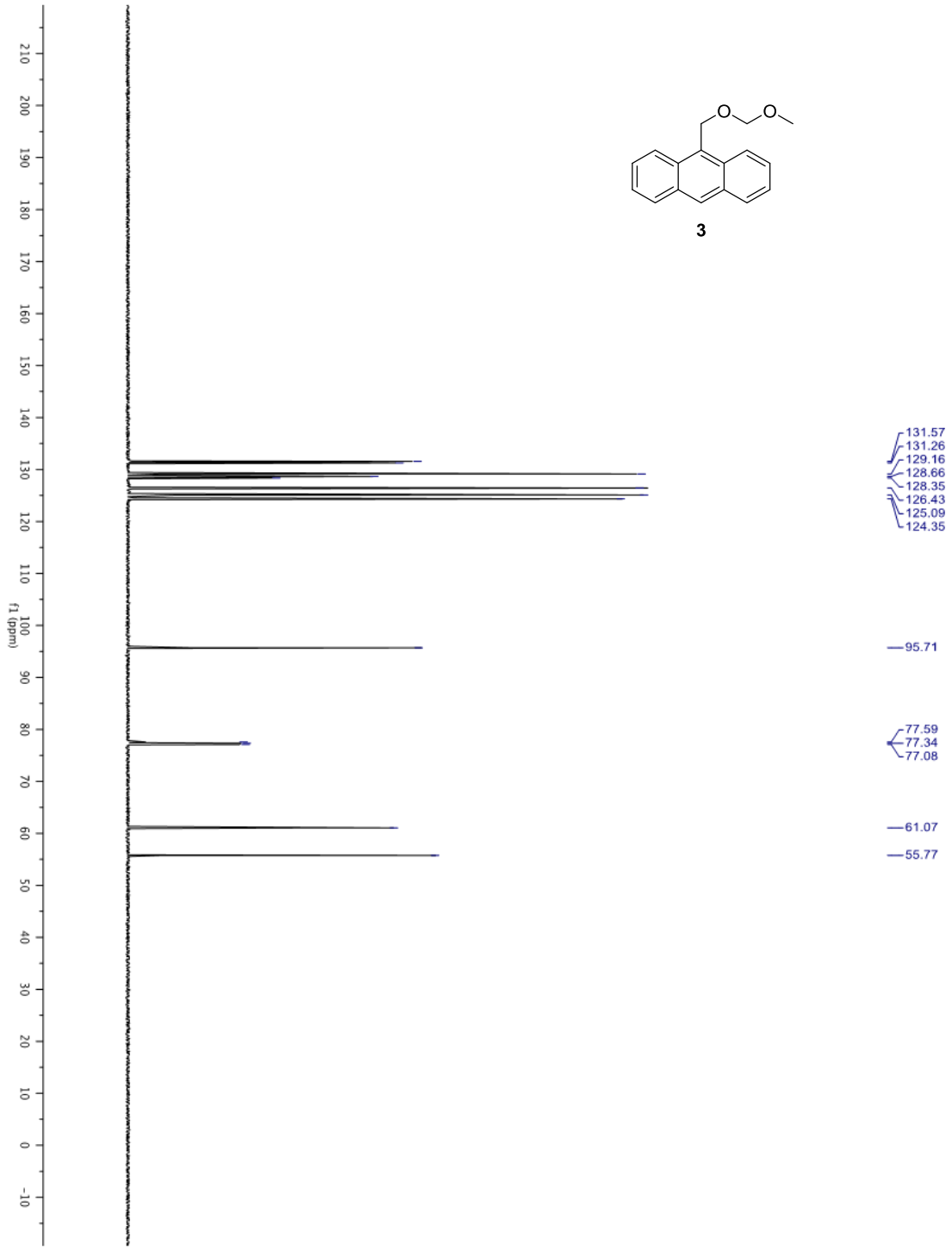

Figure A6.4. ^{1}H NMR spectrum of **4** in $CDCl_3$ (500 MHz).

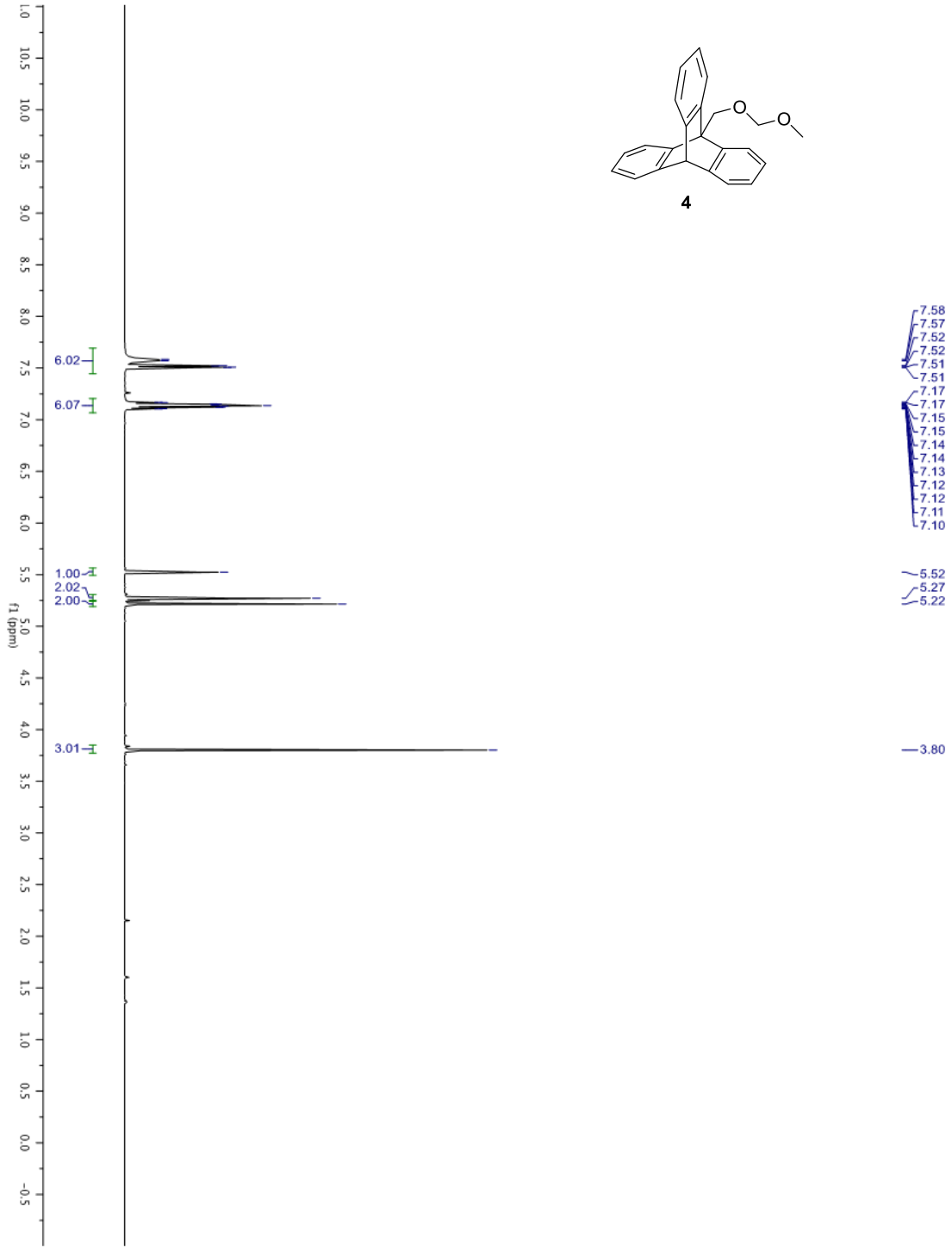

Figure A6.5. ^{13}C NMR spectrum of **4** in $CDCl_3$ (125 MHz).

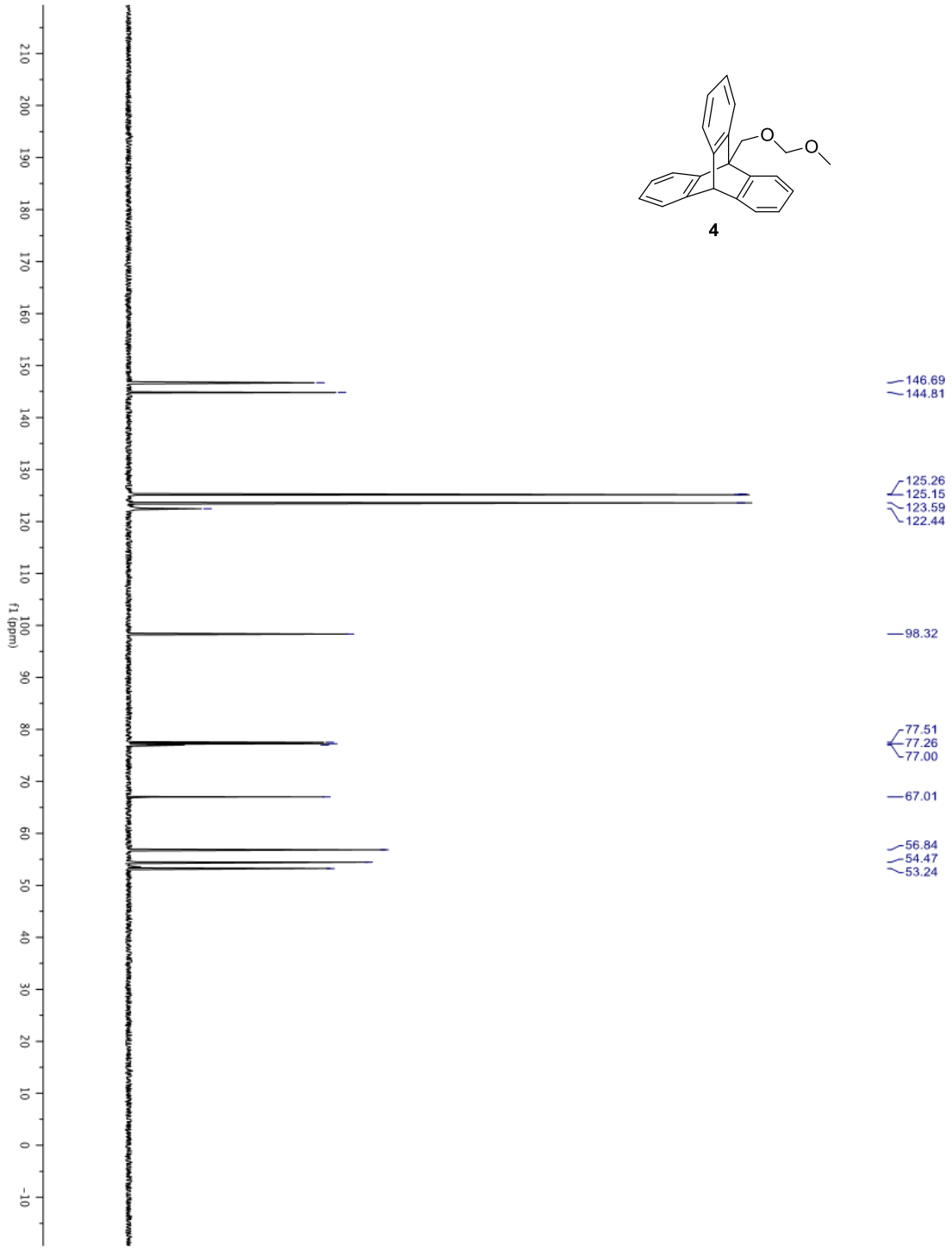

Figure A6.6. ^{1}H NMR spectrum of **5a** in $CDCl_3$ (500 MHz).

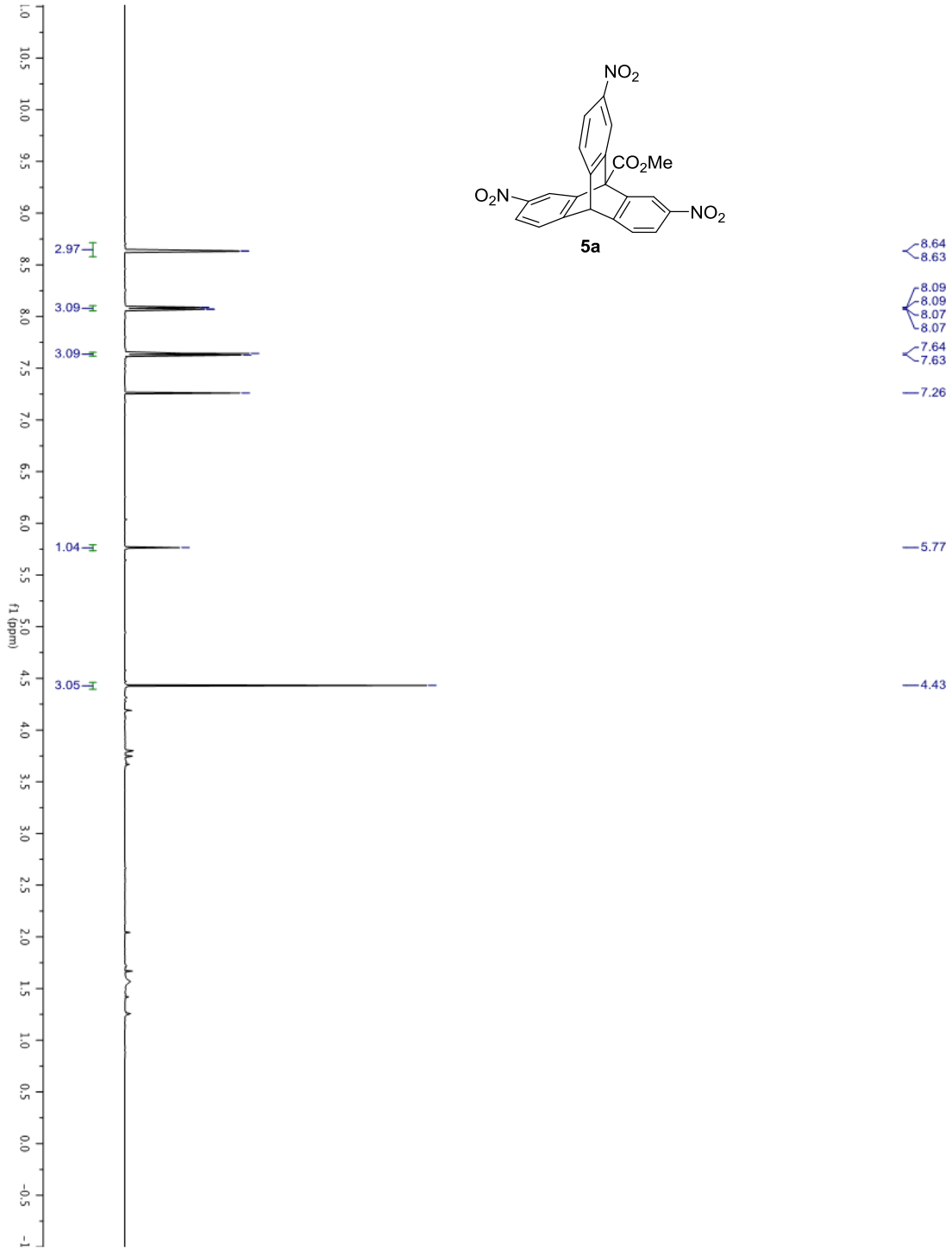

Figure A6.7. ^{13}C NMR spectrum of **5a** in $CDCl_3$ (125 MHz).

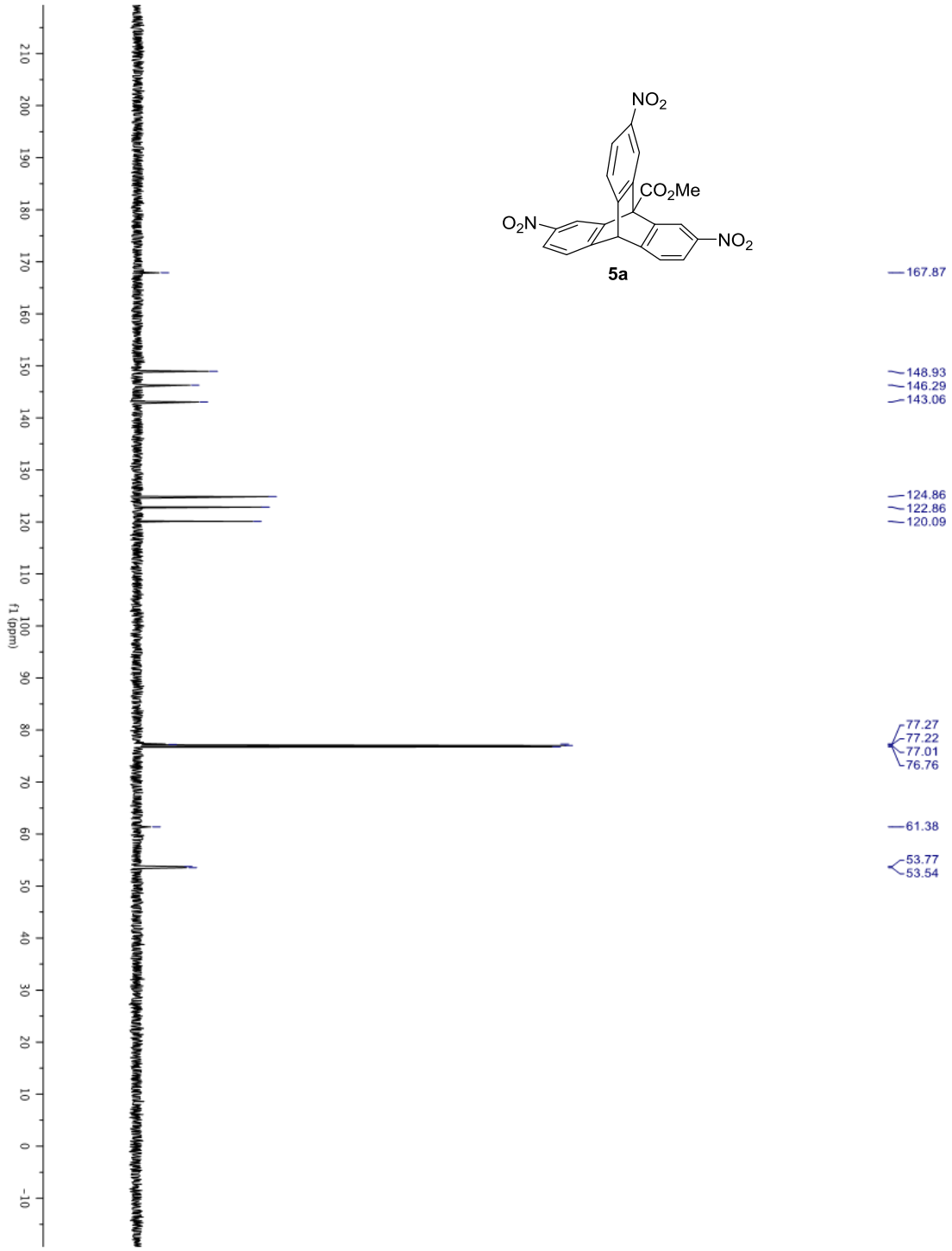

Figure A6.8. HSQC spectrum of **5a** in $CDCl_3$.

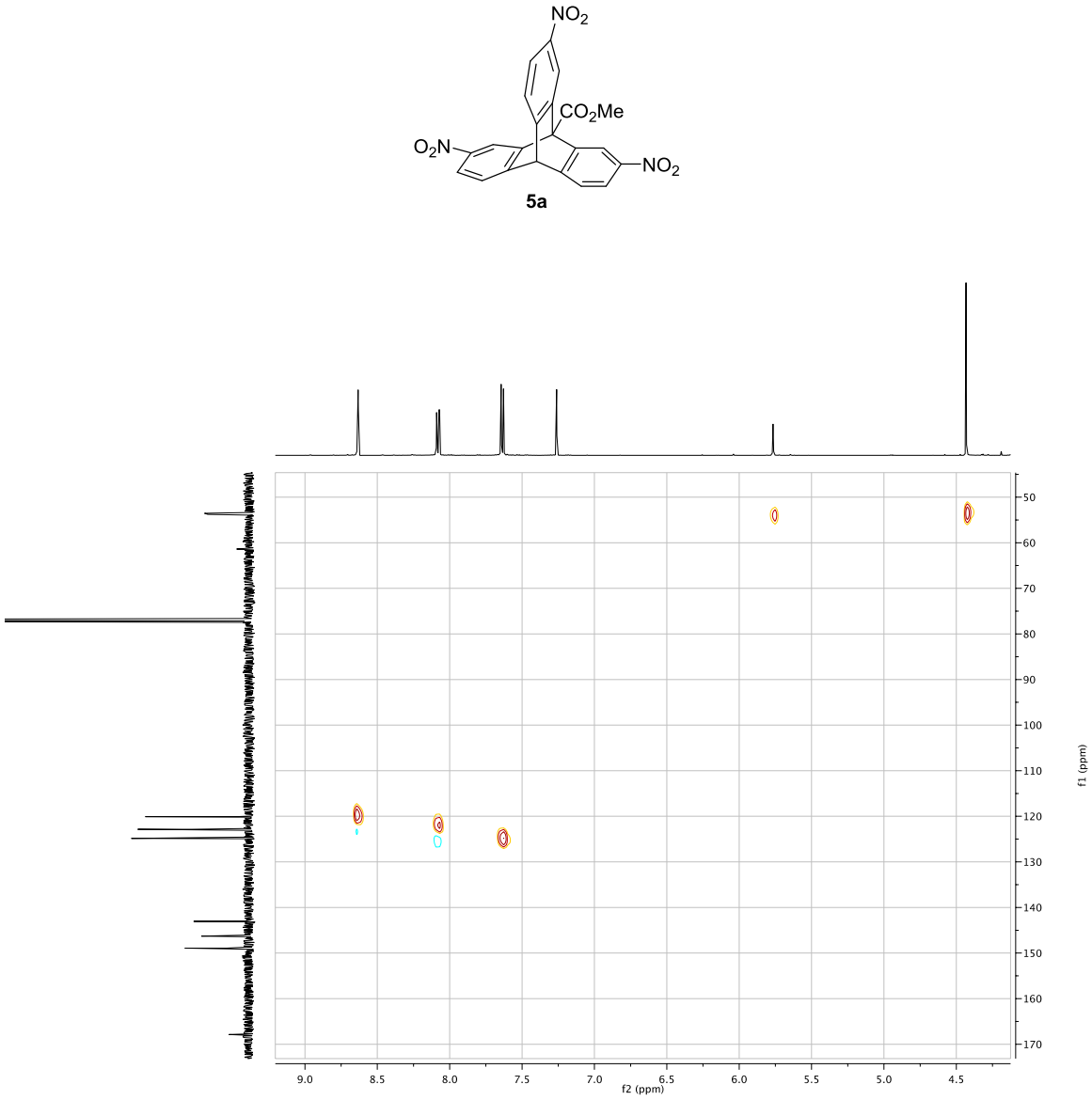

Figure A6.9. HMBC spectrum of **5a** in $CDCl_3$.

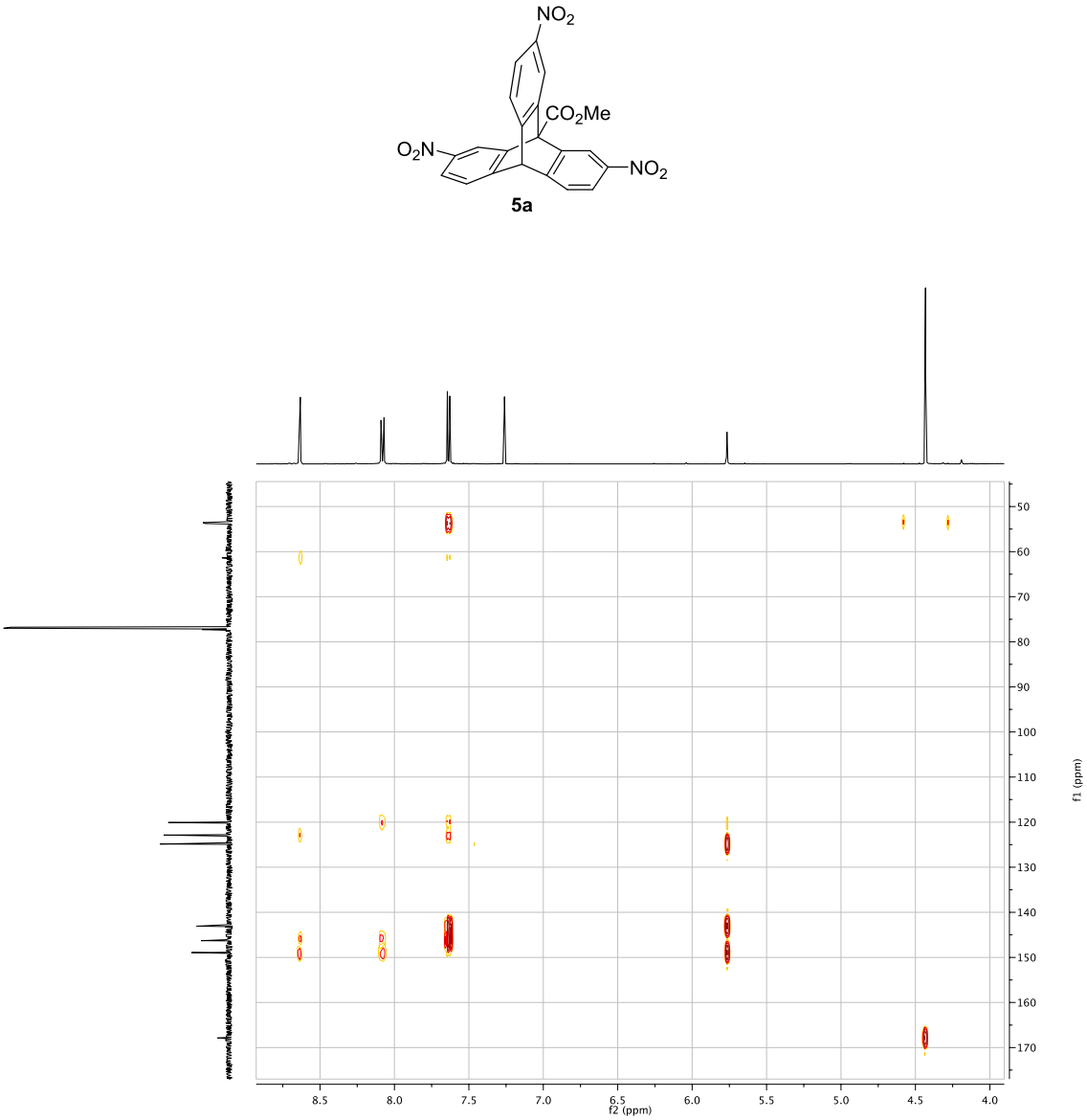

Figure A6.10. ^{1}H NMR spectrum of **5b** in $CDCl_3$ (500 MHz).

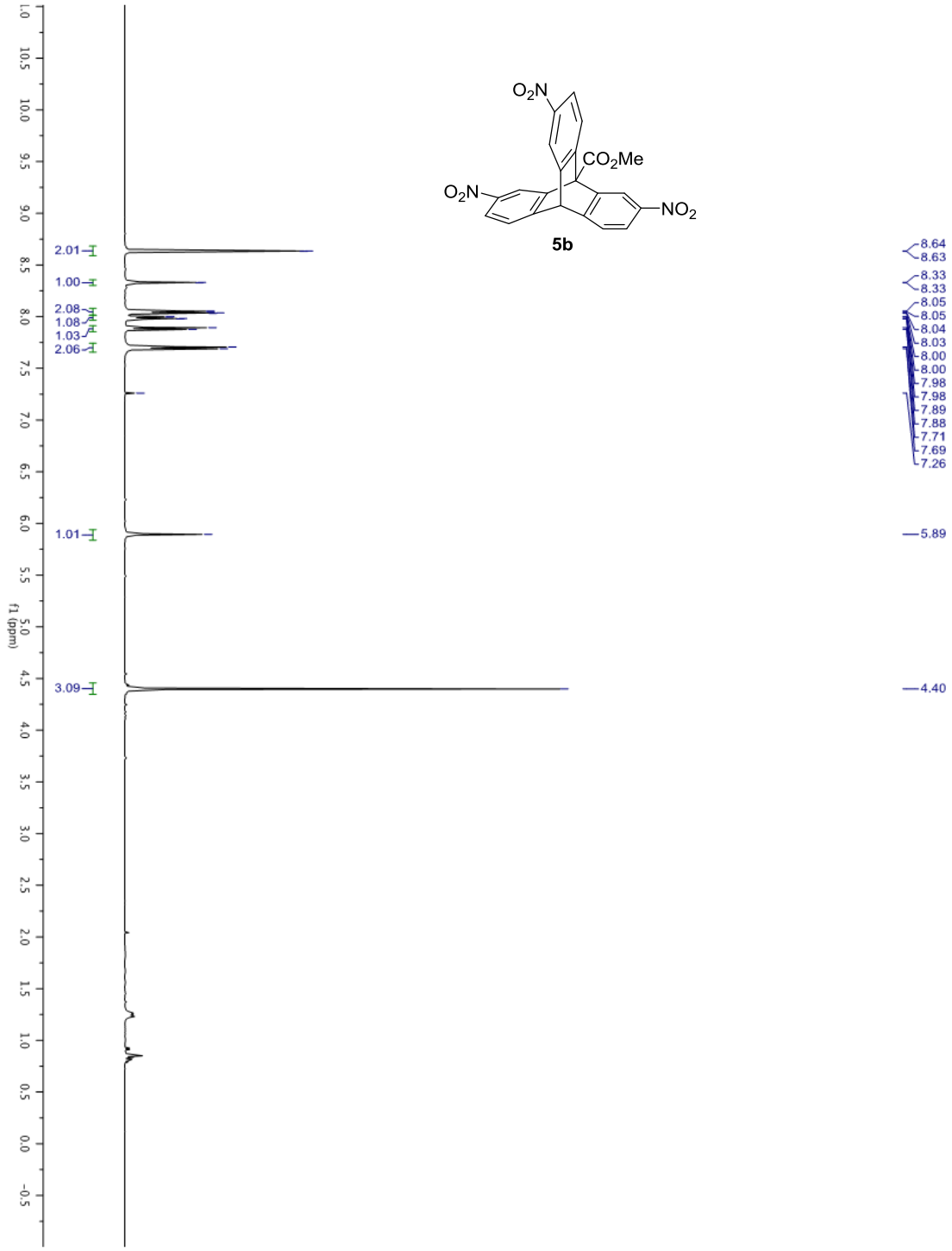

Figure A6.11. ^{13}C NMR spectrum of **5b** in $CDCl_3$ (125 MHz).

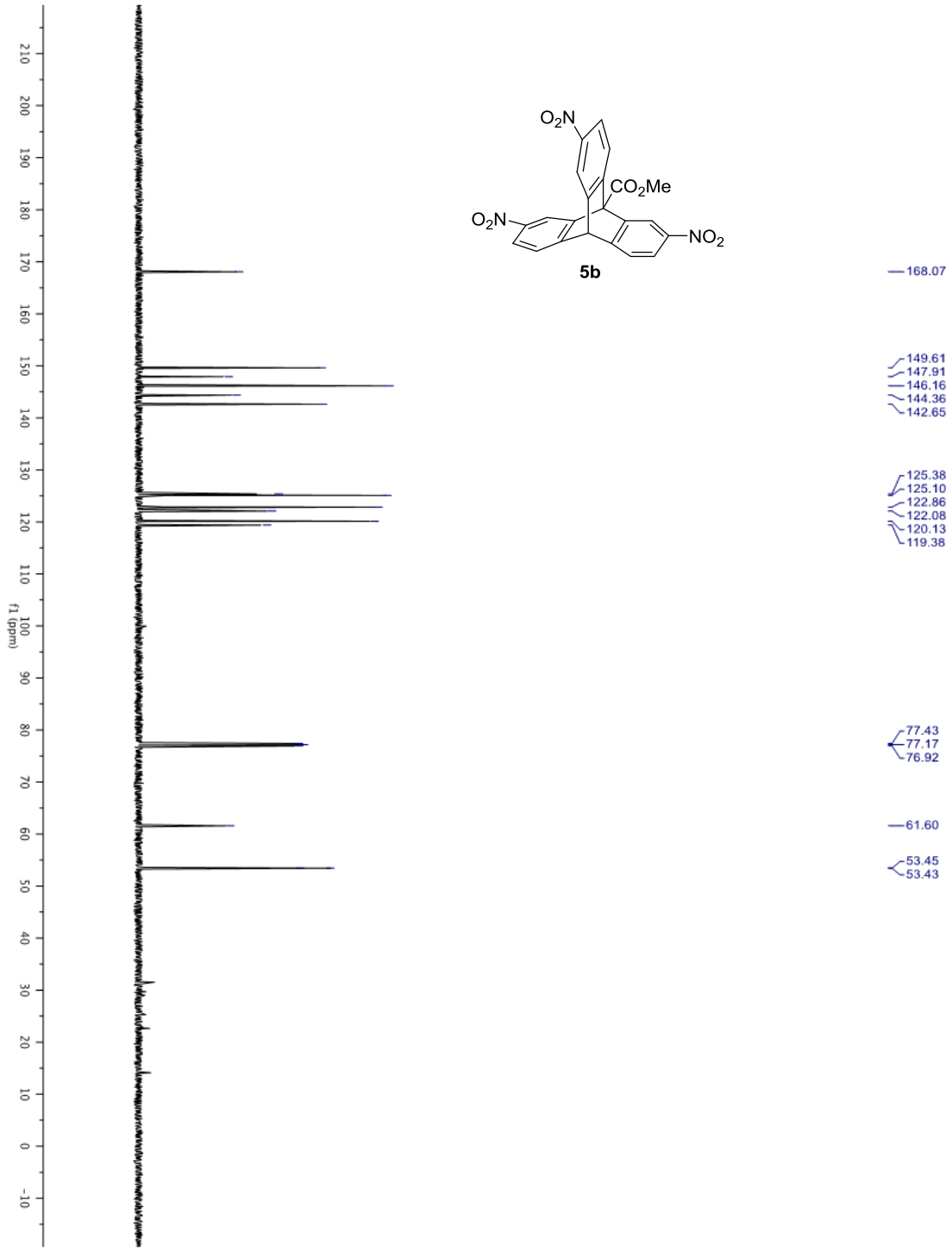

Figure A6.12. HSQC spectrum of **5b** in $CDCl_3$.

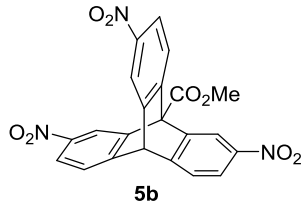

5b

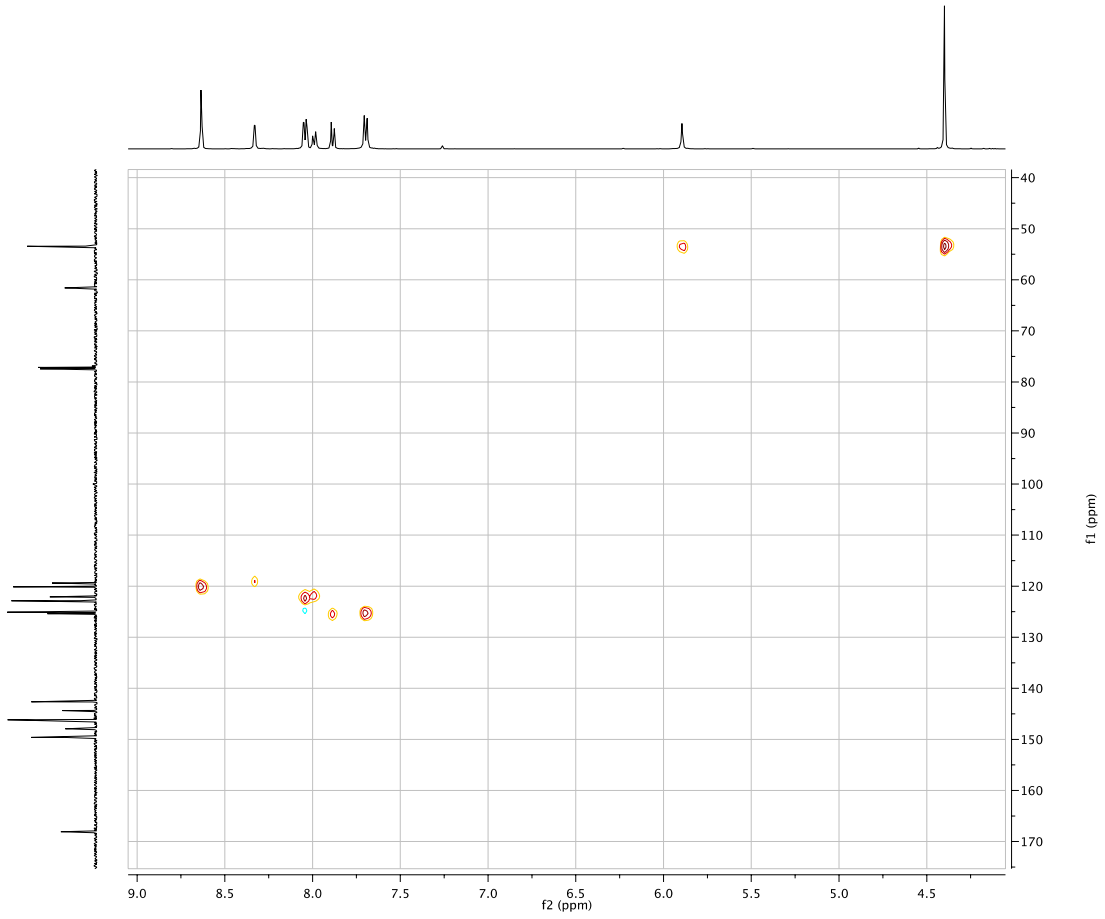

Figure A6.13. HMBC spectrum of **5b** in $CDCl_3$.

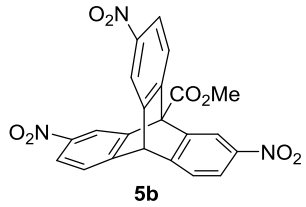

5b

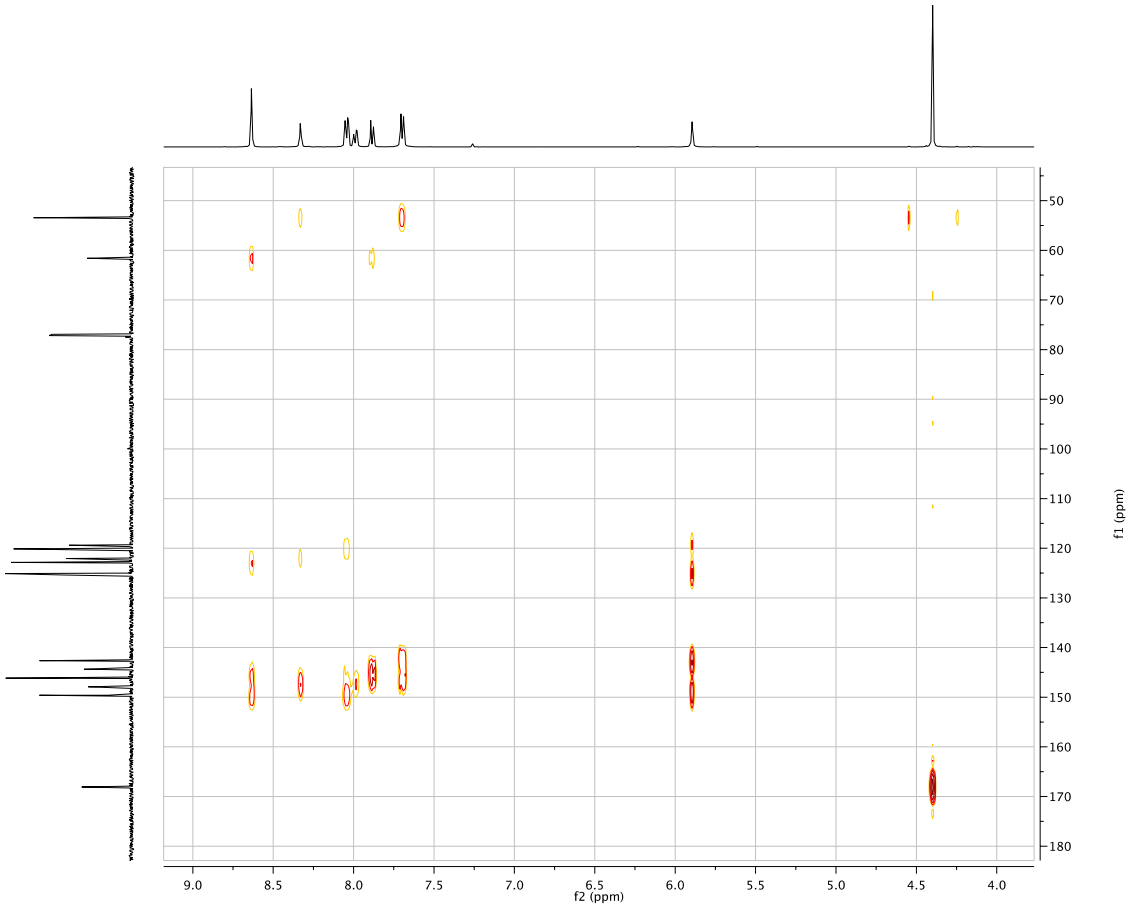

Figure A6.14. ^{1}H NMR spectrum of **5c** in $CDCl_3$ (500 MHz).

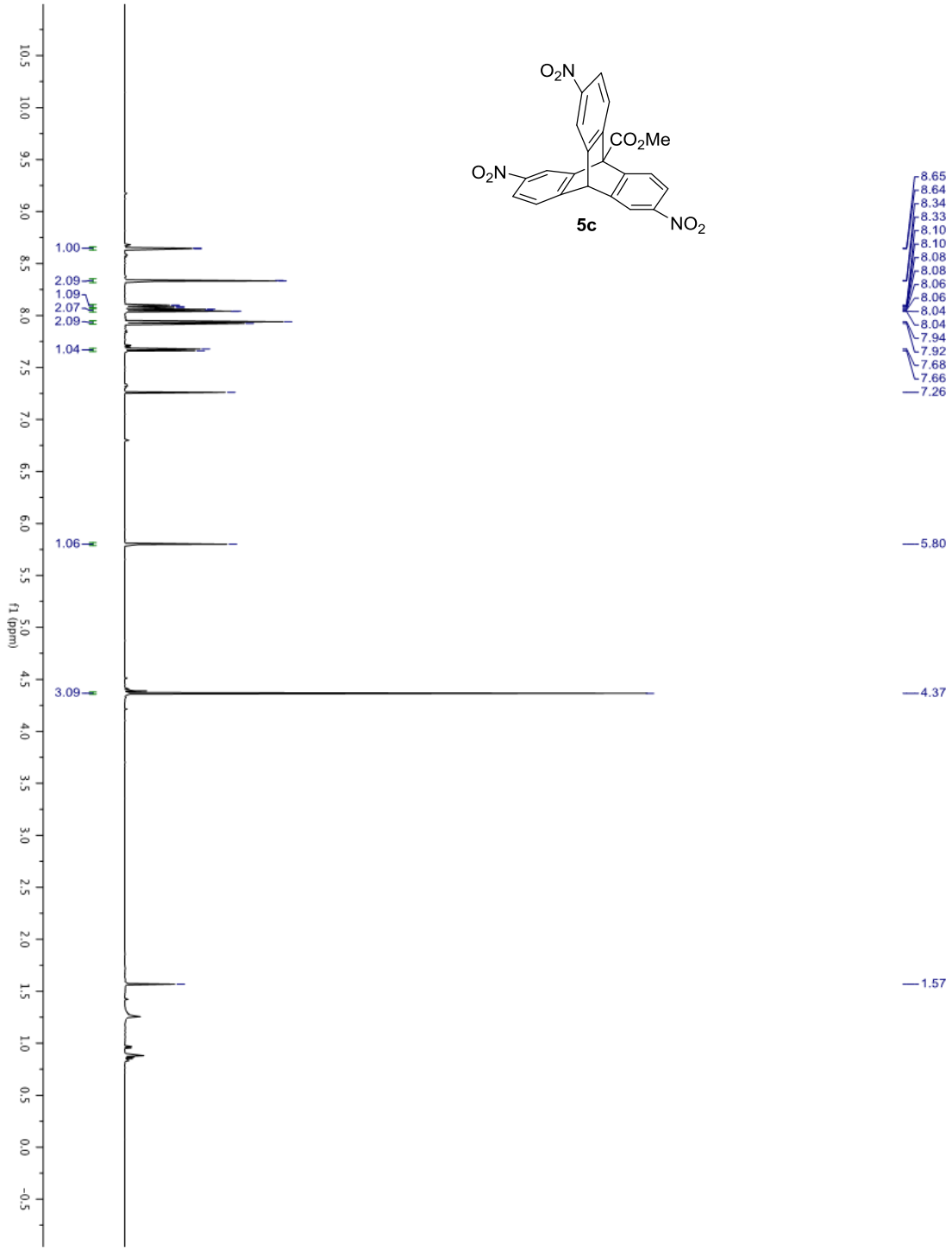

Figure A6.15. ^{13}C NMR spectrum of **5c** in $CDCl_3$ (125 MHz).

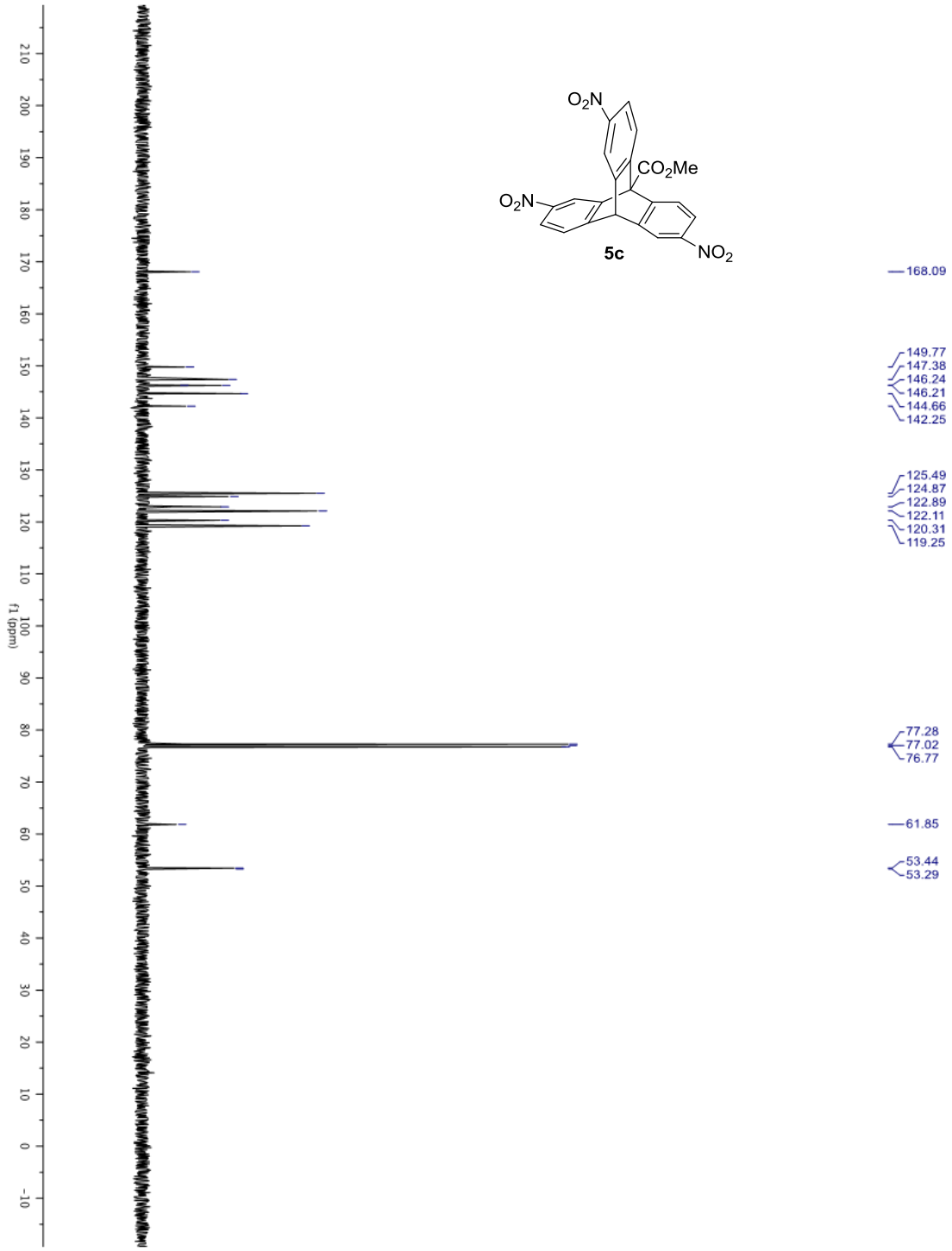

Figure A6.16. HSQC spectrum of **5c** in $CDCl_3$.

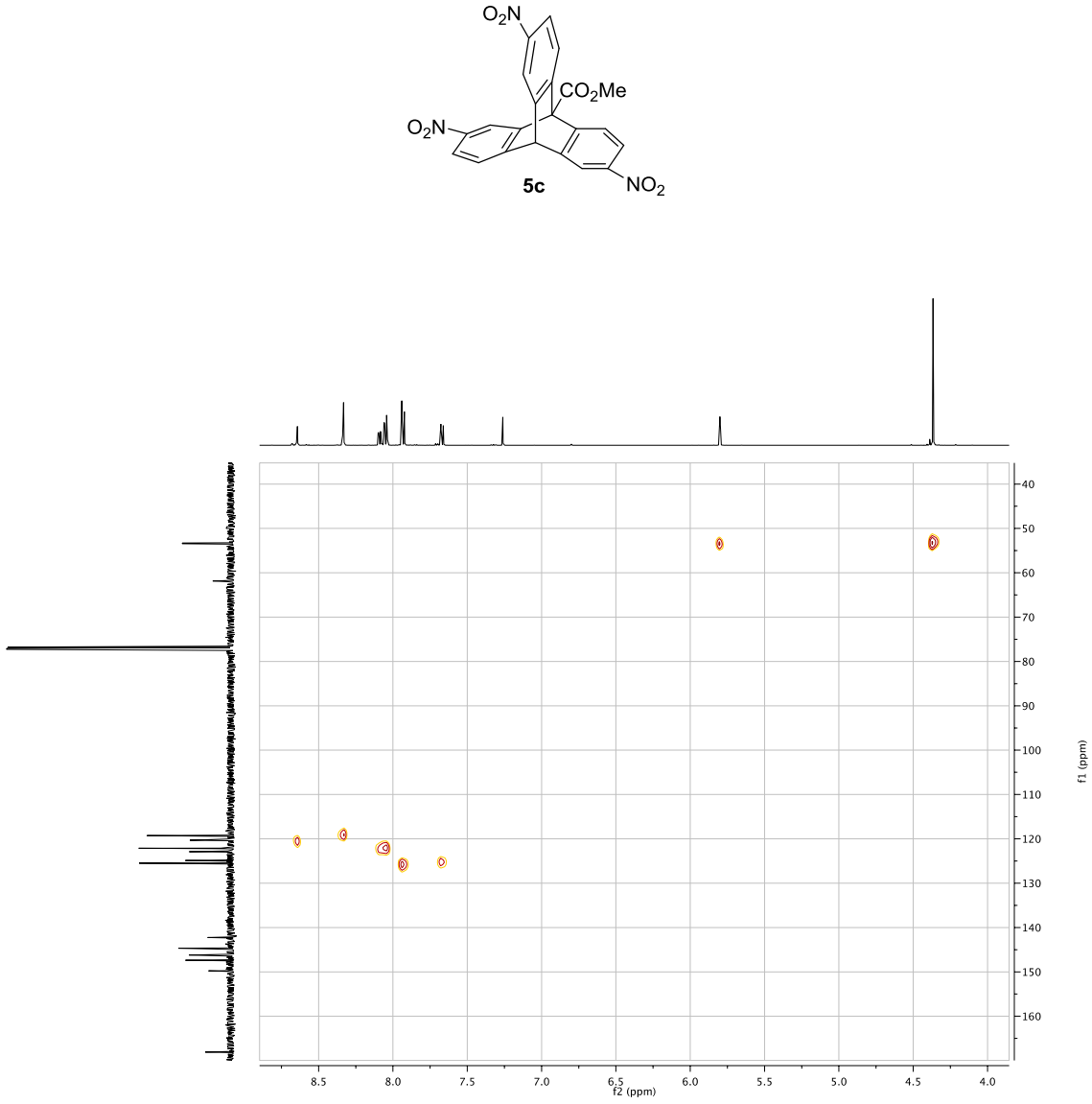

Figure A6.17. HMBC spectrum of **5c** in $CDCl_3$.

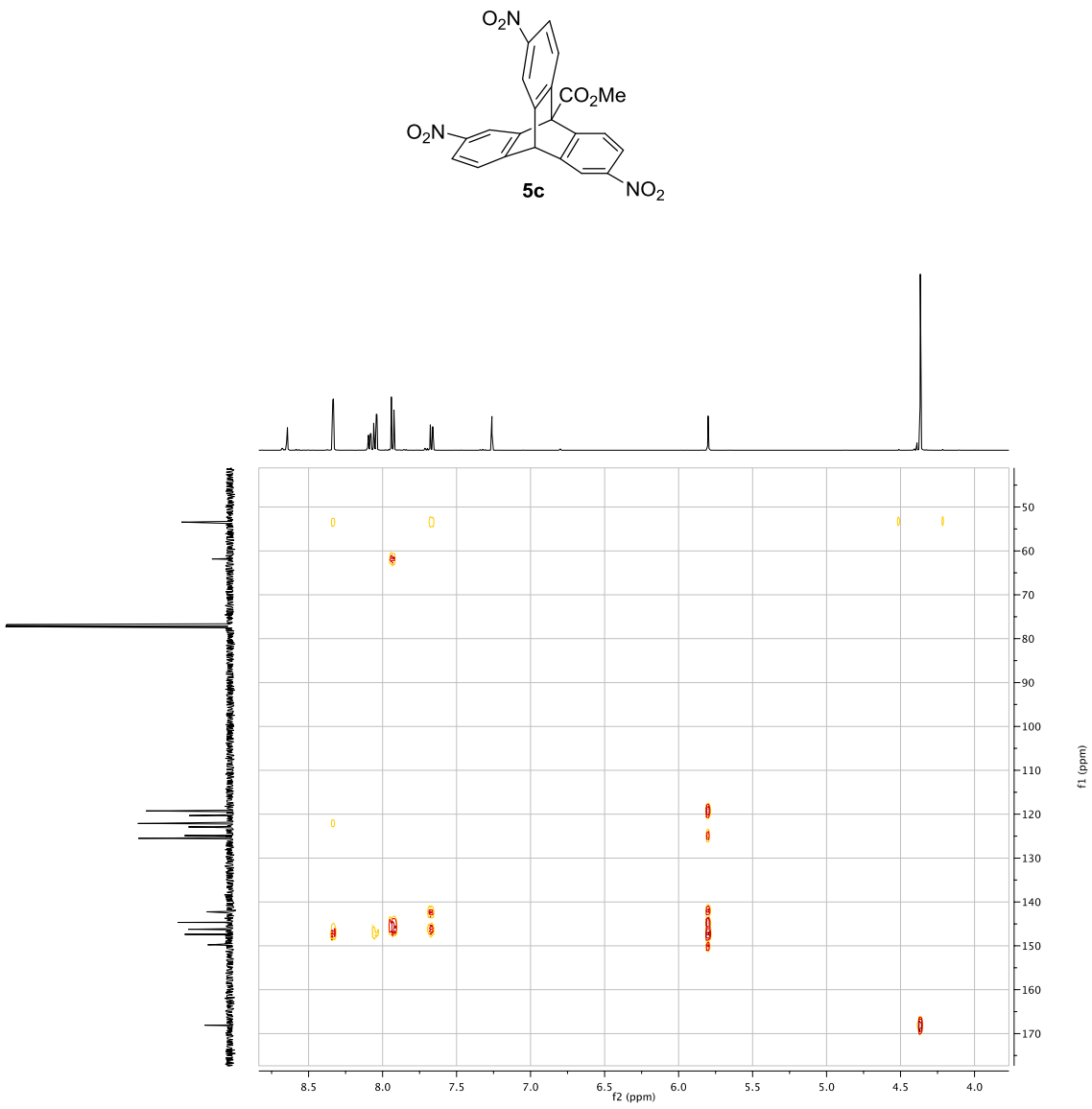

Figure A6.18. ^{1}H NMR spectrum of **6a** in $(CD_3)_2CO$ (500 MHz).

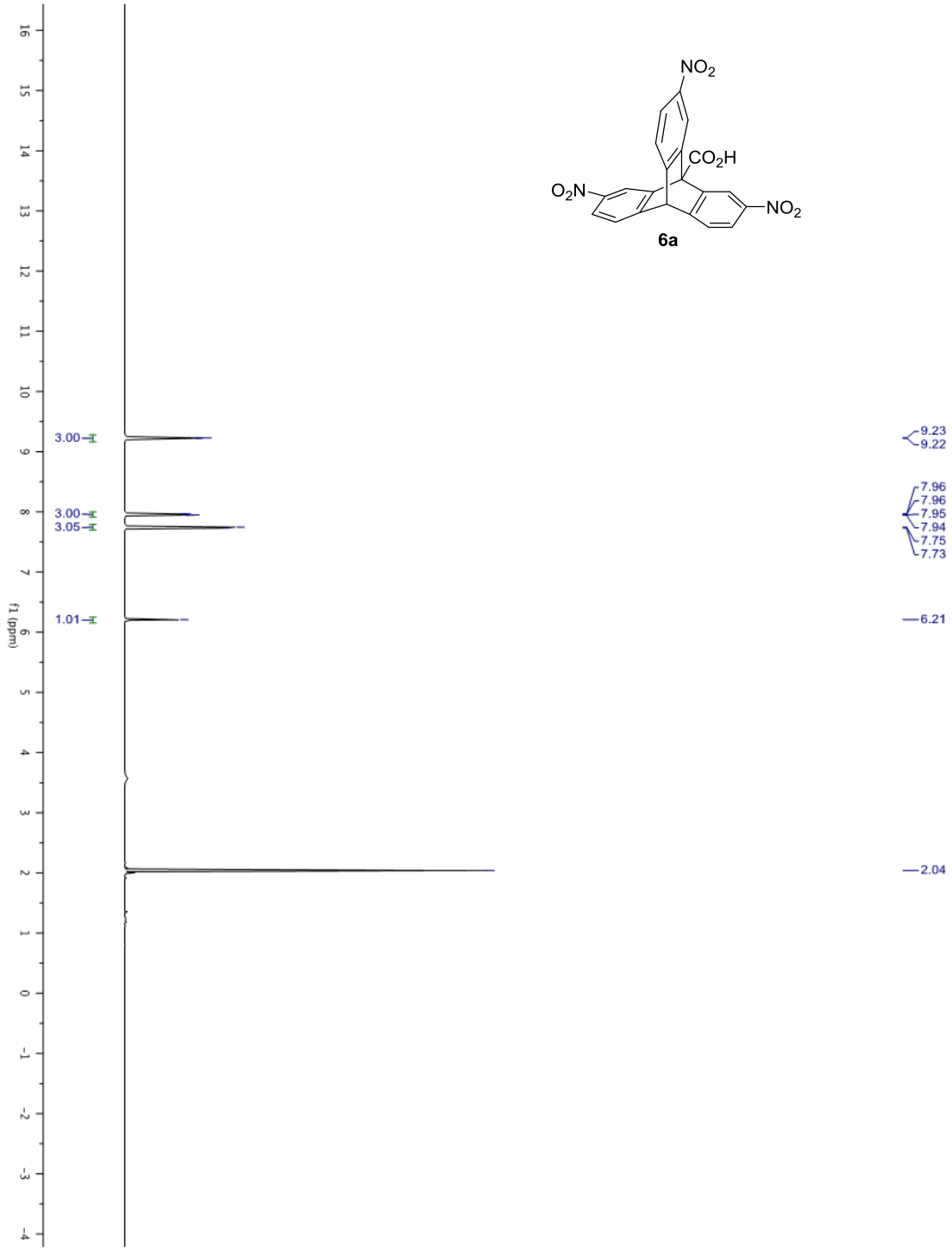

Figure A6.19. ^{13}C NMR spectrum of **6a** in $(CD_3)_2CO$ (125 MHz).

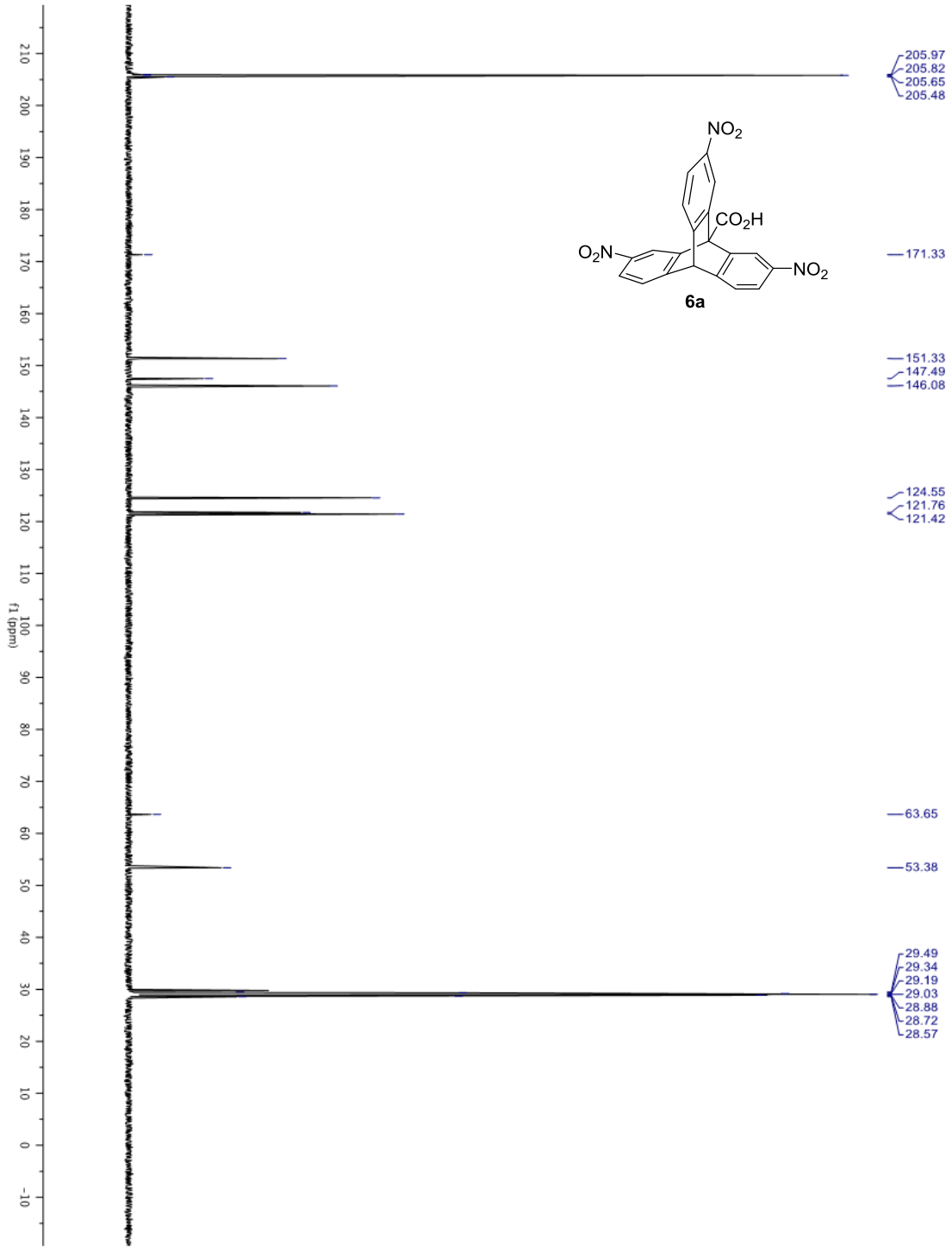

Figure A6.20. HMBC spectrum of **6a** in $(CD_3)_2CO$.

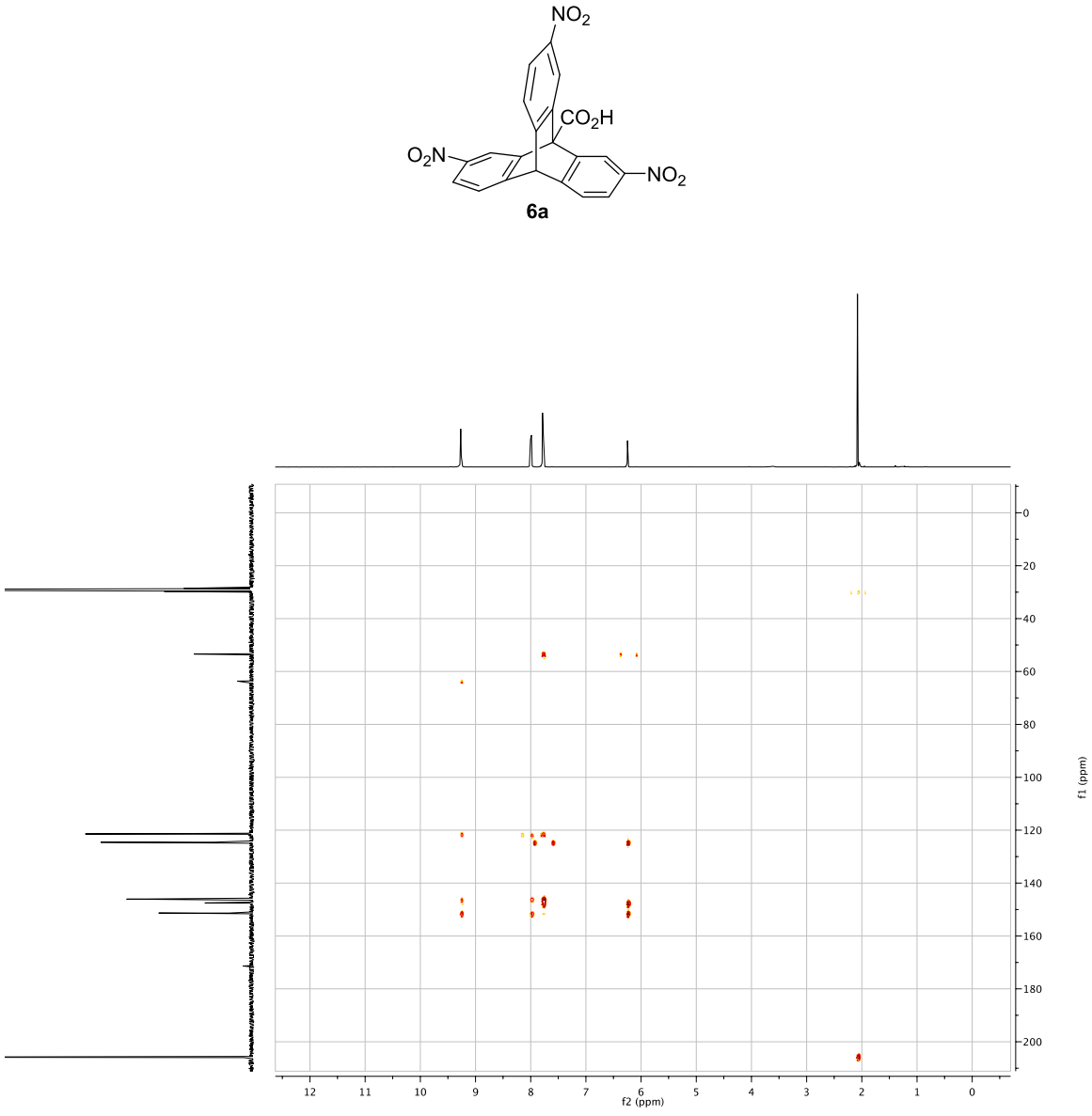

Figure A6.21. Expanded HMBC spectrum of **6a** in $(CD_3)_2CO$.

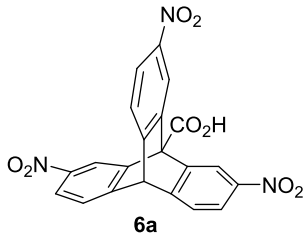

6a

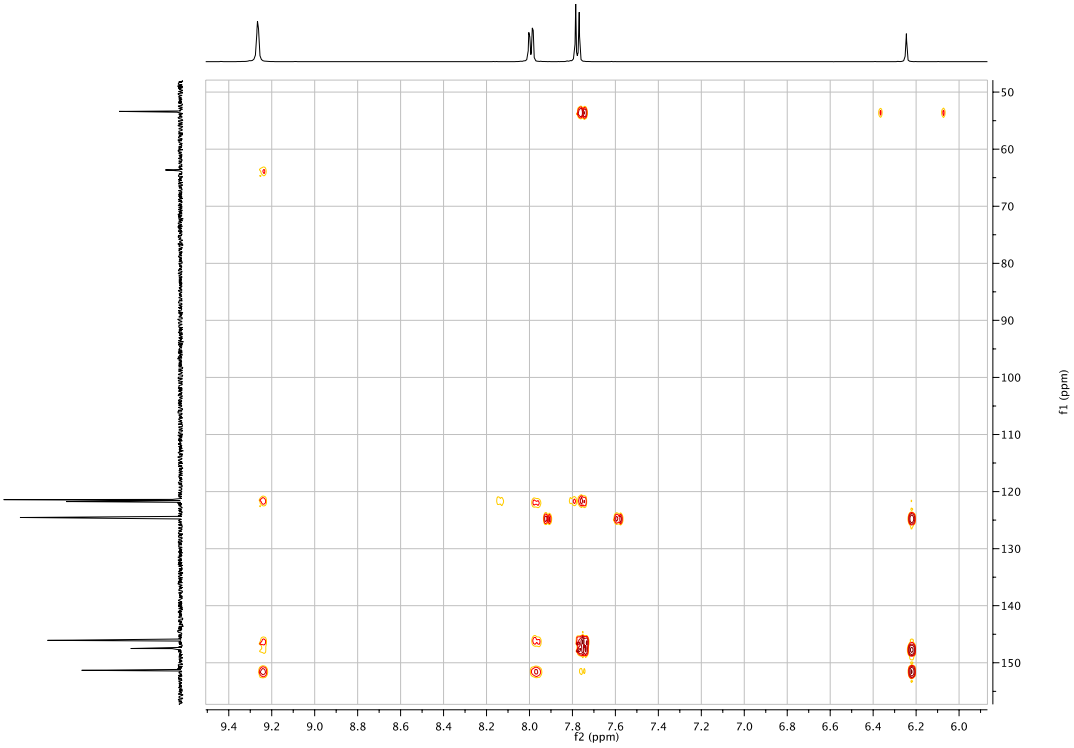

Figure A6.22. ^{1}H NMR spectrum of **6b** in $(CD_3)_2CO$ (500 MHz).

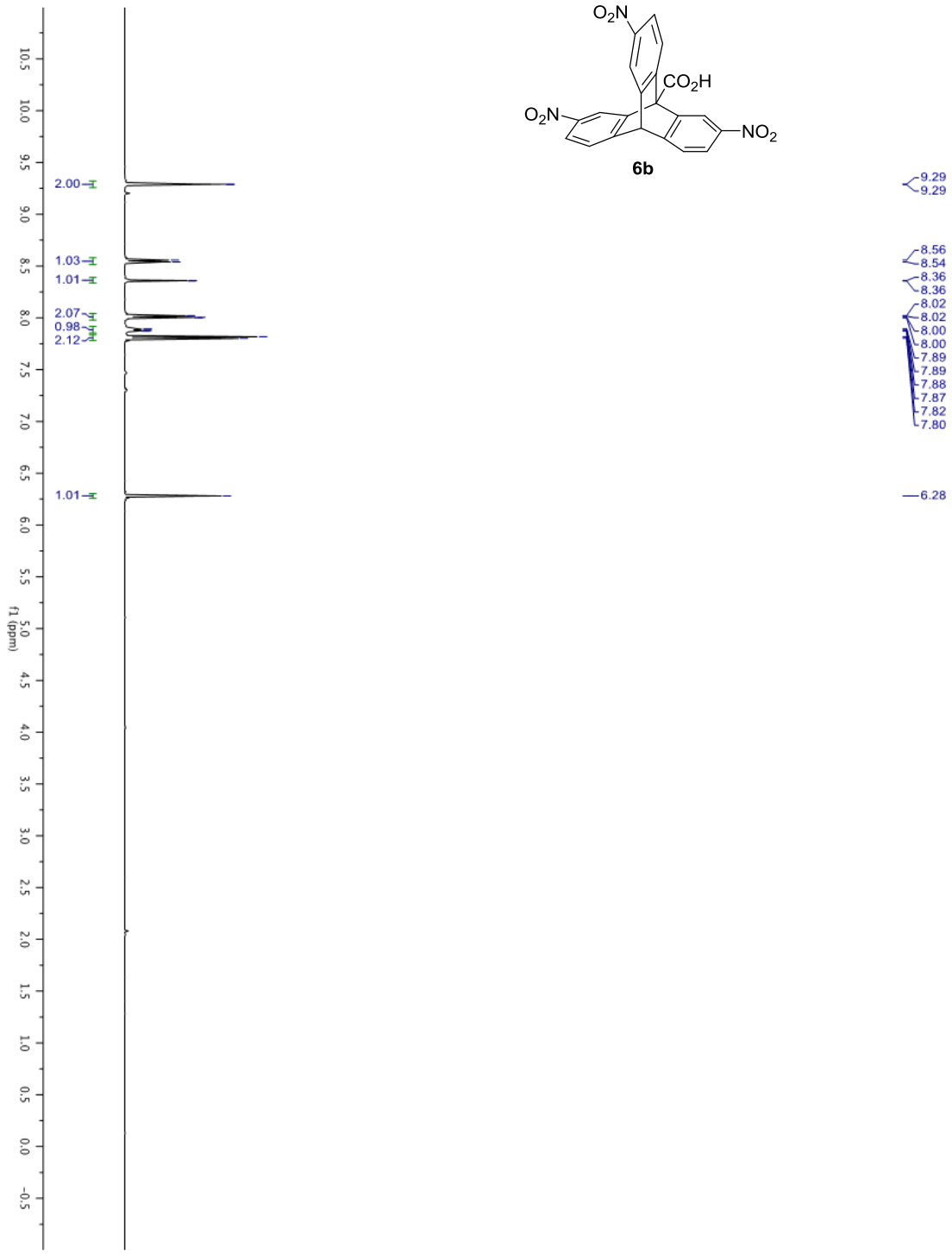

Figure A6.23. ^{13}C NMR spectrum of **6b** in $(CD_3)_2CO$ (125 MHz).

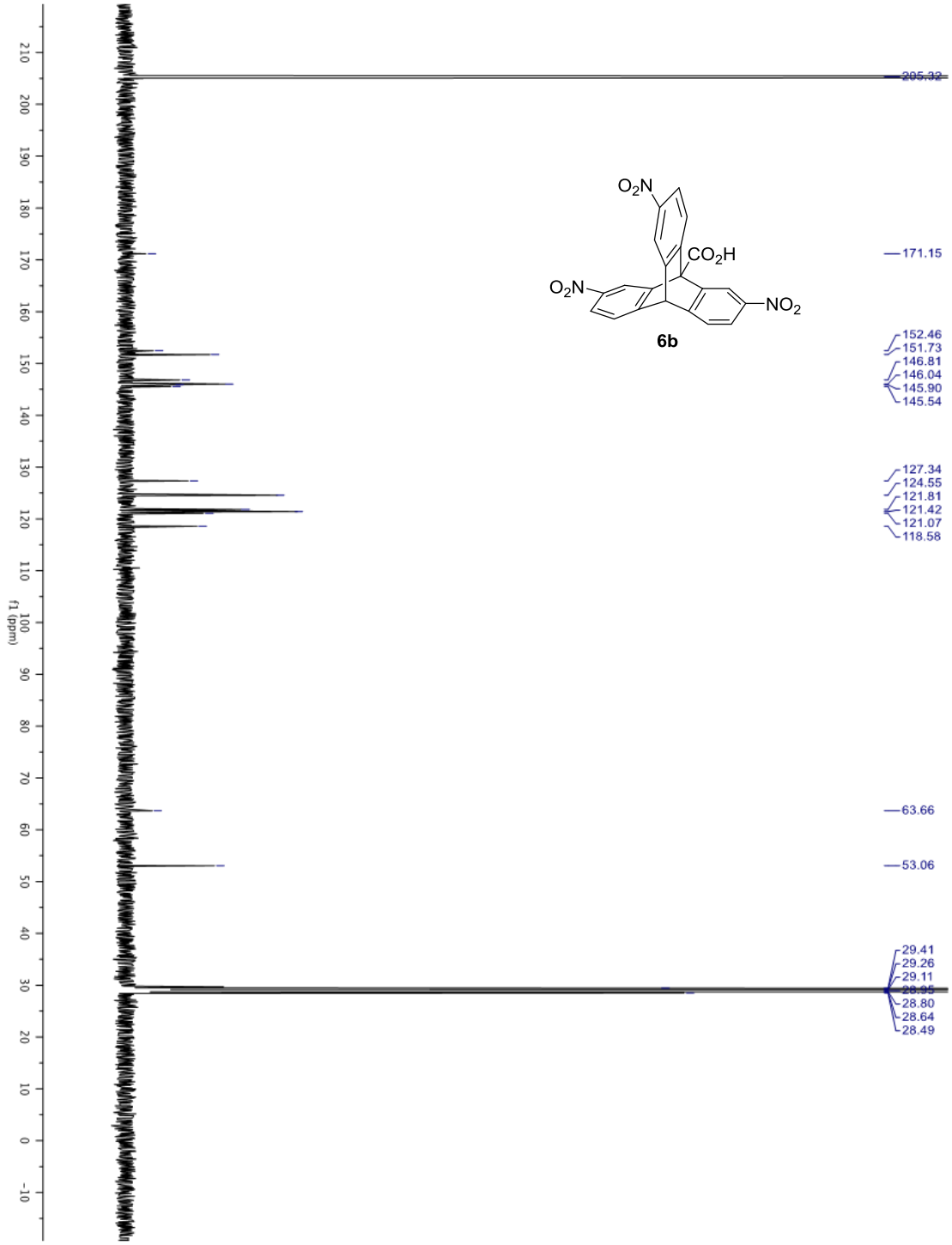

Figure A6.24. ^{1}H NMR spectrum of **6c** in $(CD_3)_2CO$ (500 MHz).

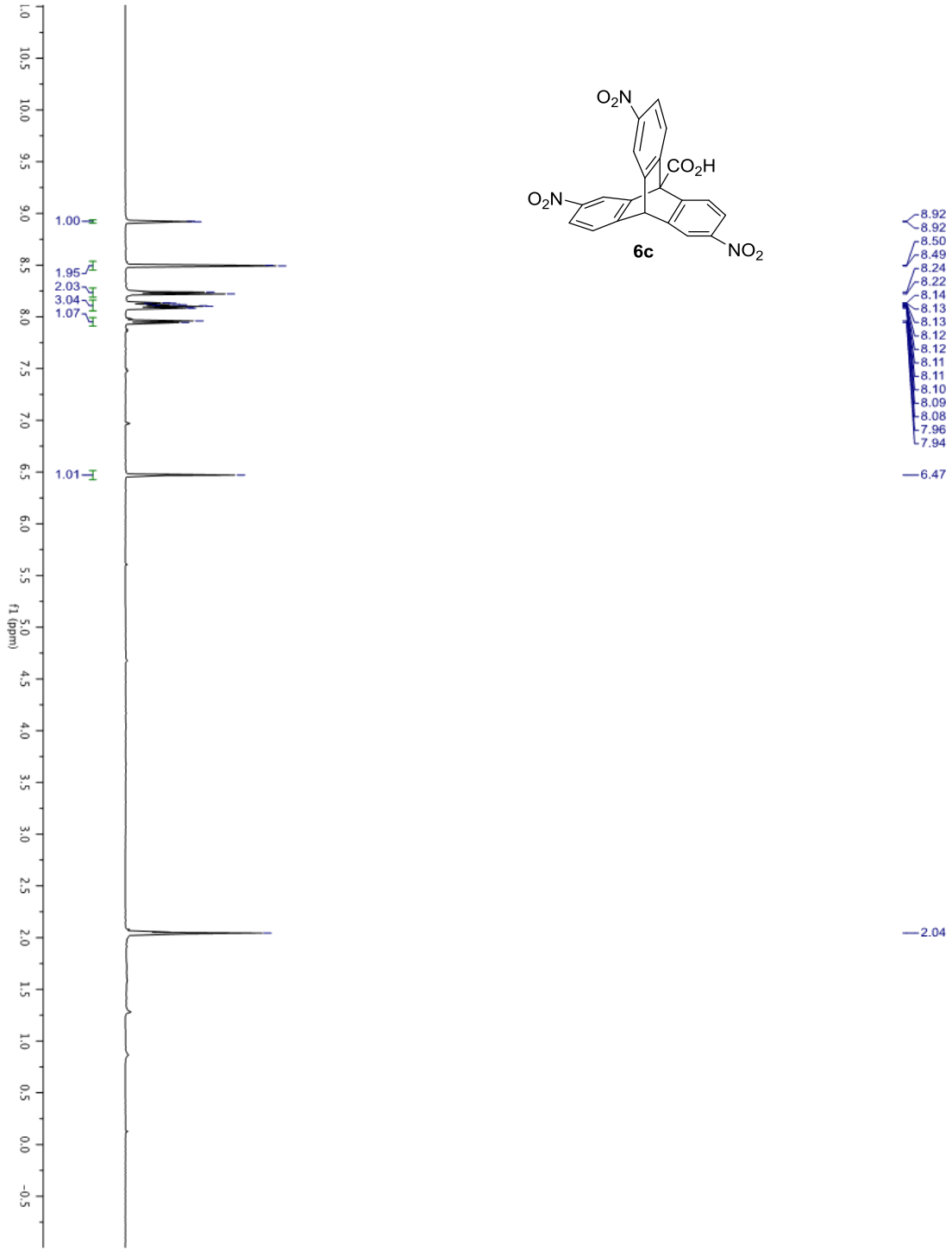

Figure A6.25. ^{13}C NMR spectrum of **6c** in $(CD_3)_2CO$ (125 MHz).

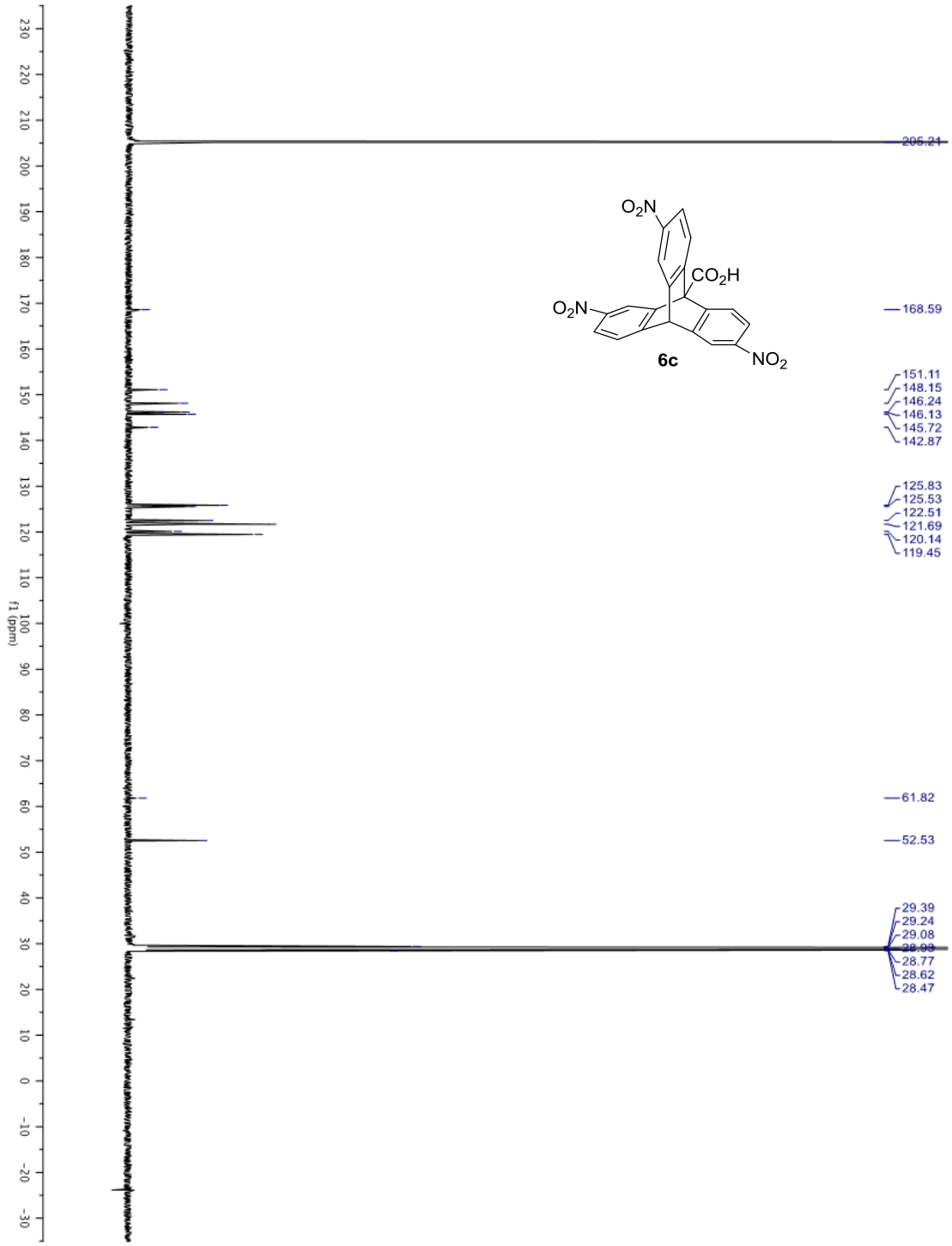

Figure A6.26. ^{1}H NMR spectrum of **7** in $(CD_3)_2CO$ (500 MHz).

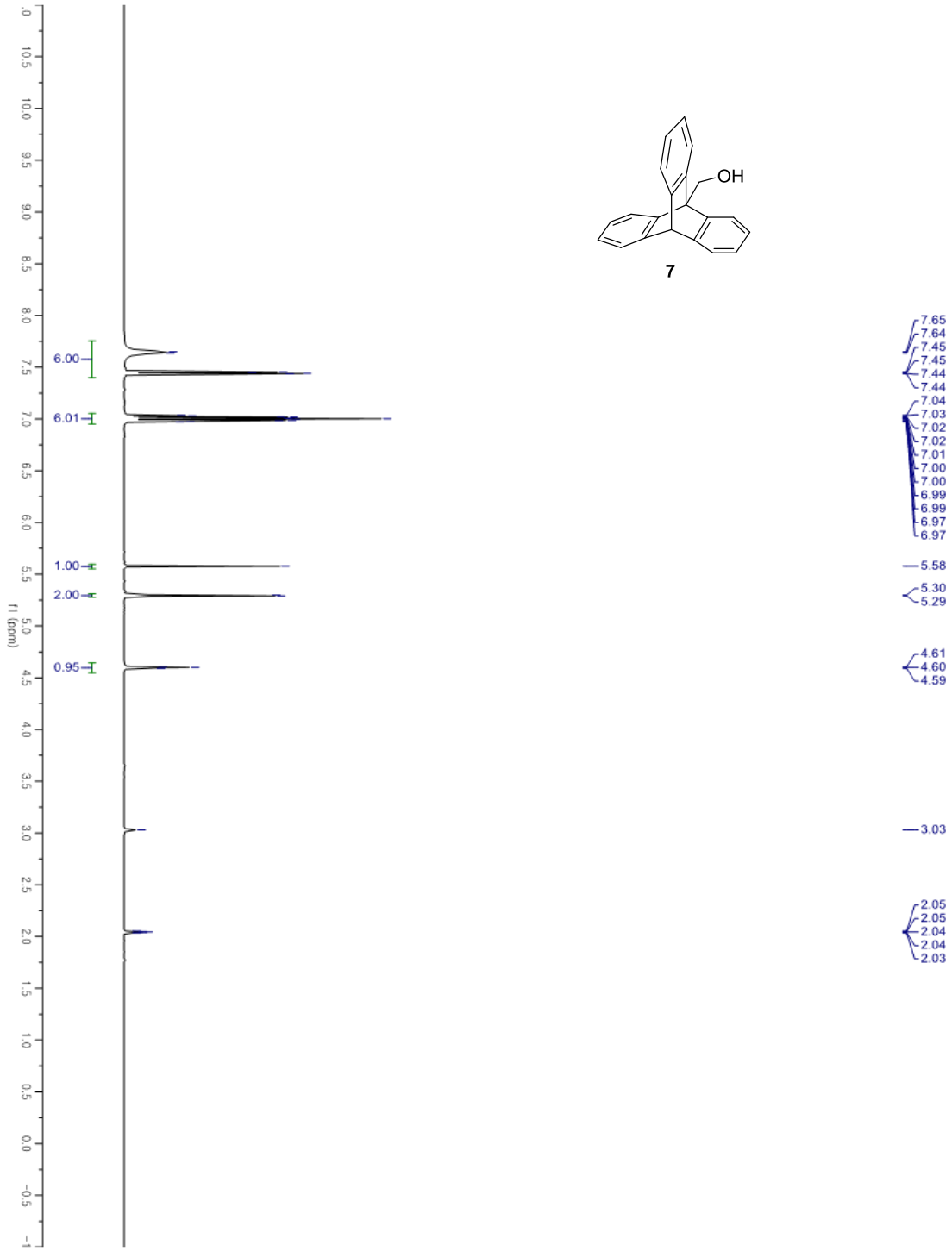

Figure A6.27. ^{13}C NMR spectrum of **7** in $(CD_3)_2CO$ (125 MHz).

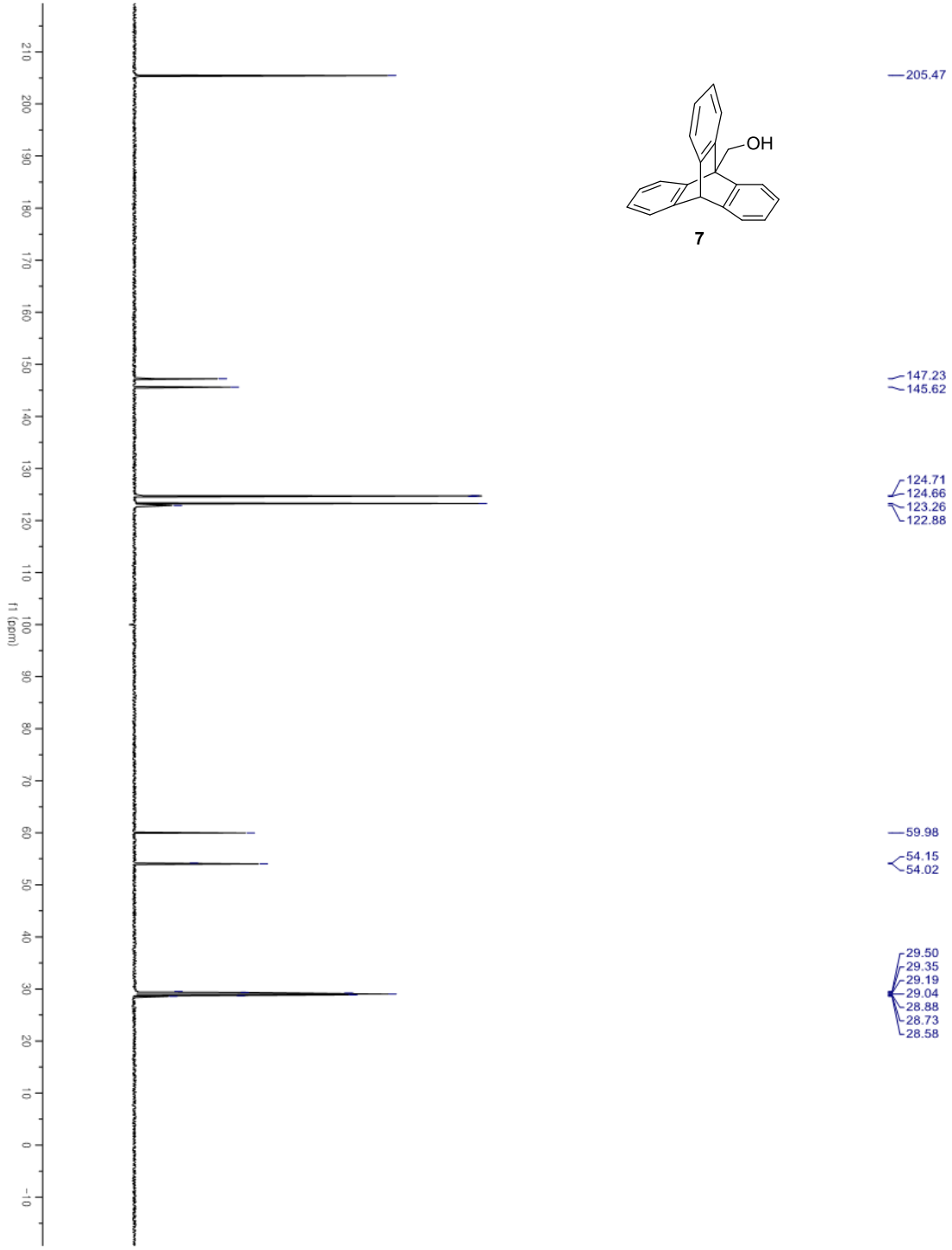

Figure A6.28. ^{1}H NMR spectrum of **8** in $(CD_3)_2CO$ (500 MHz).

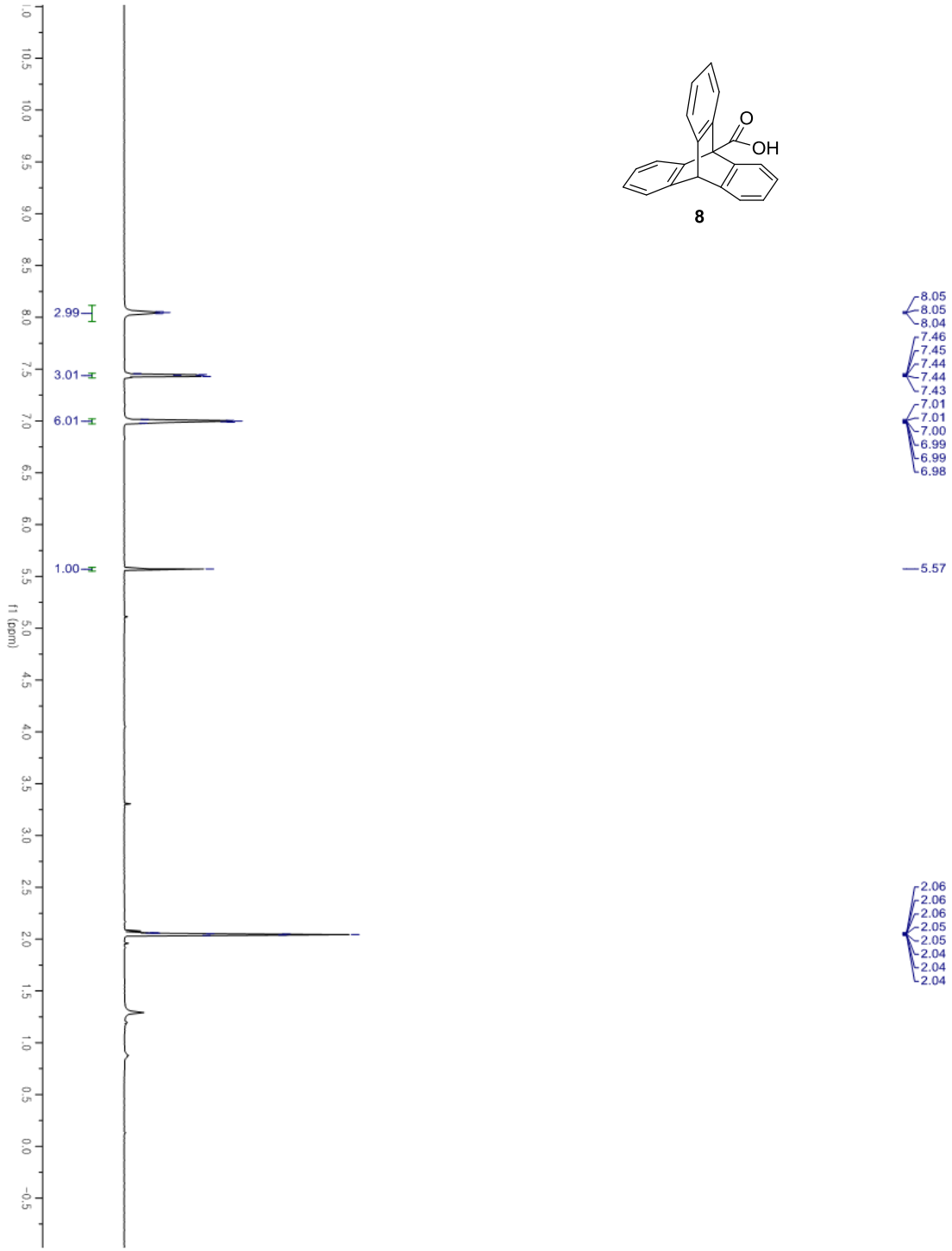

Figure A6.29. ^{13}C NMR spectrum of **8** in $(CD_3)_2CO$ (125 MHz).

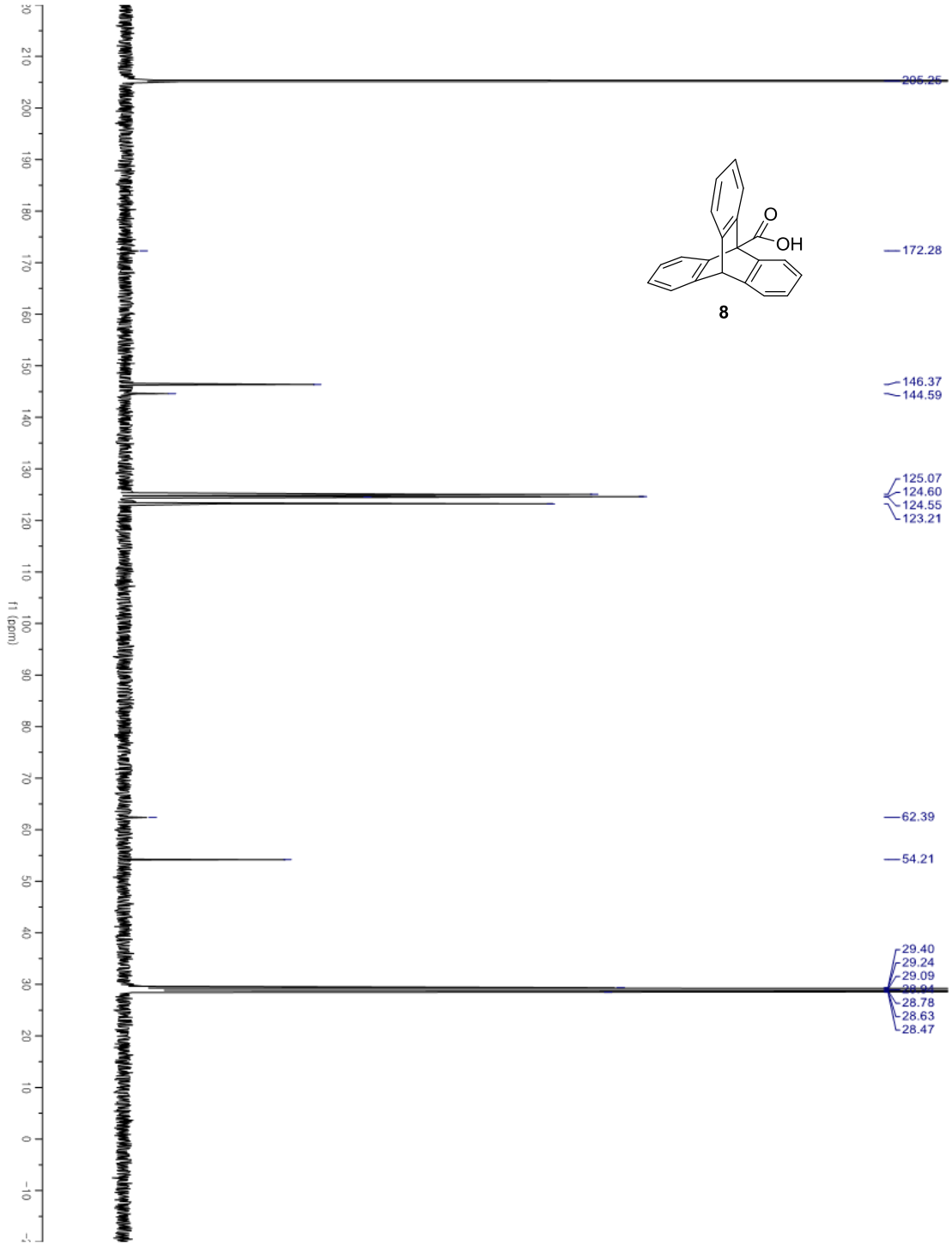

Figure A6.30. Carbonyl carbon peak (172.3 ppm) of **8** on ^{13}C NMR spectrum between 210 and 130 ppm in $(CD_3)_2CO$ (125 MHz).

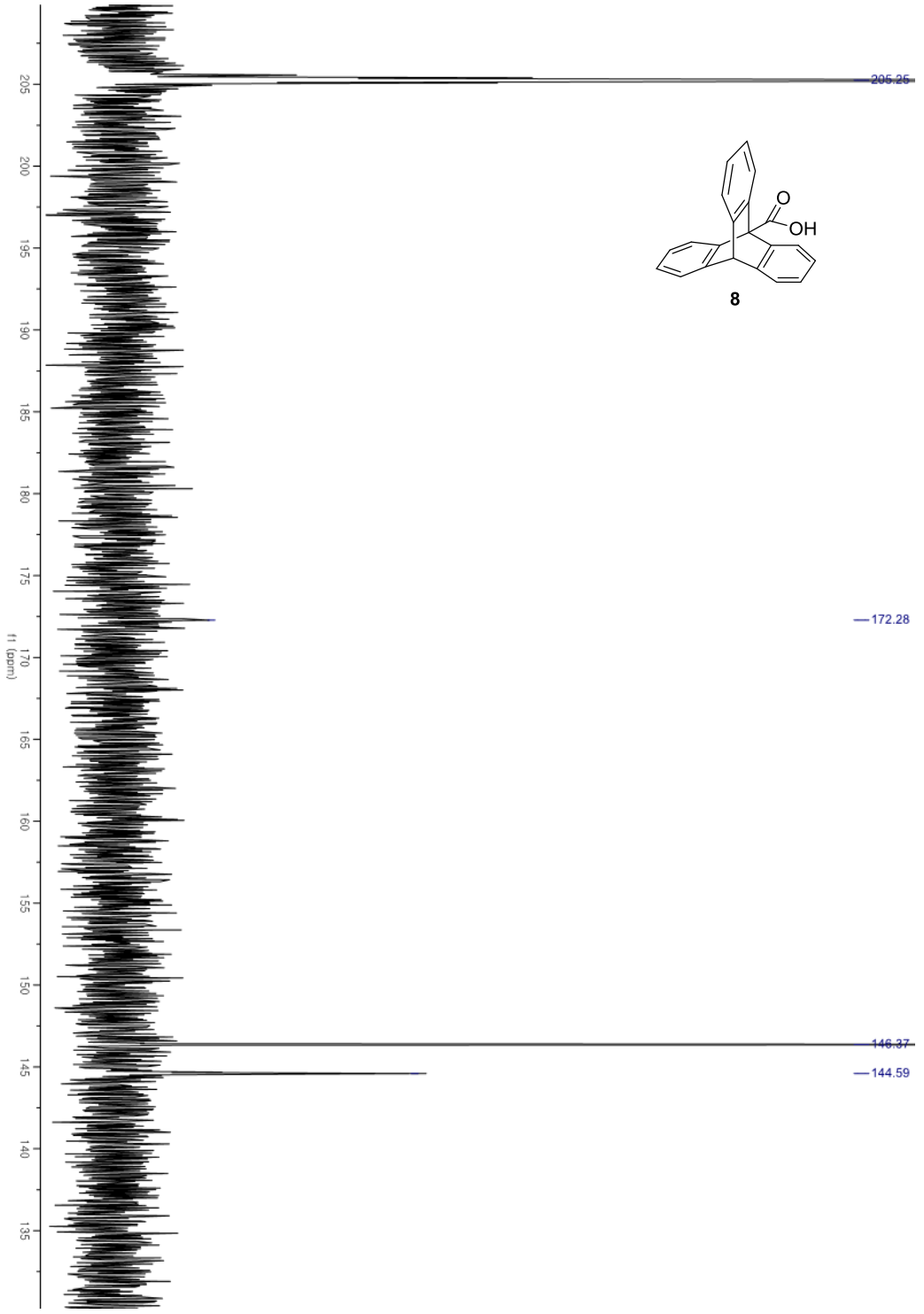

Figure A6.31. ^{1}H NMR spectrum of **9** in $(CD_3)_2CO$ (500 MHz).

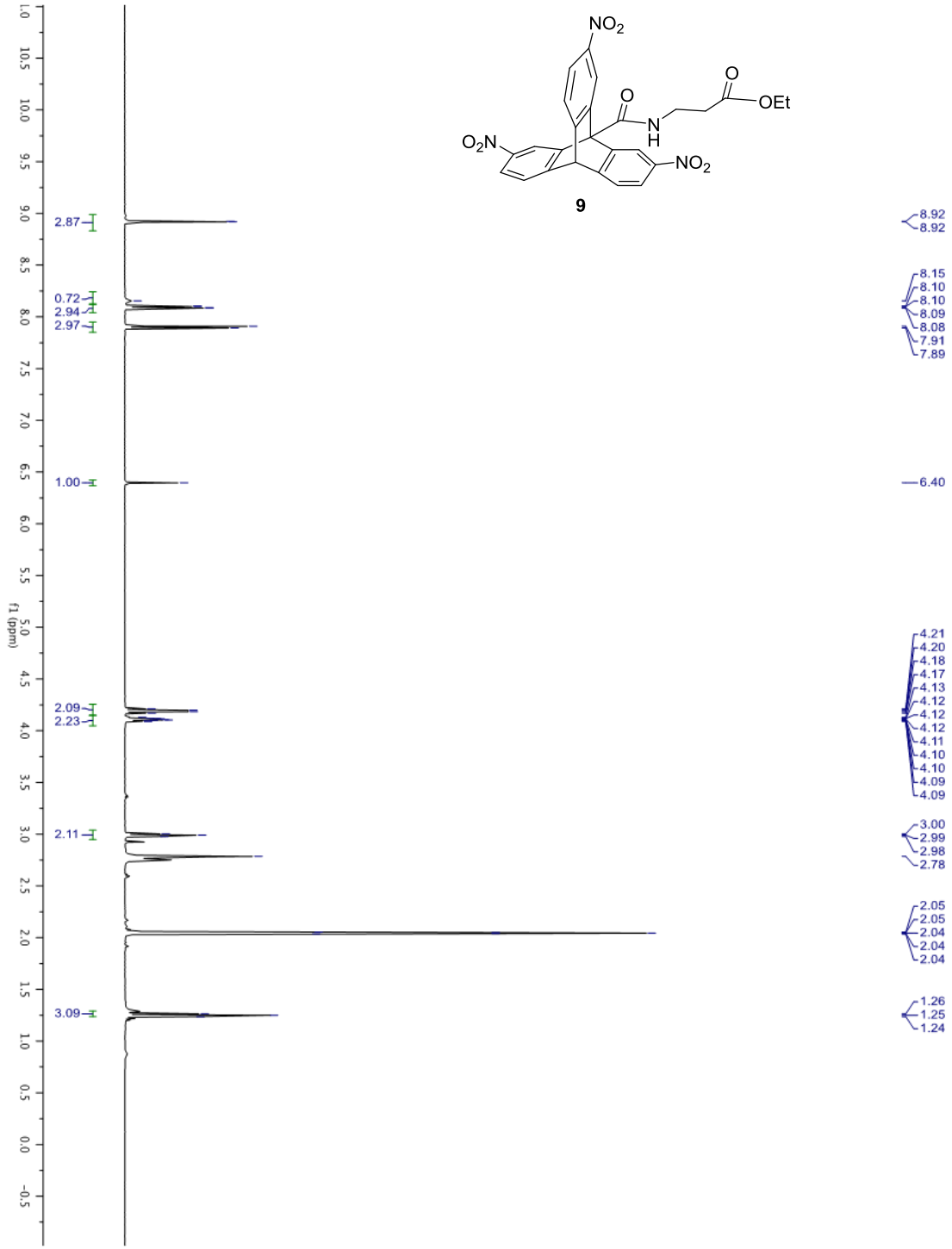

Figure A6.32. ^{13}C NMR spectrum of **9** in $(CD_3)_2CO$ (125 MHz).

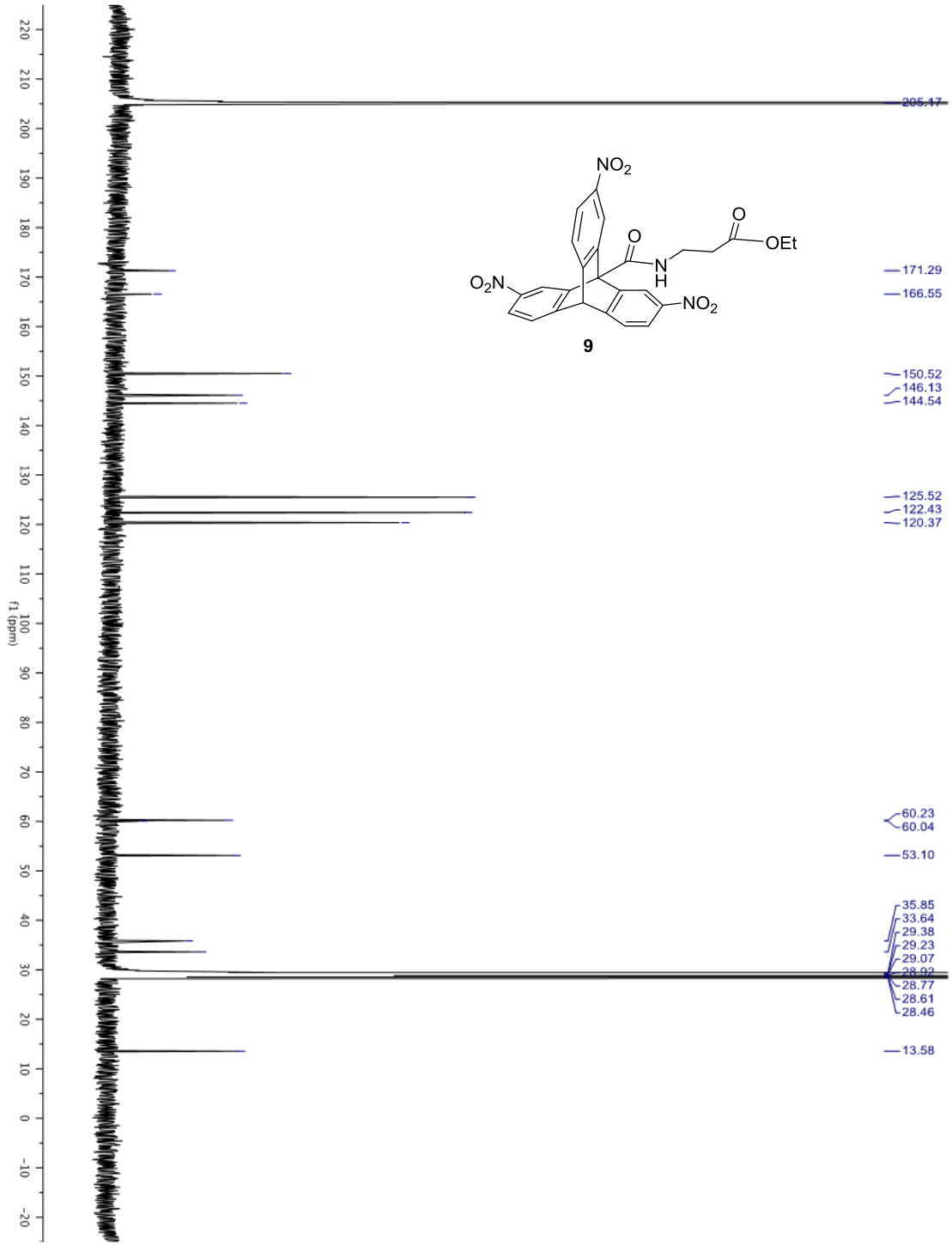

Figure A6.33. ^{1}H NMR spectrum of **11** in CD_2Cl_2 (500 MHz).

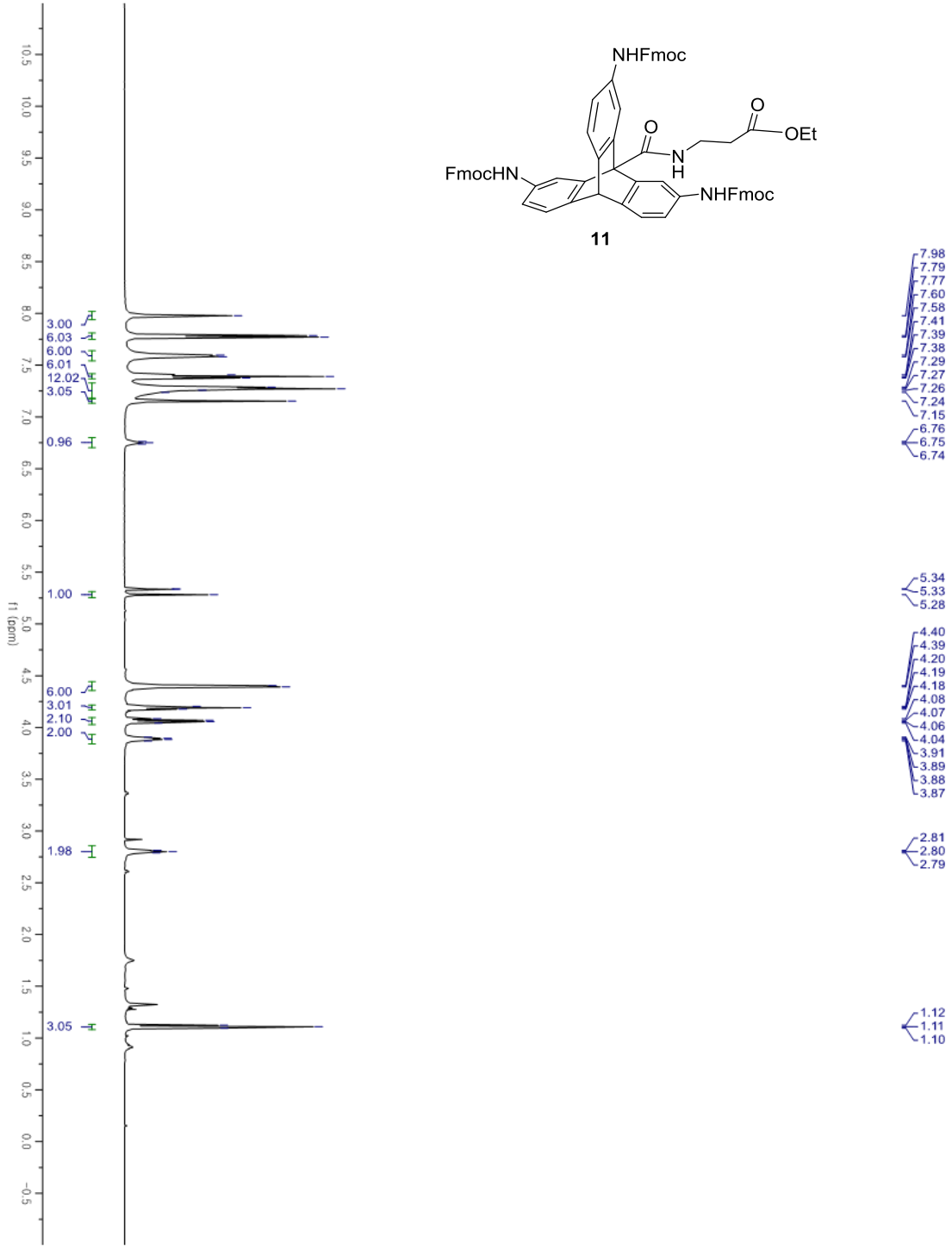

Figure A6.34. ^{13}C NMR spectrum of **11** in CD_2Cl_2 (125 MHz).

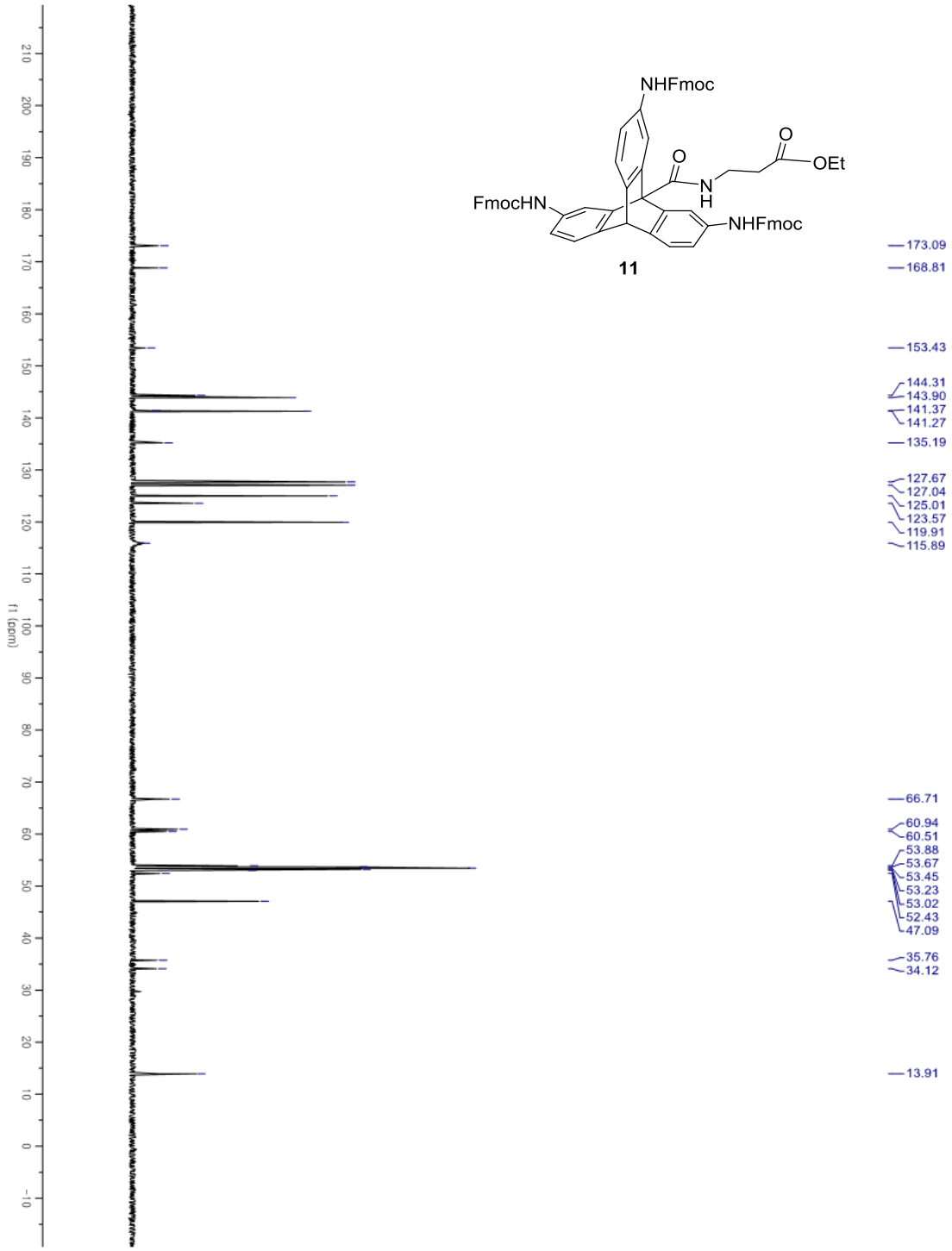

Figure A6.35. ^{1}H NMR spectrum of **12** in $(CD_3)_2SO$ (500 MHz).

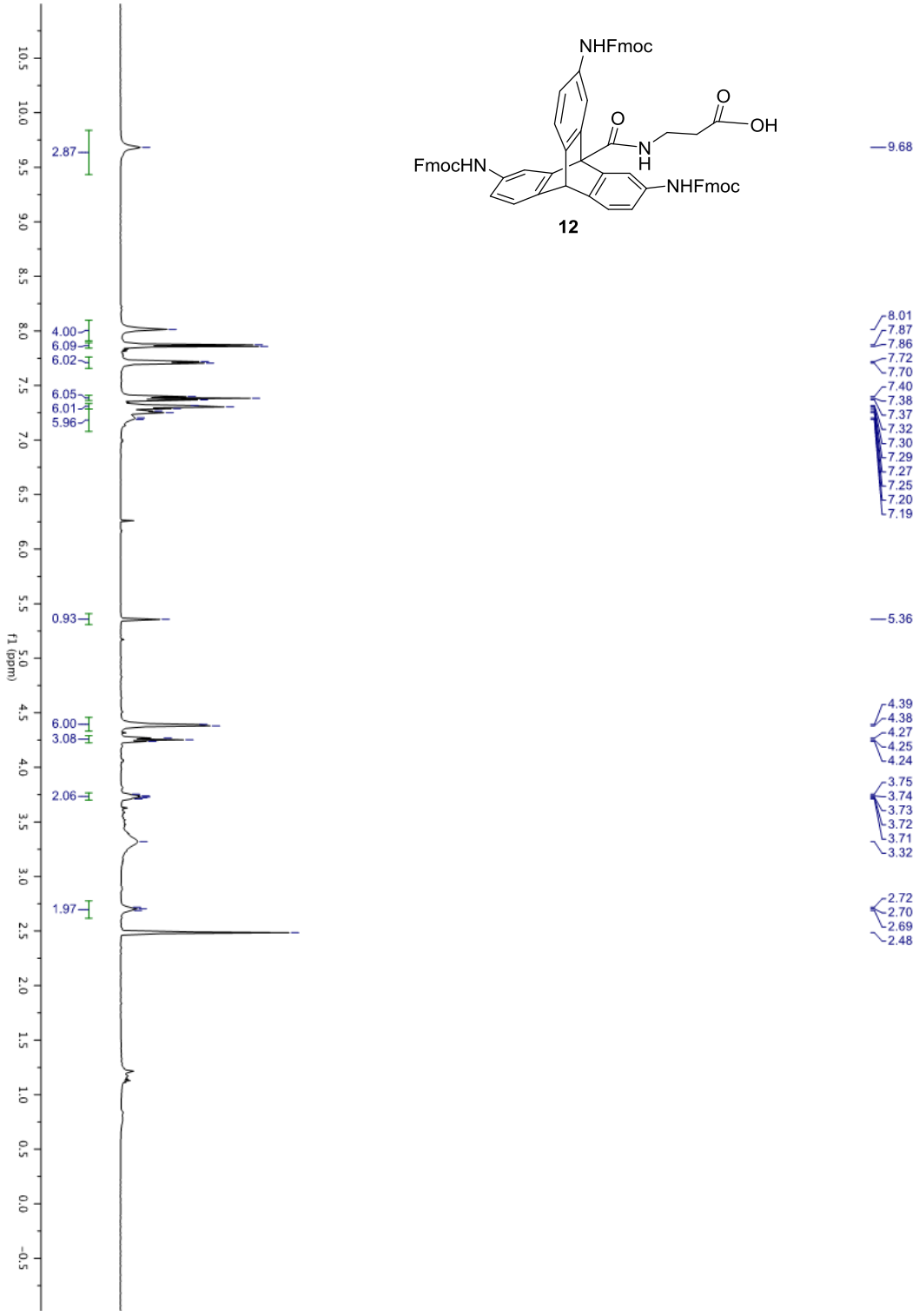

HPLC analysis of compound 5a-5c

After the nitration reaction of **4**, **7**, and **8** with nitric acid for 24 h at 80 °C, the crude mixture was cooled, neutralized with K_2CO_3, and re-acidified with 1M HCl. Ethyl acetate was added to the solution and the organic layer was extracted from the solution. The combined organic solution was dried with anhydrous sodium sulfate, and concentrated in vacuo. Crude mixtures were dissolved in acetonitrile. For quantitative analysis, 9,10-diphenylanthracene (internal standard) dissolved in acetonitrile was added to the crude mixture. All samples were then analyzed by reverse-phase HPLC. Solvent gradient method used is shown below. (A: 0.1 % CF_3CO_2H in MilliQ water, B: Methanol)

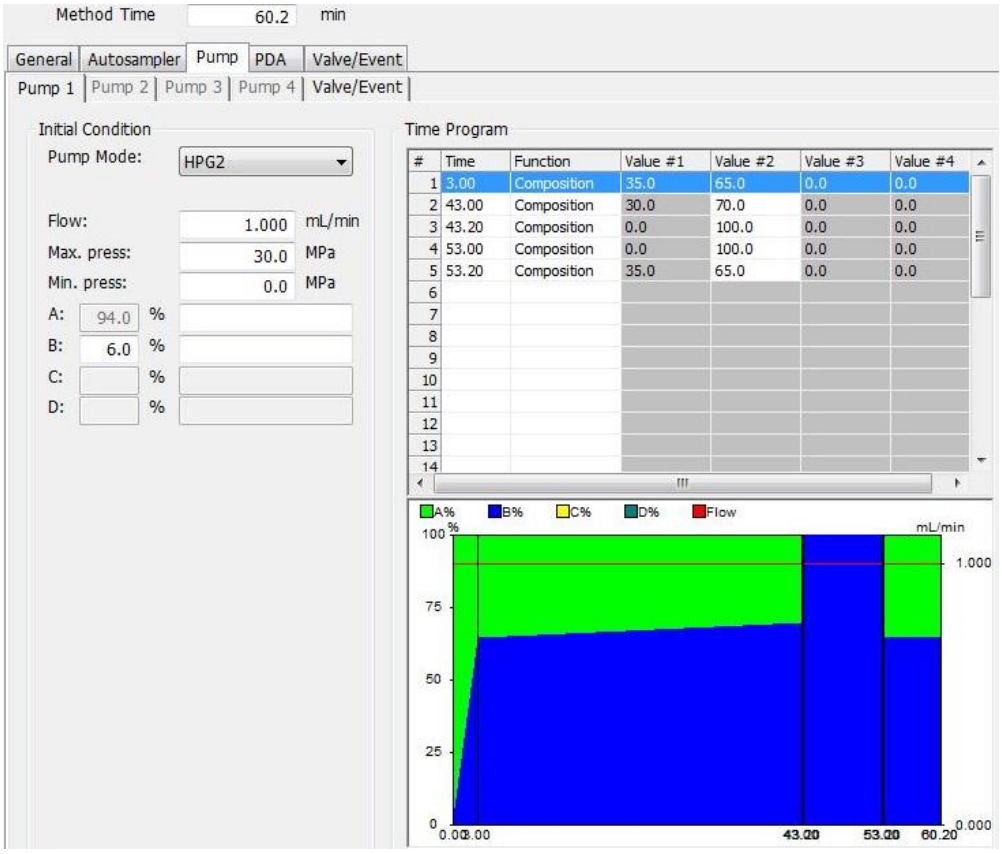

Figure A6.36. Solvent gradient method for **4**, **7**, and **8**.

Figure A6.37. Chromatogram of crude nitration mixture from compound **4.**

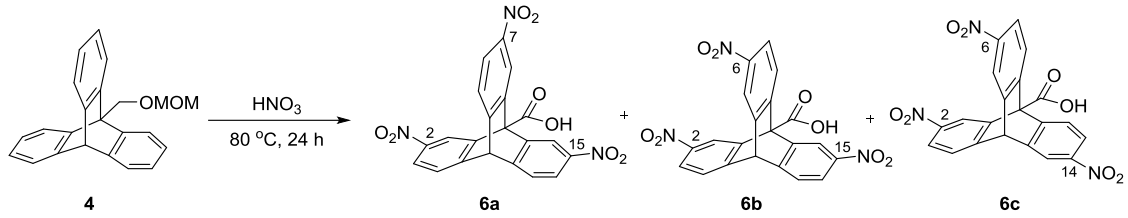

●: **6a**, ▲: **6b**, ★: **6c**, and ▪: 9,10-diphenylanthracene (internal standard)

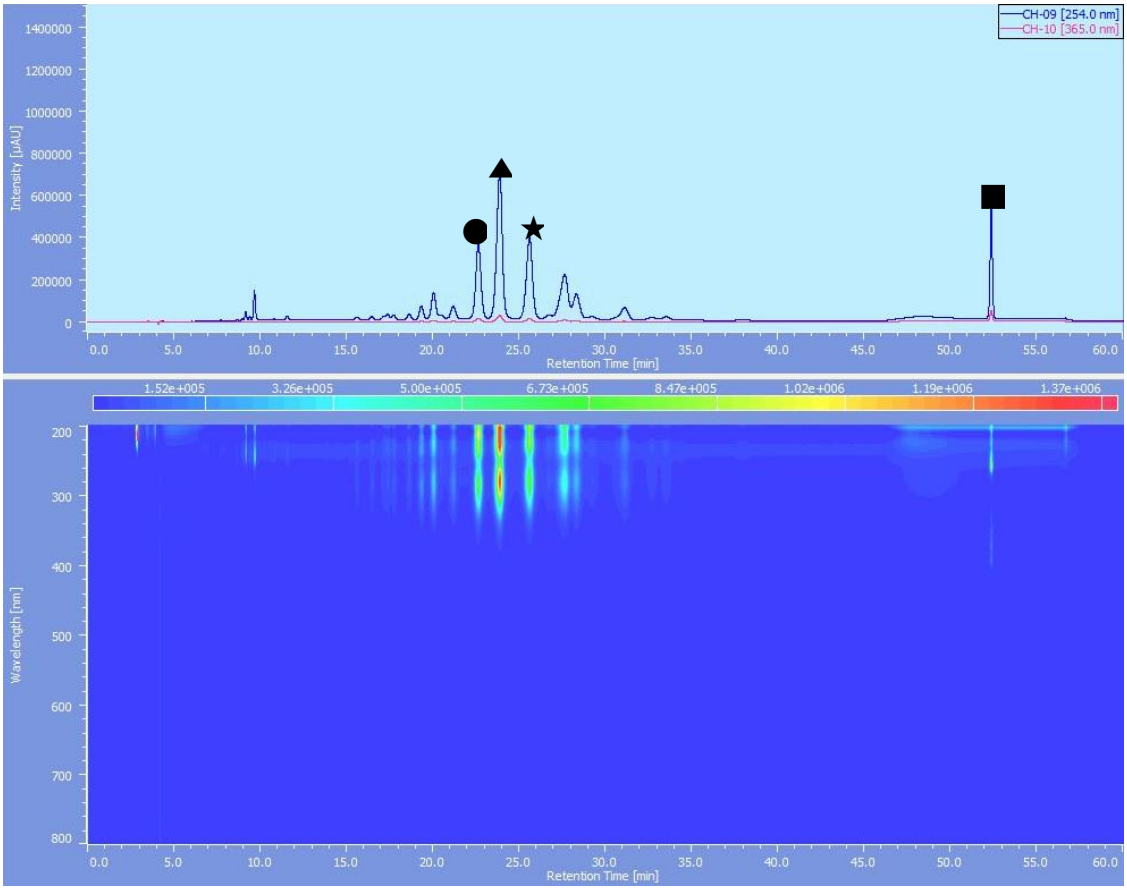

Figure A6.38. Chromatogram of crude nitration mixture from compound **7.**

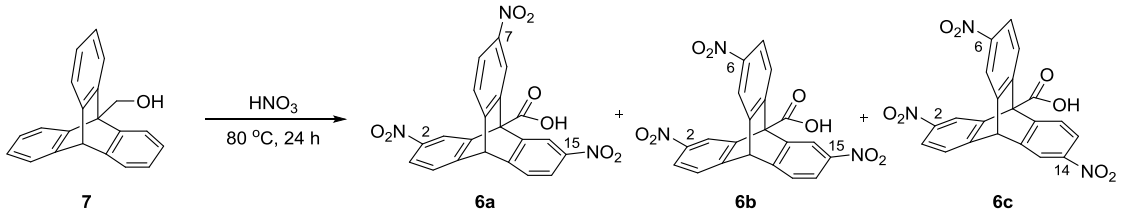

7 **6a** **6b** **6c**

●: **6a**, ▲: **6b**, ★: **6c**, and ▪: 9,10-diphenylanthracene (internal standard)

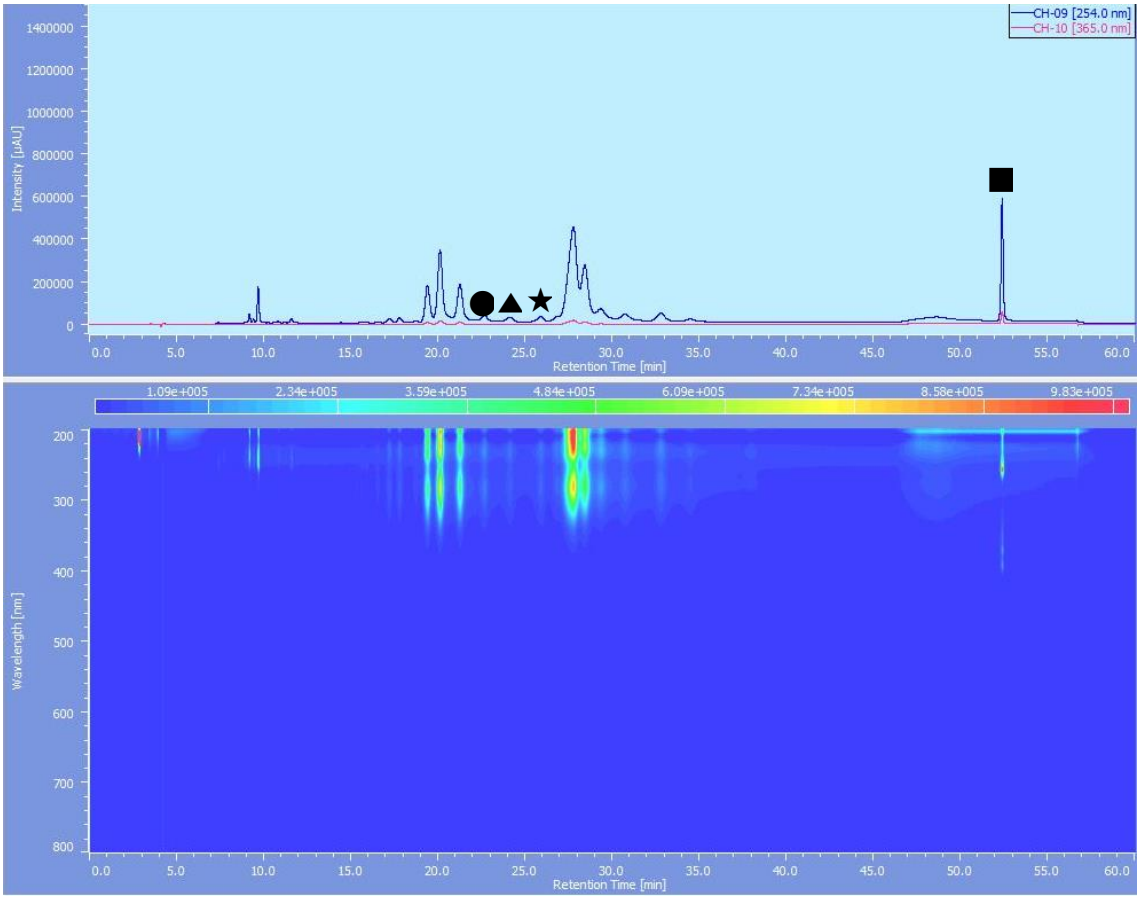

Figure A6.39. Chromatogram of crude nitration mixture from compound **8.**

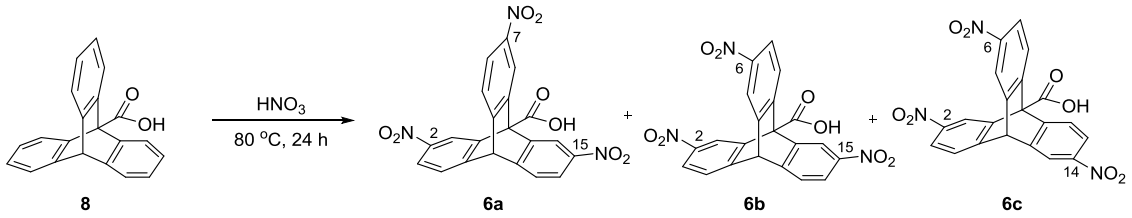

●: **6a**, ▲: **6b**, ★: **6c**, and ▪: 9,10-diphenylanthracene (internal standard)

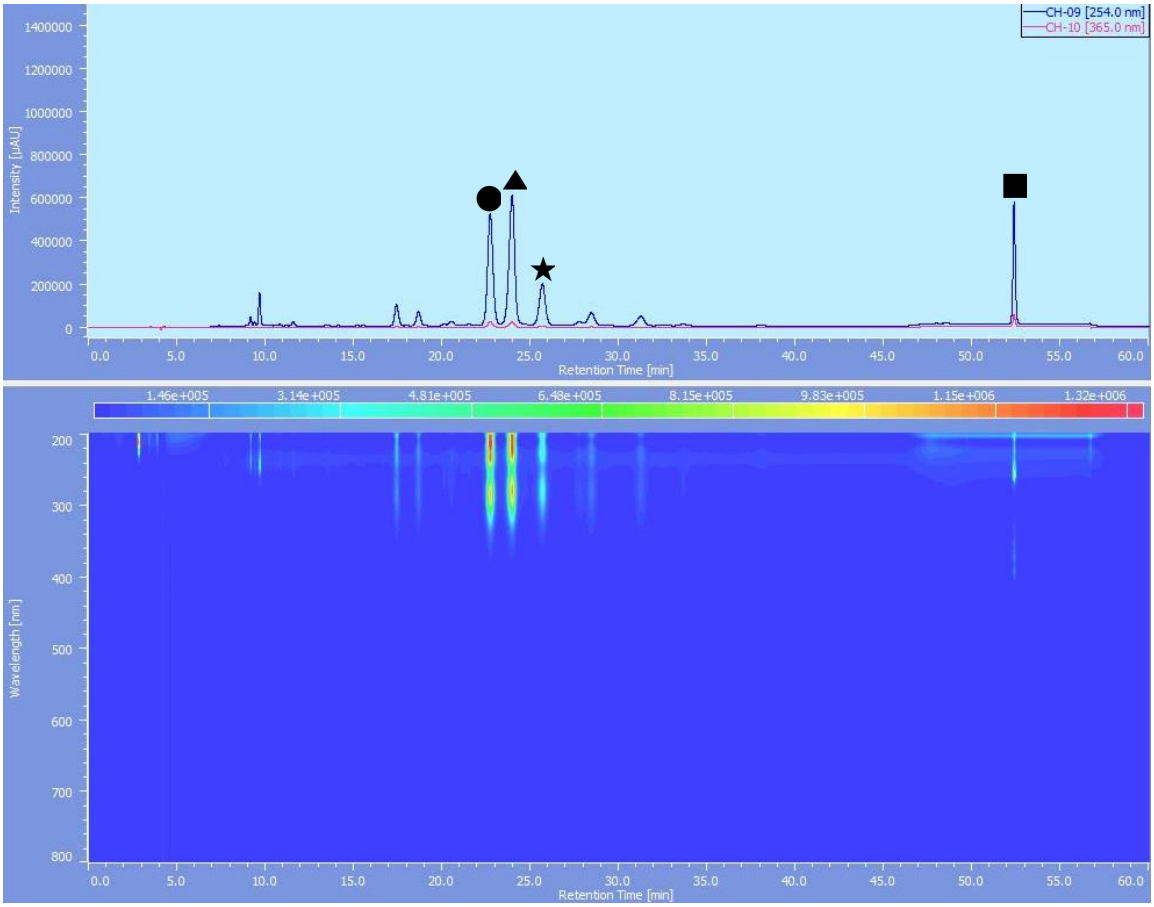

Figure A6.40. Merged chromatogram of crude nitration mixtures from compound **4**, **7**, and **8**.

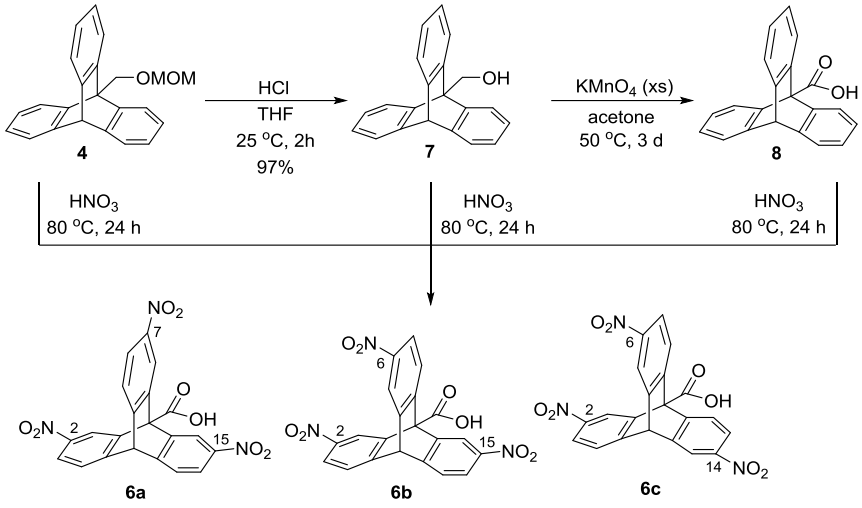

●: 6a, ▲: 6b, ★: 6c, and ▪: 9,10-diphenylanthracene (internal standard)

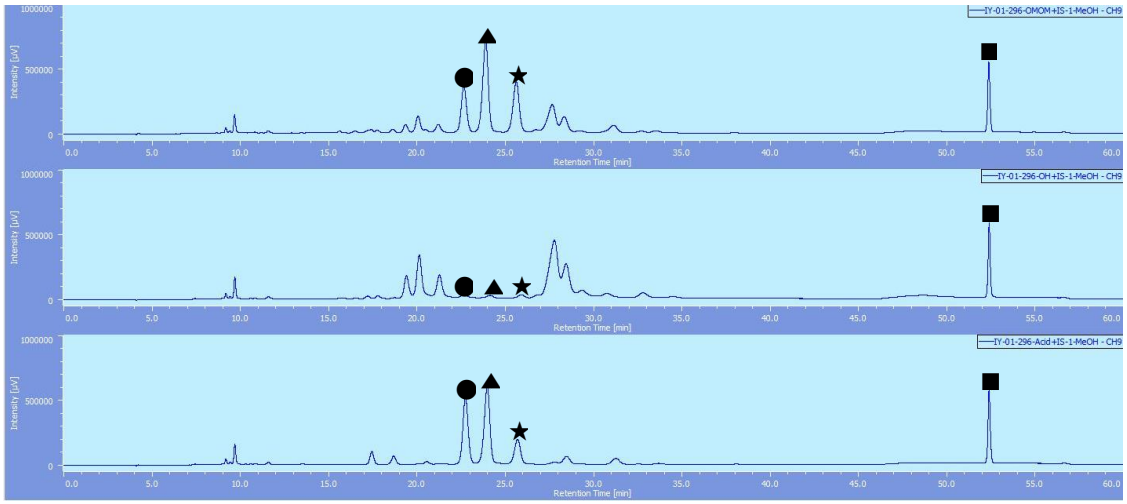

HPLC analysis of compound 12 and 17-19

The purified samples were dissolved in acetonitrile (for compound **12**) or in MilliQ water (for compounds **17-19**) and then analyzed by reverse-phase HPLC to confirm the purity of samples. Two different gradients were used as shown below (top: compound **12**, bottom: compound **17-19**, A: 0.1 % CF_3CO_2H in MilliQ water, B: Acetonitrile).

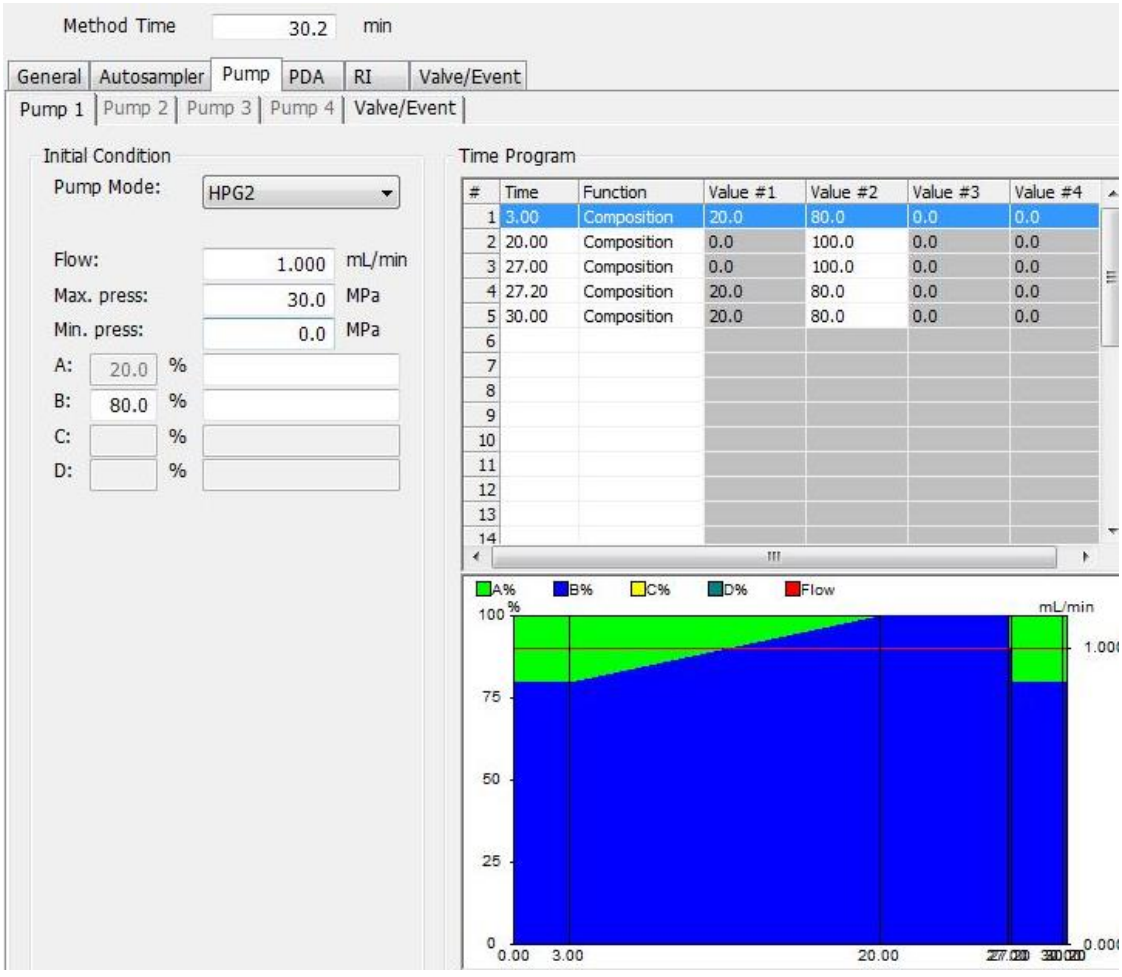

Figure A6.41. Solvent gradient method for **12**.

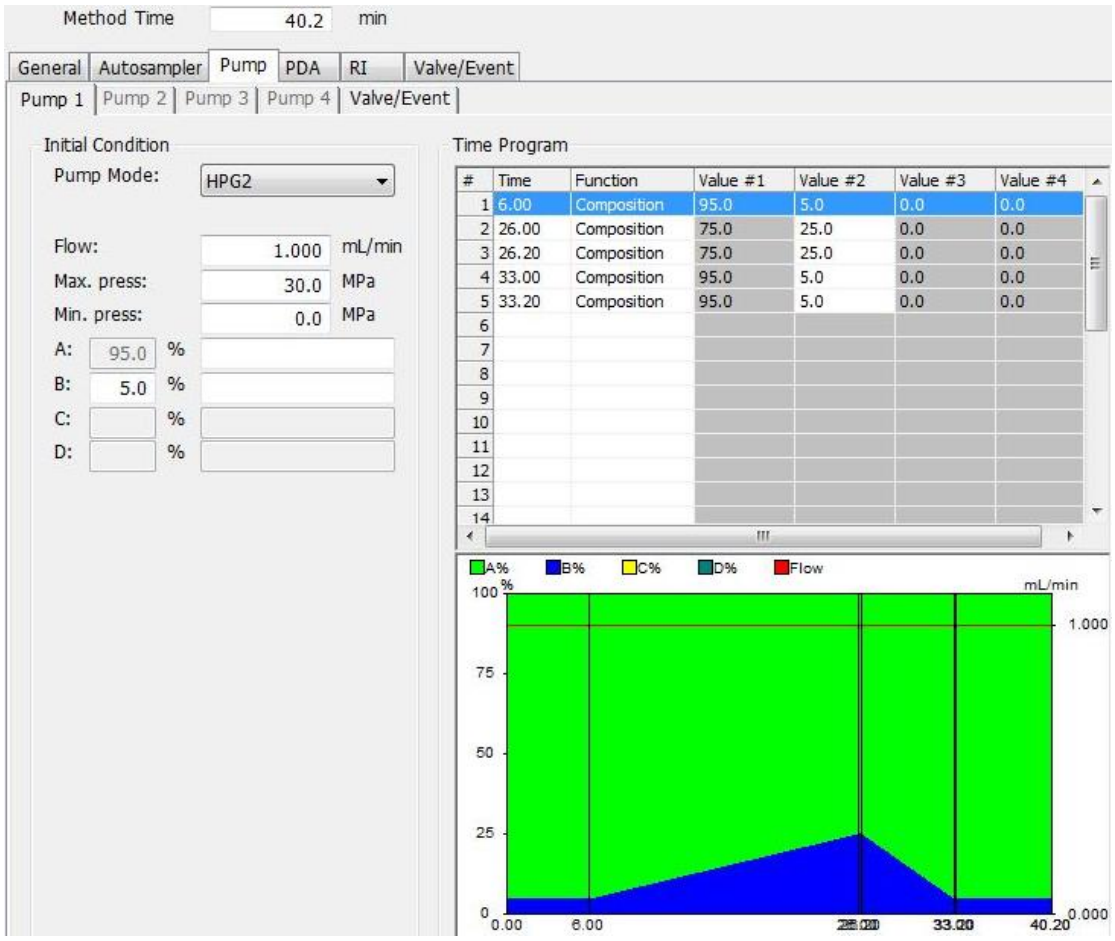

Figure A6.42. Solvent gradient method for **17-19**.

Figure A6.43. Chromatogram of analytical HPLC of compound **12**.

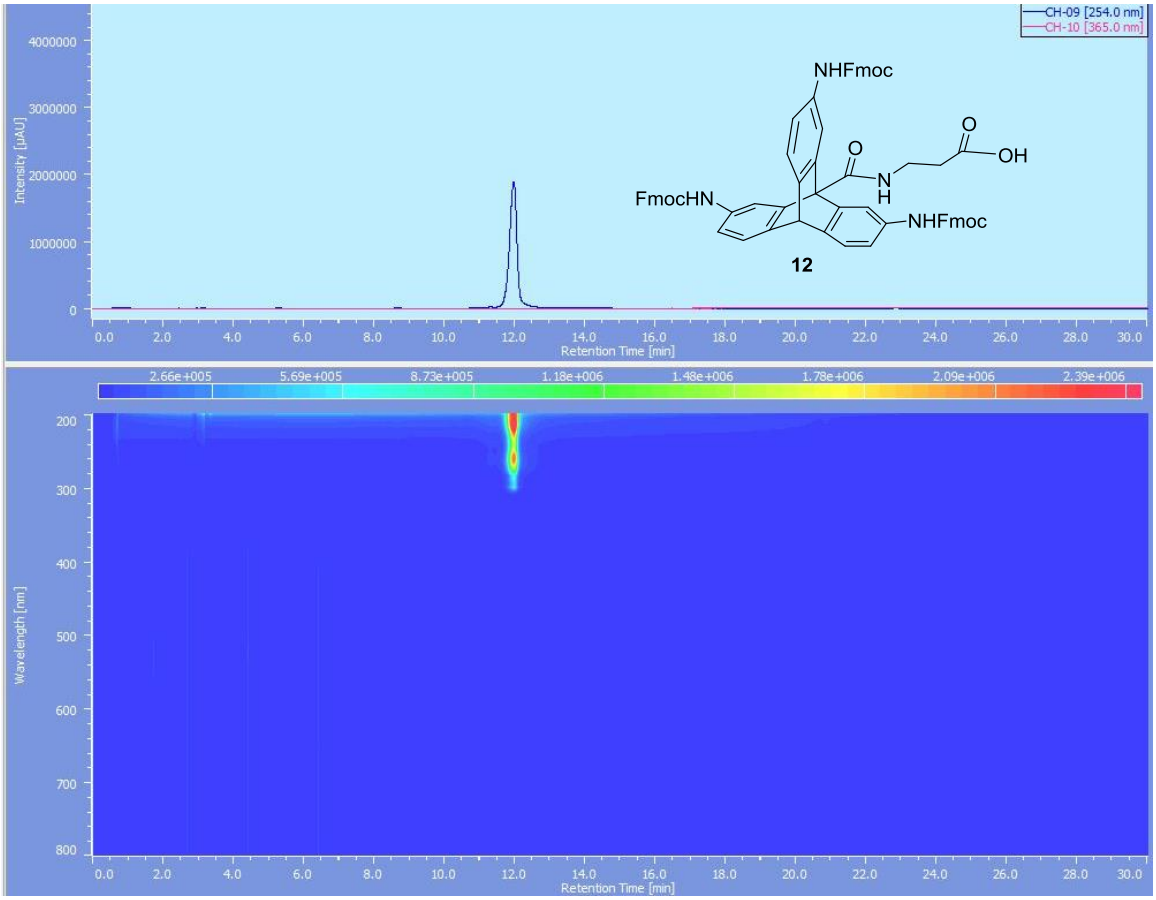

Figure A6.44. Chromatogram of analytical HPLC of compound **17**.

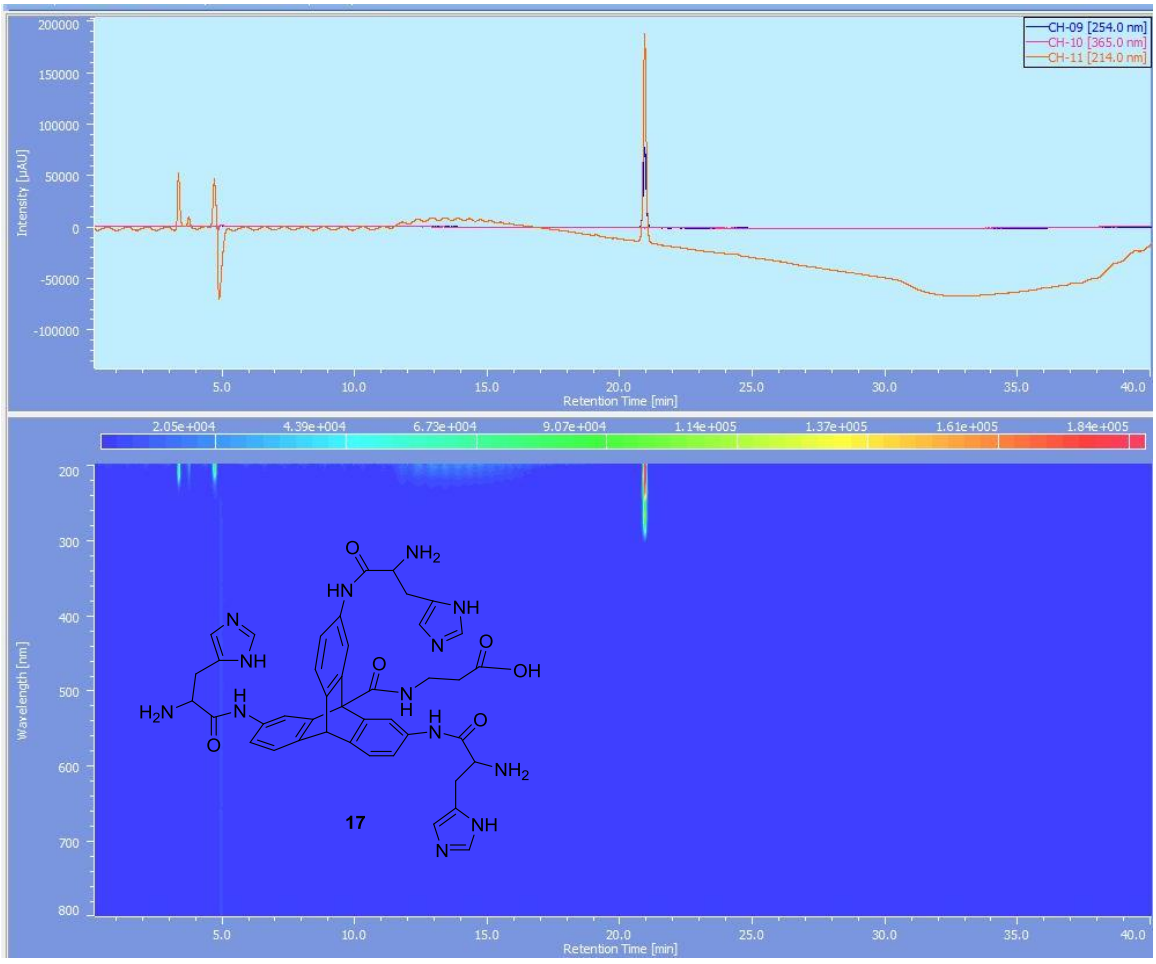

Figure A6.45. Chromatogram of analytical HPLC of compound **18**.

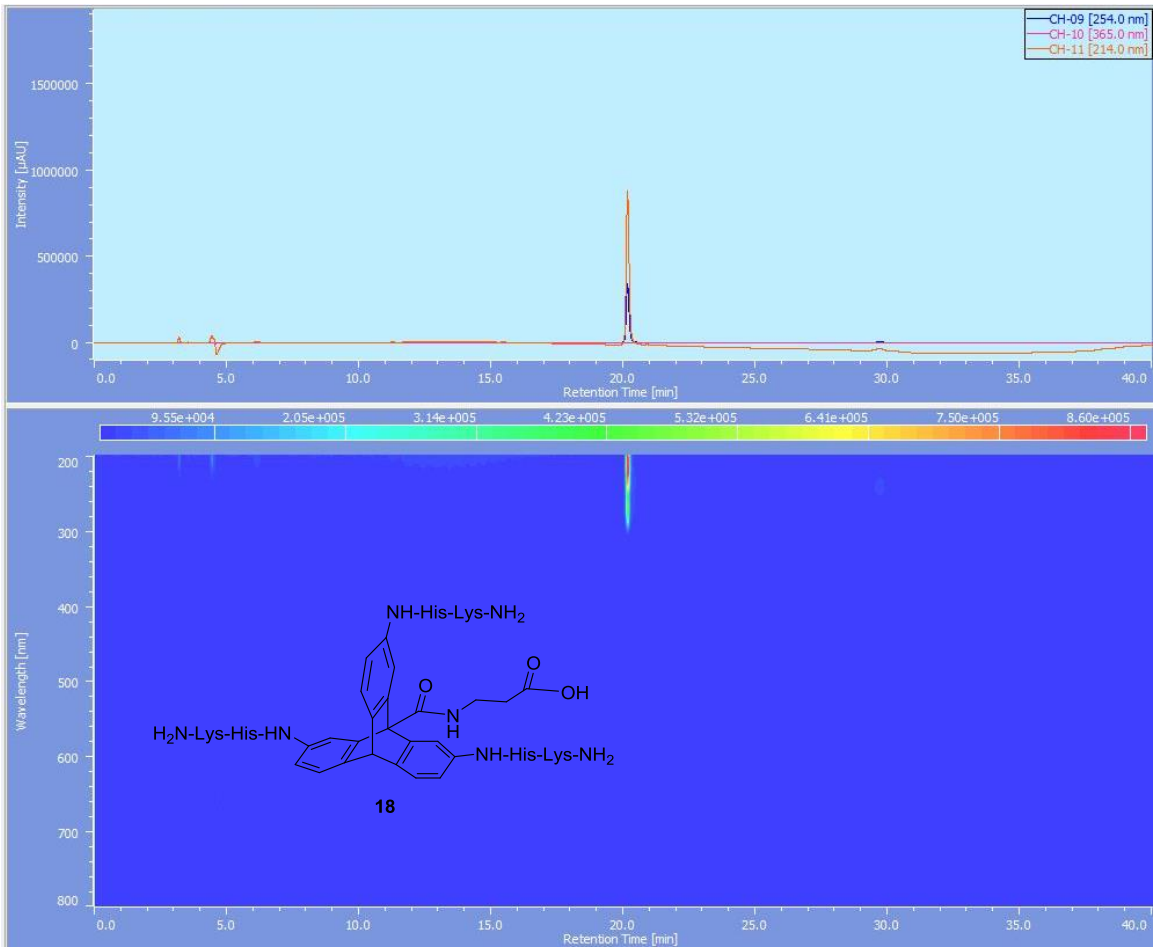

Figure A6.46. Chromatogram of analytical HPLC of compound **19**.

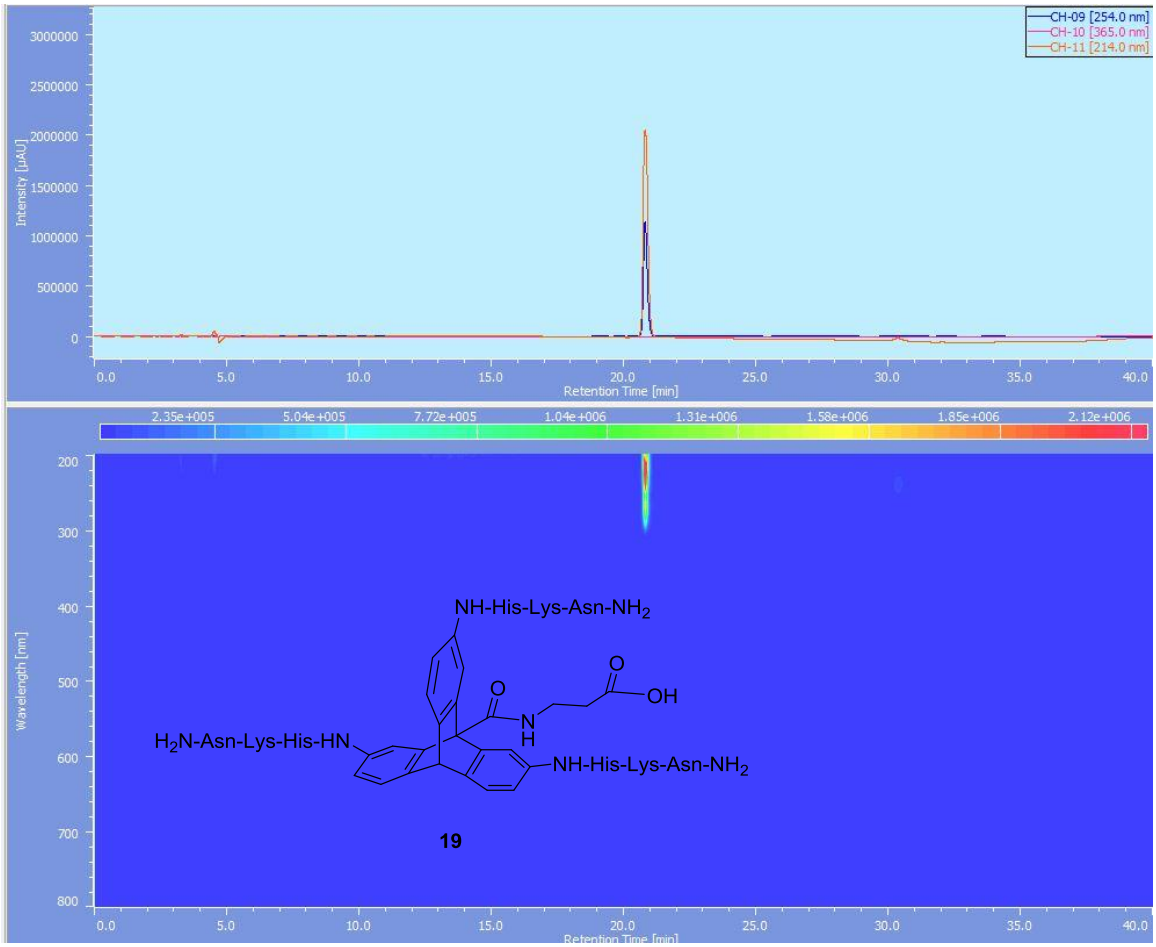

MALDI-MS analysis

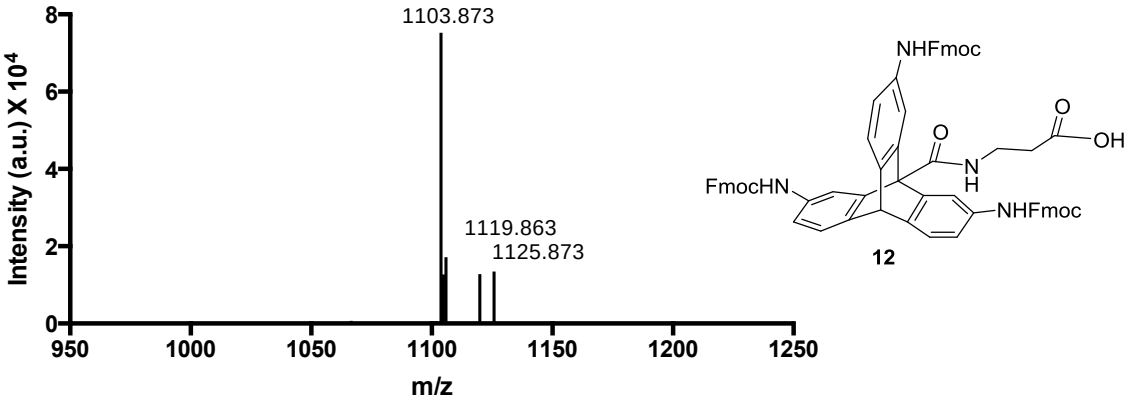

Calculated for $C_{69}H_{52}N_4NaO_9^+$ $[M+Na]^+$ 1103.363, found 1103.873.; $C_{69}H_{52}KN_4O_9^+$ $[M+K]^+$ 1119.337, found 1119.863.; $C_{69}H_{51}N_4Na_2O_9^+$ $[M-H+2Na]^+$ 1125.345, found 1125.873.

Figure A6.47. MALDI-MS data of compound **12**.

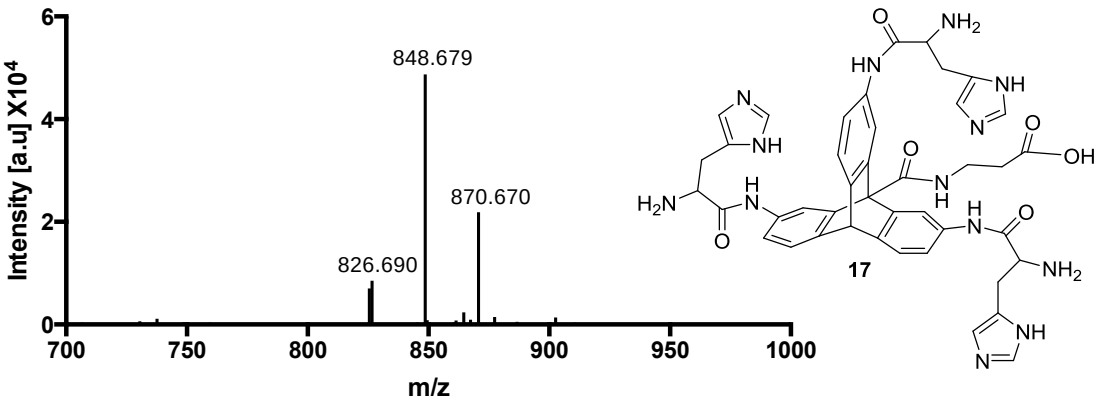

Calculated for $C_{42}H_{44}N_{13}O_6^+$ $[M+H]^+$ 826.353, found 826.690.; $C_{42}H_{43}N_{13}NaO_6^+$ $[M+Na]^+$ 848.335, found 848.679.; $C_{42}H_{42}N_{13}Na_2O_6^+$ $[M-H+2Na]^+$ 870.317, found 870.670.

Figure A6.48. MALDI-MS data of compound **17**.

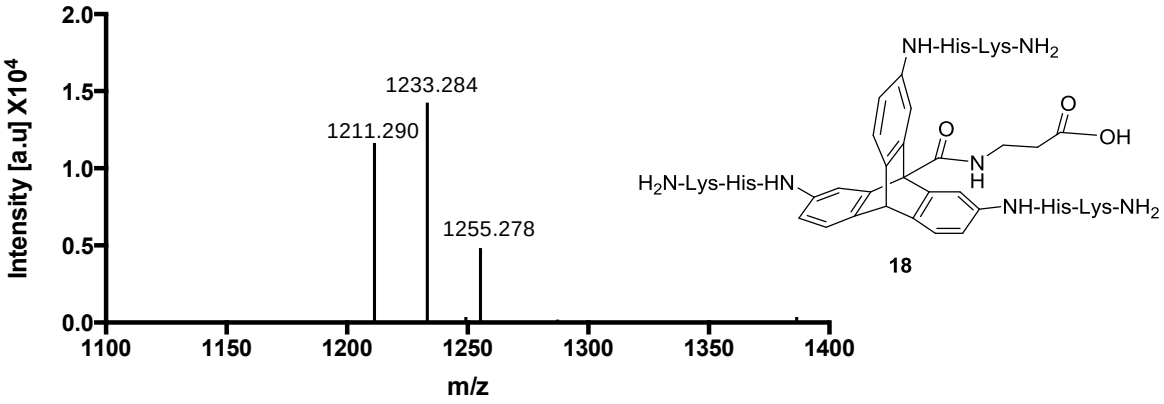

Calculated for $C_{60}H_{80}N_{19}O_9^+$ $[M+H]^+$ 1210.638, found 1211.290.; $C_{60}H_{79}N_{19}NaO_9^+$ $[M+Na]^+$ 1232.620, found 1233.284.; $C_{60}H_{78}N_{19}Na_2O_9^+$ $[M-H+2Na]^+$ 1254.602, found 1255.278.

Figure A6.49. MALDI-MS data of compound **18**.

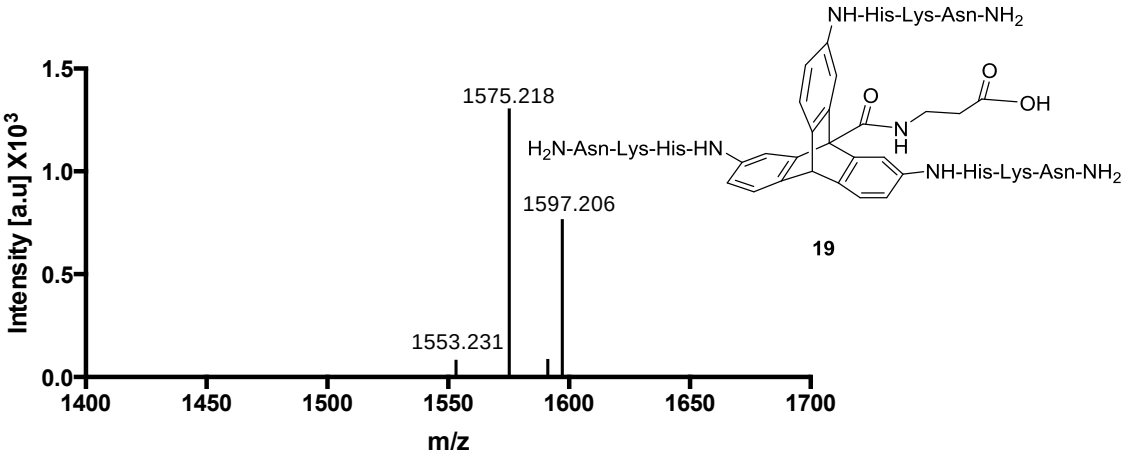

Calculated for $C_{72}H_{98}N_{25}O_{15}^+$ $[M+H]^+$ 1552.767, found 1553.231.; $C_{72}H_{97}N_{25}NaO_{15}^+$ $[M+Na]^+$ 1574.749, found 1575.218.; $C_{72}H_{96}N_{25}Na_2O_{15}^+$ $[M-H+2Na]^+$ 1596.731, found 1597.206.

Figure A6.50. MALDI-MS data of compound **19**.

Table A6.1. Crystal Data and Structure Refinement for 5c.

Empirical formula	$C_{47}H_{29}N_6O_{16}Cl_9$
Formula weight	1252.81
Temperature/K	100
Crystal system	triclinic
Space group	$P\bar{1}$
a	9.6450(4)Å
b	11.5310(5)Å
c	23.1800(9)Å
α	92.059(2)°
β	90.249(2)°
γ	95.534(2)°
Volume	2564.25(18)Å^3
Z	2
d_{calc}	1.623 g/cm^3
μ	0.569 mm^{-1}
F(000)	1268.0
Crystal size, mm	0.28 × 0.14 × 0.03
2θ range for data collection	3.55 - 50.764°
Index ranges	-11 ≤ h ≤ 11, -13 ≤ k ≤ 13, 0 ≤ l ≤ 27
Reflections collected	81802
Independent reflections	9384[R(int) = 0.0693]
Data/restraints/parameters	9384/0/706
Goodness-of-fit on F^2	1.036
Final R indexes [I>=2σ (I)]	R_1 = 0.0553, wR_2 = 0.1464
Final R indexes [all data]	R_1 = 0.0644, wR_2 = 0.1568
Largest diff. peak/hole	1.25/-1.10 eÅ^{-3}

Chapter 8

Bridgehead-Substituted Triptycenes for Discovery of Nucleic Acid Junction Binders

Adapted with permission from Barros, S. A.; Yoon, I.; Suh, S.-E.; Chenoweth, D. M. *Org. Lett.* **2016,** *18,* 2423-2426.

8.1 Introduction

Nucleic acid junctions are important structural intermediates in biology.[1–3] Junctions are present in important biological processes including replication.[4,5] These junctions also occur in viral genomes in addition to trinucleotide repeat expansions associated with numerous neurodegenerative diseases.[6–12] These structures are also present in nanostructures and aptamer-based sensors.[13–20] The ability to selectively modulate a subset of nucleic acid structures using small molecules would allow for the chemical control of cellular processes as well as the reprogramming of cellular events.[21–37] The ability to differentially stabilize predefined nucleic acid structures or to reprogram and bias the equilibrium distribution of an ensemble of structures in a precise manner could have a profound impact not only in biology but also in nucleic acid nanotechnology and materials applications.

We previously demonstrated that triptycene-based molecules can bind to three-way junctions (3WJs).[38] Additionally, we have shown that these molecules bind to d(CAG)·(CTG) repeats implicated in triplet repeat expansion diseases.[39] The ability to synthesize libraries of triptycene derivatives on solid supports will accelerate efforts to identify biologically relevant nucleic acid junction binders and provide further insight into the molecular recognition properties of triptycenes toward diverse junction sequences and topologies. To facilitate solid-phase immobilization, a point of attachment on triptycene is required. The bridgehead position provided a strategic location, as it is equidistant from the three amino groups that serve as sites of diversification (Figure 8.1a). We recently described a synthesis for bridgehead-substituted triptycene building blocks.[40] Here, we report a modified, more efficient synthesis by utilizing a

combined Heck coupling/benzyne Diels-Alder strategy. The new triptycene building block was further diversified on solid phase with short di- and tri-peptides, and the final compounds were evaluated for binding to a d(CAG)·(CTG) repeat junction. We discovered new high-affinity lead compounds for this junction motif that will form the basis of further investigations.

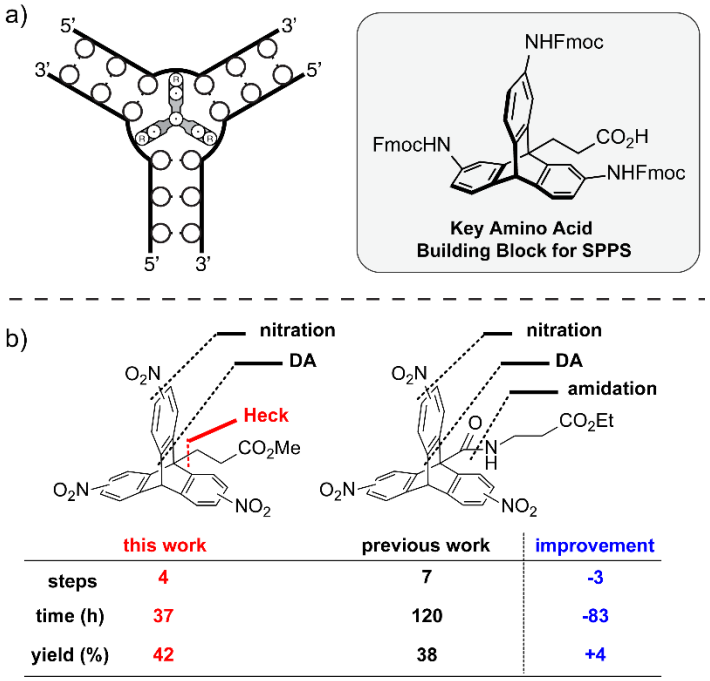

	this work	previous work	improvement
steps	4	7	-3
time (h)	37	120	-83
yield (%)	42	38	+4

Figure 8.1. (a) Schematic of triptycene bound to a three-way junction and a key triptycene building block for diversification by solid-phase synthesis. (b) Improvement of the synthesis of triptycene intermediates in this work.

8.2 Results and Discussion

Similar to our previous route, our synthetic plan relied on the reduction of nitrated triptycene, a key intermediate, to install the three key amine functional groups that serve as

points of future diversification (Figure 8.1b). The synthetic strategy presented here provides a shorter synthesis with only four steps to the key intermediate compared to seven steps in our previous route. Additionally, this method significantly reduced total reaction times from 120 h to 37 h and showed an improvement in overall yield (Figure 8.1b). Moreover, the solubility of intermediates was improved. After extending the linker at the bridgehead via an amidation reaction in the previous route, the resulting product showed poor to moderate solubility in most organic solvents. However, the intermediates in this synthetic route have good solubility, allowing easier characterization and large-scale reactions. In addition, a new regioisomer **5c** that has all three nitro groups facing away from the linker was isolated in this new synthetic route, whereas this regioisomer was not observed in the previous report.

We initiated our synthesis with a Heck reaction between 9-bromoanthracene **1** and methyl acrylate in the presence of palladium(II) acetate, tri-*o*-tolylphosphine, and triethylamine in a sealed tube. The Heck reaction proceeded cleanly and resulted in the desired product **2** in 84% yield (Scheme 8.1). Next, olefin **2** was reduced under mild conditions using palladium(II) acetate as the catalyst and potassium formate as the hydrogen source, producing **3** in 85% yield.[41] The key Diels-Alder reaction with anthracene **3** and benzyne, generated *in situ* from 2-(trimethylsilyl)phenyl trifluoromethanesulfonate and cesium fluoride, proceeded smoothly to yield bridgehead-substituted triptycene **4** in 95% yield. Nitration of triptycene resulted in hydrolysis of the bridgehead ester and four major nitrated regioisomers that proved inseparable by standard chromatographic techniques. Esterification of the crude reaction greatly facilitated the separation of the regioisomeric mixture (**5a-d**) using standard silica gel column chromatography. The nitrated triptycene regioisomers were characterized by HMBC and

HSQC (Figure A7.9-12, 15-18, 21-24, 27, 28 in Appendix 7). A crystal of triptycene **5d** was obtained in chloroform to confirm its structure by X-ray crystallography (Scheme 8.1).

Scheme 8.1. Synthesis of Bridgehead-Substituted Triptycenes 5a-d.

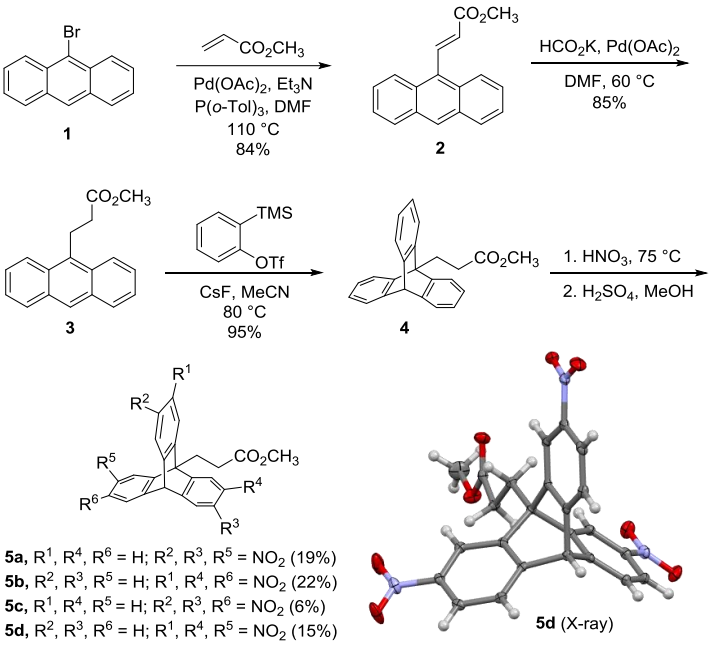

Next, isomer **5d** was utilized in subsequent transformations that were described in the previous publication.[40] Pd/C-catalyzed hydrogenation, Fmoc protection, and acid-catalyzed hydrolysis of the ester were performed to yield protected triptycene acid **7** in 78% yield over three steps. A key building block **7** was immobilized on 2-chlorotrityl chloride resin in preparation for solid-phase diversification (Scheme 8.2a). After addition of triptycene and washing of the resin, the Fmoc groups on triptycene were deprotected using piperidine in DMF (20% v/v) for 1 h. A decreased reaction time led to incomplete deprotection of all three Fmoc groups. After deprotection, the first amino acid was coupled onto the immobilized triptycene amino acids were continued until the final sequence was obtained. The final deprotection of the

Scheme 8.2. Solid-Phase Synthesis of Orthogonally Protected Building Block 7 and Fluorescence-Quenching Experiment of Triptycene-Peptides

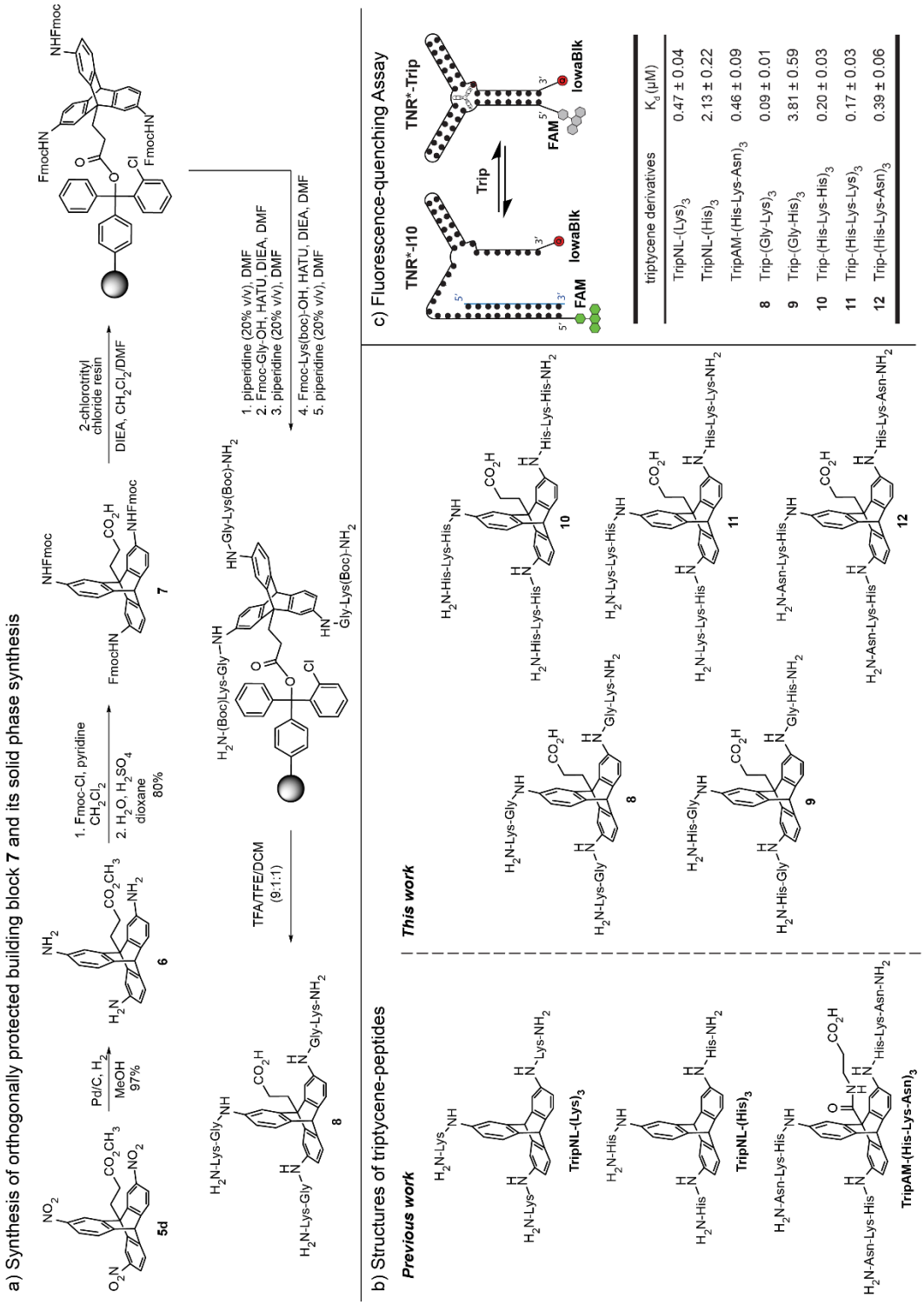

using HATU and DIEA. Overnight couplings were required for complete reaction with all three hindered aniline nitrogens. Next, subsequent deprotections followed by coupling of the desired amino acid side chain protecting groups and cleavage from resin were performed simultaneously using 9:1:1 TFA/TFE/DCM. The resulting triptycene-peptides were purified by reverse phase HPLC and characterized prior to evaluation of the junction binding properties. In this manuscript, we focused our efforts on mono, di, and tri peptides to maximize diversity while maintaining minimal molecular weight. Longer peptides can certainly be produced although cell permeability will be a consideration as the size increases.

Binding of the amino acid-substituted triptycenes was evaluated against a slipped-out d(CAG)·(CTG) repeat nucleic acid junction. Lysine and histidine containing triptycenes were synthesized due to their large presence in nucleic acid-protein interfacial interactions. Among the molecules previously tested, TripNL-$(Lys)_3$ and TripNL-$(His)_3$ exhibited the highest affinity towards the junction. Several dimeric and trimeric amino acid substituents were synthesized for comparison (Scheme 8.2b). A high-throughput assay in which the 3WJ was labelled with a fluorophore and a quencher was used to determine binding. The addition of a 10 bp oligonucleotide strand that was complementary to the 5' end of the junction (**I10**) opened the structure, resulting in a highly fluorescent state (**TNR*-I10**), as shown in Scheme 8.2c. Titration of junction-stabilizing molecules resulted in quenching of fluorescence due to displacement of the inhibitor strand and reformation of the junction (**TNR*-Trip**). To determine if increased flexibility of the amino acid may play an important role in binding, glycine was coupled directly to the triptycene core followed by lysine or histidine. Trip-$(Gly\text{-}Lys)_3$ (**8**) exhibited increased potency compared to that of Trip-$(Lys)_3$, with a K_d of 90 nM, indicating that

the increased flexibility may allow for better binding. This triptycene derivative demonstrates the highest binding affinity towards the TNR junction thus far. Interestingly, Trip-(Gly-His)$_3$ (**9**) did not exhibit improved binding compared to that of Trip-(His)$_3$. Triptycenes substituted with three amino acids were also synthesized using lysine, histidine, and asparagine. Trip-(His-Lys-His)$_3$ (**10**), Trip-(His-Lys-Lys)$_3$ (**11**), and Trip-(His-Lys-Asn)$_3$ (**12**), which only differ in their final amino acid, exhibited K_d values of 0.20 μM, 0.17 μM, and 0.39 μM, respectively. It should be noted that most triptycene derivatives synthesized in this work showed improved binding affinity compared to the most potent triptycene derivative from the previous work, which exhibited a K_d value of 0.27 μM. We also compared the binding affinity of Trip-(His-Lys-Asn)$_3$ (**12**) to that of TripAM-(His-Lys-Asn)$_3$, which have the same peptide sequence but an amide linker at the bridgehead. They exhibited similar binding affinities toward the junction. Triptycenes **8-12** were also characterized using a gel shift assay, where the inhibitor strand was incubated with unlabeled 3WJ (Figure 8.3). This change resulted in an electrophoretic shift that is consistent with a larger complex. Titration of triptycene with this complex resulted in reformation of the nucleic acid junction.

8.3 Conclusions

In summary, we have developed a shorter, more efficient synthetic strategy toward a bridgehead-substituted triptycene building block. This new synthetic route is improved in terms of solubility, enabling large-scale reactions. Moreover, this route provides an interesting new

regioisomer that was not observed through the previous route. A building block with an attachment point at the bridgehead provided rapid access to new triptycene peptide derivatives using solid-phase synthesis methods. The triptycene peptides were evaluated for nucleic acid junction binding to a triplet repeat expansion oligonucleotide using a fluorescence-based assay, which revealed the most potent binder to this junction to date. New triptycene building blocks that are amenable to solid-phase diversification provide a path for the discovery of new junction binders with superior properties. This new class of bridgehead-substituted triptycenes may allow for the generation of one-bead-one-compound combinatorial libraries for the rapid discovery of new junction binders using fluorescently labeled junctions. [42-44] Additionally, this new class of bridgehead-substituted triptycenes opens the door for the creation of pull-down probes to identify cellular targets in future studies.

8.4 Experimental Section

General information

All commercial reagents and solvents were used as received. 9-bromoanthracene, potassium formate, nitric acid, Fmoc chloride, pyridine, and acetonitrile were purchased from Sigma-Aldrich (St. Louis, MO). Methyl acrylate, triethylamine (Et_3N), tri-*o*-tolylphosphine, palladium(II) acetate, cesium fluoride, and Pd/C were purchased from Acros Organics. Methanol, dichloromethane (DCM), dimethylformamide (DMF) were purchased from Fisher Scientific (Waltham, MA). (1-[Bis(dimethylamino)methylene]-1H-1,2,3-triazolo[4,5-

b]pyridinium3-oxide hexafluorophosphate) (HATU) was purchased from Oakwood Products, Inc. (West Colombia, SC), 2-chlorotrityl chloride resin was purchased from Advanced ChemTech (Louisville, KY), diisopropylethylamine (DIEA), trifluoroacetic acid (TFA), and 2,2,2-trifluoroethanol (TFE) were purchased from Alfa Aesar (Ward Hill, MA), and piperidine was purchased from American Bioanalytical (Natick, MA). Chloroform-d, methanol-d4, dimethylsulfoxide-d6 were purchased from Cambridge Isotope Laboratories (Tewksbury, MA). Thin-layer chromatography was done using Sorbent Technologies (Norcross, GA) silica plates (250 μm thickness). Flash chromatography was performed on a Teledyne Isco (Lincoln, NE) CombiFlash R_f system using RediSep R_f silica columns.

TNR DNA 3WJ (5'-GCGGAGCAGCCCTTGGGCAGCACCTTGGTGCTGCTCCGC-3') and DNA inhibitor 10 (5'-GCTGCTCCGC-3') were purchased from Integrated DNA Technologies (IDT). HPLC-purified TNR DNA 3WJ oligo modified with a 5'-FAM and a 3'-IowaBlack was purchased from IDT.

^{1}H and ^{13}C NMR were recorded on a Bruker UNI 500 NMR at 500 and 125 MHz, respectively. High resolution mass spectra were obtained at the University of Pennsylvania Mass Spectrometry Center on a Waters LC-TOF mass spectrometer (model LCT-XE Premier) using electrospray ionization in positive or negative mode, depending on the analyte. High-performance liquid chromatography was performed on a JASCO HPLC (Easton, MD) equipped with a Phenomenx (Torrance, CA) column (Analytical: Luna 5μ C18(2) 100A; 250 x 4.60 mm, 5 μm Semi-prep: 5μ C18(2) 100A; 250 x 10.00 mm, 5 μm) using aqueous (H_2O + 0.1% CF_3CO_2H) and organic (CH_3CN) phases. Matrix-assisted laser desorption ionization

(MALDI) mass spectra were obtained on a Bruker Ultraflex III MALDI-TOF-TOF mass spectrometer (Billerica, MA) using α-cyano-4-hydroxycinnamic acid (CHCA). Fluorescence measurements were collected on a Tecan M1000 plate reader (Mannedorf, Switzerland).

Experimental procedures

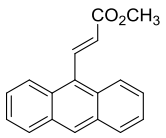

2

methyl-3-(anthracen-9-yl)acrylate (2).[45-47] A solution of 9-bromoanthracene (192 mg, 0.746 mmol), methyl acrylate (642 mg, 7.46 mmol), Et_3N (755 mg, 7.46 mmol), tri-*o*-tolylphosphine (25 mg, 0.082 mmol), and $Pd(OAc)_2$ (8.37 mg, 0.0373 mmol) in DMF (7 mL) was heated at 120 °C in a sealed tube for 5 h. Upon cooling, the mixture was filtered through Celite and washed with ethyl acetate. The filtrate was extracted with ethyl acetate and water several times. Combined organic layers were then dried over Na_2SO_4. The crude mixture was purified by column chromatography on silica gel (5% EtOAc/hexanes) to give **1** (164 mg, 84%). ^{1}H NMR (500 MHz, $CDCl_3$) δ 8.65 (d, 1H, J = 16.3 Hz), 8.45 (s, 1H), 8.25-8.23 (m, 2H), 8.03-8.01 (m, 2H), 7.53-7.48 (m, 4H), 6.45 (d, 1H, J = 16.3 Hz), 3.93 (s, 3H); ^{13}C NMR (125 MHz, $CDCl_3$) δ 167.0, 142.4, 131.4, 129.5, 129.4, 129.0, 128.4, 126.9, 126.5, 125.5, 125.3, 52.1; IR (neat) 3051, 2949, 1719, 1635, 1435, 1265, 1170, 988, 886, 733; HRMS *m/z* calcd for $C_{18}H_{15}O_2^+$ $[M+H]^+$ 263.1067, observed 263.1074.

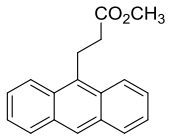

3

methyl 3-(anthracen-9-yl)propanoate (3).[45-47] To a solution of **2** (102 mg, 0.389 mmol) in DMF (5 mL) was added potassium formate (654 mg, 7.78 mmol) and $Pd(OAc)_2$ (4.4 mg, 0.02 mmol) and stirred at 60 °C for 4 h. After cooling, the mixture was filtered through Celite and washed with ethyl acetate. The filtrate was extracted with ethyl acetate and water. The combined organic layer was washed with water and brine, then dried over Na_2SO_4. The crude mixture was purified by column chromatography on silica gel (5% EtOAc/hexanes) to yield **3** (87.3 mg, 85%). ^1H NMR (500 MHz, $CDCl_3$) δ 8.38 (s, 1H), 8.28 (dd, 2H, J = 8.8, 0.6 Hz), 8.02 (dd, 2H, J = 8.4, 0.5), 7.56-7.53 (m, 2H), 7.50-7.46 (m, 2H), 4.00-3.96 (m, 2H), 3.75 (s, 3H), 2.82-2.79 (m, 2H); ^{13}C NMR (125 MHz, $CDCl_3$) δ 173.6, 132.4, 131.7, 129.6, 129.6, 126.5, 126.1, 125.1, 124.0, 52.0, 35.2, 23.4; IR (neat) 3053, 2950, 1734, 1436, 1174, 885, 732; HRMS *m/z* calcd for $C_{18}H_{17}O_2^+$ $[M+H]^+$ 265.1223, observed 265.1226.

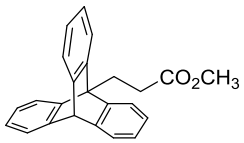

4

methyl 3-(9,10-[1,2]benzenoanthracen-9(10H)-yl)propanoate (4).[48] To a solution of **3** (443 mg, 1.68 mmol) in acetonitrile (2.8 mL) was added CsF (764 mg, 5.03 mmol) and 2-(trimethylsilyl)phenyl trifluoromethanesulfonate (1.0 g, 3.35 mmol) and stirred at 80 °C for 4 h. Upon cooling, saturated NH_4Cl solution was added to the mixture and then extracted with

dichloromethane. The combined organic layer was washed with brine and dried over Na_sSO_4. The crude mixture was purified by column chromatography on silica gel (5-10% EtOAc/hexanes) to yield **4** (542 mg, 95%). ^{1}H NMR (500 MHz, $CDCl_3$) δ 7.40-7.30 (m, 6H), 7.04-6.95 (m, 6H), 5.34 (s, 1H), 3.85 (s, 3H), 3.36-3.31 (m, 2H), 3.21-3.15 (m, 2H); ^{13}C NMR (125 MHz, $CDCl_3$) δ 174.7, 147.0, 125.2, 125.1, 123.8, 122.1, 54.6, 53.4, 52.2, 30.7, 22.7; IR (neat) 2952, 1733, 1450, 1176, 628; HRMS *m/z* calcd for $C_{24}H_{20}NaO_2^+$ $[M+Na]^+$ 363.1356, observed 363.1369.

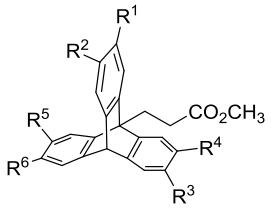

5a, R^1, R^4, R^6 = H; R^2, R^3, R^5 = NO_2; 19%
5b, R^2, R^3, R^5 = H; R^1, R^4, R^6 = NO_2; 22%
5c, R^1, R^4, R^5 = H; R^2, R^3, R^6 = NO_2; 6%
5d, R^2, R^3, R^6 = H; R^1, R^4, R^5 = NO_2; 15%

methyl 3-(trinitro-9,10-[1,2]benzenoanthracen-9(10H)-yl)propanoate (5a-5d). A solution of **4** (424.5 mg, 1.25 mmol) in concentrated HNO_3 (15 mL) was stirred at 75 °C overnight. The solution was cooled to room temperature, neutralized, and extracted with EtOAc. The organic layers were combined, washed with brine, and dried over Na_2SO_4. The crude mixture was then reesterified by stirring in methanol (50 mL) with catalytic H_2SO_4 under reflux overnight. The solution was concentrated under vacuum. Water was added and then basified by the addition of 1M NaOH. The water was extracted with EtOAc immediately. The organic layer was washed with brine and dried over Na_2SO_4. The crude mixture was purified by column chromatography on silica gel (30% EtOAc/hexanes) to give **5a** (110 mg, 19%), **5b** (130 mg, 22%), **5c** (37.2 mg,

6.3%), and **5d** (88.3 mg, 15%). **5a** ^{1}H NMR (500 MHz, $CDCl_3$) δ 8.32 (d, 2H, J = 1.3 Hz), 8.28 (s, 1H), 8.01 (dd, 3H, J = 8.3, 2.2 Hz), 7.69 (d, 1H, J = 8.1 Hz), 7.62 (d, 2H, J = 8.4 Hz), 5.87 (s, 1H), 3.91 (s, 3H), 3.52 (t, 2H, J = 7.4 Hz), 3.17 (t, 2H, J = 7.4 Hz); ^{13}C NMR (125 MHz, $CDCl_3$) δ 173.4, 151.3, 150.2, 146.2, 146.1, 145.8, 145.0, 125.2, 123.6, 122.5, 122.1, 119.4, 118.3, 54.8, 53.3, 52.7, 30.2, 22.0; IR (neat) 2953, 1734, 1523, 1344, 1201, 738; HRMS *m/z* calcd for $C_{24}H_{18}N_3NaO_8^+$ $[M+Na]^+$ 498.0908, observed 498.0919; mp 143-146 °C; **5b** ^{1}H NMR (500 MHz, $CDCl_3$) δ 8.32-8.27 (m, 3H), 8.04-7.97 (m, 3H), 7.69 (d, 2H, J = 8.1 Hz), 7.64 (d, 1H, J = 8.4 Hz), 5.88 (s, 1H), 3.92 (s, 3H), 3.56 (t, 2H, J = 7.3 Hz), 3.20 (t, 2H, J = 7.3 Hz); ^{13}C NMR (125 MHz, $CDCl_3$) δ 173.4, 150.9, 150.5, 146.2, 145.8, 145.7, 145.3 125.2, 123.6, 122.4, 122.1, 119.4, 118.1, 54.6, 53.4, 52.7, 30.2, 21.8; IR (neat) 3091, 2953, 2848, 1733, 1520, 1342, 1201, 736; HRMS *m/z* calcd for $C_{24}H_{18}N_3NaO_8^+$ $[M+Na]^+$ 498.0908, observed 498.0919; mp 139-142 °C; **5c** ^{1}H NMR (500 MHz, $CDCl_3$) δ 8.32 (d, 3H, J = 2.2 Hz), 8.03 (dd, 3H, J = 8.4, 2.2 Hz), 7.60 (d, 3H, J = 8.4 Hz), 5.79 (s, 1H), 3.92 (s, 3H), 3.48 (t, 2H, J = 7.6 Hz), 3.13 (t, 2H, J = 7.6 Hz); ^{13}C NMR (125 MHz, $CDCl_3$) δ 173.4, 149.9, 146.7, 146.4, 123.7, 122.2, 119.5, 55.2, 53.6, 52.7, 30.5, 22.6; HRMS *m/z* calcd for $C_{24}H_{16}N_3O_8^-$ $[M-H]^-$ 474.0943, observed 474.0931; **5d** ^{1}H NMR (500 MHz, $CDCl_3$) δ 8.31 (d, 3H, J = 1.7 Hz), 8.04 (dd, 3H, J = 8.1, 1.8 Hz), 7.63 (d, 3H, J = 8.1Hz), 5.78 (s, 1H), 3.96 (s, 3H), 3.57 (t, 2H, J = 7.3 Hz), 3.20 (t, 2H , J = 7.3 Hz); ^{13}C NMR (125 MHz, $CDCl_3$) δ 173.4, 150.5, 146.4, 125.2, 122.5, 118.3, 54.6, 53.8, 52.9, 30.3, 21.8; IR (neat) 3093, 2954, 2851, 1736, 1525, 1453, 1343, 1202, 1076, 903, 823; HRMS *m/z* calcd for $C_{24}H_{18}N_3NaO_8^+$ $[M+Na]^+$ 498.0908, observed $[M+Na]^+$ 498.0910; mp 147-150 °C.

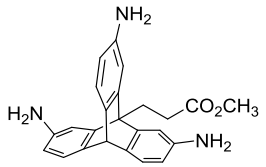

6

methyl 3-(2,7,15-triamino-9,10-[1,2]benzenoanthracen-9(10H)-yl)propanoate (6). To a solution of **5d** (259 mg, 0.544 mmol) in methanol was added Pd/C (25 mg). The solution was purged with a H_2 gas balloon and kept under H_2 gas for 1 h. The mixture was filtered through Celite and washed with methanol. The filtrate was concentrated and purified by column chromatography on silica gel (5% MeOH/DCM) to give **6** (204 mg, 97%). ^{1}H NMR (500 MHz, MeOD) δ 7.01 (d, 3H, J = 7.7 Hz), 6.79 (d, 3H, J = 1.7 Hz), 6.33 (dd, 3H, J = 7.7, 1.5 Hz), 4.98 (s, 1H), 3.85 (s, 3H), 3.18-3.13 (m, 4H); ^{13}C NMR (125 MHz, MeOD) δ 176.5, 144.6, 140.7, 124.1, 112.6, 112.2, 54.2, 53.3, 52.5, 31.4, 23.8; IR (neat) 3354, 2951, 1724, 1605, 1473, 1326, 1181, 582 HRMS *m/z* calcd for $C_{24}H_{24}N_3O_2^+$ $[M+H]^+$ 386.1863, observed 386.1848.

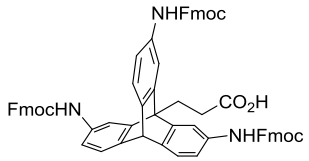

7

3-(2,7,15-tris((((9H-fluoren-9-yl)methoxy)carbonyl)amino)-9,10-[1,2]benzenoanthracen-9(10H)-yl)propanoic acid (7). To a solution of **6** (116 mg, 0.301 mmol) in DCM (2.5 mL) was added excess pyridine. The solution was cooled to 0 °C, then added Fmoc chloride in DCM (2.5 mL) slowly. The solution was allowed to warm to room temperature over time and stirred overnight. The mixture was extracted with DCM and acidic water. The organic layer was washed with brine and dried over $MgSO_4$. The crude mixture was purified by column chromatography

on silica gel (30% EtOAc/hexanes). A solution of the ester (209 mg, 0.199 mmol) in dioxane (5 mL), H_2O (5 mL), and catalytic H_2SO_4 was stirred at 80 °C overnight. The reaction mixture was neutralized and concentrated under vacuum. Water was added to the mixture and was extracted with DCM. The organic layer was washed with brine and dried over Na_2SO_4. The crude mixture was purified by column chromatography on silica gel (50% EtOAc/hexanes) to yield **7** (165 mg, 80%). ^{1}H NMR (500 MHz, DMSO-*d*6) δ 12.44 (bs, 1H), 9.58 (s, 3H), 7.89 (d, 6H, J = 7.6 Hz), 7.72 (d, 6H, J = 7.0 Hz), 7.50 (s, 3H), 7.40 (t, 6H, J = 7.4 Hz), 7.36-7.22 (m, 9H), 7.14 (bs, 3H), 5.37 (s, 1H), 4.44 (d, 6H, J = 6.7 Hz), 4.28 (t, 3H, J = 6.7 Hz), 3.13-2.92 (m, 4H) ; ^{13}C NMR (125 MHz, DMSO) δ 174.2, 153.4, 143.7, 141.3, 140.7, 135.7, 127.6, 127.1, 125.1, 123.2, 120.1, 114.4, 113.5, 65.5, 52.2, 50.9, 46.6, 29.2, 22.2 IR (neat) 3375, 3325, 3075, 2950, 1709, 1605, 1528, 1450, 1212, 738; HRMS *m/z* calcd for $C_{69}H_{52}N_3O_8^+$ $[M+H]^+$ 1038.3749, observed 1038.3737; mp 169-171 °C.

Solid Phase Synthesis:

All triptycenes were synthesized on 2-chlorotrityl chloride resin (100-200 mesh, 1.5 mmol substitution/g). The resin was added to a dry glass reaction vessel and swollen by stirring in dichloromethane (DCM) for 30 min. After swelling, the DCM was removed by vacuum and Fmoc-Trip-OH (**8d**) was coupled to the resin. Fmoc-Trip-OH (1.5 equiv) in 1:5 DMF:DCM and DIEA (5equiv) were added and stirred for 5 min. DIEA (1.5 equiv) was added and the resin was stirred overnight. The solution was then drained by vacuum and the resin was washed thoroughly with DMF, then DCM, then DMF. The beads were deprotected by treatment with

20% piperidine in DMF for 1 h with stirring. The deprotection solution was removed by vacuum and the resin was washed thoroughly with DMF, DCM, then DMF. The first Fmoc-protected amino acid was then activated with HATU (9 equiv) in the presence of DIEA (18 equiv) prior to addition to the reaction vessel and allowed to couple overnight. Subsequent deprotections and amino acid couplings were run as described above. Before cleavage from the resin, the terminal Fmoc was removed. The beads were thoroughly washed with DMF then DCM. Peptides were cleaved by addition of trifluoroacetic acid (TFA), 2,2,2-trifluoroethanol (TFE), and DCM (9:1:1). The cleavage solution was collected by vacuum and concentrated using a rotary evaporator. The crude residue was diluted in 1:1 (0.1% TFA/H_2O:MeCN), purified by reverse-phase HPLC, and analyzed by MALDI-MS.

Table 8.1. Calculated and Observed Triptycene Masses.

Triptycene	Calculted m/z $[M+H]^+$	Observed m/z $[M+H]^+$	Calculted m/z $[M+Na]^+$	Observed m/z $[M+Na]^+$
Trip-(Gly-Lys)$_3$	927.52	927.57	949.40	949.52
Trip-(Gly-His)$_3$	954.41	954.41	976.39	976.39
Trip-(His-Lys-His)$_3$	1578.81	1578.76	1600.79	1600.74
Trip-(His-Lys-Lys)$_3$	1551.92	1551.81	1573.90	1573.83
Trip-(His-Lys-Asn)$_3$	1509.76	1509.70	1531.74	1531.68

Fluorescence Quenching Assay

All experiments were conducted in 50 mM sodium phosphate buffer, pH 7.2. Fluorescence measurements were recorded with excitation at 495 nm and emission at 520 nm

using 5 nm bandwidths on a Tecan M1000 plate reader. Inhibitor strand displacement by triptycene curves were obtained by incubating 120 nM TNR DNA with 10 μM inhibitor 10 for 2 h, followed by addition of increasing concentrations of triptycenes. Samples were incubated for 2 h and measured in triplicate in a 384-well plate.

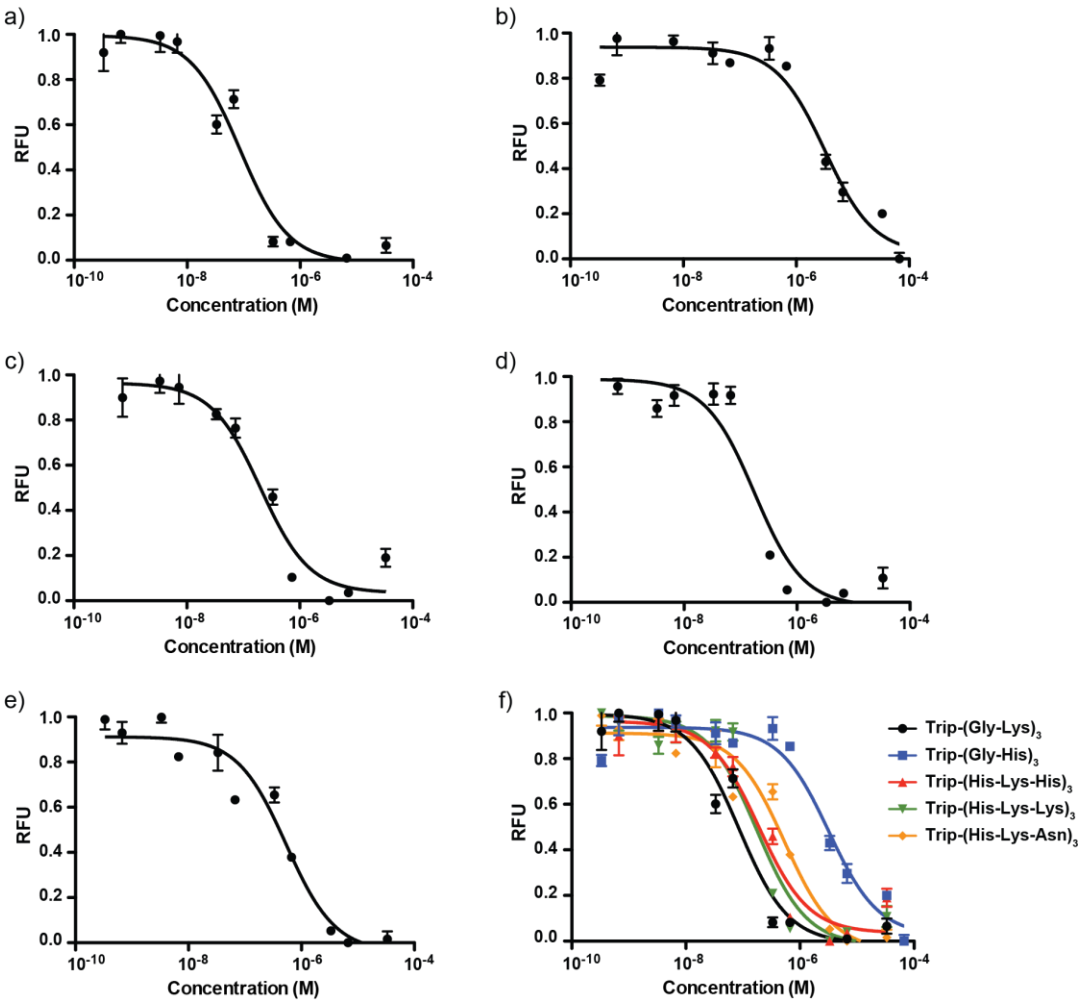

Figure 8.2. Fluorescence-quenching experiment plots. Displacement of I10 from TNR 3WJ by Trip-(Gly-Lys)$_3$ (a), Trip-(Gly-His)$_3$ (b), Trip-(His-Lys-His)$_3$ (c), Trip-(His-Lys-Lys)$_3$ (d), Trip-(His-Lys-Asn)$_3$ (e). An overlay of all plot is shown in (f).

Gel Shift Assay

Gel shift experiments were conducted in 50 mM sodium phosphate buffer, pH 7.2. Triptycene titration gels were prepared by incubating TNR 3WJ (0.5 μM) with inhibitor strand 10 (1.5 μM) for 2 h followed by titration of triptycenes and incubation at room temperature for 2 h. Samples were loaded on a 20% non-denaturing polyacrylamide gel (19:1 monomer:bis) at 50V in 1X TBR buffer at 4 °C for 10 h. Gels were imaged by staining with SYBR Gold for 15 min then visualized using a BioRad GelDoc XR+ imager.

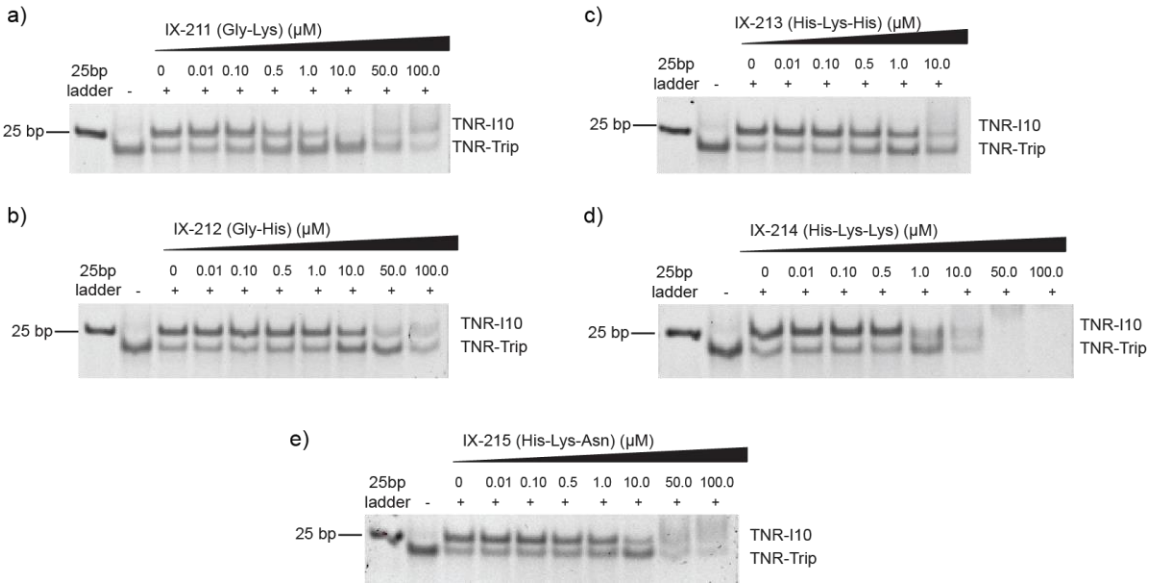

Figure 8.3. Gel shift assay in the presence of triptycenes. TNR 3WJ was incubated with I10 followed by titration of triptycene derivatives, Gly-Lys (a), Gly-His (b), His-Lys-His (c), His-Lys-Lys (d), or His-Lys-Asn (e).

8.5 Acknowledgments

Supported by funding from the University of Pennsylvania. Instruments supported by the NSF and NIH including HRMS (NIH RR-023444) and MALDI-MS (NSF MRI-0820996). We thank Pat Carroll (University of Pennsylvania) for X-ray crystallographic assistance. S.A.B. thanks NIH for funding through the Chemistry–Biology Interface Training Program (T32 GM07133). I.Y. thanks the Kwanjeong Educational Foundation for funding.

8.6 References

(1) Altona, C. *J. Mol. Biol.* **1996**, *263*, 568–581.

(2) Lilley, D. M. J. *Q. Rev. Biophys.* **2000**, *33*, 109–159.

(3) Duckett, D. R.; Lilley, D. M. J. *EMBO* **1990**, *9*. 583.

(4) Singleton, M. R.; Scaife, S.; Wigley, D. B. *Cell* **2015**, *107*, 79–89.

(5) Woods, K. C.; Martin, S. S.; Chu, V. C.; Baldwin, E. P. *J. Mol. Biol.* **2001**, *313*, 49–69.

(6) Bai, Y.; Tambe, A.; Zhou, K.; Doudna, J. a. *Elife* **2014**, *3*, e03656.

(7) Leonard, C. J.; Berns, K. I. *Nucleic Acid Res. Mol. Biol* **1994**, *48* (29-52).

(8) Liu, G.; Chen, X.; Bissler, J. J.; Sinden, R. R.; Leffak, M. *Nat. Chem. Biol.* **2010**, *6*, 652–659.

(9) Mauger, D. M.; Golden, M.; Yamane, D.; Williford, S.; Lemon, S. M.; Martin, D. P.; Weeks, K. M. *Proc. Natl. Acad. Sci.* **2015**, *112*, 3692-3697.

(10) Mirkin, S. M. *Nature* **2007**, *447*, 932–940.

(11) Slean, M. M.; Reddy, K.; Wu, B.; Nichol Edamura, K.; Kekis, M.; Nelissen, F. H. T.; Aspers, R. L. E. G.; Tessari, M.; Schärer, O. D.; Wijmenga, S. S.; Pearson, C. E. *Biochemistry* **2013**, *52*, 773–785.

(12) Watts, J. M.; Dang, K. K.; Gorelick, R. J.; Leonard, C. W.; Bess Jr, J. W.; Swanstrom, R.; Burch, C. L.; Weeks, K. M. *Nature* **2009**, *460*, 711–716.

(13) Seeman, N. C.; Lukeman, P. S. *Reports Prog. Phys.* **2005**, *68*, 237–270.

(14) Shu, D.; Shu, Y.; Haque, F.; Abdelmawla, S.; Guo, P. *Nat. Nanotechnol.* **2011**, *6*, 658–667.

(15) Porchetta, A.; Vallée-Bélisle, A.; Plaxco, K. W.; Ricci, F. *J. Am. Chem. Soc.* **2012**, *134*, 20601–20604.

(16) Wang, F.; Lu, C.-H.; Willner, I. *Chem. Rev.* **2014**, *114*, 2881–2941.

(17) Duprey, J.-L. H. a.; Takezawa, Y.; Shionoya, M. *Angew. Chem., Int. Ed.* **2013**, *52*, 1212–1216.

(18) Kato, T.; Yano, K.; Ikebukuro, K.; Karube, I. *Nucleic Acids Res.* **2000**, *28*, 1963–1968.

(19) Aldaye, F. A.; Palmer, A. L.; Sleiman, H. F. *Science* **2008**, *321*, 1795–1799.

(20) Stojanovic, M. N.; de Prada, P.; Landry, D. W. *J. Am. Chem. Soc.* **2001**, *123*, 4928–4931.

(21) Blackledge, M. S.; Melander, C. *Bioorg. Med. Chem.* **2013**, *21*, 6101–6114.

(22) Carlson, C. B.; Stephens, O. M.; Beal, P. a. *Biopolymers* **2003**, *70*, 86–102.

(23) Chenoweth, D. M.; Meier, J. L.; Dervan, P. B. *Angew. Chem., Int. Ed.* **2013**, *52*, 415–418.

(24) Dervan, P. *Bioorg. Med. Chem.* **2001**, *9*, 2215–2235.

(25) Dervan, P. B.; Edelson, B. S. *Curr. Opin. Struct. Biol.* **2003**, *13*, 284–299.

(26) Fujimoto, J.; Bando, T.; Minoshima, M.; Kashiwazaki, G.; Nishijima, S.; Shinohara, K.; Sugiyama, H. *Bioorg. Med. Chem.* **2008**, *16*, 9741–9744.

(27) Guan, L.; Disney, M. D. *ACS Chem. Biol.* **2012**, *7*, 73–86.

(28) Hartley, J. a.; Hochhauser, D. *Curr. Opin. Pharmacol.* **2012**, *12*, 398–402.

(29) Hermann, T. *Curr. Opin. Struct. Biol.* **2005**, *15*, 355–366.

(30) Hurley, L. H. *Nat. Rev. Cancer* **2002**, *2*, 188–200.

(31) Neidle, S. *Nat. Prod. Rep.* **2001**, *18*, 291–309.

(32) Palchaudhuri, R.; Hergenrother, P. J. *Curr. Opin. Biotechnol.* **2007**, *18*, 497–503.

(33) Poehlsgaard, J.; Douthwaite, S. *Nat. Rev. Microbiol.* **2005**, *3*, 870–881.

(34) Seitz, O. *Angew. Chem., Int. Ed.* **2003**, *42*, 4994–4994.

(35) Thomas, J. R.; Hergenrother, P. J. *Society* **2008**, *108*, 1171–1224.

(36) Vicens, Q.; Westhof, E. *ChemBioChem* **2003**, *4*, 1018–1023.

(37) Wilson, W. D.; Tanious, F. a.; Mathis, A.; Tevis, D.; Hall, J. E.; Boykin, D. W. *Biochimie* **2008**, *90*, 999–1014.

(38) Barros, S. A; Chenoweth, D. M. *Angew. Chem., Int. Ed.* **2014**, *53*, 13746–13750.

(39) Barros, S. A.; Chenoweth, D. M. *Chem. Sci.* **2015**, *6*, 4752-4755.

(40) Yoon, I.; Sung, S.-E.; Barros, S.A.; Chenoweth, D.M. *Org. Lett.* **2016**, *18*, 1096-1099.

(41) Zeng, B.; King, S. *Synthesis (Stuttg).* **2002**, *2*, 2335–2337.

(42) Lam, K. S., Lebl, M., Krchnak, V. *Chem. Rev.* **1997**, *97*, 411-448.

(43) Bryson, D. I.; Zhang, W., Ray, W. K., Santos, W. L. *Mol. Biosyst.* **2009**, *5,* 1070-1073.

(44) Wynn, J. E., Santos, W. L. *Org. Biomol. Chem.* **2015**, *13*, 5848-5858.

(45) Gopal, R.; Reddy, M.; Rao, J. *J. Org. Chem.* **1995**, *1*, 7966–7973.

(46) Arjunan, P.; Shymasundar, N.; Darrell Berlin, K.; Najjar, D.; Rockley, M. G. **1981**, *46*, 626–629.

(47) Cook, J. W.; Ludwiczak, R. S.; Schoental, R. **1950**, *J. Chem. Soc.*, 1112-1121.

(48) Kornfeld, E. C.; Barney, P.; Blankley, J.; Faul, W. *J. Med. Chem.* **1965**, *8*, 342–347.

Appendix 7

NMR Spectra and X-Ray Structure Data Relevant to Chapter 8

Figure A7.1. ^{1}H NMR spectrum of **2** in $CDCl_3$ (500 MHz).

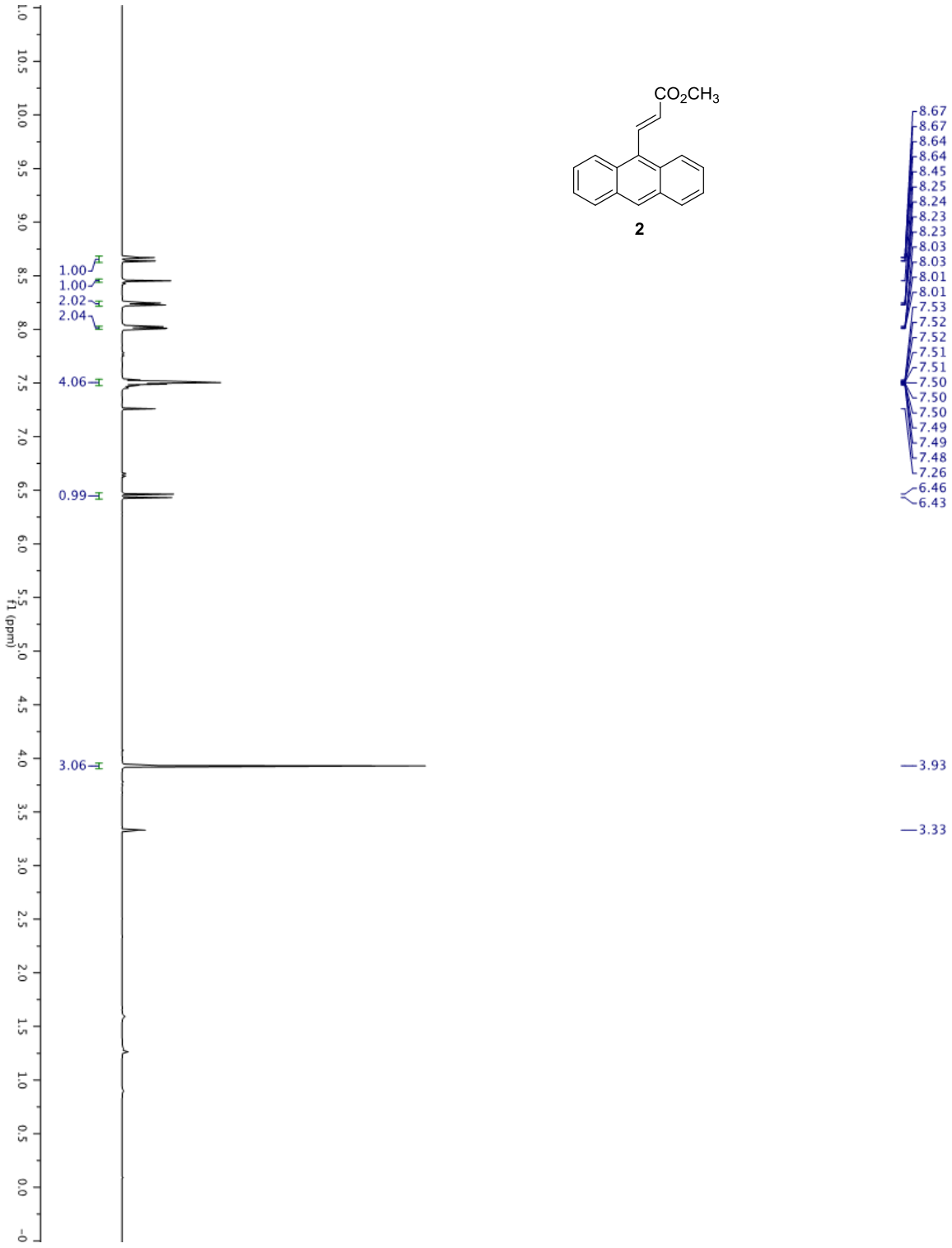

Figure A7.2. ^{13}C NMR spectrum of **2** in $CDCl_3$ (125 MHz).

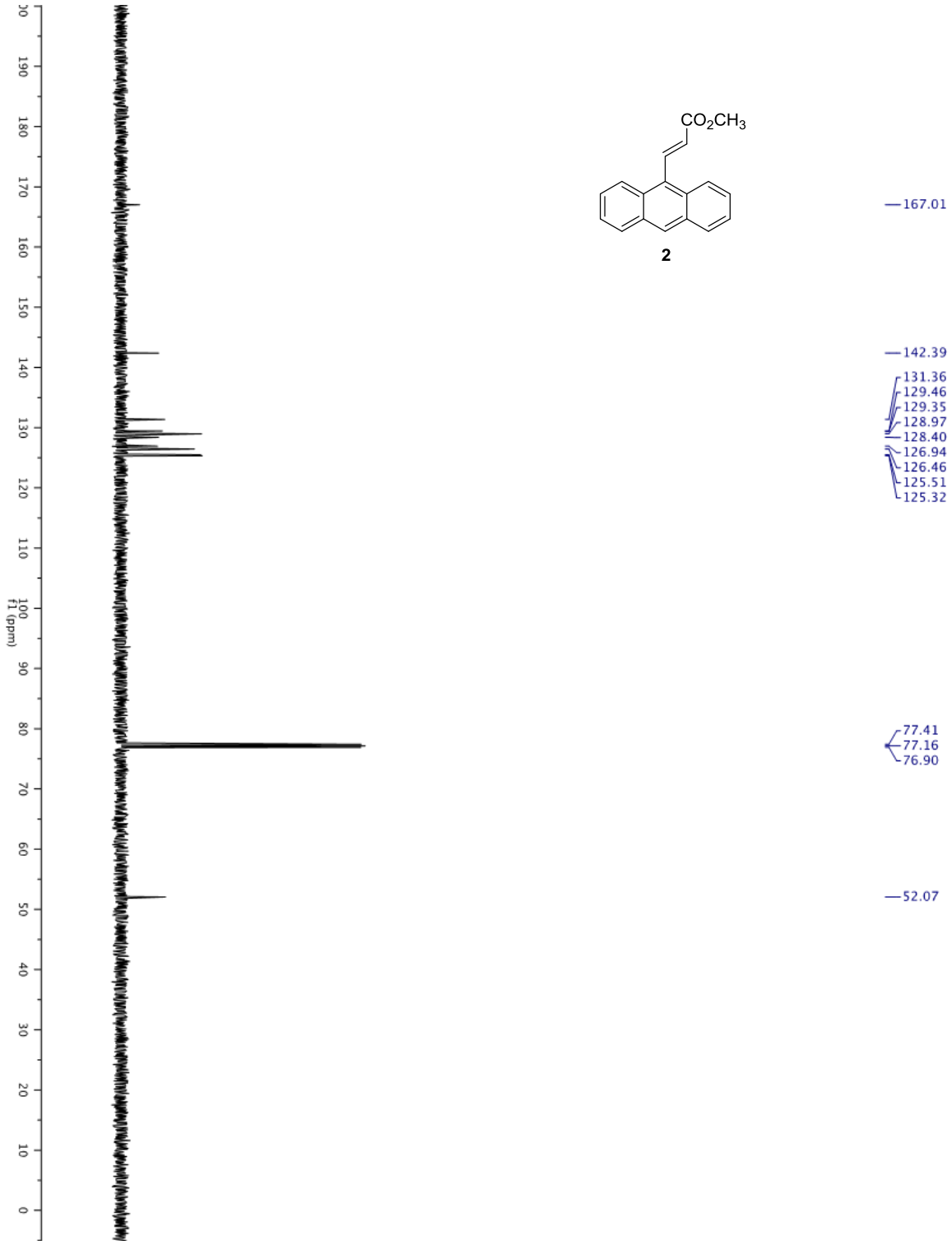

Figure A7.3. ^{1}H NMR spectrum of **3** in $CDCl_3$ (500 MHz).

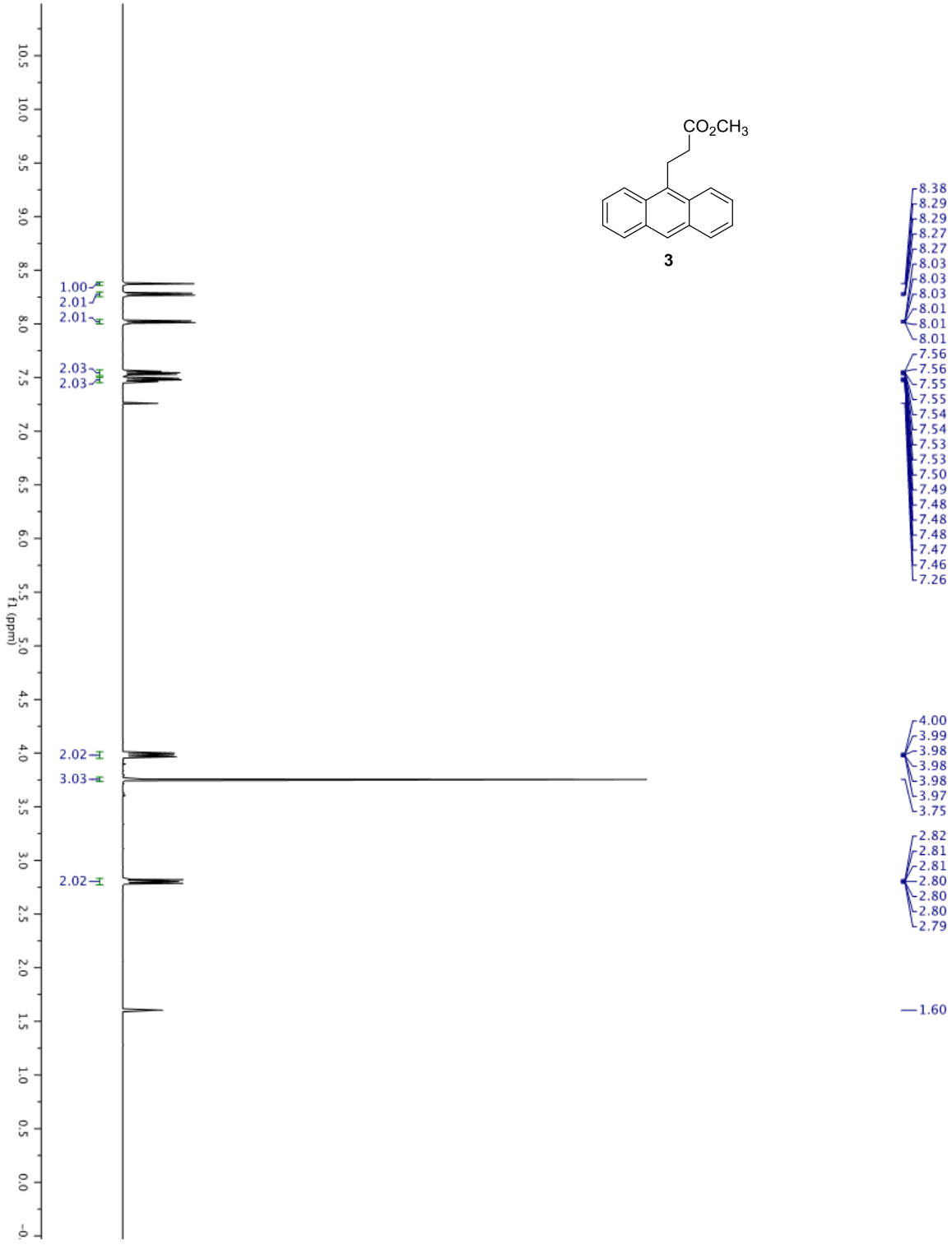

Figure A7.4. ^{13}C NMR spectrum of **3** in $CDCl_3$ (125 MHz).

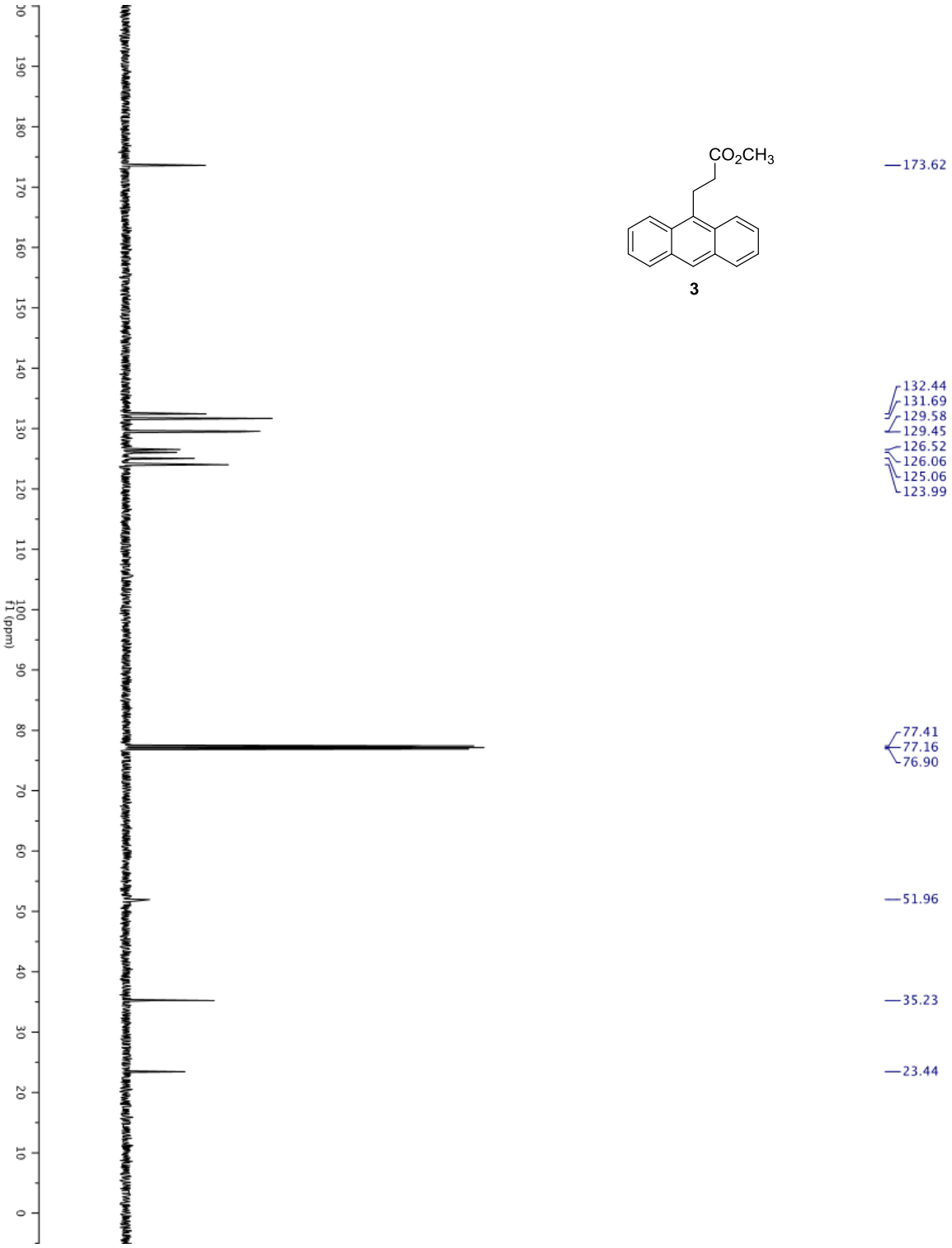

Figure A7.5. ^{1}H NMR spectrum of **4** in $CDCl_3$ (500 MHz).

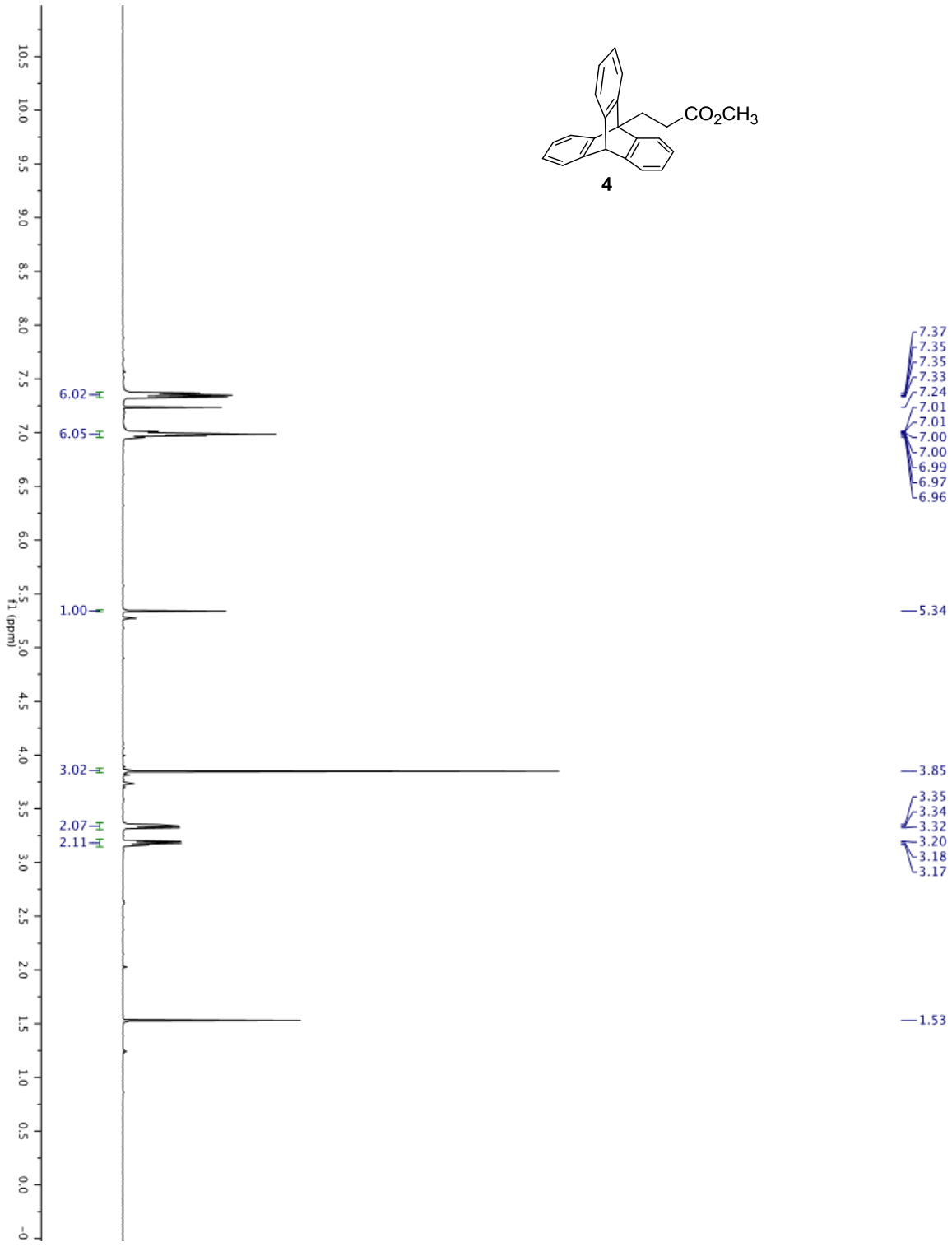

Figure A7.6. ^{13}C NMR spectrum of **4** in $CDCl_3$ (125 MHz).

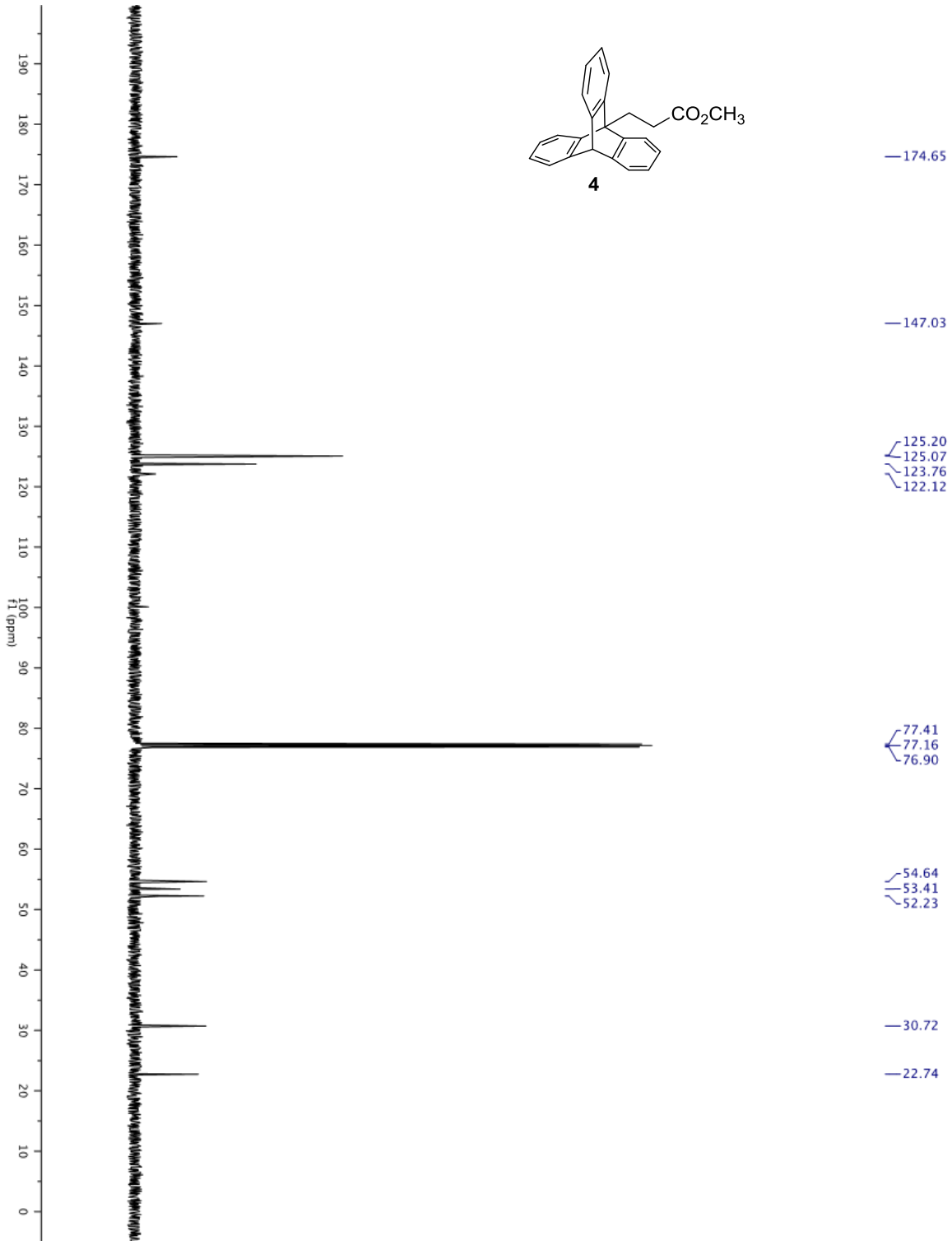

Figure A7.7. ^{1}H NMR spectrum of **5a** in $CDCl_3$ (500 MHz).

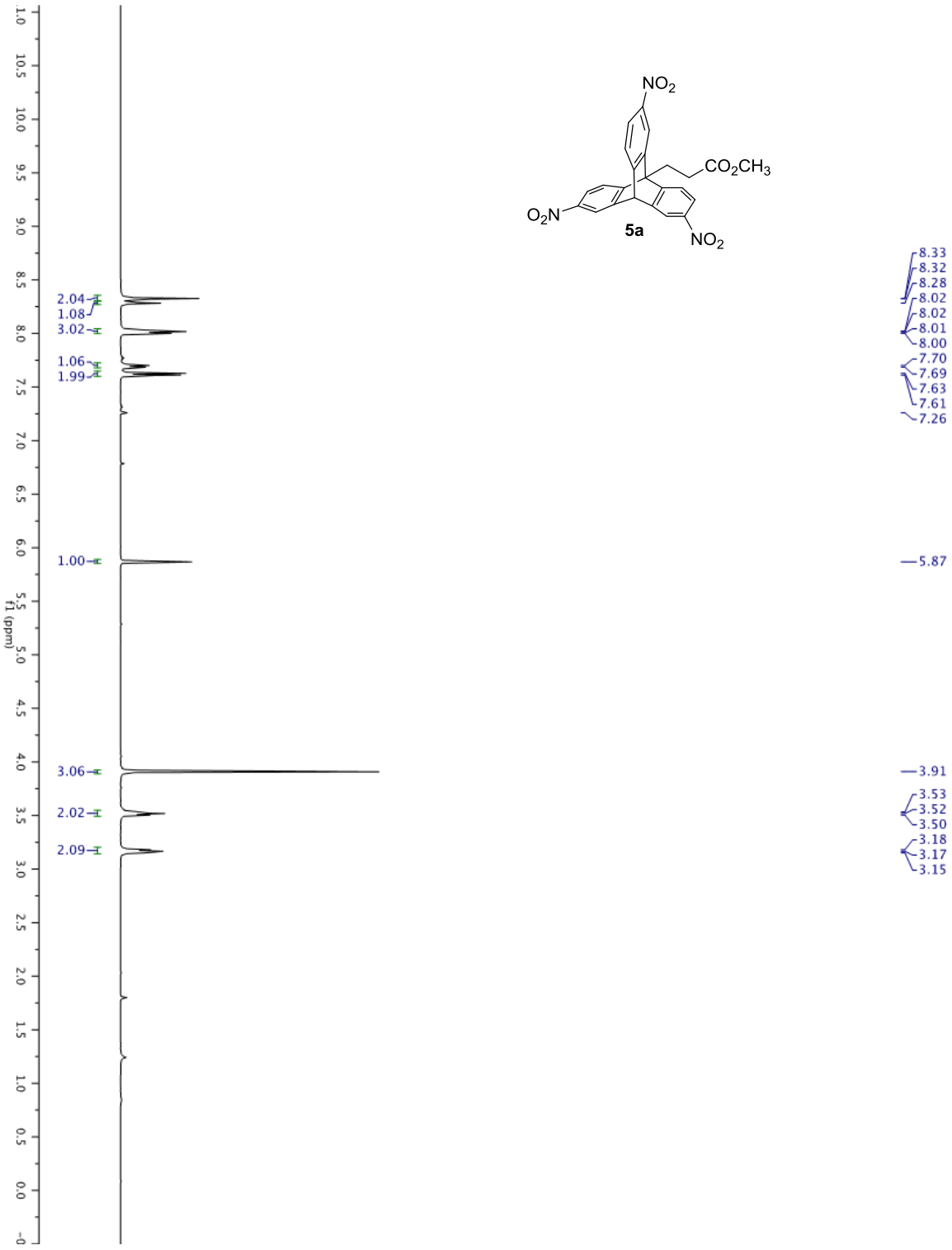

Figure A7.8. ^{13}C NMR spectrum of **5a** in $CDCl_3$ (125 MHz).

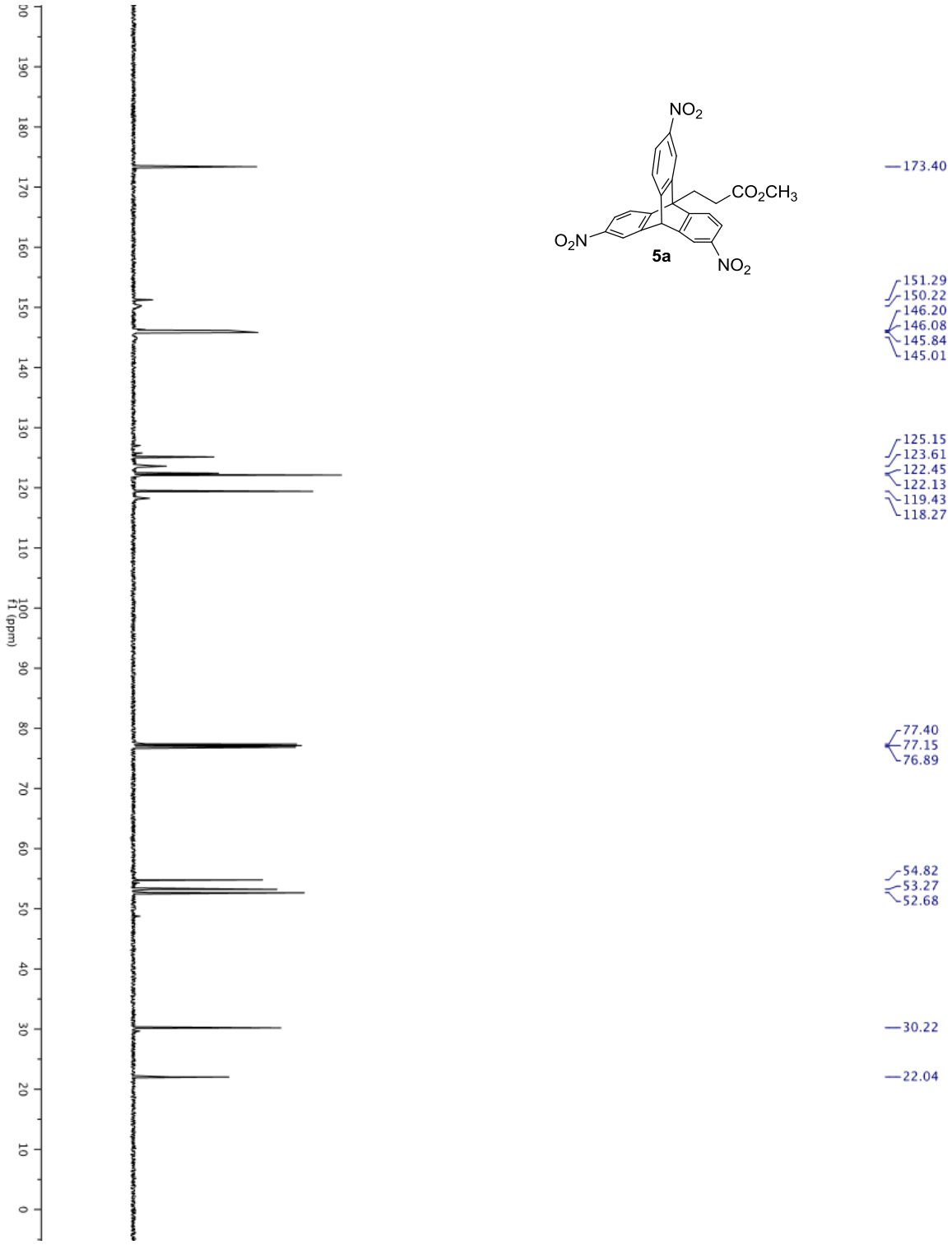

Figure A7.9. HMBC spectrum of **5a** in $CDCl_3$.

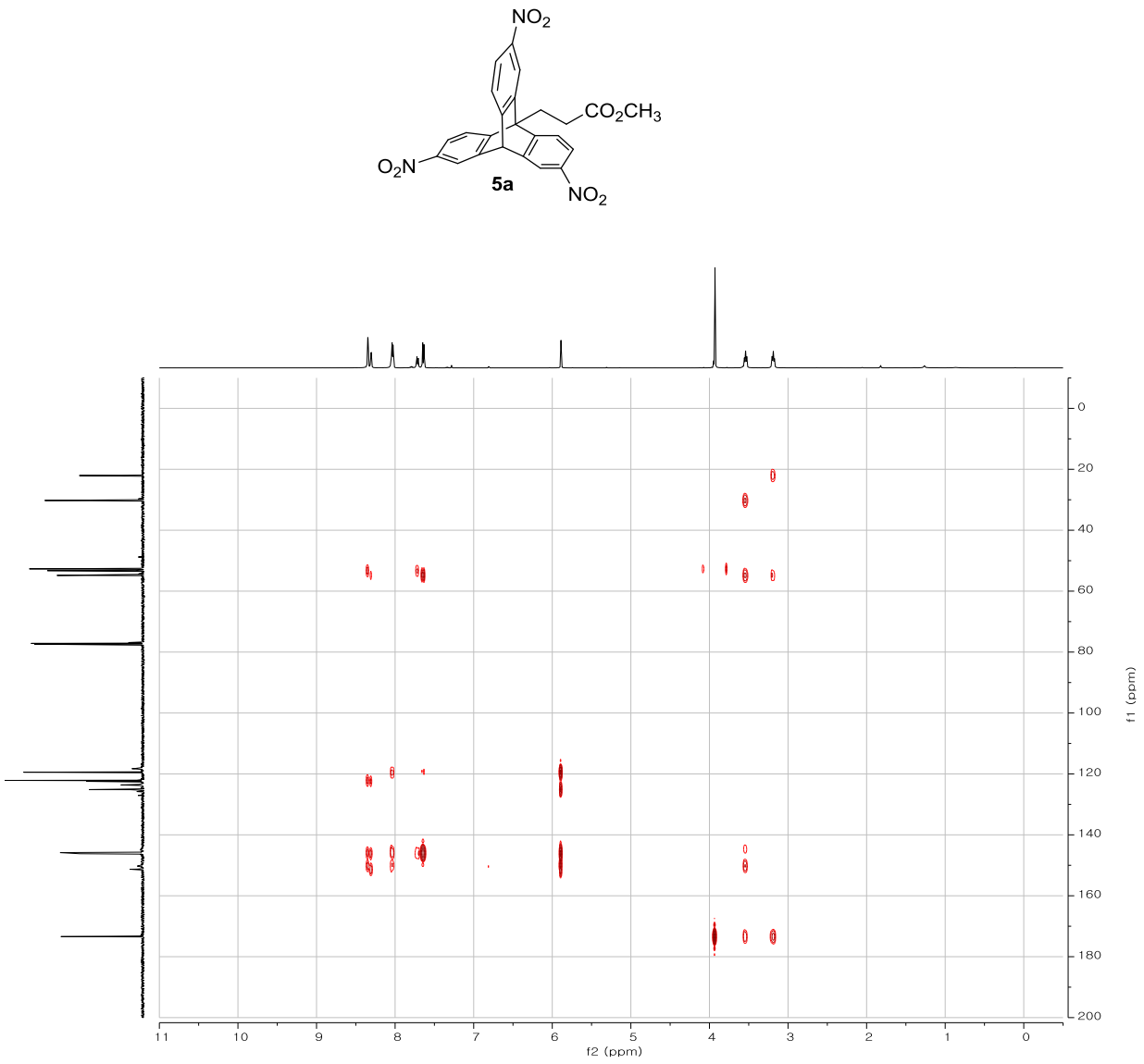

Figure A7.10. Expanded HMBC spectrum of **5a** in $CDCl_3$.

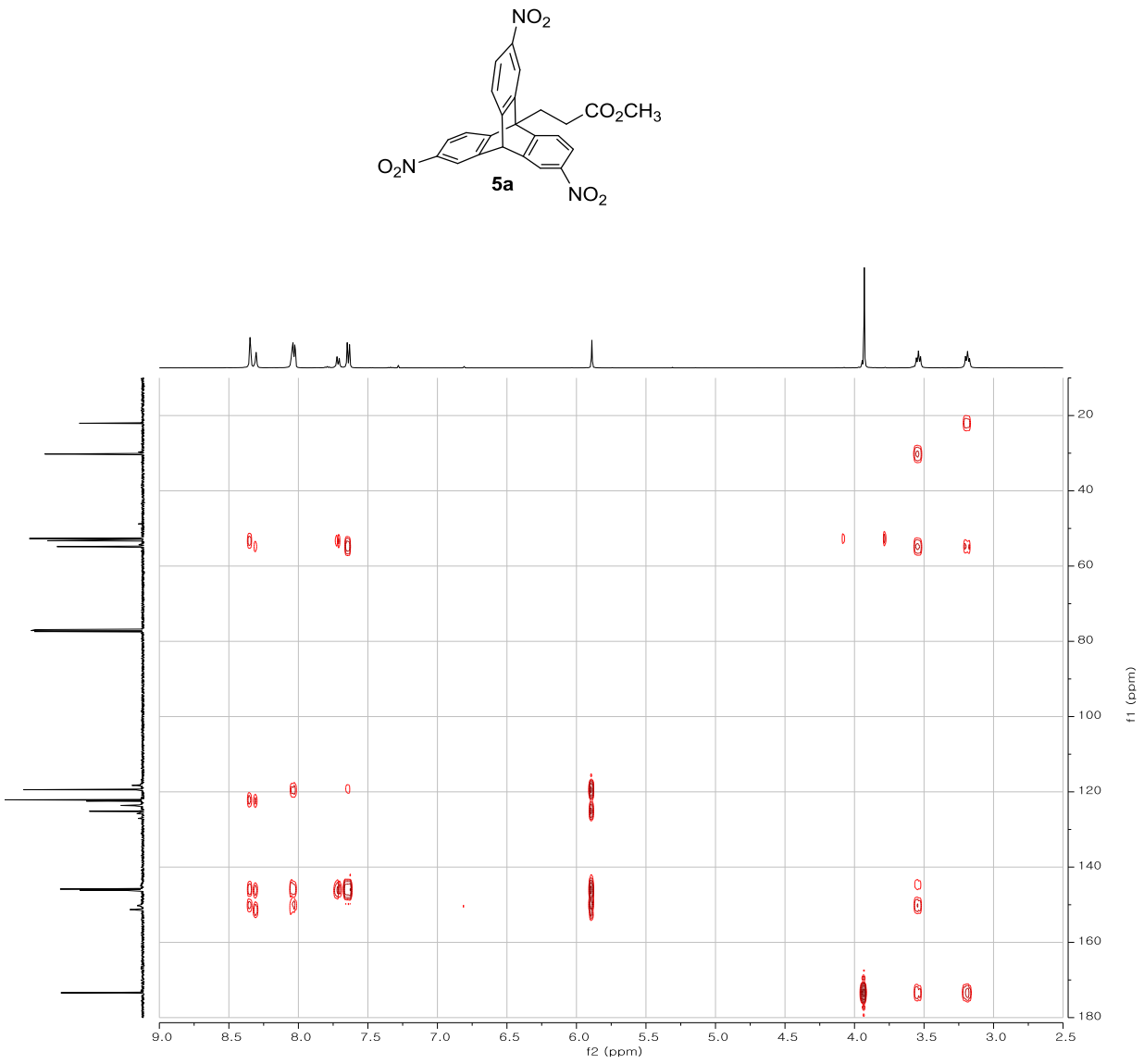

Figure A7.11. HSQC spectrum of **5a** in $CDCl_3$.

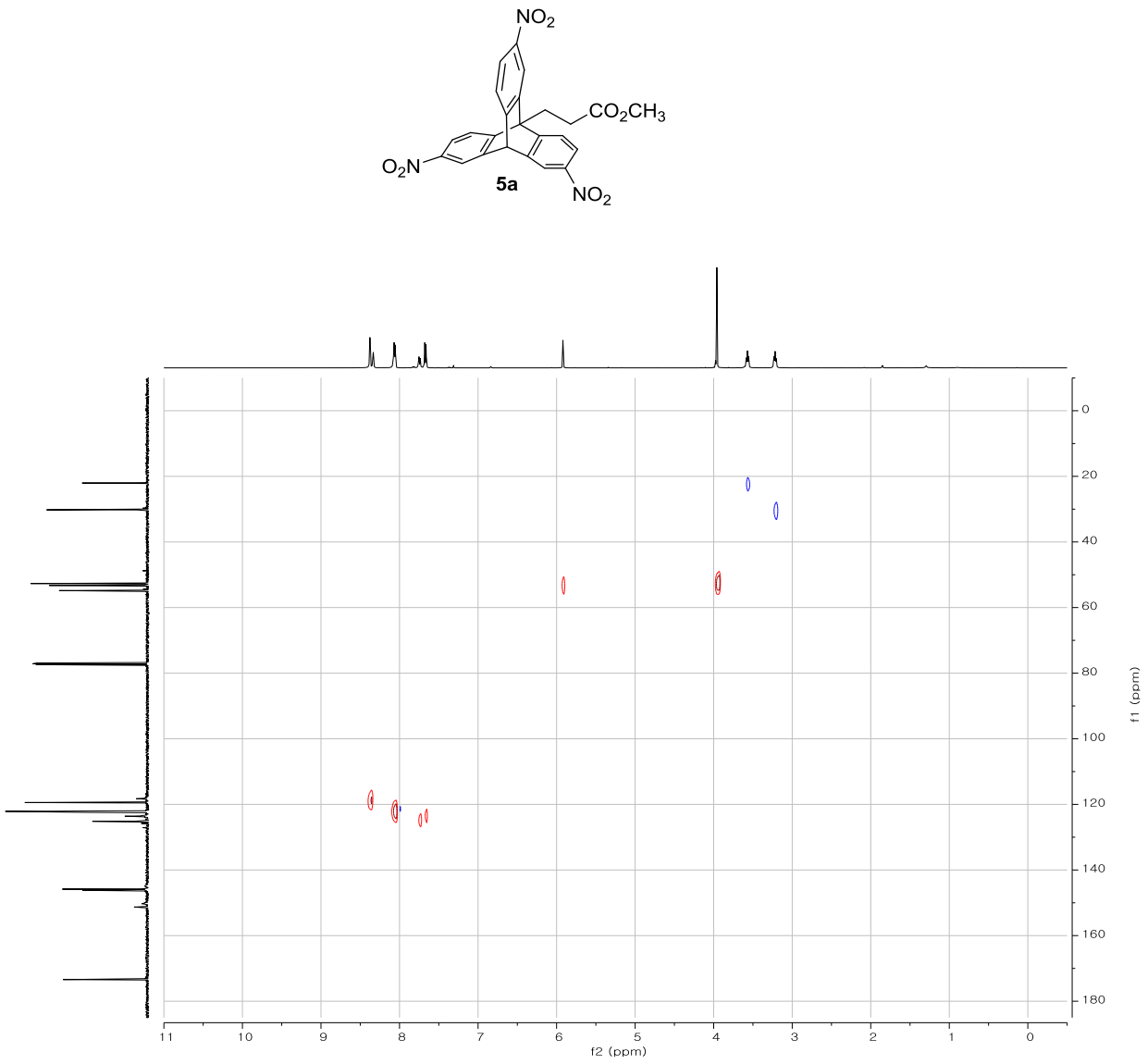

Figure A7.12. Expanded HSQC spectrum of **5a** in $CDCl_3$.

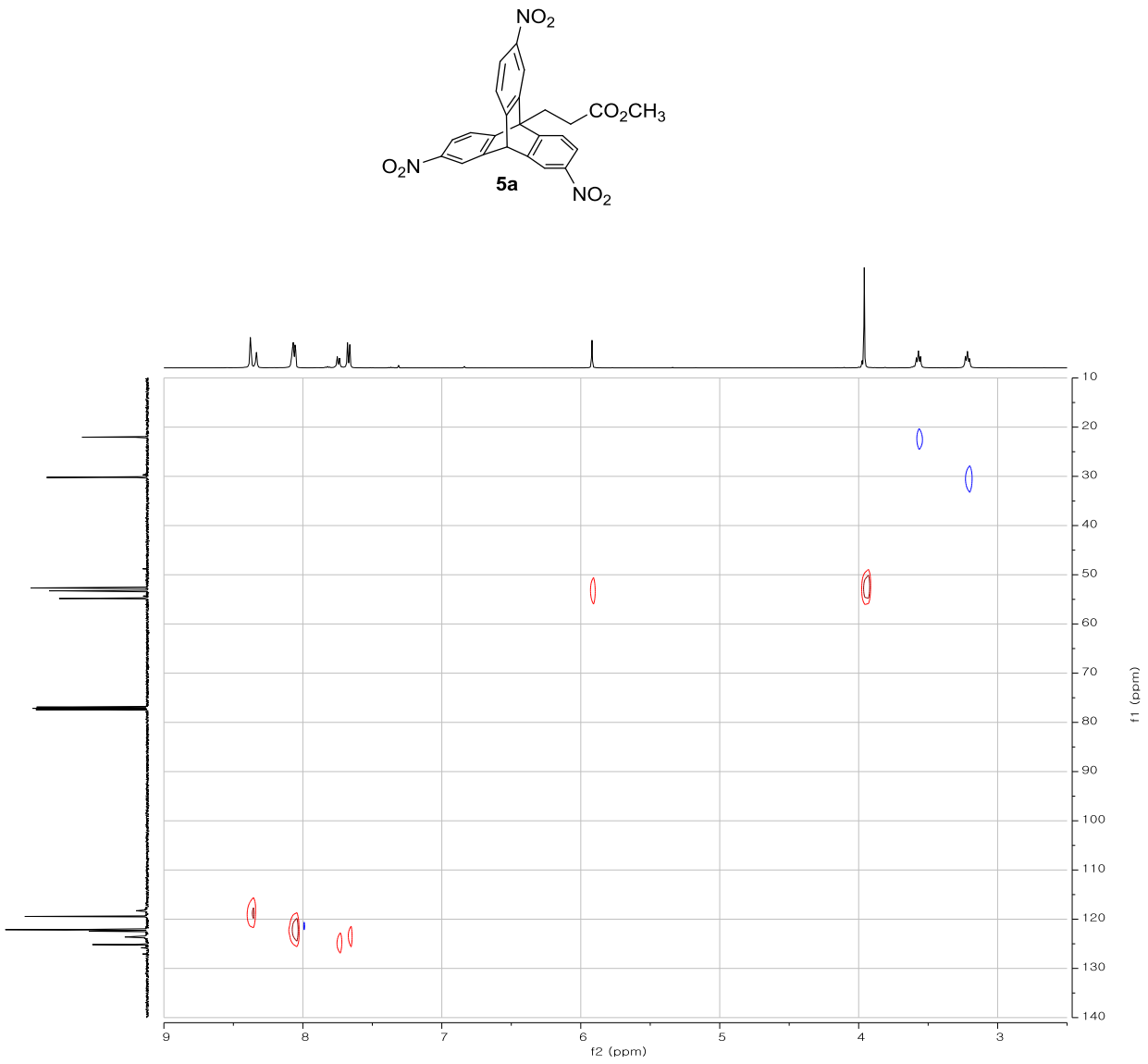

Figure A7.13. ^{1}H NMR spectrum of **5b** in $CDCl_3$ (500 MHz).

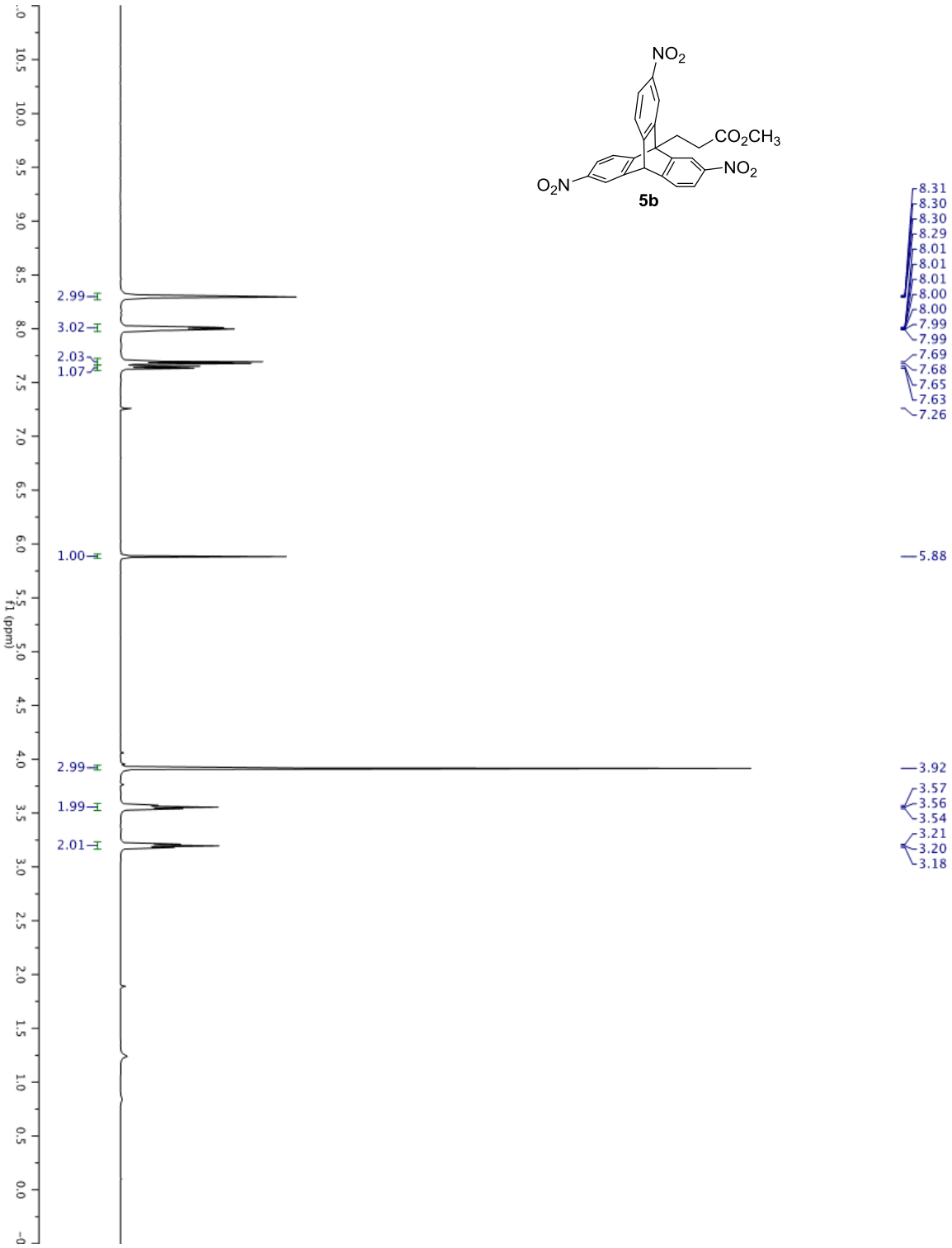

Figure A7.14. ^{13}C NMR spectrum of **5b** in $CDCl_3$ (125 MHz).

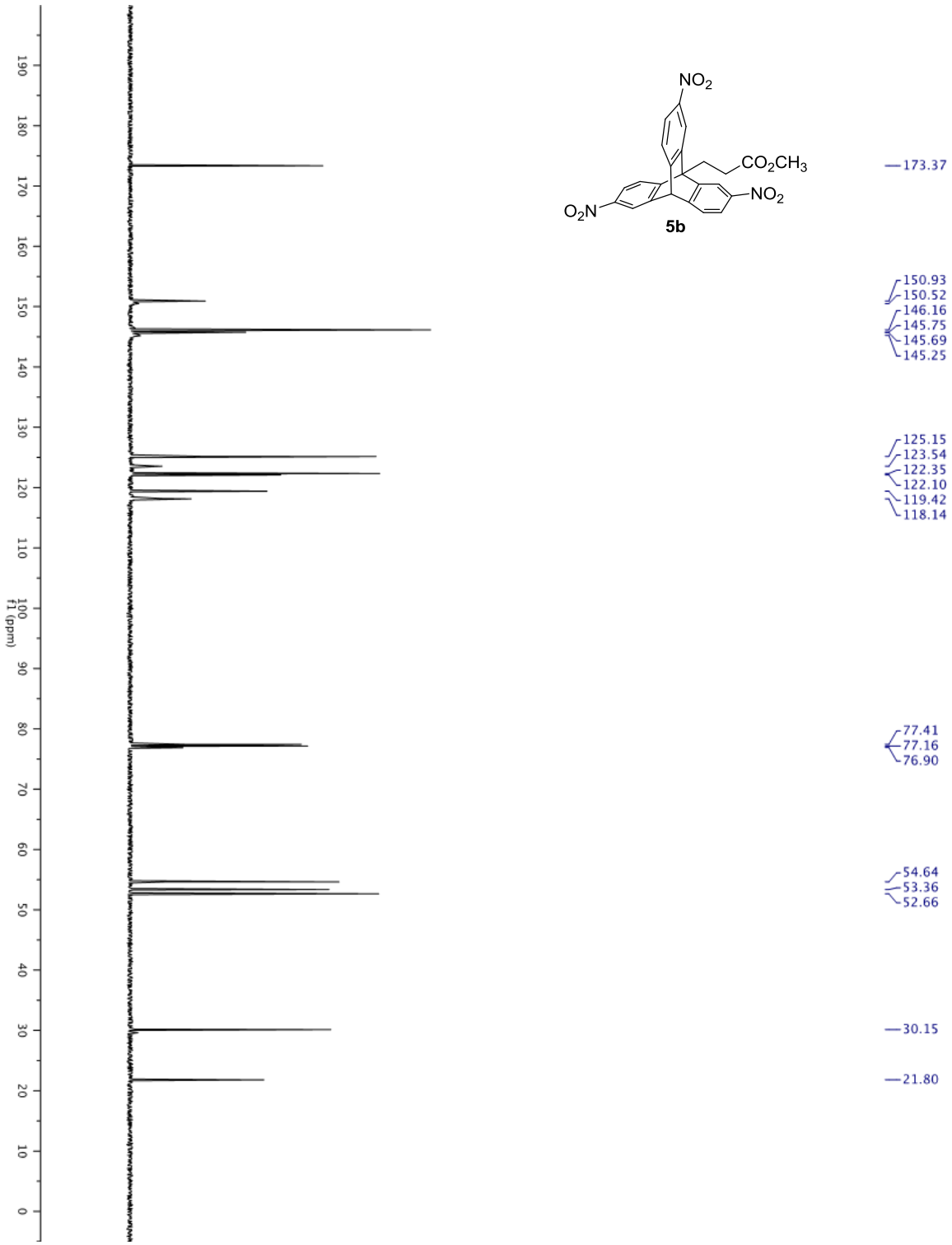

Figure A7.15. HMBC spectrum of **5b** in $CDCl_3$.

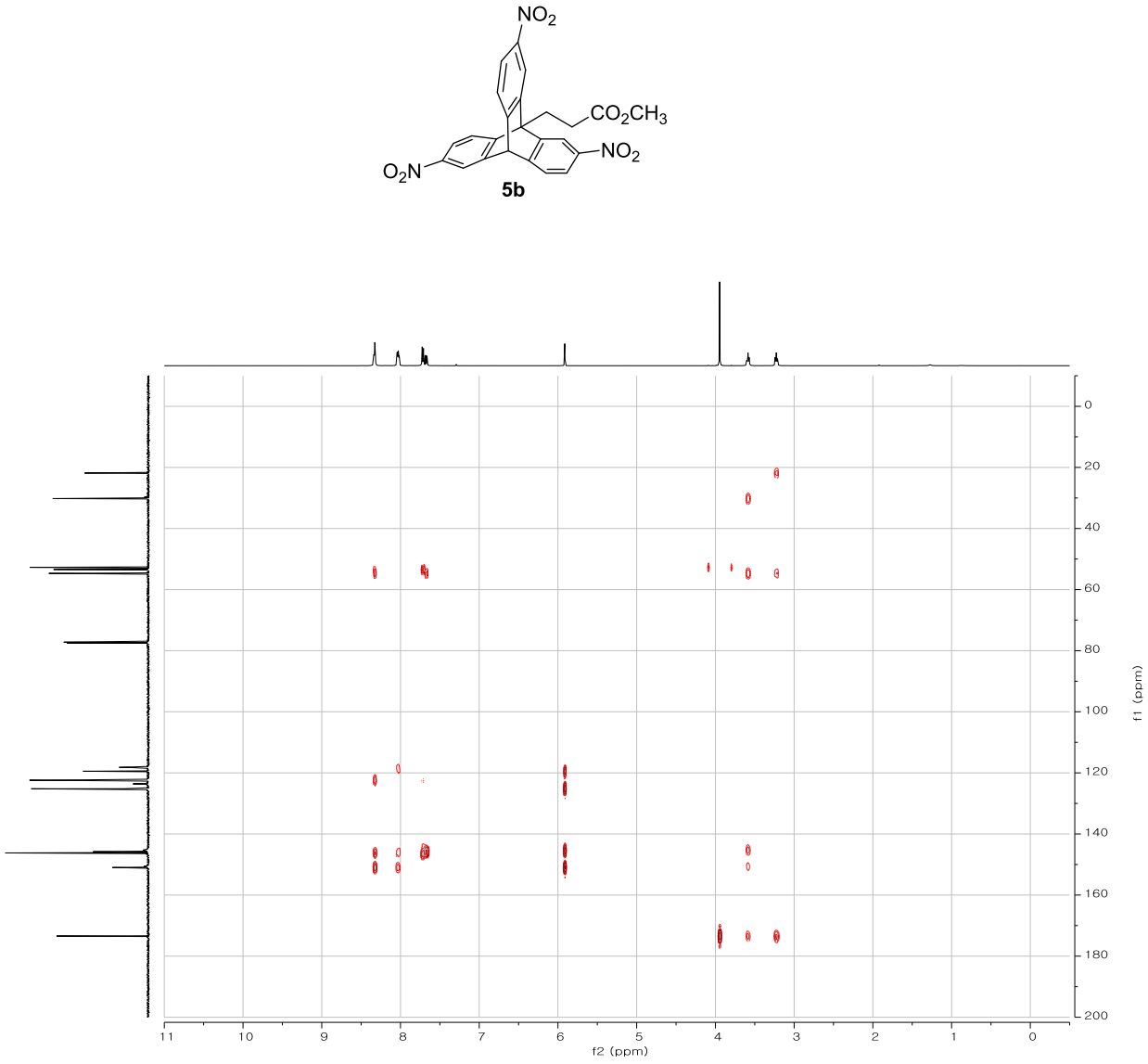

Figure A7.16. Expanded HMBC spectrum of **5b** in $CDCl_3$.

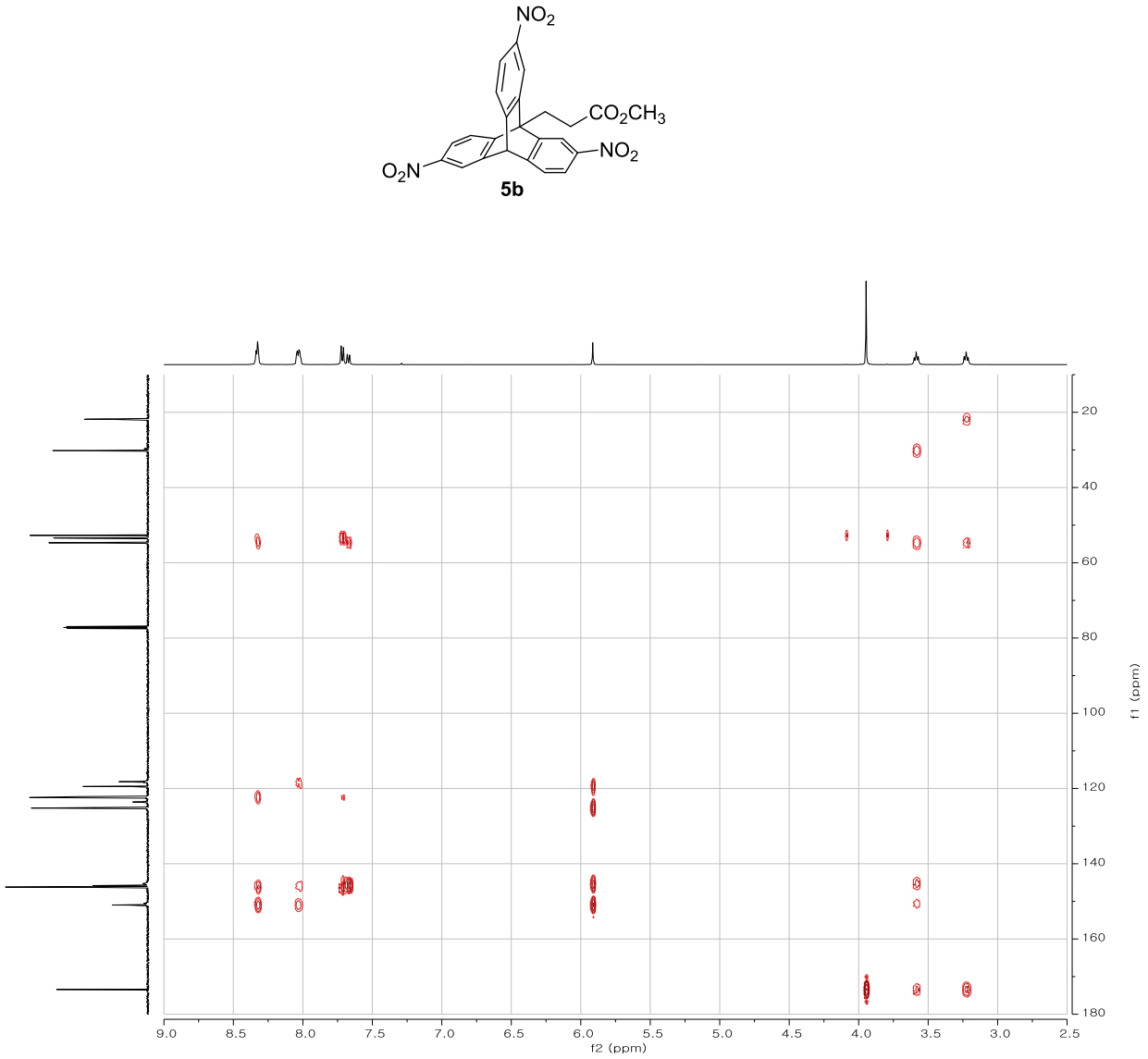

Figure A7.17. HSQC spectrum of **5b** in $CDCl_3$.

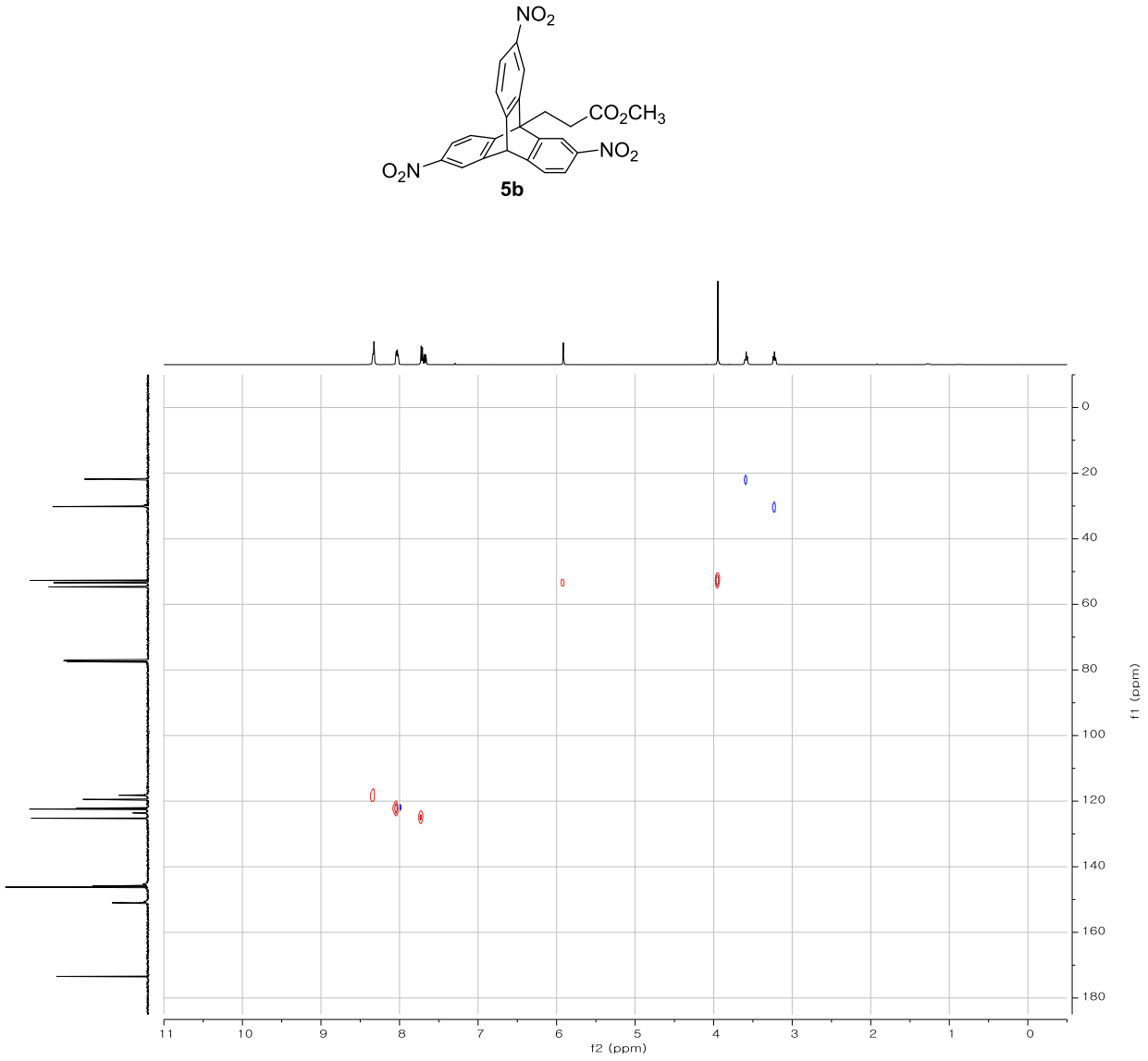

Figure A7.18. Expanded HSQC spectrum of **5b** in $CDCl_3$.

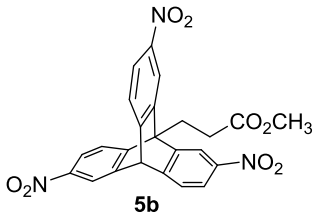

5b

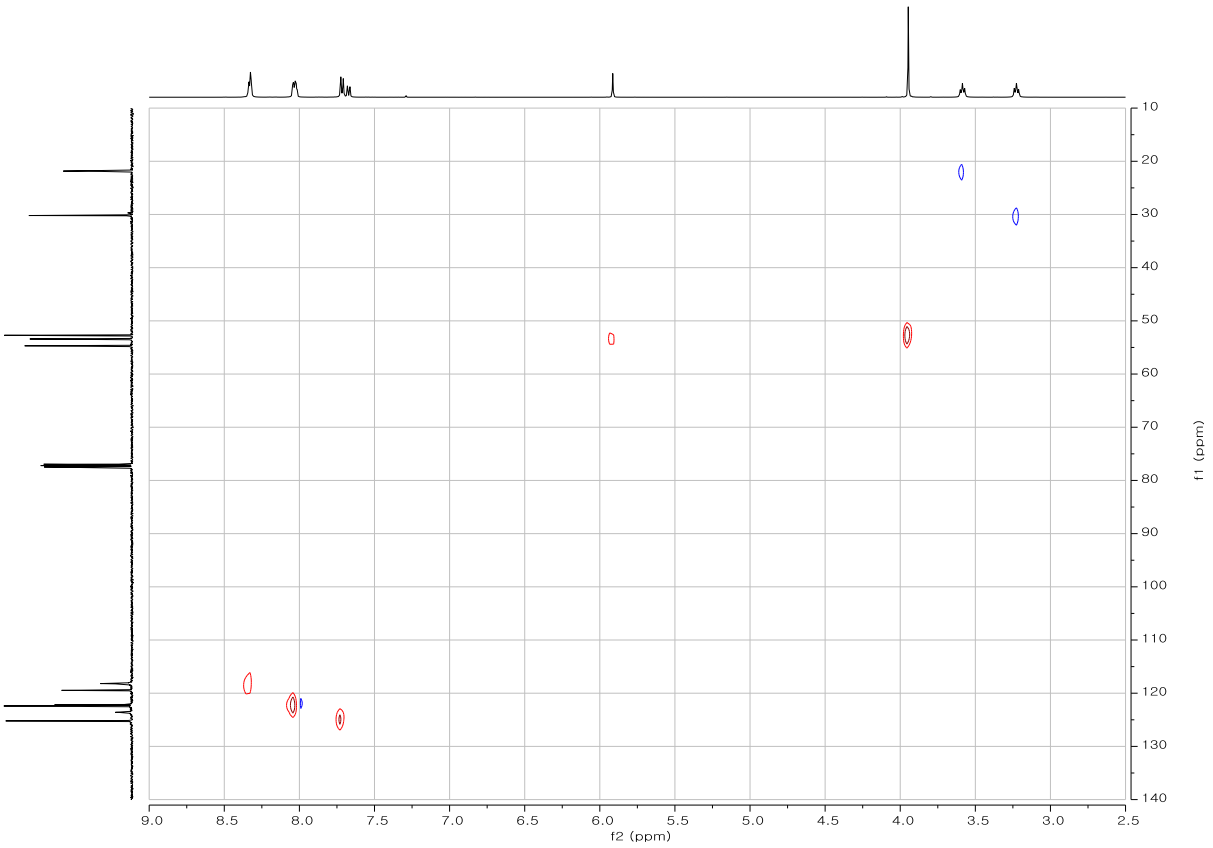

Figure A7.19. ^{1}H NMR spectrum of **5c** in $CDCl_3$ (500 MHz).

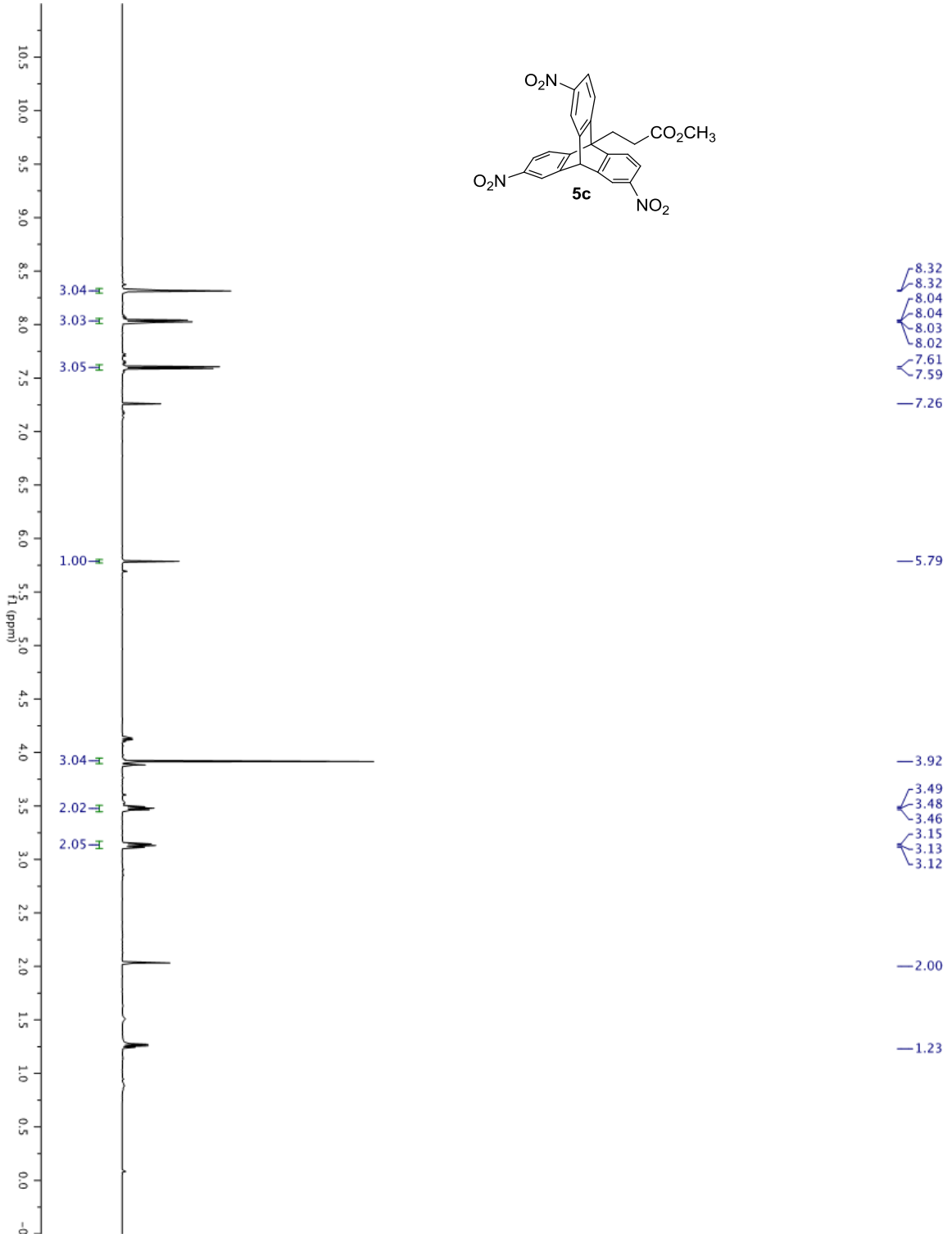

Figure A7.20. ^{13}C NMR spectrum of **5c** in $CDCl_3$ (125 MHz).

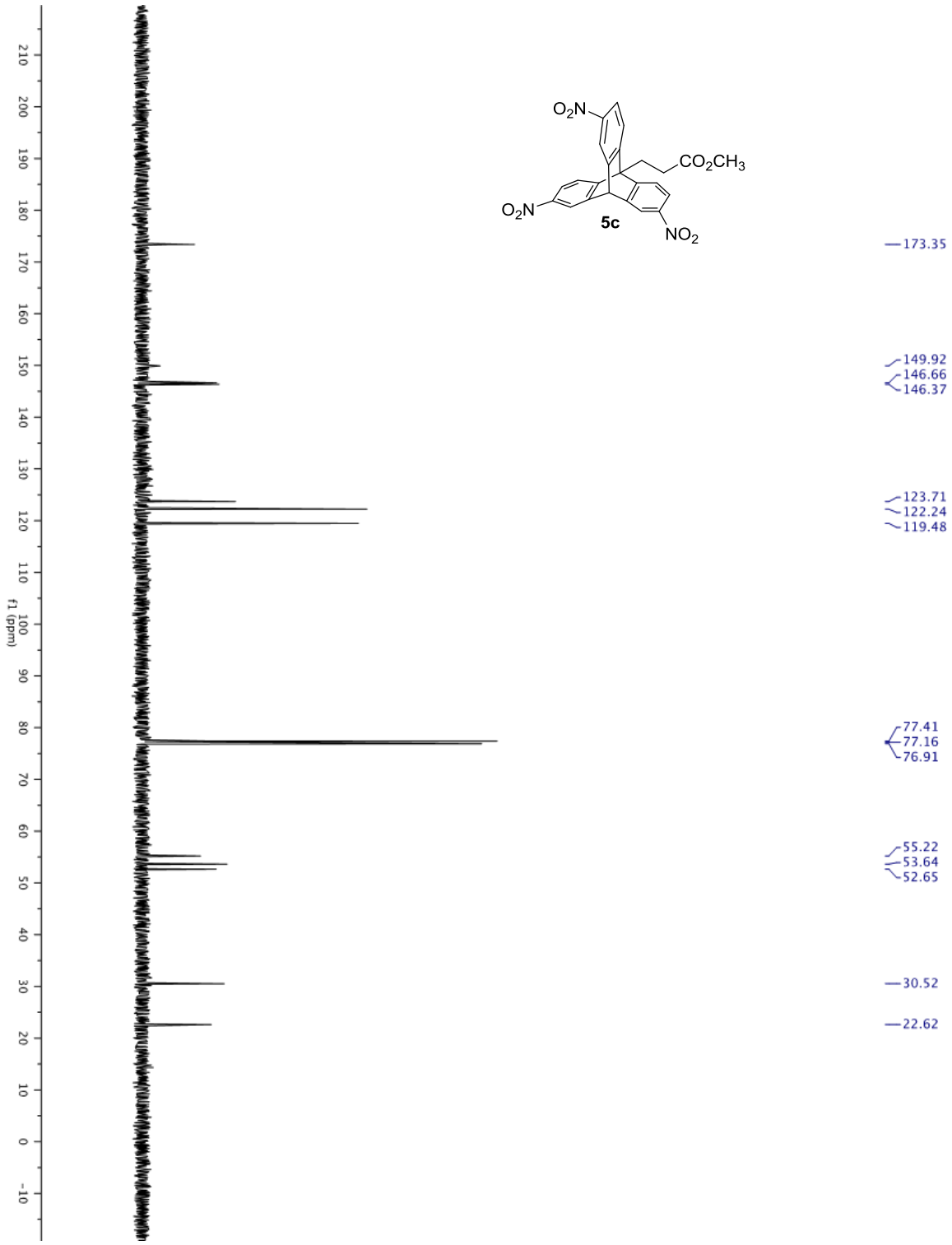

Figure A7.21. HMBC spectrum of **5c** in $CDCl_3$.

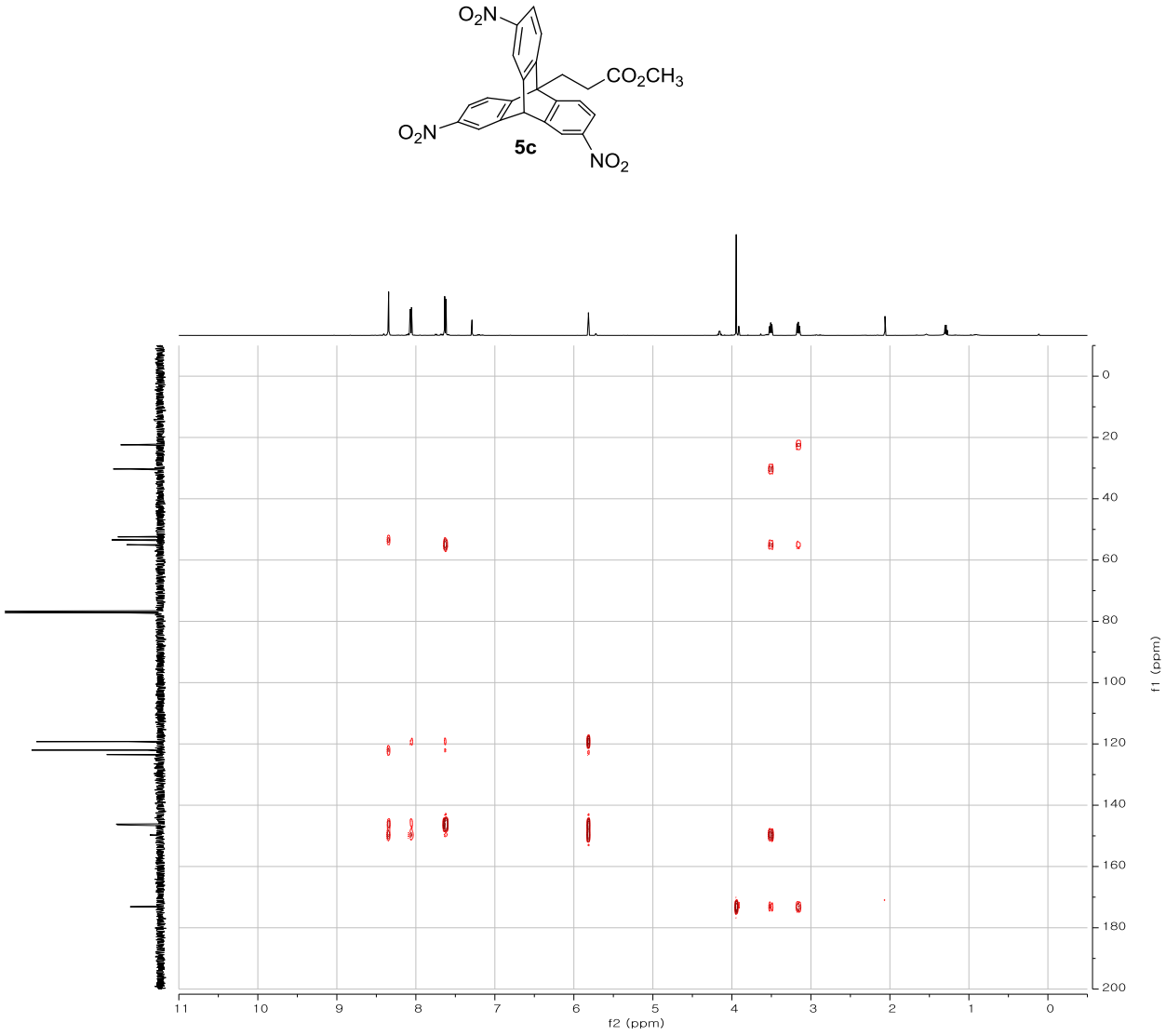

Figure A7.22. Expanded HMBC spectrum of **5c** in $CDCl_3$.

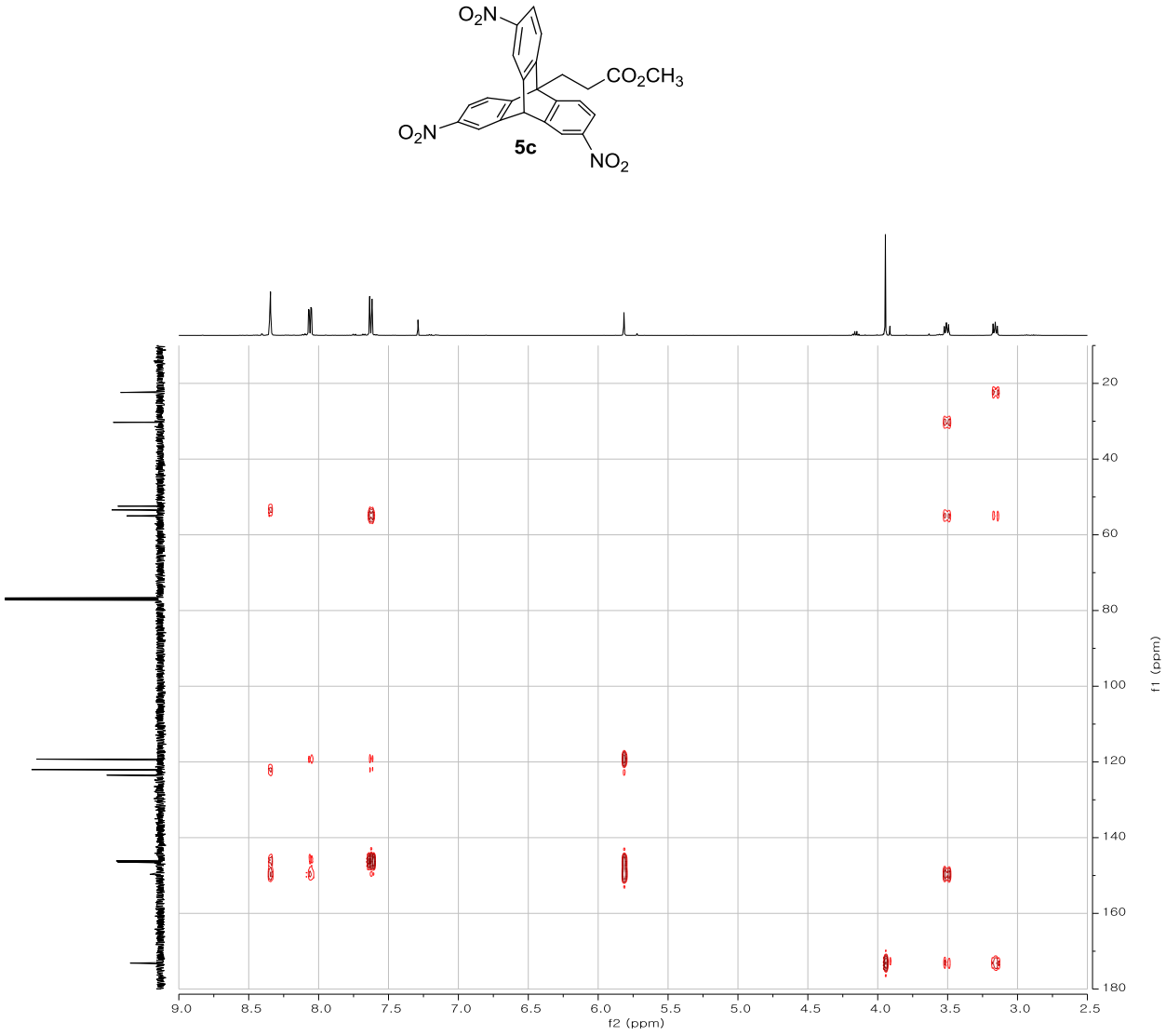

Figure A7.23. HSQC spectrum of **5c** in $CDCl_3$.

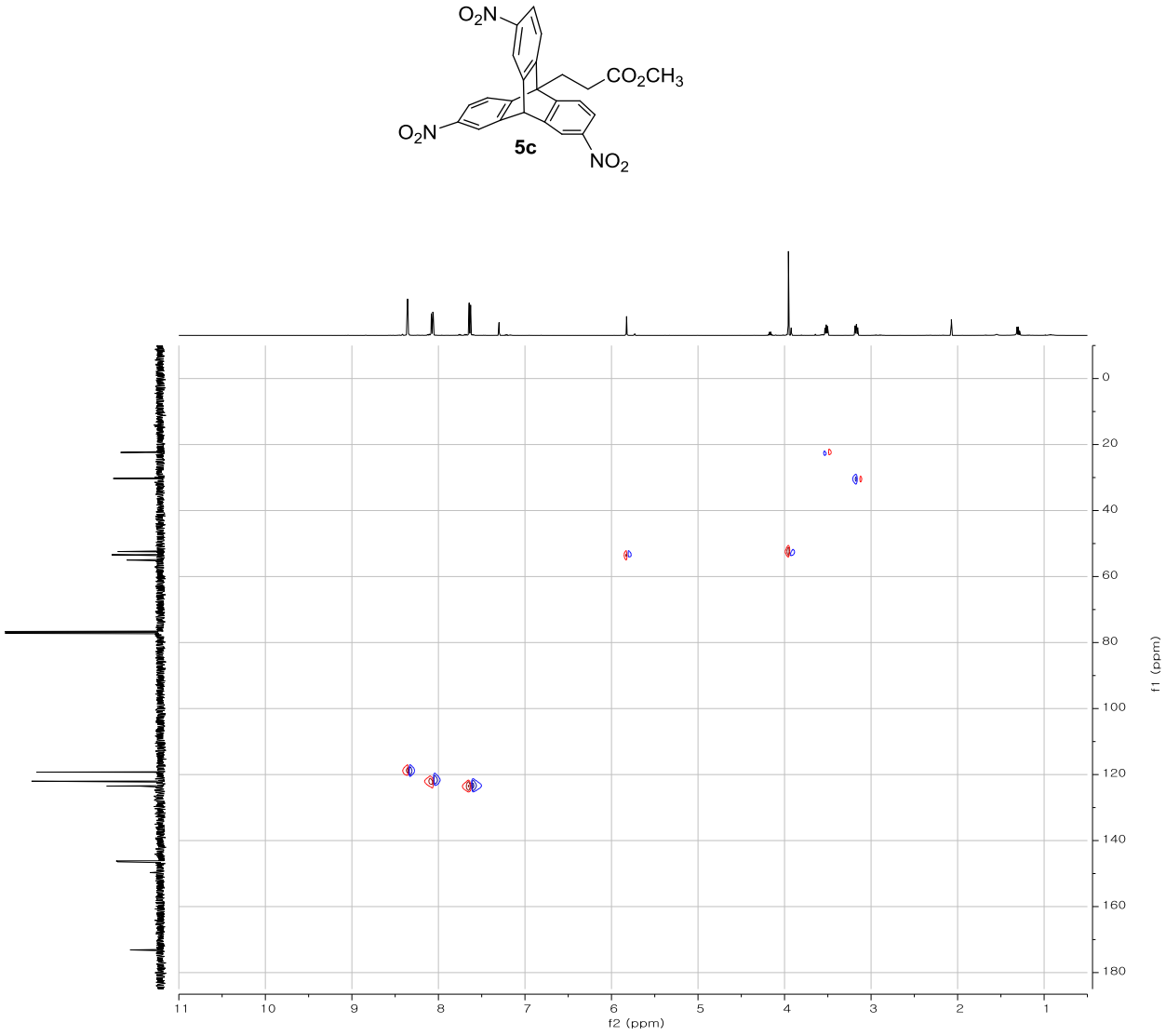

Figure A7.24. Expanded HSQC spectrum of **5c** in $CDCl_3$.

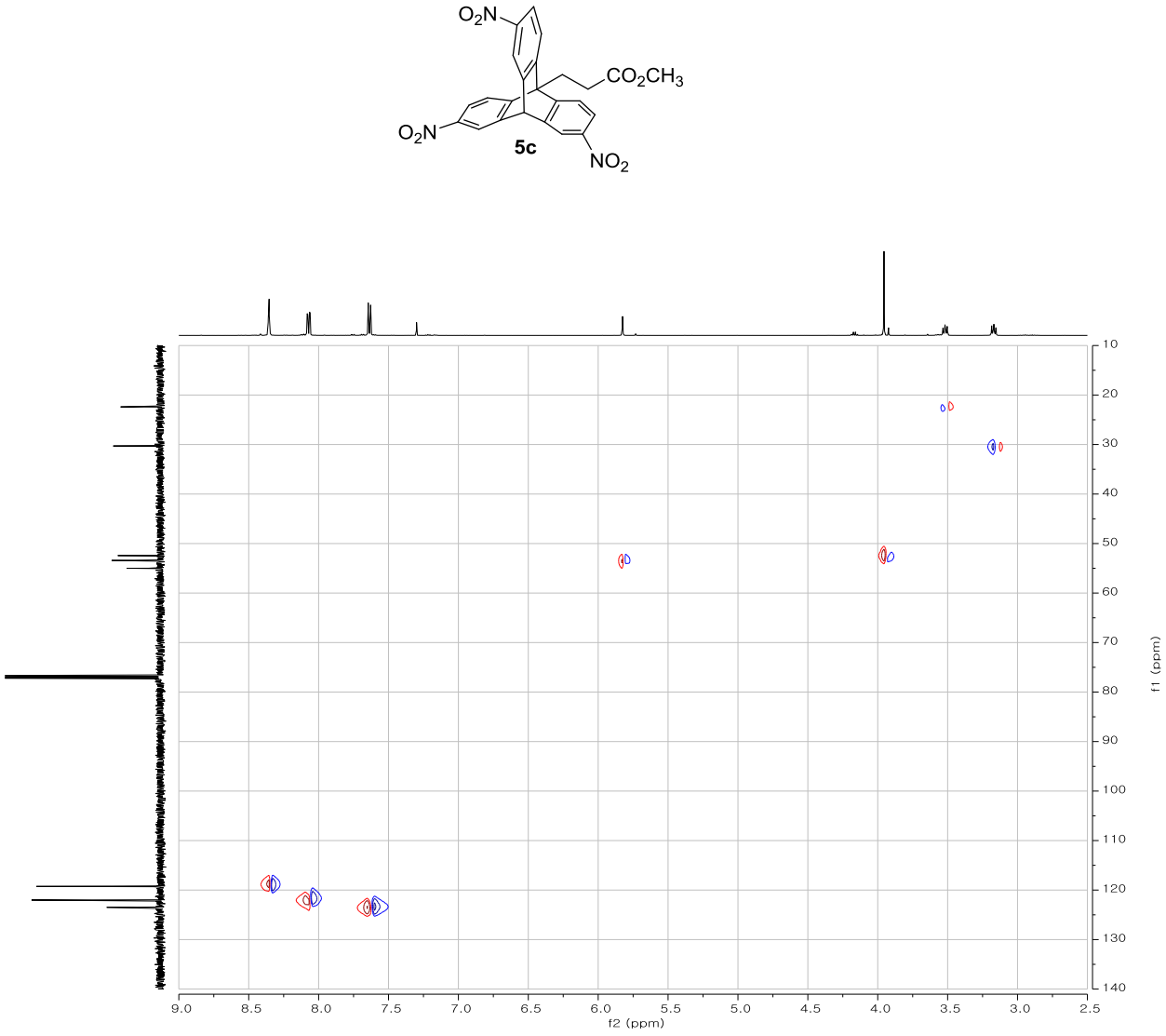

Figure A7.25. ^{1}H NMR spectrum of **5d** in $CDCl_3$ (500 MHz).

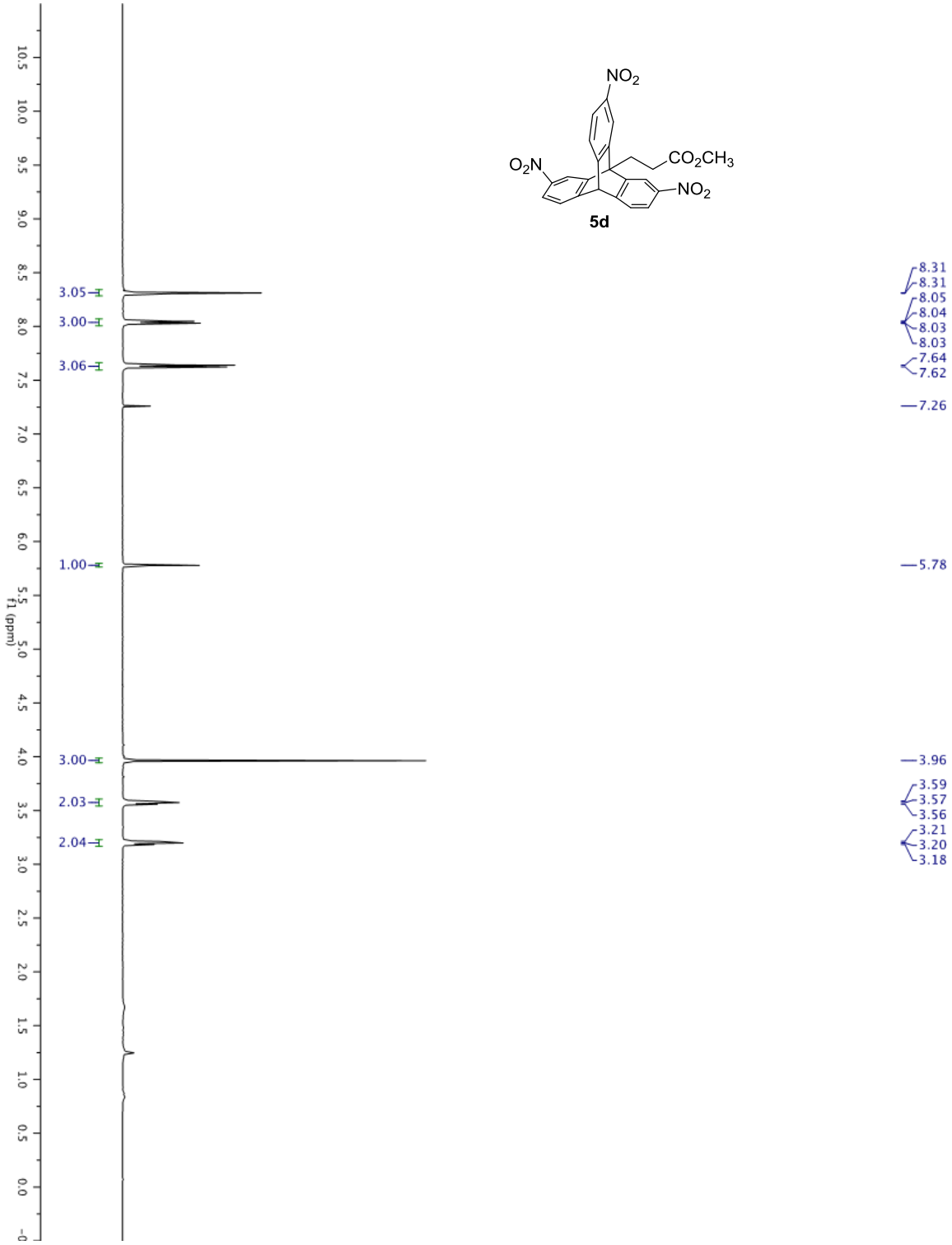

Figure A7.26. ^{13}C NMR spectrum of **5d** in $CDCl_3$ (125 MHz).

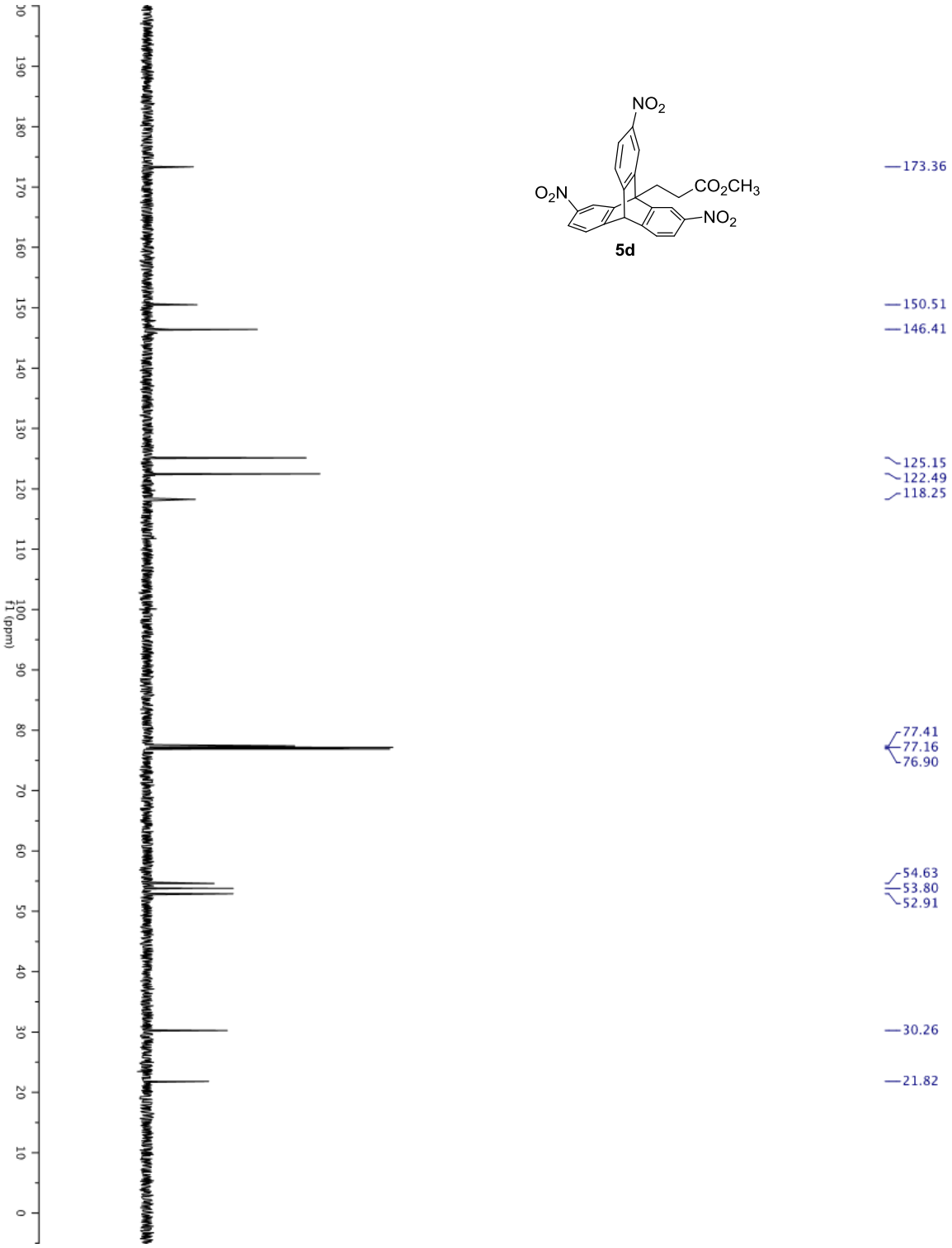

Figure A7.27. HMBC spectrum of **5d** in $CDCl_3$.

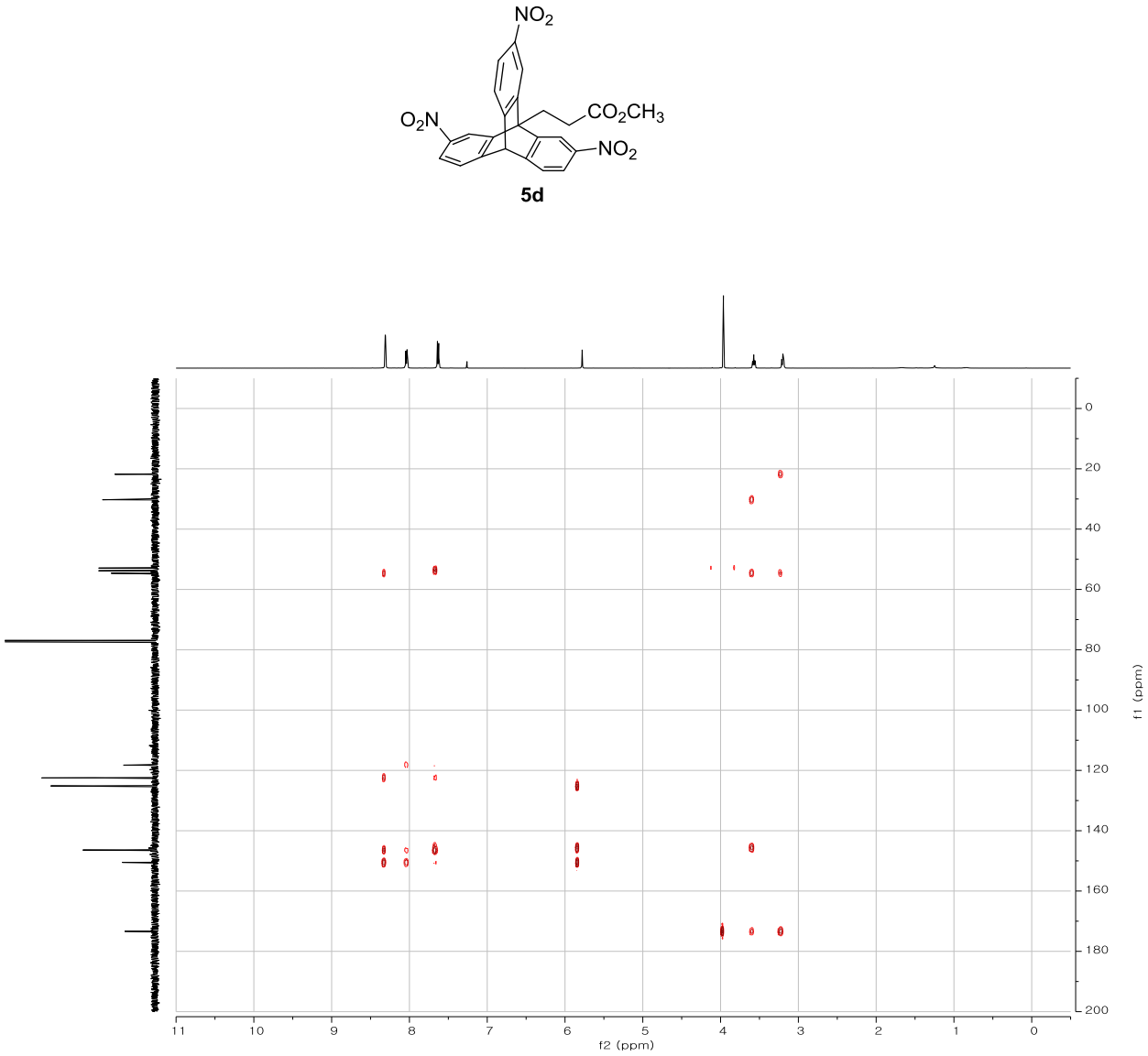

Figure A7.28. Expanded HMBC spectrum of **5d** in $CDCl_3$.

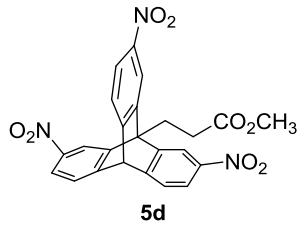

5d

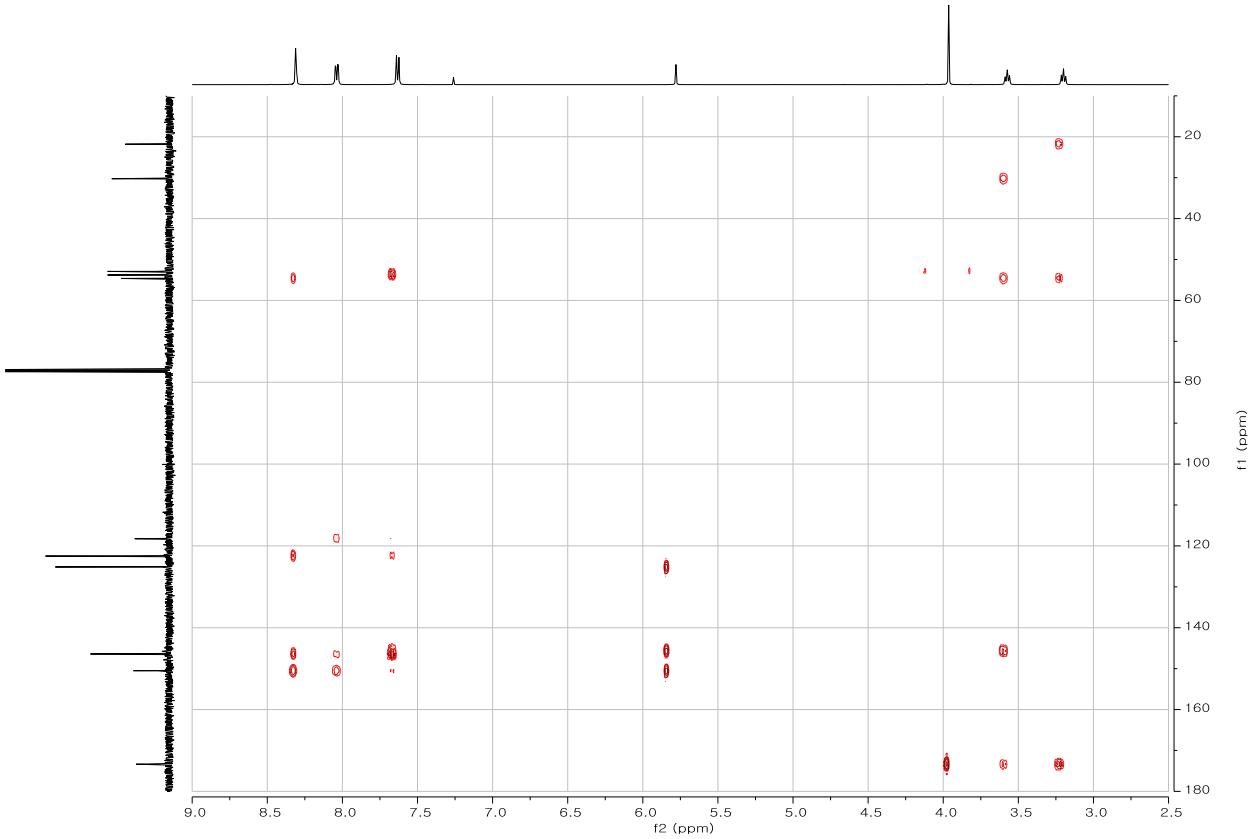

Figure A7.29. ^{1}H NMR spectrum of **6** in MeOD (500 MHz).

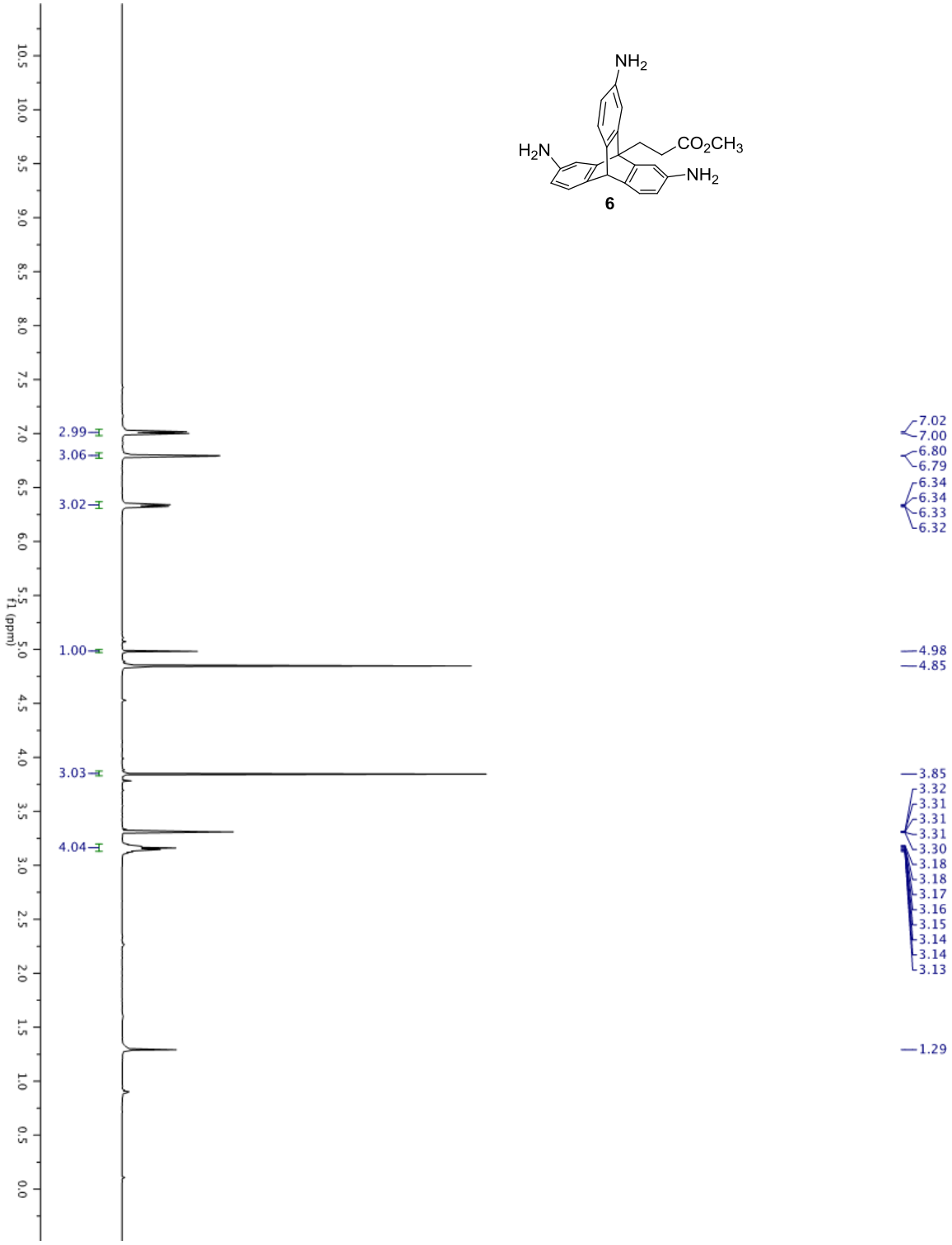

Figure A7.30. ^{13}C NMR spectrum of **6** in MeOD (125 MHz).

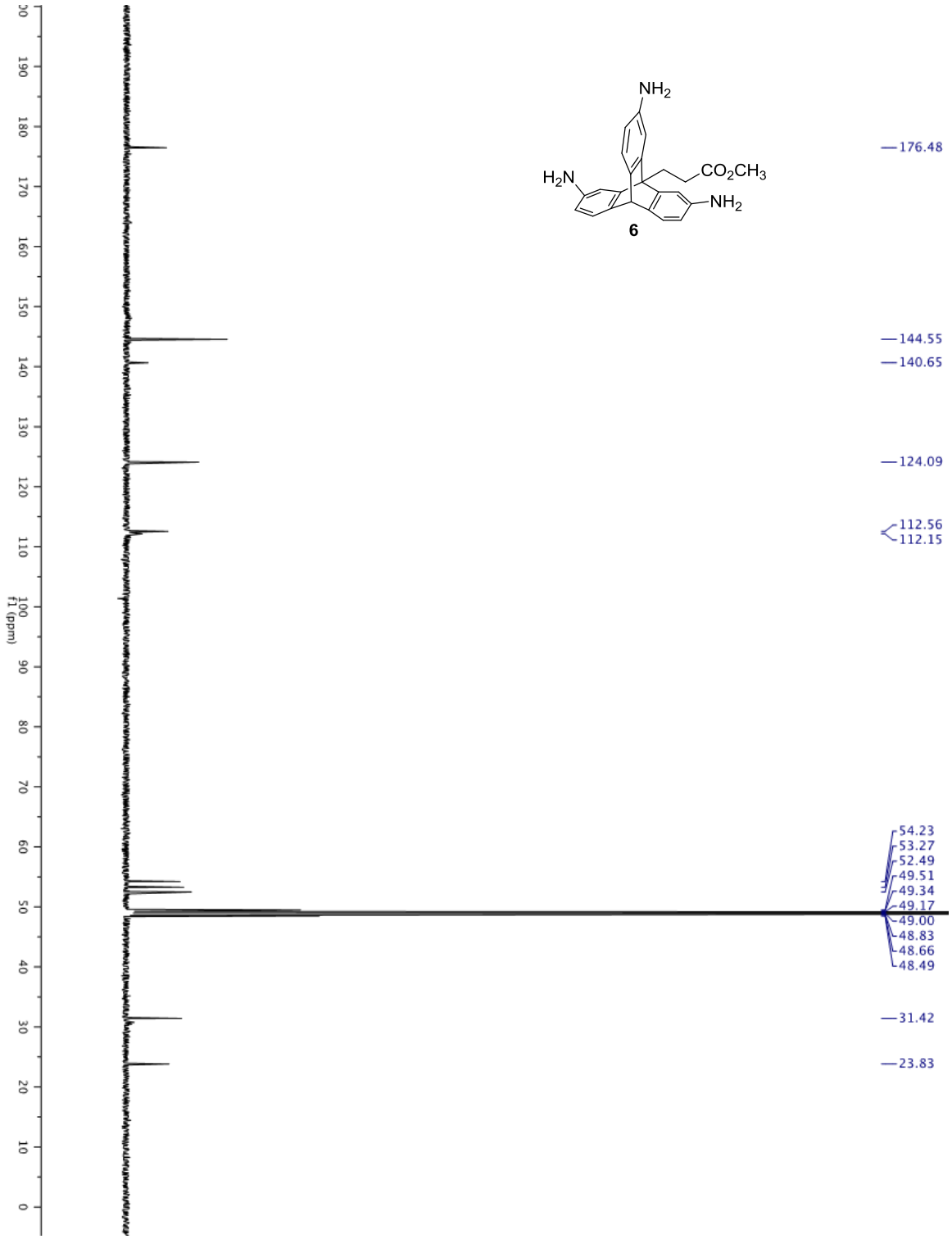

Figure A7.31. ^{1}H NMR spectrum of **7** in DMSO-*d6* (500 MHz).

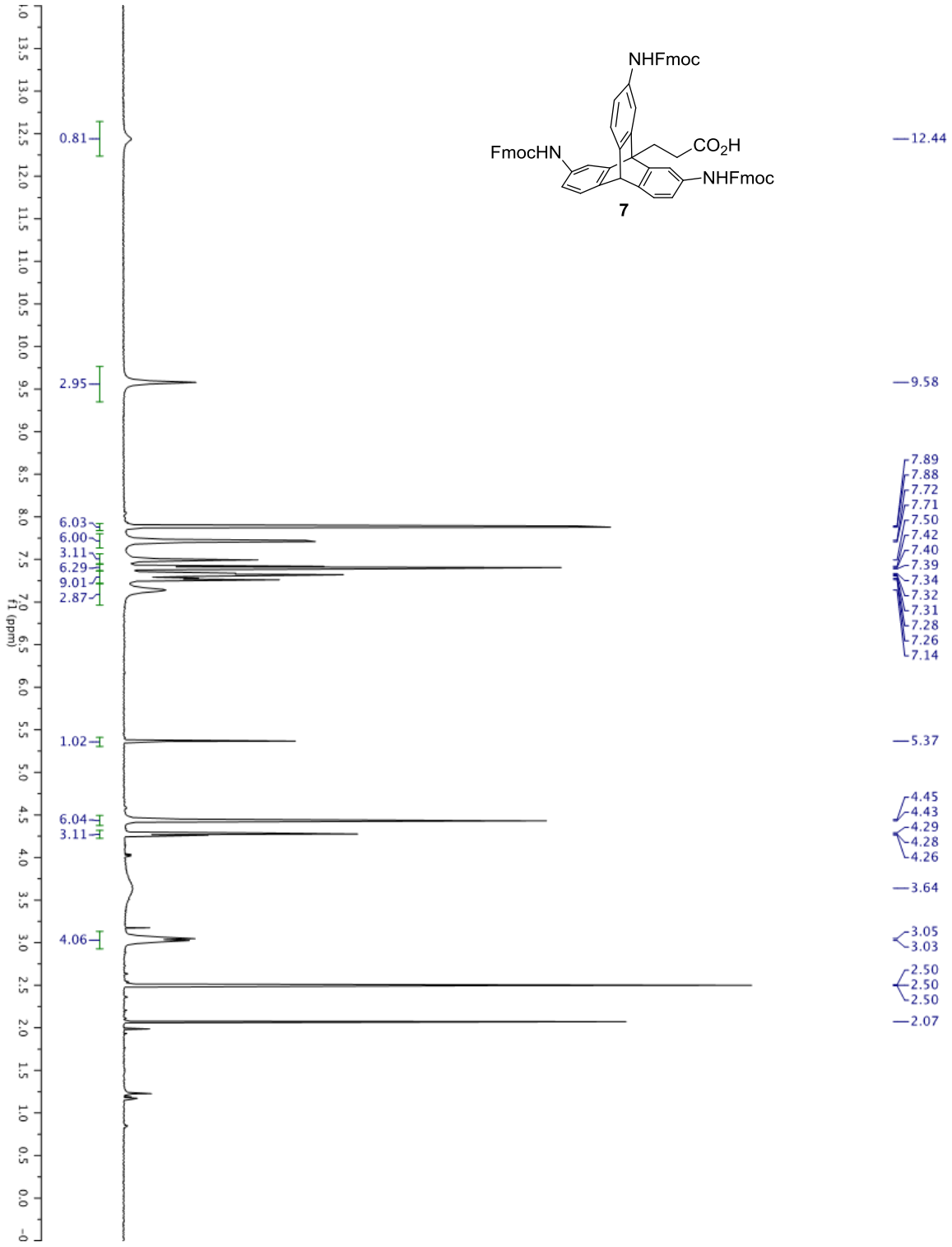

Figure A7.32. ^{13}C NMR spectrum of **7** in DMSO-*d6* (125 MHz).

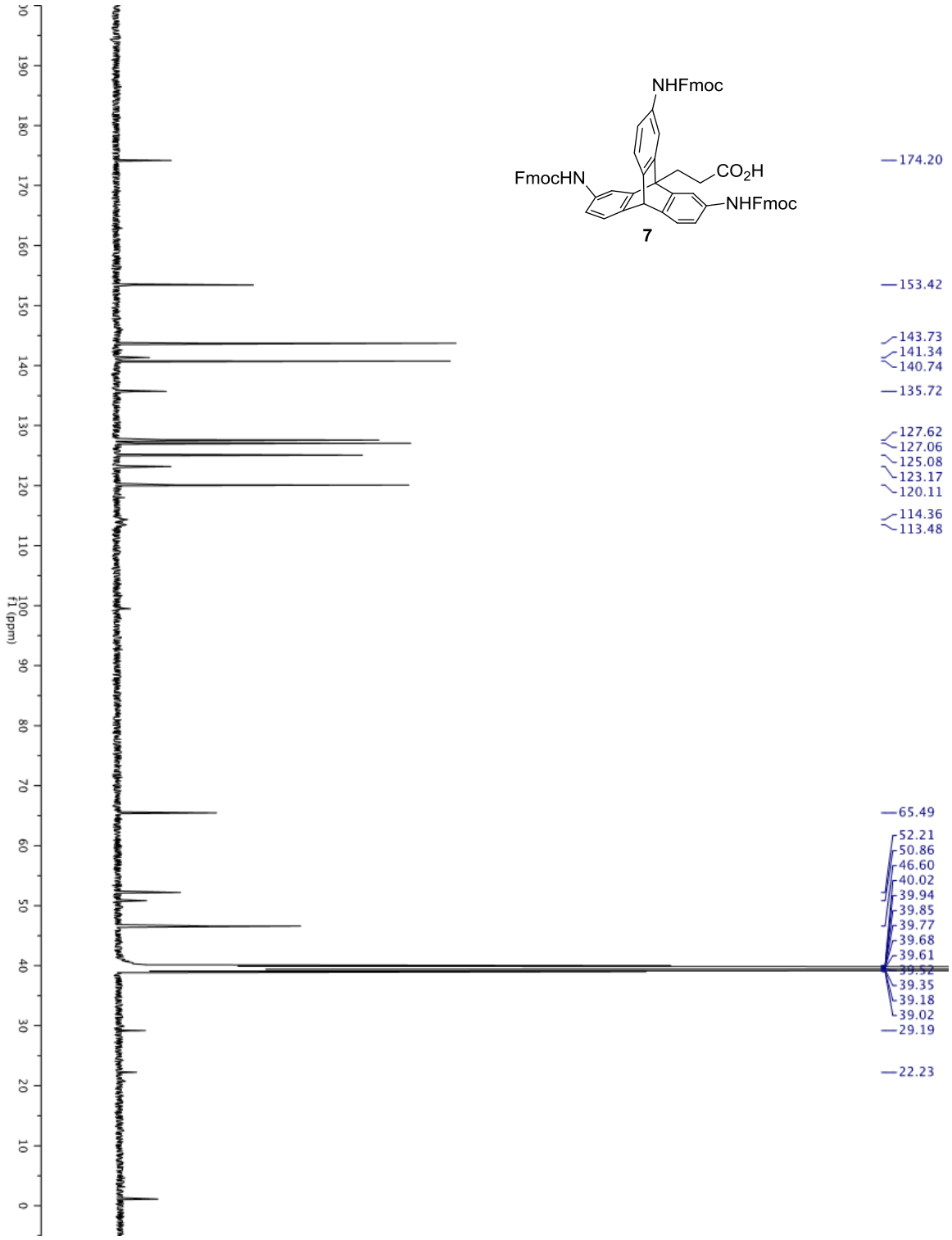

Figure A7.33. HPLC Chromatograms of the crude solution of the triptycenes **8** and **9**.

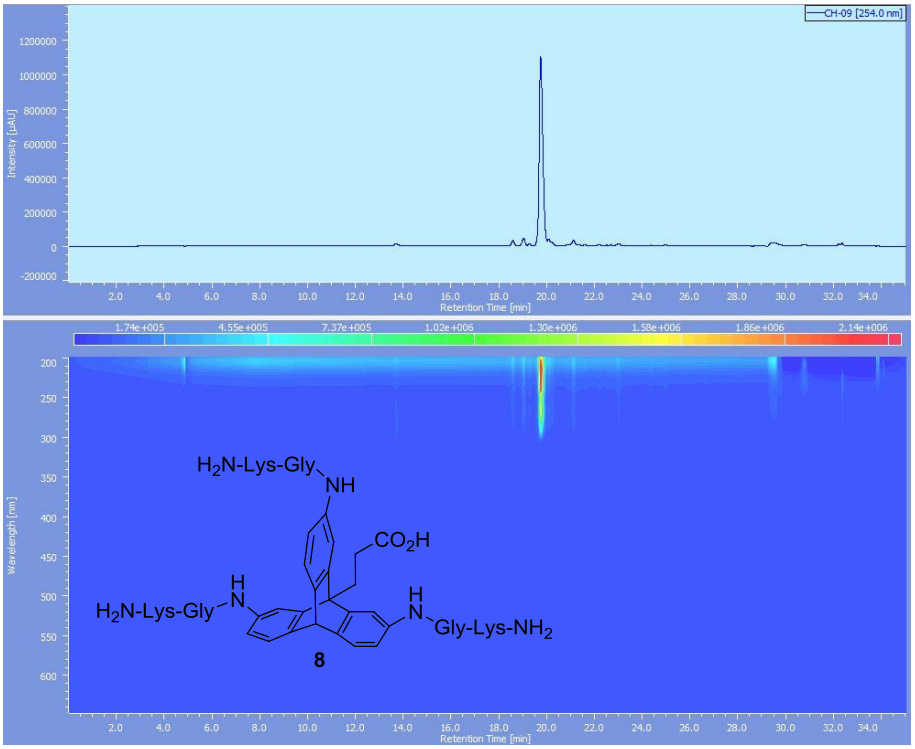

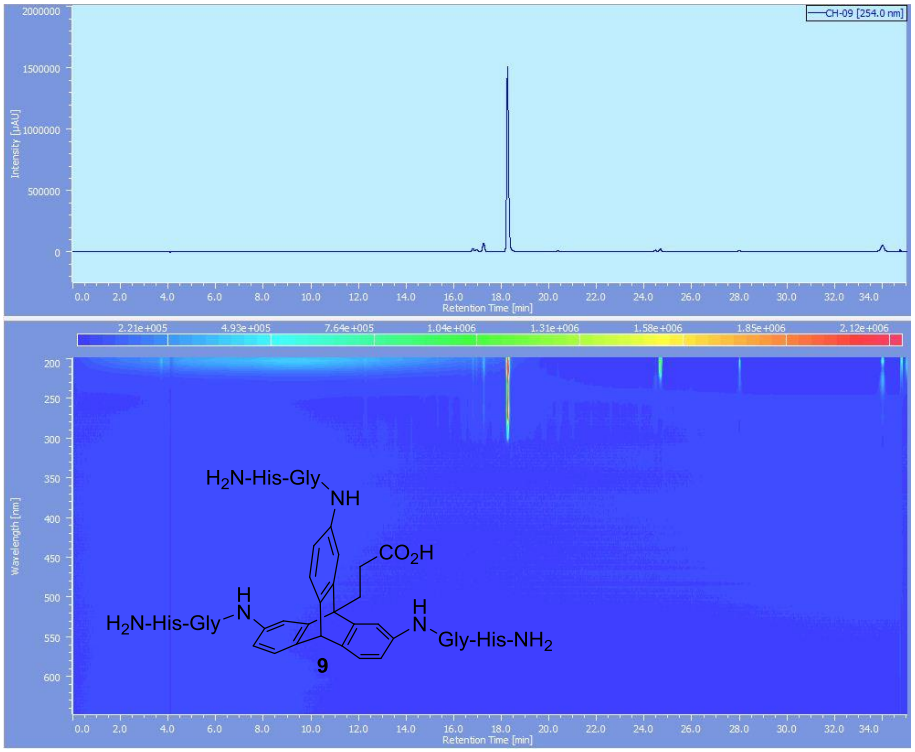

Figure A7.34. HPLC Chromatograms of the purified triptycenes **8** – **12**.

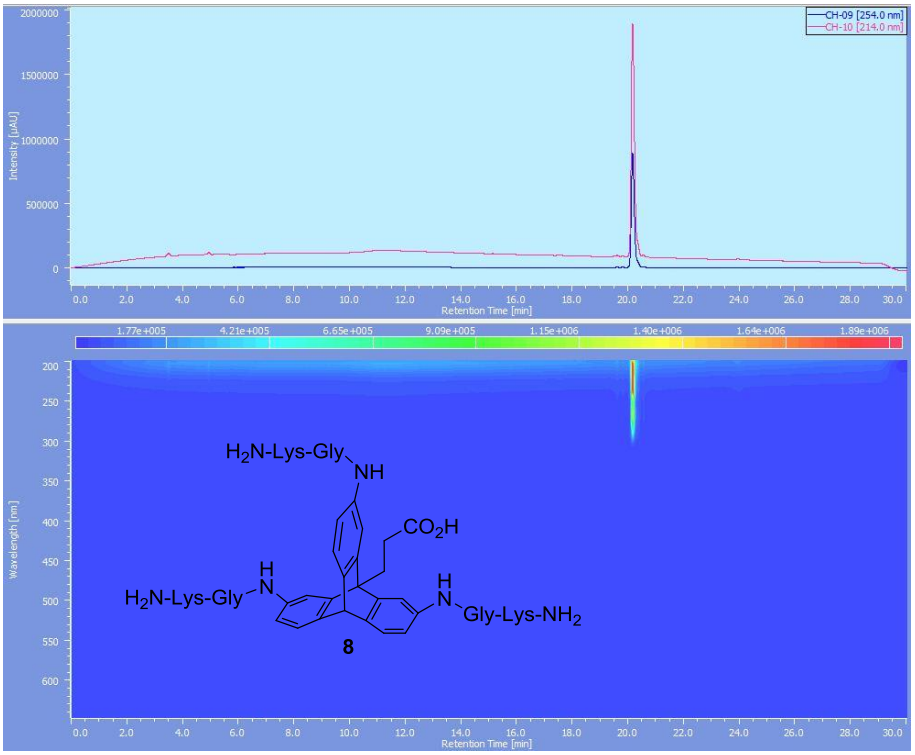

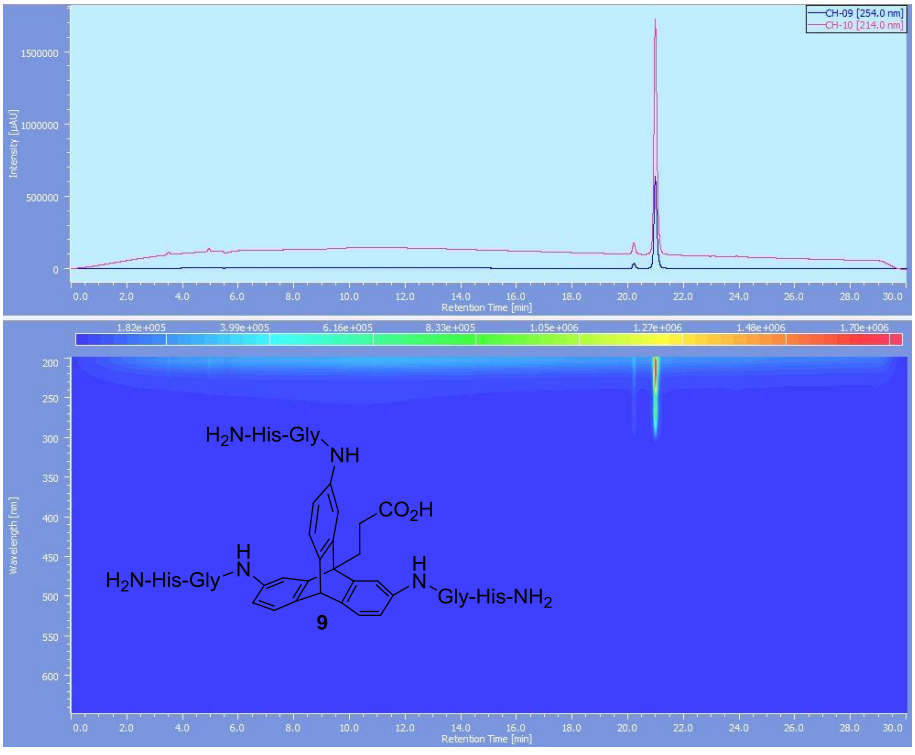

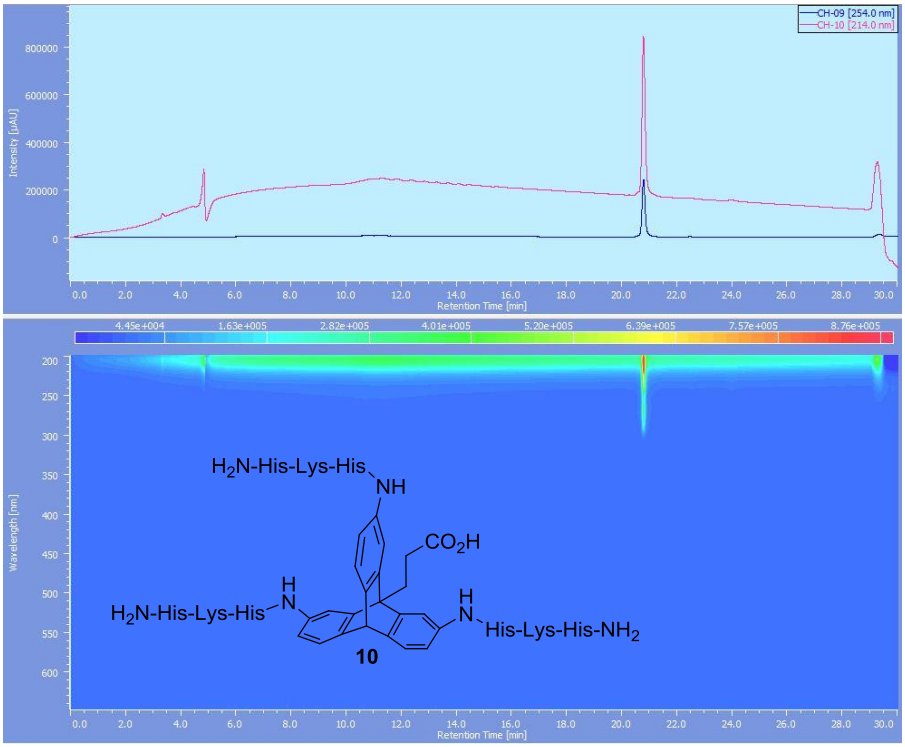
CH-09 [254.0 nm]
CH-10 [214.0 nm]
Intensity [µAU]
Retention Time [min]
Wavelength [nm]
H2N-His-Lys-His
NH
CO2H
H2N-His-Lys-His
H
N
H
N
His-Lys-His-NH2
10

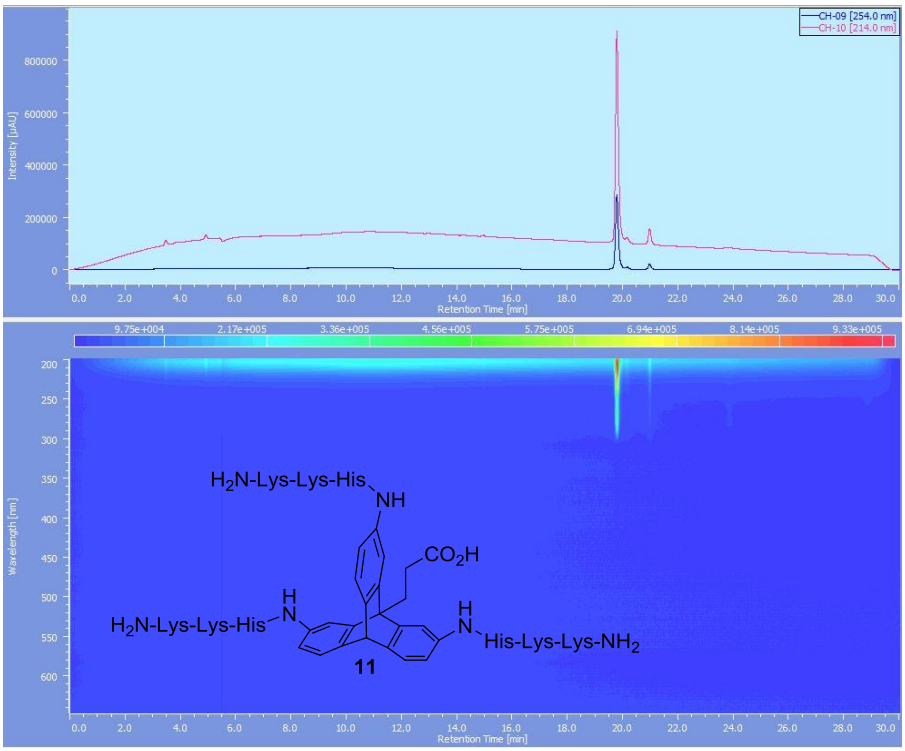
CH-09 [254.0 nm]
CH-10 [214.0 nm]
Intensity [µAU]
Retention Time [min]
Wavelength [nm]
H2N-Lys-Lys-His
NH
CO2H
H2N-Lys-Lys-His
H
N
H
N
His-Lys-Lys-NH2
11

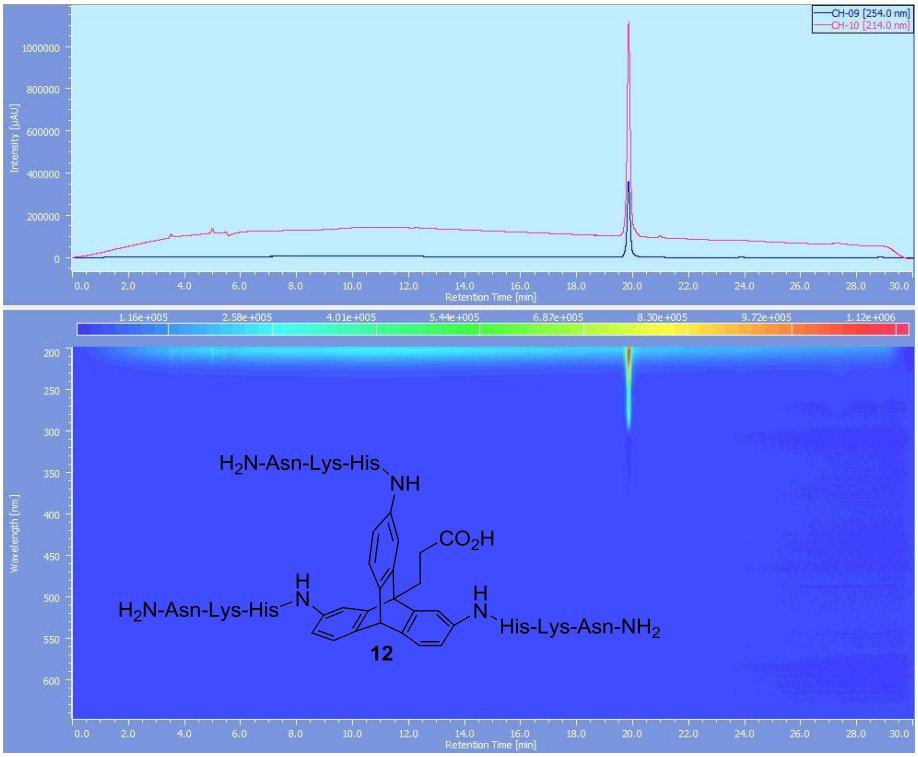
CH-09 [254.0 nm]
CH-10 [214.0 nm]
Intensity [µAU]
Retention Time [min]
1.16e+005
2.58e+005
4.01e+005
5.44e+005
6.87e+005
8.30e+005
9.72e+005
1.12e+006
Wavelength [nm]
Retention Time [min]
H2N-Asn-Lys-His
NH
CO2H
H2N-Asn-Lys-His
H
N
H
N
His-Lys-Asn-NH2
12

Table A7.1. Crystal Data and Structure Refinement for 5d.

Empirical formula	$C_{25}H_{18}N_3O_8Cl_3$
Formula weight	594.77
Temperature	100(1) K
Wavelength	0.71073 Å
Crystal system	monoclinic
Space group	C2/c
Cell constants:	
a	29.8039(12) Å
b	9.4923(4) Å
c	22.1375(9) Å
β	120.796(2)°
Volume	5379.8(4) $Å^3$
Z	8
Density (calculated)	1.469 Mg/m^3
Absorption coefficient	0.394 mm^{-1}
F(000)	2432
Crystal size	0.25 x 0.12 x 0.10 mm^3
Theta range for data collection	1.59 to 25.40°
Index ranges	$-35 \leq h \leq 32$, $-11 \leq k \leq 11$, $-26 \leq l \leq 26$
Reflections collected	39795
Independent reflections	4911 [R(int) = 0.0251]
Completeness to theta = 25.40°	99.3 %
Absorption correction	Semi-empirical from equivalents
Max. and min. transmission	0.7452 and 0.7055
Refinement method	Full-matrix least-squares on F^2
Data / restraints / parameters	4911 / 0 / 345
Goodness-of-fit on F^2	1.039
Final R indices [I>2sigma(I)]	R1 = 0.0335, wR2 = 0.0855
R indices (all data)	R1 = 0.0400, wR2 = 0.0897
Largest diff. peak and hole	0.412 and -0.525 $e.Å^{-3}$

Chapter 9

Development of Novel Irreversible Multistage Photoconvertible Fluorophore

This work was performed in collaboration with Joomyung V. Jun, a graduate student in the Chenoweth group at the University of Pennsylvania.

9.1 Introduction

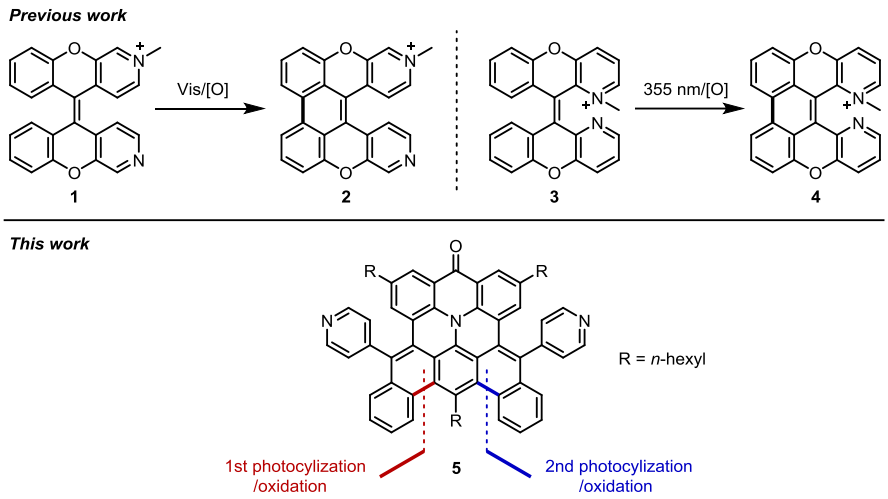

Figure 9.1. Irreversible photoconvertible fluorophores. Our previous double-stage (upper) and this multistage photoconvertible scaffolds (lower).

Photoactivatable small molecules have been used as fluorescent probes for studying biological system. The mechanism for photoactivation of small molecules are various: photoisomerization, photouncaging, photodecomposition of azides, or photoclick reactions.[1] We recently reported the synthesis of mono-methylated diazaxanthilidene derivatives **1** and **2** and their application for photoelectrocyclization-based live-cell imaging (Figure 9.1).[2] The mechanism of these novel photoconvertible fluorophores is based on the photo-induced 6 π cyclization. Changing the position of nitrogen atoms on pyridine rings, we developed different fluorescent localization pattern of mono-methylated diazaxanthilidenes in the cell. Here, on the basis of our previous result, we installed three photocyclizable sites on a single molecule to develop the multistaged photoelcetrocyclization-based fluorophore **5**.

9.2 Results and Discussion

Scheme 9.1. Synthesis of the First-Stage Compound 9.

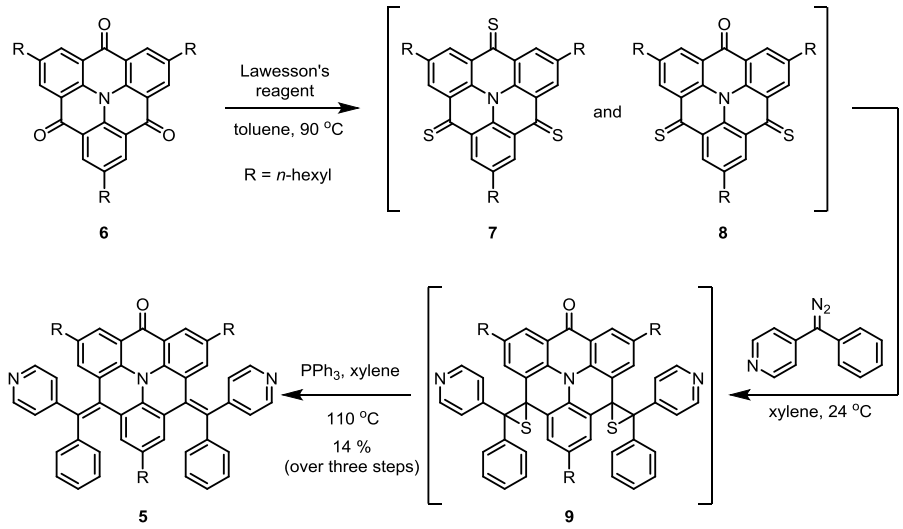

The synthesis of the thioketone **6** was reported by Kivala group in 2015 and we followed the literature procedures.[3] Anthranilic acid, the starting material, underwent ester formation using thionyl chloride to afford methyl 2-aminobenzoate. Ullmann coupling with methyl 2-iodobenzoate followed by iodination to prepare the trimethyl nitrilotrisiodobenzoate**.** After saponification and the subsequent intramolecular Friedel–Crafts reaction gave the iodinated heterotriangulene. The Negishi cross-coupling reaction of the the isodinated heterotriangulene with *n*-hexylzinc bromide gave **6**. After thionation of 6, the thioketone (**7** and **8**) went through the Barton-Kellogg olefination of the thioketone **12** with 4-(diazo(phenyl)methyl)pyridine to prepare **9**. Reduction of **9** with triphenylphosphine gave the desired product **5**. Due to (*E/Z*) isomerization of **5**, variable-temperature ^{1}H-NMR spectroscopy was performed to confirm the structure of **5**. Each multiplet peaks (δ 8.55-8.35, 8.20-8.10, and 6.80-6.70) of **5** at 25 °C was

observed as a single sharp peak at 67 °C, indicating fast exchange of (*E, E*), (*E,Z*), and (*Z,Z*) forms.

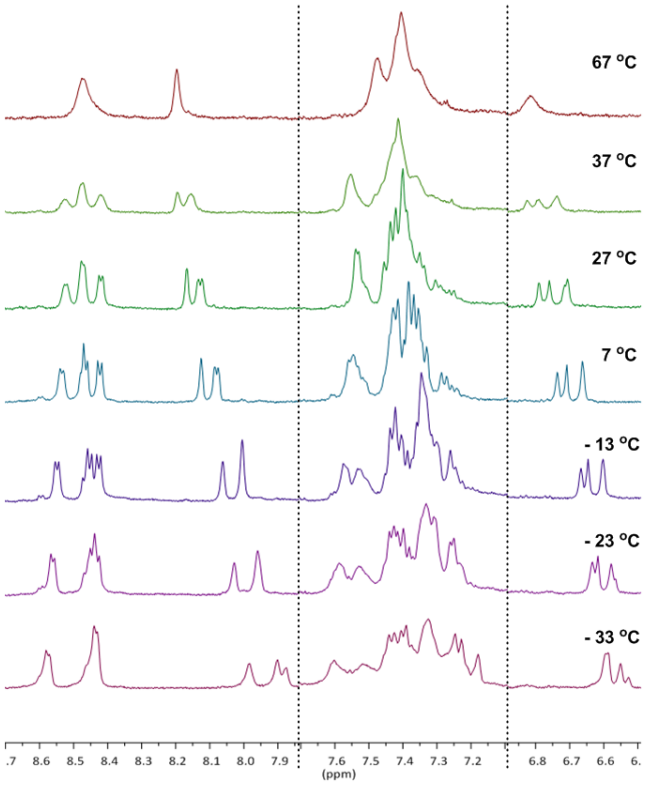

Figure 9.2. Observed isomerization of **9** on variable-temperature NMR experiment.

The compound **5** has three photocyclizable sites on a single molecule, thus, **5** was photocyclized in three discrete steps to the monocyclized product **10** and the dicyclized form **11**. The conversion of **5** to **10** and **10** to **11** was monitored by MALDI-MS analysis. According to the excitation and emission spectra of **5**, **10**, and **11** in the course of photocyclization, apparent redshift was shown (Figure 9.3).

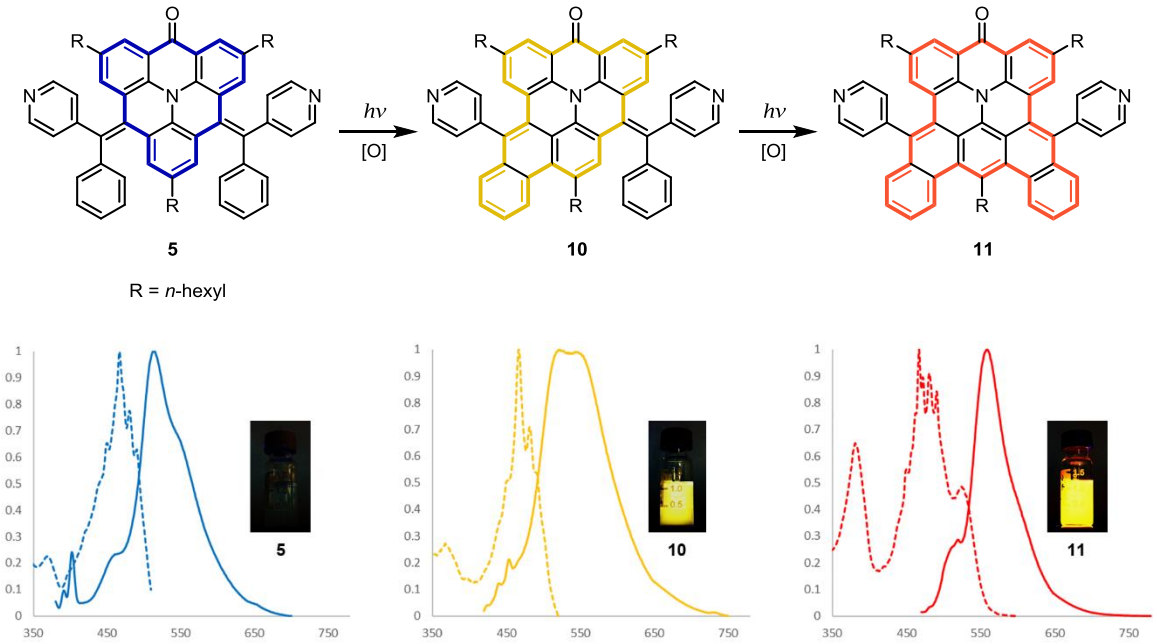

Figure 9.3. Synthesis and multistage photoactivation of **5** and emission and excitation spectra of **5**, **10**, and**11**. The dashed line represents excitation spectra and the solid line indicates emission spectra.

9.3 Conclusions

In conclusion, it has been demonstrated that the multistaged photoactivatable fluorophore **5** was synthesized and charcterized by NMR analysis. Photoconversion of **5** afforded the single-cyclized and double-cyclized products **10** and **11**. The excitation and emission spectra of **5**, **10**, and **11** have shown redshift. Mmore studies will be carried out to investigate its potential as a new tool for high-resolution optical imaging applications in addition to fluorescence lifetime imaging applications.

9.4 Experimental Section

General information

All commercial reagents and solvents were used without further purification. Flash column chromatography was done using Silicycle silica gel (55–65 Å pore diameter). Thin-layer chromatography was conducted on Sorbent Technologies silica plates (250 μm thickness). Proton nuclear magnetic resonance spectroscopy (^{1}H NMR) and carbon nuclear magnetic resonance spectroscopy (^{13}C NMR) spectra were obtained from a Bruker DMX 500 ^{1}H NMR. High performance liquid chromatography analysis was performed using a Jasco HPLC instrument equipped with a Phenomenex column (Luna 5u C18(2) 100A; 250 × 4.60 mm, 5 μm).

Experimental procedures

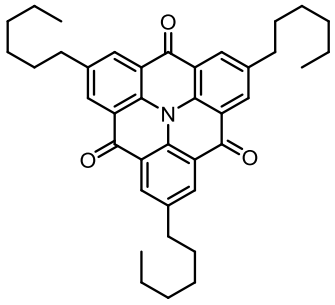

6

2,6,10-trihexyl-4H-benzo[9,1]quinolizino[3,4,5,6,7-defg]acridine-4,8,12-trione (6): 6 was prepared according to the literature procedure.[3]

^{1}H NMR (500 MHz, $CDCl_3$) δ 8.66 (s, 6H), 2.90 (t, 6H, J = 7.7 Hz), 1.79 (quint, 6H, J = 7.5 Hz) 1.46-1.31 (m, 18H), 0.91 (t, 9H, J = 7.0 Hz).

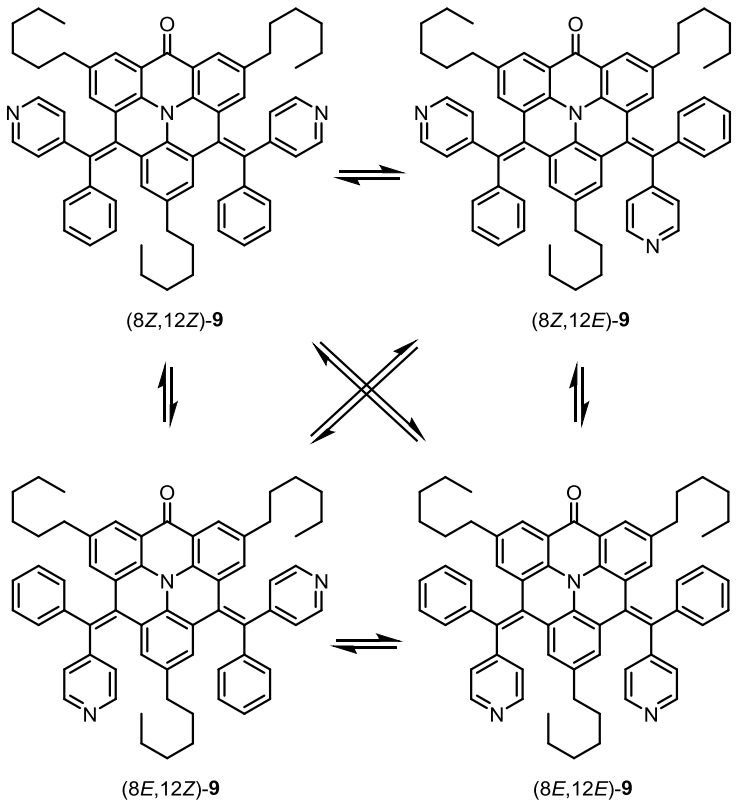

(8*Z*,12*Z*)/(8*Z*,12*E* or 8*E*,12*Z*)/(8*E*,12*E*)-2,6,10-trihexyl-8,12-bis(phenyl(pyridin-4-yl)methylene)-8,12-dihydro-4*H*-benzo[9,1]quinolizino[3,4,5,6,7-*defg*]acridin-4-one (9): A vial was charged with 10 μmol of **6** (5.8 mg), 50 μmol of Lawesson's reagent (26.6 mg) in 1.0 mL of anhydrous toluene and was heated under reflux. After 24 hours, the solution was cooled down and passed through silica gel packed filter. Blue or purple-colored fractions were collected, dried in vacuo, and used for the next step without further purification. A solution of 0.1 mmol (19.5 mg) of 4-(diazo(phenyl)methyl)pyridine in 1.0 mL of toluene was added to the crude mixture and the corresponding reaction mixture was stirred at 24 °C. After 12 hours, 0.1 mmol (33.3 mg)

of triphenylphosphine (polymer-bound) was added to the solution and stirred under reflux for 12 hours. The crude mixture was dried, redissolved in acetonitrile, and injected to HPLC for purification. 1.2 mg of 9 was isolated (14 % over three steps).

^{1}H NMR (500 MHz, CD_3OD) δ 8.73-8.47 (m, 4h), 8.27-8.07 (m, 2H), 7.92-7.64 (m, 4H), 7.60-7.28 (m, 12H), 6.96-6.78 (m, 2H), 2.62-2.28 (m, 4H), 2.11-1.81 (m, 2H), 1.39-0.64 (m, 33H).

^{13}C NMR (126 MHz, CD_3OD) δ 177.5, 160.2, 143.3, 142.7, 139.9, 138.6, 138.2, 136.7, 134.6, 134.1, 131.2, 130.9, 130.4, 130.4, 130.3, 130.0, 129.83, 129.76, 129.68, 129.60, 129.5, 129.2, 129.1, 128.6, 128.2, 128.0, 127.7, 127.58, 127.56, 127.39, 127.36, 127.0, 126.8, 126.39, 126.35, 126.33, 122.90, 122.85, 122.7, 121.4, 121.3, 119.9, 119.63, 34.60, 34.4, 34.2, 31.34, 31.30, 31.2, 31.0, 30.7, 28.5, 22.3, 22.23, 22.17, 13.04, 13.00.

Physical Property: Brown semi-solid.

9.5 Acknowledgments

This work was supported by funding from the University of Pennsylvania. We thank Dr. Charles W. Ross III, Director: Automated Synthesis and Characterization of Penn Chemistry, Ryan Kubanoff, BCRC Coordinator, and laboratory research associates, Miklos Szantai-Kis for providing chromatographic and mass spectral method development, analyses, and data interpretation.

9.6 References

(1) (a) Cho, S. Y.; Song, Y. K.; Kim, J. G.; Oh, S. Y.; Chung, C. M. *Tetrahedron Lett.* **2009**, *50*, 4769. (b) Gagey, N.; Neveu, P.; Benbrahim, C.; Goetz, B.; Aujard, I.; Baudin, J. B.; Jullien, L. *J. Am. Chem. Soc.* **2007**, *129*, 9986. (c) Faal, T.; Wong, P. T.; Tang, S.; Coulter, A.; Chen, Y.; Tu, C. H.; Baker, J. R.; Choi, S. K.; Inlay, M. A. *Mol. BioSyst.* **2015**, *11*, 783. (d) Ballister, E. R.; Aonbangkhen, C.; Mayo, A. M.; Lampson, M. A.; Chenoweth, D. M. *Nat. Commun.* **2014**, *5*, 5475. (e) Kobayashi, T.; Komatsu, T.; Kamiya, M.; Campos, C.; Gonzalez-Gaitan, M.; Terai, T.; Hanaoka, K.; Nagano, T.; Urano, Y. *J. Am. Chem. Soc.* **2012**, *134*, 11153. (f) Lord, S. J.; Conley, N. R.; Lee, H. L. D.; Samuel, R.; Liu, N.; Twieg, R. J.; Moerner, W. E. *J. Am. Chem. Soc.* **2008**, *130*, 9204. (g) Lim, R. K. V.; Lin, Q. *Acc. Chem. Res.* **2011**, *44*, 828. (h) Yu, Z.; Ho, L. Y.; Lin, Q. *J. Am. Chem. Soc.* **2011**, *133*, 11912. (i) An, P.; Yu, Z.; Lin, Q. *Org. Lett.* **2013**, *15*, 5496.

(2) (a) Rarig, R.-A. F.; Tran, M. N.; Chenoweth, D. M. *J. Am. Chem. Soc.* **2013**, *135*, 9213. (b) Tran, M. N.; Chenoweth, D. M. *Angew. Chem. Int. Ed.* **2015**, *54*, 6442. (c) Tran, M. N.; Chenoweth, D. M. *Chem. Sci.* **2015**, *6*, 4508.

(3) Hammer, N.; Shubina, T. E.; Gisselbrecht, J.-P.; Hampel, F.; Kivala, M. *J. Org. Chem.* **2015**, *80*, 2418.

Appendix 8

NMR Spectra Relevant to Chapter 9

This work was performed in collaboration with Joomyung V. Jun, a graduate student in the Chenoweth group at the University of Pennsylvania.

Figure A8.1. ^{1}H NMR spectrum of **6** in $CDCl_3$ (500 MHz).

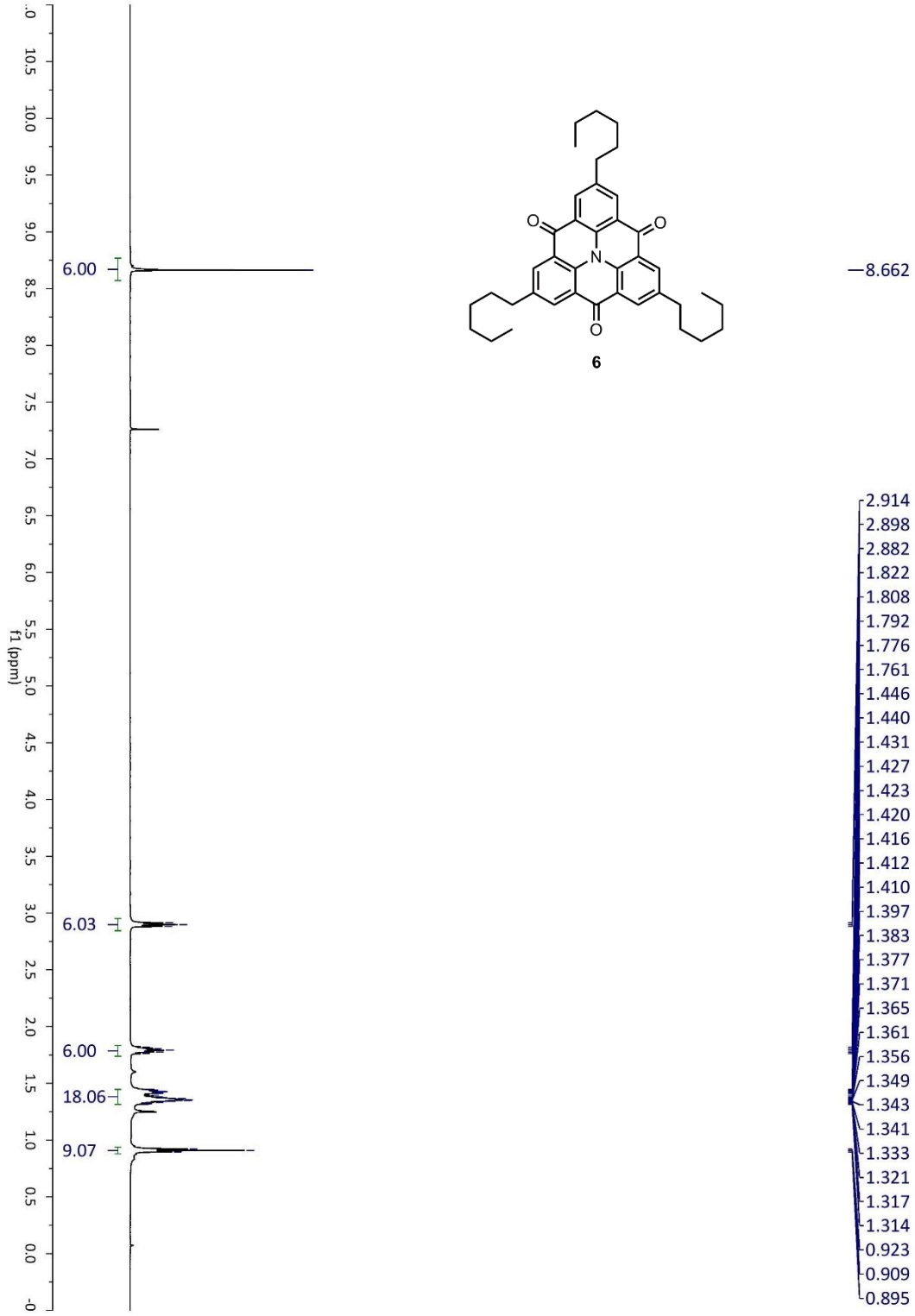

6

Figure A8.2. ^{1}H NMR spectrum of **9** in CD_3OD (500 MHz).

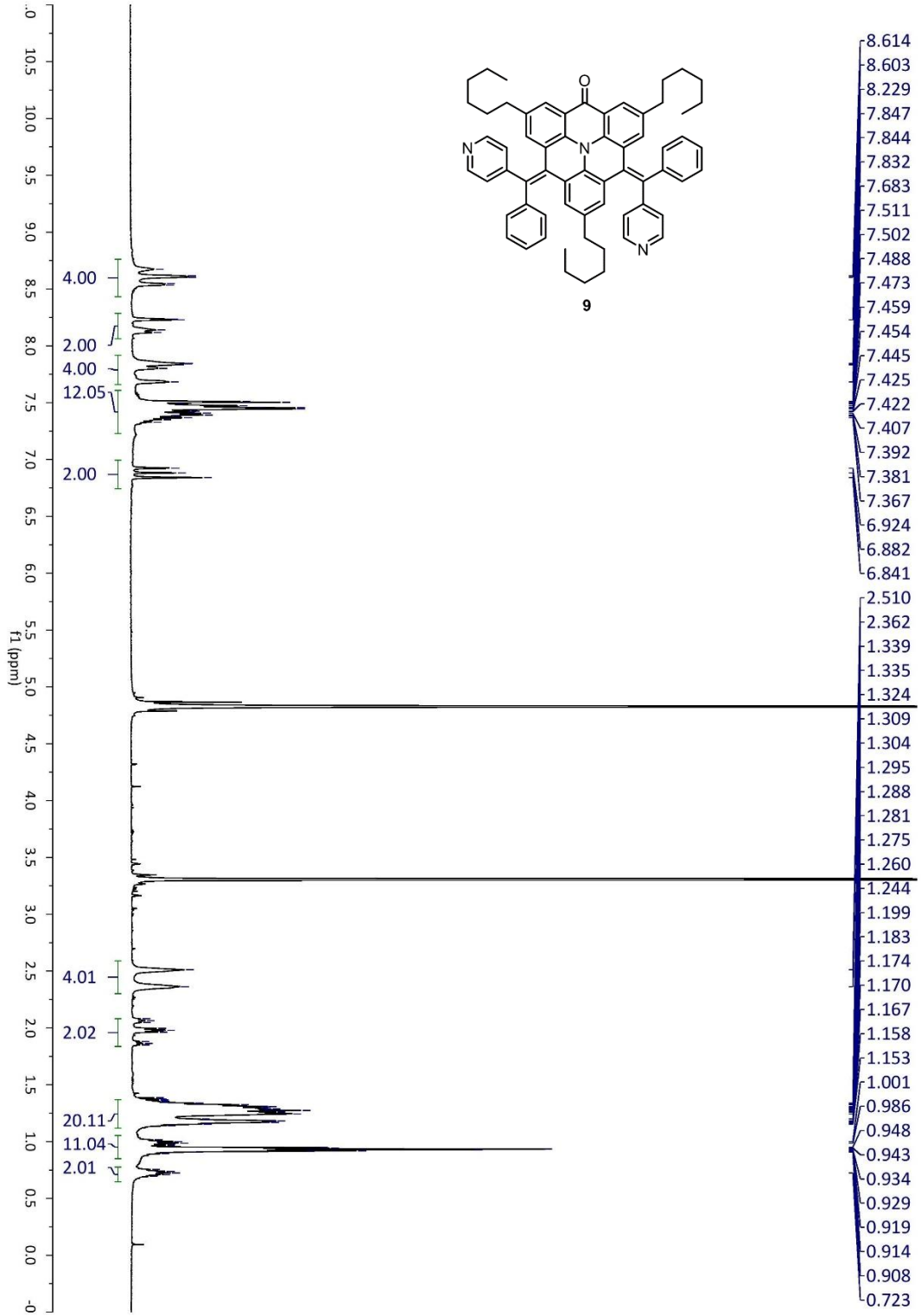

Figure A8.3. ^{13}C NMR spectrum of **9** in CD_3OD (125 MHz).